The Malaysian Journal of
ANALYTICAL SCIENCES
ISSN 1394-2506

Vol 17 No 1 (2013)

Vol 17 No 2 (2013)

Vol 17 No 3 (2013)

2013

The Malaysian Journal of Analytical Sciences Vol 17 No 1 2013

Articles 11 - 24 are selected papers from the "National Seminar on Oil and Fat (SMILE 2012)", 7 - 8 June 2012, MY Hotel, Bandar Kuah, Langkawi, Malaysia.

Guest Editors: Mohd Ambar Yarmo, Mohamed Rozali Othman, Muhammad Rahimi Yusop, Mohd Suzeren Md Jamil

		Page
1.	INFLUENCE OF HEAT TREATMENTS ON ELECTRICAL PROPERTIES AND MICROSTRUCTURE OF 10% MASS FRACTION OF SUCROSE YBCO SUPERCONDUCTOR (Kesan Rawatan Haba Ke Atas Sifat-Sifat Elektrik dan Mikrostruktur 10% Pecahan Jisim Sukrosa YBCO Superkonduktur) *S.Khalida, F.Fariesha, H.Azhan and S.Y.Yusainee*	1
2.	PENGARUH FAKTOR KERUANGAN DAN MASA DALAM MENENTUKAN KADAR PINTASAN HUJAN DI KANOPI HUTAN DIPTEROKARPA, TASIK CHINI PAHANG (Influence of Spatial and Temporal Factors in Determining Rainfall Interception at Dipterocarp Forest Canopy, Lake Chini, Pahang) *Nur Munirah Abdullah, Mohd Ekhwan Toriman, Haslinur Md Din, Nor Azlina Ab.Aziz, Mohd Khairul Amri Kamarudin, Nurul Syazwani Abdul Rani, Frankie Marcus Ata, Mohd Hafiz Saad, Noraini Wahida Abdullah Mushrifah Idris, Nor Rohaizah Jamil*	11
3.	LEACHATE CHARACTERIZATION FROM A CLOSED LANDFILL IN AIR HITAM, PUCHONG, MALAYSIA (Pencirian Air Larut Resap dari Tapak Pelupusan Ditutup Air Hitam, Puchong, Malaysia) *Nur Fatin Dahlia Mat Salleh, Ku Halim Ku Hamid*	24
4.	DEVELOPMENT OF BIO-BASED PAINT BY USING METHYL ESTERS FROM PALM OIL FOR CORROSION INHIBITOR (Pembangunan Cat Berasaskan Bio Menggunakan Metil Ester Dari Minyak Sawit Untuk Mengawal Pembentukan Karat) *Mohibah Musa, Miradatul Najwa Muhd Rodhi, Najmiddin Yaakob, Ku Halim Ku Hamid, Juferi Idris*	30
5.	AN EXPERIMENTAL DESIGN APPROACH FOR THE ANALYSIS OF LIQUID PHASE PRODUCTS IN WATER FOR HYDROGENOLYSIS OF GLYCEROL USING IMMERSED SOLID-PHASE MICROEXTRACTION (Pendekatan Reka Bentuk Eksperimen Untuk Analisis Produk Fasa Cecair Dalam Air Bagi Tindak Balas Hidrogenolisis Gliserol Menggunakan Rendaman Mikroekstraksi Fasa Pepejal) *Noraini Hamzah, Rozita Osman, Mohd Ambar Yarmo*	38
6.	ISOLATION AND CHARACTERIZATION OF COMPOUNDS FROM THE STEM BARK OF *UVARIA RUFA* (ANNONACEAE) (Pemisahan dan Pencirian Sebatian dari Kulit Batang Uvaria rufa (Annonaceae)) *Andi R. Rosandy, Laily B. Din, W .A. Yaacob, Nik Idris Yusoff, I. Sahidin, Jalifah Latip, Syarul Nataqain, Normah Mohd Noor*	50
7.	VARIATION OF RADON EMANATION IN WORKPLACES AS A FUNCTION OF ROOM PARAMETERS (Variasi Emanasi Radon Di Tempat Kerja Sebagai Fungsi Parameter Bilik) *Norafatin Khalid, Amran Ab. Majid, Aznan Fazli Ismail, Muhamad Samudi Yasir, Redzuwan Yahaya, Izzaty Azani Mustafa*	59

8. ISOLATION AND UTILIZATION OF CORN COBS HEMISELLULOSE AS CHELATING AGENT FOR LEAD IONS 71
(Pemencilan dan Penggunaan Hemiselulos Daripada Tongkol Jagung Sebagai Agen Pengkelat Untuk Ion Plumbum)
Muchlisyam, Urip Harahap, Jansen Silalahi, Zul Alfian

9. EFFECT OF SODA-ANTHRAQUINONE PULPING CONDITIONS AND BEATING REVOLUTION ON THE MECHANICAL PROPERTIES OF PAPER MADE FROM Gigantochloa scortechinii (SEMANTAN BAMBOO) 75
(Kesan Faktor-Faktor Pemulpaan Soda-Antrakuinon dan Pemukulan Ke Atas Sifat-Sifat Mekanikal Kertas Gigantochloa Scortechinii (Buluh Semantan))
Nurul Husna Mohd Hassan, Suhaimi Muhammed, Rushdan Ibrahim

10. COMPARATIVE STUDY ON CHARACTERISTICS AND POTENTIAL OF RICE STRAWS AND DRY LEAVES AS A BINDER IN REFUSE DERIVED FUEL (RDF) 85
(Kajian Perbandingan Pencirian dan Potensi Jerami Padi dan Daun Kering Sebagai Pengikat Dalam Bahan Bakar Buangan)
Othman, Z., Lias, K., Hashim, N.H., Clement, F.N.

11. SYNTHESIS OF ALKYLPOLYGLUCOSIDE FROM DEXTROSE-DECANOL IN THE PRESENCE OF SILICOTUNGSTIC ACID SOL-GEL CATALYST 91
(Sintesis Alkilpoliglukosida Daripada Dekstrosa-Dekanol Dengan Kehadiran Katalis Asid Silikotungstik Sol-Gel)
Izazi Azzahidah Amin, Mohd Ambar Yarmo, Nik Idris Nik Yusoff, Nor Asikin Mohamad Nordin, Wan Nor Roslam Wan Isahak

12. PHASE BEHAVIOR AND RHEOLOGY OF FATTY ALCOHOL SULPHATE, FATTY ALCOHOL ETHER SULPHATE FROM PALM BASED AND MIXTURES WITH OTHER SURFACTANTS 101
(Kelakuan Fasa dan Reologi Lelemak Alkohol Sulfat, Lelemak Alkohol Eter Sulfat Berasaskan Sawit dan Campuran dengan Surfaktan Lain)
Liew Kin Hong, Nur Syazani Harun, Mohd Suzeren Md Jamil, Rahimi M. Yusop

13. PENGEKSTRAKAN DAN PENCIRIAN NANOSELULOSA DARIPADA SERABUT KELAPA 109
(Extraction and Characterization of Nanocellulose from Coconut Fiber)
Nor Liyana Ahmad dan Ishak Ahmad

14. THE EFFECT OF CHEMICAL STRUCTURE ON POUR POINT, OXIDATIVE STABILITY AND TRIBOLOGICAL PROPERTIES OF OLEIC ACID TRIESTER DERIVATIVES 119
(Kesan Struktur Kimia Pada Titik Pour, Kestabilan Pengoksidaan Dan Sifat Tribological Derivatif Triester Asid Oleik)
Nadia Salih, Jumat Salimon, Emad Yousif

15. DEOXYGENATION OF PLANT FATTY ACID USING NiSnK/SiO2 AS CATALYST 129
(Penyahoksigenan Asid Lemak Tumbuhan Dengan Menggunakan NiSnK/SiO2 Sebagai Pemangkin Komposit)
L. T. Chiam and C. T. Tye

16. PHASE BEHAVIOUR OF FATTY ALCOHOL SULPHATE AND FATTY ALCOHOL ETHER SULPHATE FROM PALM BASED 139
(Kelakuan Fasa Lelemak Alkohol Sulfat Dan Lelemak Alkohol Eter Sulfat Berasaskan Sawit)
Nur Syazani Harun, Norhana Nabila Mohamed Talip, Liew Kin Hong, Mohd Suzeren Md Jamil, Rahimi M. Yusop

17. PENENTUAN KUALITI MINYAK MASAK DAN LEMAK KOMERSIAL MENGGUNAKAN TEKNIK KIMOMETIK 146
(Determination of Commercials Cooking Oils and Fats Using Chemometrics Methods)
Azwan Mat Lazim, Mohd Zuli Jaafar, Phang Wei Shong, Suzereen Jamil

18. PALM OLEIN BASED BIOLUBRICANT BASESTOCKS: SYNTHESIS, CHARACTERISATION, TRIBOLOGICAL AND RHEOLOGICAL ANALYSIS 153
(Stok Asas Biolubrikan Berasaskan Minyak Sawit Olein: Sintesis, Pencirian, Analisis Tribologi dan Reologi)
Darfizzi Derawi and Jumat Salimon

19. CHANGES ON THE SOLID FAT CONTENT OF PALM OIL/SUNFLOWER OIL BLENDS VIA INTERESTERIFICATION 164
(Perubahan Kandungan Lemak Pepejal Campuran Minyak Sawit RBD/Bunga Matahari Melalui Penginteresteran)
Suria Ramli, Azwani M. Lazim, Siti Aishah Hasbullah

20. GLYCINE AS ALTERNATIVE FUEL IN MAKING HYDROTALCITE COMPOUND BY MEANS OF COMBUSTION METHOD 171
(Glisin Sebagai Bahanapi Alternatif Dalam Pembuatan Sebatian Hidrotalsit Melalui Kaedah Pembakaran)
Shamsudin I.K, Helwani Z, Abdullah A.Z, Wiheeb A.D, Othman M.R

21. CATALYTIC CRACKING OF USED PALM OIL USING COMPOSITE ZEOLITE 176
(Peretakan Bermangkin Minyak Kelapa Sawit Terguna Menggunakan Zeolit Komposit)
W. H. Chang and C. T. Tye

22. SYNTHESIS OF ESTOLIDE 2-ETHYLHEXYL ESTER FROM RICINUS COMMUNIS 185
(Sintesis Estolida 2-Etilheksil Ester dari Ricinus Communis)
Nazrizawati Ahmad Tajuddin, Nor Habibah Rosli, Jumat Salimon, Mohd Firdaus Mohd Yusoff, Noraishah Abdullah

23. LIPIDIZATION OF SIMPLE AND DI-FUNCTIONAL AMINO ACIDS 193
(Penglipidan Asid Amino Ringkas dan Dwi-Fungsi)
Zainab Idris, Mohd. Wahid Samsudin, Salmiah Ahmad

24. PERAWATAN AIR SISA KILANG KELAPA SAWIT SECARA ELEKTROKIMIA 200
(Palm Oil Factory Wastewater Treatment Using Electrochemical Technique)
Nor Ain Mohd Aluwi, M.S Md Jamil, Rahimi M. Yusop, Bakri Din, Firdaus Ismail, Mohamed Rozali Othman

The Malaysian Journal of ANALYTICAL SCIENCES ISSN 1394-2506

INFLUENCE OF HEAT TREATMENTS ON ELECTRICAL PROPERTIES AND MICROSTRUCTURE OF 10% MASS FRACTION OF SUCROSE YBCO SUPERCONDUCTOR

(Kesan Rawatan Haba Ke Atas Sifat-Sifat Elektrik dan Mikrostruktur 10% Pecahan Jisim Sukrosa YBCO Superkonduktur)

S.Khalida[1*], F.Fariesha[2], H.Azhan[3] and S.Y.Yusainee[4]

[1]*International Education College (INTEC), UiTM Seksyen 17, 40200 Shah Alam, Selangor, Malaysia*
[2]*Faculty of Applied Sciences, Universiti Teknologi MARA Perak,, Kampus Tapah, 35400Tapah Road, Perak, Malaysia*
[3]*Universiti Teknologi MARA Pahang, 26400 Bandar Jengka, Pahang, Malaysia*
[4]*Faculty of Applied Sciences, Universiti Teknologi MARA,40450 Shah Alam, Selangor, Malaysia*

**Corresponding author: khalidasalleh@salam.uitm.edu.my*

Abstract

The influence of different heat treatments on the superconducting properties of 10% mass fraction of sucrose structure YBCO superconductor was investigated. X-Ray Diffraction (XRD) and Scanning Electron Microscopy (SEM) equipments were used to determine the phase of superconductor and structural studies respectively at10% mass fraction of sucrose. The samples were prepared via solid state (SSM) and co-precipitation (CPM) reaction methods and underwent sintering and heat treatment process at 900°C, 930°C and 960°C respectively with mixing of $C_{12}H_{22}O_{11}$ sucrose during pelletization. The $T_{C,on}$ decreases with respect to higher heat treatment temperature. The suppression of both $T_{C,on}$ and $T_{C,off}$ indicates the destruction of superconductivity trends. The best $T_{C,off}$ were achieved in pure SSM and CPM samples sintered at 950°C for 5 hours with $T_{C,off}$ 86K and 91K respectively. Comparing with pure YBCO, the 10% mass fraction of sucrose YBCO exhibited higher critical current, I_C by two times. It indicates the effect of high surface area in porous structure. The XRD results confirmed that all the samples remain in single phase, which indicates no effect of sucrose in the porous structures sample and maintaining in orthorhombic structure. Higher heat treatment at 960°C resulted in destruction on its superconductivity behavior due to the partial melt phase on its microstructure, especially in CPM. This is due to the smaller grain size of samples which trapped more heat and causing partial melting to occur rapidly. It can be deduced that, annealing temperatures at 900°C and 930°C are the best optimum heat treatments for CPM and SSM porous superconductor, respectively.

Keywords: YBCO superconductor, porous superconductor, sucrose

Abstrak

Kesan pelbagai rawatan haba ke atas sifat-sifat 10% pecahan jisim sukrosa ke atas YBCO superkonduktor telah dikaji. Peralatan seperti "X-Ray Diffraction" (XRD) dan "Scanning Electron Microscopy" (SEM) telah digunakan untuk menentukan fasa superkonduktor dan strukturnya pada 10% pecahan jisim sukrosa. Bahan ujikaji telah disediakan melalui kaedah keadaan pepejal (SSM) dan pemendakan sampingan (CPM), melalui pembakaran dan proses rawatan haba pada suhu 900°C, 930°C dan 960°C dengan mencampurkan sukrosa $C_{12}H_{22}O_{11}$ semasa proses pembentukkan pelet. $T_{C,on}$, suhu genting onset menurun dengan kenaikan suhu rawatan haba. Penurunan kedua-dua $T_{C,on}$ dan $T_{C,off}$ menunjukkan penghapusan arah aliran kesuperkonduktoran. $T_{C,off}$ yang terbaik dicapai pada sampel tulen SSM dan CPM yang dibakar pada 950°C selama 5 jam di mana $T_{C,off}$ adalah masing-masing 86K dan 91K.Apabila dibandingkan dengan YBCO tulen, 10% pecahan jisim sukrosa YBCO mempunyai arus genting, I_C yang dua kali lebih tinggi. Ia menunjukkan kesan luas permukaan yang tinggi dalam struktur berpori. Keputusan XRD mengesahkan bahawa semua bahan ujikaji kekal dalam satu fasa,yang menunjukkan sukrosa tidak membawa kesan ke atas sampel dan sampel kekal dalam struktur ortorombik. Rawatan haba yang tinggi pada 960°C mempamirkan kerosakan pada sifat kesuperkondutorannya akibat fasa separa cair pada mikro sturktur terutamanya pada CPM. Ini disebabkan oleh pengecilan saiz butir sampel yang memerangkap lebih banyak haba dan menyebabkan proses separan cair berlaku pada kadar yang tinggi. Ini boleh disimpulkan bahawa suhu pembakaran pada 900°C dan 930°C masing-masing adalah suhu optimum rawatan haba untuk CPM dan SSM pori superkonduktor.

Kata kunci: YBCO superkonduktor, pori superkonduktur, sukrosa

Introduction

Although its ability as a high field magnet has been realized, still, bulk YBCO loses its high temperature superconducting property due to low critical current densities. Despite critical current density (J_C) of thin films superconductor, for instance, exceeds bulks by at least two orders of magnitude, thin films also are not really suitable for high integral currents [1].Therefore, the applications of superconductor require material to be available in a variety of shapes and forms. Bulk and thin films superconductor reveal their own strength and weaknesses. The discovery of intermediate forms such as foams and porous superconductor has attracted many researchers to study its unique properties that are highly interesting for our modern applications. The porous pattern is believed to be the best solution for the low critical density's problems [1-6].Foams and porous superconductor have common properties where contained open pore structures that is believed to improve the performance of the superconductor which is not in bulks and thin films. Many other aspects are related to foam and porous structure, for example, more efficient heat transfer, faster oxygenation, less related micro cracking, possibility of reinforcement and of interlocking connections [2]. Although many interesting properties can be found in open porous structure, but one of the most unique properties is that it can results in higher J_C. Even though there are numbers of publications concerning methods of creating open porous superconducting structures [3,4], none focuses on its critical current. High critical current is important for various applications. Thus, this research will focus on investigating YBCO porous superconductor's unique properties and to investigate whether heat treatment and level of porosity will influence the YBCO superconducting properties, mainly on its critical current (I_C). Structural studies of the porous superconductor using powder X-Ray Diffraction (XRD) and Scanning Electron Microscope (SEM) reveal the relationship between superconducting properties and the YBCO's porous structure and microstructure.

Materials and Methods

For YBCO solid state method (SSM) sample, the precursor was prepared using powders of yttrium oxide, Y_2O_3 (Alfa Aesar, 99.90%), barium carbonate, $BaCO_3$ (Alfa Aesar, 99.80%) and copper oxide, CuO (Aldrich, 99.00%), and carefully mixed thoroughly according to its stoichiometry, $YBa_2Cu_3O_{7-x}$ in a ratio of 1: 2: 3. Then, the chemicals in grey powders were ball-milled for 24 hours to obtain fine powders and after dried in an oven for several hours. Then, the dried mixture was ground in a mortar and pestle. The mixture was then sintered at 900°C and 950°C for 5 hours respectively to get powder sample of SSM.

Co-precipitation method (CPM) sample was prepared from an aqueous solution of the salts of metals using an oxalate precipitation reagent under basic pH conditions. In this technique, a simultaneous coprecipitation of Y, Ba, and Cu oxalates by precipitating in mixture of ethanol: water (70:30) medium and using triethylammonium-oxalates (TEO) as the precipitating agent under controlled pH conditions. Stock solution of barium nitrate, Ba $(NO_3)_2$ (Aldrich, 100%), copper nitrate, $Cu(NO_3)_2$ (Hamburg chemicals, 99.90%) and yttrium nitrate, $Y(NO_3)_3$ (Aldrich, 99.90%) were prepared by dissolving the corresponding metal nitrates in distilled water. The precipitating agent, TEO $((C_2H_5)_3NH)_2C_2O_4$ was prepared by dissolving triethylamine (TEA) (Sigma-Aldrich, 99.00%) and oxalic acid (Merck, 99.00%) (2:1 mol ratio) in ethanol (System, 99.00%). After mixing the metal nitrate solution (1:2:3) in a beaker, the pH of the solution was adjusted to 4.0 by 5% solution of TEA in 70:30 ethanol:water mixtures resulting in a bluish color precipitate appeared. The solution was stirred for 30 minutes and then filtered. The crystalline precipitate was washed with ethanol and dried in an oven at 300°. The mixture was then sintered at 900°C and 950°C for 5 hours respectively to get powder sample of CPM.

Then, pressed the powder samples of SSM and CPM at 30MPa to form a pure sample pellet. To create an open pores superconductor, the crystalline sucrose (HmBg Chemicals, 99.00%) as filler was added in an amount necessary to obtain 10% mass fraction of sucrose using the mass fraction formula as in equation (1). The pores samples were then pressed to 30MPa to form pellet.

In the mass fraction formula,

$$W_A = \frac{M_A}{M_{tot}} \times 100\% \quad (1)$$

where,

W_A = mass fraction of one substance
M_A = mass of sucrose, (g)
M_{tot} = total mixture of mass (sucrose + YBCO powder), (g)

Then, the 10% mass fraction of sucrose samples of both SSM and CPM were heated at 400°C in order to burn out the sucrose completely before undergoing three different heat treatments which are 900°C, 930°C and 960°C at 5 hours respectively. The pure samples are also subjected to the same annealing heat treatment conditions for comparison.

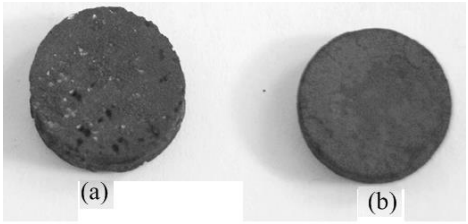


Figure 1. Different porosity of (a) 10% mass fraction of sucrose and (b) non-porous samples after underwent heat treatment.

Sample characterization process involves the electrical and structural aspects of these samples as well as its density measurement. Measurement of electrical resistance was made using four-point probe method whereas the structural and microstructural characterizations were made using X-Ray Diffraction (XRD) and Scanning Electron Micrographs (SEM).

X-Ray Diffraction (XRD) is used to study the crystal structure, particle size, phase formation and to a lesser extent, crystal defect and disorder. While in this research, XRD is used extensively in order to study the phase formation of porous YBCO in powder and pellet forms with absence of remaining sucrose filler after heated. The lattice parameter *a*, *b*, and *c* were determined using this technique. In a typical XRD, an X-Ray tube provides copper-Kα radiation that is collimated through an aperture diaphragm before the Kα radiation is absorbed by a 12μm thick nickel filter and it is then detected by standard scintillation counter. The sample rotates by a consecutive step process such that an angel of incidence of the primary beam gradually increased between present values. The detector is correspondingly moved around the sample at precise double the angular velocity ensuring that at all time the diffraction angle (2 θ) is twice the glancing angle (θ). The control of sample position and scintillation data are controlled and recorded by a computer where a real time display of the data can be viewed. Data collection times were taken in 2 or 3 hours and the scanning range 2θ is between 2° and 60°.

The porosity structures of samples are characterized by the calculation of density samples using Archimedes Principle as in equation (2) to ensure the porosity pattern.

$$\rho_s = \frac{m_s \times \rho_w}{m_w} \quad (2)$$

where,

ρ_s = density of sample
ρ_w = density of water, (g/cm^3)
m_s = mass of sample
m_w = mass of water

The dc resistivity measurements of the samples are performed on the sample between 20K and 300K with the four-probe method to obtain its critical temperature (T_C). The critical current (I_C) was also measured using the four-point probe technique. The samples was placed in a sample holder of a Cryogenic Closed Cycle cryostat by using Electrolube silver paint to allow the current flow and minimize the contact resistance, and mounted with four probes using copper wires to connect the samples to the device. The pellets were lightly polished using sandpaper before mounting to remove foreign particles and dust. A d.c current was supplied by Keithley Model 197A Autoranging Multimeter with an accuracy of $\pm$0.001 mV. The temperature of cryostat is controlled by Lakeshore Model 340 temperature controller ($\pm$0.001K). For each sample, three different current were applied and the corresponding voltages were recorded for I_C measurement. The average value of resistivity was then taken as the resistivity at 300K (room temperature).

In addition, SEM is used to study the surface of samples at very high magnification and to obtain the micrographs to give clues how the surface morphology of the samples were like. To operate SEM, samples were placed on a carbon-conductor tape on the holder. The sample is mounted inside the main chamber where the holder is attached to the main platform by sliding it to fit nicely to the holder mount. Fine electron beam is aimed at the surface of sample. The intensity of the reflected beam is then picked up by the sensor. This signal is then fed to the computer which maps the intensity of the electron reflection and thus would produce a black and white picture. For the purpose of this study, the images of the samples were magnified 15,000 times at accelerating voltage of 5 kV.

Grain size may be determined by using quadrant technique. In this method, the straight line are drawn and measured through the grains. The measured length are then is compared with the grain scale given in the micrograph pictures which is 1µm actual size of grain = 0.8 cm size of grain in the micrograph picture.

Results and Discussion

The result and discussion on this research contains results from resistance measurement, X-Ray diffraction analysis (XRD) and scanning electron microscope (SEM) micrographs from all samples, from pure to 10% mass fraction of sucrose sample, where sucrose is added after sintering at 900°C and 950°C, and then heat treated at 900°C, 930°C and 960°C at 5 hours respectively.

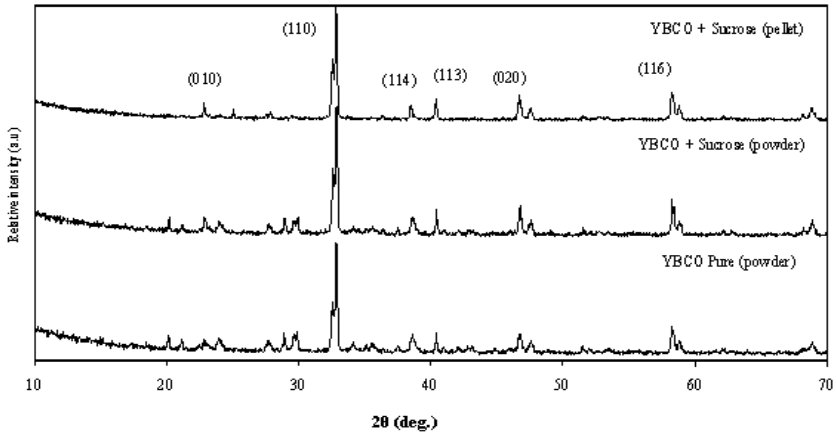


Figure 2. XRD pattern for pure YBCO and 10% mass fraction of sucrose YBCO after heated at 400°C and annealed at 930°C via CPM.

Table 1. Lattice parameter of pure and porous YBCO samples via CPM.

Sample YBCO	a (A°) ± 0.1%	b (A°) ± 0.1%	c (A°) ± 0.1%	Volume ($A°m^3$) (± 0.3%)
YBCO + Sucrose (pellet)	3.824	3.889	1.687	1.738
YBCO+Sucrose (powder)	3.818	3.890	1.668	1.732
YBCO (pure)	3.820	3.887	1.651	1.730

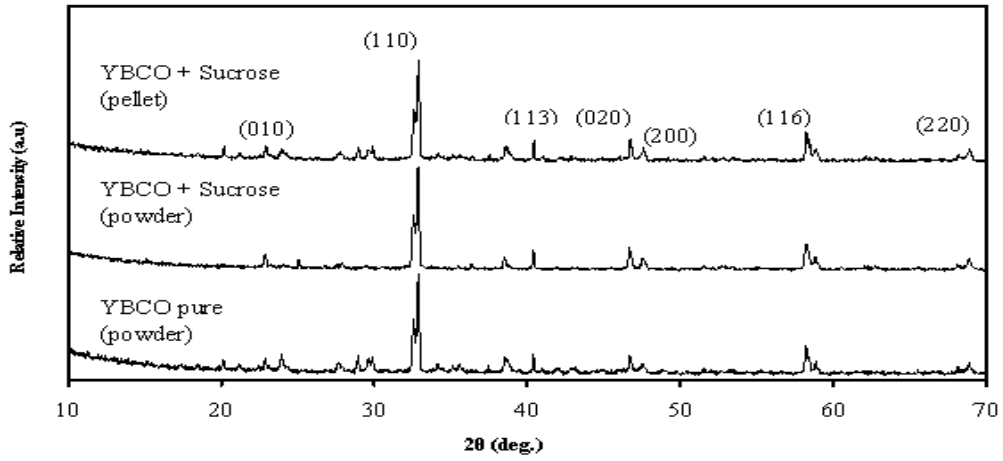


Figure 3. XRD pattern for pure YBCO and 10% mass fraction of sucrose YBCO after heated at 400°C and annealed at 930°C via SSM

Table 2. Lattice parameter of pure and porous YBCO samples via CPM.

Sample YBCO	a (A°) ± 0.1%	b (A°) ± 0.1%	c (A°) ± 0.1%	Volume ($A°m^3$) (± 0.3%)
YBCO + Sucrose (pellet)	3.827	3.893	1.699	1.743
YBCO+Sucrose (powder)	3.888	3.825	1.662	1.734
YBCO (pure)	3.820	3.887	1.651	1.730

Figure 2 and 3 above presents the XRD patterns for a reference sample (pure sample) and porous sample, after adding sucrose, heated at 400°C and annealed at 930°C for 5 hours. All samples showed a degree of single phase 123 where the $T_{c,on}$ are about 73K and 88K.

The X-Ray analysis also succeeds revealing that this orthorhombic structure of superconductor shows the absence of the remaining sucrose filler after heated. It is obviously shows that the sucrose in the YBCO samples was burned out completely.

Adding sucrose as filler had induced an increasing in surface area on open porous YBCO structures and hence reduces its density values. As shown in Table 1and Table 2, the inter-plane *c* changed practically as compared with *a* and *b* lattice. It is known that porosity had reduced the T_C and increased the unit cell volume. It is believed that the loss of oxygen content resulted in the expansion of *c* lattice. For these porous samples, it can be observed that with decreasing T_C, *a*-lattice parameter was not much affected but *c*-lattice values are increased.

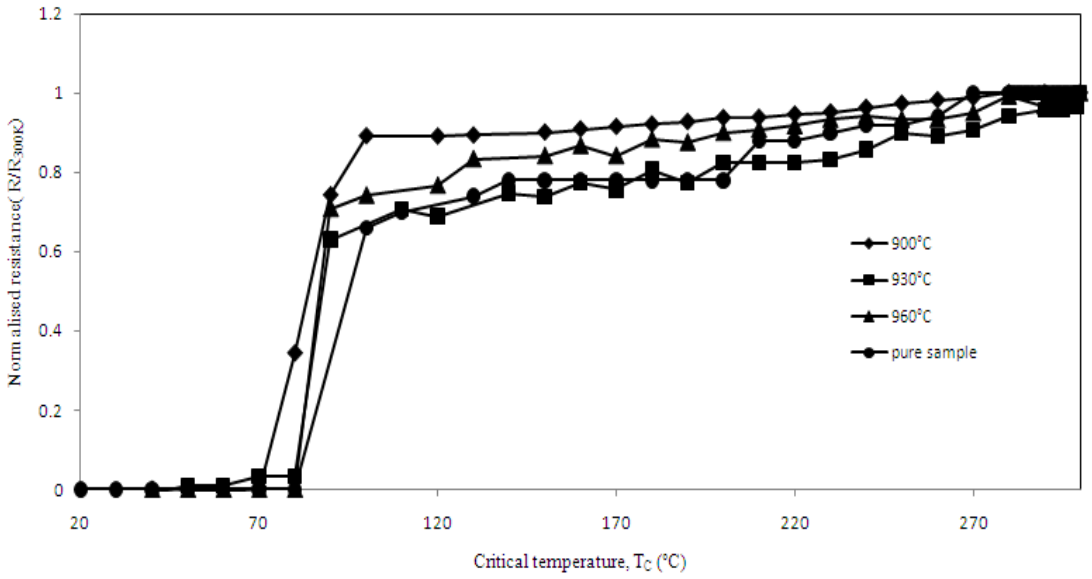


Figure 4. T_C for pure and 10% mass fraction of sucrose YBCO superconductor after annealing at 900°C, 930°C and 960°C via CPM.

The measurement of electric resistance characteristic for pure and porous samples showed metallic behavior of electric conductivity above the onset critical temperature ($T_{C,on}$)for all samples as seen in Figure 3 and 4. This shows that adding sucrose as filler does not alter the superconducting behavior of the pure YBCO superconductor but alter the electrical properties of superconductor. The highest value of onset critical temperature ($T_{C,on}$) and offset critical temperature ($T_{C,off}$) were achieved on a sucrose-free sample. For 10% mass fraction of sucrose YBCO superconductors via CPM with 900°C heat treatment is found to have the highest T_C where $T_{C,off}$ = 77K and $T_{C,on}$ = 86K. Generally, the same trend for all heat treatment series for both methods showed that the critical transition temperature (T_C) value as illustrated in Table 2 and 3 in porous superconductor is considerably decrease with increased in porosity.

Table 3. $T_{C,off}$, and $T_{C,on}$, and for pure and 10% mass fraction of sucrose YBCO heat treated sample at 900°C , 930°C and 960°C via CPM and SSM.

Heat treatment / Method	Porosity %	$T_{C,off}$ K ± 1	$T_{C,on}$ K ± 1	ΔT K ± 1
Pure CPM	0	91	97	6
900°C / CPM	10	77	86	9
930°C / CPM	10	67	85	18
960°C / CPM	10	70	100	30
Pure SSM	0	86	90	4
900°C / SSM	10	61	88	27
930°C / SSM	10	73	88	15
960°C / SSM	10	54	71	17

The effect of three different heat treatments suggested that the general performances of porous superconductor failed to improve the values of its critical temperature. Probably, the oxygen inside YBCO lattice suppressed the superconducting properties as suggested by previous researchers [7]. However, in pure YBCO samples, the remaining of copper oxide (CuO) along the [0 1 0] direction in the samples instead of YBCO itself did not cause any significant decrease in T_C. Nevertheless, in porous samples, an apparent reduction of T_C is observed and some of the sample has lower than expected T_C such as in the 10% porous YBCO. It could be due to the porous samples having an open porous structure resulting in loss vital oxygen from its structure.

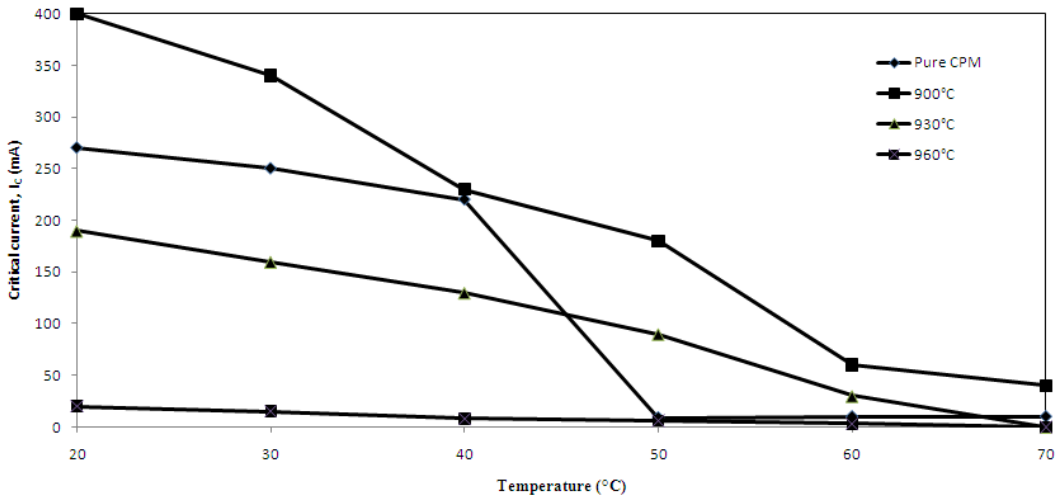


Figure 5. Critical current, I_C for 10% mass fraction of sucrose YBCO at 20K to 70K for samples heat treated at 900°C, 930°C and 960°C via CPM.

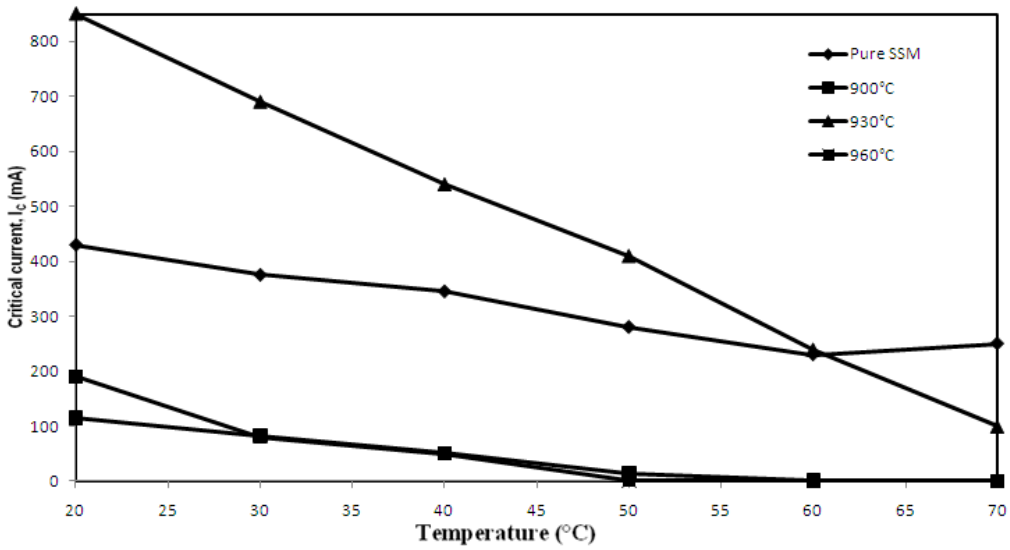


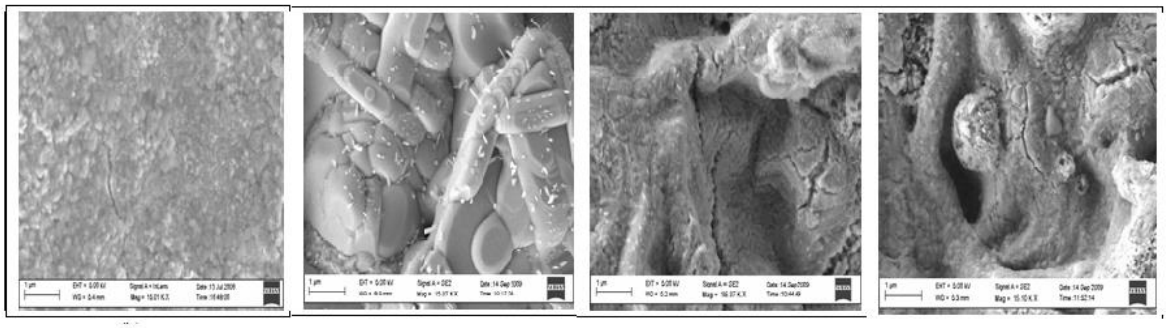
Figure 6. Critical current, I_C for 10% mass fraction of sucrose YBCO at 20K to 70K for samples heat treated at 900°C 930°C and 960°C via SSM.

Table 4. Critical current, $I_{C,}$ for pure and 10% mass fraction of sucrose YBCO heat treated sample at 900°C , 930°C and 960°C via CPM and SSM.

Heat treatment / Method	Critical current at various temperature (mA)					
	20K	30K	40K	50K	60K	70K
Pure CPM	270	250	200	90	10	10
900°C /CPM	400	340	230	180	60	40
930°C /CPM	190	160	130	90	30	-
960°C /CPM	20	15	8	6	3	-
Pure SSM	430	375	345	280	230	250
900°C / SSM	115	83	51	14	1	-
930°C / SSM	850	690	540	410	240	100
960°C / SSM	190	80	50	-	-	-

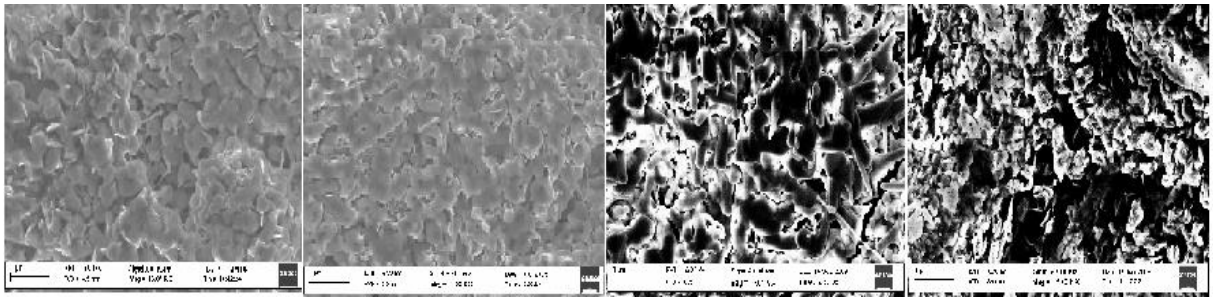
Critical current for superconductivity samples also depends on the temperature. Lower temperature of heat treatment's sample will result in higher critical current in the sample as seen in Table 4. Comparing with pure samples, the 10% mass fraction of sucrose YBCO is able to transport significantly higher critical current than the dense structure due to the increase in the surface area of porous YBCO as illustrated in Figure 5 and 6.

The I_C of samples increases in increasing porosity from pure to 10% mass fraction of sucrose for certain heat treatments. The increase of I_C may be due to the thin grain boundary and growth of grains on the sample structures as observed in 10% mass fraction of sucrose YBCO for 900°C heat treatment (CPM) and 930°C heat treatment (SSM). This porosity resulted in larger grain size hence, higher in I_C compared to others as seen in Figure 7 and 8. The existence of large, elongated grains separated by low-angle grain boundaries can increase the I_C value since it is capable to transport large amounts of currents [8]. Higher heat treatment at 960°C resulted in partial melting in the samples and thus degraded the I_C and affects its superconductivity. With increasing sintering temperature, the total number of grains will increase and consequently, the total number of intergrain weak links increases [9]. It can be obviously seen in Figure 7 to 8 that 960°C heat treatment led to microcracks presence in the sample and causes considerable reduction in I_C value [10].



(a) (b) (c) (d)

Figure 7. Micrographs of fractured surface of (a) pure and 10% mass fraction of sucrose YBCO sample that underwent heat treatment for (b) 900°C, (c) 930°C and (d) 960°C respectively via CPM.



(a) (b) (c) (d)

Figure 8. Micographs of fractured surface of (a) pure and 10% mass fraction of sucrose YBCO sample that underwent heat treatment for (b) 900°C, (c) 930°C and (d) 960°C respectively via SSM.

Different heat treatments altered the grain size and texturing. However, these samples showed a very compact structure with smaller grain size approximately in the order of 0.25 µm with addition of sucrose the grain size increase to ~ 2 µm. Pure sample tends to have higher T_C and smooth curves (Figure 4, 7 and 8).

Different heat treatments altered the grain size and texturing. However, CPM samples showed a very compact structure with smaller grain size approximately in the order of 0.25 µm with addition of sucrose the grain size increase to ~ 2 µm. Thus, CPM samples have finer size compared to the SSM samples. Pure CPM sample tends to have higher T_C and smooth curves when compared to SSM sample as seen in Figure 4.

For the 900°C heat treatment samples, the effect of sucrose addition caused the formation of porous structure. It can be concluded that, higher temperature of heat treatment up until 960°C produced smaller grain size samples and caused the partial melting occurred hence destroyed the structure of the samples. Heat treatment of 930°C is the optimum heat treatment for porous samples where it's $T_{C,on}$ and $T_{C,off}$ are almost similar to pure sample. The 10% mass fraction of sucrose enhanced grain growth and orientation in all the samples.

Conclusion

The effect of heat treatment on percentages of porous YBCO superconductor via SSM and CPM has been investigated. It can be deduced that heat treatment and porosity play important role in superconductivity of YBCO. The best superconducting behavior in terms of the critical temperature was observed in pure YBCO with no addition of sucrose as filler especially in CPM samples. The CPM method meanwhile offers some advantages over SSM such as simple to prepare and allows a rapid formation of the YBCO phase. Moreover, in CPM the particle size is easy to control and the stoichiometry ratio can be determined and thus, it showed that the CPM method produced a very fine powder. It is proved that the critical temperature decreases when the density of superconductor decreases which is in increasing of porosity. No improvement in the critical temperature behavior was observed in porous structure superconductor. However, an obvious difference between porous and non-porous superconductor is the effect of surface that is much greater in porous superconductor and hence resulted in increase of critical current up to twice as much higher compared to non-porous superconductor in for 900°C heat treatment (CPM) and 930°C heat treatment (SSM). XRD pattern showed that having sucrose as a filler phase have no effect on its structure for both CPM and SSM. It is proved that the crystallographic structure remain in orthorhombic where a, b, and c lattice were not much affected. However, higher heat treatment, 960°C will results in destruction on its superconductivity behavior due to the partial melt phase to the smaller grain size of CPM samples easily trapped more heat and caused partial melting to occur. It also led to microcracks presence in the sample and causes considerable reduction in I_C value. For this reason, it can be concluded that, heat treatment of 900°C and 930°C are the optimum heat treatment for CPM and SSM porous superconductor respectively.

Acknowledgement

The authors wish to thank the Ministry of Science Technology and Innovation (MOSTI), Malaysia, via the National Science Fellowship (NSF) and Ministry of Higher Education (MOHE), Malaysia, via the Fundamental Research Grant Scheme (FRGS) for the financial support.

References

1. Noudem, J. G., Reddy,E. S., and Schmitz, G. J. (2003). Magnetic and transport properties of $YBa_2Cu_3O_y$ superconductor foams, *Physica C*, 390: 286-290.
2. Noudem, J.G., Guilmeau, E., Chateigner, D., Lambert,S., Reddy, E.S., Ouladdiaf, B., and Schmitz, G.J. (2004). Properties of $YBa_2Cu_3O_y$-textured superconductor foams, *Physica C*, 408: 655-656.
3. Reddy, E. S., and Schmitz, G. J. (2002). Superconducting foams. *Supercond. Sci. Technol*, 15: 21-24.
4. Reddy, E. S., Herweg, M., and Schmitz, G. J. (2003). Processing of Y_2BaCuO_5 foams. *Supercond. Sci. Technol*, 16: 608-612.
5. Fiertek, P., and Sadowski, W. (2006). Processing of porous structures of $YBa_2Cu_3O_{7-\partial}$ High Temperature superconductor, *Materials Science-Poland*, 24: 1103-1108.
6. Fiertek, P., Andrzejeski, B., and Sadowski, W. (2010). Synthesis and transport properties of porous superconducting ceramics of $YBa_2Cu_3O_{7-\partial}$, Rev. *Adv. Mater. Sci*, 23: 52-56.
7. Grinenko, V., Krasnoperov, E. P., Stoliarov, V. A., Bush, A. A., and Mikhajlov, B. P. (2006). Superconductivity in porous $MgBr_2$, RRC Kurchatov Institute, Moscow, Rusia.
8. Poeppel, R. B., Goretta, K. C., Balachandran, U., Dorris, S. E., Lanagan, M. T., Picciolo, J. J., Singh, J. P., and Youngdahl, C. A. (1992). Processing and properties of bulk high temperature superconductors, *Brazillian Journal of Physics*, 22: 2.
9. Hanic, F., Cigan, A., Butcha, S., Manka, J., and Zrubec, V. (2001). A possible using of superconducting measurement to better understanding of catalytic properties of $YBa_2Cu_3O_x$. *Measurement science review* 1: 1.
10. Warrier, K. G. K., Varma, H. K., Mani,T. V., and Damodaran, A. D. (1993). Zone refining of sintered, microwave-derived YBCO superconductors, *Journal of Materials sciences*. 30: 3238 - 3241.

The Malaysian Journal of ANALYTICAL SCIENCES ISSN 1394-2506

PENGARUH FAKTOR KERUANGAN DAN MASA DALAM MENENTUKAN KADAR PINTASAN HUJAN DI KANOPI HUTAN DIPTEROKARPA, TASIK CHINI PAHANG

(Influence of Spatial and Temporal Factors in Determining Rainfall Interception at Dipterocarp Forest Canopy, Lake Chini, Pahang)

Nur Munirah Abdullah[1], Mohd Ekhwan Toriman[1]*, Haslinur Md Din[1], Nor Azlina Ab.Aziz[1], Mohd Khairul Amri Kamarudin[1], Nurul Syazwani Abdul Rani[1], Frankie Marcus Ata[1], Mohd Hafiz Saad[1], Noraini Wahida Abdullah[1] Mushrifah Idris[2], Nor Rohaizah Jamil[3]

[1] *Pusat Pengajian Sosial, Pembangunan dan Persekitaran, Fakulti Sains Sosial dan Kemanusiaan*
[2] *Pusat Pengajian Sains Sekitaran dan Sumber Alam, Fakulti Sains dan Teknologi,*
Universiti Kebangsaan Malaysia Bangi, 43600 Selangor.
[3] *Jabatan Sains Alam Sekitar,*
Universiti Putra Malaysia, Serdang, 40300 Selangor.

**Corresponding author: ekhwan@ukm.my*

Abstrak

Kehilangan air hujan oleh proses pintasan dipengaruhi oleh dua mekanisme utama iaitu ciri iklim dan ciri fisiografi tumbuhan. Ciri iklim yang mempengaruhi kehilangan pintasan adalah jumlah curahan hujan (mm), kelajuan angin (m/s) dan suhu sekitar (°C). Ciri fisiografi tumbuhan yang mempengaruhi kehilangan pintasan pula terdiri daripada ketinggian, kulit, diameter, kanopi, ranting dan dahan pokok. Dengan melihat peranan iklim dan ciri fisiografi tumbuhan dalam proses pintasan, kajian ini dijalankan untuk mengukur kadar jatuhan langsung (mm), aliran batang (mm) dan pintasan hujan (mm) serta faktor yang mempengaruhinya. Penilaian jatuhan langsung dan pintasan hujan dilakukan di atas plot kajian bersaiz 100 x 100 meter di Hutan Dipterokap Tasik Chini, Pahang. Kajian ini dilakukan bermula dari bulan Oktober 2009 hingga Januari 2010. Tiga puluh pokok telah dikenalpasti dan dipilih sebagai sampel kajian aliran batang berdasarkan spesies, famili, diameter aras dada (DBH) serta kepadatan dan saiz kanopi. Empat set jatuhan langsung digunakan untuk melakukan pengukuran jatuhan langsung. Hasil kajian mendapati nilai jatuhan langsung (TF) dan aliran batang (SF) yang direkodkan pada empat kali kejadian hujan pada bulan Oktober 2009 ialah 0.66 % (TF) dan 99.34 % (SF), November 2009 - 0.54% (TF) dan 99.46% (SF), Disember 2009 – 0.72% (TF) dan 99.28 % (SF) dan bulan Januari 2010 - 0.49% (TF) dan 99.51% (SF). Analisis statisitik juga menunjukkan wujudnya hubungan antara jumlah curahan hujan kasar dengan pintasan pada aras signifikan 0.571 (r^2) bagi bulan Disember 2009. Kajian ini membekalkan maklumat penting berkaitan dengan kitaran hidrologi dan bagaimana kanopi pokok bertindak sebagai medium pengimbang air dalam kawasan hutan.

Kata kunci: jatuhan langsung, aliran batang, pintasan, dipterokarpa, keruangan dan masa

Abstract

The reduction of rainfall by interception process is influenced by two mechanisms namely climate and plant physiographic features. Climate features that affecting the interception loss including total rainfall (mm), wind speed (m/s) and temperature (°C). Meanwhile plant physiographic features that affect interception loss consists of tree's height, skin, diameter, canopy, twigs and branches. Looking the role of climate and plant physiographic features in the interception process, this study was conducted in order to measure the throughfall, stem flow and interception loss and the factors that influence it. The assessment of throughfall and interception loss were carried out on study plot sized 100 x 100 meter in Dipterocarp Forest of Tasik Chini, Pahang. The study was conducted from October 2009 until January of 2010. Thirty tree samples are used and each tree is well-identified based on their species, family, diameter breast height (DBH), canopy size and its density. Four sets of throughfall were used to do throughfall measurements. Results of this study found that the value of throughfall and stem flow collected based on four rainfall events namely in October 2009 where 0.66 % (TF) and 99.34 % (SF), November 2009 – 0.54 % (TF) and 99.46 % (SF), December 2009 – 0.72 % (TF) and 99.28 % (SF) and January of 2010 – 0.49 % (TF) and 99.51 % (SF). Statistical analysis

also indicates the existence of the relationship between total rainfall and interception loss with significant levels in 0.571 (r^2) in December of 2009. This study provides important information that related to the hydrological cycle and how plant's canopy can be acted as a medium of water balance in the environment.

Keywords: troughfall, stem flow, interception, dipterocarp, spartial and temporal

Pengenalan

Fungsi hutan dalam mengekalkan keseimbangan proses hidrologi dilihat melalui fungsi tumbuh-tumbuhan yang mempengaruhi corak penyebaran hujan sesuatu kawasan. Sebahagian daripada jumlah hujan yang turun akan dipintas oleh daun dan lain-lain bahagian tumbuhan, lalu tersejat ke atmosfera. Jumlah air yang tidak dipintas oleh tumbuhan akan jatuh ke tanah melalui jatuhan langsung dan aliran batang pokok [1]. Justeru, peranan yang dimainkan oleh hutan dalam aspek hidrologi adalah melibatkan proses aliran batang, jatuhan langsung dan pintasan.

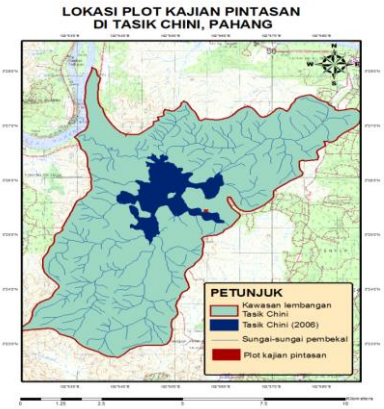
Namun begitu, kecekapan fungsi hutan dalam proses pintasan air hujan dipengaruhi oleh dua faktor utama iaitu faktor keruangan (spatial) dan masa (temporal). Perbezaan pengaruh dua faktor ini akan menghasilkan variasi dalam kadar pintasan yang dilakukan oleh sesuatu tumbuhan. Pengaruh faktor keruangan lebih menjurus kepada sifat tumbuh-tumbuhan yang menjalankan fungsi pintasan. Manakala pengaruh faktor masa pula melibatkan perbezaan dari aspek ciri meteorologi [2].

Dengan keberkesanan fungsi pintasan air hujan yang dimainkan oleh tumbuhan, pengurangan kadar larian air permukaan yang bertindak menghakis dan membawa pelbagai bentuk bahan yang dihakis menuju ke sumber air dapat dikekang. Hal ini kerana pengurangan hakisan permukaan akibat larian air permukaan merupakan indikator menentukan kualiti air yang terdapat di kawasan sumber air berhampiran.

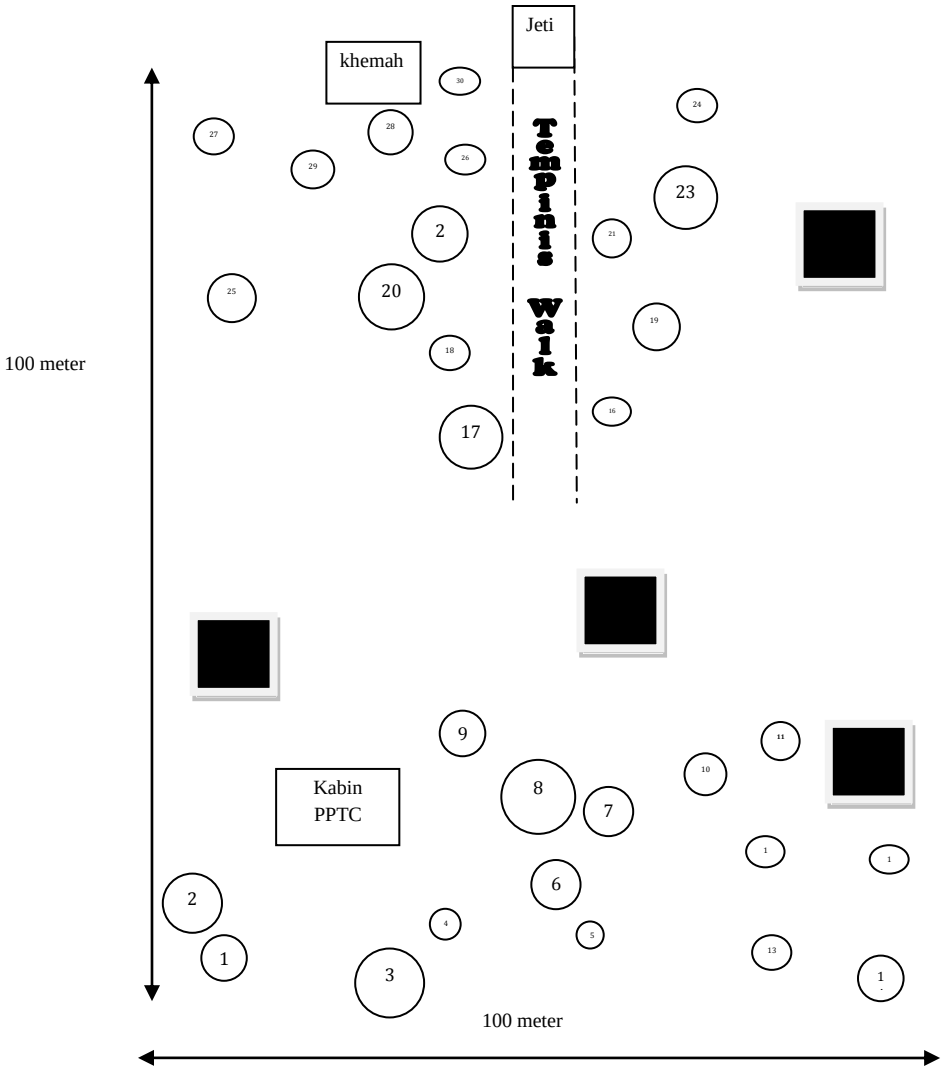
Antara objektif dalam menjalankan kajian pintasan ini termasuklah; (i) mengkaji ciri fisiografi pokok sampel di plot pintasan, (ii) mengukur kadar jatuhan langsung, aliran batang dan pintasan hujan, dan (iii) mengenalpasti faktor keruangan dan masa yang mempengaruhi kadar pintasan.

Metodologi

Tasik Chini terletak di bahagian tenggara Pahang, Malaysia yang mempunyai bacaan kedudukan pada garis lintang merangkumi 3°24'40"U hingga 3°26'42"U dan 102°52'18"T hingga 102°55'54". Juga Sinonim dengan kelebihan sebagai tasik semulajadi yang kedua terbesar di Malaysia. Dengan kedudukan plot kajian yang terletak dalam lingkungan kawasan beriklim khatulistiwa, ianya menerima taburan hujan yang sekata sepanjang tahun dengan keadaan cuaca yang panas dan lembap. Selain kadar kelembapan bandingan yang tinggi (80 %), plot kajian juga mempunyai purata suhu tahunan sebanyak 28 ^{0}C. Turut dicirikan dengan purata kelajuan angin yang rendah iaitu 0.5 m/s [3;4]. Rajah 1 menunjukan peta Tasik Chini dan kedudukan titik plot kajian. Manakala Rajah 2 pula merupakan peta kuadrat setiap pokok di plot kajian berukuran 100 meter x 100 meter pintasan Tasik Chini, Pahang.



Rajah 1. Peta Tasik Chini dan titik plot kajian pintasan di Tasik Chini, Pahang.



Rajah 2. Kedudukan kuadrat pokok sampel dan set jatuhan langsung dalam plot kajian 100 meter X 100 meter (sumber: Kerja Lapangan, 2009).

Petunjuk = Pokok sampel = Set Jatuhan Langsung

Skala 1 cm : 4 meter

Pemilihan Sampel Pokok

Sebanyak 30 batang pokok telah dipilih sebagai set aliran batang dan kriteria dalam pemilihan pokok yang diambil adalah pokok yang mempunyai ukuran lilit pokok lebih daripada 20 mm pada paras dada pengkaji. Empat set jatuhan langsung pula diletakkan secara rawak di plot pintasan untuk mendapatkan nilai jatuhan langsung (Tf). Foto 2 & 3 menunjukkan set aliran batang dan jatuhan langsung.



Foto 1: Pokok set aliran batang



Foto 2: Set jatuhan langsung

Analisis Data

Untuk mendapatkan nilai pintasan hujan, rumus yang digunakan ialah [5, 6] :

$$I = R - (Sf + Tf) \quad (1)$$

iaitu:

I = pintasan
R = hujan kasar
Sf = aliran batang
Tf = jatuhan langsung

Hasil dan Perbincangan

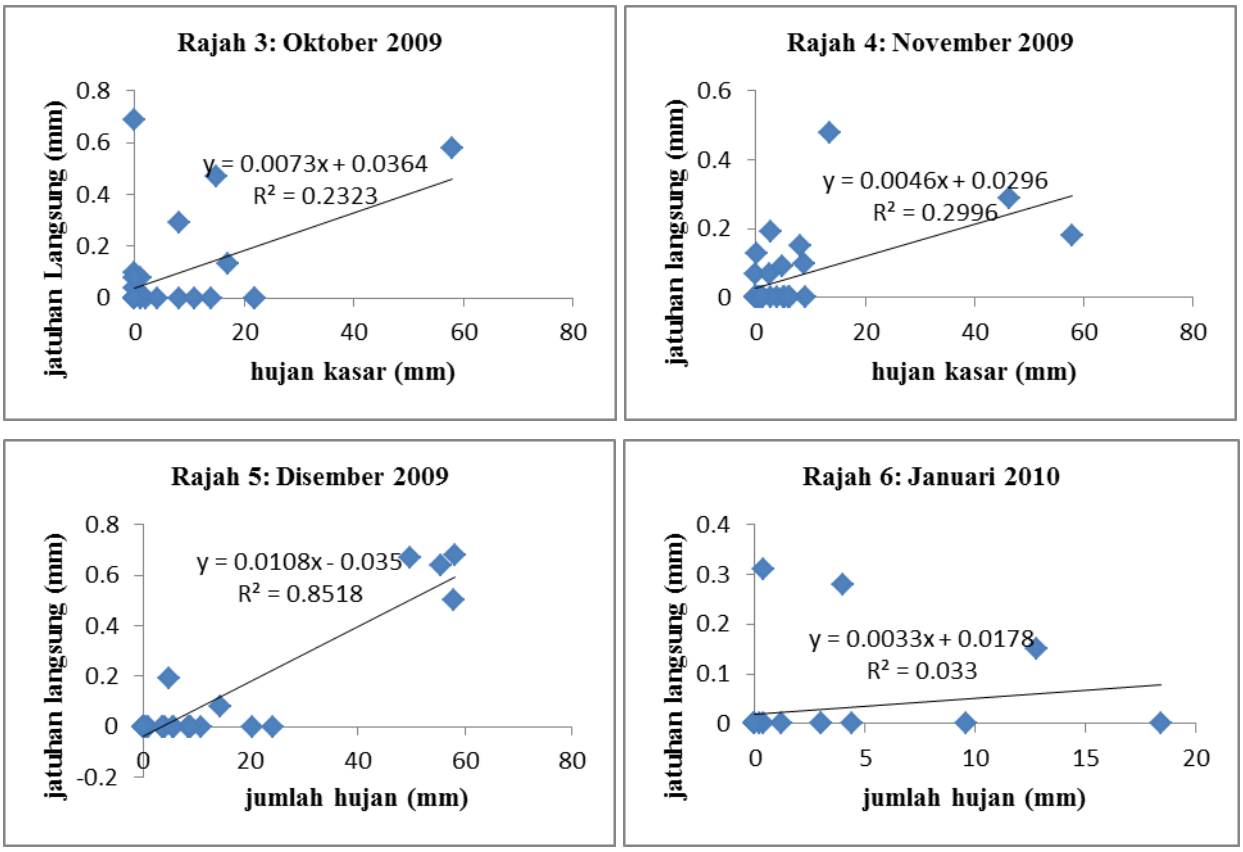
Menurut Chappell *et al*. [5] dan Crockford & Richardson [6], pintasan merangkumi tiga komponen utama iaitu jatuhan langsung (Tf), aliran batang (Sf) dan hujan kasar (R). Hubungan antara ketiga-tiga komponen dianalisis dengan ujian statistik kolerasi regrasi.

Jumlah Hujan Kasar

Hutan dipterokarpa Tasik China Pahang merupakan salah satu hutan hutan hujan tropika dan mempunyai ciri kanopi pokok yang sederhana tebal. Disebabkan kedudukannya dalam lingkungan khatulistiwa, hutan ini menerima hujan sekata sepanjang tahun disamping dipengaruhi oleh fenomena monsun. Berdasarkan kajian, jumlah hujan kasar bulan Oktober 2009 ialah 183.0 mm (sisihan piawai ±1.19 mm). Bulan November dan Disember pula masing-masing mencatatkan jumlah hujan kasar 200.1 mm (sisihan piawai ±1.30 mm) dan 356.0 mm (sisihan piawai ±1.83 mm). bulan Januari mencatatkan curahan hujan kasar sebanyak 57.4 mm (sisihan piawai ±4.26 mm).

Perilaku Hujan Dan Jatuhan Langsung

Hubungan antara jumlah jatuhan langsung yang berlaku adalah bergantung kepada jumlah curahan hujan kasar yang turun dalam suatu tempoh tertentu. Ini bermakna, semakin tinggi jumlah curahan hujan yang diterima dalam sesebuah bulan, jumlah jatuhan langsung yang dicatatkan juga adalah tinggi. Perhubungan antara jumlah jatuhan langsung dengan jumlah curahan hujan kasar bagi setiap bulan sepanjang tempoh kajian ditunjukkan pada Rajah 3-6.

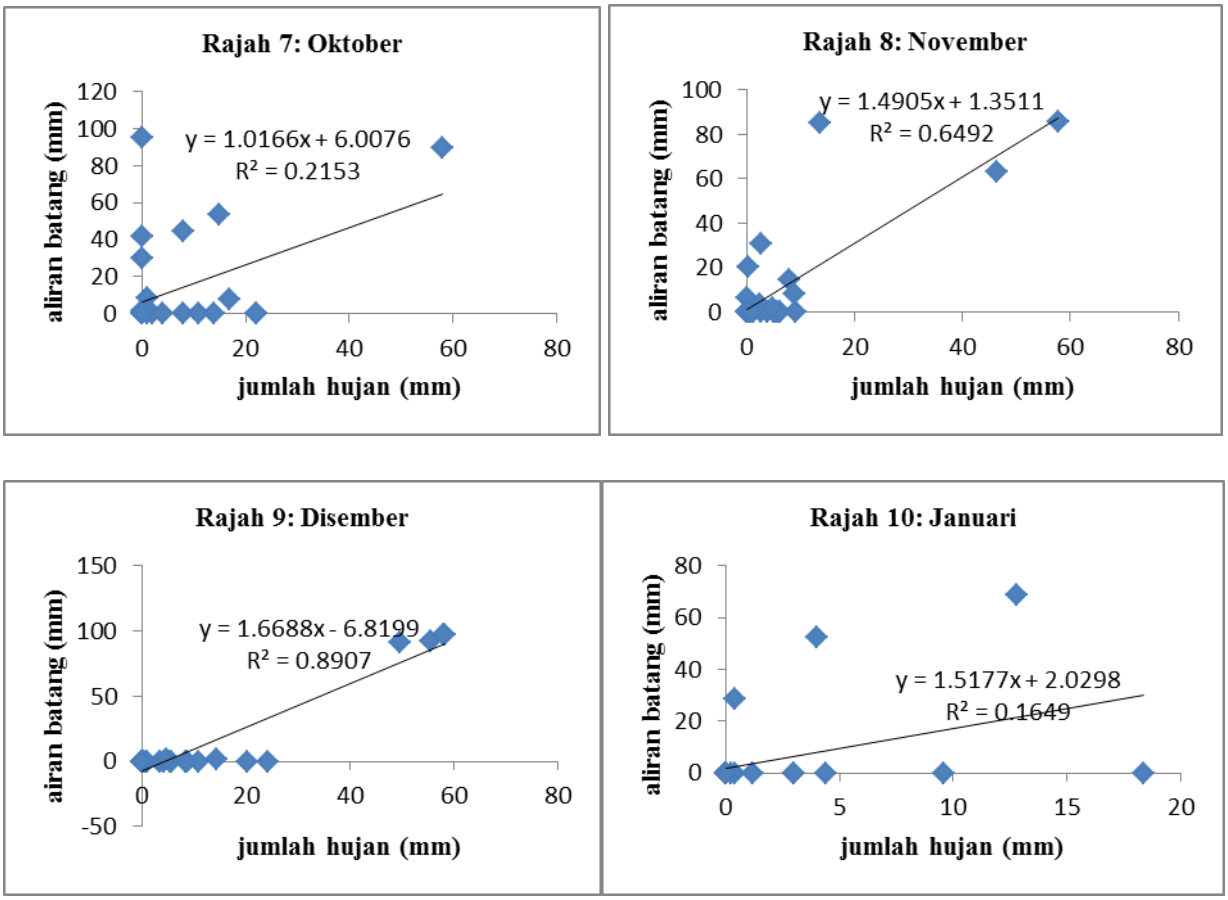


Rajah 3-6. Perhubungan antara jumlah hujan dengan jatuhan langsung bagi bulan Oktober 2009 hingga Januari 2010 (sumber: Kerja Lapangan 2009/2010).

Berdasarkan kepada Rajah 3-6, perilaku antara jumlah hujan kasar dengan jatuhan langsung adalah berbeza bagi setiap bulan mengikut musim. Melalui teknik kolerasi, hubungan yang ditunjukkan bagi perilaku hujan dan jatuhan langsung bulan Oktober 2009 adalah sangat lemah iaitu r^2=0.232. Bulan November 2009 juga menunjukkan hubungan kolerasi lemah dengan nilai pekali kolerasi r^2=0.275. Faktor hubungan yang lemah ini disebabkan kerana bulan November adalah permulaan bagi musim hujan. Bulan Disember 2009 pula mewakili musim hujan telah menunjukkan hubungan kolerasi yang tinggi antara jumlah hujan dan jatuhan langsung, iaitu r^2=0.851. Bagi bulan Januari 2010 pula, hubungan yang ditunjukkan antara komponen hujan dan jatuhan langsung tidak kuat dengan nilai pekali kolerasi r^2=0.033.

Perilaku Hujan Dan Aliran Batang

Perilaku hujan kasar dan aliran batang berdasarkan kajian adalah berbeza bagi setiap bulan. Jumlah aliran batang pada bulan Oktober ialah 372.27 mm (sisihan piawai ±2.60mm). Bulan November dan Disember pula masing-masing mencatatkan jumlah aliran batang sebanyak 319.86 mm (sisihan piawai ±2.41 mm) dan 382.67 mm (sisihan piawai ±3.23). Manakala bulan Januari pula mencatatkan jumlah aliran batang sebanyak 150.04 mm (sisihan piawai ±1.59). Nilai pekali kolerasi bagi bulan Oktober ialah 0.215 (r2), bulan November ialah 0.649 (r^2), bulan Disember ialah r^2=0.890 dan bulan Januari pula ialah r^2=0.164. Perhubungan antara jumlah hujan kasar dan aliran batang sepanjang tempoh kajian ditunjukan dalam Rajah 7 hingga 10.



Rajah 7-10. Perhubungan antara jumlah hujan dengan aliran batang dari bulan Oktober 2009 hingga Januari 2010 (sumber: Kerja Lapangan 2009/2010).

Perilaku Hujan Dan Pintasan

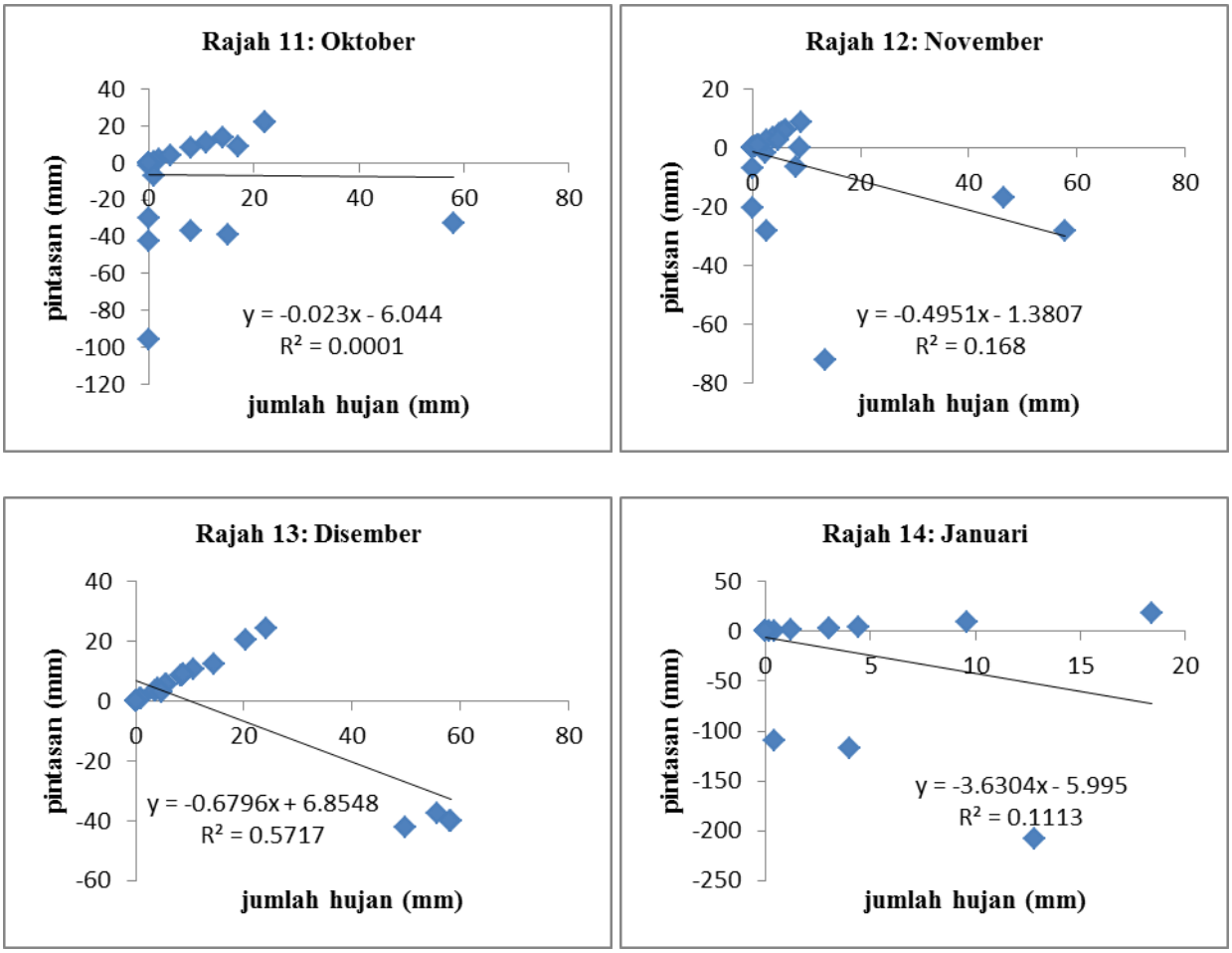
Pintasan hujan amnya merujuk kepada kehilangan air hujan sebelum ianya sampai ke permukaan bumi. Kehilangan air hujan yang berlaku adalah bergantung kepada halangan-halangan yang terdapat di sesebuah kawasan. Halangan-halangan ini boleh terdiri daripada kanopi tumbuh-tumbuhan yang akan menjalankan fungsi storan sementara yang memerangkap jatuhan air hujan supaya tidak terus jatuh ke permukaan bumi. Apabila air hujan jatuh dan dipintas oleh liputan tumbuh-tumbuhan di permukaan bumi, ianya akan mengalir melalui ranting, dahan, batang dan juga daun-daun pokok. Menurut Ismail [7], hujan yang turun di kawasan hutan akan dipintas oleh kanopi pokok sebelum sampai ke permukaan bumi. Apabila jatuhan air hujan yang turun diperangkap oleh fungsi tumbuh-tumbuhan, ianya akan memberi masa kepada tanah untuk menjalankan proses susupan air hujan dengan lebih efektif dan melengkapkan kitaran hidrologi sesebuah kawasan.

Berdasarkan kajian, nilai pintasan yang dicatatkan bagi setiap bulan adalah berbeza-beza dan ianya dipengaruhi oleh nilai jumlah hujan kasar (mm), aliran batang (mm) dan jatuhan langsung (mm) yang direkodkan bagi setiap bulan. Kajian yang dilakukan sepanjang tempoh bulan Oktober 2009 hingga Januari 2010, perilaku hujan kasar dan pintasan hujan adalah berbeza setiap bulan. Pada bulan Oktober, jumlah keseluruhan pintasan yang dicatatkan ialah -191.73 mm (sisihan piawai ±2.32 mm). Bulan November dan Disember masing-masing mencatatkan nilai pintasan sebanyak -121.51 mm (sisihan piawai ±1.61mm) dan -29.49 mm (sisihan piawai ±1.64 mm). Bulan Januari pula mencatatkan nilai pintasan -394.23 mm (sisihan piawai ±4.63 mm).

Nilai pekali kolerasi bagi bulan Oktober, November, Disember dan Januari masing-masing mencatatkan nilai r^2=0.0001, r^2=0.138, r^2=0.571 dan r^2=0.111. Perilaku perhubungan antara hujan kasar dan pintasan ditunjukan dalam Rajah 11, 12,13 & 14. Bulan Disember 2009 merupakan bulan yang mencatatkan hubungan perilaku antara hujan kasar dengan pintasan yang tinggi dengan nilai signifikan r^2=0.571 berbanding dengan bulan yang lain sepanjang tempoh kajian. Bulan Oktober 2009 pula merupakan bulan yang mencatatkan nilai signifikan paling rendah iaitu r^2=0.000. Nilai pintasan bagi bulan November 2009 dan Januari 2010 pula, masing-masing mencatatkan nilai signifikan r^2=0.168 dan r^2=0.111. Perbezaan diantara nilai signifikan perilaku hujan dan pintasan berlaku disebabkan faktor utamanya iaitu perbezaan jumlah curahan hujan yang diterima bagi setiap bulan sepanjang tempoh kajian. Hal ini berlaku kerana semakin tinggi jumlah curahan hujan yang diterima, maka semakin tinggi juga nilai pintasan yang boleh dilakukan oleh tumbuhan di sesebuah kawasan. Namun, faktor keruangan seperti ciri fisiografi pokok sampel tidak boleh diabaikan dalam menentukan kekuatan kadar pintasan yang berlaku.

Faktor Reruang Dalam Menentukan Kadar Jatuhan Langsung, Aliran Batang & Pintasan Hujan

Ciri-ciri dan sifat pokok yang mempengaruhi jumlah jatuhan langsung, aliran batang dan pintasan ialah dari segi ketinggian pokok, diameter batang (DBH), kulit pokok, kanopi, dahan serta ranting pokok. Jadual 1 menunjukan data bagi ciri fisiografi pokok sampel di kawasan kajian.



Rajah 11-14. Perhubungan antara jumlah hujan dengan pintasan bagi bulan Oktober hingga Januari (sumber: Kerja Lapangan 2009/2010).

Jadual 1. Data nama spesies, nama tempatan dan ciri fisiografi setiap pokok sampel di kawasan hutan terdedah

Pokok	Nama spesies	Nama tempatan	Ketinggian (m)	DBH (cm)	Saiz kanopi
1	*Syzygium sp*	Kelat	180.56	148	Jarang
2	*Shorea balanocarpoides*	Damar katup	235.46	193	Sederhana padat
3	*Ochanostachys amentacea*	Petaling	235.46	238	Jarang
4	*Xanthophyllum obscurum*	Minyak berok	120.78	99	Sederhana padat
5	*Hopea mengarawan*	Merawan penak	10736	88	Jarang
6	*Shorea macroptera*	Meranti melantai	192.76	158	Jarang
7	*Xanthophyllum spp*	Minya berok	195.2	160	Jarang
8	*Heritiera simplicifolia*	Mengkuang siku keluang	170.8	240	Jarang
9	*Mangifera gracilipes*	Machang	179.34	147	Jarang
10	*Shorea bracteolate Dyer*	Meranti Pa'ang	167.14	137	Jarang
11	*Hopea sangal Korth*	Merawan siput	150.06	123	Sederhana padat
12	*Palaquium hexandrum engl.*	Nyatoh jambak	150.06	123	Padat
13	*Pimeleodendron griffithianum*	Perah ikan	136.64	112	Sederhana padat
14	*Endospermum diadenum*	Sesenduk	179.34	147	Padat
15	*Gymnacranthera bancana (Miq) sinclair*	Panarahan	123.22	101	Padat
16	*Shorea macroptera*	Meranti melantai	114.68	94	Padat
17	*Shorea leprosula Miq*	Meranti tembaga	246.44	202	Sederhana padat
18	*Sarcotheca griffithii*	Pupoi	135.42	111	Sederhana padat
19	*Dyera costulata*	Jelutong	183	150	Padat
20	*Shorea sp*	Damar hitam	257.42	211	Padat
21	*Streblus elongatus*	Tempinis	150.06	123	Padat
22	*Pentaspadon motleyi*	Pelong lichin	219.6	180	Sederhana padat
23	*Dipterocarpus costulatus*	Keruing kipas	246.44	202	Padat
24	*Streblus elongatus*	Tempinis	131.76	108	Sederhana padat
25	*Dialium laurinum*	Keranji sp.	190.32	156	Jarang
26	*Dacryodes puberula*	Kedondong serong	102.48	84	Jarang
27	*Syzgium sp.*	Kelat sp	152.5	125	Sederhana padat
28	*Dipterocarpus crinitus*	Keruing sp	173.24	142	Sederhana padat
29	*Streblus elongatus*	Tempinis	143.96	118	Jarang
30	*Syzygium sp.*	Kelat	124.32	111	Padat

Wujudnya perbezaan fungsi tumbuhan dalam menjalankan pintasan mengikut ketinggian. Faktor ketinggian ini dipengaruhi oleh jumlah curahan yang turun. Pokok yang tinggi berkemampuan untuk mengalirkan aliran batang yang lebih banyak berbanding dengan pokok yang rendah [8, 9]. Keadaan ini turut disokong oleh jumlah curahan hujan yang turun. Semakin banyak jumlah curahan hujan, maka semakin tinggi aliran batang yang berlaku. Peningkatan aliran batang ini akan memberi pengaruh kepada fungsi pintasan. Apabila jumlah hujan bertambah, secara langsung akan membawa pertambahan kepada jatuhan langsung dan aliran batang. Hal ini menyebabkan tumbuhan mampu meningkatkan lagi fungsi pintasan hujan.

Selain itu, perilaku antara jumlah hujan dengan jatuhan langsung, aliran batang dan pintasan juga boleh dilihat dari segi diameter batang pokok. Pokok yang mempunyai diameter batang yang besar memerlukan curahan jumlah hujan yang tinggi untuk membolehkan berlakunya pembasahan yang sempurna pada batang pokok [10]. Apabila pembasahan batang pokok yang sempurna berjaya dilakukan, barulah permulaan aliran batang berlaku menuju ke lantai tanah. Pendapat ini bertepatan dengan analisis yang dilakukan di plot kajian melihat perbandingan antara pokok yang mempunyai diameter terbesar dan terkecil dalam musim hujan dan selepas musim hujan. Pokok yang berlabel 8 iaitu Mengkuang Siku Keluang merupakan pokok yang berdiameter terbesar iaitu 240 cm. Pengaruh diameter dapat dilihat apabila pokok ini mencatatkan jumlah aliran batang pada bulan Disember 2009 sebanyak 163.97 mm dan 98753 mm pada Januari 2010. Berbeza dengan pokok berlabel 26 yang mempunyai diameter terkecil iaitu pokok Kedondong Serong, 84 cm. Jumlah aliran batang bagi bulan Disember 2009 yang dicatatkan ialah 509.44 dan 166.67 pada Januari 2010. Keadaan ini jelas menunjukan pokok yang mempunyai diameter lebih besar akan mencatatkan aliran batang yang lebih rendah berbanding pokok berdiameter kecil. Hal ini kerana pokok yang berdiameter besar memerlukan hujan yang tinggi untuk melakukan pembasahan sempurna, lalu membolehkan aliran batang berlaku.

Kulit pokok juga memberi pengaruh besar khususnya terhadap perilaku hujan dengan aliran batang. Pokok yang mempunyai tekstur kulit yang lebih licin cenderung untuk mempunyai aliran batang yang tinggi kerana membenarkan aliran air tanpa halangan seperti pokok yang berkulit kasar [8, 11]. Berdasarkan analisis yang dilakukan, pokok yang berlabel 3 iaitu Petaling merupakan pokok yang mempunyai tekstur kulit yang kasar dan berlubang-lubang seperti yang ditunjukan pada Foto 3. Jumlah aliran batang yang dicatatkan pada bulan Disember 2009 ialah 165.41 mm. Berbeza dengan pokok berlabel 29 (foto 4) iaitu Tempinis yang mempunyai tekstur kulit yang lebih licin, aliran batang yang dicatatkan pada bulan yang sama ialah 444.15 mm. Perbezaan jumlah aliran batang akibat pengaruh tekstur kulit pokok di kawasan kajian mengukuhkan lagi hujah pengkaji terdahulu yang mengemukakan teori wujudnya pengaruh tekstur kulit pokok terhadap perilaku hujan dan aliran batang. Secara tidak langsung, pengaruh tekstur kulit pokok terhadap aliran batang akan mempengaruhi kadar pintasan yang mampu dilakukan oleh pokok.

Disamping itu, sifat tumbuhan seperti ciri kanopi dan orientasi daunnya turut mempengaruhi perilaku jumlah hujan dengan jatuhan langsung, aliran batang dan pintasan. Ciri kanopi dan orientasi daun akan menentukan berapa banyak jumlah air yang mampu disimpan oleh pokok. Kemampuan kanopi pokok untuk memerangkap hujan yang turun dikenali sebagai "crown capacity" [2]. Apabila kanopi pokok menjalankan fungsi storan sementaranya , maka aliran batang akan turun perlahan-lahan munuju ke lantai tanah. Tempoh yang diambil oleh air yang bertakung di simpanan sementara kanopi pokok ini memberi masa kepada suhu setempat untuk melakukan sejatan. Hal ini menyebabkan aliran batang yang terhasil berkurangan. Justeru, berdasarkan pemerhatian di lapangan, pokok sampel yang mempunyai saiz kanopi yang padat cenderung untuk menghasilkan aliran batang yang rendah berbanding pokok yang mempunyai kanopi yang jarang.

Contoh pengaruh kepadatan kanopi terhadap aliran batang dilihat pada pokok sampel 23 iaitu Keruing Kipas yang mempunyai kanopi yang padat seperti yang ditunjukan pada Foto 5. Jumlah aliran batang yang dicatatkan pada bulan Disember 2009 ialah 258.92 mm. Berbeza pula dengan pokok sampel 26 iaitu Kedodong Serong yang mempunyai kanopi jarang seperti yang ditunjukan dalam Foto 6. Jumlah aliran batang yang dicatatkan pada bulan yang sama ialah 508.99 mm. Jumlah aliran batang yang tinggi pada pokok sampel 26 ini didorong oleh saiz kanopi yang jarang disebabkan ketidakberkesanan kanopi menjalankan fungsi storan sementara yang memerangkap hujan

yang turun. Hujan sebaliknya terus mengalir ke batang pokok melalui tempias jatuhan langsung, lelehan di bahagian ranting dan dahan kanopi. Dengan kata lain, kanopi pokok yang mampu memerangkap jumlah air hujan yang banyak akan menghasilkan nilai pintasan yang tinggi.



Foto 3. Tekstur kulit pokok berlabel 3, Petaling.

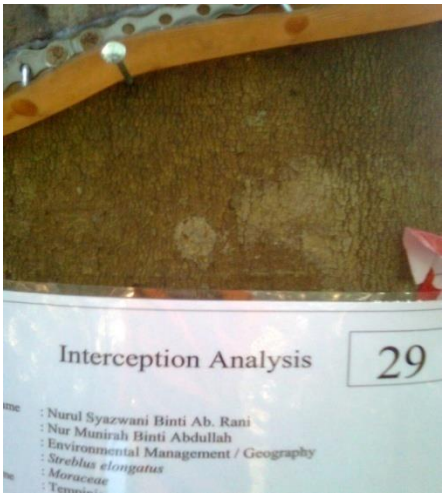


Foto 4. Tekstur kulit pokok label 29, Tempinis.

Kajian ini selari dengan hasil kajian yang dilakukan oleh penyelidik Musa [12] tentang peranan aliran batang dan jatuhan langsung dalam sistem hidrologi hutan sekunder, UKM Bangi. Kajian tersebut telah memperlihatkan bagaimana pokok yang mempunyai kanopi yang padat dan orientasi yang mencuram ke atas mempunyai keupayaan untuk mengalirkan jumlah aliran batang yang lebih tinggi. Jumlah aliran batang yang tinggi secara langsung menunjukan keberkesanan pintasan yang dilakukan oleh pokok sampel di kawasan kajian.

Dari segi dahan dan ranting pokok pula, ianya turut menentukan corak aliran jatuhan langsung dan aliran batang yang akan berlaku. Ranting yang mencuram ke atas mampu menghasilkan aliran air yang lebih banyak ke batang pokok berbanding dengan ranting pokok yang menurun ke bawah kerana ia menghalang air untuk mengalir ke batang pokok [8, 9]. Ciri dahan dan ranting dalam mempengaruhi aliran batang turut disokong oleh Ismail [7] yang mana telah menyatakan ciri dahan dan ranting yang mendatar akan mengurangkan lagi kebolehan air hujan untuk mengalir pada batang pokok.

Berdasarkan pemerhatian di lapangan juga, didapati pokok sampel kajian berada dalam kedudukan yang rapat dengan pokok bukan sampel yang lain. Kedudukan pokok yang saling berdekatan ini menyebabkan kanopi pokok cenderung untuk membesar dalam keadaan yang berlapis antara satu sama lain. Ini bermakna kanopi pokok bukan sampel boleh jadi bertindih di atas kanopi pokok sampel kajian. Pertindihan kanopi antara pokok bukan sampel di atas pokok sampel di plot kajian dilihat cenderung untuk menghasilkan jatuhan langsung dan aliran batang yang bersifat menumpang. Dengan kata lain, jatuhan langsung dan aliran batang yang dikutip boleh jadi berpunca dari kanopi pokok lain yang bertindih dengan pokok sampel.

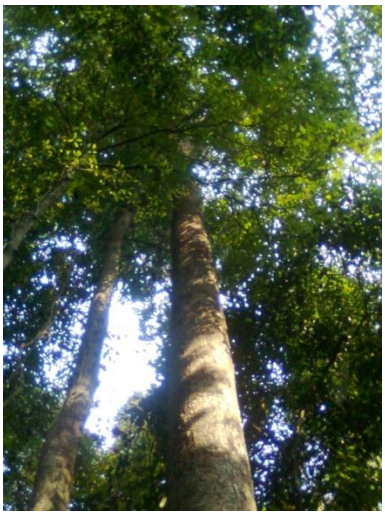


Foto 5: Kanopi sampel pokok 23, Keruing Kipas.



Foto 6: Kanopi sampel pokok 26, Kedondong Serong.

Pemerhatian adalah sama dengan kajian yang pernah dilakukan oleh penyelidik Toriman *et. al* [13] di hutan Dipterokap Tasik Chini. Dalam kajian tersebut, pokok sampel dilihat cenderung untuk membesar dalam keadaan yang hampir antara pokok-pokok yang lain sehingga menghasilkan pelbagai lapisan kanopi yang bertingkat dan bertindih. Hal ini seterusnya memberi kesan kepada nilai pintasan yang dicatatkan kerana pokok sampel cenderung untuk mengumpul jumlah aliran batang yang tinggi hasil dari pertindihan pelbagai lapisan kanopi pokok di plot kajian. Semakin besar dan padat saiz kanopi, semakin tinggi jumlah aliran batang yang dilakukan. Ini kerana kanopi pokok berjaya menjadi storan sementara yang efektif untuk menadah air hujan dan mengalirkannya perlahan-lahan ke batang pokok.

Faktor Masa Dalam Menentukan Kadar Jatuhan Langsung, Aliran Batang & Pintasan Hujan

Secara keseluruhannya, nilai jatuhan langsung, aliran batang dan pintasan di pengaruhi oleh kelajuan tiupan angin dan perbezaan jumlah hujan yang turun mengikut musim sepanjang tempoh kajian dijalankan. Pengaruh kelajuan angin terhadap jatuhan langsung menunjukan perhubungan yang positif. Nilai jatuhan langsung akan meningkat sekiranya kelajuan angin meningkat. Keadaan yang sebaliknya juga berlaku di mana jatuhan langsung akan berkurangan apabila kelajuan angin bertiup perlahan [14]. Keadaan yang sama ditunjukkan dalam perhubungan antara kelajuan angin dengan jumlah aliran batang. Semakin kuat kelajuan angin, semakin tinggi nilai aliran batang yang direkodkan. Hal ini berlaku kerana angin yang kuat mempunyai kemampuan untuk menyebarkan hujan yang bertakung di bahagian daun, kanopi, ranting dan dahan pokok. Penyebaran hujan oleh tindakan angin di sebelah atas pokok menyebabkan air hujan akan mengalir menjadi aliran batang menuju ke lantai tanah.

Namun begitu, terdapat sesetengah keadaan menunjukkan perhubungan yang negatif antara kelajuan angin dengan jumlah jatuhan langsung dan aliran batang yang seterusnya akan memberi kesan kepada fungsi tumbuhan untuk menjalankan pintasan. Menurut Jones [2], kelajuan dan perolakan angin yang kuat mampu meningkatkan lagi kadar sejat peluhan yang dilakukan oleh pokok. Hal ini menyebabkan berlakunya kegagalan tumbuhan memainkan peranan untuk melakukan pintasan dengan lebih efektif. Dengan kata lain, kelajuan dan perolakan angin yang kuat akan menganggu pemerangkapan jatuhan hujan oleh ciri-ciri fisiografi tumbuhan yang akan mengalir sebagai aliran batang.

Pengaruh iklim yang dicirikan oleh tiupan angin monsun bertepatan dengan keadaan yang berlaku pada bulan Oktober 2009 yang mencatatkan hubungan kolerasi antara jumlah hujan kasar dengan jumlah jatuhan langsung dan aliran batang yang lemah. Bulan Oktober 2009 adalah merupakan musim peralihan monsun Barat Daya ke Timur

Laut yang mana dicirikan oleh tiupan dan kelajuan angin yang kuat. Keadaan ini mempengaruhi pintasan apabila tiupan angin yang kuat semasa peralihan monsun telah menempiaskan titisan hujan yang terperangkap pada ciri fisiografi tumbuhan seperti dahan, ranting dan kanopi pokok. Peranan angin menempiaskan titisan hujan telah mengurangkan jumlah aliran batang lalu memberi kesan kepada kebolehan pokok untuk melakukan fungsi pintasan.

Bagi nilai pekali kolerasi untuk jumlah hujan dan jatuhan langsung bulan Oktober 2009 ialah r^2=0.232. hubungan kolerasi antara jumlah hujan dan aliran batang pula ialah r^2=0.215. Manakala hubungan kolerasi bagi jumlah hujan dan pintasan ialah r^2=0.000. Berdasarkan kajian, perhubungan yang lemah bagi jumlah hujan dengan jatuhan langsung, aliran batang dan pintasan pada bulan Oktober boleh dikaitkan dengan tiupan angin peralihan monsun yang berkelajuan tinggi. Tiupan angin yang kuat ini telah meningkatkan lagi kadar sejatan semasa air bertakung pada kanopi pokok. Ini bermakna, sejumlah besar air yang telah distor sementara waktu telah tersejat dalam atmosfera sebelum dipintas oleh tumbuhan melalui aliran batang dan jatuhan langsung.

Selain itu, pengaruh iklim terhadap perilaku jatuhan langsung, aliran batang dan pintasan boleh dilihat melalui hubungannya dengan jumlah hujan yang turun dalam sesuatu masa. Hubungan positif terbentuk di antara jumlah hujan dengan jatuhan langsung dan aliran batang. Hubungan yang positif ini kemudiannya akan memberi pengaruh terhadap nilai pintasan yang berlaku. Pertambahan jumlah jatuhan langsung dan aliran batang adalah selari dengan pertambahan jumlah hujan. Ini bermakna, semakin tinggi jumlah hujan, maka semakin tinggi nilai jatuhan langsung dan pintasan hujan yang dicatatkan [15].

Kajian yang dilakukan oleh Jamil *et.al* [8] di hutan sekunder Tasik Chini, Pahang menunjukkan jumlah aliran batang adalah berkadar langsung dengan suhu dan jumlah hujan. Hubungan yang berlaku menunjukkan berlakunya pertambahan aliran batang apabila jumlah hujan bertambah. Namun, pengurangan nilai aliran batang berlaku sekiranya peningkatan suhu terjadi. Hal ini kerana peningkatan suhu akan menyebabkan berlakunya sejatan yang lebih efektif terhadap simpanan air sementara di kanopi pokok. Sejatan seterusnya menyebabkan berkurangnya jumlah air yang akan dialirkan sebagai aliran batang menuju ke lantai tanah.

Kerelevanan pengaruh jumlah hujan terhadap perilaku jatuhan langsung, aliran batang dan pintasan boleh dilihat pada bulan Disember 2009 yang mencatatkan perhubungan kolerasi yang kuat. Nilai pekali kolerasi bagi hubungan jumlah hujan dengan jatuhan langsung ialah r^2=0.851. Bagi hubungan antara jumlah hujan dengan aliran batang, nilai pekali kolerasi yang dicatatkan ialah r^2=0.890. Manakala hubungan jumlah hujan dengan pintasan pula mencatatkan nilai pekali kolerasi r^2=0.571 mm. Pertambahan jumlah hujan kasar pada bulan Disember iaitu 356.0 mm (sisihan piawai ±1.83mm) telah meningkatkan lagi jumlah jatuhan langsung dan aliran batang. Peningkatan jumlah ini telah diterjemahkan dalam perhubungan kolerasi yang kuat lalu. Apabila nilai kolerasi yang kuat wujud bagi jatuhan langsung dan aliran batang, ianya membantu pokok sampel menjalankan fungsi pintasan hujan.

Kesimpulan

Terdapat dua faktor utama yang mempengaruhi ciri jatuhan langsung dan pintasan hujan di plot pintasan Tasik Chini, Pahang. Faktor tersebut terdiri daripada faktor masa seperti jumlah curahan hujan, kelajuan angin dan suhu yang sentiasa berubah-ubah mengikut musim tertentu. Selain itu, jatuhan langsung dan pintasan juga dicorakkan oleh faktor keruangan yang mana mewakili ciri fisiografi pokok sampel di lapangan. Antara ciri fisiografi pokok yang diambil kira termasuklah ketinggian, kulit, kanopi, diameter, dahan dan ranting pokok. Hubungkait di antara kedua-dua faktor iklim dan ciri fisiografi pokok telah membentuk satu bentuk perhubungan yang diterjemahkan dalam bentuk hubungan kolerasi.

Secara keseluruhannya, data sepanjang tempoh kajian yang diperolehi daripada jatuhan langsung mencatatkan jumlah 36 040.5 mm. Manakala jumlah keseluruhan aliran batang yang dicatatkan ialah 36 081.34 mm. Daripada data yang diperolehi, pokok sampel yang mencatatkan jumlah aliran batang tertinggi ialah pokok berlabel 13 iaitu spesies Perah ikan yang mencatatkan aliran batang sebanyak 1958.4 mm. Pokok label 8 iaitu spesies Mengkuang Siku Keluang pula mencatatkan jumlah aliran batang paling rendah iaitu 652.97 mm.

Berdasarkan kajian yang dilakukan, jatuhan langsung kurang memberi pengaruh dalam pintasan yang berlaku di plot kajian. Hal ini berlaku kerana jumlah jatuhan langsung yang kecil secara keseluruhannya iaitu 36 040.5 mm

dicatatkan berbanding dengan data aliran batang keseluruhannya berjumlah 36 081.34 mm. Walaupun jumlah jatuhan langsung yang dicatatkan adalah rendah, namun ia memberi pengaruh yang besar terhadap kitaran hidrologi yang berlaku di kawasan kajian. Perbezaan besar antara jumlah jatuhan langsung dan aliran batang berlaku kerana faktor ciri fisiografi yang mendorong pemerangkapan lebih banyak air hujan lalu mengalir melalui batang pokok. Selain itu, ciri iklim dengan jumlah curahan hujan sebanyak 1224.84 mm telah menambahkan lagi kecenderungan penghasilan aliran batang yang tinggi. Kira-kira 49.97 % daripada hujan kasar telah dipintas sebagai jatuhan langsung. Manakala 50.03 % adalah dalam bentuk aliran batang. Manakala jumlah pintasan maksimum (mm) bagi empat kali kejadian hujan yang dicatatkan sepanjang kajian ialah 22.0 mm (Oktober), 13.2 mm (November), 24.2 mm (Disember) dan 18.4 mm (Januari).

Rujukan

1. Majid, N. M., Hamzah, M. B. and Ahmad, S. (1979). Rainfall interception, throughfall and stemflow in a secondary forest. *Pertanika* 2(2):152-154.
2. Jones, J. A. A. (1997). *Global Hidrology: process, resources and environmental management*. England: Addison Wesley Longman Limited.
3. Jamil, N. R., Toriman, M. E., Idris, M and Jing, L. W. (2010). Pengaruh kanopi hutan sekunder terhadap kadar pintasan bagi kitaran hidrologi di Tasik Chini, Pahang,Malaysia. *Sains Malaysiana* 39(2): 181-187.
4. Rosley N. A. 2007. Analisis Pintasan, Jatuhan Langsung dan Aliran Batang di Hutan Pendidikan UKM, Bangi. Kertas Kerja Projek Ijazah Sarjana Muda, Universiti Kebangsaan Malaysia.
5. Chappell, N. A., Bidin, K. and Tych, W. (2001). Modelling rainfall and canopy controls on net-precipitation beneath selectively-Logged Tropical Forest. *Plant Ecology* 153: 215-229.
6. Crockford, R. H. and Richardson, D.P. (2000). Partitioning of rainfall into throughfall, stemflow and interception: Effect of forest type, ground cover and climate. *Hydrology Process* 14: 2903-2920.
7. Ismail W. R. 1994. *Pengantar Hidrologi*. Kuala Lumpur: Dewan Bahasa dan Pustaka.
8. Jamil, N. R., Toriman, M. E., and Idris, M. (2008). Analisis Pintasan Hujan di Hutan Sekunder Tasik Chini, Pekan Pahang. *Prosiding.* Persidangan Antarabangsa Sosial, Pembangunan dan Persekitaran. Kelab Danau UKM. 18-19 Nov 2008: 846-860.
9. Kittredge, J. (1948). *Forest Influences*. New York Mcgraw-Hill Book. Co., Inc. Volume 394.
10. Reynolds E. R. C. and Henderson C. S. (1967). Rainfall Interception by Beech, Larch And Norway Spruce. *Forestry* 40(2):165-184
11. Helvey J. D. and Patric J. H. (1967). Canpoy and litter interception of rainfall by hardwoods of Eastern United States. *Water Resource* 1: 193-206.
12. Musa S. M. S. (1998). *Pintasan: Peranan aliran batang (Steamlow) UKM Bangi.* Tesis. Bangi: Universiti Kebangsaan Malaysia.
13. Toriman, M. E., Idris, M., and Jamil, N. R. (2010). Monitoring Spatial Variability of Lowland Dipterocarp Forest in Lake Chini Catchment, Malaysia. *World Applied Sciences Journal* 8 (1): 54-60.
14. Low K. S. (1972). Interception loss in the humid forested areas (with special references to Sg. Lui catchment). *Malay National* 25: 104-111.
15. Mitchell J. A. (1930). Interception of Rainfall by Forest. *Forestry* 28: 101-102.

The Malaysian Journal of ANALYTICAL SCIENCES ISSN 1394-2506

LEACHATE CHARACTERIZATION FROM A CLOSED LANDFILL IN AIR HITAM, PUCHONG, MALAYSIA

(Pencirian Air Larut Resap dari Tapak Pelupusan Ditutup Air Hitam, Puchong, Malaysia)

Nur Fatin Dahlia Mat Salleh[1*], Ku Halim Ku Hamid[2]

[1]*Faculty of Applied Sciences,*
[2]*Faculty of Chemical Engineering,*
Universiti Teknologi MARA, 40450 Shah Alam, Malaysia

**Corresponding author: fatin_dahlia@hotmail.com*

Abstract

Leachate, wastewater that was collected from landfill is known to have pungent smell and may impose serious harm to human health and the environment. Air Hitam, Puchong Sanitary Landfill has stopped its land filling operation since December 2006 and is under post-closure maintenance stages. After several years of stopping its operation, a landfill will still produce leachate hence it needs constant monitoring and maintenance. The main aim of this paper was to characterize leachate produced from Air Hitam, Puchong Closed Landfill, according to several important parameters: pH, temperature, chemical oxygen demand (COD), ammoniacal nitrogen (NH_4-N), total organic carbon (TOC), total solids, volatile organic acids (VOA) and heavy metals content, to determine its suitability in producing methane by identifying its phase. Leachate samples were drawn weekly for a period of 3 months from three different ponds, untreated raw leachate pond 1 and treated leachate pond 2 and 3. Results obtained showed that the average values were around 25°C, average pH 8, highest COD reading was 5,248 mg/L, TOC highest at 6,797 mg/L, VOA highest at 1,424 mg/L and ammoniacal content of 3.10 mg/L the highest.

Keywords: Leachate, characterization, closed landfill, COD, Air Hitam sanitary landfill

Abstrak

Air larut resap adalah air buangan yang diperoleh dari tapak pelupusan sisa pepejal yang mempunyai bau yang tajam dan boleh mengakibatkan kemudaratan kepada kesihatan manusia dan keselamatan alam sekitar. Tapak pelupusan sanitari Air Hitam, Puchong telah dihentikan operasinya pada bulan Disember 2006 dan di bawah aktiviti penyelenggaraan selepas penutupan. Selepas bertahun-tahun beroperasi, tapak pelupusan masih akan mengeluarkan air larut resap, dan oleh itu ia memerlukan pemantauan berterusan dan penyelenggaraan. Artikel ini memberi tumpuan kepada pencirian air larut resap dari tapak pelupusan sisa pepejal yang telah ditutup menurut parameter ini: pH, suhu, parameter oksigen kimia (COD), nitrogen ammonia (NH_4-N), jumlah karbon organik (TOC), jumlah pepejal, pepejal meruap dan kandungan logam berat untuk menentukan kesesuaian air larut resap ini menghasilkan gas methana, dengan menentukan fasa air larut resap. Sample air larut resap diambil setiap minggu bagi tempoh 3 bulan daripada tiga kolam berbeza, kolam air larut resap tidak dirawat 1 dan kolam air larut resap dirawat 2 dan 3. Keputusan yang diperolehi menunjukkan bahawa suhu purata 25°C, purata pH 8, nilai -nilai tertinggi yang direkod ialah; COD 5248 mg/L, TOC 6797 mg/L, VOC 1424 mg/L dan kandungan ammonia 3.10 mg/L.

Kata kunci: Air larut resap, pencirian, tapak pelupusan sisa pepejal, COD, tapak pelupusan sisa pepejal sanitari Air Hitam.

Introduction

As the population of an area grows, the amount of wastes generated is greatly increased. Vast product innovation and as the power of buying and spending gains popularity among humans, wastes are uncontrollably produced day by day. Sanitary landfill method is widely accepted as the ultimate approach to dispose of solid waste material due

to its economic advantage [1]. Outcome from this waste management is leachate and generated by excess rainwater percolating through the waste layers in a landfill [2], and is of dark colored, it could be yellow, brown or black, due to decomposition of organic matter [3].

A sanitary landfill receives domestic waste; that are wastes from residential and offices. Hence, leachate content has a variety of chemicals as many types of wastes dumped in landfills. Landfill operators are bounded by regulations that leachate must be treated and its contents concentration comply with the limits stated in the regulation set by Malaysian government, before leachate is released to nearby river. In addition, leachate collection system is equipped with underground pipes which allow leachate to flow out of the landfill to a pond where treatment is applied. Surroundings of the underground pipes must also be monitored to avoid groundwater pollution that may impose health effects to humans. In order to apply an effective treatment to treat leachate, a thorough characterization of leachate is crucial to determine its content and their concentrations.

Landfill leachate is a potentially polluting liquid and could cause harmful effects to the surrounding surface water and groundwater due to its high concentration of toxic contents. Run-off arising from a landfill containing only soil and rubble may contain suspended solids, be turbid, and threaten fish and other aquatic organisms. Monitoring of landfill leachate provides assurance that the landfill operation will not cause harm to human as well as the environment [4].

Age of landfill is one of the important effects on leachate characteristics. As landfill age increases biological decomposition of deposited wastes altered from a relatively shorter decomposition period to a longer decomposition period, which has two sub phases; acidic and methanogenic. It is reported that leachate from these two stages has different constituents, with younger leachate having high concentration of volatile fatty acids; hence it is more likely to be in the acidic phase [5]. Younger leachate in acidic phase with age converts into methanogenic phase where fatty acids in acidic or acidogenic phase is converted into methane and carbon dioxide [6], also conversion between two phases requires a long time as organic matter needs to be decomposed into gaseous and liquid fermentation products. In this study, landfill leachate samples were taken from a closed landfill with an age of more than 10 years. Main purpose of this paper was to characterize leachate according to chosen parameters, from Air Hitam closed landfill to determine its suitability to produce methane, by identifying its phase.

Experimental

Sampling

Study area selected is a 100 acre closed landfill that is located in Air Hitam, Puchong, Malaysia and is surrounded by residential areas. This sanitary landfill received domestic wastes from 1st April 1995 and stopped its waste collection on 31st December 2006. Throughout the years, the operator, Worldwide Landfills Sdn. Bhd.[7] reported to have received a total of 6,207,684.59 ton of wastes. As of now, the landfill is undergoing post closure maintenance activity. The most crucial maintenance is the leachate collection and monitoring.

Observed in the landfill site that there are several ponds containing leachate, raw untreated leachate and treated leachate. This paper focuses on the characterization of leachate from three different ponds; first pond contains raw untreated leachate and the other two ponds contain mechanically treated leachate where Figure 1 describes the leachate flow from its generation in landfill to final discharge. Leachate samples were collected from all three ponds weekly for a period of 12 weeks, from September to December 2010. Leachate samples were stored at temperature -4°C and all analyses performed within one week.

Sample Analysis

Samples collected were analyzed and tested according to these parameters: pH, temperature, chemical oxygen demand (COD), total solids (TS), and concentration of heavy metals, ammoniacal nitrogen (NH_4-N), total organic carbon (TOC), and volatile organic acid (VOA). Tests were conducted according to the Standard Methods for the Examination of Water and Wastewater [8]. COD was measured using a HACH HR COD digestion vial and HACH DR2010 spectrophotometer was used to read the measurements. Ammoniacal nitrogen, total organic and volatile organic acid were prepared using Merck's Spectroquant test kits and measured using Spectroquant Nova 60 spectrophotometer. Heavy metals concentrations determined were As, Ca, Cd, Cr, Fe, Co, Cu, Li, Mg, Mn, Mo, Ni,

Pb, Sb, V, Zn, Al, Ba and Hg. These metals' concentrations were measured using Inductively Coupled Plasma of Optical Emission Spectrometry (ICP-OES) model Thermo Scientific iCAP 6000 series with ASX-520 auto sampler and multi-elements and Hg standard solution. Diluted leachate samples were preserved with the addition of few drops of nitric acid, for the heavy metals analysis [9]. All analyses were performed within one week of sampling to avoid the possibility of sample degradation.

Results and Discussion

Following Figure 1, it illustrates that leachate generated in landfill was collected and channeled to Pond 1, where no treatment was applied, raw untreated leachate which then channeled to Pond 2 where aeration was applied and transferred to Pond 3 for further aeration and finally, leachate was tested according to selected parameters to ensure that the concentration of leachate compositions comply to the Environmental Quality Act 1974 Second Schedule (Regulation 13) for discharge of leachate before it is discharged to nearby river.

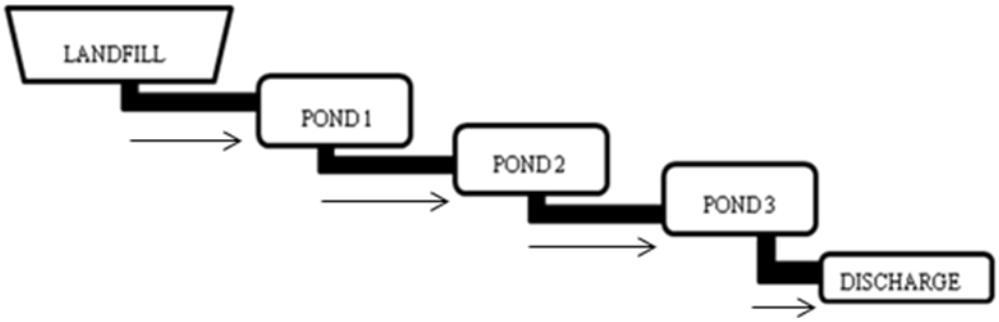


Figure 1. Schematic diagram of leachate flow

Parameter analysis for a 12 week period of leachate samples drawn from three different ponds (Pond 1, Pond 2 and Pond 3) is summarized in Table 1, which also showed significant variations of respective parameters in all three ponds. pH change from 8.49 to 6.96 was due to the high alkalinity in samples, which is typical for old landfill leachate. Occurrence of pH changes was contributed by the decomposition in the readily biodegradable organics and gas production [10]. This pH values obtained in this study offset and does not agree to the values reported by Aziz *et. al.* in 2010, which stated that mature landfills possess pH of 6.6 to 7.5 [5]. Justification for the decreased pH value after aeration process is due to the ammonification process that releases H^+ ions [11].

Ammonification is a step in the nitrogen cycle, which ammonium ion is formed by either nitrogen fixation or nitrite ammonification. Nitrogen fixation occurs in aerobic condition, due to its need for oxygen presence while nitrite ammonification is typically an anaerobic process [12]. Hence, increasing value of NH_4-N from Pond 1 to 3 was contributed by the ammonification process by nitrogen fixation, where oxygen was supplied during aeration in Pond 2 and 3.

Aeration in leachate ponds observed to have reduced COD values from 3607 mg/L to 1239 mg/L, which is about 65.7% reduction. Aeration facilitates in COD reduction due to the aerobic microorganisms consumption of the organic matter in landfill leachate, when oxygen in supplied and transformed it into new microbial biomass and partly carbon dioxide, by means of aerobic metabolism [13]. Further aeration of leachate can further reduce the COD value hence it depends on the aeration and holding time of leachate in the aeration pond. Other parameters changed as well with the application of aeration, which improves the quality of leachate and observed that %TS is also reduced from 1.15 to 0.98 %. Reduction of %TS is due to aeration also contributed by the transition from acidogenic to methanogenic phase in landfill leachate [14].

Table 1. Leachate characterization of Air Hitam Landfill

Parameter	Pond 1	Pond 2	Pond 3
pH	8.49	7.51	6.96
Temp (°C)	26.68	26.47	26.44
COD (mg/L)	3607	1461	1239
TOC (mg/L0	5337	2874	2118
VOA (as Acetic Acid, mg/L)	555	262	216
NH4-N (mg/L)	0.28	0.45	1.50
%TS	1.15	1.09	0.98
Aluminum (mg/L)	0.021	0.007	0.020
Calcium (mg/L)	0.949	1.059	1.053
Magnesium (mg/L)	0.314	0.403	0.416
Barium (mg/L)	<0.2	<0.2	<0.2
Cadmium (mg/L)	0.006	0.007	0.374
Chromium (mg/L)	0.003	0.004	0.002
Copper (mg/L)	0.013	0.011	0.011
Zinc (mg/L)	0.013	0.032	0.019
Lead (mg/L)	0.017	0.004	0.00025
Iron (mg/L)	0.080	0.159	0.045
Nickel (mg/L)	<0.2	<0.2	<0.2
Manganese (mg/L)	0.005	0.011	0.007
Molybdenum (mg/L)	0.058	0.029	0.013
Vanadium (mg/L)	<0.2	<0.2	<0.2
Antimony (mg/L)	0.020	0.012	0.012
Arsenic (mg/L)	0.011	0.016	0.232
Mercury (mg/L)	0.063	0.026	0.018

Heavy metals were observed to be of low concentrations. It was reported by [15] that heavy metals concentrations are significantly high in younger leachate, and in an acidic phase, where it could possibly be a threat. Therefore, low concentration of heavy metals is possible for older, aged leachate in methanogenic phase. However, values of heavy metals in Table 1 do not seem to have a significant pattern or trend. Cr, Cu, Pb, Fe, Hg Mo and V ions were reduced with aeration but other metals remain unchanged or slightly increased. In my opinion, it could be due to the accumulation of these metals in the aeration pond and was collected together upon sampling.

Concentration of VOA should be increasing as TOC reduced but findings in this study found that value of VOA decreased from Pond 1 to 3; 555 mg/L to 216 mg/L where it should be increasing as aerobic microorganism degraded organic matter into acetic acids. However, aeration pond at sampling location was an exposed to rain and flushing effect occurred to dilute to acetic acids that was produced [16] hence, leachate from Pond 2 and 3 is less

favorable for methane production. Another reason for VOA reduction as leachate progressed from Pond 1 through 3 is possibly to temperature change that affects microbial population and consequently changes VFA production [17].

Leachate generation was also influenced by the amount of precipitation received in the landfill site and COD and TOC values were compared to amount of precipitation received during sampling period. Precipitation data was obtained from Department of Meteorological, Malaysia [18]. Figure 2 illustrates the trend in COD reading over the 12 weeks for all three ponds compared to precipitation received one day before sampling, to allow precipitation that falls and trapped in landfill stays up to one day before it was completely discharged onto Pond 1. Note that in Figure 2, on the first week COD is high at value of ~3000mg/L, corresponds to no precipitation. Same is observed on 3rd, 4th and 5th week, no precipitation received and the COD value is at the highest of 5248 mg/L. Figure 3 shows the TOC trend over precipitation received, and the trend is dissimilar to COD, however at 7th, 8th and 9th week, no precipitation received and the TOC is at its highest at 6797 mg/L. Value of COD is significantly lower with high precipitation as water assists the redistribution of nutrients and microorganisms in within the landfill [19]. Precipitation received throughout the sampling period affects the flow of leachate.

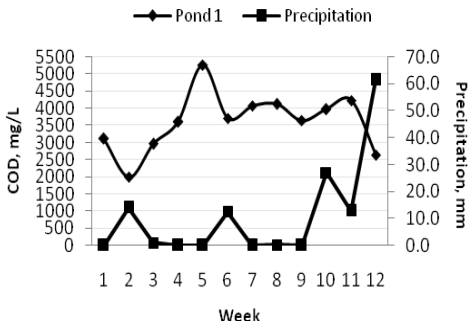


Figure 2. Relation between COD and precipitation

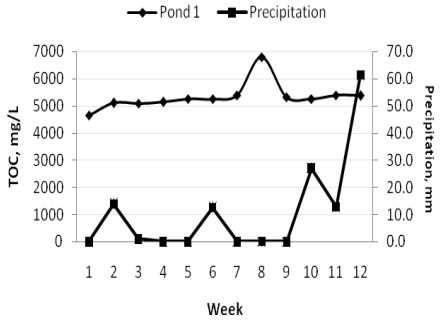


Figure 3. Relation between TOC and precipitation

Reported by B. Rincón, there are three principal digestions that occur and they are: hydrolytics, acetogenics and methanogenics [20]. In a landfill, there are two distinguished phases with the early phase called the acidogenic phase which contributes to volatile acids production. Later on, as a landfill matures, it transformed to methanogenic phase where volatile acids present are converted into biogas, methane and carbon dioxide by means of methanogenic microorganisms or methanogens [1]. Values of pH, and COD presented propose that leachate samples are in methanogenic phase and additionally, in this study Pond 1 reported to have 555 mg/L of volatile acids. It was described that methanogenic phase leachate has pH value of 7.5 to 9.0 and COD value of 500 to 4500 [21].

Conclusion

Aged leachate from a closed landfill in Air Hitam has been characterized as reported and it is found that the landfill leachate is in methanogenic phase. High content of VFA in raw untreated leachate recommended that VFA contained in leachate to be converted in methane via methanogenesis. Furthermore, parameter values differences from Pond 1 through 3 was due to the application of aeration as well as the precipitation received throughout the year considering Malaysia's tropical climate. Hence, high moisture content of the incoming waste stream at Air Hitam has a significant impact on the leachate generation and the chemical composition.

Acknowledgement

This study is made possible with the cooperation given by the operator of Air Hitam, Puchong sanitary landfill, Worldwide Landfills Sdn. Bhd. and also through the financial support from the Research Management Institute (RMI) of Universiti Teknologi MARA, as well as the expertise and facilities provided by the Center of Environmental Research laboratory, Faculty of Chemical Engineering, Universiti Teknologi MARA.

References

1. Renou, S., Givaudan, J., Poulain, S., Dirassouyan, F., & Moulin, P. (2008). Landfill leachate treatment: Review and opportunity. *Journal of Hazardous Materials 150*: 468 - 493.
2. Kjeldsen, P., Barlaz, M., Rooker, A., Baun, A., Ledin, A., & Christensen, T. (2002). Present and long-term composition of MSW landfill leachate: A review. *Critical Reviews in Environmental Science and Technology 32:4*: 297 - 336.
3. Abdul Aziz, H., Alias, S., Adlan, M.N., Faridah, Asaari, A.H., Zahari, M.S. (2007). Colour removal from landfill leachate by coagulation and flocculation processes. *Bioresource Technology 98*: 218 - 220.
4. Salem, Z., Hamouri, K., Djemaa, R., & Allia, K. (2008). Evaluation of landfill leachate pollution and treatment. *Desalination 220*: 108 - 114.
5. Aziz, S., Abdul Aziz, H., Yusoff, M., Bashir, M., & Umar, M. (2010). Leachate characterization in semi-aerobic and anaerobic sanitary landfills: A comparative study. *Journal of Environmental Management 91*: 2608-2614.
6. O'Keefe, D.M., Chynoweth, D.P. (2000). Influence of phase separation, leachate recycle and aeration on treatment of municipal solid waste in simulated landfill cells. *Bioresource Technology 72:* 55-66.
7. Air Hitam Sanitary landfill (2011). Retrieved July 2011, from www.whbenvironment.com/index.php
8. APHA; AWWA; WPCF. (2005). *Standard Methods for the Examination of Water and Wastewater 21st Edition.* Washington: American Public Health Association .
9. Al Sabahi, E., Abdul Rahim, S., Wan Zuhairi, W., Al Nozaily, F., & Alshaebi, F. (2009). Leachate composition and groundwater pollution at municipal solid waste landfill of Ibb City, Yemen. *Sains Malaysiana 38 (3)*: 295 - 304.
10. Al-Yaqout, A., & Hamoda, M. (2003). Evaluation of landfill leachate in arid climate - a case study. *Environmental International 29*: 593 - 600.
11. Chen, P. H. (1996). Assessment of leachates from sanitary landfills: Impact of age, rainfall, and treatment. *Environment International Vol 22*: 225 - 237.
12. Simon, J. (2002). Enzymology and bioenergetics of respiratory nitrite ammonification. *FEMS Microbiology Review 26*: 285 - 309.
13. Wiszniowski, J., Robert, D., Surmacz-Gorska, J., Miksch, K., & Weber, J. (2006). Landfill leachate treatment methods: A review. *Environ Chem Lett 4* : 51 - 61.
14. Bilgili, M.S., Demir, A., Ozkaya, B. (2007). Influence of leachate recirculation on aerobic and anaerobic decomposition of solid wastes. *Hazardous Materials 143:* 177 - 183.
15. Morling, S. (2010). Nitrogen removal and heavy metals in leachate treatment using SBR technology. *Hazardous Materials 174:* 679 - 686.
16. Nguyen, P.H.L., Kuruparan, P., Visanathan, C. (2007). Anaerobic digestion of municipal solid waste as a treatment prior to landfill. *Bioresource Technology 98:* 380 - 387.
17. Yuan, Q., Sparling, R., Oleszkiewicz, J.A. (2011). VFA generation from waste activation sludge: Effect of temperature and mixing. *Chemosphere 82:* 603 - 607.
18. Department of Meteorological, Ministry of Science, Technology and Innovation, Malaysia (2011). Retrieved November 2011, from http://www.met.gov.my/index.php?option=com_frontpage&Itemid=1
19. Bendz, D., Singh, V., & Akesson, M. (1997). Accumulation of water and generation of leachate in a young landfill. *Journal of Hydrology 203*: 1 - 10.
20. Rincon, B., Borja, R., Martin, M.A., Martin, A. (2009). Evaluation of the methanogenic step of a two-stage anaerobic digestion process of acidified olive mill solid residue from a previous hydrolytic-acidogenic step. *Waste Management 29:* 2566 - 2573.
21. Christensen, T., Kjeldsen, P., Bjerg, P., Jensen, D., Christensen, J., Baun, A. (2001). Biogeochemistry of landfill leachate plumes. *Applied Geochemistry 16*: 659 - 718.

The Malaysian Journal of ANALYTICAL SCIENCES ISSN 1394-2506

DEVELOPMENT OF BIO-BASED PAINT BY USING METHYL ESTERS FROM PALM OIL FOR CORROSION INHIBITOR

(Pembangunan Cat Berasaskan Bio Menggunakan Metil Ester Dari Minyak Sawit Untuk Mengawal Pembentukan Karat)

Mohibah Musa*, Miradatul Najwa Muhd Rodhi, Najmiddin Yaakob,
Ku Halim Ku Hamid, Juferi Idris

Environmental Research Centre, Fakulti Kejuruteraan Kimia,
Universiti Teknologi MARA, Shah Alam, Selangor, Malaysia

**Corresponding author: mohibah@salam.uitm.edu.my*

Abstract

Paint is used as a means of protection to prevent surfaces from being corroded over time. This research is focused on the development of a Bio-based paint made from palm oil methyl ester (POME) which originated from crude palm oil (CPO). New formulation paint has been developed to protect the pipeline from corrosion thus reducing the cost of the operation. Bio-based paint is made up of four components which are solvent, binder, additives, and pigment. The solvent in the bio-based paint is POME. The additives used are wetting and dispersing agent. The pigment used in the bio-based paint is TiO_2. The formulation was developed by using a constant amount of additives and binder but varying the amount of POME at 10 ml, 15 ml, 20 ml, 25 ml and 30 ml with addition of water. The Standard Testing Methods for measuring the corrosion rate (ASTM G5-94(2011)) was carried out for each sample. In conclusion, it is proven that in the making of bio-based paint formulation for better corrosion inhibitor; the best amount of binder, additives and de-foam that should be used is 20 ml, 10 ml and 10 ml, respectively.

Keywords: bio-based paint, additives, crude palm oil, palm oil methyl ester

Abstrak

Cat digunakan sebagai satu cara perlindungan dengan mencegah permukaan daripada berkarat dari masa ke masa. Kajian ini memberi tumpuan pada pembangunan cat berasaskan Bio-dibuat dari minyak metil ester sawit (POME) yang berasal dari minyak sawit mentah (MSM). Cat formulasi baru telah dibangunkan untuk melindungi saluran paip dari kakisan sekali gus mengurangkan kos operasi. Berasaskan Bio-cat terdiri daripada empat komponen yang pelarut, pengikat, bahan tambahan, dan pigmen. Pelarut cat berasaskan bio adalah satu POME. Aditif yang digunakan membasahkan dan ejen bersurai. Pigmen digunakan dalam cat berasaskan bio adalah TiO_2. Penggubalan telah dibangunkan dengan menggunakan jumlah berterusan tambahan dan pengikat tetapi mengubah jumlah POME di 10 ml, 15 ml, 20 ml, 25 ml dan 30 ml dengan penambahan air. Kaedah Ujian Standard untuk mengukur kadar kakisan (ASTM G5-94 (2011)) telah dijalankan bagi setiap sampel. Kesimpulannya, ia membuktikan bahawa dalam membuat perumusan cat berasaskan bio bagi perencat kakisan yang lebih baik; jumlah terbaik pengikat, aditif dan penyahbuih yang harus digunakan adalah 20 ml, 10 ml dan 10 ml, masing-masing.

Kata kunci: cat berasaskan bio, bahan tambahan, minyak sawit mentah, minyak metil ester sawit

Introduction

Mild steel has been used widely in industry as a material for reaction vessels, storage tanks, etc. However, corrosion damage on mild steel causes heavy losses on the economy and potential problems in safety at work place [1, 2]. Recently, environmental regulations on industrial consumption and development of new corrosion inhibitors have been tightened up. Thus, natural products (e.g. vegetable oil), non-toxic and environmental-friendly products, have gained much attention in regard to the development of "green corrosion inhibitors" that have high inhibition efficiency [3]. Conducting polymers properties of the bio-based paint have recently been studied as a new class of materials for the corrosion protection of metals. These polymers are non-toxic and it is anticipated that they could replace harmful anticorrosion additives based on transition metal oxides [4]. In contrast to other macromolecular

compounds used in the corrosion protection due to their barrier properties, conducting polymers have a porous structure and are highly permeable to liquids and gases [5].

Corrosion of materials continues to receive interest in the technological world. In the field of corrosion inhibition, scientists are persistent in seeking better and more efficient ways of combating the corrosion of metals. Addition of corrosion inhibitors to the corrosion environment with respect to the other methods of corrosion inhibition has been employed [6]. Corrosion inhibition of materials has been the focus of research for centuries and in many cases has been well analyzed and understood [7 - 9].

Organic compounds are well known as acid inhibitors used in industry. These organic compounds have multiple bonds in their molecules that mainly contain nitrogen, sulphur, oxygen atoms through which they are adsorbed on the metal surface [10 - 12]. In order to solve the corrosion problem, development of bio-based paint as a corrosion inhibitor is a brilliant idea, instead of use as a product colour. Basic formulation of paint consists of a pigment, binder, solvent and additives that serve different purposes to the application of paint [13 - 15]. Nowadays, all of the components in paint are made from hazardous chemicals which are harmful to the environment and the society. In 2002, paint and coatings manufacturers released 7,000 tons of volatile organic compounds (VOCs) such as formaldehyde and methane [16]. In 2003, 420 facilities in the paint and coatings manufacturing sector reported air toxics releases of 4.7 million pounds [17].

The emissions of volatile organic compounds (VOCs) and odor problem are the result from evaporation of organic solvents that are used as one of the constituents of paint ingredients. Solvent is important because it is the ingredient responsible to carry the solid components of paint which allows consistency when applying by brush, roller, and spray or dipping. The flow of the paint after it has been applied is also affected by the choice of solvent since the film develops the correct surface appearance. The paint film wets the substrate to which it has been applied thus maximizing adhesion to the surface. Most commonly used solvents are ketone and esters. However, the pitfall of using these solvents is that these solvents contain hazardous constituents that can cause serious health problem to human and environmental effects as air toxics [18]. Organic solvent based coatings are still a serious problem in the construction sector and that there are no general indications, that the problems are going to be solved. With concerns to these issues, production of bio-based paint from palm oil methyl ester (POME) is developed to overcome the emission of volatile organic compounds (VOCs) and odor problem [19].

Methodology

Polarization Curves

According to ASTM G3 and G5 reported by Najmiddin (2007) [20], Potentiostat / galvonostat Voltalab 21 was used to determine current density under steady state conditions as a function of potential. Polarization curves were obtained according to corrosion Testing Standard ASTM G3 and G5. Electrochemical tests were performed with sample coupon immersed in 1 M HCL. All potential were measured versus a saturated Calomel Electrode (SCE). For Tafel analysis, the corrosion current density, I_{corr} is calculated by the exploration of the anodic and cathodic Tafel line. The efficiency was calculated using the following equation:

$$E=100[1- (i_{add}/i_{free})]$$

where:

$i_{add} = I_{corr}$ iron electrode in the presence of coating
$i_{free} = I_{corr}$ iron electrode in the absence of coating

The main parameters for the polarization curve include the scan rate and the potential (mV). The suitable scan rate which was used in the testing was 1 mV/s. The value of potential is between -700mV to 200mV, depending on the corrosion media. In order to determine the current density (mA/cm^2), the potential that is applied to the mild steel in 1 M HCL ranges from -700 to 200mV. A current density (mA/cm^2) versus potential (mV) curve is plotted. In order to determine the E_{corr} and I_{corr}, extrapolation from Tafel curve was done.

Cell Design

According to ASTM Standard, the electrochemical cell for the corrosion measurement consists of a working electrode, reference electrode, counter electrode and electrolyte. The working electrode needs to be reproducible, representative, free from crevices free from edge effects and free from water line effect. In this work, mild steel is used as the working electrode. The reference electrode was platinum wire mesh. The auxiliary is saturated calomel electrode (SCE). The electrolyte is 1 M HCl. To complete the arrangement of the cell design, platinum wire mesh is used as the counter electrode which allows current to pass with tolerable polarization. Figure 1 shows the cell design and Figure 2 shows the equipment for corrosion test. Table 1 below indicates the sample specimen for this study.

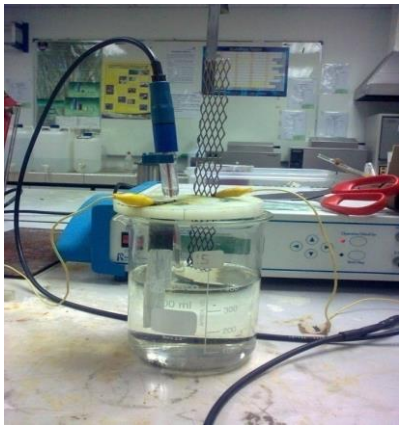


Figure 1. Cell design



Figure 2. Equipment for corrosion test

Table 1. Sample specimen for corrosion test

Sample	Binder Volume (ml)	Sample	Additives Volume (ml)	Sample	De-foamer Volume (ml)
5A	20	6A	2.0	7A	2.0
5B	30	6B	4.0	7B	4.0
5C	40	6C	6.0	7C	6.0
5D	50	6D	8.0	7D	8.0
5E	60	6E	10.0	7E	10.0

Results and Discussion

Effect of Binder to Corrosion Rate

Corrosion test with 1 M HCl and varying quantity of binder, the corrosion rate was determined in mm/y. It was found that the corrosion rate for sample 5A is 1.95 mm/y. This amount was found to be the smallest rate, thus showing that this sample is the least corrosive. As for control sample, the corrosion rate was 6.716 mm/y. The results show the differences in the corrosion rate between control sample and the sample 5A. These differences are observed due to the successful coating of sample 5A on the surface of mild steel. For sample 5E, the result was 6.008 mm/y. This result shows that sample 5E has the highest corrosion rate as compared to other samples. This higher corrosion rate was due to the unsuccessful coating of this sample on the surface of mild steel. It was found that by increasing the binder quantity, the corrosion rate increases due to less adhesion. This was concluded by observing the coating on the mild steel. The success of the coating affects the corrosion rate. For the optimum sample that was obtained by varying amount of binder, the results concluded that the sample 5A is the optimum sample for the corrosion test because of the smallest value in corrosion rate and since it adhered onto the mild steel plat. Figure 3 shows the graph of Corrosion Rate for different concentrations of paint binder.

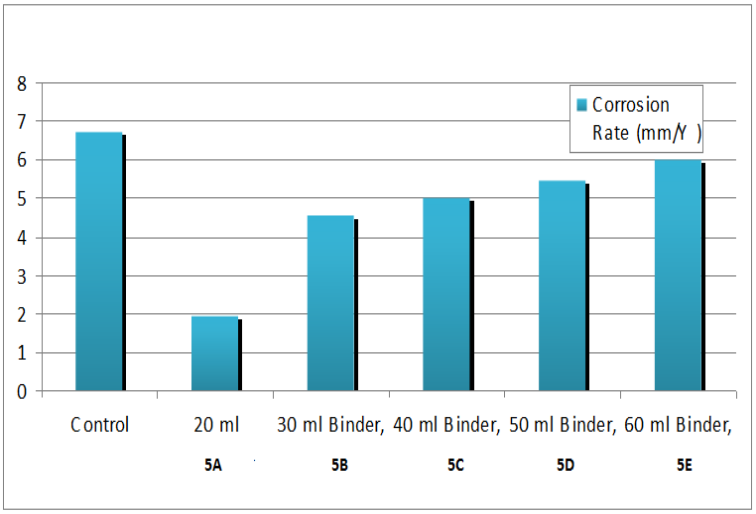


Figure 3. Corrosion Rate for different concentrations of binder

Table 2. Electrochemical corrosion parameters of mild steel in 1 M HCl various in binder

Sample	E_{corr} (mV)	I_{corr} (mA/cm^2)	R_p (ohm.cm^2)	E_1 (%)
Control	-443.4	0.7887	278.81	-
20 ml Binder, 5A	-367.2	0.2291	11.3	70.95
30 ml Binder, 5B	-357.5	0.6121	80.45	22.39
40 ml Binder, 5C	-348.9	0.5865	72.84	25.64
50 ml Binder, 5D	-348.7	0.5225	78.55	33.75
60 ml Binder, 5E	-347.1	0.7055	53.77	10.55

At constant temperature and variation in binder quantity, more electrons were released where higher dissolution of iron (Fe) was determined when higher corrosion current density (I_{corr}) was obtained. High corrosion current density would result in a high corrosion rate. This can be seen in Table 1 for control sample. The five various samples are compared in Table 2. The higher efficiency was obtained from sample 5A at 70.95% while the lowest efficiency was obtained from sample 5E at 10.55%. The lowest corrosion current density was determined from sample 5A which justified that the dissolution of Fe was retarded since fewer electrons were transferred due to the coating. Besides that, 5A sample shifted to the lowest corrosion current density (I_{corr}) which was the main criteria in determine the corrosion rate. The sample 5A adsorbed onto the surface of the mild steel plat which created a protective layer preventing corrosion due to higher polarization resistance which was determined as compared to the other samples. The formula of calculation showed in earlier equation.

Effect of Additive to Corrosion Rate

Figure 4 shows the graph of Corrosion Rate for the different amount of additives use in bio-paint development. In corrosion test of 1 M HCl with variation in additives, the corrosion rate was determined in mm/y. In this test, the corrosion rate for sample 6E was 1.941mm/y, the least corrosive sample as compared to all the other samples. The control sample has a corrosion rate of 6.716 mm/y. The results show the different of the corrosion rate between control sample and the sample 6E. These differences happened because of the successful coating of sample 6E on the surface of mild steel. For sample 6A, the result was 5.611mm/y which is the highest corrosion rate out of all samples. Higher corrosion rate was because of the unsuccessful coating on the surface of mild steel plat which is also shown in Figure 4. It was found that by increasing the amount of additives, there is a decrease in corrosion rate.

The successful coating affects the corrosion rate. As for the optimum sample with variation in additives, the results concluded that sample 6E is the optimum sample for the corrosion test rather than other samples because of the lesser corrosion rate in the corrosion test and it was adhered on the mild steel.

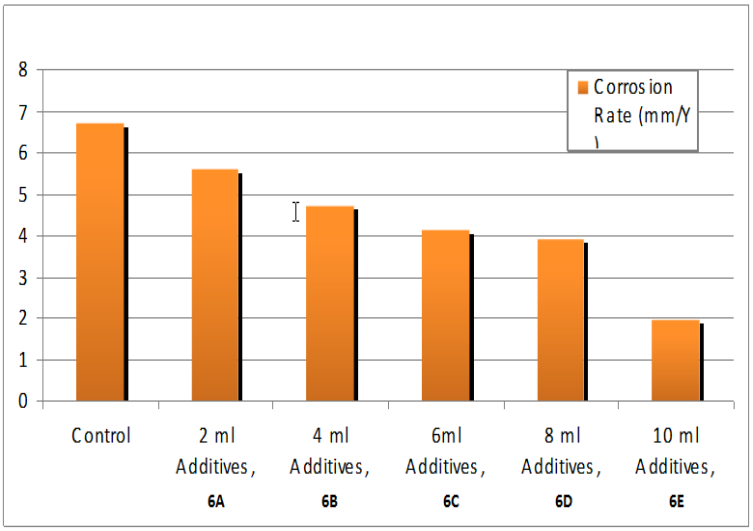


Figure 4. Corrosion Rate for Additives

Table 3. The effect of additive on electrochemical corrosion parameters of mild steel in 1 M HCl

Sample	E_{corr} (mV)	I_{corr} (mA/cm2)	R_p (ohm.cm2)	E_1 (%)
Control	-443.4	0.7887	278.81	-
2 ml additives, 6A	-365.2	0.711	80.51	[1-(0.711/0.7887)]100=9.85
4ml additives, 6B	-350.3	0.637	65.74	19.23
6 ml additives, 6C	-350.6	0.539	66.74	31.66
8 ml additives, 6D	-346.8	0.4608	140.63	41.57
10 ml additives, 6E	-379.5	0.1105	373.65	85.99

At constant temperature and varying amount of binder, more electrons were released where higher dissolution of Iron (Fe) was determined when higher corrosion current density (I_{corr}) was obtained. High corrosion current density would result in a high corrosion rate. This can be seen in Table 2 for control sample. The five various samples are compared in Table 3. The highest efficiency was obtained from sample 6E at 85.99%, lowest efficiency was obtained from sample 6A at 9.85% and lowest corrosion current density was determined from sample 6E which justified that dissolution of Fe was retarded since fewer electrons were transferred. According to high efficiency of sample 6E, it showed shifts to the lowest corrosion current density (I_{corr}) which was the main criterion to determine the corrosion rate. Sample 6E adsorbed onto the surface of the mild steel plat which creates a protective layer that prevents corrosion due to higher polarization resistance which was determined in sample 6E.

Effect of De-foam to Corrosion Rate

In the corrosion test of 1 M HCL with variation in de-foam composition; the corrosion rate was determined in mm/y. According to this test, the corrosion rate of sample 7E with 10 ml de-foam was 1.18mm/y. This shows that this sample has the smallest corrosion rate as compared to all other samples. As for the control sample, the corrosion rate was 6.716 mm/y. Different rates obtained due to the successful coating on the mild steel plat which is shown in Plate 4.3. In sample 7A, the result was 6.145mm/y and showed that sample 7A has the highest corrosion rate

between all five samples. The higher corrosion rate is due to the unsuccessful coating of this sample on the mild steel plat. It was found that increasing amount of de-foam can cause a decrease in the corrosion rate. This is due to coating on the mild steel where successful coating affects the corrosion rate. Optimum sample is obtained by varying the amount of de-foam, this sample identified to be sample 7E which has the smallest corrosion rate because this sample adheres lightly on the mild steel plat. The entire sample 7 did not adhere well onto the mild steel because lacks of de-foam in the compositions. Further studies must be conducted to improve on this shortcoming. Table 4.9 shows the corrosion rate of the mild steel plats in 1 M HCL with the different samples. Figure 3 shows the graph of Corrosion Rate for different concentrations of Defoamer.

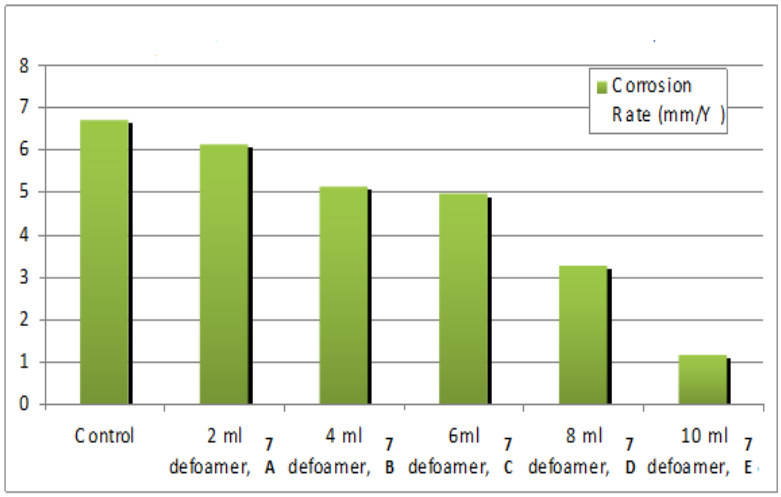


Figure 5. Corrosion Rate for different concentrations of Defoamer

Table 4. The effect of de-foam on electrochemical corrosion parameters of mild steel in 1 M HCl

Sample	**E_{corr} (mV)**	**I_{corr} (mA/cm2)**	**R_p (ohm.cm2)**	**E_1 (%)**
Control	-443.4	0.7887	278.81	-
2 ml de-foam , 7A	-347.4	0.7215	73.26	[1-(0.7215/0.7887)]100=8.52
4 ml de-foam, 7B	-346.0	0.6481	208.87	17.83
6 ml de-foam, 7C	-349.1	0.5131	69.05	34.94
8 ml de-foam, 7D	-345.3	0.2197	503.76	72.14
10 ml de-foam, 7E	-363.5	0.0387	372.84	95.1

At constant temperature and various amount of de-foam, more electrons were released where higher dissolution of Iron (Fe) was determined when high corrosion current density (I_{corr}) was obtained. High corrosion current density would result in a high corrosion rate. This can be seen in Table 3 for control sample. The five various de-foam samples are compared in Table 4. The highest efficiency was obtained from sample C_5 at 95.1 %. The 7E sample shifts to the lowest corrosion current density (I_{corr}) which is the main criterion in determining corrosion rate. The lowest efficiency was obtained from sample 7A at 8.525%, lowest corrosion current density was determined from sample 7E which justified that the dissolution of Fe was retarded since fewer electrons were transferred. Sample 7E coated the mild steel plat which creates a protective layer to prevent corrosion since high polarization resistance was determined compared to other various defoamer samples. The overall efficiency of the variation in de-foam composition from the polarization analysis with concentration 1 M HCl at constant temperature is shown in Table 3.

Conclusion

Based on Tafel analysis, the sample A_1, B_5 and C_5, performed well in 1 M HCL at room temperature when this sample recorded high value in coating efficiency as compared to other samples. The above findings are supported by the result from the Tafel analysis which showed that corrosion rate measured in mm/year in the 20 ml binders, 10 ml additives and 10 ml sample has the lowest rate as compared to all other samples.

Acknowledgement

The authors gratefully acknowledge to the Research Management Institute (RMI), Faculty of Chemical Engineering, Universiti Teknologi MARA Malaysia for providing the necessary budget, facilities and equipments to this research.

References

1. Migahed, M.A., Abdul-Raheim, A.M., Atta, A.M., & Brostow, W., (2010). Synthesis and evaluation of a new water soluble corrosion inhibitor from recycled poly(ethylene terphethalate). *Mater. Chem. Phys* 121: 208 - 214.
2. Malik, M. A., Hashim, M. A., Nabi, F., Al-Thabaiti, S. A., & Khan, Z. (2011). Anti-corrosion Ability of Surfactants: A Review. *Int. J. Electrochem. Sci*. 6: 1927 - 1948.
3. Yoo, S. H., Kim, Y. W., Chung, K., Baik, S. Y. & Kim, J. S. (2012). Synthesis and corrosion inhibition behaviour of imidazoline derivatives based on vegetable oil. *Corrosion Science* 59: 42 - 54.
4. Kalendová, A., Sapurina, I., Stejskal, J., & Vesely, D. (2008). Anticorrosion properties of polyaniline-coated pigments in organic coatings. *Corrosion Science* 50: 3549 – 3560.
5. Briegel, K. & Kane, R. (2007). Corrosion monitoring technology leads to real-time results for specialty materials: 1-2
6. Orubite-Okorosaye, K, Jack, I R, Ochei, M, & Akaranta, O. (2007). Synergistic Effect of Potassium Iodide on Corrosion Inhibition of Mild Steel in HCl Medium by Extracts of Nypa Fruticans' Wurmb. *J. Appl. Sci. Environ. Manage* 11: 27 - 31.
7. Caroline, M.M., Christian, P., Hannes, C.S., Boris, K., & Ilhan A.A., (2008). Inhibition and Promotion of Copper Corrosion by CTAB in a Micro reactor System. *Langmuir* 24: 14269.
8. El–Maksoud, S.A.Abd, (2008). The Effect of Organic Compounds on the Electrochemical Behaviour of Steel in Acidic Media. A review. *Int. J. Electrochem. Sci*. 3: 528 - 555.
9. Antonijevic, M. M & Petrovic, M. B (2008). Copper Corrosion Inhibitors: A review. *Int. J. Electrochem. Sci*. 3: 1-28
10. Kumar, A, (2008). Corrosion Inhibition of Mild Steel in Hydrochloric Acid by Sodium Lauryl Sulfate (SLS). e-*Journal of Chemistry* 5: 275 - 280.
11. Maqsood, A.M., Mohammad, A.H., Firdosa, N., Shaeel, A.T., & Zaheer, K. (2011). Anti-corrosion Ability of Surfactants: A Review. *Int. J. Electrochem. Sci* 6: 1927 - 1948.
12. Moura, E.F., Neto, A.O.W., Dantas, T.N.C., Scatena, J.H., & Gurgel, A. (2009). Applications of micelle and micro emulsion systems containing aminated surfactants synthesised from ricinoleic acid as carbon-steel corrosion inhibitors. *Colloids Surf. A.* 340: 199 - 207.
13. Bentley, J & Turner, G.P.A. (1997). Introduction to Paint Chemistry and Principles of Paint Technology. Chapman & Hall, ISBN: 9780412723308, pg 79 - 85.
14. Smith, D. G., Liu, W. H, & Nan-Tou. (2006). Laminated Coconut Palm Oil and Products Thereof, US Patent:20060078666
15. Tiarks, F., Frechen, T., Kirsch, S., Leuninger, J., Melan, M., Pfau, A., Richter, F., Schuler, B., & Zhao, C. L (2003). Formulation effects on the distribution of pigment particles in paints. *Progress in Organic Coatings* 48: 140 - 152.
16. Environmental Protection Agency's (EPA), EPA's Toxics Release Inventory. National Emission Inventory (2006) : pg 23-35
17. Johannes T.P, Derksen, F., Petrus Cuperus, & Peter Kolster, (1996). Renewable Resources in Coatings Technology: A Review. *Progress in Organic Coatings* 27: 45 - 53.
18. American Council on Science and Health, (1997) Animal Experiments, Human Cancer Risk and Regulatory.
19. Darnoko, D., & Cheryan, M. (2000). Kinetics of Palm Oil Transesterification in a BatchReactor. *Journal: Journal of The American Oil Chemists Society* 77: 1263 - 1267.

20. ASTM 1999, G 5-94, Standard Reference Test Method for making Potentiostatic and Potentiodynamic Anodic Polarization Measurements 3.01: 61-72

The Malaysian Journal of ANALYTICAL SCIENCES ISSN 1394-2506

AN EXPERIMENTAL DESIGN APPROACH FOR THE ANALYSIS OF LIQUID PHASE PRODUCTS IN WATER FOR HYDROGENOLYSIS OF GLYCEROL USING IMMERSED SOLID-PHASE MICROEXTRACTION

(Pendekatan Reka Bentuk Eksperimen Untuk Analisis Produk Fasa Cecair Dalam Air Bagi Tindak Balas Hidrogenolisis Gliserol Menggunakan Rendaman Mikroekstraksi Fasa Pepejal)

Noraini Hamzah[1,2*], Rozita Osman[1], Mohd Ambar Yarmo[2]

[1]*Faculty of Applied Sciences,*
Universiti Teknologi MARA, 40450 Shah Alam, Selangor Darul Ehsan, Malaysia
[2]*Faculty of Science and Technology,*
Universiti Kebangsaan Malaysia, 43600 Bangi, Selangor Darul Ehsan, Malaysia

**Corresponding author: norainihamzah@gmail.com*

Abstract

In this study, a response surface methodology (RSM) was applied to optimize the immersed-solid-phase microextraction (immersed-SPME) conditions for the first time using a polyacrylate (PA) coated fiber. This was to determine liquid phase compounds in water for hydrogenolysis reaction of glycerol. There are a three-factor response surface experimental design was used to evaluate the interactive effects of extraction temperature (30-70 ºC), extraction time (10-30 minutes) and desorption time (2-18 minutes) on the analysis of liquid phase compounds in water for hydrogenolysis of glycerol using immersed-solid-phase microextraction (immersed-SPME). The extraction conditions using immersed-SPME were optimized in order to achieve high enrichment of the analytes from aqueous samples. The isolated compounds from the SPME fiber were desorbed and separated on a capillary polar column of a gas chromatography-flame ionization detector (GC-FID). The extraction time and desorption time were found significant in increasing the amount of glycerol in aqueous hydrogenolysis of glycerol. Nevertheless, the effect of extraction temperature was not significant. In terms of interactions between the effects, the relation between extraction temperature and extraction time was the most significant. The optimised immersed-SPME conditions were at extraction temperature of 27 °C, extraction time of 30 minutes and 15 minutes of desorption time. Thus, the application of SPME was found to be a rapid and effective technique in the determination of glycerol and propylene glycol compounds in aqueous hydrogenolysis glycerol.

Keywords: Solid phase microextraction (SPME), Hydrogenolysis ,Glycerol, Response Surface Method (RSM)

Abstrak

Dalam kajian ini, kaedah permukaan respon telah digunakan buat pertama kalinya untuk mengoptimumkan keadaan operasi teknik rendaman mikroekstraksi fasa pepejal menggunakan fiber poliakriat (PA). Teknik ini digunakan bagi menentukan komponen dalam fasa cecair dalam air bagi tindak balas hidrogenolisis gliserol. Terdapat tiga faktor reka bentuk permukaan respon yang digunakan untuk menilai kesan interaksi suhu ekstraksi (30-70 °C), masa ekstraksi (10-30 minit) dan masa penyahjerapan (2-18 minit) terhadap analisis komponen fasa cecair dalam air untuk hidrogenolisis gliserol dengan menggunakan teknik rendaman mikroekstraksi fasa pepejal (rendaman-SPME). Keadaan ekstraksi rendaman-SPME perlu dioptimumkan bagi mendapatkan serapan analit yang maksimum daripada sampel akuas. Komponen daripada fiber SPME ternyahjerap dan di pisahkan menggunakan kolum polar kapilari gas kromatografi yang dilengkapi dengan pengesan pengionan nyala (GC-FID). Kajian ini menunjukkan bahawa faktor masa ekstraksi dan masa penyahjerapan adalah signifikan dengan pertambahan amaun gliserol dalam hidrogenolisis gliserol berakuas. Namun begitu, kesan suhu ekstraksi didapati tidak siginifikan. Dari segi interaksi antara faktor, hubungan antara suhu ekstraksi dan masa ektraksi adalah yang paling signifikan. Keadaan optimum teknik rendaman-SPME adalah pada suhu ekstraksi 27°C, masa ekstraksi 30 minit dan masa penyahjerapan 15 minit. Oleh itu, didapati aplikasi SPME yang cepat dan teknik yang berkesan dalam penentuan komponan gliserol dan propilena glikol dalam hidrogenolisis gliserol berakuas.

Kata kunci : Mikroekstraksi fasa pepejal (SPME), Hidrogenolisis, Gliserol, Kaedah permukaan respon (RSM)

Introduction

Hydrogenolysis of biomass-derived glycerol is an alternative route to sustainable production of propylene glycol. Glycerol is the main by-product of biodiesel production by the transesterification of vegetable oils and animals fats [1]. Recently, rapid development of biodiesel processes has caused some concern over the oversupply of glycerol in the market [2]. A variety of valuable chemicals can be produced from glycerol [3]. Propylene glycol or 1,2-propanediol is an important commodity chemical. It is used as biodegrable functional fluids such as de-icing reagents, antifreezes and coolants and as precusors in the synthesis of unsaturated polyester resins and pharmaceuticals [4-6].

Gas chromatogaraphy-flame ionization detector (GC-FID) [3, 5, 7] and high performance liquid chromatogarphy (HPLC) [8], are widely used to determine glycerol and liquid products in water for glycerol hydrogenolysis. However, a preconcentration step prior to the chromatogaraphic analysis is necessary in order to achieve the low levels that are presents in real samples. Recently, a new extraction technique, solid-phase microextraction (SPME) was used as an alternative to conventional techniques. SPME is a screening technique introduced by Arthur and Pawlisyn in 1990 [9]. It acts as a modern alternative to traditional sample preparation technology, is able to address many of the requirements put forward for analytical research. It has attracted great attention and is now widely accepted as a reliable technique. There are several advantages that can be pointed out in relation to this technique, such as it is solvent free, fast and uses the whole sample for analysis. Furthermore, its requires only small amounts of sample and the fibers are highly reuseable. Accordingly, it has been successfully applied for the analysis of diverse organic compounds from different matrices[10-12].

To the best of our knowledge, there is no report on the technique to extract the liquid products and glycerol in water phase for glycerol hydrogenolysis. Therefore, in this study, the possibility of using SPME coupling with GC-FID for the analysis propylene glycol and glycerol in aqueous media was proposed. A direct immersed solid-phase microextraction (immersed-SPME), combined with the gas chromatography-flame ionization detector (GC-FID), was developed and applied to detect the compounds in water medium for hydrogenolysis of glycerol. Up until now, no references have been found on the use of immersed-SPME to describe the extraction technique of compounds for hydrogenolysis of glycerol in aqueous media. Therefore, to optimize the extraction conditions, a response surface experimental design was set up to analyze the effect of three factors: extraction temperature, extraction time and desorption time. Finally, the developed method is applied to the real samples for glycerol hydrogenolysis reaction.

Experimental

Standard solution

A mixture of standard solution containing propylene glycol, ethylene glycol and glycerol with approriate concentration were prepared and this mixture was then used in order to optimize SPME condition using a face-centered central composite design.

Chemicals

Glycerol, 1,2-propanediaol (1,2-PDO) or propylene glycol and ethylene glycol (EG) were purchased from Sigma-Aldrich (Steinheim, Germany). Next, 1,4-butanediol and n-butanol were used as internal standard and these were obtained from Merck (Darmstadt, Germany).

Qualitative characterization of the isolated compounds

Qualitative analysis for liquid phase of hydrogenolysis was performed on Hewlett Packard Gas Chromatograph HP 6890 Series II Plus equipped with a flame ionization detector (FID). The column used was DB-WAX capillary column, 30 m x 0.25 mm and 0.25 μm film thickness from J & W Scientific (Pennsylvania,USA). The GC temperature and condition were as follows : initial temperature started at 45°C held for 5 minutes and increased to 250°C and held for 3 minutes with temperature ramping of 3°C min^{-1}; splitless injection port temperature at 250°C; detector temperature 280°C; carrier gas (helium) at a flow rate of 1.7 ml min^{-1}. The injector port was equipped with a glass liner designed for SPME measurement (0.75 mm i.d. splitless glass liner, Supelco). The GC-FID was used

for the optimization of the direct immersed SPME method and quantification of 1,2-PDO from hydrogenolysis of glycerol.

SPME fiber

SPME extractions were performed using 80 μm polyacrylate fiber and it was purchased from Supelco, Bellefonte, Pennsylvania, USA. The selection of this fiber was made due to its polarity and relatively high thickness. The fiber was conditioned in a gas chromatograph injection port at 250°C to remove fiber contaminants as recommended by the manufacturer.

Extraction and analysis of liquid products

A direct immersed solid phase microextraction (immersed-SPME) was employed in the extraction of samples in water for glycerol hydrogenolysis. After the reaction, the liquid phases were separated with a solid catalyst using a centrifuge at 4000 rpm for 15 min. Then, the liquid phases were filtered to remove other impurities. Finally, the liquid phases were poured into 4 ml vial for SPME extraction procedure.

After optimization, and for each SPME analysis, a volume of 4 mL of sample was placed into a 4 mL glass vial. Each sample was spiked with about 0.1 g of internal standard solution. A small magnetic stirring bar (0.8 cm x 0.2 cm) was used to mix the solution. The vial was tightly capped with a PTFE-faced silicone septum and was placed in a thermostat block on a stirrer. The sample was equilibrated for 5 minutes at sampling temperature and, after this, the SPME fiber was directly immersed in the sample. During the extraction, the sampling was stirred at constant speed (300 rpm). Upon completion of the extraction, the SPME fiber was removed from the sample vial and was placed immediately into the injection port of GC for 10 min for analysis.

Experimental Design

The Response Surface Methodology (RSM) was used as it allowed the evalution of the effects of many explanatory variables and their interactions on the response variable [13]. It also enabled one to make a reduction in the number of experiments and yet provided sufficient information for statistically acceptable results for evaluating the effect of multiple explanatory variables, alone or in a combination, on response variables [14, 15]. RSM has been used widely in research particulary for the optimization of conditions and processes[16].

In order to optimize the parameters, the response surface approach was used by using a set of experimental design was performed. A central composite design with five coded levels was applied with three experimental variables (factors), namely extraction temperature, extraction time and desorption time. This design was selected because it required four additional points outside the range which could extend this model to a wider range of variation to include the highest and the lowest value of the independent variables. The independent variables were the extraction temperature (A) , extraction time (B) and desorption time (C). The range for the independent variables was (low/high value): extraction temperature (°C), 30/70, extraction time (minutes), 10/30, and desorption time (minutes), 2/18. A set of 20 experiments was carried out. The coded levels and values of the factors set in this experiment are shown in Table 1. The response variables selected were gas chromatography area count for glycerol, 1,2-propanediol and ethylene glycol. Six replications were performed at centre point. The design matrix of the centre composite design is shown in Table 2. The order of these experiments was randomized to remove any systematic error.

Table 1. Coded level and values of the design factors

Levels	Extraction temperature (°C)	Extraction time (min)	Desorption time (min)
$-\alpha$	30	10	2
-1	40	15	5
0	50	20	10
1	60	25	15
$+\alpha$	70	30	18

The results were analyzed by Statistical software package Design Expert 6.0.6, an expert system for the design and analysis of experiments. The model permitted evaluation of the effects of linear, quadratic and interactive terms of the independent variables on the dependent variables. Three–dimensional surface plots were drawn to illustrate the main and interactive effects of the independent variables on glycerol hydrogenolysis. The optimum values of the selected variables were obtained by solving the regression and also by analyzing the response surface contour plots.

Results and Discussion

Direct immersed extraction and identification of liquids products using GC-FID

The immersed solid phase microextraction of the liquid products was directly extracted onto the SPME fiber which was later analyzed using GC-FID. This analytical method allows one to make correct identification of compounds in water. Fig. 1(A) shows a chromatogram of standard solution containing glycerol, 1,2-PDO and EG detected by GC-FID. The retention time of glycerol, 1,2-PDO and EG were 50.3 min, 26.9 minutes and 28.2 minutes respectively.The GC-FID chromatogram of liquid sample was shown in Fig. 1(B) and the retention time of the glycerol, 1,2-PDO and EG compounds was quite similar with rentention time in standard solution. Generally, these two samples could be separated well with high resolution separation. As for quantification analysis, the retention time of 8.1 min and 39.2 min corresponding to n-butanol and 1,4-butanediol was used as internal standard.

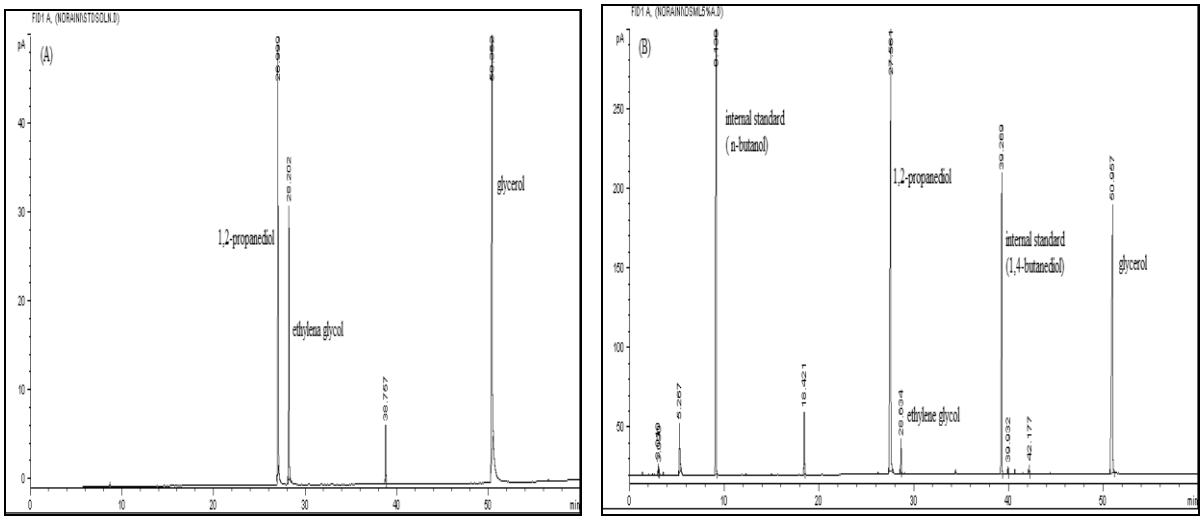


Figure 1. GC chromatogram of standard solution (A) and liquid phase sampel in hydrogenolysis of glycerol detected by GC-FID (B)

Optimization of SPME fiber for the extraction of glycerol and liquid products by RSM

The amount of analyte extracted by solid-phase microextraction could be influenced by several factors including fiber type, extraction time, extraction temperature, salt concentration, sample pH, sample volume, agitation rate, etc [16, 17]. It is well known that among these factors extraction temperature, extraction time and desorption time played the most important role in the extraction process. In this study, these three factors were therefore chosen and optimized. Traditional methods of optimization could evaluate the effect of one variable at a time, keeping all the others constant during experiments with the exception of the one being studied. However, this type of experiment does not allow one to determine what would happen if the other variables also changed. The experimental design enabled the effect of several variables to be estimated simultaneously. In particular, response surface methodology coupled with a central composite design was an effective tool for optimizing a process [18] and was therefore applied in this study.

Optimization is an important process because the immersed-SPME method is based on the principle of equilibrium. The SPME fiber will reach equilibrium with a compound at a certain time and temperature. The maximum absorption of glycerol and liquid products on the SPME fiber was optimized as it represents the equilibrium point of the compound with the fiber. RSM was applied to the immersed solid-phase microextraction of glycerol and liquid products in water from glycerol hydrogenolysis with two absorption parameters: time and temperature and desorption time as well. Table 2 lists the peak area of glycerol, 1,2-PDO and EG in each of the 20 experiment sets generated by the RSM software.

Table 2. Central composite design and experimental data for the extraction of glycerol and liquid products in water from glycerol hydrogenolysis via immersed-SPME-GC-FID

Run Order	Block	Independent variables			Response 1 Glycerol GC area	Response 2 1,2-PDO GC area	Response 3 EG GC area
		A (°C)	B (min)	C (min)			
1	1	27.00	10.00	5.00	2223.03	2269.25	1685.07
2	1	70.00	10.00	15.00	3417.48	2026.77	1562.05
3	1	27.00	30.00	15.00	7385.06	5017.2	3856.89
4	1	70.00	30.00	5.00	3604.43	3128.22	2298.06
5(C)	1	48.50	20.00	10.00	5607.48	5019.29	3578.48
6(C)	1	48.50	20.00	10.00	4505.25	3963.45	2985.67
7	2	27.00	10.00	15.00	3261.88	2515.85	1872.52
8	2	70.00	10.00	5.00	3546.22	3753.00	2684.73
9	2	27.00	30.00	5.00	4006.14	3336.97	2456.30
10	2	70.00	30.00	15.00	4452.05	2757.43	2178.12
11(C)	2	48.50	20.00	10.00	4257.46	3391.63	2469.5
12(C)	2	48.50	20.00	10.00	4038.06	2732.30	3806.61
13	3	12.34	20.00	10.00	1457.71	1665.63	1177.52
14	3	84.66	20.00	10.00	2286.51	1732.46	1320.03
15	3	48.50	3.18	10.00	1938.41	1938.58	1389.83
16	3	48.50	36.82	10.00	3020.82	2681.56	1930.79
17	3	48.50	20.00	1.59	1340.28	1311.64	927.61
18	3	48.50	20.00	18.41	2831.95	2648.83	1924.86
19(C)	3	48.50	20.00	10.00	2224.62	1988.92	1427.63
20(C)	3	48.50	20.00	10.00	2422.64	2103.88	1508.98

The six center points as shown in Table 2 produced four measures of variation known as pure error. There were four measures of variation due to the use of a block as the optimization could not be performed within the same day. Pure error represented the replication error and it was used in evaluation for the lack of fit. The significance of the equation parameters for each response variable was assessed by F-ratio at a probability (p) of 0.05. The closer the

value of R^2 to unity, the better the empirical model fitted the actual data. The fit of the RSM model was evaluated by coefficients of determination (R^2) and a test for lack of fit from ANOVA (Table 3a-c). The quadratic model is significant with a *p*-value of 0.0146 ($p < 0.05$) and the model has no lack of fit at 95% confidence level. The R^2 value of 0.8548 (Table 3a) and the observed values versus predicted values plot (Fig. 2) shows that the model is statiscally acceptable. This indicates that the model could explain 85.48% of the variability in the response. According to Bogusz and Tavares [16], the R^2 should be at least 0.80 for a good fit of a model.

Table 3a . ANOVA for response surface quadratic model for Response 1 (glycerol)

Source	Response 1 (glycerol)				
	SS	*df*	MS	*F* value	*p* value
Block	2.008E+007	2	1.004E+007		
Model	1.725E+007	9	1.916E+006	5.23	0.0146
A- Extraction Temp	1.563E+004	1	1.563E+004	0.043	0.8415
B – Extraction Time	5.696E+006	1	5.696E+006	15.55	0.0043
C – Desorption Time	4.280E+006	1	4.280E+006	11.68	0.0091
A^2	9.322E+005	1	9.322E+005	2.54	0.1493
B^2	2.263E+004	1	2.263E+004	0.062	0.8100
C^2	4.602E+005	1	4.602E+005	1.26	0.2949
AB	2.896E+006	1	2.896E+006	7.91	0.0228
AC	1.710E+006	1	1.710E+006	4.67	0.0627
BC	1.375E+006	1	1.375E+006	3.75	0.0887
Residual	2.930E+006	8	3.663E+005		
Lack of fit (model error)	2.279E+006	5	4.559E+005	2.10	0.2874
Pure error (replicate error)	6.511E+005	3	2.170E+005		
Corrected total	4.025E+007	19			
R^2	0.8548				

Table 3b . ANOVA for response surface quadratic model for Response 2 (1,2-PDO)

Source	Response 2 (1,2-PDO)				
	SS	*df*	MS	*F* value	*p* value
Block	9.044E+006	2	4.522E+006		
Model	7.975E+006	9	8.861E+005	2.11	0.1532
A- Extraction Temp	1.357E+005	1	1.357E+005	0.32	0.5853
B – Extraction Time	1.776E+006	1	1.776E+006	4.23	0.0738
C – Desorption Time	3.164E+005	1	3.164E+005	0.75	0.4107
A^2	9.830E+005	1	9.830E+005	2.34	0.1645
B^2	29479.07	1	29479.07	0.070	0.7977
C^2	3.773E+005	1	3.773E+005	0.90	0.3710
AB	1.499E+006	1	1.499E+006	3.57	0.0955
AC	2.024E+006	1	2.024E+006	4.82	0.0594
BC	9.724E+005	1	9.724E+005	2.32	0.1666
Residual	3.359E+006	8	4.199E+005		
Lack of fit (model error)	2.578E+006	5	5.156E+005	1.98	0.3046
Pure error (replicate error)	7.814E+005	3	2.605E+005		
Corrected total	2.038E+007	19			
R^2	0.7036				

Table 3c . ANOVA for response surface quadratic model for Response 3 (EG)

Source	Response 3 (EG)				
	SS	*df*	MS	*F* value	*p* value
Block	6.565E+006	2	3.283E+006		
Model	5.463E+006	9	6.070E+005	2.19	0.1414
A- Extraction Temp	5.907E+004	1	5.907E+004	*0.21*	0.6565
B – Extraction Time	1.105E+006	1	1.105E+006	*3.99*	0.0808
C – Desorption Time	2.966E+005	1	2.966E+005	*1.07*	0.3310
A^2	1.044E+006	1	1.044E+006	3.77	0.0881
B^2	2.206E+005	1	2.206E+005	*0.80*	0.3981
C^2	6.143E+005	1	6.143E+005	*2.22*	0.1747
AB	9.945E+005	1	7.914E+005	*2.86*	0.1294
AC	6.082E+005	1	9.945E+005	*3.59*	0.0947
BC	2.215E+006	1	6.082E+005	*2.20*	0.1766
Residual	1.142E+006	8	2.769E+005		
Lack of fit (model error)	1.142E+006	5	2.285E+005	0.64	0.6920
Pure error (replicate error)	1.073E+006	3	3.577E+005		
Corrected total	1.424E+007	19			
R^2	0.7115				

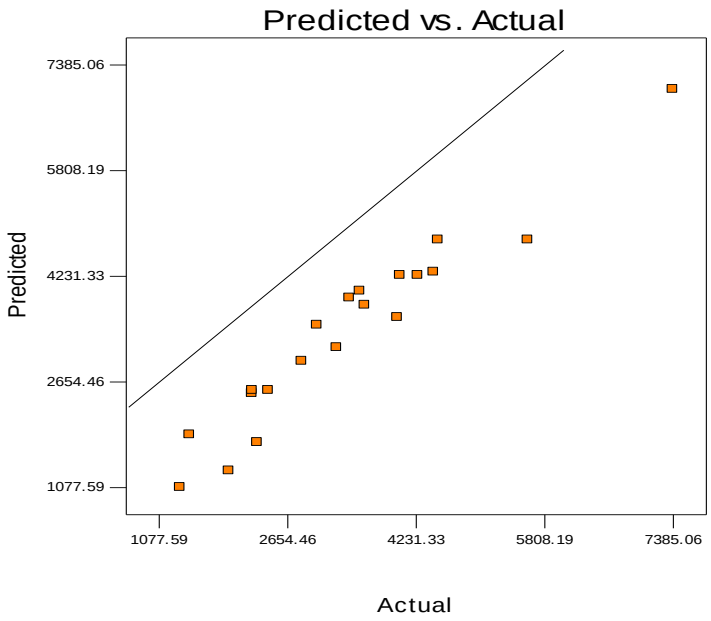


Figure 2**.** Plot to show relationships between observed values and values predicted by the model

It was found that for the recovery of glycerol at the 95% confidence level (Prob > F was less than 0.05), three parameters (extraction time (B), desorption time (C) and interaction between extraction temperature and extraction time (AB), were significant. However, no variables were significant for the recovery of 1,2-PDO and EG. Therefore, only glycerol was used to optimize the extraction of glycerol and liquid products in water for hydrogenolysis glycerol reaction. In this study, the response and explantory variables were fitted to each other by RSM. A good fit was obtained and there were no outliers observed for the quadratic model:

Peak area of glycerol = $-3799.2 + 150.79A + 133.26B + 287.76C - 0.550A^2 - 0.396B^2 - 7.151C^2 - 2.798AB - 4.30BC$

Figure 3 illustrated the relationship between the explanatory and response variables in a three-dimensional representation of the response surface and two-dimensional contour plot generated by the model. It was observed that the peak area of glycerol increased in a quadratic manner with the extension of time at room temperature. It was noted that there was an effect of interaction between the extraction time and the temperature on the peak area of glycerol.

A numerical optimization was also carried out using the Design-Expert software to determine the optimum extraction parameter (time and temperature) and desorption time of the SPME fiber for the maximum extraction of glycerol. Results showed that the estimated optimum values for extraction temperature and time and desorption time by response surface methodology were 27°C, 30 min and 15 min, respectively. To evaluate the accuracy of the results obtained by the response surface model, four experiments were carried out under the optimum conditions. Results showed, there was a good agreement between the calculated and experimental responses (Table 4).

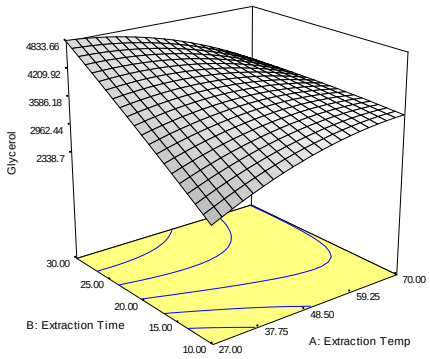


Figure 3. Response surface and contour plot for the effects of extraction time and temperature on the peak of glycerol

Table 4. Optimum response and the corresponding levels

Extraction Temperature (°C)	Extraction Time (min)	Desorption Time (min)	Optimum response (Total area)	Experimental response[a] (Total area)
27	30	15	11 072.76	10 987. 35

[a] Mean value of the measurement (n = 4)

For comparative purposes, the traditional one-at-a-time technique was also used to find the optimum conditions. Only extraction temperature was the same level as the experimental design method, except for extraction time, which was 30 minutes instead of 5.0 minutes and desorption time, which was 15 minutes instead of 10 minutes,. This might be due to the fact that the response surface model had more linear than non-linear characteristics. However, to reach the optimum conditions, much fewer experiments were needed in the experiment design compared to the one-at-a-time technique.

Analysis of Liquid Products Sample From Hydrogenolysis of Glycerol

The optimized extraction conditions (extraction temp = 27°C, extraction time = 30 minutes and desorption time = 15 minutes) were then applied in analyzing real liquid samples for glycerol hydrogenolysis reaction. The two chromatograms showed a similar paterrn for retention time from 2 to 50 minutes (Figure not shown). However, the GC-FID chromatogram showed quite different peak areas for glycerol, 1,2-PDO and EG before and after optimizing the SPME conditon (Table 5). This indicated that the optimum condition obtained using RSM gave the highest extraction of compounds in water for hydrogenolysis of glycerol.

Table 5. Peak area of glycerol, 1,2-PDO and EG compounds in water before and after optimization

Retention time (min)	Compound	Peak area analyze by GC-FID	
		Before Optimum[a]	Optimum Condition
50.6	glycerol	1450.14	2698.02
27.2	1,2-PDO	1951.06	2534.31
28.2	EG	78.94	112.51

[a] extraction temperature = 27°C, extraction time = 5 min , desorption time = 10 min

Conclusion

In this study, the effect of three operating parameters of solid phase microextraction (SPME), namely extraction temperature, extraction time and desorption time on the extraction of 1,2-propanediol and glycerol in water were evaluated using an experimental design based on central composite design approach. The optimized operating conditions for the extraction were identified using a response surface method. Consequently, this study proved that SPME coupled with GC-FID was able to provide a fast, simple and solvent-free method for the analysis of liquid products in aqueous phase glycerol hydrogenolysis reaction.

Acknowledgement

The authors would like to acknowledge Universiti Teknologi MARA(UiTM) for providing staff schlolarships and all members in the Catalysis Laboratory, UKM. The authors also would like to thanks En. Man Ghani for his contribution in this research. This study was funded by research grant UKM-ST-06-FRGS0147-2010 & UKM-GUP-BTK-08-14-306.

References

1. Furikado, I., Miyazawa, T., Koso, S., Shimao, A., Kunimori, K. Tomishige, K. (2007). Catalytic performance of Rh/SiO2 in glycerol reaction under hydrogen. *Green Chemistry* 9 (6): 582-588.
2. Miyazawa, T., Koso, S., Kunimori, K. Tomishige, K. (2007). Development of a Ru/C catalyst for glycerol hydrogenolysis in combination with an ion-exchange resin. *Applied Catalysis A: General* 318: 244-251.
3. Feng, J., Fu, H., Wang, J., Li, R., Chen, H. Li, X. (2008). Hydrogenolysis of glycerol to glycols over ruthenium catalysts: Effect of support and catalyst reduction temperature. *Catalysis Communications* 9 (6): 1458-1464.
4. Alhanash, A., Kozhevnikova, E.F. Kozhevnikov, I.V. (2008). Hydrogenolysis of glycerol to propanediol over Ru: Polyoxometalate bifunctional catalyst. *Catalysis Letters* 120 (3-4): 307-311.
5. Bolado, S., Treviño, R.E., García-Cubero, M.T. González-Benito, G. (2010). Glycerol hydrogenolysis to 1, 2 propanediol over Ru/C catalyst. *Catalysis Communications* 12, (2): 122-126.
6. Guo, L., Zhou, J., Mao, J., Guo, X. Zhang, S. (2009). Supported Cu catalysts for the selective hydrogenolysis of glycerol to propanediols. *Applied Catalysis A: General* 367(1-2): 93-98.
7. Balaraju, M., Rekha, V., Sai Prasad, P.S., Prasad, R.B.N. Lingaiah, N. (2008). Selective hydrogenolysis of glycerol to 1, 2 propanediol over Cu-ZnO catalysts. *Catalysis Letters* 126, (1-2), 119-124.
8. Roy, D., Subramaniam, B. Chaudhari, R.V. (2010). Aqueous phase hydrogenolysis of glycerol to 1,2-propanediol without external hydrogen addition. *Catalysis Today* 156 (1-2): 31-37.
9. De Oliveira, A.R.M., Cesarino, E.J. Bonato, P.S. (2005). Solid-phase microextraction and chiral HPLC analysis of ibuprofen in urine. *Chromatography B: Analytical Technologies in the Biomedical and Life Sciences* 818 (2): 285-291.
10. Bianchi, F., Careri, M., Mangia, A., Mattarozzi, M. Musci, M. (2008). Experimental design for the optimization of the extraction conditions of polycyclic aromatic hydrocarbons in milk with a novel diethoxydiphenylsilane solid-phase microextraction fiber. *Chromatography A* 1196-1197 (1-2): 41-45.

11. Ferrari, F., Sanusi, A., Millet, M. Montury, M. (2004). Multiresidue method using SPME for the determination of various pesticides with different volatility in confined atmospheres. *Analytical and Bioanalytical Chemistry* 379 (3): 476-483.
12. Larreta, J., Vallejo, A., Bilbao, U., Usobiaga, A., Arana, G. Zuloaga, O. (2007). Headspace-solid-phase microextraction preconcentration of phenols, indoles and on-fibre derivatised volatile fatty acids in liquid and gas samples from cow slurries. *Separation Science* 30 (14): 2293-2304.
13. Zhang, Y.and Zhang, J., (2008). Optimization of headspace solid-phase microextraction for analysis of ethyl carbamate in alcoholic beverages using a face-centered cube central composite design. *Analytica Chimica Acta* 627 (2): 212-218.
14. Ossiander, L., Reichenberg, F., McLachlan, M.S. Mayer, P. (2008). Immersed solid phase microextraction to measure chemical activity of lipophilic organic contaminants in fatty tissue samples. *Chemosphere* 71 (8): 1502-1510.
15. Januszkiewicz, J., Sabik, H., Azarnia, S. Lee, B. (2008). Optimization of headspace solid-phase microextraction for the analysis of specific flavors in enzyme modified and natural Cheddar cheese using factorial design and response surface methodology. *Chromatography A* 1195 (1-2): 16-24.
16. Bogusz Jr, S., de Marchi Tavares de Melo, A., Zini, C.A. Godoy, H.T. (2011). Optimization of the extraction conditions of the volatile compounds from chili peppers by headspace solid phase micro-extraction. *Journal of Chromatography A* 1218 (21): 3345-3350.
17. Negreira, N., Rodríguez, I., Rubí, E. Cela, R. (2010). Solid-phase microextraction followed by gas chromatography-mass spectrometry for the determination of ink photo-initiators in packed milk. *Talanta* 82 (1): 296-303.
18. Cam, D., Gagni, S., Lombardi, N. Punin, M.O. (2004). Solid-phase microextraction and gas chromatography-mass spectrometry for the determination of polycyclic aromatic hydrocarbons in environmental solid matrices. *Chromatographic Science* 42 (6): 329-335.

The Malaysian Journal of ANALYTICAL SCIENCES ISSN 1394-2506

ISOLATION AND CHARACTERIZATION OF COMPOUNDS FROM THE STEM BARK OF *UVARIA RUFA* (ANNONACEAE)

(Pemisahan dan Pencirian Sebatian dari Kulit Batang *Uvaria rufa* (Annonaceae))

Andi R. Rosandy[1], Laily B. Din[1], W .A. Yaacob[1]*, Nik Idris Yusoff[2], I. Sahidin[3], Jalifah Latip[1], Syarul Nataqain[4], Normah Mohd Noor[4]

[1]*School of Chemical Sciences and Food Technology, Faculty of Science and Technology, Universiti Kebangsaan Malaysia, 43600 Bangi, Selangor, Malaysia*
[2]*Pharmaceutical Chemistry Department, Kulliyyah of Pharmacy, International Islamic University Malaysia, Bandar Indera Mahkota, 25200 Kuantan, Pahang, Malaysia*
[3]*School of Pharmacy and Sciences, Haluoleo University, Kendari, Indonesia*
[4]*Metabolomic Laboratory, Institute of Systems Biology (INBIOSIS), Universiti Kebangsaan Malaysia, 43600 Bangi, Selangor, Malaysia*

**Corresponding author: wanyaa@ukm.my*

Abstract

Isolation of compounds from methanol extract of the stem bark of Uvaria rufa has been conducted by using radial chromatography. Their structures were elucidated by UV, IR, NMR and mass spectroscopy, and by comparison with the literature. Seven compounds were isolated namely benzyl benzoate (**1**), caryophyllene oxide (**2**), glutinol (**3**), 5-hydroxy-7-methoxyflavone (**4**), 5-hydroxy-6,7-dimethoxyflavone (**5**), 2,5-dihydroxy-7-methoxyflavanone (**6**) and 5,7-dihydroxyflavanone (**7**). Separation of the caryophyllene oxide (**2**), glutinol (**3**) and 5,7-dihydroxyflavanone (**7**) from Uvaria rufa has never been reported.

Keywords: *Annonaceae*, Uvaria rufa, *terpene, flavonoid*

Abstrak

Pengasingan sebatian dari ekstrak metanol kulit batang Uvaria rufa telah dilakukan dengan menggunakan kromatografi radial. Struktur semua sebatian ditentukan dengan spektroskopi UL, IM, RMN dan jisim, dan secara perbandingan dengan data kepustakaan. Tujuh sebatian telah diasingkan iaitu benzil benzoat (**1**), kariofilena oksida (**2**), glutinol (**3**), 5-hidroksi-7-metoksiflavon (**4**), 5-hidroksi-6,7-dimetoksiflavon (**5**), 2,5-dihidroksi-7-metoksiflavanon (**6**) dan 5,7-dihidroksiflavanon (**7**). Pemisahan kariofilena oksida (**2**), glutinol (**3**) dan 5,7-dihidroksiflavanon (**7**) dari Uvaria rufa belum pernah dilaporkan.

Kata Kunci: *Annonaceae*, Uvaria rufa, *terpena, flavonoid*

Introduction

Uvaria, a genus of Annonaceae family, consists of approximately 150 species that are distributed in several areas including tropical Africa, Madagascar, Indo-Malaya and Australia [30]. Most plants of the genus *Uvaria* are found to grow as vines on trees. Some are known as Larak (Malaysia), Kalak (Java) and Allagat or Hinlalaki (Luzon). *Uvaria rufa* or *U. ridleyi* is widely available in Peninsular Malaysia, and have been named by the locals as Larak or Pisang-pisang [16]. This plant was reported to be found in the north-west and southern part of Peninsular Malaysia, namely the River Tebrau in Johor and Pahang [4]. Traditionally, all parts of this plant can be used for specific purposes; the squeezed leaves afford a cinnamon bark-like smell and water decoctions can be consumed directly, while the fruits are believed to cure certain diseases like ulcers of the intestines [4]. It has also been mentioned that the water decoction of the roots are used to treat women after giving birth [11]. *Uvaria rufa* is a rich source of various new compounds as proven by the isolation of benzoylated derivatives [17], flavonoids [5] and flavonoid

glycosides [9], essential oils [3], oxygenated cyclohexanes [29] and polyoxygenated cyclohexenes [31]. In our recent study on methanol extract of the stem bark of *U. rufa*, we have successfully isolated seven compounds.

Materials and Methods

Plant material

The stem bark of *Uvaria rufa* was collected from the secondary forest in Parit, Perak, Malaysia. A herbarium specimen of BKP0001 was deposited at the Universiti Kebangsaan Malaysia Herbarium.

Extraction and Isolation

Dried ground stem bark of *Uvaria rufa* (500 g) was macerated with methanol at room temperature. The filtrate was concentrated using rotary evaporator to yield a dark green extract (13 g, 2.65 %). A 3 g portion of the extract was fractionated by using radial chromatography (RC) with 4 mm thickness silica gel on a round glass plate eluted with increasing polarity of *n*-hexane-EtOAc. The eluents that showed the same profile on thin layer chromatography (TLC) chromatogram were combined to give three fractions (I-III). Purification of fraction I (600 mg) was carried out using RC with silica gel plate of 1 mm thickness eluted with 95:5 *n*-hexane-EtOAc in 5% polarity increment to yield compounds **1** (550 mg) and **2** (26 mg). Purification of fraction II (410 mg) was conducted utilizing another RC with silica gel plate of 1 mm thickness. Elution with 9:1 *n*-hexane-EtOAc produced compounds **3** (18 mg) and **4** (36 mg). Purification of fraction III (430 mg) was then performed using RC with silica gel plate of 1 mm. Elution with 7:2:1 *n*-hexane-EtOAc-$CHCl_3$ resulted in compounds **5** (28 mg), **6** (56 mg) and **7** (12 mg).

Compound Identification

Structures of pure compounds were determined based on the spectral data recorded on Shimadzu UV-260 spectrophotometer, Frontier Perkin-Elmer FTIR/NIR spectrophotometer and Bruker NMR 600 MHz Cryo-Probe instrument that included 1-D and 2-D NMR. Melting points were measured using Stuart SMP10 melting point apparatus. ESIMSs were recorded by using GC/MS Model GC5890 Series II/MSD-5970 HP. The isolation was then carried out by radial chromatography using round glass plates of the Merck Kieselgel 60 PF_{254} (art. no. 7749) and profile was analyzed using smaller pieces from aluminium sheets 20 x 20 cm of the Merck TLC silica gel 60 F_{254} of 0.25 mm thickness (art. no. 5554) and then detected under UV light (254 nm) or by $CeSO_4$ spraying reagent followed by heating.

Benzyl benzoate (**1**): Pale yellow oily liquid (550 mg), ESIMS $[M]^+$ at *m/z* 212, FT-IR (ATR, attenuated total reflectance) ν_{max} cm^{-1}: 3034-2953 (weak), 1715, 1601-1451, 1265 and 707-695. ^1H NMR ($CDCl_3$, 600 MHz) δ_H (ppm) and ^{13}C NMR ($CDCl_3$, 150 MHz) δ_C (ppm) are tabulated in Table 1.

Caryophyllene oxide (**2**): White amorphous (26 mg), 59-61 ^oC (60-61 ^oC, Chavan et al. 2010), ESIMS $[M]^+$ at *m/z* 220, FT-IR (ATR) ν_{max} cm^{-1}: 2927-2867, 1640, 970. ^1H NMR ($CDCl_3$, 600 MHz) δ_H (ppm) and ^{13}C NMR ($CDCl_3$, 150 MHz) δ_C (ppm) are tabulated in Table 2.

Glutinol (**3**): White amorphous (18 mg), m.p. 202-203°C, ElMS $[M]^+$ at *m/z* 426, FT-IR (ATR) ν_{max} cm^{-1}: 3391, 2927, 1726 and 1072 (weak). ^1H NMR ($CDCl_3$, 600 MHz): δ_H (ppm) 0.86, 0.96, 1.00, 1.01, 1.05, 1.10, 1.15, 1.17 (each 3H, *s*, $8CH_3$), 1.23-2.05 (23H, complex, $10CH_2$ + 3CH), 3.49 (lH, *d*, J = 13.8 Hz, H-3) and 5.64 (lH, *d*, *J* = 6.6 Hz, H-6). ^{13}C NMR ($CDCl_3$, 150 MHz) δ_C (ppm) data are tabulated in Table 3.

5-Hydroxy-7-methoxyflavone (**4**): Yellow amorphous (36 mg), m.p. 164-165^oC, EIMS $[M]^+$ at *m/z* 268, UV [MeOH] λ_{max} 269 and 310 nm, [MeOH+NaOH] λ_{max} 283 and 377 nm, FT-IR (ATR), ν_{max} cm^{-1}: 3100-2800, 1652, 1600-1590, 1470-1430, 1350-1340 and 1270-1210. ^1H NMR ($CDCl_3$, 600 MHz) δ_H (ppm) and ^{13}C NMR ($CDCl_3$, 150 MHz) δ_C (ppm) are tabulated in Table 4.

5-Hydroxy-6,7-dimethoxyflavone (**5**): Yellow amorphous (28 mg), m.p. 158-159^oC, EIMS $[M]^+$ at *m/z* 298, UV [MeOH] λ_{max} 314 and 273 nm, [MeOH+NaOH] λ_{max} 314 and 384 nm, FT-IR (ATR) ν_{max} cm^{-1}: 2850-2950, 1620-1640, 1590-1600, 1430-1470, 1350-1340, and 1120-1150. ^1H NMR ($CDCl_3$, 600 MHz) δ_H (ppm) and ^{13}C NMR ($CDCl_3$, 150 MHz) δ_C (ppm) are tabulated in Table 4.

2,5-Dihydroxy-7-methoxyflavanone (**6**): Colourless crystals (56 mg), m.p. 174-176°C, EIMS $[M]^+$ at *m/z* 286, UV [MeOH] λ_{max} 289 nm, [MeOH+NaOH] λ_{max} 387 nm, FT-IR (ATR) ν_{max} cm^{-1}: 3409, 1640, 1575-1449, 1315, and 1156. ^1H NMR ($CDCl_3$, 600 MHz), δ_H (ppm) and ^{13}C-NMR ($CDCl_3$, 150 MHz) δ_C (ppm) are tabulated in Table 4.

5,7-Dihydroxyflavanone (**7**): Colourless amorphous (8 mg), m.p 285-286°C, EIMS $[M]^+$ at *m/z* 254, FT-IR (ATR) ν_{max} cm^{-1}: 3403, 1638, 1600-1590, 1447, 1317 and 1190-1156. ^1H NMR ($CDCl_3$, 600 MHz), δ_H (ppm) and ^{13}C-NMR ($CDCl_3$, 150 MHz) δ_C (ppm) are tabulated in Table 4.

Results and Discussion

Chromatographic separation of the methanol extract of the stem bark of *Uvaria rufa* on silica gel Merck $60F_{254}$ (art. no. 7749) resulted in the isolation of compounds **1-7** (Figure 1).

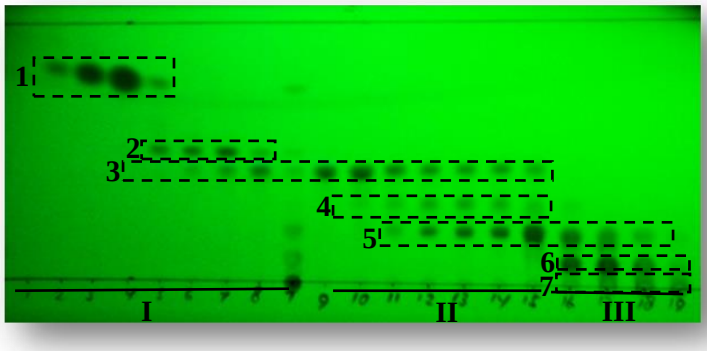
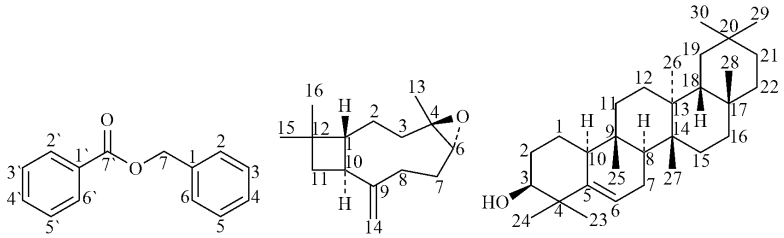
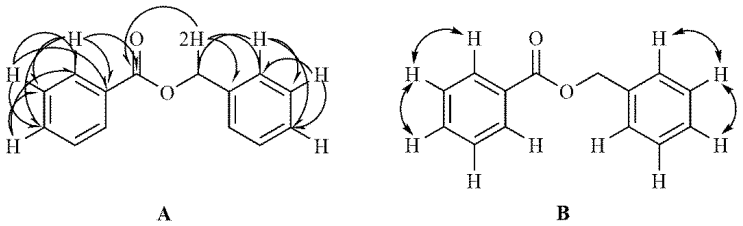


Figure.1. TLC profile of compounds present in the extract of stem bark of *Uvaria rufa* (Merck, art. no. 5554; n-hexane-EtOAc, 9:1). Combination of fractions 1-8, 9-15 and 16-19 gave respective fractions I, II and III. Similar horizontal spots designated as **1** (R_f 0.70), **2** (0.64), **3** (0.50), **4** (0.39), **5** (0.25), **6** (0.14) and **7** (0.06) represent respective benzyl benzoate (**1**), caryophyllene oxide (**2**), glutinol (**3**), 5-hydroxy-7-methoxyflavone (**4**), 5-hydroxy-6,7-dimethoxyflavone (**5**), 2,5-dihydroxy-7-methoxyflavanone (**6**) and 5,7-dihydroxyflavanone (7).



Benzyl benzoate (**1**) [1, 2; 18, 19; 23; 24] was obtained in the form of yellow pale oily liquid. The mass spectrum showed a molecular ion peak ESIMS $[M]^+$ at *m/z* 212 which was analyzed for the molecular formula $C_{14}H_{12}O_2$. FTIR (ATR) spectrum indicated that the compound contained a carbonyl group with stretching at 1715 cm^{-1}, ether at 1265 cm^{-1}, C=C aromatic at 1601-1451 cm^{-1} and *ortho* coupling in the benzene ring at 707-695 cm^{-1}. The presence of functional groups is supported by NMR analysis of 1-D (^1H, ^{13}C-NMR and DEPT) and 2-D (HSQC, HMBC and H-H COSY) data. Spectrum of ^{13}C-NMR showed 10 signals representing 14 carbons, which consisted of ten methine carbons for two phenyls at 133.1, 129.8, 128.7, 128.5, 128.3 and 128.2 ppm; a methylene carbon at 66.7 ppm; and three quaternary carbons including one carbonyl carbon at 166.4 ppm and two aromatic carbons at 136.2 and 130.3 ppm. Meanwhile, the ^1H NMR spectrum showed 7 signals representing 12 protons. Furthermore,

experiments of HMBC as shown in A and H-H COSY in **B** established the final structure of benzyl benzoate. 1-D and 2-D NMR data for benzyl benzoate (**1**) are tabulated in Table 1.



A **B**

Table 1. NMR data of benzyl benzoate (**1**)

No. of C	δ_C (ppm)	δ_H (ppm) (mult., *J* in Hz)	2-D NMR	
			HMBC	H-H COSY
1	136.2	-	-	-
2/6	128.2	7.53 (*d*, 8.1) (2H)	C-3/5, C-4, C-7	H-3/5
3/5	128.3	7.48 (*t*, 7.7) (2H)	C-2/6, C-4	H-2/6, H-4
4	128.5	7. 40 (*t*, 7.2) (1H)	C-2/6, C-3/5	H-3/5
7	66.7	5.44 (*s*) (2H)	C-7`, C-1, C-2/6	-
1`	130.3	-	-	-
2`/6`	129.8	8.17 (*d*, 8.1) (2H)	C-1`, C-3`/5`, C-4`, C-7`	H-3`/5`
3`/5`	128.7	7.45 (*t*, 7.5) (2H)	C-1`, C-2`/6`, C-4`	H-2`/6`, H-4`
4`	133.1	7.59 (*t* , 7.5) (1H)	C-2`/6`, C-3`/5`	H-3`/5`
7`	166.4	-	-	-

Caryophyllene oxide (**2**) [6; 8; 26] is a white amorphous. FT-IR (ATR) ν_{max} cm^{-1}: 1640 (epoxy), 2959-2858 (C-C cyclic aliphatic), 1541-1458 (weak, C=C), 1277 and 772 (epoxy), and ν_{max}1128-1073 (C=C olefinic). The ^{13}C-NMR data showed the presence of 15 carbon signals representing three quaternary carbons at δ_C of 151.8, 60.0 and 34.0 ppm; six methylene carbons at δ_C of 112.8, 39.8, 39.2, 30.2, 29.8 and 27.2 ppm; three methine carbons at δ_C of 63.8, 50.8 and 48.7 ppm; and three methyl carbons at δ_C of 29.9, 21.6 and 17.0 ppm. Based on the data, compound **2** can be assigned as a cyclic aliphatic sesquiterpene with an epoxy formed across C-4 and C-6, while a double bond is formed between C-9 and C-14. Meanwhile, 18 proton signals representing 24 protons appeared in the ^{1}H-NMR spectrum as shown in Table 2. Eighteen of the signals came from the three signals, one each from a methyl group at C-epoxy and the two non-equivalent gem-dimethyls at C-12; three signals from the three methine protons at C-1, C-6 and C-10; two respective signals of the saturated non-equivalent methylene protons C-2, C-3, C-7, C-8, C-11 and olefinic non-equivalent methylene protons C-14. The H-H COSY experiment indicated that protons at δ_H 4.89 and 5.00 ppm were related to each other and marked as olefinic methylene protons at C-14. Furthermore, the allylic methine proton at δ_H 2.65 ppm (C-10) was proven by an association between methine proton at C-1 (δ_H 1.77 ppm) and methylene protons at C-11 (δ_H 1.70 and 1.63 ppm). This assumption on compound **2** was highly supported by the similar parameters between ^{13}C- and ^{1}H-NMR data with those of caryophyllene oxide which was reported by Orihara et al. (1994) [20] (Table 2).

Table 2. Comparison of NMR data of caryophyllene oxide (**2)** with those of the literature*****

No. of C	δ_C (ppm)		No. of H	δ_H (ppm)
	2	*****		**2**
1	50.8	51.0	1	1.77 (*t*, 9.6)
2	27.2	27.6	2 α	1.45 (*m*)
			2 β	1.71 (*t*, 9.3)
3	39.2	39.7	3 α	2.13 (*m*)
			3 β	0.96 (*m*)
4	60.0	59.7	-	-
6	63.8	63.4	6	2.90 (*dd*)
7	30.2	30.2	7 α	1.26 (*m*)
			7 β	2.27 (*m*)
8	29.8	30.2	8 β	2.35 (*m*)
			8 α	2.11 (*m*)
9	151.8	152.4	-	-
10	48.7	49.0	10	2.65 (*m*)
11	39.8	40.0	11 β	1.70 (*dd*, 9.7, 3.6)
			11 α	1.63 (*s*)
12	34.0	34.1	-	-
13	17.0	17.4	13	1.23 (*s*)
14	112.8	113.0	14 α	4.89 (*d*, 6.6)
			14 β	5.00 (*d*, 6.6)
15	29.9	29.9	15	1.03 (*s*)
16	21.6	21.8	16	1.01 (*s*)

*****Source: Orihara et al. (1994)

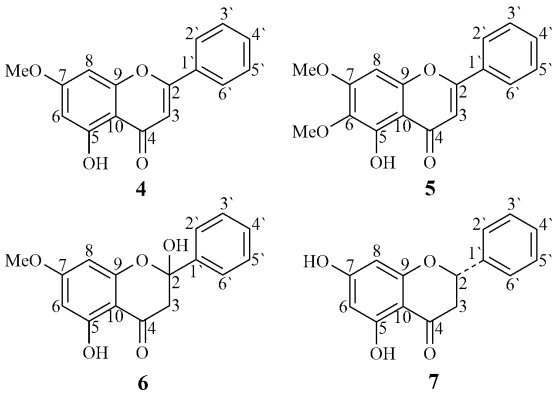
Glutinol (**3**) [13; 21; 27] is a white amorphous with m.p. 202-203°C. Its IR spectrum showed ν_{max} absorption peaks at 3525 (O-H); 2927, 2867 (C-H); 1385 (C-O) and 1453 (C=C). Compounds **3** gave positive response to Liebermann-Burchard spray reagent, which indicated the presence of a triterpenoid nucleus**.** This assumption was reinforced by the ^{13}C-NMR data that indicated the presence of thirty carbons as tabulated in Table 3 which included two olefinic carbon signals at δc 141.6 (C-5) and 122.1 (C- 6) and also one oxymethine at δc 76.3 (C-3). The ^{1}H-NMR spectrum of compound **3** displayed signals due to the eight methyls (δ_C 0.86-1.17), a carbinol proton H-3 at δ_H 3.5 and an olefinic proton H-5 at δ_H 5.6. A molecular ion peak $[M]^+$ at *m/z* 426 was exhibited in its mass spectrum data, which gave a possible molecular formula of $C_{30}H_{50}O$. The combined spectral data of ^{13}C NMR suggested that the triterpenoid was glutinol, which was further supported by comparison with the literature [28] as tabulated in Table 3.

Table 3. Comparison of ^{13}C-NMR data of glutinol (**3)** with those of the literature*****

No of C	3	**	No of C	3	**
1	18.2	18.2	16	36.0	36.0
2	27.8	27.8	17	30.1	30.1
3	76.4	76.3	18	43.1	43.1
4	40.8	40.8	19	35.1	35.1
5	141.6	141.6	20	28.3	28.2
6	122.1	122.1	21	32.1	33.1
7	23.6	23.7	22	39.0	39.0
8	47.4	47.5	23	25.5	25.5
9	34.9	34.9	24	29.0	29.0
10	49.7	49.7	25	16.2	16.2
11	34.6	34.6	26	19.6	19.6
12	30.4	30.4	27	18.5	18.4
13	39.3	39.3	28	32.0	32.0
14	37.8	37.8	29	34.5	34.5
15	33.1	32.1	30	32.4	32.4

**Source: Sule et al. 2011

The flavonoids were characterized as 5-hydroxy-7-methoxyflavone (**4**), 5-hydroxy-6,7-dimethoxyflavone (**5**) 2,5-dihydroxy-7-methoxyflavanone (**6**) and 5,7-dihydroxyflavanone (**7**) by spectroscopic methods as well as comparison of their physical and spectral data which was reported by [5], [7], [16] and [22]. The differences between compounds **4**, **5**, **6** and **7** lay on C-2, C-6 and C-7, where Compounds **4** and **6** had a methoxy bound at C-7, whereas in **5** two methoxys were bound to C-6, C-7 and also had a hydroxyl bound at C-2. For compound **7**, it had a hydroxyl at C-7 and two protons were bound to C-2 and C-6.



4 **5** **6** **7**

Table 4. NMR data of 5-hydroxy-7-methoxyflavone (**4**), 5-hydroxy-6,7-dimethoxyflavone (**5**), 2,5-dihydroxy7-methoxyflavanone (**6**) and 5,7-dihydroxyflavanone (**7**)

No. of C	δ_C (ppm)				No. of H	δ_H (ΣH, mult., *J* in Hz			
	4	**5**	6	7		4	5	6	7
-	-	-	-	-	-	-	-	-	-
2	164.0	164.0	105.7	79.3		-	-	-	5.44 (*dd*, 3, 13.2)
3	105.9	104.9	56.4	43.4	3	6.67 (*s*)	6.69 (*s*)	3.06 (*s*)	3.11 (*d*, 12.6)
								3.22 (*s*)	2.08 (*d*, 13.2)
4	182.5	182.8	183.0	195.8	-	-	-	-	-
5	162.2	157.6	159.0	164.4		-	-	-	-
6	98.2	132.0	90.7	95.5	6	6.39 (*s*)	-	6.13 (*s*)	5.86 (*br-s*)
7	165.6	158.8	163.0	164.6		-	-	-	-
8	92.7	95.9	90.7	96.8	8	6.51 (*s*)	6.45 (*s*)	6.12 (*s*)	6.02 (*s)*
9	157.8	149.5	153.4	163.2		-	-	-	-
10	105.7	105.4	105.6	102.8		-	-	-	-
1`	131.9	131.4	132.7	138.3		-	-	-	-
2`/6`	126.3	126.4	126.3	126.2	2`/6`	7.89 (*d*,7.8)	7.96 (*d*, 7.8)	7.69 (*d*, 7.8)	7.46 (*m*)
3`/5`	129.1	129.2	131.4	129.0	3`/5`	7.54 (*m*)	7.56 (*m*)	7.54 (*m*)	7.45 (*m*)
4`	126.3	126.4	129.1	126.2	4`	7.52 (*m*)	7.54 (*m*)	7.54 (*m*)	7.46 (*m*)
6OMe	-	61.7	-	-	6OMe	-	3.97 (*s*)	-	-
7OMe	55.9	56.4	55.7	-	7OMe	3.89 (*s*)	3.96 (*s*)	3.84 (*s*)	-
-	-	-	-	-	-OH	12.73 (*s*)	12.57 (*s*)	11.93 (*s*)	12.05 (*s*)

Chemotaxonomic Significance

Benzyl benzoate (**1**) and caryophyllene oxide (**2**) are the main components of essential oils that have been frequently isolated from the family Annonaceae. Compound **1** is the main precursor in the biogenesis of the highly oxidized cyclohexenoid reported earlier from the leaves of *Uvaria rufa* [29]. It has been found in most of *Uvaria* species such as *U. purpurea*, *U. versicolor*, *U. klaineana*, *U. ferruginea*, *U. pauci-ovulata*, *U. narum* and *U. chamae* [1, 2; 3; 14, 15]. Meanwhile, the sesquiterpene **2** is frequently isolated from many species of *Uvaria*, *Cyathostemma*, *Mitrephora* and *Cananga* [3]. Glutinol (**3**) is a triterpene, which was reported in *Uvaria narum* and *U. hookeri* [12; 21]. This compound was also found in the family Olacaceae, especially *Olax* oliv. group [28] and in *Acer mandshuricum* (Aceraceae) [10]. Flavonoids are molecules with antioxidant properties that are widely occurring in the plant kingdom [25]. The presence of flavonoid group is very common in *Uvaria* species. Previous studies have reported the isolation of six flavonoids from the bark and roots of *Uvaria rufa* including 5-hydroxy-7-methoxyflavone (**4**), 5-hydroxy-6,7-dimethoxyflavone (**5**), 2,5-dihydroxy-7-methoxyflavanone (**6**), 2,5-dihydroxy-6,7-dimethoxyflavanone, 5-hydroxy-7-methoxyflavanone and 7-O-methylwogonine [9]. To the best of our knowledge, this is the first time 5,7-dihydroxyflavanone (**7**) has been found from *Uvaria rufa*., which contributes to the database of flavonoids from *Uvaria* species.

Conclusion

Benzyl benzoate (**1**), caryophyllene oxide (**2**), glutinol (**3**), 5-hydroxy-7-methoxyflavone (**4**), 5-hydroxy-6,7-dimethoxyflavone (**5**), 2,5-dihydroxy-7-methoxyflavanone (**6**) and 5,7-dihydroxyflavanone (**7**) were successfully isolated from the methanol extract of *Uvaria rufa.* To the best of our knowledge, this is the first report of caryopyllene oxide, glutinol and 5,7-dihydroxyflavanone from the stem bark of *Uvaria rufa.*

Acknowledgement

We would like to thank the School of Chemical Sciences and Food Technology, Faculty of Science and Technology, Universiti Kebangsaan Malaysia (UKM); School of Pharmacy and Sciences, Haluoleo University and INBIOSIS UKM for providing research facilities and also would also like to express our gratitude to the Ministry of Higher Education Malaysia and UKM for financial support through research grants of UKM-ST-06-FRGS0149-2010 and UKM-DLP-2012-033.

References

1. Akendengue, B., Roblot, F., Loiseau, P.M., Bories, C., Ngou-Milama, E., Laurens, A. & Hocquemiller, R. 2002. Klaivanolide, An antiprotozoal lactone from *Uvaria klaineana*. *Phytochemistry* 59(8): 885-888.
2. Akendengue, B., Ngou-Milama, E., Bourobou, B.H., Roblot, E.J., Gleye, F., Laurens, C., Hocquemiller, A.R. & Loiseau, P., Bories, C. 2003. Acaricidal activity of *Uvaria versicolor* and *Uvaria klaineana* (Annonaceae). *Phytotherapy Res.* 17(4): 364-367.
3. Brophy, J.& Goldsack, R. 2004. Essential oils from the leaves of some Queensland annonaceae. *J. Essent. Oil Res*. 16: 95–100.
4. Burkill, I.H.H. 1966. *A Dictionary of The Economic Products of The Malay Peninsular*. Volume II. Governments of Malaysia and Singapore by the Ministry of Agriculture and Co-operatives. Kuala Lumpur, pp 2255-2257.
5. Chantrapromma, K., Pakawatchai, C., Skelton, B.W., White, A.H. & Worapatamasri, S. 1989. 5-Hydroxy-7-methoxy-2-phenyl-4H-1-benzopyran-4-one (tectochrysin) and 2, 5- dihydroxy-7-methoxy-2-phenyl-2, 3-dihydro-4H-1- benzopyran-4-one: Isolation from *Uvaria rufas* and X-ray structures, *Aust. J. Chem.* 42: 2289-2293.
6. Chavan, M.J., Wakte, P.S. & Shinde, D.B. 2010. Analgesic and anti-Inflammatory activity of Caryophyllene Oxide from *Annona squamosa L*. Bark, *Phytomedicine* 17(2):149-151.
7. Chopin, J., Hauteville, M., Joshi, B.S. & Gawad, D.H. 1978. A novel example of a Natural 2,5-dihydroxyflavanone from *Unona lawii*. *Phytochemistry* 17(2): 332-334.
8. da Silva, D.B., Tulli, E., Garcez,C.O., Nascimento,W.S., de Siqueira, E.A., & Joao, M. 2007. Chemical constituents of the underground stem bark of *Duguetia furfuracea* (Annonaceae). *Jour. Brazil. Chem. Soc*. 18(8):1560-1565.
9. Deepralard, K., Kawanishi, K., Moriyasu, M., Pengsuparp, T.& Suttisri, R. 2009. Flavonoid glycosides from the leaves of *Uvaria rufa* with advanced glycation end-products inhibitory activity. *Thai J. Pharm. Sci.* 33: 84-90.
10. Ding, Y., Liang, C., Kim, J.H., Lee, Y., Hyun, J., Kang, H., Kim, J., Min, B.S. & Kim, Y.H. 2010. Triterpene compounds isolated from *Acer mandshuricum* and their anti-inflammatory activity. *Bioorganic & Medicinal Chemistry Letters* 20: 1528–1531.
11. Gimlette, J.D. 1971. *A Dictionary of Malayan Medicine*, Oxford University Press, p 141.
12. Hisham, A., Pieters, L.A.C., Claeys, M., Van Den Heuvel, M., Esmans, E., Dommisse, R. & Vlietinck, A.J. 1991. Acetogenins from root bark of *Uvaria narum*. *Phytochemistry* 30(7): 2373-2377.
13. Kim, H.K., Lee, K.H., Choi, S.U., Kim, Y.H. & Lee, K.R. 2008. Terpene and phenolic constituents of *Lactuca indica* L. *Arch. Pharm. Res.* 131(8): 983-988.
14. Kodpinid, M., Chirawat, S., Chachanat, T. & Yodhathai, T. 1984. Benzyl benzoates from the root of *Uvaria purpurea*. *Phytochemistry* 23: 199-200.
15. Kodpinid, M., Thebtaranonth, C. & Thebtaranonth, Y. 1985. Benzyl benzoates and o-hydroxybenzyl flavanones from *Uvaria ferruginea*. *Phytochemistry* 24(12): 3071-3072.
16. Lojanapiwatna,V., Promsuwansiri, K., Suwannatip, B. & Wiriyachitra, P. 1981. The flavonoids of *Uvaria rufa*, *J. Sci. Soc. Thailand* 7: 83-86

17. Macabeo, A.P.G., Tudla, F.A., Alejandro, G.J.D., Kouam, S.F., Hidayat Hussain, & Krohn, K. 2010. Benzoylated derivatives from *Uvaria rufa. Biochem. Syst. Ecol*. 38 :857–860.
18. Nkunya, M.H.H., Achenbach, H.H., Renner, H., Christian, R., Reiner, W. & Weenen, H. 1990. Schefflerin and isoschefflerin: prenylated chalcones and other constituents of *Uvaria scheffleri. Phytochemistry* 29(4): 1261-1264.
19. Nkunya, M.H.H., Weenen, H., Bray, D.H., Mgani, Q.A. & Mwasumbi, L.B. 1991. Antimalarial activity of Tanzanian plants and their active constituents: the genus ***Uvaria***. *Planta Med.* 57(4): 341-343.
20. Orihara, Y., Saiki, K. & Furuya, T. 1994. Biotransformation of caryophyllene oxide by cultured cells of *Eucalyptus perriniana**. *Phytochemistry*35(3): 635-639.
21. Padmaja, V., Thankamany, V. & Hisham, A. 1993. Antibacterial, antifungal and anthelmintic activities of root barks of *Uvaria hookeri* and *Uvaria narum*. *J. Ethnopharm.* 40(3): 181-186.
22. Payakarintarungkul, K. 2005. Antioxidants from *Uvaria rufa* Bloom roots. Master Thesis, Faculty of Science, Chulalongkorn University.
23. Rameshkumar, Koranappally. B. & George, V. 2006. *Cinnamomum sulphuratum* Ness-Benzyl benzoate rich new chemotype from southern western ghats. *India J. of Essential Oil Research* 18(5): 521-522.
24. Raynaud, S. Fourneau, Christophe, Laurens, Alain, Hocquemiller, Reynald, Loiseau, Philippe & Cristian, B. 2000. Squamocin and benzyl benzoate, bcaricidal components of *Uvaria pauci-ovulata* bark extracts. *Planta Medica* 66(2): 173-175.
25. Righi, G., Antonioletti, R., Silvestri, I.P., D'Antona, A., Lambusta, D. & Bovicelli, P. 2010. Convergent synthesis of mosloflavone, negletein and baicalein from crysin. *Tetrahedron* 66: 1294–1298.
26. Seidel, V., Francois, B. & Waterman, P.G. 1999. A diterpene, a sesquiterpene and a flavonol glycoside from *Piptostigma fasciculata* (Annonaceae). *Biochem. Syst. Ecol.* 27(5): 543-545.
27. Shadid, K.A., Khozirah, S., Faridah, A., Israf, D.A., Hamzah, A.S., Syakroni, N, Khoushik, S. & Lajis, N. 2007. Cytotoxic paged-polyprenylated xanthonoids and a xanthone from *Garcinia cantleyana. Phytochemistry* 68(20): 2537-2544.
28. Sule, M.I., Hassan, H.S., Pateh, U.U. & Ambi, A.A. 2011. Triterpenoids from the leaves of *Olax mannii* Oliv. *Nigerian Journal of Basic & Applied Science*. 19(2): 193-196.
29. Tudla, F.A., Aguinaldo, A.M., Krohn, K., Hussain, H. & Macabeo, A.P.G. 2007. Highly oxygenated cyclohexene metabolites from *Uvaria rufa. Biochem. Syst. Ecol.* 35: 45-47.
30. Usher, G. 1974. *A Dictionary of Plants Used by Man*. Constable and Company Ltd. London. p 594.
31. Zhang, C.R., Yang, S.P., Liao, S.G., Wu,Y. & Yue, J.M. 2006. Polyoxygenated cyclohexene derivatives from *Uvaria rufa. Helv. Chim. Acta* 89: 1408-1416.

The Malaysian Journal of ANALYTICAL SCIENCES ISSN 1394-2506

VARIATION OF RADON EMANATION IN WORKPLACES AS A FUNCTION OF ROOM PARAMETERS

(Variasi Emanasi Radon Di Tempat Kerja Sebagai Fungsi Parameter Bilik)

Norafatin Khalid, Amran Ab. Majid*, Aznan Fazli Ismail, Muhamad Samudi Yasir, Redzuwan Yahaya, Izzaty Azani Mustafa

Nuclear Science Programme,
Faculty of Science and Technology,
Universiti Kebangsaan Malaysia, 43600 Bangi, Selangor, Malaysia

**Corresponding author: amran@ukm.my*

Abstract

Modern life style requires people to spend most of their time indoors either in a house or in the workplace. Most modern buildings are made from soil based material which may consist of low concentration of naturally occurring radioactive materials (NORM). It is known that one of the daughters of natural uranium is ^{226}Ra which eventually produce radon (^{222}Rn) gas. Recently, more evidence has linked lung cancer to exposure to high levels of radon and also to cigarette-smoking. Consequently, this research was conducted to study the radon emanation rates in different workplaces. The radon emanations in 27 rooms with three different dimension (54 m^3, 210 m^3 and 351 m^3) and different building materials were determined for 96 hours using Sun Nuclear Radon Monitor. The radon emanations in the rooms studied were found to be in the range of 20.6 Bq m^{-3} $hour^{-1}$ to 134.3 Bq m^{-3} $hour^{-1}$.The increase in humidity was found to significantly increase the radon emanation rates in the building, whereas the increase in temperature will result the decrease of radon emanation rates. In addition, the findings shows that the radon emanation rates in building were higher during the night until early in the morning which is in agreement with the findings on humidity and temperature factors.

Keywords: Radon emanation, building materials, humidity, temperature

Abstrak

Kehidupan gaya moden memerlukan manusia untuk memperuntukkan masa mereka di dalam bangunan sama ada di rumah atau di tempat kerja. Kebanyakan bangunan moden diperbuat daripada bahan berasaskan tanah yang terdiri daripada kepekatan yang rendah unsur keradioaktifan tabiinya. Seperti mana yang diketahui bahawa salah satu daripada pereputan uranium semulajadi iaitu ^{226}Ra akan membebaskan gas radon (^{222}Rn). Terbaru, lebih banyak bukti mengaitkan kanser paru-paru dengan tahap radon yang tinggi dan juga asap rokok. Oleh yang demikian, kajian ini dijalankan untuk mengkaji kadar emanasi radon di empat kerja yang berbeza-beza. Emanasi radon di 27 bilik-bilik dengan tiga dimensi yang berbeza (54 m^3, 210 m^3, 351 m^3) dan bahan-bahan binaan yang berbeza telah ditentukan selama 96 jam dengan menggunakan peralatan Pemonitoran "Radon *Sun Nuclear"*. Emanasi radon dalam bilik-bilik kajian mendapati julat berada dalam lingkungan 20.6 Bq m^{-3} jam^{-1} hingga 134.3 Bq m^{-3} jam^{-1}. Pertambahan kelembapan didapati memberi pertambahan signifikasi pada kadar emanasi radon, manakala peningkatan suhu mempengaruhi penurunan kadar emanasi radon. Di samping itu, hasil penemuan menunjukkan kadar emanasi radon dalam bangunan adalah tinggi pada waktu malam hingga awal pagi di mana bersesuaian dengan penemuan faktor kelembapan dan suhu.

Kata kunci: Emanai radon, bahan binaan, kelembapan, suhu

Introduction

Natural radionuclides of ^{40}K, ^{238}U and ^{232}Th presented naturally in the earth's crust can be found in water, soil and rocks. Radon is an inert gas that is odourless and cannot be detected without the use of appropriate equipment. Radon, (^{222}Rn) is produced by disintegration of uranium. The human respiratory system has limited filtration

system, which is unable to filter from inhaled radon gas. Radon intake will provide direct internal exposure to human. Radon is carcinogenic and one of the cause of lung cancer to human [1].

Radon easily enters the space in the building through cracks in pipelines and walls. However, building materials can also be a contributor in the radon content of building. Total radon produced depends on the concentration of uranium which is found in rock and soils. Housing development in Malaysia has increase rapidly, in line with government's objective to make Malaysia an advance country in the world. Growth in population and living standards also stimulate the increase in the number of building in Malaysia thus this also leads to greater demand for building materials. This has led to manufactures of building materials taking an initiative to use low cost, in large quantities and readily available raw material, such as the use of mixture of industrial wastes in building materials. In addition, consumers are more likely to choose the building material that have the elements of rocks and sand compared to wood based materials as they are far cheaper than wood [2].

Emanation of radon gas will occur, especially in enclosed spaces such as in rooms and buildings. Radon is one aspect that needs serious attention especially in the air quality index for most countries in the world. More individual prefer to spent their time indoors than to be outside of the building. It is therefore very important to determine the contribution of radon to the total dose received by occupants to assess acceptable risk [3].

Therefore, the main objectives in this study is to determine the level of radon emanation in different types of Malaysia's building at Universiti Kebangsaan Malaysia (UKM), the effective dose received by students and employees, the equivalent dose received by students and employees and to investigate the relationship between radon emanation with the factors of room parameters.

Materials and Methods

Research Workplace

This study was conducted to determine the effects of radon to the UKM students and employees, the selection of the study area includes buildings and buildings used by students and staff of the University.

Type of Building

Building and selected study areas were classified according to the age of the building (34 years), semi-long (16 years) and new building (2 years). There are 27 rooms with three different dimension (54 m^3, 210 m^3 and 351 m^3) and different building materials. The study area selected and the year of occupancy and age of the building is referred in Table 1.

Table 1 Study area selected and the year began of occupancy and age of the building

ID	Year of operation	Age (year)	Type of Workplace
ADM-B	1977	34	Administration Building
NSB	1995	16	Nuclear Science Building, Faculty of Science and Technology (FST)
EXT-B	2009	2	Extension Building, Faculty of Information Science and Technology (FTSM)

For each of the building studied, three types of rooms with different sizes were selected based on the following:

a) The small size of individual rooms (3 m x 6 m x 3 m)
b) The medium size such as tutorial rooms, meeting rooms, discussion rooms and operations room (7 m x 10 m x 3 m)
c) The large size such as lecture halls, laboratories, office space and seminar room (9nm x 13 m x 3m)

Three different rooms were selected for each type of area to make all the nine rooms. This makes all the nine rooms studied for each building selected. The total rooms studied are 27. Table 2, Table 3 and Table 4 show complete details of the Administration Building (ADM-B), Nuclear Science Building (NSB) and Extension Building (EXT-B).

Table 2. Information of study area for ADM-B Workplace, Administration Building

Workplace	Building	Size of studied room (m x m x m)	Rooms		Level	Ceiling	Wall	Floor
		3 x 6 x 3	ADM-B 1	Room 1, PHA	2	Asbestos	wall paper	carpet
			ADM-B 2	Room 2, PKK	2	Asbestos	cement,painted	tile
			ADM-B 3	Pantry Room	3	Asbestos	cement, painted	PVC
ADM-B	Administration	7 x 10 x 3	ADM-B 4	Meeting Room, Department of Bursary	3	Asbestos	cement,painted	carpet
	Building		ADM-B 5	Meeting Room, PHA	2	Asbestos	wall paper	carpet
			ADM-B 6	Meeting Room, PKK	2	Asbestos	cement,painted	tile
		9 x 13 x 3	ADM-B 7	Office Room, Department of Bursary	3	Asbestos	cement, painted	PVC
			ADM-B 8	Office Room, PHA	2	Asbestos	wall paper	carpet
			ADM-B 9	Office Room, PKK	2	Asbestos	cement, painted	tile

*PHA = Office of International Relations *PKK= Office of Corporate Communications

Table 3. Information of study area for NSB Workplace, Nuclear Science Building

Workplace	Building	Size of studied room (m x m x m)	Rooms		Level	Ceiling	Wall	Floor
		3 x 6 x 3	NSB 1	Room 3	1	Asbestos	cement,painted	carpet
			NSB 2	Room 4	2	Asbestos	cement,painted	PVC
			NSB 3	Lab assistant Room	1	Asbestos	cement, painted	PVC
	Nuclear							
NSB	Science	7 x 10 x 3	NSB 4	Meeting Room	1	Asbestos	wall paper	carpet
	Building		NSB 5	Resource Room	1	Asbestos	cement,painted	PVC
			NSB 6	Tutorial Room	1	Asbestos	cement,painted	PVC
		9 x 13 x 3	NSB 7	Graduate Room	1	Asbestos	cement, painted	PVC
			NSB 8	Lecture Hall 1	1	Asbestos	cement, painted, wood panel, aluminium piece	PVC
			NSB 9	Electronic Lab	2	Asbestos	cement, painted	terrazo

Table 4. Information of study area for EXT-B Workplace, Extension Building

Workplace	Building	Size of studied room (m x m x m)	Rooms		Level	Ceiling	Wall	Floor
		3 x 6 x 3	EXT-B 1	Technician Room Graduate Lab	2	Asbestos	cement,painted	tile
			EXT-B 2	Assistant Information System Officer Room	2	Asbestos	cement,painted	tile
			EXT -B 3	Information System Officer Room	2	Asbestos	cement, painted	tile
EXT-B	Extension	7 x 10 x 3	EXT -B 4	PC Recovery Workshop	1	Asbestos	cement,painted	tile
	Building		EXT -B 5	Machine Control Workshop	1	Asbestos	cement,painted	tile
			EXT -B 6	Meeting Room,	2	Asbestos	cement,painted	carpet
		9 x 13 x 3	EXT -B 7	Network Lab	1	Asbestos	cement, painted	tile
			EXT -B 8	Graduate Lab	2	Asbestos	cement,painted	tile
			EXT -B 9	Office Room	2	Asbestos	cement, painted	tile

Research Equipment

This study was conducted using radon monitor equipment by "Sun Nuclear" for model 1028 and 1029. This equipment was used to measure radon emanation in study area and the readings obtained in unit Bqm^{-3}. Continuous readings were obtained for a period of time required to meet the purpose and needs of the research. Continuously readings were taken for 96 hours which is equivalent to 4 days.

Method of Monitoring

Radon monitor was placed in the selected study area. The characteristics of the study area were identified according to the height of the study area from ground level, the estimated area of research, building materials used for walls, ceilings and floors of the study area. The sizes of area studied for each building were ensured to be similar. Figure 1 shows the measurement geometry of the recommended for radon emanation studied in an enclosed space.

The radon monitor was placed in appropriate place that suit the actual conditions on site so that it will not interfere with the working space. In addition, to avoidance of interruption during the process of monitoring. A continuous reading is taken over 96 hours and readings were taken of an interval of one hour. The readings were classified into a set of 24 hours and the unit in Bqm^{-3}. The monitoring data obtained from the area studied calculate the concentration of radon and its risks to employees in the area studied. Determination of the risk to be used to the students and employees was done by calculating the effective dose and the equivalent dose received by students and employees.

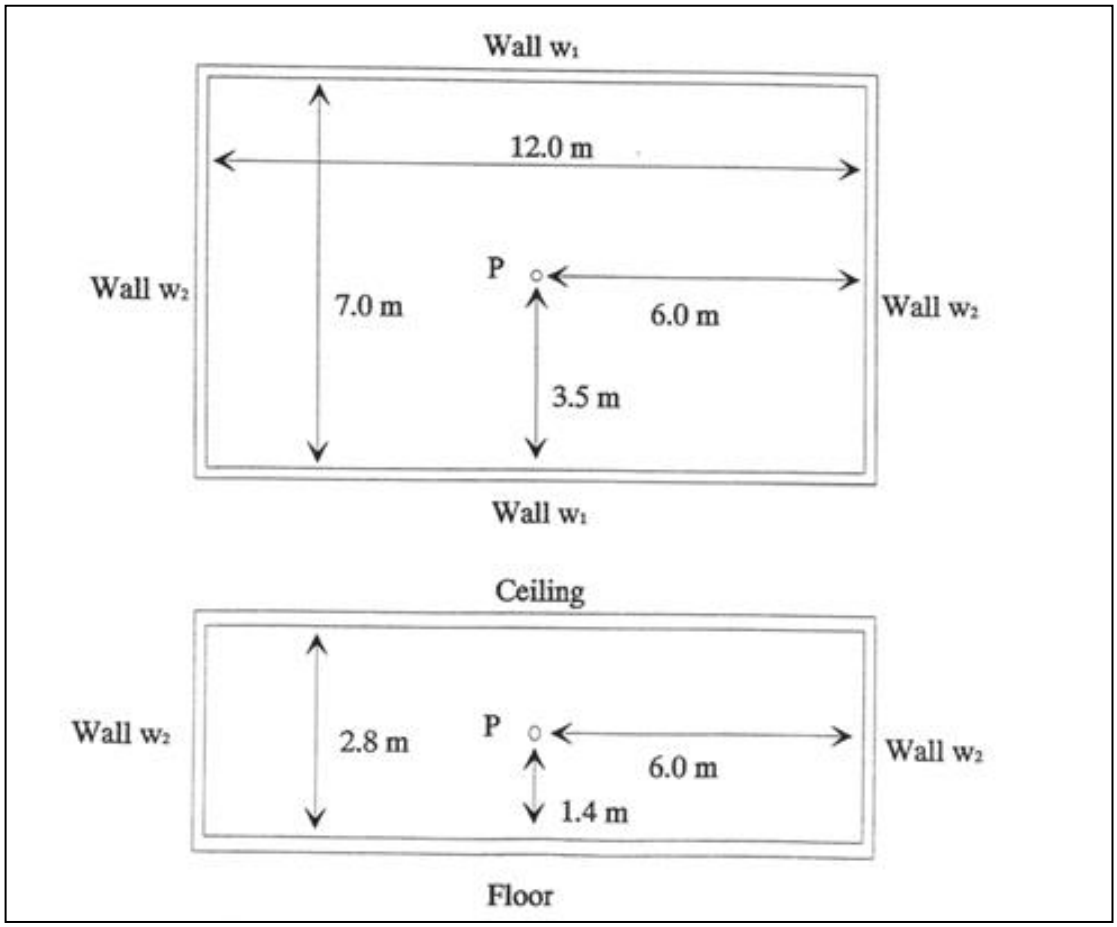


Figure 1. Geometry of the proposed for dose measurement in the building according to Finnish Centre For Radiation and Nuclear Safety, Finland Recommendation (STUK-B-STO 32, 1995).

Results and Discussion

Results and information from this study was compared with the previous studies and in accordance to the parameter studied. The results obtained were used to determine whether the concentration of radon in building around UKM, Bangi is below or above the International Recommended level.

Concentration of radon content in the study area

The radon emanation for each area studied was measured using a radon monitor that was left for 96 hours at the workplace. The reading of radon emanation ($Bqm^{-3}h^{-1}$) was obtained, recorded and classified according to study area. The value was calculated by subtracting the average reading of first three readings since they were considered unstable [1]. The average reading at each workplace were classified into a set of 24 hours, which the average concentration of radon readings taken accordingly in the time range of 0-24 hours, 25-48 hours, 49-72 hours and 73-96 hours with a standard deviation calculated for each interval of 24 hours. The average radon emanation was determined using the following equation.

$$\text{Average Reading} = \frac{\text{Total reading 96 hours (Bqm}^{-3}\text{)} - \text{3 first reading on each set of 24 hours measurement (Bqm}^{-3}\text{)}}{93 \text{ hours}}$$

Workplace ADM-B, Administration Building (1977)
Nine workplaces selected in this 34 years old building that cover the Office of International Relation (PHA), Office of Corporate Communications (PKK) and Department of Bursary. Table 5 shows average reading of radon emanation for the nine selected workplaces in this building.

Table 5. Average concentration of radon in selected area in Workplace ADM-B, Administration Building

Workplace	Level	Average Readings $Bqm^{-3}h^{-1}$
Room1, PHA	2	34.6 ± 7.5
Room 2, PKK	2	36.5 ± 5.8
Pantry Room, Department of Bursary	3	24.5 ± 5.0
Meeting Room, Department of Bursary	3	33.5 ± 4.7
Meeting Room, PHA	2	41.0 ± 5.0
Meeting Room, PKK	2	34.1 ± 7.0
Office Room, Department of Bursary	3	30.7 ± 5.1
Office Room, PHA	2	39.7 ± 7.2
Office Room, PKK	2	36.0 ± 6.0

Workplace NSB, Nuclear Science Building (1995)
For 16 years old building, the radon emanation readings were recorded in the nine areas used by students and employees of the university. Table 6 below indicates average reading of radon emanation for 9 areas in Nuclear Science Building.

Table 6. Average concentration of radon in selected area in Workplace NSB, Nuclear Science Building

Workplace	Level	Average Reading $Bqm^{-3}h^{-1}$
Room 3	1	33.6 ± 4.8
Room 4	2	26.1 ± 3.0
Lab Assistant Room	1	46.9 ± 8.5
Meeting Room	1	51.7 ± 14.4
Resource Room	1	30.6 ± 3.5
Tutorial Room 1	1	32.4 ± 2.8
Graduate Room	1	37.5 ± 2.9
Lecture Hall 1	1	36.8 ± 8.6
Electronic Lab	2	20.6 ± 1.4

Workplace EXT-B, Extension Building, FTSM (1995)
Nine of the area studied in the 2 years old building also includes areas that are often used by students and staff. Table 7 shows average reading of radon emanation for 9 areas in Extension Building, FTSM.

Table 7. Average concentration of radon in selected area in Workplace EXT-B, Extension Building, FTSM

Workplace	Level	Average Reading Bq m^{-3}
Technician Room Graduate Lab	2	134.3 ± 14.9
Assistant Information System Officer Room	2	46.0 ± 10.1
Information System Officer Room	2	78.7 ± 15.3
PC Recovery Workshop	1	30.7 ± 4.2
Machine Control Workshop	1	67.2 ± 26.4
Meeting Room	2	96.2 ± 8.5
Network Lab	1	97.2 ± 15.1
Graduate Lab	2	110.1 ± 2.8
Office Room	2	78.6 ± 29.6

The result showed that the building built two years ago recorded an average value of radon emanation higher than other buildings constructed 34 and 16 years ago. The range of radon emanation readings in building built 34 years (Administration Building), 16 years (Nuclear Science Building) and 2 years (Extension Building) recorded readings of 24.5 ± 5.0 Bq m^{-3} to 41.0 ± 5.0 Bq m^{-3}, 20.6 ± 1.4 Bq m^{-3} to 51.7 ± 14.4 Bq m^{-3} and 30.7 ± 4.2 Bq m^{-3} to134.3 ± 14.9 Bq m^{-3} respectively. Note the trends for older buildings (34 years and 16 years) showed that the lower floors revealed higher emanation of radon but not observed in newer building (2 years). This is due to the building materials and type of soils used in the older building. The older buildings were using the red bricks and other building materials that contained high NORM. It was also affected by the working practice such as factors of open-close doors, ventilation and air conditioner system applied by the workers.

Malaysia has not to set the value of radon emanation in the building, but follow International Recommended level used in this study. Among the recommendation from the U.S. Environmental Protection Agency (USEPA), which suggested the Action Level of 148 Bq m^{-3} [1], Health Protection Agency (HPA) recommends 100 Bq m^{-3} up to 200 Bq m^{-3} [2], International Commission on Radiological Protection (ICRP) recommends 300 Bq m^{-3} until 1000 Bq m^{-3} [4]. The Action Level value used in this study is according to the ICRP recommendations. Based on the results, radon emanation is still low when compared to the ICRP recommended limit.

Radon emanation
Variation of radon emanations workplaces studied has shown that The Extension Building, FTSM recorded the highest value compared to Administration Building and Nuclear Science Building. This is due to influence radon emanations in the building. Results showed radon emanation in the building was also contributed by the soil and rock in the building surrounding. The factors mentioned earlier is related to the room parameters such as types of building construction materials used for example rocks, sand, cement, tile, PVC and terrazzo. Other influences include, level of building, atmospheric layer stability, temperature and humidity.

Room Parameters

From the results obtained, this study has found that new building built two years ago (Extension Building) recorded higher average value of radon emanation than old building (34 years and 16 years). There is a connection between radon emanations with building age. Hence, the age of the building will be one of the room parameter that influences radon emanation. ANOVA statistical test was performed to determined differences in radon emanation for each building built in 34, 16 and 2 years ago. There were two different hypotheses whether there are significant differences between the samples. The two hypotheses presented as Null Hypothesis (H_0) and alternative hypothesis (H_1). Null hypothesis (H_0) states that the concentration of radon in the building is not dependent on the age of the building while the alternative hypothesis (H_1) stated that the radon concentration in building is dependent on the age of building.

ANOVA test gives results of F value and F_{crit}. If value of F> F_{crit} , Null hypothesis (H_0) will be rejected and if value of F_{crit} >F, Null hypothesis (H_0) will be accepted.

	Administration Building	Nuclear Science Building	Extension Building, FTSM
1	34.6	33.6	134.3
2	36.5	26.1	46.0
3	24.5	46.9	78.7
4	33.5	51.7	30.7
5	41.0	30.6	67.2
6	34.1	32.4	96.2
7	30.7	37.5	97.2
8	39.7	36.8	110.1
9	36.0	20.6	78.6
N	9	9	9
X	34.511	35.133	82.111
S	4.888	9.647	31.872
X_{ave}	50.585		

source	df	SS	MS	F	F crit	P-value
treatments	2	13419.176	6709.588	17.77	3.40	0.00
error	24	9062.278	377.595			
total	26	22481.454				

The statistical results gave value of F= 17.77 and the F_{crt}= 3.40 with a value of P= 0.00. If F > F_{crit} , Null hypothesis (H_0) is rejected and the alternative hypothesis (H_1) is accepted which stated that the radon emanation in the building depends on age of building. These results were in agreement with the previous studies [6], which indicated that the age of building in a contribution factor to radon concentration in building. The age of the building shows positive results since room parameter can give variation of radon emanation in the work places.

Diurnal variation of radon emanation

As in the previous studies, the emanation of radon has shown certain pattern. The radon concentration was found high at night and early morning and low during the daytime [3; 6; 7; 8; 9]. Figure 2 describe the pattern of radon production for 24 hours over three consecutive days in ADM-B, NSB, EXT-B.

Figure 2 shows that high radon concentration started at night until early in the morning and began in the early morning; radon concentration began to decrease until it reached the night time and often that it continues to increase. As in the previous studies, this was done to the stability of the atmospheric surface layer. [6]

At night until early morning, the earth's surface is in a stable condition in which the surface layer and the atmosphere have nearly the same temperature and the radon tends to accumulate near the earth's surface. In the daytime, as the temperature rises during the day it create the difference between temperature of surface to the temperature of the atmosphere. There is a heat transfer process and this process makes the atmospheric surface layer becomes unstable and produces convection. This forces radon gas upward and spread away from the surface. Then in the evening, the surface temperature began to decrease and the opposite occur for radon. This stabilizes the atmospheric conditions and radon again gathered close to the earth's surface. [3, 6]

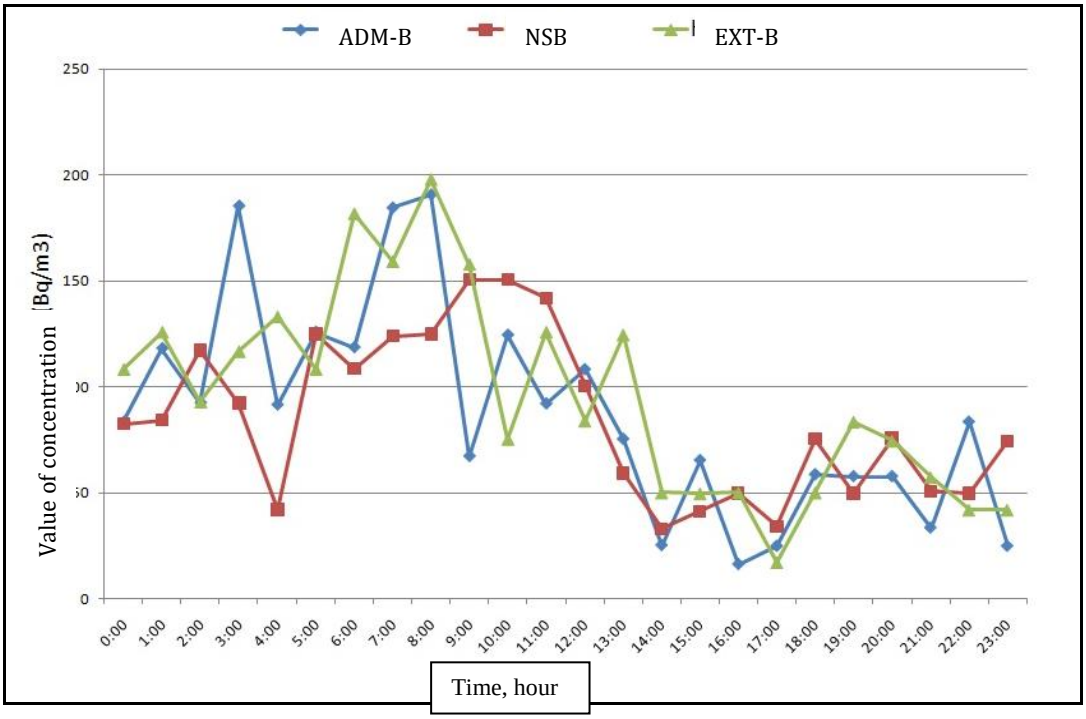


Figure 2. The diurnal variation of radon emanation in ADM-B, NSB and EXT-B

Radon in indoor air may be diluted by increased ventilation of the indoor spaces with outdoor air. This method can be done in terms of energy loss, particularly in working time. Energy loss can happen while opening and closing the doors frequently. Besides that, switching on the air conditioner in the workplace during the day may affect the radon gas decreasing as well as the indoor air is entered the air conditioner system in and out.

Temperature and Humidity

Temperature and humidity is also a part of room parameters that affect the level of radon emanation in building. The level of radon concentration with humidity factor has a positive correlation that is with the increment of humidity,

the level of radon concentration also increase. Meanwhile, for temperature there is a negative correlation with radon concentration. The rise in temperature in the building will reduce the level of radon concentration. [6, 7].

This study was found to be in agreement with the previous studies that stated that the level of radon concentration in the building will increase with the increase in humidity but radon concentration will decrease when temperature is increase. Figure 3.0 shows the distribution of radon concentration with temperature and Figure 4.0 shows the distribution of radon concentration with humidity at Electronic Lab in the Nuclear Science Building. The influence of temperature and humidity as a function of room parameters can be one of the factor that influence radon emanation.

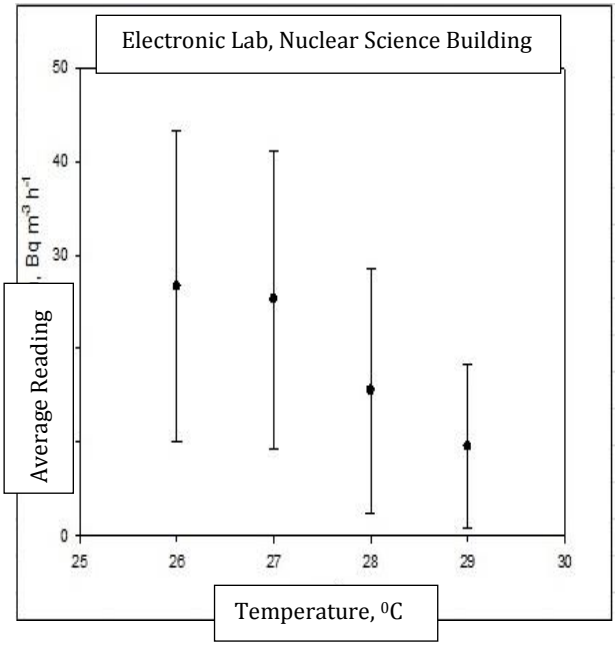


Figure 3. Pattern of radon concentration with temperature

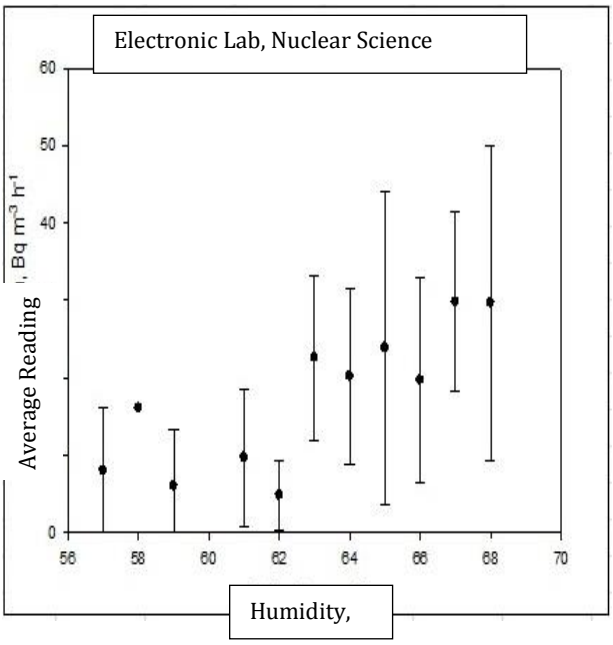


Figure 4. Pattern of radon concentration with humidity

Effective Dose

Effective dose, also called exposure dose is the total dose of radon exposure received by occupants in a year. By using the average value of radon concentration ($Bqm^{-3}h^{-1}$), annual effective dose for workers in the study area will be determined using the formula below [8].

$$D = C_{Rn} \times F \times O \times T \times D \text{ (unit = mSv)}$$

where;

C_{Rn}	average of radon concentration	Bq m^{-3}
F	equivalent factor	0.4
O	occupancy factor	0.25 (8h/24h x 100%)
D	exchange unit	9 nSv (Bq h m^{-3})$^{-1}$
T	time	8760 hour (365d x 24h)

From the results calculated, the range of effective dose for the Administration Building (34 years), Nuclear Science Building (16 years) and Extension Building (2 years) was 0.19 mSv – 0.32 mSv, 0.16 mSv – 0.41 mSv and 0.24 mSv – 1.06 mSv.

Equivalent Dose

Equivalent dose is the dose received by occupants on the type of radiation produced by radon and also with the organ and tissue involvement. It using weighting factors for alpha particle and weighting factors for lung tissue [4].

$$E = D \times wR \times WT \qquad (\text{unit} = \text{mSv y}^{-1})$$

where:

D	annual exposure dose,	mSv
wR	weighting factors for alpha particle	20
WT	weighting factors for lung tissue	0.12

From the results calculated, the range of equivalent dose for the Administration Building (34 years), Nuclear Science Building (16 years) and Extension Building (2 years) was 0.46 mSv y^{-1} – 0.77mSv y^{-1}, 0.38 mSv y^{-1} – 0.98 mSv y^{-1} and 0.58 mSv y^{-1} – 2.54 mSv y^{-1}.

Conclusion

Variation of radon emanation in workplaces was successfully studied. The radon emanations in the rooms studied were found to be in the range of 20.6 $Bqm^{-3}h^{-1}$ to 134.3 $Bqm^{-3}h^{-1}$. Several factors were found to influence the quantity radon emanation such as; room parameters that are the type and source of construction materials use, atmospheric layer stability, temperature and humidity. The radon emanation also indicated a pattern where it was higher at night and early morning but lower during daytime. The measured radon emanation values were lower than 300 Bqm^{-3}. This is a limit of radon emanation in workplace as suggested by ICRP 103. The calculated annual effective dose values and annual equivalent dose values were calculated to be in the range of 0.16 mSv to 1.06 mSv and 0.38 mSv y^{-1} to 2.54 mSv y^{-1} were still below the action levels recommended by ICRP which were 20 mSv and 10 mSv.

Acknowledgement

The authors would like to acknowledge the Universiti Kebangsaan Malaysia for funding this research through research grant UKM-GUP-PLW-08-15-056 & UKM-GUP-2011-152.

References

1. Environmental Protection Agency (EPA). (2003). EPA Assessment Of Risks From Radon In Homes. EPA 402-R03003. U.S.
2. Health Protection Agency (HPA). (2010). Limitation Of Human Exposure To Radon. *Document of the HPA,* RCE-15.
3. Segovia, N., Gaso, M.I. & Armienta, M.A. (2007). Environmental Radon Studies In Mexico. *Environ Geochem Health*, 29: 143-153.
4. International Commission on Radiological Protection (ICRP). (2007). Recommendations of ICRP.Publication 103. New York: Oxford Pergamon Press.
5. Dios, J.M.B., Ravina, A.R., Iturri, J.G. & Figueras, A. (2006). Factors Underlying Residential Radon Concentration: Results From Galicia, Spain. *Environmental Research,* 103: 185-190.
6. Kulwant, S., Manmohan, S., Surinder, S., Sahota, H.S. & Papp, Z. (2004). Variation of Radon Progeny Concentrations in Outdoor Air As A Function Of Time, Temperature And Relative Humidity. *Radiation Measurement,* 39: 213- 217.
7. Baciu, A.C. (2004). Radon and Thoron Progeny Concentration Variability in Relation To Meteorological Conditions at Bucharest (Romania). *Journal of Environmental Radioactivity,* 83: 171-189.

8. UNSCEAR. (2000). Exposures From Natural Radiation Sources. *United Nations Scientific Committee On The Effects Of Atomic Radiation*. Report To General Assembly, With Annexes. New York: United Nations.
9. UNSCEAR. (2006). Sources-To-Effects Assessment For Radon In Homes And Workplaces. *United Nations Scientific Committee On The Effects Of Atomic Radiation*. Report To General Assembly, With Annexes. New York: United Nations.

The Malaysian Journal of ANALYTICAL SCIENCES ISSN 1394-2506

ISOLATION AND UTILIZATION OF CORN COBS HEMISELLULOSE AS CHELATING AGENT FOR LEAD IONS

(Pemencilan dan Penggunaan Hemiselulos Daripada Tongkol Jagung Sebagai Agen Pengkelat Untuk Ion Plumbum)

Muchlisyam[1*], Urip Harahap[1], Jansen Silalahi[1], Zul Alfian[2]

[1]*Facultyof Pharmacy,*
[2]*Department of Chemistry, Faculty of Mathematics and Natural Sciences*
University of Sumatra Utara,Medan, Indonesia

**Corresponding author: muchlisyam@gmail.com*

Abstract

Corn cobs is an agricultural byproduct containing polysaccharide composed of cellulose, hemicellulose and lignin. Hemicellulose has a hydroxyl and carbonyl functional groups which can be used as chelating agent for metal ions. The purpose of this study was to isolate and evaluate corncobs hemicellulose as a chelating agent toward lead ion. Graphite furnace spectrofotometry at 283.3 nm was used to determine the residual lead ion in solution. The research's result showed that the highest yield of hemicellulose (12.04%) was obtained from delignication with 0,03M NaOH in 60% ethanol and 3% H_2O_2, hemicellulose isolation with 500 ml of 0.2 M NaOH, and precipitation with 1 : 4 ratio of 10% acetic acid in 95% ethanol. The 300 mg corn cobs hemicellulose has chelating effect for 40mg lead solution at (39.52 ± 0.1350) mg or 98.80%, that the corn cobs hemicellulose can be used as a chelating agent for lead.

Keywords: corn cobs, isolation, hemicellulose, Pb, chelating agent

Abstrak

Tongkol jagung adalah sisa pertanian yang mengandungi polisakarida yang terdiri daripada selulos, hemiselulos dan lignin. Hemiselulos mempunyai gugusan berfungsi karbonil dan hidroksil yang boleh digunakan sebagai agen pengkelat ion logam. Tujuan kajian ini ialah untuk mengasingkan dan menilai hemiselulos tongkol jagung sebagai agen pengkelat ion plumbum. Spektrofotometri dapur grafit digunakan bagi menentukan plumbum dalam larutan pada 283.3 nm. Hasil kajian menunjukkan hasil hemiselulos tertinggi (12.4%) diperolehi daripada nyahlignin dengan 0,03M NaOH dalam 60% ethanol dan 3% H_2O_2 dan pengasingan hemilulos dengan 500 ml 0.2 M NaOH,dan pemendekan dengan 1:4 nisbah 10% asid asetik dalam 95% ethanol. Sebanyak 300 mg hemiselulos tongkol jagung menyerap 39.52 ± 0.1350 mg (98.8%) daripada 40 mg Pb, ini menunjukkan hemiselulos tongkol jagung boleh digunakan sebagai agen pengkelat Pb.

Kata kunci: tongkol jagung, hemiselulos, Pb, agen pengkelat

Introduction

Hemicellulose is one of most abundant polymer after cellulose. However, its potential has yet to be completely recognized. Hemicellulose comprises a variety of monomers including xylosa, mannose, arabinose, glucose, glukoronic acid having hydroxyl (OH) group on each monomer [1]. In the qualitative chemical analysis of organic compounds, the OH group in both cyclical aliphatic will be able to bind metal ions to form complex salts. Hemicellulose applications in the pharmaceutical field could potentially be developed as a dietary supplement or as drug formulation excipients such as binders, disintergrator, thickeners and stabilizers. In addition, several important applications of hemicellulose have been done by making the derivatives which have pharmacological effects such as lowering cholesterol, and inhibitors of HIV [2,3,4].

Corn cobs contains hemicellulose approximately 12.5% and is the largest amount in comparison with other species [5]. Several reseaches have been performed on the separation of hemicellulose from different plant byproducts with

different methods of isolation. Isolation of hemicellulose by using alkali such as KOH or NaOH at various concentrations have been reported [2,3,5].

Lead is a toxic element because it tends to undergo a process of bioaccumulation and potential toxic amount accumulate within sensitive organs and tissues. In humans, poisoning by most of these metals causes severe dysfunction in the kidneys, reproductive system, liver, brain and central nervous system [6,7]. The aim of this study is to isolate hemicelluloses from corn cobs and to test its ability to absorb lead in solution.

Materials and Methods

Materials

Corn Cobs were obtained from local Corn in Medan, Indonesia. Pectin Technical grade (China), NaOH (E.Merck), 35% H_2O_2 (E.Merck), 96% ethanol (E.Merck), CH_3COOH (E.Merck), $Pb(NO3)_2$ (E.Merck), Lead ion 1000 ppb/ml (E.Merck), All other chemicals used were of analytical grade.

Isolation of hemisellulose from corn cobs

The extraction method was modified from the combination methods described by [2,3,5]. The corn cobs powder of 50 grams was added to 500 ml of 0.03 M NaOH in 70% ethanol and heated at 60°C and stirred for 2 hours to dissolve the lignin. The suspension was allowed to cool to room temperature and filtered through Whatman filter paper. The precipitate was added 500 ml of 0.2 M NaOH, and stirred for 8 hours at room temperature to dissolve hemicellulose, and then filtered. The filtrate was heated at a temperature of 65°C, and added 137 ml of 3% H_2O_2 in stages. Each addition of 1 ml 3% H_2O_2 to the filtrate and stirred constantly, stirring was performed until the entire 3% $H_2O_2$is used, stirring is continued until a clear solution. Solution of 10% acetic acid in 95% ethanol with a ratio of 1:4 (v / v) was added to the sample solution and left at room temperature for 6 hours until the precipitate formed. The suspension was centrifuged at a rate of 10,000 rpm for 15 minutes, and the filtrate was discarded, the precipitate was washed with 96% ethanol, and dried in vacuum dryer. The washed precipitate is hemicellulose.

Lead absorption

The absorption method was modified from the methods described by Wong et al. [8]. The hemicellulose and pectin respectively weighed 100 mg, 200 mg and 300 mg, Then each dissolved into erlenmeyer containing 25 ml solution 40 mg/ml of lead in 0.1 N nitric acid and the pH adjusted with acid pH performed at pH 2, the solution was stirred with a magnetic stirrer at room temperature for 2 hours. Then each was centrifuged at 10,000 rpm for 30 minutes. The supernatant was taken and diluted with 0.5 ml to 50 ml aquabidest then 0.25 ml of dilution was taken and diluted to 25 ml with aquabidest and lead levels were measured. The Lead in the supernatant were estimated using graphite furnace atomic absorption spectroscopy (Hitachi Analyst 100). The results are presented as mean values ± standard deviation.

Results and Discussion

Isolation of Hemicellulose

Modified isolation of corn cobs hemicellulose using 500ml of 0.03M NaOH in70% ethanol and precipitation using the solution of 10% acetic acid in 95% ethanol with a ratio of 1:4 (v/v) and corn cobs hemicellulose obtained with levels of 12.03% and in accordance with the results of Ricahana 2006 research that levels of 12:04% [5]. Chelating ability of corn cobs hemicellulose and pectin toward lead ion is shown in Table 1.

Table 1 shows that the administration of chelating agent to bind lead at pH 2, the higher the amount of chelating agent showed an increase chelating ability, but in hemicellulose from corn cobs the increase was not in proportional with the amount of hemicellulose, it is in accordance with the principle of adsorption that the adsorption process will end if there is equilibrium between the adsorbent, so the weight does not affect a significant absorbance with the increasing amount of hemicellulose for each treatment.

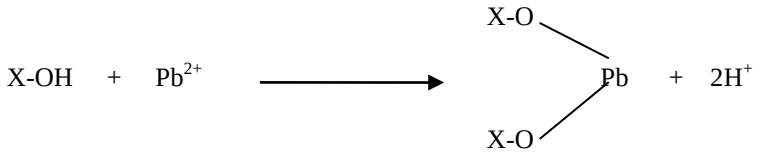
From Table 1 can be seen that there is the influence of the type of chelating agent and the weight of the chelating agent applied. Compare to hemicellulose, 100 mg pectin has the lowest binding capacity of 21.10 ± 1.08 mg of lead ion or 52.75%. But the 200 mg and 300 mg pectin will give a greater ability in binding capacity of 32.48 ±

0.71 mg or 81.20% and 37.39 ± 0.22 mg or 93.47% of lead ion respectively which show that the corn cob hemicellulose has greater chelating effect than pectin.

Table 1. Chelating effect of Corn Cobs Hemicellulose and Pectin for 40mg/25ml lead ions.

Chelating agent	Weight	Lead content in Chelating agent (mg)	Percentage lead ion in Chelating agent (%)
Hemicellulose	100 mg	35.97 ± 0.25	89.92
	200 mg	37.33 ± 1.90	93.32
	300 mg	39.53 ± 0.13	98.82
Pectin	100 mg	21.10 ± 1.08	52.75
	200 mg	32.48 ± 0.71	81.20
	300 mg	37.39 ± 0.22	93.47

Absorption characteristics between hemicelluloses and pectin are different where hemicelluloses reacts with lead ions. This suggests that the hydroxyl group of the hemicellulose causes attraction of lead ions present in solution, thus hemicellulose is more polar and has a better absorption capacity than the less polar substances. Uptake mechanism that occurs between the-hydroxyl function from hemicellulose monomer for example xylose group attached to the surface with the positively charged metal ion (cation) is an ion exchange mechanism as follows:



Metal ion in the form of lead ions, -OH groups are hydroxyl groups present on the C atom of the monomer compound in the hemicellulose and X is a matrix of hemicellulose place the-OH group attached. Interactions between the-OH group with the lead ion is also possible through the mechanism of formation of coordination complexes as atomic oxygen (O) with -OH group has a lone pair, while the lead ion has an empty orbitals. The free electron pair will occupy a empty orbital which is owned by a metal ion, thus forming a compound or complex ion [9]. Chemical bonding that occurs between the active groups in the molecules of organic substances can be explained as the behavior of Lewis acid-base interactions which produce complex on the surface of solids. In the system of binding of metal ion solution, for example the interaction is written in general form,

$$2[FH] + M^{z} \longrightarrow [F_2M^{(Z-2)}]^{+} + 2H^{+}$$

with FH is a functional group found in organic matter, and M is the ion of z valency. This means that the in-vitro hemicellulose which is an organic compound having a hydroxyl group can bind to metal of two valency in the dissolved state and acidic conditions.

Conclusion

The modified method for isolation of corn cobs hemicelluloses gave a yield of 12.03%. Corn cobs hemicelluloses have the ability to bind lead at pH2 and the capacity was influenced by the weight and the highest was shown by the 300mg corn cobs hemicelluloses with binding capacity at 39.52 ± 0.1350 mg to 40mg of lead solution, or 98.80%. Corn cobs Hemicelluloses can be used as a chelating agent for lead.

References

1. Dumitriu, S. (2005). Polysaccharides: Structural Diversity and Functional Versatility. New York: Marcel Dekker.
2. Karssalan, A. M., Tshabalala, M. A., & Buschle, D. G. (2010). Wood Hemisellulose/Chitosan-Basedsemi-Interpenetrating Networks Hydrogels: Mechanical, Swelling And Control Drug Release Properties, *J. BioResources* 5(2): 1036 - 1054.
3. Yadav, M. P., Johnston, D. B., Hotchkiss, A. T., & Hicks, K. B. (2007). Corn Fiber Gum: A Potential Gum Arabic Replacer For Beverage Flavor Emulsificatio, *Food Hydrocolloids* : 1022 – 1030.
4. Saha, C. B. (2003). Hemicellulose bioconversion. *J. Microbiol. Biotech.* 30 (16): 279 - 291.
5. Richana, N., Irawadi, T. T., & Nur, A. M. (2007). Ekstraksi Hemiselulosa Dari Tongkol Jagung. *J. Pascapanen* 4(1):38-43.
6. Casas, S. J & Sordo, J. (2006). Lead Chemistry, Analytical Aspects, Environmental Impact and Health Effects. Amsterdam: Elsevier.
7. Jickel, S. & Negrusz, A. (2008).Clarke's Analytical Forensic Toxicology. Chichago, USA.
8. Wong, W. W., Abbas, F. M. A., Liong, M. T. & Azhar, M. E. (2008). Modification of durian ring for improved biosorbent ability, *Int. Food Res. J.* 15(3): 363 - 365.
9. Pearson, R. G. (2005). Chemical hardness and density functional theory. *J. Chem. Sci.* 117(5): 369 – 377.

The Malaysian Journal of ANALYTICAL SCIENCES ISSN 1394-2506

EFFECT OF SODA-ANTHRAQUINONE PULPING CONDITIONS AND BEATING REVOLUTION ON THE MECHANICAL PROPERTIES OF PAPER MADE FROM *Gigantochloa scortechinii* (SEMANTAN BAMBOO)

(Kesan Faktor-Faktor Pemulpaan Soda-Antrakuinon dan Pemukulan Ke Atas Sifat-Sifat Mekanikal Kertas *Gigantochloa Scortechinii* (Buluh Semantan))

Nurul Husna Mohd Hassan[1]*, Suhaimi Muhammed[1], Rushdan Ibrahim[2]

[1] *Department of Wood Industry, Faculty of Applied Sciences, Universiti Teknologi MARA Pahang, 26400 Bandar Tun Abdul Razak, Jengka Pahang*
[2]*Pulp and Paper Programme, Forest Research Institute Malaysia (FRIM), 52109 Kepong, Selangor*

**Corresponding author: afna07@yahoo.com*

Abstract

The effect of soda-AQ pulping conditions and beating revolution on the mechanical properties of paper made from Semantan bamboo (*Gigantochloa scortechinii*) was studied. The bamboo chips were pulped using MK digester pulping unit with 10 to 20% alkali charge and 150 to 170^{o}C cooking temperature. The screened yield varies from 38.7 to 48.4%, and each yield went through beating process at 1000 or 8000 beating revolutions. The bamboo pulp was then made into 60 g/m^2 laboratory scale papers and their mechanical properties were assessed conforming to TAPPI standards. The results revealed that tensile index, bursting index, tearing index and folding endurance ranged from 42.04 to 91.09 Nm/g, 2.68 to 7.10 kPa.m^2/g, 11.03 to 26.64 mN.m^2/g and 30 to 1127 double folds, respectively. The highest paper properties were found from pulping condition of 15% alkali charge and 150^{o}C cooking temperature based on the fibre bonding index, with tensile index at 87.71 Nm/g, bursting index at 6.94 kPa.m^2/g, tearing index at 12.72 mN.m^2/g and folding endurance at 613 double folds. Such findings indicate that comparable high strength mechanical properties of paper can be produced from Semantan bamboo pulp with more environmentally friendly pulping process compared to the kraft pulping process that had been used in bamboo pulping.

Keywords: soda-AQ pulping, Semantan bamboo, beating, paper mechanical properties

Abstrak

Kesan faktor-faktor pemulpaan soda-AQ dan pemukulan terhadap sifat-sifat mekanikal kertas buluh Semantan (*Gigantochloa scortechinii*) telah dikaji. Cip-cip buluh dimasak menggunakan unit penghadam MK dengan peratusan alkali 10 hingga 20% dan suhu pemulpaan pada 150 hingga 170^{o}C. Hasil penskrinan yang diperolehi adalah daripada 38.7 hingga 48.4%, dan selepas itu setiap hasil pulpa menjalani proses pemukulan pulpa pada 1000 atau 8000 revolusi pemukulan. Pembuatan kertas makmal 60 g/m^2 adalah berdasarkan standard TAPPI. Keputusan ujian mendapati indeks tensil, indeks pecahan, indeks koyakan dan ketahan lipatan berada dalam julat 42.04 to 91.09 Nm/g, 2.68 to 7.10 kPa.m^2/g, 11.03 to 26.64 mN.m^2/g dan 30 to 1127 kali lipatan, masing-masing. Berdasarkan indeks ikatan antara gentian, sifat kertas yang tertinggi adalah pada tahap pemasakan yang menggunakan alkali sebanyak 15% dan suhu pemasakan pada 150^{o}C, dengan indeks tensil 87.71 Nm/g, indeks pecahan 6.94 kPa.m^2/g, indeks koyakan 12.72 mN.m^2/g dan ketahanan lipatan sebanyak 613 kali lipatan. Penemuan ini membuktikan kekuatan mekanikal kertas yang setara boleh dihasilkan daripada pulpa buluh Semantan dengan proses pemulpaan yang lebih mesra alam berbanding proses pemulpaan kraft yang biasa digunakan dalam pemulpaan buluh.

Kata kunci: pemulpaan soda-AQ, buluh Semantan, pemukulan, sifat-sifat mekanikal kertas

Introduction

Bamboo is one of the most diverse groups of plant in the grass family which belongs to the family of *Gramineae* and sub-family of ***Bambusoidae***. This fast growing monocotyledon plant can be found in temperate, subtropical and tropical areas. There are 75 genera and 1250 species of bamboo in the world and in Asia alone there are 14

genera and 120 species [1]. Ironically, bamboo exists naturally in the forest while plantation bamboo needs shorter time (3 to 5 years) to be harvested compared to hardwood or softwood fibre sources [2].

Traditionally in Malaysia, bamboo usage is very versatile in the rural areas as supplementary materials in the construction of walls for village house, ceilings and scaffoldings. Even furniture and handicrafts also used bamboo as the raw material [3-4]. Bamboo is also been used commercially or on organized scale by several industries. Most of the industries use *G. scortechinii* for manufacturing poultry cages, shade blinds, barbeque sticks, vegetable baskets, incense sticks, tooth picks, chopsticks, skewers, and joss paper [5-6].

Currently, Malaysia packaging industry used recycled paper as the main raw material for the papermaking. The problem is recycled paper has limited recycling process as it can be recycled 5 to 7 times before the fibre become shorter, stiff and difficult to collapse during papermaking process [7]. The virgin pulp need to be added to maintain the fibre strength, but imported virgin pulp such as softwood long fibre is expensive and can contribute to the increasing of the production cost. Alternative raw material of virgin pulp is needed in contribution of enhancing the recycled paper strength.

In the paper making process, the beating process is mainly to increase fibre to fibre bonding in the paper. The beating level increases the surface area of pulp fibre and it is essential towards increasing the paper strength properties [8]. Biermann [9] presented that the action of beating or refining on pulp fibre causes fibrillation, thus exposure of cellulose fibrils subsequently increases the surface area of the fibre.

The aim of this paper is to study the suitability of Semantan bamboo for papermaking with more environmentally friendly pulping process i.e. soda-AQ pulping, compared to kraft pulping. In addition, this study also looks at the paper mechanical properties enhancement through beating process. The study also investigates the effects of alkali charge and pulping temperature on the paper mechanical properties.

Experimental

Soda-AQ pulping

The bamboo chips were pulped using Soda-Anthraquinone (AQ) pulping process with variables of 10 to 20% alkali charge and 150 to 170^{o}C cooking temperature as listed in Table 1. The fixed parameters for each batch of bamboo pulping were, 90 mins to reach pulping temperature, 90 mins at pulping temperature, 0.1% AQ, 1:4 bamboo to liquor ratio.

Table 1. Soda-AQ pulping variables

Treatment	Alkali (%)	Temperature (^{o}C)
1	**10**	150
2	**10**	160
3	**10**	170
4	**15**	150
5	**15**	160
6	**15**	170
7	**20**	150
8	**20**	160
9	**20**	170

Beating process

The beating process was conducted using the PFI beater at 1000 and 8000 beating revolutions. The beating revolution was chosen based on the previous study from 1000 to 24000 beating revolution [10]. It showed that after 8000 to 24000 beating revolution, there was no significant increasing of paper mechanical properties with the increasing of the beating revolution. That is the justification of this study for using 1000 beating as the basic beating process and 8000 as the optimum beating for achieving highest paper properties. Details of beating process conducted in this study are shown in Table 2 below.

Table 2. Description of Beating process

Treatment	Alkali (%)	Temperature (^oC)	Beating (revolution)
1	**10**	150	1000 & 8000
2	**10**	160	1000 & 8000
3	**10**	170	1000 & 8000
4	**15**	150	1000 & 8000
5	**15**	160	1000 & 8000
6	**15**	170	1000 & 8000
7	**20**	150	1000 & 8000
8	**20**	160	1000 & 8000
9	**20**	170	1000 & 8000

Papermaking and paper testing

The 60 g/m^2 laboratory papermaking process was based on the TAPPI standard T205 cm-88. After the papermaking process was completed, the paper was put into the conditioning room (temperature 23 ± 1^{o}C, relative humidity 50 ± 2%) for 24 h. Then they were cut accordingly (Figure 1) for specific paper testing. Mechanical testing such as tensile, bursting, tearing, folding and zero-span testing were done to examine the influence of alkali charge, cooking temperature and beating effect on the paper properties. Table 3 shows the TAPPI standards used in the paper testing process.

Table 3. TAPPI standards for paper mechanical testing

Mechanical testing	TAPPI standards
Tearing index	T414 om-88
Folding endurance	T511 om-88
Tensile index	T404 cm-92
Bursting index	T403 om-91
Zero-span	T231 cm-96

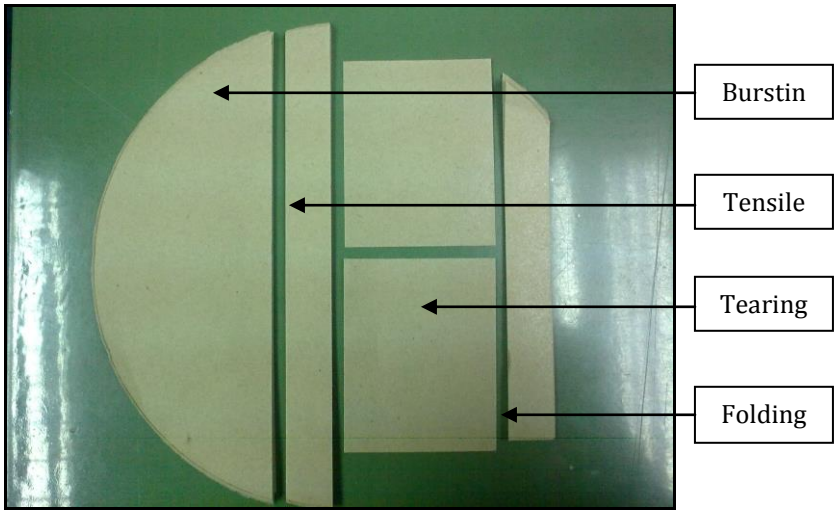


Figure 1. Paper segregation for specific testing

Results and Discussion

Soda-AQ pulping

Before the papermaking process, the pulp needed to go through a screening process. Cooked bamboochips were put through the screening machine to produce a screened yield. Only acceptable size of fibre can go through the screen plate and rejected or oversized fibre will be left on the screen plate. This process is crucial in papermaking manufacturing to ensure smooth and uniform paper texture.

Figure 2 shows the overall screened yield for soda-AQ pulping conducted in this study. As can be seen in the bar graph, there was a decreasing pattern on screened yield percentage with the increasing of the alkali charge percentage in all pulping temperature range. The highest screened yield was produced from the lowest alkali charge percentage (10%) and moderate pulping temperature (160^{o}C) i.e. treatment number 2 where by the screened yield is at 48.38%. This is good in terms of cost effeciency for commercial scale, as only small amount of chemicals and moderate energy power are needed for the pulp production, while the lowest screened yield was produced from the highest alkali charge (20%) and highest pulping temperature (170^{o}C) where only 38.70% screened yield was produced in treatment number 9 (Table 1). This might be due to the cellulose, hemicelluloses and lignin dissolved more in higher alkaline percentage and higher temperature, and thus decreasing the pulping yield.

Beating process and paper testing

Figure 3 shows the tearing index for all treatments which consist of 9 treatments for 1000 beating revolutions and also 9 treatments for 8000 beating revolutions. The tearing index slightly increased with the increasing of the alkali charge and pulping temperature as can be seen from the results in treatment 1 to 9, except for pulping conditions with 170^{o}C temperature and 20% alkaline percentage. This may due to at high temperature and active alkaline, more hemicellulose and cellulose chain were dissolved and thus produced shorter or weaker fibre. For tearing index, the 1000 beating revolutions gave higher results compared to 8000 beating revolution because the tearing index decreased with the increasing of the beating process made on the fibre. A slight beating process (1000 beating revolution) will make the fibre more flexible and can produced better bonding between fibres in the paper sheets and thus can enhance the tearing properties compared to unbeaten pulp. But, further beating process will make the fibre shorter and less bonding area between fibres can occurred, so less energy is needed to tear up the paper sheets and contribute to the decreasing of the tearing index with the increasing (8000 beating revolution) of the beating process.

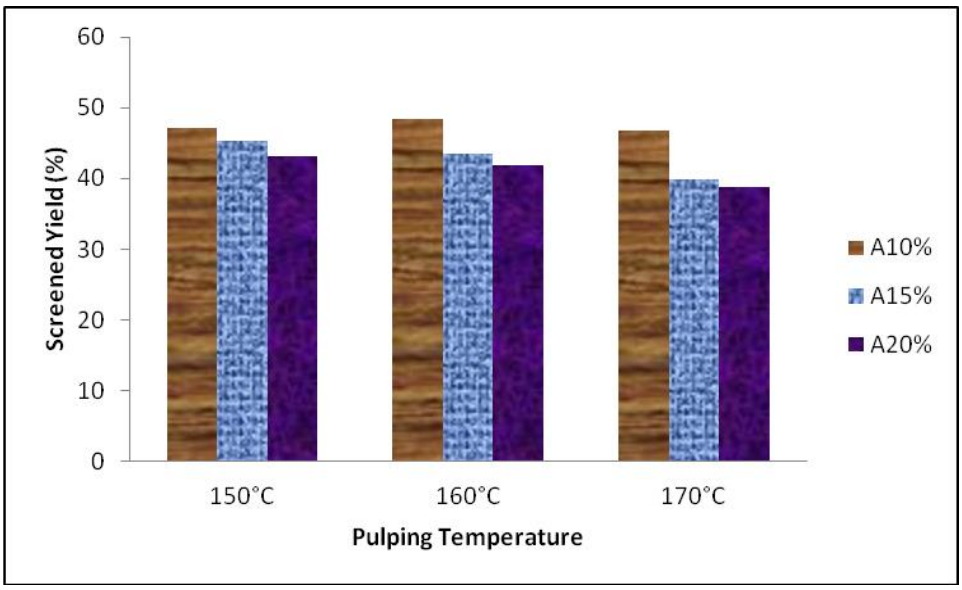


Figure 2. Soda-AQ pulping screened yield

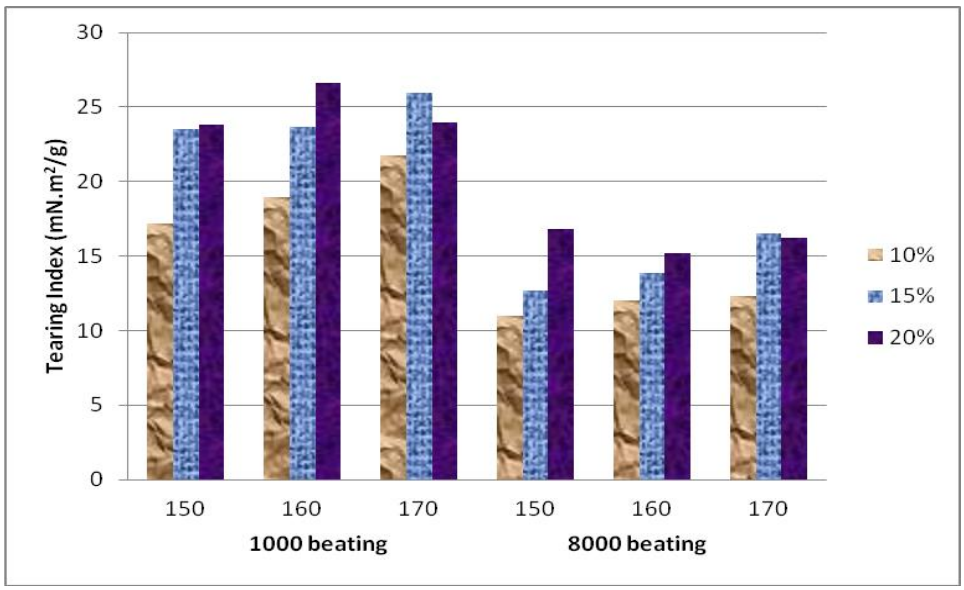


Figure 3. Tearing Index for 1000 and 8000 beating revolutions

The trend was contradicted with the tensile index whereby the trend shows that 8000 beating revolutions paper has higher tensile index compared to the 1000 beating revolutions paper as shown in Figure 4. Tensile index measures the paper resistance to being broken when the paper is stretch out from both sides. In terms of alkali charge and pulping temperature influence, the tensile index increased with the increasing of alkali charge and pulping

temperature from 10 to 15% and 150 to 160°C, but slightly decreased when the alkali charge and pulping temperature kept increasing to 20% and 170°C. This also may due to degradation of hemicelluloses and cellulose in extreme high pulping conditions. Interestingly, as can be seen in Figure 4, highest tensile index occurs at every 15% of alkaline usage regardless the pulping temperature. It means that moderate alkaline percentage is sufficient enough to produce good paper strength. For both 8000 and 1000 beating revolutions, the highest tensile index was found in treatment number 5 (alkali charge 15% and pulping temperature 160°C), which produced tensile indexes 91.09 and 53.79 Nm/g respectively. For 8000 beating revolutions paper, the fibre bonding in the paper was closer and produced higher resistance to being broken and thus produced high tensile index compared to the 1000 beating revolutions paper.

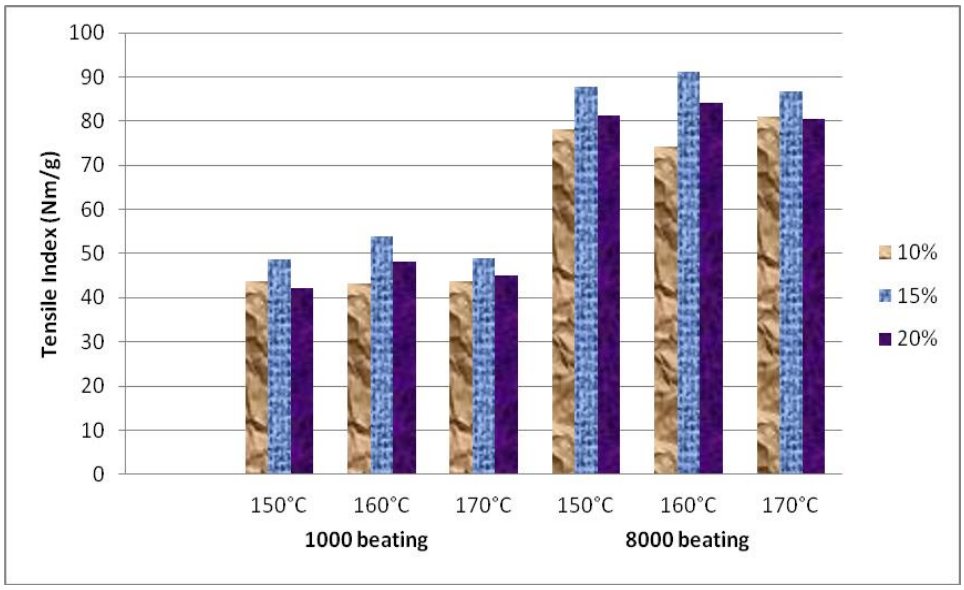


Figure 4. Tensile index for 1000 and 8000 beating revolution

The bursting indexes for 1000 and 8000 beating revolutions in Figure 5 also show the same trend as tensile index above. The bursting strength measures the paper resistance to being burst when hydraulic pressure was applied to the paper. The highest bursting strength was also found in treatment number 5 that produced 3.37 and 7.09 kPa.m^2/g for 1000 and 8000 beating revolutions respectively. Highest bursting index also occur at alkaline percentage of 15% regardless the pulping temperature. It shows that alkaline percentage has higher influence to the paper strength compared to pulping temperature. The 8000 beating revolution paper produced higher bursting strength compared to 1000 beating revolutions, due to higher inter-fibre bonding present in the 8000 beating revolutions paper. Thus the paper became more dense and more pressure was needed to break the inter-fibre bonding thus producing higher bursting index. Yusoff, *et al.* [11] reported that burst strength for 3 year old tropical bamboo *Gigantochloa scortechinii* soda pulp range from 4.5 to 4.7 kPa.m^2/g. Sadawarte *et al.* [12] revealed the highest burst index of unbleached bamboo kraft pulp occurring at 3500 revolutions, was 5 kPa.m^2/g.

Figure 6 shows the folding endurance for 1000 and 8000 beating revolutions papers from Semantan bamboo. It clearly shows that the 8000 beating revolution paper produced better folding endurance as compared to the 1000 beating revolutions paper. The folding endurance measures how many times the paper can be folded (double folds) with a 1g force being attached to it before the paper tears due to the folding action. For the 8000 beating revolutions paper, the fibre bonding in the paper was closer and the paper formation was better and could be folded many times before the paper tore compared to the 1000 beating revolutions. As in tearing, tensile and bursting index, the highest

folding endurance was found in treatment number 5, which produced 68 and 1127 double folds for 1000 and 8000 beating revolutions respectively.

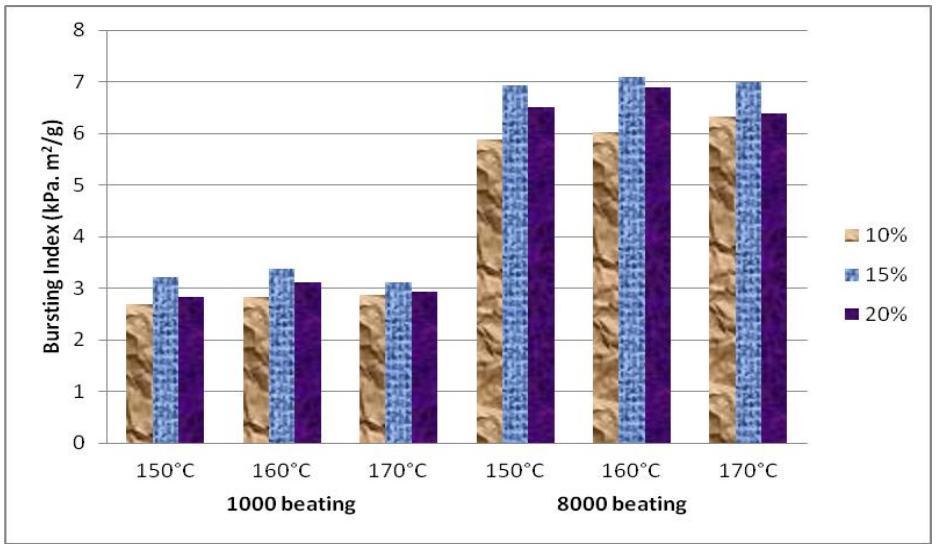


Figure 5. Bursting Index for 1000 and 8000 beating revolutions

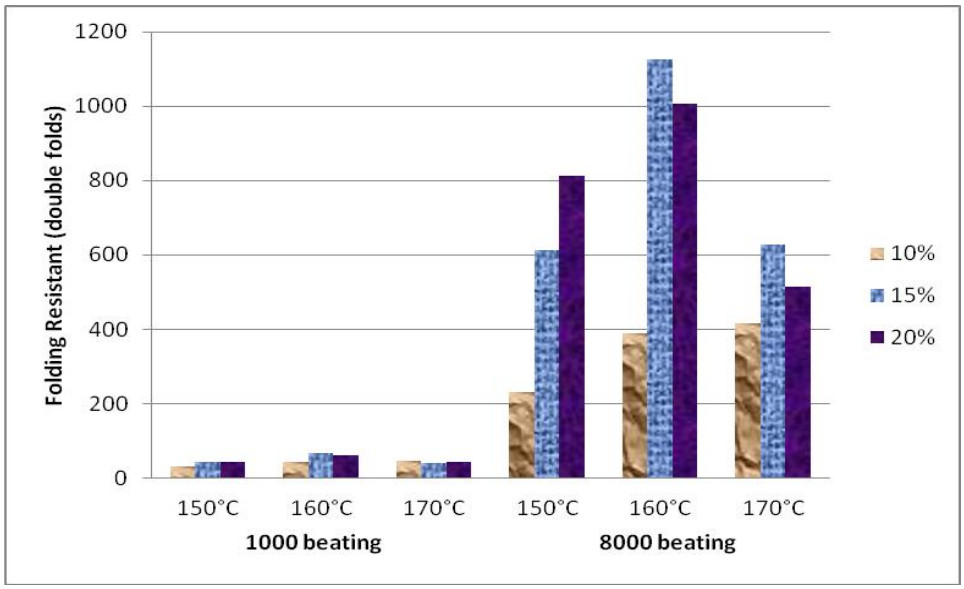


Figure 6. Folding endurance for 1000 and 8000 beating revolutions

Figure 7 shows the zero-span index for 1000 and 8000 beating revolutions paper. The zero-span strength determined the strength of individual, single fibre in the paper. The zero-span tensile test measures the tensile strength at the moment of tensile failure of fibres randomly oriented in a paper sheet. One important usage of zero-span tensile data

is to determine the maximum strength of pulp fibres when beaten under idealized laboratory conditions. The alkali charge percentage and pulping temperature gave more influence to the paper individual fibre as the zero-span index increased with the increasing of alkali charge and pulping temperature, compared to the beating effect. At this time, treatment number 6 with 1000 beating revolutions gave the highest zero-span index which was 153.01 Nm/g.

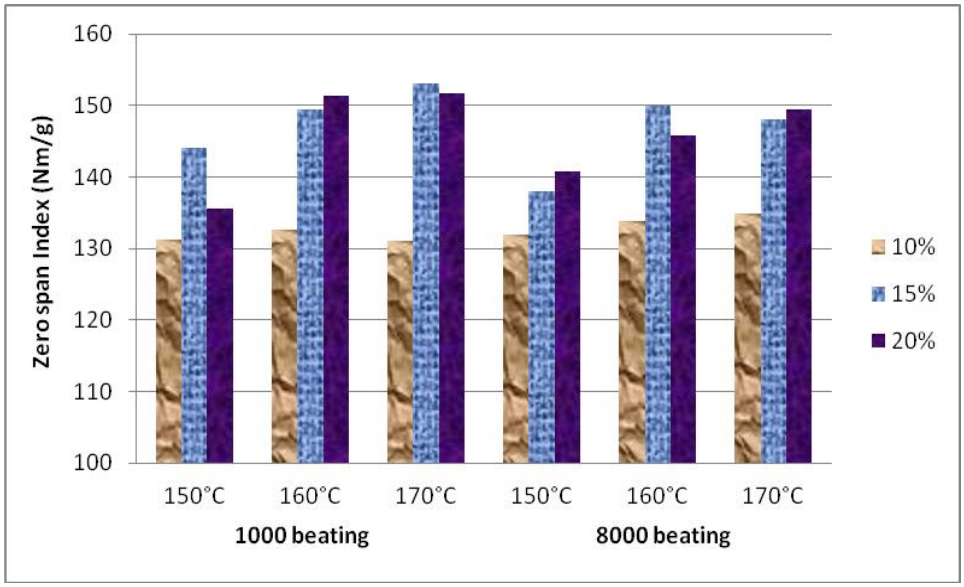


Figure 7. Zero-span Index for 1000 and 8000 beating revolutions

Figure 8 shows the fibre bonding index of the Semantan bamboo studied in this paper under the condition of 1000 and 8000 beating revolutions. The bonding index determination was based on Page's Simplified Equation, that showed the relationship between zero-span and tensile index, as stated in equation below:

$$B = \frac{8ZT}{8Z - 9T}$$

where B = bonding index, Nm/g
Z = zero-span index, Nm/g
T = tensile index, Nm/g

Although most of the paper mechanical testing results namely, tearing, tensile, bursting index and folding endurance tests showed that treatment number 5 (alkali charge 15% and pulping temperature 160^{o}C) had the highest paper properties based on the fibre bonding index, which consider the relationship between tensile index and zero-span index, it can be seen that the optimum paper mechanical properties was derived from treatment number 4, which involved alkali charge of 15% and pulping temperature of 150^{o}C.

Table 4 shows the analysis of variance for all paper mechanical properties discussed above. All the properties show significant and highly significant different between each treatment except for temperature factor for bursting index was not significant. It shows that alkaline percentage and pulping temperature have high influence in mechanical paper properties of Semantan bamboo.

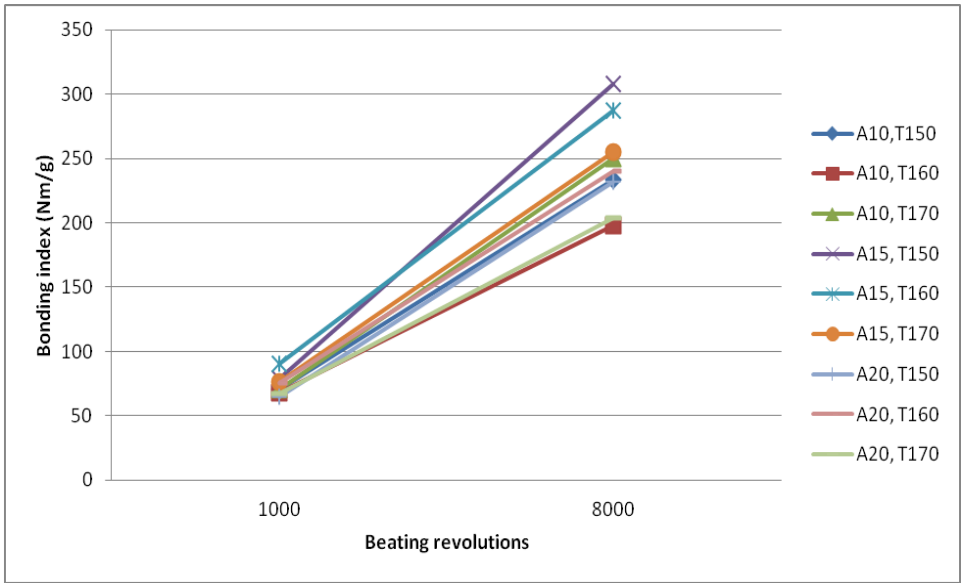


Figure 8. Fibre Bonding Index for 1000 and 8000 beating revolutions

Table 4. Summary of ANOVA for Semantan bamboo paper mechanical properties

Variables	df	Folding endurance	Tearing Index	Tensile Index	Bursting Index	Zero-span Index
Alkaline (A)	2	9.376**	51.965**	87.657**	37.797**	31.583**
Temperature (T)	2	4.966*	8.416**	5.656**	3.544ns	7.024*
Beating (B)	1	123.466**	506.299**	$4.348x10^3$**	$2.747x10^3$**	9.259*
A*T	4	1.614ns	3.143ns	8.118**	2.284ns	1.510ns
A*B	2	8.639**	3.798ns	4.047ns	8.143*	0.981ns
T*B	2	4.231*	0.993ns	2.260ns	0.013ns	0.135ns
A*T*B	4	1.286ns	2.291ns	1.606ns	0.569ns	0.556ns

Note:** - highly significant, *- significant, ns - not significant

Conclusion

Based on the studies conducted, it was found that the paper mechanical properties for the optimum condition (15% of alkali charge and 150^{o}C of pulping temperature) are as follows. Tensile index at 87.71 Nm/g, bursting index at 6.94 kPa.m^2/g, tearing index at 12.72 mN.m^2/g and folding endurance at 613 double folds. It can be concluded from these findings that comparable high strength paper can be produced from Semantan bamboo pulp with more environmentally friendly pulping process.

Acknowledgement

Author would like to thank the Young Lecture Scheme, JPbSM, UiTM for the scholarship granted throughout the study, and also thank to the Pulp and Paper Programme, Forest Research Institute Malaysia (FRIM) for providing the equipments during laboratory works.

References

1. Azmy, H.M., Norini, H. & Wan Razali, W.M. (1997). Management Guidelines and Economics of Natural Bamboo Stands, *FRIM Technical Information Handbook* No.15, Forest Research Institute Malaysia, Kepong, pp1.
2. Chen, M.C., Ho, C.C., & Tracy, M.Y.L. (2000). Bonding Moso Bamboo with Copolymer Resins Made of Biomass Residual Extracts with Phenol and Formaldehyde. *Forest Prod. J.* 50 (9):70-74.
3. Wong, K.M. (1995). The Bamboos of Peninsular Malaysia. Malaysian Forest Records, No. 41. Forest Research Institute Malaysia. pp 71.
4. Lee, A.W.C & Liu, Y. (2003). Selected Physical Properties of Bamboo Flooring, *Forest Prod. J*., 53(6):23-25
5. Wong, K.M. (1989). Current and Potential Uses of Bamboo in Peninsular Malaysia, *Journal of American Bamboo Society* 7(172):1-15.
6. Azmy, H.M. (1989). *Perusahaan Membuat Bakul Ikan dan Sayur dan Bakul Arang*, *FRIM Technical Information* No. 8, Forest Research Institute Malaysia, Kepong, pp 6 (In Malay).
7. Rushdan, I. (2003). Structural, Mechanical And Optical Properties Of Recycled Paper Blended With Oil Palm Empty Fruit Bunch Pulp. *Journal of Oil Palm Research*, Vol. 15, No. 2, December 2003, pp. 28-34.
8. Suphat, K. (2007). Preliminary Study of Anthraquinone in Sweet Bamboo (*Dendrocalamus asper* Backer) Alkaline Sulfite Pulping, *Chiang Mai J. Sci*., 34(2) : 235-247.
9. Biermann, C. J. (1993). Essential of pulping and papermaking, California: *ACADEMIC PRESS*, Inc.
10. Nurul Husna, M.H., Mansur, A. & Rushdan, I. (2010). Enhancement of Mechanical Properties of Semantan Bamboo Pulp by Beating. (Eds.) Gan, K.S., Mahmudin, S., Mohd Nor, M.Y. *In* Proceedings of the International Symposium on Forestry and Forest Product 2010. Addressing Global Concerns and Changing Societal Needs, 5 – 7 October 2010, Kuala Lumpur, Malaysia, 91 – 100.
11. Yusoff, M.N.M., Kadir, A.Abd., & Mohamed, A. H. (1992). Utilization of Bamboo for Pulp and Medium Density Board, (Eds.) Mohd W. R.W., and Mohamad A.B., *In* Proceeding of Seminar Towards the Management, Conservation, Marketing and Utilization of Bamboos, Kuala Lumpur: FRIM, 196 – 205.
12. Sadawarte, N.S., Dharwadkar, A.R., & Veeramani, H. (1982). Pulp strength properties and black liquor viscosity for kraft pulping of bamboo-bagasse blend (70:30), *In* 1982 Pulping Conference, Book. 1, Atlanta, 197 – 206.

The Malaysian Journal of ANALYTICAL SCIENCES ISSN 1394-2506

COMPARATIVE STUDY ON CHARACTERISTICS AND POTENTIAL OF RICE STRAWS AND DRY LEAVES AS A BINDER IN REFUSE DERIVED FUEL (RDF)

(Kajian Perbandingan Pencirian dan Potensi Jerami Padi dan Daun Kering Sebagai Pengikat Dalam Bahan Bakar Buangan)

Othman, Z.[1*], Lias, K.[2], Hashim, N.H.[2], Clement, F.N.[2]

[1]*Faculty of Civil Engineering,*
Universiti Teknologi MARA Pahang, 26400 Bandar Tun Abdul Razak Jengka, Pahang, Malaysia
[2]*Faculty of Applied Science,*
Universiti Teknologi MARA (Perlis), 02600 Arau, Perlis, Malaysia

**Corresponding author: zulhafizal445@pahang.uitm.edu.my*

Abstract

Integrated waste management systems are one of the greatest challenges in order to develop the green environment. In this research, two types of binder were chosen in producing of Refuse Derived Fuel (RDF) which is rice straws and dry leaves. The objective of the research is to identify which types of binder that can give the optimum performance. This two binder was mixed with paper and plastic waste with controlled mixing ratio which is 3:1 (ratio 1), 3:1.5(ratio 2) and 3:2 (ratio 3). In order to identify the optimum ratio of RDF, 45 number of samples was prepared and their properties such as moisture content, carbon content, sulfur content, chlorine content and calorific value were evaluated. Result indicated that samples with rice straw as a binder give the optimum result with the ratio of 3:1. The optimum values of the carbon content is 50.9%, moisture content is 5.5%, chlorine content is 0.0%, sulfur content is 2.1% and calorific value is 29.0 MJ/kg. Hence, rice straws shows a great potential to be used as binder in production of RDF.

Keywords: Rice Straws, Dry Leaves, Refuse Derived Fuel, Potential, Characteristics

Abstrak

Sistem pengurusan sisa pepejal bersepadu merupakan satu cabaran terbesar dalam membangunkan persekitaran mesra alam. Dalam penyelidikan ini, dua jenis pengikat telah dipilih untuk menghasilkan Bahan Bakar Buangan iaitu jerami beras dan daun-daun kering. Objektif penyelidikan ialah untuk mengenal pasti jenis pengikat yang boleh memberi prestasi yang optimum. Pengikat akan diadunkan dengan kertas dan bahan buangan plastik dengan nisbah campuran terkawal iaitu 3:1 (nisbah 1), 3:1.5 (nisbah 2) dan 3:2 (nisbah 3). Dalam mengenal pasti nisbah optimum bahan bakar buangan yang dihasilkan, sebanyak 45 sampel telah disediakan dan pencirian sampel seperti kandungan lembapan, kandungan karbon, kandungan sulfur, kandungan klorin dan nilai kalori telah dikenalpasti. Hasil menunjukkan bahawa sampel dengan pengikat jerami padi memberi hasil optimum dengan nisbah 3:1. Nilai-nilai optimum kandungan karbon ialah 50.9%, kandungan lembapan ialah 5.5%, kandungan klorin ialah 0.0%, kandungan sulfur ialah 2.1% dan nilai kalori ialah 29.0 MJ/kg. Oleh itu, jerami beras menunjukkan potensi besar untuk digunakan sebagai pengikat di pengeluaran bahan bakar buangan.

Kata kunci: Jerami Padi, Daun Kering, Bahan Bakar Buangan, Potensi, Pencirian

Introduction

The amount of solid waste generated s one of the most debatable environmental issues. In order to overcome this issue, many initiatives created such as applying the integrated waste management. Waste management is one of the ways the ways to control the production of waste. It includes six strategies which are rethink, refuse, reuse, replace, recycle and remove to pursuit environmentally sustainable development area. Lack of managing in solid waste may

affect the eco system and indirectly effect human health. Refused derived fuel (RDF) is a new and alternative way of managing waste beside incineration process.

Refuse Derived Fuel (RDF)

RDF is a solid waste which is consists of paper and plastic use as a fuel for boilers to produce steam or electricity. RDF is frequently burned in utility boilers and also been mixed and burned with coal. Generally it is a waste that has been sorted, reduced in size, and refined by removal of noncombustible such as metals and glass [1]. The concept of processing waste for the purpose of RDF production has received additional impetus in Europe [2]. The aim of the RDF preparation is to improve the quality of the waste stream in a way that the substitute fuel produced can be burned in plants without operational problems and without pollution loading. [3]. Thus process was gained from combustion process. Combustion, in its most basic sense, is the process whereby the hydrogen and carbon in fuel is combined with oxygen from the air to release heat [4]. Energy recovery as RDF is preferred option for utilizing plastic wastes when their potential recycling as raw material for product manufacturing is not possible because their physical properties damaged during long-term exposure to sunlight. However, their high calorific content (18 – 25MJ/kg) remain especially when almost dried completely during summer but purification process is still required if there are to be utilized as energy source [5].

Rice Straws

Rice straw is the residue and the excesses of production of rice that was not utilized [6].The main carbohydrate components of rice straw are hemicellulose, cellulose and lignin. For every tonne of grain harvested, about 1.35 tonnes of rice straw remain in the field. Rice straw has a high potential as a source of lignocellulosic biomass because of the high yield of rice straw per hectare [4]. Burning the rice straws away not only pollutes the environment, but also may cause the traffic accident if the field is close to the freeway. Moreover, the abandoned rice straws in the field sometimes may flow into the drainage during the rainy season and cause an obstruction of the drainage, or provide the place for the propagation of the bacteria [7]. The waste that comes from rice straws that utilize into RDF has the potential for becoming a secondary renewable energy in Taiwan [8]. Among the alternative energy resources, the biomass becomes an important renewable energy resource because it has appealing properties, such as low production cost, low greenhouse gas and low acidic gas emissions.

Dry Leaves

In India, sugarcane is harvested manually. The tops and leaves are stripped from the stalks in the field after cutting the stalks. The tops are extensively use as fodder for animals. However, dried leaves are disposed of by burning them in the open field, which is large loss of potentially useful heat energy. Gasification of these leaves offers a better option for their utilization [9].

Materials and Methods

Production of RDF briquettes

The plastics and papers wastes were shredded separately before mix together with ratio 1:1. Rice straw and dry leaves were crash and turn into paste by adding water before mixing with the wastes mixture. The weight ratio of the wastes mixture and binders (rice straw and dry leaves) were varied at 3:1 (ratio 1), 3:1.5 (ratio 2) and 3:2 (ratio 3). The total weight of each briquette is 500 gram (Table 1). The formation of briquette was conducted at room temperature using a 5-hp screw compactor at 15 MPa of compression. After the production process, they were stored under ambient conditions for 5 days before their utilization. Triplicates samples of the RDF produces were tested in the laboratory typical for moisture content, carbon content, calorific value, sulfur and chloride analysis.

Table 1. Sample Ratio

Sample Ratio	Paper + Plastic (Wastes Mixture) : Binder	
	Waste Mixtures : Dry leaves (Binder) (g)	Waste Mixtures : Rice straw (Binder) (g)
3:1	375 : 125	375 :125
3:1.5	333 : 167	333 : 167
3:2	300 : 200	300 : 200

Analyses / Characterization

a) Moisture content: The initial weight of sample was determined and the samples were dry at temperature 77^{o}C for 24 hours using oven. Then, the final weight of sample determined after drying process.

b) Carbon content: The empty ceramic crucible was weight. The sample was put in the empty ceramic crucible. The crucible with the sample was weight and the weight was recorded. The crucible was place into a furnace at room temperature and the crucible was heated for 15 minutes in the 600^{o}C. The crucible in the desiccators was cool before weighing the crucible with the sample. The differences between the initial and the final weight in the amount of volatile solid is determined as carbon content.

c) Energy content: The determination of energy content was conducted by using bomb calorimeter. 10 grams of samples was picking and put into the bomb calorimeter. Then the result of the process release from the display monitor.

d) Chloride content: Quantitatively the chloride solution was transferred into a 250ml Erlenmeyer flask. 10ml of HNO_3 was added while stirring gently during the acid addition. Then, 20ml of standard $AgNO_3$ solution was added. Stopper, mix and let the solution to stand in dark for 15 minutes and cool at room temperature. 5 to 10ml of nitrobenzene was added and shake for 1 min. 8 to 10 drops of $FeNH_4(SO_4)_2$ was added to the solution and titrate with standard KCNS solution against white background. The end point of the determination was reached when solution becomes faintly orange pink in colour.

e) Sulfur content: 5.0g of sample was weight into weight ceramic crucible. The sample was mix with 10.0g of Eschka mixture well. Another 5.0g mixture was added to cover the mixture. The crucible and its content were placed in muffle furnace. The temperature was raised gradually to 815^{o}C within 1 hour. Then, continue heating at this temperature for another one and half hours. The crucible was removed from the furnace and empties all its content into 500ml beaker. 100ml of hot distilled water was added and 15ml of concentrated hydrochloric acid. The solution was stirred for 30 to 45 minutes with occasional stirring. The solution was filter through Whatman filtered paper into 500ml beaker and washes 5 times with hot distilled water. The filtered was collected about 250ml beaker. 3 to 4 drops of methyl orange were added to the filtrate. The filtrate was neutralized with 1:1 ammonia solution until gel was formed. 1:1 hydrochloric acid was added until the solution become pink. 10ml of hot barium chloride was added and stir. The solution was boiled for 15 minutes and allowed it to stand at room temperature for overnight. The solution was filtered through Whatman filter paper and washed for 6 times with hot distilled water. The filter paper was placed in the ceramic crucible and recorded the weight, W_1. Dry in the oven. Then, the filter paper was ignited in furnace at 1000^{o}C for 45 minutes. The crucible was cool in desiccators before weighing. The crucible was weight, W_2. Calculation for the sulfur content is shown as below:

$$\text{Percentage of sulfur (\%)} = [W_1 - W_2] \times 13.738 / M$$

where: M = weight of sample used.
13.738 is the percentage of sulfur atomic weight to the molecular weight of barium sulphate.

Results and Discussion

Moisture Contents

Figure 1 showed the percent of moisture content produced from rice straw and dry leaves as a binder are 3.0% to 7.6%, respectively. Sample 2 of dry leaves which is the ratio of 3:1.5 seems to be the lowest reading with the values of 3.0% while the highest is rice straw with the ratio of 3:2 and value 7.6%. From the figure below, due to differences in morphology of the binders the readings show that the moisture contents increase exponentially with the quantity of rice straw. Researched has been founded if the material is too dry, the surface of the material may carbonize and the binder will burn before the combustion process finished completely, whereas if the material is too wet, then the moisture contained in the pressing cannot escape and enlarges the RDF volume, making it mechanically weak [10].

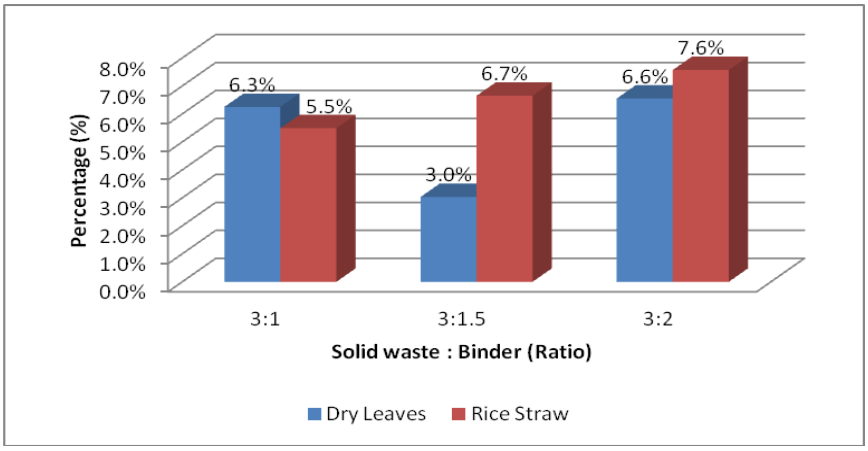


Figure 1. Moisture content

Carbon Contents

Based on the results in figure 2, the sample with ratio 3:1 of rice straw gives the highest reading which is 50.9% where by the lowest is the third sample of rice straw which is 38.6%. The higher carbon content in fuels leads to the higher combustion efficiency [11]. Carbon is present in every hydrocarbon fuel and this will react with oxygen in combustion process [4]. So that in order to choose the good RDF, this parameter must take under consideration.

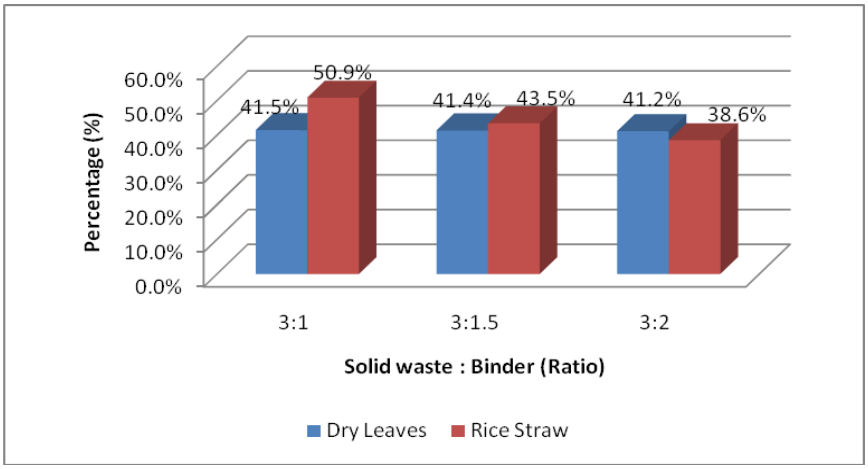


Figure 2. Carbon content

Calorific Value

Figure 3 below shows the reading of sample 1 with ratio 3:1 get the highest value which is 29 MJ/kg while the third sample shows the lowest reading that is 20.40 MJ/kg. The sample ratio 1 of rice straw gives the higher value of energy content may because of the amount of solid waste mixed is less compare to sample ratio 2 and 3. The reading for calorific value of rice straw obtained as 27.5 MJ/kg to 38.5 MJ/kg [1]. While, the calorific value of rice straw in Europe is about 15.3 MJ/kg [12]. For typical value for plastic wastes is 28 MJ/kg to 37 MJ/kg [12]. In order to produce the good performance of RDF, high energy content is required from the sample for better performance in combustion process.

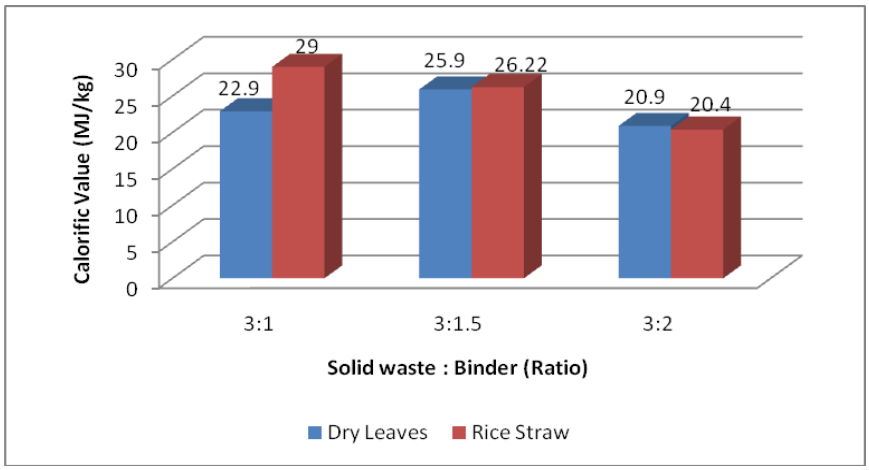


Figure 3. Energy content

Chloride Content & Sulfur Content

Table 2 illustrates the percentage of chloride and sulfur in the composition of wastes while rice straw and dry leaves which acts as the binder. Based on Table 1, the percentage of chloride varies from 0.0% to 0.01% as rice straw as a binder and dry leaves as well. The ratio 1 of rice straw as a binder gives the lowest reading 0.0% whereby the ratio 3 contains the highest amount of chloride, 0.1%. Same goes to sulfur in sample ratio 1 indicates the lowest value while the ratio 3 gives the highest value. Meanwhile, the result for dry leaves as a binder indicated the constant reading of sulfur content in all 3 ratio which is 2.2% and for chloride content showed the ratio 2 is the lowest percentage. High chlorine and sulfur can lead to higher emission of acidic gaseous pollutants such as HCl, SO_X and organic chlorinated compounds for example PCCDs and PCDFs in the incineration process [13]. With these limitations, it is suggested that the preparation of plastic wastes should be blended with other low chlorine containing materials before being used as RDF in order to comply with the specified limit [1].

Table 2. Chloride and Sulfur content

Sample	Ratio of wastes : Binder (rice straw) weight ratio		Ratio of wastes : Binder (dry leaves) weight ratio	
	Chloride Content (%)	Sulfur Content (%)	Chloride Content (%)	Sulfur Content (%)
1	0.0	2.1	0.1	2.2
2	0.0	2.2	0.0	2.2
3	0.1	2.7	0.1	2.2

Conclusion

After all the experiment have been conducted and data analyzed, the result indicated that samples with rice straw as a binder give the optimum result with the ratio of 3:1 (ratio 1) meanwhile the sample with dry leaves as a binder indicated the sample with ratio 3:1.5 (ratio 2) as the optimum result. After further consideration related to literature review such as the carbon content in ratio 2 is not so high because the higher carbon content in fuels leads to the higher combustion efficiency. Furthermore, the characteristic of energy content is also important because it shows the ability of material can be combustible and produce the energy. Hence, rice straws with ratio 3:1 have a great potential as a binder to produce refuse derived fuel (RDF) for application purpose compare to dry leaves.

Acknowledgement

Researchers want to thanks to the management of University Teknologi MARA (Perlis) for the supporting us in conducting the research. Many thanks also to our family and friends for the ideas and encouragement until this research done and lastly, to all individual who give the contribution to this research directly or not directly in order to make this research succeed.

References

1. Tchobanoglous, G., Theisen, H., Vigil, S. (1993). Integrated Solid Waste Management, Engineering Principle and Management Issues. New York: Mcgraw-Hill Inc.
2. Rotter, V. S., Kost, T., Winkler, J. And Bilitewski, B. (2004). Material Flow Analysis of RDF-Production Processes. Waste Management. 24: 1005-1021.
3. Gina-geogiana Rolea, Gheorghe Ciocea, Ion V. Ion and Florin Popescu. (2011). The Use of Reed Briquettes in a Domestic Heat. Development, Energy, Environment, Economics & Engineering. 26: 1291-1300
4. Liang Lu, Yuqi Jin et all. (2012). An investigation on Cocombustion Behaviors of Hydrothermally Treated Municipal Solid Waste with Coal Using a Drop-Tube Reactor. Journal of Combustion. 10.1155/2012/282851.
5. Chiemchaisri, C., Charnnok, B., Visvanathan. (2009). Recovery of Plastic Wastes from Dumpsite as Refuse-Derived Fuel and its Utilization in Small Gasification System. Bioresource Technology. 101:1522-1577.
6. Mohdy, F.A.A., Halim, E.S.A., Ayana, Y.M.A., El Sawy, S.M. (2009). Rice Straw as A New Resource for Some Beneficial Uses. Carbohydrate Polymers. 75: 44-51.
7. Chou, C.S., Lin, S.H., Peng, C.C., Lu, W.C. (2009). The Optimum Conditions for Preparing Solid Fuel Briquette of Rice Straw by A Piston-Mold Process Using The Taguchi Method. Fuel Processing Technology. 90: 1041-1046.
8. Wey, K.D and Hong, S.C. (2007). Refuse-Derived Fuel as A Secondary in Taiwan-Using Hotelling Space Allocation Model. Resource Policy. 31: 204-210.
9. R.J.Jorapur, A.K. Rajvanshi. (1995). Development of Sugarcane Leaf Gasifier for Electric Generation. Pergamon Biomass and Bioenergy. Vol.8. No.2: 91-95.
10. Loo Van S, and Koppejan J. (2004). Handbook of Biomass Combustion of Co-firing prepared by task 32 of the Implementing Agreement on Biomass under the auspices of the Int. Energy Agency. Tent University Press.
11. Gendebien, A., Leavens, A., Blackmore, K., Godley, A., Lewin, K., Whiting, K. J., et al. (2003). Refuse Derived Fuel, Current Practice And Perspectives Final Report. European Commission.
12. Jenkin BM. (1998). Physical properties of biomass. In Biomass Handbook. Chapter 5.2. O. Kitani and C.W. Hall, Gordon and Breach, New York.
13. Watanabe, N., Yamato O., Sakai, M., Fukuyama. J. (2004). Combustible and Incombustible Specification of Cl and S in Various Component of Municipal Solid Waste. Waste Management. 24: 623-632.

The Malaysian Journal of ANALYTICAL SCIENCES ISSN 1394-2506

SYNTHESIS OF ALKYLPOLYGLUCOSIDE FROM DEXTROSE-DECANOL IN THE PRESENCE OF SILICOTUNGSTIC ACID SOL-GEL CATALYST

(Sintesis Alkilpoliglukosida Daripada Dekstrosa-Dekanol Dengan Kehadiran Katalis Asid Silikotungstik Sol-Gel)

Izazi Azzahidah Amin[1*], Mohd Ambar Yarmo[1], Nik Idris Nik Yusoff [2], Nor Asikin Mohamad Nordin[1,3], Wan Nor Roslam Wan Isahak[1]

[1] *School of Chemical Sciences and Food Technology, Faculty of Science and Technology, Universiti Kebangsaan Malaysia, 43600 Bangi, Selangor Malaysia.*
[2] *Department of Pharmaceutical Chemistry, Kuliyyah of Pharmacy, International Islamic University of Malaysia, 25200 Kuantan, Pahang Malaysia.*
[3]*Department of Science, UTM Space, Universiti Teknologi Malaysia International Campus Jalan Semarak, 54100 Kuala Lumpur*

**Corresponding author: azzahidah_87@yahoo.com.my*

Abstract

The purpose of this study is to synthesis alkylpolyglucoside via condensation of decanol with dextrose in the presence of heterogenous catalyst. In this study, silicotungstic acid sol-gel (STSG) prepared using sol-gel was used as solid acid catalyst. The catalyst was characterized using BET surface area measurement, X-ray Diffraction (XRD) and X-ray Photoelectron Spectroscopy (XPS) surface analysis. The final product was easy to be separated from catalyst without the need of a further neutralization. Silicotungstic acid sol-gel has been found efficient to be solid catalyst for synthesis alkylpolyglucosides. Condensation reaction was carried out 8 hours at 110^{o}C-120^{o}C under vacuum condition at 10mmHg. The determination of decylglucoside has been achived by LC/ESI-MS/MS (ToF) giving a mass peak at m/z = 343.2 correspond to the m/z of $[M+Na]^{+}$. Alkylpolyglucoside produced was analysed by FTIR, ^{1}H and ^{13}C NMR spectrometric technique.

Keywords: silicotungstic acid sol-gel, alkylpolyglucosides, XPS, LC/ESI-MS/MS

Abstrak

Tujuan penyelidikan ini dilakukan adalah untuk menghasilkan alkilpoliglukosida melalui proses kondensasi di antara dekanol dan dekstrosa, dengan kehadiran mangkin heterogen. Dalam penyelidikan ini, mangkin asid silikotungstik sol-gel digunakan, yang mana disediakan menggunakan teknik sol-gel. Mangkin dicirikan menggunakan kaedah pengukuran luas permukaan BET, Pembelauan Sinar X (XRD) dan analisis permukaan Spektroskopi Fotoelektron Sinar X (XPS). Produk akhir yang diperolehi mudah untuk diasingkan daripada mangkin yang digunakan tanpa proses peneutralan. Didapati, mangkin asid silikotungstik sol-gel boleh digunakan sebagai katalis pepejal untuk penghasilan alkilpoliglukosida. Tindakbalas kondensasi dilakukan selama 8 jam pada suhu 110^{o}C-120^{o}C pada keadaan vakum 10mmHg. Penentuan dekilglukosida berjaya diperolehi menggunakan LC/ESI-MS/MS, yang mana memberikan nilai puncak m/z = 343.2, yang mana merujuk kepada $[M+Na]^{+}$. Alkilpoliglukosida yang dihasilkan dianalisa menggunakan spectrometri FTIR, ^{1}H dan ^{13}C NMR.

Katakunci: asid silikotungstik sol-gel, alkilpoliglukosida, BET, XPS, LC/ESI-MS/MS

Introduction

Alkylpolyglucosides (APGs) are non-ionic surfactants developed based on carbohydrate and fatty alcohol and categorized as environmentally non-toxic surfactant as it based on renewable resources [1]. Fischer glycosidation, a method identified by Emil Fischer more than 100 years ago, have been used widely to synthesis alkylpolyglucosides [2]. However, the method exist many drawbacks, especially the needs of final neutralization and a separation step of

the acid catalyst after the reaction [3]. Homogenous catalysts and strong mineral acids for example dinonyl naphthalenesulfonic acid, *p*-toluene sulfonic acid, and sulphuric acid have been used in tradition as acid catalyst for the synthesis of alkylpolyglucosides because of their good catalytic properties [4].

Strong acid catalyst usage also can produces alkylpolyglucosides which dark in colour and offensive smell, generate a waste that need to be managed, as well as gives a corrosion to the equipment [5]. Therefore, in order to overcome the drawbacks and achieve a green chemistry process, a solid acid catalyst has to replace the conventional liquid acid catalysts [6]. Heterogenous catalyst receives an attention due to easy separate from final products as well as gives a good catalytic [7]. Few studies have been reported on the synthesis of alkylpolyglucosides using heterogenous catalyst such as acid zeolites [8], MCM-41 [9] and dealuminated HY faujasites [10]. Y.Wu et al. (2008) reported the synthesis of alkylpolyglucosides in the presence of solid acid catalyst (H_2SO_4/SiO_2) offers high coversion and minimal environmental effect [11]. In this paper, we present the studies of the usage of silicotungstic acid sol-gel (STSG) as catalyst for synthesis of alkylpolyglucosides. Alkylpolyglucosides is produce when glucose is reacting with fatty alcohol through ether bond as shown in Figure 1.

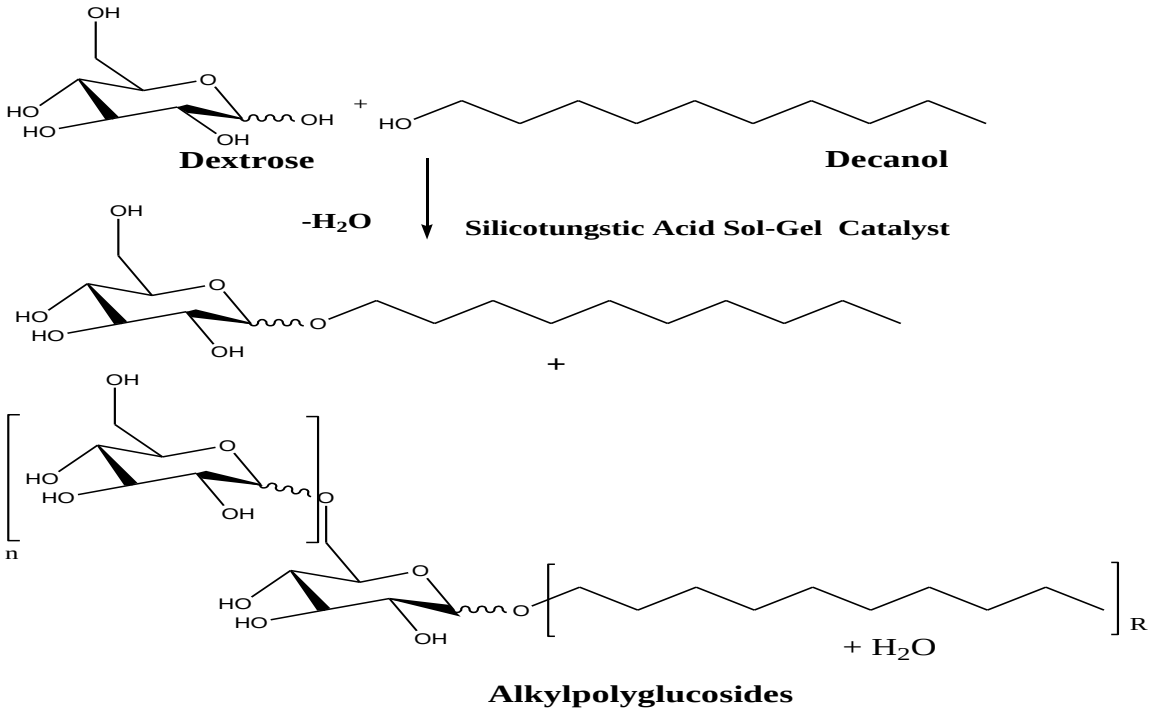


Figure 1. Synthesis of Alkylpolyglucosides [12, 13, 14]

Materials and Methods

Materials

All chemicals used are of A.R grade. TEOS is a product supplied by Merck-Schuchardt, Hohenbruhn, Germany. $H_4SiW_{12}O_{40}$ supplied by Fluka Sigma-Aldrich Chemie Gmblt, Japan.

Synthesis of silicotungstic acid sol-gel (STSG)

The preparation of STSG was carried out based on method by Izumi et al. [15] with some modification. A mixture of water (2 mol, 36.00g), 1-butanol (0.2 mol, 14.28g), and 12-silicotungstic acid hydrate ($H_4SiW_{12}O_{40}$, 5.0 x 10^{-4} mol, 1.440g) was added to tetraethyl orthosilicate (TEOS, 0.2 mol, 41.60g) and stirred for 3 hours at 80^{o}C. A

hydrogel was obtained and was dehydrated in reflux apparatus with methanol at 65°C-70°C for 72 hours, and then was heated to let the methanol to dry completely.

Catalyst Characterization

The specific surface area, S_{BET} of the catalyst was measured using a Gemini apparatus Micromeritics model ASAP 2010 and the analysis adsorptive was done at liquid nitrogen at 77 K. XRD analysis was performed on Bruker AXS D8 Advance X-ray Powder Diffractometer with Cu Kα (40 kV, 40 mA, λ=0.15406 nm) to record angle 2θ from 10° to 60°. The X-ray Photoelectron Spectoscopy (XPS) surface analysis was performed on XPS Axis Ultra from Kratos equipped along with monochromatic Al Kα radiation. The catalyst was analyzed in the analysis chamber pressure at 1×10^{-10} Pa. The binding energy of C1s, 284.5 eV was used as reference.

Synthesis of alkylpoluglucosides

The Fischer direct glycosidation process was carried out by reacting excess decanol and dextrose in a mol ratio of 4:1 and the presence of meoporous silica sol-gel (10%wt of reactant) as catalyst. The reaction was carried out at 110°C-120°C and connected to the vacuum in order to remove water as by product which can cause hydrolysis of product [11]. After 8 hours, the reaction was terminated and the reaction product was dissolve in methanol; the catalyst was removed by simple filtration. Purification was carried using solid-liquid chromatography to isolate the alkylpolyglucosides from excess alcohol and unreacted dextrose [16].

Analysis and Characterization of Alkylpolyglucosides

The structure of the prepared alkylpolyglucosides was confirmed by:

1. The presence of ether linkage was confirmed by Fourier transform infrared spectroscopy (FTIR) model Perkin Elmer Model GC 1605.
2. ^{1}H and ^{13}C Nuclear Magnetic Resonance (NMR) was measured in DMSO-d_6 on on FT-NMR 600MHz Cryoprobe Model Bruker/Advance III 600 MHz equipped with TOPSPIN 2.1 software and pulse programme zg30 for proton and zgpg 30 for ^{13}C.
3. LC/ESI-MS/MS (ToF) analysis was performed on a Dionex Ultimate 3000 separation module filter with an auto injector (20-µL injection loop), coupled via an electrospray interface and a Bruker micrOTOF-Q mass spectrometer. A C18-reversed phase column chromatography was carried out with a column (150 mm x 3.9 mm, RP18) supplied by XTerra. Parameter for separation method; gradient of water and methanol was applied, the linear gradient started from 30% of methanol reaching 100% of methanol after 10 min. The latter concentration was maintained for 10 min; with the mobile phase flow rate was 0.5 ml min-1. The electrospray source potentials were: capillary 4 kV, end plate offset -0.5 kV, collision cell RF 250.0 Vpp; the source temperature was 190°C. Nitrogen was used as the nebulizing and at flow rates of 0.6 lh1.

Results and Discussion

Surface Area Analysis by BET

The surface area analysis of showed that the surface area of STSG catalyst was 794.1 m^2/g while raw material, silicotungstic acid bulk (STAB) was 0.98 m^2/g. By using the sol-gel technique, STSG catalyst prepared gave a higher surface area with higher porosity. These properties will give a catalyst result in higher adsorption and higher catalytic activity. Figure 2 shows the sorption of the STSG which exhibited a type-IV isotherm and a presence of hysterisis loop indicated a capillary condensation in mesoporous material.

Crystalline Determination by XRD.

From Figure 3, the XRD patterns of STSG catalysts show an amorphous phase, no crystalline material characteristic due to the presence of SiO_2 layers. Broader diffraction peaks at 25° correspond to the Si-O-Si bond.

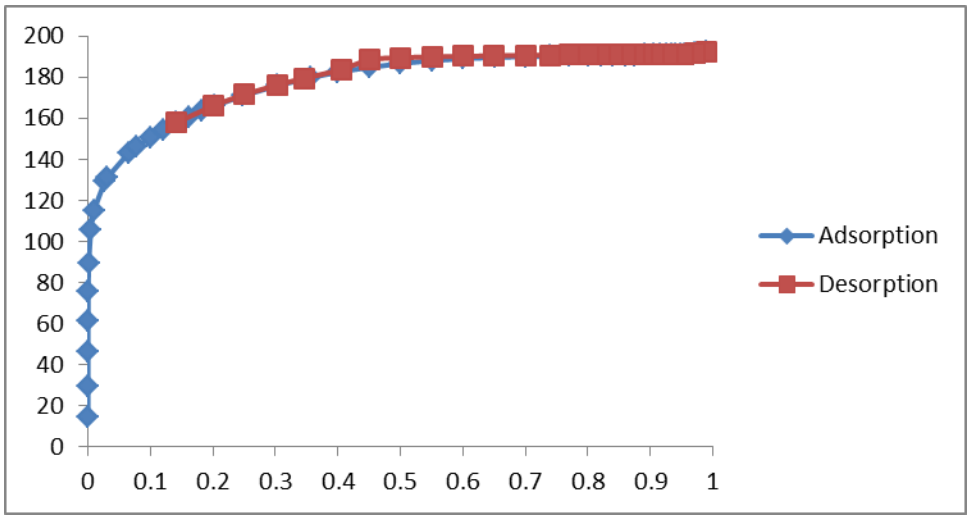


Figure 2. Nitrogen sorption of STSG catalyst

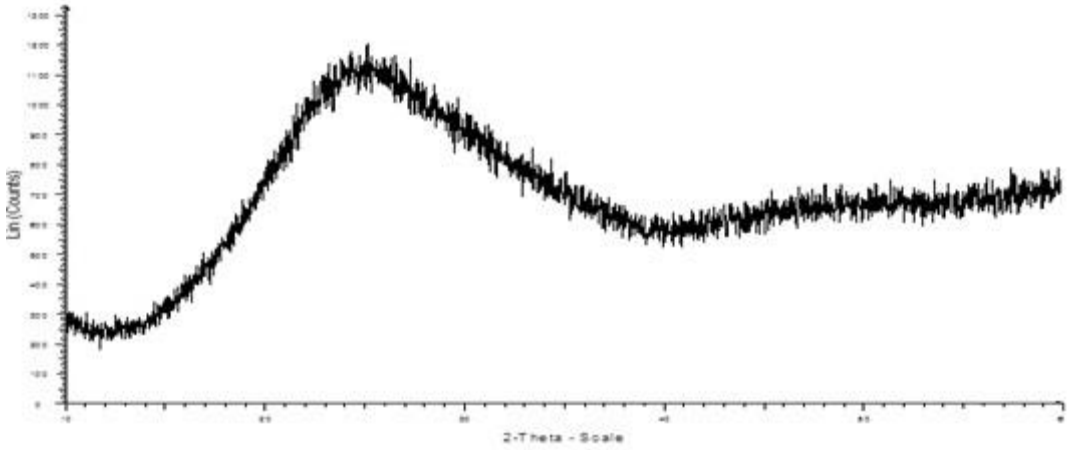


Figure 3. XRD patterns of STSG

Surface Analysis by XPS

The surface composition and binding energy (BE) of the C1s, O1s, and Si2p of STSG and STAB were obtained using XPS analysis. Figure 4 shows the XPS wide scan spectra of STSG and STAB. The photoelectron peaks show the presence of C1s, O1s, Si2p and W4f as expected. The percentage of mass concentration and binding energy of C1s, O1s, and Si2p of STSG obtained were summarized in Table 1.

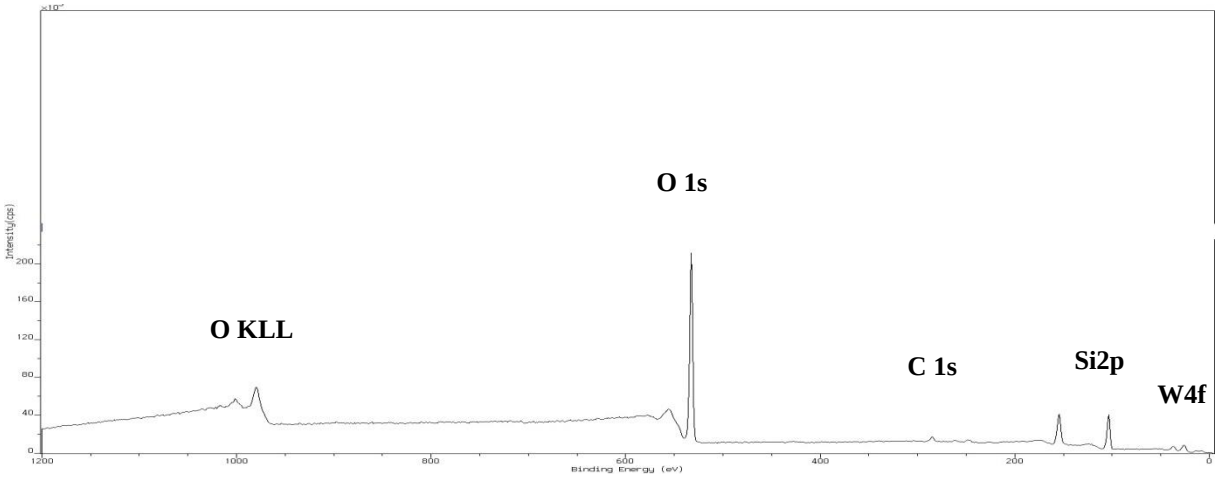


Figure 4. XPS wide scan spectra of STSG

Table 1. Binding energy (eV) and mass concentration (%) from wide scan analysis of the elements of STSG.

Catalyst	O1s		Si2p		W4f	
	Binding energy, eV	Mass concentration, %	Binding energy, eV	Mass concentration, %	Binding energy, eV	Mass concentration, %
STSG	532.9	56.41	103.8	31.8	26.9	8.01

Figure 5(a) shows XPS narrow scan for O1s of STSG and found that O1s binding energy of STAG, 534.0 eV and 535.6 eV. It is due to the adsorbed water, $SiOH_2^+$.

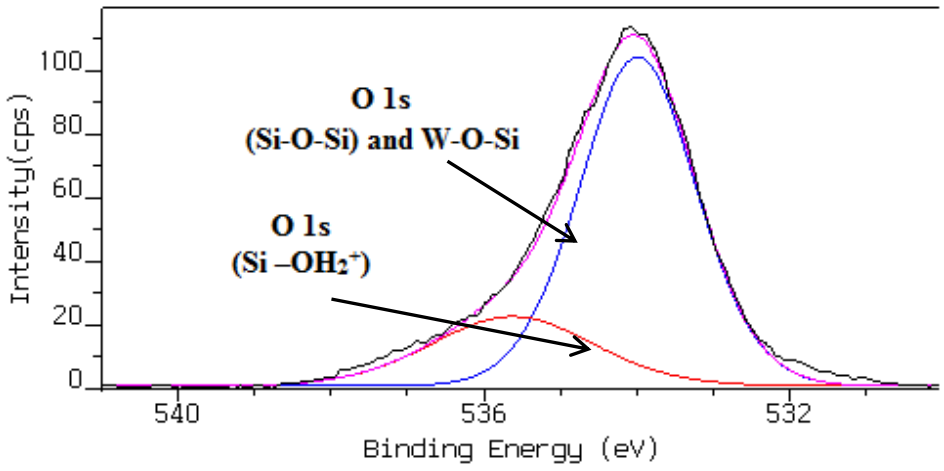


Figure 5(a). Narrow scan for O1s of STSG

Figure 5(b) shows XPS narrow scan for Si2p of STSG and found that Si2p binding energy of STSG, 103.0 eV and 104.1 eV. The Si2p binding energy, 103.0 eV corresponds to the Si in the matrix SiO_2 while 104.1 eV correspond to the appearance of $SiOH_2^+$.

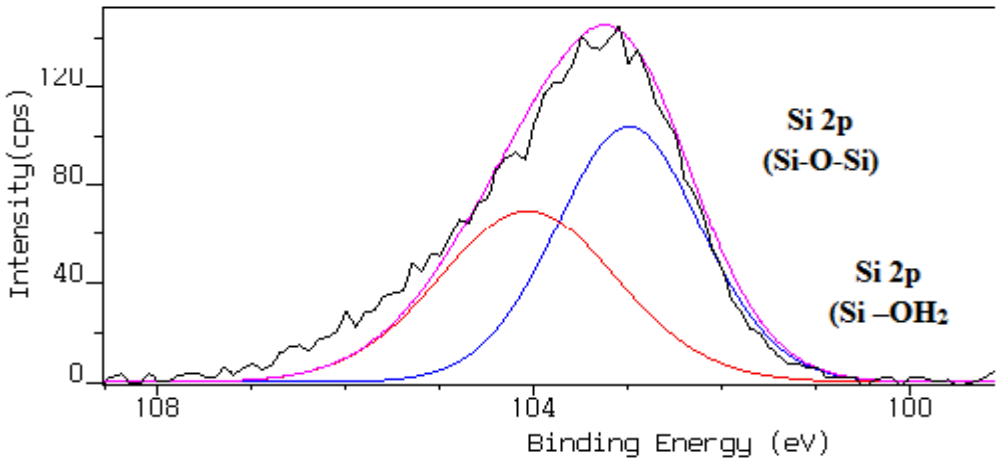


Figure 5(b). Narrow scan for Si2p of STSG

Figure 5(c) shows XPS narrow scan for W4f of STSG. Found that W4f binding energy corresponds to two different W contributions, a spin doublet at 35.9 eV ($W4f_{7/2}$) and 37.6 eV ($W4f_{5/2}$) respectively. The binding energy 37.6 eV corresponds to the formation of an oxide, WOx.

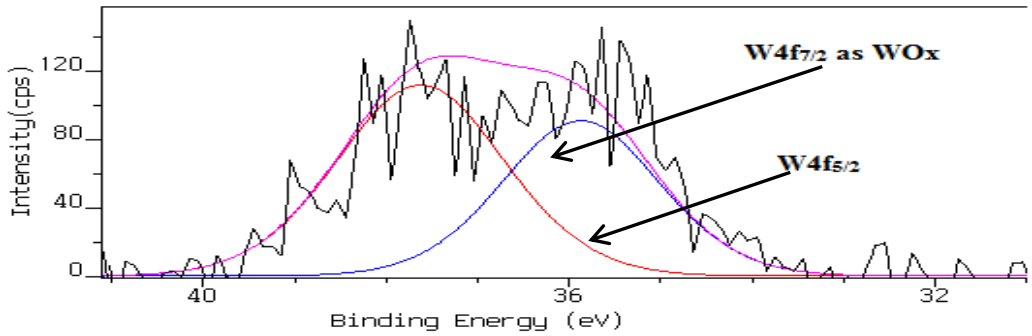


Figure 5(c). Narrow scan for W4f of STSG

FTIR spectroscopy of alkylpolyglucosides.

Ether linkage formed as condensation among OH groups of trehalose and decanol happend. This showed by existence of prominent band at wavenumber 1034-1051 cm^{-1} for the ether linkage (C-O-C), while at 3391 cm^{-1} for the OH bond, 2924-2855 cm^{-1} for CH bond in $–CH_2$ or $-CH_3$, 1458 cm^{-1} for $-CH_2$, 1378 cm^{-1} for CH_3, and 721 cm^{-1} for $(CH)_2$ as shown in Figure 6.

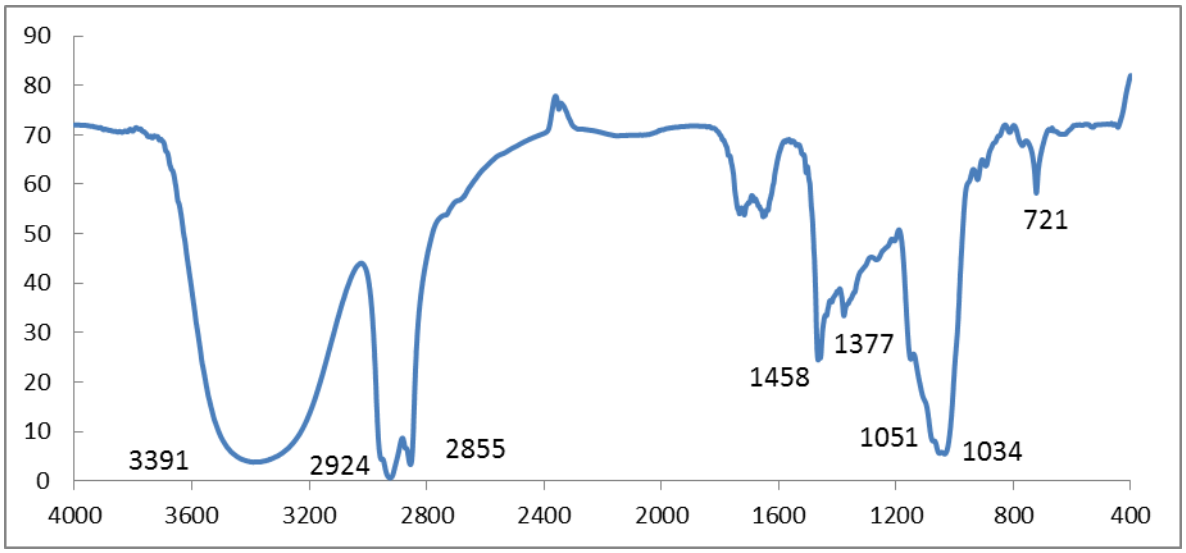


Figure 6. FTIR spectroscopy spectra of alkylpolyglucosides

NMR spectroscopy of alkylpolyglucosides.

Figure 7(a) shows the ^{1}H-NMR spectrum. It showed protons of the alkyl CH_3 groups (t, 3H, CH_3 $(CH_2)_9$), at δ = 0.85 ppm, the CH_2 protons of alkyl chain (16H, CH_3-$(CH_2)_8$) dominated the spectrum at δ = 1.24- 1.52 ppm. The protons of the hydroxyl groups (OH) of dextrose are found at δ = 4.3 ppm. The alkyl CH_2 protons attached to dextrose (m, 2H, O-$CH_2(CH_2)_8$), are found at δ = 3.35 ppm and CH protons of the dextrose moieties are found as multiplet at δ = 3.38 ppm.

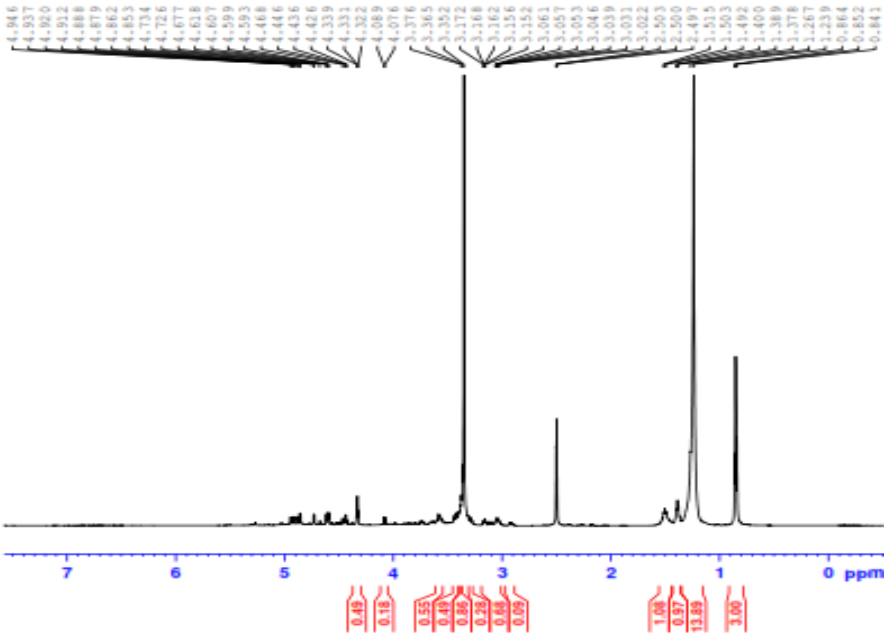


Figure 7(a). ^{1}H NMR spectroscopy spectrum of alkylpolyglucosides

Figure 7(b) shows the ^{13}C-NMR spectrum. It showed the terminal CH_3 are found at δ = 14 ppm, the methylene carbons are found between δ = 22 ppm and δ = 33 ppm, the peak at δ = 61 ppm is carbon atom of CH_2OH (of glucose ring). The remaining peak at δ = 67- 77 ppm are the carbon atom of CH-O which directly attached to the dextrose ring and the carbon atoms of the dextrose ring, with the exception of the anomeric carbon. Anomeric carbon attached to two oxygen atoms and deshielded at δ = 99 ppm and δ = 103 ppm, each for α- and β-anomer respectively.

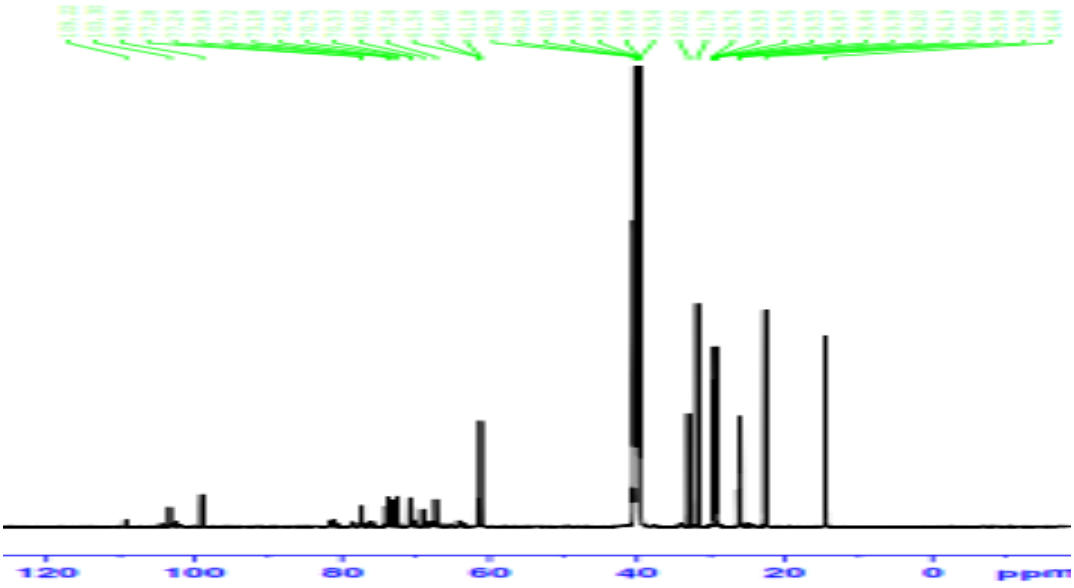


Figure 7(b). C^{13} NMR spectroscopy spectrum of alkylpolyglucosides

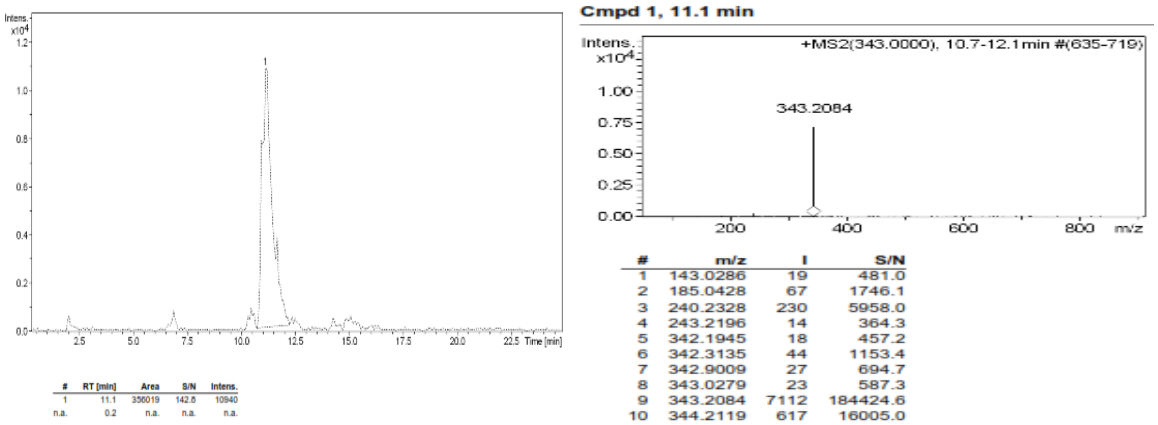


Figure 8. LC/ ESI-MS-MS (ToF) chromatogram of decylmonoglucoside

LC/ESI-MS/MS of alkylpolyglucosides

Alkylpolyglucosides were characterized by positive-mode LC/ESI-MS/MS (ToF) spectra. Alkylpolyglucosides was identified by their protonated molecules, the m/z value of the adduct ions $[M + Na]^+$. At retention time 11.1 min corresponding to alkylmonoglucosides, m/z = 343.21 as $[M+Na]^+$. The mass spectrum confirms the structure based on the proposed fragmentation mechanism pathway. Mass spectrum of alkylpolyglucosides is shown in Figure 8. Molecular ion peak at m/z 343.2 correspond to the protonated parent ions $[M+ Na]^+$, which confirmed the structure as decylglucoside. Elimination of one proton generated positive ions at m/z 342.9. Elimination of C_nH_{2n} and one protons generate the positive ions at m/z = 243.2, followed by elimination of three protons to give the positive ions at m/z = 240.2. Elimination of O-C_nH_n generated the ions at m/z = 185.0 and elimination of two molecule water and 6 protons generated positive ions at m/z =143.0. Figure 9 shows the proposed fragmentation mechanisms pathway of decylpolyglucoside [1].

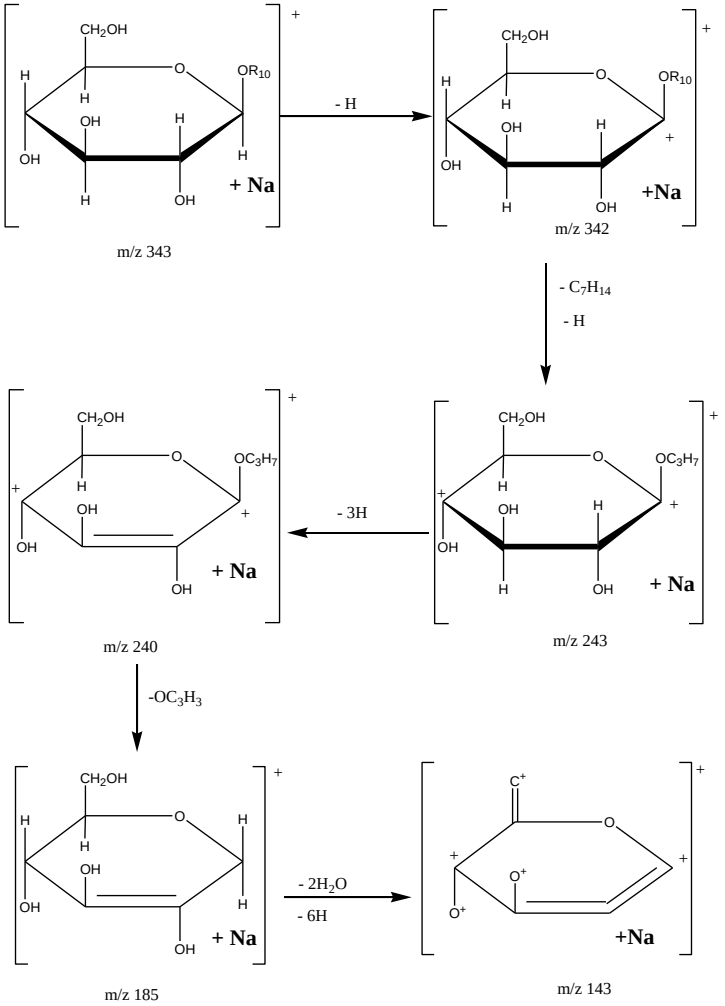


Figure 9. Proposed fragmentation mechanism pathway of decylglucoside

Conclusion

From this study, showed that the silicotungstic acid sol-gel (STSG) catalyst prepared by sol-gel technique has a catalytic activity as well as can be used as a catalyst to prepare alkylpolyglucoside by glycosidation, without the need of a further neutralization and separation process. This sol-gel catalyst can be applied as an alternative heterogenous catalyst instead of using homogenous acid catalyst. Decylglucoside, m/z = 343.2 as $[M+Na]^+$ have been successfully synthesis from dextrose and decanol in the presence of silicotungstic acid sol-gel (STSG) catalyst.

Acknowledgement

The authors thanks to National University of Malaysia (UKM) for funding this project under grant number UKM-GUP-NBT-08-27-109, UKM-GUP-BTK-08-14-306 and OUP-2012-138 and to Centre for Research and Instrumentation Management (CRIM-UKM) for FT-NMR, LC/ESI-MS/MS (ToF), XRD and XPS spectrometer analysis.

References

1. J. Zembrzuska, A. Zgola-Grzeskowiak, M. Franska, (2005). "Alkali Metal Cationization of Alkyl glucosides under Electrospray Ionization Conditions". *Tenside Surf. Det*. 42 Pt 4, 226 – 228.
2. B. Roy, B. Mukhopadhyay, (2007). "Sulfuric acid immobilized on silica: an excellent Fischer type glycosylation". *Tetrahedron Letters*. 48, 3783 – 3787.
3. A. Corma, S. Iborra, S. Miquel, J.Primo, (1996). "Preparation of Environmentally Friendly Alkylglucoside Surfactants Using Zeolites as Catalysts". *Journal of Catalysis*, 161, 713 – 719.
4. S. Shanmugam, B. Viswanathan, T.K. Varadarajan, (2011). "Esterification by solid acid catalysts - a comparison". *Journal of Molecular Catalysis A: Chemical*, 223, 143 – 147.
5. Z. Yang, L. Niu, X. Jia, Q. Kang, Z. Ma, Z.Lei, (2011). "Preparation of silica-supported sulfate and its application as a stable and highly active solid acid catalyst". *Catalysis Communications*, 12, 798 – 802.
6. F. M. Moghaddam, M. Akhlaghi, L. Hojabri, M.G. Dekamin, (2009). "A New Eco-Friendly and Efficient Mesoporous Solid Acid Catalyst for the Alkylation of Phenols and Naphthols Under Microwave Irradiation and Solvent-Free Conditions". *Transactions C: Chemistry and Chemical Engineering*, 16, 81 – 88.
7. M.A. Camblor, A. Corma, S. Iborra, S. Miquel, J. Primo, S.Valencia, (1997). "Beta Zeolite as a Catalyst for the Preparation of Alkyl Glucoside Surfactants: The Role of Crystal Size and Hydrophobicity". *Journal of Catalysis*, 172, 76 – 84.
8. A. Corma, S. Iborra, S.Miquel, J. Primo, (1998). "Preparation of Long-Chain Alkyl Glucoside Surfactants by One-Step Direct Fischer Glucosidation, and by Transacetalation of Butyl Glucosides, on Beta Zeolite Catalysts". *Journal of Catalysis*, 180, 218 – 224.
9. M.J. Climent, A. Corma, S. Iborra, S. Miquel J. Primo, and F. Rey, (1999). "Mesoporous Materials as Catalysts for the Production of Chemicals: Synthesis of Alkyl Glucosides on MCM-41". *Journal of Catalysis*, 183, 76 – 82.
10. J. Chapat, A. Finiels, J. Joffre, C. Moreau, (1999). "Synthesis of Butyl-α and β-D-Glucopyranosides in the Presence of Dealuminated H–Y Faujasites: Kinetic Study, Mechanism, Stereoelectronic Effects, and Microreversibility Principle". *Journal of Catalysis*, 185, 445 – 453.
11. Y. Wu, G.Y. Jiu, F.M. Xiao, S.Z. Jian, (2007). "An efficient and facile procedure for synthesis of of octyl polyglucoside". *Chinese Chemical Letters*, 18, 1173 – 1175.
12. W.von. Rybinski and K. Hill, (1998). "Alkyl Polyglycosides - Properties and Applications of a new Class of Surfactants". *Angew. Int. Ed*., 37,1328 – 1345.
13. M.M.A. El-Sukkary, N.A. Syed, I.Aiad, and W.I.M. El-Azab, (2008). "Synthesis and Characterization of some Alkyl Polyglycosides Surfactants". *Journal of Surfactant Detergent*, 11, 129 – 137.
14. T. Benvegnu, D. Plusquellec and L. Lemiegre in: Surfactant from Renewable Sources: Synthesis and Applications, edited by M.N. Belgacem and A.Gandini, Monomers, Polymers and Composites from Renewable Resources, chapter, 7; Elsevier (2008).

The Malaysian Journal of ANALYTICAL SCIENCES ISSN 1394-2506

PHASE BEHAVIOR AND RHEOLOGY OF FATTY ALCOHOL SULPHATE, FATTY ALCOHOL ETHER SULPHATE FROM PALM BASED AND MIXTURES WITH OTHER SURFACTANTS

(Kelakuan Fasa dan Reologi Lelemak Alkohol Sulfat, Lelemak Alkohol Eter Sulfat Berasaskan Sawit dan Campuran dengan Surfaktan Lain)

Liew Kin Hong, Nur Syazani Harun, Mohd Suzeren Md Jamil, Rahimi M. Yusop*

School of Chemical Science and Food Technology, Faculty of Science and Technology
Universiti Kebangsaan Malaysia, 43600 Bangi, Selangor, Malaysia

**Corresponding author: rahimi@ukm.my*

Abstract

The phase diagrams of fatty alcohol sulphate (FAS)/ fatty alcohol ether sulphate (FAES)/soap (4.5:4.5:1.0)/propylene glycol/water mixtures were established at 60˚C. The birefringence was observed under cross polarisers and their phases changes examined under a polarized microscope. The results showed that the liquid crystalline region for FAS and FAES occurred only in a small region. The optical patterns of lamellar liquid crystal were identified as oily streaks structure. The rheological tests of lamellar liquid crystal were carried out in the region of 4.5/4.5/1 FAES/FAS/soap with 0% PG and 10% of water. The rheological tests used were flow curve, 3 interval thixotropy test (3ITT), oscillation (dynamic test) stress sweep test and frequency sweep test measurement done using a cone-plate sensor (25mm, 1^{o}). The flow curve was fitted to a Casson model to obtain values for the consistency coefficient and the flow behavior index. The lamellar liquid crystal show typical flow behavior and stress influenced the recovery of the structure. Linear visco-elastic (LVE) range analysis show the critical stress value at 0.475%, and elastic modulus was dominant over an angular frequency range studied.

Keywords: Lamellar liquid crystal, FAS, FAES, ternary phase diagram, rheology

Abstrak

Gambarajah fasa campuran lelemak alcohol sulfat (FAS)/lelemak alcohol eter sulfat (FAES)/sabun (4.5:4.5:1.0)/propelina glikol/air telah dibina pada suhu 60^{o}C. Dwibiasan telah diperhatikan melalui pengutub bersilang manakala perubahan fasa telah dikaji dengan menggunakan mikroskop berkutub. Keputusan menunjukkan hablur cecair bagi FAS dan FAESterbentuk pada kawasan yang kecil. Ciri optikal bagi hablur cecair lamella didapati mempunyai struktur carikan berminyak. Kajian reologi yang dijalankan seperti lengkuk aliran, tiksotropi 3 tahap (3ITT), tegasan perubahan dan frekuensi perubahan di ukur dengan menggunakan gelendung (25mm, 1^{o}). Lengkuk aliran dibina berdasarkan model Casson untuk memperolehi nilai koefisien dan indek lengkuk aliran. Struktur hablur cecair lamella menunjukkan kelakuan aliran dan tegasan mempengaruhi pembentukan semula strukturnya. Julat visko-elastik linear (LVE) menunjukkan nilai nilai tegasan kritikal pada 0.475%, dan modulus elastic dominan terhadap frekuensi yang dikaji.

Kata kunci: Hablur cecair lamella, FAS, FAES, gambarajah fasa tenari, reologi

Introduction

Soap and anionic surfactants have traditionally been the major constituents in many cleaning agents [1]. Fatty alcohol sulphates and fatty alcohol ether sulphates derived from palm oil were produced from Chemiton technology in Malaysian Palm Oil Board (MPOB). Preliminary pilot plant trials for these surfactants showed low activity and therefore the two surfactants were mixed to obtain a synergistic effect in their properties. Many other works on other mixtures have shown the advantages of using mixed surfactants in terms of enhancing the performance of

single surfactants [2-6]. To further understand the physico-chemical behaviour of surfactants systems, a study of ternary phase system was carried out to identify the contribution of the different components to a formulator for developing new products [7]. The phase behaviour and other properties of mixed surfactants have been carried out by Hofman et al. [8-10]. The mesophase change can be described from phase diagrams. The type of liquid crystal has a major influence on product properties. About seven different classes of liquid crystals have now been recognised, the major ones being lamellar, hexagonal, cubic, nematic and gel phase [11]. Surfactant liquid crystal is commonly used in products such as detergents, shampoos, and household cleaners [7].

Mixtures of anionic and nonionic surfactants are used in products such as laundry detergents, dishwashing detergents and cleaners. The phase behavior and rheological properties of these mixtures play an important role in the formulation and use of product. The phase behavior of surfactant systems is also a crucial factor in the production of product and in the choice of emulsifiers [12]. Investigation has already been conducted on the phase behavior of many commercially interesting individual surfactants [13] and mixtures [14].

Rheology is the study of the deformation and flow of matter. Solids and fluids exhibit different flow behaviors under shear. Solid store mechanical energy and are elastic, whereas fluids dissipate energy and are viscous. Knowledge of the complete flow and viscosity curve over a broad shear rate range is crucial for practical application whereas knowledge of the viscoelastic properties which can be determined by dynamic oscillating experiments is useful for elucidating structure effect principles in surfactants-containing formulation [13,15]. The characteristics and concentrations of surfactants are important factors affecting the structure and the rheological properties [16]. There has been no known systematic investigation into the rheological properties of lamellar liquid crystals. However, investigations into shear viscosity and its dependence on temperature have been published [17]. The rheological properties, in addition to characteristics and concentration of the surfactants, are affected by the interfacial rheology of the surfactants film, volume fraction of the disperse phase, viscosity of disperse droplets, droplets size distribution as well as viscosity and chemical composition of the medium [18]. The viscoelastic properties provide a deep insight into structural and dynamic aspect of structure systems. Besides characterizing the optically anisotropic liquid crystalline range, dynamic oscillating experiments are also able to describe the optically isotropic regions, which cannot be detected by polarization microscopy, such as viscoelastic networks of rod micelles or cubic gel phases [19]. The aim of this work is to identify the phase behaviour in ternary system using FAES/FAS /soap (4.5:4.5:1.0)/PG/ water mixtures and rheological properties of lamellar liquid crystal.

Materials and Methods

Materials

FAS and FAES were obtained from Advanced Oleochemical Technology Centre (AOTC), Malaysian Palm Oil Board (MPOB). The specification of these compounds is shown in Table 1. Soap was obtained from Unichema Sdn. Bhd. and its specification as shown in Table 2. Propylene glycol (PG) was 99% purity. These materials were used without further purification.

Table 1. Specification of FAS and FAES

Properties	FAES	FAS
Active	27.37 %	27.65
Unsulphonated matter	0.32%	0.74%
Moisture	68.62%	71.77%
Color	0.4 R,	2.0 R,
Petroleum ether extraction	3.7 Y	10.0 Y
PH (10%)	-	1.13%
	-	9.61

Table 2. Specification of soap

Properties	
Total fatty matter %	9-81
Moisture %	10.5-12.5
Free fatty acids %	1.3 max
Sodium chloride %	0.4-0.6
Glycerol %	0.1-0.2
Sequestrants	Present
Typical titer (Fatty acids) deg. C	44-47

Phase diagram

Phase diagram of FAES/FAS/soap (4.5:4.5:1.0)/PG/water mixtures were prepared at 60˚C (to dissolve the soap component). 0.5g mixtures was placed in a test tube. Approximately 0.5% (total mixtures) deionised water was added into the mixture and homogenized at 4000 rpm for 15 minutes (Jouan CR3I) to homogenate and eliminate the air bubbles. Each sample was centrifuged for at least 3 times. The sample was then allowed to equilibrate in water bath at 60˚C for at least 15 minutes. Then the phases were identified by visual observation between polarized film and crossed polarizing microscope in combination with a heating stage (Olympus AX70). More water was added to the test tube and the procedure repeated.

Rheology

Rheological properties were determined using a MCR 300 rheometer equipped with US 200 software. The cone-plate module with 25 mm in diameter and cone angle of 1° was used. Measuring temperature was maintained at 60.00±0.01°C by a Peltier Plate temperature controller (Model Viscotherm VT2). The tests perform were flow curve, 3-interval thixotropy test (standard test rotational), oscillation stress sweep test and frequency sweep test. The flow curve was fitted to a Casson model because it gives the lower standard deviation (±2.66) compared with Bingham, instead the result cannot be calculated by Herschel-Bulkley model.3ITT test was used to determine how far the structure of a material can be re-built after shear or how long time the recovery takes. To be able to do this, the sample is measured with a three-interval test: rest-shear-rest. The first and the third interval usually have identical measurement parameters. The first interval is necessary to obtain a reference value for sample properties at rest (1Pa), during the second interval the material is sheared (50Pa, 75Pa and 100Pa) and the third interval (1Pa) the recovery of the structure can be observed. The calculate structure recovery after is a method that used for calculation of recovery interval. This method calculates the degree of recovery by comparing the viscosity after a selected period with the value at the end of the rest interval. The structure recovery is given in percent.

Dynamic test

In the oscillation stress sweep the stress was increased from 0.1 to100 Pa and the frequency was kept constant (1 Hz). The linear viscoelastic region of each sample was determined with oscillation stress sweep test. In the linear viscoelactic region the ratio of stress and strain is a function of time alone [20]. Small-amplitude, oscillatory frequency sweep were conducted using a constant applied strain of 0.1% over a angular frequency range 0.1-100 $rads^{-1}$. The strain amplitude was found to be within the LVE range for the samples tested.

Results and Discussion

Phase diagram

The ternary system of FAES/FAS/ water is plotted at 60°C. Using the same ratio at equal amount of FAES and FAS, soap was added. The ratio of this study was 4.5:4.5:1.0 of mixed FAS, FAES and soap respectively as shown in Figure 1. Result showed that the LC region formed at 100% FAS/FAES with soap in 4% to 14% water. The phase transition results are summarized in Table 3. The optical patterns of LC are observed as shown in Figure 2. The texture of lamellar liquid crystal obtain was comparable with literature [7, 8].

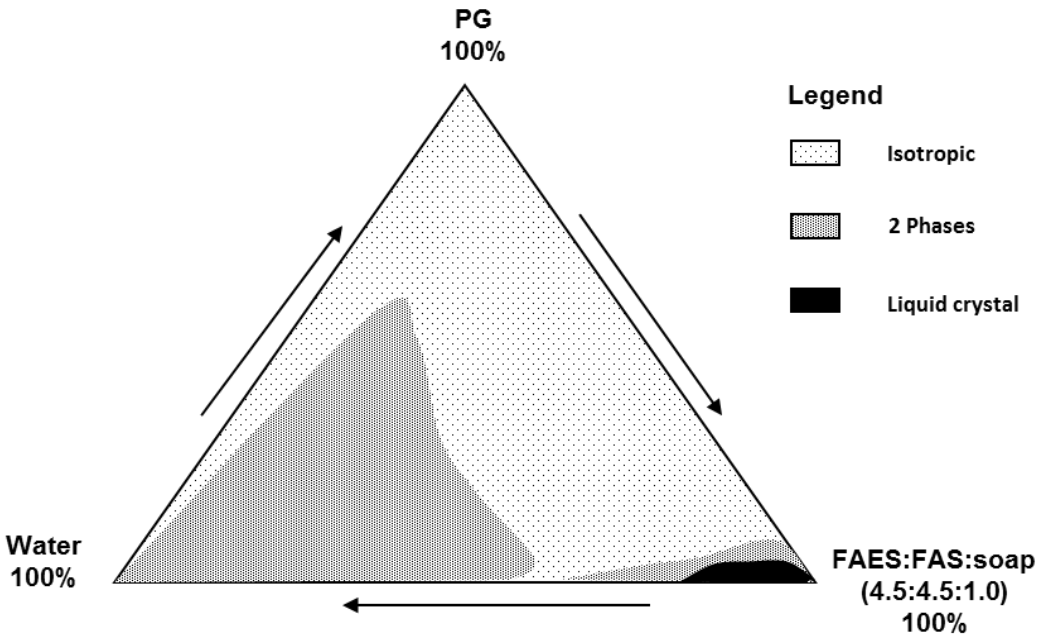


Figure 1. Phase diagram of (FAES:FAS:soap)/PG/water at 60^0C

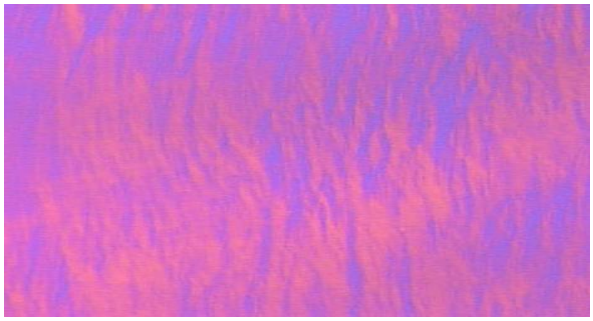


Figure 2. Optical pattern of oily streaks textureof 4.5/4.5/1 FAES/FAS/soap with 0% PG and 10% of water, 100x magnification.

Flow curve

The flow behavior of liquid crystal can be described by flow or viscosity curve. In flow curves, the shear stress of a sample is plotted against the shear rate which produces shearing. The Casson equation describes the flow curve of a material with yield stress and a non-newtonion behavior at stress above the yield stress. It often provides a good fit for blood and for food product. The yield stress is given as the analysis result. As seen in Figure 3, shear stress as a function of the shear rate and the consistency curve for a pseudoplastic material with low yield stress (1.5376E-6 Pa). Yield stress is a minimum stress to make substance flow. At stress below the yield stress, the substances act as an elastic material. The shear stress of a pseudoplastic substance increase with increasing shear rate. The curved rheogram for pseudoplastic materials results from a shearing action on the long-chain molecules of materials such as linear polymers. As the shearing stress is increased the normally disarranged molecules begin to align their long axes in the direction of flow. This orientation reduces the internal resistance of the material and allows a greater shear rate at each successive shear stress [21].

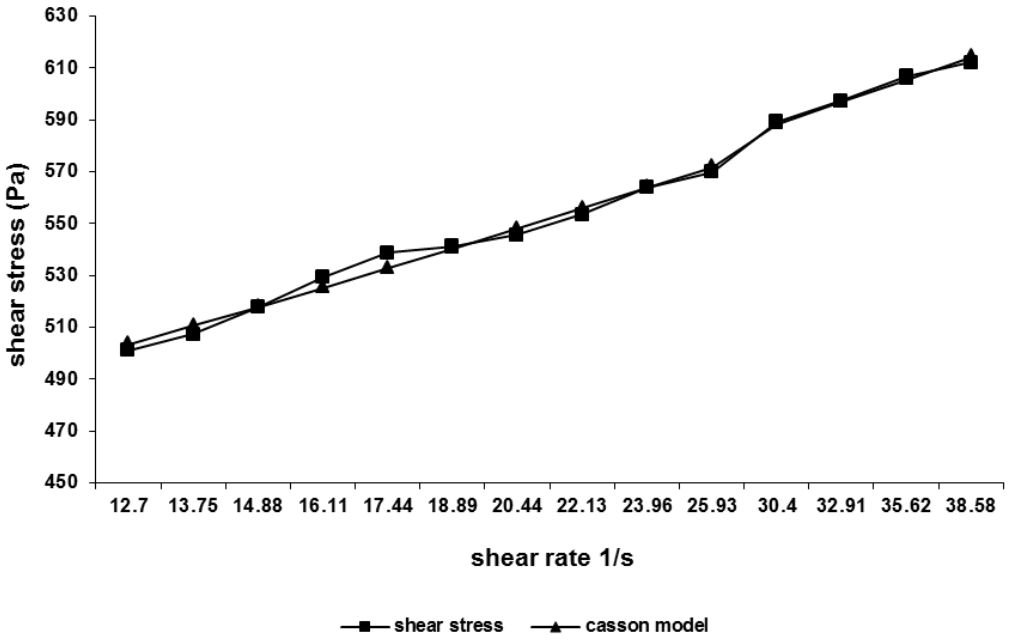


Figure 3. Flow curve of liquid crystal of 4.5/4.5/1 FAES/FAS/soap with 0% PG and 10% of water.

Thixotropic

Figure 4 shows the results of 3ITT for the sample, which is, differ by load interval 50 Pa, 75 Pa, 100 Pa respectively. The calculation for recovery was compared with the value at the end of the rest interval and the value at the end of recovery interval (100 seconds after stress). The recovery after stress is 51.57%, 48.10% and 46.16% of 50 Pa, 75 Pa, and 100 Pa respectively. At load interval, there was a significant difference between 3 stress-applied show the viscosity was decreased with stress. The consequences by load influenced the structure recovery, which indicates low recovery after high stress.

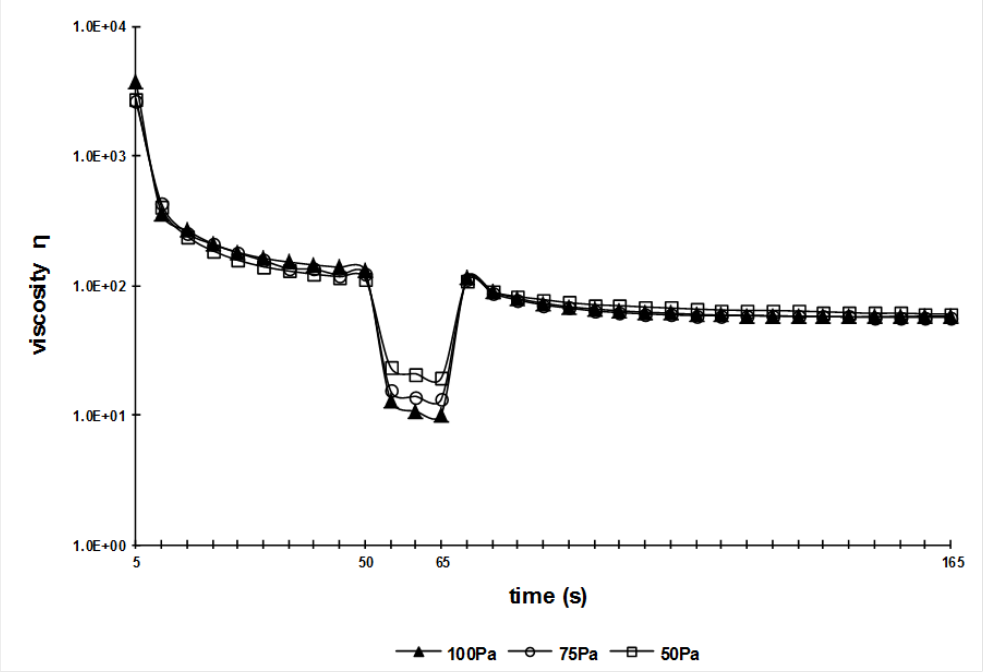


Figure 4. 3 Interval Thixotropy Test of liquid crystal of 4.5/4.5/1 FAES/FAS/soap with 0% PG and 10% of water at stress of 50Pa, 75Pa and 100Pa.

Stress sweep

In order to determine the strain amplitude range over which linear visco-elastic (LVE) prevails, stress sweep experiments were carried out at a frequency of 1 Hz in the overall strain amplitude of 0.1%-100%. Figure 5 shows a linear of the storage modulus G′ and loss modulus G″ at low strain, followed by a sharp decrease when the system passes from linear to nonlinear viscoelastic regime. The G′ and G″ started to decrease continuously at slightly higher strain amplitudes. That point is called critical strain. The critical strain characterizing the limit of the LVE regime. The critical strain at 0.475%, and 0.1% strain were used in the frequency sweep as suggested by the LVE range analysis. The lamellar liquid crystal had the low critical stress and the optical microphotographs show a clearly weak structure (Figure 2). In the theory of LVE, the relevant equations are linear differential equations and the coefficients of the time differential are constants, i.e. are material constant. Leaving this LVE range by selecting higher amplitudes and consequently higher stress means no accountable deviation for the measured data of the materials tested linked to the chosen test parameter and the instrument used. Under these conditions the sample is deformed to the point that the internal temporary bonds of molecules or of aggregates are destroyed.

Frequency sweep

Having determined the amplitude that keeps test of a particular sample safety within the LVE region, one can then proceed with further test using the frequency sweep to measure the sample's visco-elastic behavior and predict the storage stability of suspensions. This necessitates using low-deformation oscillatory measurements. The data obtained hold valuable information about the particle-particle interaction. Figure 6 show the frequency dependence (rad/sec) of the viscoelastic parameters, G′ and G″. The results show the elastic or storage modulus, G′, is the dominant response over the frequency range investigated. At low frequencies the sample are elastic, i.e., the storage modulus G′ is higher than the loss modulus G″, the phase angle is below 45°. At high frequencies, the samples are also elastic but showed greater deviation. The G′ and G″ values show a small frequency dependant over the frequency range. These are characteristics of a strongly associated, but stable viscoelastic liquid crystal.

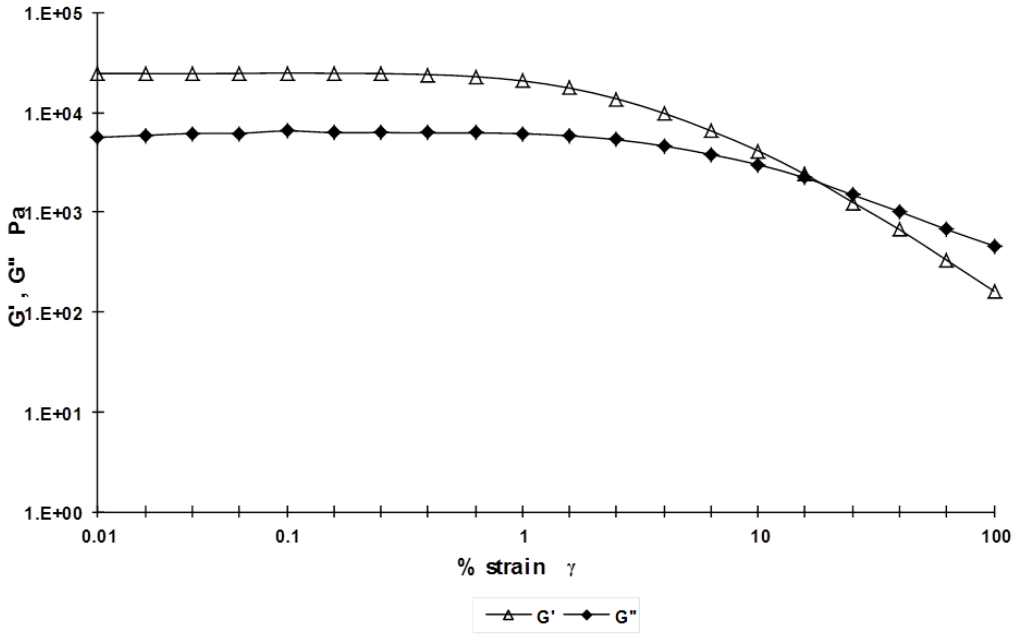


Figure 5. Dynamic stress sweep of liquid crystal of 4.5/4.5/1 FAES/FAS/soap with 0% PG and 10% of water at 1Hz

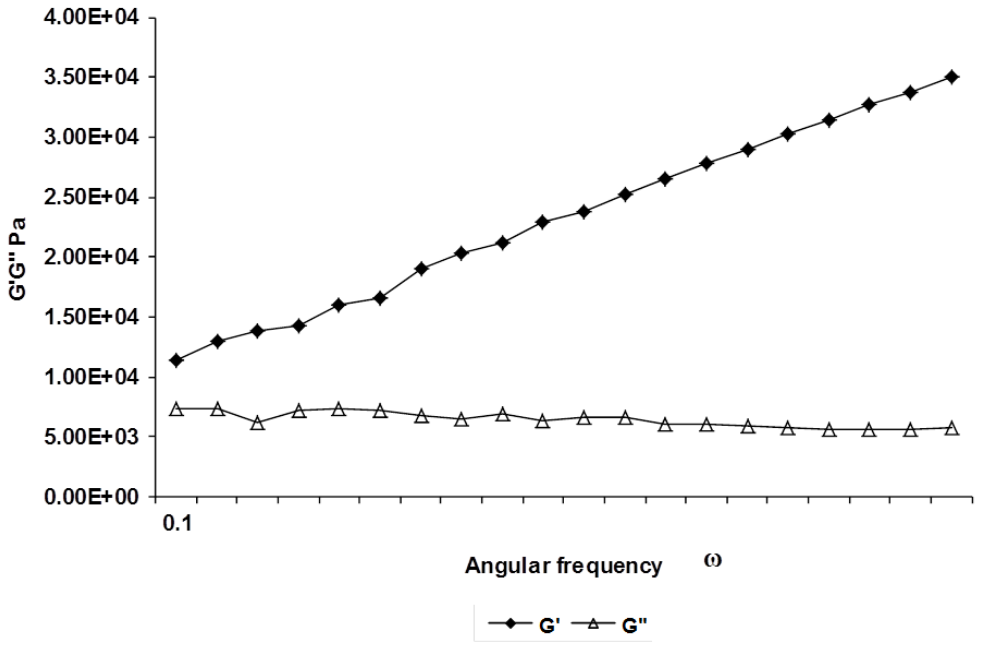


Figure 6. Dynamic frequency sweeps of liquid crystal of 4.5/4.5/1 FAES/FAS/soap with 0% PG and 10% of water at 0.1% strain.

Conclusion

In conclusion, the phase diagrams of fatty alcohol sulphate /fatty alcohol ether sulphate/soap /propylene glycol/water mixtures were established at 60˚C. The results showed that the liquid crystalline region for FAS and FAES occurred only in a small region and the optical patterns of lamellar liquid crystal were identified as oily streaks structure. The rheological tests show typical behavior of liquid crystal and it is very useful to be used in development of household products.

Acknowledgement

This work was supported financially by the Government of Malaysia grant no. GGPM-2012-010, FRGS/1/2012/ST01/UKM/02/1, GUP-2012_070. We are grateful to Abd Halim for his helpful advice regarding the rheology measurement.

References

1. Lynn, J. 1991. *Detergency.* John Wiley & Sons, New York: 1072-1117.
2. Scamehorn, J.F., & J.H. Harwell. 1993. *Precipitation of Surfactant Mixtures, in Mixed Surfactant systems*, . New York: 283-312.
3. Scamehorn, J.F.1986. *An overview of Phenomena Involving Surfactant Mixtures, in Phenomena in Mixed Surfactants Systems*: 1-27 .
4. Cheryl, H., Rodriguez, Chanin, C., Scamehorn, J.F., Chintana, S., and Sumaeth, C.1998. Precipitation in Solutions Containing Mixtures of Synthetic Anionic Surfactants and Soap. *J. Surf. Det.* 1: 321-325.
5. Michael F. Cox, Nelson F. Borys and Ted P. Matson.1985. Interactions between LAS and Nonionic Surfactants. *J. Am. Oil Chem. Soc*. 62:1139-1143.
6. Scamehorn, J.F., and J.H., Harwell.1993. Precipation of surfactants mixtures, in Mixed Surfactant Systems, edited by K.Ogino and M. Abe, Marcel Dekker, Inc., New York: 283-312.
7. Comellas, F., Megias, V., Sanches, J., Parra, J.L., Coll, J., Ballaguera, F. and Pelejero, C. 1989. Applications of ternary systems in specific cosmetic formulation. *Int. J. of Cosmetic Sci*. 11: 5-19.
8. Hauthal, H.G. 2001. *48th SEPAWA Congress 2001, J. Applied Sci.* 127: 8-12.
9. Caroline. 1999. *Liquid crystal in cosmetic emulsion*, Personal Care Ingredients Asia, Step publishing limited: 120-129.
10. Nielsen, M., Drews, B. 2001. Lamellar liquid crystals in o/w cosmetic emulsion. *Int.l J. Applied Sci.* 127: 8-12.
11. Hauthal, H.G. 2001. Würzburg conference-Progress on Detergents, Würzburg conference-Progress on Detergents, *Int. J. Applied Sci*. 127: 8- 12.
12. Foster, T.H., Rybinski, V,W., Wadle, A. 1995. *Advanced Colloid Interface Sci*.: 119-120.
13. Hofmann, R.; Nickel, D., VonRybinski, W. 1994. Interfacial properties and phase behaviour of fatty acid alcohol sulphate, Tenside Surf. Det. 31:63-67.
14. Friberg, S. E., Chiu, M. 1992. Rheology of surfactant system. *J. Am. Oil Chem. Soc*. 69: 653-6654.
15. Platz, G.; Pölike, J., Thuning, C., Hofmann, R.; Nickle, D., von Rybinski, W. 1995. Phase behavior of anionic surfactants. *Langmuir*. 11:4250.-4255
16. Korhonen, M., Hellen, L., Hirvonen, J. 2001. Rheological properties of creams with four different surfactant combinations-effect of storage time and conditions. *Int. J. Pharm*. 221: 187-196.
17. Oswald P. and Allain M. 1988. Surface tension of surfactant system. *J. Coll. Interface Sci*.: 126:45-49.
18. Tadros, T.F.1994. Fundamental principles of emulsion rheology and their applications. *Colloid. Surf. Physicochem. Eng. Aspects*: 39-55
19. Hofmann, R.; Moser, J.; VonRybinski. 1997. W. Phase behaviour and rheology of fatty alcohol sulphate and mixtures with other surfactants. *Henkel-Referate.* 33:22-28.
20. Kobayashi,M.,Ishikawa, S., Samejima, M. 1982. Application of nonlinear viscoelactic analysis by the oscillation method to some pharmaceutical ointments in the Japanese Pharmacopeia. *Chem. Pharm. Bull*. 30:4468-4478.
21. Gebhard, S. 1994. A Practical Approach to Rheology and Rheometry. Gebrueder Haake: 3-50

The Malaysian Journal of ANALYTICAL SCIENCES ISSN 1394-2506

PENGEKSTRAKAN DAN PENCIRIAN NANOSELULOSA DARIPADA SERABUT KELAPA

(Extraction and Characterization of Nanocellulose from Coconut Fiber)

Nor Liyana Ahmad dan Ishak Ahmad*

Pusat Pengajian Sains Kimia dan Teknologi Makanan, Fakulti Sains dan Teknologi, University Kebangsaan Malaysia, 43600 Bangi, Selangor, Malaysia

**Corresponding author: gading@ukm.my*

Abstrak

Pengubahsuaian kimia telah dijalankan ke atas serabut kelapa untuk mengekstrak nanohablur selulosa daripadanya. Antara rawatan yang dilakukan adalah rawatan alkali, rawatan penambahan peluntur dan akhirnya hidrolisis menggunakan asid sulfurik pekat. Kesan setiap rawatan kimia terhadap serabut kelapa dianalisa menggunakan spektroskopi inframerah transformasi Fourrier (FTIR) dan analisis pembelauan sinar-X (XRD). Seterusnya perubahan morfologi permukaan dikaji menggunakan mikroskop imbasan elektron (SEM) manakala kestabilan terma gentian serabut kelapa dikaji melalui analisis termogravimetrik (TGA). Hasil analisis menunjukkan pengubahsuaian kimia yang dilakukan dapat menyingkirkan hemiselulosa dan lignin daripada serabut kelapa. Analisis XRD juga telah menunjukkan peningkatan kehabluran serabut selepas setiap peringkat rawatan. Nanoselulosa yang terhasil daripada proses hidrolisis menggunakan asid sulfurik dianalisis menggunakan mikroskop transmisi elektron (TEM) bagi mengenal pasti saiz nanoselulosa yang diperoleh. Didapati purata diameter nanoselulosa daripada serabut kelapa adalah 13.7 ± 6.2 nm manakala panjangnya adalah 172.34 ± 8.4 nm. Selulosa nanohablur mempunyai pelbagai potensi dalam aplikasi seperti bioperubatan, jerapan minyak, membran, farmasi dan biokomposit.

Kata kunci: serabut kelapa, nanohablur selulosa, lignin, hemiselulosa

Abstract

Coconut husk fibers has been modified by some chemical treatments to extract cellulose nanocrystals (CNC), which are alkali treatment, bleaching and acid hydrolysis using concentrated sulphuric acid. The effect of the treatments on the coconut husk fibers has been analysed using Fourier transform infrared (FTIR) and X-Ray diffraction (XRD). Meanwhile, the morphology observation and thermal stability of the fiber have been analysed by scanning electron microscopy (SEM) and thermogravimetric analysis (TGA) respectively. The analyses show that the chemical modification could eliminate some of the lignin and hemicelluloses of the fiber. Nanocellulose extracted from acid hydrolysis has been analysed using transmission electron microscopy (TEM) to define the size of extracted nanocellulose. The cellulose nanocrystals from coconut fibre has the average diameter and length in the range 13.7 ± 6.2 nm and 172.3 ± 8.4 nm, respectively. The obtained nanocellulose may have the potential applications in the fields of biomedical, oil adsorption, membrane, pharmaceutical and biocomposites.

Keywords: Coconut husk fiber, cellulose nanocrystals (CNC), lignin, hemicelluloses

Pengenalan

Serabut semulajadi banyak digunakan sebagai bahan penguat dalam komposit polimer kerana ia mudah didapati, murah, menggunakan tenaga yang rendah, boleh diperbaharui dan terbiodegradasi. Kelapa atau nama saintifiknya *Cocos nucifera* berasal daripada famili *Arecacae* (*Palmae*) merupakan antara serabut semulajadi yang mempunyai ketumpatan yang rendah, iaitu antara 1.0 hingga 1.3 g/cm^3 dan terikan yang tinggi iaitu kira-kira 40%. Sifat ini menjadikan ia sesuai digunakan sebagai bahan komposit [1]. Bahan komposit daripada serabut semulajadi juga mempunyai aplikasi yang besar dalam pembuatan barangan kegunaan harian dan seterusnya menjadi pengganti kepada penggunaan gentian kaca. Walau bagaimanapun, terdapat beberapa kelemahan untuk menggabungkan serabut semulajadi dengan polimer yang bersifat hidrofobik, iaitu keserasian antara serabut dan polimer itu sendiri.

Justeru beberapa pengubahsuaian perlu dilakukan ke atas serabut dan polimer untuk meningkatkan kualiti bahan komposit [2].

Selulosa merupakan komponen utama serabut semulajadi seperti flaks, kapas, jut dan tebu. Selain itu, terdapat juga komponen bukan selulosa iaitu hemiselulosa dan lignin. Serabut kelapa mengandungi kandungan lignin yang tinggi berbanding serabut semula jadi yang lain. Walau bagaimanapun penambahan serabut kelapa dalam komposit dapat mengurangkan kadar aliran terma seterusnya menghasilkan bahan yang berketumpatan rendah. Serabut kelapa yang dirawat terlebih dahulu sebelum diadun dengan matriks juga dapat meningkatkan perlekatan antara serabut dan matriks dalam penghasilan komposit [3].

Pengekstrakan nanoselulosa daripada serabut semulajadi semakin mendapat perhatian kerana dapat menghasilkan bahan yang mempunyai sifat mekanik yang tinggi dan nisbah dimensi yang tinggi [4]. Kajian ini dijalankan untuk mengekstrak nanoselulosa daripada serabut kelapa dan mengkaji kesan rawatan kimia yang dijalankan terhadap serabut ini.

Bahan dan Kaedah

Bahan

Serabut kelapa yang digunakan dalam kajian ini diperoleh daripada hasil industri. Bahan kimia yang digunakan terdiri daripada natrium hidroksida (NaOH) dan asid asetik (CH_3COOH) yang dibekalkan oleh Systerm, natrium klorit ($NaClO_2$) daripada Sigma-Aldrich dan asid sulfurik (H_2SO_4) daripada Univar.

Pengekstrakan nanoselulosa

Serabut kelapa yang diperoleh daripada industri dibersihkan dan direndam semalaman untuk menghilangkan bendasing dan kotoran. Kemudian, serabut kelapa dikisar dan ditapis untuk mendapatkan serabut dengan saiz 100-250 µm. Rawatan alkali dijalankan melalui kaedah refluks dengan menggunakan 4% NaOH yang dicampurkan dengan 5% kandungan serabut kelapa daripada jumlah larutan yang digunakan di dalam kelalang dasar bulat. Refluks dijalankan selama 2 jam dengan suhu minyak silikon 90^oC. Selepas refluks, campuran dibasuh dengan air suling sehingga larutan tanpa warna terhasil dan ditapis untuk rawatan seterusnya. Serabut kelapa yang telah dirawat dikeringkan semalaman. Proses rawatan alkali ini diulang sebanyak empat kali.

Seterusnya, serabut kelapa yang telah menjalani rawatan alkali akan mengalami rawatan penambahan bahan peluntur. Proses ini turut menggunakan kaedah refluks tetapi mengunakan tiga jenis larutan yang berbeza, iaitu $NaClO_2$, larutan penimbal CH_3COOH dan NaOH, serta air suling. Campuran yang digunakan untuk penyediaan larutan penimbal ini adalah 2.7 g NaOH dan 7.5 mL asetik asid dalam 100 mL air suling. Larutan penimbal ini seterusnya dicampurkan 1.7%brt $NaClO_2$ dan air suling.

Proses rawatan bahan peluntur menggunakan ketiga-tiga jenis larutan ini dengan isipadu yang sama dan mengikut nisbah serabut kepada larutan adalah 1:20. Proses refluks untuk rawatan bahan peluntur dijalankan selama 4 jam dengan suhu minyak silikon 90^oC. Proses ini diulang sebanyak empat kali sehingga serabut kelapa dilunturkan warnanya kepada warna putih. Serabut yang telah direfluks turut dibasuh dan dikeringkan pada suhu bilik. Serabut yang telah mengalami proses rawatan dan dikeringkan akan dihantar untuk dianalisis.

Pengekstrakan nanoselulosa dijalankan dengan kaedah hidrolisis menggunakan 64 %brt H_2SO_4. Proses hidrolisis ini dijalankan selama 30 minit pada suhu 45^oC sambil dikacau berterusan. Kemudian, campuran diletakkan di dalam bekas berais selama 30 minit sebelum diemparkan. Proses pengemparan dijalankan selama 10 minit pada suhu 10^oC dengan kelajuan 10 000 rpm untuk mengasingkan asid daripada selulosa yang telah diekstrak. Kemudian selulosa dimasukkan ke dalam sel membran dan didialisis dengan air ternyahion sehingga mencapai nilai pH neutral. Larutan juga dihomogenkan menggunakan penghomogen Ultra Turrax T25 sebelum dihantar untuk dianalisis.

Analisis pencirian serabut kelapa

Kajian morfologi permukaan sampel serabut kelapa tanpa rawatan dan yang telah mengalami rawatan alkali dan rawatan pelunturan dianalisis menggunakan mikroskop imbasan elektron (SEM) model Philips XL-series XL-30. Nanoselulosa yang telah diekstrak pula dianalisis menggunakan mikroskop transmisi elektron (TEM) Philips CM12

yang beroperasi pada voltan 3 kV. Sampel nanoselulosa yang telah diletakkan di atas grid kuprum dititiskan dengan 2% uranil asetat akueus dan dikeringkan sebelum dianalisis.

Analisis spektroskopi inframerah transformasi Fourrier (FTIR) dijalankan untuk mengetahui perubahan terhadap kumpulan berfungsi bagi sampel serabut kelapa yang telah dirawat. Analisis dijalankan menggunakan spektrometer Perkin-Elmer (Spektrum GX) pada julat 4000-500 cm^{-1} dengan resolusi imbasan 8 cm^{-1}. Sampel berbentuk serbuk dicampurkan dengan serbuk kalium bromide, KBr, sebelum dianalisis.

Kehabluran sampel serabut kelapa dikenal pasti berdasarkan analisis pembelauan sinar-X (XRD) menggunakan difraktometer model Bruker AXS D8 Advance dengan Cu-Kα (λ=0.5141 nm) pada 40 kV, 40 mA . Data direkod dengan julat 2θ adalah 5 hingga 60 ^{o}C. Peratus kehabluran (I_h) sampel dikira menggunakan kaedah [5] seperti berikut:

$$I_h = \frac{I_{002} - I_{am}}{I_{002}} \times 100$$

di mana I_{002} ialah keamatan maksimum pembelauan pada kekisi (0 0 2) iaitu di antara puncak 22^{o} dan 23^{o}, I_{am} ialah keamatan minimum pada bahagian amorfus sampel iaitu pada puncak 2θ = 18^{o} dan 19^{o}.

Analisis termogravimetrik (TGA) dijalankan menggunakan penganalisa termogravimetrik Mettler Toledo Model TGA/SDTA851 untuk menentukan kestabilan terma serabut kelapa pada keadaan yang berbeza.

Keputusan dan Perbincangan

Gambaran serabut kelapa secara fizikal yang dianalisis dalam kajian ini ditunjukkan dalam Rajah 1. Warna serabut kelapa yang telah dirawat dengan alkali menjadi semakin cerah dan seterusnya berwarna putih setelah rawatan pelunturan dilakukan. Hal ini disebabkan penyingkiran hemiselulosa dan lignin yang berlaku dalam rawatan kimia tersebut. Keadaan ini dapat dibuktikan melalui analisis yang dijalankan dalam kajian ini.



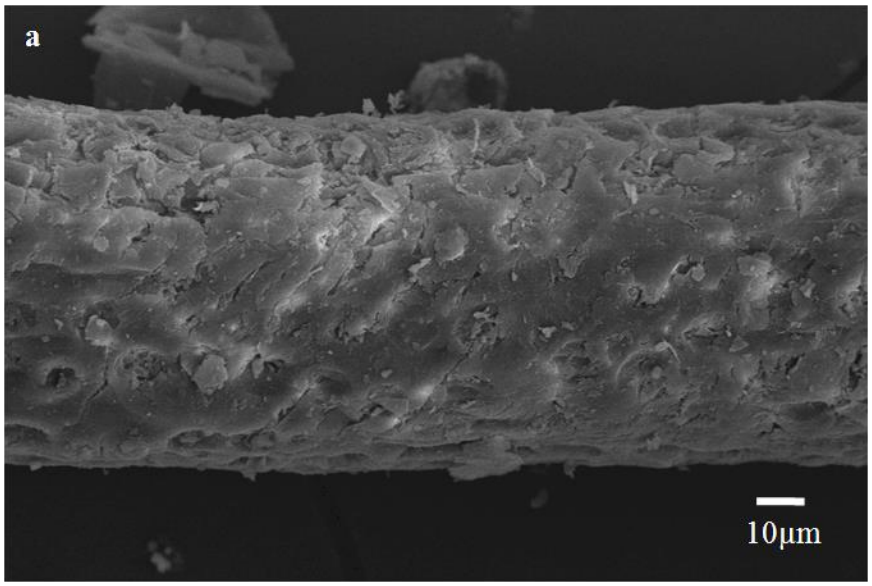
(a) (b) (c) (d)

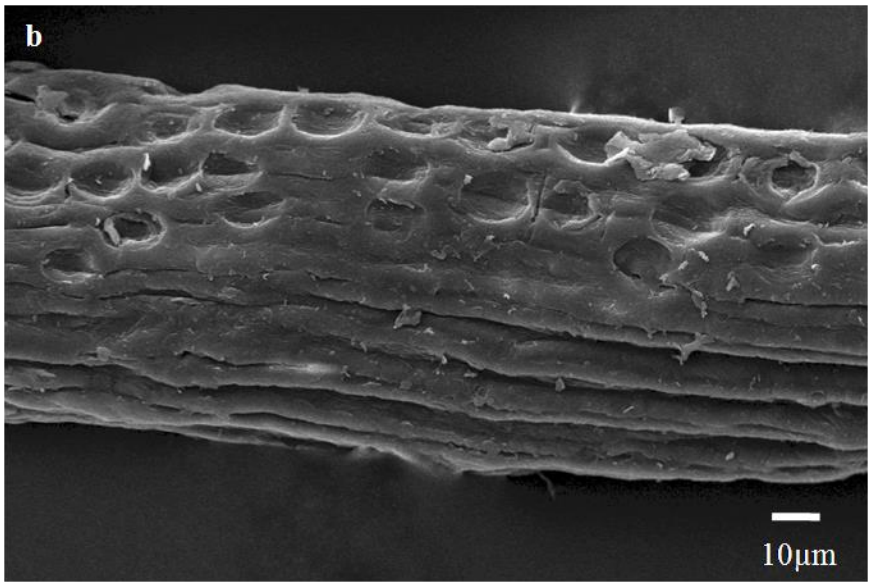
Rajah 1. Gambar serabut kelapa (a) tanpa rawatan, (b) dengan rawatan alkali, (c) dengan rawatan peluntur dan (d) nanoselulosa.

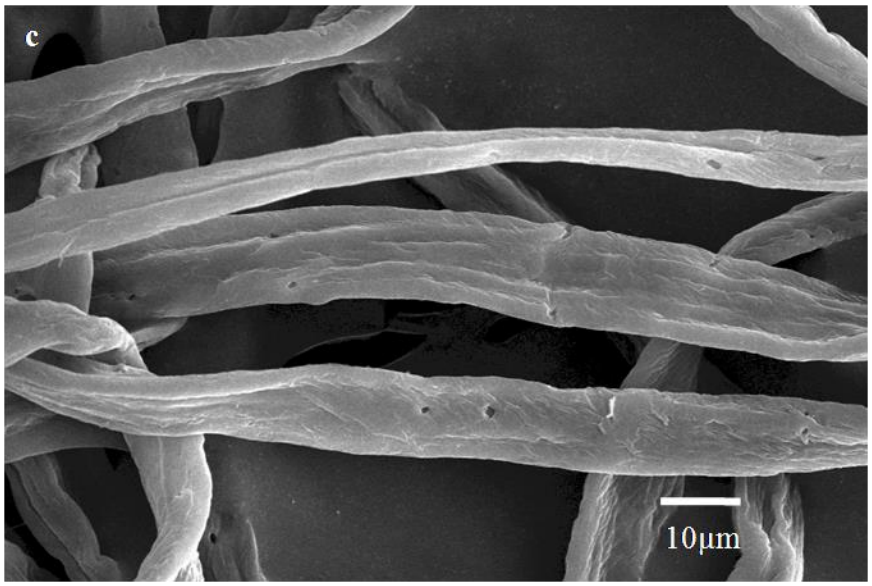
Analisis morfologi permukaan

Pemeriksaan morfologi permukaan serabut kelapa dijalankan menggunakan mikroskop imbasan elektron (SEM) seperti yang ditunjukkan dalam Rajah 2. Permukaan serabut kelapa tanpa rawatan kelihatan tidak sekata dan diselaputi oleh bendasing seperti hemiselulosa, lignin, pektin dan bahan berlilin. Serabut kelapa tanpa rawatan ini juga terdiri daripada fibril yang diikat oleh lignin. Morfologi permukaan serabut kelapa yang telah mengalami rawatan alkali dilihat lebih kasar berbanding serabut tanpa rawatan. Hal ini disebabkan berlakunya penyingkiran hemiselulosa semasa rawatan alkali. Bintilan berbentuk lubang kosong pada serabut kelapa dengan rawatan alkali pula disebabkan penyingkiran unjuran globul pada serabut kelapa tanpa rawatan [6].

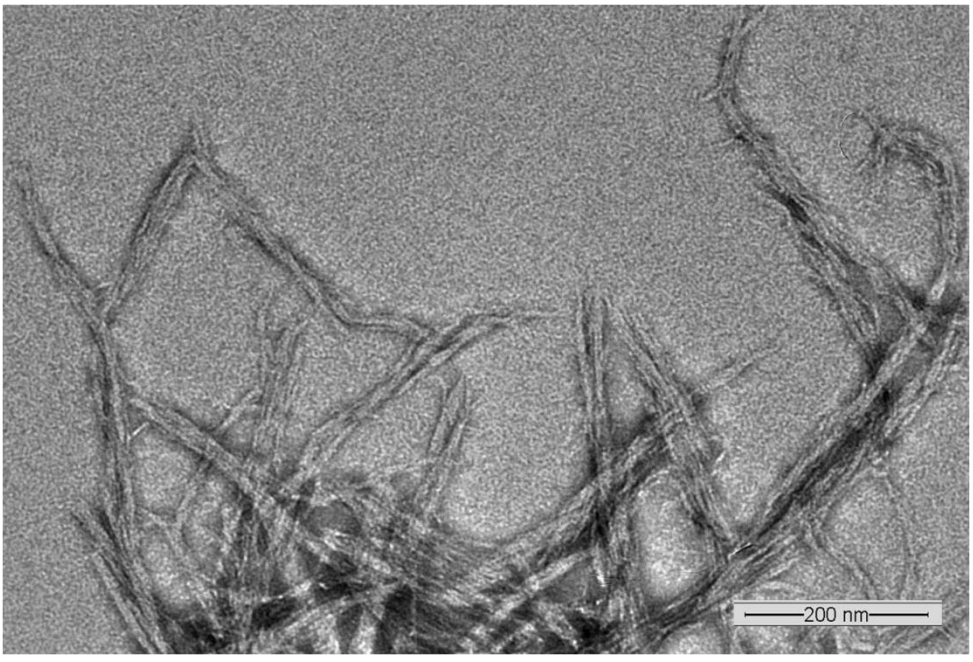
Selepas rawatan pelunturan, permukaan serabut menjadi semakin licin berikutan penyingkiran lignin pada serabut kelapa, berbanding serabut kelapa tanpa rawatan dan dengan rawatan alkali. Keadaan ini juga memudahkan perlekatan antara serabut kelapa dan matriks dalam penghasilan komposit. Gumpalan antara serabut yang diikat dengan lignin juga dilihat telah terpisah dan bertukar kepada diameter yang lebih kecil, iaitu sekitar 5-15 µm.







Rajah 2. Mikrograf SEM serabut kelapa (a) tanpa rawatan, (b) dengan rawatan alkali, dan (c) dengan rawatan peluntur.



Rajah 3. Nanoselulosa yang diekstrak daripada serabut kelapa.

Rajah 3 menunjukkan dimensi nanoselulosa yang telah diekstrak daripada serabut kelapa. Imej ini menunjukkan keberkesanan proses hidrolisis asid di mana ampaian akueus nanoselulosa terdiri daripada fibril berbentuk seperti jarum dan sedikit gumpalan [7-8]. Pengukuran terhadap dimensi nanoselulosa yang diekstrak daripada serabut kelapa ditunjukkan dalam Jadual 1. Umumnya, saiz nanoselulosa mempunyai purata diameter 13.7 ± 6.2 dan panjangnya 172.34 ± 8.4 nm [9]. Nanoselulosa yang berjaya diekstrak dalam kajian ini mempunyai purata nisbah dimensi 14.23 ± 8 nm.

Jadual 1. Dimensi nanoselulosa yang telah diekstrak selepas hidrolisis yang diukur berdasarkan mikrograf TEM.

Panjang, L /nm	Diameter, D /nm	Nisbah dimensi (L/D)
201.17	24.18	8.32
188.96	12.24	15.63
73.02	9.52	7.63
226.24	8.93	25.33

Analisis spektrum FTIR

Analisis terhadap kumpulan berfungsi pada serabut kelapa yang mengalami rawatan kimia yang berbeza ditunjukkan dalam Rajah 4. Puncak yang mempunyai perubahan yang ketara adalah pada 1723 cm^{-1} yang menunjukkan getaran kumpulan asetil dan ester uronik hemiselulosa atau rantaian ester daripada kumpulan karbosilik ferulik dan asid p-kumerik daripada lignin. Puncak pada 1630 cm^{-1} mewakili getaran rangka aromatik C=C lignin, manakala puncak 1252 cm^{-1} menerangkan regangan C-O hemiselulosa dan lignin [10]. Puncak ini yang semakin hilang bagi serabut kelapa yang telah mengalami rawatan kimia dan naoselulosa menunjukkan bahawa rawatan kimia yang dijalankan berjaya menyingkirkan kandungan lignin dalam serabut kelapa.

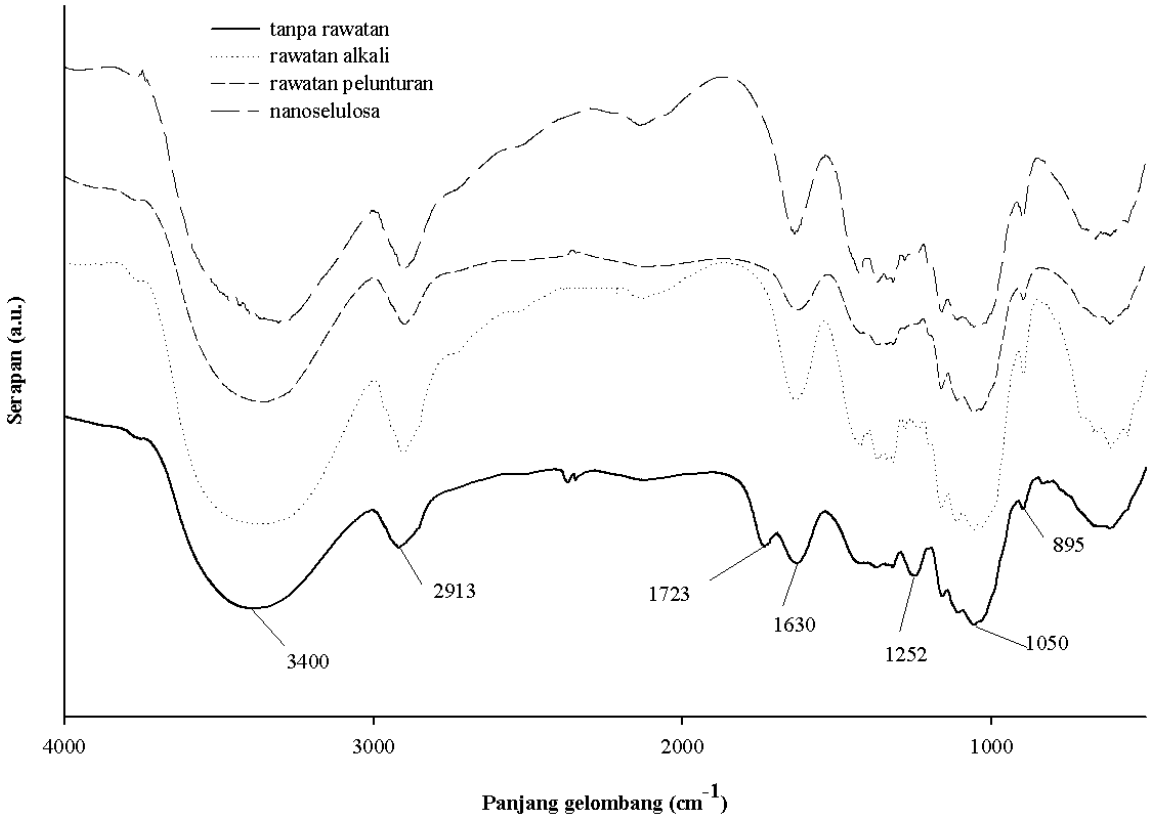
Jalur serapan yang lebar pada puncak 3330 cm^{-1} dan 3400 cm^{-1} menunjukkan getaran O-H bebas oleh kumpulan hidroksil dalam molekul selulosa, manakala puncak pada 2913 cm^{-1} yang juga terdapat pada keempat-empat sampel mewakili getaran regangan C-H. Regangan C-O pada puncak 1050 cm^{-1} yang semakin berkurang kelebarannya bagi sampel nanoselulosa menunjukkan berlakunya penyingkiran lignin dan hemiselulosa semasa rawatan kimia dijalankan. Puncak 1630 cm^{-1} mewakili regangan C=C bagi rantai aromatik lignin. Puncak ini semakin tajam bagi serabut kelapa terawat alkali namun semakin berkurang bagi rawatan pelunturan. Serapan pada puncak ini merujuk serapan air pada sampel serabut kelapa [11].

Puncak bagi selulosa dapat dilihat pada puncak 895 cm^{-1} yang semakin berkurang bagi nanoselulosa. Puncak ini menerangkan regangan gelang glukosa, iaitu deformasi C-H bagi selulosa dan hemiselulosa. Penyingkiran lignin yang banyak semasa rawatan pelunturan menyebabkan bahagian amorfus terdedah kepada serangan asid. Hal ini menjadikan nisbah puncak lignin kepada selulosa bertambah disebabkan pengurangan kandungan selulosa, seterusnya mengurangkan penyerapan spektrum pada puncak 895 cm^{-1} [12].

Analisis difraktometer X-ray

Difraktogram kehabluran bagi serabut kelapa ditunjukkan dalam Rajah 5. Serabut kelapa tanpa rawatan, serabut kelapa yang telah mengalami rawatan alkali dan pelunturan serta nanoselulosa menunjukkan puncak utama pada puncak belauan $2\theta = 15.8^{o}$, 22.7^{o} dan 34.6^{o}. Puncak pada $2\theta = 22.7^{o}$ mewakili kehabluran selulosa pada satah (2 0

0). Puncak bagi serabut kelapa dengan rawatan pelunturan adalah lebih tajam berikutan penyingkiran lignin semasa rawatan pelunturan. Pertambahan intensiti pada puncak $2\theta = 16.5^{o}$ dan 22.7^{o} menunjukkan pola serapan bagi selulosa I [13].

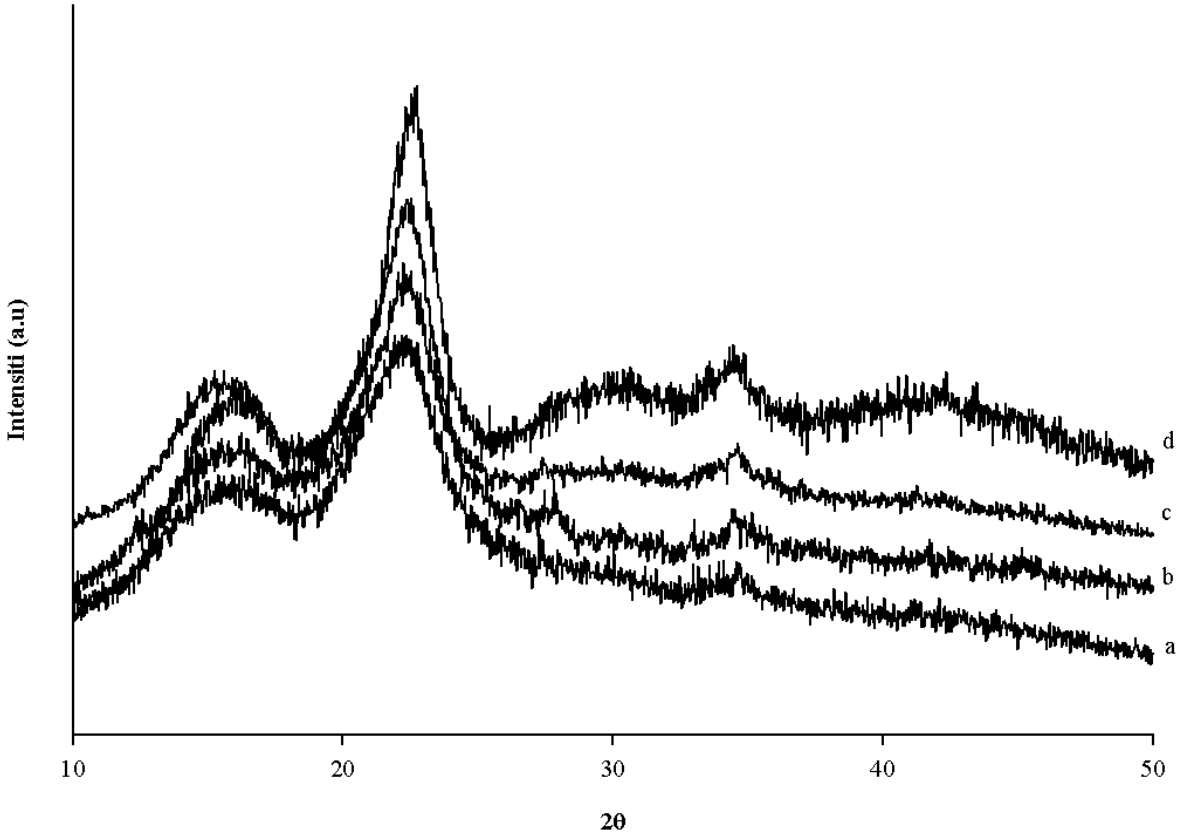


Rajah 4. Spektrum serabut kelapa tanpa rawatan, dengan rawatan alkali, dengan rawatan peluntur, dan nanoselulosa.

Berdasarkan Jadual 2, indeks kehabluran bagi sampel serabut kelapa semakin meningkat dengan rawatan kimia yang dijalankan. Hal ini menunjukkan bahawa proses penyediaan sampel mempengaruhi kehabluran nanoselulosa. Di samping itu, tempoh hidrolisis selama 30 minit merupakan tempoh yang sesuai untuk penyediaan nanoselulosa ini kerana rawatan dengan asid yang mangambil masa yang lama bukan sahaja boleh memusnahkan bahagian amorfus selulosa tetapi turut merosakkan bahagian hablurnya [14].

Jadual 2. Indeks kehabluran serabut kelapa.

Sampel serabut kelapa	Indeks kehabluran, I_h (%)
Serabut kelapa tanpa rawatan	51.18
Serabut kelapa dengan rawatan alkali	54.71
Serabut kelapa dengan rawatan pelunturan	59.71
Nanoselulosa	63.18

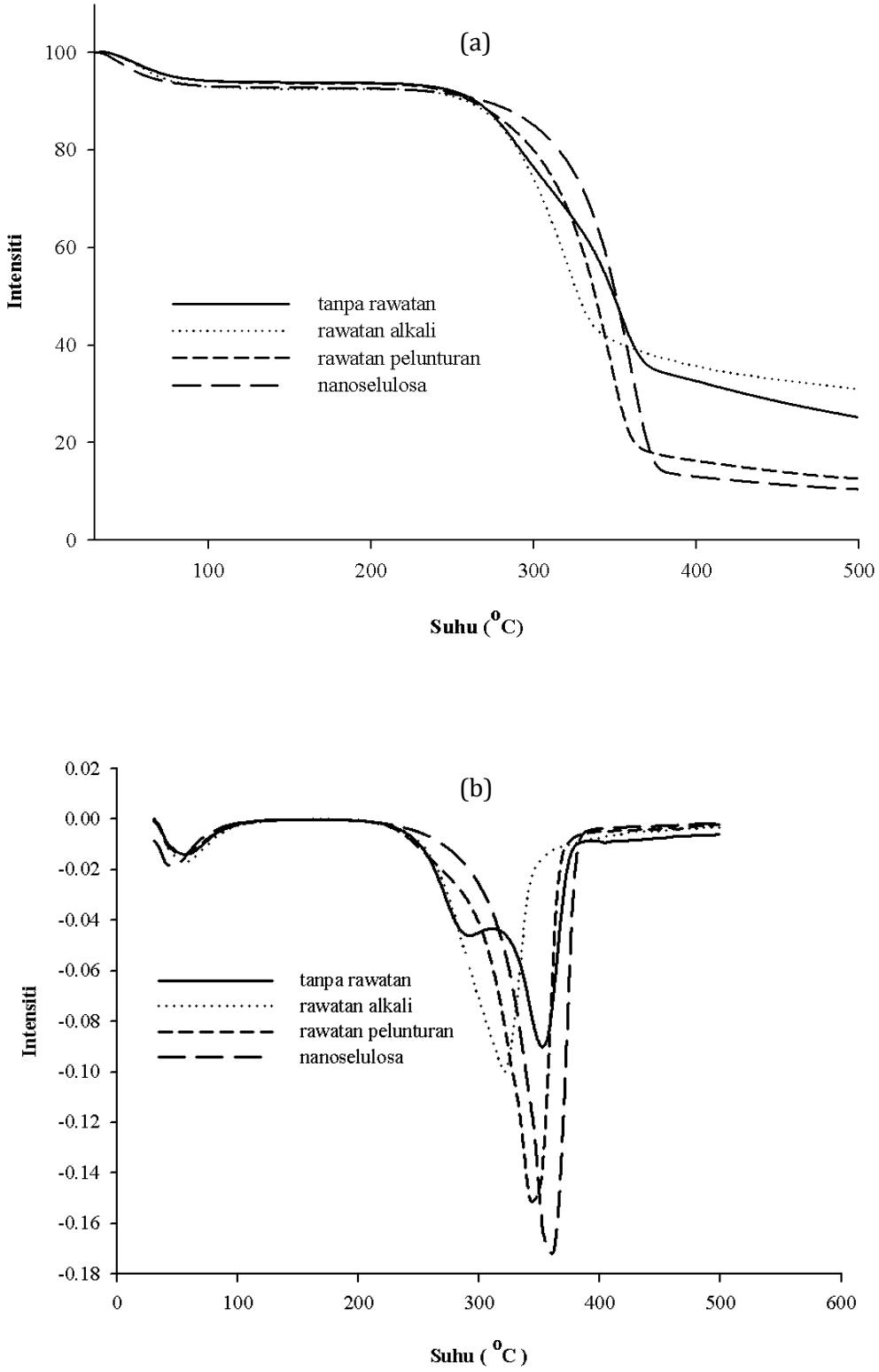


Rajah 5. Difraktogram serabut kelapa (a) tanpa rawatan, (b) dengan rawatan alkali, (c) dengan rawatan peluntur, dan (d) nanoselulosa.

Analisis kestabilan terma

Kestabilan terma bagi setiap serabut kelapa dikaji daripada analisa termogravimetrik TGA dan DTG seperti dalam Rajah 6. Lengkung TGA menunjukkan empat tahap degradasi, iaitu proses penyejatan lembapan, proses degradasi hemiselulosa, selulosa dan lignin. Berat sampel semakin berkurangan bermula pada suhu 34^{o}C disebabkan oleh dehidrasi atau penyejatan lembapan yang berlaku pada setiap sampel. Degradasi selulosa bermula pada suhu 260^{o}C dan berterusan sehingga 380^{o}C. Penyingkiran lignin ditunjukkan pada tempoh degradasi antara suhu 345^{o}C dan 500^{o}C, di mana tahap degradasi semakin berkurang dengan rawatan kimia yang dijalankan ke atas serabut kelapa. Hal ini juga dapat dilihat pada lengkuk DTG pada suhu 285 ^{o}C bagi serabut kelapa tanpa rawatan semakin hilang bagi sampel serabut kelapa yang telah mengalami rawatan kimia dan nanoselulosa. Keadaan ini juga disokong oleh spektrum hasil analisis FTIR sebelumnya. Julat suhu yang panjang semasa penguraian lignin turut dipengaruhi oleh sifat ikatan kimia pada struktur serabut kelapa.

Kehilangan berat yang ketara dapat dilihat pada suhu yang lebih tinggi. Sampel dengan rawatan pelunturan menunjukkan peningkatan kestabilan terma berbanding sampel tanpa rawatan dan sampel rawatan alkali. Keadaan ini disebabkan kehadiran lignin, hemiselulosa dan pektin dalam serabut kelapa tanpa rawatan dan serabut kelapa dengan rawatan alkali. Komposisi ini mempunyai tahap degradasi yang rendah berbanding selulosa. Namun penyingkiran komponen ini meningkatkan kestabilan terma serabut kelapa dan nanoselulosa. Kestabilan terma bagi serabut kelapa dengan rawatan alkali kelihatan lebih tinggi daripada serabut kelapa tanpa rawatan disebabkan baki lignin yang masih ada pada sampel rawatan alkali. Oleh itu, pembasuhan yang bersih sangat dititik beratkan dalam penyediaan sampel.



Rajah 6. Rajah kestabilan terma (a) TGA dan (b) DTG serabut kelapa tanpa rawatan, dengan rawatan alkali, dengan rawatan peluntur, dan nanoselulosa.

Kesimpulan

Selulosa telah diperolehi daripada serabut kelapa menggunakan rawatan alkali dan bahan peluntur dan dicirikan menggunakan spektroskopi FTIR dan pemerhatian mikroskopi. Seterusnya selulosa nanohablur telah berjaya diektraks menggunakan asid sulfurik (H_2SO_4)pekat pada kepekatan 64% H_2SO_4. Analisis pembelauan sinar-X (XRD) menunjukkan peningkatan kehabluran selepas setiap rawatan di mana selulosa nanohablur menunjukkan peratus kehabluran yang paling tinggi dengan indeks kehabluran 63.18. Analisis terma telah menunjukkan peningkatan suhu penguraian selepas setiap rawatan dengan celulosa nanohablur menunjukkan peningkatan suhu degredasi yang sangat tinggi.

Penghargaan

Penulis merakamkan penghargaan kepada Kementerian Sains, Teknologi dan Inovasi dan Universiti Kebangsaan Malaysia atas pembiayaan projek ini.

Rujukan

1. Defoirdt, N., Biswas, S., De Vries, L., Tran, L. Q. N., Van Aker, J., Ahsan, Q., Gorbatikh, L., Van Vuure, A. & Verpoest, I. 2010. Assessment of the tensile properties of coir, bamboo and jute fibre. *Composites A.* 41: 588-595.
2. Geethamma, V. G., Kalaprasad, G., Gabriel, G., Sabu, T. 2005. Dynamic mechanical behavior of short coir fiber reinforced natural rubber composites. *Composites.* 36: 1499-506.
3. Asasutjarit, C., Charoenvi, S., Hirunlabh, J. & Khedari, J. 2009. Materials and mechanical properties of pretreated coir-based green composites. *Composites: Part B.* 40: 633-637.
4. Li, R., Fei, J., Cai, Y., Li, Y., Feng, J., & Yao, J. 2009. Cellulose whiskers extracted from mulberry: A novel biomass production, carbohydrate polymers. *Carbohydrate Polymers* 76: 94–99.
5. Segal, L., Creely, L., Martin, A.E., Conrad, C.M. 1959. An empirical method for estimating the degree of crystallinity of native cellulose using X-ray diffractometer. *Text. Res. J.* 29: 786–794.
6. Rout, J., Misra, M., Tripathy, S. S., Nayak, S. K. & Mohanty, A. K. 2001. The influence of fibre treatment on the performance of coir-polyester composites. *Composites Science and Technology*. 61: 1303-1310.
7. Azizi, M. A. S., Alloin, F., & Dufresne, A. 2005. Review of recent research into cellulosic whiskers, their properties and their application in nanocomposite field. Biomacromolecules. 6(2): 612-616.
8. Lai-Kee-Him, H., Chanzy, H., Muler, M., Putaux, J. L., Imai, T. & Bulone, V. 2002. In vitro versus in vivo cellulose microfibrils from plant primary wall synthases: Structural differences. The Journal of Biological Chemistry, 277(40): 36931-36939.
9. Bondenson, D., Kvien, I. & Oksman, K. 2006. Strategies for preparation of cellulose whiskers from microcrystalline cellulose (MCC) as reinforcement. In: Oksman, K., Sain, M., editors. Cellulose nanocomposites: processing, characterization and properties. ACS symposium series, jilid 938. Oxford: Oxford University Press.
10. Zuluanga, R., Putaux, J. L., Cruz, J., Velez, J., Mondragon, I., Ganan, P. 2009. Cellulose microfibrils from banana rachis: effect of alkaline treatments on structural and morphological features. *Carbohydrate Polymer*. 76: 51-59.
11. Moran, J. I., Alvarez, V. A., Cyras, V. P. & Vazquez, A. 2008. Extraction of cellulose and preparation of nanocellulose from sisal fibers. *Cellulose*. 15: 149-159.
12. Socrates, G. 2004. Infrared and raman characteristic group frequencies. New York: John Wiley & Sons. p. 366.
13. Marchessault, R. H., & Sundararajan, P. R. 1993. In G. O. Aspinall (Ed.), The polysaccharides. 2. New York: Academic Press. p. 44.
14. M.F. Rosa, E.S. Medeiros, J.A. Malmonge, K.S. Gregorski, D.F. Wood, L.H.C. Mattosa, G.Glenn, W.J. Orts & S.H.Imam. 2010. Cellulose nanowhiskers from coconut husk fibers: Effect of preparation conditions on their thermal and morphological behavior. *Carbohydrate Polymers* 81: 83-92.

The Malaysian Journal of ANALYTICAL SCIENCES ISSN 1394-2506

THE EFFECT OF CHEMICAL STRUCTURE ON POUR POINT, OXIDATIVE STABILITY AND TRIBOLOGICAL PROPERTIES OF OLEIC ACID TRIESTER DERIVATIVES

(Kesan Struktur Kimia Pada Titik Pour, Kestabilan Pengoksidaan Dan Sifat Tribological Derivatif Triester Asid Oleik)

Nadia Salih[1], Jumat Salimon[1]*, Emad Yousif[2]

[1]*School of Chemical Sciences and Food Technology, Faculty of Science and Technology, Universiti Kebangsaan Malaysia, 43600 Bangi, Selangor, Malaysia*
[2]*Department of Chemistry, College of Science, Al-Nahrain University, Baghdad, Iraq*

**Corresponding author: jumat@ukm.my*

Abstract

Due to the strict regulations imposed on non-biodegradable mineral oil-based lubricants, the development and applications of biolubricants are increasing daily. Plant oils are being investigated as a potential source of environmentally favorable lubricants because of their biodegradability, renewability, viscosity-temperature relationship, low volatility and excellent lubrication performance. However, the use of plant oils has some restriction, the most critical being oxidative stability and low-temperature problems. This paper presents systematic modifications to improve the physicochemical and tribological properties of plant oil derivatives. The results showed that among the oleic acid-based triester compounds, 2-ethylhexyl 9-(myristoxy)-10-(heptanoyloxy)octadecanoate (**9**) had the lowest pour point (-47.19 ˚C) while 2-ethylhexyl 9-(caprooxy)-10-(heptanoyloxy)octadecanoate (**5**) had the highest onset temperature (103.10 ˚C). Overall, the data indicate that the biolubricant basestocks based on this chemical modification offer great potential for the development of industrial products application.

Keywords: Plant oils, pour point, physicochemical properties, biolubricant basestocks

Abstrak

Perkembangan dan penggunaan biopelincir telah meningkat saban hari disebabkan oleh penguatkuasaan yang lebih ketat dikenakan keatas minyak pelincir berasaskan minyak mineral yang takterbiourai. Minyak tumbuhan telah dikaji sebagai sumber yang berpotensi untuk minyak pelincir disebabkan oleh sifat terbiourai, terganti semula, hubungan kelikatan-suhu yang baik, kemeruapan yang rendah dan prestasi pelinciran yang cemerlang. Walaubagaimana pun penggunaan minyak tumbuhan mempunyai kelemahan terutamanya sifat kestabilan oksidatif and sifat suhu rendah yang rendah. Kertas kerja ini membentangkan pengubahsuaian kimia secara sistematik untuk meningkatkan sifat-sifat fizikokimia dan tribologi terbitan minyak tumbuhan. Hasil kajian menunujukkan bahwa diantara sebatian berasaskan asid oleik, 2-etilheksil 9-(miristoksi)-10-(heptanoiloksi)oktadekanoat (**9**) mempunyai takat tuang terendah (-47.19 ˚C) sementara 2-etilheksil 9-(kaproksi)-10-(heptanoiloksi)oktadekanoat (**5**) mempunyai suhu onset tertinggi (103.10 ˚C). Secara keseluruhan, hasil kajian menunjukkan stok asas biopelincir berasaskan pengubahsuaian kimia ini memberikan potensi yang tinggi untuk pembangunan produk kegunaan industri.

Kata kunci: Minyak tumbuhan, takat tuang, sifat fisikokimia, minyak asas biopelincir

Introduction

Stronger environmental concerns and growing regulations over contamination and pollution will increase the need for renewable and biodegradable lubricants [1]. Most lubricants originate from petroleum stock, which is environmentally toxic and difficult to dispose of. Because of the growing environmental concerns over petrochemical disposal, plant oils and their derivatives are finding a place as lubricants in industrial and

transportation applications. Plant oils with high oleic acid content and synthetic ester derivatives are considered to be potential candidates to replace conventional mineral oil-based lubrication oils and synthetic esters [2].

There are several reasons to use plant oils or plant oil derivatives as biolubricants. Because as much as 40% [3] of a lubricant can be lost to the environment, the inherent biodegradability of plant oils reduces their environmental impact. Other advantages include low volatility, superior lubricity and good anticorrosion properties [4].

The majority of plant oils consist primarily of triacylglycerols (TAGs), which are glycerol molecules with three fatty acid (FA) chains attached at the hydroxyl groups via ester linkages. The fatty acids vary in the length of their hydrocarbon chains and in their degree of unsaturation [5]. Triacylglycerol molecules orient themselves with their polar end at the solid surface making a close-packed monomolecular or multimolecular layer [6], which results in a surface film that is believed to inhibit metal-to-metal contact and the progression of pits and asperities on the metal surface. Furthermore, this lubricant film helps in reducing both friction and wear.

Despite the many advantages of plant oils, there are two major problems, inadequate oxidative stability and poor low-temperature properties, that restrict their use as biolubricant basestocks [7]. Low-temperature studies have shown that most plant oils undergo cloudiness, precipitation, poor flow, and solidification at -10 ˚C, the temperature considered the benchmark for long-term exposure to cold, which is in contrast to the behavior of mineral oil-based fluids [8].

The chemical modification of plant oils is an attractive way to solve these problems. Transforming alkene groups in plant oils to other stable functional groups could improve their oxidative stability, whereas, the reducing structural uniformity of the oil by attaching alkyl side chains would improve its low-temperature performance [9].

Based on our previous research on the development of biolubricant basestocks, the ring-opening reaction of epoxidized oleic acid followed by the estrification of the resulting hydroxyl groups improved the physicochemical and tribological properties of the synthetic product oils [10]. The objective of this work was to prepare new synthetic biolubricants basestocks from epoxidized oleic acid and to study their low-temperature and thermo-oxidative properties and other physicochemical properties, such as their tribological properties. In this study, the addition of heptanoic acid to the oxirane moiety of epoxidized oleic acid (EOA) at elevated temperature (100 ˚C) is the key step in a four-step sequential reaction (Fig. 1). The utilization both head-group manipulation and branching strategies allowed the major physical properties of these lipid-based materials to be improved.

Materials and Methods

Materials

Formic acid (88%) was obtained from Fisher Scientific (Pittsburgh, PA) and oleic acid (92%) from ChemaR (Poland). All other chemicals and reagents were obtained from Aldrich Chemical (Milwaukee, WI). All materials were used without further purification and all organic extracts were dried using anhydrous magnesium sulfate (Aldrich Chemical).

Characterization

^{1}H and ^{13}C NMR spectra were recorded using a JEOL JNM-ECP 400 spectrometer operating at a frequency of 400.13 and 100.77 MHz, respectively, using a 5-mm broadband inverse Z-gradient probe in DMSO-d_6 (Cambridge Isotope Laboratories, Andover, MA) as the solvent. Each spectrum was Fourier-transformed, phase-corrected, and integrated using MestRe-C 2.3a (Magnetic Resonance Companion, Santiago de Compostela, Spain) software. FTIR spectra were recorded directly on a Thermo Nicolet Nexus 470 FTIR system (Madison, WI) with a Smart ARK accessory containing a 45 ZeSe over a scanning range of 650-4,000 cm^{-1} using 32 scans to give a spectral resolution of 4 cm^{-1}.

The pour point and the cloud point

Pour points (PP) and cloud points (CP) were measured using the ASTM D5949 [11] and ASTM D5773 [12] methods, respectively, with a Phase Technology Analyzer, Model PSA-70S (Hammersmith Gate, Richmond, B.C., Canada). The pour point of a sample is the lowest temperature at which it will pour or flow as an oil under the

prescribed conditions. It is a rough indication of the lowest temperature at which oil is readily pumpable. The cloud point is the temperature at which dissolved solids, such as paraffin wax, are no longer completely soluble, instead precipitating as a second phase giving the fluid a cloudy appearance. In the petroleum industry, the presence of solidified waxes thickens the oil, causing clogs in the fuel filters and injectors of engines. Waxes also accumulate on cold surfaces and form an emulsion with water. Therefore, the cloud point indicates the tendency of oil to plug filters or small orifices at cold operating temperatures. All runs were carried out at least in duplicate and the average values were reported with their standard deviations (± SD).

The flash point

The flash point (FP) measures the tendency of a specimen to form a flammable mixture with air under controlled laboratory conditions. The flash point of a volatile liquid is the lowest temperature at which it will vaporize to form an ignitable mixture in air. The lower the flash point, the easier it is to ignite the material. The flash point is an important component of a number of properties that should be considered when assessing the overall flammability hazard of a material. The flash points were determined by ASTM D56-05 [13]. All runs were carried out at least in duplicate and the average values were reported with their standard deviations (± SD).

Viscosity index measurements

Automated multi-range viscometer tubes HV M472 obtained from Walter Herzog (Germany) were used to measure viscosity. Measurements were run in a Temp-Trol (Precision Scientific, Chicago, IL, USA) viscometer bath set at 40.0 or 100.0 ˚C. The viscosity and the viscosity index were calculated using ASTM methods D445-97 [14] and D2270-93 [15], respectively. Triplicate measurements were made and the average values were reported with their standard deviations (± SD).

The pressure differential scanning calorimetry (PDSC) method

The experiments were performed using a DSC 2910 thermal analyzer from TA Instruments (New Castle, DE). Typically a 1.5-2.0 mg sample was taken in a hermetically sealed-type aluminum pan with a pinhole lid for interaction of the sample with the reactant gas (dry air). A film thickness of less than 1 mm was required to ensure proper oil-air interaction and eliminate gas-diffusion limitations. Dry air (Gateway Airgas, St Louis, MO) was pressurized in the module at a constant pressure of 1379 kPa. A 10 ˚C/min heating rate from 50 to 350 ˚C was used during each experiment. The onset temperature (OT, ˚C) and the signal maximum temperature (SMT, ˚C) of the oxidation were calculated from the exotherm for each sample. Each sample was run in triplicate and the average values were reported with their standard deviations (± SD).

The density determination method

Density determinations were made at 20 ˚C based on the ASTM method D1298-99 [16], using a glass hydrometer provided by Lanxi Comp., Shanghai, China.

The volatility determination method

The volatility was determined in agreement with ASTM method D6184 [17] in an electrical stove using glass pans of 4 cm in diameter.

The tribological test method

Tribological determinations were performed according to ASTM method D4172-94 [18] using the four-ball method (Anton Paar Physica MCR301, Germany) via a Rheoplus/ 32 V3.40 software. Each sample was run in triplicate and the average values were reported with their standard deviations (± SD).

Synthesis Peocedure

Epoxidized oleic acid (EOA) (2)

Hydrogen peroxide solution (30 % in H_2O, 8.0 mL) was slowly added into a stirred solution of oleic acid (OA) (92 %, 15 g) in formic acid (88 %, 14 mL) at 4 ˚C (ice bath). The reaction proceeded at room temperature with vigorous stirring (900 rpm) until the formation of a powdery solid was observed in the reaction vessel (2-5 h). The solid was collected via vacuum filtration, washed with H_2O (chilled, 3×10 mL), and placed under high vacuum for 12 h to produce epoxidized oleic acid (EOA) as a colorless, powdery solid.

9-Hydroxy-10-heptanoxyoctadecanoic acid (HHODA) (3)
Heptanoic acid (6 g) was added to a mixture of EOA (31 g) and 5 g of *p*-toluenesulfonic acid (PTSA) in toluene over a period of 1.5 h in order to keep the reaction mixture temperature under 70-80 ˚C. The reaction mixture was subsequently heated to 90-100 ˚C and held there for 3 h. After termination of the reaction, the heating was stopped and the mixture was left to stand overnight at room temperature. The mixture was washed with water. The organic layer was dried over anhydrous magnesium sulfate and the solvent was removed using a vacuum evaporator.

2-Ethylhexyl 9-hydroxy-10-heptanoxyoctadecanoate (EHHHOD) (4)
Sulfuric acid (conc. H_2SO_4, 10 mol-%) was added to a stirred suspension of 9-hydroxy-10-heptanoxyoctadecanoic acid (3.35 mmol) in 2-ethylhexanol (3.35 mL). The suspension was heated with stirring at 60 ˚C for 10 h. Hexanes (5 mL) was added, and the solution was washed with $NaHCO_3$ (sat. aq., 1 × 0.5 mL) and brine (2 × 1 mL), dried ($MgSO_4$), filtered, concentrated *in vacuo* and placed for 6 h under vacuum to yield the title product.

2-Ethylhexyl 9-(acyloxy)-10-(heptanoyloxy)octadecanoate (EHAHOD) (5-9)
Either caproic acid (5 g), octanoic acid (5 g), capric acid (5 g), lauric acid (5 g) or myristic acid (5 g) was added to a solution of 2-ethylhexyl 9-hydroxy-10-heptanoxyoctadecanoate (5 g) and sulfuric acid (10% H_2SO_4) in a two-neck round-bottomed flask equipped with a magnetic stir bar at room temperature; then the reaction mixture was heated to reflux with stirring for 10 h. After the reaction was transferred to a separatory funnel, the lower aqueous phase was removed and hexane (20 mL) was added to the upper oily phase. The organic phase was washed with $NaHCO_3$ (sat. aq., 2 × 5 mL) and brine (2 × 5 mL), dried ($MgSO_4$), filtered, concentrated *in vacuo*, and placed under high vacuum for 6 h to provide the triesters as clear oils, which were stored over molecular sieves to mitigate potential hydrolysis.

Results and Discussion

Synthesis
Based on our previous studies, we found that increasing the mid-chain ester group length improved the low-temperature properties but had a negative effect on oxidative stability [19]. Therefore, we continued researching chemically modified biolubricant basestocks.

In the present work, we describe the synthesis of the monoester derivative through a two-step reaction (epoxidation of oleic acid and oxirane ring opening) to afford monoester 9-hydroxy-10-heptanoxyoctadecanoic acid (**3**). Furthermore, esterification of the carboxylic acid hydroxyl group with 2-ethylhexanol gave diester 2-ethylhexyl 9-hydroxy-10-heptanoxyoctadecanoate (**4**), and finally, esterification of the resulting α-hydroxy group in diester **4** with caproic, octanoic, capric, lauric or myristic acids yielded triesters 2-ethylhexyl 9-(acyloxy)-10-(heptanoyloxy)octadecanoate **5**-**9**, respectively (Fig. 1). The straightforward epoxidation of oleic acid was closely monitored to avoid the synthesis of the undesired 9,10-dihydroxyoctadecanoate, which will form if the reaction is performed at elevated temperature or the reaction is allowed to progress for too long.

The low-temperature fluidity of EOA (**1**) is low, and its pour point is 0 ˚C (Table 1). The low pour point of plant oil prevents its use at low operating temperatures. A method to improve the low-temperature flow property is to introduce branching sites at the epoxy carbons. The branched products have significantly improved low-temperature flow characteristics and friction-wear properties compared with EOA or olefinic analogs [19]. Furthermore, the elimination of the unsaturated double bond in oleic acid through an epoxidation reaction improves the oxidation stability of the resulting products [20]. It has been established that the presence of multiple double bonds in plant oil fatty acid chains accelerates oxidative degradation. However, a balance must be obtained between improving the oxidative stability and preserving the lubricating properties of the plant oils. Too many modifications may destroy the properties that make plant oils useful in the first place.

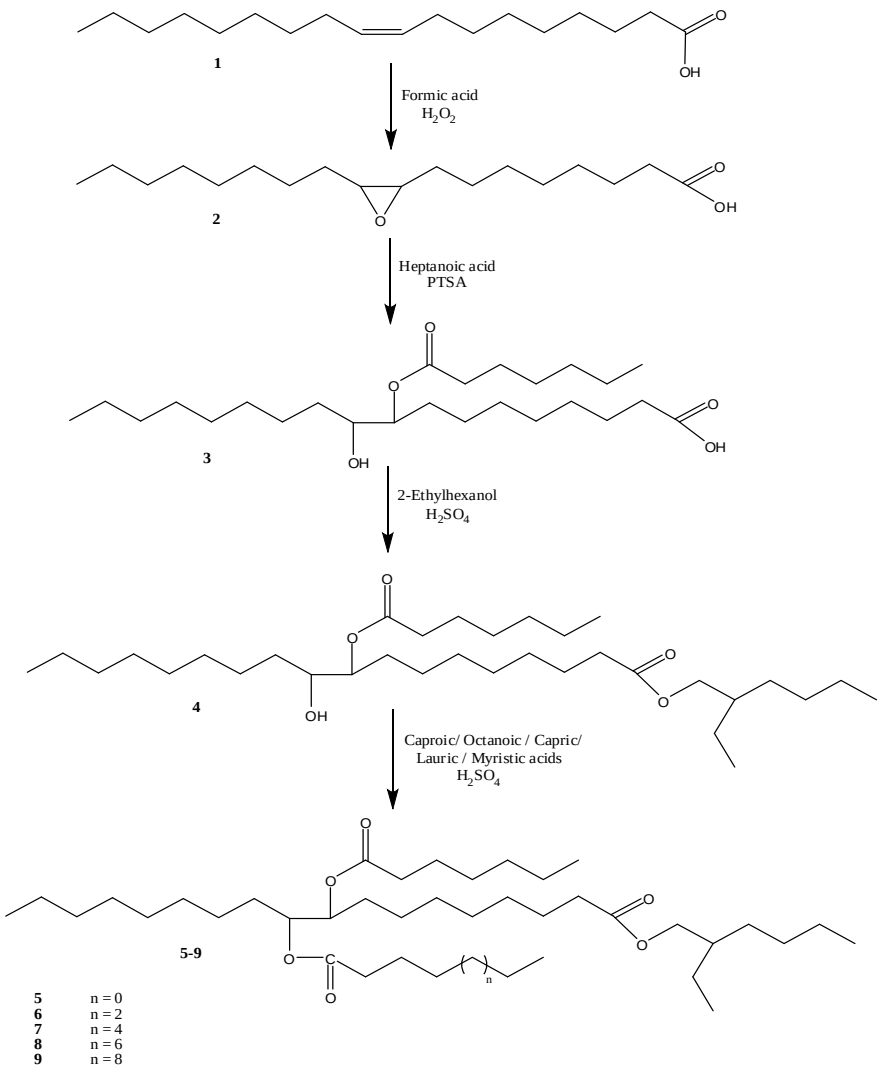


Fig. 1. The reaction scheme for triester formation.

Characterization

The FTIR spectrum of EOA (**2**) shows the characteristic peaks of an epoxy group at 826 and 845 cm^{-1}. The other important peaks observed in the FTIR spectrum are: 720 (methylene in-phase rocking); 1380 (methyl symmetric deformation); 1465 (methyl antisymmetric deformation) and 1742 cm^{-1} (the C=O stretch) [21].

In the FTIR spectra of compounds **3-9**, the absorption bands from the epoxy group (826 and 845 cm^{-1}) are not observed. This result suggests that **2** undergoes complete ring opening under the reaction conditions. Bands representing C=O groups (~722, 1748 cm^{-1}), CH_3 groups (~1370-1462 cm^{-1}), OH groups (~3473-3450 cm^{-1}) and the C-O-C bands of esters (~998-1105 cm^{-1}) are clearly visible in the spectra [22].

The structures of all synthesized compounds were also verified by ^{1}H and ^{13}C NMR spectroscopy. Significant signals in the ^{1}H spectrum of EOA (**2**) at ~2.8-2.10, ~9.26-9.29 and ~2.05-3.71 ppm were due to the quaternary hydrogens of the oxirane ring, the OH group, and the $–CH_2-$ groups, respectively. Furthermore, in the ^{13}C spectrum,

the signals at ~56.87-56.90 ppm were due to the carbons of the oxirane ring. On the other hand, in the ^{1}H NMR spectra of triesters 2-ethylhexyl 9-(acyloxy)-10-(heptanoyloxy)octadecanoate (**5-9**), there were no signals from an OH proton. Furthermore, in the ^{13}C NMR spectra, the signals at approximately ~174-178 ppm are attributed to the ester carbonyl groups [21]. These signals provide evidences for the proposed structures.

Low-temperature fluidity, flash point, and viscosity index measurements

The pour point (PP) and cloud point (CP) of a biolubricant are good indicators of its low-temperature fluidity. The cold flow properties of unmodified plant oils are poor and this limits their use at subzero temperatures. At low temperatures, plant oils have a tendency to form macro crystalline structures through uniform stacking of the "bent" triglyceride backbone. Such macro-crystals restrict the easy flow of the system due to the loss of kinetic energy of the individual molecules during self-stacking. Branching on the fatty acid chains may disrupt this stacking process and result in improved low-temperature properties [3]. This approach is used here to improve the low-temperature flow behavior of fatty acid triesters. The ester branching is attached at the mid- and end-sites on the fatty acid chains as shown in Fig. 2.

The attachment of an ester side chain of optimum length at the 9 or 10 position of the fatty acid chain improved the pour point significantly [23]. While EOA has a pour point of 0 ˚C and a cloud point of 10.24 ˚C; all the synthesized esters (**3-9**) have much better pour points, in the range of -16.12 to -47.19 ˚C, and CPs in the range -13.11 to -45.63 ˚C. Attachment of myristic acid to produce 2-ethylhexyl 9-(myristoxy)-10-(heptanoyloxy)octadecanoate (**9**) showed the most effective decrease in the pour point and cloud point to -47.19 and -45.63˚C, respectively. It can be assumed that the presence of a large branching group at the mid-point of a fatty acid chain creates a steric barrier around the individual molecule and inhibits crystallization, the result of which is lower pour and cloud points (Table 1).

The flash point is useful in determining the volatility and fire resistance of a biolubricant. It can be used to determine the transportation and storage temperature requirements for biolubricants. The flash point should be high, to ensure the safe operation and minimum volatilization at the maximum operating temperature. For the most demanding applications, such as in aviation jet engines, an effective flash point range of greater than 300 ˚C may be required (Salimon et al., 2010 b). In this work, the highest flash point was 285.80˚C for 2-ethylhexyl 9-(myristoxy)-10-(heptanoyloxy)octadecanoate (**9**) (Table 1).

The viscosity index (VI) of an oil indicates the effect of temperature on the viscosity of the oil. A low viscosity index signifies a relatively large change of viscosity with temperature. In other words, the oil becomes extremely thin at high temperatures and extremely thick at low temperatures. On the other hand, a high viscosity index signifies relatively little change in viscosity over a wide temperature range. Ideal oil, for most purpose, is one that maintains a constant viscosity during temperature changes. The importance of the viscosity index can be easily shown by considering automotive lubricants. Oil having a high viscosity index resists excessive thickening when the engine is cold and consequently promotes rapid starting and prompt circulation. It resists excessive thinning when the motor is hot and thus provides full lubrication and prevents excessive oil consumption. From Table 1, we can see that the viscosity index (VI) increased as the substitution of the oil increased in the order monoesters < diesters < triesters which can be rationalized by an overall increase in the molecular weight of the products with the increasing chain length from newly added ester group.

Oxidative stability measurements

Differential scanning calorimetry (DSC) is an effective technique for determining the effect of temperature on a material's properties. DSC represents these effects as an exothermic or endothermic peak that is a function of temperature. In general, chemical decomposition and oxidation cause exothermic peaks, while physical properties such as melting and boiling cause endothermic peaks. Pressure differential scanning calorimetry (PDSC) is an effective method for measuring the oxidative tendencies of biolubricant base oils, plant oils, and oleochemicals, in rapid fashion.

Table 1. The physicochemical properties of the synthesized products

Samples	Density (g/cm^3)	Volatility 120 ˚C (%)	Pour point/˚C [a]	Cloud point/˚C [a]	Flash point/˚C [a]	Viscosity index (VI) [a]
2, EOA	0.804	1.05	0	10.24 ± 0.68	113.15 ± 4.78	45.10 ± 0.94
3, HHODA	0.825	0.95	-16.12 ± 0.61	-13.11 ± 0.53	145.16 ± 5.24	65.70 ± 1.67
4, EHHHOD	0.831	0.88	-24.33 ± 0.45	-21.37 ± 0.21	187.34 ± 4.89	77.89 ± 1.89
5, EHCOHOD	0.841	0.82	-31.57 ± 0.25	-27.68 ± 0.35	192.27 ± 10.78	80.57 ± 2.67
6, EHOHOD	0.848	0.73	-36.48 ± 0.77	-32.54 ± 0.64	234.79 ± 9.56	92.59 ± 3.11
7, EHCIHOD	0.856	0.69	-40.40 ± 0.24	-36.42 ± 0.75	257.10 ± 6.42	156.61 ± 6.87
8, EHLHOD	0.862	0.63	-44.74 ± 0.39	-41.81 ± 0.40	277.56 ± 8.90	178.90 ± 8.38
9, EHMHOD	0.869	0.55	-47.19 ± 0.58	-45.63 ± 0.58	285.80 ± 7.46	213.53 ± 10.21

2, EOA = Epoxidized oleic acid; **3**, HHODA = 9-Hydroxy-10-heptanoxyoctadecanoic acid; **4**, EHHHOD = 2-Ethylhexyl 9-hydroxy-10-heptanoxyoctadecaoate; **5**, EHCOHOD = 2-Ethylhexyl 9-(caprooxy)-10-(heptanoyloxy)octadecanoate; **6**, EHOHOD = 2-Ethylhexyl 9-(octanoxy)-10-(heptanoyloxy)octadecanoate; **7**, EHCIHOD = 2-Ethylhexyl 9-(caproxy)-10-(heptanoyloxy)octadecanoate; **8**, EHLHOD = 2-Ethylhexyl 9-(lauroxy)-10-(heptanoyloxy)octadecanoate; **9**, EHMHOD = 2-Ethylhexyl 9-(myristoxy)-10-(heptanoyloxy)octadecanoate.

[a] Mean ± SD

Depending on the number of double bonds it has, fatty acids are categorized as saturated, monounsaturated or polysaturated. Double bonds are oxidized more easily than fully saturated hydrocarbon chains. Free radicals attack the allylic hydrogen located next to the double bond [24]. When using the PDSC technique at high air pressure, i.e., 1379 KPa, the oxygen concentration is in excess and in equilibrium with the sample. Thus, any inconsistencies due to the access rate of oxygen or the egress rate of volatile degradation products are effectively eliminated.

Epoxidized oleic acid (**2**), 9-hydroxy-10-heptanoxyoctadecanoic acid (**3**), 2-ethylhexyl 9-hydroxy-10-heptanoxyoctadecanoate (**4**) and 2-ethylhexyl 9-(acyloxy)-10-(heptanoyloxy)octadecanoate (**5-9)** were screened for oxidation stability using pressurized differential scanning calorimetry through the determination of the onset temperature (OT) and the signal maximum temperature (SMT). The onset temperature is the temperature at which we observed the rate of oxidation rapidly increase. It is obtained by extrapolating the tangent of the steepest slope of the reaction exotherm down to the baseline. A high onset temperature would suggest that the oxidation stability of oil is high. The signal maximum temperature is the temperature at which maximum heat output is observed in the sample during oxidative degradation. A higher signal maximum temperature does not necessarily correlate with improved oxidation stability.

The results in Table 2 indicate that an improvement in oxidation stability was observed as the chain length of the mid-chain ester decreased because longer side chains have more accessible sites that are prone to oxidation, which makes them more susceptible to cleavage than short chains [25].

Tribological measurements

The tribological interactions of a solid surface's exposed face with interfacing materials and the environment may result in a loss of material from the surface. The process leading to a loss of material is known as "wear". Major types of wear include abrasion, friction (adhesion and cohesion), erosion, and corrosion. Wear can be minimized by modifying the surface properties of solids by one or more "surface finishing" processes or by the use of lubricant for frictional or adhesive wear.

An important property of biolubricants is their ability to maintain a stable lubricating film at the metal contact zone. The long fatty acid chain and presence of polar groups in the structure of plant oil makes it amphiphilic in nature, therefore allowing it to be used as both boundary and hydrodynamic biolubricants. To meet the increasing demands for stability during various tribological processes, oil structures have to withstand extremes of temperature variation

and shear degradation and maintain excellent boundary lubricating properties through strong physical and chemical adsorption to the metal surface. The ester ends of the fatty acid chain adsorb to metal surfaces thus permitting monolayer film formation with the hydrocarbon end of fatty acids oriented away from the metal surface. The fatty acid chain thus offers a sliding surface that prevents direct metal-to-metal contact and the formation of pits and asperities on the metal surface. The strength of the film and the extent to which it is adsorbed on the metal surface dictate the efficiency of the biolubricant's performance. If the film is not formed, direct metal contact may result in high-temperatures at the contact zones between moving parts causing adhesion, scuffing, or even metal-to-metal welding. Under lubricated conditions, the hydroxyl and ester group of the products offers active oxygen sites that bind to the metal surface [26]. Table 3 shows the tribological results for the synthesized compounds.

The results indicated that an improvement in anti-wear properties (lower scar test values) occurred with longer mid-chain esters and increased polar ester functional group substitution, i.e., triesters > diesters > monoesters (Table 3). The branching structure of the biolubricant and increasing the polar functional groups increased the strength of the tribological film at the metal contact zone thereby increasing its efficiency at reducing wear.

Table 2. The PDSC data of the samples showing the onset of oxidation and the signal maximum temperatures

Samples	Onset temperature (OT)/°C [a]	Signal maximum temperature (SMT)/°C [a]
2, EOA	75.12 ± 1.38	164.40 ± 4.70
3, HHODA	122.67 ± 5.90	198.63 ± 6.29
4, EHHHOD	116.34 ± 4.71	122.46 ± 3.78
5, EHCOHOD	103.10 ± 4.34	203.02 ± 9.65
6, EHOHOD	97.65 ± 3.52	88.53 ± 2.24
7, EHCIHOD	90.33 ± 2.88	169.15 ± 4.90
8, EHLHOD	85.89 ± 1.93	267.69 ± 11.87
9, EHMHOD	80.46 ± 1.67	138.34 ± 4.45

2, EOA = Epoxidized oleic acid; **3**, HHODA = 9-Hydroxy-10-heptanoxyoctadecanoic acid; **4**, EHHHOD = 2-Ethylhexyl 9-hydroxy-10-heptanoxyoctadecaoate; **5**, EHCOHOD = 2-Ethylhexyl 9-(caprooxy)-10-(heptanoyloxy)octadecanoate; **6**, EHOHOD = 2-Ethylhexyl 9-(octanoxy)-10-(heptanoyloxy)octadecanoate; **7**, EHCIHOD = 2-Ethylhexyl 9-(caproxy)-10-(heptanoyloxy)octadecanoate; **8**, EHLHOD = 2-Ethylhexyl 9-(lauroxy)-10-(heptanoyloxy)octadecanoate; **9**, EHMHOD = 2-Ethylhexyl 9-(myristoxy)-10-(heptanoyloxy)octadecanoate.

[a] Mean ± SD

Table 3. The tribological properties of the synthesized compounds in the four-ball test

Samples	Four ball wear scar, 40 daN, 1 h (mm) [a]	Coefficient of friction (μ)
2, EOA	0.89 ± 0.11	0.58
3, HHODA	0.81 ± 0.10	0.51
4, EHHHOD	0.75 ± 0.12	0.45
5, EHCOHOD	0.62 ±0.10	0.39
6, EHOHOD	0.50 ±0.10	0.30
7, EHCIHOD	0.43 ±0.11	0.24
8, EHLHOD	0.33 ± 0.10	0.16
9, EHMHOD	0.21 ±0.10	0.12

2, EOA = Epoxidized oleic acid; **3**, HHODA = 9-Hydroxy-10-heptanoxyoctadecanoic acid; **4**, EHHHOD = 2-Ethylhexyl 9-hydroxy-10-heptanoxyoctadecaoate; **5**, EHCOHOD = 2-Ethylhexyl 9-(caprooxy)-10-(heptanoyloxy)octadecanoate; **6**, EHOHOD = 2-Ethylhexyl 9-(octanoxy)-10-(heptanoyloxy)octadecanoate; **7**, EHCIHOD = 2-Ethylhexyl 9-(caproxy)-10-(heptanoyloxy)octadecanoate; **8**, EHLHOD = 2-Ethylhexyl 9-(lauroxy)-10-(heptanoyloxy)octadecanoate; **9**, EHMHOD = 2-Ethylhexyl 9-(myristoxy)-10-(heptanoyloxy)octadecanoate.

[a] Mean ± SD

Conclusion

The present work describes a systematic approach to the chemical modification of oleic acid oils to yield basestocks capable of operating under a range of conditions. Based on the results obtained, an increase of the chain length of the mid-chain ester had a positive influence on the low-temperature properties because it created a steric barrier around individual molecules that inhibited crystallization, the result of which was an in lower pour point. An increase in the chain length of the mid-chain ester also had a positive influence on the tribological properties of the molecules. However, the trends for PP run counter to those of thermo-oxidative stability as shown in the PDSC and TFMO results, i.e., increasing the chain length is a benefit to the PP but a detriment to the thermo-oxidative stability.

Furthermore, it is evident that hydrogen bonding is a critical parameter influencing the physicochemical and tribological properties of synthetic esters. Removal of unstable double bonds from fatty acid acyls, increasing the molar weight and changing their molecular structure results in an increased of the viscosity index of the synthesized esters. In addition, the flash point and volatility values show that synthetic ester oils have a low potential as a fire hazard. Furthermore, increasing the polar functionality in the plant oil structure has a positive impact on wear protection, the result of stronger absorption potential on the metal surface and a greater lateral interaction between the ester chains. This advantage was achieved by increasing the polarity through the chemical modification of triester products. Chemical modification is necessary to improve the performance of plant oils by reducing the limitations imposed by the native oil structure. Specifically, we focus on improving the oxidative stability of these structures by eliminating the bis-allylic hydrogen functionalities in the polyunsaturated methylene chain. In general, the oleic acid-based triester derivatives have improved physicochemical and tribological properties when compared to their precursors, making them a good candidate for the general biolubricant used in chain saws, brake fluid and transmission oil. Our research suggests that these modification pathways might appreciably improve the overall properties of biolubricant basestocks.

Acknowledgement

We are grateful to Universiti Kebangsaan Malaysia for funding ("Code UKM-GUP-NBT-08-27-113", "UKM-GGPM-NBT-164-2010" and "OUP-2012-139") and to the support staff from the School of Chemical Sciences and Food Technology and the Faculty of Science and Technology, Universiti Kebangsaan Malaysia.

References

1. Rhee, I.. 1996. Evolution of environmentally acceptable hydraulic fluids. NLGI Spokesman 60 (5), 28.
2. Randles, S.J., Wright, M., 1992. Environmentally considerable ester lubrication for the automotive and engineering industeries. *J. Synth. Lubr*. 9: 145-161.
3. Castro, W., Perez, J.M., Erhan, S.Z., Caputo, F., 2006. A study of the oxidation and wear properties of vegetable oils: Soybean oil without additives. *J. Am. Oil Chem. Soc*. 83: 47-52.
4. Doll, K.M., Sharma, B.K., Erhan, S.Z., 2007. Synthesis of branched methyl hydroxy strearates including an ester from bio-based levulinic acid. *Ind. Eng. Chem. Res*. 46: 3513-3519.
5. Rudnick, L., 2002. Biobased industrial fluids and lubrication. AOCS Press, Champaign, IL.
6. Fuks, G.I., 1963. Research in surface forces, New York, Consultants Bureau, pp. 29-88.
7. Asadauskas, S., Perez, J.M., Duda, J.L., 1996. Oxidative stability and antiwear properties of high oleic vegetable oils. *Lub. Eng.* 52: 877-882.
8. Schuster, H., Rios, L.A., Weckes, P.P., Hoelderich, W.F., 2008. Heterogenouse catalyst for the production of new lubricants with unique proprties. *Appl. Catalysis A: Gen.* 348: 266-270.
9. Salih, N., Salimon, J., Yousif, E., 2011 a. The physicochemical and tribological properties of oleic acid based triester biolubricants. *Ind. Crops Prod.* 33: 1089-1096.
10. Salih, N., Salimon, J., Yousif, E., 2011 b. Synthesis of oleic acid based esters as potential basestock for biolubricant production. *Turk. J. Eng. Env. Sci.* 35: 115-123.
11. American Society for Testing Materials, 2011 a. Standard test method for pour point of petroleum products (automatic pressure pulsing method). ASTM, West Conshohcken, PA (USA).
12. American Society for Testing Materials, 2011 b. Standard test method for cloud point of petroleum products (constant cooling rate method). ASTM, West Conshohcken, PA (USA).

13. American Society for Testing Materials, 2011 c. Standard test method for flash point by Tag Closed Cup Tester. ASTM, West Conshohcken, PA (USA).
14. American Society for Testing Materials, 2011 d. Standard Test Method for kinematic viscosity of transparent and opaque liquids. ASTM, West Conshohcken, PA (USA).
15. American Society for Testing Materials, 2011 e. Standard practice for calculating viscosity index from kinematic viscosity at 40 and 100 ˚C. ASTM, West Conshohcken, PA (USA).
16. American Society for Testing Materials, 2011 f. Standard test method for density, relative density (specific gravity), or API gravity of crude petroleum and liquid petroleum products by hydrometer method. ASTM, West Conshohcken, PA (USA).
17. American Society for Testing Materials, 2011 g. Standard test method for measure the volatility of petroleum products. ASTM, West Conshohocken, PA (USA).
18. American Society for Testing Materials, 2011 h. Standard test method for wear preventive characteristics of lubricating fluid (four-ball method). ASTM, West Conshohocken, PA (USA).
19. Salimon, J., Salih, N., Yousif, E., 2011 a. Synthetic biolubricant basestocks from epoxidized ricinoleic acid: improved low temperature properties. *Kem. Ind.* 60 127-134.
20. Salimon, J., Salih, N., Yousif, E., 2011 b. Chemically modified biolubricant basestocks from epoxidized oleic acid: Improved low temperature properties and oxidative stability. *J. Saudi Chem. Soc.* 15, 195-201.
21. Sliverstien, R., Bassler, G., Morrill, T., 2005. Spectrometric identification of organic compounds. 7th ed., John-Wiley, New York.
22. Salimon, J., Salih, N., 2010. Modification of epoxidized ricinoleic acid for biolubricant base oil with improved flash and pour points. *Asian J. Chem*. 22: 5468-5476.
23. Hwang, H.-S., Erhan, S.Z., 2001. Modification of epoxidized soybean oil for lubricant formulations with improved oxidative stability and low pour point. *J. Am. Oil Chem. Soc.* 78: 1179-1184.
24. Zhang, Y.Y., Ren, T.H., Wang, H.D., Yi, M.R., 2004. A comparative study of phenol-type antioxidant in methyl oleate with quantum calculations and experiments. *Lub. Sci.* 16: 385-392.
25. Randals, S.J., 1999. Esters. In: Rudnick, L.R., Shubkin, R.L. (Eds.), Synthetic lubricants and high performance functional fluids. Marcel Dekker, New York, pp. 63-102.
26. Sharma, B.K., Adhvaryu, A., Liu, Z., Erhan, S.Z., 2009. Friction and wear behavior of thioether hydroxyl vegetable oil. *Tribology Int.* 42 353-358.

The Malaysian Journal of ANALYTICAL SCIENCES ISSN 1394-2506

DEOXYGENATION OF PLANT FATTY ACID USING NiSnK/SiO_2 AS CATALYST

(Penyahoksigenan Asid Lemak Tumbuhan Dengan Menggunakan NiSnK/SiO_2 Sebagai Pemangkin Komposit)

L. T. Chiam and C. T. Tye*

School of Chemical Engineering, Engineering Campus,
Universiti Sains Malaysia, 14300 Nibong Tebal, Pulau Pinang, Malaysia

**Corresponding author: chcttye@eng.usm.my*

Abstract

Environmental friendly bio-oil which offers supply reliability as a potential alternative fuel, has spurred to rapid development of biofuels technology. Palm oil is a potential renewable energy source for biofuels production in the future and Malaysia is one of the world largest palm oil producers. However, undesired oxygen content in the plant fatty acid that contributes to low energy density, high viscosity, and low stability, makes the palm oil not effective to be used as biofuels directly. In the present study, the performance of silica supported trimetal catalyst, NiSnK/SiO_2, on deoxygenation of used palm oil was evaluated. In addition, the effects of operating parameters, such as reaction temperature and weight hourly space velocity were investigated. Conversion of palmitic acid as high as 90% was achieved in deoxygenation of used palm oil at reaction temperature 350^{o}C. In order to have a better understanding on the deoxygenation reaction, model compound system using the major saturated fatty acid in the used palm oil, palmitic acid was also carried out. Palmitic acid was found mainly decarboxylated into n-pentadecane with some decarbonylation and isomerizations products.

Keywords: Deoxygenation, used palm oil, palmitic acid, NiSnK/Silica

Abstrak

Minyak-bio mesra alam yang menawarkan kebolehpercayaan bekalan sebagai bahan api alternatif yang berpotensi, telah membawa perkembangan pesat dalam teknologi bahan-api-bio. Minyak kelapa sawit adalah sumber tenaga boleh diperbaharui yang berpotensi bagi pengeluaran bahan-api-bio pada masa akan datang, dan Malaysia merupakan salah satu pengeluar minyak sawit yang terbesar di dunia. Namun, kandungan oksigen dalam asid lemak tumbuhan yang tidak diingini menyumbang kepada ketumpatan tenaga yang rendah, kelikatan yang tinggi, dan kestabilan yang rendah, menjadikan minyak sawit tidak berkesan untuk digunakan sebagai bahan api secara langsung. Dalam kajian ini, prestasi pemangkin, NiSnK/SiO_2 untuk penyahoksigenan minyak kelapa sawit dinilai. Di samping itu, kesan parameter operasi, seperti suhu tindak balas dan halaju ruang berat setiap jam (WHSV) telah dikaji. Penukaran asid palmitik setinggi 90% telah dicapai apabila penyahoksigenan minyak kelapa sawit dijalankan pada suhu tindak balas, 350^{o}C. Untuk mendapatkan pemahaman lanjut mengenai tindak balas penyahoksigenan, sistem sebatian model menggunakan asid lemak tepu utama dalam minyak kelapa sawit terguna, asid palmitik, telah dijalankan. Asid palmitik didapati dinyahkarbosilan terutamanya kepada n-pentadekana dan beberapa produk penyahkarbonilan dan pengisomeran.

Kata kunci: Penyahoksigenan, minyak kelapa sawit terguna, asid palmitik, NiSnK/Silika

Introduction

Biofuels are renewable energy derived from biological carbon fixation, predominantly produced from biomass, which can be used as a substitute for depleting petroleum fuels. Natural plants and animals fats are promising source as fuel owing to their energy contents of the carbon chain. Biofuels refers to solid biomass (bio-char), liquid fuels (bioethanol, vegetable oil and biodiesel) or various gaseous (biogas, biosyngas, and biohydrogen) [1]. From energy security standpoint, utilization of biofuels displaces significant amounts of fossil fuels, and offers supply reliability. In terms of climate change mitigation, environmental friendly and biodegradable biofuels are attractive to reduce

greenhouse gas emissions, and hence reduce air pollution. For economic aspects, development of biofuels protects trade balances and promotes foreign exchange savings through reduce the dependency on imported petroleum. Biofuels create prospect of new economic opportunity for people in rural areas by increasing number of rural manufacturing and farming jobs [1-4].

Malaysia is the world's second largest palm oil producer, accounting for 42.3% of worldwide production. Furthermore, Malaysia is also world's largest palm oil exporter, accounting for 48.3% of world's total exports of palm oil [3]. The optimization of land usage for oil palm cultivation without deforestation has proven the sustainability of oil palm [4]. Thus, palm oil is most productive energy crops with abundant sources and hence a good candidates to enhance into excellent renewable energy in Malaysia [5]. Used cooking oil price is 2.5-3.5 times cheaper than virgin vegetable oils due to no market available for used cooking oil [1]. In order to avoid the fuel and food issue, used palm oil (UPO) is more suitable to be biofuels feedstock than edible palm oil.

However, the biofuels have oxygen levels from 10 to 45 percents. The undesired oxygen content produced especially insoluble impairs engine performance such as plugging of fuel filter, fouling of injector, sticking of ring, and formation of deposit in engine. Removal of oxygen contents inside plant fatty acid is required to improve biofuels quality; increase energy density, reduce viscosity, and stabilize biofuels [6-8]. Removal of carboxyl oxygen can be achieved via deoxygenation or hydrodeoxygenation. During reaction, hydrogen is consumed not only for hydrodeoxygenation, but also for side reaction such as methanation and water-gas shift reaction [9]. Therefore, hydrodeoxygenation is not economically applicable due to high consumption of excess hydrogen and hence high operating cost since raw material constitutes high percentage in expenses of a production line. Besides that, avoid utilization of hydrogen ensure a higher safety. Deoxygenation reactions of fatty acid in the absence of hydrogen flow can occur through two pathways, which are direct decarboxylation and decarbonylation. Direct decarboxylation removes carboxyl group and hence yields carbon dioxide and paraffinic hydrocarbon (alkane with one carbon atom less than original fatty acid), while direct decarbonylation yields carbon monoxide, water and olefinic hydrocarbon (alkene with one carbon atom less than original fatty acid) [10].

In 2006, Snåre et al. [11] evaluated a series of active metals supported on either aluminium oxide, silicon oxide, chromium oxide, magnesium oxide, or activated carbon as catalyst for deoxygenation of stearic acid to desired paraffin product, heptadecane. The comparison results of metal catalyst tested on similar supports by normalizing the metal content revealed the following order Pd>Pt>Ni>Rh>Ir>Ru>Os. In addition, 5% of palladium loading was reported to give the highest conversion of stearic acid and selectivity toward deoxygenated heptadecane. Later in 2008, 5 wt% Pd/C was reported deactivated due to coking and poisoning. Catalyst reactivation with hydrogen did not restore the catalyst activity [12].

Do et al. compared performance of 1 wt% platinum supported on gamma alumina (Pt/Al_2O_3) and titania (Pt/TiO_2) for deoxygenation of methyl octanoate and methyl stearate. The results showed that higher selectivity of heptadecane was achieved by utilization of Pt/Al_2O_3 as catalyst. Deactivation study was also carried out. Deactivation was reported due to oligomerization of unsaturated hydrocarbons and heavy compounds to coke which blocked the active site of catalysts [13]. Recently, catalytic deoxygenation of triglycerides to paraffins and olefins was carried out in a semibatch reactor with reactive distillation fashion, in which products were quickly removed from reaction mixture in flowing Helium. PtSnK/silica was found to be best catalyst for deoxygenation of triglycerides and methyl ester to olefins. Addition of tin was found to reduce sites that interact with hydrogen and CO strongly and consequently reduce selectivity to side reaction hydrogenation /hydrogenolysis by products [14].

Significant effect of tin addition on catalyst performance has reported before for linear olefin production from saturated fatty acid. The catalytic system consisted of nickel catalyst and at least a metal selected from the group consisting of tin, germanium or lead group. The nickel carrier preferably non-acidic silica, titanium oxide, or zinc oxide. NiSn catalyst achieved 65%, the highest selectivity to C_{15} olefin, with no thermal cracking that resulted in product with less carbon number and hence low in energy density. Without tin addition, the olefin yield reduced to 6% only, and large fraction of cracking products produced [15].

Due to high cost of palladium and platinum catalyst, it is not suitable from economical view. A modified trimetal catalyst, $NiSnK/SiO_2$ for deoxygenation of plant fatty acid is being investigated in detail in the present study. The catalyst performance was evaluated over UPO and its model compound, palmitic acid.

Materials and Methods

Catalyst preparation

In this study, $NiSnK/SiO_2$ catalysts were prepared based on [14, 16]. SiO_2 support used was obtained commercially. Metal was loaded onto the support by incipient wetness impregnation method. The weight ratio of Ni:Sn:K was 1:1.3:1.5. Firstly, desired amount of nickel (II) nitrate hexahydrate, $Ni(NO_3)_2.6H_2O$ (ACROS, 99%) and tin (II) chloride, $SnCl_2.2H_2O$ (MERCK, 98%) were dissolved in distilled water, impregnated to silica support and followed by drying in air at 120°C for 16 hrs in oven [16]. Then, calcination was carried out in a muffle furnace at 700°C for 8 hrs. Potassium was then incorporated onto the prepared $NiSn/SiO_2$ catalyst with the same procedure by using KOH (MERCK, 85%) as the potassium precursor, but calcined for 2 hrs at 400°C in the air [14].

Catalyst characterization

Catalyst specific surface are, pore size and pore volume were measured by nitrogen adsorption–desorption at liquid nitrogen temperature using a Micrometrics ASAP 2020 System. Prior to the measurements, samples were degassed at 77 K for 4 hrs. Pore size distributions was obtained using Barrett-Joyner-Halenda (BJH) model applied to desorption isotherms data. The micropores area were estimated using the correlation of *t*-plot method [17].

X-ray diffraction (XRD) analysis was carried out by a Philips X-Ray Diffractometer. The diffraction patterns were recorded using Cu-Kα radiation and taken in the range of 10-90° (2θ).

Catalyst activity test

The deoxygenation reactions were conducted in a fixed-bed reactor with outer diameter of ½ inch. Schematic diagram of the reactor system is shown in Figure 1.

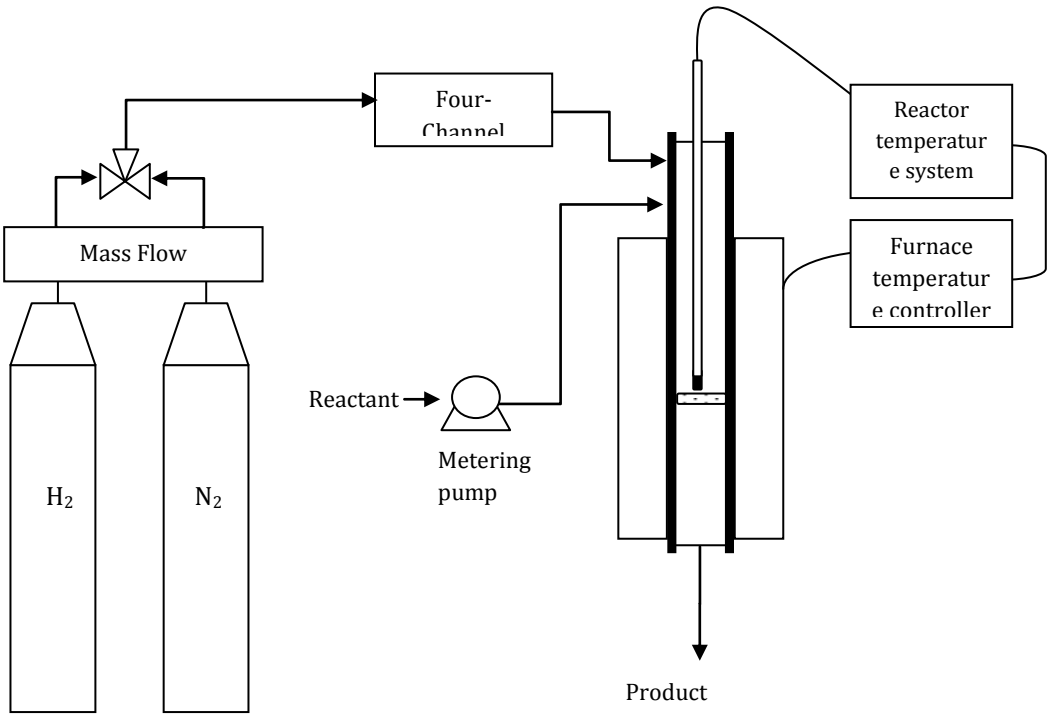


Figure 1. Schematic diagram of fixed-bed reactor system

Prior to reactions, the catalyst was activated based on [18], reduced in flowing H_2 ($100cm^3$ (STP) min^{-1}) for 2 hrs at 200^oC. Then, the reactor was replaced by 10 ml/min nitrogen flow. The flow of hydrogen and nitrogen gas was controlled by mass flow controller (MKS Instrument model M100B). The reactor was heated up to the desired temperatures in a tube furnace (Nabertherm B170).

When reaching desired temperature, feedstock (UPO without solvent, or palmitic acid dissolved in dodecane solvent) was pumped into the reactor from the top by using a metering pump. The feed rate was determined based on weight hourly space velocity (WHSV) of the reaction. Liquid sample from reactor outlet was collected in every half an hour interval continuously for 3 hours. The liquid product was analyzed by an offline gas chromatography (Perkin Elmer) equipped with a flame ionization detector (FID) and HP-INNOWAX capillary column (30m x 0.25mm x 0.25 µm).

Results and Discussion

Used Palm Oil (UPO)

The feed, UPO was analyzed by using a gas chromatograph-mass spectrometry (GC-MS). It showed that the major components were oleic acid and palmitic acid, which is in agreement with major components reported [19, 20], as shown in Table 1. Impurities of aldehyde (such as dodecanal, and 9-octadecanal) and alcohol (such as 2-methyl-1-hexadecanol and 1-heptadecanol) existed in small concentration have also been found in the current research. It is due to the presence of oxygen atoms in fatty acid which undergo oxidation into alcohol, aldehyde and insolubles. The degraded chains will polymerize and hook together into insoluble gums and hence cause clogging parts in engine if the oil is applied as engine fuel [21].

Table 1. Major composition of fatty acid in UPO (waste cooking oil) [20]

Fatty acid common name	Abbreviation*	Composition (wt %)
Palmitic acid	16:0	22.47
Stearic acid	18:0	12.51
Oleic acid	18:1	27.64
Linoleic acid	18:2	14.58

*Abbreviation was referred to number of carbon atoms: number of double bonds.

Deoxygenation of fatty acid leads to hydrocarbon production. After a non-catalytic thermal reaction, significant amount of alkane and alkene have been found in the liquid product from GC-MS analysis. It can tell that deoxygenation of fatty acid to alkane and alkene has occurred during the reaction. Therefore, it can be deduced that higher conversion of fatty acid lead to higher deoxygenation of the system. Due to complex mixture of different types of fatty acid present in the UPO, deoxygenation of major saturated fatty acid of UPO, which is palmitic acid was focus in the present study.

Catalyst characterization

The results of nitrogen adsorption surface analysis were summarized in Table 2. The catalyst was found to have large 60 Å pore size with 84.81 m^2/g BET surface area. Nitrogen adsorption isotherm for the catalyst is shown in Figure 2. It is a type IV isotherm with hysteresis loop. The initial part of the Type IV isotherm was attributed to monolayer-multilayer adsorption [22].

Table 2. Physical properties of $NiSnK/SiO_2$ catalyst

Particular	Amount
BET surface area	84.81 m^2/g
t-plot micropore area	4.85 m^2/g
BJH Desorption average pore diameter	60 Å
BJH Desorption pore volume	0.18 cm^3/g

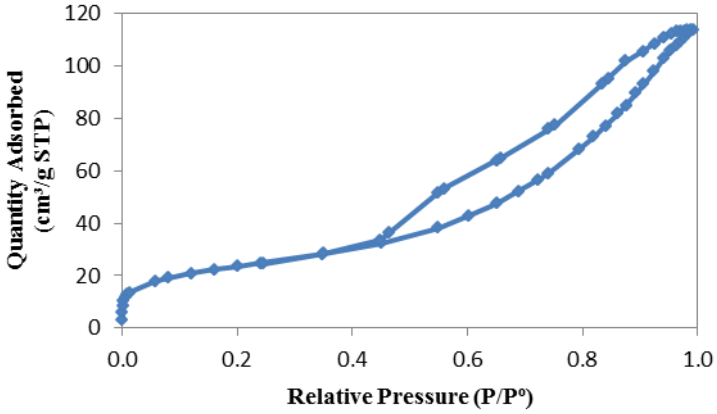


Figure 2. Nitrogen adsorption-desorption isotherm of $NiSnK/SiO_2$ catalyst

The XRD pattern of the catalyst is shown in Figure 3. Three different phases of the crystalline structure were identified, which were silicon oxide (SiO_2), nickel tin (NiSn) and potassium oxide (K_2O_2). Diffraction peak of silica used as support in the present study, appeared at 2Θ of 22°, 34°, 52°, 63° and 65°. Diffraction peaks of nickel tin (NiSn) were observed at 2Θ of 43° and 79°. Another phase identified was potassium oxide. The diffraction peaks of potassium oxide were observed at 2Θ of 27°, 42° and 55°.

NiSn was observed and this could be due to both metal precursor of Ni and Sn were mixed and impregnated together during catalyst preparation. K_2O_2 was found because of oxidation of outer layer of potassium coating on $NiSn/SiO_2$ catalyst in the presence of air. Only potassium existed in oxide form. Potassium is more reactive than Ni and Sn, and hence more easily undergoes oxidation.

Deoxygenation of UPO

A catalytic deoxygenation reaction with $NiSnK/SiO_2$ as catalyst carried out at WHSV of 4 hr^{-1} at 300°C was compared to a thermal reaction for the conversion of palmitic acid within UPO. The conversions of palmitic acid for both tests are showed in Figure 4. The conversions for both reactions seem to increase even after 3 hours of continuous reaction. This could be due to the system has yet reaching the steady state condition. Generally, reaction with catalyst had a higher conversion compared to that of without catalyst. The conversion of palmitic acid collected at 180 minutes for catalytic test was 84.96% compared to 62.13% in a non-catalytic test. The conversion has increased by 22.83% in the presence of catalyst, $NiSnK/SiO_2$. Therefore, deoxygenation reactions were further carried out for the effects of operating parameters.

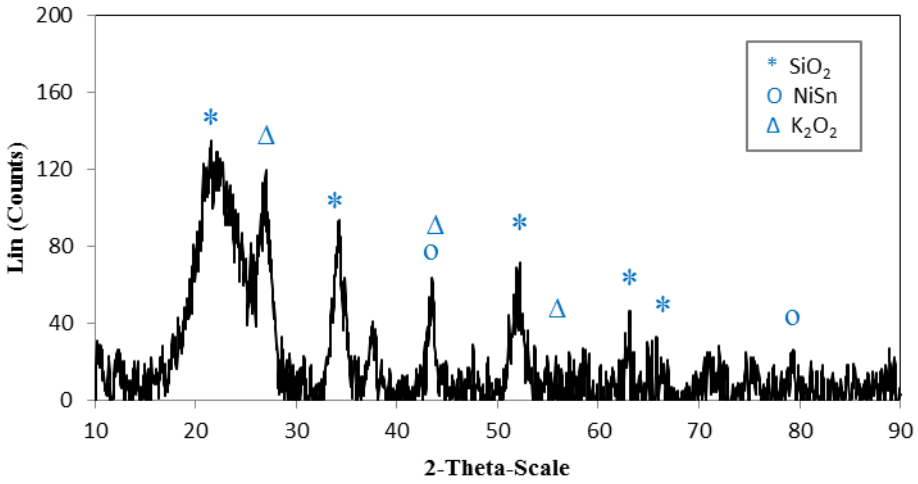


Figure 3. X-ray diffraction pattern for NiSnK/SiO_2.

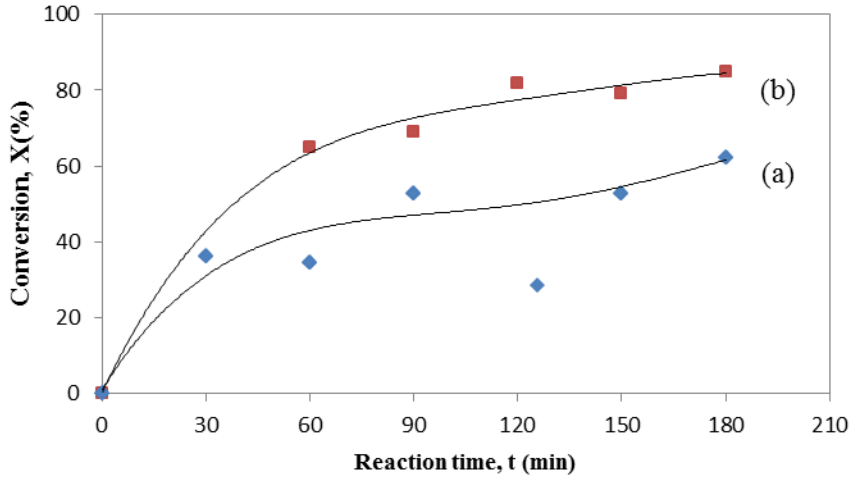


Figure 4. Conversions of palmitic acid for (a) thermal and (b) catalytic deoxygenation (300^{o}C, WHSV = 4 hr^{-1}).

Effect of WHSV on deoxygenation of UPO

In the present study, WHSV was varied by manipulating the flow rate of UPO while keeping the catalyst mass fix. The catalyst bed was kept in cylindrical shape at middle part of reactor with diameter of 0.8 cm and thickness of 1 cm. The size of catalyst bed was fixed in the present study in order to wipe out other factors that could have influenced the reaction rate such as mass transfer resistance and pressure drop. The effects of WHSV at 4, 6, and 8 hr^{-1} on deoxygenation of UPO were studied and the results are presented in Figure 5. A linear decreasing trend in conversion of palmitic acid with WHSV was observed as expected. The trend obtained in this research was in agreement with Priecel et al. [23].

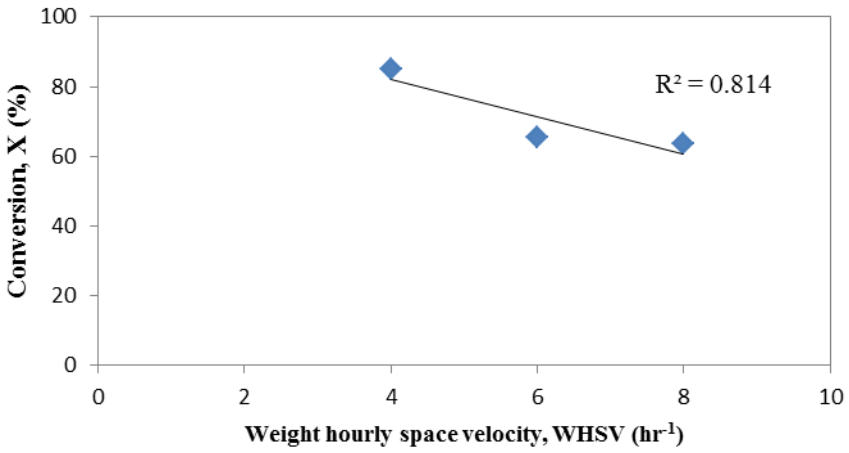


Figure 5. Effects of WHSV on the conversion of palmitic acid (sample collected at 180 mins, 300°C).

Effect of reaction temperature on deoxygenation of UPO

Three different reaction temperatures, 250°C, 300°C, and 350 °C were studied in deoxygenation of UPO using $NiSnK/SiO_2$ as the catalyst. WHSV of 4 hr^{-1} was applied in this study since the highest conversion of palmitic acid was achieved with this WHSV. The effect of temperature on the conversion of palmitic acid is shown in Figure 6. A linear increasing trend of palmitic acid conversion with reaction temperature was observed. Similar trend had also been observed by other researchers [12, 18, 24, 25].

Higher conversion of palmitic acid achieved at higher temperature was expected as the deoxygenation reaction is endothermic and the reaction rate increase with the temperature. The conversion was the highest at 350°C proved that thermal stability of $NiSnK/SiO_2$ is reasonable. The catalyst able to withstand high temperature and maintains its catalytic activity at 350 °C.

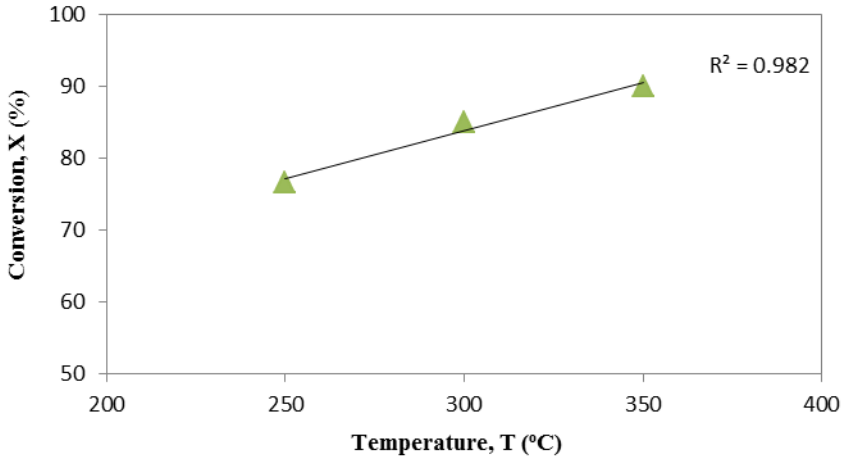


Figure 6. Effect of temperature on conversion of palmitic acid (sample collected at 180 mins, WHSV= 4 hr^{-1}).

Deoxygenation of palmitic acid

Palmitic acid was used as model compound of UPO in order to obtain further understanding on deoxygenation of UPO. WHSV was varied in order to observe products formed under different contact time. From the analysis, n-pentadecane product, $C_{15}H_{32}$ was detected in samples for all the reactions. N-pentadecane is an alkane with 15 carbon atoms, one carbon less than palmitic acid. Thus, it was produced via decarboxylation.

$$C_{15}H_{31}COOH \xrightarrow{\text{decarboxylation}} C_{15}H_{32} + CO_2$$

When the contact time for reaction was increased, additional three isomers of pentadecane were observed (2,5-dimethyltridecane, 4,8-dimethyltridecane and 2,7,10-trimethyldodecane). Besides that, pentadecene ($C_{15}H_{30}$) and its isomer, alkene with a double bond and one carbon less than palmitic acid was also observed. This was found to be the product of decarbonylation. Thus, the reaction mechanism for deoxygenation of palmitic acid is proposed, as shown in Figure 7.

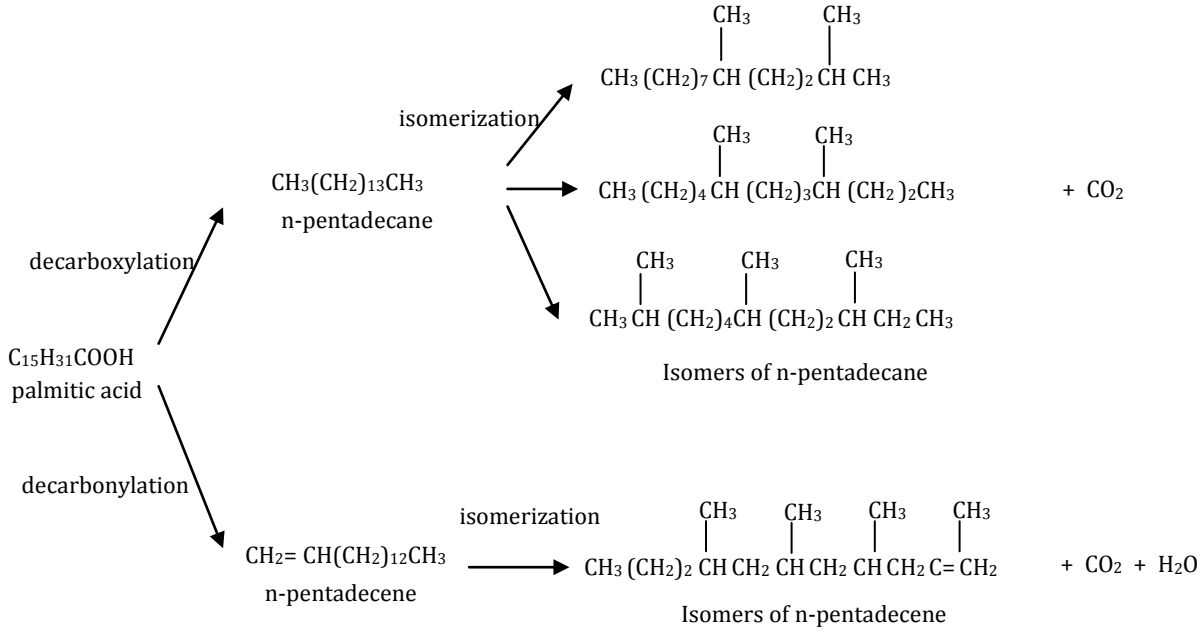


Figure 7. Reaction mechanism for deoxygenation of palmitic acid.

Conclusion

Deoxygenation of UPO with NiSnK/SiO_2 catalyst for the production of diesel-like hydrocarbon was investigated. NiSnK/SiO_2 was found to be an effective catalyst for the reactions. Conversion of palmitic acid, the major fatty acid in UPO was found to increase with reaction temperature and decrease with space velocity as expected. The highest conversion of palmitic acid in UPO, 90.08% was achieved in the present study at 350 ^{o}C. Reactions of palmitic acid model compound system proof that deoxygenation was via decarboxylation and decarbonylation.

Acknowledgement

The authors acknowledge the financial support provided by Universiti Sains Malaysia under RU Grant (814130).

References

1. Ayhan, D. (2009). Political, economic and environmental impacts of biofuels: A review. *Applied Energy*, 86(1): S108-S117.
2. Timilsina, G.R. & Shrestha, A. (2011). How much hope should we have for biofuels? *Energy*, 36(4): 2055-2069.
3. Zhou, A. & Thomson, E. (2009). The development of biofuels in Asia. *Applied Energy*, 86(1): S11-S20.
4. Lam, M. K., Tan, K. T., Lee, K. T. & Mohamed, A. R. (2009). Malaysian palm oil: Surviving the food versus fuel dispute for a sustainable future. *Renewable and Sustainable Energy Reviews*, 13(6-7): 1456-1464.
5. Sumathi, S., Chai, S. P. & Mohamed, A. R. (2008). Utilization of oil palm as a source of renewable energy in Malaysia. Renewable and Sustainable Energy Reviews, 12(9): 2404-2421.
6. Kwon, K. C., Mayfield, H., Marolla, T., Nichols, B. & Mashburn, M. (2011). Catalytic deoxygenation of liquid biomass for hydrocarbon fuels. *Renewable Energy*, 36(3): 907-915.
7. Rakopoulos, C. D., Antonopoulos, K. A., Rakopoulos, D. C., Hountalas, D. T. & Giakoumis, E. G. (2006). Comparative performance and emissions study of a direct injection Diesel engine using blends of Diesel fuel with vegetable oils or bio-diesels of various origins. *Energy Conversion and Management*, 47(18-19): 3272-3287.
8. Ayhan, D. (2003). Biodiesel fuels from vegetable oils via catalytic and non-catalytic supercritical alcohol transesterifications and other methods: a survey. *Energy Conversion and Management*, 44(13): 2093-2109.
9. Lestari, S., Mäki-Arvela, P., Beltramini, J., Lu, G. Q. M. & Murzin, D. Y. (2009). Transforming triglycerides and fatty acids into biofuels. ChemSusChem, 2(12): 1109-1119.
10. Immer, J. G., Kelly, M. J. & Lamb, H. H. (2010). Catalytic reaction pathways in liquid-phase deoxygenation of C18 free fatty acids. *Applied Catalysis A: General*, 375(1): 134-139.
11. Snåre, M., Kubic Ková, I., Mäki-Arvela, P., Eränen, K. & Murzin, D. Y. (2006). Heterogeneous catalytic deoxygenation of stearic acid for production of biodiesel. *Industrial & engineering chemistry research*, 45(16): 5708-5715.
12. Mäki-Arvela, P., Mäki-Arvela, P., Snåre, M., Eränen, K., Myllyoja, J. & Murzin, D. Y. (2008). Continuous Decarboxylation Of Lauric Acid Over Pd/C Catalyst. *Fuel*, 87(17-18): 3543-3549.
13. Do, P.T., Chiappero, M., Lobban, L. L. & Resasco, D. E. (2009). Catalytic deoxygenation of methyl-octanoate and methyl-stearate on Pt/Al_2O_3. *Catalysis letters*, 130(1): 9-18.
14. Chiappero, M., Do, P. T. M., Crossley, S., Lobban, L. L. & Resasco, D. E. (2011). Direct conversion of triglycerides to olefins and paraffins over noble metal supported catalysts. *Fuel*, 90(3): 1155-1165.
15. Stern, R. & Hillion, G. (1985). Process for manufacturing a linear olefin from a saturated fatty acid or fatty acid ester. United States Patents, Pat No. 4,554,397
16. Penkova, A., Bobadilla, L., Ivanova, S., Domínguez, M. I., Romero-Sarria, F., Roger, A. C., Centeno, M. A. & Odriozola, J. A. (2011). Hydrogen production by methanol steam reforming on NiSn/MgO–Al2O3 catalysts: The role of MgO addition. *Applied Catalysis A: General*, 392(1-2): 184-191.
17. Kubička, D. & Kaluža, L. (2010). Deoxygenation of vegetable oils over sulfided Ni, Mo and NiMo catalysts. *Applied Catalysis A: General*, 372(2): 199-208.
18. Bernas, H., Eränen, K., Simakova, I., Leino, A.-R., Kordás, K., Myllyoja, J., Mäki-Arvela, P., Salmi, T. & Murzin, D. Y. (2010). Deoxygenation of dodecanoic acid under inert atmosphere. *Fuel*, 89(8): 2033-2039.
19. Hoekman, S.K., Hoekman, S. K., Broch, A., Robbins, C., Ceniceros, E. & Natarajan, M. (2012). Review of biodiesel composition, properties, and specifications. *Renewable and Sustainable Energy Reviews*, 16(1): 143-169.
20. Ong, Y.K. & Bhatia, S. (2010). The current status and perspectives of biofuel production via catalytic cracking of edible and non-edible oils. *Energy*, 35(1): 111-119.
21. Jain, S. & Sharma, M.P. (2010). Stability of biodiesel and its blends: A review. *Renewable and Sustainable Energy Reviews*, 14(2): 667-678.
22. Sing, K., Everett, D., Haul, R., Moscou, L., Pierotti, R., Rouquerol, J. & Siemieniewska, T. (1985). Reporting physisorption data for gas/solid systems. *Pure Appl. Chem*, 57(4): 603-619.
23. Priecel, P., Kubička, D., Čapek, L., Bastl, Z. & Ryšánek, P. (2011). The role of Ni species in the deoxygenation of rapeseed oil over NiMo-alumina catalysts. *Applied Catalysis A: General*, 397(1-2): 127-137.

24. Snåre, M., Kubičková, I., Mäki-Arvela, P., Chichova, D., Eränen, K. & Murzin, D. Y. (2008). Catalytic deoxygenation of unsaturated renewable feedstocks for production of diesel fuel hydrocarbons. *Fuel*, 87(6): 933-945.
25. Simakova, I., Simakova, O., Mäki-Arvela, P., Simakov, A., Estrada, M. & Murzin, D. Y. (2009). Deoxygenation of palmitic and stearic acid over supported Pd catalysts: Effect of metal dispersion. *Applied Catalysis A: General*, 355(1-2): 100-108.

The Malaysian Journal of ANALYTICAL SCIENCES ISSN 1394-2506

PHASE BEHAVIOUR OF FATTY ALCOHOL SULPHATE AND FATTY ALCOHOL ETHER SULPHATE FROM PALM BASED

(Kelakuan Fasa Lelemak Alkohol Sulfat Dan Lelemak Alkohol Eter Sulfat Berasaskan Sawit)

Nur Syazani Harun, Norhana Nabila Mohamed Talip, Liew Kin Hong,
Mohd Suzeren Md Jamil, Rahimi M. Yusop*

School of Chemical Sciences and Food Technology, Faculty of Science and Technology, Universiti Kebangsaan Malaysia, 43600 Bangi Selangor, Malaysia

**Corresponding author: rahimi@ukm.my*

Abstract

The phase diagrams of fatty alcohol sulphates (FAS)/ fatty alcohol ether sulphates (FAES)/water and mixed FAS:FAES (1:1)/propylene glycol/water were constructed at room temperature. Another phase diagram of mixed FAES/FAS/soap (4.5:4.5:1.0)/propylene glycol/water were established at 60˚C. Birefringence was observed under cross-polarized light and their phase changes examined under a polarized microscope. The liquid crystalline region for FAES and FAS occurred only in a small region. The optical patterns of lamellar liquid crystal observed were oily streaks and a typical fine cross-striated structure.

Keywords: lamellar liquid crystal, FAS, FAES, anionic surfactant, ternary phase diagram

Abstrak

Gambarajah fasa campuran lelemak alcohol sulfat (FAS)/lelemak alcohol eter sulfat (FAES)/sabun (4.5:4.5:1.0)/propelina glikol/air telah dibina pada suhu bilik. Selain itu, gambarajah fasa FAS/FAES/sabun (4.5:4.5:1.0)/propilena glycol/air turut dibina pada suhu 60˚C. Dwibiasan telah diperhatikan melalui pengutub bersilang manakala perubahan fasa telah dikaji dengan menggunakan mikroskop berkutub. Keputusan menunjukkan hablur cecair bagi FAS dan FAESterbentuk pada kawasan yang kecil. Ciri optikal bagi hablur cecair lamella didapati mempunyai struktur carikan berminyak.

Kata kunci: hablur cecair lamella,FAS,FAES, surfaktan anionik, gambarajah fasa tenari

Introduction

Soap and anionic surfactants have traditionally been the major constituents in many cleaning agents [1]. FAS and FAES derived from palm oil are produced from Chemiton technology in the Malaysian Palm Oil Board (MPOB). However, they show low activity and were therefore mixed for a synergistic effect on their properties. Many other works on other mixed have shown the advantages of using mixed surfactants in terms of enhancing the performances of single surfactants [2-6]. But for the mixing to be successful, it is necessary to understand the physico-chemical behaviour of the surfactants, and a study of their ternary phase systems was carried out to identify the contributions of the different components in the formulation of new products [7]. The phase behaviour and other properties of mixed surfactants have been studied by Hoffman *et al*. [8-10]. The mesophase changes can be described from phase diagrams. The type of liquid crystal has a major influence on product properties. About seven different classes of liquid crystals have now been recognised, the major ones being lamellar, hexagonal, cubic, nematic and gel phase [11]. Liquid crystal surfactants are common in products such as detergents, shampoos and household cleaners. The aim of this work was to identify the phase behaviour in ternary systems of FAES/FAS/water, FAES/FAS (1:1)/PG/water and FAES/FAS/soap (4.5:4.5:1.0)/PG/ water.

Materials and Methods

Materials

The surfactants were FAS and fatty alcohol ether sulphate (FAES), obtained from the Advanced Oleochemicals Technology Centre (AOTC), MPOB (Figure 1). The specifications of these compounds are shown in Table 1. Soap was obtained from Unichema Sdn Bhd and its specifications shown in Table 2. Propylene glycol (PG) was of 99% purity. All these chemicals were used without further purification.

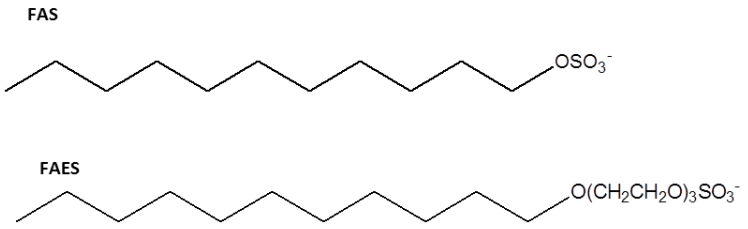


Figure 1. Structures of FAS and FAES

Table 1. Specification of FAS and FAES

Properties	FAES	FAS
Active	27.37 %	27.65
Unsulphonated matter	0.32%	0.74%
Moisture	68.62%	71.77%
Color	0.4 R,	2.0 R,
Petroleum ether extraction	3.7 Y	10.0 Y
PH (10%)	-	1.13%
	-	9.61

Table 2. Specification of soap

Properties	
Total fatty matter %	9-81
Moisture %	10.5-12.5
Free fatty acids %	1.3 max
Sodium chloride %	0.4-0.6
Glycerol %	0.1-0.2
Sequestrants	Present
Typical titer (Fatty acids) deg. C	44-47

Three phase diagrams, FAES/FAS/ water (phase diagram 1), FAES/FAS (1:1)/PG/water (phase diagram 2) and FAES/FAS/soap (4.5:4.4:1.0)/PG/water (phase diagram 3), were prepared at room temperature (25˚C) with the exception of phase diagram 3 which was prepared at 60˚C to dissolve the soap component. The procedure of preparation was the same with only the components and their ratios different. 0.5 g mixtures were placed in test tubes, approximately 0.5% deionised water added and the mixture homogenized at 4,000 rpm for 15 minutes (Jouan CR3I) to eliminate air bubbles. Each sample was centrifuged for at least 3 times and then allowed to equilibrate in a water bath at 25˚C for at least 15 minutes. The phases were identified by observation through polarized film and crossed polarizing microscope with a heating stage (Olympus AX70). More water was added to the test tube and the procedure repeated.

Results and Discussion

Phase diagram 1

The ternary system of FAES/FAS/ water was plotted at room temperature (Figure 2). The phase changed from lamellar liquid crystalline phase (LC) → two-phase region (2p) → isotropic region (1p) with the results summarized in Table 3. liquid crystal region were observed in 80/20, 70/30, 60/40, 50/50 and 40/60. The optical patterns observed under a microscope for each phase transition are shown in Figure 3. The texture of the lamellar liquid crystal obtained was comparable with those in the literature (7 and 8).

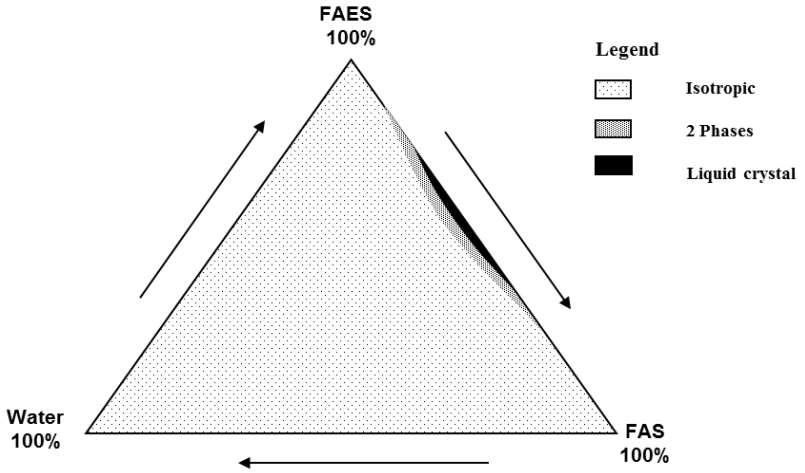


Figure 2. Phase diagram of FAES:FAS:Water at room temperature

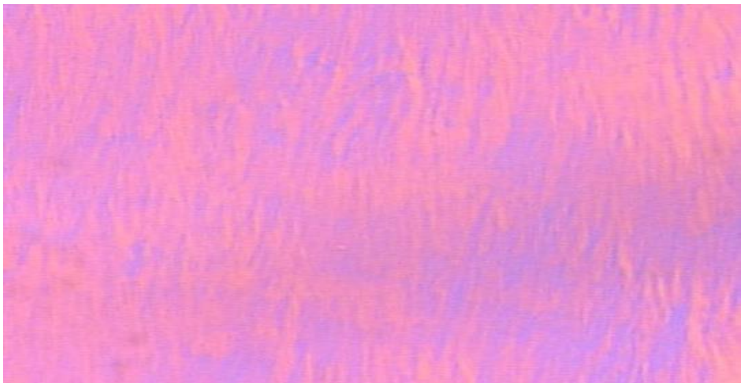


Figure 3. The optical patterns of FAES:FAS:Water at room temperature.

Table 3. Phase transition summary of FAES/FAS/water at room temperature

FAES/FAS (w/w%)	Phase Transition
100/0	1p
90/10	1p
80/20	LC →2p →1p
70/30	LC →2p →1p
60/40	LC →2p →1p
50/50	LC →2p →1p
40/60	LC →2p →1p
30/70	1p
20/80	1p
10/90	1p
0/100	1p

Phase diagram 2

Based on phase diagram 1, the liquid crystalline regions of FAES and FAS at 1:1 ratio were selected for further study of their phase behaviour by adding PG. The ternary system of FAES/FAS (1:1)/PG/water at room temperature was plotted as in Figure 4. The smallest liquid crystalline region was obtained in 100% FAS without PG. The rest of ratios started from 100/0 to 10/90 exhibit isotropic region. The phase transition results are summarized in Table 4. The optical patterns of LC, 2p and 1p observed are shown in Figure 5.

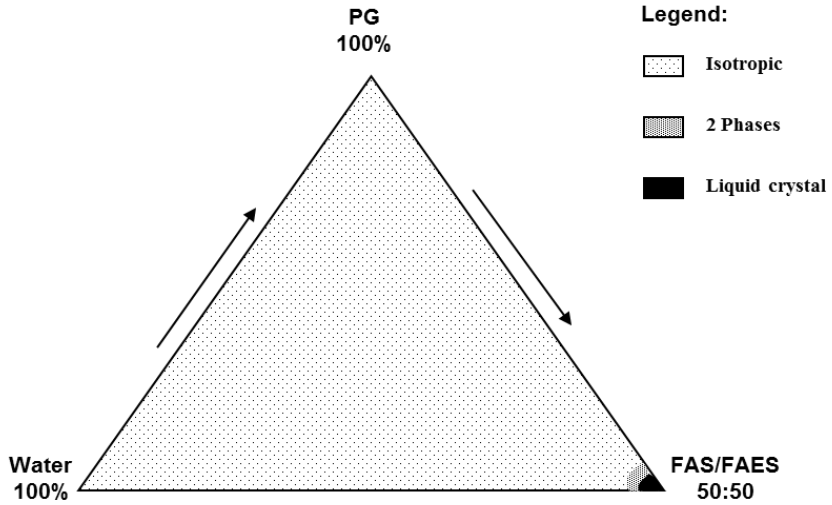


Figure 4. Phase diagram of FAES/FAS:PG:Water at room temperature

Table 4. Phase transition summary of mixed FAES/FAS(1:1)PG/water at room temperature

(FAES/FAS)/PG (w/w%)	Phase Transition
100/0	1p
90/10	1p
80/20	1p
70/30	1p
60/40	1p
50/50	1p
40/60	1p
30/70	1p
20/80	1p
10/90	1p
0/100	LC→2p →1p

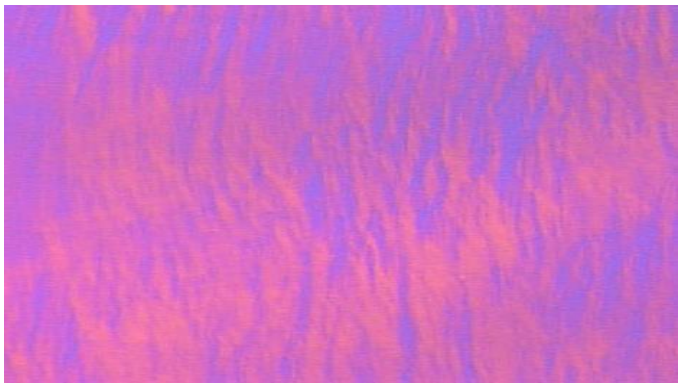


Figure 5. The optical patterns of FAES/FAS:PG:Water at room temperature.

Phase diagram 3

Using the same amounts of FAS and FAES, soap was added, i.e. a ratio of 4.5:4.5:1.0 of mixed FAS:FAES:soap, as shown in Figure 6. The LC region formed at 100% FAS with soap in 4% to 14% water. The phase transition results are summarized in Table 5. The optical patterns of LC, 2p and 1p observed were as shown in Figure 7. Mixtures of FAES and FAS with water as the third component, a large LC area was found compared to the mixture of FAES, FAS and soap. When water was replaced with PG, no improvement in LC region occurred as in phase diagrams 1 and 2. The surfactant mixtures of FAES/FAS/water exhibited oily streaks and a fine cross-striated texture implying a lamellar liquid crystal structure.

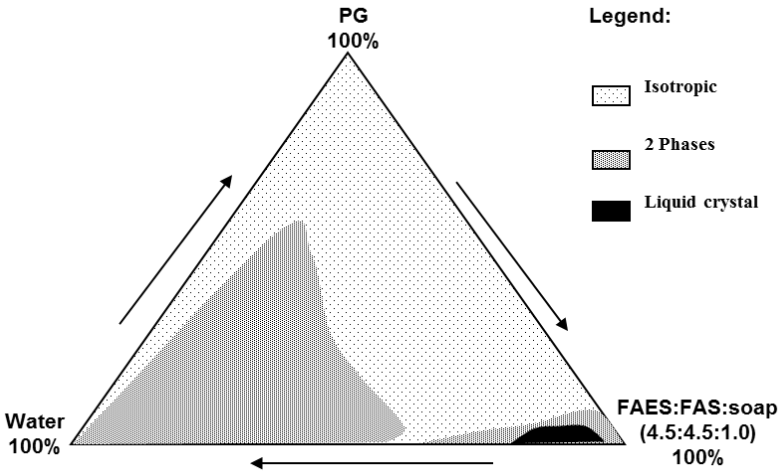


Figure 6. Phase diagram of (FAES/FAS:soap):PG:Water at 60°C

Table 5. Phase transition summary of the ternary system of (FAES/FAS/soap)/PG/water at 60°C

(FAES/FAS/soap) /PG (w/w%)	Phase Transition
100/0	1p
90/10	1p→2p
80/20	1p→2p
70/30	1p→2p
60/40	1p→2p
50/50	1p→2p
40/60	1p→2p
30/70	1p→2p
20/80	1p→2p
10/90	2p→ 1p→2p
0/100	2p→ LC → 2p→1p →2p

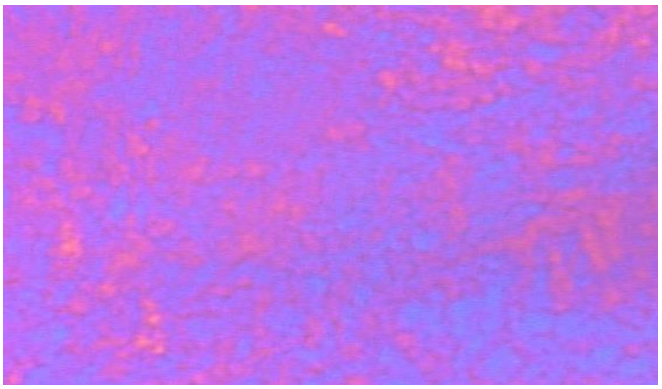


Figure 7. The optical patterns of (FAES/FAS:soap):PG:Water at 60^{o}C.

Conclusion

In conclusion, the phase diagrams based on various combination of fatty alcohol sulphates , fatty alcohol ether sulphates, water, propylene glycol and soap were constructed at different condition. Birefringence was observed under cross-polarized light and their phase changes examined under a polarized microscope showed formation of lamellar liquid crystal identified as oily streaks and a typical fine cross-striated structure.

Acknowledgement

This work was supported financially by the Government of Malaysia grant no. GGPM-2012-010, FRGS/1/2012/ST01/UKM/02/1, GUP-2012_070. We are grateful to Zaihanif Hussin for his helpful advice regarding the microscopic study.

References

1. Lynn, J. 1991. *Detergency.* John Wiley & Sons, New York: 1072-1117.
2. Scamehorn, J.F., & J.H. Harwell. 1993. *Precipitation of Surfactant Mixtures, in Mixed Surfactant systems*, . New York: 283-312.
3. Scamehorn, J.F.1986. *An overview of Phenomena Involving Surfactant Mixtures, in Phenomena in Mixed Surfactants Systems*: 1-27 .
4. Cheryl, H., Rodriguez, Chanin, C., Scamehorn, J.F., Chintana, S., and Sumaeth, C.1998. Precipitation in Solutions Containing Mixtures of Synthetic Anionic Surfactants and Soap. *J. Surf. Det.* 1: 321-325.
5. Michael F. Cox, Nelson F. Borys and Ted P. Matson.1985. Interactions between LAS and Nonionic Surfactants. *J. Am. Oil Chem. Soc*. 62:1139-1143.
6. Scamehorn, J.F., and J.H., Harwell.1993. Precipation of surfactants mixtures, in Mixed Surfactant Systems, edited by K.Ogino and M. Abe, Marcel Dekker, Inc., New York: 283-312.
7. Comellas, F., Megias, V., Sanches, J., Parra, J.L., Coll, J., Ballaguera, F. and Pelejero, C. 1989. Applications of ternary systems in specific cosmetic formulation. *Int. J. of Cosmetic Sci*. 11: 5-19.
8. Hauthal, H.G. 2001. *48th SEPAWA Congress 2001, J. Applied Sci.* 127: 8-12.
9. Caroline. 1999. *Liquid crystal in cosmetic emulsion*, Personal Care Ingredients Asia, Step publishing limited: 120-129.
10. Nielsen, M., Drews, B. 2001. Lamellar liquid crystals in o/w cosmetic emulsion. *Int.l J. Applied Sci.* 127: 8-12.
11. Hauthal, H.G. 2001. Würzburg conference-Progress on Detergents, Würzburg conference-Progress on Detergents, *Int. J. Applied Sci*. 127: 8- 12.

The Malaysian Journal of ANALYTICAL SCIENCES ISSN 1394-2506

PENENTUAN KUALITI MINYAK MASAK DAN LEMAK KOMERSIAL MENGGUNAKAN TEKNIK KIMOMETIK

(Determination of Commercials Cooking Oils and Fats Using Chemometrics Methods)

Azwan Mat Lazim[1]*, Mohd Zuli Jaafar[2], Phang Wei Shong[1], Suzereen Jamil[1]

[1]*Pusat Pengajian Sains Kimia & Teknologi Makanan, Fakulti Sains & Teknologi, Universiti Kebangsaan Malaysia, 43600 Bangi,Selangor, Malaysia*
[2]*Universiti Teknologi MARA, 72007 Kuala Pilah, Negeri Sembilan*

**Corresponding author: azwani79@ukm.my*

Abstrak

Dalam kajian ini, kaedah kimometrik telah digunakan bagi menentukan kualiti beberapa jenis minyak masak komersil daripada dua jenama yang berbeza. Sampel minyak masak yang telah digunakan ialah minyak zaitun, minyak bunga matahari dan mentega dalam dua keadaan yang berbeza, iaitu segar dan digoreng. Kaedah konvensional dilakukan untuk menentukan kualiti minyak, iaitu peratus asid lemak bebas, nilai iodin dan nilai peroksida. Sebanyak 12 sampel minyak telah dianalisis menggunakan spektroskopi inframerah fourier transformasi (FTIR) pada jalur 4000-400 cm^{-1}. Stimulasi komputer telah dilakukan berdasarkan pencaman corak FTIR dan data pencaman corak dioptimumkan kepada model analisis komponen utama (PCA) dan kuasa dua terkecil separa (PLS). Model PCA digunakan dalam kajian ini bagi membezakan sifat-sifat antara minyak komersial segar dan minyak digoreng. Kemudian model PLS digunakan untuk mendapatkan ujian pengesahan antara kedua-dua minyak. Ujian ini dapat membandingkan hasil yang diramal oleh kaedah PLS dengan nilai yang diperoleh menggunakan kaedah konvensional. Keputusan yang diperoleh menunjukkan ujian pengesahan bagi minyak komersial mempunyai nilai kecerunan graf iaitu 0.90. Ini menunjukkan kaedah kimometik adalah signifikan dengan kaedah konvensional.

Kata kunci : Kimometrik; kualiti minyak; PCA; PLS

Abstract

In this study, chemometric method has been used in determining the oil quality. The samples used were olive oil, sunflower oil and butter from two different brands. Two different conditions were applied, either it was fresh or fried. Titratio, a conventional method was used to determine free fatty acids content (FFA), iodine value (IV), and peroxide value (PV). Twelve samples were then used for analysis and their FTIR spectra were measured at 4000-400 cm^{-1}. The computer stimulation was used to process the data based on their pattern recognition which optimized by principal component analysis (PCA) and partial least squares (PLS). PCA model was used to distinguish the properties between fresh and fried oil. The PLS model was used to predict the value for validation test in comparison with conventional results. Results showed the validation value for fresh oil was 0.90. This indicated the chemometric method was in agreement with conventional method.

Keywords: Chemometric; Oil quality; PCA; PLS

Pengenalan

Pada awal tahun 50an Sinclair et. al. (1952) telah mempelopori usaha menggunakan kaedah infra merah bagi menentukan kualiti minyak [1]. Beliau telah menyatakan hubungan linear antara bilangan ikatan ganda dua *cis* bagi satu siri asid lemak metal ester (FAME) dengan menggunakan julat serapan pada 2920 cm^{-1} dan 3020 cm^{-1} bagi merujuk kepada getaran regangan kumpulan –CH dan olefinik =CH-. Pada tahun 1971 Arnold dan Hartung memperkenalkan gabungan antara serapan infra merah dengan kaedah kimometik di mana nilai darjah ketidak tepuan minyak ditentukan dengan menggunakan nisbah serapan getaran regangan –CH olefinik (3030 cm^{-1}) dan

alifatik pada nilai serapan 2857 cm^{-1}[2]. Kaedah ini diperbaharui dengan menggunakan serapan lemah regangan C=C [3].

Modifikasi telah dilakukan menggunakan puncak serapan regangan C-H pada jalur 3010 cm^{-1} dan 2854 cm^{-1} yang diperoleh menggunakan spektrofotometer ATR/FTIR. Kaedah ini diperbaiki dengan menggabungkan kaedah kemometrik iaitu *partial least square (PLS*). Selanjutnya, pelbagai kajian telah dilaporkan menggunakan asas PLS dalam menentukan kualiti minyak seperti menggunakan serapan regangan pada 3200-2600 cm^{-1} dan 1600 – 1000 cm^{-1} bagi penentuan iodin [4], 3450 cm^{-1} bagi penentuan nilai pengoksidaan [5] dan nilai asid lemak bebas [6]. Beberapa kajian terdahulu melaporkan bahawa kaedah kemometrik adalah model yang amat kompeten bagi mengesan dan meramalkan nilai campuran minyak masak [7] dan ketengikan minyak [8].

Dalam kajian ini, kaedah konvensional digunakan untuk mendapat data parameter kualiti minyak. Data-data parameter kualiti minyak akan digunakan untuk membuat perbandingan antara kaedah konvensional dengan kaedah kimometrik. Jika perbandingan data antara dua kaedah adalah hampir sama, ini membuktikan bahawa kaedah kimometrik adalah sesuai dan boleh menjadi alternatif menggantikan kaedah konvensional (eksperimen makmal) dalam penentuan kualiti minyak.

Bahan dan Kaedah

Bagi menentukan kualiti minyak masak bahan-bahan kimia berikut telah digunakan seperti penunjuk kanji, natrium tiosulfat, natrium hidroksida, kalium iodida, larutan wijs (iodin monoklorida) dan larutan dietileter : alkohol, larutan asid asetik – kloroform. Sampel-sampel minyak zaitun minyak bunga matahari dan mentega pula telah dibeli dari pasaran.

Kaedah

Bagi menentukan kualiti minyak masak, kaedah piawaian MPOB telah digunakan.

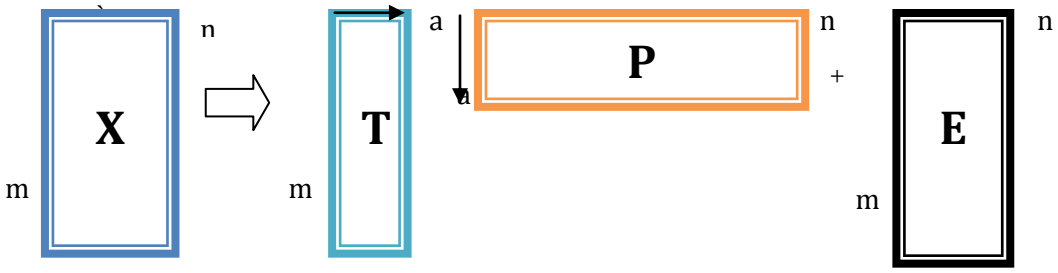
Analisis FTIR

Penganalisisan sampel minyak digunakan instrumen spektrometer FTIR. Semua spektrum inframerah (4000-400 cm^{-1}) telah diambil dengan Perkin Elmer Spektrum 100 spektrometer FTIR (Perkin Elmer Inc. Wellesley, MA). Instrumen ini telah dilengkapi dengan aksesori *Horizontal Attenuated Total Reflectance* (HATR) (Kristal ZnSe) dan pengesan *Deuterated Tri-glycerine Sulphate* (DTGS). Aksesori HATR digunakan untuk mengumpul data spektrum minyak. Resolusi ditetapkan pada 2 cm^{-1} dan bilangan imbasan yang dikumpul untuk setiap spektrum adalah sebanyak 128.

Analisis Kimometrik

Pengoptimuman data pencaman corak daripada spektrometer FTIR dilakukan dengan stimulasi komputer. Perisian komputer MATLAB 7.60 berversi RX2008a digunakan untuk analisis data tersebut . Pakej perisian MATLAB digunakan untuk aplikasi kepada model PCA dan PLS serta untuk penerokaan data analisis awal.

Analisis Komponen Utama (Principal Component Analysis, PCA)



Rajah 1: Skema PCA kepada bilangan sampel, m dan bilangan pemboleh ubah, n.

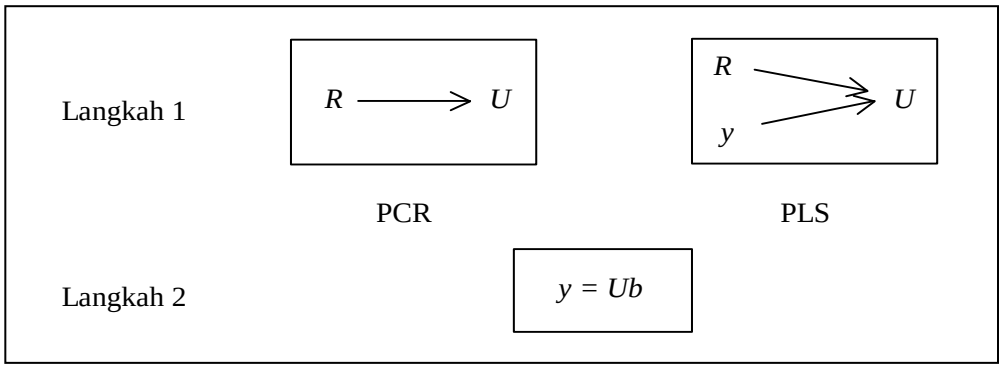
Setiap komponen kepada model PCA dicirikan daripada tiga pelengkap, iaitu varian, muatan (*loading*) dan skor [9]. Varian adalah pelengkap pengukuran ralat dan muatan menerangkan struktur data dalam segi pemboleh ubah kolerasi manakala skor pula adalah menerangkan pencirian, perbezaan atau persamaan dengan sampel. Selain itu, skor komponen utama dilakarkan bertujuan mendedahkan corak dan kelompok dalam sampel. Gambar rajah skema PCA yang diberikan dalam Rajah 1. Bagi data matrik X [m × n], T [m × p]adalah matriks skor , P [p × n] adalah matriks muatan dan E [m × n] adalah ralat.

Regresi Kuasa Dua Terkecil Separa (Partial Least Square Regression, PLS)

Merujuk kepada dalam kaedah MLR, kesukaran terjadi dalam pembinaan model apabila matrik $R^T R$ tidak boleh disongsangan iaitu matrik $(R^T R)^{-1}$ tidak wujud kerana kolineariti pemboleh ubah *x*. Analisis komponen utama mengatasi masalah kolineariti pemboleh ubah *x* dengan pembinaan satu matrik baru *U* yang mempunyai ciri lajur kombinasi linear dengan lajur matrik *R*. Menggunakan matrik baru *U* boleh disongsangkan, model baru boleh ditulis sebagai persamaan 2.1.

$$y = U\tilde{b} \tag{2.1}$$

Kaedah PLS menggunakan matrik *R* dan matrik *y* bagi menghasilkan matrik *U*. Kovarian matrik *y* dan varian matrik *R* diambil kira untuk menghasilkan matrik *U* (Leardi & Gonzalez 1998) [10]. Kaedah PCR hanya mempertimbangkan matrik *y* sahaja semasa pembentukan matrik *U*. Perbezaan kaedah PLS dan kaedah PCR dijelaskan dalam Rajah 2.



Rajah 2. Ilustrasi perbezaan antara PLS dan PCR

Matrik *U* sebagai hasil daripada peralatan atau perisian semasa penghasilan pemboleh ubah *R* yang mempunyai komponen atau faktor PLS sejajar dengan pengukuran *y*. Matrik skor berkait dengan matrik *R* seperti persamaan 2.2.

$$R = USV^T \tag{2.2}$$

dengan *U* adalah matrik skor, *V* matrik yang mengandungi muatan (*loading*) dan *S* adalah matrik diagonal. Matrik *U* diperolehi dengan menyelesaikan persamaan 1.10 dan akan diperolehi persamaan 2.3.

$$U = RVS^{-1} \tag{2.3}$$

Kemudian, model PLS diperolehi apabila vektor pekali moldel regresi $\tilde{b}$ dikenal pasti menerusi persamaan 2.4.

$$\tilde{b} = U^T y \tag{2.4}$$

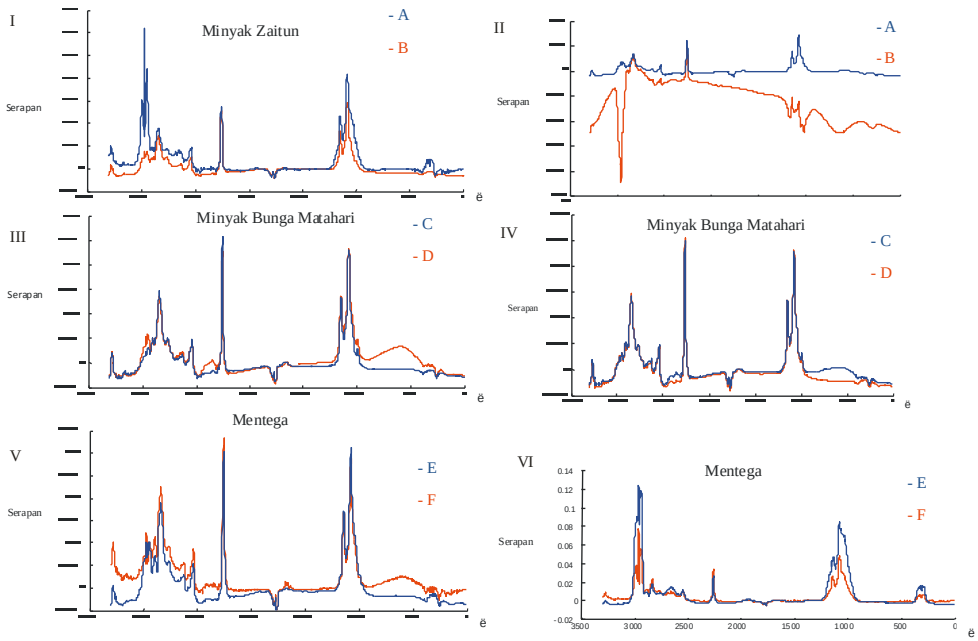
Akhir sekali, vektor regrasi $\tilde{b}$ tersebut boleh digunakan untuk membuat ramalan ke atas aktiviti biologi, $y_{i,p}$ bagi sebatian yang tidak diketahui. Pekali korelasi, R^2 memberikan ukuran tahap kebolehgunaan persamaan kepada data atau mengukur tahap ketinggian korelasi. Nilai R^2 yang sempurna bernilai +1 (korelasi positif) atau –1 (korelasi negatif) dan nilai 0 bermakna tiada korelasi. Kaedah kiraan R^2 diberikan oleh persamaan 2.5.

$$R^2 = \frac{\left[\sum xy - \frac{\sum x \sum y}{n}\right]^2}{\left[\sum x^2 - \frac{(\sum x)^2}{n}\right]\left[\sum y - \frac{(\sum y)^2}{n}\right]} \qquad 2.5$$

dengan x dan y adalah pemboleh ubah tak bersandar dan bersandar masing-masing. R^2 juga disebut sebagai peratus varian yang dapat diterangkan oleh model regresi. Nilai yang memuaskan bagi R^2 adalah sekitar 0.90.

Keputusan dan Perbincangan

Rajah 3 menunjukkan spektrum serapan tipikal FTIR bagi tiga jenis sampel minyak komersial (segar) dan sampel minyak yang telah digoreng menggunakan jenama yang berbeza. Keputusan menunjukkan spektrum yang diperoleh adalah hampir sama walaupun menggunakan jenama yang berbeza. Dengan menggunakan kaedah FTIR, pencirian bagi setiap minyak dapat diperolehi oleh nombor gelombang spektrum inframerah pada serapan yang tertentu seperti nilai iodin, nilai peroksida dan nilai keasidan [5].



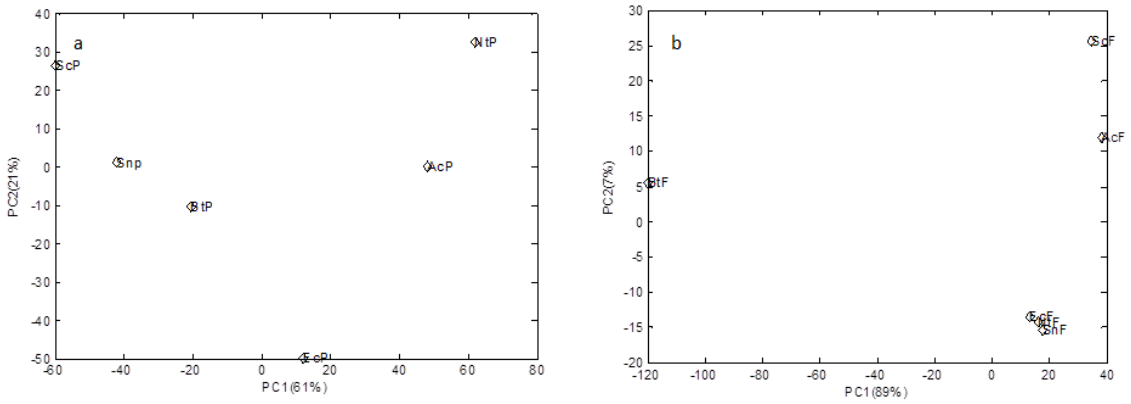
Rajah 3. Spektrum serapan FTIR bagi sampel minyak daripada jenama yang berbeza (A – F) pada dua keadaan iaitu segar (I, III, V) dan yang telah digoreng (II, IV, VI).

Nilai iodin selalunya ditentukan menggunakan keluk serapan pada nombor gelombang 3006, 1654 dan 968 cm^{-1} yang merujuk kepada regangan cis =CH, regangan cis C=C dan bengkokan trans C=C [11]. Rajah 3 (I dan II) menunjukkan perbandingan kualiti minyak komersial dan minyak digoreng dan didapati minyak yang telah digunakan untuk menggoreng secara umumnya merosot. Ini dapat dilihat pada serapan pada jalur sekitar 3000-2800 cm^{-1} yang merujuk kepada nilai iodin [4].

Bagi menentukan nilai peroksida, perubahan nilai boleh dirujuk kepada regangan OH di jalur 3440 cm^{-1}. Setiap spektrum terdapat serapan regangan pada jalur 3050-2800 cm^{-1} merujuk kepada cis C=C, CH_2 dan CH_3. Jalur pada rantau sekitar 1744 cm^{-1} merupakan serapan karbonil bagi rangkaian ester. Apabila proses pengoksidaan berlaku, jalur 3800-3200 cm^{-1} yang merujuk regangan O-H menjadi lebar dan rantau bagi serapan karbonil dan regangan kumpulan CH akan berkurang [5]. Dari Rajah 3(II, IV, VI) boleh diperhatikan bahawa spektrum untuk setiap minyak digoreng mempunyai jalur serapan OH lebih lebar berbanding dengan minyak segar. Ini menunjukkan nilai peroksida kepada minyak digoreng adalah lebih tinggi daripada minyak komersial. Selektiviti spektrum infra merah adalah penting untuk menunjukkan pencirian atau parameter kualiti bagi sesuatu minyak. Oleh itu, spektrum yang dipilih akan digunakan sebagai data input sebelum diproses menggunakan kaedah kimometrik.

Penganalisisan kaedah kimometrik

Selepas pra-pemprosesan data dilaksanakan, PCA telah dilakar plot skor untuk sampel minyak segar dan digoreng. Plot skor adalah plot yang menunjukkan pola atau taburan sampel yang mungkin wujud seperti ditunjukkan dalam Rajah 3.



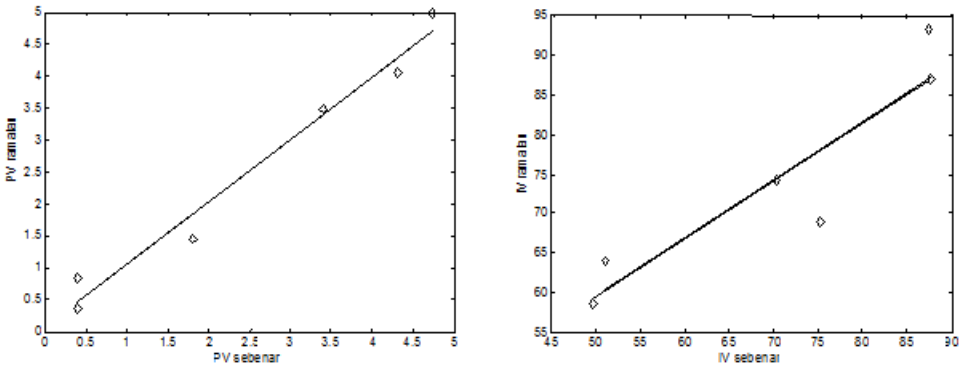
Rajah 4. Plot skor PCA minyak komersial segar (a) manakala minyak yang telah digoreng (b) dengan akronim yang digunakan; SnP- Minyak Bunga Matahari C, EcP- Minyak Bunga Matahari D, NtP- Minyak Zaitun A, BtP- Minyak Zaitun B, AcP- Mentega F, ScP- Mentega E

Rajah 4 menunjukkan plot skor adalah plot taburan sampel bagi enam jenis minyak komersial segar dan yang telah digoreng. Keputusan menunjukkan minyak segar daripada jenis yang berbeza mempunyai jarak taburan yang berbeza. Ini menunjukkan setiap jenis minyak komersial mempunyai perbezaan dalam segi kimia dan fizikal. Plot skor PCA kepada minyak digoreng agak berbeza dengan minyak segar. Lazimnya, skor kepada setiap dua minyak berjenama lain adalah hampir sama. Pada Rajah 4b menunjukkan skor dua minyak berjenamayang berbeza seperti minyak bunga matahari dan minyak zaitun boleh diplot dalam kategori yang sama. Ini kerana kedua-dua minyak tersebut mempunyai komposisi minyak yang sama. Namu begitu, bagi sampel mentega keputusan yang diperoleh adalah berbeza. Hasil ini mungkin disebabkan oleh bahan tambah yang diperkaya dalam setiap jenama yang berbeza.

Ujian Pengesahan

Rajah 5 menunjukkan ujian pengesahan kepada model pemboleh ubah terpilih PV dan IV bagi minyak komersial. Satu garis lurus diperolehi dengan kecerunannya adalah 0.90 dengan dapat beberapa titik berada pada satu garis

lurus. Nilai kecerunan ini menunjukkan bahawa keputusan yang diperoleh adalah persis (March et al. 1999). Selain daripada itu, nilai R^2_{CV} diperolehi adalah 0.975 menunjukkan kaedah konvensional dan kaedah kimometrik adalah sepadan. Bagi ujian pengesahan kepada model pemboleh ubah terpilih IV bagi minyak digoreng ditunjukkan dari Rajah 5. Satu garis lurus juga diperolehi dengan kecerunan yang rendah iaitu 0.90. Nilai kecerunan ini menunjukkan keputusan adalah persis setara dengan minyak komersial. Nilai R^2_{CV} yang diperolehi pula adalah 0.847.



Rajah 5. Ujian pengesahan antara nilai peroksida serta nilai iodin ramalan dengan nilai sebenar kepada minyak komersial.

Kesimpulan

Berdasarkan keputusan eksperimen makmal, kaedah konvensional adalah selalu digunakan untuk menentukan kualiti minyak sekiranya terdapat kebanyakan keputusan daripada eksperimen makmal agak sama dengan data daripada rujukan. Walaubagaimanapun, kaedah konvensional dilakukan dalam kajian ini masih mendapat ralat dari segi bacaan dan sistem. Melalui kaedah konvensional mendapati setiap dua minyak jenis sama walaupun jenamanya berlainan mempunyai perbezaan dari segi fizikal dan kimia. Selain itu, pencirian minyak komersial yang telah digunakan untuk menggoreng agak berbeza dengan minyak komersial. Keadaan ini disebabkan oleh tindak balas pengoksidaan dan hidrolisis berlaku pada minyak komersial semasa menggoreng.

Bagi analisis kimometrik pula, pencaman corak FTIR daripada setiap 12 sampel minyak dioptimumkan untuk membina model PCA dan PLS. Dalam kajian ini, perbandingan keputusan yang dibuat antara nilai pencirian minyak yang diramalkan oleh PLS dengan nilai pencirian minyak komersial yang ditentukan dalam kaedah konvensional. Satu garis lurus dengan kecerunan 0.90 diperoleh dengan sekiranya beberapa titik berada satu garis lurus manakala nilai pekali korelasi pengesahan silang, R^2_{CV} adalah menghampiri satu. Kaedah ini memberikan alternatif kepada kaedah konvensional bagi menentukan kualiti minyak masak.

Penghargaan

Penyelidik ingin mengucapkan terima kasih kepada Kementerian Pengajian Tinggi Malaysia atas geran FRGS/1/2011/SG/UKM/02/25dan Universiti Kebangsaan Malaysia atas geran penyelidikan UKM-GGPM-NBT-030-2011.

Rujukan

1. Sinclair, R.G., McKay, A.F., Myers, G.S. & Jones, R.N. (1952). The Infrared Absorption Spectra of Unsaturated Fatty Acids and Esters1. *Journal of the American Chemical Society*, 74 (10): 2578-2585.
2. Arnold, R.G. & Hartung, T.E. (1971). Infrared spectroscopic determination of degree of unsaturated of fats and oils. *Journal of Food Science*, 36 (1): 166-168.
3. Bernard, J.L. & Sims, L.G. (1980). IR spectroscopy for determination of total unsaturation.:
4. Voort, F.R., Ismail, A.A., Sedman, J., Dubois, J. & Nicodemo, T. (1994). The determination of peroxide value by fourier transform infrared spectroscopy. *Journal of the American Oil Chemists' Society*, 71 (9): 921-926.

5. Ho, M.M. & Sue, T.T., *A review on the quantitative analysis of fats and oils using FTIR*, M.P.O.B. (MPOB), Editor 1999. p. 30-37.
6. Moh, M.H., Che Man, Y.B., Badlishah, B.S., Jinap, S., Saad, M.S. & Abdullah, W.J.W. (1999). Quantitative Analysis of Palm Carotene Using Fourier Transform Infrared and Near Infrared Spectroscopy. *JAOCS, Journal of the American Oil Chemists Society*, 76 (2): 249-254.
7. Hussein, M.Z., Tarmizi, R.S.H., Zainal, Z., Ibrahim, R. & Badri, R.M. (1996). Preparation and characterization of active carbons from oil palm shells. *Carbon*, 34 (11): 1447-1453.
8. Wesolowski, M., Suchacz, B. (2001). Classification of rapeseed and soybean oils by use of unsupervised pattern-recognition methods and neural networks. *J.Anal Chem*, 3 (30): 323-371.
9. Brereton, R.G., *Chemometrics: Data Analysis for the Laboratory and Chemical Plant*. 2003, Chichester, UK: John Wiley & Sons, Ltd.
10. Riccardo Leardi, A.L.G. (1998). Genetic Algorithms applied to feature selection in PLS Regression : how and when to use them. *Chemometrics and Intelligent Laboratory Systems*, 41: 195-207.
11. Guillén, M.D. & Cabo, N. (1997). Infrared spectroscopy in the study of edible oils and fats. *Journal of the Science of Food and Agriculture*, 75 (1): 1-11.

The Malaysian Journal of ANALYTICAL SCIENCES ISSN 1394-2506

PALM OLEIN BASED BIOLUBRICANT BASESTOCKS: SYNTHESIS, CHARACTERISATION, TRIBOLOGICAL AND RHEOLOGICAL ANALYSIS

(Stok Asas Biolubrikan Berasaskan Minyak Sawit Olein: Sintesis, Pencirian, Analisis Tribologi dan Reologi)

Darfizzi Derawi[1,2] and Jumat Salimon[1*]

[1]*School of Chemical Sciences and Food Technology, Faculty of Science and Technology, Universiti Kebangsaan Malaysia, 43600 UKM Bangi, Selangor, Malaysia*
[2]*International Education College (INTEC), UiTM Section 17 Campus, 40200 Shah Alam, Selangor, Malaysia*

**Corresponding author: jumat@ukm.my*

Abstract

Palm olein (PO_o) was modified through chemical reaction to produce biolubricant basestock (di-oleate-PO_o and oleate-ether-PO_o). PO_o was epoxidised to produce epoxidised palm olein (EPO_o), then ring opening process were performed by hydrolysis and alcoholysis to produce di-hydroxy-PO_o and hydroxy-ether-PO_o. Both intermediate products were esterified with oleic acid to produce di-oleate-PO_o and oleate-ether-PO_o. Detection analyses were done by using fourier transformation infra-red (FTIR), proton and carbon nuclear magnetic resonance (^{1}H-NMR and ^{13}C-NMR). Di-oleate-PO_o recorded of its oxidative stability (140 ^{o}C), pour point (-5 ^{o}C), flash and fire point (215 ^{o}C and 245 ^{o}C), kinematic viscosity about 417.5 cSt (40 ^{o}C) and 45.4 cSt (100 ^{o}C) with the viscosity index of 166. While, oleate-ether-PO_o recorded of its oxidative stability (178 ^{o}C), pour point (1 ^{o}C), flash and fire point (190 ^{o}C dan 210 ^{o}C), kinematic viscosity about 113.7 cSt (40 ^{o}C) and 21.5 cSt (100 ^{o}C) with the viscosity index of 217. The biolubricant basestocks grade of ISO VG 460 (di-oleate-PO_o) and ISO VG 100 (oleate-ether-PO_o) were successfully produced. Di-oleate-PO_o and oleate-ether-PO_o were Newtonian and non-Newtonian fluid. Both products were hydrodynamic lubricant with low friction coefficients at 40 ^{o}C and 100 ^{o}C.

Keywords: Biolubricant Basestock, Palm Olein, Tribology, Rheology

Abstrak

Minyak sawit olein (PO_o) dimodifikasi melalui tindak balas kimia untuk menghasilkan stok asas biolubrikan (di-oleate-PO_o dan oleate-eter-PO_o). PO_o diepoksidakan untuk menghasilkan minyak sawit olein terepoksida (EPO_o), kemudian dijalankan proses pembukaan gelang secara hidrolisis dan alkoholisis untuk menghasilkan di-hidroksi-PO_o dan hidroksi-eter-PO_o. Kedua-dua produk pertengahan tersebut dijalankan pengesteran dengan asid oleik untuk menghasilkan di-oleate-PO_o dan oleate-eter-PO_o. Analisis pengecaman menggunakan transformasi fourier infra-merah (FTIR), resonans magnetik nukleus proton dan karbon (^{1}H-NMR and ^{13}C-NMR) telah dilakukan. Di-oleate-PO_o mencatatkan kestabilan oksidatif (140 ^{o}C), takat tuang (-5 ^{o}C), takat kilat dan api (215 ^{o}C dan 245 ^{o}C), kelikatan kinematik sebanyak 417.5 cSt (40 ^{o}C) dan 45.4 cSt (100 ^{o}C) dengan indeks kelikatan 166. Oleate-eter-PO_o mencatatkan kestabilan oksidatif (178 ^{o}C), takat tuang (1 ^{o}C), takat kilat dan api (190 ^{o}C dan 210 ^{o}C), kelikatan kinematik sebanyak 113.7 cSt (40 ^{o}C) dan 21.5 cSt (100 ^{o}C) dengan indeks kelikatan 217. Stok asas biolubrikan bergred ISO VG 460 (di-oleate-PO_o) dan ISO VG 100 (oleate-eter-PO_o) telah berjaya dihasilkan. Di-oleate-PO_o dan oleate-eter-PO_o adalah bendalir Newtonian dan bukan Newtonian. Kedua-dua produk merupakan lubrikan hidrodinamik dengan pekali geseran yang rendah pada suhu 40 ^{o}C and 100 ^{o}C.

Kata kunci: Stok Asas Biolubrikan, Minyak Sawit Olein, Tribologi, Reologi

Introduction

Since industrial revolution, lubricants are widely used in all sectors of industry for lubricating their machines and materials. Reports indicate that nearly 38 million metric tons of lubricants were used globally in 2005, with a projected increase of 1.2% over the next decade [1]. Approximately 85% of lubricants being used around the world

are petroleum based oils [2]. Generally, lubricants are made by combining basestock oil with suitable additives that enhance oil inherent characteristics or to impart new performance properties to the blend. The basestock oil is the main constituent and has traditionally been of mineral or synthetic nature [3]. These petroleum based basestocks present a potential danger when they are not readily biodegradable and thus tend to persist in the environment, having, a negative impact on the ecosystem [4,5]. The major negative effect is particularly linked to their inappropriate use, which results in surface water and groundwater contamination, air pollution, soil contamination, and consequently, agricultural product and food contamination [6]. In this sense, environmental concerns have risen considerably worldwide during the last 25 years and, consequently, there is growing interest in the use of environmentally friendly products such as biolubricants.

For these reasons, the uses of vegetable oils as basestock oils represent an important alternative in environmentally sensitive applications. These vegetable oils can be considered as a source of biolubricant. Vegetable oils are tri-esters of straight-chained, mostly unsaturated fatty acids with glycerol and have higher levels of biodegradability and lower toxicity than conventional mineral or synthetic oils [7]. In addition, vegetable oils have others advantages such as very low volatility, good high lubricity and high viscosity index, as well as lower cost than synthetic oils [8, 9, 10]. Unfortunately they have low thermal and oxidative stabilities, narrow viscosity range and higher pour points than both mineral or synthetic oil-based lubricants, so their use in industry is not yet extensive [11, 12, 13].

In Malaysia, palm oil as a major crop product has the possibility to be used as industrial lubricating oil. Palm oil is a vegetable oil, which is biodegradable, and also has a high production rate, which could fulfill the demand for vegetable-based lubricating oil in the future. One hectare of palm trees can produce almost 10 times as much oil compared to other sources of vegetable oil [14]. Therefore, palm oil has the potential to fulfill the supply volume in the demand for vegetable-based lubricants. One of refined products by palm oil is palm olein (PO_o). PO_o contains higher unsaturated triacylglycerol (TAG) compared to the saturated TAG [15]. These unsaturated TAGs chains give a large potential in chemical modification to produce biolubricants.

Previously, some of researchers in Malaysia carried out research on the palm oil based lubricant products. A palm based hydraulic fluid was produced with the lubricant grade of ISO VG 46 [16]. Food grade palm oil based lubricants also produced as spindle oil (ISO VG 15 and ISO VG 22), hydraulic fluid (ISO VG 32, ISO VG 46 and ISO VG 68) and circulating oil (ISO VG 100) [17]. But mostly, PO_o was not used as raw materials in chemical modification because of its usage in food industries as cooking oils.

In this paper, palm olein used as a raw material to produce biolubricant basestocks (di-oleate-PO_o and oleate-ether-PO_o) via chemical modifications. Detection analyses were done by using Fourier Transformation Infra-red (FTIR), proton and carbon nuclear magnetic resonance (^{1}H, ^{13}C-NMR). Then, both biolubricant basestocks were characterized and analysed their tribological and rheological properties.

Materials and Methods

Raw materials

Palm olein (PO_o) (Seri Murni Brand, FFM Marketing Sdn. Bhd.) was purchased directly from market. 1-Decanol was supplied by Emery Oleochemicals (M) Sdn. Bhd, Teluk Panglima Garang, Selangor. Oleic acid (90 % of purity) was obtained from Sigma Aldrich.

Chemical reactions

The first reaction is epoxidation of PO_o to produce epoxidised palm olein (EPO_o) by using generated *in situ* performic acid with mol ratio of PO_o:HCOOH:H_2O_2 (1:5:2) [18]. Then, EPO_o was performed ring opening reaction by two approaches which that by water hydrolysis and alcoholysis with 1-decanol to produce di-hydroxy-PO_o and hydroxy-ether-PO_o. Both intermediate products were performed esterification process by using oleic acid to produce biolubricant basestocks (di-oleate-PO_o and oleate-ether-PO_o). Each level of products were detected and compared by using FTIR, ^{1}H-NMR and ^{13}C-NMR. Then, the biolubricant basestocks were characterised and analysed on their tribology and rheology properties.

Detection tests

FTIR spectrometer (GX model) was used to detect the differences of functional groups by using the NaCl salt window method. The wavenumber of vibrations absorption was ranged between 4000 – 700 cm^{-1}. Proton and carbon analysis was performed by using FT-NMR spectrometer 600 MHz Cryo-Probe (Advance 111 600MHz model). Sample was prepared by using chloroform ($CDCl_3$) as a solvent [18].

Characterisation tests

Di-oleate-PO_o and oleate-ether-PO_o characterised of their moisture contents (A.O.C.S. Tb 2-64), pour point (ASTM D 97-66) [19], oxidative stability [20], flash and fire point, kinematic viscosity at 40 ^oC and 100 ^oC (ASTM D 445-79) [19], viscosity index (ASTM D2270) [21], then their lubricant grade were determined [22].

Tribology and rhelogy analysis

Tribological properties of di-oleate-PO_o and oleate-ether-PO_o were determined by using Anton Paar rheometer (Physica MCR 301 model) with one ball geometry. The sliding speed was manipulated between 10^{-1} – 10^3 mm/s at temperature 40 ^oC and 100 ^oC [23]. The tribological properties were discussed based on their Stribeck curves at 40 ^oC and 100 ^oC (Figure 1).

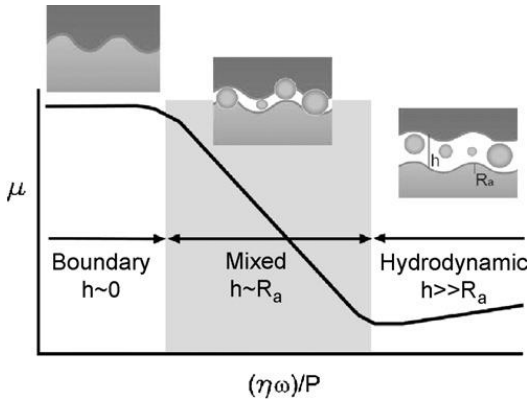


Figure 1. Sketch of a Stribeck curve relating friction coefficient; h: fluid film thickness, R_a: average surface roughness

Rheological properties of di-oleate-PO_o and oleate-ether-PO_o were observed by the same rheometer with cone and plate geometry [24]. The cone spindle used was CP 25-2 with diameter 0.051 mm. The shear rate was manipulated between 0 – 100 s^{-1} at temperature 25 ^oC. A plot of shear rate vs. shear stress shown as Figure 2.

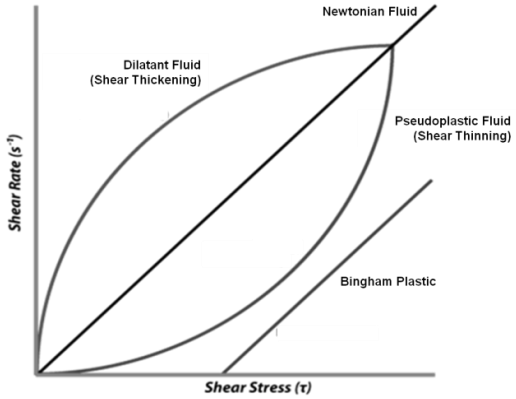


Figure 2. Shear rate vs. shear stress plots of Newtonian and non-Newtonian fluid

Results and Discussion

Figure 3 shows the overall chemical modification processes that were involved to produce biolubricant basestocks. By using chemical modifications, the unsaturated bond of palm olein (PO_o) was converted to a new functional group that can be further the modification process to produce biolubricant basestocks (di-oleate-PO_o and oleate-ether-PO_o). At the epoxidation process, double bonds of PO_o were converted to oxirane ring to produce epoxidised palm olein (EPO_o). Then, oxirane ring cleavage done to produce hydroxyl and ether groups. At the end of modification, both ring opening products (di-hydroxy-PO_o and hydroxy-ether-PO_o) undergo esterification with oleic acid to produce ester group of di-oleate-PO_o and oleate-ether-PO_o.

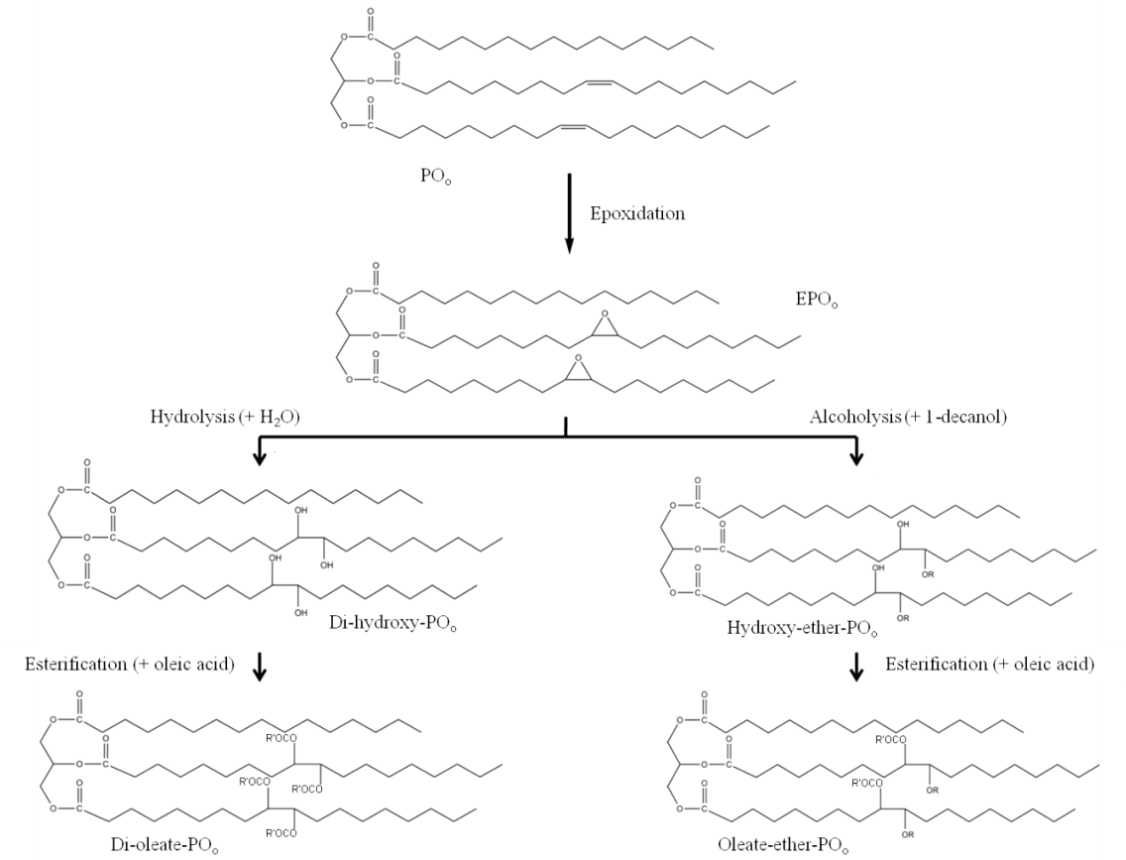


Figure 3. Chemical modifications of PO_o to produce biolubricant basestocks

Epoxidation of palm olein (PO_o) was carried out by using generated *in situ* performic acid (HCOOOH). HCOOOH was a peroxy acid which prepared by mixing of formic acid (HCOOH) as oxygen carrier and hydrogen peroxide (H_2O_2) as oxygen donor. Preparation HCOOOH as epoxidation agent was carried out as *in situ* since the reaction condition is highly exothermic and not stable [18, 25]. The epoxidation process involved of electrophilic addition mechanism as Figure 4. Unsaturated bond at triacylglycerol (TAG) PO_o was converted to oxirane ring to produce epoxidised palm olein (EPO_o).

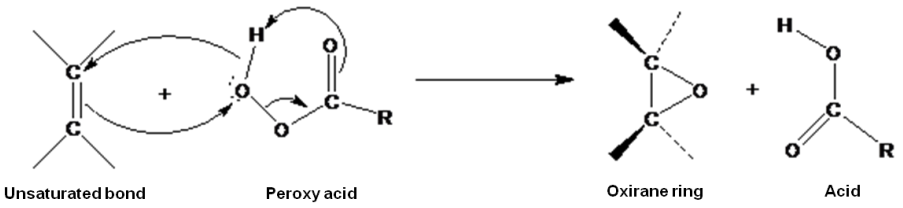


Figure 4. Electrophilic addition mechanisms on unsaturated bond to give oxirane ring

First ring opening process involved water hydrolysis by using perchloric acid as catalyst [26]. EPO_o was converted to di-hydroxy-PO_o. At the first step, oxirane ring was protonised to produce a strong electrophile. Then, back-side electrophilic attack happened to make oxirane cleavage. Finally, de-protonisation occurred to produce diol. Figure 5 shows the mechanisms of water hydrolysis.

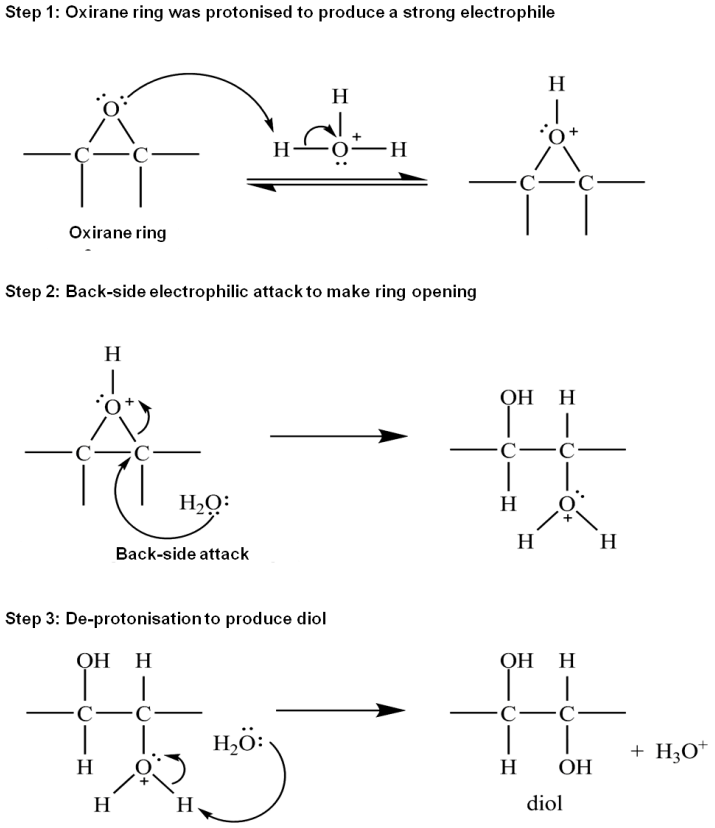


Figure 5. Ring opening mechanisms through water hydrolysis

Second ring opening process via alcoholysis with 1-decanol. 1-decanol is a medium chain fatty alcohol with ten carbon chains. EPO_o was converted to hydroxy-ether-PO_o. This reaction used sulphuric acid as catalyst. At the first step, oxirane ring was protonised to produce a strong electrophile. Then, electrophilic attack happened to make ring opening and produce hydroxyl group. Finally, de-protonisation occurred to produce ether group. Figure 6 shows the mechanisms of alcoholysis process to produce hydroxy-ether compound.

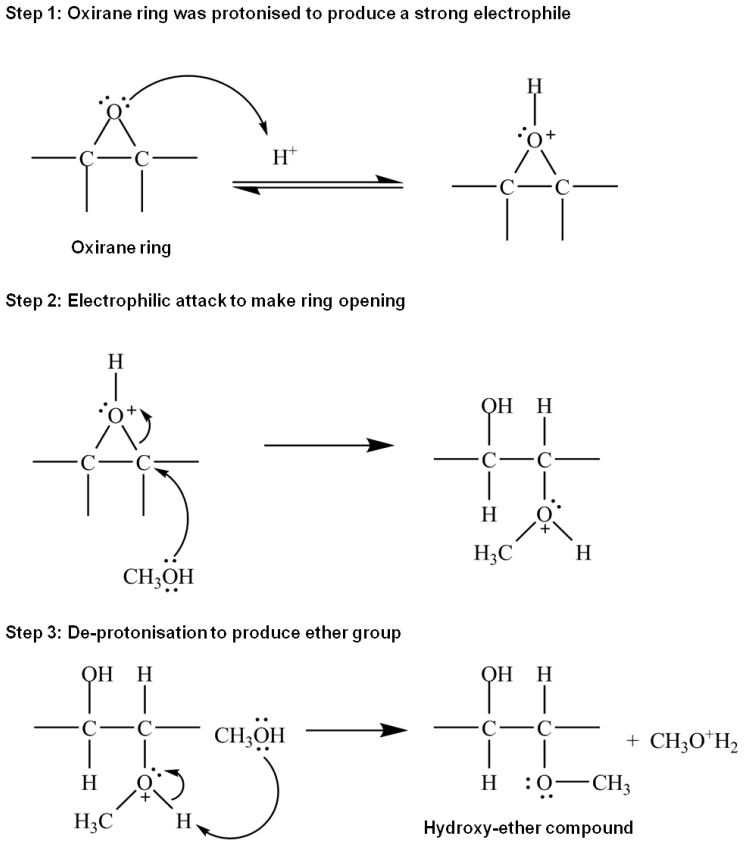


Figure 6. Ring opening mechanisms through alcoholysis

Both ring opening products reacted with oleic acid through esterification process. This process used a mineral acid such as sulphuric acid or hydrochloric acid. An oxygen atom at carbonyl group of carboxylic acid was protonised by mineral acid to give positive charge on the carboxylic acid in order to make it more reactive. Then, the reactive carboxylic acid was attacked by alcohol to release water and forming ester compound [26]. Figure 7 shows the mechanisms of esterification.

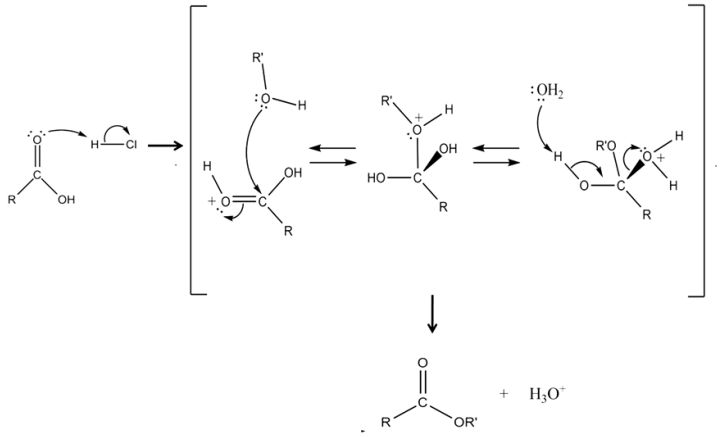


Figure 7. Mechanisms of esterification process

FTIR Analyses

The comparison data of FTIR analyses shown at Table 1. PO_o contains of unsaturated functional group where the chemical reactions can be occurred. The peak of sp^2 C-H (=C-H) and double bond were appeared at wavenumber 3003 cm^{-1} and 1600 cm^{-1}. For EPO_o, oxirane ring peaks presence at wavenumber 844 cm^{-1} and the double bond peaks were disappeared. All of the double bonds were totally converted to oxirane ring [27]. While, both ring opening products (di-hydroxy-PO_o and hydroxy-ether-PO_o) showed the presence of stretching vibration peaks of hydroxyl group and hydrogen bonded of hydroxyl group at wavenumber 3650-3600 cm^{-1} and 3400-3300 cm^{-1}. The stretching vibration of C-O (ether) hydroxy-ether-PO_o supposes to be appeared at wavenumber 1260-1000 cm^{-1} but due to the highly intensity of -CH_2- and -CH_3 bending of TAGs chains, the peaks were overlapped with each other. Di-oleate-PO_o and oleate-ether-PO_o showed the presence of unsaturated stretching region of sp^2 =C-H, HC=CH and =C-H (oop) at wavenumber 3003, 1600 and 960 cm^{-1} [28]. So, all of the hydroxyl group were converted to ester group and the presence of oleic acid chain in the biolubricant basestocks were confirmed.

Table 1. Comparison Data of FTIR analyses

Compound	Wavenumber (cm^{-1})	Wavenumber, Ref. (cm^{-1})[28]	Conclusion
PO_o	3003	> 3000	sp^2 C-H (=C-H)
	1600	1600	HC=CH
EPO_o	844 (sharp)	950 – 815	-C-O-C- (oxirane ring)
Di-hydroxy-PO_o	3650-3600 (sharp)	3650 – 3600	stretch. vib. (O-H)
	3400-3300 (broad)	3400 – 3300	stretch. vib. H-bonded (O-H)
Hydroxy-ether-PO_o	3650-3600 (sharp)	3650 – 3600	stretch. vib. (O-H)
	3400-3300 (broad)	3400 – 3300	stretch. vib. H bond (O-H)
Di-oleate-PO_o	3003 (small)	> 3000	sp^2 =CH
	1600 (sharp)	1600	HC=CH
	960	900 – 690	=C-H (oop)
Oleate-ether-PO_o	1600 (sharp)	1600	HC=CH
	960	900 – 690	=C-H (oop)

^{1}H-NMR and ^{13}C-NMR analyses

The comparison data of ^{1}H-NMR and ^{13}C-NMR shown at Table 2 and 3. Proton analysis of PO_o showed that the presence of proton attached to the carbon double bond (δ 5.3 ppm) and proton attached to the carbon that attached to carbon double bond (2.0 ppm). While, proton attached to carbon (oxirane ring) appeared at δ 2.9 ppm for the EPO_o. So, the double bond of PO_o was totally converted to oxirane ring to produce EPO_o [18]. Di-hydroxy-PO_o and hydroxy-ether-PO_o recorded the presence of proton peaks that attached to the carbon next to the hydroxyl group at δ 3.4 and 3.6 ppm. The presence of proton peaks of hydroxyl group was at δ 4.6 and 4.8 ppm. For hydroxy-ether-PO_o, the peaks attached to carbon (ether) showed at δ 3.5 and 3.2 ppm. Both of the biolubricant basestock products showed the presence of proton peaks attached to carbon double bond (δ 5.3, 5.4 ppm) and peaks attached to carbon next to the carbon double bond (δ 2.0 ppm) [28].

Carbon analysis of PO_o showed that the presence of carbon double bond peaks at δ 130 ppm. While the carbon peaks of oxirane ring of EPO_o appeared at δ 57 and 54 ppm [18]. For both ring opening products, there was carbon peaks attached to hydroxyl group at δ 75 ppm. For carbon (ether) peaks of hydroxy-ether-PO_o appeared at δ 71 and 82 ppm. Di-oleate-PO_o and oleate-ether-PO_o were recorded the presence of carbon double bond peaks at δ 130 ppm [28]. These proved that the oleic acid chains are presence in the biolubricant basestock products.

Characterisation, tribological and rheological properties

Comparison of characterisation between PO_o, di-oleate-PO_o and oleate-ether-PO_o shown at Table 4. Oxidative stability of di-oleate-PO_o lower than oleate-ether-PO_o. This is due to the higher number of double bond at its structure. Both biolubricant products showed lower temperature properties of their flash and fire points compared to the PO_o. The pour point of di-oleate-PO_o and oleate-ether-PO_o were improved compared to the PO_o. Both of

products recorded of high kinematic viscosity (40 ^{o}C and 100 ^{o}C) and good viscosity index. Based on their kinematic viscosity at 40 ^{o}C, di-oleate-PO_o and oleate-ether-PO_o can be considered as ISO VG 460 and ISO VG 100.

Table 2. Comparison Data of ^{1}H-NMR analyses

Compound	Chemical Shift, δ (ppm)	Chemical Shift, δ Ref. (ppm)[28]	Conclusion
PO_o	2.0	1.6 – 2.6	C=C-C-**H**
	5.3	4.5 – 6.5	C=C-**H**
EPO_o	2.9	2.5 – 3.5	**H**-C-O-C-**H** (oxirane ring)
Di-hydroxy-PO_o	3.4	3.2 – 3.8	**H**-C-OH
	4.6	0.5 – 5.0	C-O-**H**
Hydroxy-ether-PO_o	3.5, 3.2	3.2 – 3.8	R-O-C-**H**
	3.6	3.2 – 3.8	**H**-C-OH
	4.8	0.5 – 5.0	C-O-**H**
Di-oleate-PO_o	2.0	1.6 – 2.6	C=C-C-**H**
	5.3	4.5 – 6.5	C=C-**H**
Oleate-ether-PO_o	2.0	1.6 – 2.6	C=C-C-**H**
	3.5, 3.2	3.2 – 3.8	R-O-C-**H**
	5.4	4.5 – 6.5	C=C-**H**

Table 3. Comparison Data of ^{13}C-NMR analyses

Compound	Chemical Shift (ppm)	Chemical Shift, Ref. (ppm)[28]	Conclusion
PO_o	130	100 – 150	**C**=**C**
EPO_o	57, 54	40 – 80	**C**-O-**C** (oxirane ring)
Di-hydroxy-PO_o	75	40 – 80	H-**C**-OH
Hydroxy-ether-PO_o	72	40 – 80	RH_2-**C**-O-C
	75	40 – 80	H-**C**-OH
	82	40 – 80	R_2H-**C**-O-C
Di-oleate-PO_o	130	100 – 150	**C**=**C**
Oleate-ether-PO_o	71	40 – 80	RH_2-**C**-O-C
	82	40 – 80	R_2H-**C**-O-C
	130	100 – 150	C=C

Table 4. Characterisation of PO_o, di-oleate-PO_o and oleate-ether-PO_o

Parameter	Unit	PO_o	Di-oleate-PO_o	Oleate-ether-PO_o
Moisture content	%	0.22	0.46	0.45
Oxidative stability	^{o}C	179.7	155.8	178.3
Flash point	^{o}C	> 320	215	190
Fire point	^{o}C	> 320	245	210
Pour point	^{o}C (± 2 ^{o}C)	5	-5	1
Pour point (+additive)	^{o}C	-	-10	-13
Kinematic viscosity (40 ^{o}C)	cSt (± 5 ^{o}C)	45.9	417.5	113.7
Kinematic viscosity (100 ^{o}C)	cSt (± 5 ^{o}C)	9.4	45.4	21.5
Viscosity index	-	195	166	217
Lubricant grade (ISO VG)	-	46	460	100

Comparison of tribological properties between PO_o, di-oleate-PO_o and oleate-ether-PO_o shown at Figure 8. By referring to Figure 1, the Stribeck curve has three types of lubricant conditions which are boundary, mixed and hydrodynamic lubricant. In the middle between mixed and hydrodynamic lubricant condition, there was a elastohydrodynamic lubricant which is the friction coefficient decreasing during the increasing of parameter [29]. All of the samples showed low friction coefficient at 40 ^oC. But PO_o recorded a higher friction coefficient than di-oleate-PO_o and oleate-ether-PO_o at 100 ^oC. The friction coefficient of di-oleate-PO_o and oleate-ether-PO_o still below than 0.5. This showed that both biolubricant basestock products had a better quality of their tribological properties even the temperature was increased compared to the PO_o.

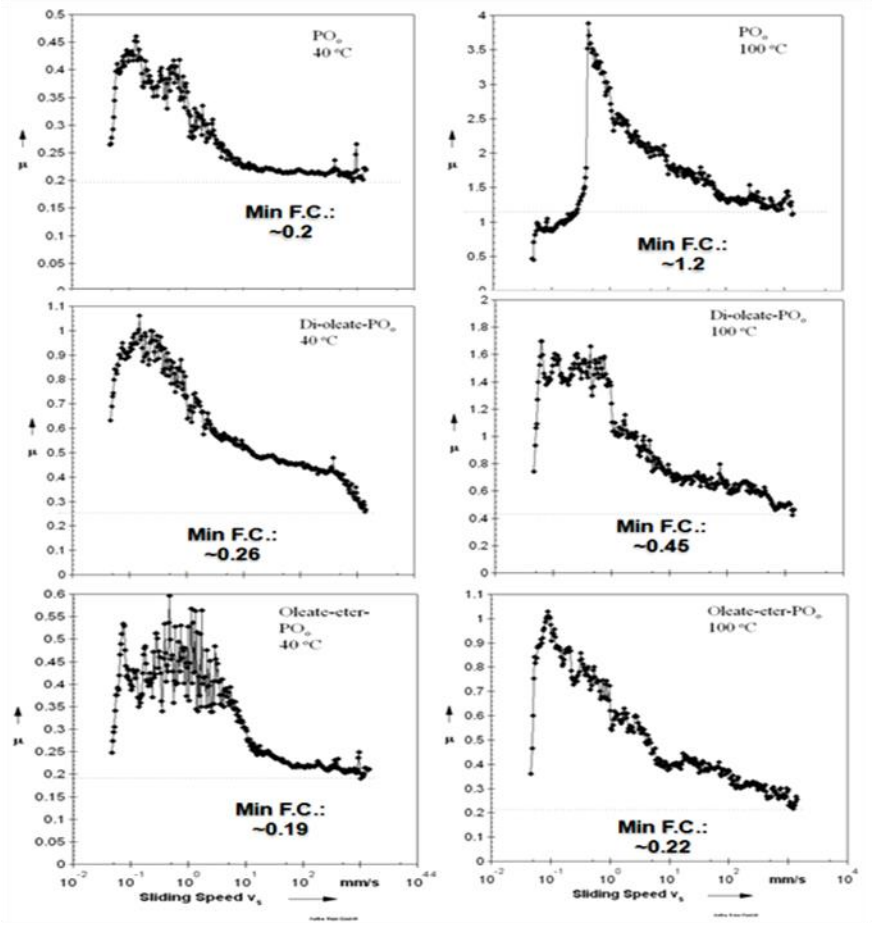


Figure 8. Comparison of Stribeck curves between PO_o, di-oleate-PO_o and oleate-ether-PO_o (40 ^oC and 100 ^oC)

Rheology analysis of samples produced shear stress vs. shear rate plot (Figure 9). From this plot, a fluid can be decided as Newtonian or non-Newtonian fluid. Newtonian fluid was classified as a fluid that has a constant viscosity by increasing shear rate and *vice versa* for non-Newtonian fluid [30]. Based on figure given, PO_o and oleate-ether-PO_o are non-Newtonian fluids. While di-oleate-PO_o is a Newtonian fluid.

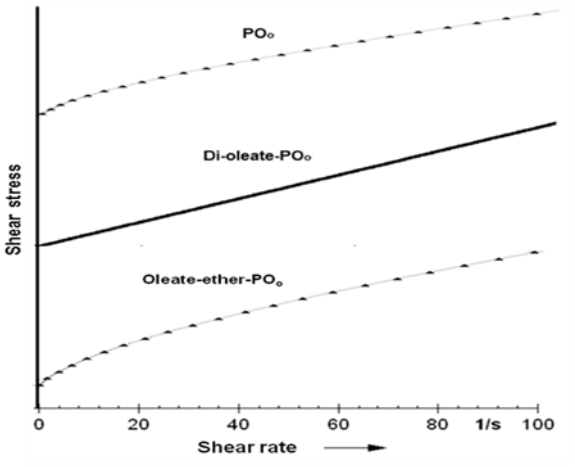


Figure 9. Shear stress vs. shear rate plots of PO_o, di-oleate-PO_o and oleate-ether-PO_o (25 ^oC)

Conclusion

Biolubricant basestocks grade ISO VG 460 (di-oleate-PO_o) and ISO VG 100 (oleate-ether-PO_o) were successfully synthesized from palm olein and characterized their lubrication, tribological and rheological properties. These products are having potential to be used as a lubricant basestock in the industrial field at moderate operation temperature in tropical countries.

Acknowledgement

The authors would like to thank to the Universiti Kebangsaan Malaysia for the financial support via research grant no. UKM-OUP-NBT-29-150/2010 and Ministry of Science, Technology and Innovation (MOSTI) for the National Science Fellowship (NSF) scholarship support. We would also like to thank to the Emery Oleochemicals (M) Sdn. Bhd. for sponsoring raw materials in this research.

References

1. Kline & Company Inc. 2006. Competitive intelligence for the global lubricants industry 2004–2014, Kline & Company, Inc.
2. Loredana P., Cosmina P., Geza B., Gabriela V., Remus N. 2008. Basestock oils for lubricants from mixtures of corn oil and synthetic diesters. *J Am Oil Chem Soc*. 85: 71–6.
3. Erhan, S.Z., Adhvaryu, A. 2002. Vegetable-based base stocks. In: Erhan, S.Z., Perez, J.M. (Eds.), Bio-Based Industrial Fluids and Lubricants. Champaign, USA, AOCS Press.
4. Lawate, S. 2006. Environmentally friendly hydraulic fluids. In: Rudnick, L.R. (Ed.), Synthetics, Mineral Oils, and Bio-Based Lubricants. Chemistry and Technology, Taylor & Francis, CRC Press, PA, USA.
5. Sharma, B.K., Adhvaryu, A., Liu, Z., Erhan, S.Z. 2006. Chemical modification of vegetable oils for lubricant applications, *JAOCS*, 83: 129–136.
6. Birova A, Pavloviova A, Cvengro J. 2002. Lubricating oils based on chemically modified vegetable oils, *J Synth Lubr.* 18: 291.
7. Adhvaryu, A., Erhan, S.Z. 2002. Epoxidized soybean oil as a potential source of high temperature lubricants, *Ind. Crop Prod.* 15: 247–254.
8. Erhan, S.Z., Asadaukas, S. 2000. Lubricants base stocks from vegetable oils, *Ind. Crop Prod.* 11: 277–282.
9. Erhan, S.Z., Adhvaryu, A., Sharma, B.K. 2006. Chemically functionalized vegetable oils. In: Rudnick, L.R. (Ed.), Synthetics, Mineral Oils, and Bio-Based Lubricants. Chemistry and Technology, Taylor & Francis, CRC Press, PA, USA.
10. Campanella, A., Rustoy, E., Baldessari, A., Baltanas, M.A. 2010. Lubricants from chemically modified vegetable oils. *Bioresour. Technol*. 101: 245–254.
11. Erhan, S.Z., Asadaukas, S. 2000. Lubricants base stocks from vegetable oils, *Ind. Crop Prod*. 11: 277–282.

12. Sharma, B.K., Stipanovic, A.J. 2003. Development of a new oxidation stability test method for lubricating oils using high-pressure differential scanning calorimetry, *Thermochim. Acta* 402: 1–18.
13. Duangkaewmanee, S., Petsom, A. 2011. Synergistic and antagonistic effects on oxidation stability of antioxidants in a synthetic ester based oil *Tribol. Int.* 44: 266–271.
14. Ming KK, Chandramohan D. 2002. Palm oil industry at crossroad and its future direction, *Oil Palm Industry Economic Journal* 2: 10–5.
15. Ramli, M. R., Siew, W. L., Cheah, K. Y., 2009. Production of high oleic palm oils on a pilot scale, *J. Am. Oil. Chem. Soc*. 86: 587-594.
16. Yeong, S. K., Ooi, T. L., Salmiah, A., 2005. Palm-Based Hydraulic Fluid, MPOB, KL.
17. Loh, S. K., Choo, Y. M., 2006. Food-Grade Palm-Based Industrial Lubricants, MPOB, KL.
18. Derawi, D., Salimon, J., 2010. Optimization on epoxidation of palm olein by using performic acid, *E-J.Chem.* 7(4): 1440-1448.
19. Emery, 1983. Emery Analytical Testing Procedures, Emery Industries, USA.
20. Fox, N.J., Stachowiak, G.W. 2007. Vegetable oil-based lubricants—A review of oxidation, *Tribology International* 40: 1035–1046.
21. Stachowiak, G. W., Batchelor, A. W. 2005. Engineering Tribology, Elsevier Inc., UK.
22. ISO 3448, 1975. International Standard, Industrial Liquid Lubricants, ISO Viscosity Classification.
23. Kalin, M., Velkavrh, I., Vizintin, J. 2009. The Stribeck curve and lubrication design for non-fully wetted surfaces, Wear 267: 1232-1240.
24. Coussot, P., Tocquer, L., Lanos, C., Ovarlez, G., 2009. Macroscopic vs local rheology of yield stress fluids. J. Non-Newtonian Fluid Mech., 158: 85-90.
25. Gunstone, F.D. 2004. The Chemistry of Oils and Fats: Sources, Composition, Properties and Uses, Blackwell Publishing Ltd., U.K.
26. Wade, L. G., 2006. Organic Chemistry, 6th ed., Pearson Prentice Hall, United States.
27. Derawi, D., Salimon, J. 2011. Effect of Performic Acid Concentration on Epoxidation of Palm Olein, *Sains Malaysiana* 40(9): 1023-1027
28. Pavia, D. L., Lampman, G. M., Kriz, G. S. 2001. Introduction to spectroscopy, Thomson Learning, Inc., USA.
29. Hironaka, S., 1984. Boundary Lubrication and Lubricants., Three Bond Co. Ltd., Japan.
30. Batchelor, G. 2000. An Introduction to Fluid Mechanics, Cambridge University Press, UK.

The Malaysian Journal of ANALYTICAL SCIENCES ISSN 1394-2506

CHANGES ON THE SOLID FAT CONTENT OF PALM OIL/SUNFLOWER OIL BLENDS VIA INTERESTERIFICATION

(Perubahan Kandungan Lemak Pepejal Campuran Minyak Sawit RBD/Bunga Matahari Melalui Penginteresteran)

Suria Ramli*, Azwani M. Lazim, Siti Aishah Hasbullah

School of Chemical Science and Food Technology, Faculty of Science and Technology
Universiti Kebangsaan Malaysia, 43600 UKM Bangi, Selangor, Malaysia

**Corresponding author: su_ramli@ukm.my*

Abstract

Physicochemical characteristics of binary blends containing refined-deodorized-bleached palm oil (RBDPO) and sunflower oil (SFO) were studied before and after chemical interesterification at different temperature (110 ^{o}C (CIE1) and 80 ^{o}C (CIE2)) using sodium methoxide as catalyst. Thirty-three samples with different ratios were analyzed for triacylglycerol (TAG) composition, fatty acid composition (FAC) and solid fat content (SFC) profile. Upon CIE, extensive rearrangements of fatty acids among triacylglycerol (TAG) were seen. Generally, CIE not induced enormous changes in the TAG compositions of ratio 8:2 and 5:5 of RBDPO:SFO blends. However, CIE induced enormous changes in the TAG compositions of the 9:1, 7:3, 6:4, 4:6, 3:7, 2:8 and 1:9 blends, which some of the TAGs were increasing while the other decreasing. These changes in TAG profiles resulted in some changes in the physical properties (especially SFC) of the blends. Generally, the SFC of interesterified blend were decreased after CIE1 and increased after CIE2, except for sample 10:0, 8:2, 7:3, 5:5 and 9:1 which were decreased after CIE1 and CIE2. As a conclusion, CIE1 and CIE2 successfully changed the physicochemical characteristics of the binary blends.

Keywords: palm oil, sunflower oil, interesterification, blending, solid fat content

Abstrak

Ciri-ciri fiziko-kimia adunan duaan langsung minyak sawit tertapis, terluntur dan ternyahbau/minyak bunga matahari (RBDPO/SFO) dikaji sebelum dan selepas penginteresteran kimia pada suhu berbeza (110 ^{o}C (CIE1) dan 80 ^{o}C (CIE2)) dengan menggunakan mangkin natrium metoksida. Sebanyak 33 adunan dengan nisbah yang berbeza dianalisis menggunakan kaedah penentuan komposisi triasilgliserol (TAG), komposisi asid lemak (FAC) dan kandungan lemak pepejal (SFC) yang dilakukan sebelum dan selepas penginteresteran kimia. Penyusunan semula asid-asid lemak pada molekul-molekul TAG dikesan selepas penginteresteran kimia. Umumnya, penginteresteran kimia merangsang perubahan yang tidak begitu ketara di dalam komposisi TAG adunan 8:2 dan 5:5. Walaubagaimanapun, penginteresteran kimia telah merangsang perubahan yang agak besar bagi adunan 9:1, 7:3, 6:4, 4:6, 3:7, 2:8 dan 1:9 dengan beberapa jenis TAG meningkat, manakala yang lainnya menurun. Perubahan di dalam profil TAG menyebabkan perubahan ke atas sifat-sifat fizikal terutamanya kandungan lemak pepejal adunan duaan minyak. Kandungan lemak pepejal bagi adunan-adunan yang terinterester menurun selepas CIE1 dan meningkat selepas CIE2, kecuali bagi adunan 10:0, 8:2, 7:3, 5:5 dan 9:1 yang menurun selepas CIE1 dan CIE2. Keseluruhannya, CIE1 dan CIE2 berjaya mengubah ciri-ciri fiziko-kimia adunan minyak.

Kata kunci: minyak sawit, minyak bunga matahari, adunan, kandungan lemak pepejal

Introduction

Most native vegetable oils have specific characteristic in their original forms due to their specific chemical composition that reflect specific physical properties and nutritional value, which limit their applications. To enlarge the usage of these oils, they have been modified either chemically (interesterfication or hydrogenation) or physically (fractionation) [1].

Chemical interesterification is an important process for the oils and fats industry. This reaction modifies physical properties of oils by rearrange the distribution of fatty acids on the glycerol backbone without changing their chemical composition [2]. On the other words, the process induces changing on TAG composition. The modified TAG will clearly reflect on solid fat content, which is every type of TAG have their own physical properties like melting point and crystallization.

The objective of this study was to investigate a correlation of simple and chemically interesterified blends containing RBDPO and SFO in TAG composition and solid fat content.

Materials and Methods

Source materials

Refined – deodorized - bleached palm oil (RBDPO) was obtained from Intercontiremtd Specialty Fats Sdn. Bhd. Sunflower oil (SFO)was purchased from a local grocery store (Sunbeam brand) and used without further treatment. All solvents and chemicals used were of analytical grade.

Blend Preparation

RBDPO and SFO were mixed in proportions ranging from 100% RBDPO to 100% SFO in 10% increments (w/w). Nine blend samples with different ratios were prepared [90:10, 80:20, 70:30, 60:40, 50:50, 40:60, 30:70, 20:80, 10:90], identified by the mass ratio of RBDPO to SFO.

Chemical Interesterification

Portions (250 g) of the blends, RBDPO and SFO were dried at temperature of 110 ^{o}C for 30 minutes, followed by thorough nitrogen flush to remove moisture and air. Then, the blends were mixed with 0.2% (w/w) sodium methoxide. The interesterification reaction was performed at 110^{o}C (CIE1) and 80^{o}C (CIE2) in a stoppered flask using water bath with constant agitation for one hour. To terminate the reaction, flasks were cooled to below than 60 ^{o}C, followed by addition of citric acid solution (20%) to neutralize the catalyst. The citric acid and sodium methoxide were removed with hot distilled water (3 x 150 mL). Water residual was removed with excess anhydrous sodium sulfate, followed by filtration through a Whatman no. 2 filter. Non-interesterified is abbreviated as DB (direct blending) while chemically interesterified known as CIE.

Pulsed Nuclear Magnetic Resonance (pNMR)

Solid fat content (SFC) was measured by pNMR using Bruker NMR/ND 1844 (Bruker, Germany). This method consists of heating the samples to 70 ^{o}C for 30 minutes and then cooling down to 0 ^{o}C for 90 minutes. The samples were conditioned for 30 minutes at the chosen measurement temperature. During this study, the samples were evaluated at (0, 15, 20, 25, 30, 35 and 40) ^{o}C.

High-Performance Liquid Chromatography (HPLC)

Triacylglycerol composition was determined by HPLC using Waters 1515 Isocratic HPLC Pump, Waters 2414 refractive index (RI) detector. The column used was a Nova-Pak C_{18} (250 mm x 4.6 mm) Waters packed with a particle size of 5 μm. The mobile phase was a mixture of acetone/acetonitrile (63.5:36.5) and the flow rate was 1 mL/min. Triacylglycerol peaks were identified based on the retention time of TAG standards and results ofNoor Lida et al. (2001), Tan & Che Man (2000), Zainal & Yusoff (1999) and Lai et al. (1998) [3-6].

Gas Chromatography (GC)

GC determines fatty acid compositions. The blends were esterified into fatty acid methyl ester (FAME). About 1 μL of the FAME was injected into a Shimadzu (model GC-17A), equipped with a flame-ionization detector (FID), fitted with a polar capillary column BPX70 (0.25 mm internal diameter x 30 cm length x 0.25 μm film thickness). The detector and injector port temperatures were 240 ^{o}C. Carrier gas was nitrogen at 0.3 mL/min. The column temperature was isothermal at 180 ^{o}C.

Results and Discussion

Fatty Acid Composition (FAC)

Table 1 and Figure 1 show fatty acid compositions of RBDPO, SFO and their blends. RBDPO and their blends containing high proportion of RBDPO were characterized by higher content of palmitic and oleic acids. This is because palmitic and oleic are the major fatty acids in RBDPO. While, SFO and blends with high portion of SFO showed a higher content of linoleic acid as the major fatty acid in SFO. The fatty acid compositions of the interesterified blends are not shown as CIE neither affects the degree of saturation nor causes isomerization of fatty acid double bond. Thus, it does not change the fatty acid profile of the starting material [7-9].

Triacylglycerol Composition

Triacylglycerol (TAG) composition of RBDPO and SFO before and after CIE is shown in Figure 2 and 3. The main TAGs in RBDPO were PPO (30.76%), POO (24.09%), POL/SLL (9.46%), PPL (7.97%), PPP (5.87%), POS (5.31%) and OOO (4.19%) (P, palmitic; S, stearic; O, oleic and L, linoleic). The major TAGs of SFO were LLL (28.03%), OLL (27.19%), POL/SLL (11.27%), OOL (10.74%) and PLL (10.05%). Generally, CIE induced only small changes in the TAG composition of RBDPO and SFO.

Table 1. Fatty compositions of RBD palm oil, sunflower oil and their blends in various ratios

RBDPO:SFO ratios	**FAC (wt. %)**						
	C 12:0	C 14:0	**C 16:0**	**C 18:0**	**C 18:1**	**C 18:2**	**C 18:3**
ADB [10:0]	0.289	1.045	44.803	4.042	40.224	8.816	0.152
BDB [9:1]	0.251	0.956	41.561	3.988	38.741	13.605	0.141
CDB [8:2]	0.243	0.906	38.868	3.787	36.614	18.500	0.141
DDB [7:3]	0.252	0.900	36.304	3.627	34.479	23.154	0.126
EDB [6:4]	0.182	0.690	30.744	3.765	34.290	29.141	0.168
FDB [5:5]	0.148	0.561	25.866	3.796	33.220	35.440	0.156
GDB [4:6]	0.123	0.462	21.921	3.735	31.524	41.293	0.154
HDB [3:7]	0.096	0.358	17.978	3.666	29.996	46.416	0.180
IDB [2:8]	0.070	0.267	14.033	3.606	28.878	52.582	0.166
JDB [1:9]	0.046	0.170	10.075	3.538	26.797	58.287	0.174
KDB [0:10]	-	0.068	6.126	3.411	24.863	63.186	0.082

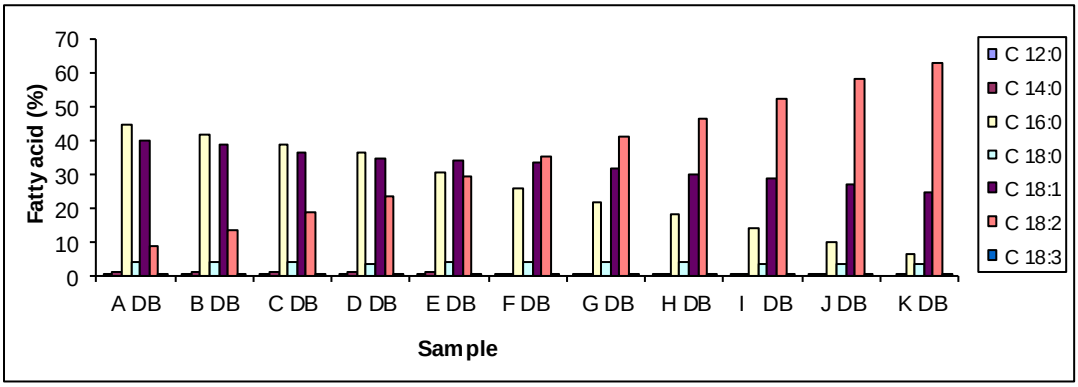


Figure 1. Fatty acid compositions of RBDPO, SFO and their blends in various ratios

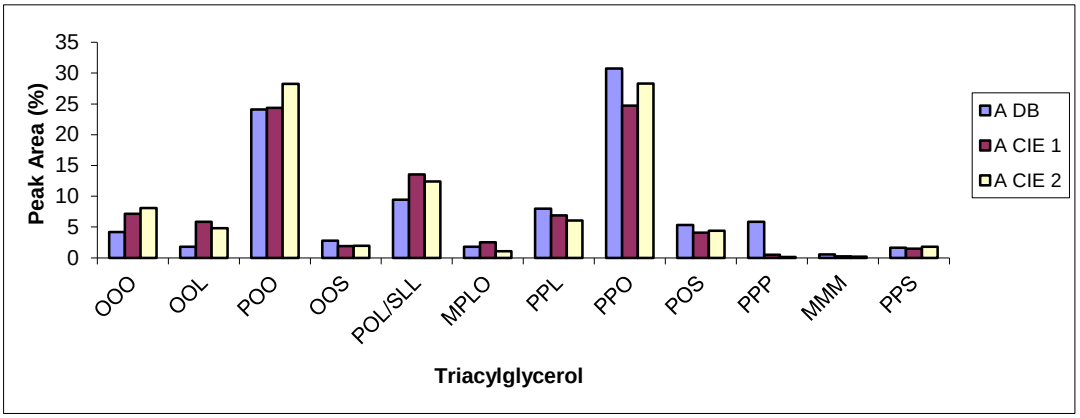


Figure 2. Triacylglycerol compositions of RBDPO before and after interesterification

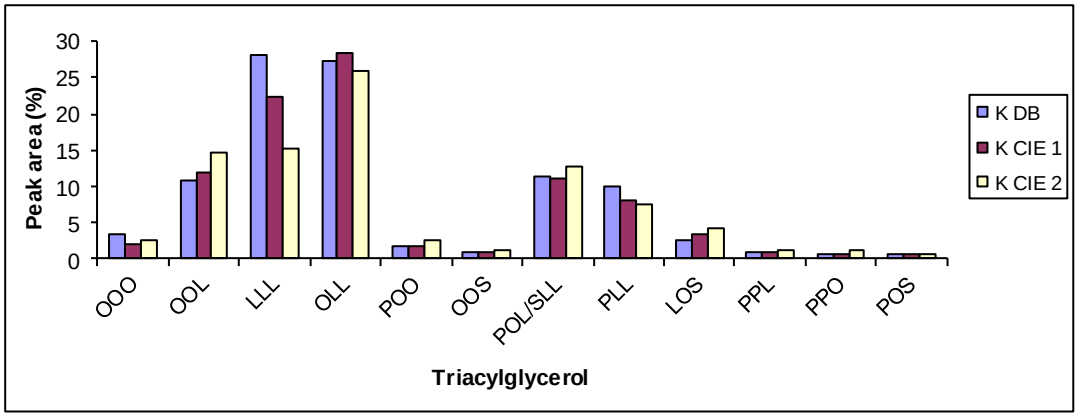


Figure 3. Triacylglycerol compositions of SFO before and after interesterification

Figure 4 shows the TAG composition of some of the binary blends before and after interesterfication of RBDPO/SFO in various ratios. TAG composition of the simple blends of RBDPO/SFO represents a linear combination of the oil component in the blends. For example, as the proportion of SFO increases in the blends, so does the proportion of OOL, LLL, OLL, PLL and LOS. CIE induced enormous changes in the TAG composition of the some samples (G, H and J), but induced a little change for the rest of the samples.

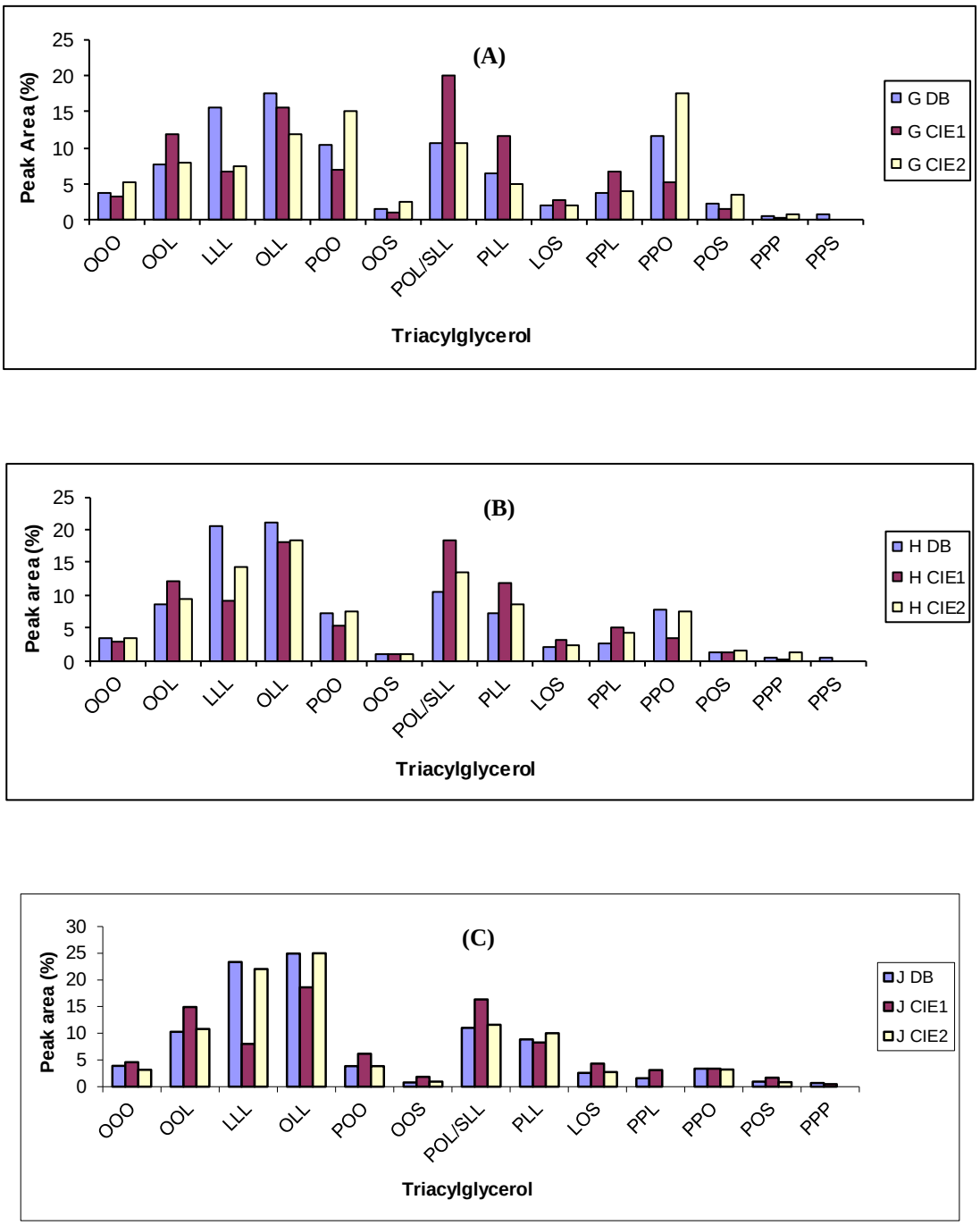


Figure 4. Triacylglycerol compositions of binary blends of RBDPO/SFO before and after interesterification: (A) sample G, (B) sample H and (C) sample J

For example, the proportions of the main TAGs in the sample G DB (containing 40% of RBDPO and 60% of SFO), i.e. the POL/SLL and PLL had increased in CIE1 (86.58% and 81.55% respectively), but decreased in CIE2 (1.03% and 23.47% respectively). CIE1 and CIE2 had resulted increasing in PPL (84.8% and 12.15% respectively) and

OOL (51.99% and 1.67% respectively). However, LLL and OLL had dropped as much as 57.00% and 11.49% respectively in CIE1, and 53.29% and 31.44% respectively in CIE2. PPO, POO and OOO had decreased in CIE1 (55.00%, 33.49% and 12.30% respectively), but increased in CIE2 (51.00%, 44.78% and 37.70% respectively).

Generally, the TAG profiles of the interesterified blends show relative concentrations of several TAGs increased, others decreased, and several new TAGs might also have been synthesized.

Solid fat content (SFC)

The SFC profiles of the simple blend and chemically interesterified RBDPO and their blends in various ratios are shown in Figure 5. The SFC profiles of each sample were significantly changed. The rate of SFC evaluation was dependent on both temperature and proportion of oil in the blends. RBDPO was the hardest fat with 3.12% of SFC at 40 ^{o}C. This was due to the high proportion of saturated TAG with respect to the content of palmitic acid as describe in Table 1 compared to SFO. Enormous changes can be seen at temperature from 20 ^{o}C to 40 ^{o}C, and 5 ^{o}C increasing induced dropping more than 40% of SFC. Thus, a little change in temperature induced enormous changes in SFC profile.

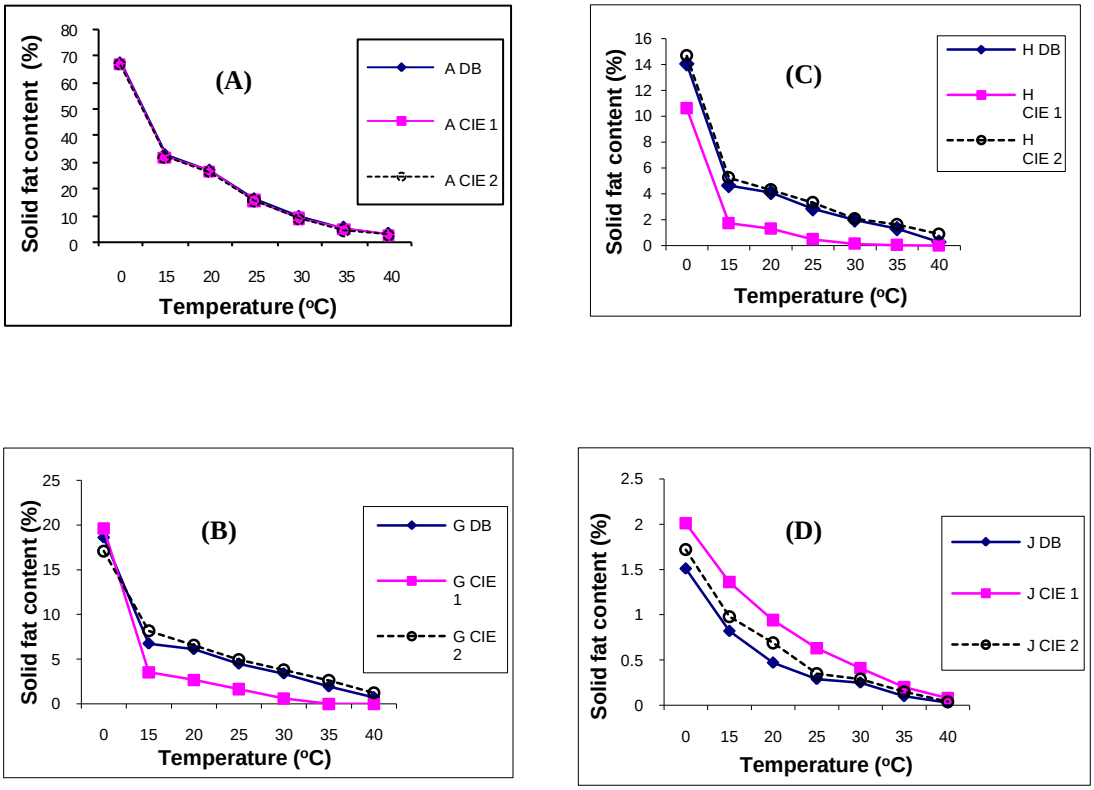


Figure 5. Solid fat content profiles: (A) sample A, (B) sample G, (C) sample H and (D) sample J

SFO is rich in linoleic acid which has very low of melting point. At 15 ^{o}C, SFC value of SFO was 0%. Depending on Noor Lida (2001)[3], SFO was fully liquid at temperatures as low as 5 ^{o}C, as it was in polyunsaturated fatty acids.

Any changing on TAG composition of the interesterified blends effect the SFC profile. However, TAG composition of RBDPO and SFO after CIE was not much seen. As a result, there was also not much change in their SFC profiles. However, interesterified blends showed various SFC profile due to various type of TAG formed. Enormous changing can be seen in sample G, H and J. For example, sample G DB showed SFC profile higher than sample G CIE1, but lower than G CIE2. Increasing in OOL, POL/SLL and PLL, and decreasing in PPO, POS and PPP for sample G CIE1 alter this result. However, sample G CIE2 decreased in LLL, OLL, POL/SLL and PLL, but increased in PPO, POS and PPP.

SFC profiles of sample H DB was higher than sample H CIE1, but lower than H CIE2. This situation resulted by increasing of OOL, POL/SLL, PLL and LOS, and decreasing of PPO, POS and PPP in sample H CIE1. However, sample H CIE2 has decreased in LLL and OLL, but increased in PPL, PPO, POS and PPP.

SFC profiles of sample J DB was lower than interesterified blends (J CIE1 and J CIE2). It was due to enormous reduction in triunsaturated TAGs (LLL and OLL), but increasing in PPL, LOS and POS for J CIE1. While, sample J CIE2 has decreased in LLL, OOO and OLL.

Conclusion

This study showed that different temperature of interesterification process will produce different interesterified blends. The properties of the interesterified blends cannot be predicted due to randomization of the chemical interesterification. However, SFC profile has direct correlation to TAG composition of the interesterified blends.

Acknowledgement

This work was supported by the Universiti Kebangsaan Malaysia (UKM). The authors would like to thank research grant GUP-2012-076.

References

1. Basiron, Y., Jalani, B. S. & Chan, K. W. (2000). Advances in Oil Palm Research. Malaysia Palm Oil Board: Malaysia.
2. Petrauskaite, V., De Greyt, W., Kellens, M. & Huyghebaert, A. (1998). Physical and Chemical Properties of Trans-Free Fats Produced by Chemical Interesterification of Vegetable Oil Blends. *Journal of the American Oil Chemists Society*, *75*, 489-493.
3. Noor Lida, H. M. D., Siew, W. L., Chong, C. L. & Kalyana, S. (2001). Characteristics of Simple and Chemically Interesterified Blends Containing Palm Stearin, Sunflower Oil and Palm Kernel Olein and Their Potential Application of The Blends in Fats Spread Formulation. *Oil Palm Bulletin*, *43*, 38-49.
4. Zainal, Z. & Yusoff, M. S. A. (1999). Enzymatic Interesterification of Palm Stearin and Palm Kernel Olein. *Journal of the American Oil Chemists Society*, *76*, 1003-1008.
5. Tan, C. P. & Man, Y. B. C. (2000). Differential Scanning Calorimetric Analysis of Edible Oils: Comparison of Thermal Properties and Chemical Composition. *Journal of the American Oil Chemists Society*, *77*, 143-155.
6. Lai, O. M., Ghazali, H. M. & Chong, C. L. (1998). Physical Properties of Pseudomonas and Rhizomucor Miehei Lipase-Catalyzed Transesterified Blends of Palm Stearin Palm Kernel Olein. *Journal of the American Oil Chemists Society*, *75*, 953-959.
7. Allen, D. A. (1996). Interesterification - A Vital Tool for The Future? *Lipid Technology*, 11-15.
8. Haumann, B. F. (1994). Tools: Hydrogenation and interesterification. *INFORM*, *5*, 668-678.
9. Rozendaal, B. F. (1994). Interesterification of Oil and Fats. In *Edible fats and oil: Basic principle and modern practice*, pp. 152-157.

The Malaysian Journal of ANALYTICAL SCIENCES ISSN 1394-2506

GLYCINE AS ALTERNATIVE FUEL IN MAKING HYDROTALCITE COMPOUND BY MEANS OF COMBUSTION METHOD

(Glisin Sebagai Bahanapi Alternatif Dalam Pembuatan Sebatian Hidrotalsit Melalui Kaedah Pembakaran)

Shamsudin I.K[1], Helwani Z[1,2], Abdullah A.Z[1], Wiheeb A.D[1,3], Othman M.R[1]*

[1]*School of Chemical Engineering,*
Universiti Sains Malaysia, 14300 Nibong Tebal, Pulau Pinang, Malaysia
[2]*Department of Chemical Engineering,*
Riau University, Pekanbaru 28293, Indonesia
[3]*Department of Chemical Engineering, College of Engineering,*
University of Tikrit, Salah ad Din, Iraq

**Corresponding author: chroslee@eng.usm.my*

Abstract

Hydrotalcite is anion compound capable of exchanging ions; it has the potential as a catalyst and adsorbent for variety of applications. Hydrotalcite can be prepared through several approaches, depending on the specific need and the characteristics of the compound. In this study, hydrotalcite was prepared through combustion method using glycine as fuel for the first time. Glycine was selected as opposed to urea so that hydrotalcite is safe for use in food processing or health. Hydrotalcite that was successfully obtained via combustion technique using glycine as fuel showed interesting characteristics. The compound demonstrated high thermal endurance and highest alkalinity, which suited the application for biodiesel production from vegetable oil and hydrogenation in the making of fats. However, the surface area was low in comparison with the same compound obtained from co-precipitation and sol-gel techniques.

Keywords: hydrotalcite, catalyst, sol gel technique, combustion method, co-precipitation method, bio-diesel

Abstrak

Hidrotalsit adalah sebatian beranion yang berkebolehan dalam penukaran ion; berprestasi sebagai pemangkin dan bahan penjerap untuk pelbagai kegunaan. Hidrotalsit boleh disediakan melalui beberapa kaedah bergantung kepada keperluan spesifik dan sifat-sifat sebatian. Dalam kajian ini, hidrotalsit telah disediakan melalui kaedah pembakaran dengan menggunakan glisin sebagai bahan api buat kali pertamanya. Glisin dipilih berbanding urea supaya hidrotalsit selamat digunakan untuk pemerosesan makanan atau kesihatan. Hidrotalsit yang telah berjaya dihasilkan melalui teknik pembakaran menggunakan glisin sebagai bahanapi telah menunjukkan ciri-ciri yang menarik. Sebatian ini mempamirkan daya tahan terma tinggi dan alkaliniti yang tertinggi, sesuai digunakan untuk aplikasi pengeluaran biodiesel daripada minyak sayuran dan juga penghidrogenan dalam pembuatan lelemak. Namun, luas permukaannya rendah berbanding sebatian yang sama yang dihasilkan daripada kaedah se-mendakan dan sol-gel.

Kata kunci: hydrotalsit, mangkin, kaedah sol-gel, kaedah pembakaran, kaedah se-mendakan, bio-diesel

Introduction

Hydrotalcite (HT) compounds are double-layered hydroxide that was first found in 1915 [1]. Its structure consists of consecutive layers of brucite, $Mg(OH)_2$ and gibbsite, $Al(OH)_3$ [2]. It was reported that both layers constituted of localized cations [3] where M^{2+} cations are substituted by M^{3+} cations and interlayers containing the charge balancing anions and water molecules. HT is also called layered double hydroxides (LDHs) [4] because it consists of hydroxyl ions held together by van der Waal's force. When a fraction of Mg^{2+} ions in the brucite is substituted by trivalent cations such as Al^{3+}, hydroxide layers exhibit anionic mobility [5], anion exchange and sorption properties [6] in addition to surface basicity. These properties make HT highly potential for base-catalysed reactions [7] such

as transesterification of oil into biodiesel. HT materials are also known to exhibit biodegradability and naturally mild materials [8]. Their microstructures and properties have been actively researched and developed over the years. Realizing their reactive behaviour towards certain species and their desirable micro-structural characteristics such as permanent anion exchange, high adsorption capacity, mobility of their interlayer anions and water molecules, large surface areas, stability and homogeneity of the materials; HTs have been exploited for use in a wider range of applications such as adsorbent for liquid ions and gas molecules [9,10,11,12,13, 14].

HTs may occur naturally but are scarcely found. The usual synthetic method for mass production is through co-precipitation [4, 15]. A more recent methods are sol-gel and decomposition-recrystallization, urea method and microwave irradiation [16, 17, 18, 19]. Conventional preparative routes involve oxide precipitation in the presence of alkali hydroxide and carbonates [20, 21, 22, 23]. This presents problem of alkali contaminants in the finished HT [20]. The contaminants were reportedly K [21] or Na [24] residues. This contamination was found to complicate performance comparison [25] of HT.

Combustion method is preferred prior due to the short period of heating required whilst saving significant amount of energy and time. This method involves very rapid chemical process as it is based on the explosive decomposition of organic fuels. The fuels typically used were urea [19. 26] and sugar [27]. The combusted mixed oxides were recrystallized as layered double HT by contacting with sodium carbonate solution. The reaction was initiated with heat. A network of Mg^{2+}-O^{2-} was initially formed while the aluminium was progressively incorporated into a mixed oxide with a periclase-like structure [27]. The combusted HT prepared in this manner was reportedly able to adsorb and desorb CO_2 in pressure swing adsorption (PSA) over 50 times with insignificant capacity loss [28].

The present work is dedicated to preparing of HT from 3 different methods. Their observed properties were compared in order to identify relevant applications.

Materials and Methods

Samples from co-precipitation were purchased from Tomita Pharmaceutical. The samples were pretreated by heating it up in a furnace at 450°C, 650°C and 850°C, respectively.

Samples prepared from sol-gel method started by mixing aluminium tri-sec-butylate ($C_{12}H_{27}AlO_3$) and magnesium methoxide $(CH_3O)_2Mg$ at 3:1 atomic ratio with deionized water. The alkoxides were hydrolyzed under vigorous stirring at 70-90 °C to form sol. Then, 9.5ml 1M potassium carbonate (K_2CO_3) was added to the mixture, followed by peptization of the sol using molar composition of the alkoxide, acid and water at 1:0.07:100. Polyvinyl alcohol (PVA) (4g PVA/100ml H_2O) was added to increase sol's strength. The peptized sol was allowed to cool steadily for hydroxylation, alkoxilation or condensation. A small amount of the resulting mixture was poured onto a polypropylene petri dish, dried under ambient and highly humid conditions to obtain a hardened dried gel. The resulting paste was later placed into furnace and heated at 450°C, 650°C and 850°C, respectively to obtain mixed oxides.

Sample prepared from combustion method started by mixing magnesium nitrate and aluminum nitrate with deionized water at Mg/Al atomic ratio of 3:1. The nitrates were hydrolyzed separately for approximately 30 minutes under vigorous stirring at 70^{o}C. Then, the sodium carbonate (Na_2CO_3) of 0.10 to 0.20 per gram of solid mixture was added. 10% of glycine per gram of mixture was added and the mixture was allowed to be suspended in water. The solution was heated at 80 °C. About 5ml of polyvinyl alcohol (PVA) (4g PVA/100ml H_2O) was added to the heating mixture until water was evaporated. The resulting paste was heated at 450 °C, 650 °C and 850 °C, respectively.

Results and Discussion

Figure 1a shows XRD pattern of a mixed oxide of hydrotalcite and Fig. 1b to 1d, show the XRD patterns of the mixed oxides after they were contacted with the carbonate solution. It is obvious that the mixed oxides were disordered in nature but they returned to the more ordered state after being in contact with carbonate solution to form HT. The peaks that correspond to hydrotalcite are 11.4, 22.9, 34.6, 38.9, 45.9, 60.2, and 61.7. The intercalated structure with at least a mono-molecular layer is described by the distinguished peak at 2θ of less than 20° [8]. The

heat released per mole of burned glycine, $C_2H_5O_2N$ was reportedly 528 kJ/mol [28]. Although it is low when compared to other fuels such as saccharose (5646.7kJ/mol), fructose (2826.7 kJ/mol) and glucose (2815.8 kJ/mol) [28], the energy from glycine was found to be sufficient to form complexes with the metal ions to form mixed oxides and later HT upon contact with carbonate solution. The enthalpy required to form Mg-O and Al-O bonds is 363.2 and 511 kJ/mol, respectively, lower than the energy provided by glycine.

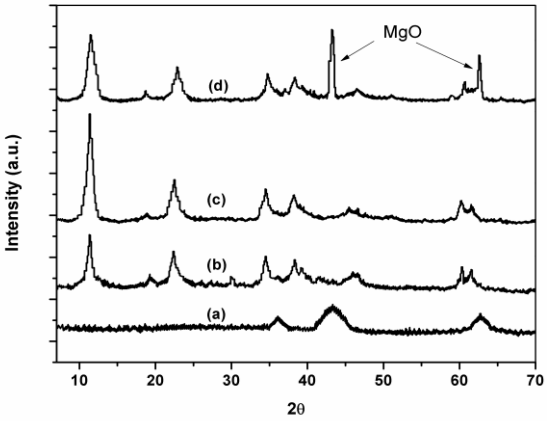


Figure 1. XRD pattern of (a) mixed oxide of hydrotalcite at 450°C, (b) hydrotalcite at 450°C (c) hydrotalcite at 650°C and (d) hydrotalcite at 850°C.

Table 1 compares the results of the characterization that describe the most desirable properties (smallest pores, highest BET surface area, etc). The results suggest that HT from co-precipitation is suitable for application such as in filtration that requires extremely small pores. HT from sol-gel method is suitable as catalyst for biodiesel production from oil due to its highest BET surface area. Whereas, HT from combustion is suitable for application requiring thermal endurance such as adsorption of CO_2 from hot flue gas. However, due to high crsytallinity level and the highest alkalinity, HT from combustion is also suitable for use as base catalyst in biodiesel production via transesterification of vegetable oils and hydrogenation to convert liquid vegetable oils to solid or semi-solid fats, such as margarine and shortening.

Table 1. Comparisons of as-synthesized HT from different approaches

	Characteristics	HTcp	HTcomb	HTsg
1.	Minimum pore size (nm)	1.5	1.9	4.1
2.	Maximum BET surface area (m^2/g)	58.86	22.21	273.8
3.	Particle size (μm)	15.81	28.22	20.91
4.	Specific surface area (m^2/g)	0.77	1.10	1.49
5.	Crystallinity*	Moderate	High	High
6.	Stability temperature (^oC)	600	624	550
7.	pH of HT	9.02	13.6	9.35

*Low - below 100Å; Moderate - 100-300Å; High - 301Å and above

Conclusion

The results suggest that HT from co-precipitation using glycine as fuel is suitable for application requiring thermal endurance such as adsorption of CO_2 from hot flue gas. HT from combustion is also suitable for use as base catalyst in biodiesel production via transesterification of oil and hydrogenation to convert liquid vegetable oils to solid or semi-solid fats, such as margarine and shortening due to its high crsytallinity level and the highest alkalinity.

Acknowledgement

The supports from the Universiti Sains Malaysia through Research University, Short Term and Research Cluster grants are gratefully acknowledged.

References

1. Manasse, E. (1915). Rocce eritree e di aden della collezione issel. Atti Soc. oscana. Sc. Nat., Proc. Verb. 24: 92
2. Feitknecht, W. (1942). The Formation of Double Hydroxide between Bivalent and Trivalent Metals Helv. *Chim.Acta* 25: 131 and 555.
3. Almann, R. (1968).The crystal structure of pyroaurite, *Acta Cryst.* 24: 972
4. Cavani, F., Trifiro, F., Vaccari A. (1991). Hydrotalcite-type anionic clays: preparation, properties and applications. *Catal. Today* 11: 173.
5. Oesten, R. and Bohm, H. (1993). Ionic mobility in basic double salts. Part 1: Hydrotalcites.*Solid State Ionics* 62: 199.
6. Ookubo A, Ooi H, Hayashi K. (1993). Preparation and phosphate ion-exchange properties of a hydrotalcite-like compound. *Langmuir* 9:1418.
7. Reichle, W.T. (1986). Synthesis of anionic clay minerals (mixed metal hydroxides, hydrotalcite). *Solid State Ionics*. **22**: 135 – 141.
8. Lee, W.F., Chen Y.C. (2006). Effects of intercalated hydrotalcite on drug release behaviour for poly(acrylic acid-co-N-isopropyl acrylamide)/intercalated hydrotalcite hydrogels. *Eur Polymer J* 42:1634.
9. Aramendia, M.A., Aviles, Y., Benitez, J.A., Borau, V., Jimenez, C., Marinas, J.M.,Ruiz, J.R. and Urbano, F.J. (1999). Comparative study of Mg/Al and Mg/Ga layered double hydroxides. *Microporous and Mesoporous Materials* 29: 319 – 328.
10. Yong, Z. and Rodrigues, A. E. (2002). Hydrotalcite – like compounds as adsorbents for carbon dioxide. *Energy Conversion and Management* 43 :1865 – 1874.
11. Yamamoto, T., Kodama, T., Hasegawa, N., Tsuji, M. and Tamaura, T. (1995). Synthesis of hydrotalcite with high layer charge for CO_2 adsorbent. *Energy Conversion Management* 36 : 637 – 640.
12. Ding, Y. and Alpay, E. (2000). Equilibria and kinetics of CO_2 adsorption on hydrotalcite adsorbent. *Chemical Engineering Science* 55: 3461 – 3474.
13. Othman, M.R., Rasid, N.M., Fernando, W.J.N. (2006). Effects of thermal treatment on the micro-structures of co-precipitated and sol-gel synthesized (Mg-Al) hydrotalcites. *Microporous and Mesoporous Materials* 93: 23-28.
14. Othman M.R., Fernando W.J.N, Kim, J. (2009). The conversion of an organometallic compound into an intercalated thin-layer amorphous structure. *Appl. Organometal Chem*. 23: 403-408.
15. Lopez – Salinas, E., Torres – Garcia, E. and Garcia – Sanchez, M.(1997). Thermal behavior of hydrotalcite – like $[Mg_{1-x}\,Ga_{\,x}\,(OH)_2]\,(CO_3)_{x/2}\,.\,mH_2O$ as a function of Galium content. *Journal Physical Chemistry Solids*. 58(6): 919 – 925.
16. Fetter, G., Hernandez, F., Maubert, A.M., Lara, V.H., Bosch, P. (1997). Microwave irradiation effect on hydrotalcites synthesis, *J. Porous Mater*. 4:27
17. Yang, W., Kim, Y., Liu Paul, K.T., Tsotsis, T.T. and Sahimi, M. (2002). A study by in situ techniques of the thermal evolution of the structure of a $Mg – Al – CO_3$ layered double hydroxide. *Chemical Engineering Science* 57 : 2945 – 2953.
18. Patil, K.C., Aruna, S.T., Ekambaram, S. (1997). Combustion synthesis, *Solid State Mater. Sci.* 2: 158.
19. Cruz, D., Bulbulian, S. (2003). Synthesis of lithium silicate tritium breeder powders by a modified combustion method, *J. Nucl. Mater*. 312: 262.
20. Constantino, U., Mamottini, F., Nocchetti, M., Vivani, R. (1998). New synthetic routes to hydrotalcite-like compounds-characterisation and properties of obtained materials, *Eur. J. Inorg. Chem*. 10:1439.

21. Diez, V.K., Apesteguia, C.R., and J.I. Di Cosimo (2003). Effect of the chemical composition on the catalytic performance of MgyAlOx catalysts for alcohol elimination reactions. *J. Catal.* 215: 220-233.
22. Mistra, C., Perrotta, A. (1992). Composition and properties of synthetic hydrotalcites, *Clays Clay Miner*. 40: 145.
23. Kagunya, W., Hassan, Z., Jones, W. (1996). Catalytic Properties Of Layered Double Hydroxides and Their Calcined Derivatives, *Inorg. Chem* 35: 5970.
24. Prinetto, F., Ghiotti, G., Graffin, P. and Tichit, D. (2000). Synthesis and characterization of sol gel Mg/Al and Ni/Al layered double hydroxides and comparison with co-precipitated samples. *Microporous and Mesoporous Materials* 39 : 229 – 247.
25. Cantrell, D.G., Gillie, L.J., Lee, A.F., Wilson, K. (2005). Structure-reactivity correlations in MgAl hydrotalcite catalyst for biodiesel synthesis, *Applied Catalysis A*: Gen. 287, 183-190.
26. Erickson, K.L., T.E. Bostrom, and R.L. Frost (2004). A study of structural memory effects in synthetic hydrotalcites using environmental SEM. *Materials Letters*, 59(2-3): 226-229.
27. Davila, V., Lima, E., Bulbulian, S., Bosch, P. (2008). Mixed Mg(Al)O oxides synthesized by the combustion method and their recrystallization to hydrotalcites, *Microporous and Mesoporous Materials* 107: 240-246.
28. Martunus, Othman, M.R., Fernando, W.J.N. (2011). Elevated temperature CO_2 capture via reinforced metal hydroxide, *Microporous and Mesoporous Materials*, 138:110-117.

The Malaysian Journal of ANALYTICAL SCIENCES ISSN 1394-2506

CATALYTIC CRACKING OF USED PALM OIL USING COMPOSITE ZEOLITE

(Peretakan Bermangkin Minyak Kelapa Sawit Terguna Menggunakan Zeolit Komposit)

W. H. Chang and C. T. Tye*

School of Chemical Engineering, Engineering Campus, Universiti Sains Malaysia, 14300 Nibong Tebal, Pulau Pinang, Malaysia

**Corresponding author: chcttye@eng.usm.my*

Abstract

The rapid expansion of human society implies greater energy demand and environmental issues. In face of depletion energy resources, research is being carried out widely in order to convert the plant oil into biofuel. In this research, the production of liquid biofuels via catalytic cracking of used palm oil in the presence of composite zeolite was studied. The performance of composite zeolite of different properties in the reaction has been evaluated. The catalytic cracking reactions were carried out in a batch reactor at reaction temperature of 350^{o}C for an hour. In the present study, adjusting the ratio of mesoporous coating to microporous zeolite and magnesium loading on composite zeolite catalyst were found to be able to increase the gasoline fraction and overall conversion of the reaction.

Keywords: Catalytic cracking, used palm oil, composite zeolite

Abstrak

Perkembangan pesat masyarakat manusia menyebabkan permintaan tenaga yang lebih tinggi dan isu-isu alam sekitar. Untuk menghadapi masalah kehabisan sumber tenaga, penyelidikan sedang dijalankan secara meluas untuk menghasilkan bahan api hijau daripada minyak tumbuhan. Dalam kajian ini, pengeluaran bahan api hijau cecair daripada peretakan bermangkin minyak sawit terguna dengan kehadiran zeolit komposit telah dikaji. Prestasi sifat zeolit yang berbeza dalam tindak balas ini telah dinilai. Tindak balas peretakan bermangkin telah dijalankan dalam reaktor kelompok pada suhu 350^{o}C selama satu jam. Dalam kajian ini, penyelarasan nisbah salutan berliang-meso kepada zeolit berliang-mikro dan muatan magnesium pada mangkin zeolit komposit didapati boleh meningkatkan pecahan gasolin and penukaran keseluruhan tindak balas.

Kata kunci: Peretakan bermangkin, minyak kelapa sawit terguna, zeolit komposit

Introduction

Biofuel production is undergoing rapid technological reforms in industries and academia. This has become more obvious with the growing awareness of the issues of environmental sustainability and the fossil fuel over-dependency. The feedstock for biofuel production is mainly vegetable oil. Vegetable oil can be divided into edible and non-edible oil. Edible oil such as crude palm oil and soybeans oil and non-edible oil such as used palm oil, are commonly accepted as raw material to produce biofuel. Used palm oil is used as the utilization of used edible oil would not divert resources from the food supply [1]. Conversion of biofuel from vegetable oil via catalytic cracking process has been carried out. Catalytic cracking is preferable compared to thermal cracking as catalytic cracking can take place at a much lower temperature, produces high octane gasoline and lowers the yield of heavy fuel oils and light gases [2].

Zeolite with microporous structure, ZSM-5 is commonly used as a catalyst to boost the gasoline octane number. Various types of zeolite catalysts were reported in catalytic cracking for the production of biofuels from vegetable oil. These findings show that zeolite possess a great potential as solid acid cracking catalyst due to its structure, acidity and high selectivity for the production of biofuels from vegetable oils. Catalytic cracking of palm oil over HZSM-5 was found to produce organic liquid rich in gasoline fraction from the catalytic cracking of palm oil based

fatty acid mixture [3] but the selectivity for gaseous products was also high [4]. It was found that MCM-41, a mesoporous catalyst is more selective for C_{5+} olefin products producing high octane fuels comparing to the performance with ZSM-5 [4]. The selectivity of MCM-41 mesoporous materials towards particular liquid hydrocarbons such as gasoline, kerosene or diesel in the cracking of palm oil was found strongly depended on the pore size and the surface area of mesoporous material. Due to the higher accessibility of reactants in mesoporous MCM-41 as compared to zeolite, it is suitable for catalytic reactions dealing with large molecules. However, the cracking activity of MCM-41 is lower than ZSM-5 zeolite due to lower acidity and shape selectivity of the mesoporous materials [4].

Zeolite can be more effective for larger reactant molecules by combining their microporous structure with mesoporous materials having higher adsorption capacity. The role of HZSM-5 in catalytic cracking unit was an octane-boosting additive due to its higher selectivity towards aromatic hydrocarbons [4]. However, HZSM-5 has tendency to produce gaseous product compare to other zeolite catalysts in palm oil cracking [4]. Hence, mesoporous materials were introduced as a diluting component to moderate the activity of the zeolite. Composite catalyst of mesoporous and microporous zeolite is desired as it contains the characteristic of both the mesoporous molecular sieve and microporous zeolite [4]. It is reported that MCM-41/Beta zeolite composite catalyst was more selective towards liquid fuel gasoline and enriched with olefins [5]. Composite material (MCM-41/ZSM-5) gave similar yield as HZSM-5 but lower gaseous products [4].

The modification of zeolite with Zn, Cu and rare earth metal (RE) could increase the total acidity of zeolite [6]. ZSM-5 zeolites modified with transition metals, such as Cu, Zn, and Ag increase the yield of aromatics. The loading of rare earth metal into Y zeolite catalyst improved the ability of the catalyst to withstand high temperature, leading to the catalytic stability and increasing the catalyst activity and gasoline selectivity [7]. Introducing rare earth metal in zeolite USL, was believed to increase the yield of total liquid products (LPG, gasoline and diesel) and improving the quality of gasoline. It has not only enhanced the content of isoparaffins, aromatic hydrocarbons and RON number in gasoline, but also decreased the olefin content in gasoline [8].

The objective of the present study is to develop a suitable metal loaded composite zeolite catalyst for catalytic cracking of used palm oil to produce liquid fuel.

Materials and Methods

Catalyst preparation

Metal loaded zeolite catalyst

Metal loaded zeolite catalyst was prepared by impregnation method. Zeolite catalysts loaded with three different metals (magnesium, zinc, copper) were prepared in the present study. To load magnesium on zeolite, first, magnesium chloride, $MgCl_2$ (Merck) was dissolved in decationized water and mixed with zeolite. The mixture was stirred at room temperature for 12 hrs. Then, the mixture was dried in an oven at 120^{o}C for 24 hrs. Next, the mixture was calcined in a muffle furnace at 550 ^{0}C for 2 hrs. The same procedure has been used to load zinc and copper on the zeolite by using zinc chloride, $ZnCl_2$ (Merck) and copper (II) nitrate, $Cu(NO_3)_2.3H_2O$ (Merck) as the metal precursor, respectively.

Composite zeolite *(CMZ)*

The composite materials were prepared by coating commercially obtained zeolite ZSM-5 (Acros) by a layer of mesoporous material. The procedure was based on Twaiq et al. [4]. First, cetyltrimethylammonium hydroxide, CTMA-OH (Acros, 25% in methanol) and SiO_2.NaO (Aldrich, 20% in water) was dissolved in deionized water. Then another mixture of metal loaded ZSM-5 and cetyltrimethylammonium chloride (CTMA-Cl) (Aldrich, 25% in methanol) which undergo medium mixing rate for overnight to form gel was added to the solution. 0.15 wt% of Al_2O_3.NaO (Aldrich) aqueous solution was added to the reaction gel mixture after 15 mins. The amount of chemical used, CTMAOH: H_2O: SiO_2.NaO: Al_2O_3.NaO followed the mole ratio of 1:97.23:1.15:0.058. The reaction gel mixture was stirred vigorously for 1 hr. The resulting mixture was loaded in a Teflon liner autoclave and kept for 24 hrs at 150^{o}C under 150 rpm. The solid was filtered and washed by water, followed by drying overnight at room temperature. The solid was then calcined at 440 ^{0}C for 6 hrs.

Acidification of zeolite

The zeolite was acidified by reflux zeolite with 0.1M of ammonium chloride aqueous solution with solution to solid ratio of 20 at 80 ^{0}C with continuous overnight stirring. The zeolite was then recovered and dried in air overnight, followed by calcination at 550 ^{0}C for 4 hrs. The prepared composite catalyst was coded as *X*-CMZ (*W*, *Y*)- P% where *X* referred to the metal, *W* referred to the mesophase to zeolite ratio in the synthesis gel, *Y* referred to Al/Si ratio in the mesophase and *P* referred to metal loading.

Catalyst characterization

BET surface area was measured by nitrogen adsorption-desorption analysis using Micromeritics ASAP 2020 at 77 K. XRD patterns of catalysts were carried out in a range of 20^o-80^o with Cu target Kα-ray by using a Philips diffractometer.

Catalyst activity test

The feedstock, used palm oil (UPO) for the catalytic cracking reaction was waste cooking oil obtained in local café. The catalyst performance in catalytic cracking was evaluated in a batch reactor (Parr 4570). 100 ml of used palm oil and 0.5 wt% of catalyst were loaded into the reactor. The reactor was purged with nitrogen before heated up to 350^{o}C and maintained for 1 hr. The stirrer speed was set at 350 rpm after the reactor temperature reach 350^{o}C. After 1 hr, the reactor was cooled down to room temperature by passing water through the cooling coil. Then, the liquid and solid product was recovered. The coke formation was defined as the acetone insoluble after dried in oven at 100^{o}C for 24 hrs.

The liquid products boiling points distribution were analyzed by using ASTM D86 distillation. The composition of cracking liquid product was defined according to boiling range of petroleum products such as gasoline (< 180^{o}C), kerosene (180°C - 240°C), diesel (240°C - 340°C) and palm oil residue (>340°C). The performance of catalysts was evaluated in terms of conversion, product yield and liquid product fraction distribution. The conversion and liquid product fraction are defined as follow:

$$\text{Conversion (wt \%)} = \frac{\text{residue (>340°C) in feedstock - residue (>340°C) after cracking}}{\text{residue (>340°C) in feedstock}} \text{ x 100 \%} \quad (1)$$

$$\text{Liquid product yield (wt \%)} = \frac{\text{weight of distillate}}{\text{weight of liquid before distillation}} \text{ x 100\%} \quad (2)$$

$$\text{Liquid product fraction (vol \%)} = \frac{\text{volume of distillate fraction}}{\text{total volume of distillate obtained}} \text{ x 100\%} \quad (3)$$

Results and Discussion

Result of UPO analysis

The feed, UPO was analyzed for its boiling range fraction. The result is given in Table 1. There is no gasoline boiling range fraction obtained in the UPO. The largest volume fraction was diesel (72 vol%) followed by palm oil residue (22 vol%) and kerosene (6 vol%).

Table 1. UPO boiling range fraction

Temperature (^{0}C)	Liquid fraction (vol %)
<180 (gasoline)	0
180-240 (kerosene)	6
240-340 (diesel)	72
>340 (palm oil residue)	22

Catalytic cracking of UPO with different metal loaded HZSM-5 catalyst

Three metals i.e. magnesium, zinc and copper was loaded on zeolite and tested for their respective activity in catalytic cracking of UPO. These metals were reported to increase the total acidity of zeolite and thus increase the gasoline fraction [6]. The product yield of different catalyst in the catalytic cracking of used palm oil is shown in Table 2. As expected, the liquid product yield (72.11 wt%) for thermal cracking of used palm oil was the lowest. Meanwhile, the gas yield (16.65 wt%) was the highest. However, when comparing the catalytic cracking reaction with the presence of different catalyst, ie. H-ZSM5, Cu-HZSM5, Zn-HZSM5, Mg-HZSM5, there was negligible coke formation in thermal cracking of used palm oil. Coke formation was observed for all catalytic cracking of used palm oil. Similar observation was also reported by Ong and Bhatia [2].

Table 2. Performance of different catalyst on catalytic cracking of UPO

	Liquid product (wt%)	**Residue (wt%)**	**Coke (wt%)**	**Gases (wt%)**	**Conversion (wt%)**
UPO without catalyst	-	10.58	-	-	-
HZSM-5	72.11	11.24	Negligible	16.65	1.192
Cu-HZSM-5	83.28	10.46	0.48	6.26	22.67
Zn-HZSM-5	80.6	10.81	0.348	8.59	15.68
Mg-HZSM-5	75.94	8.2	0.056	15.804	26.74
	84.7	9.647	0.37	5.633	14.5

Reaction with the presence of Mg-HZSM5 catalyst gave the highest liquid product yield (84.70 wt%) and lowest gas yield (5.63 wt%) among the four catalysts used. Mg-HZSM5 catalyst gave the highest liquid product could be due to the low secondary cracking reaction to a low gas yield (5.63 wt%).

Among the catalyst studied, the highest gas yield (16.65 wt%) was obtained from the reaction running in the presence of Zn-HZSM5. This was followed by the reaction with Cu-HZSM5 as the catalyst (8.59 wt%). Zinc and copper are transition metals that were reported to increase the Lewis acid site of catalyst and promote the dehydrogenative cracking which leading to the yield of light olefins [7]. This could be reason for high gas yield obtained in these two reactions.

As shown in Table 2, thermal cracking of UPO at 350^{o}C gave the lowest conversion (1.19 wt%). Among the four catalyst, catalyst Zn-HZSM5 gave the highest conversion (26.74 wt%) followed by HZSM-5 (22.67 wt%) in catalytic cracking of UPO while Mg-HZSM and Cu-HZSM both gave lower conversion, at 14.5 wt% and 15.68 wt% respectively. It was reported that loading of magnesium did not decrease the strength of acidity but reduced the Bronsted acid sites and the conversion of UPO was influenced by the disappearance of Bronsted acidity [9].

The liquid product distribution that obtained with different catalyst is shown in Figure 1. Mg-HZSM5 gave the highest gasoline fraction which was 9 vol% compared to that of HZSM-5 (5 vol%), Cu-HZSM5 (4.5 vol%) and Zn-HZSM5 (2 vol%). The gasoline fraction obtained with the presence of Zn-HZSM5 catalyst is the lowest. It is believed that most of the gasoline fraction was cracked to gas product since highest gas yield was obtained in the reaction. H-ZSM5 catalyst gave the highest kerosene fraction (7 vol%) while Mg-HZSM5 catalyst had the highest diesel fraction (72.5 vol%) in the catalytic cracking reactions in the present study.

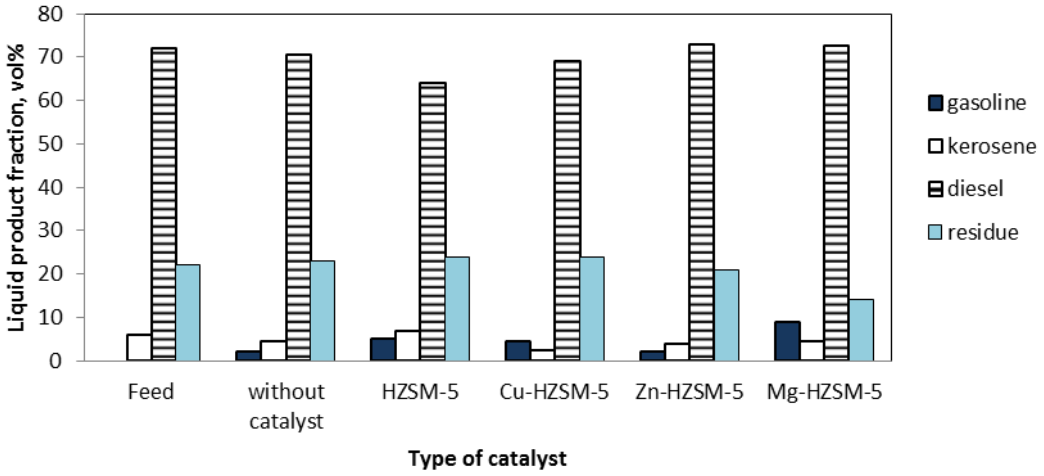


Figure 1. Liquid product fraction distribution for different catalysts (reaction condition: 350 ^{0}C, 1 atm, 0.5wt% catalyst and retention time 1 hour).

Effect of ratio of mesophase to microphase in composite zeolite for catalytic cracking of UPO

As illustrated in Table 3, the ratio of mesophase to microphase in composite zeolite had not much effect on the liquid product yield. As the ratio of mesophase to microphase in composite zeolite increase, the conversion of UPO was found to decrease. The gasoline fraction obtained was also having the similar trend, decrease with increasing of the ratio. This was in agreement with the result reported by Twaiq et al. [4] that increasing the coating in the composite catalyst would decrease the gasoline fraction while increase the kerosene fraction as lower ratio of mesophase coating in composite zeolite can improve the gasoline fraction. Lower ratio of mesophase coating increase the conversion as thinner coating layer is preferable in order to allow reactants to access the micropores [4]. Although the liquid product yield in the presence of HZSM-5 is higher than another three composite zeolites, the conversion is lower.

Table 3. Effect of mesoporous/microporous ratio in composite zeolite and HZSM-5 on liquid and gas yield and conversion

	Liquid product (wt%)	**Residue (wt%)**	**Coke (wt%)**	**Gases (wt%)**	**Conversion (wt%)**
HZSM-5	83.28	10.46	0.48	6.26	22.67
CMZ (0.1, 0.15)	78.90	10.50	0.38	10.22	35.00
CMZ (0.15, 0.15)	79.20	10.47	0.39	9.94	33.00
CMZ(0.2,0.15)	79.31	8.97	0.41	11.31	26.7

As shown in Figure 2, when the ratio of mesophase to microphase in composite zeolite decrease, the gasoline fraction and diesel fraction increase while the kerosene fraction decrease. The gasoline fraction for three composite zeolite is higher than catalyst NZSM-5. The fraction of gasoline is higher than the fraction of kerosene in each of the composite zeolite. CMZ(0.10, 0.15) composite catalyst even gave a gasoline fraction as high as 18 vol%.

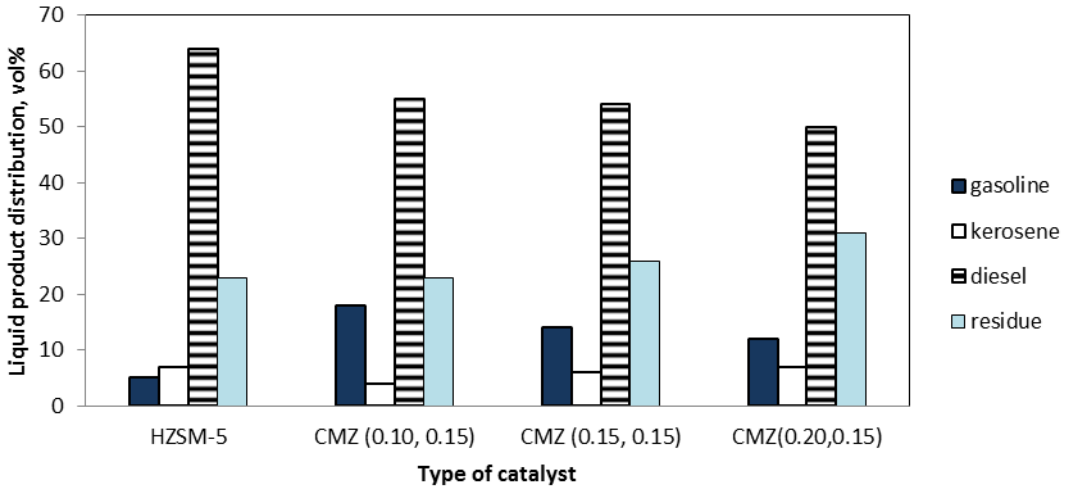


Figure 2. Effect of ratio of mesoporous to microporous in composite zeolite on product fraction (reaction condition: 350 ^{0}C, 1 atm, 0.5wt% catalyst and retention time 1 hour)

Magnesium loaded composite zeolite for catalytic cracking of UPO

The liquid yield for CMZ(0.1,0.15) catalyst (78.9 wt%) and Mg-CMZ(0.1,0.15)-5% (77.8 wt%) were almost similar. However, Mg-CMZ(0.1,0.15)-5% catalyst gave lower yield of coke (0.3 wt%) and lower yield of residue (10.5 wt%) compared to CMZ(0.1,0.15) catalyst.

As shown in Figure 3, the gasoline fraction for CMZ(0.1,0.15) catalyst (18 vol%) and Mg-CMZ(0.1,0.15)-5% catalyst (17 vol%) were similar but higher than feed which does not have any gasoline fraction. The diesel fraction for Mg-CMZ(0.1,0.15)-5% (60 vol%) was higher than CMZ(0.1,0.15) catalyst which gave 55 vol% of diesel. The feed contains the highest diesel fraction which is 72 vol%. The conversion for the catalytic cracking reaction in the presence of Mg-CMZ(0.1,0.15)-5% catalyst (58.89 wt%) was higher than CMZ(0.1,0.15) catalyst (35 wt%).

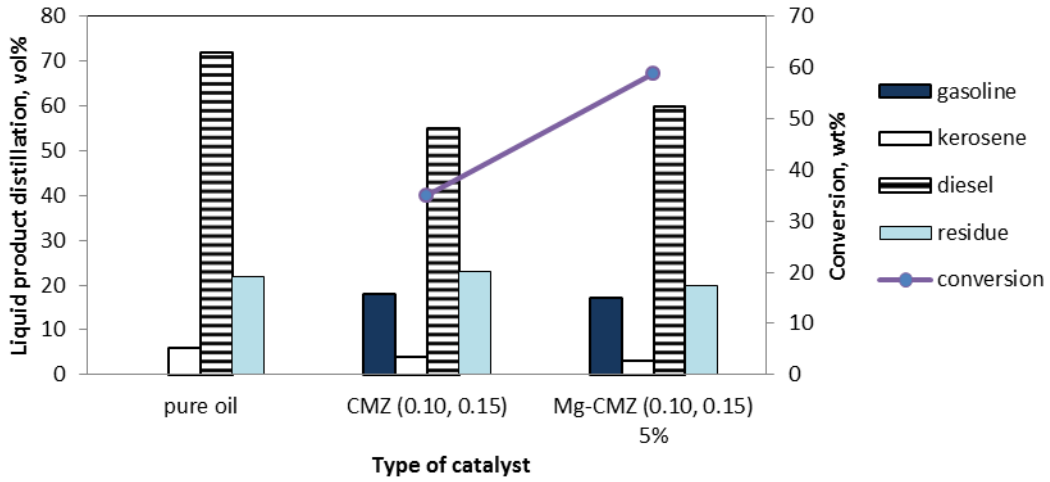


Figure 3. Effect of 5% magnesium loaded in composite zeolite CMZ(0.10,0.15) on product fraction and conversion (reaction condition: 350 ^{0}C, 1 atm, 0.5wt% catalyst and retention time 1 hour).

Properties of catalyst

The physical properties of CMZ(0.10, 0.15) catalyst was obtained from the nitrogen adsorption-desorption analysis. The result is presented in Table 4. The composite catalyst zeolite was found to have large BET surface area of 272 m^2/g and also large average pore size of 29 nm.

Table 4. Physical properties of CMZ(0.10, 0.15) catalyst.

Properties	**value**
BET surface area (m^2/g)	272.55
Pore volume (cm^3/g)	0.10
Pore Size (nm)	29.58

Figure 4 shows the nitrogen adsorption desorption isotherms of CMZ(0.10, 0.15) catalyst. Type IV isotherm is observed. Type IV isotherm are very common and show characteristic hysteresis loops which arise from different adsorption and desorption mechanism in mesoporous. The sharp and steep initial rise in the first part indicated that the composite catalyst contains microporous material as the sharp and steep initial rise is associated with capillary condensation in micropores [10].

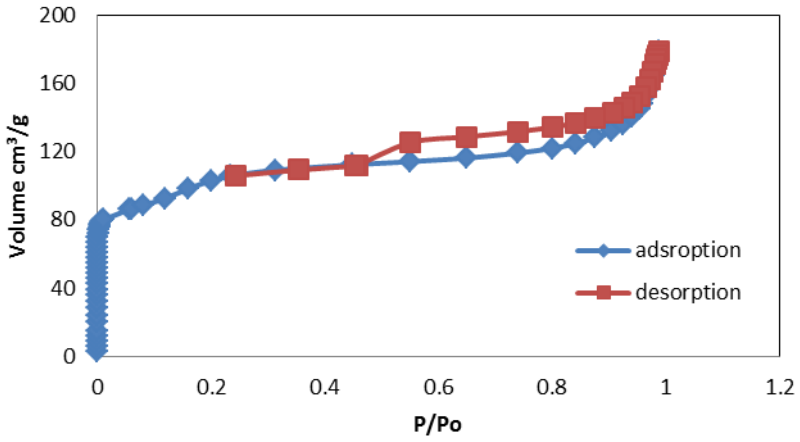


Figure 4: Nitrogen adsorption-desorption of CMZ(0.10, 0.15) catalyst.

The XRD pattern of Mg-CMZ(0.1, 0.15) -5% catalyst is presented in Figure 5. There are peaks that represent two components, which are zeolite and magnesium alumina silicate. The triangle symbol referring to the zeolite peaks while the peaks with a circle symbol referring to magnesium alumina silicate. The shape for zeolite was orthorhombic while for magnesium alumina silicate was hexagonal. From the XRD results, it showed that the active magnesium component on the zeolite is magnesium alumina silicate instead of magnesium oxide.

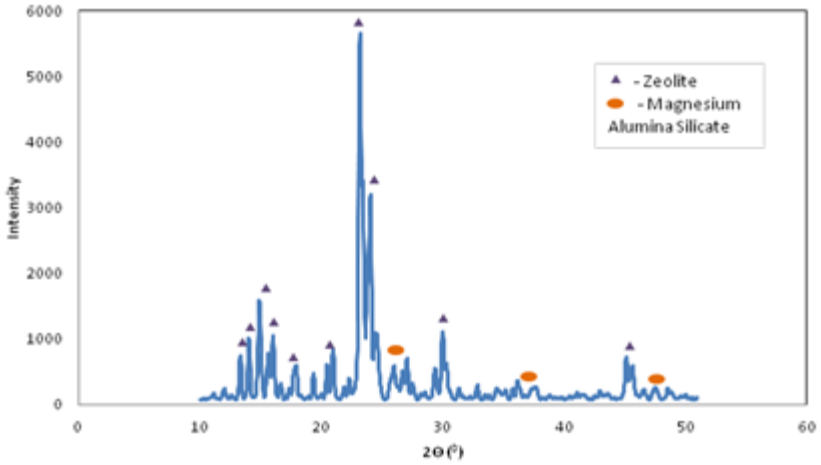


Figure 5. XRD pattern of catalyst Mg-CMZ(0.1, 0.15)-5%

Conclusion

Among the three metal loaded zeolite catalysts, Mg-HZSM5 gave the highest liquid product yield (84.7 wt%) and gasoline fraction (8 vol%). Zn-HZSM5 catalyst gave the highest conversion (26.74 wt%). Ratio of mesophase to microphase in composite catalyst plays an important role in increasing the gasoline fraction and conversion in catalytic cracking of UPO. When the ratio decreased, the gasoline fraction and the conversion of UPO was found to increase. In the present study, CMZ(0.1, 0.15) composite catalyst with 5 wt% of magnesium were found to be active in catalytic cracking of UPO.

Acknowledgement

The authors acknowledge the financial support by Universiti Sains Malaysia under RU grant (814130).

References

1. Taufiqurrahmi, N., Mohamed A. R. & Bhatia, S. (2011). Production of biofuel from waste cooking palm oil using nanocrystalline zeolite as catalyst: Process optimization studies. *Bioresource Technology,* 102(22): 10686-10694.
2. Ong, Y. K. & Bhatia, S. (2010). The current status and perspectives of biofuel production via catalytic cracking of edible and non-edible oils. *Energy*, 35(1): 111-119.
3. Ooi, Y. S., Zakaria, R., Mohamed, A. R. & Bhatia, S. (2004). Catalytic conversion of palm oil-based fatty acid mixture to liquid fuel. *Biomass and Bioenergy*, 27(5): 477-484.
4. Twaiq, F. A. A., Mohamad, A. R. & Bhatia, S. (2004) Performance of composite catalysts in palm oil cracking for the production of liquid fuels and chemicals. *Fuel Processing Technology*, 85(11): 1283-1300.
5. Ooi, Y. S., Zakaria, R., Mohamed, A. R. & Bhatia, S. (2004). Synthesis of composite material MCM-41/Beta and its catalytic performance in waste used palm oil cracking. *Applied Catalysis A: General*, 274(1-2): 15-23.
6. Pang, X., Zhang, L., Sun, S., Liu, T. & Gao, X. (2007). Effects of metal modifications of Y zeolites on sulfur reduction performance in fluid catalytic cracking process. *Catalysis Today,* 125(3-4): 173-177.
7. Rahimi, N. & Karimzadeh, R. (2011). Catalytic cracking of hydrocarbons over modified ZSM-5 zeolites to produce light olefins: A review. *Applied Catalysis A: General*, 398(1-2): 1-17.
8. Pan, H., Wei, G., Yuan, H., Huo, Q., Li, Q., Pan, X., Wang, W. & Yu, X. (2007). Studies on catalytic cracking catalyst of hydrocarbons with a new type of zeolite L, in Studies in Surface Science and Catalysis, Elsevier. p. 1392-1398.

9. Twaiq, F. (2002) Synthesis, characterization and activity of microporous and mesoporous aluminosilicate molecular sieve materials for the conversion of palm oil to liquid fuels. PhD Thesis, Universiti Sains Malaysia.
10. Sing, K.S.W., Everett D.H. & Haul R.A. (1985). Reporting physisorpton data for gas/solid systems with special reference to the determination of surface are and porosity. *Pure Application Chemistry*, 57(4): 603-619.

The Malaysian Journal of ANALYTICAL SCIENCES ISSN 1394-2506

SYNTHESIS OF ESTOLIDE 2-ETHYLHEXYL ESTER FROM *RICINUS COMMUNIS*

(Sintesis Estolida 2-Etilheksil Ester dari *Ricinus Communis*)

Nazrizawati Ahmad Tajuddin[1,2]*, Nor Habibah Rosli[1], Jumat Salimon[2], Mohd Firdaus Mohd Yusoff [2], Noraishah Abdullah[2]

[1]*Department of Chemistry, International Education College, UiTM Section 17, 40200 Shah Alam, Selangor, Malaysia*
[2]*Oleochemistry Programme, School of Chemical Science and Food Technology, Faculty of Science and Technology, Universiti Kebangsaan Malaysia,43000 Bangi, Selangor, Malaysia*

**Corresponding author: nazriza@salam.uitm.edu.my*

Abstract

Estolide 2-ethylhexyl ester synthesized through condensation reaction between ricinoleic acid from castor oil (*Ricinus communis*) and lauric acid, and then capped with 2-ethylhexyl alcohol. The reaction was continuously conducted under vacuum for 24 hours. Product of 2-ethylhexyl ester was characterized by using Fourier Transform Infrared (FTIR) to determine functional group and Nuclear Magnetic Resonans (NMR) for structure's determination. The presence of ester group at 1738.23 cm^{-1} wavenumber indicates that the formation of estolide ester has occurred. The vibration peak of C-O at 1174.60 cm^{-1} and 1117.10 cm^{-1} support the formation of ester. The presence of CH_2 bending indicated the long-chain compound. The ester methine signal at 3.8669 ppm indicated the estolide linkage in the ^{1}H-NMR spectrum while the ^{13}C-NMR showed two carbonyl signals at 173.41 ppm for acid and 173.56 ppm for ester.

Keywords: Castor oil, ricinoleic acid, estolide ester, biodegradable, biolubricant study

Abstrak

Estolida 2-etilheksil ester disintesis melalui tindakbalas kondensasi antara asid risinoleik dari minyak jarak (*Ricinus communis*) dan asid laurik yang kemudiannya ditutup dengan 2-etilheksil alkohol. Tindakbalas ini dijalankan secara berterusan selama 24jam. Hasilan 2-etilheksil alkohol ester dikenalpasti dengan menggunakan Fourier Transform Infrared (FTIR) untuk pengecaman kumpulan berfungsi dan Magnetic Resonan Nuclear (NMR) digunakan untuk menentukan struktur estolida yang terhasil. Getaran C-O pada puncak 1174.60 cm^{-1} dan1117.10 cm^{-1} mengesahkan kehadiran ester di dalam sebation yang terbentuk. Kehadiran CH_2 bengkokan menunjukkan kehadiran kompaun berantai panjang. Signal ester methane yang hadir pada 3.8669 ppm dalam ^{1}H-NMR spectrum dan signal karbonil pada 173.56 ppm dalam ^{13}C-NMR mengesahkan kompaun terhasil adalah ester.

Kata kunci: Minyak jarak, asid risinoleik, estolida ester, biodegradasi, kajian biolubrikan

Introduction

The depletion of the world's crude oil reserve, increasing crude oil prices, and issues related to conservation have brought about renewed interest in the use of bio-based materials. Emphasis on the development of renewable, biodegradable, and environmentally friendly industrial fluids, such as lubricants, has resulted in the widespread use of natural oils and fats for non-edible purposes. The desire to replace petroleum-based material with environmental friendly and sustainable alternatives has stimulated the development of vegetables oil-based materials as biolubricants [1] such as castor oil.

Castor bean oil contains ricinoleic acid, a hydroxy monounsaturated fatty acid as main constituent of its fatty acid profile [2]. Ricinoleic acid, a monounsaturated, 18-carbon fatty acid, is unusual in that it has a hydroxyl functional

group on the 12th carbon. This functional group causes ricinoleic acid and castor oil to be unusually polar, and also allows chemical derivatization that is not practical with most other seed oils. It is the hydroxyl group which makes castor oil and ricinoleic acid valuable as chemical feedstocks. Estolide have been shown to have certain physical characteristics that could eliminate common problems associated with vegetable oils as functional fluids [3].

Ref [4] reported that vegetable oil-based lubricants and derivatives have excellent lubricity and biodegradability properties for which they are being more closely examined as a base stock for lubricants and functional fluids. However, vegetable oil as functional fluids has two major problems; low resistance to thermal oxidative stability [5] and poor low temperature properties [6]. The properties still can be improved but only at the sacrifice of biodegradability, toxicity and cost.

An estolide is a unique oligomeric fatty acid that contains secondary ester linkage on the alkyl backbone of the molecule [7,8,9]. These linkages are more resistance to hydrolysis than those of triglycerides. Estolides are formed when the carboxylic acid functionality of one fatty acid links to the site of unsaturation of another fatty acid to form oligomeric ester [10]. Typically, estolides were synthesized by homo-polymerization fatty acid from vegetable oil acidic conditions.

Estolide from oleic and saturated fatty acids and their 2-ethylhexyl ester have excellent low temperature properties when synthesized at 45°C. These estolide esters were more suitable as a base stock for biodegradable lubricants and functional fluids than commercial materials [11] So far, there is no reference on ricinoleic acid from castor oil being synthesize with 2-ethylhexyl alcohol have been reported. In this paper we synthesized estolide 2-ethylhexyl ester from ricinus communis and being capped by 2-ethylhexyl alcohol for biolubricant purposes where perchloric acid has been used as catalyst.

Materials and Methods

Materials

Samples (castor bean) were collected from four different areas; Meru-Kapar (Klang); Salak Tinggi(KL); Sungai Chua (Kajang) and Plant House (UKM, Bangi). 2-ethylhexyl alcohol, lauric acid and percholoric acid were purchased from Sigma-Aldrich, USA. Hexane (for extraction) and potassium hydroxide were obtained from SYSTERM.

Extraction of Castor Oil

The samples went under pretreatment of drying (80^{o}C, 8 hours) and grinding before being extracted using Soxhlet Extractor apparatus. Castor oil was extracted according to Soxhlet method and hexane being used as solvent. Extraction was carried out for 6-12 hours at 65°C in order to assure the oil was fully extracted. The collected oil was separated by using rotavapor.

Hydrolysis of Castor Oil

Hydrolysis was performed to produce fatty acid of ricinoleic acid. 25 g of castor oil was added with 65 ml ethanol, 5.71g KOH and 11 ml distilled water. The mixture were reflux for 1 hour with maintain temperature 50°C. Then 50 ml distilled water was added and quenched with 100 ml hexane (2x). Soap matter was acidized to pH 1 by using 25 ml HCl 6N. The product was quenched again with 50 ml hexane. Sodium sulphate was added and the process proceeded with rotavapor. Isolation been done by adding 40 ml ethanol and 60 ml distilled water. The mixture was quenched with 40 ml hexane. The final product was added with sodium sulphate and rotavap.

Synthesis of Estolide Ester

Synthesis of estolide 2-ethylhexyl ester were conducted based on Ref [10] with modification by using ricinoleic acid as first fatty acid reacted with lauric acid and capped with 2-ethylhexyl alcohol. Ricinoleic acid (50 g, 177 mmol) and saturated fatty acid, lauric (17.75g, 88.5 mmol) were combined together and heated to 60 ^{o}C under vacuum. Once the desired temperature was reached, 11.5 ml perchloric acid was added and stirred for 24 hours. All the reactions were conducted in a three-neck round flask, connected to a recirculating vacuum in a fume hood. After 24 hours, 2-ethylhexyl alcohol (33.75 ml, 228.8 mmol, 29.8 g) was added to the vessel, vacuum was restored and the

mixture was stirred for 2 additional hours. The complete reaction was quenched by 25 g KOH in 90% ethanol/water (10 ml) solution.

The reactor was disconnected from the circulating bath and the solution was allowed to cool for 30 minutes. The organic layer was dried over sodium sulphate and filtered. The material was distilled at 105^{o}C to remove any excess alcohol and water contents.

Analysis and Characterization

Fourier Transform Infrared Spectroscopy (FTIR)

FTIR spectroscopy analysis was carried out to determine the functional group presence in estolide ester based on the spectrum peaks. In this analysis, Perkin Elmer GX FTIR Spectrophotometer was used to get the information of all functional groups in each sample. Samples which were in liquid form were sandwiches between two sodium chloride (NaCl) plates while samples in solid form were diluted before being placed between two potassium bromide (KBr) plates.

The functional group to be monitored for is ester carbonyl (1735 cm^{-1}), hydroxyl –OH (2900-3300 cm^{-1}), sp^3 stretching carbon (2800-3000cm^{-1}), long chain (720cm^{-1}) and other functional groups which may appear as a characteristic of the product. Spectrums for all raw materials (ricinoleic acid and 2-ethylhexyl alcohol) were compared to product's to observe the differences between each spectrum.

Nuclear Magnetic Resonance (NMR)

NMR spectroscopy been used to detect ^{1}H proton and carbon ^{13}C in the estolide structure. Samples were eluted in chloroform and injected in Delta NMR ECP 400 (1D complex) using probe proton/carbon (400 MHz ^{1}H/100.61 MHz ^{13}C).

Results and Discussion

Synthesis of Estolide Ester

Generally, formation of estolide ester is influences by two major factors; acid catalyst and the reaction temperature used. Perchloric acid was added in this reaction act as catalyst. Perchloric acid provide significantly faster rate (5-8 times) of estolide formation compare to sulphuric acid and produce more yield of estolide [7]. Addition of sulphuric acid to unsaturated fatty acid will produce sulfated oils. The sulfated oil is stable at low temperature (≤20°C) in the presence of acid, but at elevated temperature (50°C), the sulphate esters quickly decompose, estolides and lactones are observed.

Estolide esters formation also influences by the temperature. At room temperature (27°C), the rate of reaction catalyzed by perchloric acid becomes slow. However, at higher temperature, the formation become too fast due to the rate is accelerated even though the concentration of perchloric acid is reduced and the side reactions begin to predominate, chiefly the formation of lactones [7]. Hence, an optimum temperature, 60°C has been applied in this study. Synthesis was carried out within 24 hours in order to assure all the reactions are complete.

Figure 1 shows C7 on ricinoleic acid tend to interact with OH group from lauric acid to form ester and also for capping the chain. Carbonyl group tends to form bonding with OH because carbonyl group are easier to disconnect compared to double bond, which is more stable. By capping the fatty ester, the compounds no longer had the opportunity to undergo either intra- or intermolecular hydrogen bond interaction [11]. Yield produced is about 82.25%.

FTIR Characterization of Estolides

Synthesis of estolide 2-ethylhexyl ester was expected to produce unsaturated estolides as shown in Figure 1. To prove that condensation had occurred, FTIR spectra of estolide 2-ethylhexyl ester and reaction product were compared. The FTIR spectrum shows a strong stretching band at 1738.23 cm^{-1}. This peak indicates the presence of ester group in the estolide as ester shows a strong peak at range 1750-1735 cm^{-1} [12]. This assumption was supported by the presence of two C-O streching bonds.

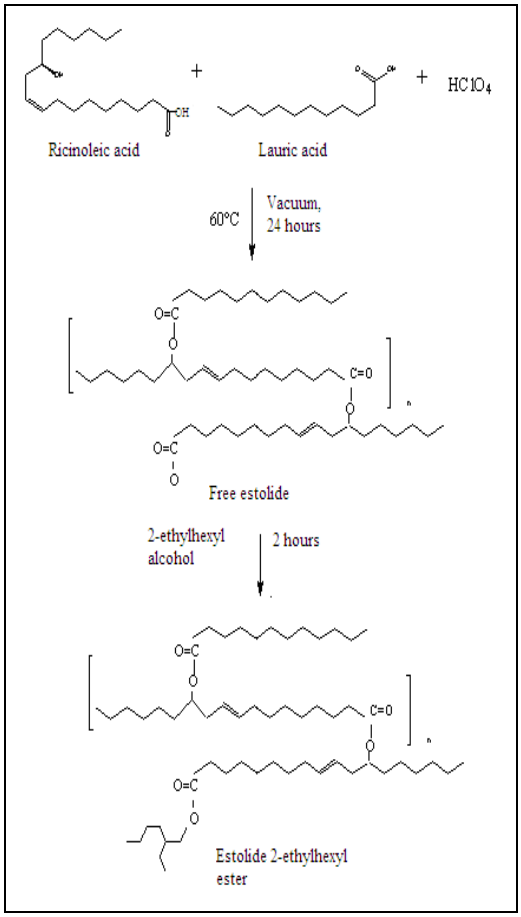


Figure 1. Reaction of estolide 2-ethylhexyl ester

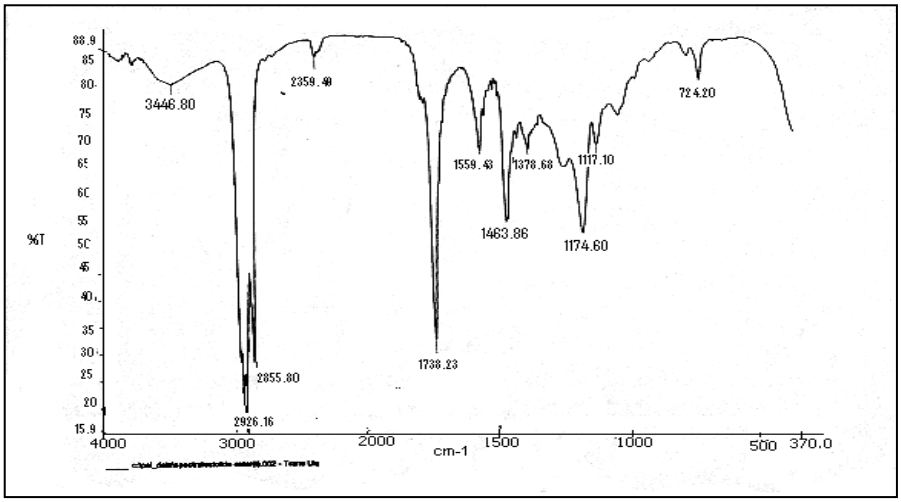


Figure 2. Estolide 2- ethylhexyl ester

At 1174.60 cm^{-1} wavenumber which is more electronegative as the C-O group bonded to the acid backbone while ester with is less electronegative, which is C-O ester bonded to the ester backbone appeared at 1117.10 cm^{-1}.

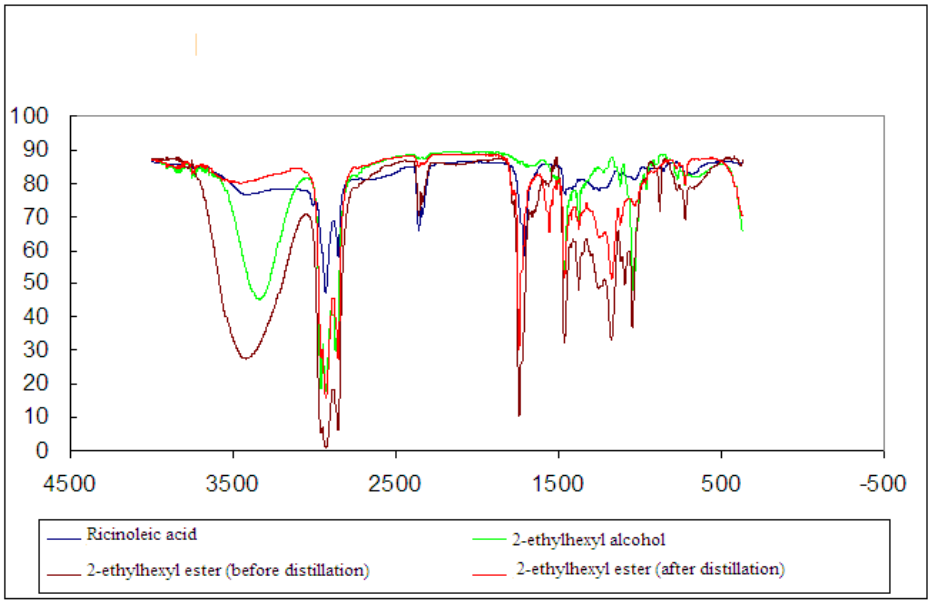


Figure 3. Differentiate spectrum in formation of estolide ester before and after distillation

NMR Characterization of estolide 2-ethylhexyl ester

The 1H-NMR spectrum for estolide 2-ethylhexyl ester shows in Figure 4 contains the expected estolide signals. The ester methine signal (Hm) at 2.157 ppm indicates the estolide linkage. Another distinctive feature is the α-methelyne proton shift at 4.5438 ppm adjacent to the acid and the α- methelyne proton shift at 3.8669 ppm adjacent to the ester (Table 1).

Table 1. Data elucidation of NMR ^{1}H spectrum

Node	Shift (ppm)	Group
CH_3	0.7712	Methyl
CH_2	1.1641	Methylene ($CDCl_3$ peak)
	1.4929	Methylene
	4.5438	Methylene (α- acid)
CH	2.1570	Methine (ester linkage)
	3.8669	Methine (α-ester)

Although the ratio of α- ester/ α- acid can be used as a means to determine the estolide number (EN), the method cannot be applied for this compound since the NMR is more complex [8]. The ^{13}C NMR spectrum for estolide 2-ethylhexyl ester shows in Figure 5 contains some of the key features for a typical estolide and all the shift data are listed in Table 2. There are two carbonyl signals at 173.4091 ppm (acid) and 173.5697 ppm (ester). Methine carbons were appeared at 76.9122-77.5545 ppm which is common to estolides. Estolide ester is supposed to have ethylene peak at 130.6 ppm in the spectrum due to double bond from ricinoleic acid. However, spectrum of estolide 2-ethylhexyl ester shows inverse result where there is no ethylene peak or very small signal observed [10] expected cause by the impurity of ricinoleic acid**.**

Table 2 Data elucidation of NMR ^{13}C spectrum

Node	Shift (ppm)	Group
CH_3	10.8630-13.9675	Methyl
CH_2	22.9137-30.43	Methylene
	64.7010-66.3602	Methylene
CH	38.7722	Methine
	76.9122-77.5545	Methine ($CDCl_3$ peak)
C-O	173.4091	Carbonyl (acid)
	173.5697	Carbonyl (ester)

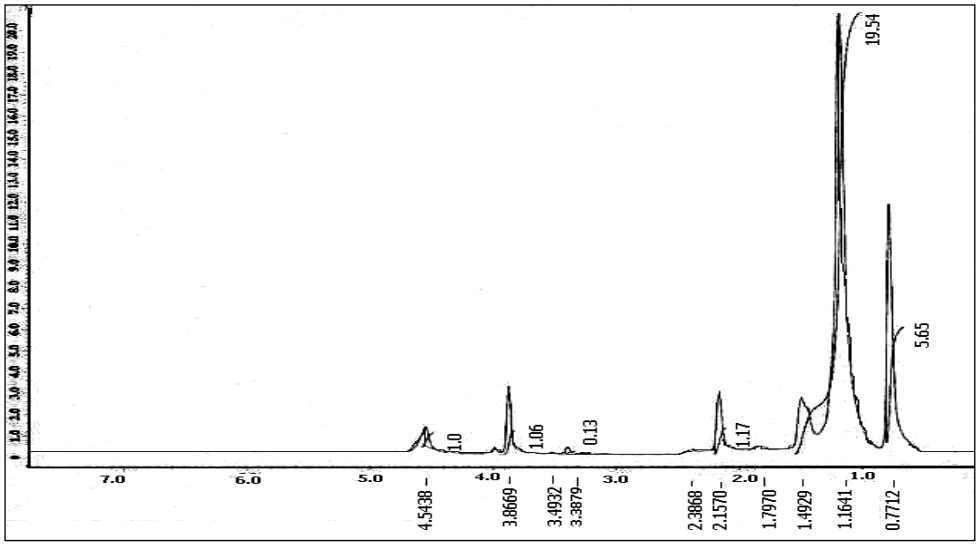


Figure 4. Spectrum of NMR ^{1}H estolide 2-ethylhexyl ester.

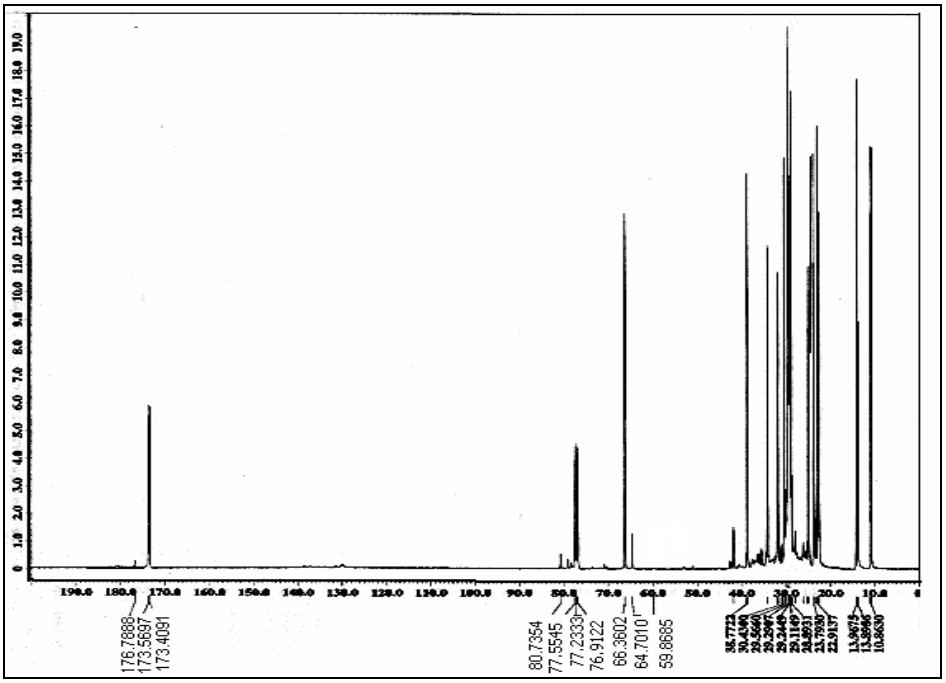


Figure 5. Spectrum of NMR ^{13}C estolide 2-ethylhexyl ester.

Conclusion

Estolide 2-ethylhexyl ester was successfully synthesized between ricinoleic acid from castor oil and lauric acid with addition of 2-ethylhexyl alcohol where perchloric acid acted as catalyst. Data elucidation from FTIR and NMR described the characteristic of the product. The result shows significant value with the estimation and matched with the molecular structure, hence possibly been use as biolubricant material.

Acknowledgement

Thanks to Universiti Kebangsaan Malaysia for research funding, OUP-BTT-28/2007 and supporting staff of Science and Technology Faculty for expert technical assistance. And thank you to International Education College, UiTM Section 17 for Accommodation & Travelling sponsored.

References

1. Lin, J.T. & Chen, G.Q. 2010. Acylglycerols Containing Trihydroxy Fatty Acids in Castor Oil and the Regiospecific Quantification of Triacylglycerols. *Journal of the American Oil Chemists' Society*. 87:1371-1379
2. Jumat, S., Neeranjini, N., Nadia, S. & Bashar, M.A. 2011. Synthesis and Physical Properties of Estolide Ester Using Saturated Fatty Acid and Ricinoleic Acid. *Journal of Automated Methods and Management in Chemistry*.2011: 1-4
3. Cermak, S.C. & Isbell, T.A. 2002. Physical prop of saturated estolides and their 2-ethylhexyl ester. *Industrial Crops Products*. 16: 119-127.
4. Zaher, F.A. & Nomany, H.M. 1988. Vegetable oils and lubricants. *Grases Aceities (Seville).* 39: 235-238
5. Becker, R. & Knorr, A. 1996. An evaluation of antioxidants for vegetable oil at elevated temperatures. *Lubri. Sci.* 8: 95-117.
6. Asadauskas, S. & Erthan, S.Z. 1999. Depression of pour points of vegetable oils by blending with diluents used for biodegradable lubricants. *J.Am.Oil Chem.Soc.* 76: 313-316.
7. Isbell, T.A., Kleiman, R. & Plattner, B.A. 1994. Acid.Catalyzed Condensation of Oleic Acid into Estolides and Polyestolides. *J.Am.Oil Chem.Soc*: 71.

8. Isbell, T.A. & Kleiman, R. 1994. Characterization of Estolides Produced from the Acid-Catalyzed Condensation of Oleic Acid. *New Crops Research.* 71:379-383.
9. Cermak, S.C. & Isbell, T.A. 2001. Synthesis of estolides from oleic and saturated fatty acids. *J.Am.Oil.Chem.Soc.* 78: 557-565.
10. Cermak, S.C. & Isbell, T.A. 2003. Synthesis physical properties of estolide-based functional fluids. *Industrial Crops Products.* 18:183-196.
11. Cermak, S.C., Brandon, K.B. & Isbell, T.A. 2006. Synthesis and physical properties of estolides from lesquerella and castor fatty acid esters. *Industrial Crops Products*.23:54-64.
12. Pavia, D.L., Lampman, G.M. & Kriz, G.S. 2001. Introduction to spectroscopy, 3rd ed. America:Thomson Learning.

The Malaysian Journal of ANALYTICAL SCIENCES ISSN 1394-2506

LIPIDIZATION OF SIMPLE AND DI-FUNCTIONAL AMINO ACIDS

(Penglipidan Asid Amino Ringkas dan Dwi-Fungsi)

Zainab Idris, Mohd. Wahid Samsudin* and Salmiah Ahmad

School of Chemical Sciences and Food Technology, Faculty of Science and Technology
Universiti Kebangsaan Malaysia, 43600 UKM Bangi, Selangor, Malaysia

**Corresponding author: wahid@ukm.my*

Abstract

This paper discuss the modification of azelaic acid into its applicable form by attachment of both its carboxyl sites to N-terminal of amino acid ethyl ester forming amide linkages in anhydrous medium. Acylation of glycine ethyl ester hydrochloride with azelaic acid dichloride was best conducted in a 100% anhydrous medium. L-amino acid ethyl ester bearing a primary hydroxyl group on its side chain gave mixtures of product and variation in composition depending on the mole ratio of reactants used. Reduction in purity was also observed for L-amino acid ethyl ester with primary –SH group on its side chain as compared to L-amino acid ethyl ester having $–SCH_3$ group on the L-amino acid side chain. The diamidoester of azelaic acid with L-alanine ethyl ester, L-valine ethyl ester, L-leucine ethyl ester and L-glutamic acid diethyl ester were in good yield when prepared through the modified Schotten-Baumann reaction conditions.

Keywords: Azelaic acid dichloride, L-amino acid ethyl ester, Schotten-Bauman condition, Glycine ethyl ester hydrochloride

Abstrak

Perbincangan membabitkan pengubahsuaian molekul dwi-asid karboksilik melalui lekatan pada kedua-dua kumpulan karboksil oleh terminal N-asid amino etil ester di dalam pelarut organik. Proses asilasi yang melibatkan tindakbalas di antara glisina etil ester hidroklorida dan asid azelik diklorida memberikan hasil dwi-amidoester tertinggi sekiranya dijalankan melalui proses asilasi di dalam 100% media organik kontang. L-asid amino yang mempunyai kumpulan sisi hidroksil primer memberi pelbagai campuran produk dan peratus komposisi yang berbeza bergantung pada nisbah reaktan yang digunakan. Penurunan dari segi ketulenan hasil diperolehi bagi L-asid amino yang mempunyai kumpulan sisi –SH berbanding dengan L-asid amino etil ester yang mempunyai kumpulan sisi $–SCH_3$. Dwi-amidoester asid azelik dari L-alanina etil ester, L-valina etil ester, L-leusina etil ester dan L-asid glutamik dietil ester adalah agak tinggi juga jika disediakan melalui proses asilasi melalui kaedah Schotten-Baumann yang diubahsuai.

Kata kunci: Asid azelik diklorida, L-asid amino etil ester, kaedah Schotten-Bauman, glisina etil ester hidroklorida

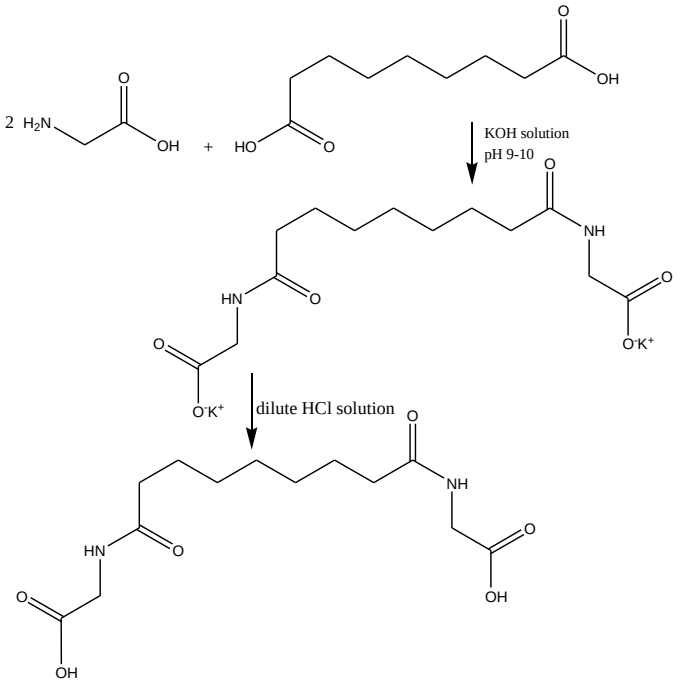
Introduction

Azelaic acid is a well known compound incorporated into topical cream medication formulation to treat patient with acne and skin diseases [1-5]. However, due to its crystalline form which melts at temperature as high as 103^{o}C, incorporation of azelaic acid into cream formulation is, therefore, difficult at standard conditions. In addition, efficacy was only observed when 15% and above of azelaic acid was incorporated [6,7].

Maralmadi and Esposito (2002) [8] reported that modification of azelaic acid by attachment of glycine through amide linkages and converting one of the carboxylic acid group into potassium carboxylate has enhanced not only the technical property of azelaic acid, but also the functional performance of the resulting modified azelaic acid. Their studies showed that the modified azelaic acid, known as potassium azeloyl diglycinate, exhibited anti-acne, sebum regulatory and skin lightening properties on the treated skin.

The compound of interest has already been commercialized by Sinerga Italy and sold under the tradename Azeloglicina™. Attachment of glycine was performed through the conventional Schotten-Baumann reaction

condition i.e. by reacting 1 mol of azelaic acid dichloride with 2 mols of glycine in aqueous medium with regular pH control of 10.00 to 11.00. The di-potassium azeloyl diglycinate formed was then partially acidified with dilute hydrochloric acid solution to final pH of 5.5 to 6.0. The product was sold as 31% pale yellow solution. The reaction scheme is as illustrated in Scheme 1.



Scheme 1

In view of this valuable technical transformation of azelaic acid into its multifunctional tasks, we foresee the interest in producing this compound into its crystal form for ease of handling and transportation and to extend the method with other L-amino acid ethyl ester.

Materials and Methods

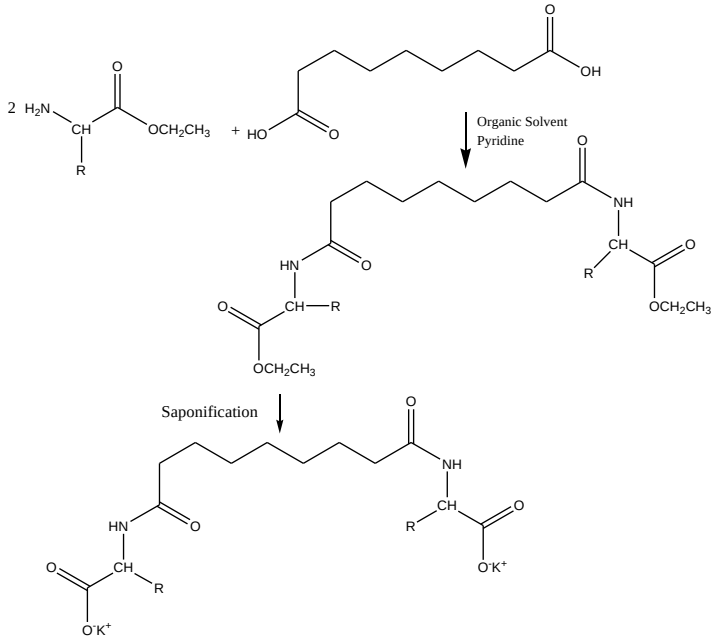
Glycine ethyl ester hydrochloride, L-serine ethyl ester hydrochloride and azeloyl dichloride with purity of above 98 % were purchased from Sigma-Aldrich Chemie GmbH (Switzerland). L-alanine and L-valine ethyl ester hydrochloride of purity above 99 % were purchased from Acros Organics, (USA). L-leucine ethyl ester hydrochloride and L-glutamic acid diethyl ester hydrochloride of GR Grade were purchased from TCI (Japan). L-cysteine ethyl ester hydrochloride of 98 % purity was purchased from Aldrich (Germany). All solvents used were of Analytical Grade.

Functional group characterization was conducted on FTIR instrumentation (Nicolet, MAGNA-IR 550 series II, Japan). The samples to be analyzed were first affixed on KBr pellet. Purity of the product isolated was determined using established HPLC methods [JASCO (Column: ODS-3(250mm x 4.6 mm) , Mobile phase: 35% acetonitrile and 65% H_2O, Detector: UV detector at 210 nm)].

^{1}H NMR-spectra of the isolated products was recorded on JEOL JNM-ECP400 FT NMR system (JEOL Ltd., Japan) with internal standard used was tetramethylsilane (TMS).

Reaction Between Azelaic Acid Dichloride and Glycine Ethyl Ester Hydrochloride in Anhydrous Medium

The method to produce diamidoester of azelaic acid with glycine ethyl ester was conducted according to process as described by Idris et al., (2009) [9]. The general reaction was as illustrated in Scheme 2.



Scheme 2

To evaluate the effect of amino acids with non polar side chain versus amino acids with polar side chain, the above reaction were also conducted using L-valine ethyl ester hydrochloride, L-alanine ethyl ester hydrochloride, L-leucine ethyl ester hydrochloride, L-glutamic acid diethyl ester hydrochloride, L-methionine ethyl ester hydrochloride, L-serine ethyl ester hydrochloride and L-cysteine ethyl ester hydrochloride as nucleophile. Their crude product mixtures were then analysed for their composition using HPLC system .

Saponification and Acidification of Diamidoester of Azelaic Acid with Glycine Ethyl Ester

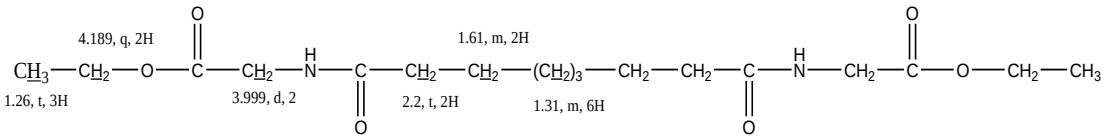
The procedure to saponify the diamidoesters of azelaic acid with glycine ethyl ester was conducted according to the method described by Idris et al. (2009). The product was evaluated for its composition by HPLC, amide functionality and chemical formula confirmation by CHNO-S and ^{1}H and ^{13}C NMR.

Results and Discussion

Amidation in Anhydrous Medium with In-Situ Treatment of Amino Acid Ethyl Ester Hydrochloride

The reaction mixture was found to be homogeneous in aprotic solvent medium. As the reaction proceeded, slurry of salts crystals was formed. After recrystallization from isopropanol, the purity of the diamidoester was 97% (HPLC) with 50% recovery after first cycle of recrystallization from isopropanol.

Azeloyl diglycinate ethyl ester **:** Yield: 80.43%; Needle-like soft crystals flake. Melting point = 116.97^{o}C. FTIR (KBr) (Figure 1a): 3318, 3085, 2985, 2930, 2850, 1751, 1644, 1544, 1377, 1350, 1190, 1022, 722 cm^{-1}. ^{1}H NMR (400Mhz, $CDCl_3$) (Figure 2):δ 1.26 (t, 6H), 1.30 (m, 6H), 1.61 (m, 4H), 2.21(t, 4H), 4.00(dd, 4H), 4.1 9(q, 4H), 6.21(s, 2H). Analysis: Calculated for $C_{17}H_{36}N_2O_6$: C, 56.97; H, 8.44; N, 7.82, Other, 26.78. Found: C, 57.52; H, 8.57; N, 7.90, Others, 23.48.



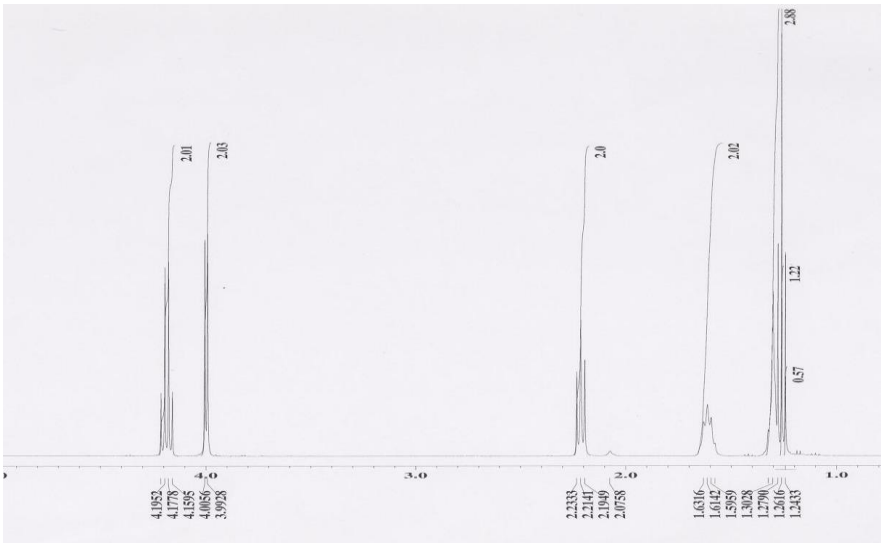


Figure 1. Overlayed FTIR spectrum of azeloyl diglycinate and its derivatives.

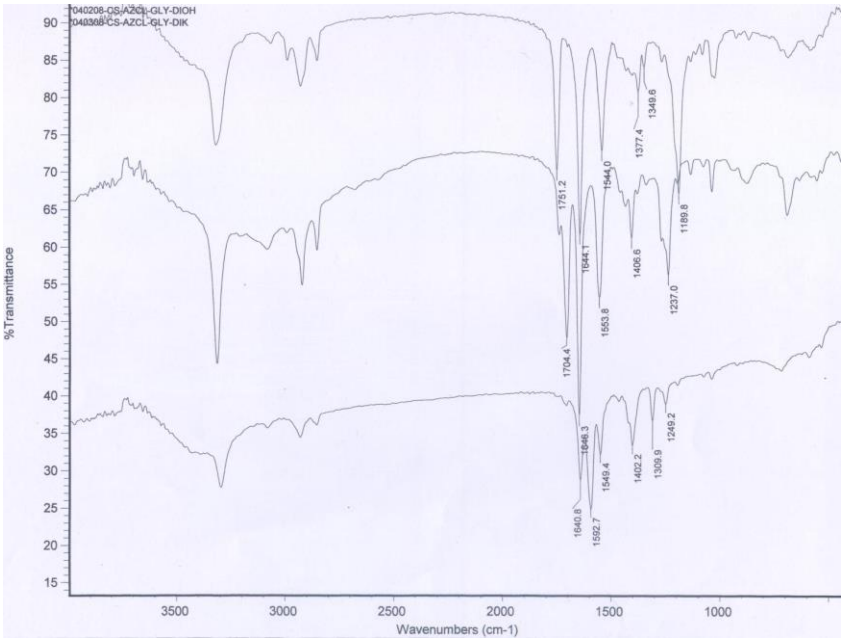
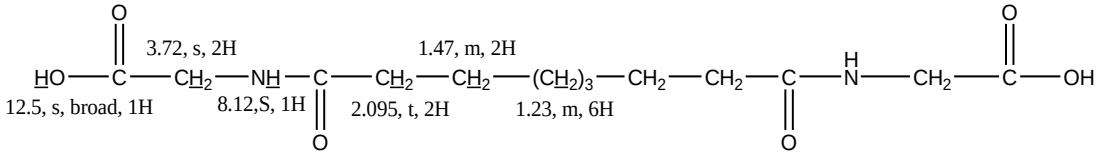


Figure 2. The ^{1}H NMR spectrum of azeloyl diglycinate ethyl ester with its predicted structural illustration above the spectrum

Saponification and Acidification

Diamidoester of azelaic acid with glycine ethyl ester was saponified through the usual saponification procedure to form its dipotassium carboxylate compound. Further derivatization through acidification in aqueous solution with dilute hydrochloric acid gave a product of diamido glycinate of azelaic acid. The following analysis results indicated that the amide linkages on both sides of azelaic acid were retained through the process.

Azeolyl diglycinate:Yield: white soapy granulated solid; Melting point= Nil; ash residue: 10.86%. FTIR (KBr)(Figure 1c): 3295, 3085 (weak), 2930, 2850, 1751(weak), 1641, 1593, 1549, 1402, 1310, 1190 (weak), 718, cm^{-1}. ^1H NMR ($CDCl_3$)(Figure 3): δ1.28 (m, 6H), 1.56 (m, 4H), 2.25 (t, 4H), 3.70 (s, 4H).. Analysis: Calculated for $C_{13}H_{20}K_2N_2O_6$: C, 40.25; H, 5.33; N, 7.40; Others, 46.02. Found: C, 39.19; H, 5.69; N, 7.66; Others, 47.46.



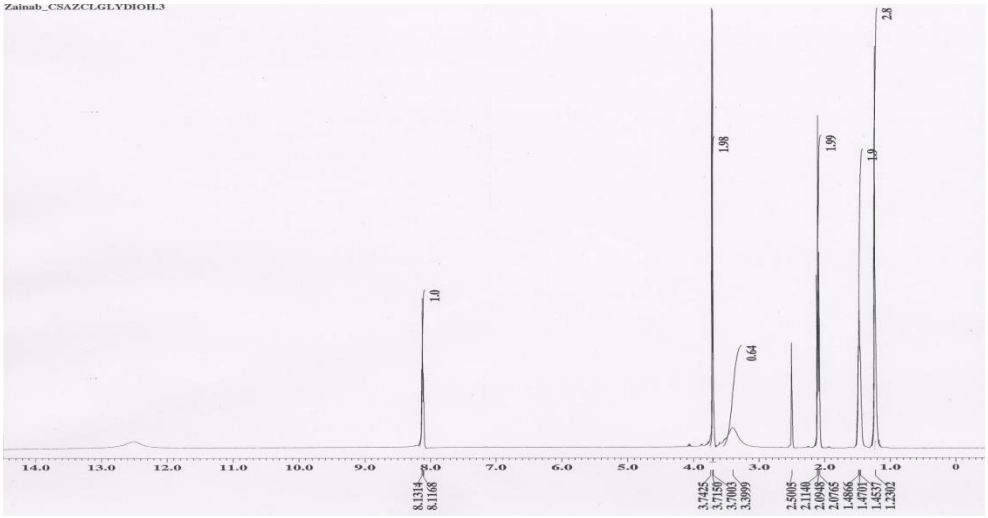


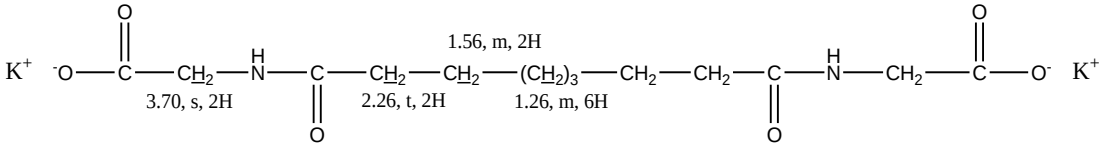
Figure 3. The ^1H NMR spectrum of azeloyl diglycinate with its predicted structural illustration above the spectrum

Dipotassium azeolyl diglycinte:Yield: Fine white powder; melting point = 189. 6°C. FTIR (KBr)(Figure 1b): 3295, 3066 (weak), 2990 (weak), 2930, 2850, 1751(weak), 1704, 1646, 1553, 1407, 1237, 1190 (weak), 688 (stronger) cm^{-1}. ^1H NMR ($DMSO_4$-D_6)(Figure 4): δ1.23 (m, 6H), 1.47 (m, 4H), 2.09 (t, 4H), 3.40 (s, 2H), 3.72 (dd, 4H), 8.12 (t, 2H), 12.51 (s, 1H). .Analysis: Calculated for $C_{13}H_{22}N_2O_6$: C, 51.65; H, 7.33; N, 9.27; Others, 31.75. Found: C, 51.87; H, 7.38; N, 9.67; Others, 29.97

Effect of Non Polar Side Chain Versus Polar Side Chain Of Amino Acid Ethyl Ester

Based on the data in Table 1, it was interesting to note that among all the L-amino acid ethyl ester studied, L-serine ethyl ester possessing a primary alcohol side chain was found to be the most reactive to side chain reactions. With 2:1 mole ratio of L-serine ethyl ester to azeloyl dichloride, only 9.58 % of the organic soluble fraction was isolated

as crude product. The rest of the fraction was soluble in the aqueous phase and was discarded during the washing process. The major component in organic soluble fraction was 51% pure. On the other hand, reaction conducted with 1:1 mole ratio gave a higher crude yield but the purity of the major peak detected for 2:1 ratio was drastically reduced to 6.20 % and could have been converted to a less polar component which appears at the far end of the HPLC acquisition time. The side chain of neutral amino acid ethyl esters: L-valine ethyl ester, L-alanine ethyl ester, L-leucine ethyl ester and L-glutamic acid diethyl ester seemed to be the least affected as their purity was above 80 %. This was because the side chain of the first three L-amino acid ethyl esters was purely hydrocarbon, while that of L-glutamic acid diethyl ester, the carboxylic acid functionality on the side chain was protected by presence of an ethyl ester group.



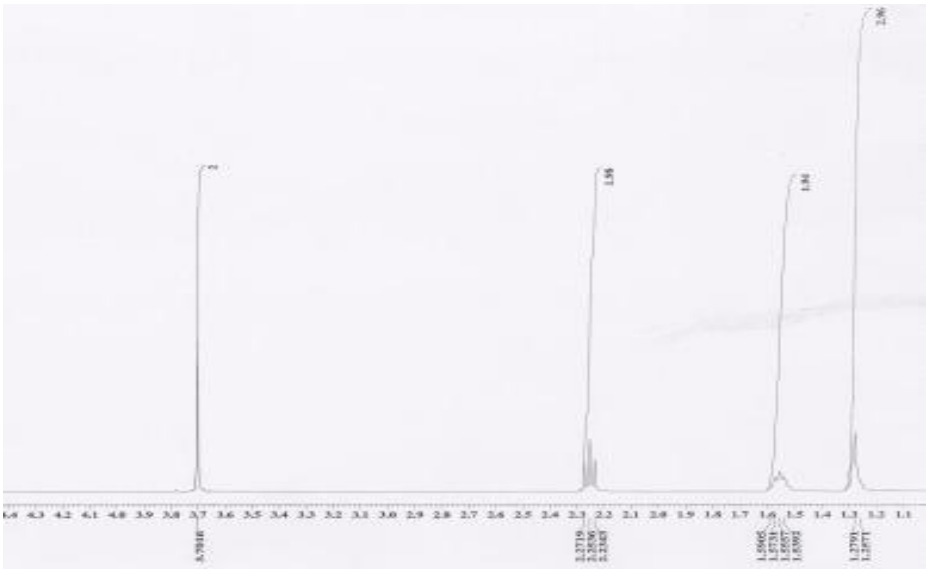


Figure 4. The ^{1}H NMR spectrum of dipotassium azeloyl diglycinate with its predicted structural illustration above the spectrum

Table 1. Characterization of reaction products for reaction between various L-amino acid ethyl ester hydrochloride and azeloyl dichloride

Types of L-amino acid ethyl ester hydrochloride	Crude yield[a] (%)	Purity[b] (HPLC) (%)
L-valine ethyl ester	76.38	81.76
L-alanine ethyl ester	87.01	86.74
L-leucine ethyl ester	83.64	82.20
L-serine ethyl ester (2:1)[c]	9.58	50.78*
L-serine ethyl ester (1:1)[d]	44.00	6.20*
L-cysteine ethyl ester	76.92	49.10*
L-methionine ethyl ester	75.53	70.56
L-glutamic acid diethyl ester	79.27	89.89

[a]Crude yield was calculated based on the expected yield of diamidoester of respective amino acid ethyl ester.
[b]The % purity was based on the % area of the major peak appearing at the earliest retention time of HPLC chromatogram. [c]Reaction between L-serine ethyl ester and azeloyl dichloride at 2:1 mole ratio. [d]Reaction between L-serine ethyl ester and azeloyl dichloride at 1:1 mole ratio

Conclusion

The amidation of azeloyl dichloride and glycine ethyl ester in 100% anhydrous medium has provided a simpler method in producing diamidated azelaic acid with purity of above 97%. Organic base can be used to remove the hydrochloric acid molecules both from glycine ethyl ester hydrochloride and that resulting from the reaction itself. Unreacted organic base and the resulting hydrochloride salts were easily removed through subsequent washing with diluted HCl solution and followed by water. Aprotic solvent medium and its traces could be completely removed by vacuum evaporation followed by saponification in ethanolic potassium hydroxide and then acidification by dilute acid resulting in precipitation of precipitating the azeloyl diglycinate out from the aqueous media.

Acknowledgement

The authors wish to thank the Director-General of MPOB for his permission to publish this article.

References

1. Addo-Boadu, K., Wojta, J. Christ, G, Itufnagl, P., Pehamberger, H. and Binder, B.R. (1996). Azelaic acid decreases the fibronolytic potential of cultured human melanoma cells in vitro. Cancer Lett. 103(2):125-129
2. Bojar, R.A., Cunliffe, W.J. and Holland, K.T. (1994). Distruption of the transmembrane pH gradient- a possible mechanism for the antibacterial action of azelaic acid in Propionibacterium acnes and Staphylococcus epidermis. Journal of Antimicrobial Chemotheraphy. 34:321-330.
3. Thiboutot, D. (2000). New treatment and therapeutic strategies for Acne. Arch Fam. Med. 9(2):174-187.
4. Gollnick, H. P. M and Krautheim, A. (2003). Topical Treatment in Acne: Current Status and Future Aspects. Dermatology. 206:29-36.
5. Akamatsu, H., Komura, J., Asada, Y., Miyachi, Y. and Niwa, Y. (1991). Inhibitory effect of azelaic acid on neutrophil functions: a possible cause for its efficacy in treating phatogenetically unrelated diseases. Arch Dermatol. Res. 283:162-166.
6. Webster, G. (2000). Combination of azelaic acid therapy for Acne vulgaris. J. Am. Acad Dermatol 43(2 pt 3):S47-50.
7. Hermanns, J.F., Petit, L, Piérard-Frachchimont, C., Paquet, P. and Piérard, G.E. (2002). Assessment of Topical Hypopigmenting agents on Solar Lentigenes of Asian. Dermatology. 204:281-286.
8. Maralmadi, G. and Esposito, M. (2002). Potassium azeloyl diglycinate. Cosmetic & Toil. 117(3):43-50.Roeske, R. (1963). Preparation of t-butyl esters of free amino acids. J. Org. Chem. 28(5):1251-1253
9. Idris, Z., Ahmad, S., Abu Hassan, H., Yeong S.H. Samsudin, M.W. (2009). A method of producing derivative of azelaic acid. Malaysian Patent Application. PI 2009 1437.

The Malaysian Journal of ANALYTICAL SCIENCES ISSN 1394-2506

PERAWATAN AIR SISA KILANG KELAPA SAWIT SECARA ELEKTROKIMIA

(Palm Oil Factory Wastewater Treatment Using Electrochemical Technique)

Nor Ain Mohd Aluwi, M.S Md Jamil, Rahimi M. Yusop, Bakri Din, Firdaus Ismail, Mohamed Rozali Othman*

Pusat Pengajian Sains Kimia dan Teknologi Makanan, Fakulti Sains dan Teknologi
Universiti Kebangsaan Malaysia, 43600 UKM Bangi, Selangor, Malaysia

**Corresponding author: rozali@ukm.my*

Abstrak

Kajian ini dilakukan untuk merawat air buangan yang diambil dari sumber sisa air buangan kilang kelapa sawit secara elektrokimia menggunakan besi tahan karat sebagai elektrod dalam 0.1 M NaCl. Sampel yang dielektrolisis dianalisis menggunakan UV-Vis dan penentuan nilai COD. Disamping sisa cecair, sisa pepejal yang diperolehi turut dianalisis menggunakan FTIR dan penganalisa CHNS. Hasil kajian mendapati warna air buangan tersebut dapat dikurangkan sehingga 50% dan paras COD dikurangkan sehingga 80% untuk tempoh elektrolisis selama 3 jam dan dikenakan keupayaan setinggi 10 V.

Kata kunci: Rawatan air buangan, elektrolisis

Abstract

A study was carried out to determine the suitability of palm oil factory wastewater treatment using electrochemical technique with stainless steel as both working and counter electrode in 0.1 M NaCl. Treated liquid samples were later analysed using UV-Vis and COD determination. While solid samples formed during the electrolysis process were analyse using FTIR and CHNS analyser. Results obtained showed than electrochemical technique with the above condition able to reduced color and COD level of the waswater up to 50% and 80% respectively after 3 h electrolysis time with 10 V applied voltage.

Keywords: Wastewater treatment, electrolysis

Introduction

Minyak kelapa sawit adalah satu daripada minyak sayuran yang penting di pasaran dunia [1]. Malaysia adalah antara pengeluar dan pengeksport terbesar minyak kelapa sawit dunia, merangkumi 11% pengeluar minyak dan lemak dunia dan 27% pasaran eksport [2]. Pokok kelapa sawit mengeluarkan dua jenis minyak, iaitu minyak sawit mentah dan minyak isirung kelapa sawit mentah [2]. Namun, tidak terkecuali industri ini juga sentiasa mengeluarkan air buangan ke sistem saliran dalam proses untuk mendapatkan minyak dari buahnya.

Air buangan kilang kelapa sawit mengandungi komponen yang tidak larut air seperti buah kelapa sawit dan bahan termendak seperti gentian kelapa sawit dan minyak. Disamping itu, air buangan ini juga mengandungi gas metana, sulfat, gas nitrogen, halogen dan pepejal ion organik atau tak organik yang melebihi paras ambangnya [1]. Kandungan bahan organik, terutamanya lipid, karbohidrat, minyak & gris juga tinggi. Kehadiran minyak dan gris menyebabkan air sisa menjadi asidik dan menjadi bahan pencemar kerana ianya sukar diuraikan. Minyak adalah masalah utama dalam rawatan biologi sisa kelapa sawit [3].

Ciri-ciri fizikal air buangan sisa ini ialah panas dan berasid sekitar pH 4 dan 5. Air sisa ini berwarna perang yang likat dan mempunyai mendakan. Niali pH sisa akan bertukar kepada alkali sejurus biodegradasi mengambil alih [4]. Secara keseluruhan, air sisa kelapa sawit mengandungi 40–500 mgL^{-1} jumlah pepejal, 4,000 mgL^{-1} minyak & gris, 50,000 mgL^{-1} COD dan 2,5000 mgL^{-1} BOD [5 – 8]. Tidak kurang juga bahan-bahan mineral yang wujud seperti

fosforus, kalium, magnesium dan kalsium yang terdapat dalam air sisa dengan setiap satunya berkepekatan 18, 2270, 615 dan 439 mgL^{-1}. Air buangan dari kilang kelapa sawit ini memberi kesan buruk kepada alam sekitar termasuklah kepada tanah, air dan hidupan akuatik. Walaupun ianya boleh dibiodigredasi kerana kehadiran sisa-sisa minyak yang masih wujud dalam air tersebut, namun air buangan ini perlu dirawat terlebih dahulu kerana keadaannya yang berasid dan mempunyai nilai BOD yang tinggi.

Sistem rawatan yang digunakan sekarang untuk merawat air buangan ini adalah melalui sistem penghadaman anaerobik, proses aerobik lanjutan, sistem perkolaman, sistem bioreaktor dan sistem pengkompos [9]. Dalam sistem penghadaman anaerobik, efluen akan dibiarkan didalam *acidification buffering pond* selama dua ke tiga hari, kemudian dirawat dalam kolam anaerobik dengan masa tahanan hidrolik 30-80 hari mengikut kilang rawatan [1]. Cecair kemudiannya dirawat dalam kolam fakultatif sebelum dilepaskan.

Proses lanjutan aerobik adalah untuk menurunkan nilai BOD air sisa yang tinggi. Dalam proses ini, jumlah mikro-organisma diperbanyakkan untuk menukarkan bahan pencemar kepada tenaga, karbon dioksida dan air. Mendakan aerobik diuruskan di tangki untuk memastikan penghasilan sisa yang bersih. Kebaikan rawatan ini adalah ianya tidak sensitif kepada perubahan persekitaran, stabil dan memastikan keupayaan biodigradasi mencecah 95% [1]. Masalah sistem pengolahan kolam adalah penyingkiran pepejal yang kurang memuaskan disamping pengeluaran gas metana dan karbon dioksida [6]. Dalam rawatan menggunakan bioreaktor, air sisa dirawat dengan cara yang hampir sama dengan cara lama kecuali ianya menggunakan masa pengekalan yang lebih singkat dengan menggunakan sistem hidrolik. Rawatan ini juga memerlukan ruang yang lebih kecil dan lebih mesra alam.

Kaedah pengkomposan vermi juga adalah antara kaedah yang baik untuk digunakan bagi rawatan air buangan kilang kelapa sawit. V*ermicast* adalah kaya nutrien dan menolong mengitar nutrisi tumbuhan disamping membantu tanah daripada terdegredasi [5]. Rawatan air sisa juga boleh dilakukan menggunakan sistem membran UF [10]. Peningkatan dalam penurunan nilai COD, warna dan kekeruhan juga didapati dengan tekanan transmembran 0.5 bar [10]. Rawatan menggunakan kaedah membran dapat meningkatkan kualiti air sisa dan membran UF memainkan peranan penting dalam mengurangkan bahan pencemar yang hadir dalam air sisa.

Pihak industri akan senantiasa mencari jalan untuk menggunakan kaedah yang paling menjimatkan perniagaan mereka disamping memastikan air sisa terkawal semasa dilepaskan ke persekitaran. Antara kaedah yang selalu digunakan adalah dengan penghadaman sistem anaerobik, lanjutan proses aerobik dan sistem bioreaktor. Antara kaedah lain adalah dengan menggunakan teknologi membran dan proses elektrokimia, yang menggunakan teknik pengoksidaan.

Dalam kajian ini, proses elektrokimia digunakan. Semasa proses elektrokimia dijalankan, proses pengoksidaan dan penurunan akan berlaku pada anod dan katod [11]. Proses pengoksidaan adalah proses dimana suatu spesis itu akan kehilangan elektron bagi mencapai keadaan pengoksidaan yang lebih tinggi, manakala proses penurunan pula adalah proses dimana suatu spesis mengalami pertambahan elektron bagi mencapai keadaan pengosidaan yang lebih rendah [12]. Penghasilan bahan pengoksida iaitu daripada NaCl yang digunakan sebagai elektrolit penyokong dihasilkan dalam larutan pukal secara *in-situ* melalui tindak balas [13]:

$$2\,Cl^- \longrightarrow Cl_2 + 2e^-$$
$$Cl_2 + H_2O \longrightarrow HOCl + H^+ + Cl^-$$
$$HOCl \longrightarrow H^+ + OCl^-$$

Sisa semasa elektrolisis dipisahkan oleh tiga lapisan, iaitu lapisan paling atas adalah buih, pepejal seni dan minyak [3]. Lapisan tengah adalah cecair yang mengandungi pepejal terlarut dan minyak, manakala lapisan terbawah adalah *flocks.*

Dalam kajian ini, proses pengoksidaan yang berlaku mampu menukar dan memutuskan rantai-rantai molekul yang boleh membahayakan persekitaran kepada molekul yang lebih kecil dan lebih mudah terbiodegredasi. Terdapat dua proses yang berlaku semasa elektrolisis dijalankan iaitu proses pengoksidaan anodik terus, dimana bahan pencemar akan melekat pada elektrod dan dimusnahkan dengan tindak balas pengaliran anodik [13]. Proses yang keduanya

adalah proses pengoksidaan tidak langsung, yang menggunakan bahan pengoksida kuat seperti hiperklorit yang dihasilkan melalui proses elektrokimia tersebut.

Bahan dan Kaedah

Bahan kimia

Semua reagen yang digunakan adalah bergred Analar (R & M Chemicals) dan digunakan tanpa penulinan lanjut.

Sampel, persampelan dan pra-pengolahan sampel

Air sisa kilang kelapa sawit diperolehi dari kilang kelapa sawit di FELDA Kemahang, Tanah Merah, Kelantan. Sampel ini diambil dari saluran paip yang mengalirkan air buangan dari kilang ke kolam rawatan. Sampel kemudiannya disejukkan ke suhu bilik dan dilindungi dari cahaya matahari dengan meletakkannya di tempat gelap. Sampel yang diambil dibahagikan kepada dua iaitu sampel mentah yang tidak dituras dan yang dituras terlebih dahulu menggunakan kertas turas gentian kaca berliang 0.45 µm.

Proses elektrolisis dan pencirian hasil elektrolisis

Proses elektrolisis ke atas 25 mL sampel air buangan dilakukan menggunakan besi tahan karat sebagai elektrod kerja dan elektrod lawan dengan keupayaan setinggi 10 V selama tiga jam digunakan dalam 0.1 M NaCl sebagai elektrolit penyokong dalam bikar 100 mL. Keupayan dibekalkan menggunakan pembekal kuasa DC (TTi PSU Bench CPX 400). Pengacauan dilakukan sepanjang tempoh elektrolisis. Bagi air buangan yang dituras, analisis menggunakan UV-Vis akan dijalankan sebelum dan selepas elektrolisis, manakala bagi air buangan yang tidak dituras, sampel hanya akan dianalisis selepas rawatan dijalankan.

Untuk menentukan peratus penyahwarnaan dan kepekatan bahan penyerap yang ada, Spektrofotometer UV-Vis digunakan, manakala FTIR digunakan untuk melihat kumpulan berfungsi yang masih tinggal selepas elektrolisis. Nilai COD ditentukan sebelum dan selepas elektrolisis menggunakan kaedah piawai [14].

Spektrometer UV-Vis dua alur yang digunakan untuk menentukan keberkesanan proses rawatan disamping mengkaji penurunan warna air buangan. Pengukuran peratus penyingkiran warna dikira melalui persamaan [11]:

$$Abs(\%) = [(Abs_{\lambda i}-Abs_{\lambda f}) / Abs_{\lambda i}] \times 100$$

dimana $Abs_{\lambda i}$ dan $Abs_{\lambda f}$ masing-masingnya adalah serapan pada panjang gelombang tertentu sebelum dan selepas rawatan dijalankan

Peratus penyingkiran COD dikira melalui persamaan:

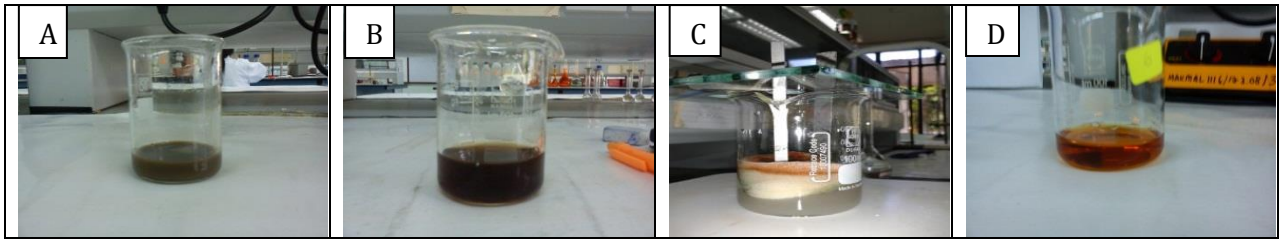
$$COD(\%) = [(COD_i-COD_f) / COD_i] \times 100$$

dimana COD_i dan COD_f adalah nilai COD sebelum dan selepas rawatan

Hasil dan Perbincangan

Sisa bahan pepejal

Sisa cecair sebelum elektrolisis dituras terlebih dahulu menggunakan kertas turas gentian kaca 0.45 µm untuk mendapatkan sisa pepejal untuk analisis. Daripada pemerhatian didapati pepejal akan terbentuk apabila proses elektrolisis dijalankan ke atas air sisa yang telah dituras atau tidak dituras sebelumnya (Rajah 1). Kedua-dua sisa pepejal yang diperolehi sebelum dan selepas proses eleklisis ini dibiarkan kering ini dibiarkan kering pada suhu bilik sebelum dianalisis menggunakan penganalisa CHNS, spektroskopi FT-IR dan ujian keterlarutan menggunakan pelarut air dan metanol.



Rajah 1. Bentuk air buangan yang tidak dituras (A), selepas dituras (B), semasa elektrolisis (C) dan selepas elektrolisis (D).

Proses elektroflokulasi dan elektrokoagulasi dijangka terjadi semasa proses elektrolisis berjalan, dimana zarahan yang lebih besar saiznya akan terbentuk. Kejadian ini berlaku apabila zarahan menjadi kurang stabil dan membentuk zarahan baru yang lebih besar. Penyahstabilan ini adalah proses flokulasi sebelum membentuk zarahan baru**.** Proses koagulasi membolehkan pepejal seni bergabung menghasilkan pepejal yang lebih besar akibat proses penyahstabilan [6]. Ini menyebabkan jumlah pepejal terlarut dapat dikurangkan dengan efektif. Proses elektrokoagulasi ini adalah lebih baik berbanding kaedah koagulasi kimia kerana ianya lebih mesra alam [3]. Elektrokoagulasi telah dikaji menggunakan beberapa jenis air buangan yang berbeza dan membuktikan ianya berguna dalam menyingkirkan sisa pepejal terlarut, logam berat dan penyingkirkan bahan organik komplek [3, 15 – 17].

Analisis keunsuran

Analisis telah dijalankan keatas sisa pepejal yang diperolehi untuk melihat kandungan unsur menggunakan alat penganalisa CHNS. Sebelum rawatan, sisa pepejal menunjukkan nilai peratus karbon yang sangat tinggi, manakala selepas rawatan, nilai peratus karbon menjadi lebih rendah (Jadual 1). Ini menunjukkan walaupun sampel dituras terlebih dahulu sebelum rawatan, pepejal yang terlarut dalam sampel masih ada dan mempunyai nilai karbon yang tinggi. Perkara yang sama terjadi terhadap kandungan nilai peratus nitrogen dan hidrogen. Analisis ini menunjukkan ketidakhadiran sulfur dalam sampel pepejal sisa. Jadual 1 menunjukkan bahawa pepejal yang terhasil semasa proses elektrolisis dijalankan mengandungi kandungan unsur C, N dan N yang jauh lebih rendah daripada pepejal yang diperolehi sebelum elektrolisis. Ini menunjukkan bahawa pepejal berkenaan adalah merupakan bahan yang berbeza. Keputusan ini menunjukkan bahawa andaian yang dikatakan bahawa berlakunya proses elektroflokulasi dan elektrokoagulasi sebelum ini adalah tidak tepat, tetapi sebaliknya bahan baru hasil pengoksisaan secara elektrokimia yang terbentuk. Bahan yang pertama mungkin sisa sabut dan tempurung buah kelapa sawit, manakala pepejal yang terbentuk semasa elektrolisis mungkin merupakan sebatian amida yang tidak larut dalam air yang terbentuk daripada sisa minyak atau kandungan asid lemak dalam sampel air buangan. Ini merujuk kepada sampel yang telah dituras terlebih dahulu.

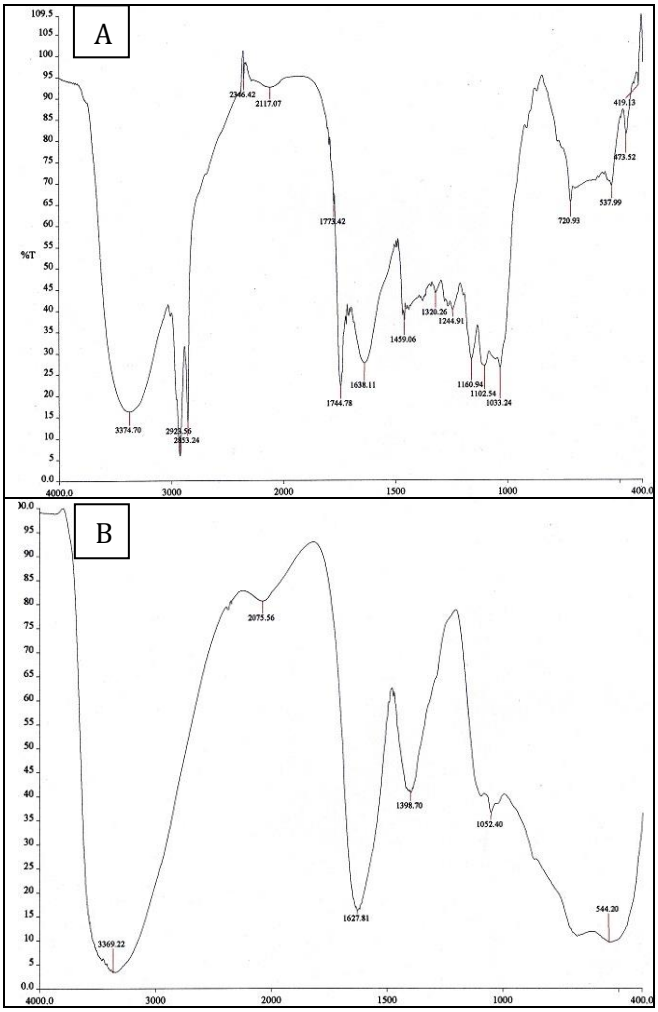
Jadual 1. Keputusan analisis sisa pepejal yang diperolehi sebelum dan selepas elektrolisis

Parameter	Analisis unsur	Tidak dituras		Dituras	
		Sebelum elektrolisis	Selepas elektrolisis	Sebelum elektrolisis	Selepas elektrolisis
Kelarutan dalam air		nd	4 mendakan terhasil	2	4 mendakan terhasil
Kelarutan dalam metanol		nd	4 mendakan terhasil	2	4 mendakan terhasil
Kandungan unsur (%)	C	nd	17.06	48.04	8.82
	N	nd	0.41	1.48	0.27
	H	nd	3.80	7.19	3.68
Berat** (g)		nd	1.355	0.345	0.992

nd- tidak ditentukkan; *julat 1-5 : 1- paling tidak larut, 5- larut sepenuhnya

Analisis Spektroskopi FTIR

Secara puratanya, analisis spektroskopi FTIR memberikan puncak pada 3,370.74 cm^{-1} dan 1,630.06 cm^{-1} yang merujuk kepada regangan N-H dan C=O amida. Untuk sisa sebelum rawatan, spektrum menunjukkan kehadiran kumpulan alkana pada nombor gelombang 2,923.56 cm^{-1} dan 2,853.24 cm^{-1} bagi regangan alkana (Rajah 2). Ini menunjukkan bahawa rantaian alkana yang wujud pada awalnya telah dapat diputuskan dan pengoksidaan elektrokimia yang berlaku telah menyebabkan kumpulan berfungsi tertentu telah bertukar kepada kumpulan amida.



Rajah 2. Spektrum FTIR untuk sisa pepejal yang diperolehi sebelum (A) dan selepas elektrolisis (B)

Analisis Keterlarutan dalam Air dan Metanol

Kedua-dua pelarut organik dak tak organik digunakan untuk menguji kelarutan pepejal yang telah diperolehi sebelum dan selepas elektrolisis. Hasil analisis menunjukkan bahawa semuanya larut dalam air dan metanol. Sebelum rawatan, sisa ini hanya larut sedikit dalam pelarut dengan hanya memberikan perubahan warna yang sangat sedikit terhadap kedua-dua pelarut. Manakala bagi sampel pepejal selepas rawatan menunjukkan keterlarutan yang agak tinggi kerana dapat merubah warna pelarut menjadi perang. Namun, setelah beberapa ketika, mendakan terhasil dan warna perang menjadi lebih pudar.

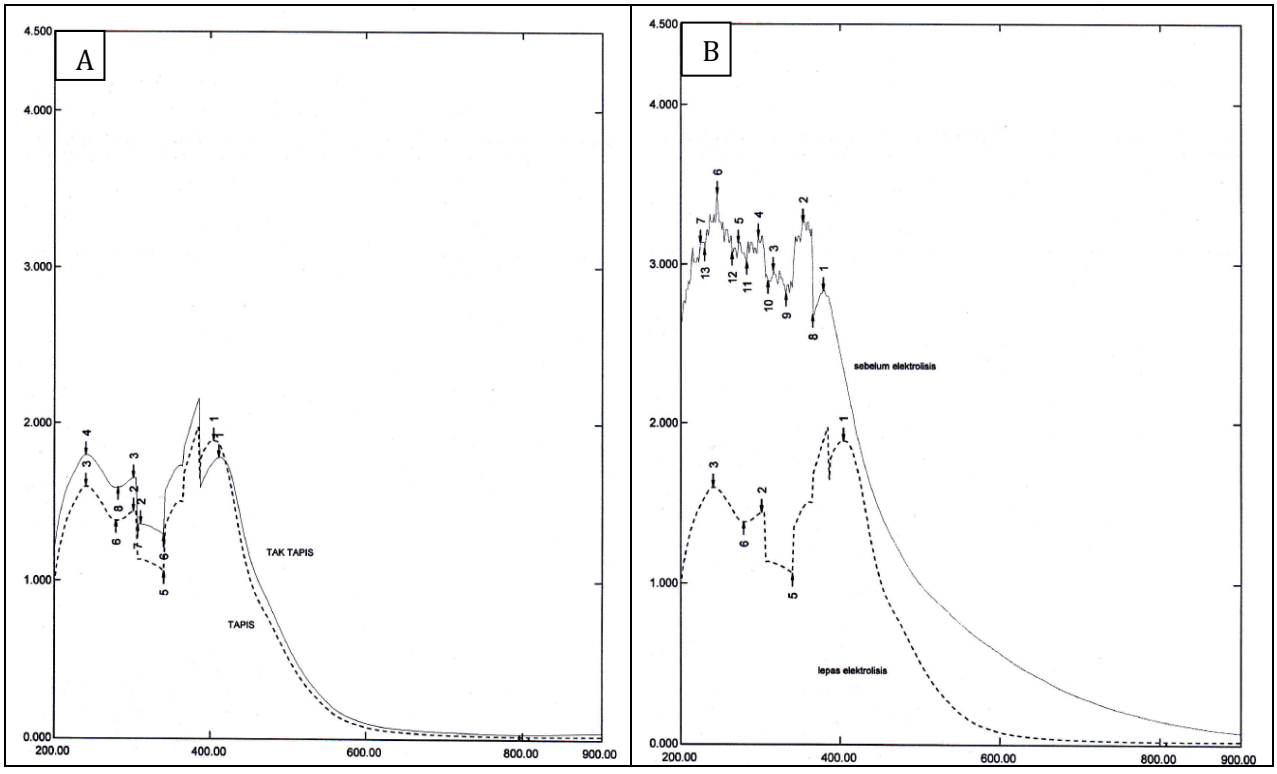
Molekul yang bersifat terkutub akan larut dalam air, manakala pelarut metanol akan melarutkan larutan yang mengandungi bahan-bahan organik. Ujian keterlarutan ini juga membuktikan sisa pepejal mempunyai bahan-bahan yang terkutub dan organik dalam komposisinya.

Sisa cecair

Sisa hasil cecair merujuk kepada analisis terhadap sisa dalam fasa cecair sebelum dan selepas elektrolisis. Untuk mendapatkan sampel cecair, sampel air buangan yang belum dan telah dirawat perlu dituras terlebih dahulu untuk mengasingkan sisa cecair ini daripada mendakan dan bahan pepejal yang terhasil semasa proses elektrolisis. Antara analisis yang digunakan adalah kajian terhadap serapan menggunakan spektroskopi UV-Vis, spektroskopi FTIR dan penentuan COD menggunakan kaedah refluks terbuka. Analisis menggunakan spektroskopi FTIR dijalankan dengan mengeringkan sisa cecair tadi pada suhu bilik sebelum analisis dijalankan.

Analisis spektrum UV-Vis

Warna asal sisa buangan, iaitu perang gelap bertukar kepada perang muda selepas elektrolisis. Bagi spektrum sisa sebelum elektrolisis, larutan menyerap dalam julat panjang gelombang 378 nm sehingga 225 nm. Sebanyak tujuh puncak ditemui. Bagi spektrum selepas elektrolisis, serapan hanya berlaku dalam julat panjang gelombang 404 nm hingga 241nm dan hanya tiga puncak yang wujud. Spektrum bagi sampel yang tidak dituras menunjukkan empat puncak yang menyerap pada julat panjang gelombang 411 nm hingga 241 nm (Rajah 2).



Rajah 3. Spektrum UV-Vis sisa cecair yang dituras dan tidak dituras (A) serta spektrum UV-Vis sisa cecair sebelum dan selepas elektrolisis (B)

Rajah 3(A) menunjukkan perbezaan antara air sisa selepas elektrolisis bagi air buangan yang tidak dituras dan sampel yang dituras terlebih dahulu sebelum dirawat. Serapan sisa tidak banyak berbeza kecuali serapan bagi yang tidak dituras lebih tinggi sedikit daripada lawannya. Manakala Rajah 3(B) menunjukkan perbezaan spektrum bagi sampel sebelum rawatan dijalankan dan selepas rawatan. Spektrum ini menunjukkan dengan jelas bahawa serapan bahan-bahan kromofor dalam larutan telah menurun dengan begitu ketara. Peratus penyahwarnaan sampel yang berlaku adalah seperti yang diringkaskan aalam Jadual 2.

Jadual 2. Peratus penyahwarnaan dan nilai COD air buangan yang dirawat secara elektrokimia

Parameter	Keadaan sampel	Julat panjang gelombang (nm)	Sebelum elektrolisis	Selepas elektrolisis	Peratus penyingkiran (%)
Warna	Tidak dituras	378.00-411.00	nd	1.783	nd
		298.00-302.00	nd	1.653	nd
		241.00-246.00	nd	1.799	nd
	Dituras	378.00-411.00	2.834	1.892	33.24
		298.00-302.00	3.175	1.438	54.71
		241.00-246.00	3.436	1.597	53.52
COD	Tidak dituras		nd	7,660.8	nd
	Dituras		37,632.0	6,643.2	82.35

Analisis COD

Analisis COD telah dijalankan menggunakan kaedah refluks terbuka terhadap sisa sebelum dan selepas elektrolisis untuk melihat perbandingan kandungan bahan organik yang wujud dalam sisa. Air buangan yang belum dan telah dirawat dicairkan dengan air suling dengan nisbah 1:49. Seperti yang ditunjukkan dalam Jadual 2, peratus penyingkiran COD adalah mencapai sehingga 82.35% dengan nilai COD bagi sebelum rawatan adalah 37,632.0 mgL^{-1} dan sisa selepas rawatan adalah 6,643.3 mg^{-1}, manakala COD bagi sisa selepas elektrolisis yang tidak dituras adalah 7,660.8 mg^{-1}, dimana nilainya tinggi daripada yang dituras. Nilai-nilai COD yang masih tinggi ini menunjukkan masih banyak bahan organik yang wujud walaupun setelah rawatan dijalankan.

Kerajaan tidak menetapkan nilai COD yang perlu dipatuhi untuk membebaskan sisa kelapa sawit ke persekitaran, namun nilai ini masih terlampau tinggi ini dilepaskan.

Kesimpulan

Paras COD dan bahan berwarna dapat dikurangkan selepas elektrolisis masing-masingnya sebanyak 82.3% dan 54.7%, disamping itu juga didapati pepejal terbentuk selepas elektrolisis. Namun memandangkan ini hanya kajian awal tidak dapat dipastikan samada pepejal yang terbentuk itu disebabkan terjadinya proses elektrokoagulasi atau disebabkan pembentukan sebatian yang tidak larut air. Warna air sisa yang terbentuk pada akhir proses elektrolisis adalah mungkin disebabkan oleh warna yang terhasil apabila pepejal yang terbentuk melarut sedikit dalam air. Ujian FTIR yang dijalankan menunjukkan bahawa sebatian yang terbentuk itu merupakan sebatian amida.

Penghargaan

Pembiayaan daripada Universiti Kebangsaan Malaysia melalui geran UKM-AP-2011-21 dan UKM-DLP-2012-024 amat dihargai.

Rujukan

1. Igwe, J.C. and Onyegbado, C.C. (2007), A Review of Palm Oil Mill Effluent (Pome) Water Treatment. *Global J. Environ. Res.* 1(2), 54 - 62
2. MPOC. 2011. http://www.mpoc.org.my/The_Oil_Palm_Tree.aspx. [13 Disember 2011].
3. Chantaraporn, P., Junpita, M., Kanita, I. and Boonyarit, N. (2010), Pretreatment of palm oil mill effluent by electrocoagulation and coagulation *Sci. Asia* 36, 142 – 149

4. Okwute, L.O. and Isu, N.R. (2007), The environmental impact of palm oil mill effluent (pome) on some physico-chemical parameters and total aerobic bioload of soil at a dump site in Anyigba, Kogi State, Nigeria *Afr. J. Agr. Res.* 2(12), 656 – 662
5. Parveen Fatemah Rupani, Rajeev Pratap Singh, M. Hakimi Ibrahim and Norizan Esa. (2010*),* Review of Current Palm Oil Mill Effluent (POME) Treatment Methods: Vermicomposting as a Sustainable Practice *World Appl. Sci. J.* 11(1), 70
6. Ta, Y.W., Abdul Wahab Mohammad, Jamaliah Md. Jahim and Nurina Anuar. (2010), Pollution control technologies for the treatment of palm oil mill effluent (POME) through end-of-pipe processes *J. Environ. Manage.* 91, 1467 - 1490
7. Wong, Y.S., Kadir, M.O.A.B. and Teng, T.T. (2009), Biological kinetics evaluation of anaerobic stabilization pond treatment of palm oil mill effluent *Bioresour. Tech.* 100(21), 4969 – 4975
8. Wood, B.J., Pillai, K.R. and Rajaratnam, J.A. (1979), Palm oil mill effluent disposal on land.*Agr. Wastes* 1, 103 - 127
9. APOC. 2003. http://www.americanpalmoil.com/ [23 November 2011]
10. Munirat Abolore Idris, Mohammed Saedi Jami and Suleyman Aremu Muyibi. (2010), Tertiary treatment of biologically treated palm oil mill effluent (POME) using UF membrane system: effect of MWCO and transmembrane pressure. *Inter. J. Chem. Environ. Eng.* 1(2), 108 - 112
11. Usha, N.M., Rekha, H.B. and Bhavya, J.G. (2011), *2011 Inter. Conf. Environ. Comput. Sci.* 19, 64
12. Ramli Ibrahim, Ilyas Md Isa and Anuar Kassim. (2003), *Kimia Analisis*. Edisi 1. Tanjong Malim: Penerbit UPSI.
13. Rajkumar, D. and Palanivelu, K. 2004. Electrochemical treatment of industrial wastewater. *J. Hazard. Mater.* B 113, 123
14. APHA (1995), Standard Methods for the Examination of Water and Wastewater (19$^{ed.}$), American Public Health Association, Washington, D.C (1995)
15. Abuzaid, N.S., Bukhari, A.A. and Al-Hamouz, Z.M. (1998), Removal of bentonite causing turbidity by Electrocoagulation *J. Environ. Sci. Heal. A* 33(7), 1341 - 1358
16. Bukhari, A. (2008). Investigation of the electro-coagulation treatment process for the removal of total suspended solids and turbidity from municipal wastewater *Bioresour. Tech.* 99(5), 914

The Malaysian Journal of Analytical Sciences Vol 17 No 2 2013

Page

1. ANALYSIS OF CHROMIUM, MERCURY, SILVER AND ZINC IN HAIR SAMPLES FROM DENTISTS PRACTICING IN BENGHAZI, LIBYA 208
(Analisis Kromium, Raksa, Perak dan Zink Dalam Sampel Rambut Doktor Gigi di Benghazi, Libya)
Intisar Alakili, Aiman. M. Bobaker, Sukiman. B. Sarmani

2. SINTESIS DAN PENENTUAN STRUKTUR KOMPLEKS DI-TERT-BUTILSTANUM (IV) DITIOKARBAMAT 214
(Synthesis and Structure Determination of Di-tert-butyltin (IV) Dithiocarbamate)
Amirah Faizah Abdul Muthalib, Ibrahim Baba, Yang Farina Abdul Aziz, Mohd Wahid Samsudin

3. COMPARISON BETWEEN WATER QUALITY INDEX (WQI) AND BIOLOGICAL WATER QUALITY INDEX (BWQI) FOR WATER QUALITY ASSESSMENT: CASE STUDY OF MELANA RIVER, JOHOR 224
(Perbandingan di antara Indeks Kualiti Air (WQI) dan Indeks Kualiti Air Biologi (BWQI) bagi Penilaian Kualiti Air: Kajian Kes Sungai Melana, Johor)
Nor Zaiha Arman, Mohd. Ismid Mohd. Said, Salmiati, Shamila Azman, Muhammad Hazim Mat Hussin

4. DISCRIMINATION OF BLACK BALLPOINT PEN INKS BY HIGH PERFORMANCE LIQUID CHROMATOGRAPHY (HPLC) 230
(Diskriminasi Pen Mata Bola Berdakwat Hitam Menggunakan Kromatografi Cecair Berprestasi Tinggi)
Mohamed Izzharif Abdul Halim, Norashikin Saim , Rozita Osman , Halila Jasmani , Nurul Nadhirah Zainal Abidin

5. PENENTUAN SIFAT KEFUNGSIAN SERBUK RUMPAI LAUT *KAPPAPHYCUS ALVAREZII* 236
(Determination of the functional properties of *Kappaphycus alvarezii* seaweed powder)
Sjamsiah, Nazaruddin Ramli, Rusli Daik, Mohd. Ambar Yarmo

6. SORPTION OF Au (III) AND Ag (I) ON AMINO- AND MERCAPTO-SILICA HYBRID COLUMNS 244
(Jerapan Au (III) dan Ag (I) pada Turus Hibrid Amino- dan Merkapto-silika)
Nuryono, Nurma Y. Indriyanti, Julita B. Manuhutu, Narsito, Shunitz Tanaka

7. STRUCTURE ELUCIDATION OF FLAVONOID COMPOUND FROM THE LEAVES OF *COLEUS ATROPURPUREUS* BENTH USING 1D- AND 2D-NMR TECHNIQUES 255
(Elusidasi Struktur Sebatian Flavonoid Dari Daun *Coleus Atropurpureus* Benth Menggunakan Teknik 1D- Dan 2D-NMR)
Sovia Lenny, Tonel Barus, Lamek Marpaung, M.Pandapotan Nasution

8. TANDEM SOLID PHASE EXTRACTION FOR THE DETERMINATION OF PHARMACEUTICALS IN WASTEWATER 262
(Pengekstrakan Fasa Pepejal Secara Penggabungan Katrij Untuk Analisis Farmaseutikal Dalam Air Sisa Buangan)
Licaberth Ismail, Rozita Osman, Norashikin Saim

9. SUBCRITICAL WATER EXTRACTION OF MONOSACCHARIDES FROM OIL PALM FRONDS HEMICELLULOSES 272
(Pengekstrakan Air Subgenting Daripada Monosakarida Dari Hemiselulosa Pelepah Kelapa Sawit)

R., Norsyabilah, S. Sabiha Hanim, M. H., Nor Suhaila, A. Noraishah, A.K., Siti Kartina

10. PHENOLIC COMPOUNDS FROM THE FRUITS OF *ORANIA SYLVICOLA* 276
(Sebatian Fenol daripada Buah *Orania sylvicola*)
Solihah Sukari, Ikram M. Said

11. STEROIDAL COMPOUNDS FROM THE ROOTS OF *HOLARRHENA CURTISII* 281
(Sebatian Steroid daripada Akar *Holarrhena curtisii*)
Noor Fazila Zahari, Ikram M. Said

12. PETROLEUM HYDROCARBON IN SURFACE SEDIMENT FROM COASTAL AREA OF PUTATAN AND PAPAR, SABAH 286
(Petroleum Hidrokarbon di Dalam Sedimen Permukaan daripada Pesisiran Pantai Putatan dan Papar, Sabah)
Siti Aishah Mohd Ali, Rohana Tair, Soon Zhi Yang, Masni Mohd Ali

13. OPTIMIZATION OF A DISTILLATION UNIT IN TERMS OF POTENTIAL ENVIRONMENTAL IMPACT AND ECONOMICS 291
(Pengoptimuman Unit Penyulingan dari Segi Potensi Impak Ekonomi dan Alam Sekitar)
Alhassan Salami Tijani, Naveed Ramzan

14. LIPID PEROXIDATION IN RAT LIVER USING DIFFERENT VEGETABLE OILS 300
(Peroksidaan Lipid Pada Hati Tikus yang Menggunakan Minyak Sayuran yang Berbeza)
Eqbal Dauqan, Aminah Abdullah, Halimah Abdullah Sani

15. SPECTROPHOTOMETRIC DETERMINATION OF LAMOTRIGINE IN PHARMACEUTICAL PREPARATIONS AND URINE SAMPLES USING BROMOTHYMOL BLUE AND BROMOPHENOL BLUE 310
(Penentuan Spektrofotometrik Lamotrigina dalam Persediaan Farmaseutikal dan Sampel Urin Mengunakan Bromotimol Biru dan Bromofenol Biru)
Fadhil M. Najib, Kosar H. H. Aziz

16. EFFECT OF TEMPERATURE ON KAFFIR LIME OIL BY USING HYDRO-DIFFUSION STEAM DISTILLATION SYSTEM 326
(Kesan Suhu Ke Atas Minyak Limau Purut Dengan Menggunakan Sistem Penyulingan Penyebaran Hidro)
Zakiah Mohd Yusoff, Zuraida Muhammad, Nurhani Kasuan, Mohd Hezri Fazalul Rahiman, Mohd Nasir Taib

17. STEAM DISTILLATION WITH INDUCTION HEATING SYSTEM: ANALYSIS OF KAFFIR LIME OIL COMPOUND AND PRODUCTION YIELD AT VARIOUS TEMPERATURES 340
(Penyulingan Wap Dengan Sistem Pemanasan Aruhan: Analisis Komposisi Minyak Limau Purut Dan Hasil Pengeluaran Pada Suhu Pelbagai)
Zuraida Muhammad, Zakiah Mohd Yusoff, Mohd Noor Nasriq Nordin, Nurhani Kasuan, Mohd Nasir Taib, Mohd Hezri Fazalul Rahiman, Zaibunnisa Abdul Haiyee

The Malaysian Journal of ANALYTICAL SCIENCES ISSN 1394-2506

ANALYSIS OF CHROMIUM, MERCURY, SILVER AND ZINC IN HAIR SAMPLES FROM DENTISTS PRACTICING IN BENGHAZI, LIBYA

(Analisis Kromium, Raksa, Perak dan Zink Dalam Sampel Rambut Doktor Gigi di Benghazi, Libya)

Intisar Alakili[1]*, Aiman. M. Bobaker[1], Sukiman. B. Sarmani[2]

[1]*Department of Chemistry, Benghazi University, Benghazi, Libya*
[2]*School of Chemical Sciences and Food Technology, Faculty of Science and Technology, Universiti Kebangsaan Malaysia, 43600 UKM Bangi, Selangor D.E., Malaysia*

**Corresponding author: mneimm@hotmail.com*

Abstract

The measurements of mercury, zinc, chromium and silver in hair samples of dentists and control group were carried out by neutron activation analysis. Our results showed that, the level of mercury (mean ± standard deviation) in hair samples of dentists were 5.99 ± 2.64 mg/kg (range of 3.44 – 776 mg/kg) and for control group were 2.45 ± 0.62 mg/kg (range of 1.70 – 3.48 mg/kg) and the difference between the two groups was significant. A high level of zinc in hair samples of dentist and control group was also observed. The level of zinc in dentist was 1081.14 ± 495.36 mg/kg (range of 315 – 1770 mg/kg) while the mean level of zinc was 1862±1581.76mg/kg for the control group (ranged from 688 to 5256 mg/kg) which was found to be significantly higher than those for dentists. The mean levels of chromium and silver show no significant difference between dentists and control group. The hair mercury level of dentists was correlated to the number of weekly working hours, experience in years and age while gender, fish consumption and the number of dental amalgam in mouth of dentists were found to be uncorrelated to the level of mercury.

Keywords: dental amalgam, mercury, hair, dentist

Abstrak

Pengukuran kandungan raksa,zink, kromium dan perak dalam sampel rambut doktor gigi dan kumpulan kawalan dilakukan dengan kaedah analisis pengaktifan neutron. Hasil yang diperolehi menunjukkan kandungan raksa (min ± sisihan piawai) sampel rambut doktor gigi ialah 5.99 ± 2.64 mg/kg (julat 3.44 – 776 mg/kg) dan bagi kumpulan kawalan ialah 2.45 ± 0.62 mg/kg (julat 1.70 – 3.48 mg/kg) yang menunjukkan perbezaan bererti di antara dua kumpulan tersebut. Kandungan zink yang tinggi bagi kedua-dua kumpulan juga diperhati, kandungan zink dalam sampel rambut doktor gigi ialah 1081.14 ± 495.36 mg/kg (julat 315 – 1770 mg/kg) manakala bagi kumpulan kawalan ialah 1862±1581.76mg/kg (julat 688 - 5256 mg/kg). Terdapat perbezaan bererti dalam kandungan zink bagi kumpulan kawalan berbanding dengan kumpulan doktor gigi. Kandungan kromium dan perak tidak menunjukkan perbezaan bererti bagi kedua-dua kumpulan tersebut. Kandungan raksa doktor gigi mempunyai korelasi dengan jumlah jam berkerja seminggu, bilangan tahun pengalaman dan usia walau bagaimanapun tiada korelasi dengan kekerapan pengambilan ikan dan bilangan amalgam gigi.

Kata kunci: amalgam gigi, raksa, rambut, doktor gigi

Introduction

Hair analysis have been used as a bio-monitor for many elements, both toxic and essential, for assessing environmental exposures and body nutritional status, as well as diagnosis of diseases. Dental amalgam is well known as a major source of mercury exposure in dentistry. An amalgam is a restorative material generally contains 50% mercury (Hg) in complex mixture of other metals. Dentist and dental personnel who work with amalgam are chronically exposed to mercury which is readily absorbed into the body through the skin during handling and by inhalation. Mercury has been demonstrated to have damaging effects on the kidney, central nervous system and

cardiovascular system. The effect of the mercury is to block or inhibit most essential enzymatic processes at very low levels of exposure. Possible adverse effects of mercury exposure in dentistry have been discussed in several studies. To our knowledge, no studies have examined the mercury levels in hair samples of Libyan dentists. The purpose of this study was to assess the levels of exposure to mercury in dentists in Benghazi, Libya to show if the level of mercury in the hair of the dentists exceeded the level of mercury set by WHO [1].

Materials and Methods

Sample collection

Thirty two dentists were included in this study. There were randomly selected from 4 dental clinics (2 private, 2 public) in Benghazi, Libya. Each dentist was asked to complete a questionnaire detailing age, gender, number of working hours per week, number of years in experience as a dentist, number of dental amalgam in dentist mouth and frequency of fish consumption per week.

A group of 25 respondents representing the students and the lectures in the faculty of science, Benghazi University was assigned as the control group. The control group members were also asked to complete a questionnaire similar to that of dentists but excluding questions specifically relating to dentists work.

Preparation of hair samples

Hair samples were collected from donors by single cutting from the occipital region with a pair of clean stainless steel scissors in accordance with the IAEA protocols. The hair samples were cut to lengths of about 2-5 mm. The hair samples were then washed according to the standard procedure recommended by the IAEA: wash hair in acetone, thrice in water and once more in acetone. The samples were then dried overnight in an oven at 60˚C.

Table 1. Description of the study population

	Male N = 16		Female N = 16		All Dentists N = 32		Control Group N = 25	
	Mean ± stdv	Range	Mean ± stdv	Range	Mean ± stdv	Range	Mean ± stdv	Range
Age (years)	32.06 ±4.06	25 – 38	28.14 ±2.21	24 - 32	30.20 ±3.85	24 -38	27.83±9.20	19 - 40
Number of dental amalgam	3.5 ±1.90	0 – 8	1.86 ±1.51	0 - 5	2.27 ± 1.73	0 -8	1.5 ± 1.05	0 - 3
Fish Consumption (Meal/week)	2	1 – 3	1	0 - 2	1	0 -3	1	0 - 3
Working Hours/week	38 ± 13.95	18 – 60	26.21 ± 10.11	18 - 50	32.50 ± 13.50	18 - 60	-	-
Experience (years)	6.60 ± 3.70	1 – 12	3.42 ± 1.51	1 – 6.5	5 ± 3.3	1 - 12	-	-

Hair analysis

Samples were analysed by neutron activation analysis with the kayzero standardization methods. About 0.1 gram of each hair sample and Al-Au wire and Zr monitors were irradiated in a neutron flux of 2.1 x 10^6 n $cm^{-2}s^{-1}$ in the

PUSPATI TRIGA MKII Reactor for about 6 hours. After a decay period of three days activated samples were analysed by a gamma spectroscopy system consisting of a HPGe detector and the associated electronics. Detail of the analysis has been reported earlier [2-5].

Results and Discussion

General description of the study population

The total sample was made up of 32 dentists and 25 controls live in the same general geographical area. For dentists, the results of the survey revealed that 50% of the participating dentists within the two types of gender had ages of 24 – 38 years old. The mean age (± standard deviation) was 30.20± 3.85 years. The number of fish meal consumed weekly by this group varied from 0 to 3 times with an average of 1 time/week. The average number of dental amalgam was 2 in the range of 0 – 8.

For the control group, the population consisted of 11 male (44%) and 14 female (56%). Their mean age was 27.83± 9.20 years in the range of 19 – 40 years. Details description of the population studied are summarized in Table 1.

Hg, Zn, Cr and Ag level in hair of dentists and control group

The mean (±standard deviation) of total mercury levels in hair samples for whole participating dentists was 5.99±2.64 mg/kg in the range of 3.44 – 776 mg/kg. For male, the mean (±standard deviation) of the total mercury in their hair samples was 6.22±1.32mg/kg in the range of 3.82 – 12.40 mg/kg. For female, the mean level was 6.60 ±4.46 mg/kg in the range of 3.44 – 776 mg/kg. The frequency distribution of mercury concentration for the participating dentists is shown in Figure 1.

For control group, the mean (± standard deviation) of total mercury level in their hair samples was 2.45± 0.6 mg/kg in the range of 1.70 – 3.48 mg/kg. For male, the mean of mercury level (±standard deviation) was 2.19±0.42 mg/kg in the range 1.70 – 2.48 mg/kg. for female, the mean of mercury level (± standard deviation) was 2.70±0.77 ranged from 1.95 – 3.48 mg/kg.

High levels of zinc were found in hair samples of dentists and control. The mean level (±standard deviation) of zinc in hair samples of dentists was 1081.4 ± 495.36 mg/kg in the range of 315–1770 mg/kg. For control group, the mean zinc level was 1862.18 ± 1581.76 mg/kg in the range of 688 – 5256 mg/kg.

The mean level of chromium and silver (±standard deviation) in the participating dentists were 2.60±1.87mg/kg (ranged from 1.25 –13.7mg/kg) and 3.54±1.17 mg/kg (ranged from 0.51 – 4.53mg/kg), respectively. For control group, the mean level of chromium and silver (±standard deviation) were 2.83±1.94 mg/kg (ranged from 0.13 – 12.2mg/kg) and 3.13 ±2.55mg/kg (ranged from 1.78 – 13.3 mg/kg), respectively. No significant difference was found in the level of chromium and silver between dentist and control group. The level of total mercury, zinc, chromium and silver in hair samples of participating dentists and control group were summarized in Table 2.

Our results indicated that, there was a significant difference between hair mercury concentration of dentists and controls. The mean concentration of hair mercury for dentists was about two times that for the control group. In this study, 65% of the participating dentists had level of mercury in their hair exceeded the level of mercury of 5mg/kg which sets by the WHO [1].

Although zinc is an essential element that is found in almost every cell and low level will cause health problem especially for children growth, a high level of zinc can produce acute and chronic effects of toxicity. In this study a very high level of zinc were found in hair of dentists and control group. In contrast to mercury, the mean level in control group hair was found to be significantly higher than that for dentists. However, the source of zinc in both the samples is not known. Further investigation of the blood levels in order to assess internal contamination must be carried out. No significant difference was found between the level of Cr and Ag in hair of dentists and those for control group.

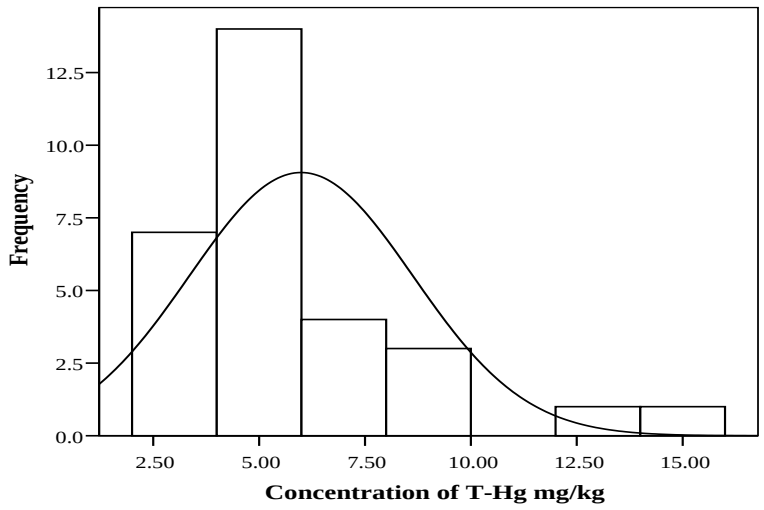


Figure 1. Frequency distribution of total mercury concentration for the participating dentists

The relation between the number of weekly worked hours by dentists and hair mercury concentrations was examined by Pearson correlation. The results showed a significant correlation between the number of weekly worked hours and hair mercury level ($r = 0.561$, $p = 0.001$). Similar correlation was reported by Scarlett et al. [6] but not with Harakeh et al. [7] who found no correlation between hair mercury levels and working hours. While in other study, a significant correlation between urinary mercury and the number of worked hours but no correlation between that and concentrations of mercury in head hair. In this study, Zn, Cr and Ag in dentist's hair were not correlated to weekly worked hours.

Table 2. The level of Hg, Zn, Cr and Ag in hair samples of participating dentists and the control group (mg/kg)

Group	Hg		Zn		Cr		Ag	
	Mean	Range	Mean	Range	Mean	Range	Mean	Range
Dentists	5.99±2.64	3.44-776	1081 ±495	315-1770	2.60±1.87	1.25 –13.7	3.54±1.17	0.51 – 4.53
Control Group	2.45±0.62	1.70-3.48	1862 ±1581	688-5256	2.83±1.94	0.13 -12.2	3.13 ±2.55	1.78 – 13.3

Our results showed a significant positive correlation between the hair mercury levels in dentists and the number of years of their experience at 0.05% level (r=0.447, p=0.013). This is in agreement with Scarlet et al. [6] but contradicts with what was reported by Harakeh et al. [7]. Duncan et al. [8] found that, staff working in dental practices for more than five years had small but discernible increases in head hair mercury concentration.

Age was found to be correlated to hair mercury level of dentists at 0.01 level (r=0.531, p=0.001). This finding contrast to that of Ott et al. [9] who found no correlation between mercury level in hair samples of dentists and their age. Tabatabaei et al. [10] found a positive relation between urine mercury and age (p=0.008). For control group, age correlated only with the concentration of zinc in their hair.

The mean mercury level in hair samples of male dentists was higher than that for female. However, the difference was not significant. In control group, gender had effect on the level of mercury and zinc. The level of mercury and zinc in hair of females were significantly higher than those for male. In this study, two samples one male dentists and one female dentists were found to have high level of mercury in their hair (12.40 and 15.80 mg/kg, respectively). This may due to contaminated environment in their work place, where both work in the same clinic. Another two female dentists have a very high level of hair mercury (423 and 776 mg/kg). However, the reason of these high levels wasn't known. In those cases blood test would have confirmed the internal exposure to mercury.

Our results revealed no significant correlation between mercury level in hair of dentists and the number of dental amalgam in their mouth. This comparable to what was reported elsewhere [7] and similar finding was found for Zn, Cr and Ag.

Although fish consumption is a major source mercury exposure, in this study fish consumption had no effect on the level of mercury in dentists or control group hair and this finding accords with Harakeh [7]. A significant correlation between hair mercury level and fish consumption have been reported in our previous study in other nation [2]. The absence of correlation between hair mercury level and fish consumption may be due to low frequency of fish consumption in Libya.

Conclusion

This study showed that the occupational exposure to mercury in dentists poses a potential risk of increasing systematic mercury level. There is a need for further investigation including environment monitoring of Hg, evaluation and test for neuro-behavior to detect early effects of mercury poisoning. It is important to enforce personnel safety measures to control the exposure. Apart from mercury, our results showed a high level zinc contamination in the hair of dentist and control group. Detail studies need to be carried out to asses the level of zinc in the population of Benghazi and in other cities in general and to investigate the source of contamination.

References

1. WHO (1994). *Recommendation for Epidemiological Research on Mercury.* Geneva: World Health Organisation.
2. Sarmani, S & Alakili, I. (2004). Determination of total mercury and methylmercury in hair samples from residents of Kuala Lumpur, Malaysia by neutron activation analysis. *Journal of Radioanalytical and Nuclear Chemistry* 259(2): 261-264
3. Khoo, K. S., Sarmani, S.B., & Abugassa, I. O. (2007). Determination of thermal to epithermal neutron flux ratio (f), epithermal neutron flux shape factor (alpha) and comparator factor (Fc) in the TRIGA Mark II Reactor. *Journal of Radioanalytical and Nuclear Chemistry* (271)2: 419-424.
4. Abugassa, I. O., Khrbish, Y.S., Ben Faid, N., Basir, A. T., & Sarmani,S. B. (2007). Installation of Kayzero-INAA standardization in the TNRC and its applications for trace elements determination in different materials. *Journal of Radioanalytical and Nuclear Chemistry* 271(1): 27-33.
5. Yavar Alireza, Sukiman Sarmani, Abdul Khalik Wood, Nurul Syakireen Zainal, Kok Siong Khoo,(2012). Development and implementation of Høgdahl convention and Westcott formalism for k0-NAA application at Malaysian Nuclear Agency reactor. *Journal of Radioanalytical and Nuclear Chemistry* 291:521–527.

6. Scarlett, J.M., Gutenmann, W. H., & Lisk, D., J. (1988). A study of mercury in the hair of dentists and dental-related professionals in 1985 and subcohort comparison of 1972 and1985 mercury hair levels. *Journal of Toxicology and Environmental Health*. 25(3): 373-81.
7. Harakeh,S., Sabra, N., Kassak, K., & Doughan, B. (2002). Factors influencing total mercury levels among Lebanese dentists. *Science of Total Environment* 297:153 - 160
8. Duncan, A., O'Reilly, D. S., McDonald, E. B., Watkins, T. R., & Taylor, M. (2011). Thirty-five year review of a mercury monitoring service for Scottish dental practices. *British Dental Journal* 12(3): 210.
9. Ott, K., H., Grimmeisen, J., Alt, F., Messerschmidt, J., & Tölg, G. (1991). Mercury in the hair of dentists and dental personnel. *Dtsch Zahnarztl Z*. 46(2):154-8.
10. Tabatabaei, M., Golbabaei, F., & Shariatei, B. (2006). Evaluation of urine mercury level of dentists in Tehran and its influencial factors. *Journal of Dental Medicine* 19(3): 66 – 75.

The Malaysian Journal of ANALYTICAL SCIENCES ISSN 1394-2506

SINTESIS DAN PENENTUAN STRUKTUR KOMPLEKS DI-*TERT*-BUTILSTANUM (IV) DITIOKARBAMAT

(Synthesis and Structure Determination of Di-*tert*-butyltin (IV) Dithiocarbamate)

Amirah Faizah Abdul Muthalib, Ibrahim Baba*, Yang Farina Abdul Aziz, Mohd Wahid Samsudin

Pusat Pengajian Sains Kimia dan Teknologi Makanan, Fakulti Sains dan Teknologi, Universiti Kebangsaan Malaysia, 43600 UKM Bangi, SelangorD.E.

**Corresponding author:aibi@ukm.my*

Abstrak

Kompleks diorganostanum(IV) ditiokarbamat baru telah disintesis daripada di-*tert*-butilstanum(IV) diklorida dengan kehadiran bersama *N*-dialkilamina dan karbon disulfida. Analisis unsur dan gravimetri menunjukkan formula umum bagi kompleks ini ialah $(t\text{-}C_4H_9)_2Sn[S_2CNR_1R_2]_2$ (R_1 = CH_3, C_2H_5, C_7H_7 dan R_2 = C_2H_5, C_6H_{11}, iC_3H_7, CH_3, C_2H_5, C_4H_9, C_7H_7). Struktur kesemua kompleks ditentukan dengan menggunakan spektroskopi inframerah, ultralembayung, ^1H, ^{13}C dan ^{119}Sn RMN dan kristalografi sinar-X. Analisis termogravimetri bagi kompleks yang telah diperoleh juga turut dibincangkan. Spektrum inframerah semua kompleks ini menunjukkan tiga jalur *ν*(C ---- N), *ν*(C ---- S) dan *ν*(Sn-S) yang wujud masing-masing pada julat 1447-1496, 947-988 dan 352-370 cm^{-1}. Spektroskopi ^{13}C RMN menunjukkan anjakan kimia untuk $\delta(N^{13}CS_2)$ berada pada julat 199.1–201.8 ppm. Struktur hablur tunggal sinar-X bagi kompleks $(t\text{-}C_4H_9)_2Sn[S_2CN(CH_3)(iC_3H_7)]_2$ menunjukkan atom pusat stanum berkoordinat enam dan hablur mempunyai sistem *monoklinik* dengan kumpulan ruang *P2/n*, dengan *a* = 11.2934(11) Å, *b* = 7.0175(7) Å, *c* = 15.6894(15) Å; β = 95.016(1)°. Manakala kompleks (*N*-benzil-*N*-etilditiokarbamato)klorido di-*tert*-butilstanum(IV) dan (*N*,*N*-dibenzilditiokarbamato)klorido-di-(*tert*-butil)stanum(IV) hanya mempunyai satu ligan ditiokarbamat dan satu atom klorin dengan membentuk struktur lima koordinatan. Hablur (*N*-benzil-*N*-etilditiokarbamato)klorido di-*tert*-butilstanum(IV) bersistem *triklinik* di mana *a* = 8.6140 (2) Å, *b* = 10.9604 (3) Å, *c* = 11.4765 (3) Å; α = 91.858 (2)˚, β = 96.193 (2)˚, γ = 96.011 (2)˚, dengan kumpulan ruang *P*1. Manakala (*N*,*N*-dibenzilditiokarbamato)klorido-di-(*tert*-butil)stanum(IV) bersistem *monoklinik* di mana *a* = 9.0600 (2) Å, *b* = 10.9238 (2) Å, *c* = 12.7845 (3) Å; β = 102.759 (2)˚ serta berkumpulan ruang $P2_i$.

Kata kunci: *di-tert-butilstanum(IV), ditiokarbamat*

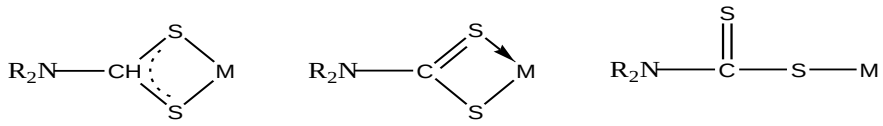
Abstract

New diorganotin(IV) dithiocarbamate complexes have been synthesized from di-*tert*-butyltin(IV) dichloride, N-dialkylamine and carbon disulphide. Elemental and gravimetric analysis confirmed the general formula of these complexes as $(t\text{-}C_4H_9)_2Sn[S_2CNR_1R_2]_2$ (R_1 = CH_3, C_2H_5, C_7H_7 dan R_2 = C_2H_5, C_6H_{11}, iC_3H_7, CH_3, C_2H_5, C_4H_9, C_7H_7). The structures of these complexes have been elucidated on the basis of infrared, ultraviolet, ^1H, ^{13}C & ^{119}Sn NMR spectroscopy and X-ray crystallography. The infrared spectra of these complexes showed three main peaks for *ν*(C ---- N), ν(C ---- S) and *ν*(Sn-S) bands that appeared in the region of 1447-1496, 947-988 and 352-370 cm^{-1}, respectively. The ^{13}C NMR spectrum showed the chemical shift for $\delta(N^{13}CS_2)$ in the range of 199.1–201.8 ppm. X-ray single crystal structure $(C_4H_9)_2Sn[S_2CN(CH_3)(iC_3H_7)]_2$ demonstrated a six-coordination geometry around the tin atom adopting a *monoclinic* system with a space group of *P2/n* with *a* = 11.2934(11) Å, *b* = 7.0175(7) Å, *c* = 15.6894(15) Å; β = 95.016(1)°. The (*N*-benzyl-*N*-ethyldithiocarbamato)chlorido di-*tert*-butyltin(IV) and (*N*,*N*-dibenzyldithiocarbamato)chlorido-di-(*tert*-butyl)tin(IV) formed a different geometry with one dithiocarbamate ligand and one chlorine atom attached to the tin centre to form a five-coordinate structure. Crystal of (*N*-benzyl-*N*-ethyldithiocarbamato)chlorido di-*tert*-butyltin(IV) adopts a *triclinic* system with space group of *P*1 and cell parameter of *a* = 8.6140 (2) Å, *b* = 10.9604 (3) Å, *c* = 11.4765 (3) Å; α = 91.858 (2)˚, β = 96.193 (2)˚, γ = 96.011 (2)˚, while (*N*,*N*-dibenzyldithiocarbamato)chlorido-di-(*tert*-butyl)tin(IV) adopts a *monoclinic* system with space group of $P2_i$ with cell parameter *a* = 9.0600 (2) Å, *b* = 10.9238 (2) Å, *c* = 12.7845 (3) Å; β = 102.759 (2)˚.

Keywords: *di-tert-butyltin(IV), dithiocarbamate*

Pengenalan

Ditiokarbamat adalah kompleks tak organik dengan setengah asid karbonik yang ditemui pada awal sejarah kimia organosulfur. Debus (1850) [1] adalah penyelidik pertama yang melaporkan sintesis asid ditiokarbamik diikuti dengan perbincangan awal kompleks ditiokarbamat oleh Thorn dan Ludwig (1962) [2]. Penyelidikan terhadap kompleks di-*tert*-butilstanum(IV) dengan menggunakan dimetilditiokarbamat sebagai ligan pemula juga telah dilaporkan [3]. Penggunaan dan juga potensi kompleks organostanum ditiokarbamat telah banyak dilaporkan berdasarkan kepada penggunaannya dalam pelbagai bidang. Pelbagai ligan ditiokarbamat seperti dietilditiokarbamat diketahui penggunaannya sebagai antidot HIV [4]. Kompleks logam ditiokarbamat juga diketahui mempunyai kegunaan dalam pemvulkanan getah dan pestisid [5, 6].



(I) (II) (III)

Anion ditiokarbamat $R_1R_2NCS_2^-$ adalah sejenis bes lemah yang boleh bersifat ligan bidentat berkelat dengan kekuatan ikatan atom sulfur yang berbeza dalam kumpulan yang sama [7]. Ligan ditiokarbamat organostanum(IV) boleh berkoordinat kepada atom stanum dalam tiga mod, iaitu bidentat (I), anisobidentat (II) atau monodentate (III) [8]. Geometri kompleks heksakoordinat akan terbentuk apabila ditiokarbamat bertindak sebagai bidentat dan berkoordinat kepada atom Sn melalui dua atom sulfur [9].

Bahan dan Kaedah

Bahan Kimia

Kesemua bahan kimia dan pelarut yang digunakan dalam eksperimen ini telah diperoleh daripada pembekal pada gred yang 98% tulen dengan tidak melakukan sebarang penulenan: *N*-metiletilamina (Aldrich, 98%), *N*-metilsikloheksilamina (Aldrich, 98%), *N*-etilsikloheksilamina (Aldrich, 98%), *N*-metilisopropilamina (Aldrich, 98%), *N*-etilisopropilamina (Aldrich, 98%), *N*-benzilisopropilamina (Aldrich, 98%), *N*-metilbenzilamina (Aldrich, 98%), *N*-etilbenzilamina (Aldrich, 98%), *N*-metilbutiamina (Aldrich, 98%), *N*-dibenzilamina (Aldrich, 98%) dan di-*tert*-butilstanum(IV) diklorida bersama dengan karbon disulfida, kloroform dan etanol (Merck, 98%).

Peralatan

Takat lebur telah diukur menggunakan alat jenama Electrothermal model IA 9100. Analisis unsur telah dilakukan menggunakan peralatan jenama Fison model EA 1108. Alat jenama Perkin Elmer model GX telah digunakan untuk merekod spektrum inframerah dengan menggunakan pelet KBr untuk julat 4000 - 400 cm^{-1} dan nujol bersama dengan pelet polietilena untuk julat inframerah jauh 400-250 cm^{-1}. Bagi pencirian struktur kompleks ditiokarbamat, spektrum RMN ^1H, ^{13}C dan ^{119}Sn telah dikutip dengan menggunakan model JEOL JNM-ECP 400 MHz dengan pelarut kloroform terdeuderat, $CDCl_3$ dan tetrametilsilana, TMS telah digunakan sebagai piawai. Spektrum RMN ^1H telah dicerap pada frikuensi 400 Hz manakala RMN ^{13}C pada frikuensi 100 Hz. Difraktometer Bruker SMART APEX2 dan Oxford Diffraction Xcaliber EOS Gemini telah digunakan untuk penentuan struktur hablur tunggal dengan menggunakan perhidmatan analisis X-ray masing-masing daripada Jabatan Kimia, Universiti Malaya (UM) dan Jabatan Kimia, Universiti Putra Malaysia (UPM).

Sintesis Kompleks

Kaedah sintesis yang telah digunakan untuk kesemua kompleks di-*tert*-butilstanum(IV) ditiokarbamat adalah merupakan kaedah tindak balas terus [10]. Kompleks di-*tert*-butilstanum(IV) ditiokarbamat telah disediakan melalui tindak balas berstoikiometri 1:2 di antara di-*tert*-butilstanum(IV) diklorida dengan amina dan karbon disulfida secara *in-situ* pada suhu 277 K (Skema 1). Kompleks di-*tert*-butilstanum(IV) ditiokarbamat yang disintesis terdiri daripada $(t\text{-}C_4H_9)_2Sn[S_2CNR'R'']_2$ (R' = CH_3, C_2H_5, C_7H_7; R'' = C_2H_5, C_6H_{11}, iC_3H_7, CH_3, C_2H_5, C_4H_9, C_7H_7). Sebanyak 10 mmol amina dilarutkan terlebih dahulu ke dalam 20 mL etanol sejuk selama 30 minit. Tindak balas ini dilakukan dalam takungan ais dan dikacau dengan menggunakan pengacau bermagnet pada suhu 277 K. Selepas

dikacau, 10 mmol larutan karbon disulfida dititiskan secara perlahan-lahan ke dalam larutan amina tersebut menyebabkan warna campuran bertukar menjadi kekuningan selepas beberapa minit dan dibiarkan selama satu jam. Sebanyak 5 mmol di-*tert*-butilstanum(IV) klorida dalam etanol sejuk (277 K) dititiskan secara perlahan-lahan ke dalam campuran ligan dan dibiarkan selama satu jam. Mendakan putih yang terbentuk dituras dengan menggunakan pam vakum serta dibilas beberapa kali dengan menggunakan etanol sejuk dan dibiarkan kering dalam desikator.

a. $(t\text{-}C_4H_9)_2SnCl_2 + 2R'R''NH + 2CS_2 \rightarrow (t\text{-}C_4H_9)_2Sn(S_2CNR'R'')_2 + 2HCl$

b. $(t\text{-}C_4H_9)_2SnCl_2 + R'R''NH + CS_2 \rightarrow (t\text{-}C_4H_9)_2SnCl(S_2CNR'R'') + HCl$

Skema 1. Tindak balas di antara amina sekunder, karbon disulfida dan di-*tert*-butilstanum(IV) klorida

Kajian Kristalografi

Hablur yang sesuai untuk pengumpulan data belauan sinar-X diperoleh dengan pemeruwapan secara perlahan-lahan dalam pelarut campuran etanol dan kloroform pada nisbah 1:2. Perkakasan dan perisian yang digunakan untuk pengumpulan dan olahan data: APEX2 [11]; pembaikan sel: SAINT [11]; penurunan data: SAINT; penyelesaian struktur: SHELXS97 [12]; program untuk pembaikan struktur: SHELXL97 [12]; grafik molekul: XSEED [13]. Manakala makmal kristalografi UPM pula telah menggunakan perisian CrysAlis PRO bagi penurunan semula data manakala perisian SHELXS97 [12] telah digunakan bagi penentuan struktur.

Keputusan dan Perbincangan

Kompleks di-*tert*-butilditiokarbamat telah disintesis dengan tindak balas di antara amina sekunder, karbon disulfida dan di-*tert*-butilstanum(IV) diklorida pada keadaan suhu rendah (4^0C) dalam pelarut etanol [14]. Kesemua kompleks yang disintesis adalah dalam bentuk pepejal berwarna putih, tulen dan larut dalam campuran pelarut etanol dan kloroform. Berdasarkan Jadual 1, kandungan setiap unsur di dalam kompleks yang diperoleh dibandingkan dengan nilai sebenar adalah kecil dengan peratusan nilai, iaitu dalam lingkungan ±3 peratus sahaja. Perbezaan kecil ini juga membuktikan bahawa kesemua kompleks ditiokarbamat tersebut adalah tulen. Keputusan analisis ini juga membuktikan bahawa stoikiometri pada nisbah 1:2 bagi logam kepada ligan untuk semua kompleks di-*tert*-butilstanum(IV) ditiokarbamat. Spektrum ultralembayung dan boleh tampak untuk kesemua kompleks menunjukkan jalur serapan peralihan π - π^* bagi kumpulan N⋯C⋯S terletak dalam julat 251 - 254 nm yang menunjukkan peralihan cas berlaku di kawasan cahaya nampak [15]. Kromofor bagi kumpulan NCS_2 dalam pengkompleksan akan menyebabkan jalur serapan teranjak ke panjang gelombang rendah [16].

Jalur serapan di sekitar julat 1447-1496 cm^{-1} untuk kompleks di-*tert*-butilstanum(IV) ditiokarbamat dikenali sebagai jalur 'tioreida' adalah hasil daripada getaran ν(C⋯N) bagi moeti $S_2C{=}NR_2$ [17, 18]. Kedudukan jalur tioreida telah memberi gambaran bahawa ikatan C-N bagi setiap kompleks mempunyai ciri ikatan separa ganda dua, iaitu ν(C⋯N) kerana nilai getaran ν(C=N) dan ν(C-N) masing-masing terletak pada julat 1640-1690 cm^{-1} dan 1250-1350 cm^{-1} [19].

Data inframerah kompleks menunjukkan jalur penting ν(C⋯S) terletak dalam julat 947-988 cm^{-1}, iaitu kawasan yang dijangkakan untuk kumpulan tersebut [20]. Kewujudan satu puncak tajam dalam julat ini membuktikan wujudnya ikatan bidentat yang simetri dalam pengkompleksan berbanding dengan puncak yang terbelah dua yang menunjukkan keadaan ikatan tak simetri bagi moeti ditiokarbamat [21]. Manakala kompleks lain pula terdapat puncak dublet pada kawasan 952 cm^{-1} yang jelas menunjukkan ikatan ligan bidentat yang tidak simetri [22]. Jalur lain adalah puncak tioureda yang berada pada kawasan 1447-1496 cm^{-1} yang menunjukkan kombinasi ν(C-N) dan ν(C=N) disebabkan kewujudan atom sulfur yang kaya dengan elektron menyebabkan berlakunya sifat nyahelektron pada kawasan keseluruhan NCS_2 [23]. Puncak penting lain menunjukkan kewujudan ikatan logam-ligan boleh dicerap dalam kawasan 352-370 cm^{-1} disebabkan getaran daripada Sn-S [23].

Kompleks di-*tert*-butilstanum ditiokarbamat menunjukkan kehadiran isyarat proton ^{1}H pada kawasan yang dijangkakan, iaitu enam isyarat proton yang berikat dengan atom nitrogen seperti metil, etil, butil, isopropil, sikloheksil dan benzil serta kumpulan di-*tert*-butil yang berikatan dengan logam stanum.

Jadual 1. Sifat fizik dan nilai analisis unsur kompleks di-*tert*-butilstanum (IV) ditiokarbamat.

Kompleks	Hasil akhir (%)	Takat lebur (ºC)	Analisis Unsur (%) C	H	N	S	Sn*
$(t\text{-}C_4H_9)_2Sn[S_2CN(CH_3)(C_2H_5)]_2$	94	72-74	38.35	6.14	5.79	25.79	22.15
			38.33	**6.83**	**5.59**	**25.58**	**23.67**
$(t\text{-}C_4H_9)_2Sn[S_2CN(CH_3)(C_6H_{11})]_2$	87	82-90	47.12	7.73	4.55	18.33	20.13
			47.29	**7.61**	**4.60**	**21.04**	**19.46**
$(t\text{-}C_4H_9)_2Sn[S_2CN(C_2H_5)(C_6H_{11})]_2$	84	105-106	47.68	7.90	4.53	15.27	19.73
			48.97	**7.90**	**4.39**	**20.11**	**18.63**
$(t\text{-}C_4H_9)_2Sn[S_2CN(CH_3)(iC_3H_7)]_2$	90	85-86	40.79	7.42	5.36	25.24	23.14
			40.83	**7.23**	**5.29**	**24.22**	**22.43**
$(t\text{-}C_4H_9)_2Sn[S_2CN(C_2H_5)(iC_3H_7)]_2$	85	90-92	43.62	7.55	4.90	25.55	21.52
			43.09	**7.59**	**5.03**	**23.01**	**21.28**
$(t\text{-}C_4H_9)_2SnCl[S_2CN(C_7H_7)(iC_3H_7)]$	74	184-186	46.78	6.29	2.88	12.51	23.41
			46.31	**6.55**	**2.84**	**13.01**	**24.09**
$(t\text{-}C_4H_9)_2SnCl[S_2CN(CH_3)(C_7H_7)]$	78	172-174	43.17	5.99	2.47	12.51	24.73
			43.94	**6.07**	**3.01**	**13.80**	**25.55**
$(t\text{-}C_4H_9)_2Sn[S_2CN(CH_3)(C_4H_9)]_2$	91	79-81	43.60	7.73	4.96	19.66	20.32
			43.09	**7.59**	**5.02**	**23.01**	**21.29**
$(t\text{-}C_4H_9)_2SnCl[S_2CN(C_7H_7)_2]$	71	202-204	51.37	4.43	2.58	11.42	20.64
			51.08	**5.96**	**2.59**	**11.86**	**21.95**
$(t\text{-}C_4H_9)_2SnCl[S_2CN(C_2H_5)(C_7H_7)]$	76	178-180	46.09	5.79	3.09	12.95	24.12
			45.16	**6.32**	**2.93**	**13.40**	**24.80**

Nilai huruf tebal merupakan nilai teori, ***Sn** ditentukan dengan kaedah gravimetrik

Spektroskopi RMN ^{13}C merupakan salah satu teknik analisis penting yang dapat menentukan struktur sesuatu kompleks organologam [24]. Nilai anjakan kimia yang wujud dalam julat δ 199.1 – 201.8 ppm merupakan nilai anjakan kimia untuk $N^{13}CS_2$ yang merupakan isyarat penting dalam pencirian kompleks ditiokarbamat [25]. Saiz ion logam memainkan peranan penting dalam penentuan nilai anjakan bagi isyarat karbon CS_2 di mana saiz ion logam yang besar akan menyebabkan ikatan logam-sulfur lebih kuat dan ketumpatan elektron pada moieti NCS_2 lebih tinggi dan menyebabkan nilai $\delta(N^{13}CS_2)$ teranjak pada medan yang lebih tinggi.

Spektroskopi RMN ^{119}Sn merupakan kaedah yang terbaik dalam penentuan struktur dan pencirian kompleks yang mempunyai atom stanum di samping RMN ^{119}Sn ini juga boleh memberi gambaran persekitaran elektronik pada logam stanum [26]. Anjakan kimia bagi RMN ^{119}Sn yang bervariasi kuat boleh berkolerasi dengan setiap perubahan pada atom stanum sebanyak -2338 sehingga +3301 ppm [27]. Nilai di antara +200 sehingga -60 ppm adalah anjakan bagi kompleks empat koordinat, manakala -90 sehingga -190 ppm pula untuk lima koordinat dan -210 sehingga -400 ppm adalah untuk enam koordinat [28]. Kesemua kompleks yang terpilih mempunyai anjakan kimia di antara -274.5 dan -428.5 ppm yang mencadangkan bahawa kompleks ini mempunyai atom pusat stanum yang berkoordinat enam [29].

Jadual 2. Puncak λ maks ultralembayung dan puncak serapan inframerah kompleks di-*tert*-butilstanum(IV) ditiokarbamat.

Kompleks	**UV**		**FTIR - Nombor gelombang (cm^{-1})**			
	λ maks (nm)	**Perl. Elektronik**	**ν(C····N)**	**ν(N-C)**	**ν(C····S)**	**ν(M-S)**
$(t\text{-}C_4H_9)_2Sn[S_2CN(CH_3)(C_2H_5)]_2$	248	π - π*	1487m	1139s	950s	354s
$(t\text{-}C_4H_9)_2Sn[S_2CN(CH_3)(C_6H_{11})]_2$	247	π - π*	1470m	1139s	974s	370s
$(t\text{-}C_4H_9)_2Sn[S_2CN(C_2H_5)(C_6H_{11})]_2$	250	π - π*	1468s	1196s	947s	354s
$(t\text{-}C_4H_9)_2Sn[S_2CN(CH_3)(i\text{C}_3H_7)]_2$	248	π - π*	1446m	1139s	972s	352m
$(t\text{-}C_4H_9)_2Sn[S_2CN(C_2H_5)(i\text{C}_3H_7)]_2$	252	π - π*	1466m	1189s	952s	353m
$(t\text{-}C_4H_9)_2SnCl[S_2CN(C_7H_7)(i\text{C}_3H_7)]$	249	π - π*	1447m	1167s	982s, 961s	351m
$(t\text{-}C_4H_9)_2SnCl[S_2CN(CH_3)(C_7H_7)]$	251	π - π*	1485m	1196s	968s	351s
$(t\text{-}C_4H_9)_2Sn[S_2CN(CH_3)(C_4H_9)]_2$	250	π - π*	1485m	1138s	968s	352m
$(t\text{-}C_4H_9)_2SnCl[S_2CN(C_7H_7)_2]$	252	π - π*	1487s	1154s	988s, 960m	351s
$(t\text{-}C_4H_9)_2SnCl[S_2CN(C_2H_5)(C_7H_7)]$	252	π - π*	1496m	1185s	950s	351s

Petunjuk: s = kuat, m = sederhana, w = lemah, br = lebar

Jadual 3. Data spektrum RMN ^1H dan ^{13}C untuk kompleks di-*tert*-butilstanum(IV) ditiokarbamat.

Kompleks	**Anjakan Kimia, δ (ppm)**			
	^1H	**^{13}C**		**^{119}Sn**
	Sn-C_4H_9	**Sn-C_4H_9**	**N$^{13}CS_2$**	**δ (ppm)**
$(t\text{-}C_4H_9)_2Sn[S_2CN(CH_3)(C_2H_5)]_2$	1.58(s)	12.1, 30.6	199.7	-324.2
$(t\text{-}C_4H_9)_2Sn[S_2CN(CH_3)(C_6H_{11})]_2$	1.57(s)	25.7, 36.4	199.4	-318.0
$(t\text{-}C_4H_9)_2Sn[S_2CN(C_2H_5)(C_6H_{11})]_2$	1.51(s)	14.5, 41.3	199.1	-316.8
$(t\text{-}C_4H_9)_2Sn[S_2CN(CH_3)(i\text{C}_3H_7)]_2$	1.57(s)	19.9, 35.0	199.4	-317.8
$(t\text{-}C_4H_9)_2Sn[S_2CN(C_2H_5)(i\text{C}_3H_7)]_2$	1.56(s)	14.6, 43.1	199.2	-316.9
$(t\text{-}C_4H_9)_2SnCl[S_2CN(C_7H_7)(i\text{C}_3H_7)]$	1.18(s)	20.6, 52.5	201.6	-211.2
$(t\text{-}C_4H_9)_2SnCl[S_2CN(CH_3)(C_7H_7)]$	1.55(s)	31.3	201.8	-230.8
$(t\text{-}C_4H_9)_2Sn[S_2CN(CH_3)(C_4H_9)]_2$	1.57(s)	14.0, 43.1	200.0	-236.9
$(t\text{-}C_4H_9)_2SnCl[S_2CN(C_7H_7)_2]$	1.58(s)	30.5	201.1	-235.2
$(t\text{-}C_4H_9)_2SnCl[S_2CN(C_2H_5)(C_7H_7)]$	1.54(s)	11.9, 30.4	201.2	-236.4

Merujuk kepada data termogravimetri kompleks di-*tert*-butilstanum(IV) ditiokarbamat menunjukkan kesemua kompleks terurai lengkap pada suhu di bawah 370°C. Termogram bagi kompleks $(t\text{-}C_4H_9)_2Sn[S_2CN(C_2H_5)(C_6H_{11})]_2$, $(t\text{-}C_4H_9)_2Sn[S_2CN(CH_3)(i\text{C}_3H_7)]_2$ dan $(t\text{-}C_4H_9)_2Sn[S_2CN(C_7H_7)(i\text{C}_3H_7)]_2$ menunjukkan kompleks ini mengurai secara satu peringkat diikuti oleh kompleks $(t\text{-}C_4H_9)_2Sn[S_2CN(CH_3)(C_2H_5)]_2$, $(t\text{-}C_4H_9)_2Sn[S_2CN(CH_3)(C_6H_{11})]_2$, (*t*-

$C_4H_9)_2Sn[S_2CN(C_2H_5)(iC_3H_7)]_2$ (Rajah 1) dan (t-$C_4H_9)_2SnCl[S_2CN(C_2H_5)(C_7H_7)]$ yang mengurai secara dua peringkat. Kompleks (t-$C_4H_9)_2Sn[S_2CN(CH_3)(C_4H_9)]_2$ dan (t-$C_4H_9)_2SnCl[S_2CN(C_7H_7)_2]$ menunjukkan kestabilan yang agak tinggi oleh kerana ia mula mengurai pada suhu melebihi 130°C di samping mempunyai tiga peringkat penguraian diikuti oleh kompleks (t-$C_4H_9)_2SnCl[S_2CN(CH_3)(C_7H_7)]$ yang menghasilkan kadar penguraian yang tertinggi, iaitu sebanyak empat peringkat. Untuk aspek kestabilan pula, kesemua kompleks di-*tert*-butilstanum(IV) ditiokarbamat adalah stabil untuk dilakukan ujian analisis pada suhu bilik kerana penguraian kompleks berlaku bermula di sekitar suhu 90-160°C.

Jadual 4. Data analisis termogravimetri kompleks di-*tert*-butilstanum(IV) ditiokarbamat.

Kompleks	**Julat suhu (ºC)**	**% Residu akhir (SnS_2)**	**Perbezaan % residu dari eksperimen berbanding kiraan**
(t-$C_4H_9)_2Sn[S_2CN(CH_3)(C_2H_5)]_2$	130-196, 196-288	17.1 **(36.5)**	-19.3
(t-$C_4H_9)_2Sn[S_2CN(CH_3)(C_6H_{11})]_2$	130-198, 198-305	18.8 **(30.0)**	-11.2
(t-$C_4H_9)_2Sn[S_2CN(C_2H_5)(C_6H_{11})]_2$	120-302	20.2 **(28.7)**	-8.5
(t-$C_4H_9)_2Sn[S_2CN(CH_3)(iC_3H_7)]_2$	120-300	22.7 **(34.5)**	-11.8
(t-$C_4H_9)_2Sn[S_2CN(C_2H_5)(iC_3H_7)]_2$	132-190, 190-300	16.7 **(32.8)**	-16.2
(t-$C_4H_9)_2SnCl[S_2CN(C_7H_7)(iC_3H_7)]$	100-340	29.7 **(37.0)**	-7.3
(t-$C_4H_9)_2SnCl[S_2CN(CH_3)(C_7H_7)]$	90-170, 170-220 220-286, 286-355	18.0 **(39.3)**	-21.3
(t-$C_4H_9)_2Sn[S_2CN(CH_3)(C_4H_9)]_2$	130-214, 214-262 262-350	19.8 **(32.7)**	-12.8
(t-$C_4H_9)_2SnCl[S_2CN(C_7H_7)_2]$	155-238, 238-290 290-370	9.7 **(33.7)**	-24.0
(t-$C_4H_9)_2SnCl[S_2CN(C_2H_5)(C_7H_7)]$	98-290, 290-362	16.0 **(38.1)**	-22.0

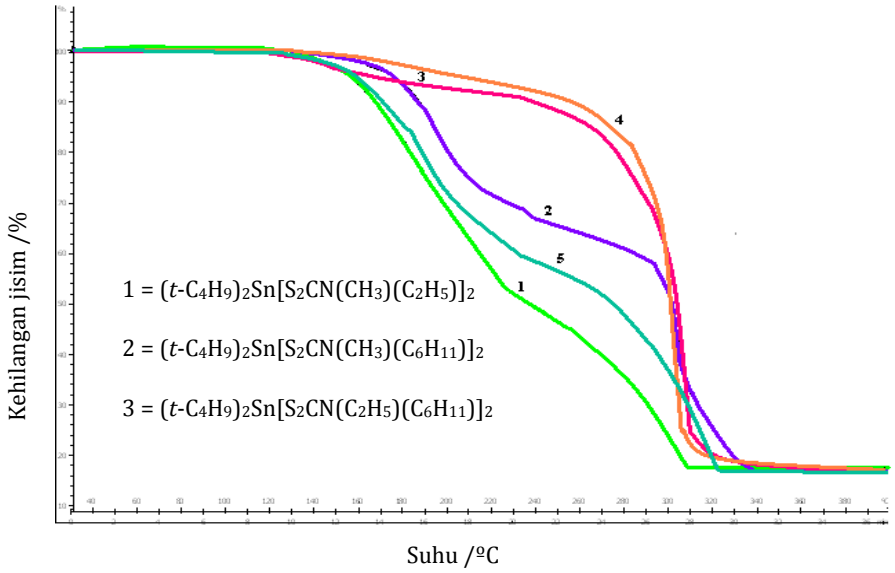
Nilai huruf tebal merupakan nilai jangkaan.

Tiga struktur hablur kompleks di-*tert*-butilstanum(IV) ditiokarbamat (Rajah 2) yang diperoleh bersetuju dengan data analisis unsur, spektroskopi inframerah, ultralembayung dan RMN (^1H, ^{13}C dan ^{119}Sn) untuk kesemua kompleks di-*tert*-butilstanum(IV) ditiokarbamat. Hablur tunggal kompleks (t-$C_4H_9)_2Sn[S_2CN(CH_3)(iC_3H_7)]_2$ [30], (t-$C_4H_9)_2SnCl[S_2CN(C_2H_5)(C_7H_7)]$ [31] dan (t-$C_4H_9)_2SnCl[S_2CN(C_7H_7)_2]$ [32] telah diperoleh dengan cara pemeruwapan secara perlahan campuran perlarut etanol:kloroform pada nisbah 1:2 selama 4-5 hari pada suhu bilik. Plot ORTEP untuk ketiga-tiga struktur ini ditunjukkan dalam Rajah 2.

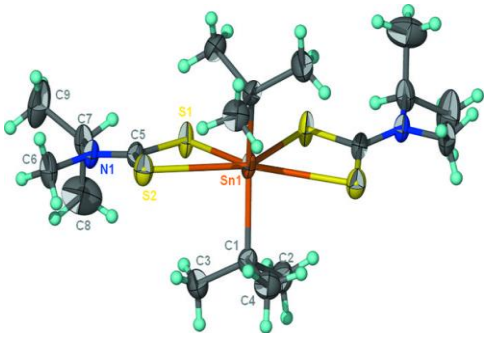
Kompleks (t-$C_4H_9)_2Sn[S_2CN(CH_3)(iC_3H_7)]_2$ (Rajah 2a) menunjukkan enam koordinat dengan mod pengkoordinatan secara bidentat kelat. Hablurnya adalah bersistem *monoklinik* dengan kumpulan ruang *P2/n* di mana a = 11.2934(11) Å, b = 7.0175(7) Å, c = 15.6894(15) Å; β = 95.016(1)º. Panjang ikatan Sn-S yang berbeza mencadangkan pengkoordinatan yang berbeza bagi ligan kepada atom Sn. Geometri bagi kompleks ini adalah trapezoidal bipiramid dengan kumpulan *tert*-butil mengisi kedudukan paksi dan kumpulan NCS_2 daripada ligan ditiokarbamat mengisi pada kedudukan khatulistiwa trapezoidal.

Struktur (*N*,*N*-dibenzilditiokarbamato)klorido-di-(*tert*-butil)stanum(IV) pula bersistem *monoklinik* dengan kumpulan ruang $P2_i$ di mana a = 9.0600 (2) Å, b = 10.9238 (2) Å, c = 12.7845 (3) Å, β = 102.759 (2)˚ (Rajah 2c), bergeometri segiempat piramid terherot dengan atom klorin, Cl yang berkedudukan pada mercu. Dua kumpulan *tert*-butil serta dua atom sulfur berada pada kedudukan khatulistiwa. Ligan ditiokarbamat pula terikat pada atom stanum secara bidentat tidak simetri di mana ikatan Sn-S1 = 2.486 (10) Å dan Sn-S2 = 2.737 (10) Å.

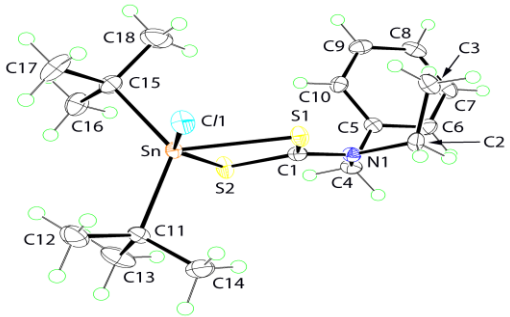
Manakala struktur (*N*-benzil-*N*-etilditiokarbamato)klorido di-*tert*-butilstanum(IV) (Rajah 2b) pula terbentuk dengan satu ligan ditiokarbamat sahaja bersama satu atom klorin yang tidak tertukarganti dengan ligan ditiokarbamat menyebabkan kompleks ini hanya membentuk lima koordinatan. Hablur kompleks ini tidak berwarna, bersistem *triklinik* dengan kumpulan ruang *P*1 di mana *a* = 8.6140 (2) Å, *b* = 10.9604 (3) Å, *c* = 11.4765 (3) Å; α = 91.858 (2)˚, β = 96.193 (2)˚, γ = 96.011 (2)˚. Struktur lima koordinatan yang terikat pada ligan ditiokarbamat secara bidentat tidak simetri oleh kerana panjang ikatan Sn-S yang tidak sama, iaitu Sn1- S1 = 2.476 (4) Å; Sn1-S2 = 2.741 (4) Å. Satu atom klorin yang tidak tertukarganti dengan ligan ditiokarbamat beserta dengan dua atom karbon masing-masing daripada kumpulan *tert*-butil telah mendorong kepada pembentukan struktur hablur lima koordinatan.



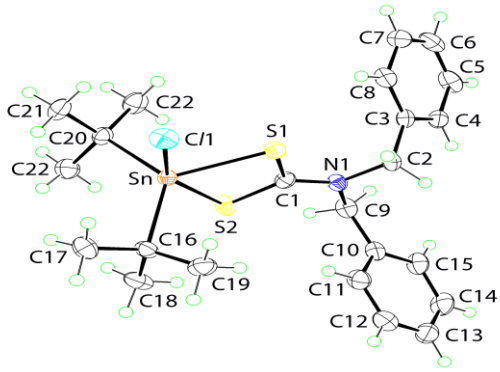
Rajah 1. Lengkung termogravimetri untuk lima kompleks terpilih di-*tert*-butilstanum(IV) ditiokarbamat dalam gas nitrogen.



(a)



(b)



(c)

Rajah 2. Plot ORTEP (a) Di-*tert*-butilbis(*N*-isopropil-*N*-metilditiokarbamato-κ^2S,S')stanum(IV) (b) (*N*-benzil-*N*-etilditiokarbamato)klorido-di-(*tert*-butil)stanum(IV) dan (c) (*N, N*-dibenzilditiokarbamato)klorido-di-(*tert*-butil)stanum(IV) pada paras kemungkinan 50%.

Kesimpulan

Data unsur, spektroskopi dan kristalografi telah membuktikan bahawa sepuluh kompleks di-*tert*-butilstanum(IV) ditiokarbamat telah berjaya disintesis dalam keadaan tulen. Kajian kristalografi untuk tiga kompleks, iaitu bis(*N*-isopropil-*N*-metilditiokarbamato-κ^2S,S')di-*tert*-butilstanum(IV) menunjukkan ligan ditiokarbamat membentuk enam koordinatan kepada atom stanum dalam kedudukan bidentat. Manakala kompleks (*N*-benzil-*N*-etilditiokarbamato)klorido di-*tert*-butilstanum(IV) dan (*N,N*-dibenzilditiokarbamato)klorido-di-(*tert*-butil)stanum(IV) pula membentuk hanya lima koordinatan dengan satu ligan ditiokarbamat dan satu atom klorin.

Penghargaan

Penghargaan dan terima kasih ditujukan kepada Universiti Kebangsaan Malaysia untuk gran UKM-GUP-NBT-08-27-111 dan Kerajaan Malaysia untuk gran Science Fund 06-01-02-SF0539. Ucapan terima kasih juga kepada rakan akademik dan pembantu makmal yang sama-sama membantu dalam menjayakan kerja penyelidikan ini.

Rujukan

1. Debus, H. (1850). Uber die Verbindungen der sulfocarbamisaur. *Agnew Chemistry* (Liebigs), 73: 26.
2. Thorn, G.D. and Ludwig, R.A. 1962. *The Dithiocarbamates and Related Compounds*. Amsterdam-New York: Elsevier Publishing Company.
3. Kim, K., Ibers, A.J., Jung, O.S. and Sohn, S.Y. (1987). Structure of Di(tert-butyl)bis(N,N-dimethyldithiocarbamato)tin(IV). *Acta Crystallographica,* C43: 2317-2319.
4. Frank, N., Christmann, A. and Frei, E. (1995). Comparative studies on the pharmacokinetics of hydrophilic prolinedithiocarbamate, sarcosinedithiocarbamate and the less hydrophilic diethyldithiocarbamate. *Toxicology*, 95: 113-122.
5. Gandhi, N., Jain, R. and Kaushik, N. K. (1996). Thermal studies on germanium(IV) compounds of N-alkylcyclohexyldithiocarbamates. *Thermochimica Acta*, 282/283: 501-508.
6. Gessner, T. and Jakubowski, M. (1972). Diethyldithiocarbamic acid methylester *1: A metabolite of disulfiram. *Biochemical Pharmacology,* 21(2): 219-230.
7. Radha, K., Aravamudan, G., Rajalakshmi, A., Rout, G.C. and Seshasayee M. (1986). Synthesis and properties of tris(bis(2-hydroxyethyl)-dithiocarbamato)halotellurium(II) ('halo'=SCN^-, Br^-, I^-) and the crystal structure of the thiosyanato-S complex, $[Te_2\{(HOCH_2CH_2)_2NCS_2\}_3SCN]$. *Australian Journal Chemical Society*, 39: 847-854.

8. Okamoto, K., Kirchoff, J.R., Ho, D.M. and Deutsch, E. (1993). Preparation, characterization and electrochemical properties of technetium(II) complexes with 1, 2-bis(diethylphosphino) ethane (DEPE) and dithiocarbamate ligands. Single crystal analysis of [Tec{$(CH_3)_2NCS_2$}$(DEPE)_2(PF_6)$]. *Polyhedron* 12(12): 1559-1568.
9. Shahzadi, S., Ali, S. and Fettouhi, M. (2006). Dimethylbis(4-methylpiperidine-1-dithiocarboxylato-κ^2*S*,*S*')tin(IV). *Acta Crystallographica* E62: 1178.
10. Thirumaran, S., Venkatachalam, V., Manohar, A., Ramalingam, K., Bocelli, G. and Cantoni, A. (1998). Synthesis and characterization of bis(*N*-Methyl-*N*-ethanoldithiocarbamato)M(II)(M = Zn, Cd, Hg) and bis(*N*,*N*-(iminodiethylene)bisphthalimidedithiocarbamato)M(II) (M = Zn, Cd, Hg) complexes. Single crystal X-ray structure of bis(di(2-hydroxyethyl)dithiocarbamato)zinc(II). *Journal of Coordination Chemistry* 44: 281-288.
11. Bruker. (2009). APEX2 and SAINT. Bruker AXS Inc., Madison, Wisconsin, USA.
12. Sheldrick, G. M. (2008). Software reference manual, Siemens Analytical X-ray System, Madison, WI, USA.
13. Barbour, L. J. (2001). E-Seed – A software tool for supramolecular crystallography. *Journal Supramolecular Chemistry*, 1: 189–191.
14. Jung, O.S. and Sohn, S.Y. (1988). Coordination Chemistry of Organotin(IV) Dithiocarbamate Complexes. *Bulletin of the Korean Chemical Society*, 9: 356-368.
15. Chauhan, H.P.S. and Shaik, N.M. (2005). Synthetic, spectral, thermal and antimicrobial studies on some mixed 1,3-dithio-2-stannacyclopentane derivatives with dialkyldithiocarbamates. *Journal of Inorganic Biochemistry*, 99: 538–545.
16. Singh, R. and Kaushik, N.K. (2008). Spectral and thermal studies with anti-fungal aspects of some organotin(IV) complexes with nitrogen and sulphur donor ligands derived from 2-phenylethylamine. *Spectrochimica Acta Part A*, 71: 669–675.
17. Jian, F. F., Wang, Z. X., Bai, Z. P., You, X. Z., Fun, H. K., Chinnakali, K. (1999). Structure of bis(dipropyldithiocarbamate) cadmium(II). *Journal of Chemical Crystallography*, 29: 227 – 231.
18. Sharma, C. P., Kumar, N., Khandpal, M. C., Chandra, S. and Bhide, V. G. (1981). Studies on the preparation and characterization of bis-dithiocarbamato derivatives of di-*n*-butyl- and di-*n*-hexyl Sn(IV). *Journal Inorganic Nuclear Chemistry*, 43: 923-930.
19. Casas, J. S., Sanchez, A., Bravo, J., Fontan, S., Castellano, E. E., Jones, M., (1989). Cadmium(II) coordination chemistry related to chelate therapy. *Inorganica Chemica Acta*, 158: 119 – 126.
20. Cea-Olivares, R., Toscano, R.A., Silvestru, C., Garcia-García, P., López-Cardoso, M., Blass-Amador, G. and Nöth, H. (1995). Synthesis and structural characterization of phenoxarsin-10-yl dithiocarbamates, $O(C_6H_4)_2AsS_2CN(CH_2CH_2)_2$, a compound containing an asymmetric mononuclear biconnective 1,1-dithiolato ligand. *Journal of Organometallic Chemistry*, 493: 61-67.
21. Khan, S., Nami, S.A.A., Siddiqi, K.S. (2008). Mononuclear indolyldithiocarbamates of $SnCl_4$ and R_2SnCl_2: Spectroscopic, thermal characterizations and cytotoxicity assays in vitro. *Journal of Organometallic Chemistry* 693: 1049–1057.
22. Shaheen, F., Badshah, A., Gielen, M., Dusek, M., Fejfarova, K., de Vos, D. and Mirza, B. (2007). Synthesis, characterization, antibacterial and cytotoxic activity of new palladium(II) complexes with dithiocarbamate ligands: X-ray structure of bis(dibenzyl-1-S:S0-dithiocarbamato)Pd(II). *Journal of Organometallic Chemistry*, 692: 3019–3026.
23. Husaina, A., Nami, S.A.A. and Siddiqia, K.S. 2009. Interaction of organotin with piperazine derived self-assembled cylindrical bisdithiocarbamates: Spectral and thermal investigations. *Spectrochimica Acta Part A* 73: 89–95.
24. Van Gaal, H. L. M., Diesveld, J. W., Pijpers, F. W and Vander Linden, J. G. M. (1979). ^{13}C NMR spectra of dithiocarbamates. Chemical shift, carbon-nitrogen stretching vibration frequencies, and p bonding in the NCS_2 fragment. *Inorganic Chemistry*, 18(11): 3251-3260.
25. Nomura, R., Takabe, A. and Matsuda, H. (1987). Facile synthesis of antimony dithiocarbamate complexes. *Polyhedron*, 6(3): 411-416.
26. Agustin, D. and Ehses, M. (2009). ^{119}Sn NMR spectroscopic and structural properties of transition metal complexes with terminal stannylene ligands. *Comptes Rendus Chimie*, 12: 1189-1227.
27. Schiemenz, B., Huttner, G., Zsolnai, L., Kircher, P. and Diercks, T. (2006). Two Extremes in Tin Chemistry: A Non-bonding Sn–Sn Distance of 285 pm and a ^{119}Sn-NMR Shift δ = 3301 in Organometallic derivatives of Sn(0). *European Journal of Inorganic Chemistry* 128(2): 187-191.

28. Holecek, J., Nadvornik, M., Handlir, K., Lycka, A. (1986). ^{13}C and ^{119}Sn NMR spectra of Di-n-butyltin(IV) compounds. *Journal of Organometallic Chemistry*, 315: 299-308.
29. Zhang, R., Sun, J. and Ma, C. 2005. Structural chemistry of mononuclear, tetranuclear and hexanuclear organotin(IV) carboxylates from the reaction of di-*n*-butyltin oxide or diphenyltin oxide with rhodanine-*N*-acetic acid. *Journal of Organometallic Chemistry*, 690: 4366-4372.
30. Muthalib, F.A., Baba, I., Samsudin, W.M. and Ng, W.S. (2010). Di*tert*-butylbis(N-isopropyl-N-methyldithiocarbamato-κ^2S,S')tin(IV). *Acta Crystallographica*, E66:m356.
31. Muthalib, A. F. A., Baba, I., Tahir, M. I. M., Ng, S. W. and Tiekink, E. R. T. (2011a). (N-Benzyl-N-ethyldithiocarbamato)-di-*tert*-butylchloridotin(IV). *Acta Crystallographica*, E67: 372-373.
32. Muthalib, A. F. A., Baba, I., Tahir, M. I. M., Ng, S. W. and Tiekink, E. R. T. (2011b). Di-*tert*-butylchlorido(*N*,*N*-dibenzyldithiocarbamato)tin(IV). *Acta Crystallographica*, E67: 386.

The Malaysian Journal of ANALYTICAL SCIENCES ISSN 1394-2506

COMPARISON BETWEEN WATER QUALITY INDEX (WQI) AND BIOLOGICAL WATER QUALITY INDEX (BWQI) FOR WATER QUALITY ASSESSMENT: CASE STUDY OF MELANA RIVER, JOHOR

(Perbandingan di antara Indeks Kualiti Air (WQI) dan Indeks Kualiti Air Biologi (BWQI) bagi Penilaian Kualiti Air: Kajian Kes Sungai Melana, Johor)

Nor Zaiha Arman[1], Mohd. Ismid Mohd. Said[2], Salmiati[1], Shamila Azman[2], Muhammad Hazim Mat Hussin[2]

[1]*Institute of Environmental and Water Resource Management,*
[2]*Department of Environmental Engineering,*
Faculty of Civil Engineering
Universiti Teknologi Malaysia, 81310 Skudai, Johor D.T.

**Corresponding author: salmiati@utm.my*

Abstract

A study of water quality in Melana River, Johor was carried out in three consecutive months (March - May 2012). This study aims to determine the comparative results through biological monitoring as well as conventional method (physical and chemical analysis). Assessment is carried out through collection and identification of the biological indicator which comprises of macrobenthos based on Biological Water Quality Index (BWQI). Comparison was done based on two methods namely invertebrate analysis and also laboratory analysis. For invertebrate analysis, Melana River consist of three types of Family groups namely Nymphs, Larvae and Molluscs. The result for Water Quality Index (WQI) and also Biological Water Quality Index (BWQI) analysis showed that the level of Melana River is polluted and classified in Class III. This study shows that even though different methods were used, the similar results were obtained for both rivers and can be applied to any river to identify their level of cleanliness.

Keywords: Melana River, benthic macroinvertebrate, Water Quality Index, Biological Water Quality Index

Abstrak

Satu kajian kualiti air di Sungai Melana, Johor telah dijalankan dalam tiga bulan berturut-turut (Mac - Mei 2012). Tujuan kajian ini dijalankan adalah untuk melihat perbandingan hasil melalui kaedah pemonitoran biologi serta konvensional (analisis fizikal dan kimia). Penilaian dijalankan melalui pengumpulan dan mengenal pasti penunjuk biologi yang terdiri daripada makrobentos berdasarkan Indeks Kualiti Air Biologi (BWQI). Perbandingan telah dilakukan berdasarkan kepada dua kaedah iaitu invertebrat analisis dan juga analisis makmal. Untuk analisis invertebrat, Sungai Melana terdiri daripada tiga jenis kumpulan Famili iaitu Nimfa, Larva dan Moluska. Hasil analisis Indeks Kualiti Air (WQI) dan Indeks Kualiti Air Biologi (BWQI) menunjukkan bahawa tahap Sungai Melana adalah tercemar dan dikelaskan dalam Kelas III. Kajian ini menunjukkan bahawa walaupun kaedah yang berbeza telah digunakan, hasil yang sama telah diperolehi bagi kedua-dua sungai dan boleh digunakan untuk mana-mana sungai bagi mengenal pasti tahap kebersihan sungai tersebut.

Kata kunci: Sungai Melana, bentik makroinvertebrat, Indeks Kualiti Air, Indeks Kualiti Air Biologi

Introduction

The purpose of this paper is to determine the effectiveness of the method using macrobenthos as biological indicator in determining the level of water pollution in terms of assessment and results and compared with conventional methods commonly used. This method is taken as an alternative way for determining the level of pollution of a river. The results of this study can help in reducing river pollution by increasing public awareness among the community.

River rehabilitation program has become an important issue for water authorities and river manager in many countries throughout the world. Term 'rehabilitation' is referring to reinstatement of feature of the river ecosystem, be it structural or functional; that may have been impaired or lost [1]. The objective for river rehabilitation program is for protection against flood, nature development to enhance the amenity and recreational potentials of a river, and improvement of reverie fish habitats and communities to improve water quality [2]. The implementation of river rehabilitation program has shown positive effect and significantly improved the water quality conditions of our stream and river, at the same time enhance the amenity and landscapes of the riverside.

River water quality monitoring is important in achieving the objectives of river rehabilitation program. Water quality data were used to determine the water quality status whether in clean, slightly polluted or polluted category and to classify the rivers in Class I, II, III, IV or V based on Water Quality Index (WQI) every year. Water Quality Index (WQI) is computed based on six main parameters which are Biochemical Oxygen Demand (BOD), Chemical Oxygen Demand (COD), Ammonia Nitrogen (AN), Acidic and Alkaline (pH), Dissolved Oxygen (DO) and Total Suspended Solids (TSS). In addition, river water quality status also can be determined by using macrobenthos based on Biological Water Quality Index (BWQI). The reason in choosing macrobenthos as the indicator because they are varying in their adaptation to environmental conditions and their tolerance of sensitivity to pollution and can be used to reflect environmental quality. Besides, water quality status also can be predicted using water quality modeling. The main objective of water quality modeling is to describe and predict the observed effects of a change in the river system [3].

Materials and Methods

Study Area

This study is located at Melana River catchment (Figure 1). This river started from Gunung Pulai until Skudai River reach at Taman Perling district of Johor Bahru. Melana River is one of network in Skudai River basin. This watershed is located in Mutiara Rini area, Skudai in Johor Bahru district. The area of Melana watershed is about 22.92 km^2 with many changes occurred in this area because of vast development. Many housing area and light industry being constructed in this watershed such as Taman Teratai, Taman Universiti, Taman Mutiara Rini, Taman Sri Pulai, and Taman Pulai Perdana to cater the increasing of population. The river substrates were mainly muddy type with murky and smelly water.

Methodology

A rectangular dip net with 500µ mesh size attached with long pole was used to collect the macrobenthos. Dip net was placed resting on the river bed with the opening mesh against the current flow. The substrates were disturbed and rock and boulders were rubbed by hand in order to dislodge the organisms. Samples collected were put into polyethelene bottles and preserved with 70% alcohol for further analysis in laboratory using light microscopy. In the laboratory, speciments were washed with tap water, sorted, enumerated and identified. Finally, samples were analysed and calculated according to Biological Water Quality Index, BWQI [4], as shown below:

$$BWQI = \Sigma S / \Sigma J \quad (1)$$

where:

BWQI = Biological Water Quality Index,
S = Total score,
J = Number of animal type

River morphology and water quality parameters (temperature, conductivity, depth, width, DO and pH) were measured in-situ. Dissolved oxygen and pH were determined using YSI 55 Proplus meter (Multi sensor) while others (BOD, COD, TSS and AN) were analysed in laboratory. These parameters were then calculated to obtain the water quality index based on equation below:

$$WQI = 0.22*SIDO + 0.19*SIBOD + 0.16*SICOD + 0.15* SIAN +0.16*SISS + 0.12*SipH \quad (2)$$

where:

WQI = Water Quality Index,
DO = Dissolved oxygen,
BOD = Biochemical oxygen demand,
COD = Chemical oxygen demand,
AN = Ammonia Nitrogen,
SS = Suspended solids,
pH = acidic value

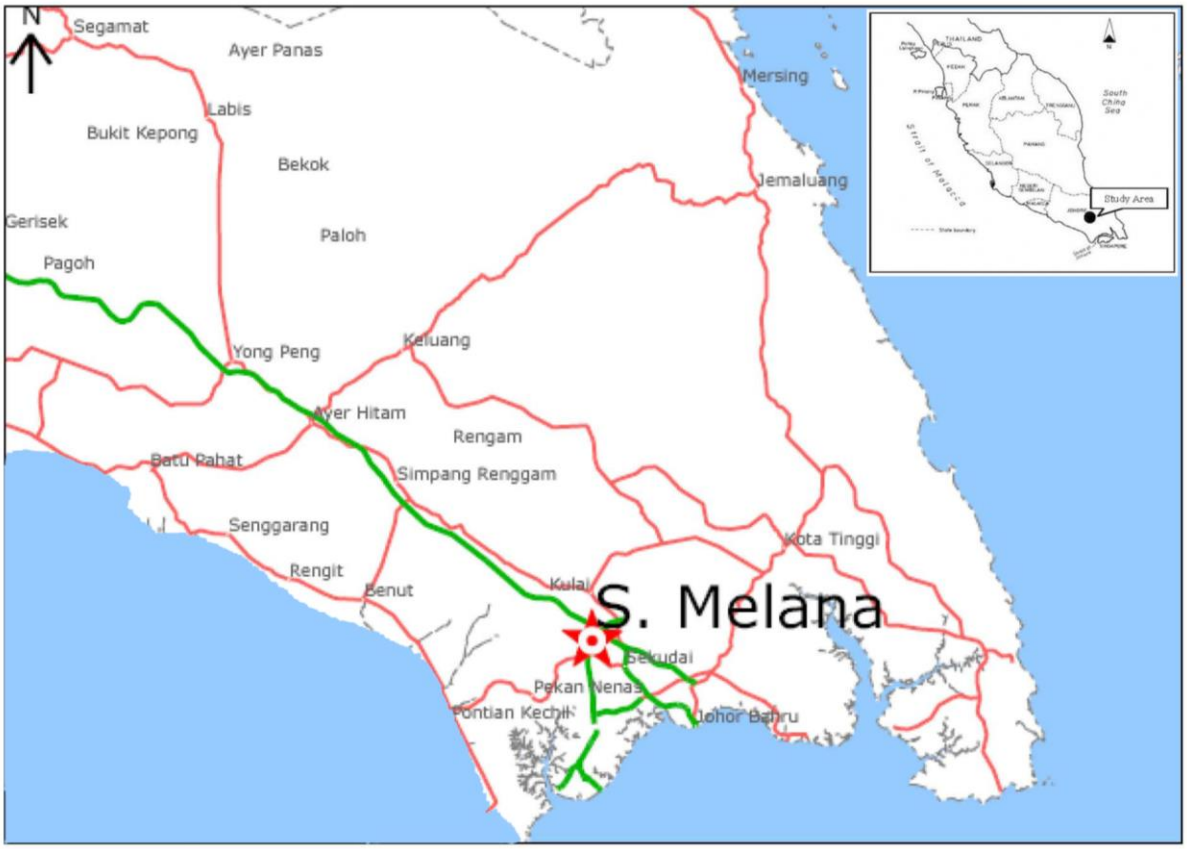


Figure 1. Study area of Melana River, Johor

Results and Discussion

Physico-chemical Water Quality

Dissolved Oxygen (DO) is the most important parameter in classifying a river's class in WQI. Based on the coefficient of DO, it influence the water quality index by 22% [5]. When the value of DO is lower, WQI tends to have lower value and if the value of DO is higher, it is vice versa. The average DO recorded for Melana River was 3.16 mg/L. The highest concentration of DO (4.07 mg/L) was recorded on April at Station 3 whereas the lowest DO

(2.33 mg/L) was on March at Station 2. The value of DO depends on the activities at those stations. The town area is the main cause of the depletion of DO content in the river due to the high organic pollutants released from the town center. The rubbish, detergent, grease as well as suspended solids tend to accumulate on the surface of the river which directly affects the surrounding oxygen from dissolving into the river. According to [6] during high tide, the flow of the river is stronger and faster therefore more oxygen can easily dissolve in the water, making DO concentration higher compared to during low tide where the flow is quite stagnant.

BOD is related to the dissolved oxygen content in the river and is the main indicator of the organic pollution in the river. A decrease in the DO value usually denotes an increase in the BOD value. BOD is also the second most important parameter in classifying a river in the Water Quality Index as it holds 19% of the classification [5]. Based on study conducted, the average concentration of BOD for Melana River was 13.16 mg/L. The highest BOD (16.47 mg/L) was observed on March at Station 2 while the lowest BOD (10.14 mg/L) was on May at Station 1. BOD concentration was higher in Melana River due to the commercial activities as well as the residential areas along the river. The untreated sewage from squatters and food waste which is disposed directly into the river will also increase the BOD content in the river [7].

The accountability of Chemical Oxygen Demand (COD) to the WQI is the third most important parameter when determining a river's WQI as it takes up 16% together with suspended solid (SS) [5]. Generally, the average value for COD in rivers are usually ranged from 0 to 150mg/L. This study found that the average COD concentration for Melana River was 33.3 mg/L. The highest COD was recorded on May at Station 2 with 40.6 mg/L while the lowest COD was 24.0 mg/L on April at Station 1. This result indicated that there were much organic substances which are non-biodegradable and reactive. Even domestic waste also contributes to high COD content. All these effluents are toxic and harmful to living things [7].

Total Suspended Solid (TSS) contribute 16% of the amount to the value of WQI. TSS include all the suspended particle which will not pass through the filter paper during the laboratory experiment in determining the TSS. The average of TSS for Melana River was 44.3 mg/L. The highest TSS was on March at Station 3 (132.5 mg/L) meanwhile the lowest (2.6 mg/L) was on April at Station 1. Significant difference in the value of the two month period is influenced by rainfall factor. Sampling in March was done in rainy season. Rain cause water to carry any particle on land into the river, thus contribute in increasing of suspended solid in river.

Ammonia Nitrogen (NH_3N) contribute 15% of the amount to the value of WQI. One of the sources of NH_3N in a river is come from the microbial degradation of nitrogenous organic material. The other sources of this compound are come from the sewerage treatment plant, the using of fertilizer for agriculture as well as other by products which flow into the river. The average NH_3N for Melana River was 2.86 mg/L. The highest NH_3N obtained was 3.72 mg/L at Station 3 while the lowest was 1.47 mg/L at Station 1. The level of NH_3N significantly increase as it meets with connecting tributaries and drains indicating that the pollutant carried by them is very high.

Biological Water Quality Index (BWQI)

Using the macrobenthos as a biological indicator is another way in determining the class and status of river. This method classified the river based on the Biological Water Quality Index (BWQI). The analysis of macrobenthos as a biological indicator is an easy, fast and low cost method. Anyone can do it due to this method does not need any special tools. This method requires collecting of macrobenthos at the river with appropiate tools for safety and environmental purpose, and stored it for further identification. The identification on types of macrobenthos is based on the Identification Index as provided by Jabatan Pengairan dan Saliran Malaysia. Table 1 shows the status of Melana River based on macroinvertebrate analysis.

This study found that, there were four types of macrobenthos with three family groups which were Nymphs, Larvae and Molluscs populated at vicinity of Melana River. The types of macrobenthos were dragonfly nymphs, rat-tailed maggots, mosquito larvae as category as other fly larvae and pagoda snails. All those types of macrobenthos can live in clean and average river water. Family group Larvae got the highest score of macrobenthos with the value of 8. The rat-tailed maggots and mosquito larvae were grouped in same family. Rat-tailed maggots breathe fresh air through long extending 'tails' for their survival. Dragonfly nymphs and pagoda snails shared the same score with

the value of 3. However, the dragonfly nymphs belong to the nymphs family meanwhile pagoda snails belongs to molluscs family. Dragonfly nymphs are very active hunters with large jaws. They feed on insect, tadpoles and even small fish, and are probably important natural pest controllers of animals such as mosquitoes and blackflies. The pagoda snails from molluscs family were collected with 5 individuals. Pagoda snails are shell animal that survive by eating plant.

Table 1. Classification of water quality in Melana River, Johor based on biological index

Total Score	Number of Animals Type	BWQI	Class	Status
20	4	5.0	III	Rather dirty - average

Water Quality Index (WQI)

Water Quality Index (WQI) is used to classify the class and status of river. The value of WQI depends on the value of the sub index for each parameter. According to Table 2, Melana River was classed in Class III with status as polluted river based on WQI. There are many factors contributing to the water pollution of Melana River either from point source or non-point source. Sewerage treatment plant is one of the point source contributing pollution to Melana River. The discharge of sewerage treatment plant that has contaminant entered the river, cause changes in the ecosystem of the river. Furthermore, Melana River is sourrounded by residential area, sewerage treatment plant, and also the huge industrial area at the downstream of rivers. The materials used for the enrichment plant would normally flow and seep into the ground and then into rivers. The major source of pollution is from animal manure, agricultural and domestic waste. Surface runoff from the heavy rains act as non-point source pollution to the Melana River as the surface runoff carried contaminant with it before entering the river.

Table 2. Classification of water quality in Melana River, Johor based on water quality index

SIDO	SIBOD	SICOD	SISS	SIAN	SIpH	WQI	Class	Status
48	51	62	14	75	99	56	III	Polluted

Conclusion

As a whole, Melana River can be categorized as polluted or Class III based on the assessment of Water Quality Index (WQI) and Biological Water Quality Index (BWQI). The level of pollution at this river was found affected by its surrounding. From the observation, many activities contribute to river pollution such as industrial, commercial and residential activities. On the other hand, by using biological monitoring can give the information on biological conditions of water body which is consist of survey or other direct measurement for aquatic life. Based on group of macrobenthos sampled, the composition of macrobenthos as biological indicator is very important to determine the level of river pollution because macrobenthos live in water for all or most of their life and they only live in area which suitable for their survival. From the macrobenthos analysis, Larvae were major group of macrobenthos found along the Melana River.

Acknowledgement

We would like to express our appreciation to Ministry of Higher Education, MOHE (No. Q.J130000.7122.00H99) and Universiti Teknologi Malaysia (UTM) for the financial support of this research. We are also indebted to laboratory staff for their assistance during the sampling.

References

1. Cottinham P., Bond N., Lake P.S. and Outhet D. (2005) Recent lessons on river rehabilitation in eastern Australia. Technical report, CRCFE, Canberra.
2. Nienhuis, P. H. & R. S. E. W. Leuven (2001). River restoration and flood protection: controversy or synergism. *Hydrobiologia* 444: 85–99.
3. IPASA (2008). Water Quality Models in River Management. Institute of Environmental and Water Resource Management. Universiti Teknologi Malaysia.
4. Jabatan Pengairan dan Saliran (1996). Towards the Making of River Rich in Nature. Foundation for riverfront improvement and restoration, Kuala Lumpur.
5. DOE (1986). Classification of Malaysian Rivers. Department of Environment, Malaysia
6. Sholkovitz, R.R. (1985). Redox Related Geochemical in Lakes: Alkali Metals, Alkaline Earth Element and 137Cs. In Stum, W. Chemical Processes in Lakes. John Wiley, New York.
7. Lung, D.S. (2001). *Kajian Kualiti Air Sungai Kempas*. Universiti Teknologi Malaysia, Johor Bahru: Projek Sarjana Muda Kejuruteraan Awam.

The Malaysian Journal of ANALYTICAL SCIENCES
ISSN 1394-2506

DISCRIMINATION OF BLACK BALLPOINT PEN INKS BY HIGH PERFORMANCE LIQUID CHROMATOGRAPHY (HPLC)

(Diskriminasi Pen Mata Bola Berdakwat Hitam Menggunakan Kromatografi Cecair Berprestasi Tinggi)

Mohamed Izzharif Abdul Halim*, Norashikin Saim, Rozita Osman, Halila Jasmani, Nurul Nadhirah Zainal Abidin

Faculty of Applied Sciences
Universiti Teknologi MARA, 40450 Shah Alam,Selangor

**Corresponding author: izzharif@salam.uitm.edu.my*

Abstract

In this study, thirteen types of black ballpoint pen inks of three major brands were analyzed using high performance liquid chromatography (HPLC). Separation of the ink components was achieved using Bondapak C-18 column with gradient elution using water, ethanol and ethyl acetate. The chromatographic data obtained at wavelength 254.8nm was analyzed using agglomerative hierarchical clustering (AHC) and principle component analysis (PCA). AHC was able to group the inks into three clusters. This result was supported by PCA, whereby distinct separation of the three different brands was achieved. Therefore, HPLC in combination with chemometric methods may be a valuable tool for the analysis of black ballpoint pen inks for forensic purposes.

Keywords: ballpoint inks, principle component analysis, HPLC, chemometric

Abstrak

Dalam kajian ini, tiga belas jenis dakwat pen mata bulat daripada tiga jenama di analisis menggunakan kromatografi cecair prestasi tinggi (HPLC). Pemisahan komponen-komponen dakwat diperolehi menggunakan turus "Bondapak C-18" secara elusi berperingkat mengunakan kombinasi air, etanol dan etil asetat. Data kromatografi yang diperolehi pada panjang gelombang 254.8 nm dianalisis menggunakan pengelompokan hierarki agglomerative, (AHC) dan analisis komponen prinsip, (PCA). AHC membolehkan sample dakwat dikelaskan kepada tiga kelompok. Hasil daripada analisis AHC disokong oleh PCA yang juga menunjukkan pemisahan yang jelas bagi tiga kelompok mengikut jenama. Oleh itu, gabungan di antara HPLC dengan kaedah kemometrik merupakan teknik yg berguna untuk analisis dakwat pen mata bulat bagi tujuan forensik.

Kata kunci: dakwat pen mata bulat, analisis komponen prinsip, HPLC, kimometrik

Introduction

Over recent years, technological developments have rapidly expanded the range of pen designs and ink composition used throughout the world [1].Quill and nib pens have given way to other classes of writing instruments such as the ballpoint, roller ball and gel pens which have different requirements for the properties of their writing inks [2]. These inks may contain many substances aiming to improve ink characteristic [3]. Although all black ballpoint pen inks may look the same, there can be some important differences in their chemical composition, constituent and substances. This study emphasizes on black ballpoint pen inks available in Malaysian market as these pens are often used in the occasion of signing important documents. Black ballpoint pen inks are also used in documents with significant financial value like checks, insurance claims, wills, contract and tax return [4]. The examination of inks is often performed to evaluate the authenticity of these document. A ballpoint pen ink consists of synthetic dyes in (acidic and/or basic), pigments (organic and/or inorganic) and a range of additives [5]. Inks of similar color may consist of different dye composition and are frequently the subjects of forensic examinations. The inks can be discriminated by non-destructive or destructive methods [3, 6] depending on whether a sample needs to be taken

from the document, a process that would alter it. Destructive methods include high performance liquid chromatography (HPLC), thin layer chromatography (TLC), capillary electrophoresis (CE), gas chromatography/mass spectroscopy (GC/MS) and fourier transform infrared (FTIR) Spectroscopy [2,3,6]. Non-destructive methods include scanning electron microscopy (SEM), video spectral comparative (VSC) and Raman Spectroscopy [3,6,7]. In this study, HPLC was used as this method is able to provide detailed information regarding the components of the inks. The data obtained was subjected to chemometric methods as these techniques allow the extraction of more information based on the similarities and differences among samples in a data set [8]. The application of chemometric techniques such as agglomerative hierarchical clustering (AHC) and principle component analysis (PCA) helps in the interpretation of complex chromatographic data sets to better understanding of the studied subject. The goal of AHC is to identify relatively similar, that is, homogeneous, group of objects (ink samples) in the space of measured features. Combination of PCA and AHC could be used to investigate the measurable variability between the same colors of pens of different brands by matching the ink's components provided in the chromatograms.

Materials and Methods

Chemicals and Reagents

Ethanol 95% was purchased from Merck (Darmstadt, Germany), Ethyl acetate and acetone were obtained from System (ChemAR).

Samples

Thirteen black ballpoint pens of three major brands consisting of different types were purchased from local stores (Table 1).

Table 1. Types of pens from three major brands

Sample	Brand	Type
CbH1	CARERA	Carera B3 II
CbH2	CARERA	Carera B7
CbH3	CARERA	Carera B8
CbH4	CARERA	Carera B6
SbH1	STABILO	Stabilo galaxy 818 F
SbH2	STABILO	Stabilo liner 308 F
SbH3	STABILO	Stabilo liner 308 M
SbH4	STABILO	Stabilo galaxy 818 XF
SbH5	STABILO	Stabilo Point 88
PbH1	PILOT	Pilot BP – SF
PbH2	PILOT	Pilot BP – SM
PbH3	PILOT	Pilot supergrip M
PbH4	PILOT	Pilot supergrip F

Sample preparation
Ink samples were obtained by cutting 1.0 cm of each ink barrel. Each ink barrel was placed into different vial and 5 ml of ethanol was added into each vial. The sample was sonicated for about 15minutes and the solution was analyzed by HPLC.

High Performance Liquid Chromatography (HPLC)
The gradient elution employed for HPLC separation is shown in the Table 2. The column used was µ Bondapak C-18, 30 cm x 3.9mm. Detection was done by a dual wavelength UV monitoring at 254.8 nm.

Table 2. Gradient elution for HPLC system

Time range	Solvent Composition	Flow Rate	Temperature
0 min – 8 min	water-ethanol-ethyl acetate (55:40:5)	1.0ml/min	27 ˚C
8 min – 13 min	water-ethanol-ethyl acetate (40:40:20)	1.0ml/min	27 ˚C
13 min – 25 min	water-ethanol-ethyl acetate (35:40:25)	1.5ml/min	27 ˚C

Chemometric analysis of the HPLC data
The selected retention times for each sample were subjected to AHC and PCA using XLSTAT 2012 software.

Result and Discussion

Fig. 1 shows a chromatogram obtained from one of the ink samples. Major components selected (based on retention times) in black ballpoint pen inks are shown in the Table 3.

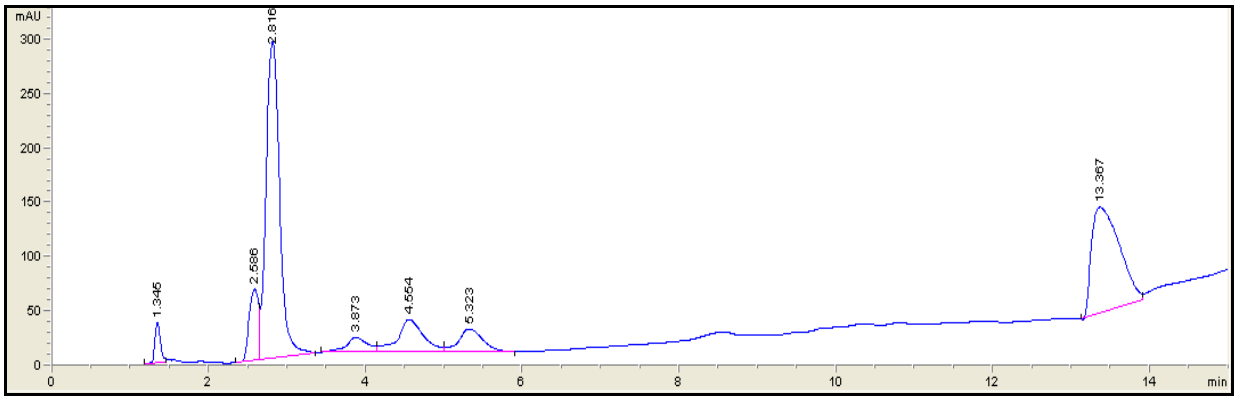


Figure 1. Chromatogram of ink sample (PbH4)

Table 3. Major components selected for chemometric analysis

Retention time range	Assigned component name
1.2 – 1.5 min	Component A
2.1 – 2.3 min	Component B
2.3 – 2.6 min	Component C
2.6 – 2.9 min	Component D
3.6 – 3.9 min	Component E
4.3 – 4.6 min	Component F
5.0 – 5.3 min	Component G
5.3 – 5.6 min	Component H
11.8– 12.0 min	Component I
12.0 – 15.0 min	Component J

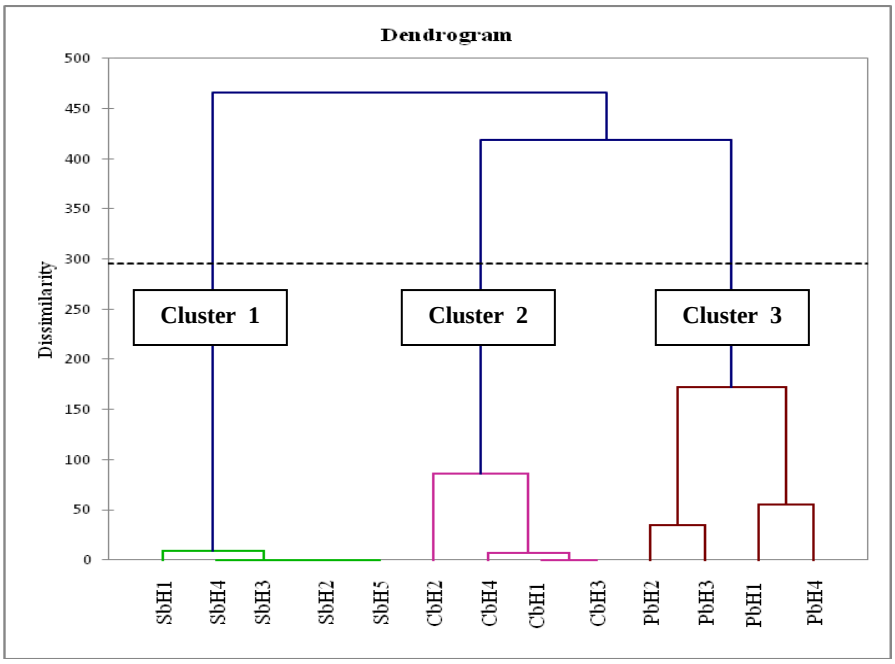


Figure 2. Dendrogram of inks samples based on HPLC data.

Agglomerative Hierarchichal Clustering (AHC)

AHC is a process of subdividing a set of entities into subsets in which the members are similar to each other, but different from members of other subsets. A shown in the dendogram in Figure 2, three clusters representing the three brands of inks were obtained. The various types of inks from Stabilo pens were grouped in cluster 1. Cluster 2 and 3 are formed by inks from Carera and Pilot pens, respectively. Therefore, the AHC analysis on the HPLC chromatogram data indicates that this approach is suitable to classify inks of different brands.

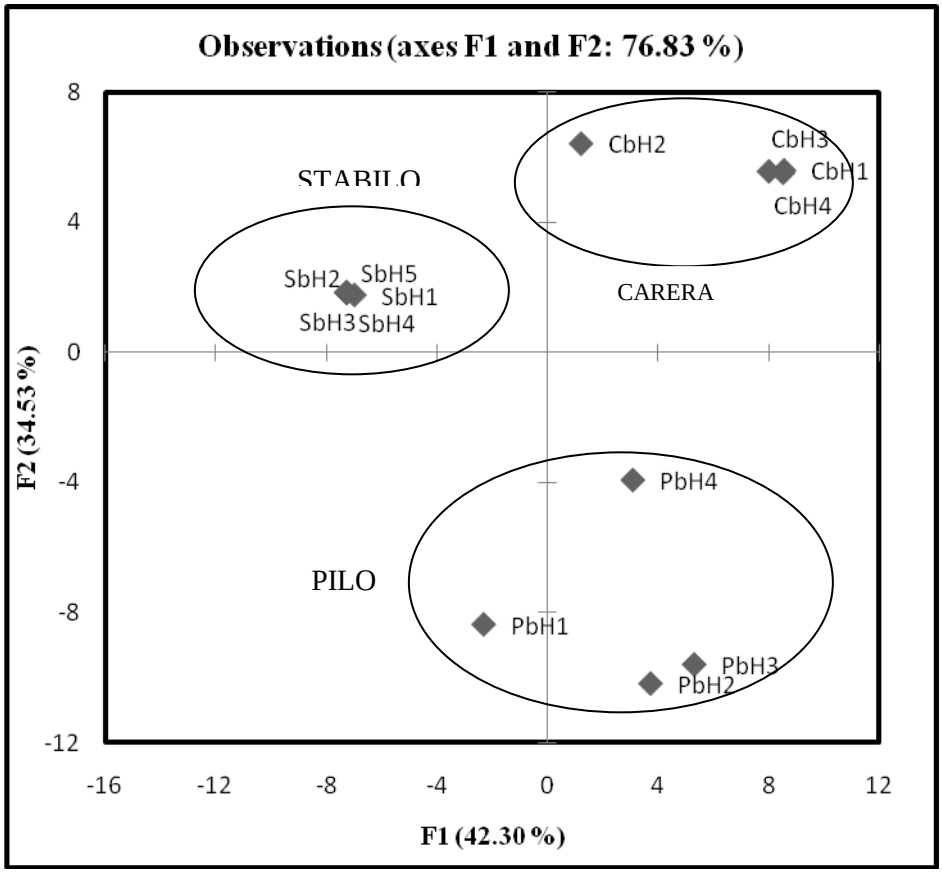


Figure 3. Score plot of F1 versus F2

Principal component analysis (PCA)

Principal component analysis provides information on the most meaningful parameters that describe the whole data sets rendering data reduction with a minimum loss of original information [9]. The PCA technique allowed the identification of an association between variables, thus reducing the dimensionality of the data sets. It is a powerful technique for pattern recognition that attempts to explain the variance of a large set of inter-correlated variables and transform them into a smaller set of independent (uncorrelated) variables (principal components). Based on the eigenvalue criterion, only the PCs with eigenvalue greater than one are considered important. This criterion is based on the fact that the average eigenvalue of the autoscaled data is just one [10].

PCA analysis, applied to HPLC inks sample datasets, resulted in three latent factors explaining 76.83% of the total variance. Figure 3 shows the PCA scores plot obtained showing a clear separation of ink samples from different brands for the first two principle components (F1 and F2). All the Stabilo inks are clustered in the left region of the

plot. Most of the Carera inks are grouped in the upper-right region, white Pilot inks are clustered together in the lower-right part of the plot. The results are strongly supported the AHC analysis discussed earlier.

Conclusion

In this study, the application of chemometric techniques (agglomerative hierarchical clustering and principle component analysis) on HPLC data can successfully evaluate the variations of thirteen types of black ballpoint pen inks of different brands. These results suggest that the HPLC profile of inks of different brands differ due to their similarities and differences in the chemical compositions. AHC grouped the various types of inks into three clusters of similar ink component's characteristic of each brand. The results concurred with the PCA. Combination of HPLC and chemometric techniques provided a more objective interpretation of the results for the analysis of black ballpoint pen inks for forensic purposes.

Acknowledgement

The authors would like to acknowledge the financial support obtained from Ministry of Higher Education (MOHE), Malaysia for this project (Project number: 600-RMI/ST/FRGS/5.3.Fst/6/2010) and Universiti Teknologi MARA.

References

1. Adam, C.D., Sheratt, S.L. & Zholobenko, V.L. (2008). Classification and individualization of black ballpoint pen inks using principle component analysis of UV-vis absorption spectra. *Forensic Science International,* 174(1): 16-25.
2. Wahab Williams, M.R., Moody, C., Arceneaux, L.A., Rinke, C., White, K. & Sigman, M.E. (2009). Analysis of black writing ink by electrospray ionization mass spectrometry. *Forensic Science International,* 191(1-3): 97-103.
3. Thanasoulias, N.C., Parisis, N.A. & Evmirids, N.P. (2003). Multivariate chemometrics for the forensic discrimination of blue ball-point pen inks based on their Vis Spectra. *Forensic Science International,* 138(1-3): 75-84.
4. Djozan, D., Baheri, T., Karimian, G. & Shahidi, M. (2008). Application of the micro–FTIR spectroscopy, Raman spectroscopy and XRF method examination of inks. *Forensic Science International,* 158(2-3): 164-172.
5. Denman, J. A., Skinner, W.M., Kirkbride, K..P. & Kempson, I.M. (2010). Organic and inorganic discrimination of ballpoint pen inks by ToF-SIMS and multivariate statistics. *Applied Surface Science*, 256(7): 2155–2163.
6. Dirwono, W., Park, J.S., Agustin-Camacho, M.R., Kim, J., Park, H-M., Lee, Y. & Lee, K-B. (2010). Application of micro-attenuated total reflectance FTIR spectroscopy in the forensic study of questioned documents involving red seal inks. *Forensic Science International,* 199(1-3): 6-8.
7. Senvaitiene, J. & Beganskiene and Kareiva, A. (2005). Spectroscopic evaluation and characterization of different historical writing inks. *Vibrational Spectroscopy*, 37(1): 61-67.
8. Gallidabino, M., Weyermann, C. & Marquis, R. (2011). Differentiation of blue ballpoint pen inks by positive and negative mode LDI-MS. *Forensic Science International,* 204(1-3): 169-178.
9. Kowalkowski, T., Zbytniewski, R., Szpejna, J. & Buszewski, B. (2006). Application of chemometrics in river water classification. *Water Research*, 40(4): 744-752.

The Malaysian Journal of ANALYTICAL SCIENCES ISSN 1394-2506

PENENTUAN SIFAT KEFUNGSIAN SERBUK RUMPAI LAUT *KAPPAPHYCUS ALVAREZII*

(Determination of the functional properties of *Kappaphycus alvarezii* seaweed powder)

Sjamsiah[1,2*], Nazaruddin Ramli[1,3], Rusli Daik[1], Mohd. Ambar Yarmo[1]

[1]*Pusat Pengajian Sains Kimia dan Teknologi Makanan, Fakulti Sains dan Teknologi*
Universiti Kebangsaan Malaysia, 43000 UKM Bangi, Selangor D.E.
[2]*Jurusan Kimia, Fakultas Sains dan Teknologi*
Universitas Islam Negeri Alauddin Makassar, Indonesia
[3]*Pusat Innovasi Teknologi Manisan (MANIS), Fakulti Sains dan Teknologi*
Universiti Kebangsaan Malaysia, 43000 UKM Bangi, Selangor D.E.

**Corresponding author: sjamsiahuca@yahoo.com*

Abstrak

Serbuk rumpai laut *Kappaphycus alvarezii* yang diperolehi secara pengeringan semburan (SD), sejuk-beku (FD) dan pengeringan cahaya matahari (SND) telah ditentukan sifat kefungsiannya iaitu keupayaan membengkak (SWC), keupayaan memegang air (WHC), keupayaan memegang minyak (OHC), kelikatan dan kekuatan gel. Hasil kajian memperlihatkan bahawa serbuk rumpai laut *Kappaphycus alvarezii* yang diperolehi secara FD dan SND mempunyai keupayaan membengkak masing-masing 25 mL/g dan 50 mL/g manakala serbuk SD memberikan hasil campuran yang sekata dan sangat likat (SWC 100 mL/g). Hasil penentuan WHC serbuk SND (30.67 g/g) didapati lebih tinggi ($p<0.05$) daripada serbuk FD (21.33 g/g) dan serbuk SD (4.67 g/g). Nilai OHC serbuk FD (19.81 g/g) adalah lebih tinggi ($p<0.05$) daripada serbuk SD (5.11g/g) dan serbuk SND (4.67 g/g). Manakala nilai kelikatan serbuk FD, SND dan SD masing-masing adalah 0.22, 0.17 dan 0.06 Pa.s. Sementara itu, kekuatan gel serbuk SD (82.77 gf) adalah lebih tinggi ($p<0.05$) daripada serbuk FD (57.1 gf) dan serbuk SND (35.01 gf). Hasil penentuan sifat kefungsian ini menunjukkan bahawa serbuk SD paling berpotensi untuk diaplikasikan sebagai pengubahsuai kelikatan pada pembuatan produk minuman.

Kata kunci: pengeringan**,** serbuk rumpai laut, *Kappappycus alvarezii***,** sifat kefungsian

Abstract

Seaweed *Kappaphycus alvarezii* powder prepared by spray drying (SD), freeze drying (FD) and sun drying(SND) were determined their functional properties such as swelling capacity (SWC), water holding capacity (WHC), oil holding capacity (OHC), viscosity and gel strength. The study showed that the *Kappaphycus alvarezii* seaweed powder obtained by FD and SND have the ability to swell to 25 mL/g and 50 mL/g respectively, while the SD powder formed a homogeneous solution and it exhibited highly viscous solution (SWC 100 mL/g). The WHC of SND powder (30.67 g/g) was higher ($p<0.05$) than the FD (21.33 g/g) and SD (4.67 g/g) powders. The OHC of FD powder (19.81 g/g) was higher ($p<0.05$) than the SD (5.11g/g) and SND (4.67 g/g) powders. While the viscosity of the FD, SND and SD powders were 0.22, 0.17 and 0.06 Pa.s respectively. Meanwhile, the gel strength of the SD powder (82.77 gf) was higher ($p<0.05$) than the FD (57.1 gf) and SND (35.01 gf) powders. These results on determination of functional properties shows that the SD powder had the most potential to be applied as a viscosity modifier in the manufacturing of beverages.

Keywords: drying, seaweed powder, *Kappappycus alvarezii*, functional properties

Pengenalan

Kappahycus alvarezii adalah sejenis rumpai laut yang banyak ditanam di kawasan perairan Sabah, Malaysia. Ia merupakan komoditi yang mempunyai nilai ekonomi yang tinggi dan merupakan sumber penghasilan kappa-karagenan serta sumber penting gentian diet [1, 2]. Dalam struktur rumpai laut, polisakarida mampu mengikat air hingga 20 kali lebih besar daripada isi padunya dan keupayaan ini berkait rapat dengan struktur panjang dan tebal partikel serat rumpai laut itu [2]. Polisakarida yang memiliki afiniti tinggi terhadap air (hidrokoloid) menunjukkan

sifat kefungsian unik seperti sifat gel dan kelikatan yang berperanan penting dalam pembaikan tekstur, pembentukan gel, kelikatan dan sebagainya[2, 3].

Pada masa kini, beberapa serbuk hidrokoloid seperti gam arabik, gam xantan, karagenan dan karboksilmetil selulosa telah digunakan secara meluas di dalam industri makanan, minuman dan juga industri bukan makanan [4]. Sebagai contoh dalam industri makanan dan minuman, hidrokoloid digunakan dalam pembuatan produk jeli, sos, konfeksi, sirap, puding, dodol, makanan sejuk-beku, produk susu dan lain-lain [5, 6]. Dalam industri makanan, hidrokoloid digunakan sebagai kontrol sifat kefungsian produk makanan [7].Walaupun penggunaannya dalam jumlah kecil (0.01-2%) namun ia dapat memberikan perubahan pada tekstur produk makanan [6, 8]. Beberapa sifat kefungsian yang penting larutan hidrokoloid adalah kelikatan dan kemampuan mengikat air [8]. Selain itu, hidrokoloid juga digunakan dalam formulasi makanan sebagai penstabilan emulsi, menghindari pengkristalan ais dan pembaikan nilai sensori [8, 9].

Ciri-ciri gentian diet rumpai laut yang berkaitan dengan sifat fizikokimianya seperti keupayaan membengkak (SWC), keupayaan memegang air (WHC) dan keupayaan memegang minyak (OHC) sangat penting untuk memperbaiki sifat-sifat kefungsian di dalam makanan dan minuman [10]. Sifat kefungsian rumpai laut tersebut sangat sensitif terhadap kaedah penyediaan dan proses pengeringan [3, 11]. Oleh itu, kajian ini bertujuan untuk menentukan sifat kelikatan, kekuatan gel, keupayaan memegang air, keupayaan membengkak dan keupayaan memegang minyak serta bentuk morfologi serbuk rumpai laut *Kappaphycus alvarezii* yang dihasilkan secara pengeringan matahari, semburan dan sejuk-beku. Kajian ini akan membantu memahami hubungan antara proses pengeringan dan sifat fungsi serbuk rumpai laut *Kappaphycus alvarezii* dan juga memberikan maklumat yang bermanfaat mengenai aplikasinya dalam industri makanan.

Bahan dan Kaedah

Rumpai laut *Kappaphycus alvarezii* kering diperolehi dari kawasan perairan Sabah Malaysia. Sebelum dianalisis, rumpai laut *Kappaphycus Alvarezii* dibasuh dengan air paip yang mengalir untuk membersihkan kotoran dan bendasing seperti garam, pasir, kekerang dan lain-lain. Kemudian, ia direndam dalam air suling selama semalaman (24 jam) untuk melunturkan warna kekuningan daripada rumpai laut menjadi tidak berwarna (jernih). Seterusnya sampel ditapis dan dikeringkan di bawah cahaya matahari selama 3 hari. Rumpai laut yang telah dikeringkan dipotong kecil-kecil sebelum dikisar menggunakan pengisar tukul dengan saiz lubang penapis 3 mm, dan penapis 0.25 mm untuk mendapatkan serbuk rumpai laut yang halus. Dalam kajian ini, serbuk rumpai laut dihasilkan dengan menggunakan peralatan *spray dryer* jenama Lab Plant SD-05, England UK dan alat pengeringan sejuk beku model Epsilon 1-8 D Christ, Germany. Parameter-parameter yang digunakan dalam kajian telah diubahsuai mengikut keberkesanan proses pengeringan dan kualiti serbuk rumpai laut yang dihasilkan.

Mikroskopi Elektron Imbasan (SEM)

Mikroskopi elektron imbasan (S E M, model LEO 1450 VP Jenama LEO) digunakan untuk melihat bentuk permukaan dan saiz serbuk rumpai laut yang diperolehi dengan kaedah pengeringan matahari, semburan dan sejuk-beku.

Keupayaan membengkak (SWC)

Keupayaan membengkak (SWC) sampel rumpai laut diukur melalui penentuan isi padu lapisan (*bed volume*) selepas keseimbangan dalam pelarut berlebihan [12]. Sampel serbuk rumpai laut 100 mg dimasukkan dalam silinder 25 ml, ditambah 10 ml air suling nyah ion dan campuran dikacau secara bersungguh-sungguh. Silinder penyukat dibiarkan selama 24 jam pada suhu 25°C. Pembengkakan atau pengembangan isipadu diukur dan dinyatakan sebagai mililiter sampel bengkak per gram sampel.

Keupayaan memegang air (WHC)

Keupayaan memegang air oleh sampel serbuk rumpai laut diukur dengan kaedah pengemparan yang diubahsuai [13]. Air suling nyah ion sebanyak 10 mL ditambah ke dalam tiub pengempar bersenggat yang mengandungi100 mg sampel, kemudian digetar (150 rpm) dalam rendaman air selama 24 jam pada suhu 25°C . Pada akhir masa getaran, tiub diempar pada 10,000 rpm pada suhu 25°C selama 30 minit (menggunakan alat pengempar model Centrifuge

5810 R). Isipadu lapisan bahagian atas diukur dan keupayaan memegang air dinyatakan sebagai berat gram air yang dipegang oleh 1 gram berat sampel serbuk rumpai laut kering.

Keupayaan memegang minyak (OHC)

Keupayaan memegang minyak sampel serbuk rumpai laut ditentukan dengan kaedah yang dijelaskan oleh Capres et al. [14] dan Wong & Cheung [15] dengan sedikit pengubahsuaian. Sebanyak 150 mg sampel serbuk rumpai laut diletakkan dalam tiub emparan bersenggat dan ditambahkan minyak jagung sebanyak 10 mL. Tiub dibiarkan selama 30 minit pada suhu 25 °C dengan getaran 150 rpm. Campuran kemudiannya diempar pada 4000 rpm selama 30 minit. Lapisan minyak dikeluarkan dan isipadunya diukur. Keupayaan memegang minyak sampel serbuk rumpai laut dinyatakan sebagai gram minyak dipegang oleh 1 g sampel serbuk rumpai laut kering. Ketumpatan minyak jagung adalah 0.92 g/ml.

Kelikatan

Kelikatan diukur mengikut kaedah Monuz et al. [16]. Sampel serbuk rumpai laut 30 mg dilarutkan dalam 20 mL air suling nyah ion panas (sebaran1.5% w/v) bersuhu 90 °C dan digerak-gerakkan menggunakan pengacau magnet selama 20 minit. Kelikatan sebaran rumpai laut 1.5 % (w/v) diukur menggunakan alat Anton Paar, Physica MCR 301, kon pengukur CP50-1.

Kekuatan gel

Serbuk rumpai laut sebanyak 45 mg dilarutkan dalam 30 mL air suling nyah ion panas (larutan sebaran1.5% w/v) pada suhu 90 °C dan digerak-gerakkan menggunakan pengacau magnet selama 20 minit. Larutan yang terhasil dituang ke dalam botol kaca acuan 50 mL dengan diameter dalaman 4 cm, dibiarkan dingin kemudian disimpan dalam petisejuk pada suhu 4°C semalaman (18 jam). Analisis kekuatan gel menggunakan Texture Analyzer, Autograph, Shimadzu, dengan sebuah lekapan dan prob analisis 1 cm ditekan pada sampel hingga kedalaman 70% daripada tinggi asalnya dan kelajuan 1 mms^{-1}. Setiap pengukuran dilakukan sebanyak tiga kali.

Hasil dan Perbincangan

Mikroskopi Elektron Imbasan (SEM)

Analisis Mikroskopi Elektron Imbasan (SEM) dilakukan untuk melihat bentuk permukaan dan saiz serbuk rumpai laut yang diperolehi secara pengeringan semburan (SD), sejuk-beku (FD) dan cahaya matahari (SND). Hasil menunjukkan ketiga-tiga kaedah pengeringan memberikan bentuk permukaan serbuk yang berbeza (Rajah 1). Serbuk SD mempunyai bentuk teratur seperti bola dan berdiameter sekitar 1.5-14.2 µm. Serbuk FD dan serbuk SND mempunyai bentuk tidak teratur yang disebabkan oleh potongan pengisar yang digunakan pada proses pemerolehan serbuk halus. Namun serbuk FD mempunyai bentuk lembaran yang lebih nipis, halus dan ringan berbanding dengan serbuk SND. Hal ini mungkin disebabkan oleh proses pengeringan FD di mana sampel kering yang digunakan terlebih dahulu dibuat sebaran rumpai laut 0.5 % w/v kemudian disejuk-bekukan dan dikeringkan dengan proses pemejalwapan.

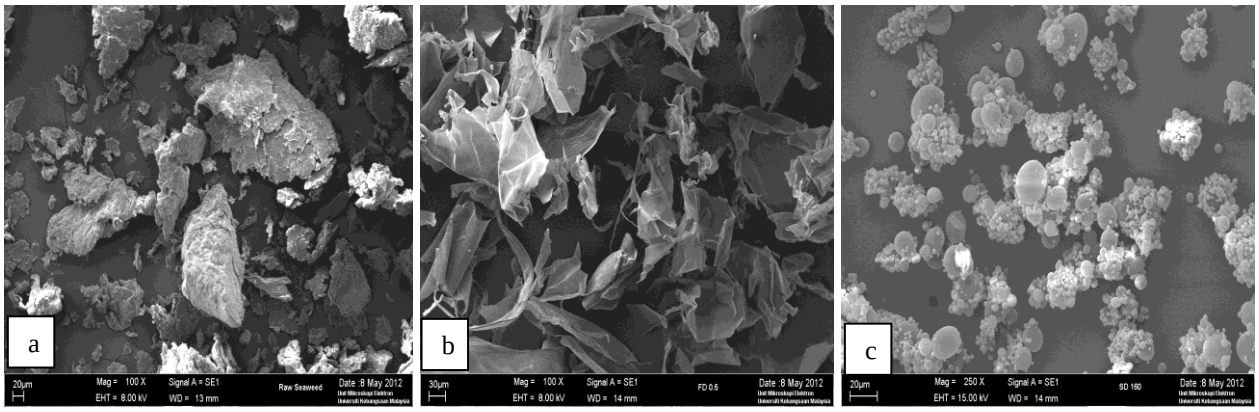
Bentuk struktur permukaan dan saiz serbuk rumpai laut *Kappapphycus alvarezii* yang diperolehi dengan kaedah pengeringan yang berbeza menunjukkan terdapatnya hubung-kait dengan sifat kefungsiannya. Hal ini sesuai dengan kajian lepas yang menyatakan bahawa keupayaan memegang air oleh polisakarida rumpai laut berkait rapat dengan struktur panjang dan tebal partikel serat rumpai laut [2].

Sifat kefungsian

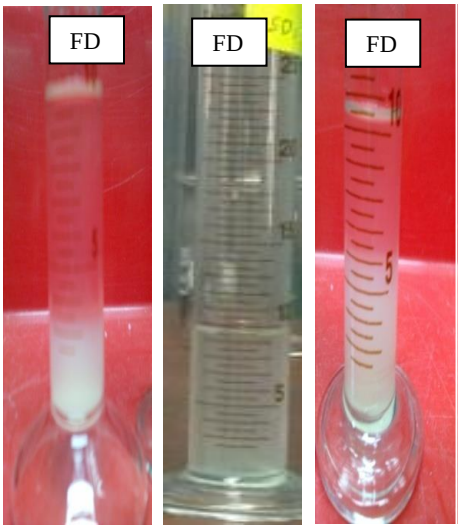
Secara amnya, serbuk rumpai laut yang kaya serat ditentukan sifat penghidratannya, SWC (*swelling capacity*), WHC (*water holding capacity*) dan OHC (*oil holding capacity*) [10]. Hasil kajian sifat SWC ditunjukkan pada Rajah 2, di mana serbuk SD memperlihatkan suatu campuran yang sekata dan likat sehingga boleh dikatakan bahawa serbuk SD mempunyai nilai SWC 100 mL/g. Sementara itu, sebaran serbuk rumpai laut FD dan SND memperlihatkan ada lapisan bahagian bawah yang membengkak. Rajah 3 menunjukkan nilai SWC serbuk SD (100 mL/g) paling tinggi berbanding serbuk SND (50 mL/g) dan serbuk FD (25mL/g).

Sifat WHC dan OHC serbuk rumpai laut ditunjukkan pada Rajah 4. Hasil pengamatan menunjukkan WHC serbuk SND (30.67 g/g) lebih tinggi daripada serbuk FD (21.33 g/g) dan serbuk FD lebih tinggi daripada serbuk SD (4.67

g/g). Manakala sifat fungsi OHC serbuk FD (19.81 g/g) lebih tinggi daripada serbuk SD (5.11 g/g) dan serbuk SD lebih tinggi daripada serbuk SND (4.67 g/g). OHC adalah sifat fungsi bahan makanan yang digunakan dalam formulasi makanan. Serbuk rumpai laut dengan nilai OHC yang tinggi memberikan kestabilan ke atas emulsi dan makanan yang berlemak tinggi [9, 15].



Rajah 1. SEM serbuk rumpai laut *Kappaphycus alvarezii* keringan matahari (a), sejuk-beku (b) pada pembesaran 100x dan semburan (c) pada pembesaran 250x

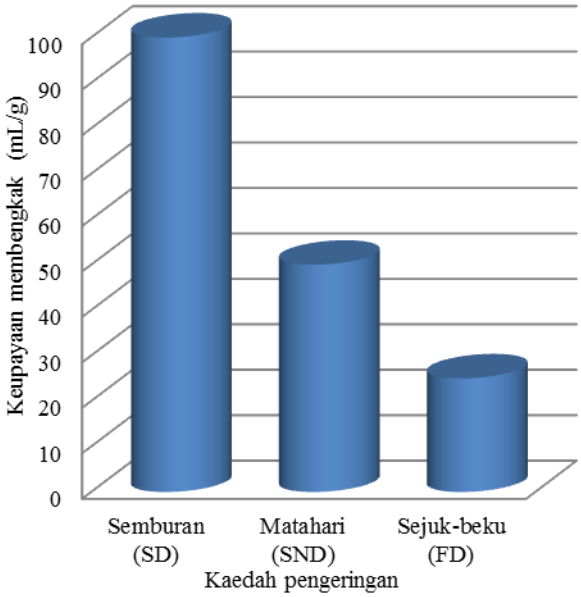


Rajah 2. Sebaran rumpai laut 1 % w/v membentuk *swelling* (bengkak)

Hasil kajian sifat fungsi SWC, WHC dan OHC daripada serbuk rumpai laut *Kappaphycus alvarezii* yang diperolehi secara SD, FD dan SND telah memberikan nilai yang berbeza. Hal ini disebabkan oleh bentuk permukaan dan saiz serbuk rumpai laut yang berbeza. Untuk nilai SWC yang tertinggi dimiliki oleh serbuk SD di mana bentuk butiran serbuk SD menyerupai bola yang seragam serta mempunyai saiz diameter kecil (1.5 µm) yang banyak sehingga

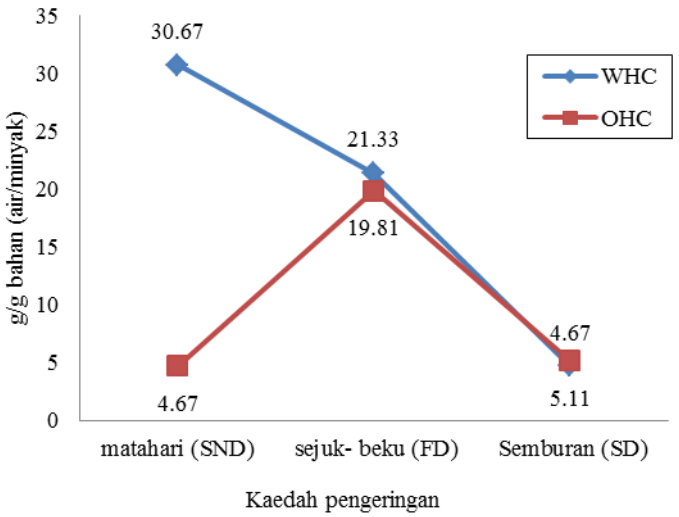
mampu menyerap air secara rata dan membengkak kemudian seterusnya membentuk larutan yang sangat likat. Manakala nilai WHC yang tertinggi adalah serbuk SND di mana bentuk dan saiz partikel serbuk SND lebih tebal dan panjang sehingga mampu memegang air lebih banyak. Hasil kajian mendapati bahawa semakin tebal dan panjang partikel serat rumpai laut maka semakin tinggi keupayaan memegang air. Sementara itu, serbuk FD memberi nilai OHC yang tertinggi. Pada dasarnya mekanisme OHC disebabkan oleh pemerangkapan fizikal minyak oleh tarikan kapilari [17]. Selain itu, menurut Elleuch et al. [9] sifat OHC adalah berkaitan dengan sifat-sifat permukaan, ketumpatan, juzuk lipofilik dan hidrofilik.

Beberapa kajian lepas melaporkan bahawa nilai-nilai fungsi SWC, WHC dan OHC sukar untuk dibandingkan antara satu rumpai laut dengan yang lain disebabkan mereka tergantung pada kaedah penyediaan sampel, kaedah pengeringan, saiz dan keporosan sampel serta keadaan eksperimen (masa, suhu dan kadar pengemparan) [9, 10, 15].

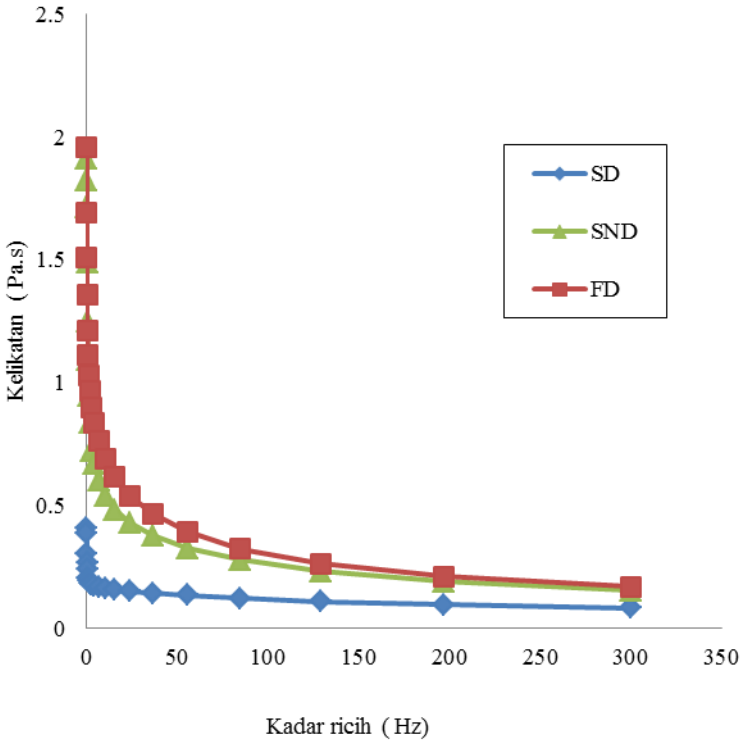


Rajah 3. Keupayaan membengkak serbuk rumpai laut *Kappaphycus alvarezii*

Hasil pengukuran kelikatan sebaran rumpai laut *Kappaphycus Alvarezii* 1.5% w/v ditunjukkan pada Rajah 5. Sifat aliran sebaran rumpai laut *Kappaphycus Alvarezii* 1.5 %w/v menurun dengan meningkatnya kadar ricih. Ini menandakan bahawa aliran bersifat pseudoplastik (penipisan ricih). Kelikatan serbuk FD pada kadar ricih 100 Hz, suhu 25°C (0.22 Pa.s) lebih tinggi daripada serbuk SND (0.17 Pa.s) dan serbuk SND lebih tinggi daripada serbuk SD (0.06 Pa.s).. Ini kemungkinan disebabkan adanya perlakuan suhu tinggi pada pengeringan semburan yang boleh merosakkan struktur biopolimer, seperti yang dilaporkan oleh [3] bahawa suhu udara masuk dan kelajuan penggabus yang tinggi pada pengeringan semburan mempunyai sifat kelikatan dan penipisan kadar ricih yang kecil. Suhu udara masuk yang tinggi dapat mempengaruhi keadaan biopolimer dan menyebabkan degradasi terma struktur molekul, seperti meruapnya sulfat bersama air. Menurut Kinsella [17] *Kappaphycus alvarezii* sebagai penghasil karagenan yang mempunyai sifat kental dan likat bergantung pada kepekatan, suhu, pH, kehadiran molekul-molekul lain, kaedah perlakuan, jenis karagenan dan jisim molekulnya.

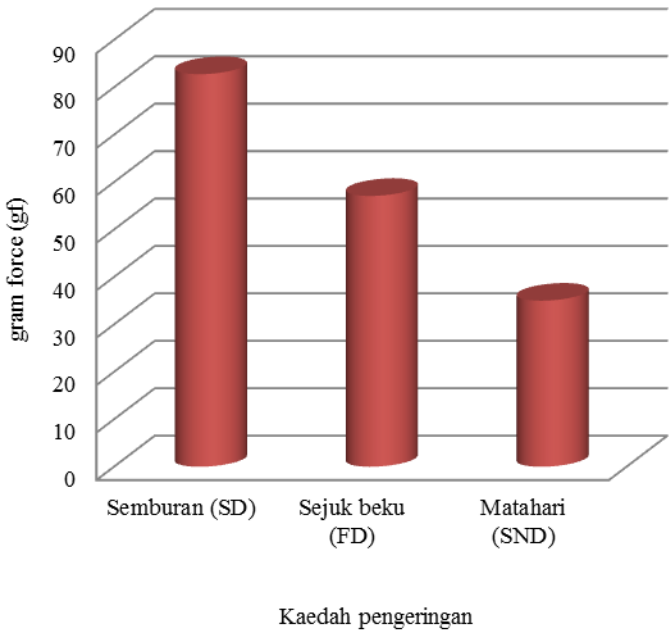


Rajah 4. Keupayaan serbuk rumpai laut memegang air dan minyak



Rajah 5. Kelikatan sebaran rumpai laut *Kappaphycus alvarezii*1.5% (w/v)

Kekuatan gel merupakan salah satu sifat serbuk rumpai laut yang utama kerana kekuatan gel menunjukkan kemampuan serbuk rumpai laut dalam pembentukan gel. Hasil pengukuran kekuatan gel ditunjukkan pada Rajah 6. Serbuk SD mempunyai kekuatan gel yang tinggi (82.77 gf) dibandingkan dengan serbuk FD (57.1 gf) dan serbuk FD lebih tinggi daripada SND (35.01 gf). Tinggi kekuatan gel pada serbuk SD dibandingkan dengan serbuk FD dan SND disebabkan oleh penggunaan suhu tinggi (160°C) yang boleh mempengaruhi penyusutan kandungan sulfat. Menurut Towle [18], peningkatan kekuatan gel berkadar terus dengan banyaknya kandungan kumpulan 3,6-anhidrogalaktosa dan berkadar songsang dengan kandungan sulfatnya. Semakin kecil kandungan sulfatnya semakin kecil pula kelikatannya tetapi kekuatan gelnya semakin meningkat.



Rajah 6. Kekuatan gel rumpai laut *Kappaphycus alvarezii*1.5 % w/v

Kesimpulan

Dalam kajian ini, sifat kefungsian dari serbuk rumpai laut yang diperolehi secara pengeringan semburan, sejuk-beku dan cahaya matahari telah diselidiki. Ketiga-tiga jenis serbuk menunjukkan sifat fungsi yang unik dan berbeza disebabkan oleh kesan kaedah pengeringan yang berbeza. Serbuk keringan semburan dalam sebaran 1 % w/v memiliki sifat seperti larutan yang sekata dan mempunyai nilai kekuatan gel yang tinggi sehingga ia berpotensi sama ada sebagai pembentuk gel mahupun sebagai pengubah kelikatan. Manakala serbuk keringan matahari mempunyai keupayaan memegang air yang tinggi sehingga ia berpotensi untuk meningkatkan sifat fizik dan struktur di dalam produk makanan. Sementara itu, serbuk keringan sejuk-beku mempunyai keupayaan memegang minyak yang tinggi sehingga ia berpotensi untuk digunakan sebagai penstabil emulsi makanan.

Penghargaan

Penulis ingin merakamkan penghargaan dan terima kasih kepada pihak UKM dan Jabatan Perikanan Malaysia atas sokongan kewangan (Kod No: STGL-007-2010) serta kemudahan penyelidikan yang diberikan.

Rujukan

1. Webber, V., de Carvalho S.M.,Burreto P.L.M. 2012. Molecular and rheological characterization of carrageenan solutions extracted from *Kappaphycus alvarezii*. *Carbohydrate Polymers* 90: 1744-1749.

2. Venugopal, V. 2009. Marine Products for healthcare. *Functional and bioacticenutraceutical Compounds from the ocean*, 261-311.
3. Wang, Y.,Li D.,Wang L-J., Li, S-J., Adhikari, B. 2010. Effects of drying methods on the functional properties of flaxseed gum powders. *Carbohydrate Polymers* 81: 128-133.
4. Karazhiyan, H., Razavi,S.M.A., Philips, G.O., Fang, Y. 2009. Rheological properties of *Lepidium sativum* seed extract as a function of concentration, temperature and time. *Food Hdrocolloids* 23:2062-2068.
5. Prabhasankar, P., Ganesan, P., Bhaskar, N., Hirose, A.,Stephen, N., Gowda, L.R. 2009. Edible Japaneze seaweed, wakame (*Undaria pinnatifida*) as an ingredient in pasta: Chemical, functional and structural evaluation. *Food Chemistry*, 115: 501-508.
6. Glicksman, M.1983. Food hydrocolloids volume II, 21-95.
7. Garcia-Abuin, A., Gomez-Diaz, D., Navaza, J.M.,Quitans-Riveiro, L.C. 2010. Viscosimetric bahaviour of carboxymethyl cellulose-arabic gum mixtures. A. new step to modeling. *Carbohydrate Polymers* 80: 26-30.
8. Mishra, S., Rai, T. 2006. Morphology and functional properties of corn, potato and tapioca starches. *Food Hdrocolloids* 20:557-556.
9. Elleuch, M., Bedigian, D., Roiseux, O., Besbes, S., Blecker, C. 2011.Dietary fibre and fibre-rich by-products of food processing: Characterization, technological functionality and commercial applications: A review. *Food Chemistry*, 124: 411-421.
10. Benjana, O., Masniyom, P. 2011. Nutritional composition and physicochemical properties of two green seaweeds (*Ulva pertusa and U. intestinalis*) from the Pattani Bay in Southern Thailand. *Songklanakarin J. Sci.Technol*. 33: 575-583.
11. Leon-Martinez, F.M., Mendez-Lagunas, L.L, Rodriguez-Ramirez, J. 2010. Spray drying of nopal mucilage (*Opuntia ficus-indica*): Effects on powder properties and characterization.*Carbohydrate Polymers.* 81: 864-870.
12. Kuniak, L., Marchessault, R.H.1972. Study of the cros-linking reaction between epichlohydrin and starch. *Die Starke* 4: 110-116.
13. Suzuki, T., Ohsugi, Y., Yoshie, Y., Shirai, T., Hirano, T. 1996. Dietary fiber content, water holding capacity and binding capacity of seaweeds. *Fisheries Science* 62: 454-641.
14. Caprez, A., Arrigoni, E., Amado,R.,Neukom, H. 1986.Influence of different types of thermal treatment on the chemical composition and physical properties of wheat bran. *Journal of Cereal Science*, 4: 233-239.
15. Wong K. & Cheung P.C. 2001. Influence of Drying treatment on three *Sargassum* species. Proximate composition, amino acid profile and some physic-chemichal properties. *Journal of Applied Phycology* 13:43-50.
16. Monuz, J., Freile-Pelegrin, Y., Robledo, D. 2004. Mariculture of *Kappaphycus alvarezii* (Rhodophyta, Solieriaceae) color strains in tropical waters of Yucatan, Mexico. *Aquaculture* 239: 161-177.
17. Kinsella, J.P.1976. Functional properties of protein in foods:A surfey. *Journal of Food Sciences and Nutrition*7: 219-280.
18. Towle GA. 1973. Carragenan. Di dalam: Whister RL (editor). Industrial Gums. Second edition. New York. Academic Press. 83-114.

The Malaysian Journal of ANALYTICAL SCIENCES ISSN 1394-2506

SORPTION OF Au (III) AND Ag (I) ON AMINO- AND MERCAPTO-SILICA HYBRID COLUMNS

(Jerapan Au (III) dan Ag (I) pada Turus Hibrid Amino- dan Merkapto-silika)

Nuryono[1]*, Nurma Y. Indriyanti[2], Julita B. Manuhutu[3], Narsito[1], Shunitz Tanaka[4]

[1]*Department of Chemistry, Faculty of Mathematics and Natural Sciences*
Universitas Gadjah Mada, Sekip Utara, Yogyakarta 55281, Indonesia
[2]*Study Program of Chemical education, Faculty of Teacher Training and Education*
Universitas Sebelas Maret Surakarta 57126, Indonesia
[3]*Study Program of Chemistry, Faculty of Educational Sciences*
Universitas Pattimura Ambon, Indonesia
[4]*Division of Environmental material Science, Faculty of Environmental Earth Science,*
Hokkaido University, Japan

**Corresponding author: nuryono_mipa@ugm.ac.id*

Abstract

Adsorption-desorption of Au(III) and Ag(I) ion on amino-silica hybrid (ASH) and mercapto-silica hybrid (MSH) in a column system has been studied. Adsorption was conducted in a 0.5-g adsorbent packed column passing through 30 mL solution of Au(III)/Ag(I)/Cu(II) ions 10 mg/L for MSH and Au(III)/Ag(I)/Ni(II) for ASH with three repetitions. Desorption used eluent of thiourea in HCl solution with volume of 10 mL each. Concentration of metal ions in the eluent was analyzed with flame atomic absorption spectroscopy and the amount of metal ions desorbed was calculated. The results showed that metal ions loaded in the columns were adsorbed completely in both adsorbents. However, the amount of metal ions desorbed for first three fractions is depended on the concentration of eluent. Thiourea 1M in 1M HCl solution eluted 96.7% and 59.1% of Au(III) ion from MSH and ASH, respectively; and Ag(I) was desorbed 79.2% from MSH and 97.6% from ASH. Metal ions of Cu(II) and Ni(II) are not easily eluted with that eluent; only 45.8% of Cu(II) was eluted from MSH and 5.0% of Ni(II) from ASH. Repetition of process in three-time use indicates the highly stability of the adsorbents; hence those are potential for solid phase extraction application.

Keywords: sorption, gold, silver, silica, rice hull ash

Abstrak

Dalam kajian ini, jerapan dan nyahjerapan ion Au (III) dan Ag (I) pada hibrid amino-silika (ASH) dan hibrid merkapto-silika (MSH) telah dikaji dalam sistem turus. Jerapan dilakukan dalam turus padat 0,5 g penjerap dengan mengalirkan 30 mL larutan ion Au(III)/Ag(I)/Cu(II) masing-masing 10 mg/L untuk MSH dan Au (III)/Ag(I)/Ni(II) untuk ASH dengan tiga kali ulangan. Nyahjerapan dilakukan dengan menggunakan eluen tiourea dalam larutan HCl dan setiap 10 mL. Kepekatan ion logam dianalisis mengunakan spektroskopi serapan atom nyalaan dan jumlah ion logam yang ternyahjerap dihitung. Hasil penelitian menunjukkan bahawa semua ion logam yang melalui turus akan terjerap sempurna pada kedua adsorben. Namun, jumlah ion logam yang ternyahjerap untuk tiga bahagian pertama bergantung pada kepekatan eluen yang digunakan. Tiourea 1M dalam larutan HCl 1M mengelusi 96.7% dan 59.1% ion Au(III) dan Ag(I) ternyahjerap 79.2% dan 97.6% masing-masing dari MSH dan ASH. Ion logam Cu(II) dan Ni(II) tidak mudah dielusi dengan eluen, hanya 45.8% Cu(II) dielusi dari MSH dan 5.0% Ni(II) dari ASH. Pengulangan proses di dalam tiga kali penggunaan menunjukkan kestabilan penjerap adalah sangat tinggi, sehingga berpotensi untuk diaplikasikan pada pengekstrakan fasa pepejal.

Kata kunci: sorpsi, emas, perak, silika, abu sekam padi

Introduction

Precious metals such as gold, silver, platinum and palladium are widely used in many fields like catalysts in various chemical processes, in electrical and electronic industries, in medicine and in jewelry [1]. The increasing demand for the precious metals is of great economical interest to the recovery of these metals from aqueous and waste

solutions since mineral stocks have started to decline. There are several methods, such as liquid–liquid extraction, membrane filtration and solid phase extraction (SPE), available in the literature for the removal of precious metals from aqueous solutions. Comparatively, SPE seems to be the most suitable method for the recovery of those metals in the case of low concentration due to low cost and high efficiency. Due to the technical and economical point of view, now much attention has been focused on lost cost adsorbents for the removal and recovery of precious metal ions.

In comparison with liquid-liquid extraction of metal ions, the solid phase extractions have two major advantages. First, they are more ecofriendly and second, it is easier to reuse them [2]. Ion-exchangers and chelating resin are the two most important classes of solid phase extractors (adsorbents). However, the later ones are attractive due to their selectivity. Several ligand immobilized organic polymeric matrices have been studied as chelating resins in the recent past [3]. The modified silica gel generally exhibits sorption capacities higher than those of organic polymer based resins. On silica gel reactive sites exist in large number, and therefore, the number of organic molecules immobilized is high, which results in good sorption capacity for metal ions.

Silica gel functionalized with 8-hydroxyquinoline [4], salicyldoxime [5], 1-(2-thiazolylazo)-2-naphthol [6], dithizone [7], acidred-88 [8], acid alizarin violet-N [9], didecylami-noethyl-b-tridecylammonium [10], 3-methyl-1-phenyl-4-stearoyl-5-pyrazolone [11], formylsalicylic acid [12], thiourea [13], 2-mercaptoben-zothiazole [14], dithiocarbamate [15], salicyldehyde [16], o-vanillin [17] and 2-hydroxy-5-nonylacetopheneoxime [18] is reported as a chelating collector for heavy metal ions. Separation and preconcentration methods for gold have been reported, in which the common adsorbents of gold were silica gel modified with mercaptobenzothiazole [19], nanometer titanium dioxide [20], thioethericsites [21], benzoylthiourea [22] and aminopropyltrimethoxysilane [23].

Selectivity of adsorption for the target metal ions may be improved by imprinting the target metal ion in the modified silica. Imprinting of silica with Au nanoparticles using aminosilanes was achieved at high loadings [24, 25] and phenyl-functionalized silica gels with embedded gold particles were also prepared in a basic medium, albeit with particle sizes larger than 10 nm [26]. Sakti et al. [23] reported synthesis of ionic imprinting amino-silica hybrid (Im-ASH) for adsorption of gold ion in a batch system. The result shows that Im-ASH increases selectivity in absorbing Au (III) but reduces the capacity. The selectivity of this hybrid silica-based materials mainly depends on the structure of the immobilized organic compound, the nature of the incorporated donor atoms (O, N, S and P), the positioning of the functional groups along the surface of the silica support and the steric requirements of the complex formed after uptake of the desired metal ion. In the present paper, we report sorption characteristic of two active sites namely mercapto (-SH) and amino (-NH_2) immobilized on silica toward multimetal ions Au(III)/Ag(I)/Cu(II) and Au(III)/Ag(I)/Ni(II), respectively, in a dynamic (column) system. In addition, reusability of the adsorbents loaded column is examined as well.

Materials and Methods

Chemicals

Sodium silicate solution, as the source of silica, from rice husk ash was prepared using a procedure reported by Sakti et al.[23]. As site active sources two precursors namely 3-aminopropyltrimethoxysilane (APTMS) and 3-mercaptopropyltrimethoxysilane (MPTMS) were supplied from Merck. Standard Au(III) solution 1000 mg/L in HCl solution was purchased from Merck and solution of Ag(I), Ni(II) and Cu(II) were prepared by dissolving salts of metal nitrate (Merck). Eluent for desorption of metal ions was prepared by dissolving thiourea (Merck) in HCl solution. All above chemicals were used without further purification.

Apparatus

A solid phase extraction set consisting of a chamber for fitting the bottom side of the SPE polyethylene column and reaction tubes below the column for collecting the eluat and a vacuum pump was used in this research. A flame atomic absorbance spectrophotometer (FAAS) (Perkin Elmer 3110) was used analysis of metal ions and Fourier transform infrared (FTIR) spectrophotometer (Shimadzu FTIR-8210 PC) were used for identification of functional group present in the adsorbents.

Procedures

Synthesis of adsorbent with sol-gel process

A mixture of 40 mL sodium silicate solution and 10 mL APTMS was added with 3 M HCl solution dropwise with constant stirring until pH of the mixture reached 7.0. The resulting gel was aged for one night, washed with demineralized water, and dried in an oven at 70 °C for 2 h. The resulting dry gel was ground and sieved 200 mesh in size. The product then used for further experiment was called adsorbent of amino-silica hybrid (ASH). The similar work was carried out to obtain mercapto-silica hybrid (MSH) by replacing APTMS with MPTMS. The hybrids were characterized with FTIR spectrophotometer dan XRD.

Packing of solid phase extraction (SPE) column

A SPE column (100 mm long x 5 mm inlet diameter) completed with a 20-µm polyethylene frit in the bottom was washed with water and ethanol prior use. Adsorbent 0.5 g suspended in 5 mL ethanol was homogenized in an ultrasonic bath for 5 min. The suspension then was poured into the column with help of a vacuum pump at a flow rate of 0.6 mL/min and the second frit was put above the adsorbent in the column.

Adsorption-desorption of metal ions in SPE column

A 10-mL aliquot of Au(III)/Ag(I)/Cu(II) solution (10 mg/mL, each) was passed through the column at a flow rate of 0.5 mL/min. The loading was repeated three times. Metal ions in the filtrate were analyzed with FAAS to calculate the amount of metal ions un-adsorbed. The adsorbed ion was eluted with 1.0 M thiourea solution in 0.5 M HCl at an elution rate of 1.0 mL/min. The metal ion in each fraction (10 mL) of elution was determined with FAAS and the recovery percentage was calculated. The cycle of adsorption-desorption was repeated 3 times using the same column to evaluate stability and reusability of the adsorbent.

Results and Discussion

Characteristics of adsorbent

The presence of amine ($-NH_2$) groups in ASH and thiol (-SH) in MSH was confirmed with FTIR spectra (Figure 1). In Figure 1(a) (silica gel, SG) bands observed at 3426, 1636, and 957 cm^{-1} indicate vibration of O–H from silanol group (Si–OH), and at 1088 and 463 cm^{-1} come from Si–O–Si vibration of the siloxane groups. Those bands are also observed in spectra of ASH and MSH. The characteristic spectra of ASH (Figure 1(b)) are seen at 1528 cm^{-1} from N–H and at 2940 cm^{-1} from C–H band. Similar spectra were also observed for MSH in Fig. 1(c). A sharp band at 2931.8 cm^{-1} was originated from C-H vibration and a weak band of S-H is observed at 2553.75 cm^{-1}.

The structure of materials was identified with XRD. The patterns resulted (not presented) show that there is a broad peak at $2\theta = 21\text{-}22^{o}$ for all three materials (SG, ASH and MSH) indicating the amorphous structure [27]. These results reveal that the modification with the silane reagent does not alter the nature of amorphous silica.

Adsorption of multimetal ion in column

In this study, the adsorption was carried out three repetitions in separated columns. The adsorption result was presented in Table 1.

Adsorption metal ions on ASH

Table 1(a) shows that the total metal ions adsorbed on ASH reaches 100 %. It is consistent with the capacity of ASH in adsorbing those metal ions in a batch system reported by previous researchers. Sakti et al. [23] found that ASH is able to adsorb 132 mg/g of Au(III) and Nuryono et al. [28] reported that the capacity of adsorption for Ni(II) and Ag(II) are 21 and 154 mg/g, respectively. In this study, the pH of the solution multilogam used for the adsorption process is 4.0. This is consistent with previous studies reporting that the maximum adsorption capacity of Au(III) on amino silica hybrids occur between pH 3-5 [23]. At this pH range, amino ($-NH_2$) groups on the ASH surface are protonated to form ammonium ($-NH_3^+$) groups and interact with Au(III) in $AuCl_4^-$ form.

Possible interactions between the metal Au(III) with amino silica hybrid is through ionic interactions presented in Figure 2. This leads to Au(III) to be adsorbed more than Ag(I) and Ni(II). In this study, multimetal adsorption of Au(III), Ag(I) and Ni(II) was conducted in the medium of water leading to tendency metal ions to form octahedral

complexes. Ion Au(III) dissolved in HCl solution forms complex anion of $[AuCl_4]^-$ while Ni(II) and Ag(I) complexes form $[Ni(H_2O)_6]^{2+}$, $[Ag(H_2O)_6]^+$ [29].

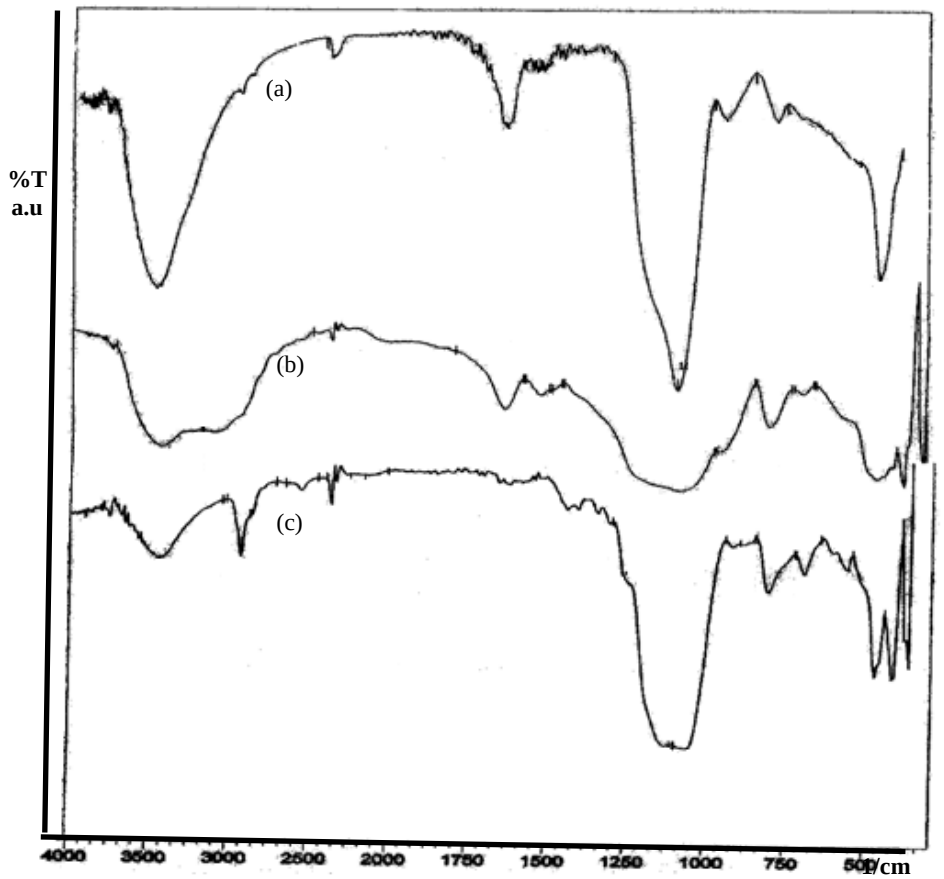


Figure 1. Infrared spectra of SG (a), ASH (b) and MSH (c)

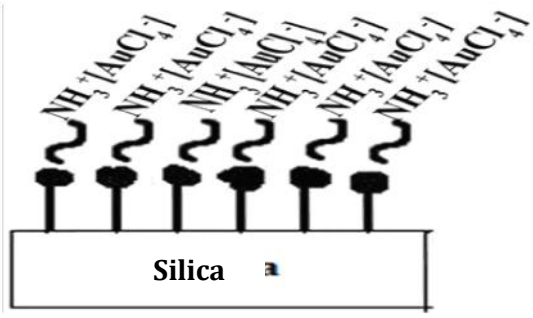


Figure 2. Model of ionic interaction between ammonium groups and anion of Au(III)

Ni(II) and Ag(I) cations with the ammonium groups are expected to repel each other and adsorption would not occur. However, Table 1 shows that Ag(I) and Ni(II) are adsorbed in high percentage (90 %). This is probably due to substitution of proton on ammonium groups by metal cation to form metal ion-amine complexes followed by removal of water molecule hydrated on the metal ions. Another possibility is that adsorption occurs through hydrogen bonding between silanol groups remaining on silica and water molecule hydrated on the metal ions.

Table 1. Amount of metal ions adsorbed on column loaded with adsorbent.

a. Adsorbent ASH

Ion	Column	Total metal Ion		
		Loaded	Adsorbed	
		(mg)	(mg)	(%)
	I	0.42	0.41	98.7
Au(III)	II	0.41	0.40	97.6
	III	0.39	0.39	100
	I	0,42	0.38	90.5
Ag(I)	II	0.42	0.40	95.2
	III	0.48	0.48	100
	I	0.38	0.37	98
Ni(II)	II	0.38	0.37	98
	III	0.39	0.39	100

b. Adsorbent MSH

Ion	Column	Total metal Ion		
		Loaded	Adsorbed	
		(mg)	(mg)	(%)
	I	0.30	0.30	100
Au(III)	II	0.30	0.30	100
	III	0.30	0.27	90
	I	0.36	0.29	81
Ag(I)	II	0.35	0.34	97
	III	0.35	0.35	100
	I	0.35	0.35	100
Cu(II)	II	0.35	0.35	100
	III	0.35	0.35	100

Adsorption of metal ions on MSH

Similar result is also observed for adsorption of Au(III)/Ag(I)/Cu(II) on MSH (Table 1(b)) that all metal ions are adsorbed. It is also consistent with data resulted for the batch system. In that system, adsorption capacity of MSH for Au(III) is 203.4 mg/g [29] and for Ag (I) and Cu (II) is 359.54 mg/g and 48.83 mg/g, respectively [30]. Probably interaction between Au(III) and adsporbent MSH is expressed in Figure 3. It seems that Au(III) is adsorbed through complex formation between S as electron donor atom and Au(III) as acceptor.

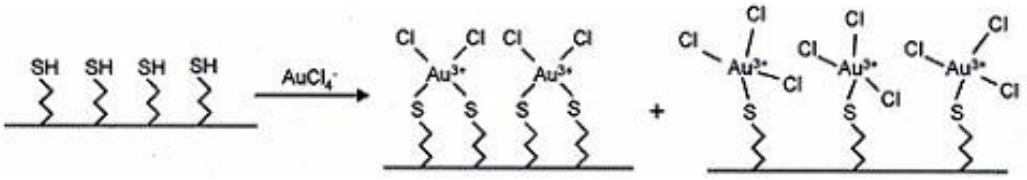


Figure 3. Model of complex formation between anion of Au(III) and MSH

Based on the HSAB concept, the active groups thiol (-SH) present on the surface of the MSH is a soft base, so it may adsorb the soft metal, Au(III). Theoretically, adsorption HMS multilogam system will only adsorb Au(III) ions and will not adsorb Cu(II) and Ni(II), which are intermediate acid. However, based on Table 1(b) shows that Cu(II) and Ni(II) adsorbed on HMS is much lower than that of Au(III). This is possible because according to FTIR spectra the surface of HMS is covered not only by thiol groups but also silanol, -OH. The atom O in the silanol groups may act as harder electron donor than S atom on the HMS. Therefore silanol groups are be able to bind metal ions Cu(II) and Ni(II), intermediate acids. According to Lam [31] the adsorbed Au(III) on the surface of the adsorbent at acidic conditions (pH ~ 2-3) provides a partial negative charge on the surface of the adsorbent, since at that pH range Au(III) ions present in $AuCl_4^-$. Partial negative charge on the surface of the adsorbent allow to interact with Cu(II) and Ni(II) ions, which is positively charged in water medium.

Desorption

To study performance of the SPE column in separating/extracting Au(III) ion from the adsorbent, in this research elution with 1M thiourea in different concentration of HCl (0.5 and 1 M) was conducted. Thiourea solution has a low toxicity and desorption runs faster compared to conventional cyanide solution [32]. The addition of thiourea led to Au (III) is unstable then reduced to Au(I). Metal ion Au(I) is then used to react with thiourea to form a stable complex by the reaction:

$$Au^+ + 2\ SC(NH_2)_2 \rightarrow [Au(SC(NH_2)_2)_2]^+ \quad (1)$$

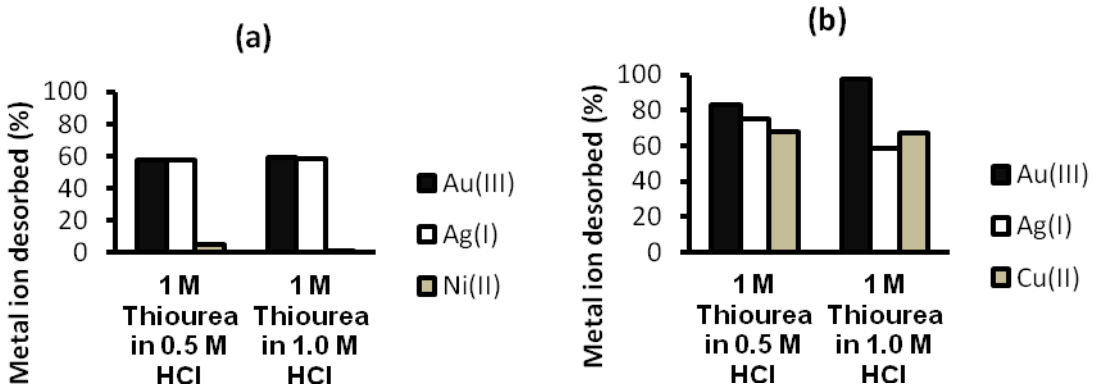


Figure 4. Diagram of metal ions desorbed from adsorbent ASH (a) dan MSH (b) using eluent of 1 M thiourea in 0.5 M HCl and in 1.0 M HCl

Desorption also aims to evaluate the selectivity of thiourea in HCl solution in eluting the metal ions from the column. The total percentage of metal ions desorbed from the adsorbent with both eluents in the first three fractions can be seen in Figure 4.

Desorption of metal ions from ASH

Figure 4(a) shows that Au(III) and Ag(I) are desorbed in similar amount and Ni(II) is practically not desorbed from the ASH column. As mentioned previously, S atom acting as desorbing agent is categorized into soft base so that soft metal ions i.e. Au(III) and Ag(I) form complexes with thiol groups much more stable than Ni(II) categorized as a borderline acid. In addition, a ligand with large donor atom such as S is not readily to form strong interaction with small metal ion. Complexes formed by small metal ions lead to low coordination since those metal ions should provide large space to accommodate the ligand large atom [33]. Based on the size of the ion, the order is Au (III)>Ag (I)>Ni (II); hence Au (III) forms a complex with thiourea more stable than Ag (I). However, both ions Au (III) and Ag (I) in the system multimetal Au (III)/Ag (I)/Ni (II) are desorbed only about 50%. This is probably due

to slow rate of complex formation and competition of multimetal ions present in the solution to form complexes with thiourea.

Desorption of metal ions from MSH

From Figure 4(b) can be seen that 84.61% of Au (III) in multimetal Au (III)/ Ag (I)/Cu (II) can be eluted using a solution of 1 M thiourea in 0.5 M HCl and almost complete amount (96.00%) of Au (III) is desorbed with 1 M thiourea in 1.0 M HCl. Metal ion of Cu (II) 68.12% is eluted with the first eluent and 66.67% with the second eluent. A similar trend is also seen for Ag (I), in which 74.28% is eluted with 1M thiourea in 0.5 M HCl and only 57.14% with 1M thiourea solution in 1M HCl.

From the results of desorption the increase of the HCl concentration did not significantly improve the percentage of Cu (II) and Ag (I) desorbed. The eluent of 1 M thiourea in 1 M HCl solution desorbs Au(III) in the highest amount among the investigated metal ions for the multilmetal system of Au (III)/Ag (I)/Cu (II). Based on the HSAB concept the softness of S atom in thiourea may act as good desorbing groups for soft metal ions. Hence, thiourea forms more stable complex with Au (III) than with Cu (II) and Ag (I). Also in the solution, the ligands with large donor atoms such as S may limit their ability to form stable complexes with smaller metal ions.

According to Lacoste-Boucet [34] addition of acid may stabilize and prevent thiourea degraded, thereby reducing the consumption of thiourea. Chloride ions (Cl^-) derived from the addition of HCl serves as a competing agent (competitors) for Au-Cl complexes on the surface so that Au(III) may be desorbed from HMS [35]. Higher concentration of HCl increases the amount of chloride ions as competitor. These results give similar trend to that done in a batch system [29]. Elution process in three fractions yield percentage of metal ions desorbed as presented in Figure 5.

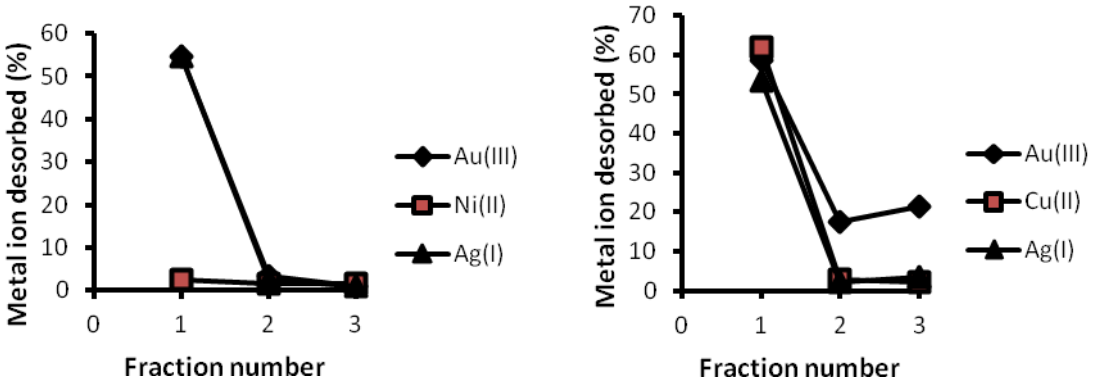


Figure 5. Curves of metal ions desorbed from adsorbent ASH (a) and MSH (b) versus fraction number of elution using 1 M thiourea in 1 M HCl

Figure 5(a) shows that two metal ions namely Au (III) and Ag (I) are eluted together with large amount in the first fraction. However, Ni (II) is not easily desorbed from the column. Based on HSAB, Ni (II) is categorized into hard acid, as well as donor atom N is hard base. Therefore, those acid and base may interact strongly, and difficult to be broken by soft base such as S atom in thiourea. In contrary, interaction between soft acid Ag (I) and hard base N atom is very weak; hence this metal ion is eluted fast. Ionic interaction between ammonium cation and Au (III) anion is ready to be broken by S atom due to complex bonding formation.

From Figure 5(b) can be seen that in the first fraction the amount of ions desorbed for all metals shows the same percentage. It is probable desorption occurs for metal ions adsorbed on the MSH through trapping interaction. In this case, the amount of Au (III) bounded on MSH is not difference from other metal ions. However, in the second and third fractions, percentage of Ag (I) and Cu (II) eluted drops drastically in comparison to that of Au (III). This is

probable due to the un-effective contact between the adsorbent and metal ions in the column. Low stability constant of Cu-thiourea complexes (log $\beta = 2.3 \pm 0.1$) causes Cu (II) not easily to be eluted with this eluent and this also happens for Ag (I). In contrary, the stability constant of gold-thiourea complex is log $\beta \approx 24$ [36].

Table 2. Amount of metal ions desorbed from column in three repetitions.

a. ASH

Ion	Cycle	Total metal ions		
		Adsorbed	Desorbed	
		(mg)	(mg)	(%)
Au (III)	1	0.41	0.29	96.7
	2	0.37	0.36	96.8
	3	0.39	0.38	98.6
Ag (I)	1	0.38	037	96.6
	2	0.38	0.36	94.4
	3	0.36	0.35	98.1
Ni (II)	1	0.48	0.06	0.37
	2	0.42*	0.05	12.2
	3	0.37*	0.04	9.50

b. MSH

Ion	Cycle	Total metal ions		
		Adsorbed	Desorbed	
		(mg)	(mg)	(%)
Au (III)	1	0.30	0.29	96. 7
	2	0.30	0.29	96.7
	3	0.27	0.27	100
Ag (I)	1	0.29	0.23	79.3
	2	0.34	0.27	79.0
	3	0.35	0.26	74.3
Cu (II)	1	0.35	0.16	45.7
	2	0.19*	0.04	21.1
	3	0.15*	0.01	6.70

* The column was not reloaded with the ion logam since not all metal ion was eluted in the previous elution

Reusability of Adsorbent

Regeneration of the adsorbent for reuse is a key in the improvement of the economic process. Additionally, study on reusability of adsorbent in the column is used to evaluate the stability of the adsorbent during the adsorption-desorption process. To determine the reusability adsorbent in SPE columns was used for adsorption-desorption process (cycle) in several times. Elution was performed in ten fractions (10 mL each) and the adsorption-desorption cycle was repeated 3 (three) times. The results can be seen in Table 2. From the data in Table 2 can be seen that in three repetitions the metal ions are desorbed in the similar amount for the both adsorbents. It indicates the higher chemical stability, and within three months from the first usage performance of columns does not change significantly. Similar to the previous result, three metal ions (Au (III)/Ag (I)/Cu (II)) absorbed on ASH column are eluted in different amount (Table 2(a)). Au (III) and Ag (I) are desorbed completely but Ni (II) is difficult to be desorbed from the ASH column. It can be stated that ASH column and eluent of thiourea in HCl solution give highly selectivity for the separation of Au (III) from Ni (II) but not from Ag (I).

Different from ASH, three metal ions adsorbed on MSH are eluted with the order of desorbed percentage Au (III)>Ag (I)>Cu (II). This result is different from the data of the first three fractions (Figure 2(b), in which the order is Au (III)>Cu (II)>Ag (I). Ion Cu (II) is eluted faster than Ag (I); in the first three fractions elution of Cu (II) has reached maximum amount and Ag (I) may be eluted up to ten fractions. Competition between S atom from –SH in adsorbent and from thiourea makes removal of Ag (I) from adsorbent occurs slowly and need a lot amount of eluent/fraction. Similar to ASH, MSH selective for Au (III) toward Cu (II) but not toward Ag (I), even though Au (III) and Ag (I) can still be separated since Au (III) is easier eluted than Ag (I).

Conclusion

Adsorption of metal ions investigated from multimetal ion solution on the adsorbents ASH and HMS in a column technique shows almost the same results, in which three metal ions in solution are adsorbed completely on the adsorbents if the metal ions loaded are less than capacity calculated in a batch system. The process of separation of Au(III) through the desorption of gold metal ion in the multimetal system Au(III)/Ag(I)/ Cu(II) from MSH surfaces using a solution of thiourea-HCl shows high selectivity (97% desorbed) toward Ag(I) and Cu(II). However, desorption of Au (III) from the adsorbent ASH gives low selectivity toward Ag (I) but excellent to Ni (II). Adsorbents developed in the separation of metal Au (III) from multimetal system in column technique with three adsorption-desorption cycles show no decrease in performance of adsorption-desorption characteristic indicating high stability of the adsorbents. Therefore, those adsorbents may be reusable and potential for solid phase extraction application in the future.

Acknowledgement

The authors would like to thank the Directorate of Research and Community Services, Directorate General of Higher Education (DP2M-DIKTI), Ministry of Culture and Education, Republic of Indonesia for providing funding in this research through the program of International Collaboration Research No. 180/SP2H/PL/ Dit.litabmas/IV/2012.

References

1. Goswami A., & Singh, A. K., (2002).1,8-Dihydroxyanthraquinone anchored on silica gel: synthesis and application as solid phase extractant for lead(II), zinc(II) and cadmium(II) prior to their determination by flame atomic absorption spectrometry, *Talanta*, 58, 669 - 678.
2. Ramesh, A., Hasegawa, H., Sugimoto, W., Maki, T. & Ueda, K. (2008). Adsorption of gold(III), platinum(IV) and palladium(II) ontoglycine modified crosslinked chitosan resin, *Bioresource Technology*, 99: 3801 – 3809.
3. Zih-Pere ´nyi, K., Lasztity, A., Horvath, Z., Levai, A. (1998). Use of a new type of 8-hydroxyquinoline-5-sulphonic acid cellulose (sulphoxine cellulose) for the preconcentration of trace metals from highly mineralised water prior their GFAAS determination, *Talanta*, 47: 673 - 679.
4. Kasahara, I., Willie, S. N., Sturgeon, R. E., Berman, S. S., Taguchi, S., Goto, K. (1993). Preparation of 8-quinolinol immobilized adsorbents with minimum contamination for the preconcentration of trace metals in water, *Bunseki Kagaku*, 42: 107-110.
5. Sarkar, A. R., Datta, P. K. & Sarkar, M. (1996). Sorption recovery of metal ions using silica gel modified with salicylaldoxime, *Talanta*, 43: 1857-1862.
6. Zaporozhets, O. A., Nadzhafova, O. Y., Zubenko, A. I. & Sukhan, V. V. (1994). Analytical Application of Silica Gel Modified with Didecylaminoethyl-β-Tridecylammonium Iodide, *Talanta*, 41, 2067 - 2071.
7. Zaporozhets, O., Petruniock, N. and Sukhan, V. (1999). Determination of Ag(I), Hg(II) and Pb(II) by using silica gel loaded with dithizone and zinc dithizonate, *Talanta*, 50: 865 - 872.
8. Kocjan, R. (1999). Retention of Some Metal Ions and Their Separation on Silica Gel Modified with Acid Red 88, *Microchim. Acta*, 131: 153-158.
9. Ferreira, S. L. C., & de Brito, C. F. (1999). Separation and Preconcentration of Cobalt after Sorption onto Amberlite XAD-2 Loaded with 2-(2-Thiazolylazo)-*p*-cresol, *Anal. Sci.*, 15: 189 - 192.
10. Zaporozhets, O., Petruniock, N., Bessarabova, O., Sukhan, V. (1999). Determination of Cu(II) and Zn(II) using silica gel loaded with 1-(2-thiasolylazo)-2-naphthol, *Talanta*, 49: 899 - 906.
11. Tong, A., Akama, Y. & Tanaka, S. (1990). Pre-concentration of copper, cobalt and nickel with 3-methyl-1-phenyl-4-stearoyl-5-pyrazolone loaded on silica gel, *Analyst*, 115: 947 - 949.
12. Mahmoud, M. E. & Soliman , E. M. (1997). Silica-immobilized formylsalicylic acid as a selective phase for the

extraction of iron(III), *Talanta*, 44: 15 - 22.
13. P. Liu, Q. Pu, Z. Su, (2000), Synthesis of silica gel immobilized thiourea and its application to the on-line preconcentration and separation of silver, gold and palladium, *Analyst*, 125: 147 - 150.
14. Liu, P., Pu, Q. & Su, Z. (1998). Application of 2-mercaptobenzothiazole-modified silica gel to on-line preconcentration and separation of silver for its atomic absorption spectrometric determination, *Analyst*, 123: 239 - 243.
15. Mahmoud, M. E. (1999). Selective solid phase extraction of mercury(II) by silica gel-immobilized-dithiocarbamate derivatives, *Anal. Chim. Acta*, 398: 297 - 302.
16. Kubota, L. T., Moreira, J. C., Gushikem, Y. (1989). Adsorption of metal ions from ethanol on an iminosalicyl-modified silica gel, *Analyst*, 114: 1385 - 1388.
17. Garg, B. S., Sharma, R. K., Bist, J. S., Bhojak, N. & Mittal, S. (1999). Separation and preconcentration of metal ions and their estimation in vitamin, steel and milk samples using *o*-vanillin-immobilized silica, *Talanta*, 48 (1): 49 - 55.
18. Kim, J. S. & Yi, J. (1999). The Removal of Copper Ions from Aqueous Solutions Using Silica Supports Immobilized with 2-Hydroxy-5-nonylacetophenoneoxime, *Sep. Sci. Technol*., 34: 2957 – 2971.
19. Pu, Q. S., Su, Z. X., Hu, Z. H., Chang, X. J. & Yang, M. J. (1998). 2-Mercaptobenzothiazole-bonded silica gel as selective adsorbent for preconcentration of gold, platinum and palladium prior to their simultaneous inductively coupled plasma optical emission spectrometric determination, *Journal of Analytical Atomic Spectrometry*, 13: 249 – 253.
20. Liu, P., Pu, Q. S., & Su, Z. X. (2000) Synthesis of silica gel immobilized thiourea and its application to the on-line preconcentration and separation of silver, gold and palladium, *Analyst (London)*, 125: 147 – 150.
21. Gentscheva, G., Tzvetkova, P., Vassileva, P., Lakov, L., Peshev, O. & Ivanova, E. (2007). Analytical characterization of a silica gel sorbent with thioethericsites, *Mikrochimica Acta*, 156: 303 – 306.
22. Bozkurt, S. S. & Merdivan, M. (2009). Solid phase extraction of gold(III) on silica gel modified with benzoylthiourea prior to its etermination by flame atomic absorption spectrometry, *Environ Monit Assess*, 158: 5 – 21.
23. Sakti, S.C.W., Siswanta, D. & Nuryono (2013), Adsorption of Gold(III) on Ionic Imprinted Amino-Silica Hybrid Prepared from Rice Hull Ash, *Pure Appl. Chem.*, 85 (1): 211 - 223.
24. Bonnemann, H., Endruschat, U., Tesche, B., Rufinska, A., Lehmann, C. W., Wagner, F. E., Filoti, G., Parvulescu, V. and Parvulescu, V. I. (2000) An SiO_2-Embedded Nanoscopic Pd/Au Alloy Colloid, *Eur. J. Inorg. Chem*., 5: 819 - 822.
25. Xie, Y. W., Quinlivan S. & Asefa, T. (2008). Tuning Metal Nanostructures in Mesoporous Silica by a Simple Change of Metal Complexes and by Reduction with Grafted Imines and Hemiaminals, *J. Phys. Chem*. 112: 9996 - 10003.
26. Hall, S. R., Davis S. A. & Mann, S. (2000). Cocondensation of Organosilica Hybrid Shells on Nanoparticle Templates: A Direct Synthetic Route to Functionalized Core−Shell Colloids, *Langmuir*, 16: 1454 - 1456.
27. Kalapathy, U., Proctor, A. & Shultz, J. (2000). A simple method for production of pure silica from rice hull ash, *Bioresource Technology*, 73: 257 - 262.
28. Nuryono, Bassir, M., Setyaningsih, A. & Narsito (2007). *Synthesis of Amino-Silica Hybrid from Rice Hull Ash for Heavy Metal Ion Adsorption*, Presented at International Conference of Chemical Sciences (ICCS) Held by Department of Chemistry, Universitas Gadjah Mada and School of Chemistry, University Sains Malaysia on 24-25 May 2007, In Yogyakarta, Indonesia.
29. Hamdiani, S., Nuryono, Rusdiarso, B. & Sakti, S. C. W. (2010). *Kajian Adsorpsi-Desorpsi Au(III) Pada Hibrida Merkapto Silika (HMS)*, Prosiding Seminar Nasional Penelitian, 15 Mei 2010 (Indonesian)
30. Mujiyanti, D. R., Nuryono & Kunarti, E.S. (2007). *Simultaneous Adsorption Of Ag(I), Pb(II), Cu(II), Cr(III), And Ni(II) On Mercapto Immobilized Rice Hull Ash Silica*, Presented at International Conference of Chemical Sciences (ICCS) Held by Department of Chemistry, Universitas Gadjah Mada and School of Chemistry, University Sains Malaysia on 24-25 May 2007, In Yogyakarta, Indonesia.
31. Lam, K. F., Fong, C. M., Yeung, K. L. & Mckay, G. (2008). Selective adsorption of gold from complex mixtures using mesoporous adsorbent, *J. Chem. Eng*., 145: 185 – 195
32. Groenewald, T. (1976). The Solution of Gold in Acidic Solutions Thiourea, *Hydrometallurgy*,1: 277 - 290.
33. Martell, E.A. & Hancock, R.D. (1996). *Metal Complexes in Aqueos Solution*, Plenum Press, New York.
34. Lacoste-Bouchet, P., Deschenes, G. and Ghali E. (1998). Thiourea Leaching of a Copper-Gold Ore Using

Statistical Design, *Hydrometallurgy*, 47: 189 - 203.
35. Ertan, E. & Gulfen, M. (2009). Separation of Gold(III) from Copper(II) and Zinc(II) Ions Using Thiourea-Formaldehyde or Urea-Formaldehyde Chelating Resins. *J. Appl Polym Sci*., 111: 2798 – 2805.
36. Puddephat, R. J., (1978), *The Chemistry of Gold*, Elsevier Scientific Publishing Company, Amsterdam.

The Malaysian Journal of ANALYTICAL SCIENCES ISSN 1394-2506

STRUCTURE ELUCIDATION OF FLAVONOID COMPOUND FROM THE LEAVES OF *COLEUS ATROPURPUREUS* BENTH USING 1D- AND 2D-NMR TECHNIQUES

(Elusidasi Struktur Sebatian Flavonoid Dari Daun *Coleus Atropurpureus* Benth Menggunakan Teknik 1D- Dan 2D-NMR)

Sovia Lenny[1]*, Tonel Barus[1], Lamek Marpaung[1], M.Pandapotan Nasution[2]

[1]*Department of Chemistry,*
[2]*Faculty of Pharmacy,*
University of Sumatera Utara, Medan, Republic of Indonesia

**Corresponding author: sovialeni@yahoo.com*

Abstract

Isolation of flavonoid compound from ethylacetate extract of the leaves of *Coleus atropurpureus* Benth using column chromatography have been carried out. Structure elucidation of the isolated compounds was done by one-and two-dimensional NMR (^{1}H, ^{13}C, DEPT, COSY, HMQC and HMBC). Analysis of 1D-NMR spectra (^{1}H-NMR showed signals at δ 6-8 ppm for the aromatic region of the flavonoid aglycone and ^{13}C-NMR showed signals for three carbon atoms of the flavonoid ring C at δ 182.8 ppm (C-4), 103.9 ppm (C-3), 166.4 ppm (C-2) and DEPT showed the presence of CH and CH_2 group). Analysis of 2D-NMR spectra (COSY showed correlation of proton at δ 7.86 and 6.92 ppm and HMBC showed correlation between proton at δ 6.61 with 166.4 ppm and 6.92 with 123.3 ppm).

Keywords: *Coleus atropurpureus* Benth, column chromatography, flavonoid, structure elucidation, 1D- and 2D-NMR techniques

Abstrak

Pengasingan flavonoid dari ekstrak etilasetat daun *Coleus atropurpureus* Benth menggunakan kromatografi turus telah dijalankan. Elusidasi struktur sebatian yang telah diasingkan dilakukan dengan teknik 1D- and 2D-NMR (^{1}H, ^{13}C, DEPT, COSY, HMQC and HMBC). Analisis spektrum 1D-NMR (^{1}H-NMR menunjukkan isyarat δ 6-8 ppm untuk kumpulan aromatik dari aglikon flavonoid dan ^{13}C-NMR menunjukkan adanya isyarat tiga atom karbon dari cincin C flavonoid pada δ 182.8 ppm (C-4), 103.9 ppm (C-3), 166.4 ppm (C-2) and DEPT menunjukkan adanya kumpulan berfungsi CH and CH_2). Analisis spektrum 2D- NMR (COSY menunjukkan korelasi proton pada δ 7,86 and 6,92 ppm and HMBC menunjukkan korelasi antara proton pada δ 6.61 dengan 166.4 ppm dan 6.92 dengan 123.3 ppm).

Kata kunci: *Coleus atropurpureus* Benth, kromatografi turus, flavonoid, elusidasi struktur, teknik 1D- and 2D-NMR

Introduction

Iler (*Coleus atropurpureus* Benth) is a species of the genus Coleus in family Lamiaceae. Typical secondary metabolites of Lamiaceae include various terpenoids, especially mono-, sesqui- di- and tri-terpenes. Also various phenolic compounds, especially phenolic acids, such as rosmarinic acid and flavonoids are abundant. Nitrogen containing secondary metabolite play a minor role, such as stachydrine and other simple alkaloids [1]. Exudate flavonoids in the Lamiaceae concern flavones with a strong tendency towards 6-substitution and/or 8-substitution [2,3].

Flavonoid compounds have a variety of structures with interesting biological activity and is a major component of the family Lamiaceae. The systematic and phylogenetic analysis of plants was traditionally based on macroscopic

and microscopic morphological characters. Since secondary metabolites are often similar within members of a clade, their occurrence or absence might be taken as an indication of common descent and thus relatedness[1].

Study of the molecular structure of flavonoid compounds using ^{1}H-NMR and ^{13}C-NMR has become the method of choice for structure elucidation of flavonoid compounds. Chemical shifts and signal multiplicity of specific atoms and clutch with other atoms in the molecule allows for the identification of aglycone structure, glycosylation pattern and identification of the sugar cluster [4].

NMR spectroscopy in chemistry is not based on the ability to distinguish the elements in the compound, but it is based on the ability to learn certain core with respect to their chemical environment in the molecule would produce a signal expressed in resonance chemical shift. Based on the chemical shifts, the NMR spectroscopy yield important data that can be used to determine the molecular structure of a compound [5].

The purpose of a standard ^{1}H-NMR experiment is to record chemical shift, spin–spin coupling, and integration data, thus providing information about the relative number of hydrogen atoms. Applied to a flavonoid, this information may help in identifying the aglycone and acyl groups, the number of monosaccharides, and the anomeric configuration of the monosaccharides. However, for most flavonoids the information provided by a standard ^{1}H-NMR experiment is insufficient for complete structural elucidation. Thus, ^{13}C-NMR experiments combined with various 2D NMR experiments, especially those using gradient techniques that imply increased sensitivity, have to be used for assignments of all ^{1}H and ^{13}C-NMR signals. Two-dimensional NMR spectra are mainly produced as contour maps. These maps may be best imagined as looking down on a forest where all the trees (representing peaks in the spectrum) have been chopped off at the same fixed height. Two-dimensional NMR spectra are produced by homonuclear and heteronuclear experiments [4, 6].

NMR spectroscopy is an important method for the elucidation of the complete structure of flavonoid compounds based on the chemical shift (δ) and coupling constants (*J*) that they have with the ^{1}H-NMR and ^{13}C-NMR. 1D and 2D NMR spectroscopy supported by homo-and heteronuclear correlation crosspeaks. NMR spectroscopic method development has been made in determining the structure of the natural compound material which techniques such as DEPT 1D and 2D techniques such as COSY, HMBC and HMQC. 2D-NMR spectrum provide more information on the molecular 1D-NMR spectrum and is useful in determining the molecular structure [7]. Although the ^{13}C-NMR is usually not the method of choice to differentiate the flavonoid compounds, but can be useful in differentiating types of aglycone by aromatic carbon resonance chemical shift and three carbon atoms in the ring C are typical [8].

Experimental

Air-dried and powdered of the leaves of *Coleus atropurpureus* Benth (1.2 kg) were extracted at room temperature with methanol as solvent. Further partition with *n*-hexane and etylacetate. The ethylacetate extract (9.6 g) was subjected to column chromatography (CC) over silica gel as stationary phase using mixtures of *n*-hexane-etylacetate and ethylacetate as mobile phase based of gradient elution system or an increase in the polarity rise. Fractions with similar TLC patterns are combined and the solvent evaporated.

Fractions which showed positive results containing flavonoids then performed purification using preparative TLC with eluent *n*-hexane: ethylacetate (6:4 v/v). The pure isolate were determined by spectral analysis, i.e. 1D- and 2D-NMR techniques using a spectrometer JEOL 500 MHz to 1D-NMR (^{1}H-NMR, ^{13}C-NMR, DEPT) and 2D-NMR spectra (COSY, HMQC, HMBC).

Results and Discussion

The ethylacetate extract of the leaves of *Coleus atropurpureus* Benth were separated into its components using column chromatography with silica gel 60 as stationary phase and *n*-hexane-ethylacetate (6:4 v/v) as mobile phase. A pure isolate was obtained as an amorphous yellowish solid (37.5 mg). The structure of the pure isolate were determined by spectral 1D- and 2D-NMR experiments.

The ^{1}H-NMR spectrum of the isolated compound showed signals at chemical shifts of aromatic region δ 6-8 ppm as shown in Figure 1. The ^{1}H-NMR spectrum of the isolated compound displayed two meta-coupled doublets at δ 6.46

ppm (d, J = 2.0 Hz, 1H) and δ 6.21 ppm (d, J = 2.0 Hz, 1H) respectively for aromatic protons H-6 and H-8 on the ring A. The position of H-6 and H-8 are meta to each other. This is evidenced by the coupling constant values (*J*) 2.0 Hz, which is *Jmeta* 1-3 Hz [9]. This also proves the ring A contain two substituents at position C-5 and C-7.

Two doublet signals at δ 6.92 ppm (d, J = 9.1 Hz, 1H) and δ 7.86 ppm (d, J = 9.1 Hz, 1H) showed the orientation of the ortho proton signal for the proton H-3', 5' and H-2', 6' ring B with the substituents at position C-4'. A singlet signal at δ 6.61 ppm (1H, s) showed proton H-3 in ring C has isolated proton. The ^{1}H-NMR spectrum exhibited proton signals characteristic of flavone nucleus [2, 3].

Based on the chemical shifts of the aromatic rings indicated that the isolated compound is a flavone compound with substituents at position C-5, C-7 and C-4' (Figure 2). It is also based on the phytochemical of Lamiaceae family that the main flavonoids found in these families were flavone compound.

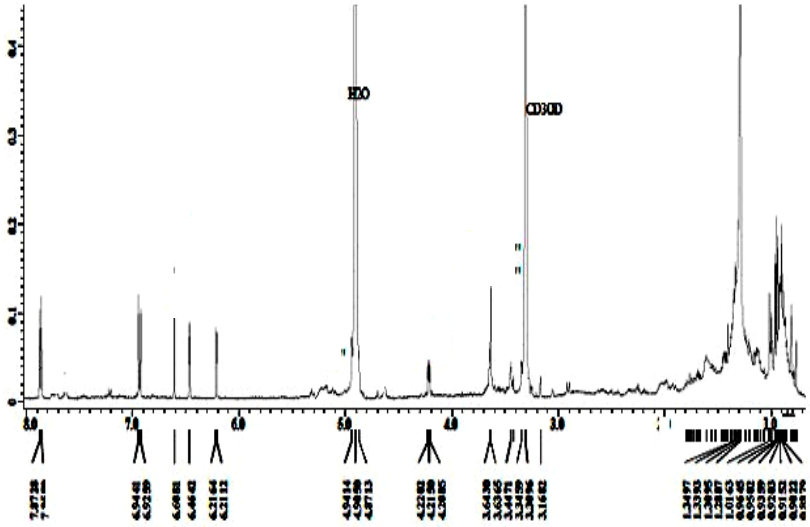


Figure 1. ^{1}H-NMR spectrum

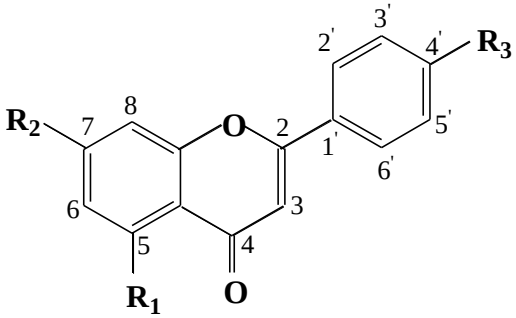


Figure 2. The isolated compound

The ^{13}C-NMR spectrum of the isolated compounds as shown in Figure 3. The signal for C-4 ' appears a singlet at δ 162.9 ppm for 4'-oxygenated ring B and the chemical shifts for the ortho carbon (C-3', 5') at 117.1 ppm, meta carbon (C-2', 6')) at δ 129.6 ppm and para carbon (C-l') at δ 123.3 ppm. It is closely related to the spectrum of 5-hidroxyflavone which the changes occur primarily to the carbon atoms in the ring B.

The chemical shift for the carbon of ring A appears on chemical shift 100.2 ppm (C-6) and 95.1 ppm (C-8). This is because of oxygenation at C-7 which will cause the signal of the ortho positions C-6 and C-8 shift towards upfiled about 13 ppm of the chemical shifts of compounds 5.4'-dihidroxyflavone 111.43 ppm for C-6 and 95.6 ppm for C-8. It is also influenced by the effects of the ortho and para hydrogen bonds OH at C-5 to C-6 carbon and C-8. Thus, C-6 is represented by signals at higher chemical shift region (downfield) than the C-8 atom. In the isolated compound C-3 signal appears at δ 103.9 and 105.6 ppm for C-10 similar to the signal for the compound 5,7,4 '-trihidroxyflavone at 104.3 ppm ascribed to C-3 and signal 105.1 ppm for C-10.

The chemical shifts for the signals of the carbon C-5 and C-9 shifted to downfield to 158.9 ppm and 163.2 ppm from 158.7 ppm and 162.0 ppm due to the influence meta position of hydroxyl group on the C-5 to the C-9 signal shift towards downfield [10].

The chemical shifts for the ring C of C-2 signal at δ 166.4 ppm, while the core compound flavone C-2 signal appears at 163.2 ppm, this is caused by the presence of 5-hydroxyl group so the C-2 downfield shifted signal. Atom C-3 signal appear at δ 103.9 ppm (104.3 ppm). The carbonyl carbon C-4 appeared as a less intense peak or very low in the region 182.8 ppm. Chemical shift downfield region only remaining 163.4 ppm signal is thus ascribed to C-7 [10].

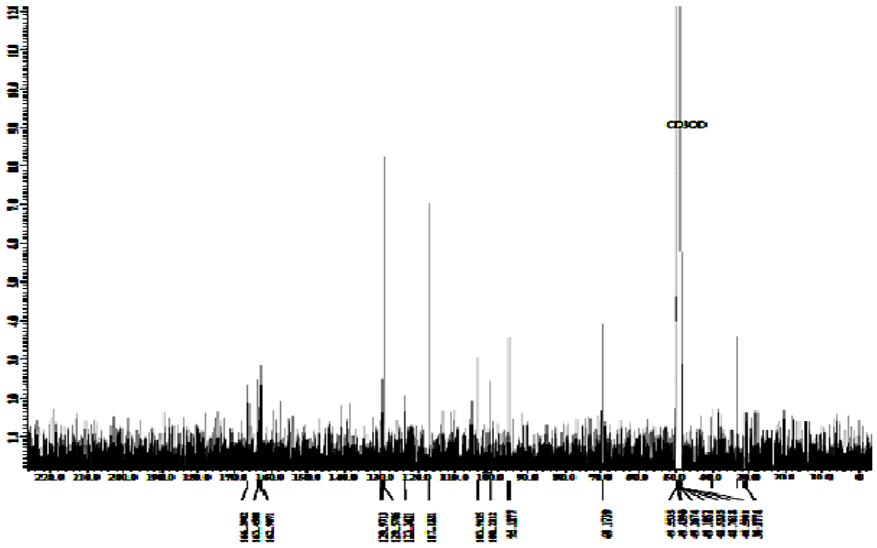


Figure 3. ^{13}C-NMR spectrum

DEPT spectrum of the isolated compound shows the number of CH_2 groups and CH/CH_3 groups. DEPT spectrum showed the presence one of methylene carbon (CH_2) at δ 69.2 ppm , twelve of metin carbon (CH) at δ 129.6 ppm (C-2',6'), 117.1 ppm (C-3',5'), 103.9 ppm (C-3), 100.2 ppm (C-6,1"), 95.1 ppm (C-8), 71.4 ppm (C-2",3",5") and 69.2 ppm (C-4") with peaks to up and eight quaternary carbon as shown in Figure 4.

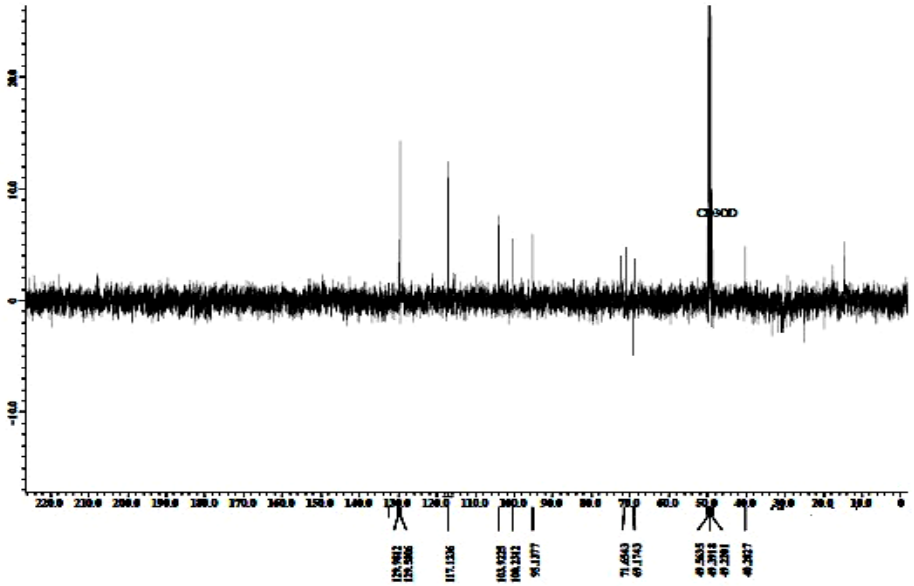


Figure 4. DEPT spectrum

^{1}H-NMR spectrum of the isolated compound can be explained in detail by using two-dimensional NMR spectrum (2D) correlation spectrum are homonuklir (^{1}H-^{1}H COSY) as shown in Figure 5. Figure 5 shows the correlations between proton H-2' and H-6' at δ 7.86 ppm with proton H-3' and H-5' at δ 6.92 ppm doublet which generates a signal which describes a system of aromatic monosubstitution on ring B. Correlation proton to the isolated compound just described for the proton H-2', 6' with proton H-3', 5'. ^{1}H-^{1}H COSY spectrum shows the correlations between the four protons in the form of vicinal protons.

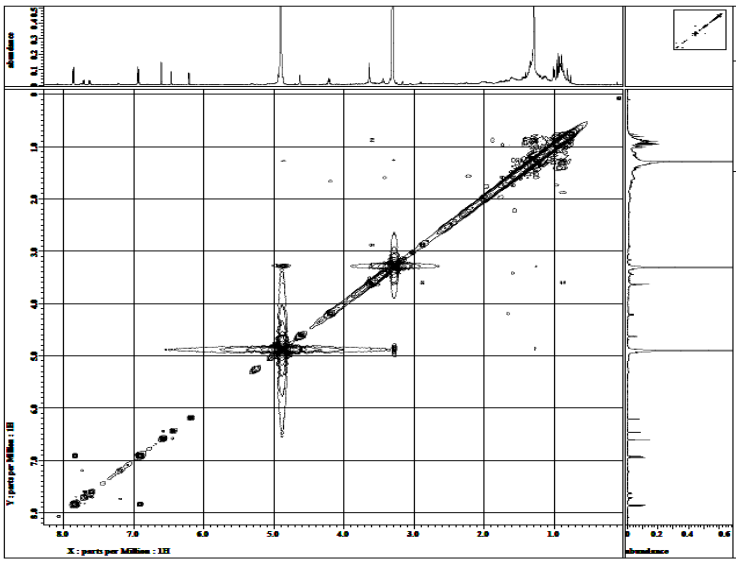


Figure 5. COSY spectrum

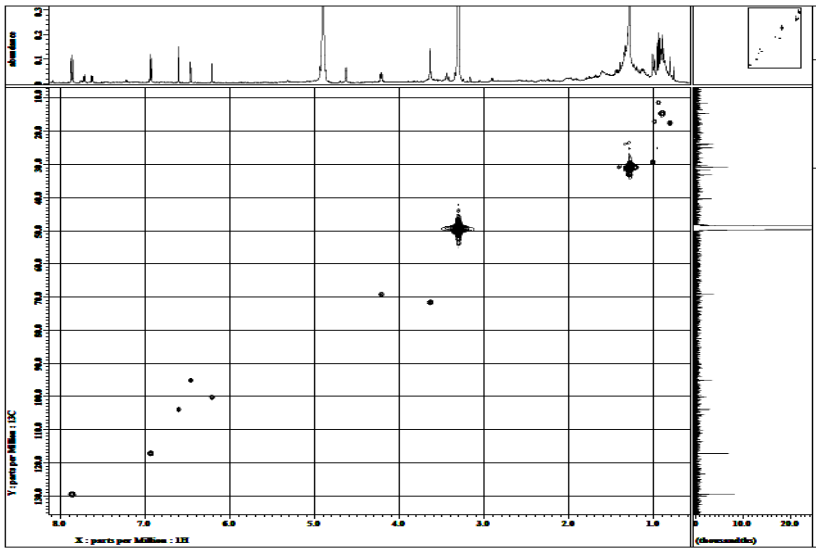


Figure 6. HMQC spectrum

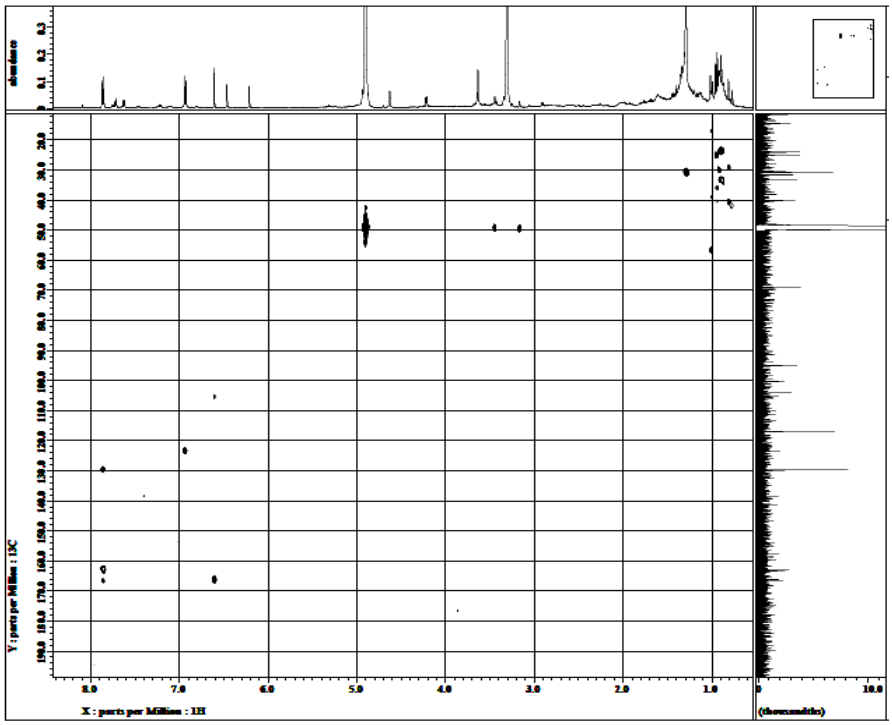


Figure 7. HMBC spectrum

HMQC spectrum (Figure 6) shown correlation between carbon and protons of skeleton of flavone compounds from the isolated compound. Characteristic of flavone compounds is the presence of a proton at position C-3 of ring C are indicated by the correlations between proton at δ 6.61 ppm (H-3) with δ 103.9 (C-3). The chemical shifts of aromatic protons in ring B at δ 7.86 (H-2', 6') correlated with a carbon at δ 129.6 ppm (C-2', 6') and proton at 6.92 ppm (H-3', 5') correlated with a carbon at δ 117.1 ppm (C-3',5').

The chemical shifts of the proton at ring A showed a correlation between proton at δ 6.21 ppm (H-6) with a carbon at δ 100.2 ppm (C-6) and proton at δ 6.46 ppm (H-8) with a carbon at δ 95.1ppm (C-8). Based on the correlations between proton and carbon of the isolated compound indicated that structure of the compound has only a hydrogen atom at position C-3, 6, 8, 2 ', 3', 5 ' and 6' while the atom C-5, 7 and 4 ' are substituent. Further evidence regarding the skeleton and substitution pattern of isolated compounds obtained from HMBC data analysis as shown in Figure 7.

Figure 7 shows long-range correlations between the singlet at δ 6.61 ppm (H-3) with a carbon at δ 166.4 ppm (C-2). The aromatic proton doublet signal at δ 7.86 ppm (H-2' and H-6') showed long-range correlations with two quaternary carbon atoms at δ 162.9 ppm (C-4') and δ 166.4 ppm (C-2) and correlated well with the carbon atom δ 129.6 ppm (C-6' and C-2'). This suggests that the presence of substituents on the atom C-4'. The HMBC spectrum also showed a correlation between aromatic protons at δ 6.92 ppm (H-3' and H-5') with a quaternary carbon at δ 123.3 ppm (C-1'). From the data HMBC shows the structure of flavone ring B substituted at C-4'.

Conclusion

On the basis of ^{1}H-NMR, ^{13}C-NMR, DEPT, COSY, HMQC and HMBC data the isolated compound were identified as flavone compound with substituents at C-5, C-7 and C-4'.

References

1. Wink, M. (2003). Evolution of Secondary Metabolites from and Ecological and Molecular Phylogenetic Perspective, *Phytochemistry* (64), 3-19.
2. Valant-Vetschera,K.M., Roitman,J.N. and Wollenweber,E. (2003). Chemodiversity of exudates flavonoids in some members of the Lamiaceae, *Biochemical Systematics and Ecology* (31), 1279-1289.
3. Skaltsa. H., Karioti, A., Heilmann, J., and Sticher, O. (2003). Acylated Flavonoid and Phenylethanoid Glycosides from *Marrubium velutinum*, *Phytochemistry* (64), 655-660.
4. Fossen, T. and Andersen, Q.M. (2006). Spectroscopic Techniques Applied to Flavonoids, In Markham, K.R. and Andersen, Q.M., At Flavonoids : Chemistry, Biochemistry, and Applications, CRC Press.
5. Sastrohamidjojo, H. (1994). Spektroskopi Resonansi Magnetik Inti (Nuclear Magnetic Resonance, NMR), Liberty Yogyakarta.
6. Stobiecki, M. and Kachlicki, P. (2006). Isolation and Identification of Flavonoids, In Grotewold, E., At The Science of Flavonoids, The Ohio State University Columbus, Ohio, USA.
7. Rossomando, P.C. (2009). NMR, In Sampietro, D.A., Catalan, C.A.N., Vattuone, M.A, At Isolation, Identification and Characterization of Allelochemicals/Natural Products, Science Publishers, Enfield, USA.
8. Markham, K.R., Chari, V.M., and Marby, T.J. (1982). Carbon-13 NMR Spectroscopy of Flavonoids, In Harborne, J.B. and Marby, T.J., At The Flavonoids : Advances in Research, Chapman and Hall, London.
9. Silverstein, R.M., Bassler, G.C. and Morril, T.C. (1991) Spectrometric Identification of Organic Compounds, 5th ed, John Wiley & Sons.
10. Ternai, B and Markham, K.R. (1976). Carbon-13 NMR Studies of Flavonoids-I : Flavones and Flavonols, *Tetrahedron* Vol. 32, 565-569.

The Malaysian Journal of ANALYTICAL SCIENCES ISSN 1394-2506

TANDEM SOLID PHASE EXTRACTION FOR THE DETERMINATION OF PHARMACEUTICALS IN WASTEWATER

(Pengekstrakan Fasa Pepejal Secara Penggabungan Katrij Untuk Analisis Farmaseutikal Dalam Air Sisa Buangan)

Licaberth Ismail*, Rozita Osman, Norashikin Saim

Faculty of Applied Sciences, Universiti Teknologi MARA, 40450 Shah Alam, Selangor

**Corresponding author: lica.ismail@yahoo.com*

Abstract

In this study, a simple and rapid tandem solid phase extraction (SPE) was developed for the analysis of seven pharmaceuticals (acetaminophen, caffeine, carbamazepine, diclofenac, naproxen, ibuprofen and metoprolol) in wastewater sample. The novel aspect of coupling SPE cartridge in tandem is the ability to simplify the SPE procedure (sample introduction step) as no single sorbent was able to retain and concentrate all selected compounds since these compounds are of different physicochemical properties. A tandem SPE cartridges using Oasis HLB and octadecyl bonded silica (C_{18}) was found to be efficient with the advantages of minimizing sample volume and reducing analysis time. Using this approach, carbamazepine, diclofenac, naproxen and metoprolol were trapped in the Oasis HLB while acetaminophen, caffeine and ibuprofen were trapped in the second cartridge (C_{18}). The instrumental limits of detection (LOD) ranged from 0.01 to 0.04 µg/L and satisfactory recoveries were obtained between 76% to 104%. The calibration curves were linear from 0.1 to 5.0 µg/mL, with correlation coefficients (R^2) in the range of 0.995 to 0.999. The developed method was applied to the analysis of pharmaceuticals in wastewater samples. The amount of pharmaceuticals detected in wastewater samples varied from 0.4 to 24.5 mg/L.

Keywords: pharmaceuticals, solid phase extraction, Oasis HLB, wastewater

Abstrak

Dalam kajian ini, pengekstrakan fasa pepejal (SPE) yang ringkas dan cepat telah dibangunkan untuk menganalisa tujuh jenis farmaseutikal (acetaminophen, kaffein, carbamazepin, diclofenak, naproxen, ibuprofen dan metoprolol) dalam sampel air sisa buangan. Aspek novel penggabungan katrij SPE secara berturutan ialah meringkaskan prosedur pengekstrakan disebabkan tiada satu penjerap yang boleh mengekstrak dan memekatkan kesemua farmaseutikal dalam satu ekstraksi kerana sifat fizikokimianya yang berbeza. Penggabungan katrij secara berturutan iaitu Oasis HLB dan silica terikat oktadesil (C_{18}) didapati lebih cekap dengan kelebihan dapat mengurangkan isipadu sampel dan tempoh masa analisis. Dengan menggunakan pendekatan ini, carbamazepin, diclofenak, naproxen dan metoprolol diperangkap dalam Oasis HLB manakala acetaminophen, kaffien dan ibuprofen diperangkap dalam katrij yang kedua (C_{18}). Had pengesanan instrumentasi yang diperolehi ialah dari 0.01-0.04 µg/L and peratus perolehan semula farmaseutikal ialah di antara 76% -104%. Graf kalibrasi yang diperolehi adalah linear dari 0.1-5.0 µg/mL,dengan nilai pemalar kolerasi (R^2) dari 0.995 -0.999. Kaedah yang dibangunkan ini telah diaplikasikan untuk menganalisa farmaseutikal dalam sampel air sisa buangan. Kepekatan farmaseutikal yang diperolehi adalah di antara 0.4 to 24.5 mg/L.

Kata kunci: farmaseutikal, pengekstrakan fasa pepejal, Oasis HLB, air sisa buangan

Introduction

From a global perspective, Malaysia has made considerable headway in environmental issues compared to other countries. In the 2010 Environmental Performance Index, Malaysia ranked 54th out of 163 examined countries and performed better than other countries like Poland, the US and Belgium in addressing environmental challenges. Rapid development and industrialization over the last few years have resulted in an increase of industrial and domestic discharges into the water system. Realizing the importance of environmental protection, the Malaysian

government once again focuses on environmental aspects in its 10th Malaysian Plan (2011-2015) called "Building an environment that enhances quality of life" that promises to introduce new legislation and incentives to ensure that all industries and consumers comply with the measures necessary to take on the country's environmental problems. The sources of water pollution can be categorized as point and non-point sources. Point sources include sewage treatment plants, manufacturing and agro-based industries and animal farms, whereas non point sources are mainly diffused sources such as agricultural activities and surface runoffs. In the year of 2010, the Department of Environment (DOE) has reported 20,348 water pollution sources comprise of sewage treatment plant (49.27%), manufacturing industries (44.57%), animal farms (3.7%) and agro-based industries (2.46%). In the recent years, worldwide focus of environmental research has widened from universal pollutants such as polycyclic aromatic hydrocarbons and pesticides to emerging pollutants such as pharmaceuticals and personal care products. Pharmaceuticals are classified as the so-called emerging contaminants which referred to previously unknown or unrecognized pollutants. Great concern towards these emerging contaminants is the fact that they may be carcinogenic, mutagenic and reproductively toxic [1]. Sewage treatment plants (STPs) are not able to remove pharmaceuticals and their excretion metabolites completely, and thus, they are discharged to different environmental compartments at concentrations ranging from μg/L to ng/L.

Commonly used pharmaceuticals selected in this study are anti-inflammatory drugs/analgesics (i.e. acetaminophen, diclofenac, and naproxen, ibuprofen), β_1 receptor blocker (i.e. metoprolol), stimulant drug (i.e. caffeine) and antiepileptic drug (i.e. carbamazepine). Sample preparation prior to the analysis of pharmaceuticals in wastewater sample requires effective, selective and rapid extraction technique to ensure optimum enrichment of the analytes of interest, as pharmaceuticals present at trace levels in wastewater compartment. Togola and Budzinski [2, 3] reported the use of octadecyl bonded silica (C_{18}), Oasis HLB and MCX as SPE cartridges for the extraction of several pharmaceuticals, whereby the use of MCX cartridge gave highest recoveries. However, MCX was able to give higher selectivity and sensitivity for basic compounds with cation exchange groups. In this study, C_{18} and HLB were chosen for the analysis of pharmaceuticals with different polarity, basicity, and acidity. Reversed phase (RP) materials (C_{18}) are clearly advantageous in terms of cost. However, its application towards polar species is restricted to weakly acidic or basic compounds. For polar compounds and strongly acidic and basic pharmaceuticals, Oasis HLB will significantly improve the extraction. The work presented here dealt with the development of simple and rapid tandem solid phase extraction (SPE) in analyzing pharmaceuticals in water. The chromatographic analysis was done using two types HPLC; HPLC with diode array detector (HPLC-DAD) and HPLC with fluorescence detector (HPLC-FLD). Fluorescent pharmaceuticals were analyzed using HPLC-FLD due to higher sensitivity and selectivity [4]. The proposed method was applied to wastewater samples to determine the occurrence these pharmaceuticals in the environment.

Materials and Methods

Reagent

Seven pharmaceuticals (as tabulated in Table 1) were purchased from respective supplier. Acetaminophen and naproxen were purchased from Sigma-Aldrich (St.Louis, USA, purity assay in range of 98-101%). Carbamazepine was obtained from Sigma-Aldrich (China, purity assay ≥ 98%). Ibuprofen was purchased from Sigma-Aldrich (Belgium, purity assay ≥ 98%). Diclofenac and metoprolol in their salt form were bought from Sigma-Aldrich (Steinheim, Italy, purity assay ≥ 98%). Methanol, acetonitrile of HPLC-grade and ultrapure water were purchased from Merck (Darmstafd, Germany). Phosphate buffer solution was prepared from phosphate buffer tablet obtained from CALBIOCHEM, Germany. SPE cartridges, packed with 1 g of C18 and 60 mg of Oasis HLB were purchased from Biotage (Europe) and Waters (Milford, MA, USA). Ultrapure water purchased from Merck (Darmstafd, Germany) was used to prepare the spiked water sample.

Instrumentation

HPLC-DAD was performed on Agilent 1200 Series (Germany) equipped with diode array detector 3 using Acclaim Polar Advantage2 (C_{18} column), 150 mm x 4.6 mm internal diameter with 5 μm particles. For fluorescent compounds, separation was carried out on Agilent 1200 Series (Germany) with fluorescence detector using ZORBAX Rx-SIL column, 250 mm x 4.6 mm internal diameter with 5 μm particles.

Chromatographic Conditions

Chromatographic analysis of acetaminophen and caffeine, methanol and water were used as mobile phases and detection were done at 254 nm and 280 nm, respectively. Diclofenac and naproxen were analysed using acetonitrile and phosphate buffer adjusted to pH 3 with detection at 235 nm and 280 nm. For carbamazepine, acetonitrile and water was used as mobile phases and detected at 280 nm. All analysis was done at 40 °C and flow rate of 1.0 mL/min. For chromatographic analysis of ibuprofen, mobile phase was acetonitrile (30):25 mM phosphate buffer (70), flow rate of 1.2 mL/min, excitation wavelength at 263 nm, and emission wavelength at 288 nm. Separation of metoprolol was achieved using acetonitrile (70):25 mM phosphate buffer (30), flow rate of 1.0 mL/min, excitation and emission wavelength at 229 nm and at 298 nm, respectively. The retention time registered for all pharmaceuticals is tabulated in Table 1.

Preparation of Standard Solution

A stock solution of 1000 mg/L for each pharmaceutical was prepared by dissolving standard pharmaceuticals using methanol (HPLC-grade), ethyl acetate: acetone (50:50, v/v), and deionized water. The standard solutions were prepared for calibration purposes by diluting the stock solution in the range of 0.01 to 50 mg/L.

Solid Phase Extraction (SPE)

The target pharmaceuticals were extracted from water samples using two types of SPE cartridges (C_{18} and Oasis HLB). The pharmaceuticals (2 mg/L and 3 mg/L) were spiked using ultrapure water for the recovery test. The elution procedure for C_{18} was adapted from the study conducted by Togola and Budzinski [3]. The extraction procedures were improved by connecting SPE cartridges (C_{18} and Oasis HLB) in tandem arrangement with Oasis HLB on top of that C_{18}. The conditioning step was done separately, whereby C_{18} is conditioned using 3 ml of 50:50 (ethyl acetate: acetone), 3 mL of methanol and 3 ml of deionized water. For Oasis HLB, conditioning was done by 3 mL of methanol, followed by 3 mL of deionized water. Water sample (500 mL) was loaded onto the tandem cartridges at 15 mL/min. After sample loading, cartridges were separated and let to dry for 30 minutes. Washing of cartridges was done using 6 ml deionized water and 6 mL of methanol and once again were let to dry for 1 hour. Elution of pharmaceuticals from C_{18} and Oasis HLB was done using 9 ml of 50:50 (ethyl acetate: acetone) and 6 mL of methanol, respectively. Pharmaceuticals obtained from each cartridge were evaporated to 1 mL prior to chromatographic analysis.

Method Validation

In order to apply the proposed method to environmental samples, the instrumental method was validated based on several parameters as follows:

Linearity

Ten different low level concentrations (0.1-5.0 μg/mL) of each pharmaceutical were chosen for linearity studies. The responses were measured as peak areas versus concentration.

Precision

The injection of repeatability was determined by five replicates of each standard pharmaceutical. The precision of the method was established by five replicates of the spiked water sample.

Limit of Detection and Limit of Quantification

The limit of detection (LOD) and limit of quantification (LOQ) were established by injection of seven replicates of very low concentration for each pharmaceutical

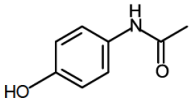
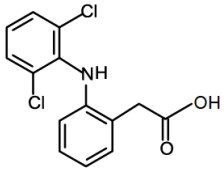
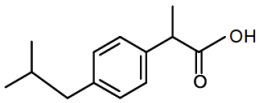
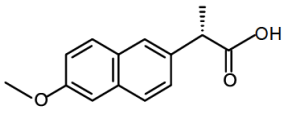
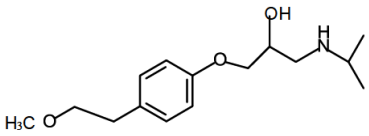
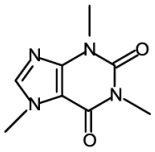
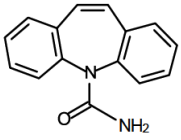
Preparation of Spiked Sample

Distilled water (100 mL) was adjusted to pH 2.0 and filtered through 0.45 μm glass fibre filter (Whatman International Ltd Maidstone, England). Sample was then spiked with the working standard solution of seven pharmaceuticals (3 μg/mL). Spiked sample was agitated for 1-2 min prior to SPE extraction.

Preparation of Water Sample

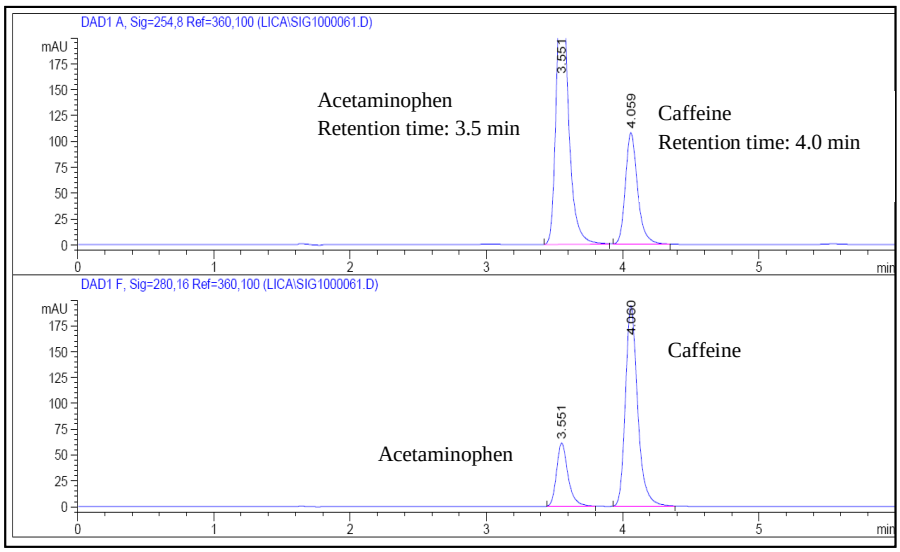
Wastewater samples obtained from wastewater treatment plant (WWTP) of Indah Water Consortium and Universiti Teknologi MARA (UiTM, Shah Alam, Selangor) were filtered through 0.45 μm glass fiber filter to remove suspended matter. Samples were stored in amber bottles at 4 °C until analysed.

Table 1. Studied pharmaceuticals with various parameters (therapeutic group, chemical properties, structure, molecular weight, pKa and retention time).

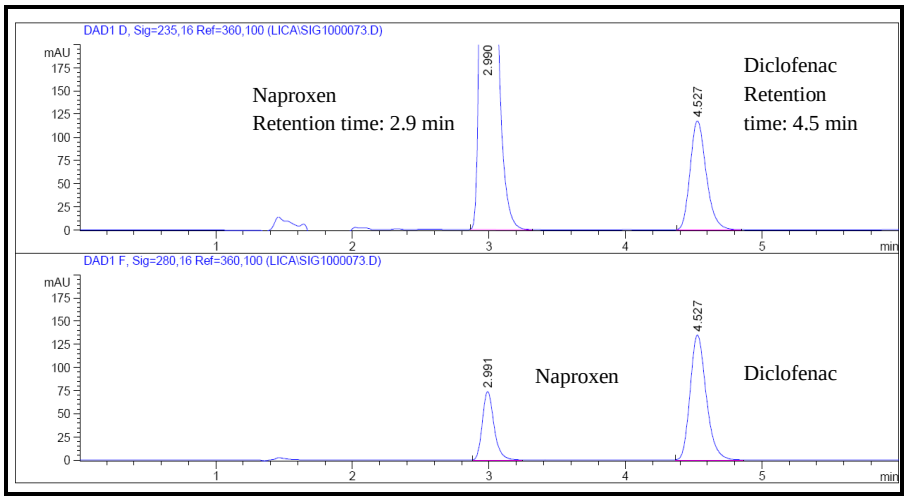
Pharmaceuticals	Therapeutic group	Chemical properties	Structure	MW (g/mol)	pKa	Retention Time
Acetaminophen	Anti-inflammatory/ analgesics	Acidic		151	9.5	3.2-3.4
Diclofenac	Anti-inflammatory/ analgesics	Acidic		194	14.0	3.9-4.0
Ibuprofen	Anti-inflammatory/ analgesics	Acidic		236	13.4	2.7
Naproxen	Anti-inflammatory/ analgesics	Acidic		295	4.0	4.0-4.1
Metoprolol	β1receptor blocker	Basic		230	4.4	2.9
Caffeine	Stimulant	Basic		206	4.2	1.8
Carbamazepine	Antiepileptic drug	Basic		267	9.68	5.4

Data of DIC, IBU, NAP, MET and CBZ from [5], Data of ACT and CAF from [6]

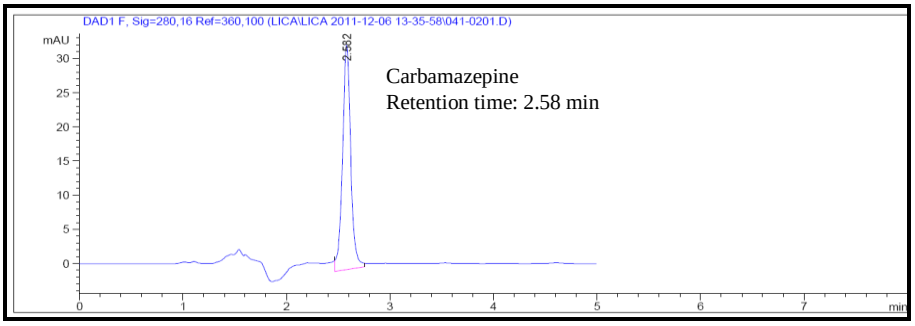
Figure 1 shows the chromatogram of standard pharmaceuticals analysed using HPLC-DAD at wavelength of 235 nm, 254 nm and 280 nm.



(a)



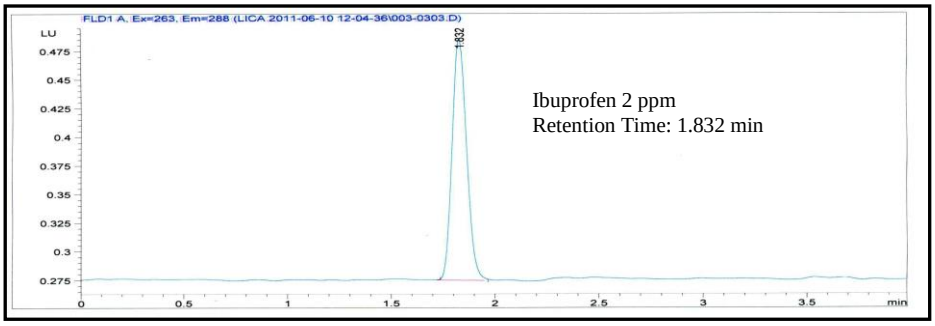
(b)



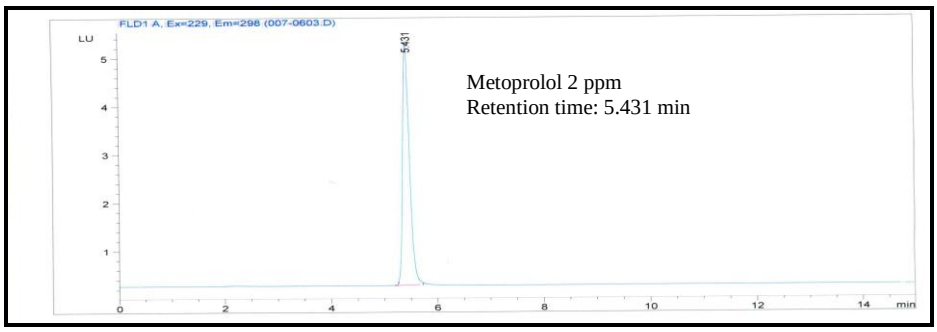
(c)

Figure 1. Chromatogram of standard pharmaceuticals separated using HPLC-DAD; (a) Acetaminophen at 254 nm and ibuprofen at 280 nm; (b) Naproxen at 235 nm and diclofenac at 280 nm; (c) Carbamazepine at 280nm.

Figure 2 (a) and (b) show the chromatogram of standard ibuprofen and metoprolol separated using HPLC-FLD.



(a)



(b)

Figure 2. Chromatogram of standard ibuprofen and metoprolol using HPLC-FLD.

Results and Discussion

HPLC Separation

In this study, two types of liquid chromatography were used to analyse seven pharmaceuticals; HPLC-DAD and HPLC-FLD. HPLC-DAD was used to separate caffeine, acetaminophen, diclofenac, naproxen, and carbamazepine, while HPLC-FLD was used to separate ibuprofen and metoprolol. Selection of wavelengths for the detection of these compounds was based on previous studies [7, 8]. Column temperature for HPLC-DAD was set at 40 °C in order to increase column efficiency and decrease retention time. Common solvents; methanol, acetonitrile (ACN), phosphate buffer and deionized water were used as mobile phases. However, due to the different physicochemical properties of these compounds, separation was done separately using various compositions of mobile phases. Acetaminophen and caffeine were separated using deionized water: methanol with 70:30 ratios, while diclofenac and naproxen was separated using ACN: phosphate buffer (pH 3) with 70:30 ratio. Separation of carbamazepine was achieved using ACN: deionized water with 60:40 ratios. Ibuprofen and metoprolol was separated using ACN and phosphate buffer (pH 7.4) with ratio of 30:70 and 70:30, respectively.

Linearity study was done using individual standard or standard mixtures with concentration ranges from 0.1 - 5.0 µg m/L. In order to justify the applicability of the proposed method, calibration curve was prepared using the least square regression analysis between average area and concentration of pharmaceuticals. Linear relationship of the correlation coefficients (R^2) in the range of 0.995 to 0.999 was obtained for all studied pharmaceuticals (Table 2). The linearity of the calibration curves gave an indication on the suitability of the chromatographic method over a wide range of concentration for the studied pharmaceuticals. The repeatability of the HPLC injection system as well as the developed method is determined by the values of the relative standard deviation for five replicates injection of the standard solution of the studied pharmaceuticals. The relative standard deviation (RSD) is presented in Table 2. Low RSD (< 1%) was obtained for all pharmaceuticals, showing good precision.

The instrumental LOD and LOQ were determined and expressed as µg/L, varied from 0.007 to 0.054 and the LOQ was determined from the calculated LOD, ranged from 0.023 to 0.374. This low value of LOD and LOQ shows the method is applicable to be used for the analysis of pharmaceuticals in wastewater sample. Considering the sample enrichment (0.5 L water sample will be reconcentrated to 1000 µL) obtained and environmental concentrations reported for the studied pharmaceuticals, we can propose the application of this HPLC method to study the occurrence of pharmaceuticals in the water compartments as it enable the detection of studied pharmaceuticals at trace levels (ng/mL)

Table 2. Method Validation Parameters

Pharmaceuticals	Retention Time (min)	LOD (µg/L)	LOQ (µg/L)	Precision (% RSD)	Coefficient Correlation, R^2
Acetaminophen	3.4	0.013	0.041	0.025	0.999
Caffeine	4.0	0.013	0.041	0.025	0.999
Carbamazepine	2.7	0.037	0.374	0.159	0.998
Diclofenac	4.0	0.007	0.023	0.136	0.999
Ibuprofen	1.8	0.054	0.161	0.027	0.998
Naproxen	2.8	0.007	0.023	0.099	0.995
Metoprolol	5.4	0.021	0.067	0.525	0.999

Arrangement of Tandem Cartridges

The capability of SPE cartridges was evaluated using water sample spiked with the working standard solution of seven pharmaceuticals (3 μg/mL). Since no single sorbent was able to retain and concentrate compounds with different physicochemical properties, preliminary study was conducted to evaluate the performance of C_{18} and Oasis HLB on the retention of the selected pharmaceuticals. C_{18} was chosen as it is advantageous in terms of cost, although its application towards polar species is restricted to weakly acidic or basic compounds. Oasis HLB is used for the extraction of polar compounds and strongly acidic and basic pharmaceuticals to overcome the limitation of C_{18}. Retention mechanism of both C_{18} and Oasis HLB is based on reversed phase [9]. However, Oasis HLB is more specific to hydrophobic compounds with some hydrophilic functionality, especially aromatics (lipophilic divinylbenzene). Hydrophilic N-vinylpyrrolidone provides retention of polar analyte. Carbamazepine, diclofenac, naproxen and metoprolol were efficiently trapped in the Oasis HLB (Table 3), while acetaminophen, caffeine and ibuprofen were trapped in C_{18}. Based on these results, tandem SPE cartridges approach was developed. Positioning Oasis HLB on top of $C_{18,}$ specific pharmaceuticals (carbamazepine, diclofenac, naproxen and metoprolol) were retained by Oasis HLB, while the pharmaceuticals (acetaminophen, caffeine and ibuprofen) poorly retained by Oasis HLB will pass through and retain by the second cartridge, C_{18}. Retention mechanism of C_{18} is based on the attractive forces between the carbon-hydrogen bonds in the analyte and the functional groups on the sorbent surface. However, if the positioning of C_{18} is above Oasis HLB, only some of the hydrophobic compounds will be trapped, while other will pass through. This resulted in poor recoveries of some pharmaceuticals (carbamazepine, diclofenac, naproxen and metoprolol). The proposed tandem SPE approach with Oasis HLB on top of C_{18} successfully retained seven pharmaceuticals selected in this study as tabulated in Table 3. Satisfactory and comparable recoveries of pharmaceuticals were obtained using both single cartridge and arrangement in tandem approaches.

Table 3. Recoveries (%) of pharmaceuticals using different approach of SPE extraction.

Pharmaceuticals	Single Cartridge (n=3)		Tandem Cartridges (C_{18}-Oasis HLB) (n=3)	
	C_{18}	Oasis HLB	C_{18}	Oasis HLB
Acetaminophen	94.5 ± 0.9	nd	90.5 ± 1.5	nd
Caffeine	104.6 ± 4.1	nd	87.4 ± 15	nd
Ibuprofen	60.4 ± 3.3	nd	76.6 ± 1.6	nd
Carbamazepine	nd	95.7 ± 0.1	nd	89.0 ± 1.4
Diclofenac	nd	88.9 ± 0.6	nd	104.7 ± 0.1
Naproxen	nd	102.3 ± 3.6	nd	90.2 ± 3.5
Metoprolol	nd	89.1 ± 2.0	nd	85.3 ± 2.0

nd = not detected (below the limit of detection)

Acetaminophen gave good recovery (90.5%) using the tandem cartridges approach as compared to single cartridge Oasis HLB approach reported by Justin *et al.* [10] with 52.8% recovery. The tandem cartridges approach also gives good recovery of caffeine (87.4%) as compared to that (67.7%) obtained by Martin *et al.* [1]. Improved recovery of ibuprofen was obtained using tandem SPE cartridges as compared to single cartridge approach, and the recovery of this pharmaceutical (60.4%-76.6%) concurred with previous studies conducted by Azzouz *et. al* and Yu & Wu [4,8]. Recoveries of carbamazepine, diclofenac, naproxen and metoprolol using Oasis HLB single cartridge were in the range of 88.9%-102.3%, comparable to the recoveries obtained using tandem SPE cartridges approach (85.3%-104.7%). This result showed that the use of tandem cartridges can significantly simplify the extraction procedures by using one-step sample loading for seven pharmaceuticals with different physicochemical properties, thus reducing the analysis time with an advantage of minimising sample volume.

Analysis of wastewater samples

The developed method was applied for the analysis of pharmaceuticals in wastewater samples from Indah Water treatment plant and Universiti Teknologi Mara (UiTM) treatment plant in Shah Alam, Selangor. Table 4 shows the amount of pharmaceuticals detected in samples from these wastewater treatment plants. Acetaminophen and caffeine were found in high concentrations in influent wastewater sample obtained from UiTM (10.7 mg/L and 24.5 mg/L), respectively compared to wastewater sample from Indah Water (8.5 mg/L and 11.3 mg/L), respectively. The results showed high consumption of these pharmaceuticals among the students' community. Ibuprofen and naproxen were found in higher concentration from wastewater sample of Indah Water (3.4 mg/L and 1.5 mg/L) compared to water sample of UiTM (0.7 mg/L and 0.43 mg/L), respectively. Concentrations of 1.5 µg/L for naproxen and 85 µg/L for ibuprofen have been found in some STP effluents [6] and low removal efficiencies (between 15% and 69%) for diclofenac [11] have been reported by several researchers. The concentration of diclofenac from the wastewater sample of Indah Water was 2.0 mg/L, but was not detected in wastewater sample of UiTM as this pharmaceutical is used for reducing inflammation and as analgesic reducing pain for arthritis or acute injury, which may not be commonly used by the students. Prolonged exposure to diclofenac has been reported to cause toxic effects and bioaccumulation in fish [12]. The concentration of carbamazepine was below LOD in both wastewater treatment plant samples. Metoprolol, used for the treatment of hypertension, angina pectoris and arrhythmia was detected from the wastewater sample of UiTM (1.2 mg/L), but not from the wastewater sample of Indah Water. The reported concentrations of all pharmaceuticals were significantly higher and not in the same order with those reported in European countries [6, 9, 13]. However, significant amounts of these pharmaceuticals were detected from water samples of both treatment plants suggested that they can be good chemical markers for human contamination and may be a very promising alternative for verification of consumption of pharmaceuticals in local communities.

Table 4. Concentrations of the pharmaceuticals in the WWTP of Indah Water and UiTM.

Pharmaceuticals	Concentration of Pharmaceuticals (mg/L), n=3	
	UiTM	Indah Water
Acetaminophen	10.7 ± 1.0	8.5 ± 0.8
Caffeine	24.5 ± 1.5	11.3 ± 0.2
Ibuprofen	0.7 ± 2.6	3.4 ± 4.0
Naproxen	0.4 ± 2.6	1.5 ± 1.2
Diclofenac	nd	2.0 ± 4.0
Carbamazepine	nd	nd
Metoprolol	1.2 ± 0.02	nd

nd = not detected (below the limit of detection)

Conclusion

A rapid and selective (SPE) using tandem-cartridges Oasis HLB and octadecyl, C_{18} for the determination of seven pharmaceuticals in wastewater sample was developed. The Oasis HLB sorbent retained the polar compounds and strongly acidic and basic pharmaceuticals (carbamazepine, diclofenac, naproxen and metoprolol), while the weakly acidic or basic compounds (acetaminophen, caffeine and ibuprofen) were poorly retained in Oasis HLB will pass through and retained by the C_{18}. The developed SPE procedure using tandem SPE cartridges approach of Oasis HLB and C_{18} was found to be efficient with the advantage of minimizing sample volume and reducing analysis time. This developed tandem SPE cartridges approach has allowed simultaneous extraction using two different sorbents in a single sample loading. The application of the developed method on wastewater sample from two treatment plants was able to detect the significant amount of the studied pharmaceuticals with acceptable repeatability. The amount of pharmaceuticals in wastewater may be applied in the estimation of the usage of pharmaceuticals in a community.

Acknowledgement

The authors would like to acknowledge the financial support obtained from Universiti Teknologi MARA for this project (Project number: 600-RMI/DANA 5/3/SG (1/2012).

References

1. Martín, J., Santos, J.L., Aparicio, I., Alonso, E. (2010). Multi-residue method for the analysis of pharmaceutical compounds in sewage sludge and sediments by sonication-assisted extraction and LC determination. *Journal of Separation Science, 33,* 1786-1766
2. Togola, A., Budzinski, H. (2007). Analytical development for analysis of pharmaceuticals in water samples by SPE and GC-MS. *Analytical and Bioanalytical Chemistry, 338,* 627.
3. Togola, A., Budzinski, H. (2008). Multi-residue analysis of pharmaceutical compounds in aqueous samples. *Journal of Chromatography A, 1177,* 150–15.
4. Malaysia Environmental Quality Report (2010). Department of Environment. Ministry of Natural Resources and Environment, Malaysia
5. Azzouz, A., Souhail, B., Ballesteros, E. (2010). Continuous solid-phase extraction and gas chromatography–mass spectrometry determination of pharmaceuticals and hormones in water samples. *Journal of Chromatography A, 1217,* 2956–2963
6. Kosma, C.I., Lambropoulou, D.A., Albanis, T.A., (2010). Occurrence and removal of PPCPs in municipal and hospital wastewaters in Greece. *Journal of Hazardous Material, 179, 804–817.*
7. Damiani, P.C., Bearzotti, M., Cabezon, M.A. (2001). Spectrofluorometric determination of ibuprofen in pharmaceutical formulations. *Journal of Pharmaceuticals and Biomedical Analysis, 25,* 679-683.
8. Huber, U. (1998). Application Notes: Analysis of Anti-inflammatory Drugs by HPLC. Agilent Technologies, Waldbronn, Germany.
9. Yu, Y., Wu, L. (2011). Comparison of four extraction methods for the analysis of pharmaceuticals in wastewater. *Journal of Chromatography A, 1218,* 2483–2489.
10. Justin M.C., Steven J.S., Scott A.K., Sean M.R. (2008). Rapid liquid chromatography–tandem mass spectrometry method for the determination of a broad mixture of pharmaceuticals in surface water. *Journal of Chromatography A, 1185,* 206–215.
11. Heberer, T., Feldman, D. (2005). Contribution of effluents from hospital and private households to the total loads of diclofenac and carbamazepine in municipal sewage effluents – modeling versus measurements. *Journal of Hazard Mater 122,* 211–21.
12. Richardson, S.D., Ternes, T.A. (2005). Emerging Contaminants and Current Issues. *Analytical Chemistry, 77,* 3807-3838.
13. Zorita, S., Mårtensson, L., Mathiasson, L., (2009). Occurrence and removal of pharmaceuticals in municipal sewage treatment system in the south of Sweden. *Science Total Environment, 407,* 2760-2770.

The Malaysian Journal of ANALYTICAL SCIENCES ISSN 1394-2506

SUBCRITICAL WATER EXTRACTION OF MONOSACCHARIDES FROM OIL PALM FRONDS HEMICELLULOSES

(Pengekstrakan Air Subgenting Daripada Monosakarida Dari Hemiselulosa Pelepah Kelapa Sawit)

R., Norsyabilah, S. Sabiha Hanim*, M. H., Nor Suhaila, A. Noraishah, A.K., Siti Kartina

Faculty of Applied Sciences,
Universiti Teknologi MARA, 40450 Shah Alam, Selangor D.E. , Malaysia

**Corresponding author: sabihahanim@salam.uitm.edu.my*

Abstract

Oil palm plantations in Malaysia generate more than 36 million tones of pruned and felled oil palm fronds (OPF) and are generally considered as waste. The composition of monosaccharide in oil palm frond can be extracted using hydrothermal treatment for useful applications. The objectives of this study were to quantify the yield of monosaccharides at various reaction conditions; temperature 170 °C to 200 °C, pressure from 500 psi to 800 psi, reaction time from 5 to 15 min using subcritical water extraction and to determine the composition of oil palm frond hemicelluloses at optimum condition. The monosaccharides composition of oil palm frond hemicellulose were analysed using High Performance Liquid Chromatography (HPLC). The highest yield of monosaccharides can be extracted from OPF at temperature of 190 °C, pressure of 600 psi and 10 min of contact time which is xylose the most abundant composition (11.79 %) followed with arabinose (2.82 %), glucose (0.61 %) and mannose (0.66 %).

Keywords: oil palm fronds; monosaccharide; subcritical water extraction; HPLC

Abstrak

Ladang kelapa sawit di Malaysia telah menghasilkan lebih daripada 36 juta tan buah sawit yang masak dan juga pelepah sawit di mana ianya di kategorikan sebagai sisa-sisa tanaman kelapa sawit. Kandungan monosakarida yang terdapat dalam pelepah kelapa sawit ini boleh diekstrak dengan menggunakan hidrotermal proses untuk pelbagai aplikasi yang berguna. Objektif-objektif kajian ini adalah untuk menetukan hasil monosakarida pada keadaan yang berbeza dari segi suhu 170 °C hingga 200 °C, tekanan pengekstrakkan 500 psi hingga 800 psi dan masa 5 hingga 15 min dengan menggunakan kaedah pengekstrakkan "subcritical water extraction" dan untuk mengkaji komponen-komponen monosakarida yang terdapat dalam hemiselulosa pelepah kelapa sawit dalam keadaan yang optimum. Komponen dalam monosakarida dianalisis dengan menggunakan Kromatografi Cecair Berprestasi Tinggi (HPLC). Hasil pengektrakan monosakarida pelepah kelapa sawit yang tertinggi adalah pada suhu 190 °C, tekanan 600 psi dan masa10 min di mana kandungan xilosa adalah yang paling banyak (11.7902 %) diikuti dengan arabinosa (2.8202 %), glukosa (0.6076 %) dan mannosa (0.6618 %).

Kata kunci: pelepah kelapa sawit; monosakarida; "subcritical water extraction"; HPLC

Introduction

Nowadays, agriculture waste from Oil palm tree reached an abundant of waste because of the oil palm tree is a most important commercial crop in Malaysia. The most generated oil palm biomass is oil palm fronds, which is produce 83 million tonnes per year, and it also can be obtained daily during replanting or pruning season for harvesting empty fruit bunch [1]. Currently, there are lots of studies focusing on the oil palm by-product such as oil palm fronds because it consists of high carbohydrate, which is simple sugar and less component of heavy metal [2]. Simple sugar might be produced as recycling nutrient with appropriate method or treatment. Hemicellulose is the second abundant in biomass component, and they are containing several types of monosaccharide as known as simple sugars units with different structure. An enrichment component of the hardwood is a carbohydrate.

Monosaccharide and oligosaccharides which are produced by the carbohydrate decomposition and it can be converted into such as biofuel, additive food or valuable product [3]. Solubilized monosaccharide can be converted to others polymer [4]. Subcritical water extraction (SWE) is an extractant as known as uncatalyzed hydrothermal treatment for hemicelluloses oil palm fronds extraction. The principle of SWE can maintain in a liquid phase at the high temperature with suitable pressure during the extraction process within the range that was given. It also can call as an environmental process because no chemical added instead of deionised water. Hydrothermal treatment is an effective process, especially in hydrolysis of hardwood processes and minor effect to softwood [5]. Monosaccharides can be separated and quantified by chromatographic methods [6].

Materials and Methods

Oil palm fronds were collected from local oil palm plantation in Selangor area. The raw materials were washed with deionised water to remove the impurities like sand or other small particle and then were dried in oven at 40 °C for 24 hours. The samples were cut, ground and sieved to achieve fine fibres with a size of <0.5 mm. The samples were then stored at room temperature.

Extraction of hemicelluloses

SWE was carried out at Block G laboratory, UiTM Shah Alam. SWE was performed using an accelerated solvent system ASE 200 from Dionex Corporation. In the extraction process, the subcritical water extractions were focused on three parameters, which were extraction temperature (180, 190 and 200 °C), pressure (500, 600 and 700 psi) and extraction time (5, 10 and 15 min). The oil palm fronds chips (2.0 g) were added in the extraction cell. Approximately, 60 mL of water was filled in the cell and heated at those parameters. The extracts were collected, centrifuged at 8000 rpm for 15 min and then the liquid extract was filtered with 0.45 µm cellulose acetate membrane filter (Minisart, Sartorius, Germany). The extracts were freeze-dried prior to analyse using high performance liquid chromatography (HPLC).

Quantification of monosaccharide sugars using HPLC

Monosaccharide compositions were determined by HPLC (Agilent, USA). Deionized water was used as a mobile phase at flow rate of 0.5 mL/min, temperature 80 °C and 35 °C for column Bio-rad Aminex HPX 87H (7.8 mm x 300 mm) and refractive index detector, respectively. Freeze dried hemicelluloses was dissolved in deionized water and filtered through a 0.45 µm cellulose acetate membrane filter (Minisart, Sartorious, Germany) before injecting (20 µL) into the column. The mixture of xylose, glucose, arabinose, and mannose were used as a standard.

Statistical Analysis

The data were determined by the Duncan multiple range test from one-way analysis of variance (ANOVA), and the significance of the differences between means was determined, where $p < 0.05$ of sample was considered statistically significant. The SPSS (Statistical Package for Social Science) statistical computer package was used to analyze the experimental data (SPSS, Inc., Chicago, IL, USA) [6].

Results and Discussion

Effect of temperature on monosaccharide yield

Temperature is an important factor that influenced the extraction process on monosaccharide [7]. SWE extraction process was carried out at different temperature, which were 180 °C, 190 °C and 200 °C, while the pressure and extraction time were fixed at 600 psi and 10 min, respectively.

Clearly, xylose is the most of highest composition (11.79 %) followed with arabinose (2.82 %) and the minor quantity were glucose (0.61 %) and mannose (0.66 %) at temperature of 190 °C. The same finding was reported from the previous study which xylose was found to be the main constituent in the extracts of flax shives using PLPW at extraction temperature of 180 °C [8]. Based on the previous studies, extraction temperature of 190 °C was selected as an optimum temperature due to high total sugar content. It showed that the trend of the total monosaccharide yield was proportionally increased when the temperature was increased [9]. Statistical analysis showed that significant differences existence between temperature of 180 °C and 200 °C ($P<0.05$) but there was no significant difference between temperature of 190 °C and 200 °C ($P>0.05$). Therefore, 190 °C was selected as the

optimum point of extracting temperature in the response surface methodology (RSM) experiment. Different agricultural wastes had different structure and they also had different responses to experimental condition [10].

Table 1. Design matrix and the yield of monosaccharides obtained

Treatment Condition			**Percent yield of monosaccharides (%)**			
Temperature (^{O}C)	Pressure (psi)	Time (min)	Xylose	Glucose	Mannose	Arabinose
180	500	10	11.79	1.77	0.94	1.79
190	500	10	10.67	1.60	0.86	1.79
200	500	10	7.14	3.32	0.57	1.99
190	600	10	11.79	0.61	0.66	2.83
190	700	10	2.49	1.27	2.46	8.16
190	600	5	4.16	0.17	2.25	3.29
190	600	15	10.67	1.60	0.87	1.79

Effect of pressure on monosaccharide yield

To investigate the effect of pressure on the monosaccharide yield, the experiment was conducted at constant temperature (190 $^{\circ}$C) and time (10 min) with the pressure between 500, 600 and 700 psi. The result showed that the percent yield of monosaccharides increased proportionally with pressure between arabinose and mannose at different condition compared to xylose and glucose. It was reported that steam pressure could help to optimise and obtain an intermediate hemicelluloses product for high-value utilization induced by modification of remarkable structural in the treatment process [11].The highest total monosaccharide was obtained at 600 psi. According to previous study, the yield of monosaccharide was increased between 500 to 600 psi and decreased when pressure higher than 600 psi [9]. The statistical analysis showed that there were significant differences ($P<0.05$) between 500, 600 and 700 psi of pressure. Therefore, 600 psi was selected as the optimum point of extracting contact time in the response surface methodology (RSM) experiment.

Effect of contact time on monosaccharide yield

Another factor that influences the extraction efficiency and selectivity of fluid is contact time. The results showed that the yield of xylose, arabinose, glucose and mannose was high at 10 min. Similar results were observed from the previous study [8]. The total yield of monosaccharide composition was increased when increasing time from 5 to 10 min and decrease slightly after 10 min. Statistical analysis showed that significant differences existence between 5 and 10 min ($P<0.05$) but there was no significant difference between 10 min and 15 min ($P>0.05$). Longer time can be affected the structure of monosaccharide [12]. Furthermore longer reaction time of the extraction process can cause more decomposition of monosaccharide content [13]. Therefore, 10 min was selected as the optimum point of extracting contact time in the response surface methodology (RSM) experiment.

Conclusion

In conclusion, the highest monosaccharide's composition can be extracted from OPF using subcritical water extraction at temperature of 190 $^{\circ}$C, pressure of 600 psi and 10 min of contact time which is xylose the most abundant composition (11.79 %) followed with arabinose (2.82 %), glucose (0.61%) and mannose (0.66 %).

Acknowledgement

The authors are grateful to the Faculty of Applied Sciences, Research Management Institute (RMI), UiTM Shah Alam and Ministry Of Higher Education (MOHE) Malaysia for the financial support under the Fundamental Research Grant Scheme (FRGS):600-RMI/ST/FRGS 5/3/Fst (211/2010). The authors are also grateful to the Analytical Unit, Faculty of Pharmacy, UiTM Puncak Alam for using HPLC equipment.

References

1. Abu Hassan., Ishida, M., Mohd, I., Shukri., Ahmad Tajuddin, Z. (2000). Oil-palm fronds as a roughage feed source for ruminants in Malaysia. Research division. Malaysian Agriculture Research and Development Institute (MARDI).
2. Mior, AK., Mohd Zahari., Mohd Rafein, Z., Hidayah, A., Mohd Noriznan, M., Jailani, S., Yoshihito, S., Mohd Ali H. (2012). Renewable sugars from oil palm frond juice as an alternative novel fermentation feedstock for value-added products. *Bioresource Technology*, 110: 566–571.
3. Matsunaga, M., Matsui, H., Otsuka, Y., Yamamoto, S. (2008). Chemical conversion of wood by treatment in semi-batch reactor with subcritical water. *Journal of Supercritical Fluids*, 44: 364-369.
4. Xiao, B., Sun, X.F., RunChans, Sun. (2001). Chemical, structural and thermal characterizations of alkaline-soluble and hemicelluloses, and cellulose from maize stems, rye straw and rice. *Polymer Degradation and Solubility*, 74: 307-319.
5. Tsuyoshi, S., Hiroyuki, I., Shinichi, Y., Takashi, E., Shigeki., Sawayama. (2008). Combining hot-compressed water and ball milling pretreatments to improve the efficiency of the enzymatic hydrolysis of eucalyptus. *Biotechnology for fuels*, 186: 1754-5834.
6. Vuorinen, T., Alén, R. (1999). Analytical Methods in Wood Chemistry, Pulping and Papermaking. *Journal of carbohydrate*, 38–75.
7. Kronholm, J., Hartonen, K. & Riekkola, M.(2007)**.** Analytical extractions with water at elevated temperatures and pressures. *Trends in Analytical Chemistry*, 26
8. Buranov AU, Mazza G (2010). Extraction and characterization of hemicelluloses from flax shives by different methods. *Carbohydr Polym* 79: 17–25.
9. Sabiha, S.H., Norsyabilah, R., Nor Suhaila, M.H., Noraishah, A., Siti Kartina, A. K.(2012). Effects of temperature, time and pressure on the hemicelluloses yield extracted using subcritical water extraction. *Procedia Engineering*, 42: 616-619.
10. Alpinar, O., Levent, O., Sabanci, S., Uysal, R. S., Sapci B. (2011). Optimization and comparison of dilute acid pretreatmentof selectedagricultural residues for recovery of xylose. Peer-reviewed *Bioresources*.
11. Wang, K., Xin, J. J., Xu, F., Cang, S. R., Baird, M. S. (2010). Influence of steam pressure on the physicochemical properties of degraded hemicelluloses obtained from steam exploded Lespedeza stalk. Peer-reviewed *Bioresource*.
12. Cai, W., Gu, X. & Tang J. (2008). Extraction, purification, and characterization of the polysaccharides from Opuntia milpa alta. *Carbohydrate Polymers*, 71: 403-410.
13. Itziar, E., Cristina, S., Inaki, M., Jalel, L. (2012). Effect of alkaline and autohydrolysis processes on the purity of obtained hemicelluloses from corn stalk. *Bioresource technology*, 103: 239-248.

The Malaysian Journal of ANALYTICAL SCIENCES ISSN 1394-2506

PHENOLIC COMPOUNDS FROM THE FRUITS OF *ORANIA SYLVICOLA*

(Sebatian Fenol daripada Buah *Orania sylvicola*)

Solihah Sukari*, Ikram M. Said

School of Chemical Sciences and Food Technology, Faculty of Science and Technology, Universiti Kebangsaan Malaysia, 43600 UKM Bangi, Selangor Darul Ehsan, Malaysia

**Corresponding author: solihah_sukari@yahoo.com*

Abstract

Fruits of *Orania sylvicola* (Arecaceae) were extracted with methanol and partitioned with chloroform and n-butanol. Investigation of the chloroform and n-butanol partitions by repetitive chromatographic method resulted in the isolation of two known compounds, namely, 5-hydroxy-7,4'-dimethoxyflavone (**1**) and 4-hydroxybenzoic acid (**2**). Compound **1** was isolated from chloroform fraction while compound **2** was presented in n-butanol fraction. 4-hydroxybenzoic acid is the major phenolic compound and has been used as a chemotaxonomic marker for the Arecaceae family. Their structures were elucidated with UV-VIS, IR, NMR (^{1}H, ^{13}C, HSQC, HMBC, COSY and NOESY) and MS.

Keywords: Arecaceae, *Orania sylvicola*, 4-hydroxybenzoic acid, 5-hydroxy-7,4'-dimethoxyflavone

Abstrak

Buah *Orania sylvicola* (Arecaceae) diekstrak menggunakan metanol dan dipartisikan kepada bahagian kloroform dan n-butanol. Kajian ke atas partisi kloroform dan n-butanol dengan kaedah kromatografi yang berulangan telah menemui dua sebatian yang diketahui, iaitu 5-hidroksi-7,4'-dimetoksiflavon **(1)** dan asid 4-hidroksibenzoik (**2**). Sebatian **1** dipencilkan daripada fraksi kloroform manakala sebatian **2** hadir di dalam fraksi n-butanol. Asid 4-hidroksibenzoik ialah sebatian fenol yang utama dan bertindak sebagai penanda kemotaksonomi bagi famili Arecaceae. Struktur sebatian ini dikenal pasti melalui UV-VIS, IM, RMN (^{1}H, ^{13}C, HSQC, HMBC, COSY and NOESY) dan JM.

Kata kunci: Arecaceae, O*rania sylvicola*, asid 4-hidroksibenzoik, 5-hidroksi-7,4'-dimetoksiflavon

Introduction

Orania, genus from family Arecaceae (palm tree) have been identified previously as consisting of 28 species [1]. Most of the species in genus *Orania* show a robust canopy while a few exist as a small understory palm, distributed from Malaysia to the Philippines, New Guinea, Australia, Indonesia and West Irian, but mostly it is found in New Guinea [2]. *Orania* species can be found at lowland coastal swampy heath forest about 10 m above sea level and highland tropical humid rainforest about 1220 m above sea level [1]. There is little economic use, in some species, the fruits and buds are said to be poisonous [3 - 5]. *Orania sylvicola* species or in ancient times known as *O. macrocladus*, locally called 'Ibul' is one of the poisonous fruit [6]. *O. sylvicola* is found in Malaysia and Indonesia notably in Ulu Kesial (Kelantan), Melaka, Pahang, Pulau Pangkor, Cameron Highland, Perlis, Fraser Hill and Jawa [5 - 6]. It is a solitary large palm about 60 feet tall and 18 inch diameter [5]. Fruits are globose with 4.5 - 5 cm diameter, dull green when young and yellowish green when mature [1]. There has been no work done on the chemical constituents for any species of *Orania*. In this paper, we investigate the chemical substituents of *O. sylvicola* fruits where two phenolic compounds were isolated and their structures elucidated with various spectroscopic techniques.

Materials and Methods

General Experimental Procedure

All solvents used for chromatography were of analytical reagent grade. Silica gel 60 for CC and radial chromatography were purchased from Merck (Darmstadt, Germany). ^{1}H, ^{13}C, HSQC, HMBC, COSY and NOESY

NMR spectra were taken on a Bruker/ Avance 111 600 MHz Cryoprobe spectrometer in $CDCl_3$ and MeOD with TMS as internal standard. UV-VIS spectra were recorded on a Shimadzu UV-VIS Spectrophotometer- 2450. IR spectral data were measured on a Perkin Elmer Fourier Transform Infrared 400 Attenuated Total Reflectance (ATR) and sampel used are in solid state. Mass spectra were obtained from direct injection ESI-MS Bruker MicroTOF Q with flow rate 180 µL/hour using syringe pump.

Plant material

A fruit of O. sylvicola were collected from Perlis, Malaysia and was identified by Herbarium of Taman Botani, Putrajaya (voucher specimen, HTBP 2577). Mature fruits were de-shelled and dried under room temperature. It was then ground to fine meal using a grinder.

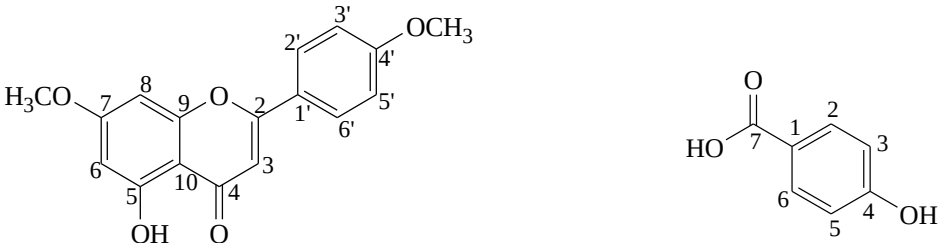
Extraction and Isolation

The fine meal (2 kg) was extracted by cold extraction method with n-hexane (3 L) followed by methanol (3 L), successively. After two days extraction, the mixture was filtered to separate the soluble and residue. The extraction was repeated three times. MeOH extracts were combined and evaporated to dryness by rotary evaporator. The dried MeOH extract (44 g) was dissolved in 80% MeOH and 20 % H_2O, and partitioned between $CHCl_3$ and n-BuOH by liquid-liquid extraction yielding chloroform fraction (1.18 g), n-butanol fraction (8.90 g) and the methanol aqueous fraction (27.85 g).

Separations on the chemical components of the chloroform fraction start with injection on column chromatography. The eluent consisting a mixture of diethyl eter: chloroform: methanol (6: 3.5: 0.5 v/v) at normal phase silica gel. By observation with thin layer chromatography (TLC), seven combination fractions were pooled. The third fraction was applied to a silica gel column chromatography eluted with hexane: chloroform: methanol (2.5: 7: 0.5, v/v), yielding compound 1 (0.5 mg), which was purified with repeated radial chromatography using 100% chloroform. For the n-butanol fraction, the crude extract was injected on silica gel column chromatography and eluted with hexane: chloroform: methanol (3.5: 6: 0.5, v/v) with increasing polarity, yielded six fractions. Purification of fraction two by repeated radial chromatography afforded compound 2 (7.9 mg).

Results and Discussion

Two known phenolic compounds were isolated where compound 1 was from chloroform fraction while compound 2 was from n-butanol fraction.



5-hydroxy-7,4'-dimethoxyflavone (**1**) 4-hydroxybenzoic acid (**2**)

Fig. 1. Structures of compound **1** & **2**

Compound **1**, a white amorphous solid having molecular formula $C_{17}H_{14}O_5$, deduced from positive ESIMS at m/z 321.0518 $[M+Na]^+$ and m/z 299.0713 $[M+H]^+$. The skeleton of 1 was further supported by the presence of 17 carbons in its ^{13}C NMR spectrum. UV absorption of 1 in MeOH at 269 nm and 326 nm is typical of a flavone structure [7]. The IR spectrum exhibited a broad vibrational band due to hydroxyl group at 3418 cm^{-1} and a carbonyl band at 1738 cm^{-1}. From ^1H NMR, two signals for two aromatic methoxy groups appeared at δ3.90 and δ3.89 were

placed at C-7 and C-4', respectively as they showed ^{3}J correlation with these carbons at δ165.4 and δ162.6 ppm in its HMBC spectrum. Strong NOE correlations of the δ3.90 methoxy proton with H-6 and H-8, and correlation with H-3' and H-5' for δ3.89 methoxy protons were observed at ring-B in its NOESY spectrum. One proton singlet at δ6.59 was assigned to H-3 which showed correlation with H-6' in the NOESY spectrum. Two *ortho*-coupled doublets at δ7.85 and δ7.02 and two meta-coupled doublets at δ6.38 and δ6.49 were assigned to H-2' and H-6', and H-3' and H-5', and H-6 and H-8, respectively on the basis of HSQC and HMBC studies. From the COSY spectrum, there were correlations between protons at H-2' and H-3' or H-5' and H-6'. The singlet at δ12.82 corresponded to a chelated hydroxy group at H-5. Thus from the foregoing spectral features, the structure of 1 was established as 5-hydroxy-7,4'-dimetoxyflavone (Table 1, Fig. 1 and Fig. 2). This analysis was also consistent with other reports in the literature for 1 [8 - 10].

Compound **2** was obtained as a white amorphous solid and its molecular formula suggested as $C_7H_6O_3$, deduced from negative ESIMS at m/z 137.0235 $[M+H]^+$. The IR absorption bands of 2 showed signals for hydroxyl group (3462 cm^{-1}) and carbonyl group (1654 cm^{-1}). Broad absorption band at frequency from 3400 cm^{-1} to 2400 cm^{-1} showed the presence of carboxylic acid. ^{1}H NMR spectrum for 2 in $CDCl_3$ showed two signals for proton resonance at aromatic ring. Two *ortho*-coupled doublet of triplet at δ 7.89 and δ 6.84, each integrating for two protons, H-2 and H-6, and H-3 and H-5 respectively. The proton NMR spectrum was in agreement with the literature [13] while ^{13}C NMR spectrum (Table 1), exhibited seven carbons resonance at five different signals. Signals at δ131.6 and δ114.7 ppm, each corresponding to two carbons, C-3 and C-5, and C-2 and C-6. The signal at δ 168.8, is correlated to carbon at C-7 or COOH. The above spectral analysis strongly indicates that the structure of compound 2 is 4-hydroxybenzoic acid or *p*- hydroxybenzoic acid (Table 1 and Fig. 1). From the literature, compound 2 was used as a chemotaxonomic marker for the family Arecaceae [12]. Besides, compound 2 also has been reported in *Euterpeoleracea martius* (acai) and *Calamus quiquesetinervius* Burret [13, 14].

Table 1: 1H & 13C (600 MHz) NMR data for compound **1** (MeOD) and **2** ($CDCl_3$)

Position	**1**			**2**	
	δ_H (mult, *J* in Hz)	**δ_C**	**HMBC (δ ^{1}H)**	**δ_H (mult, *J* in Hz)**	**δ_C**
1					121.3
2		164.1	H-3; H-2', H-6'	7.89 (dt, *J* =2.4, 9)	131.6
3	6.59 (s)	104.4		6.84 (dt, *J* =2.4, 9)	114.7
4		182.5	H-3		161.9
5				6.84 (dt, *J* =2.4, 9)	114.7
6	6.38 (d, *J* =2.4)	98.1		7.89 (dt, *J* =2.4, 9)	131.6
7		165.4	OCH_3-7; H-6; H-8		168.8
8	6.49 (d, *J* =2.4)	92.7			
9		157.7	H-8		
10		105.6	H-3; H-6; H-8; 5-OH		
1'		123.6	H-3'; H-5'		
2'	7.85 (d, *J* =9)	128.1			
3'	7.02 (d, *J* =9)	114.5			
4'		162.6	OCH_3-4'; H-2'; H-3'; H-5'; H-6'		
5'	7.02 (d, *J* =9)	114.5			
6'	7.85 (d, *J* =9)	128.1			
5-OH	12.82 (s)	162.2	H-6		
7-OMe	3.90 (s)	55.8			

4'-OMe	3.89 (s)	55.6

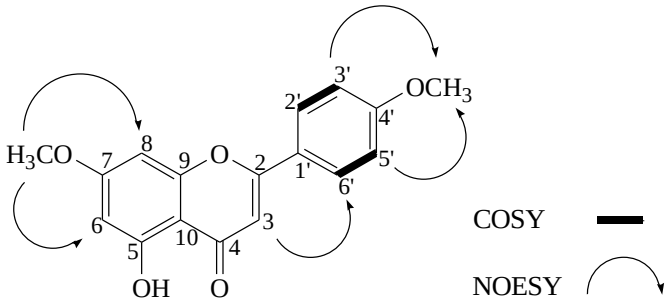


Fig. 2. 1H-1H COSY and NOESY correlation for **1.**

Conclusion

In the studies of chemical components from *Orania sylvicola* fruits, two known phenolic compounds, 5-hydroxy-7,4'dimetoxyflavone (1) and 4-hydroxybenzoic acid (2) were isolated and successfully identified. 4-hydroxybenzoic acid has been used as a chemotaxonomic marker of Arecaceae family. While, 5-hydroxy-7,4'dimetoxyflavone has not been reported yet from this family. Particularly, both compounds is now reported for the first time from the fruits of the species *O. sylvicola*.

Acknowledgement

The research was partially supported by the grant UKM-PNI-NBD0009-2007 and gratefully acknowledged.

References

1. Keim, A. P & Dransfield, J. (2012). A monograph of the genus Orania (Arecaceae: Oranieae). *The Board of Trustees of the Royal Botanic Gardens, Kew Bulettin*, 67: 127-190.
2. Essig, F. B. (1980). The genus *Orania Zipp* (Arecaceae) in New Guinea. *Lyonia*, 1 (5): 211-233.
3. McCurrach, J. C. (1960). *Palms of the World*. Harper and Brothers, New York.
4. Ridley, H. N. (1925). *Flora of the Malay Peninsula*. V. L. Reeve & Co., Ltd., London.
5. Whitmore, T. C. (1973). *Palms of Malaya*. Oxford Univ. Press, London.
6. Gimlette, J. D. (1915). *Malay Poison and Charm Cures*. Oxford University Press. Kuala Lumpur.
7. Mabry, T.J., Markham, K.R., Thomas, M.B. (1970). *The Systematic Identification of Flavonoids*. Springer Verlag, New York.
8. Herrera, J. C., Romero, A. J. R., Crescente, O. E., Acosta, M. & Pekerar, S. (1996). Analysis of 5-hydroxy-7-methoxyflavones by normal-phase high performance liquid chromatography. *Journal of Chromatography A*, 740: 201-206.
9. Kolak, U., Hacibekiroglu, I., Ozturk, M., Ozgokce, F., Topcu, G. & Ulubelen, A. (2009). Antioxidant and anticholinesterase constituents of *Salvia poculata*. *Turk J Chem*, 33: 813-823.
10. Rossi, M. H., Yossida, M. & Maia, J. G. S. (1997). Neolignans, Strylpyrones and Flavonoids from an Aniba Species. *Phytochemistry*, 45(6): 1263-1269.
11. Tan, J., Bednarek, P., Liu, J., Schneider, B., Svatos, A. & Hahlbrock, K. (2004). Universally occurring phenylpropanoid and species-specific indolic metabolites in infected and uninfected *Arabidopsis thaliana* roots and leaves. *Phytochemistry*, 65: 691–699.
12. Chakraborty, M., Das, K., Dey, G. & Mitra, A. (2006). Unusually high quantity of 4-hydroxybenzoic acid accumulation in cell wall of palm mesocarps. *Biochemical Systematics and Ecology*, 34: 509 - 513.

13. Chang, C. L., Wang, G. J., Zhang L. J., Tsai, W. J., Chen, R. Y., Wua, Y.C. & Kuo, Y. H. (2010). Cardiovascular protective flavonolignans and flavonoids from *Calamus quiquesetinervius*. *Phytochemistry*, 71: 271 - 279.
14. Pacheco-Palencia, L. A., Duncan, Ch. E. & Talcot, St. T. (2009). Phytochemical composition and thermal stability of two commercial acai species, *Euterpe oleracea* and *Euterpe precatoria*. *Food Chem*, 115: 1199–1205.

The Malaysian Journal of ANALYTICAL SCIENCES ISSN 1394-2506

STEROIDAL COMPOUNDS FROM THE ROOTS OF *HOLARRHENA CURTISII*

(Sebatian Steroid daripada Akar *Holarrhena curtisii*)

Noor Fazila Zahari*, Ikram M. Said

School of Chemical Science and Food Technology, Faculty of Science and Technology
Universiti Kebangsaan Malaysia, 43600 UKM Bangi, Selangor D.E.

**Corresponding author: fazilazahari@yahoo.com*

Abstract

Two known steroidal compounds namely pregnenolone (**1**), an androstane steroid [3-hydroxypreg-5-en-20-one] and stigmasterol (**2**) [stigmasta-5,22-dien-3β-ol] have been isolated from methanol extract of the roots of *Holarrhena curtisii* by using several chromatographic means. Their structures were elucidated through a combination of NMR, IR and GC-MS techniques by comparison with the data obtained from the literature. Separation of pregnenolone and stigmasterol from the *Holarrhena curtisii* has never been reported.

Keyword: Apocynaceae, *Holarrhena curtisii*, roots, steroids, pregnenolone, stigmasterol

Abstrak

Dua sebatian steroid yang diketahui iaitu pregnenolon, sebatian steroid androstana (3-hydroxypreg-5-en-20-one) dan stigmasterol telah diasingkan daripada ekstrak methanol akar *Holarrhena curtisii* dengan menggunakan pelbagai kaedah kromatografi. Struktur sebatian berikut telah ditentukan melalui kombinasi teknik RMN, IM, dan KG-SJ secara perbandingan dengan data daripada kajian lepas. Pemisahan sebatian pregnenolon dan stigmasterol daripada *Holarrhena curtisii* belum pernah dilaporkan.

Kata kunci: Apocynaceae, *Holarrhena curtisii*, akar, steroid, pregnenolone, stigmasterol

Introduction

Numerous drugs with steroidal ring structures have neen isolated from plant sources. The limited yield of some bioactive compounds in plants however gives a significant challenge for drug development. The use of plants and their preparations to treat infectious diseases is an age-old practice. *Holarrhena curtisii* which is locally know as ”Pulai Tanah” is a native plant of Malaysia [1]. It has been used traditionally for the treatment of dysentery especially amoebic dysentry [2, 3]. This decidious tree [4] belongs to a very important alkaloid family Apocynaceae [5] and provide mainly steroidal alkaloids of the aminopregnane type [6]. Alkaloids isolated from *H. curtisii* are used as antibiotics [7] while the non-alkaloid extract exhibited significant cytotoxic activity [8].

The purpose of this study is to identify and characterize the bioactive principles from the roots of *Holarrhena curtisii*. This paper describes the isolation and structural elucidation of two unreported steroid compounds from this species which are identified as pregnenolone (1) and stigmasterol (2) on the basis of spectroscopic evidence.

Experimental

General Experimental Procedures

Solvents used are from analar grade. Thin layer chromatography (TLC) was carried out on a silica gel 60 F_{254}. Reagents used are 5% H_2SO_4, Vanillin and 5% H_2SO_4 in EtOH. ^{1}H, APT and 2D NMR spectra were recorded in $CDCl_3$ on a FT-NMR 600MHz Cryoprobe Model Bruker/AVANCE III equipped with TOPSPIN 2.1 software. Chemical shifts are given in δ (ppm) values referred to the internal standards, tetramethylsilane (TMS) while

coupling constant in Hz. IR spectra were measured on FTIR Model Perkin Elmer GC1605 spectrophotometer. GC-MS were determined on an Agilent 7890A gas chromatograph directly coupled to the mass spectrometer system of an Agilent 5975C inert MSD with triple-axis detector.

Plant Material

Roots of *Holarrhena curtisii* were collected from Perlis. A voucher specimen UKMB21593 is deposited at the herbarium of National University of Malaysia.

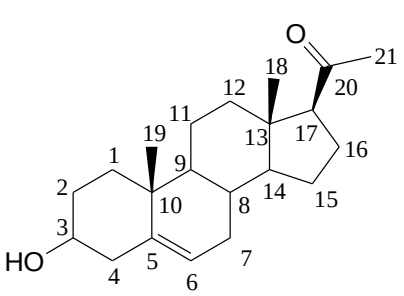
Extraction and Isolation

The roots of *Holarrhena curtisii* (573.3g) were powdered and percolated with MeOH at room temperature for 3 days x10. The concentrated MeOH extract (29.0g) was acidified with 5% HOAc. Two fractions obtained from this acidic process contain the alkaloid and non-alkaloid (4.88g) components. The alkaloidal fraction was basified with Na_2C0_3 to pH9 and partitioned with $CHCl_3$ followed by drying with Na_2SO_4 (anhydrous). The concentrated alkaloid extract (2.93g) was subjected to vacuum liquid chromatography (VLC) by using silica 7749 and eluted with $CHCl_3$: MeOH in order of increasing polarity resulting in 6 fractions. The first fraction was re-chromatograph using column chromatography (CC) (Alumina, Merck) with eluent 9Hex:1Diethylether yielded pregnenolone (1) 1.7mg. While, stigmasterol (2) was attained from the non-alkaloid part using CC that was eluted with 9Hex:1Aceton as a solvent system. Compound 2 was purified and recrystallized to yield white needle crystals (4.8mg).

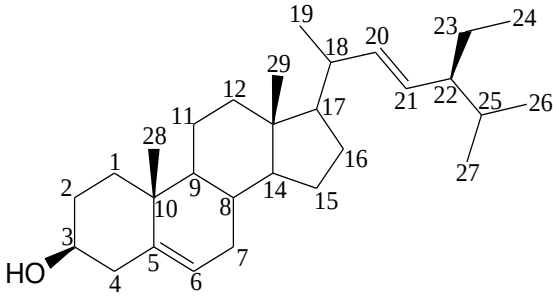
Results and Discussion

Two compounds obtained from the roots of *Holarrhena curtisii* were identified as pregnenolone (1) and stigmasterol (2). These two compounds showed mass spectral data of the steroid aglycone and gave GCMS data in agreement with the proposed structures. Their IR data showed absorptions for OH and C=O functions. The NMR data of 1 and 2 can be seen in Table 1. The spectra were assigned based on the application standard of 2D NMR methods (HSQC, HMBC, COSY) and with reference to related compounds that have been previously reported [9 - 11].

Compound (1), $C_{21}H_{32}O_2$ appeared as a colourless needle-like crystal which gave a positive response with reagents vanillin followed by 5% H_2SO_4 in EtOH for a steroid. The ^{1}H NMR spectrum showed the presence of two methyl singlets (δ 0.64 and δ 0.99) , 8 complicated methylene envelope (between δ 1.02 and δ 2.31) and a vinylic proton multiplet at δ 5.36 suggesting the possibility of a steroidal moiety in 1. Additionally, one OH group at δ 3.54 and one OMe group at δ 2.13 implied that 1 is a steroidal aglycone. The APT NMR spectrum showed the presence of a total 21 carbons consistent with a C-21 pregnane skeleton. IR spectra showed absorptions for OH, C=O and C=C functions at 3383 cm^{-1} (OH), 1702 cm^{-1} (C=O) and 1460 cm^{-1} (C=C). The existance of C=C also was indicated by the presence of vinylic H-6 signal at δ 5.36 in the ^{1}H NMR spectrum and the olefinic carbon resonances at δ 140.7 and δ 121.4 in the APT NMR spectrum. Moreover, the presence of a 2^o OH group was suggested by the oxymethine resonance at δ 71.7 in the APT NMR. Determination of the OH location was also supported by HSQC and COSY data which confirmed the CH_2-CH(OH)-CH_2 fragments corresponding to the structure of C2-C3-C4 as shown in structure 1. Compound (1) was comfirmed as 3-hydroxypreg-5-en-20-one by GC-MS data at m/z 316.2.



1



2

Table 1. APT and ^{1}H NMR spectral data of pregnenolone (**1**) and stigmasterol (**2**) from roots of *H. curtisii*

	1		**2**	
Position	**APT**	**^{1}H**	**APT**	**^{1}H**
1	37.3	1.02 (4H, *s*) 1.19 (3H, *m*) 1.87 (2H, *m*)	37.3	1.04 1.17 (5H, *m*) 1.84 (1H, *m*)
2	31.8	1.58 (10H, *m*) 2.02 (2H, *m*)	31.7	1.84 (1H, *m*) 1.99 (2H, *m*)
3	71.7	1.19 (3H, *m*) 1.58 (10H, *m*) 3.54 (1H, *m*)	71.8	3.53 (1H, *m*)
4	42.3	2.21 (2H, *m*) 2.31 (1H, *m*)	42.3	2.29 (1H, *m*)
5	140.7	-	140.8	-
6	121.4	5.36 (1H, *m*)	121.7	5.36 (1H, *br-s*, *J* = 5.32 Hz)
7	31.9	1.58 (10H, *m*) 2.02 (2H, *m*) 2.13 (3H, *s*)	31.9	1.47 1.99 (2H, *m)*
8	29.7	1.87 (2H, *m*)	31.7	1.47
9	50.0	1.02 (4H, *s*)	50.2	1.01 (2H, *s*)
10	36.5	-	36.5	-
11	21.1	1.58 (10H, *m*)	21.1	1.47
12	38.8	1.58 (10H, *m*) 2.02 (2H, *m*)	39.7	1.17 (1H, *m*)
13	44.0	-	45.4	-
14	56.9	1.19 (3H, *m*)	56.9	1.01 (2H, *s*)
15	24.5	1.19 (3H, *m*) 1.58 (10H, *m*)	24.4	1.56 1.06
16	22.8	1.87 (2H, *m*) 2.21 (2H, *m*)	29.0	1.17 (5H, *m*) 1.71 (1H, *m*)
17	63.7	2.54 (1H, *t*)	55.9	1.17 (5H, *m*)
18	13.3	0.64 (3H, *s*)	40.5	1.19 (2H, *m*)
19	19.4	1.02 (4H, *s*)	21.9	1.01 (2H, *s*)
20	209.6	-	138.4	5.15 (1H, *dd*)
21	31.6	2.13 (3H, *s*)	129.3	5.01 (1H, *dd*)
22	-	-	51.3	5.15 (1H, *dd, J* = 15.2, 8.5 Hz)
23	-	-	25.4	1.17 (5H, *m*) 1.47 5.01 (1H, *dd, J* = 15.2, 8.5 Hz)
24	-	-	11.9	0.83 (4H, *m*)
25	-	-	31.3	1.47
26	-	-	19.0	0.83 (4H, *m*)
27	-	-	21.2	0.83 (4H, *m*)
28	-	-	19.4	1.01 (2H, *s*)
29	-	-	17.4	0.70 (1H, *s*)

Compound (2), $C_{29}H_{48}O$ is the major compound obtained from the non-alkaloid extract and gave positive result for a steroid when tested with reagents vanillin followed by 5% H_2SO_4 in EtOH. Compound 2 is a white crystalline needles with melting point 144-146°c [10]. The ^{1}H NMR spectrum of 2 indicated the presence of 6 methyl peaks of H-18, H-27, H-29, H-26, H-21 and H-19 that appeared at respective δ 1.19, 0.83, 0.70, 0.83, 5.01 and 1.01. The hydroxymethine proton H-3 appeared as a multiplet at δ 3.53 and revealed the existance of signals for olefinic proton at δ 5.36, 5.15, 5.01 and 3.53. Angular methyl proton at δ 0.70, 0.83 and 1.01 corresponds to C18 and C19 proton respectively [12, 13]. The APT NMR has shown recognizable signals at 145.2 and 121.7 ppm which are assigned to the C5 and C6 double bonds. The value at 21.9 ppm corresponds to angular C19. APT spectra showed 29 carbons signal including 6 methyls, 9 methylenes, 11 methane and 3 quaternary carbons. The alkene carbons appeared at 140.8, 121.4, 138.4 and 129.3 ppm [12 - 14]. Compound 2 is similar to compund 1 from C1-C17, C28-C29 except for C18-C27. The structure of compound 2 was further confirmed by its MS spectral data which showed a mass at 412.4.

Conclusion

The isolation and identification of pregnenolone (1) and stigmasterol (2) from the roots of *Holarrhena curtisii* was the first ever to be reported from this plant. The work was carried out by utilizing several kinds of chromatographic separation techniques and spectroscopy analyses.

Acknowledgement

This work was partially supported by a grant from UKM-PNI-NBD009-2007. We wished to extend our gratitude to the School of Chemical Sciences and Food Technology, National University of Malaysia for the provision of laboratory facilities and technical assistance. We are also grateful to the CRIM for providing facilities for spectral characterization of compound.

References

1. Georges, M., Mackay, D. & Fraser-Reid, B. (1984). Stereocontrolled Routes to *cis*-Hydroxyamino Sugars. Part VII.[1] A Synthesis of Holacosamine[2]. *Can. J. Chem*, 62: 1539.
2. Bhutani, K. K., Ali, M., Sharma, S. R., Vaid, R. M. & Gupta, D. K. (1988). Three New Steroidal Alkaloids from The Bark of *Holarrhena antidysentrica*. *Phytochem*, 27 (3): 925 - 928.
3. Siddiqui, B. N., Usmani. S. B., Begum. S. & Siddiqui. S. (1993). Steroidal Alkaloids and An Androstane Derivatives from The Bark of *Holarrhena pubescens*. *Phytochem*, 33: 925 - 928.
4. Chakraborty, A. & Brantner, H. A. (1999). Antibacterial Steroid Alkaloids from The Stem Bark of *Holarrhena pubescens*. *J. Ethnopharmacol*, 68: 339 – 344.
5. Cannon, J. R., Ghisalberti, E. L. & Lojanapiwatna, V. (1980). The Alkaloids of *Holarrhena curtisii* King and Gamble. *J. Sci. Soc. Thai*, 6: 81 - 89.
6. Jamal, A. K., Yaacob, W. A. & Din, L. B. (2009). A Chemical Study on *Phyllanthus columnaris*. *Eur. J. Sci. Res*, 28 (1): 76 - 81.
7. Jannot, M. M., Khauong, H. Q., Honneret, C., Kabore, I., Hildeshein, I., Gero, S. D., et al. (1970). Alkaloidal Steroid C and Holantosine A & B Isolated from The Leaves of *Holarrhena antidysentrica. Tetrahedron*, 26: 1695 - 1709.
8. Loukaci, A., Kayser, O., Bindseil, K. U., Siems, K., Frevert, J. & Aberu, P. M. (2000). New Trichothecenes Isolated from *Holarrhena floribunda. J. Nat. Prod*, 63: 52 - 56.
9. Kamboj, A. & Saluja, A. K. (2011). Isolation of Stigmasterol and β-Sitosterol from Petroleum Ether Extract of Aerial Parts of *Ageratum conyzoides* (Asteraceae). *Int. J. Pharm. Sci*, 3 (1): 94 - 96.
10. Wasylyk, J. M., Martin, G. E., Weinheimer, A. J. & Alam, M. (1989). Isolation and Identification of A New Pregnene Glycoside from The Gorgonian *Pseudoplexaura wagenaari. J. Nat. Prod*, 52 (2): 391 - 394.
11. Yahya, M. A. A., Yaacob, W. A. & Nazlina, I. (2011). Isolation of Chemical Constituents from Rhizomes of *Etlingera sphaerocepala* Var. *Grandiflora*. *Malays. J. Analyt. Sci*, 15 (1): 22 - 26.
12. Kam, T. S. (1999). Alkaloids from Malaysian Flora. In. Pelletier, S.W. (editor). *Alkaloids: Chemical & Biological Perspectives*, pg. 324 - 326. UK: Elsevier.
13. Pateh, U. U., Haruna, A. K., Garba, M., Iliya, I., Sule, I. M., Abubakar, M. S. & Ambi, A. A. (2009). Isolation of Stigmasterol, β-Sitosterol, and 2-Hydroxyhexadecanoic Acid Methyl Ester from Rhizomes of *Stylochiton lancifolius* Pyer and Kotchy (Aeaceae). *Niger. J. Pharm. Sci*, 7 (1): 19 - 25.

14. Agarwal, P. K., Jain, D. C., Gupta, R. K. & Thakur, R. S. (1985). Carbon-13 NMR Spectroscopy of Steroidal Sapogenins and Steroidal Saponins. *Phytochem*, 24: 2476 - 2496.

The Malaysian Journal of ANALYTICAL SCIENCES ISSN 1394-2506

PETROLEUM HYDROCARBON IN SURFACE SEDIMENT FROM COASTAL AREA OF PUTATAN AND PAPAR, SABAH

(Petroleum Hidrokarbon di Dalam Sedimen Permukaan daripada Pesisiran Pantai Putatan dan Papar, Sabah)

Siti Aishah Mohd Ali[1*], Rohana Tair[1], Soon Zhi Yang[1], Masni Mohd Ali[2]

[1]*Water Research Unit, School of Science and Technology,*
Universiti Malaysia Sabah, Jalan UMS, 88400 Kota Kinabalu, Sabah, Malaysia
[2]*School of Environmental and Natural Resource Sciences, Faculty of Science and Technology,*
Universiti Kebangsaan Malaysia, 43600 UKM Bangi, Selangor D.E., Malaysia

**Corresponding author: ctaishah@ums.edu.my*

Abstract

Total petroleum hydrocarbons (TPH) and percent total organic carbon (TOC) were investigated in surface sediments from coastal area of Papar and Putatan, Sabah. Samples were collected in five different stations in each area by using Ponar grab sampler. Samples were extracted with Soxhlet, concentrated and analyzed by using UV/VIS spectrophotometer. The overall mean and range of TPH concentrations in the sediments from coastal area of Papar and Putatan were 1.95 (0.53 – 4.59 mg/kg dw Miri crude oil equivalents) and 0.85 (0.26 – 1.64 mg/kg dw Miri crude oil equivalents) respectively. Meanwhile, the TOC ranged from 0.81 – 2.32% and 0.35 – 0.81% respectively. Statistical analysis using Pearson correlation showed no significant differences between TPH and TOC ($p < 0.05$) in both areas.

Keywords: Total petroleum hydrocarbons, surface sediment

Abstrak

Jumlah petroleum hidrokarbon (TPH) dan peratus jumlah karbon organik (TOC) telah dikaji dalam sedimen permukaan dari kawasan pesisiran pantai Papar dan Putatan, Sabah. Sampel dikumpul dari lima stesen yang berbeza di setiap kawasan dengan menggunakan *Ponar grab sampler*. Sampel telah diekstrak menggunakan Soxhlet, dipekatkan dan dianalisis menggunakan UV / VIS spektrofotometer. Nilai min dan julat keseluruhan kepekatan TPH dalam sedimen dari kawasan persisiran pantai Papar dan Putatan adalah 1.95 (0.53 – 4.59 mg/kg bk, setara dengan minyak mentah Miri) dan 0.85 (0.26 - 1,64 mg/kg bk, setara dengan minyak mentah Miri) masing-masing. Sementara itu, julat TOC adalah di antara 0.81 – 2.32% dan 0.35 – 0.81% masing-masing. Analisis statistik menggunakan korelasi Pearson menunjukkan tiada perbezaan yang signifikan di antara TPH dan TOC ($p < 0.05$) di kedua-dua kawasan.

Kata kunci: jumlah petroleum hidrokarbon, sedimen permukaan

Introduction

Hydrocarbons are ubiquitous constituents in aquatic sediments, relatively stable in the marine environment and often accumulate in biological communities and ecosystems, thus representing a human health hazard [1, 2]. Their sources can be either natural or anthropogenic. Hydrocarbons generated by biological or diagenetic processes naturally occur at low content in sediments, and are part of the natural hydrocarbon baseline of an ecosystem [3]. Aliphatic hydrocarbons derive from a variety of natural sources including terrestrial plants and marine algae [4] but they are also major components of petroleum. In marine sediments, especially in coastal areas, human activities are believed to be an important influence on hydrocarbons. Those activities include oil transportation and spill, shipping, and industrial, storm water and domestic discharge.

The subject of the research is sediment because sediment and sand is a good indicator for oil pollution in an area than the assessment of hydrocarbon in the water [5]. Bottom sediments of most aquatic systems are known to act as

a reservoir or sink for petroleum hydrocarbons, trace metals, and some other pollutants [6]. Moreover, sediments are composite materials, which consist of inorganic components, mineral particulates and organic matter in various stages of decomposition, and are well known for their sensitive indicators between natural and anthropogenic variables [7]. The organic matter content of sediments, quantified by the concentration of total organic carbon (TOC), is thought to play an important role in the accumulation and release of different micro pollutants [8]. The input of organic matter to coastal systems is indeed the triggering mechanism leading to ecological concern [9]. TOC measurement provides information on all organic substance content in water or sediments [10, 11]. These substances either from natural sources, such as humic acids, mineral oils, solvents, pesticides, poly aromatic hydrocarbons or chlorinated organic compounds [12]. However, the quantity of TOC in the sediments/soils depends on the amount of organic matter added, sediment texture such as clay content, and climatic conditions [13].

Due to the lack of information regarding the concentration of petroleum hydrocarbons in the sediments of the coastlines of Sabah, this study was designed to determine the total hydrocarbon concentration (TPH) and total organic carbon (TOC) in the surface sediment of Papar and Putatan, Sabah (Table 1). Correlations with surface sediment TPH and TOC from sampling stations are discussed.

Table 1. Description of station in Papar and Putatan, Sabah.

Area	Station	Coordinate
Papar	A1	N 05°44.016', E 115°53.387'
	A2	N 05°44.925', E 115°53.672'
	A3	N 05°45.744', E 115°54.323'
	A4	N 05°45.823', E 115°55.594'
	A5	N 05°46.412', E 115°56.731'
Putatan	B1	N 05°51.518', E 116°02.043'
	B2	N 05°51.854', E 116°02.168'
	B3	N 05°52.235', E116°02.331'
	B4	N 05°52.715', E116°02.514'
	B5	N 05°53.079', E116°02.250'

Experimental

This study was conducted in January 2011. Surface sediment samples (0-1 cm) were collected using Ponar grab sampler from 5 stations in each area as shown in Table 1. Analysis of the top (1-2 cm) surface layer provides baseline data for present-day pollution [8, 14, 15, 16]. 10 g of sediments was dried in the oven at 105 °C for 2 hours for the moisture content analysis. The procedure used for TPH analysis was standard method sediment/sludge APHA 5520E [17]. 10 g of sediment was extracted with saturated hydrochloric acid (HCl) and 15 g magnesium sulphate ($MgSO_4$). After mashing the whole sediment sample, the sample was extracted with Soxhlet for 4 hours with 250 ml petroleum ether. The extracts were saturated using rotary evaporator and cleaned-up on silica gel columns. The eluate from the columns was concentrated with pure nitrogen and the TPH were analysed by using UV/VIS spectrophotometer Lambda 25 Perkin Elmer (excitation was at 239 nm and emission at 259 nm). A calibration curve was generated using Miri crude oil as arbitrary standard. Percentage of TOC was measured based on United Nations Environment Programme (UNEP)/MAP Athens (2006) method [18].

Results and Discussion

Table 2 shows the concentration of TPH and percentage of TOC in sediment collected along the coastal area of Papar and Putatan, Sabah. The overall range and mean of the TPH concentrations in both areas were 0.26 - 4.59 and 1.40 mg/kg dw Miri crude oil equivalents respectively, while TOC were 0.35 - 2.32% and 1.15% respectively.

Table 2. The TPH concentrations and TOC in sediment from Papar and Putatan, Sabah.

Area	Station	TPH (mg/kg) dw	TOC (%)
Papar	A1	2.82	0.81
	A2	4.59	1.91
	A3	0.79	2.09
	A4	1.05	2.32
	A5	0.53	1.04
	Mean	**1.95**	**1.63**
Putatan	B1	0.26	0.64
	B2	1.64	0.75
	B3	1.44	0.35
	B4	0.39	0.81
	B5	0.54	0.81
	Mean	**0.85**	**0.67**

The result shows that the higher TPH concentrations are found at station A2 which is Papar area. The range of TPH concentration at Papar area is 0.53 – 4.59 mg/kg dw and the mean is 1.95 mg/kg dw Miri crude oil equivalents. Meanwhile, the lower TPH concentrations are found at station B1 which is Putatan area. The range of TPH concentration at Putatan area is 0.26 – 1.64 mg/kg dw and the mean is 0.85 mg/kg dw Miri crude oil equivalents. The ranged of the TOC percentage in Papar and Putatan are 0.81 – 2.32% and 0.35 – 0.81% respectively. The highest level of TOC was recorded at station A4 (2.32%), meanwhile the lowest level was recorded at station B3 (0.35%). The mean of TOC at Papar area (1.6%) was twice the amount of TOC at Putatan area (0.67%).

The mean TPH concentration at Papar area was found to be twice higher than the mean at Putatan area. This is due to the main activity of fishing by boat. Papar area is well-known as a place which produces dried anchovy and dried salted fish. Boat is used as the main transportation to travel from land to reach the *bagang* (the traditional house made by wood at the ocean to catch anchovy). In addition, the water flushing out from the Papar River may contribute to the sources of hydrocarbon from land activities and vehicles which is close to the station A2. According to Tahir *et al*. [19], the variation between estuarine and coastal area may attribute to an insignificant input from inland hydrocarbon sources or due to efficient mixing in the estuarine zone. Alfred *et al.* [20] stated that the migration of hydrocarbon in sediment associate mainly with hydrothermal minerals and deep ground waters. So, the difference TPH concentrations in Papar and Putatan area may due to the differences in physical and biological characteristic of coastal area such as the sediment size, the composition of sediment and the species of organism present.

A comparison of the TPH from the present study with values reported in other parts in Malaysia is presented in Table 3. The results indicate that the TPH levels in Papar and Putatan is much lower than that found in Peninsular Malaysia [19, 21, 22, 23, 24]. The main contribution to the hydrocarbon pollution in Peninsular Malaysia was by shipping activities, illegal discharge of oily waste water by vessels and through the routine handling of crude oil at the terminals of refineries [22, 23, 24]. Tahir *et al*. [19] conducted a survey in coastal water and sediment of east coast Peninsular Malaysia and their study showed significant differences in the levels of TPH could be directly attributed to much higher maritime activities and major oil production companies along the east coast of Peninsular Malaysia. Abdullah [21] stated that the hydrocarbon concentrations are related not only due to possible sources of hydrocarbon but also the physical characteristic of the sediment samples. Clayey sediment contains more hydrocarbons compared to sandy sediment.

The sources and transportation of sedimentary organic matter composition can be used as physical indicator to the hydrocarbon concentration or organic pollution [25, 26, 27]. However, Simpson *et al.* [28] stated that the relationship between TPH and organic matter of sediment was only significant in a highly contaminated site. Al-Ghadban *et al.* [29] also stated that the efficiency of TOC in indicating TPH level and considered it to be authentic when TPH is present in high concentration. Statistical analysis of the result using Pearson correlation revealed that

there is no significant difference between TPH and TOC at both areas ($P < 0.05$). It means that the level of TPH observed in the sediments of the coastlines of Papar and Putatan do not correlate significantly with TOC content in various stations.

According to the Food and Agricultural Organization [30], sediments containing hydrocarbon levels less than 100 mg/kg dry weight can be classified as unpolluted. Based on this classification, it can be stated that the levels of TPH obtained from the present investigation in both Papar and Putatan area are still below the alarming pollution level.

Table 3. Comparison of petroleum hydrocarbon levels in Papar and Putatan sediment with levels reported in other part in Malaysia.

Location	Petroleum Hydrocarbon in Sediment (mg/kg dw)	References
East coast Peninsular Malaysia	0.8 – 20.0	[19]
Straits of Johor	14.259 – 361.371	[22]
Port Dickson	21.73 – 74.50	[23]
Pulau Langkawi, Pulau Ketam, Tanjung Piai, Pulau Tioman and Kemaman.	18.2 – 847.4	[21]
Straits of Malacca	52 - 128	[24]
Papar and Putatan, Sabah	0.26 - 4.59	Present study

Conclusion

TPH and TOC in sediment from coastal area of Papar and Putatan, Sabah were quantified and compared. The mean TPH and TOC in surface sediment from Papar coastal area are 1.95 mg/kg dw Miri crude oil equivalents and 1.63% while at Putatan area are 0.85 mg/kg dw Miri crude oil equivalents and 0.67% respectively. The sediment samples in both areas can be concluded as non-polluted by petroleum hydrocarbon based on with FAO (1982) standard.

Acknowledgement

The authors would like to acknowledge the financial support from Universiti Malaysia Sabah and Miri Crude Oil Terminal (MCOT) in this study.

References

1. Lipiatou, E. & Saliot, A. (1991). Hydrocarbon contamination of the Rhone delta and western Mediterranean. *Marine Pollution Bulletin*, 22: 297-304
2. Wakeham, S.G. (1996). Aliphatic and polycyclic aromatic hydrocarbons in Black Sea sediments. *Marine Chemistry*, 53: 187-205.
3. Commendatore, M.G. & Esteves, J.L. (2004). Natural and anthropogenic hydrocarbons in sediments from the Chubet River (Patagonia, Argentina). *Marine Pollution Bulletin*, 48: 910-918.
4. Saliot, A. (1981). *Natural hydrocarbons in sea water in Marine Organic Chemistry*. E. Duursma & R. Dawson. Eds. Elsevier. Amsterdam, 327-374.
5. Law, A.T. & Ravinthar V. (1989). Petroleum hydrocarbon along the coastal areas of Port Dickson. *Pertanika*, 12(3): 349-355.
6. Horowit, A.J. (1991). *A primer on sediment-trace element chemistry*. 2nd edition. Chelsea, MI: Lewis Publishers.
7. Kucuksezgin, F., Kontas, A., Altay, O., Uluturhan, E. & Darilmaz, E. (2006). Assessment of marine pollution in Izmir Bay: Nutrient, heavy metal and total hydrocarbon concentrations. *Environment International*, 32: 41-51.

8. Massoud, M.S., AI-Abdali, F. & AI-Ghadban, A.N. (1996). Bottom sediments of the Arabian Gulf; II. TPH and TOC contents as indicators of oil pollution and implications for the effect and fate of Kuwait oil slick. *Environmental Pollution*, 93(3): 271-284.
9. Dell'Anno, A., Mei, M.L., Pusceddu, A. & Danovaro, R. (2002). Assessing the trophic state and eutrophication of coastal marine systems: a new approach based on the biochemical composition of sediment organic matter. *Marine Pollution Bulletin*, 44: 611–622.
10. Dojlido, J. & Best, G. (1993). *Chemistry of water and water pollution*. Ellis Horwood Limited England.
11. Zerbe J. (1993). Hydrocarbons and its derivatives in water. Environmental and Natural Resources Protection.
12. Al Darwish, H.A., Abd El-Gawad, E.A., Mohammed, F.H. & Lotfy, M.M. (2005). Assessment of organic pollutants in the offshore sediments of Dubai, United Arab Emirates. *Environmental Geology*, 48: 531–542.
13. Jenkinson, D.S. (1990). Studies on the decomposition of plant material in soil, IV: The effect of rate of addition. *Journal of Soil Science*, 28: 417.
14. AI-Abdali, F., Massoud, M.S. & A1-Ghadban, A.N. (1996). Bottom sediments of the Arabian Gulf; IIL Trace metal contents as indicators of pollution and implications for the effect and fate of Kuwait oil slick. *Environmental Pollution*, 93(3): 285-301.
15. Literathy, P. & Foda, M. (1985). KISR activities on Nowruz oil slick. EESGEN Report KISR 1827. Kuwait: Kuwait Institute for Scientific Research.
16. Michel, J., Hayes, M.O., Keenan, R.S., Sauer, T.C., Jensen, J.R. & Narumalani, S. (1993). Contamination of nearshore subtidal sediments of Saudi Arabia from the Gulf War oil spill. *Marine Pollution Bulletin*, 27: 109-116.
17. American Public Health Association (APHA). (2005). Standard Methods for the Examination of Water and Wastewater. 21st edition. American Public Health Association.
18. United Nations Environment Programme (UNEP). (2006). Methods for Sediment Sampling and Analysis. United Nations Environment Program.
19. Tahir, N.M., Abdullah, A.R. & Shanmugam, S. (1997). Determination of total hydrocarbon concentration in coastal waters and sediments off the east coast of Peninsular Malaysia. *Environmental Geochemistry and Health*, 19: 67-71.
20. Alfred, R.G., Richterb, B., Pikovskiic, Y.I., Chernyanskyc, S.S. & Alexeevac, T.A. (2006). Polycyclic aromatic hydrocarbons as evidence of hydrocarbon migration in marine and lagoon sediments of a recent rift zone (Skjá lfandi and Öxarfjörjur), Iceland. *Chemie der Erde Geochemistry*, 66: 213–225.
21. Abdullah, M. P. (1997). Hydrocarbon pollution in the sediment of some Malaysian coastal areas. *Environmental Monitoring and Assessment*, 44: 443-454.
22. Abdullah, A.R., Woon, W.C. & Bakar, R.A. (1996). Distribution of oil and grease and petroleum hydrocarbons in the Straits of Johor, Peninsular Malaysia. *Bulletin of Environmental Contamination and Toxicology*, 57: 155-162.
23. Law, A.T., Ravinthar, V. & Yeong, C.H. (1990). Oil pollution in the coastal waters off Port Dickson, Straits of Malacca. *Pertanika*, 13: 381-387.
24. Zakaria, M.P. & Takada, H. (2007). *Case study: Oil spills in the Strait of Malacca, Malaysia*. In: Wang, Z. & Stout, S.A. (eds.) Oil spill environmental forensics. Elsevier, Inc., pg. 489-504.
25. Karichknofff, S.W., Brown, D.S. & Scott, T.A. (1996). Sorption of hydrophobic pollutants. *Water Research*, 13: 241–248.
26. Pionke, H.B. & Chester, G. (1973). Pesticide sediment water interactions. *Journal of Environmental Quality*, 2: 29–45.
27. Rudolf, J., Ahmed, I.R., Medeiros, P.M. & Bernd, R.T.S. (2006). Natural product biomarkers as indicators of sources and transport of sedimentary organic matter in a subtropical river. *Chemosphere*, 64: 1870–1884.
28. Simpson, C.D., Mosi, A.A., Cullen, W.R. & Reimer, K. (1996). Composition and distribution of polycyclic aromatic hydrocarbons in surficial marine sediments from Kitimat Harbour. *Science Total Environment*, 181: 265-278.
29. Al-Ghadban, A.N., Jacob, P.G. & Abdali, F. (1994). Total organic carbon in the sediments of the Arabian Gulf and need for biological productivity investigations. *Marine Pollution Bulletin*, 28: 356–362.
30. Food & Agriculture Organisation (FAO). (1982). The Review of the Health of the Oceans. FAO/IMCO/UNESCO/WMO/WHO/IAEA/UNEP Joint Group of Experts on Scientific Aspects of Marine Pollution (GESAMP).

The Malaysian Journal of ANALYTICAL SCIENCES ISSN 1394-2506

OPTIMIZATION OF A DISTILLATION UNIT IN TERMS OF POTENTIAL ENVIRONMENTAL IMPACT AND ECONOMICS

(Pengoptimuman Unit Penyulingan dari Segi Potensi Impak Ekonomi dan Alam Sekitar)

Alhassan Salami Tijani[1*], Naveed Ramzan[2]

[1]*Faculty of Mechanical Engineering*
Universiti Teknologi MARA, 40450 Shah Alam, Selangor, Malaysia.
[2]*Department of Chemical Engineering,*
University of Engineering and Technology, G.T Road Lahore (54890) Lahore-Pakistan

**Corresponding author: alhassan@salam.uitm.edu.my*

Abstract

Process energy integration and continuous improvement of process technology are increasing issues to ensure profitability of chemical productions. These objectives are increasingly important due to long-term environmental impact of energy degradation, such as resource depletion, emissions and the release of "waste" heat. The earlier energy conservation, process economics and environmental aspects are integrated into the process development, the easier and less expensive it is to improve the process design. In this work different distillation process design alternatives have been considered with respect to evaluations of process economics and potential environmental impacts. "Optimum design alternatives" are analyzed related to these objectives. A multi-criteria decision making technique such as (Analytic Hierarchy Process) AHP is applied for ranking the alternatives. This method reveals that the heat pump distillation unit which has the highest score of 52 % is the best alternative when compare with base case. In terms of the effluent streams the base case has a less potential environmental impact (PEI) compared with heat pump. The lower total PEI/kg (7.45E-01) of the base case illustrates that the material utilization efficiency of the base case is better than the heat pump whose PEI/kg is 8.14E-01.

Keywords: economic, thermodynamic efficiency, distillation unit, waste reduction (WAR) algorithm

Abstrak

Peningkatan yang berterusan dalam integrasi proses tenaga dan proses teknologi adalah isu-isu yang semakin diperbincangkan untuk memastikan keuntungan dalam pengeluaran kimia. Objektif ini semakin penting disebabkan kesan jangka panjang terhadap alam sekitar akibat kemerosotan tenaga, seperti kehabisan sumber, pelepasan dan pembebasan haba "sisa". Pemuliharaan tenaga yang lebih awal, proses ekonomi dan aspek-aspek alam sekitar disepadukan ke dalam proses pembangunan, lebih mudah dan lebih murah untuk memperbaiki proses rekabentuk. Dalam kejian ini proses rekabentuk alternatif yang berbeza telah dipertimbangkan dalam kombinasi dengan penilaian proses ekonomi dan kesan terhadap alam sekitar yang berpotensi. "Alternatif reka bentuk optimum" telah dianalisis seiring dengan objektif ini. Teknik membuat sesuatu keputusan pelbagai kriteria seperti (Proses Hierarki Analisis) AHP diaplikasikan untuk memperbaharui kedudukan. Kaedah ini mendapati bahawa rekabentuk pam haba yang mempunyai skor tertinggi sebanyak 52% adalah alternatif terbaik. Dari segi asas pengaliran pengeluaran kumbahan ianya mempunyai kesan yang kurang berpotensi terhadap alam sekitar (PEI) berbanding dengan pam haba. Jumlah PEI / kg (7.45E-01) yang lebih rendah dalam penggunaan bahan asas menunjukkan bahawa kecekapan penggunaan bahan asas adalah lebih baik daripada pam haba (PEI / kg 8.14E-01).

Kata kunci: ekonomi, kecekapan termodinamik, penyulingan unit, pengurangan sisa (PERANG) algoritma

Introduction

Currently the chemical process industries rely on distillation processes to separate chemical mixtures into pure products. Due to their high energy-intensive, energy–efficient design and operation are therefore important issues. The importance of alternative energy efficient design distillation columns has become more necessary not only due to the continuous depletion of limited fossil fuel stock but also consideration of better environmental system during

early design or retrofitting stages. Traditionally, chemical process design and optimization are more focus towards economic objective such as total annualized cost (TAC). Less attention has been given to environmental impact of process design; they are generally integrated into traditional design as end of-pipe treatment [1]. As a result of newly issued environmental regulations, there is a growing interest of minimizing environmental impacts of chemical process design.

Energy efficient design process can help reduce the quantity of pollution or waste generated during operation of a manufacturing process. However, a design with less waste does not necessarily have lower impacts on the environment, since the wastes may have a higher contribution to the potential environmental impacts than another design with a larger amount of waste but a lower environmental effect [2]. Hui et al. [1] suggested that there are two ways of integrating environmental perspectives into traditional design and optimization, the most popular method is to treat environmental considerations as constraints, for example Dantus et al. [3] did developed a methodology based on economic to minimise waste and reduce energy consumption, however Cano-Ruiz [4] stated that "the main problem with incorporating environmental considerations as constraints is that the proposed solutions may not address the underlying environmental concerns". The other alternative is to treat environmental requirement as objective. Among the most recent systematic methods for the assessment of environmental impacts of chemicals processes includes, life cycle assessment (LCA) [5], the environmental fate and risk assessment tool [6], thermodynamic analysis method (emergy and exergy) [7] and waste reduction (WAR) algorithm introduced by Hilaly and Sikdar [8]. Later Young and Cabezas [9] extended the PEI balance to include the consumption of energy of the process into the environmental evaluation. Morais et al. [10] did study the potential environmental impacts (PEIs) and economic potentials of alkali-catalysed trans-esterification process; they apply the Waste Reduction algorithm (WAR) to evaluate the potential environmental impacts (PEIs) of process alternatives. More recent studies on environmental impact assessment of chemical process plants can be found in [11, 12].

In this paper, the evaluation of energy related optimization of a technical multi-component distillation unit is presented. For every design alternative, the optimum solution is identified based on cost objective function. Environmental performance index based on WAR algorithm is used to evaluate environmental effects. Finally, a multi-criteria decision making technique such as (Analytic Hierarchy Process) AHP is applied for ranking the alternatives. The analysis is based on steady state simulation using Aspen Plus^{TM}. A case study of a Hydrocarbon Recovery (HCR) plant is discussed to highlight the proposed methodology.

Methodology

As a first step in the design methodology, the design starts with framing of the problem (see Figure 1). This step consists of gathering thermodynamic data of the process flow sheet (base case) model. The process is modelled using Aspen Plus^{TM} simulator. Mass and energy data from the Aspen Plus^{TM} model are used to compute the exergy of the streams and thermodynamic efficiency. The process data from Aspen Plus^{TM} are entered into the WAR Graphical user interface (GUI) in order to compute environmental criteria of the base case model. The process data information includes the chemicals used, the flow rates of the streams entering and leaving the process, and the energy usage of the process. The successive quadratic programming algorithm (SQP) in Aspen Plus^{TM} is used for economic optimization. The next step is the generation and evaluation of alternatives which includes identifying energy saving alternatives. Finally, in the last step a multi-criteria decision making technique such as AHP is applied for ranking the alternatives.

Case study

This paper concentrates on the stripping column which is part of a Hydrocarbon Recovery (HCR) unit. Figure 2 provides a simple schematic illustration of the distillation unit (steam stripping column) unit from a real chemical plant. The main components of the feed stream are water, acetone, methanol, and acetic acid etc. The feed stream, which is close to its bubbling point enters the stripping column on tray 17. The column has a diameter of 0.728 m and 35 trays, where the rectifying section includes trays 1-15 and the stripping section 16-35. The column is operated with steam (550 - 650 kg/hr, 140^{o}C and 3.75 bars) injection into the bottom below stage 35. The top pressure is 1.01 bar with reflux ratio of 0.7 (operating plant) and feed flow rate of 4000 kg/hr.

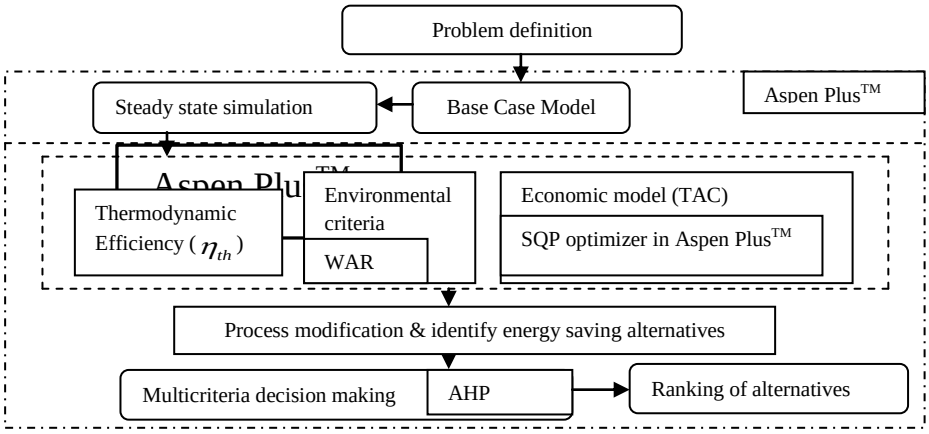


Figure1. Procedure of the integrated methodology.

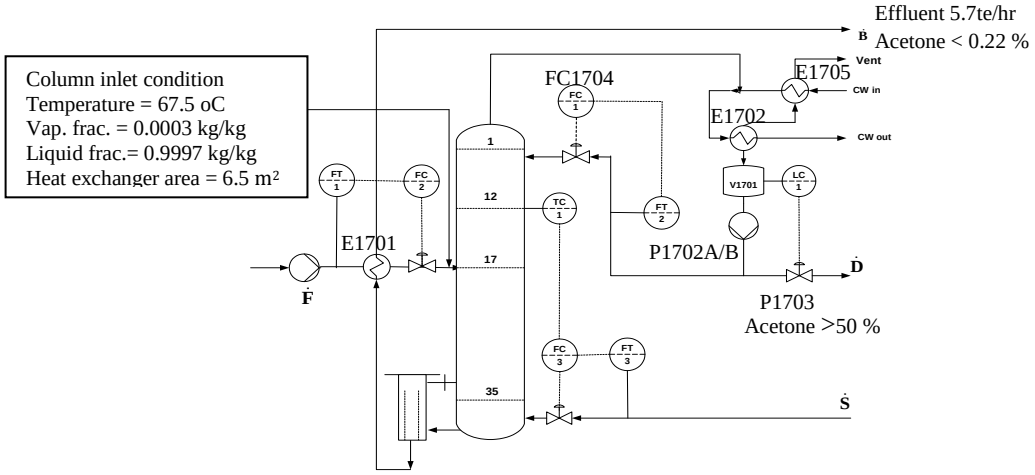


Figure 2. Base case flow sheet of a hydrocarbon recovery (HCR) unit.

The operating targets are as shown below:

Distillate: $x_{Water} < 10\ \%$ (percentage of water by mass at distillate should be less than 10%), $x_{Acetone} > 50\ \%$
Bottom: $x_{Acidity} < 3\ \%$, $x_{Acetone} < 0.22\ \%$, $x_{Methanol} < 2\ \%$

The acidity is the sum of the mass fraction of the acids i.e. acetic acid, formic acid and propionic acid. Acetone is the key component for the bottom and distillate qualities. The design alternative studied in this work is the heat pump distillation unit (see Figure 3). The head product is condensed in heat exchanger E1702 with the vent passing through heat exchanger E1705 to the atmosphere and the liquids are collected by reflux drum V1701. Using pump P1702A/B the reflux is transferred under flow control back into the column on stage 2. Since the feed flow rate changes continuously the set point of reflux control valve (FC1704) is fixed to high rates to prevent hydrocarbon from slipping through the base at different feed rates. The remaining crude acetone is pumped through product

control valve (P1703) and sent to the acetone recovery storage unit. The liquid level in V1701 is set to 50% under normal operating conditions.The base product passes the heat exchanger E1701 for cooling and is then discharged into the in-plant effluent pit.

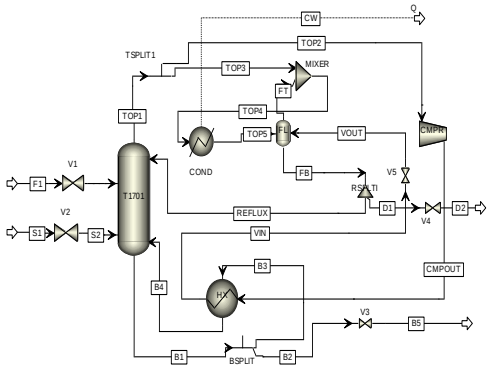


Figure 3. Aspen model for heat pump design alternative.

Environmental Criteria

The potential environmental impacts (PEI) of each alternative are evaluated using the waste reduction (WAR) algorithm developed by Young and Cabezas [12]. These environmental impact scores reflect the potential environmental harm of each chemical in the effluent stream (bottom stream) of the distillation column. These PEI categories are human toxicity by ingestion (HTPI) and by dermal/inhalation exposure (HTPE), terrestrial toxicity potential (TTP), aquatic toxicity potential (ATP), photo oxidation chemical potential (POCP), acidification potential (AP), global warming potential (GWP) and ozone depletion potential (ODP). The chemical PEI of each impact category is given by:

$$PEI_i = \sum_{i}^{Envt\ cat} w_i \cdot \dot{M}_b \cdot \sum_{j}^{comps} X_{kj} \cdot \psi_{ki} \qquad \text{(PEI/kg product)} \qquad (1)$$

PEI_i= PEI of category i,
w_i = weighting factor associated with PEI for each category I,
$\dot{M}_b$ = mass flow rate of effluent (bottom stream),
X_{kj} = mass fraction of chemical (component) k in base stream,
ψ_{ki} = Normalized impact score of chemical component k for category i.

The weighting (w_i) factors are used to combine PEI categories into a single PEI index. They represent the relative or site-specification concerns of the user. For instance, Douglas et al. [13] did mentioned that, if a user was evaluating a process that was located in the Los Angeles area the weighting factor for smog formation (PCOP) would probably receive a high value. Whereas, if the user was evaluating a process in the Northeast the weighting factor for acid rain (AP) would probably receive a high value, they concluded that since their case study has no specific site in mind, they assigned a weighting factor of unity for all the categories. This paper also follows this procedure of assigning a weighting factor of unity for all the categories. This gives the basis for assigning each category a weighting factor of unity in this paper.

Economic Model

In all stages of design process, estimation of Total annualized cost (TAC) is very important for the evaluation of process alternatives. In this section both the base case and heat pump distillation structures where investigated. Optimal operating conditions are determined for these distillation structures. TAC (Operational cost + Annualized

capital investment cost) is considered in this paper as the economic objective function. The estimation of the purchase cost of the distillation column, trays, condenser, compressor heat exchanger and the cost of their installation is considered as the Capital investment cost. The bare-module concept introduced by Seider [14] was used in the estimation of capital investment cost of each equipment. The total Capital investment ($\dot{C}_{TCI}$) cost is given by:

$$\dot{C}_{TCI} = \left(C_{cond} + C_{col} + C_{tray} + C_{comp} + C_{HX} + C_{flashdrum}\right) \cdot \dot{d} \tag{2}$$

C_{cond}=cost of condenser ($),
C_{col}=cost of distillation column ($),
C_{tray}=cost of tray ($),
C_{comp}=cost of compressor ($),
C_{HX}=cost of heat exchanger ($),
$C_{flush\ drum}$=flush drum ($),

where $\dot{d}$ is the depreciation or capital recovery factor and normally varies from 15 to 20% of the total fixed capital investment.

Operating cost

Operating cost is estimated in terms of utility cost of cooling water, steam and electrical energy consumption. The operating cost is formulated according to Douglas [15] as follows:

$$\dot{C}_{utility} = c_S \cdot \dot{M}_S \cdot (8000\,hr/yr) + c_{cw} \cdot \dot{M}_{cw} \cdot (8000\,hr/yr) + c_{el} \cdot \dot{P}_{el} \cdot (8000\,hr/y) \tag{3}$$

$\dot{C}$ = cost per year ($/yr),
c_s=cost of steam ($/kg),
c_{cw}=cost of cooling water ($/kg),
c_{el}=cost of Electricity ($/kW),
$\dot{M}_s$ =Mass flow rate of steam (kg/hr),
$\dot{M}_{cw}$ =Mass flow rate of cooling water (kg/hr),
$\dot{P}_{el}$ =electrical power (kW).

The operating cost is estimated using the following utility prices in Table 1. For the examples studied in this paper, low pressure steams as well as cooling water costs data are taken from Douglas [15] and are assumed to be available as shown in Table 1.

Table 1. Economic data considered

Utility	cost
Cooling water, c_{cw}	0.07 \$/10^3kg
Low-pressure steam (5-10bar), c_S	8.8 \$/10^3kg
Electricity, c_{el}	0.04 \$/kWhr
Operating hours per year	8000 hr/yr

Thus total annualized cost is

$$\dot{C}_{TAC} = \dot{C}_{utility} + \dot{C}_{TCI} \tag{5}$$

Results and Discussion

In chemical processes, the operating conditions are often varied due to influence of market needs and price variations. It is therefore important to know what extent the distillation unit will tolerate to changes in its nominal operating condition and still maintain lower cost (TAC). Figure 4 shows the variation of steam flow rate with acetone recovery at the distillate. It can be observed that the target percentage of acetone recovery (55 % by mass) at the distillate is achieved with steam flow rate of 550kg/hr. Further increase in steam flow rate does not result in any significant increase in the acetone recovery instead it increases the operating cost which leads to increase in TAC (see Figure. 5). TAC can however be at it's minimum of $351x10^3$ (\$/yr) at steam rate within the range of 550 to 560kg/hr.

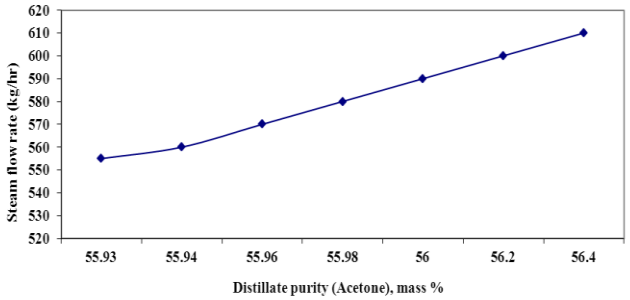


Figure 4. Variation of acetone recovery due to steam flow rate.

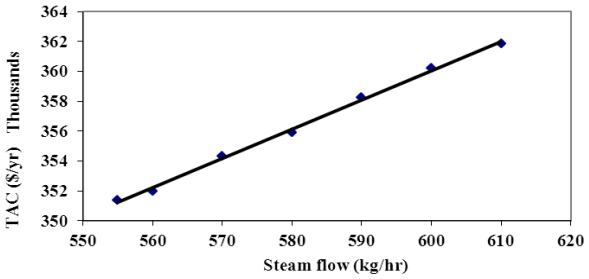


Figure 5. Variation of TAC due to steam flow rate

Environmental assessment

The contribution to the total potential environmental impacts (see Table 2) due to energy consumption decreases as the level of energy integration increases because energy consumption (steam) decreases. This result shows that the energy consumption of the heat pump has 30% decrease in total PEI when compared to the base case. Table 3 shows the comparison of PEI for both design alternatives on the basis of effluent stream discharge. A higher value of this index means a less efficient process with regard to materials utilization The lower total PEI/kg (7.45E-01) of the base case illustrates that the material utilization efficiency of the base case is better than the heat pump (PEI/kg 8.14E-01).

Table 2. Normalized PEI score associated with the energy generation process.

Case	HTPI	HTPE	TTP	ATP	GWP	ODP	PCOP	AP	TOTAL
Base Case	5.94E-01	9.26E-03	5.94E-01	2.01E+00	1.46E+00	1.54E-05	5.36E-04	4.54E+01	5.01E+01
Heat Pump	3.25E-01	5.07E-03	3.25E-01	1.10E+00	8.02E-01	8.43E-06	2.94E-04	2.48E+01	2.74E+01

Table 3. Normalized Total PEI of effluent stream (bottom stream) per mass of products (PEI/kg product).

Case	HTPI	HTPE	TTP	ATP	GWP	ODP	PCOP	AP	TOTAL
Base Case	1.53E-01	1.98E-03	1.53E-01	7.32E-03	1.59E-03	1.67E-08	3.79E-01	4.92E-02	7.45E-01
Heat Pump	1.73E-01	2.23E-03	1.73E-01	7.15E-03	9.78E-04	1.03E-08	4.28E-01	3.03E-02	8.14E-01

Optimal operating conditions of base case model

Each potential environmental impacts category are caused by energy consumption and effluent streams. An optimization study was conducted for the base case model and the results show that as energy consumption (steam flow rate) increases the effluent streams decreases but the environmental impact due to energy and TAC increases. An optimum steam rate that satisfies both the environment and the TAC for base case model was reached as shown in Figure 6.

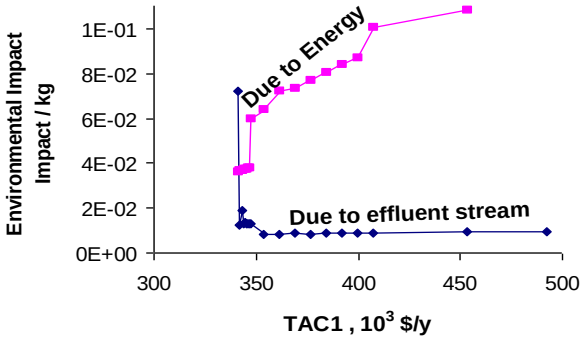


Figure 6. Effect of process variable (steam) on environment and TAC for base case.

The result also shows that steam consumption has more influence on PEI due to energy than due to effluent stream (see Figure 6). In terms of the effluent streams the base case has less PEI compared with heat pump (see Table 4). The lower total PEI/kg (7.45E-01) of the base case illustrates that the material utilization efficiency of the base case is better than the heat pump (PEI/kg 8.14E-01). The total exergy loss in the column decreased from 49.90kW for base case to 45.31kW for heat pump. The lower exergy loss of the heat pump model accounts for its higher thermodynamic efficiency (18.47%) (see Table 4). The product purity was within the target range as shown in Table 5.

Table 4. Cost and exergy analysis

Alternatives	Base case	Heat pump
Steam rate kg/hr	550.0	315.56
Reflux ratio	0.586	0.620
TAC [$/y]	351, 000	402, 000
n_{th} %	14.30	18.47
Exergy loss kW	49.92	45.31
PEI/kg	7.45E-01	8.14E-01

Table 5. Product purity

Product purity	Base case	Heat pump
Distillate compositions mass %		
X_{water}<10 %	2.19	2.75
$X_{acetone}$<50 %	55.9	63.20
Bottom compositions mass %		
$X_{methanol}$<2 %	1.48	1.67
$X_{acidity}$<3 %	2.49	2.69

Ranking of alternatives

The economic and environmental results were aggregated into a single-objective function as stated by Hui et. al. [1] (see equation 7). The economic index (TAC) and the process composite environmental index were normalized and the results are converted to quantitative scores. As part of the AHP method, the values of the pairwise comparison are determined by using a scale proposed by Satty [16]. The numerical values of this sacle are used to calculate the priority weights of each criteria (economic or environment). The result of the pairwise comparison shows that economic, environment and thermodynamic efficiency (n_{th}) criteria have the following weights; 0.57, 0.29 and 0.16 respectively. The weighting results closely agree with the result of Hui et. al. [1], who computed the qualitative weighting factors of 0.82 and 0.18 for economic and environment respectively. According to Satty [16], the best alternative is indicated by:

$$A_{AHP-score} = \max_{i} \sum_{j=1}^{n} a_{ij} \cdot w_j, \quad for\ i = 1,2,3,..m \tag{6}$$

The entry $a_{ij,}$ represents the relative value of alternative A_i (base case or heat pump) when it is considered in terms of criteria C_j (economic or environment). Equation 6 was further modified by Hui et. al. [1]:

$$A_{AHP-Score} = (Score \cdot Weight) + Score \cdot Weight) \tag{7}$$

Economic Environment

When equation 7 is applied, the following scores were obtained for each alternative $A_{1,\ AHP\text{-}score}$= 0.48, $A_{2,\ AHP\text{-}score}$= 0.52

Therefore the best alternative is alternative A_2 (heat pump) because it has the highest AHP score; 0.52. This value is achieved because of low operating cost of the heat pump and also because of the higher thermodynamic efficiency of the heat pump.

Conclusion

There were a number of tradeoffs found in this study. As the level of energy integration increases the PEI increases. On the other hand as the level of heat integration increases, the column performance increases due to the higher thermodynamic efficiency of the heat pump (18.47 %) compared with the base case (14.30 %), which is evidence from the lower exergy loss of the heat pump distillation. The TAC of the heat pump was greater compared with the base case, this is due to the integration of process equipment such as heat exchanger and process machinery such as compressor to the heat pump design. With these trade-offs, the application of AHP method shows that the heat pump is the better alternative.

References

1. Hui Chen, Ya Wen, Michelle D. Waters, and David R. Shonnard. (2002). Design Guidance for Chemical Processes Using Environmental and Economic Assessments. *Ind. Eng. Chem. Res, 41, 4503-4513*.
2. Teresa M. Mata, Raymond L. Smith, Douglas M. Young, Carlos A.V. Costa. (2003). Evaluating the environmental friendliness, economics and energy efficiency of chemical processes: heat integration, *Clean Techn Environ Policy* 5, 302–309.
3. Dantus, M. M.; High, K. A. (1996). Economic Evaluation for the Retrofit of Chemical Processes through Waste Minimization and Process Integration. *Ind. Eng. Chem. Res.*, *35*, 4566.
4. Cano-Ruiz, J. A.; McRae, G. J. (1998). Environmental Conscious Chemical Process Design. *Annu. Rev. Energy Environ. 23*,499.
5. Lou, H.H., Kulkarni, M.A., Singh, A. and Hopper, J.R. (2004). Sustainability assessment for industrial systems. Ind Eng Chem Res, 43(15): 4233–4242.
6. Achour, M.H., Haroun, A.E., Schult, C.J., et al. (2005). A new method to assess the environmental risk of a chemical process Gasem. Chem Eng Process, 44(8): 901–909.
7. Hau, J.L., Yi, H.S. and Bakshi, B.R., (2007). Enhancing life cycle inventories via reconciliation with the laws of thermodynamics. J Ind Ecol, 11(4): 1–21
8. J. Rafael Alca´ntara-Avila, Manabu Kano, Shinji Hasebe. (2012). Environmental and economic optimization of distillation structures to produce anhydrous ethanol, *22nd European Symposium on Computer Aided Process Engineering*, 30: 712–716.
9. Wang, M., Shi, Y., Xia, X., Li, D., Chen, Q. (2013). Life-cycle energy efficiency and environmental impacts of bioethanol production from sweet potato. doi: http:// dx.doi.org/10.1016/*j.biortech*.01.067.
10. Gomez-Castro, F. I., Rico-Ramirez, V., Segovia-Hernandez, J. G., Hernandez-Castro, S., & El- Halwagi, M. M. (2013). Simulation Study on Biodiesel Production by Reactive Distillation with Methanol at High Pressure and Temperature: Impact on Costs and Pollutant Emissions, *Computers and Chemical Engineering* doi:10.1016/j.compchemeng.01.007.
11. Hilaly AK, Sikdar SK. (1994) Pollution balance: a new method for minimizing waste production in manufacturing processes. *J Air Waste Manag. Assoc* 44:1303–1308.
12. Young DM, Cabezas H. (1999). Designing sustainable processes with simulation: the waste reduction (WAR) algorithm. *Comput Chem Eng* 23:1477–1491.
13. Douglas Young, Richard Scharp, Heriberto Cabezas. (2000). The waste reduction (WAR) algorithm: environmental impacts, energy consumption, and engineering economics Waste Management 20 (2000) 605±615.
14. Seider, W. D., Seader, J.D., Lewin, D.R., 2003, Product and Process Design principles, Synthesis, Analysis and Evaluation, John Willey & Sons, Inc., New York. Pg. 142-145.
15. Douglas, J. M., (1988). Conceptual Design of Chemical Processes. McGraw-Hill Book Company, New York, pg.425-432.
16. Satty, T. (1980). The Analytic Hierarchy Process; McGraw-Hill: New York, pg. 560-601.

The Malaysian Journal of ANALYTICAL SCIENCES ISSN 1394-2506

LIPID PEROXIDATION IN RAT LIVER USING DIFFERENT VEGETABLE OILS

(Peroksidaan Lipid Pada Hati Tikus yang Menggunakan Minyak Sayuran yang Berbeza)

Eqbal Dauqan[1*], Aminah Abdullah[2], Halimah Abdullah Sani[1]

[1]School of Biosciences and Biotechnology,
[2]School of Chemical Sciences and Food Technology,
Faculty of Science and Technology
Universiti Kebangsaan Malaysia, 43600 UKM Bangi, Selangor D.E., Malaysia

**Corresponding author: edouqan@yahoo.com*

Abstract

The objective of the study was to evaluate the effect of different vegetable oils (Red Palm Olien (RPO), Palm Olein (PO), Corn Oil (CO) and Coconut Oil on lipid peroxidation of rat liver. One hundred and thirty two Sprague Dawley male rats were randomly divided into two groups. The first group contains seventy two rats were divided into twelve groups of 6 rats per group and were treated with different concentrations of RPO (5%, 10% and 15%) for 2, 4 and 8 weeks. The second group contains sixty male rats were randomly divided into ten groups of 6 rats per group and were treated with 15% of RPO, PO, CO and COC for 4 and 8 weeks. The results shows that after 8 weeks of treatment the malondialdehyde (MDA) value in RPO group was significantly lower ($P \leq 0.05$) than control or vegetable oils studied. These experiments suggested that red palm olein antioxidants present in rat diets may better attenuate peroxyl radical than other vegetable oil studied.

Keywords: **:** lipid peroxidation, malondialdehyde (MDA), vitamin E, β-carotene, vegetable oils, antioxidants

Abstrak

Satu siri kajian telah dijalankan untuk menilai kesan minyak sayuran yang berbeza pada peroksidaan lipid pada hati tikus Satu ratus tiga puluh dua ekor tikus Sprague Dawley jantan telah dibahagi kepada dua kumpulan. Kumpulan pertama mempunyai 72 ekor tikus dan dibahagi kepada dua belas kumpulan 6 ekor tikus setiap kumpulan. Tikus-tikus diberi makan *ad libitum* dengan pelet komersial yang mengandungi kepekatan olein sawit merah (RPO) yang berbeza selama 2, 4 dan 8 minggu. Kumpulan kedua mengandungi 60 ekor tikus jantan yang dibahagi secara rawak kepada 10 kumpulan 6 ekor yang masing masing telah diberi 15% RPO, olein sawit (PO), jagung minyak (CO) dan kelapa sawit (COC) dan kawalan selama 4 dan 8 minggu. Selepas 8 minggu perlakuan nilai malondialdehida (MDA) dalam kumpulan RPO adalah jauh lebih rendah ($P \leq 0.05$) daripada kawalan atau kumpulan minyak sayur-sayuran yang dikaji. Keputusan eksperimen ini menunjukkan minyak olein sawit merah yang mengandungi banyak antioksidan dalam diet tikus dapat mengurangkan pembentukan radikal peroksi dengan lebih baik berbanding minyak sayuran lain yang dikaji.

Kata kunci: peroksidaan lipid, malondialdehida (MDA), vitamin E, β-karotena, minyak sayuran, antioksidan

Introduction

Vegetable oils in particular are natural products of plant origin consisting of ester mixtures derived from glycerol with chains of fatty acid contain about 14 to 20 carbon atoms with different degrees of unsaturation [1]. Vegetable oil is very common, affordable and used by majority of people across the globe especially in the tropics. Its use as antidote to prevent some oxidative stress related diseases and a complication is advocated [2]. Palm oil contains approximately an equal amount of saturated and unsaturated fatty acids. Amongst the former, palmitic and stearic acid account for 45% and 5% of the total fatty acids, respectively. Palm oil has a wide range of applications and it is commonly fractionated into olein and stearin [3]. The different properties of palm oil and it's fractions allow the products to be used for different purposes [4]. Palm olein oil, a liquid fraction obtained from the refining of palm oil, is rich in oleic acid (42.7– 43.9%), β-carotene and vitamin E (tocopherols and tocotrienols) [5]. It is rich in

tocotrienol which has been reported to be natural inhibitors of cholesterol synthesis. Tocopherols are very important minor components of oils and fats because of their antioxidant properties [6].

Red Palm Oil (RPO) contains 50% saturated fatty acids, 40% monounsaturated fatty acids and 10% polyunsaturated fatty acids. The RPO is the only vegetable oil with a balanced composition of saturated and unsaturated fatty acids both in the processed and unprocessed forms [7]. It contains carotenoids, phosphatides, sterols, tocopherols and trace metals. They have shown to be effective against oxidative stress in vitro and in vivo [8]. Red palm oil (RPO) is the oil obtained before refining. The characteristic colour of RPO is due to the abundance of carotenoids (500 – 700 mg / L) in the crude oil [9]. Most of the β-carotene is destroyed during processing the oil in palm oil refineries [10]. The carotenoids, together with vitamin E, ascorbic acid, enzymes and proteins, are members of the biological antioxidant network converting highly reactive radicals and free fatty peroxyl radicals to less active species [11] thus, protecting against oxidative damage to cells. Besides providing high energy density in the diet, β-carotene is the most abundant carotenoids which can be converted to vitamin A; which is an important in the visual process. In addition, it is an antioxidant that destroys singlet oxygen and free radicals [12]. Red Palm Oil is also a rich source of vitamin E, which is about 559 to 1000 ppm. Vitamin E acts as a potent antioxidant serving to protect cellular membranes from free radical-catalyzed lipid peroxidation [12].

Coconut oil is commercially a major source of lauric acid [13]. Coconut oil contains approximately 90% saturated fats. [14]. Coconut oil contains medium chain fatty acids such as lauric, caprylic and myristic acids. Of these three, coconut oil contains 40% lauric acid, which has the greater antiviral activity of these three fatty acids [15]. Corn oil provides essential fatty acids, mostly linoleic acid. Linoleic acid is necessary for the integrity of the skin, cell membranes, and the immune system, and for synthesis of eicosanoids. [16]. Corn oil is a good source of essential fatty acids and its nutritional properties are excellent and the fatty acids found in corn oil are palmitic acid, stearic acid, oleic acid, linoleic acid, and linolenic acid [17].

Reactive oxygen species (ROS) are highly reactive and in the absence of any protective mechanism they can disrupt normal metabolism through oxidative damage to lipids, protein and nucleic acids [18]. Peroxidation of lipids is a binding process connected with the formation of aldehydes and one of them is malondialdehyde (MDA). Thibarbituric acid (TBA) assay is the most common method to be used to measure MDA activity [19]. It is known that the quantity of MDA is an intensity index of peroxidation process of polyunsaturated fatty acids (PUFAs) contained in food [20, 21]. MDA is one of the final products of polyunsaturated fatty acids peroxidation in the cells, increase in free radicals causes overproduction of MDA. Malondialdehyde level is commonly known as a marker of oxidative stress and the antioxidant status [20, 22, 23]. Mohammad et al. [24] reported that the level of lipid peroxidation can be determined by measuring the level of malondialdehyde (MDA) which is a stable lipid peroxidation product. Therefore the the main objective of this work was to compare the effect of different concentrations (5%, 10% and 15%) of RPO and four vegetable oils (red palm olein, palm oil, corn oil and coconut oil) added to commercial pallet on lipid peroxidation of rats fed until 8 weeks of growth.

Materials and Methods

Instruments

The following instruments were used in this study: (i) High-speed homogenizer (DI18 basic, IKA, Germany) (ii) centrifuge (Kubota 2010, Malaysia) (iii) UV-Visible spectrophotometer (Hitachj U-1800 single, Germany).

Chemicals

Potassium chloride (KCl), thiobarbituric acid ($C_4H_4N_2O_2S$), tetraeethoxypropane (TEP), acetic acid ($C_2H_4O_2$), butanol ($C_4H_{10}O$) were obtained from Sigma (USA) while sodium dodecyl sulfate ($C_{12}H_{25}O_4S$) was obtaind from sigma-aldrich, Japan. Pyridin (C_5H_5N) were from Hopkin and Williams chemicals campony.

Experimentals Diets

The evaluated RPO samples consist of carotino. It is provided by Carotino SDN BHD company Palm olein (Seri Murni), corn oil and coconut oil were obtained commercially. For first group the test diet was prepared by mixing vegetable oils with normal commercial rat pellet to contain 15% of the vegetable oils. The 15% diet was prepared by adding 15g RPO, PO, CO or COC to 85g rat pallet, and mixed manually and the diets were then left to absorb the

vegetable oils at room temperature overnight and stored at 20^{o} C before the feeding trial was conducted. For second group the test diet was prepared by mixing RPO with normal commercial rat pellet to contain 5%, 10% and 15% of the red palm olein (RPO). The 5% diet was prepared by adding 5g RPO to 95g rat pallet, and mixed manually and the diets were then left to absorb the RPO at room temperature overnight and stored at 20^{o} C before the feeding trial was conducted. Similar process was conducted with 10%, and 15% RPO.

Animals

One hundred and thirty two Sprague Dawley male rats each weighing between 170-250g and approximately 80 days old were obtained from the animal house of the Faculty of Science and Technology, Universiti Kebangsaan Malaysia. They were randomly divided into two groups. The first group contains seventy two rats were divided into twelve groups of 6 rats per group. The rats were fed *ad libitum* with commercial rat's food containing different concentrations of RPO (5%, 10% and 15%) for 4 and 8 weeks. The second group contains sixty Sprague Dawley male rats were randomly divided into ten groups of 6 rats per group and were treated with 15% of RPO, PO, CO and COC for 4 and 8 weeks. Rats in control group were given normal rat pellet only while in treated groups 5%, 10% and 15% of additional RPO for first group were given and 15% of additional different vegetable oils for second group were given.

MDA Standard

Depend on Oxford biomedical research [25] method the MDA standard was provided as tetraethoxypropane (TEP) because MDA is not stable. However, the TEP standard was provided as a 20 mM stock solution. For a standard curve, pipette the volumes shown in table 1 to give a total of 200 µL of standard. The concentrations of MDA were determined from standard curve, which was constructed as follows:

Malondialdehyde was calculated using the following equation:

$$[\text{MDA } (\mu\text{mol/g})] = A_{532} \times V_T / Vs],$$

where: V= Total value
Vs= Sample value

Table 1. Standard Curve Dilution Volumes

Target concentration of standard (µM)	0	0.25	0.5	1.0	2.0	4.0
Volume of 20 µM standard (µL)	0	25	50	100	150	200
Volume of water, µL	200	175	150	100	50	0

The clear supernatant was transferred to a cuvette and was absorbent at 586 nm. A plot of A_{586} nm vs. [MDA] for the standards was constructed Figure 1.

Statistical Analysis

Results were expressed as mean values ± SEM (n=6). Means of six samples were compared by analysis of variance (ANOVA). Significant differences between means were determined by Tukey's least significant difference ($p \leq 0.05$). The software used was MINITAB® (14.20).

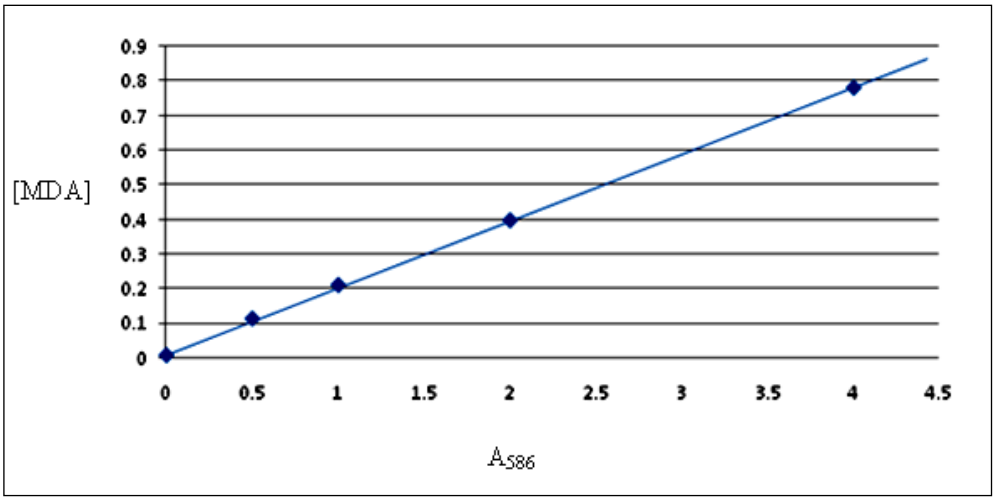


Figure 1. Malondialdehyde Standard curve

Determination of Lipid peroxidation (MDA)

Liver sample for malondialdehyde (MDA) was prepared by 1 g of liver cut to small pieces. Tissue was suspended in 9 ml of 1.15% KCl, and was homogenized using a mixer at top speed for 3 min. Thiobarbituric acid reactive substances (TBARS) will be measured by the modified spectrophotometric assay as Ohkawa at el. [26]. The reaction mixture contained 0.2 ml of 8.1% sodium dodecyl sulfate (SDS), 1.5 ml of 20% acetic acid solution, 1.5 ml of 0.8% aqueous solution of thiobarituric acid (TBA), and homogenate (10%, 0.1 ml). The mixture was finally made up to 4.0 ml with distilled water, and heated at $95C^0$ for 60 min. After cooling with tap water, 1.0 ml of distilled water was added and the red pigment produced was extracted with 5.0 ml of the mixture of n-butanol and pyridine (15:1, v/v), and the mixture was shaken vigorously. After centrifugation at 4000 rpm for 10 min, the absorbance of the organic layer (upper layer) was measured at 532 nm.

Results and Discussion

Malondialdehyde and other aldehydes are generally considered the end products of lipid peroxidation and are widely measured as the indexes of lipid peroxidation [21].

Effect of Different Concentrations of Red Palm Olein on Lipid Peroxidation of Rat Liver

The results of MDA level of rat liver with different concentrations (5%, 10% and 15%) of RPO for 2, 4 and 8 weeks of treatment are summarized in Figures 2, 3 and 4. After 2 weeks of treatment the results of MDA level was no significant different ($P \geq 0.05$) between control group and rat liver treated with 5%, 10% and 15% RPO groups. At 4 weeks the MDA level of treated rat increased in all concentrations compared to the control group but there was no significant different ($P \geq 0.05$) in MDA level of treated rat of RPO (5% and 10%) while there was significant increase ($P \leq 0.05$) in MDA level of treated rat of RPO (15%) compared to the control group. The mean ± SEM of lipid peroxidation as determined with MDA activity in the treated rat liver in control, 5%, 10% and 15% of RPO groups were 42.8µmol/g, 42.5µmol/g, 55.7µmol/g and 67.1µmol/g respectively.

At 8 weeks the MDA level was decreased with all concentrations compared to the control group. There was no significant different ($P \geq 0.05$) between control and 5% RPO but were significantly higher ($P \leq 0.05$) than 10% or 15% RPO treated liver samples. The mean ± SEM of lipid peroxidation as determined with MDA activity in the treated rat liver in control, 5%, 10% and 15% of RPO groups were 46.5µmol/g, 45.3µmol/g, 23.6µmol/g and 21.9µmol/g respectively. The results of the present study showed that after 2 weeks of treatment did not decrease MDA level.

The two weeks of treatment was not suitable for investigation because the time of treatment too short to see the effect.

Lipid peroxidation is widely used as an indicator to reflect oxidative stress and cell membrane damage [27]. Free radicals like superoxide anion and hydroxyl radical exert their toxic effect by acting on lipids. Feeding dietary oils rich in unsaturated fatty acids makes target tissues more vulnerable to peroxidative damage [28]. This is reflected in higher lipid peroxidation production in livers of animals fed these diets. However, in this study suggested that the presence of high level of dietary vitamin E used may have protected the liver tissues from peroxidative damage.

There is increasing evidence that carotenoids are very effective quenchers of peroxyl radicals [29], but the mechanism of their action has not yet been defined. One might expect that the reaction of β-carotene with a peroxyl radical would form a carotenoid radical species shown in equation 1 [30, 31].

$$\beta\text{-carotene} + ROO^{\cdot} \longrightarrow \beta\text{-carotene} + ROOH \quad (1)$$

β-Carotene may react directly with a peroxyl radical to form a resonance-stabilized carbon-centered radical (equation 2).

$$\beta\text{-carotene} + ROO^{\cdot} \longrightarrow ROO\text{-}\beta\text{-carotene} \quad (2)$$

Thus, providing an explanation of the antioxidant effect of β-carotene on lipid peroxidation induced by peroxyl radicals, In the presence of oxygen, the β-carotene radical in the equation (1) would combine with oxygen to form a carotenoid-peroxyl radical (equation 3).

$$\beta\text{-carotene} + O2 \longrightarrow \beta\text{-carotene-}OO^{\cdot} \quad (3)$$

This reaction would be dependent on the oxygen tension in the system. If the oxygen tension is sufficiently low, the equilibrium of reaction (3) shifts to the left, reducing the amount of chain-carrying peroxyl radical. In addition, the β-carotene-peroxyl complex could react with another peroxyl radical, leading to a termination reaction, as shown in reaction (4).

$$\beta\text{-carotene-}OO^{\cdot} + ROO^{\cdot} \longrightarrow \text{inactive products} \quad (4)$$

On the other hand, if the oxygen tension is high, the equilibrium of reaction (3) would shift to the right and form a peroxyl radical capable of acting as a prooxidant. The last reaction is also referred to as autoxidation of β-carotene [31]. Eder et al. [32] showed that the relationship between the vitamin E intake and level lipid peroxidation can be explained by the fact that oils with highest content of antioxidant (vitamin E and β-carotene). Tamara et al. [33] suggested that the animals on the vitamin E diet had 40% lower hepatic malondialdehyde levels in liver male mice which treated with a diet high vitamin E. Peng and Stanley [34] reported that the effect of β-carotene, tocopherol in protecting membranes from oxidative damage relative to different oxygen tensions. Hence, current study found that during treatment with 15% RPO for 8 weeks the lipid peroxidation level was inhibited in the rat liver.

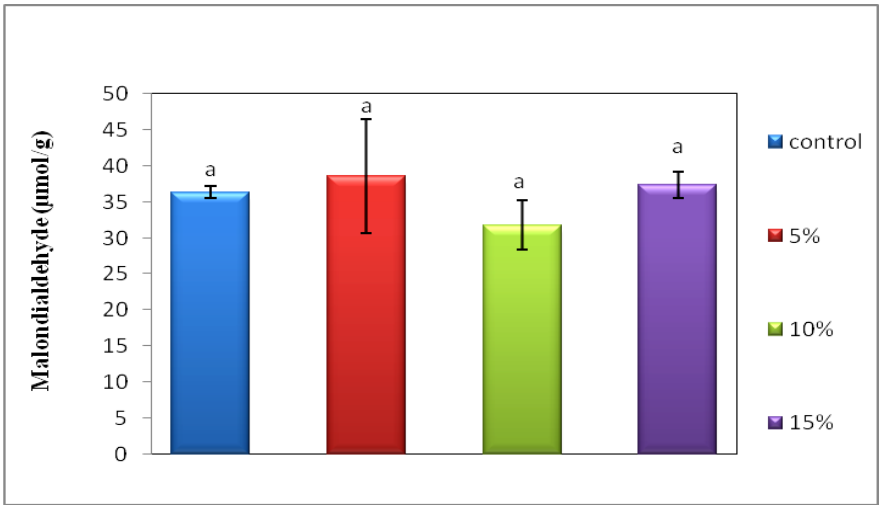


Figure 2. The malondialdehyde (MDA) in liver of rat fed with different concentrations of red palm olein for 2 weeks. Bars are mean ±SEM (n=6), no significantly different (P≥0.05).

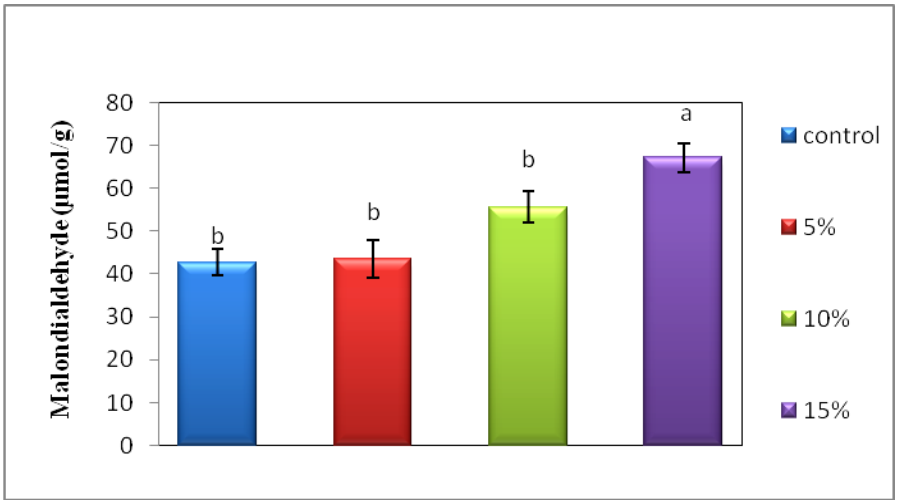


Figure 3. The malondialdehyde (MDA) in liver of rat fed with different concentrations of res palm oilein for 4 weeks. Bars are mean ±SEM (n=6), different alphabet an each bar indicate significant different (P≤0.05).

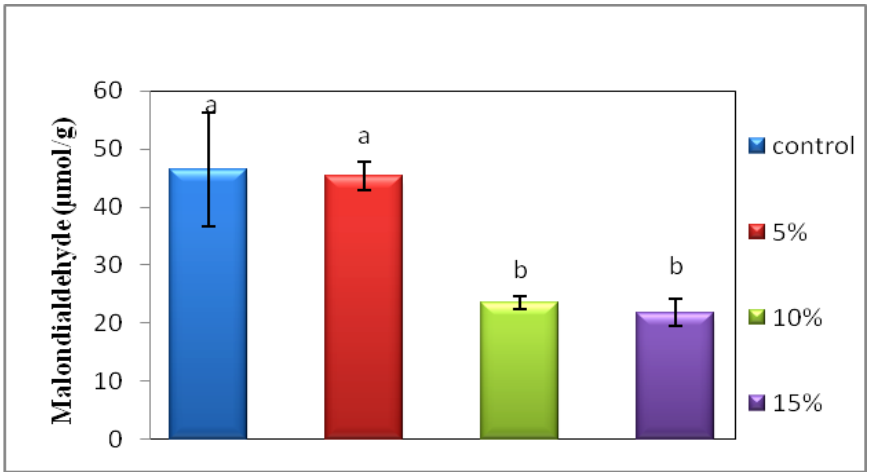


Figure 4. The malondialdehyde (MDA) in liver of rat fed with different concentrations of red palm oilein for 8 weeks. Bars are mean ±SEM (n=6), different alphabet an each bar indicate significant different (P≤0.05)

Effect of Four Different Vegetable Oils (RPO, PO, CO and COC) on Lipid Peroxidation of Rat Liver

The results of MDA level of rat liver with 15% of different vegetable oils for 4 and 8 weeks of treatment are summarized in Figures 5 and 6. At 4 weeks of treatment with different vegetable oils showed that MDA level of treated rat was increased in RPO, PO and CO groups whereas there was no significant difference (P≥0.05) in MDA level of rats treated in COC group compared to the control group. The mean ± SEM of lipid peroxidation as determined with MDA activity in the treated rat liver of control, RPO, PO, CO and COC groups were 27.3µmol/g, 92µmol/g, 54µmol/g, 47.4µmol/g and 72.6µmol/g respectively. The results at 8 weeks showed a decline in MDA level of treated rat in RPO group and there was significant increased at CO and COC groups but there was no significant different (P≥0.05) in MDA level of treated rat in PO group compared to control group. The mean ± SEM of lipid peroxidation as determined with MDA activity in the rat liver of control, RPO, PO, CO and COC groups were 31.5µmol/g, 25.2µmol/g, 43.4µmol/g, 50.1µmol/g and 48.3µmol/g respectively.

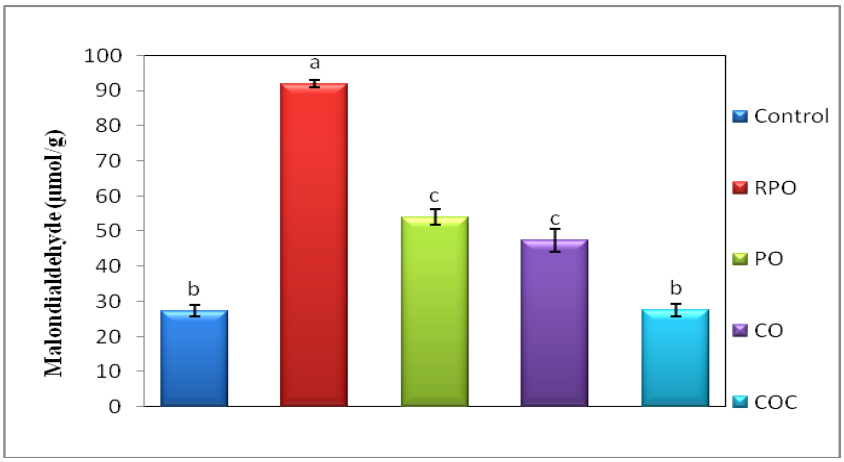


Figure 5. The malondialdehyde (MDA) in liver of rat fed with different vegetable oils for 4 weeks. Bars are mean ±SEM (n=6), different alphabet an each bar indicate significant different (P≤

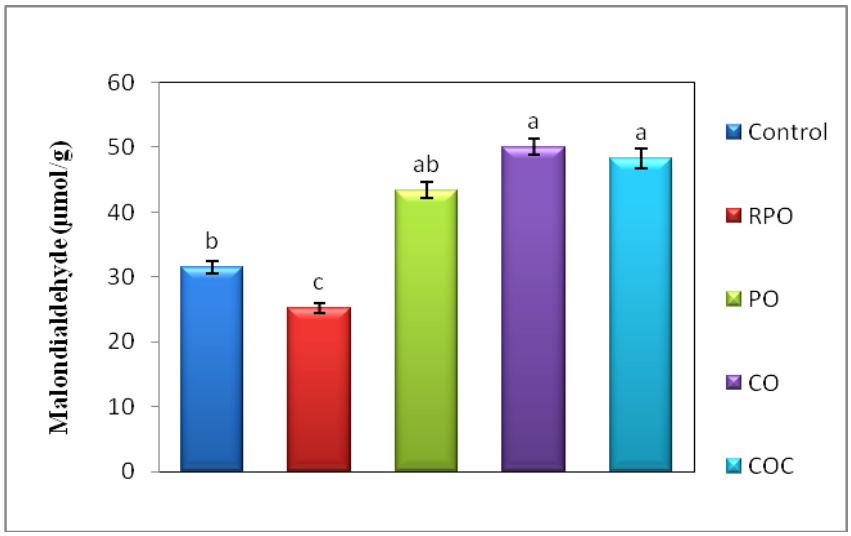


Figure 6. The malondialdehyde (MDA) in liver of rat fed with different vegetable oils for 8 weeks. Bars are mean ±SEM (n=6), different alphabet an each bar indicate significant different (P≤0.05)

The findings from present study that MDA level increased in RPO and PO groups compared to the control group after 4 weeks. This increase could be due to that it has been linked with oxidative stress and increased lipid peroxidation product expressed as level MDA. Thus, the present study could be explained on the basis of increased lipid peroxidation while the reduction in the level in RPO and PO groups after 8 weeks could be a result of the antioxidant property of palm oil. This property is conferred to palm oil by its possession of high level of α-tocopherol and other antioxidant vitamin [2].

Hence, in the second group there was significant decrease (P≤0.05) in MDA level of treated rats liver in RPO group while there was no significant decreased (P≥0.05) in MDA level of rat treated in PO group because RPO which used in this study contains vitamin E (0.10%) and PO (0.10%). Vitamin E is one of the most effective antioxidants in animals and it is composed of various subfamilies that include tocopherols and tocotrienols. These compounds have antioxidant properties [35]. Red palm olein contains β-carotene 542 ppm but PO does not contain β-carotene. Other suggests that generation of singlet oxygen during lipid peroxidation might be attributed to breakdown reactions of lipid hydroperoxy free radicals. Therefore, the β-carotene and α-tocopherol, act as potent antioxidants in protecting biological membranes or lipids against free radical damage [34].

Vitamin E as a lipid soluble, chain breaking antioxidant plays a major role against oxidative stress and prevents the production of lipid peroxides by scavenging free radicals in biological membranes [36]. Siti Khadijah et al. [19] showed that palm oil which contains high amount of monounsaturated fatty acids (MUFA) is less susceptible to oxidation. The results of MDA level of rat liver with 15% of CO for 4 and 8 weeks of treatment are increased. It seems probable that, the CO which uses in this study contains small amounts of vitamin E and β-carotene (0.03% and 0.913ppm) respectively compared to RPO and PO. Similar to the reported case of study that the increase in MDA levels observed could be due to increased oxidative stress from various sources or decrease in antioxidant defense mechanism [37]. Corn oil has a relatively high proportion of fatty acids, polyunsaturated (PUFA) [38].

Due to the high levels of unsaturation, these fats are highly susceptible to free radical oxidative reactions giving rise to the formation of lipid peroxide [39]. CO is the most unsaturated oils among widely consumed oils. It is rich in oleic, linoleic and linolenic acids. Therefore, they are easily affected by free radical reactions [40, 41]. The results of MDA level of rat liver with 15% of COC for 8 weeks of treatment are increased because the COC which uses in this study does not contain any antioxidants as vitamin E or β-carotene compared to other vegetable oils. Odutuga & Amballi [42] used male albino rat which treated with 5% of coconut oil for 14 weeks of treatment. They reported

that the saturated fatty acids consumption and malondialdehyde formation in rat tissues has been studied. It is less vulnerable to lipid peroxidation than their unsaturated counterparts [43].

Conclusion

The results conclude that after 8 weeks of treatment with different vegetable oils (RPO, PO, C and COC) the malondialdehyde value in 15% red palm olein was lower than control or other oils studied. Thus, after eight weeks the lipid peroxidation was decreased in rat liver treated with 15% red palm olein. Therefore, the presence of vitamin E and beta carotene in the RPO could be the reasone of low lipid peroxidation compared to other vegetable oils studied.

Acknowledgement

This work was supported by the Organization for Women in Science for the Developing World (OWSDW) and the research was funded by UKM-GUP-NBT-27-103, UKM-HEJIM-Industri-16-2010 and UKM OUP-NBT-29-139/2011. We grateful thank to caroteno sdn bhd Malaysia for providing red palm olein sample.

References

1. Emmanuel, O. A. & Mudiakeoghene O. 2008. The use of antioxidants in vegetable oils – A review. *African Journal of Biotechnology*, 7(29): 4836-4842
2. Ogugua, V. N. & Ikejiaku, C. A. 2005. Effect of palm oil on some oxidative indices of alloxan induced diabetic rabbitic rabbits. *Animal Research International* 2: 227 – 230
3. Pramod, K. 2006. Palm Oil: a nutritional overview. *AgroFOOD industry hi-tech*. Anno 17 - No. 3
4. Flingoh, C. H. O. H., & Chong, Chiew Let, 1992. Surface tensions of palm oil, palm olein and palm stearin. *Elasia*, 4(1).
5. Deepak, N., Subeena, S., Mathew, K. T., Amit, K. D. & Subir, K. M. 2004. Effect of dietary palm olein oil on oxidative stress associated with ischemic-reperfusion injury in isolated rat heart. *BMC Pharmacology* 4:29: 2210-2429
6. Che Man, Y. B., Ammawath, W. & Mirghani, M. E. S. 2005. Determining α-tocopherol in refined bleached and deodorized palm olein by Fourier transform infrared spectroscopy. *Food Chem*. 90: 323-327
7. Edem, D. O. & Akpanabiatu, M. I. 2006. Effects of palm oil-containing diets on enzyme activities of rats. *Pak. J. Nutr*. 5(4): 301-305
8. Aboua, Y. G., Brooks, N., Awoniyi, D. O. &. Plessis, S. S. 2009. Red palm oil: A natural good Samaritan for sperm apoptosis. *Medical Technology Sa.* 23: 8-10
9. Edem, D. O. 2009. Haematological and histological alterations induced in Rats by Palm Oil-Containing Diets. *Eur. J. Sci. Res.* 32: 405-418
10. Edem, D. O. 2009. Haematological and histological alterations induced in Rats by Palm Oil-Containing Diets. *Eur. J. Sci. Res.* 32: 405-418
11. Peng, Z. & Stanley, T. O. 2001. β-Carotene: interactions with α-tocopherol and ascorbic acid in microsomal lipid peroxidation. *Journal of Nutritional Biochemistry* 12: 38–45
12. Edem, D.O. 2002. Palm oil: Biochemical, physiological, nutritional, hematological and toxicological aspects: A review. *Plant Food for Human Neutrinos* 57:319-343
13. Gregorio C. Gervajio 2005 Fatty Acids and Derivatives from Coconut Oil, *John Wiley & Sons, Inc.* 1-56
14. Sabitha, P., Vaidyanathan, K., Vasudevan, D. M. & Kamath, P. 2009. Comparison of lipid profile and antioxidant enzymes among South Indian men consuming coconut oil and sunflower oil. *Indian J Clin Biochem*. 24(1):76–81
15. Lita, L. 2001. Coconut oil-why it is good for you, Raymond Peat. Chapter 29, page 175
16. Cedomila, M., Robert, D., Marin, T., Jasminka, G., Mira, C., Biserka, R. E. & Zlatko, C. 2001. Effect of olive oil- and corn oil-enriched diets on the tissue mineral content in mice. *Biological Trace Element Research* 82: 201-210
17. Michael, J. P. & David, F. W. 1975. Monosomic analysis of fatty acid composition in embryo lipids of zea maysl. *Genetics* 81: 277-286
18. Hatice, G., C. Cem, K. Murat, K. Muge, C. Asuman, & E. Atilla 2008. Peroxidase activity and lipid peroxidation in strawberry (*Fragaria* X *ananassa*) plants under low temperature. *J. Biol. Environ. Sci.* 2: 95-100

19. Siti Khadijah, A., Nik, A. S., Abdul, G. M. T. & Kamsiah, J. 2007. Heating reduces vitamin E content in palm and soy oils. *Malaysian Journal of Biochemistry and Molecular Biology* 15(2): 76-79
20. Alan A. H. and Lester P. 1970 Interactions Between Malondialdehyde and Rat Liver Mitochondria, *journal of Gerontology*. 25(3):199-204
21. Niedworok, E. & Bielaszka, A. 2007. Comparison of the effect of vitamins A and E on aging processes of edible vegetable oils. *Polish J. of Environ. Stud. 16(6): 861-865*
22. Jarmila Z., Jiri S., Katerina K., Anna K., Tomas H., Vaclav Z. and Alena F. 2004 Effects of Oxidised Dietary Cod Liver Oil on the Reproductive Functions of Wistar Rat, *Czech J. Food Sci.* 22(3): 108–120
23. Fakher S. H., Djalali M., Tabei S. M. B., Zeraati H., Javadi E., Sadeghi M. R., Mostafavi E., Fatehi F. 2007 Effect of Vitamins A, E, C and Omega-3 Fatty Acids on Lipid Peroxidation in Streptozotocin Induced Diabetic Rat, *Iranian J Publ Healt*. 36(2): 58-63.
24. Muhammad, A. B. & Muhammad, T. 2008. Correlation of nigella sativa of and sunflower doet intake in albino rats. *Professional Med. J. Dec.* 2008 15(4): 500-507
25. Oxford biomedical research, 2003. Colorimetric assay for lipid peroxidation. 1-7 (20/2/2011)
26. Ohkawa, H., Nobuko, O. & Kunio, Y. 1979. Assay for lipid peroxides in animal tissues acid reaction. *Anal. Biochem*. 95: 351-358
27. Halliwell, B. & Gutteridge, J. M. 1989. Free radicals in biology and medicine. 2nd ed. Oxford: Clarendon Press
28. Jaya, T. V., Poomchai, A., Neera, S. & Gabriel, F. 1998. Effects of dietary n-6 and n-3 lipids on antioxidant defense system in livers of exercised rats. *J. Am. Coll. Nutr.* 17: 586-594
29. Sophie, B., Bruno, F. & Gabriele, S. 2006. Do carotenoid-based sexual traits signal the availability of non-pigmentary antioxidants?. *The Journal of Experimental Biology* 209: 4414-4419
30. Graham, W. B. 1989. Antioxidant Action of Carotenoids. *J.Nutr* 119:109-111.19
31. Hussain, A. M. Z. I., Hydrie, B. & Claussen, S. A. 2010. Type 2 Diabetes and obesity: A review. *Journal of Diabetology* (1:2):1-7
32. Eder, E., Wacker, M., Lutz, U., Nair, J., Fang, X., Bartsch, H., Beland, F.A., Schlatter, J. & Lutz, W. K. 2006. Oxidative stress related DNA adducts in the liver of female rats fed with sunflower-, rapeseed-, olive- or coconut oil supplemented diets. *Chemico-Biological Interactions* 159: 81–89
33. Tamara, R. K., Marc, W., Anwar, F. & Hartmut, J. 2003. Role of lipid peroxidation as a mechanism of liver injury after acetaminophen overdose in mice. *Toxicological Science* 76: 229–236
34. Peng, Z. & Stanley, T. O. 2001. β-Carotene: interactions with α-tocopherol and ascorbic acid in microsomal lipid peroxidation. *Journal of Nutritional Biochemistry* 12: 38–45
35. Mazlan, M., Abd Halim, F., Mat Top, G. & Wan, Z. 2002. Effect of vitamin E on plasma malondialdehyde, antioxidant enzyme levels and the rates of wound closures during wound healing in normal and diabetic rats. *Asia Pac. J. Clin. Nutr*. 11: 448-451
36. Saalu, L. C., Oluyemi, K. A. & Omotuyi, I. O. 2007. a-Tocopherol (vitamin E) attenuates the testicular toxicity associated with experimental cryptorchidism in rats. *African Journal of Biotechnology* 6 (12):1373-1377
37. Kato J, Alice A. R., Sekharjit S. S., Bilasini D. S., Ibetombi D. Th. and Gyaneshwar S. W. 2007 Lipid Peroxidation and Antioxidant Vitamins in Urolithsis, *Indian Journal of Clinical Biochemistry*. 22 (1): 128-130.
38. Jinah, H. 2009. Diets with corn oil and/or low protein increase acute acetaminophen hepatotoxicity compared to diets with beef tallow in a rat model. *Nutrition Research and Practice* 3(2): 95-101.
39. Valls, M. G. V., Mun, P., Saez, G. T. & Cabo, J. R. Effect of corn oil and vitamin E on the oxidative status of adipose tissues and liver in rat. *Food Chemistry* 81(2): 281-286
40. Nobuko I., Eiko F. and Yohko K. 1979 Effect of Corn Oil Feeding on Lipid Peroxidation in Rats , the journal of nutration,558: 924-930.
41. Recep G. K. E, Udris A., Mustafa Y. N., Mahmut A. Y., Ahmet G. R., Osman A., Said, B. & Serdar E. 2000. Effects of dietary oils on lipoproteins, lipid peroxidation and thromboxane A2 production in chicks. *Turk. J. Vet. Anim. Sci.* 24: 473-478
42. Odutuga A.A. and Amballi A.A. 2007 Lipodystrophic and Lipo-Peroxidative Effects of Hydrogenated Coconut Oil Diet in Rats, Pakistan Journal of Nutrition. 6 (6): 593-596.
43. Leonard, T. R., Gregory, W. T., Michael, L. C., Gerald, C., Raphael, B. & David B. 2004. Lipid Peroxidation and the thiobarbituric acid assay: Standardization of the assay when using saturated and unsaturated fatty acids. *Journal of Biochemistry and Molecular Biology* 37(6): 749-752

The Malaysian Journal of ANALYTICAL SCIENCES ISSN 1394-2506

SPECTROPHOTOMETRIC DETERMINATION OF LAMOTRIGINE IN PHARMACEUTICAL PREPARATIONS AND URINE SAMPLES USING BROMOTHYMOL BLUE AND BROMOPHENOL BLUE

(Penentuan Spektrofotometrik Lamotrigina dalam Persediaan Farmaseutikal dan Sampel Urin Mengunakan Bromotimol Biru dan Bromofenol Biru)

Fadhil M. Najib*, Kosar H. H. Aziz

Chemistry Department, College of Science,
Sulaimani University, Sulaimani, Kurdistan Region, Iraq

**Corresponding author: fadhil.najib@univsul.net*

Abstract

Two simple and sensitive spectrophotometric methods have been developed for the determination of the antiepileptic drug lamotrigine (LMT) in pharmaceutical preparations and urine samples. The methods are based on the interaction of LMT with two sulphonphthalein dyes, namely, bromothymol blue (BTB) and bromophenol blue (BPB) in dichloromethane (DCM) medium to form stable and yellow-colored ion-pairs with λ_{max} 410 and 413 nm respectively. The ion-pair LMT-BPB has been extracted from aqueous solutions at pH 3.25±0.25 using DCM; while LMT-BTB ion-pair was directly prepared in DCM. Interferences from the compounds of the urine samples, in case of LMT-BPB were removed using a suppressing solution (S.S.) prepared from the salts of the interfering ions. In LMT-BTB method, the urine of normal person not taking LMT, was used as a blank to remove the effect of interferences. Under optimum conditions, the calibration curve of LMT-BTB was linear over the range of 1–12 μg.ml^{-1}, **ε** =1.97×10^4 L.mole^{-1}.cm^{-1}, r^2 = 0.9983, and D.L of 0.13 μg.ml^{-1}. The corresponding values for (LMT-BPB) ion-pair were 0.5–12 μg.ml^{-1} linear range, **ε** =1.92× 10^4, r^2= 0.9980, and D.L= 0.24 μg.ml^{-1}. The stoichiometry of the ion-pairs were found to be 1:1, based on Job's , mole ratio and slope ratio methods. The recoveries (%R) for both methods were in the range of 97%-101.8% and 95%-97.1% with RSD ≤ 1.68% and 3.1% respectively. For LMT- spiked urine samples, the recoveries were 98.5%- 106.6% with RSD ≤ 1.66%. Interferences from phenobarbital and carbamazepine were in the range of 25 – 40 folds. Statistical comparison of the results with a published method using F and t-tests showed no significant differences between each of the two methods and the reported one at 95% confidence level. A standard addition method, gave high accuracy with LMT-BPB method. The proposed methods were successfully applied for the determination of LMT in pharmaceutical preparation and urine samples.

Keywords: lamotrigine, bromothymol blue, bromophenol blue, farmaceutical formulation, urine sample

Abstrak

Dua kaedah spektrofotometri mudah dan peka telah dibangunkan bagi penentuan ubat anti-epileptik lamotrigine (LMT) di dalam persediaan farmaseutikal dan sampel air kencing (urin). Kaedah ini berasaskan kepada interaksi di antara LMT dengan dua pewarna sulfonftalein iaitu bromotimol biru (BTB) dan bromofenol biru (BPB) dalam medium diklorometana (DCM) membentuk pasangan ion yang stabil dan berwarna kuning dengan λ_{max} masing – masing 410 dan 413 nm. Pasangan ion LMT-BPB telah diekstrak daripada larutan akueus pada pH 3.25 ± 0.25 menggunakan DCM. Manakala pasangan ion LMT-BTB disediakan langsung di dalam DCM. Gangguan matriks air kencing, bagi kes LMT-BPB, disingkirkan menggunakan larutan penghalang (SS) yang disediakan daripada garam ion penganggu. Bagi kaedah LMT-BTB, air kencing daripada orang biasa yang tidak mengambil LMT, digunakan sebagai blank bagi menyingkirkan gangguan. Pada keadaan optimum, keluk tentukuran LMT-BTB adalah linear dalam julat 1-12 μg.ml^{-1}, ε = 1.97 × 104 vL.mol^{-1}.cm^{-1}, r^2 = 0.9983 dan DL = 0.13 μg.ml^{-1}. Bagi pasangan ion LMT-BPB julat linear adalah 0.5-12 μg.ml^{-1}), ε = 1.92 × 104, r^2 = 0.9980, dan DL = 0.24 μg.ml^{-1}. Stoikiometri pasangan ion adalah 1:1 berdasarkan kaedah-kaedah plot Job, nisbah mol dan nisbah cerun. Perolehan semula (% R) untuk kedua-dua kaedah adalah dalam lingkungan 97% -101.8% dan 95% -97.1% dengan RSD masing – masing adalah ≤ 1.68% dan 3.1%. Perolehan semula sampel air kencing yang dipaku dengan LMT adalah 98.5 - 106.6% dengan RSD ≤ 1.66%. Gangguan daripada phenobarbital dan carbamazepine adalah dalam lingkungan gandaan 25 - 40. Analisis statistik perbandingan menggunakan Ujian

F dan Ujian t pada aras keyakinan 95%, menunjukkan tiada perbezaan yang bererti di antara setiap kaedah. Kaedah tambahan piawai memberikan kejituan yang tinggi bagi kaedah LMT-BPB. Kaedah yang dicadangkan telah berjaya digunakan bagi penentuan LMT di dalam persediaan farmaseutikal dan sampel air kencing.

Kata kunci: lamotrigine, bromotimol biru, bromofenol biru, persediaan farmaseutikal, sampel urin

Introduction

Lamotrigine (LMT) or Lamictal, [6-(2,3-dichlorophenyl)-1,2,4-triazine-3,5diamine] is an antiepileptic drug of the phenyltriazine class, is chemically unrelated to other anticonvulsants [1,2] it has a pKa of 5.7 and its chemical structure shown in Figure 1. It is slightly soluble in water, a little more in HCl and H_2SO_4 at 25□C and of good solubility in methanol and acetone [3-5].

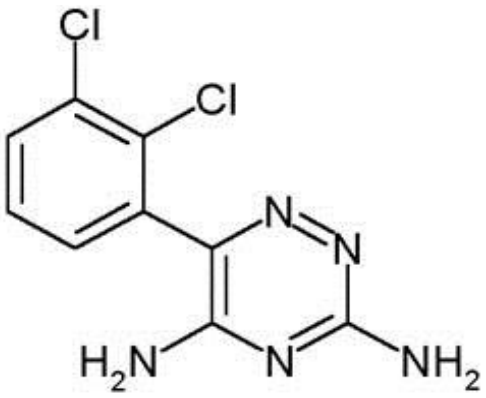
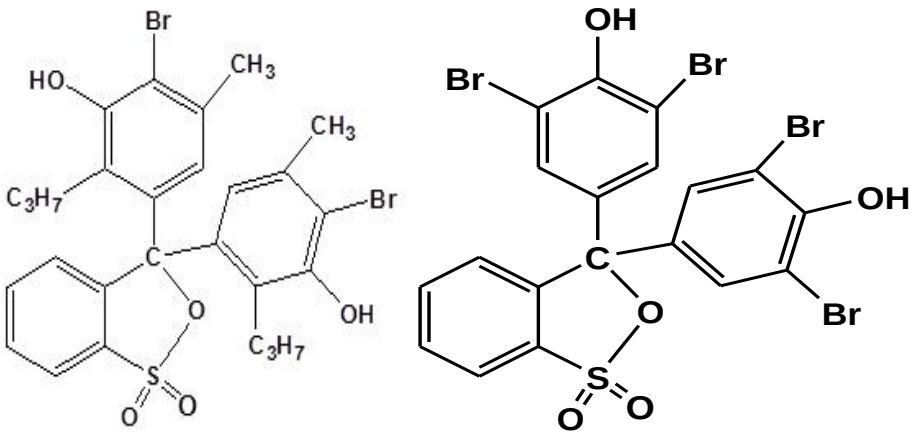


Figure 1**.** The chemical structure of lamotrigine (LMT)

LMT is used in the treatment of epilepsy as monotherapy or adjunct with other antiepileptic drugs [6]. It is rapidly and completely absorbed with elimination half-life of about 24 hours of the administered dose, 70% can be recovered in urine 90% of which is in the form of glucuronide conjugate and 10% unchanged LMT [7]. Various analytical techniques to estimate LMT in dosage forms and biological fluids have been reported in the literature. But most of the methods utilized HPLC techniques, due to their suitability, either normal or reversed-phase [8–11] and Gas chromatography too [12] in a mixture or with its metabolized species. Electroanalytical methods, including Ion-selective electrodes [13] and differential pulse adsorptive stripping voltammetry [14, 15] were among selective and sensitive methods used for the analysis of this drug. Extensive search in the literature has shown few spectrophotometric methods (absorption or emission) for the determination of LMT [2-6,16,17].

The emission method [2] in pharmaceutical formulations and biological fluids has been based on reaction of LMT with o-phthalaldehyde in the presence of 2-mercaptoethanol in borate buffer of pH 9.8 to yield a highly fluorescent derivative. Some of the absorption methods were in the UV region at 275 nm [5] and 307 nm [16] in bulk and in dosage form. In the visible region, however, charge transfer ion pair formation [17], p-chloranilic acid, Bromocresol green, Bromocresol purple, Chlorophenol red, and Bromophenol blue in chloroform or dichloromethane solvents [3-6,17] after extraction with chloroform and more recently the reagent 7,7,8,8-tetracyanoquinodimethane (TCNQ), as π-electron acceptors have been used for the spectrophotometric determination of LMT [18]. Although most of the methods applied for determination of LMT are sensitive and selective, but they require expensive instrumental set up. The aim of the present work was to develop easy spectrophotometric methods. Practical tests on many reagents revealed that sulphonphthalein dyes, namely bromophenol blue (BPB) and bromothymol blue (BTB), of the chemical structures shown in Figure 2 [19] were two suitable reagents to form colored ion-pair complexes with LMT.



I.bromothymol blue (BTB) II.bromophenol blue (BPB)

Figure 2. The chemical structures of (I) BTB and (II) BPB.

Materials and Methods

Materials

All spectra and absorbance measurements were taken with (Heλiosα UV-visible spectrophotometer V4.6) with 1cm path length quartz cells. (OAKTON pH-meter) with combined glass electrode (1100/2100) bench top meter USA. Shaker (Yamato, model SA-3IR) Micropipetspretech (variable and fixed). Sensitive balance (Sartorius) model: BL210S. Propipet controller accu-jet.Dispensette E.CAL. (0.2-2 mL, 1-10 mL) Germany.

Chemicals and Preparations

All chemicals used were analytical reagent grade and were from (Fluka, Rohm and Haas, Alpha chemika, Scharlauchemie S.A, Gainland Chemical Company GCC, and Merck) without further purification. Pure and standard powder of lamotrigine was obtained from the (Hikmacompany, Jordan). Both standard carbamazepin and Phenobarbital were obtained from (Samarra drug-company-Iraq).

Two concentrations of standard LMT were prepared: (I) 0.02 mg/mL LMT in CH_2Cl_2 and (II) 0.1mg/mL LMT in 10 mL 0.1M HCl, completing the volume to 1L with D.W in a volumetric flask. Bromothymol blue (BTB 624.4 g/mole) 5×10^{-3}M was prepared by dissolving 0.3122 g BTB in about 60 ml CH_2Cl_2 completing the volume to 100 ml in a volumetric flask with the same solvent. Bromophenol blue (BPB 670 g/mole) 4×10^{-3}M and 10^{-3}M were prepared by dissolving 0.67 g or (0.1675 g) BPB in 10 mL methanol and the volumes were completed to 250 mL in volumetric flasks with D.W. The buffers citrate, tartarate, phthalate and phosphate were prepared according to [20] and adjusted to the desired pH by NaOH or HCl.

The suppressing Solution (S.S.):was prepared by dissolving a mixture of 1.8825 g .Na_2HPO_4,1.4515 g. K_2 HPO_4, and 0.15 g. creatinine, which give 6100, 6500 and1500 ppm each of Na^+, K^+ and creatinine, respectively in100 mL volumtric flask. The pH of the solution was adjusted to 6 with 0.1M HCl.

Deproteinization of samples:

This was performed as follows:**1).** Five mL of LMT- spiked urine were collected in a beaker. **2).** Three mL of 0.15M $Ba(OH)_2$ were added to the urine sample followed by 3 mL of 2.5% w/v $ZnSO_4.7H_2O$ and mixed well. **3)-** The mixture was filtered through a whatman no.41 filter paper and the filtrate was diluted to 100 mL by D.W in a volumetric flask [21].

Preparation of tablet samples:
Ten tablets were accurately weighed and grounded into a fine powder. A quantity of the powder Equivalent to 5.0 mg of LMT was dissolved in 50 mL CH_2Cl_2 and transferred quantitatively into a 100 mL volumetric flask. Then content was shaken thoroughly for 20-25 min. then filtered through a Whatman No.41 filter paper and washed three times with 5mL portions of CH_2Cl_2. The filtrate was diluted to 100 mL in a volumetric flask with CH_2Cl_2.

Preparation of urine samples for analysis by using BPB:
In order to decrease the effect of those interferences present in urine samples, after deproteinization mentioned before, the filtrate was diluted to 100 mL with D.W.in a volumetric flask ready for analysis.

Determination of LMT using BPB; In Tablets and Urine Samples:
A volume of 1.5 mL 4×10^{-3}M BPB reagent was added to a mixture of a series of 0.25, 0.5, 0.75 till 6 mL of 0.01 $mg.mL^{-1}$ LMT standard or a suitable volume of the sample solutions of the tablet or of urine containing between (0.5-12 $\mu g.mL^{-1}$) LMT with 1mL buffer (pH 3.25). This is followed by adding 1mL 0.1M NaCl (plus 0.2mL S.S in, case of urine samples only). The mixture was mixed well and diluted to 10 mL in a volumetric flask using D.W. The resulting ion-pair formed between LMT and the reagent was transferred into a separating funnel (100 mL capacity) and extracted using 5 mL CH_2Cl_2 in two portions to wash out the volumetric flasks for quantitative transfer of the solution. The separating funnel was shaken for 2 min. After separation, the organic layer was used for drawing calibration curves and for spectrophotometric measurements of LMT at 413 nm. The blanks were run in exactly the same way throughout the whole procedure. The LMT concentration was obtained from the standard calibration curve.

Determination of LMT using BTB
In Tablets
The calibration curve between absorbance and the concentration of LMT, was prepared by taking aliquots of 0.5, 1, 1.5 and 6.0 mL, accurately from (0.02 mg/mL) standard LMT solution in CH_2Cl_2, into a series of 10 mL volumetric flasks, or a suitable volume of the tablet sample solutions. To each flask, 1mL of 5×10^{-3}M BTB was added, diluted to the mark with CH_2Cl_2 and mixed well. The absorbance of the resulting yellow color ion-pair was measured against the reagent blank. The content of LMT in each tablet was calculated from the prepared calibration curve.

In human urine:
A calibration curve was first prepared from fresh urine collected from a healthy volunteer. A series of 1 mL of this urine was spiked with 0.2, 0.4, 0.8,----, 2.8 mL, 0.1 mg/mL standard solution of LMT plus 0.5 g NaCl salt, 3 mL of phosphate buffer, to adjust pH to 7.0. Each solution, and in the same way the urine sample of the patient, was transferred to a separating funnel quantitatively and 10 mL of CH_2Cl_2 were added and shaken for 10 min. The two phases were allowed to separate, then a 5 mL of the CH_2Cl_2 layer was transferred into a10 mL volumetric flask followed by addition of 1 mL 5×10^{-3}M BTB and diluted to the mark with CH_2Cl_2. The absorbance of each solution was measured at 410 nm against the corresponding blank, which was prepared exactly in the same way without addition of LMT.

Results and Discussion

Many experiments and conditions were tried to perform this study of LMT determination with the two selected reagents BTB and BPB, in aqueous medium without any indication of colored ion-pair formation. Therefore it was decided to follow the mechanism route of LMT with one of the reagents starting from aqueous medium while organic for the other. Thus, the necessity of searching for an organic solvent suitable, favorably, for both of them to understand similarities and differences between the two mechanisms.

Choice of a suitable organic solvent
Several organic solvents such as (chloroform, carbon tetrachloride, diethyl ether, acetone methanol, ethanol, dichloromethane cyclohexane, xylene, toluene, acetophenon and benzene) for extracting the ion-pairs formed between BPB and BTB with LMT were tested. Among these solvents, dichloromethane was preferred as the most suitable solvent for both reagents. To choose one of them for extraction from aqueous solution, as was pointed out,

it was found that LMT-BPB more suitable for this purpose. This was because in case of LMT-BTB the aqueous and organic phases could not be separated well.

The Absorption Spectra:

The absorption spectra of the complexes LMT-BTB and LMT-BPB against blank and of the reagents BTB and BPB against dichloromethane are shown in Figures 3(A) and 3(B) respectively. The solution of LMT in both dichloromethane and aqueous solution was nearly colorless therefore the absorption bands appeared in the visible region after the addition of the dyes BTB or BPB to fixed concentrations of the drugs in dichloromethane indicated the formation of ion-pair complexes between the drug and the dyes. The absorption maximum of the ion-pair LMT-BTB complex in dichloromethane without extraction was 410 nm. While that of LMT-BPB ion-pair was also obtained in CH_2Cl_2 but after extraction from aqueous solution. The optimum pH 3.25 of the aqueous phase, which will be shown in the next section, was applied to extract the ion-pair LMT-BPB into dichloromethane and the absorption maximum was 413 nm. The absorbance of the reagent blank was insignificant in both methods. This is a useful phenomenon to enhance the sensitivity of LMT determination. The reagent blank and the complexes with most of the other solvents were of the same absorbance. Therefore dichloromethane was a chosen solvent.

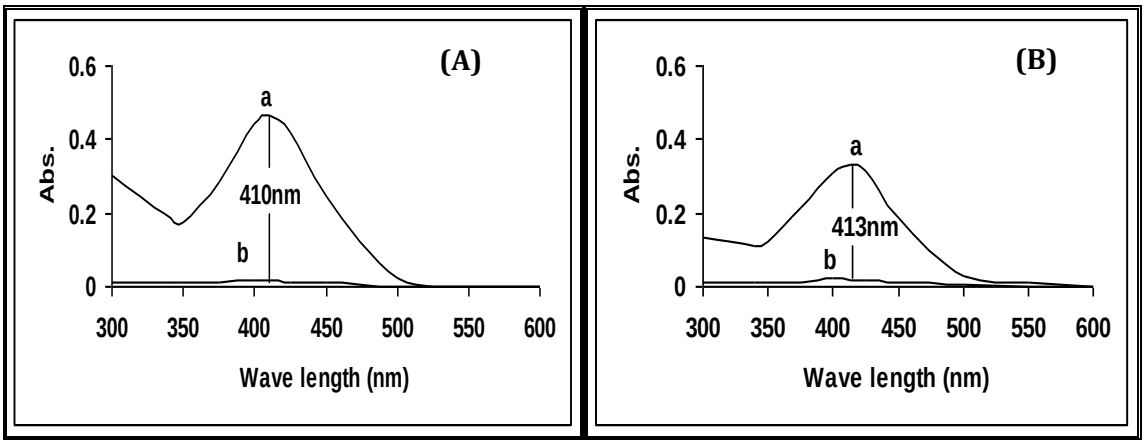


Figure 3. The absorption spectra of: A- (LMT-BTB) and B- (LMT-BPB) ion-pair complexes against the corresponding blank (a) and the reagents alone (b) against the solvent CH_2Cl_2

Optimum pH and choice of a buffer for LMT-BPB extraction

A constant pH between 3 to 3.5 was observed and the pH chosen was 3.25. The buffers examined for pH adjustment were Tartarate, Citrate, KH-phthalate and Citric acid-Na_2HPO_4. The experiments were performed by the addition of 1ml of each buffer and the basic procedure was applied for two levels of LMT concentration. Citric acid-NaOH buffer that has pH 3.18 was found suitable. The volumes between (0.5 to 3 mL) were added to a constant drug concentration and a constant absorbance region was obtained between 1-3 mL, hence 1mL of this buffer was used for all subsequent experiments

Optimization of the extraction conditions

The influence of the concentration of BTB and BPB on the intensity of the color developed at the selected wave length and constant drug concentration was studied by using different amounts (0.2 - 2 mL) of 5×10^{-3}M BTB and (1 - 9 mL) of 10^{-3} M BPB and found that 1 mL and 6 mL were the best respectively.

Under optimum conditions, the volume of dichloromethane for the extraction of the (LMT-BPB) drug-dye complex from aqueous solution was studied between 3 - 8 mL with shaking time from 0.5 - 4 min. After the first extraction,

the absorbance of the organic layer was negligibly small. Hence a single extraction with 5 mL CH_2Cl_2 and 2 min shaking time were found suitable and also sufficient to complete the analysis.

The following salting-out agents [KCl, KNO_3, KSCN, NH_4Cl, $(NH_4)_2SO_4$, $MgSO_4$, $MgCl_2$, and NaCl] were tested to enhance the distribution constant for a better extraction of the ion-pair into the organic phase. The results indicated that NaCl was suitable and the presence of 1 mL 0.1 M NaCl was the optimum amount to be used.

All possible orders of addition of the LMT, BPB, NaCl, and the buffer were tried after completing all other optimizations. The study performed on 0.5 mL and 4 ml of 0.01 mg/mL LMT, revealed that the best order of addition was when LMT is added first, then the buffer followed by BPB and NaCl the last.

The nature of LMT-BPB ion pair, stability and stoichiometry

Although, the structure of the reagent BPB at pH 3.25 behaves as an anion (Scheme II) and LMT as a cation, it was decided to verify this behavior, especially their combination product and to prove whether or not the (LMT-BPB) ion pair can form in aqueous solution as was pointed out earlier. For this purpose, cation and anion exchanger resins were used as the easiest and available technique. The reagent, the analyte and their reaction products were passed through the resins and the basic procedure was applied on the eluents. Comparisons between absorbance before and after passing through the resins showed that LMT was in a cation form that is why it has been retained on the cation type resin. In a similar way BPB was in anion form. Clear information was obtained after passing (LMT-BPB), ion-pair through both types of the resins, and that was the cation or anion part of the complex has retained on the corresponding resin. This has indicated that the complex is not sufficiently stable in aqueous solution that is why it should be extracted into the organic phase.

The stability of the ion-pair complexes formed between LMT and BTB or BPB was performed by measuring the absorbance against time. The optimum reaction time for the development of the color at room temperature was found to be instantaneous with both reagents. The color formed was stable for at least 60 min. in both cases. However, semi-quantitative measurements have shown that the ion-pair complexes are stable for at least 24 hours.

The stoichiometry of the ion-pair complexes formed between LMT and reagent dyes (BTB and BPB) were examined by three methods namely, (a) Job's continuous variation, (b) mole ratio, and (c) slope ratio methods, at wave lengths of 410 and 413 nm respectively. In Figure 4, the plot reached a maximum value at mole fraction of 0.5 indicating a molar ratio of 1**:**1. The mole ratio method, in Figure 5, also, shows that one mole of each of the reagent and the analyte participated in the ion-pair formation. Still, more confirmation by slope ratio method indicated the formation of 1:1 ion pair complex. Accordingly, the composition of the ion-pair complexes were suggested and shown in Figure 6. The anionic dyes BTB and BPB have formed ion-pair complexes with the positively charged nitrogen containing molecule LMT.

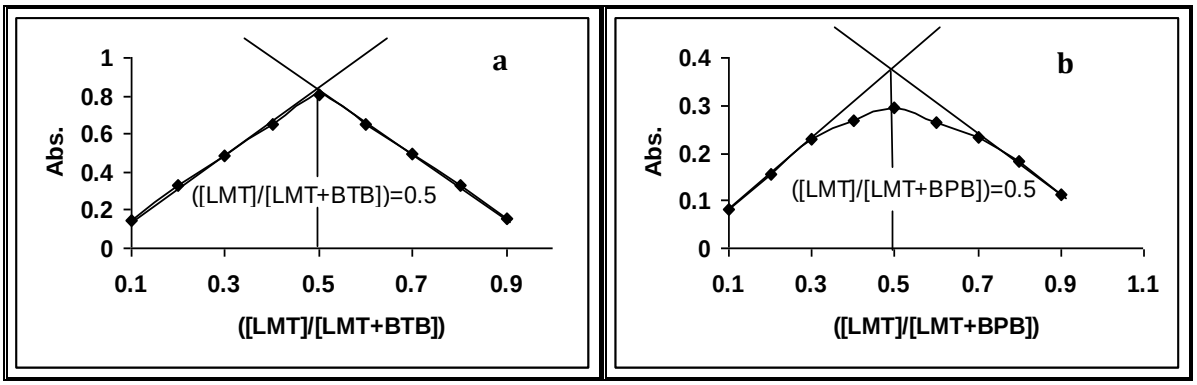


Figure 4**.** Job's plot for the ion-pair complexes (a) (LMT-BTB and (b) for (LMT-BPB).

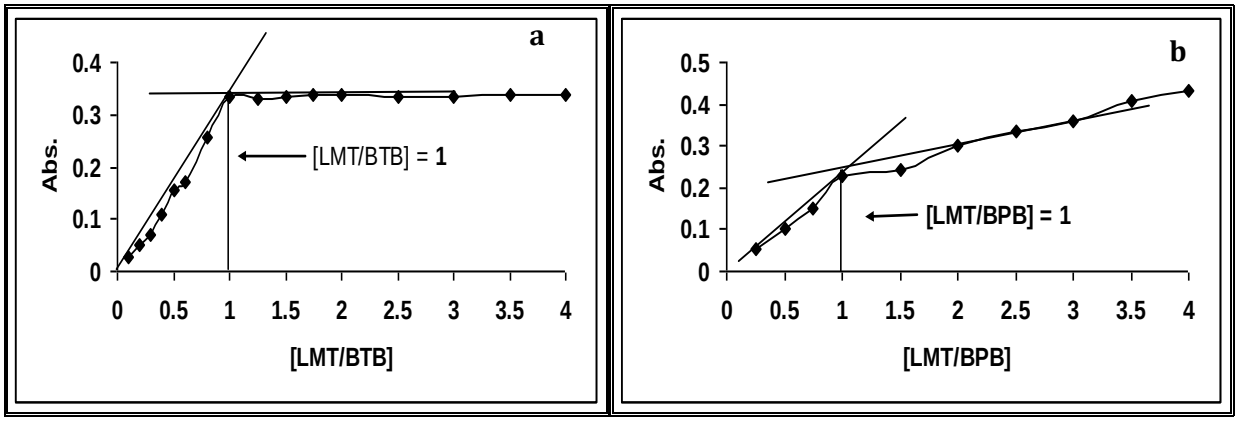


Figure 5. The mole ratio determination of the stoichiometry of (a) the (LMT – BTB) and (b) for (LMT-BPB) ion pair complexes. BTB and BPB were of constant No. of moles.

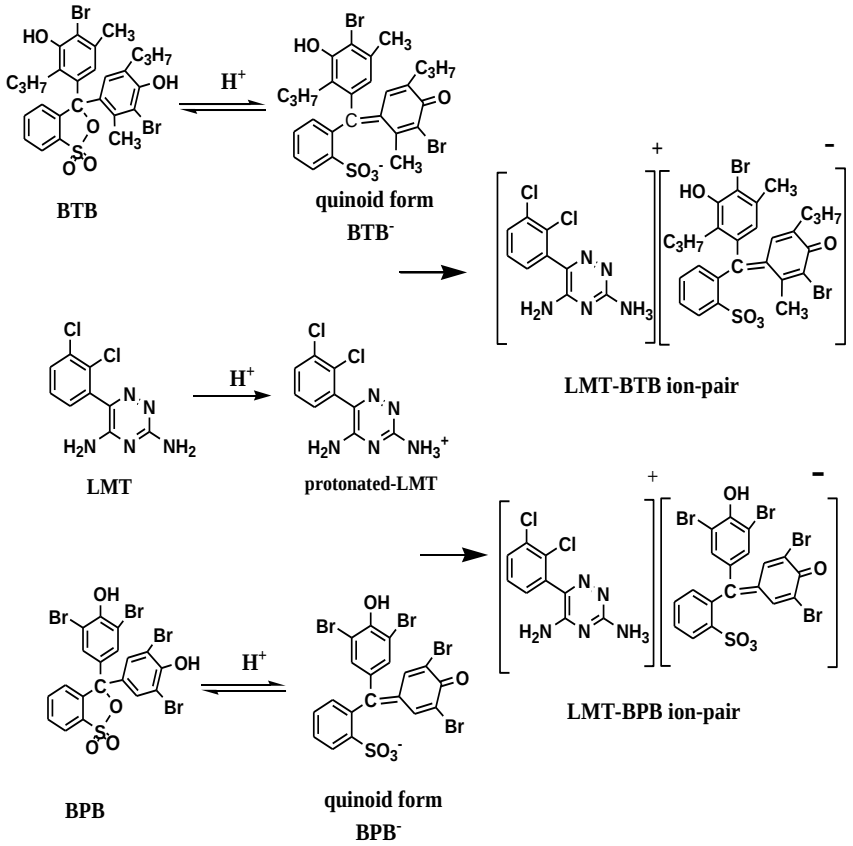


Figure 6. The suggested mechanism of the reaction pathway to form ion-pair complex between the drug and reagent dyes. Positively charged nitrogen of LMT and negatively charged sulfonate of BTB or BPB forms an ion-pair complex in dichloromethane.

Calibration curves, precision and accuracy of the methods:
Calculations showed molar absorptivity of 1.97×10^4 and 1.92×10^4 $L.mole^{-1}.cm^{-1}$ and the detection limit (D.L.) of 0.13 and 0.24 µg/mL (n=10) (LMT- BTB) and (LMT-BPB) respectively. Other properties of the calibration curves are given in Table 1. The table also shows the precision of LMT determination by both reagents BTB, and BPB. Both methods show reasonable precision but, slightly lower in case of (LMT-BPB) due to the extraction steps.

Table 1. Properties of the calibration curves in this study.

Method	LMT taken µg/ml	LMT found n=3	%R	Lin. range µg/ml	r^2	Molar abs.	D.L.	% RSD	
								type A	Type B
LMT-BTB At 410nm.	2	1.94	97.1	1 - 12	0.9983	1.97×10^4	0.13	0.71	1.68
	10	10.18	101.8					0.37	0.66
LMT-BPB At 413nm.	2	1.90	95.0	0.5 -1 2	0.9980	1.92×10^4	0.24	0.70	3.1
	10	9.71	97.1					0.47	1.47

Recovery (%r), linear range (lin.range), correlation coefficient (r^2) and relative standard deviation (%rsd): type a: 10 times repeating of the same product, and type b: 10 times repeating of the whole procedure.

Percentage recovery for the determination of known concentrations of standard LMT solution, shown in the table, is quite reasonable for both methods. Calculations also showed the difference between the mean ($\overline{X}$) and the true value (µ) tested for the existence of a systematic error in the results of the table. These were obtained by comparing the actual difference ($\overline{X}$ - µ) and the term [t.S /√N] at 95% confidence limit DOF = 2 using t-test. The difference was not significant at 95% C.L for (LMT-BTB), indicating the existence of no or a very small systematic error. In the case of (LMT-BPB), however, the difference was significant at high concentration (10 µg/ml) indicating the existence of a systematic error which was mainly due to the extraction steps. But the errors were still within the allowable values and required no treatments.

Selectivity of the methods
Study of interferences on LMT-BPB ion-pair complex
The interfering effects expected in the most common antiepileptic drugs administrated as an adjunct with LMT were examined with both reagents BTB and BPB. The ions and compounds expected to be present in urine and pharmaceutical preparations were also studied. These ions did not have any effect on LMT determination by BTB, since this method was performed in an organic medium. Interferences of the most common antiepileptic drugs co-administered with LMT, such as phenobarbital and carbamazepine, showed that phenobarbital did not interfere in the range of 1 to 40 folds, while the effect was more severe in the presence of carbamazepine. The effects were 25 and 32 folds on each of BTB and BPB respectively for 5% maximum error (tolerance level T.L), which are quite acceptable.

Results of Table 2 show the effects of the most possible ions present in urine and also those additives usually used in pharmaceutical preparations, on the determination of LMT in those samples using BPB. The table shows the maximum quantity of the interference on 2 mg/L of lamotrigine, which can cause not more than 5% error (T.L.). The cations chosen were (Na^+, K^+, Ca^{2+}, Mg^{2+}, and Fe^{3+}) in the forms of (Cl^-, HPO_4^{2-}, HCO_3^- and NO_3^-). It was found that the effect is mostly due to creatinine which was present in urine at a high level and some cations and anions. The separation of creatinine from the urine was tried by using phosphotungstic acid which forms a

precipitate with creatinine. The attempt was not successful because LMT itself formed a precipitate with phosphotungstic acid at high concentration.

The effect of the cation interferences was confirmed by examination of the first four cations in the table (Na^+, K^+, Mg^{2+}, and Fe^{3+}) all in chloride form showing that K^+ and Mg^{+2} have lower tolerance level than other cations. The cations [Na^+, K^+, and Ca^{2+}] were more effective when they were in the form of (HPO_4^{-2}). This has indicated that the effect of HPO_4^{-2} was more severe than the other anions and sodium lauryl sulfate which was used as an additive in tablets gave effective error in the negative direction.

The table also shows the effect of the compounds [urea, starch, glucose, fructose, and sucrose], which are either present in urine or as an additive in pharmaceutical preparations. These compounds showed very small interferences, in which their tolerance level ranged between 2000 – 5000 folds.

Table 2. The tolerance levels (T.L.) of interferences on 2 ppm of LMT.

Cations	**Salts of cations**	**T.L (folds)**	**Error direction**
Na^+	NaCl	16	-ve
K^+	KCl	8	-ve
Mg^{2+}	$MgCl_2.6H_2O$	6	-ve
Fe^{3+}	$FeCl_3$	> 500	------
Na^+	$NaHCO_3$	22.5	-ve
Na^+	Na_2HPO_4	6	-ve
K^+	K_2HPO_4	2.5	-ve
Ca^{2+}	$CaHPO_4.2H_2O$	8	-ve
K^+	KNO_3	18	-ve
Ca^{2+}	$Ca(NO_3)_2.4H_2O$	100	-ve
Mg^{2+}	$Mg(NO_3)_2.6H_2O$	3.6	-ve
Fe^{3+}	$Fe(NO_3)_3.9H_2O$	56	-ve
Na^+	Na-lauryl sulfate	2	-ve
Creatinine	$C_4H_7N_3O$	1	+ve
Glucose	$C_6H_{12}O_6$	> 2000	-------
Urea	$(NH_2)_2CO$	> 5000	-------
Fructose	$C_6H_{12}O_6$	>2500	-------
Sucrose	$C_{12}H_{22}O_{11}$	>2500	-------
Starch	-------	No effect	-------
Uric acid	$C_5H_4N_4O_3$	> 2500	-------

To remove interferences a suppressing solution, which was named by the present authors as a (suppressing solution, S.S.) was proposed. This solution was containing all of the interferences (the cations were in HPO_4^{-2} form), with concentrations that thought to be present in the urine sample in the normal range [22]. The use of suppressing solution will be discussed in the next section.

Removing interferences using suppressing solution (S.S)

The basic principle of this idea is of two approaches: First, is that, those interferences which are expected to be present in urine sample are also added to the calibration standards and to the blank. The net result will be subtraction of their effect from the sample. In addition to that, however, the second approach is that all interferences were of negative effect as was shown in table 2, except creatinine which has a positive effect. Thus suppressing the effect of negative errors by compensation. This solution will be added only when the urine sample is analyzed. Studying the quantity of this solution needed to be mixed with (0.8 ml) of 10 $mg.L^{-1}$ LMT was 0.2 mL. as an optimum volume of S.S for removing the effect of interferences including creatinine.

Application of the methods for real samples:

Determination of LMT in tablets

The proposed methods were applied for the determination of LMT in commercial tablets and the results obtained were compared with those of a published method [17] applying F-test and t-test. Results of Table 3 show that, calculated F-values and t-test are less than the tabulated values at 95 % confidence level, which indicate that the difference between the two methods is not significant. This is an indication that the proposed methods were as good as the published method and reliable for the determination of LMT in commercial tablets.

Table 3. Statistical comparison of the proposed and the published methods for the determination of LMT in tablets. Results are the mean of 3 determinations.

Tablet brand name (mg/tablet)	% Found ± SD (n=3)		
	Published method	BTB method	BPB method
Loxol-Hikmajordan 100	97.3±0.892	97.95±0.862 F =1.07 t =0.91	98±1.100 F =1.52 t =0.86
Lametec-India 100	99.1±1.09	98.4±1.39 F =1.63 t =0.70	97.8±0.91 F =1.43 t =1.59
BioGran-German 200	97.1±0.412	95.98±1.041 F =6.38 t =1.73	96.2±0.526 F =1.63 t =2.33
Lamictal-Glaxo U.K 50	102.24±0.891	102.14±0.56 F =2.53 t =0.16	103±0.8 F =1.24 t =1.1

F table(2,2) 95% CL =19, t table, DOF 4 at 95% CL = 2.77

Determination of lamotrigine in urine sample

The proposed methods were also applied for the determination of lamotrigine in urine samples with different procedures

Using BTB:

Optimum conditions for extraction of LMT from urine samples including pH, ionic strength and volume of dichloromethane were examined.The effect of pH on the extraction of LMT from urine was studied in the range of pH 1 to 9 using HCl or NaOH. The results showed that maximum extraction was obtained at pH 7.0. Thus, the pH was adjusted to 7 using phosphate buffer. Again NaCl was chosen as a salting out agent, and that 0.5 g was optimum amount to be added. For the volume of dichloromethane solvent optimization, different volumes of the solvent between (5-14 mL) were used. A volume of 10 ml of the solvent was found suitable and sufficient for extraction of LMT from urine.

Using BPB with a Suppressing Solution (S.S):

Because no patient taking LMT could be found, a 5 mL portion of fresh urine was spiked with a known amount of standard solution of LMT. After deproteinization, the filtrate was diluted to 100 mL in volumetric flasks by D.W. in order to lower the effect of interferences present in the urine sample). An amount of 0.8 mL of this solution was taken plus 0.2 mL suppressing solution and the basic procedure was followed. The results were compared with the same concentration of standard LMT solution with and without 0.2 mL S.S. It was found that correct result in the presence of S.S.was obtained when the filtrate of urine sample was diluted to 100 ml (20 folds dilution) after deproteinization.

The calibration curves were drawn for the (LMT-BTB) and (LMT-BPB) ion-pairs accordingto optimizations of the previous sections and the results of Table 4 show reasonable linearity and sensitivity of the methods. The correlation coefficient was found to be 0.9974 and 0.9964 for the (LMT-BTB) and (LMT-BPB) methods respectively. By comparing the results of this table with those of normal calibration curves in table 1, it is observed that the sensitivity and linearity of normal calibration curves in both methods were better than the calibration curves obtained for urine assay. Furthermore, it is indicated that the suppressing solution has slightly lowered the sensitivity in case of the (LMT-BPB) ion-pair compared with the results of Table 1.

Table 4. Sensitivity and Linearity for Determination of LMT in Urine Samples.

Parameter	Method of (BTB)	Method of (BPB) with S.S
λ_{max}.	410	413
Linear range (µg/mL)	1 - 14	1 – 13
r^2	0.9974	0.9964
Molar absorptivity $L.mole^{-1}.cm^{-1}$	1.6×10^4	1.86×10^4
D.L (µg/mL) n=10	0.43	0.41

Accuracy and precision of the methods:
Urine samples were taken from normal persons not taking LMT or other drugs followed by adding a known amount of standard solution of LMT and were then determined by both methods. The % recovery was calculated from the calibration curves for both methods. The results obtained were statistically compared with those obtained using a published method [17] and shown in table 5. This method involves spectrophotometric determination of lamotrigine using bromocresol purple in chloroform at 415 nm.[17]. It is worth mentioning that the published method has used urine of normal persons as a blank for removing interferences. This is not an easy task compared to the suppressing solution used in the present study, although the published method has been used in the present work with modification, in case of (LMT-BTB) ion pair only.

Statistical analysis of the results, using F-test and t-test shown in table 5, revealed no significant difference between the performance of the proposed and published methods**,** because the calculated values of F and t-tests at 95 % confidence level are less than the tabulated values.

These tests have also been performed to compare between the two methods developed in the present work and the results are shown in Tables 5 and 6. The differences between the means of any two pairs of the proposed methods at 2 and 10 mg/L levels LMT, of Table 5, were calculated by comparing the values ($\overline{X}_1$- $\overline{X}_2$), with the term

$$\left\{ \mathbf{t}.\mathbf{S}_{\text{pooled}} \times \left[\sqrt{(N1+N2)/N1N2} \right] \right\}$$

at 95% C.L, DOF = 18. The results show no significant difference at 2 mg/L but significant in case of 10 mg/L. This may be due to insufficient amount of S.S for such higher value of 10 mg/L LMT. But as shown in the table the % error did not exceed 6.6%, and this value is approximately close to the allowable limit of error, therefore, more treatments were not needed.

More comparison tests of the two methods are presented in Table 6. Two series of ten urine samples mentioned before have been spiked with 2 mg/L and 10 mg/L standard LMT solution and determined by both methods. The low values of the %RSD and %Error with good %Recovery indicate high precision and good accuracy of the methods. The accuracy of the (LMT-BTB) method was better than the (LMT-BPB) method which may be due to the effect of the blank solution. In the first method the urine of the healthy person was used as a blank while in the second method the effect of interferences were minimized by using S.S. The %Error in case of 10 mg/L of LMT-BPB method was slightly more than 5%. The difference between the mean ($\overline{X}$) and the true value (μ) was performed to test for the existence of a systematic error in the results. The difference between ($\overline{X}$ - μ) and [t.S /√N] was significant at 95% C.L in both methods, mentioned before. But the % error did not exceed 6.6% in case of 10 mg/L, and as mentioned above, more treatment were not needed.

Table 5. Statistical Comparison of the Proposed Methods and the Published Method for the Determination of LMT In Urine Samples.

Methods	sample	LMT added (µg/mL)	LMT found (µg/mL)	% recovery	Mean % recovery±SD
Published method	Urine(1)	2	1.93	96.5	97.5±0.87
		4	3.92	98	
		6	5.88	98	
	Urine(2)	2	2.1	105	101.86±3.4
		4	3.93	98.25	
		6	6.14	102.33	
LMT + BTB	Urine(1)	2	1.96	98	98.86±3.1
		4	4.09	102.25	**F** =12.7
		6	5.78	96.33	**t** =0.73
	Urine(2)	2	2.11	105.5	103.03±2.19
		4	4.09	102.25	**F** =2.41
		6	6.08	101.33	**t** =0.62
LMT + BPB	Urine(1)	2	1.97	98.5	102.19±3.3
		4	4.13	103.25	**F** =14.39
		6	6.29	104.83	**t** =2.38
	Urine(2)	2	2.05	102.5	105.25±2.75
		4	4.21	105.25	**F** =1.53
		6	6.48	108	**t** =1.34

$F_{(2,2)}$ table at 95% CL is 19, t table at 95% CL and DOF 4 is 2.77
Urines 1&2 were taken from healthy volunteers not taking any drug.

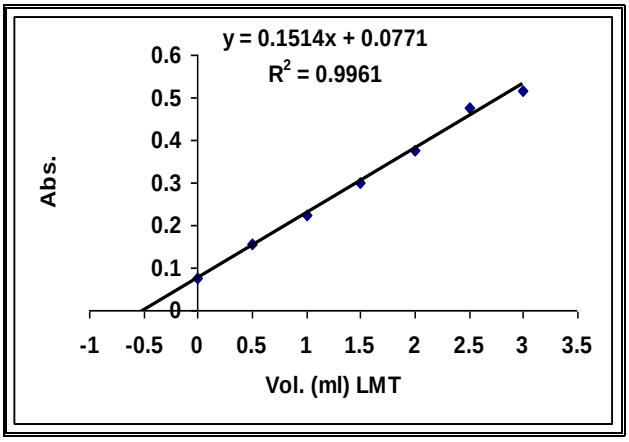


Fig. 4. Standard addition for the determination of LMT in urine sample after deproteinizationand in the presence of (S.S) solution LMT taken was (1µg/ml).

Application of standard addition method for (LMT-BPB) ion-pair method:

Standard addition method was performed on urine samples, in the presence of suppressing solution, and by using BPB reagent after deproteinization. The % recovery calculated from the graph in Fig. 4 was 101.85%, indicating that the standard addition method has improved the accuracy.

Table 6. Statistical Comparison between Accuracy and Precision of Both Methods.

Method	LMT added (µg/mL)	LMT found (µg/mL) ±SD n=10	%Recovery	%Error	%RSD	$(\overline{X} - \mu)$	$[t.S / \sqrt{N}]$
LMT-BTB	2	2.05±0.034	102.5	2.5	1.66	0.05	0.024
	10	9.85±0.12	98.5	-1.5	1.22	0.15	0.086
LMT-BPB	2	2.07±0.028	103.5	3.5	1.36	0.07	0.02
	10	10.66±0.16	106.6	6.6	1.5	0.66	0.11

The value of t-table at 95% confidence level and DOF = 9 is 2.26

Conclusion

Two sensitive and simple Spectrophotometric methods were developed for the determination of the drug (lamotrigine) in a pure form, tablets, and urine, through the formation of ion-pair complexes with the both Bromothymol blue and Bromophenol blue complexing reagents in dichloromethane. Interferences expected to be present in the urine samples could be removed by addition of a suppressing solution to the both samples and blank solutions in case (LMT-BPB) or by using urine of a normal person not taking the drug LMT as a blank in case of (LMT-BTB) method. The additives present with the tablets did not make any interference because most of them were removed through the dissolution and filtration. Also the proposed methods are selective for the determination of LMT in the presence of other co-administered antiepileptic drugs such as phenobarbital and carbamazepine. The suppressing solution was prepared from the salts of most interfering ions in case of the (LMT-BPB) method. The stoichiometry for the ion-pair complexes was found by Job's method, mole ratio and slope ratio methods; and all gave 1:1 composition of the drug: reagent.

The proposed methods were compared with another spectrophotometric method available for LMT determination in the literature, with no significant difference at 95% C.L. Visible spectrophotometric methods based on ion-pair formation published in the literature are only applicable for the determination of LMT in tablets and the spectrophotometric technique in UV region are also only applicable for the determination of LMT in tablets and less sensitive than the present methods. The use of suppressing solution in the present study in the case of (LMT-BPB) method for the determination of LMT in urine samples was much easier task compared to the use of urine of a normal person as a blank in the case of (LMT-BTB) method. In contrast to other complicated and expensive methods for the determination of LMT, the proposed methods require only dyes as reagents with some other materials which are cheaper and readily available, can be applied at ambient temperature, color development is instantaneous, with almost the similar sensitivity, accuracy and precision. The two methods can also be useful in quality control as well as reliability for urine analysis.

Acknowledgement

The authors would like to thank the Chemistry Department, College of Science and the Presidency of Sulaimani University for their kind support to perform this study.

References

1. Griner-sosanko E, Lower DR, Virji MA, Kraswski MD. Simultaneous determination of lamotrigine, zonisamide and carbamazepine in human plasma by high-performance liquid chromatography. Biomed Chromatogr. 2007; 21: 225-228
2. El-Enany NM, El-Sherbiny DT, Abdelal AA, Belal FF. Validated spectrofluorimetric method for the determination of lamotrigine in tablets and human plasma through derivatization with o-phthalaldehyde. J. Fluorescence. 2010; 20: 463-472
3. Vinay KB, Revanasiddappa HD, Rajendraprasad N. Development and validation of spectrophotometric methods for the sensitive and selective determination of lamotrigine in pharmaceuticals using bromocresol purple. J. Food and Drug Anal. 2009; 17: 424-433.
4. Rajendraprasad N, Basavaiah K, Vinay KB. Micro and nanogram determination of lamotrigine in pharmaceuticals by visible spectrophotometry using bromophenol blue. Indian J. Chem Technol. 2010; 17: 220-228.
5. Youssef NF, Taha EA. Development and validation of spectrophotometric, TLC and HPLC methods for the determination of lamotrigine in presence of its impurity. Chem. Pharm. Bull. 2007; 55: 541-545
6. Rajendraprasad N, Basavaiah K, Vinay KB. Sensitive spectrophotometric determination of lamotrigine in bulk drug and pharmaceutical formulation using bromocresol green. Ecl. Quim. Säopaulo 2010; 35: 55-66.
7. Morris RG, Black AB, Harris AL, Batty AB, Sallustio BC. Lamotrigine and therapeutic drug monitoring. Br J ClinPharmacol. 1998: 46: 547-551.
8. Lee W, Kim JH, Kim HS, Kwon OH, Lee BI, Heo K. Determination of lamotrigine in human serum by high-performance liquid chromatography-tandem mass spectrometry.Neurol Sci.2010; 14: 1–4.

9. Puvvada PK, Murugan VG, Kumar SV, Padarthi PK. RP-HPLC Method Development and Validation of Lamotrigine. Derpharma Chemical 2010; 2: 104-108.
10. Vidya SK, Prsanth NY, Suresh S, Anusha C, Somnath D, Aneela S. A new simultaneous RP-HPLC method for development and validation of lamotrigine tablets. J. Chem. Pharm. Res., 2011; 3: 651-658.
11. Contin M, Mohamed S, Candela C, Albani F, Riva R, Baruzzi A. Simultaneous HPLC-UV analysis of rufinamide, zonisamide, lamotrigine, oxcarbazepine monohydroxy derivative and felbamate in deproteinized plasma of patients with epilepsy. J. Chromatogr B: Anal Technol in the Biomed and Life Sci. 2010; 878: 461-465.
12. Queiraz ME, Silva SM, Carvalbo D, Lancas FM. Determination of lamotrigine simultaneously with carbamazepine, carbamazepine epoxide, phenytoin, phenobarbital, and primidone in human plasma by SPME-GC-TSD.J.Chromatogr. Sci., 2002; 40: 219- 223.
13. Gupta VK, Singh AK, Gupta B. Development of membrane electrodes for selective determination of some antiepileptic drugs in pharmaceuticals, plasma and urine. Anal. BioanalChem. 2007; 389: 2019- 2028.
14. Dominguez-Renedo O, Arcos Martinez M.J, Burgoa Calvo ME. Determination of lamotrigine by adsorptive stripping voltammetry using silver nanoparticle-modified carbon screen-printed electrodes. Talanta 2007; 74:59- 64.
15. Dominguez-Renedo O, Burgoa Calvo ME, Arcos Martinez MJ. Determination of lamotriginein pharmaceutical preparations by adsorptive stripping voltammetry using screen printed electrodes. Sensors. 2008; 8: 4201-4212.
16. Navdeep S, Koyal S. Quantitative determination of lamotrigine in bulk and dosageformby UV spectrophotometry. J. Appl. Pharm. Sci., 2011; 1: 113-116.
17. Alizadeh N., Khakinahad R., Jabbari A.; Pharmazie, Sectrophotometric determination of lamotrigine in pharmaceutical preparations and urine by charge-transfer complexation. J. Pharm. Sci. 2008, **63**, 791–795.
18. Sevgi Tatar Ulu. Sensitive and Simple Spectrophotometric Method for the Determination of Lamotrigine in Pure and Pharmaceutical Preparations of Charge-transfer Complex. Rev.Chim.(Bucharest). 2011; 62: 261-264.
19. Bishop E: Indicators. 1st.Ed. Germany: Pergamon Press; 1972.
20. Perrin DD, Boyd Dempsey: Buffers for pH and Metal Ion Control. 1st.Ed. Chapman and Hall;1974.
21. Abolfathi Z, Belanger PM, Gilbert M, Rouleau JR. Improved high-performance liquid chromatographic assay for the stereoselective determination of mexiletine in plasmaJ.Chromatogr.. 1992; 579: 366.
22. Ranjna C: Practical Clinical Biochemistry, methods and interpretations, 3rd. Ed. RK Yadav; 2003.

The Malaysian Journal of ANALYTICAL SCIENCES ISSN 1394-2506

EFFECT OF TEMPERATURE ON KAFFIR LIME OIL BY USING HYDRO-DIFFUSION STEAM DISTILLATION SYSTEM

(Kesan Suhu Ke Atas Minyak Limau Purut Dengan Menggunakan Sistem Penyulingan Penyebaran Hidro)

Zakiah Mohd Yusoff*, Zuraida Muhammad, Nurhani Kasuan, Mohd Hezri Fazalul Rahiman, Mohd Nasir Taib

Faculty of Electrical Engineering,
Universiti Teknologi MARA (UiTM), 40450 Shah Alam, Selangor D.E., Malaysia

**Corresponding author: zakiah_darwisy@yahoo.com or hezrif@ieee.org*

Abstract

Extraction temperature is one of an important parameter that can give large effect on output yield and quality of essential oils. For that reason, temperature is chosen as a process variable in this study. Fruit of kaffir limes was collected from orchards around Dengkil area around January 2013. Fresh peels of kaffir lime undergo weighing process. A 0.35 kg grounded kaffir lime peels for each steam temperature setting which are 80 ^{o}C, 90 ^{o}C, 95 ^{o}C and uncontrolled temperature (100 ^{o}C). The steam temperature setting was achieved by using a HFPID controller scheme by controlling the voltage fed to the heater. The proposed research applied the concept of hydro diffusion where steam and extract (water and essential oil) move naturally downwards by earth gravity downwards to the condenser. The hydro diffusion steam distillation plant enhances oil recovery by minimizing oil waste in boiling water and its opposite from the conventional steam extraction where steam goes upward. From the results, it can be concluded that different temperature will give different effects on the quality and quantity of essential oil. For each steam temperature setting, it produces a different composition of the constituents.

Keywords: essential oil, steam distillation system, hydro-diffusion

Abstrak

Suhu pengekstrakan adalah salah satu parameter penting yang boleh memberi kesan yang besar ke atas hasil pengeluaran dan kualiti minyak pati. Atas sebab itu, suhu telah dipilih sebagai proses pembolehubah dalam kajian ini. Buah limau purut telah dikutip dari kebun di sekitar kawasan Dengkil sekitar Januari 2013. Kulit segar limau purut menjalani proses timbang berat. Sebanyak 0.35 kg kulit limau purut yang telah dikisar untuk setiap tetapan suhu wap iaitu 80 ^{o}C, 90 ^{o}C, 95 ^{o}C dan suhu yang tidak terkawal (100 ^{o}C). Tetapan suhu wap telah dicapai dengan menggunakan satu skim pengawal HFPID dengan mengawal voltan yang disalurkan kepada pemanas. Penyelidikan ini menggunakan konsep penyebaran hidro dimana wap dan pati (air dan minyak pati) bergerak secara semula jadi ke bawah oleh graviti bumi, ke bawah ke pemeluwap. Kaedah penyebaran hidro meningkatkan perolehan minyak dengan mengurangkan sisa minyak tertinggal dalam air mendidih dan bertentangan dari pengeluaran stim konvensional di mana wap pergi ke atas. Daripada keputusan, boleh dibuat kesimpulan bahawa suhu yang berbeza akan memberi kesan yang berbeza terhadap kualiti dan kuantiti minyak pati. Bagi setiap tetapan suhu wap, ia menghasilkan komposisi yang berbeza.

Kata kunci: minyak pati, sistem penyulingan wap, penyebaran hidro

Introduction

Essential oils sometimes called volatile oil are aromatic substances [1-3] represent a small friction of plant's composition which can be found mostly in leaves and flowers [4]. It is multi-component chemicals that will produce a product that is highly aromatic and more concentrated than the original plant [2]. Essential oils and extracts obtained from various botanical plants have recently gained a great popularity and science interest. Essential oils have a wide range of uses and promises various significant benefits to human and industrial such as in aromas and fragrances [5-7], medical activities [3, 8, 9], as insect repellents and pesticides [10-12], cosmetics [11, 13], as a natural additive for food flavoring [4, 14], pharmaceutical industries [1-3, 5, 11] according to the composition of the

oil. The quality of essential oil can be identified based on main compound found in the substance via Gas Chromatography-Mass Spectrometry (GC-MS) analysis [10].

Kaffir lime from the Rutaceae family contains two types of essential oils, makrut leaf oil and makrut (fruit peel) oil [15]. Kaffir lime is a well known herb used in the industry and get high demand in commercialization such as aromatherapy, potential use in medicine, cosmetic industry in making anti-dandruff shampoo and in the food industry as an ingredient in processing chili paste [194-196]. The compounds in the kaffir lime peels such as α-pinene, camphene, β-pinene, sabinene, mycrene, limonene, ɣ-terpinene, terpinolene, trans-sabinene hydrate, copaene, linalool, citronellal, terpinen-4-ol, citronellol, geraniol and δ-cadinene with the refractive index (RI) is 1.4729 [16]. Fruit peels are more aromatic and moisture compared to leaves. It also contributes to oil production in steam distillation [10].

The selection of manipulated variable and process variable of a particular control system is very important because these parameters can significantly influence production yield and chemical composition of essential oil. There are some parameters under considerations such as temperature, pressure, flow rate, extraction time, particle size of extract material and raw state material (dry or natural) [17-20]. The parameters under study showed different influences on the volatile oil extracted [17]. Some previous studies on essential oils stressed that temperature, extraction time and extract material condition have the most significant effect on the production yield [18, 21, 22]. But, pressure and flow rate give less influence to output yield as compared to the temperature, extraction time and size of material [21, 23, 24]. Controlling the temperature of the extraction is important since a slight variation of a few degrees may result in big losses of oil as well as in oils with very different chemical characteristics, making them either efficient or not, according to the purpose they will serve [11].

Materials and Methods

Sample preparations

Fruit of kaffir limes were purchased from orchards around Dengkil area during mid of January 2013. The fresh peels of kaffir lime were put at room temperature around 23 ^{o}C and it was protected from direct light. Then, peels of kaffir lime undergo weighing process. A 0.35kg grounded kaffir lime peels for each steam temperature setting which are 80 ^{o}C, 90 ^{o}C, 95 ^{o}C, and uncontrolled temperature which is 100 ^{o}C . The steam temperature setting was achieved using hybrid fuzzy plus PID (HFPID) controller scheme by controlling the voltage fed to the heater via power controller.

The extraction method by using hydro-diffusion steam distillation system

The hydro-diffusion steam distillation essential oil extraction system developed in this work is intended for extracting the essential oil by steam distillation technique to improve the quality of output yield and get high quantity of essential oil as compared with the conventional steam distillation. Hydro-diffusion steam distillation essential oil extraction system is visualized as in Figure1 and installed in Distributed Control System Laboratory (DCS) in the University Technology Mara, Malaysia. It consists of two main part which is distillation column itself and material tray. Heating element in this system is electrical heater and was placed in the distillation column to boil the water in order to produce the steam. The distillation column and material tray were design using stainless steel material.

This work demonstrates a new method for extracting the essential oils. The proposed research applied the concept of hydro diffusion where steam and extract (water and essential oil) move naturally downwards by earth gravity downwards to the condenser. It's opposite from the conventional steam extraction where steam goes upward. By using conventional steam distillation, the steam is not fully used for extraction. As steam is passed through the material tray, it condenses in the first element before going to the next and so on, where it releases its enthalpy of vaporization. The steams that release their enthalpy have the probability to return back to the distillation column. This can be proved by examining the water in the distillation column. The hydro-diffusion steam distillation plant enhances oil recovery by minimizing oil waste in boiling water. Some literature reports that by using a conventional steam distillation process, residual oil dissolved in the water will cause an odor nuisance and waste of the valuable product in the water stream [18]. Redistilling or cohobating is the process to optimize the recovery of essential oil in

the wastewater. But the process offers high cost mainly heating and energy costs [18]. Hydro-diffusion also can prevent pollution [25].

The distillation column with 10 litre water is heated by electrical heater to produce steam. By using the hydro-diffusion system, the kaffir lime peels were placed in the material tray inside hydro-diffusion steam distillation plant. Pressurized steam from the top of the plant and passed through the botanical materials to vaporize the volatile oils in the plant material. Material tray was attached to a condenser build from copper material and water oil separator. The steam and oil vapor mixture is then going down through the small tube to the condenser. The volatile components were collected in a container. The collected essential oils were separated from water by using sodium anhydrous acid and dichloromethane which acted as catalysts using Vacuum Rotavap. The genuine oil then stored in sealed containers under refrigeration prior to analysis. . Extraction was performed approximately 2 hours because not much essential oil produces over 2 hours and save energy consumption. A schematic diagram of the complete system setup is shown in Figure 2.



Figure 1. Hydro-diffusion steam distillation system

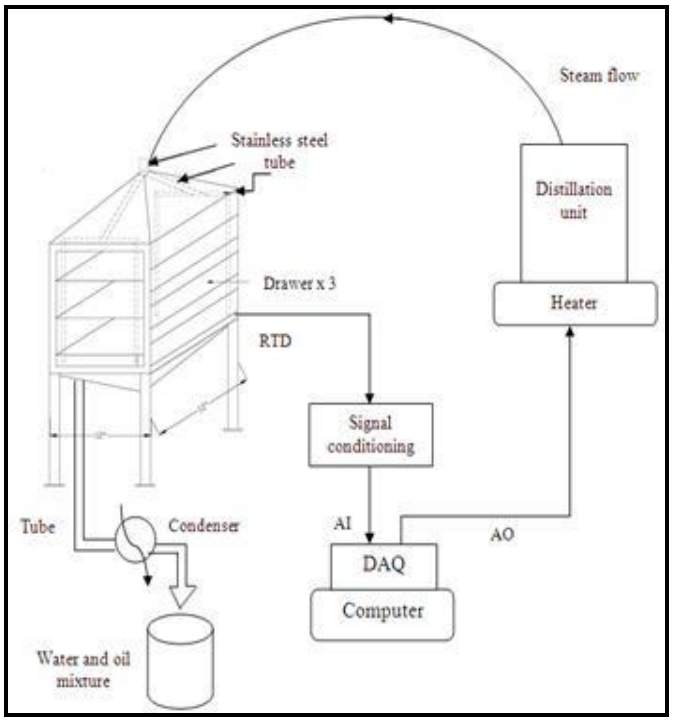


Figure 2. Schematic diagram of hydro-diffusion steam distillation system

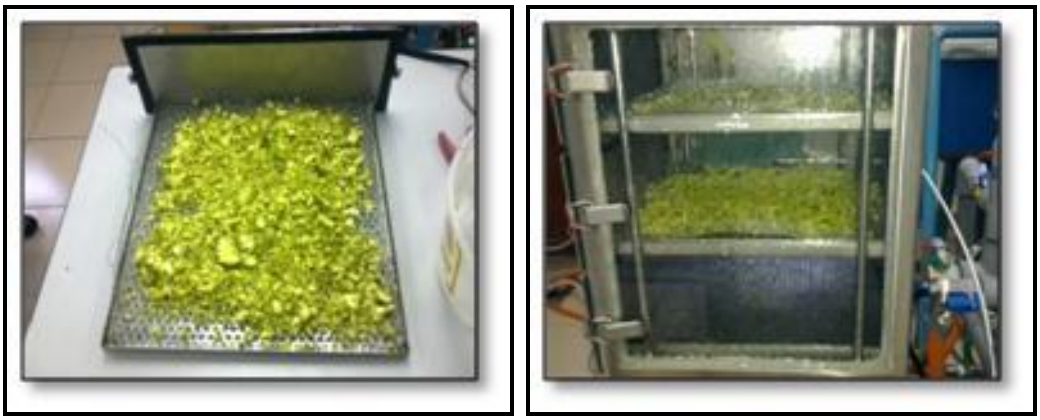


Figure 3. Sample preparations

The yield of the essential oil produced was estimated based on a wet weight basis. In order to measure the quantity of the collected oils, the percentage yields of essential oil were calculated as follows:

$$Yield\,(\%) = \frac{Weight\ of\ extract\ recover}{Weight\ of\ fresh\ citrus\ peels} \times 100$$

where the oil density of kaffir lime oil is 0.871g/mL [26]. So, the weight of extracting oil recovered in grams can be derived as:

$$Weight\ of\ extract\ recover\ (in\ gram) = volume\ of\ oil\ collected\ (mL) \times density\ of\ kaffir\ lime\ oil\left(\frac{0.871g}{mL}\right)$$

GC-MS conditions

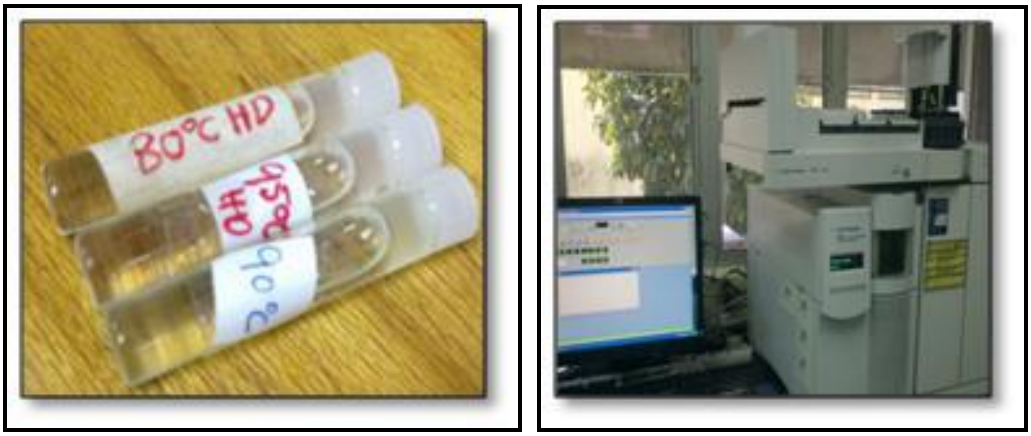


Figure 4. GC-MS analysis

The composition of kaffir lime peel oil was tested by GC and GC/MS for qualitative analysis to identify active constituents. For GC analysis, a Shimadzu GC 2010 Gas Chromatograph which equipped with a FID detector and fused silica capillary column CBP5 (30m x 0.25mm, 0.25µm film thickness) was employed. The GC/MS analyses were carried out by using Agilent 5975C Mass Selective Detector equipped with an Agilent 7890A Gas Chromatograph. A HP-5MS fused silica capillary column (30m x 0.25mm) with 0.25µm film thickness was used. The carrier gas for GC is He with flow rate of 1ml/min and temperature programming as tabulated in Table 1 below:

Table 1. Setting for GC-MS analysis

Injector temperature	250 ^oC
Detector temperature	280 ^oC, with mass range recorder from 45-450 mass-to ratios, with electron energy of 70eV.
Oven temperature	The column oven was set to 60 ^oC for 3 minutes, and then the temperature was gradually increased up to 230 ^{o}C at a rate 3^oC/min. For 230 ^{o}C till 325 ^{o}C, the rate was maintained at 30 ^{o}C/min.

Identification of the chemical compounds

The identification of the chemical compounds was done by matching their mass spectra with existing data in the HPCH2205.L, Wiley7 Nist05.L and NIST05a.L library search data. Their retention indices were compared with Adam, 2007 library. Then, the major compounds in the kaffir lime peel were compared with those reported in the literature.

Results and Discussion

Comparative analysis of the effect of temperature on the production rate of Kaffir Lime peel oil

Figure 5 presents the production yield of kaffir lime peel using hydro-diffusion steam distillation essential oil extraction system. The extraction process was performed for 2 hours. From the experiment, the production yield start produced approximately after 50 minutes. As shown in Figure 5, two layers form after extraction process where the top layer is hydrosol and water at the bottom of the container. The oils were collected for every 10 minutes with the objective to see the flow rate of production yield. From Figure 5, it is interesting to note that the yield of essential oil is rapidly produced at the early stage of extraction as shown in container 1. The yield in container 1 was collected after 50 minute process started. Another important finding was that the yields start decreasing as time increasing. As shown in container 5, very poor amount of yield was collected after 2 hours.

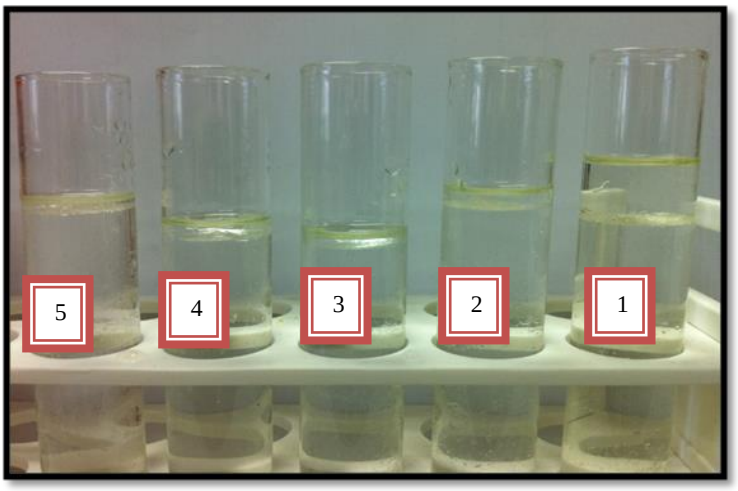


Figure 5. The production yield of kaffir lime peel

Table 2 tabulated the accumulated amount of percentage yield for each steam temperature control based on a wet weight basis. It means that no drying process involved during the sample preparation stage.

Table 2. Percentage of extracting kaffir lime essential oil

Steam temperature, (^oC)	**Production yield, (mL)**	**Percentage yield, (w/w)**
80	2.8	0.70
90	8.8	2.19
95	11.8	2.94
Uncontrolled	12.5	3.11

Referring to Table 2, by using hydro-diffusion steam distillation system for 2 hour extraction process, the percentage of kaffir lime oil yields at temperatures of 80 ^oC, 90 ^oC, 95 ^oC and uncontrolled temperature were 0.70% (w/w), 2.19% (w/w), 2.94% (w/w), and 3.11% (w/w), respectively. It was notable that the percentage yield increased as steam temperature increased. Uncontrolled steam temperature yielded the highest amount of essential oil. However, the observed difference of percentage yield between uncontrolled steam temperature and steam temperature at 95 ^oC is very small. The lowest yield was obtained at steam temperature of 80 ^oC. The most interesting finding was that the oil yields quite lucrative at 90 ^oC and showed 77.2% significant difference as compared to the oil yield at 80 ^oC. The graphical comparison of percentage yield at various steam temperature is shown in Figure 6.

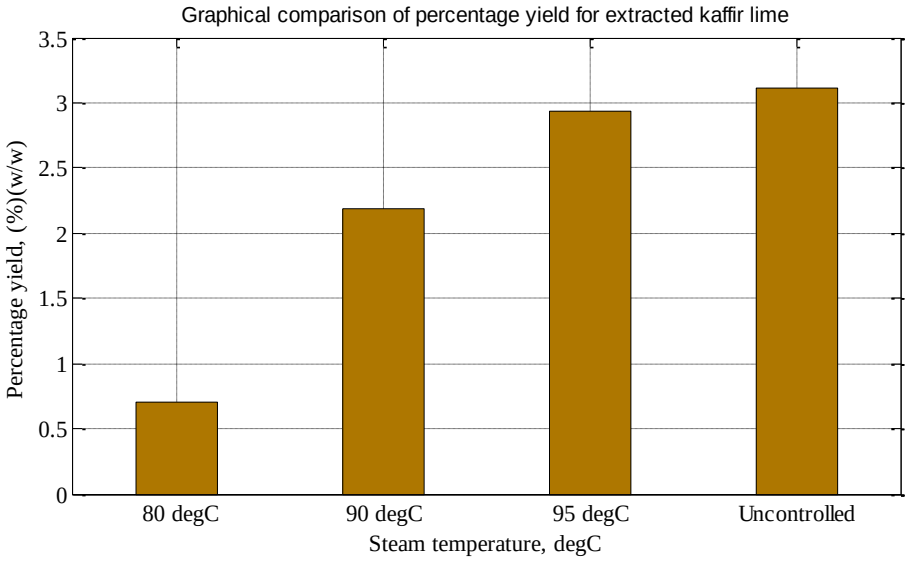


Figure 6. Graphical comparison of percentage yield for extracted kaffir lime peel using hydro-steam distillation system.

Figure 7 presents the production curves of kaffir lime oil yield at four different steam temperatures as a function of time where the oil yield was collected for every 10 minutes. The curves show that the extraction yield seems to have an asymptotic shape. It is apparent from this figure that oil yield was aggressively produced at an early stage of extraction process for all steam temperature settings. From the result, there are 3 different saturation times which are 60 min, 80 min and 90 min for a temperature of 80 ^oC, 90 ^oC, 95 ^oC and uncontrolled temperature, respectively. It was found that 80 ^oC has the fastest saturation time among all but produced the smallest oil yield. An extraction time of 60 min at 95 ^oC provide 3 times more yields as compared to those obtained by 80 ^oC.

Analysis of essential oil of kaffir lime by Gas Chromatography- Mass Spectrometry (GC-MS)

The analysis of essential oil from kaffir lime peels for each temperature was done by using Gas Chromatography-Mass Spectrometry (GC-MS). The chromatogram of GC-MS analysis for all temperature studies are presented in Figure 8 until Figure 11 for temperature 80 ^oC, 90 ^oC, 95 ^oC and uncontrolled temperature, respectively. The relative peak area in percentage (%) was calculated by comparing the peak ratio in chromatograms of GC and GC-MS. The compounds of essential oil obtained from kaffir lime peels from different temperature profile are summarized in Table 3. All the compounds were listed based on a retention index (RI).

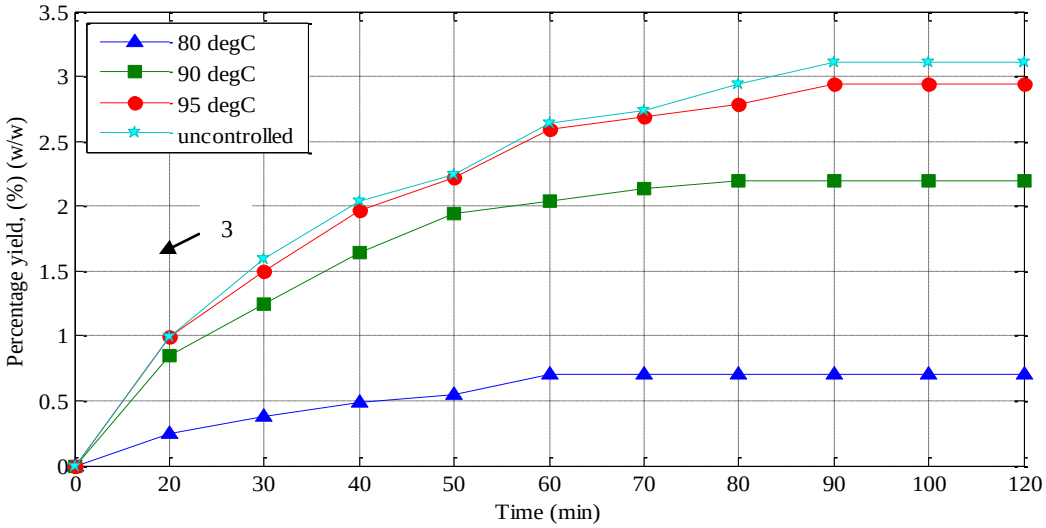


Figure 7. Production curves of kaffir lime oil yield at various steam temperature settings.

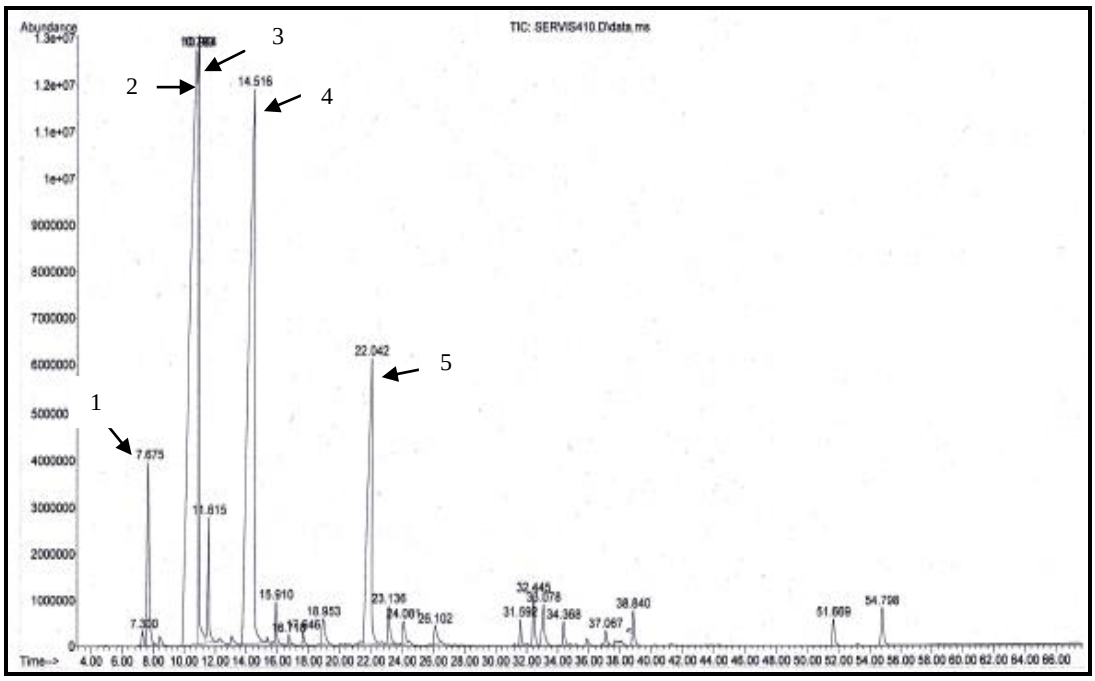


Figure 8. The GC-MS chromatogram of volatile compound from kaffir lime peel essential oil at 80 ^{o}C. The major compounds marked as (1) α-pinene, (2) Sabinene, (3) β-pinene, (4) Limonene, (5) Citronellal.

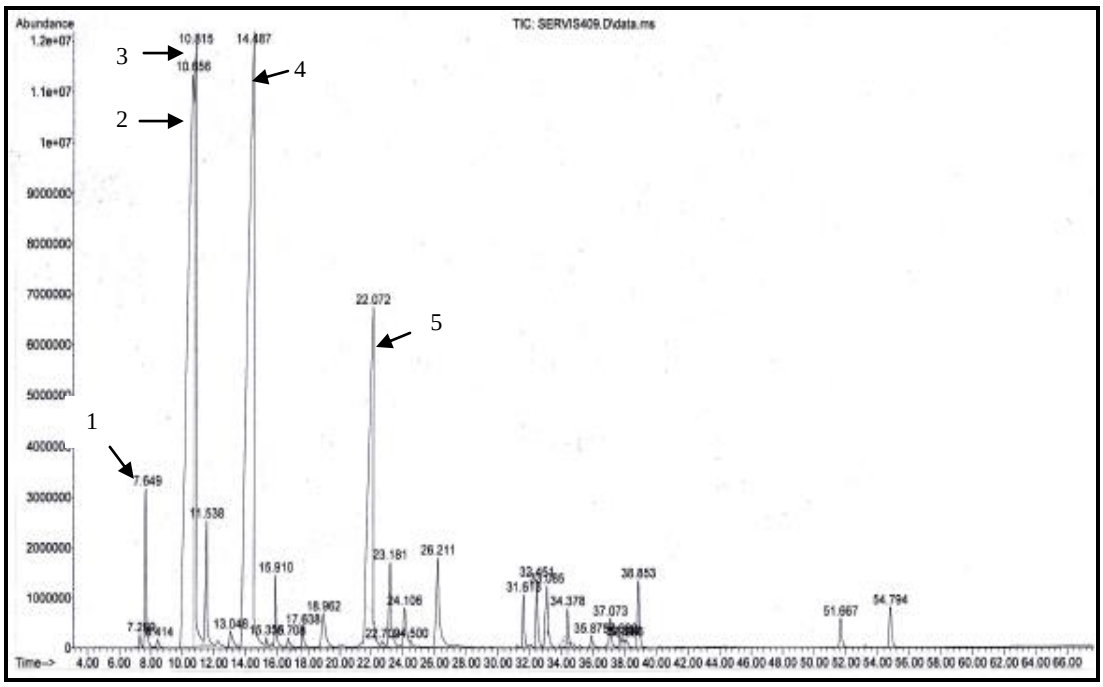


Figure 9. The GC-MS chromatogram of volatile compound from kaffir lime peel essential at 90 ^{o}C. The major compounds marked as (1) α-pinene, (2) Sabinene, (3) β-pinene, (4) Limonene, (5) Citronellal.

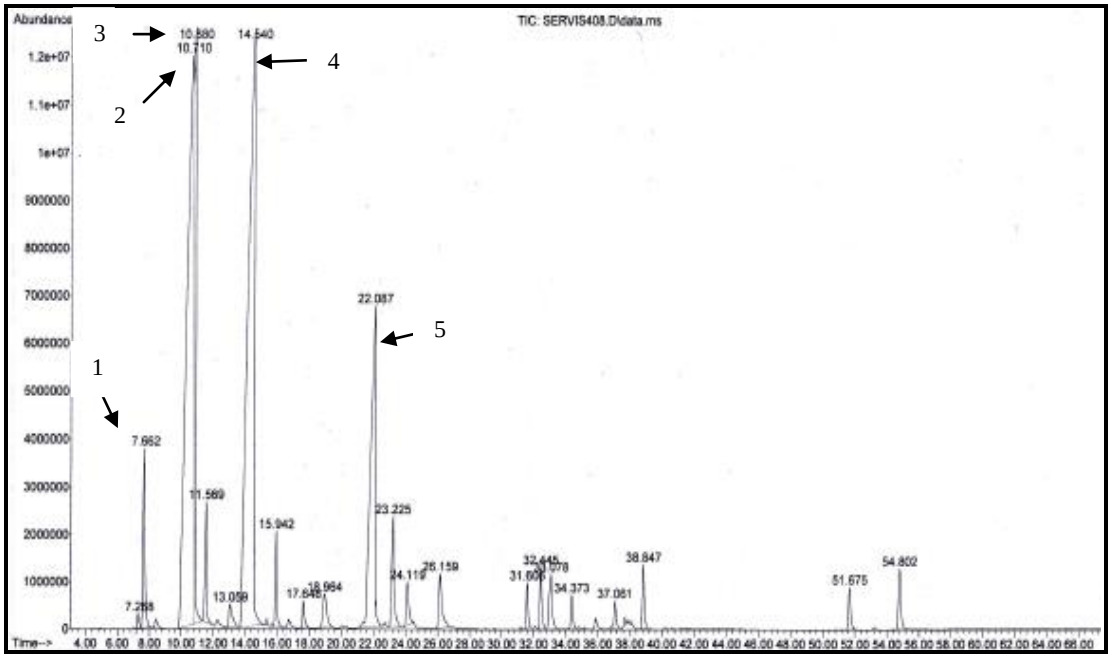


Figure 10. The GC-MS chromatogram of volatile compound from kaffir lime peel essential at 95 ^{o}C. The major compounds marked as (1) α-pinene, (2) Sabinene, (3) β-pinene, (4) Limonene, (5) Citronellal.

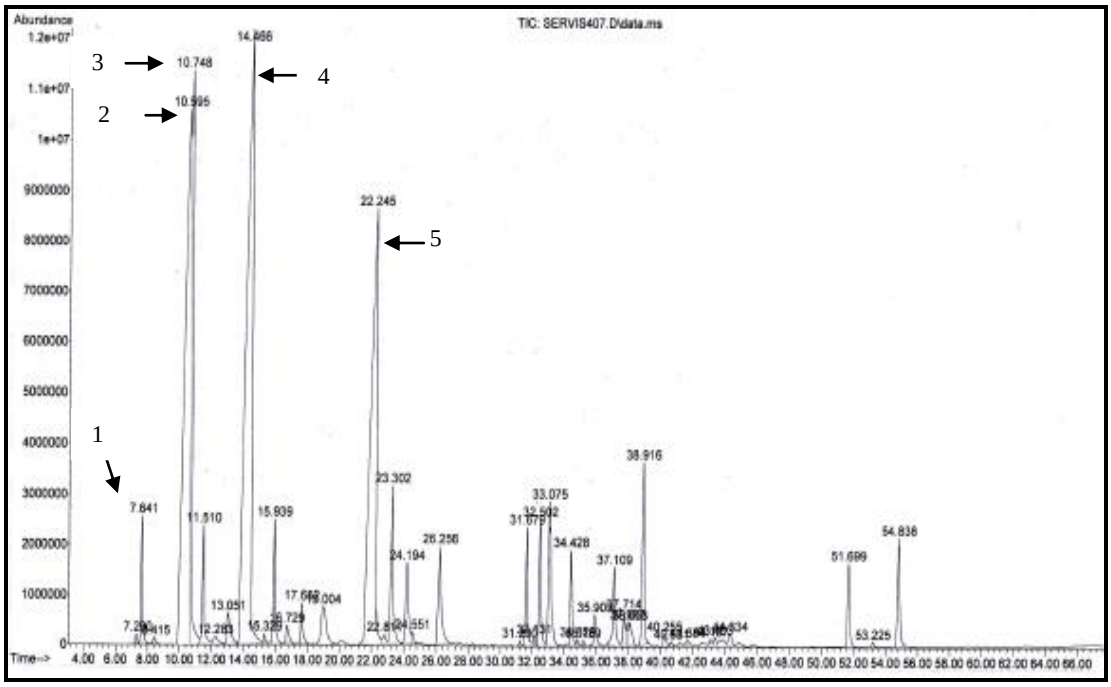


Figure 11. The GC-MS chromatogram of volatile compound from kaffir lime peel essential at uncontrolled temperature. The major compounds marked as (1) α-pinene, (2) Sabinene, (3) β-pinene, (4) Limonene, (5) Citronellal

It can be seen from the data in Table 3 that a total of 26 compounds was found in kaffir lime peels extracted using hydro-diffusion steam distillation system start with α-Thujene (0924) until δ-Cadinene (1522). Different numbers of compounds were extracted where a total of 19 compounds, 24 compounds, 19 compounds and 24 compounds were identified in temperature 80 *ºC*, 90 *ºC* and 95 *ºC* and uncontrolled temperature, accordingly. Therefore, the temperature at 90 ^{o}C and uncontrolled temperature can extract more chemical compounds. It is apparent from this table that 17 compounds appear in all temperature conditions such as α-Thujene, α-Pinene, Sabinene, β-Pinene, myrcene, δ-2-Carene, limonene, ɣ-Terpinene, linalool, citronellal, terpinene-4-ol, α-Terpineol, citronellol, α-Copaene, caryophyllene, citronellyl propanoate and germacrene D. All the major compounds of the kaffir lime peel oils such as α-pinene, sabinene, β-pinene, limonene and citronellal were detected for each temperature profile. Figure 12 presents the graphical major compounds in each temperature setting.

As refer to Figure 12, the major constituent of α-pinene at 80 ^{o}C, 90 ^{o}C, 95 ^{o}C and uncontrolled temperature were 2.515%, 1.806%, 2.207% and 1.255%, accordingly. The sabinene compound that indicates the spicy taste of the oil contributes the highest concentration among all with 45.594%, 36.394%, 37.481% and 27.498% at 80 ^{o}C, 90 ^{o}C, 95 ^{o}C and uncontrolled temperature, respectively. The third major compound is β-pinene which provide distinctive aroma where 8.974%, 8.597%, 8.714% and 7.147 were identified in respective temperature. Limonene that give a distinctive aroma of oranges provide 28.649%, 32.455%, 32.232% and 28.722% concentration at 80 ^{o}C, 90 ^{o}C, 95 ^{o}C and uncontrolled temperature, accordingly. Meanwhile, for citronellal compound which indicates the micro and insect repellent activity present 8.293%, 10.775%, 9.647% and 17.487% concentration. What is interesting in this data is that it is obvious for compound α-pinene, sabinene, β-pinene and limonene where the controlled temperature can extract more chemical compounds than uncontrolled temperature. The significant difference between these two

conditions may due to oil experience thermal degradation which consequently losing some significant compounds in uncontrolled temperature. In contrast to earlier findings, citronellal was notably high in the oils collected from uncontrolled temperature. Figure 13 shows the color of the oils varies from light brown to dark brown as temperature increase. This finding supports previous research where different temperature will give an effect to the number of compounds extracted and quantity of essential oil [18, 21-22].

Table 3. Compound of essential oils obtained from the kaffir lime peel.

			Relative peak area (%)			
NO	**COMPOUNDS**	**RETENTION INDEX (RI)**	**80 *°C***	**90 *°C***	**95 *°C***	**Uncontrolled temperature**
1	α-Thujene	0924	0.27	0.18	0.22	0.11
2	**α-Pinene**	**0932**	**2.515**	**1.806**	**2.207**	**1.255**
3	**Sabinene**	**0969**	**45.594**	**36.394**	**37.481**	**27.498**
4	**β-Pinene**	**0974**	**8.974**	**8.597**	**8.714**	**7.147**
5	Myrcene	0988	1.786	1.655	1.656	1.547
6	δ-2-Carene	1001	0.109	0.062	0.086	0.070
7	**Limonene**	**1024**	**28.649**	**32.455**	**32.232**	**28.722**
8	ɣ-Terpinene	1054	0.310	0.498	0.705	0.988
9	Terpinolene	1086	-	0.152	0.205	0.300
10	Trans-Sabinene hydrate	1098	0.146	0.136	-	0.273
11	Linalool	1095	0.541	0.810	0.802	0.921
12	**Citronellal**	**1148**	**8.293**	**10.775**	**9.647**	**17.487**
13	Terpinene-4-ol	1174	0.471	1.120	1.452	2.028
14	α-Terpineol	1186	0.350	0.583	0.668	1.242
15	Citronellol	1223	0.429	1.784	1.012	1.809
16	α-Copaene	1374	0.345	0.494	0.400	0.953
17	Caryophyllene	1417	0.280	0.313	0.258	0.725
18	Citronellyl propanoate	1444	0.185	0.391	0.315	0.909
19	Cis muurola-3, 5diene	1448	0.212	-	0.380	1.156
20	α-Humulene	1452	-	0.097	-	0.242
21	Geranyl propanoate	1476	-	-	-	0.810
22	Germacrene D	1484	0.091	0.430	0.162	0.517
23	β-Selinene	1489	-	0.032	-	-
24	Bicyclogermacrene	1500	-	0.073	-	0.256
25	α-Muurolene	1500	-	0.045	-	0.122
26	δ-Cadinene	1522	-	0.424	-	-
		TOTAL	**19**	**24**	**19**	**24**

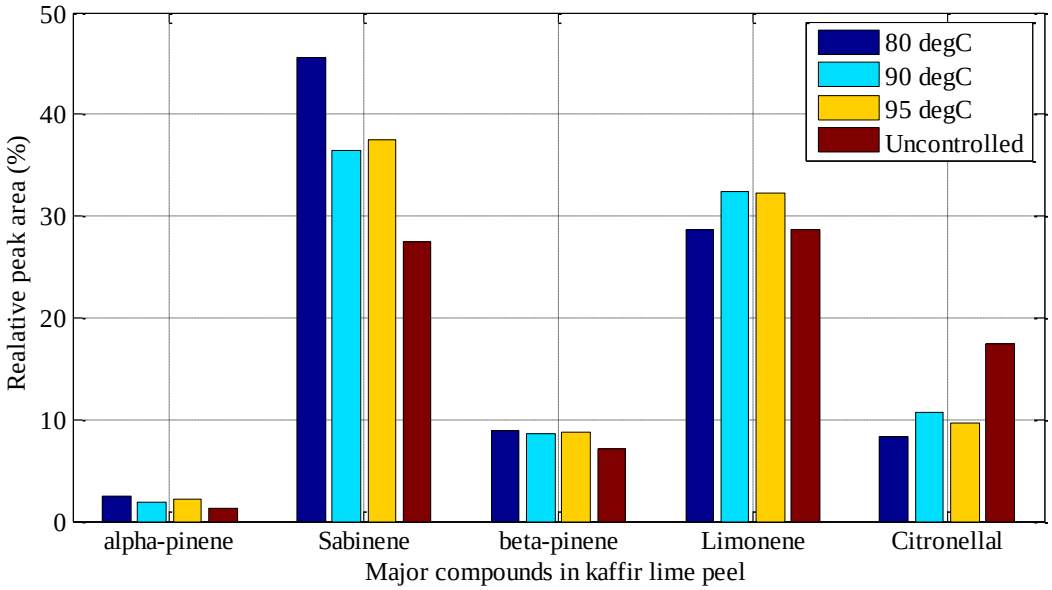


Figure 12. Major compounds in the kaffir lime peel



Figure 13. The pure essential oil from the kaffir lime peels

Conclusion

The comparative studies of production rate and quality of kaffir lime oil based on different steam temperatures have been studied. From the findings, it can be concluded that the percentage yield increased as steam temperature increased. Uncontrolled steam temperature yielded the highest amount of essential oil. However, the discrepancy between uncontrolled steam temperature and steam temperature at 95 °C is not obvious. A total of 26 compounds has been found in kaffir lime oil extracted using hydro-diffusion steam distillation system. The controlled temperature can extract more chemical compounds than uncontrolled temperature especially major compounds such as α-pinene, sabinene, β-pinene and limonene. Overall, the aims of this study to control the hydro-diffusion steam distillation system essential oil extraction system have been successfully achieved.

Acknowledgement

The authors would like to thank and acknowledged the staff of Faculty of Electrical Engineering, Research Management Institute, and Human Resource Department UiTM Shah Alam; and Forest Research Institute Malaysia (FRIM).

References

1. A.Arce, A.Pobudkowska, O.Rodriguez, and A.Soto (2007). Citrus essential oil terpenless by extraction using 1-ethyl-3-methylimidazolium ethylsulfate ionic liquid: Effect of temperature. *Chemical Engineering Journal* 133: 213-218.
2. J. M. Roldan-Gutierrez, J. Ruiz-Jimenez, and M. D. L. d. Castro (2008). Ultrasound-assisted dynamic extraction of valuable compounds from aromatic plants and flowers as compared with steam distillation and superheated liquid extraction. *Talanta* 75: 1369–1375.
3. M. E. Lucchesi, F. Chemat, and J. Smadja (2004). Solvent-free microwave extraction of essential oil from aromatic herbs: comparison with conventional hydro-distillation. *Journal of Chromatography A* 1043: 323–327.
4. N. Bousbia, M. A. Vian, M. A.Ferhat, E. Petitcolas, B. Y.Meklati, and F. Chemat (2009). Comparison of two isolation methods for essential oil from rosemary leaves:Hydrodistillation and microwave hydrodiffusion and gravity. *Journal of Food Chemistry :* 114: 355-362.
5. A. Donelian, L. H. C. Carlson, T. J. Lopes, and R. A. F. Machado (2009). Comparison of extraction of patchouli *(Pogostemon cablin)* essential oil with supercritical CO2 and by steam distillation. *The Journal of Supercritical Fluids* 48: 15–20.
6. F. Chemat, M. E. Lucchesi, J. Smadja, L. Favretto, G. Colnaghi, and F. Visinoni (2006). Microwave accelerated steam distillation of essential oil from lavender: A rapid, clean and environmentally friendly approach. *Analytica Chimica Acta,* vol. 555, pp. 157–160.
7. M. Khajeh, Y. Yaminib, and S. Shariati (2010). Comparison of essential oils compositions of *Nepeta persica* obtained by supercritical carbon dioxide extraction and steam distillation methods. *Food and Bioproducts Processing* 88: 227–232.
8. H. Ebrahimzadeh, Y. Yamini, F. Sefidkon, M. Chaloosi, and S. M. Pourmortazavi (2003). Chemical composition of the essential oil and supercritical CO2 extracts of *Zataria multiflora* Boiss. *Food Chemistry* 83: 357–361.
9. E. S. Giray, S. Kirici, D. A. Kaya, M. Turk, O. Sonmez, and M. Inan (2008). Comparing the effect of sub-critical water extraction with conventional extractipn methods on the chemical composition of Lavandula stoechas. *Talanta* 74: 930-935.
10. N. Kasuan, M. Yunus, M. H. F. Rahiman, S. R. S.Aris, and M. N. Taib (2009). Essential Oil Composition of Kaffir Lime: Comparative analysis between Controlled Steam Distillation and Hydrodistillation Extraction Process. *Proceedings of 2009 Student Conference on Research and Development (SCOReD 2009).*
11. E. L. Galvão, H. B. d. Sant'Ana, H. N. M. Oliveira, A.V.Souza, and E. M. B. D. Sousa. Influence of Temperature in the Kinetics Extraction of the Cymbopogon Winterianus j. oil with Dense Carbon Dioxide. *2nd Mercosur Congress on Chemical Engineering, 4th Mercosur Congress on Process Systems Engineering*.
12. S. Sayyar, Z. Z. Abidin, R. Yunus, and A. Muhammad (2009). Extraction of Oil from Jatropha Seeds-Optimization and Kinetics. *American Journal of Applied Sciences* 6: 1390-1395.
13. B. Marongiu, A. Piras, S. Porcedda, and A. Scorciapina (2005). Chemical composition of the essential oil and supercritical CO_2 extract of Commiphora myrrha(Nees) Eng. and of Acorus calamus L.. *Journal of Agricultural and food chemistry* 53: 7939-7943.
14. G. Wenqiang, L. Shufen, Y. Ruixiang, T. Shaokun, and Q. Can (2007). Comparison of essential oils of clove buds extracted with supercritical carbon dioxide and other three traditional extraction methods. *Food Chemistry* 101: 1558–1564.
15. V. Srisukh, C. Tribuddharat, V. Nukoolkarn, N. Bunyapraphatsara, K. Chokephaibulkit, S. Phoomniyom, S. Chuanphung, and S. Srifuenfung (2012). Antibacterial activity of essential oils from Citrus hystrix (makrut lime) against respiratory tract pathogens. *Science Asia* 38: 212-217.

16. B. M.Lawrence, J. W.Hogg, and S. J.Terhune (1970). Constituents of the leaf and peels oils of Citrus Hystrix, D.C.. *Phytochemistry* 10: 1404-1405.
17. C. Grosso, V. Ferraro, A. C. Figueiredo, J. G. Barroso, J. A. Coelho, and A. M. Palavra (2008). Supercritical carbon dioxide extraction of volatile oil from Italian coriander seeds. *Food Chemistry* 111: 197-203.
18. P. Masango (2005). Cleaner production of essential oils by steam distillation. *Journal of Cleaner Production* 13: 833-839.
19. A. Ammann, D. Hinz, R. Addleman, C.Wai, and B.Wenclawiak (1999). Superheated water extraction, steam distillation and SFE of peppermint oil. *Fresenius' Journal of Analytical Chemistry* 364: 650-653.
20. M. Kristiawan V. Sobolik, and K. Allaf 92008). Isolation of Indonesian cananga oil using multi-cycle pressure drop process. *Journal of Chromatography A* 1192: 306-318.
21. M. H. Eikani, F. Golmohammad, and S. Rowshanzamir (2007). Subcritical water extraction of essential oils from coriander seeds (Coriandrum sativum L.). *Journal of Food Engineering* 80: 735-740.
22. L. Wang and C. L. Weller (2006). Recent advances in extraction of nutraceuticals from plants. *Trends in Food Science & Technology* 17: 300-312.
23. S. Rezzoug (2009). Optimisation of Steam extraction of oil from maritime pine needles. *Journal of Wood Chemistry and Technology* 29: 87-100.
24. V. Louli, G. Folas, E.Voutas, and K. Magoulas (2004). Extraction of parsley seed oil by supercritical CO2. *The Journal of Supercritical Fluids* 30: 163-174.
25. M. A. Vian, X. Fernandez, F. Visinoni, and F. Chemat (2008). Microwave hydrodiffusion and gravity, a new technique for extraction of essential oils. *Journal of Chromatography A* 1190: 14-17.
26. J. Adamiec, C. Borompichaichartkul, G. Srzednicki, W. Panket, S. Piriyapunsakul, and J. Zhao (2012). Microencapsulation of kaffir lime oil and its functional properties. *Drying Technology* 30: 912-920.

The Malaysian Journal of ANALYTICAL SCIENCES ISSN 1394-2506

STEAM DISTILLATION WITH INDUCTION HEATING SYSTEM: ANALYSIS OF KAFFIR LIME OIL COMPOUND AND PRODUCTION YIELD AT VARIOUS TEMPERATURES

(Penyulingan Wap Dengan Sistem Pemanasan Aruhan: Analisis Komposisi Minyak Limau Purut Dan Hasil Pengeluaran Pada Suhu Pelbagai)

Zuraida Muhammad[1]*, Zakiah Mohd Yusoff[1], Mohd Noor Nasriq Nordin[1], Nurhani Kasuan[1], Mohd Nasir Taib[1], Mohd Hezri Fazalul Rahiman[1], Zaibunnisa Abdul Haiyee[2]

[1]Faculty of Electrical Engineering,
[2]Faculty of Applied Sciences,
Universiti Teknologi MARA, 40450 Shah Alam, Selangor D.E., Malaysia

**Corresponding author: muhammad_zuraida@yahoo.com*

Abstract

The steam temperature during the extraction process has a great influence on the essential oil quality. .This study was conducted to analyze the compound of kaffir-lime oil during extracting at different steam temperature using GC-MS analysis. The extraction was carried out by using steam distillation based on induction heating system at different extraction temperature such as 90^0C, 95^0C and 100^0C, the power of the induction heating system is fixed at 1.6kW. Increment of the steam temperature will increase the oil yield. In terms of oil composition, extraction at lower temperature resulted high concentration for four marker compounds of kaffir-lime oil which are α-pinene, sabinene, limonene, β-pinene.

Keywords: Kaffir-lime oil, GC-MS analysis, and steam distillation-based induction heating system

Abstrak

Suhu wap semasa proses mengekstrak mempunyai pengaruh yang besar bagi kualiti minyak pati. .Kajian ini dijalankan untuk menganalisis sebatian minyak limau purut semasa diekstrak pada suhu wap yang berbeza dengan menggunakan analisis GC-MS. Pengekstratan telah dijalankan dengan menggunakan wap penyulingan berasaskan sistem pemanasan aruhan pada suhu pengekstrakan yang berbeza iaitu pada 90^0C, 95^0C dan 100^0C, kuasa sistem pemanasan aruhan adalah 1.6kW. Meningkatkan suhu wap akan menyebabkan peningkatan hasil minyak. Dari segi komposisi minyak, pengekstraktan pada suhu yang lebih rendah menyebabkan kepekatan yang tinggi terhadap empat kompaun utama minyak limau purut iaitu α-pinene, sabinena, limonene, β-pinene.

Kata kunci: minyak limau purut, analisis GC-MS dan penyulingan wap berasaskan system pemanasan aruhan

Introduction

Essential oil is mostly used for flavouring, as perfumes or as fragrance[1] in many applications. Initially, several significant parameters should be considered to contribute the output yield and quality of the production. Have been noted, the significant parameters concern during extraction process is temperature, extraction time, and extract material condition [2-7].

The steam distillation is the conventional method used to obtain the essential oil from plant material because cleanliness, cheap, simple, ease design to compare to others advance technique [8, 9]. Countless research has been dictated highlight the effect of temperature to the production of essential oil and temperature plays important role in the extraction process [2, 7, 10-15].

Therefore, for every single of extraction method have focussed on temperature extraction either is fixed[5, 13-18] or vary with temperature[2-4, 11, 19-21] and from the analysis shows temperature will affect the yield of essential oil[3, 5, 21, 22]. Based on that point, the temperature becomes important rule and selected as the process variable in this study. Currently, steam distillation mostly used in industries of extraction essential oil. By using the basic idea of steam distillation, many techniques are extending suppose to optimize the performance of steam distillation in the process of extraction. Although this method known always become of benchmarking technique to others technique[1-3, 7, 10, 11, 23], but this method is the most popular technique in industrial and research work due to low cost, cleanliness, high production yield, simple operating procedure[24].

There has several numbers of research efforts denoted in order to control the steam temperature of steam distillation system to offer high output yield essential oil [25-27]. In this case study, application of PID controller has always be more popular technique since it's simple, ease of design, and cost required relatively low[25]. Another advanced technique also derived in optimized the output response of steam temperature such as hybrid fuzzy- PD plus PID controller, and self tuning PID controller [26, 27].

High Efficient Steam Distillation System

The conventional steam distillation system is modified to achieve the higher performance during the extraction process. Conventionally, the heating element applies to the plant steam distillation are electrical heating or gasses. But in this developed plant, induction heating system is introduced as heating element to the extraction process. Selection of the induction heating system because of their working principle which is a high efficiency, cleanliness and safe compared to other heating element.

Figure 1 shows a sketch of steam distillation system with induction based and in Figure 2 show the block diagram of the experiment setup for this system.

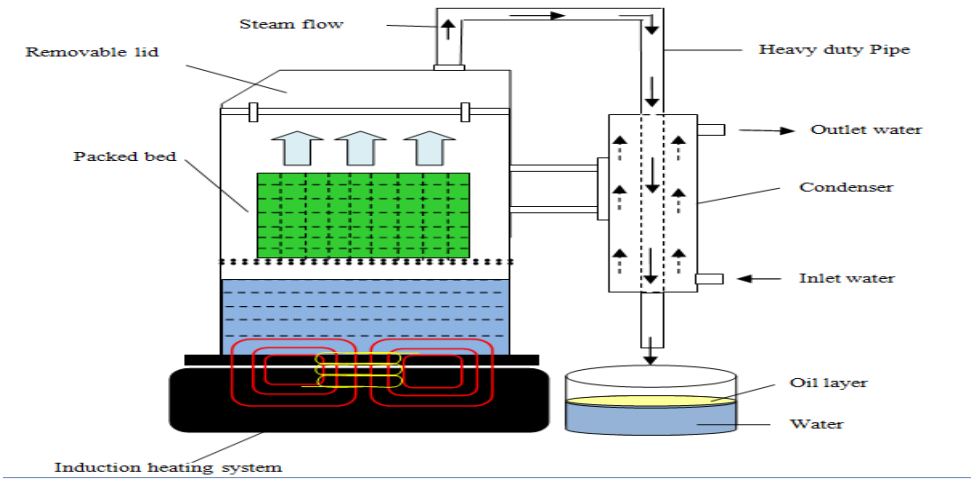


Figure 1. Distillation pot system prototype sketch

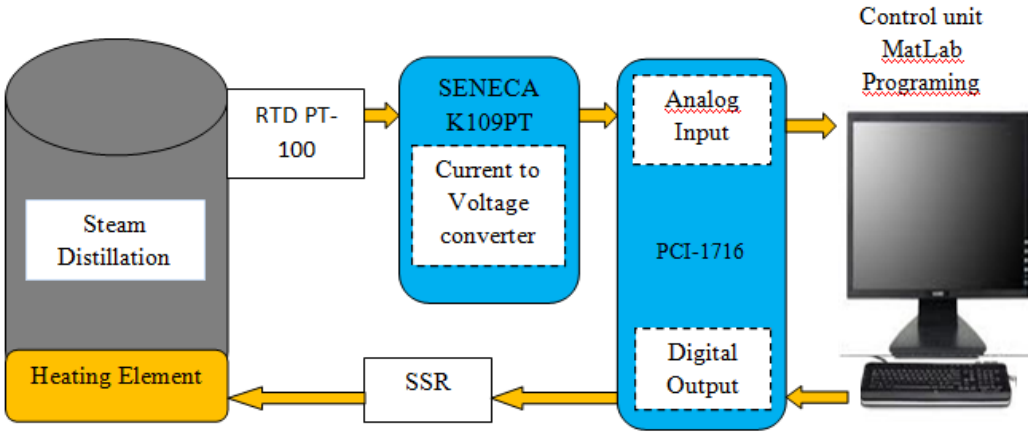


Figure 2. Experiment setup and system interface

The temperature of extraction will control by using Fuzzy plus P, I, and D proposed in [28] that give good performance which improve system response and uncertainties [29, 30].

Materials and Methods

Raw Materials

The extraction process starting with the preparation raw materials which are fruits of kaffir lime were collected at the mature stage from fruit orchards around Dengkil, Selangor. The essential oils of kaffir lime are obtaining used the kaffir lime peels because it had much of aromatic sense and more moisture compared to leaves of kaffir lime[31] which are contained high major volatile component such as limonone, citronellal and α-β pinane. Kaffir lime peels (350g) consistently are grounded to ensure the volatile compounds expose easily for each experiment running.

Extraction Procedures

The 350g ground material was stored in packed bed inside the steam distillation pot. Before the process run, 3000ml water at room temperature is adding into steam pot to produce a steam during the extraction process. The steam produce will become as transportation medium of volatile compound and enhance the production yield of essential oil. The steam produced will bring the volatile compound through condenser before condensed and become a layer of oil and hydrosol. The hydrosol produced had follow isolation process where the sample was transferred to separator funnel and dichloromethane was added to separate between oil and liquid. After funnel was shaking, the oil layer appeared at top and liquid at bottom layer.

In this conducted work, induction heating system used 1.2kW to boil the water inside the steam pot until the steam temperature achieves the set point such as 90^0C,95^0C and 100^0C. The control strategies and technique used to control the extraction temperature as introduced in the previous work[28]. The extraction time is stopped after 2 hours because not much produces essential oil when it approximately achieves saturated extraction point and avoid energy waste. The quantity of oil yield will be determined based on follower equation.

$$yield\% = \frac{Weight\ of\ extract\ recovered\,(kg)}{Weight\ of\ fresh\ kaffir\ limr\ peel\,(kg)}\ x\ 100$$

Chromatographic Analysis

The separation of essential oil volatile compound was performed on a Hewlett-Packed gas chromatograph with flame ionization detector using a fused silica capillary column HP5-MS (30m x 0.25mm internal diameter with 0.25μm film thickness). The injector temperature was 250^0C. The oven was set 60^0C for three minutes and temperature was programmed to increase from 60^0C to 200^0C at a rate of 6^0C/min and from 200^0C to 325^0C at a rate of 30^0C/min. The carrier gas was helium at a flow rate of 1.0mL/min, and the sample volume injected was 0.1 ml of the pure oil [10].

Identification of essential oil compounds was based on comparison of the mass spectra obtained in the gas chromatography with those of compounds registered in the NIST MS (National Institute Standard and Technologies Mass Spectra of the standard Wiley Register of Mass Spectra), library database of the GC-MS. The chromatography was performed on a gas chromatograph (Model Agilent 7890), using a fused silica capillary column HP5-MS, coupled to a selective mass detector (Model 5975C). The detector temperature was 280^0C, and the ionization mode was electron impact at70Ev [10].

Results and Discussion

The experiment of extraction kaffir-lime oil is conducted to see and evaluate the quantity and quality of the output yield by applying the control scheme towards the process. In this work, the oil yield of kaffir-lime was found out and volatile compound of the kaffir-lime has been identified. The volatile compound is identified through GC-MS and GC analysis provided.

The effect of temperature on production yield of kaffir-lime essential oil

In the experiment of extraction kaffir lime essential oil, the yield of oil produced is monitored by taking a reading of oil yield for every 15 minutes. Eight different tubes are used within 2 hour extraction process to separate the oil produces every 15 minutes. The layer of oil appears on top of separator tube with physical oil is clear liquid appearance. The oil that appears on top easily to suctioned and stored in the bottle. Yield of essential oil is calculated based on a wet weight basis since the drying process is escaped during pre-process the raw material preparation. The experiment was repeated three times for every different temperature The oil yield accumulated in percentage during the extraction process at different temperature is tabulated in Table 1 below/.

Table 1. Oil yield of Kaffir lime with different temperature parameter

Experiment	90 ^{o}C	95 ^{o}C	100 ^{o}C
Yield1(%)	1.738	3.249	3.517
Yield2(%)	1.652	3.114	3.544
Yield3(%)	1.822	3.331	3.445
Mean of yield(%)	1.737	3.231	3.502
Standard deviation of yield(%)	0.069	0.089	0.042

From the result, the oil yield accumulated along the extraction process is increased when the temperature is increased. For temperature control at 90^0C, the yield is not impressed when the steam is controlled at low temperature by giving yield equal 1.737%. When the temperature is controlled at 95^0C, the yield is increased to 3.231%. A last experiment conducted without control element and give yield equal 3.502%. It shows that the yield

of essential oil is proportional to the temperature. From the standard deviation, a small standard deviation of oil yield indicates that the percentage yield for every experiment have values that are very close to the mean value.

Table 2. Kaffir-lime oil compound from GCMS analysis

No	Compounds	Retention Index (RI)	Relative Peak Area (%)		
			90 °C	95 °C	Uncontrolled (100 °C)
1	α-Thujene	0924	0.072	0.158	0.105
2	**α-Pinene**	**0932**	**3.223**	**3.109**	**2.959**
3	**Sabinene**	**0969**	**48.5**	**46.165**	**46.349**
4	**β-Pinene**	**0974**	**10.088**	**9.321**	**8.759**
6	**Myrcene**	**0988**	**1.469**	**1.446**	**1.338**
6	δ-2-carene	1001	-	0.057	-
7	**Limonene**	**1024**	**27.714**	**26.446**	**25.742**
8	γ-terpinene	1054	0.053	0.190	0.168
9	Terpinolene	1086	0.095	0.079	0.042
10	Linalool	1095	0.028	0.687	0.781
11	**Citronellal**	**1148**	**3.247**	**6.633**	**7.146**
12	**Terpinen-4-ol**	**1174**	**0.457**	**1.054**	**0.888**
13	α-terpineol	1186	0.163	0.438	0.473
14	Citronellol	1223	-	0.097	0.435
15	Citronellyl acetate	1350	0.117	-	0.222
16	α- copaene	1374	0.092	0.365	0.302
17	β- copaena		-		0.309
18	Gemacrene D	1484	0.185	0.206	0.035
19	δ- cadinane	1513	0.081	0.266	0.233

The effect of temperature control on quality of kaffir-lime essential oil

This analysis is carried out to identify the volatile compound in kaffir-lime oil during extracted in different temperature control parameters. This part of the analysis consists of Gas Chromatography (GC) and Gas Chromatography-Mass Spectrometry (GC-MS) test toward the experimental sample.

Five marker compounds that fanned out from this analysis have marked for each GCMS result. Data GCMS shows that the main compound in kaffir-lime oil is appeared for all experimental samples. The marker compounds in kaffir-lime oil are α-pinene, sabinene, β-pinene, limonene and citronellal.

Based on two tests conducted, nineteen volatile compounds are identified as tabulated in Table 2. The compound that derives from the kaffir-lime oil start with the compound α-thujene at retention index 0924 and finish by δ-cadinene at retention index 1513. In kaffir-lime oil, there have five marker compounds that contribute to the odour, colour and flavour which are α-pinene, Sabinene, β-pinene, limonene and citronellal varies in between retention index from 0932 until 1148.

During the temperature control at 90^0C, the coefficient of marker compound is relative high except citronellal. For uncontrolled temperature parameter, coefficient of marker compound shows it relative low except the fifth compound which is citronellal contribute high coefficient. In kaffir-lime oil, the quality oil depends on the existing of marker compound that have high coefficient. But, high coefficient of citronellal will affect the odour of kaffir-lime oil with rancid smell. Overall, the quality of kaffir-lime oil is better when the temperature parameter is control compared without temperature control

Conclusion

From the experiment conducted, it can be concluded that by increasing the steam temperature, the oil yield has also been increased. However this increment is not always a good indicator since some of the undesired compound i.e citronelal has also increased. By controlling the steam at lower temperature, it produced high value kaffir-lime marker compound such as α-pinene,sabinene, β-pinene and limonene as compared to the oil without temperature control. It can also be noticed that by applying temperature control technique, citronelal compound can be reduced.

Acknowledgement

This work was conducted on the data gathered at the Faculty of Electrical Engineering, UiTM Shah Alam with the support of Human Resource Department and Research Management Institute UiTM . The authors would also like to express their gratitude to Dr Norazah from Forest Research Institute Malaysia (FRIM) for her advices, detailed and helpful comments.

References

1. M. Khajeh, Y. Yaminib, and S. Shariatic (2010). Comparison of essential oils compositions of Nepeta persica obtained by supercritical carbon dioxide extraction and steam distillation methods. *Food and Bioproducts Processing* 88: 227-232.
2. A. Ammann, D. Hinz, R. Addleman, C. Wai, and B. Wenclawiak (1999). Superheated water extraction, steam distillation and SFE of peppermint oil. *Fresenius' Journal of Analytical Chemistry* 364: 650-653.
3. M. Z. Ozel and H. kaymaz (2004). Superheated water extraction, steam distillation and Soxhlet extraction of essential oils of origanum onites. *Anal Bional Chem* 379: 1127-1133.
4. A. G. Badalyan, G. T. Wilkinson, and B.-S. Chun, (1998). Extraction of Australian ginger root with carbon dioxide and ethanol entrainer. *The Journal of Supercritical Fluids* 13: 319-324.
5. E. E. Stashenko, B. E. Jaramillo, and J. R. MartÄÌ • nez (2004). Comparison of different extraction methods for the analysis of volatile secondary metabolites of Lippia alba (Mill.) N.E. Brown, grown in Colombia, and evaluation of its in vitro antioxidant activity. *Journal of Chromatography A:* 1025: 93-103.
6. A. C. Kimbaris, N. G. Siatis, D. J. Daferera, P. A. Tarantilis, C. S. Pappas, and M. G. Polissiou (2006), Comparison of distillation and ultrasound-assisted extraction methods for the isolation of sensitive aroma compounds from garlic (Allium sativum). *Ultrasonics Sonochemistry* 13: 54-60.

7. H. Ebrahimzadeh, Y. Yamini, F. Sefidkon, M. Chaloosi, and S. M. Pourmortazavi (2003). Chemical composition of the essential oil and supercritical CO2 extracts of Zataria multiflora Boiss. *Food Chemistry* 83: 357-361.
8. E. Cassel and R. M. F. Vargas (2006). Experiments and Modeling of the Cymbopogon winterianus Essential Oil Extraction by Steam Distillation. *J. Mex. Chem. Soc.* 50(3): 126-129.
9. E. Cassel, R. M. F. Vargas, N. Martinez, D. Lorenzo, and E. Dellacassa (2009). Steam distillation modeling for essential oil extraction process. *Industrial Crops and Products* 29: 171-176.
10. A. Doneliana, L. H. C. Carlsonb, T. J. Lopes, and R. A. F. Machado. (2009). Comparison of extraction of patchouli (Pogostemon cablin) essential oil with supercritical CO2 and by steam distillation. *J. of Supercritical Fluids* 48: 15-20.
11. M. Z. Ozel, F. Gogus, J. F. Hamilton, and A. C. Lewis (2005). Analysis of volatile components from Ziziphora taurica subsp. Taurica by steam distillation, superheated-water extraction, and direct thermal desorption with GCxGCTOFMS. *Anal Bioanal Chem* 382: 115-119.
12. L. Ramos1, J. Taberab, L. M. HernaÂndeza, and M. J. GonzaÂlez (1998). Selective extraction of polychlorinated biphenyls from dairy products using steam distillation solvent extraction at normal pressure. *Analytica Chimica Acta* 376: 313-323.
13. J. M. Roldan-Gutierrez, J. Ruiz-Jimenez, and M. D. L. d. Castro (2008). Ultrasound-assisted dynamic extraction of valuable compounds from aromatic plants and flowers as compared with steam distillation and superheated liquid extract *Talant*.
14. F. Sefidkon, M. Dabiri, and A. Rahimi-Bidgoly (1999). The effect of distillation methods and stage of plant growth on the essential oil content and composition of Thymus kotschyanus Boiss. & Hohen *Flavour and Fragrance Journal* 14: 405-408.
15. M. R. Tellez, I. A. Khan, B. T. Schaneberg, S. L. Crockett, A. M. Rimando, and M. Kobaisy (2004). Steam Distillation - Solid-phase Microextraction for The Detection of Ephedra Sinica in Herbal Preparations. *Journal of Chromatography A:* 51-56.
16. G. O. Adegoke and B. A. Odesola (1996). Storage of maize and cowpea and inhibition of microbial agents of biodeterioration using the powder and essential oil of lemon grass (Cymbopogon citratus). *International Biodeterioration and Biodegradation* 37: 81-84.
17. S. Scalia, L. Giuffreda, and P. Pallado (1999). Analytical and preparative supercritical fluid extraction of Chamomile flowers and its comparison with conventional methods. *Journal of Pharmaceutical and Biomedical Analysis* 21: 549-558.
18. F. Chemat, M. E. Lucchesi, J. Smadja, L. Favretto, G. Colnaghi, and F. Visinoni (2006). Microwave accelerated steam distillation of essential oil from lavender: A rapid, clean and environmentally friendly approach. *Analytica Chimica Acta* 555: 157-160.
19. M. Z. Özel and A. A. Clifford, (2004). Superheated water extraction of fragrance compounds from Rosa canina. *Flavour and Fragrance Journal* 19: 354-359.
20. P. Richter, B. Sepulveda, K. C. R. Oliva, and R. Seguel (2003). Screening and determination of pesticides in soil using continuous subcritical water Chromatography-mass spectrometry. *Journal of Chromatography A:* 169-177.
21. V. Louli, G. Folas, E. Voutsas, and K. Magoulas (2004). Extraction of parsley seed oil by supercritical CO2. *The Journal of Supercritical Fluids* 30: 163-174.
22. C. Doneanu and G. Anitescu (1998). Supercritical carbon dioxide extraction of Angelica archangelica L. root oil. *The Journal of Supercritical Fluids* 12: 59-67.
23. J. M. Rold´an-Guti´errez, J. Ruiz-Jim´enez, and M. D. L. d. Castro (2008). Ultrasound-assisted dynamic extraction of valuable compounds from aromatic plants and flowers as compared with steam distillation and superheated liquid extraction. *Talanta* 75: 1369–1375.
24. P. Masango (2005). Cleaner production of essential oils by steam distillation. *Journal of Cleaner Production* 13: 833-839.
25. M. Tajjudin, N. Ishak, M. H. F. Rahiman, N. M. Arshad, R. Adnan, and H. Ismail (2012). Steam temperature regulation with self-tuning PID based on pole-assignment method, in *Signal Processing and its Applications (CSPA), 2012 IEEE 8th International Colloquium on*, pp. 174-177.
26. N. Tajjudin, Z. Yusuf, M. H. F. Rahiman, and M. N. Taib (2010). Self tuning PID controller for steam distillation essential oil extraction system, in *Signal Processing and Its Applications (CSPA), 2010 6th*

International Colloquium on, pp. 1-4.
27. N. Kasuan, Z. Yusuf, M. N. Taib, M. H. F. Rahiman, N. Tajuddin, and M. A. A. Aziz (2010). Robust Steam Temperature Regulation for Distillation of Essential Oil Extraction Process using Hybrid Fuzzy-PD plus PID Controller. *World Academy of Science, Engineering and Technology* 71: 927 -932.
28. Z. Muhammad, Z. M. Yusoff, M. N. N. Nordin, M. H. F. Rahiman, and M. N. Taib (2012). Implementation of real -time steam temperature control for high efficient induction- based extraction essential oil using hybrid fuzzy-PD plus PID controller, in *Control and System Graduate Research Colloquium (ICSGRC), 2012 IEEE*, pp. 282-287.
29. N. Threesinghawong, P. Sanposh, N. Chinthaned, and P. Srinophakun (2008). Temperature control of Koji process by using fuzzy PD controller, in *Electrical Engineering/Electronics, Computer, Telecommunications and Information Technology, 2008. ECTI-CON 2008. 5th International Conference on*, 2008, pp. 669-672.
30. Hisbullah, M. A. Hussain, and K. B. Ramachandran (2003). Design of a Fuzzy Logic Controller for Regulating Substrate Feed to Fed-Batch Fermentation. *Food and Bioproducts Processing* 81: 138-146.
31. N. Kasuan, M. Yunus, M. H. F. Rahiman, S. R. S. Aris, and M. N. Taib (2009). Essential oil composition of Kaffir lime: Comparative analysis between controlled steam distillation and hydrodistillation extraction process," in *Research and Development (SCOReD), 2009 IEEE Student Conference on*, pp. 479-482.

The Malaysian Journal of Analytical Sciences Vol 17 No 3 2013

Page

1. ANALYTICAL METHOD DEVELOPMENT AND VALIDATION FOR SIMULTANEOUS ESTIMATION OF ARTEMETHER AND LUMEFANTRINE IN PURE AND PHARMACEUTICAL DOSAGE FORM USING RP-HPLC METHOD 348
(Pembangunan dan Validasi Kaedah Analisis bagi Anggaran Serentak Artemether dan Luefantrine dalam Keadaan Tulen dan Dos Farmaseutikal Mengunakan Kaedah KCPT-Fasa Terbalik)
Mannur Vinodh, Mastiholimath Vinayak, Patware Pankaj, Kharya Rahul and Mascarenhas Renita

2. EXTRACTION OF CITRUS HYSTRIX D.C. (KAFFIR LIME) ESSENTIAL OIL USING AUTOMATED STEAM DISTILLATION PROCESS: ANALYSIS OF VOLATILE COMPOUNDS 359
(Pengekstrakan Minyak Citrus Hystrix D.C. (Limau Purut) Menggunakan Kaedah Penyulingan Wap Automatik: Analisa Komposisi Hasil Minyak)
Nurhani Kasuan, Zuraida Muhammad, Zakiah Yusoff, Mohd Hezri Fazalul Rahiman, Mohd Nasir Taib, Zaibunnisa A. Haiyee

3. EFFECT OF ESSENTIAL OIL OF ATTARASA LEAVES (Litsea cubeba Lour. Pers) ON PHYSICO-MECHANICAL AND MICROSTRUCTURAL PROPERTIES OF BREADFRUIT STARCH-ALGINATE EDIBLE FILM 370
(Kesan Pati Minyak Daun Attarasa (Litsea Cubeba Lour. Pers) ke atas Sifat Fiziko-Mekanikal dan Mikrosturktur Pati Sukun-Alginat Filem yang boleh dimakan)
Cut Fatimah Zuhra, Jamaran Kaban, Marpongahtun and Erman Munir

4. KAJIAN AWAL PENGGUNAAN JARINGAN NEURAL TIRUAN (ANN) BAGI MENENTUKAN NILAI PEROKSIDA TIGA MINYAK SAWIT KOMERSIL BERDASARKAN SPEKTRUM FTIR 376
(Preliminary Study on Application of Artificial Neural Networks (ANN) for Determining the Peroxide Value of Three Commercial Palm Oil Based FTIR Spectrum)
Azwan Mat Lazim, Musa Ahmad, Zuriati Zakaria, M. Suzeren Jamil Suria Ramli, Faiz Zainuddin, Mohd Nasir Taib, M. Nasir Mat Arip

5. DEVELOPMENT AND VALIDATION OF RP-HPLC METHOD FOR THE ESTIMATION OF CLOPIDOGREL BISULPHATE 387
(Pembangunan dan Penentusahkan Kaedah RP-HPLC Terhadap Klopidogrel Bisulfat)
Bhagat Dimple, Mannur Vinodh, Mastiholimath Vinayak

6. DETERMINATION OF ANILINE DEGRADED FROM SUDAN I IN CLOTHS 394
(Penentuan Anilin Yang Terurai Daripada Sudan I Dalam Kain)
Chong Kian Wei, Loke Chui Fung and Chan Kar Men

7. ANALYSIS OF HIGH QUALITY AGARWOOD OIL CHEMICAL COMPOUNDS BY MEANS OF SPME/GC-MS AND Z-SCORE TECHNIQUE 403
(Analisa Bahan Minyak Gaharu Berkualiti Tinggi Dengan Cara Z-Score)
Nurlaila Ismail, Mohd Ali Nor Azah, Mailina Jamil, Mohd Hezri Fazalul Rahiman, Saiful Nizam Tajuddin, Mohd Nasir Taib

8. SYNTHESIS OF RUBBER SEED OIL AND TRIMETHYLOLPROPANE BASED BIOLUBRICANT BASE STOCKS 414
(Penghasilan Stok Asas Biopelincir Berasaskan Minyak Biji Getah dan Trimetilolpropana)
Ainaatul Asmaa' Ishak and Jumat Salimon

9. PREPARATION AND ACTIVATION OF SPIROPYRAN-MEROCYANINE SYSTEM 422
(Penyediaan dan Pengaktifan bagi Sistem Spiropiran-Merosianin)
Rumaisa Nordin, Azwani Mat Lazim, Atisya Rohadi, Siti Aishah Hasbullah

10. ISOLATION OF ASTILBIN FROM LEAVES OF CRATOXYLUM ARBORESCENS 430
(Pemencilan Komponen Astilbin dari Daun Cratoxylum arborescens)
Samsiah Jusoh, Zuriati Zakaria and Laily B. Din

11. DETERMINATION OF HOT SPRINGS PHYSICO-CHEMICAL WATER QUALITY POTENTIALLY USE FOR BALNEOTHERAPY 436
(Penentuan Kualiti Fizik-Kimia Air Kolam Air Panas Yang Berpotensi Digunakan Untuk Balneoterapi)
Zaini Hamzah, Nurul Latiffah Abd Rani, Ahmad Saat and Ab Khalik Wood

12. MORPHOLOGICAL CHARACTERIZATION OF PHOTOSYNTHETIC MICROBIAL GRANULE FROM PALM OIL MILL EFFLUENT (POME) 445
(Pencirian Morfologi Granul Mikrob Fotosintetik Daripada Efluen Kilang Minyak Sawit (POME))
M.Z. Mohamed Najib, Z. Ujang, Salmiati

13. THE EFFECT OF GAMMA IRRADIATION ON THE CHEMICAL STRUCTURE AND SURFACE CHARACTERISTICS OF DIPALMITOYLPHOSPHATIDYLCHOLINE (DPPC) 454
(Kesan Sinaran Gama ke atas Struktur Kimia dan Ciri Permukaan Dipalmitoilfosfatidilkolina (DPPC))
Hur Munawar Kabir Mohd, Ainee Fatimah Ahmad, Faizal Mohamed, Nursaidatul Syafadillah Kamaruzaman, Ng Wei Ling, Poh Roe Jin, Muhamad Samudi Yasir, Mohd Hafez Mohd Isa, Suria Ramli, Shahidan Radiman and Irman Abdul Rahman

14. MINERALOGICAL RESPONSE OF THE POSTHARVEST MANGO (MANGIFERA INDICA L.) TO DIFFERENT LEVELS OF BAVISTIN DF 461
(Tindak balas Minerologi Lepas Tuai Terhadap Mangga (Mangifera Indica L.) Pada Tahap Bavistin DF Berbeza)
Md. K. Islam, N. Absar, M. A. R. Sarkar, M. Z. H. Khan, S. Yeasmin and K. A. Hakim

15. GRAPHENE COLLOIDAL DISPERSION IN VARIOUS ORGANIC SOLVENTS 475
(Penyerakan Koloid Grafin dalam Pelbagai Pelarut Organik)
Ainee Fatimah Ahmad, Fatin Humaizah Abd Moin, Hur Munawar Kabir Mohd, Irman Abdul Rahman, Faizal Mohamed, Chia Chin Hua, Suria Ramli, Shahidan Radiman

16. SYNTHESIS AND CHARACTERIZATION OF pH SENSITIVE HYDROGEL USING EXTRACTED PECTIN FROM DRAGON FRUIT PEEL 481
(Sintesis Dan Pencirian Hidrogel pH-Sensitif Berasaskan Ekstrak Pektin Kulit Buah Naga)
Azwan Mat Lazim, Farahain Mokhtar, Siti Fairus Mohd Yusof, Ishak Ahmad, Adil Hakam

17. DIFFERENTIATING AGARWOOD OIL QUALITY USING ARTIFICIAL NEURAL NETWORK 490
(Perbezaan Kualiti Minyak Gaharu Menggunakan Rangkaian Neural Tiruan)
Nurlaila Ismail, Nor Azah Mohd Ali, Mailina Jamil, Mohd Hezri Fazalul Rahiman, Saiful Nizam Tajuddin and Mohd Nasir Taib

18. POSTHARVEST QUALITY OF MANGO (MANGIFERA INDICA L.) FRUIT AFFECTED BY DIFFERENT LEVELS OF GIBBERELLIC ACID DURING STORAGE 499
(Kesan Kandungan Asid Giberelik Berbeza ke atas Kualiti Buah Mangga (Mangifera Indica L.) Lepas Tuai Semasa Penyimpanan)
Md. K. Islam, M. Z. H. Khan, M. A. R. Sarkar, S. Yeasmin, Md. K. Ali, M. H. Uddin

The Malaysian Journal of ANALYTICAL SCIENCES ISSN 1394-2506

ANALYTICAL METHOD DEVELOPMENT AND VALIDATION FOR SIMULTANEOUS ESTIMATION OF ARTEMETHER AND LUMEFANTRINE IN PURE AND PHARMACEUTICAL DOSAGE FORM USING RP-HPLC METHOD

(Pembangunan dan Validasi Kaedah Analisis bagi Anggaran Serentak Artemether dan Luefantrine dalam Keadaan Tulen dan Dos Farmaseutikal Mengunakan Kaedah KCPT-Fasa Terbalik)

Mannur Vinodh*, Mastiholimath Vinayak, Patware Pankaj, Kharya Rahul and Mascarenhas Renita

Department of Quality Assurance,
KLE University's College of Pharmacy, Belgaum- 590 010, Karnataka, India

**Corresponding author: vinodhmannur@yahoo.com*

Abstract

A simple, rapid, precise and cost effective reversed phase-high performance liquid chromatography (RP-HPLC) method was developed for the simultaneous estimation of Artemether (AT) and Lumefantrine (LU) in pure drug and pharmaceutical dosage forms. The separation was carried out using BDS Hypersil C18 (150 × 4.6 mm i.d. 3 µm particle size) column, with mobile phase comprising of 0.01M tetra butyl ammonium hydrogen sulphate and acetonitrile in the ratio of 20 : 80 (v/v). The flow rate was 1.0ml/min and the detection was carried out using UV-visible detector at 222 nm. The method was validated by evaluation of different parameters such as accuracy, precision, linearity, ruggedness, and robustness, limit of detection (LOD) and limit of quantification (LOQ). The retention time were found to be 4.19 and 5.22 min for AT and LU, respectively. Correlation coefficient (r^2) of 0.999 for both over concentration range of 3.2-19.2µg/ml and 16-96µg/ml for AT and LU, respectively. Parameters like mobile phase ratio, wavelength, flow rate, etc. were deliberately varied. It was observed that there were no marked changes in chromatograms, which demonstrated that the developed RP-HPLC method is robust. Intra and inter day precision reproducibility study was carried out and it was checked by determining precision on the same instrument, but by a different analyst. The percentage recovery for AT and LU were ranged between 99.18-100.19 and 99.96-100.07, respectively. The LOD for AT and LU were found to be 0.201 and 2.99 µg/ml and the LOQ were 0.609 and 9.086 µg/ml respectively. Method was found to be reproducible with relative standard deviation (RSD) for intra and inter day precision less than 2%.

Keywords: Artemisinin-Based Combination Therapy, Artemether, Lumefantrine, High Performance Liquid Chromatography (HPLC), Validation.

Abstrak

Satu kaedah kromatografi cecair berprestasi tinggi (HPLC) – fasa terbalik yang mudah, cepat, tepat dan kos efektif telah dibangunkan bagi anggaran serentak Artemether (AT) dan Lumefantrine (LU) di dalam ubat-ubatan bentuk tulen dan dos farmaseutikal. Pemisahan dilakukan menggunakan turus BDS Hypersil C18 (150 × 4.6 mm i.d 3 partikel saiz), dengan fasa bergerak terdiri daripada 0.01M tetra butyl ammonium hidrogen sulfat dan asetonitril pada nisbah 20:80 (v/v). Kadar aliran adalah 1.0 ml/min dan pengesanan dibuat menggunakan pengesan UV yang boleh diukur pada 222 nm. Kaedah divalidasi oleh ujian penilaian parameter yang berbeza seperti ketepatan, kejituan, linear, kekasapan dan keteguhan, had pengesanan (LOQ) dan had kuantifikasi (LOQ). Masa pengekalan didapati pada minit 4.19 dan 5.22 masing – masing untuk AT dan LU. Pekali korelasi (r^2) 0.999 kedua-duanya pada julat kepekatan masing – masing 3.2 - 19.2µg/ml dan 16 - 96µg/ml bagi AT dan LU. Parameter seperti nisbah fasa bergerak, panjang gelombang, kadar aliran, dan lain-lain telah dijalankan. Diperhatikan bahawa tiada terdapat sebarang perubahan ketara bagi kromotogram, yang membuktikan bahawa kaedah fasa terbalik-KPCT ini adalah baik kadar kekasapannya. Ujian kebolehulangan inter dan intra hari telah dijalankan dan ia adalah ketepatan telah ditentukan pada instrumen yang sama oleh penganalisa berbeza. Perolehan semula bagi AT dan LU adalah masing – masing di antara 99.18 -

100.19 dan 99.96 - 100.07. Had pengesanan, LOD bagi AT dan LU didapati pada 0.201 dan 2.99 µg/ml dan LOQ masing-masing adalah 0.609 dan 9.086 µg/ml. Kaedah ini didapati nilai kebolehulangannya dengan kejituan sisihan piawai relatif (RSD) bagi intra dan inter – hari kurang daripada 2%.

Kata kunci: Kombinasi terapi berasaskan-artemisinin, Artemether, Lumefantrine, kromatografi cecair prestasi tinggi (KCPT), Validasi

Introduction

Due to the widespread resistance of *Plasmodium falciparum* to conventional antimalarial drugs, many countries are facing problems regarding the treatment of uncomplicated malaria [1]. The main therapy now recommended by the World Health Organization (WHO) is artemisinin-based combination therapy (ACT), a combination of an artemisinin derivative and another structurally-unrelated and slowly-eliminated antimalarial lumefantrine [2]. The advantages of ACT relates to the properties of artemisinin compounds, which include rapid reduction of the parasite biomass with fast resolution of clinical symptoms, effectiveness against multidrug-resistant *falciparum* malaria, resistance not being documented yet, and a good safety profile. They also reduce gametocyte carriage, which in some settings may lower malaria transmission [3]. Artemether is chemically (3R,5aS,- 6R,8aS,9R,10S,12R,12aR)-Decahydro-10-methoxy- 3,6,9- trimethyl- 3,12-epoxy-12H-pyrano [4,3-j]-1,2- benzodioxepin[4] and is used as antimalarial agent. Lumefantrine is chemically 2, 7-Dichloro-9-[(4- chlorophenyl) methylene]-α-[(dibutylamino) methyl] - 9H-fluorene-4-methanol [5] and is used in the treatment of uncomplicated *falciparum* malaria.

Artemether-lumefantrine (AT-LU) (Figure 1) is the most common ACT used in malaria endemic areas. The rationale is that Artemether will rapidly reduce parasitaemia, resulting in symptomatic relief, and Lumefantrine will eliminate the remaining parasites [6]. WHO recommends this combination as first line therapy for *falciparum* malaria in endemic areas [7]. Increasing use of (AT-LU) combination as an effective treatment for malaria demands the need of analytical methods to simultaneously quantify these drugs in tablets in order to evaluate its quality. Some of the studies have described the analysis of AT in plasma, based on HPLC with electrochemical [8, 10] or mass spectrometry detection [11]. Few methods are available to assay AT in pharmaceutical products [12, 13]. The quantitative determination of lumefantrine in plasma has been described using HPLC with UV detection [14, 15]. However, there is lack of methods regarding the simultaneous quantitation of AT and LU. Hence, the aim of this study was to develop and validate a reversed phase-high performance liquid chromatography (RP-HPLC) method, using UV detection, to simultaneously quantify Artemether and Lumefantrine in fixed dose combination tablets. The structure of Artemether and Lumefantrine is as shown below in Figure 1.

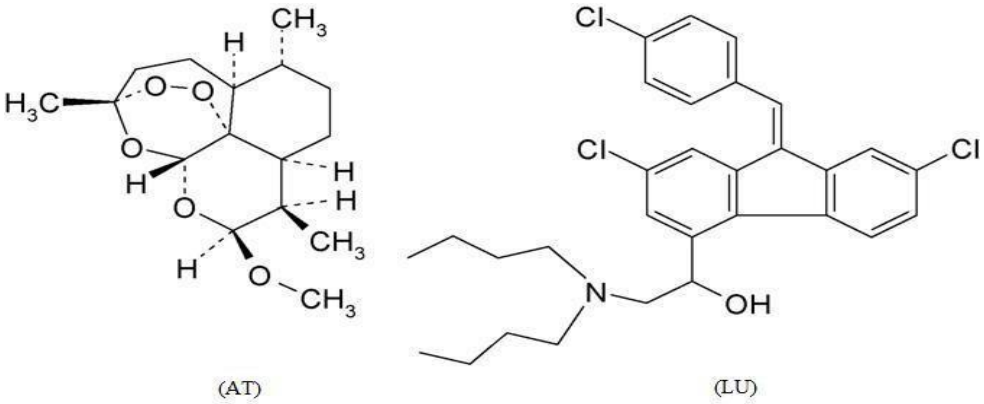


Figure 1. Structure of Artemether and Lumefantrine

Materials and Methods

Reagents

AT and LU reference standards were obtained as a gift sample from Ipca Pvt ltd. Mumbai. Market formulation LUMERAX-80 (AT and LU, combination) from Ipca Laboratories Ltd, Ratlam with a label claim of 80mg AT and 480mg LU, was purchased. Tetra butyl ammonium hydrogen sulphate of analytical-reagent grade was purchased from Leonil Chemicals Pvt Ltd, Bangalore, India. HPLC grade acetonitrile (ACN) and water were purchased from Merck Specialities Pvt Ltd, Mumbai. All buffers and solutions were prepared with HPLC grade water.

Instrumental

The separation was carried out using A HPLC unit that consisted of a LC-20AT Shimadzu pumps combined with a SPD-20A Prominence UV-VIS detector. The column used was BDS Hypersil C-18 (150×4.6mm i.d.; 3µm particle size). Analyte weighing was done on a microbalance, Shimadzu AY220. All mobile phase solutions were degassed ultrasonically by "Fast Clean" sonicator before use. The HPLC system was controlled by a PC workstation using Spinchrom software.

Chromatographic conditions

The HPLC was operated under isocratic elution with acetonitrile-0.01M tetrabutylammonium hydrogen sulphate buffer (80:20, v/v) as a mobile phase at a flow rate of 1.0 ml/min. The mobile phase was premixed, filtered through a 0.45 µm membrane filter to remove any particulate matter and degassed by sonication before use. The separation of AT and LU was good enough (Figure 2) and further it was free from any interference at 222 nm. Hence, the eluted peaks were detected at 222 nm for both, AT and LU. Moreover, the effects at different levels of all these factors were systematically addressed on system suitability parameters such as resolution, theoretical plates, retention time, separation factor, asymmetry, and Height Equivalent to Theoretical Plate (HETP) etc.

Preparation of buffer

Dissolve 0.33954 gm of tetra butyl ammonium hydrogen sulphate in small amount of distilled water, transferred into 100ml volumetric flask and made up to the final volume with HPLC grade water.

Preparation of mobile phase

200ml (20%) of the above buffer was mixed with 800 ml of acetonitrile (80%). Mobile phase will be filtered first using 0.45 µm membrane filter and then degassed in an ultrasonic water bath for 5 minutes prior to use.

Diluent Preparation

Mobile phase [0.01M tetra butyl ammonium hydrogen sulphate & acetonitrile (20:80%v/v)] used as a diluent.

Standard solution preparation

Accurately weighed and transferred 4mg of AT reference standard and 24mg of LU reference standard to 25ml volumetric flask, added appropriate quantity of diluent and sonicated to dissolve it completely and the volume was made up to the mark with the same diluent, to obtain a solution of 160µg/ml of AT and 960µg/ml of LU, resultant solution was ultra sonicated for 5min and filtered through 0.45µ filter paper.

Sample solution preparation

Five tablets of AT and LU were weighed and finely powdered. A quantity equivalent to 4mg of AT and 24mg of LU was transferred into 25 ml volumetric flak and appropriate amount of diluent was added. The contents were sonicated to dissolve AT and LU completely and the volume was made up to the mark with diluent and filtered through 0.45µm membrane filter.

Results and Discussion

Optimization of chromatographic conditions

The mobile phase conditions, such as the type and composition of the organic modifiers significantly affect the chromatographic separation, therefore before selecting the conditions for optimization, a number of preliminary trials were conducted with different combinations of different organic solvents and buffers at various pH, mobile phase compositions and flow rate to check the retention time, shape, resolution, and other chromatographic parameters. The chromatographic parameters were initially evaluated using a inertsil ODS C18 (150x4.6; 5µ)

column and a mobile phase composed of acetonitrile and water (50:50), since no peaks were obtained for both the drugs, thus water was replaced by a tetra butyl ammonium hydrogen sulphate (0.01 M). Mixture of acetonitrile and tetra butyl ammonium hydrogen sulphate buffer in different ratios (60:40, 70:30 and 80:20) was tried as mobile phase. From those experiments the mobile phase combination of acetonitrile and tetra butyl ammonium hydrogen sulphate buffer in the ratio of 80:20 was found to be more appropriate.

The retention time obtained for AT and LU is 4.19 and 5.22 respectively thus indicating the developed method is rapid compared to T.M Kalyankar *et al* method having retention time of 6.15 min and 11.31min, for AT and LU respectively [16], The retention times of Artemether and Lumefantrine were 13.888 min and 7.207 min respectively in Sridhar B. *et al* method [17]. The retention times were 13.887 and 7.218 mins for Artemether and Lumefantrine, respectively in Sunil J. *et al* method [18].Thus proving the developed method to be more cost effective, rapid and precise. A typical chromatogram of Artemether and Lumefantrine is as shown in Figure 2.

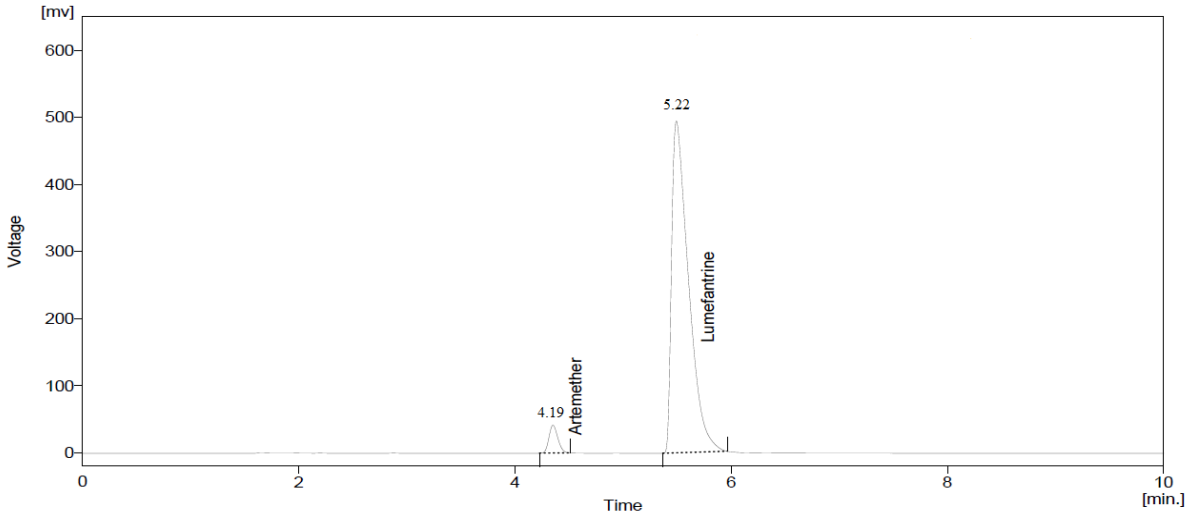


Figure 2. A typical chromatogram of Artemether and Lumefantrine

Method Validation

Once the chromatographic method was developed and optimized, it must be validated. After optimization of the chromatographic conditions, the parameters of linearity, precision, accuracy, ruggedness, robustness, limit of detection and limit of quantitation were evaluated to validate the process. The validation of an analytical method verifies that the characteristics of the method satisfy the requirements of the application domain. The proposed method was validated as per ICH Guidelines [19].

System suitability

System suitability tests are an integral part of chromatographic method. They were used to verify the adequate reproducibility of chromatographic system for analysis. To ascertain its effectiveness, system suitability tests were carried out on freshly prepared standard stock solution of Artemether and Lumefantrine and the parameters like column efficiency, resolution, peak area and tailing factor of the peaks were calculated. For all the samples analyzed, the efficiency, %RSD and USP tailing factor were found to be $\geq$ 2000 theoretical plates, $\leq$ 2% and $\leq$ 2 respectively. System suitability test results are as shown in Table 1.

Table 1. System suitability test for Artemether and Lumefantrine

Artemether				Lumefantrine			
Area (mV)	**RT**	**TF**	**TP**	**Area (mV)**	**RT**	**TF**	**TP**
1448.917	4.190	1.258	5755	3994.438	5.227	1.538	5037

Linearity

The standard solutions containing 3.2 µg/ml to 19.2 µg/ml of AT and 19.2 µg/ml to 115.2µg/ml of LU in each linearity level were prepared and injected. In the simultaneous determination, the calibration curves were found to be linear for both the analytes in the mentioned concentrations. The analytical curve with peak area versus concentration was plotted and the obtained data were subjected to regression analysis. The coefficient of correlation (r^2) was found to be 0.999 for AT and LU. Calibration curve of Artemether and Lumefantrine at 222 nm is shown in Figure 3 and 4 respectively and linearity result for Artemether and Lumefantrine is as shown in Table 2 and Table 3 respectively.

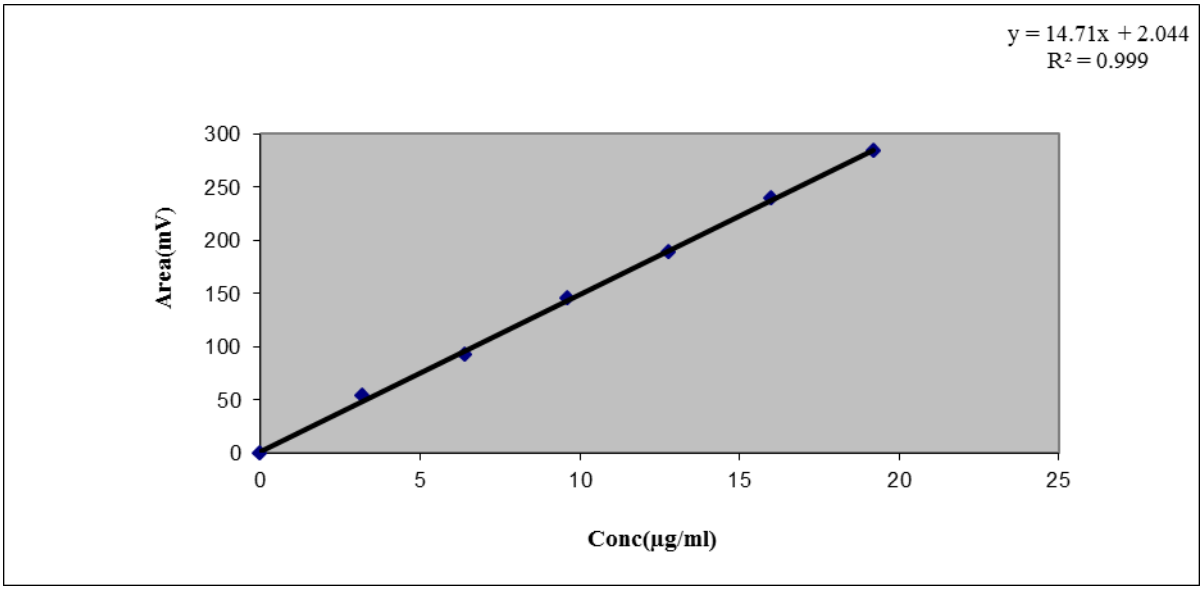


Figure 3. Calibration curve of Artemether at 222 nm

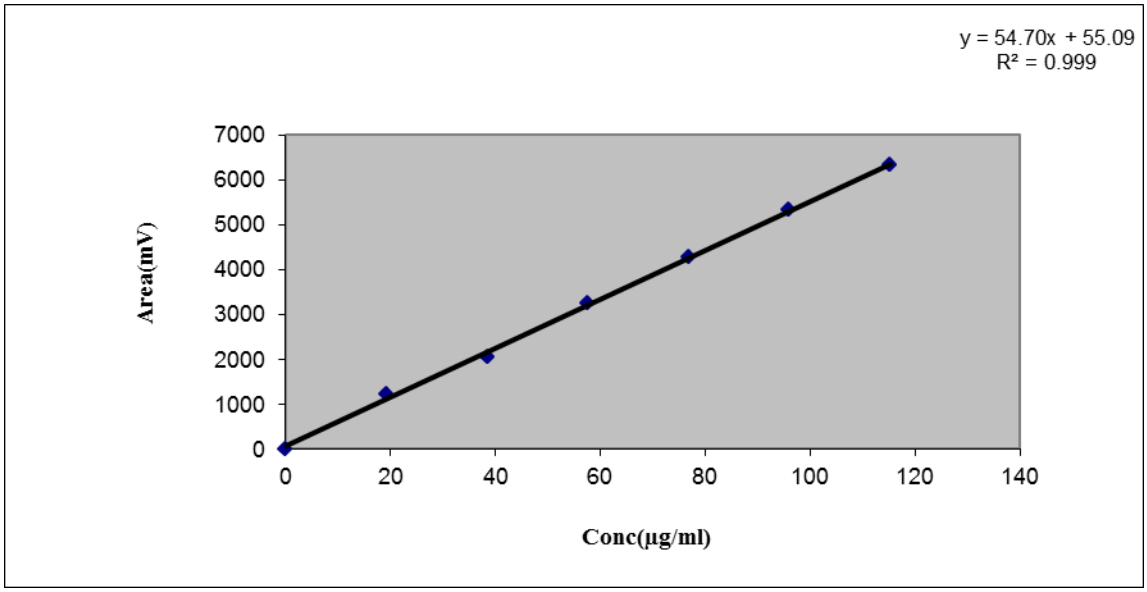


Figure 4. Calibration curve of Lumefantrine at 222 nm

Table 2. Linearity result for Artemether

Sample No.	Concentration(µg/ml)	Area(mV)
1	19.2	1222.24
2	38.4	2048.86
3	57.6	3236.65
4	76.8	4283.97
5	96.0	5331.53
6	115.2	6317.87

Table 3. Linearity result for Lumefantrine

Sample No.	Concentration (µg/ml)	Area(mV)
1	3.2	53.537
2	6.4	92.728
3	9.6	144.805
4	12.8	189.063
5	16.0	239.394
6	19.2	283.343

Precision

The precision of the method was demonstrated by inter-day and intra-day variation studies. The intra-day precision was evaluated by injecting six times each of the standard solution i.e.16µg/ml of AT and 96µg/ml of LU. Similarly, the inter-day precision was evaluated in five consecutive days. The AT and LU concentrations were determined and the relative standard deviations (R.S.D.) were calculated. Intra-day and Inter-day precision result for Artemether and Lumefantrine is as shown in Table 4 and Table 5 respectively.

Table 4. Intra-day precision result for Artemether and Lumefantrine

Injection No.	**Artemether**		**Lumefantrine**	
	Area(mV)	**RT**	**Area(mV)**	**RT**
1	238.008	4.343	5372.668	5.490
2	238.749	4.360	5373.642	5.513
3	241.630	4.357	5373.611	5.510
4	240.339	4.340	5367.166	5.487
5	238.402	4.350	5365.531	5.493
Average	239.426	4.35	5370.524	5.499
SD	1.517	0.0086	3.874	0.012
% RSD	0.630	0.190	0.072	0.210

Table 5. Inter-day precision result for Artemether and Lumefantrine

Injection No.	**Artemether**		**Lumefantrine**	
	Area(mV)	**RT**	**Area(mV)**	**RT**
1	241.313	4.353	5477.071	5.487
2	241.049	4.33	5376.734	5.46
3	239.156	4.347	5374.384	5.487
4	240.222	4.353	5361.259	5.493
5	239.739	4.343	5357.487	5.487
Average	240.296	4.345	5389.387	5.483
SD	0.897	0.009	49.705	0.013
%RSD	0.370	0.220	0.920	0.240

Accuracy

For studying the accuracy of the proposed analytical method, and for detecting the interference from excipients used in the dosage forms, recovery experiments were carried out by the standard addition method. Known concentration of working standard was added to the fixed concentration of the pre-analyzed tablet solution. Percent recovery was calculated by comparing the area before and after the addition of working standard. For both the drugs, recovery was performed in the same way. The recovery studies were performed in triplicate. At 80%, 100% and 120% level and the percentage recovery was calculated. Percent recovery indicates that the method was accurate. Recovery results for Artemether and Lumefantrine is as shown in Table 6 and Table 7 respectively.

Table 6. Recovery results for Artemether

Accuracy level (%)	Amount added in µg	Area	Amount recovered in µg (Average)	% Recovery (Average)	SD	%RSD
80	14.4	218.152	14.29	99.25	1.511	0.697
100	17.6	264.151	17.46	99.18	0.815	0.308
120	20.8	316.796	20.84	100.19	1.732	0.548

Table 7. Recovery results for Lumefantrine

Accuracy level	Amount added in µg	Area	Amount recovered in µg (Average)	% Recovery (Average)	SD	%RSD
80	86.4	4831.711	86.46	100.07	3.517	0.072
100	105.6	5908.646	105.62	100.02	3.360	0.056
120	124.8	6978.117	124.75	99.96	5.604	0.080

Sensitivity

LOD and LOQ were estimated from the signal-to-noise ratio. The LOD for AT and LU were found to be 0.201 and 2.99 µg/ml and the LOQ were 0.609 and 9.086 µg/ml respectively.

Ruggedness (Reproducibility)

In addition to intra and inter day precision reproducibility study was also carried out and it was checked by determining precision on the same instrument, but by a different analyst. Results for Ruggedness are shown in Table 8.

Table 8. Ruggedness studies of Artemether and Lumefantrine

	Artemether		**Lumefantrine**	
Sample No.	**Analyst 1 Area(mV)**	**Analyst 2 Area(mV)**	**Analyst 1 Area(mV)**	**Analyst 2 Area(mV)**
1	238.008	238.749	5372.668	5373.642
2	237.894	238.344	5373.374	5299.893
3	238.016	237.995	5354.612	5362.331
Average	237.972	238.362	5366.884	5345.288
SD	0.068	0.377	10.634	39.718
% RSD	0.028	0.158	0.198	0.743

Robustness

To evaluate robustness of the developed method, few parameters like mobile phase ratio, wavelength, flow rate, etc. were deliberately varied. It was observed that there were no marked changes in chromatograms, which demonstrated that the developed RP-HPLC method is robust. Robustness results for Artemether and Lumefantrine is as shown in Table 9 and Table 10 respectively.

Table 9. Robustness results for Artemether

Condition	**Modification**	**Mean Area ± SD***	**% RSD**
Flow Rate (ml/min)	0.9	269.590 ± 1.35	0.50
	1.0	240.079 ± 0.968	0.403
	1.1	219.149 ± 0.543	0.247
Wavelength (nm)	220	262.031 ± 0.632	0.241
	222	240.079 ± 0.968	0.403
	224	217.075 ± 0.725	0.333

* Average of three determinations.

Table 10. Robustness results for Lumefantrine

Condition	Modification	Mean Area ± SD*	% RSD
Flow Rate (ml/min)	0.9	6080.142 ± 82.522	1.357
	1.0	5364.53 ± 46.67	0.869
	1.1	4801.298 ± 6.624	0.137
Wavelength (nm)	220	5349.852 ± 4.492	0.083
	222	5364.53 ± 46.67	1.357
	224	5704.685 ± 11.54	0.202

*Average of three determinations.

Conclusion

Considering the increasing use of ACT to treat malaria in endemic areas, the availability of simple and rapid analytical method is essential to evaluate the quality of formulas being used currently. From the present study it can be concluded that the optimized and validated RP-HPLC method was simple, sensitive, precise, accurate and reproducible, hence it can be used in routine analysis for the simultaneous determination of Artemether and Lumefantrine in bulk as well as in pharmaceutical preparations.

Acknowledgement

The authors are grateful to Chandra Labs, Analytical research laboratory, Hyderabad, (A.P.), India for providing the facilities to carry out this research work.

References

1. Martensson, J., Stromberg, C., Sisowath, M. I., Msellem, J. P., Gil, S. M., Montgomery, P., Olliaro, A. S., Ali. & A., (2005). Efficacy of artesunate plus amodiaquine versus that of artemether-lumefantrine for the treatment of uncomplicated childhood Plasmodium falciparum malaria in Zanzibar, Tanzania, *Clin. Infect. Dis*. 41: 1079 – 1086.
2. WHO (2001). Antimalarial *Drug Combination Therapy. Report of a WHO Technical Consultation, 4-5 April,* (WHO/CDS/RBM/2001.35). Geneva: WHO.
3. Nosten, F. & White, N.J., (2007). Artemisinin based combination treatment of falciparum malaria, Am. *J. Trop. Med. Hyg*. 77: 181 – 192.
4. Martindale: The complete drug reference 36th edition, Pharmaceutical press, Lambeth High Street, London, (2009); 598 - 599.
5. Martindale: The complete drug reference 36th edition, Pharmaceutical press, Lambeth High Street, London, (2009); 605.
6. Omari, A.A., Gamble, C. & Garner, P., (2004). Artemether-lumefantrine for uncomplicated malaria: a systematic review, *Trop. Med. Int. Health*. 9: 192 – 199.
7. World Health Organization, WHO Expert Committee on Malaria, 20th Report, WHO Technical Report Series – 892, Geneva, 2000; 71.
8. Navaratnam, V., Mansor, S.M., Chin, L.K., Mordi, M.N., Asokan, M., Nair & N.K., (1995). Determination of artemether and dihydroartemisinin in blood plasma by high-performance liquid chromatography for application in clinical pharmacological studies, *J. Chromatogr. B*, 669: 289 – 294.

9. Karbwang, J., Na-bangchang, K., Molunto, P., Banmairuroi, V. & Congpuong, K., (1997). Determination of artemether and its major metabolite, dihydroartemisinin, in plasma using high-performance liquid chromatography with electrochemical detection, *J. Chromatogr. B*, 690: 259 – 265.
10. Sandrenan, A., Sioufi, J., Godbillon, C., Netter, M., Donker, V. & Valkenburg., (1997). Determination of artemether and its metabolite, dihydroartemisinin, in plasma by high-performance liquid chromatography and electrochemical detection in the reductive mode, *J. Chromatogr. B*, 691: 145 – 153.
11. Souppart, C., Gauducheau, N., Sandrenan, N. & Richard, F., (2002). Development and validation of a high-performance liquid chromatography-mass spectrometry assay for the determination of artemether and its metabolite dihydroartemisinin in human plasma, *J. Chromatogr. B*, 774: 195 – 203.
12. Green, M.D., Mount, D.L. & Wirtz, R.A., (2001). Authentication of artemether, artesunate and dihydroartemisinin antimalarial tablets using a simple colorimetric method, *Trop. Med. Int. Health*, 6 : 980 – 982.
13. Atemnkeng, M.A., De Cock, K. & Plaizier-Vercammen, J., (2007). Quality control of active ingredients in artemisinin derivative antimalarials within Kenya and DR Congo, *Trop. Med. Int. Health*, 12: 68 – 74.
14. Mansor, S.M., Navaratnam, V., Yahaya, N., Nair, N.K., Wernsdorfer, W.H. & Degen, P.H., (1996). Determination of a new antimalarial drug, benflumetol, in blood plasma by high-performance liquid chromatography, *J. Chromatogr*. B, 682: 321 – 325.
15. César I, Nogueira F. & Pianetti G, (2008). Simultaneous determination of artemether and lumefantrine in fixed dose combination tablets by HPLC with UV detection, *J. of Pharm. Biomed. Analysis*. 45: 951 - 954.
16. Kalyankar T.M. & Kakde R.B. (2011) Reversed-phase liquid chromatographic method for simultaneous determination of artemether and lumefantrine in pharmaceutical preparation. *International Journal of ChemTech Research*, 3(3): 1722 - 1727.
17. Sridhar B., Rao K.H., Srinivas T.V.S., Madhuri V.S., Madhuri K. & Rao J.V.L.N.S.(2010). A validated reverse phase hplc method for the simultaneous estimation of artemether and lumefantrine in pharmaceutical dosage forms. *An International Journal of Advances In Pharmaceutical Sciences* 1(1): 95 - 99.
18. Sunil J., Nath M.S., .M & Moorthy U.S. (2010) HPLC method development and validation for simultaneous estimation of artemether and lumefantrine in pharmaceutical dosage forms. *International Journal of Pharmacy and Pharmaceutical Sciences.* 2(4): 93 - 96.
19. CMPM/ICH/381/95, ICH Topic Q2B Validation of Analytical Procedures: Methodology. Step 4 consensus guideline, (1996); Nov: 1-9

The Malaysian Journal of ANALYTICAL SCIENCES ISSN 1394-2506

EXTRACTION OF *CITRUS HYSTRIX* D.C. (KAFFIR LIME) ESSENTIAL OIL USING AUTOMATED STEAM DISTILLATION PROCESS: ANALYSIS OF VOLATILE COMPOUNDS

(Pengekstrakan Minyak *Citrus Hystrix D.C.* (Limau Purut) Menggunakan Kaedah Penyulingan Wap Automatik: Analisa Komposisi Hasil Minyak)

Nurhani Kasuan[1]*, Zuraida Muhammad[1], Zakiah Yusoff[1], Mohd Hezri Fazalul Rahiman[1], Mohd Nasir Taib[1], Zaibunnisa A. Haiyee[2]

[1]Faculty of Electrical Engineering,
[2]Faculty of Applied Science,
Universiti Teknologi MARA, 40450 Shah Alam, Malaysia

**Corresponding author: nurhani.kasuan@ieee.org*

Abstract

An automated steam distillation was successfully used to extract volatiles from *Citrus hystrix* D.C (Kaffir lime) peels. The automated steam distillation integrated with robust temperature control can commercially produce large amount of essential oil with efficient heating system. Objective of this study is to quantify the oil production rate using automated steam distillation and analyze the composition of volatiles in Kaffir lime peels oil at different controlled and uncontrolled temperature conditions. From the experimentation, oil extraction from Kaffir lime peels only took approximately less than 3 hours with amount of oil yield was 13.4% more than uncontrolled temperature. The identified major compounds from Kaffir lime peels oil were sabinene, β-pinene, limonene, α-pinene, camphene, myrcene, terpinen-4-ol, α-terpineol, linalool, terpinolene and citronellal which are considered to have good organoleptic quality. In contrast with uncontrolled temperature, oil analysis revealed that some important volatile compounds were absent such as terpinolene, linalool, terpinen-4-ol due to thermal degradation effect from fast heating of extracted material.

Keywords: automated steam distillation, *citrus hystrix* D.C., kaffir lime, volatile compounds, quality

Abstrak

Satu penyulingan wap automatik telah berjaya digunakan untuk pengekstrakan minyak pati dari kulit *Citrus hystrix D.C.* (Limau purut). Penyulingan wap automatik bersepadu dengan kawalan suhu membolehkan penghasilan minyak pati lebih efisien dengan sistem pemanasan yang cekap. Objektif kajian ini adalah untuk mengukur kadar pengeluaran minyak menggunakan penyulingan wap automatik dan menganalisis komposisi minyak pati kulit limau purut pada keadaan suhu yang berbeza secara terkawal dan tidak terkawal. Melalui eksperimen ini, pengekstrakan minyak dari kulit limau purut hanya mengambil masa 3 jam dengan jumlah hasil minyak adalah 13.4 % lebih daripada suhu yang tidak terkawal. Komposisi bahan utama dari minyak pati kulit limau purut minyak adalah sabinena , β-pinene, limonene, α-pinene, camphene , myrcene , terpinen-4-ol, α-terpineol , linalool, terpinolene dan citronellal. Analisis komposisi minyak dari eksperimen suhu tidak terkawal menunjukkan bahawa beberapa komponen penting tidak hadir seperti terpinolene, linalool, terpinen-4-ol disebabkan oleh kesan kemusnahan haba daripada pemanasan proses berkadar cepat.

Kata kunci: pengulingan wap automatik, *citrus hystrix* D.C., limau purut, komposisi kandungan minyak, kualiti

Introduction

In many developing countries, one of valuable natural resources is aromatic plant. The benefit of plant resources to humanity, besides basic needs, contributes to economic advantages in food industries, flavors, fragrances, health care product and so forth. Essential oil from aromatic plants is valuable and high in demand. The feasibility to

produce essential oil in mass quantity can be achieved by designing an automated process that enable to attain high production in efficient way and easy to operate. In this research, an automated steam distillation was designed to serve public users even in rural area where most of aromatic plant located. The steam distillation process is still preferred because of its low system cost, cleanliness, high production and low operational cost [1] compared to other advance extraction methods. In assessing reliability of automated steam distillation system, Kaffir lime peels is used as extraction material to quantify oil production rate at different operated temperature and also identifying major compounds of extracted oil in justifying oil quality. This study is important to obtain abundant of production oil yield and at the same time ensuring the oil quality yield is in good grade. The botanical material being analyzed in this study is Kaffir Lime or its scientific name *Citrus hystrix D.C.* from Rutaceae family. Kaffir lime has great potential in research and commercialization for aromatherapy and spa practices, solution for insect repellent, making shampoo, antioxidants compound and beauty product [2-6]. The quality of Kaffir lime peel essential oil is assessed based on the chromatographic profile of presence compound using Gas Chromatography (GC) and Gas Chromatography-Mass Spectrometry (GC-MS) [7-8]. The right compounds with standard concentration should present to ensure that the quality of essential oil is pure and good in organoleptic profile.

Steam distillation extraction process is a popular extraction method and suitable for most plant materials [1,9]. The duration of common steam distillation process is within 3 to 8 hours [10-12] on quantity and particle size of raw materials to be extracted. The steam distillation process is considerably cheap compared to other methods [9] and has potential for commercialization [13] due to its reliability in producing mass oil production. Several studies were carried out to compare the essential oil quality profiles and its production rate gained by steam distillation with several other extraction methods. Based on [14, 22], the relative chemical composition of volatile compound obtained by steam distillation and superheated water extraction (SWE) were proven similar. In fact, steam distillation itself can produce 0.24% more oil production in contrast with superheated water extraction. Moreover, Scalia et al. [15] proved that qualitative profile of essential oils obtained by the supercritical fluid extraction (SFE) was comparable with those produced by steam distillation process. Indeed, Ammann *et al*. [13] was concluded that steam distillation was the most effective technique as compared to SFE and SWE. While, comparing with supercritical carbon dioxides methods, steam distillation had produced more yields and in fact the quality of oil extracted by both methods is similar. Additionally, by taking advantage of operational and system cost-effective, automated steam distillation may execute desired outcome. This paper focused on how steam temperature, as controlled parameter, influence oil quality and productivity. In previous study by Li *et al*. [16], temperature exhibited the most significant effect on yield production followed by extraction time and particle size. Moreover, Silou *et al.* [17] revealed that the extraction rate in steam distillation had been decreased as the temperature and extraction time increased. If the extracted botanical plant is exposed to high temperature or prolong heating during extraction process, the essential oil may experience thermal degradation [14-15]. As a result, quality of oil will reduce and degrade the oil aromatic profiles and its physical color.

Materials and Methods

Kaffir lime Sample Preparation

Fresh Kaffir lime fruits ware obtained from Dengkil, Selangor. Peels of fresh Kaffir lime were used for all the experimental extraction. Prior to extraction, the Kaffir lime peels were weighted at 350 grams and then roughly ground to 2-4 mm mesh particles. After extraction took place, the essential oil samples is stored at chilled temperature before undergo further quality analysis.

Extraction Method

Kaffir lime essential oil extraction was carried out using automated steam distillation process. Basically, automated steam distillation processing plant is made up of three main modules i.e. distillation column, a condenser and heating system that illustrated in Figure 1. In the schematic diagram, 10 litre of filtered water is filled inside distillation column and a packed bed contained of Kaffir lime peels is located at the upper compartment of the column. For heating system, an embedded immersion type of heater is used to boil the water and level of water tank is kept at constant i.e. above the heating element. Water coolant for condenser is reused to substitute loss of water tank and sustain desired water level. By doing this, it will reduce wasted water and also minimize the temperature difference between water tank and water flow-in.

Steam passes through plant material and transporting tiny particles of essential oil to the condenser which then transform back to liquid mixture contained essential oil and water. The mixture is deposited in oil separator and undergone further water separation procedure. The advantage of this automated steam distillation process is to provide proper temperature control to meet user requirement and selection of suitable temperature profiles for associated plant during extraction process with reasonable cost operation. Additionally, this operation can extract essential oil in large volume with less human intervention or labor supervision due to computer monitoring module.
In the experiment, steam temperature inside the distillation column was controlled with pre-condition setting correspond to desired temperature profile. There were four temperature profiles under test i.e. 80^{o}C, 85^{o}C, 90^{o}C and uncontrolled temperature. In the case of controlled temperature (i.e. 80^{o}C, 85^{o}C, 90^{o}C), the trajectory of temperature response is well monitored and the response are allowed to fluctuate within ± <1^{o}C with respect to the set point. However, in uncontrolled condition, the heater is undergone fast heating response until saturated temperature. Without control strategy, the process response suffers from non-uniform temperature trajectory and experienced temperature fluctuation due to disturbances and process variations. The study will be assessed on the influence of all mentioned conditions towards extracted oil compositions and their productivity.

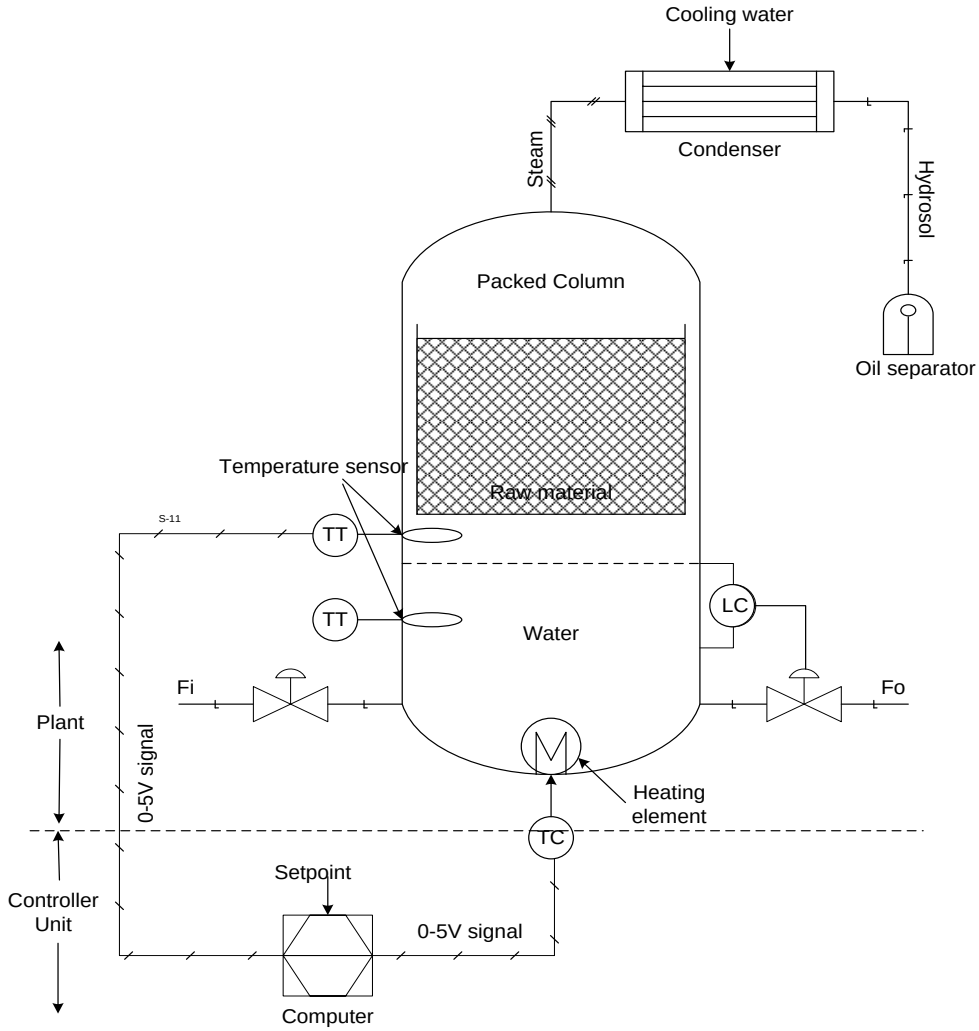


Figure 1. Steam Distillation Process for Essential Oil Extraction

Kaffir lime Essential Oil

The production yield was obtained approximately 50 minutes after process started. Two layers where formed, the top layer corresponds to oil while bottom layer is water. The oil sample was transferred into separating funnel. Dichloromethane was added into the funnel to form immiscible solvent where the oil and dichloromethane solvent at the bottom layer and water at the upper layer. The oil at lower layer was taken and the liquid at the upper layer was discarded. The evaporating process was continued to dry up remaining water contained in oil layer. Sodium anhydrous acid and dichloromethane acted as catalyze to accelerate the evaporating process using Vacuum Rotavap. Finally, the genuine extracted oil sample was ready for Gas Chromatography (GC) and Gas Chromatography – Mass Spectrophotometry (GC-MS) analysis.

Analysis of volatile compound.

the volatile compounds of kaffir lime peel were analyzed using shimadzu gc-2010 gas chromatography system for source identification. then, the chemical compound was further analyzed using agilent gcms 7890a equipped with agilent 5975c mass selective detector and using hp-5ms column (30m x0.25mm x 0.25µm film thickness). the carrier gas for gc was helium with flow rate of 1.0ml/min and the apparatus was programmed as tabulated in Table 1.

Table 1. GC-MS conditions for Kaffir lime oil analysis

Injector Temperature	250ºC
Detector Temperature	280ºC, with mass range recorded from 45-450 mass- to ratios, with electron energy of 70eV
Oven Temperature	The oven was set to 60ºC for ten minutes, and then the temperature was gradually increased up to 230ºC at a rate of 3ºC/min. For post run temperature is 50ºC.

The identification of oil chemical compounds was referred to mass spectral library HPCH2205.L, Wiley 7 NIST 05.L and NIST 05a.L database. The chromatograms from GC and GC-MS captured of existence sample oil constituents in terms of peak area count. For quantitative measurement, the percentage yield of extracted oil in wet weight basis can be calculated using Equation (1).

$$\text{Yield (\%)} = \frac{\text{Weight of essential oil recovered}}{\text{Weight of fresh citrus peels}} \times 100\% \quad (1)$$

The weight of extracted material was based on fresh Kaffir lime peels. The density of Kaffir lime oil is in range of 0.871g/mL [21]. Therefore, the mass (in grams) of Kaffir lime oil can be derived from known volume (mL) x density of Kaffir lime oil (0.871g/mL).

Results and Discussion

Analysis on Production Rate of Kaffir lime Oil Based on Different Distillation Temperature Using Automated Steam Distillation Process.

Based on previous study [18], production yield of Kaffir lime peels contained richer oil compared to oil from Kaffir lime leaves. The essential oil extorted from Kaffir lime peels was quite lucrative even though the duration of distillation only took approximately 2 hours (120 minutes). The amount of percentage oil yield was calculated based on wet weight basis. Wet basis define that the raw material contained high moisture where no drying process was involved during pre-processing stage. The accumulated amount of percentage yield is summarized in Table 2 below for different controller temperature.

Table 2. Percentage yield of Kaffir lime essential oil extracted

	Controller Steam Temperature (^oC)			
	80	85	90	Uncontrolled
%Yield (w/w)	1.87	2.19	4.26	3.36

Table 2 shows that when the temperature increased, more extracted oil was produced. At controlled temperature (90^oC), oil percentage yield is 4.26 (w/w). At lower temperature i.e. 80^oC, percentage oil yield is only 1.87 (w/w). When steam temperature regulated at 85^oC, the extracted oil yield get 2.19 (w/w). Interestingly, the increased in temperature to 90^oC really boost the oil yield almost up to 94.52% compared to yield during 85^oC (2.19 (w/w)). Even though the yield for uncontrolled steam temperature condition was greater than yield at 80^oC and 85^oC, but the extraction unable to drive system to produced maximum oil as much as yield at 90^oC.

Figure 3 presents production curves for extracted Kaffir lime oil for four different temperature profiles. The accumulated amount of oil was plotted for every 15 minutes. The overall oil production curve signifies that the Kaffir lime oil was aggressively extracted during first 30 minutes. Specifically, the production rates during this interval are approximately: 0.16ml/min, 0.3ml/min, 0.6ml/min, 0.56ml/min for 80^oC, 85^oC, 90^oC and uncontrolled temperature conditions respectively. The higher the steam temperature, the richer the oil extracted. After 75 minutes, the production curves converged to a steady value. The uncontrolled temperature, which the yield still cannot achieve to maximum production compared to 90^oC, might be due to temperature fluctuation and instable during extraction.

Analysis on the Quality of Kaffir lime Oil Based on Different Distillation Temperature Using Automated Steam Distillation Process.

This section is to investigate on how steam temperature influenced the quality of Kaffir lime peels oil based on different controlled temperature conditions. The concentration amount of compounds in Kaffir lime oil was identified using Gas Chromatography (GC) and Gas Chromatography – Mass Spectrometry (GC-MS) for each experimental sample. The chromatograms executed the peak ratio and each of peaks corresponds to particular compound at their respective retention time. Table 3 shows list of major volatile compounds derived in this experiment starting with α-Thujene occurred at lowest retention index 924 until Citronellol at 1223 of retention index. In the case of uncontrolled temperature, some important compounds were not found. The discrepancy may due to incomplete extraction process or the oil experienced thermal degradation that consequently losing some significant volatile compounds such as linalool and terpinen-4-ol.

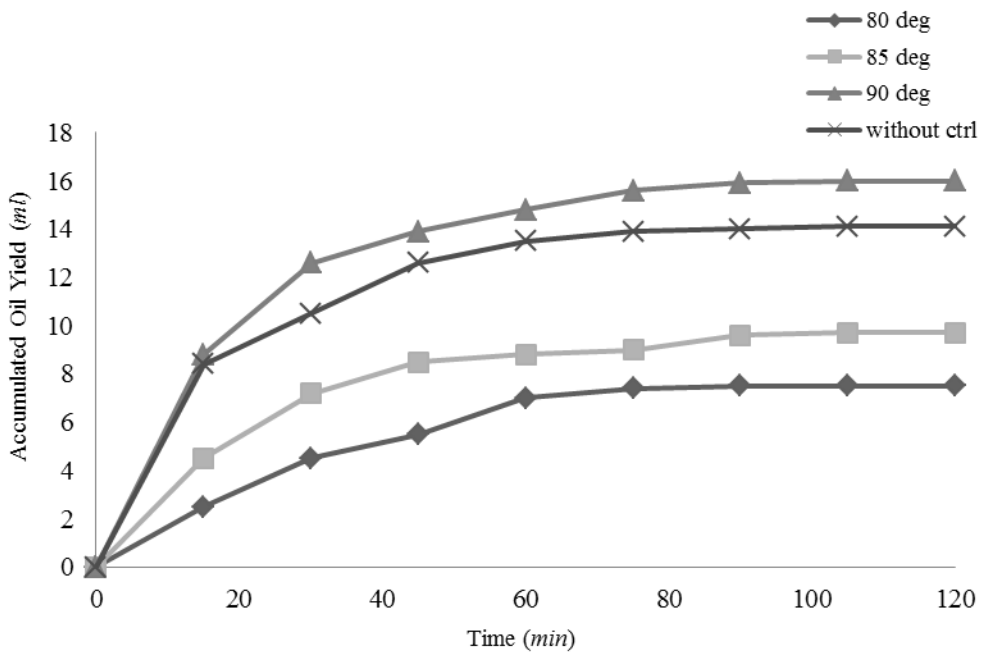


Figure 3. Cumulative quantity of Kaffir lime extracted essential oil based on different temperature control.

Table 3. Major compounds of Kaffir lime oil collected from Selangor, Malaysia.

No	Retention time (RT)	Compounds	Retention Index (RI)*	Relative Peak Area (%)			
				80°C	85 °C	90 °C	Uncontrolled temperature
1	7.27±0.02	α-Thujene	0924	0.238	0.227	0.233	0.194
2	7.65±0.04	α-Pinene	0932	3.546	3.047	3.262	3.338
3	8.40±0.03	Camphene	0946	0.180	0.151	0.155	0.135
4	10.62±0.22	Sabinene	0969	45.590	35.203	46.573	31.224
5	10.80±0.22	β-Pinene	0974	16.835	19.601	13.509	32.967
6	11.50±0.13	Myrcene	0988	1.985	1.807	1.804	1.735
7	13.02±0.05	δ-2-carene	1001	0.578	1.123	0.758	0.263
8	14.21±0.18	Limonene	1024	17.733	19.831	17.232	20.687
9	15.86±0.06	γ-terpinene	1054	1.045	1.775	1.354	0.735
10	17.60±0.04	Terpinolene	1086	0.318	0.497	0.383	-
11	18.95±0.06	Linalool	1095	0.633	1.044	1.156	-
12	21.92±0.16	Citronellal	1148	4.616	7.829	7.809	7.531
13	23.18±0.06	Terpinen-4-ol	1174	1.823	2.822	2.418	-
14	24.12±0.05	α-terpineol	1186	0.438	0.702	0.907	0.938
15	26.13±0.03	Citronellol	1223	-	0.118	-	-

*refer to [23]

The results obtained from the GCMS analysis are illustrates in Figure 4 – Figure 7. The figures of chromatograms correspond to four different controlled temperature conditions i.e. 80°C, 85°C, 90°C and uncontrolled temperature respectively. The peaks for each compound executed in chromatograms of four experimental samples occurred almost near to each retention time within certain range. The retention time is the time at which the compound elutes from the column in GC. As can be seen, altogether, there were 27 compounds identified. From the findings, the major compounds found from the oil samples are sabinene, α- pinene, limonene, myrcene, citronellal and terpinen-4-ol. The highest peak of GC-MS chromatogram is β-pinene and followed by sabinene. However, sabinene contributes highest concentration in extracted oil samples and the presence of sabinene indicates spiciness taste in the oil. The next important compounds are limonene and β- pinene. Both compounds provide distinctive aroma where limonene gives strong smells of oranges while β- pinene gives woody-green odor to the oil sample. Meanwhile, presence of citronellal indicates that the oil possesses antifungal quality and can be agent for insect repellent.

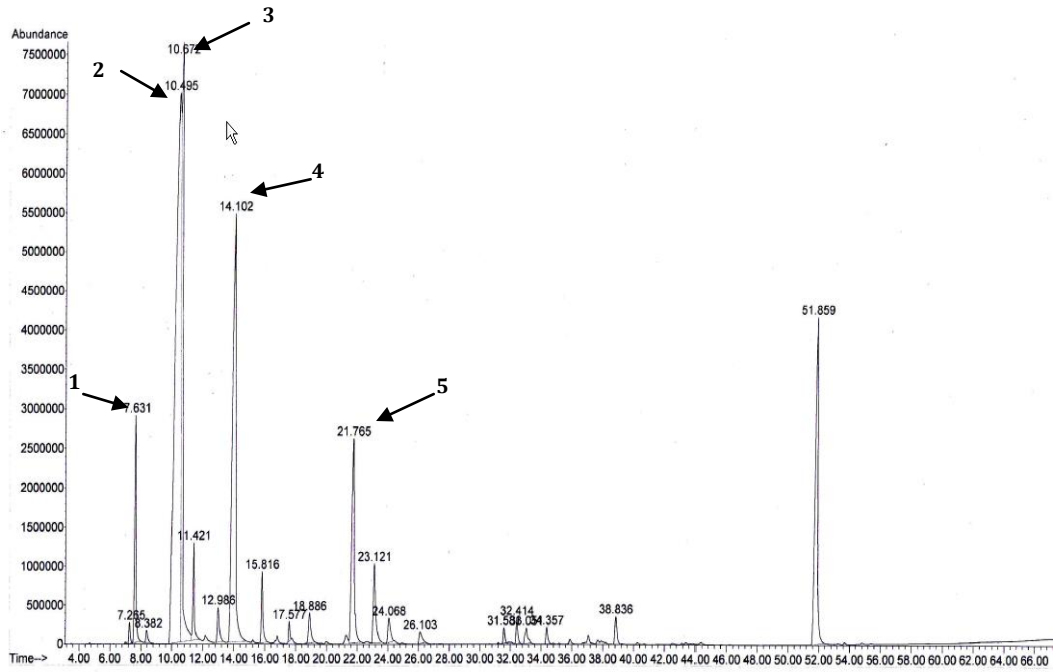


Figure 4. GCMS chromatogram of volatiles compounds from Kaffir lime peels oil (80°C). Major compounds peaks marked: α-Pinene(1), Sabinene(2), β-pinene(3), Limonene(4), Citronellal(5).

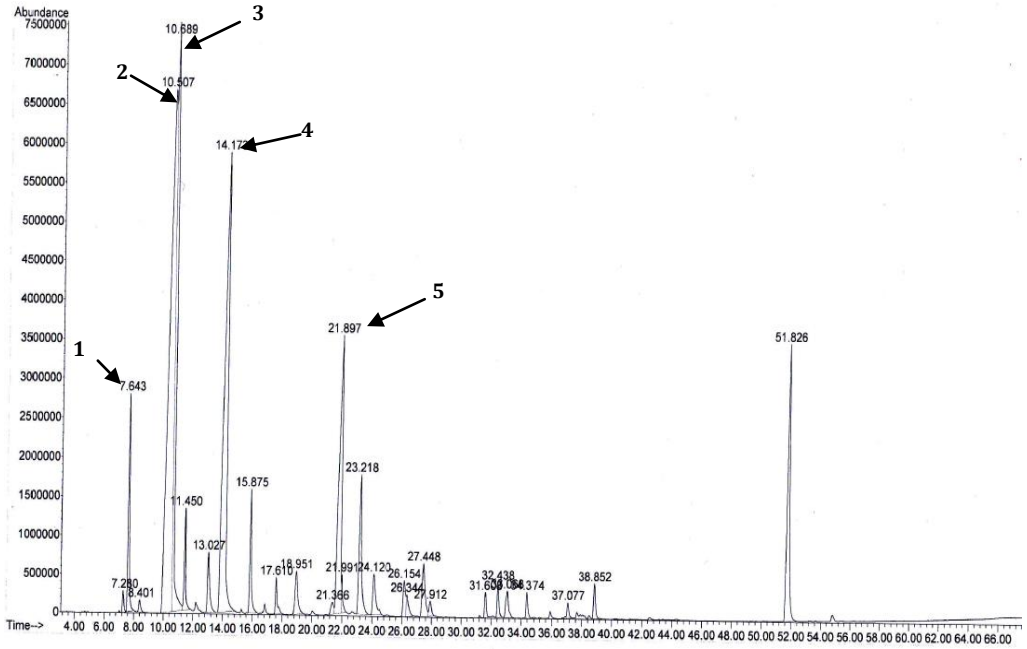


Figure 5. GCMS chromatogram of volatiles compounds from Kaffir lime peels oil (85°C). Major compounds peaks marked: α-Pinene(1), Sabinene(2), β-pinene(3), Limonene(4), Citronellal(5).

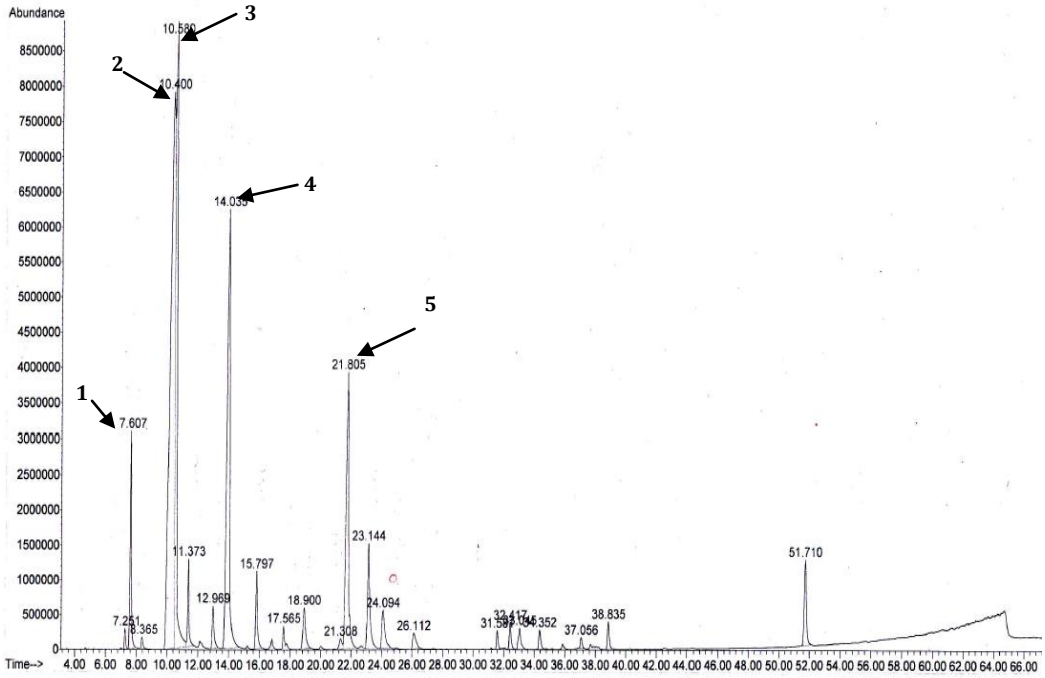


Figure 6. GCMS chromatogram of volatiles compounds from Kaffir lime peels oil (90°C). Major compounds peaks marked: α-Pinene(1), Sabinene(2), β-pinene(3), Limonene(4), Citronellal(5).

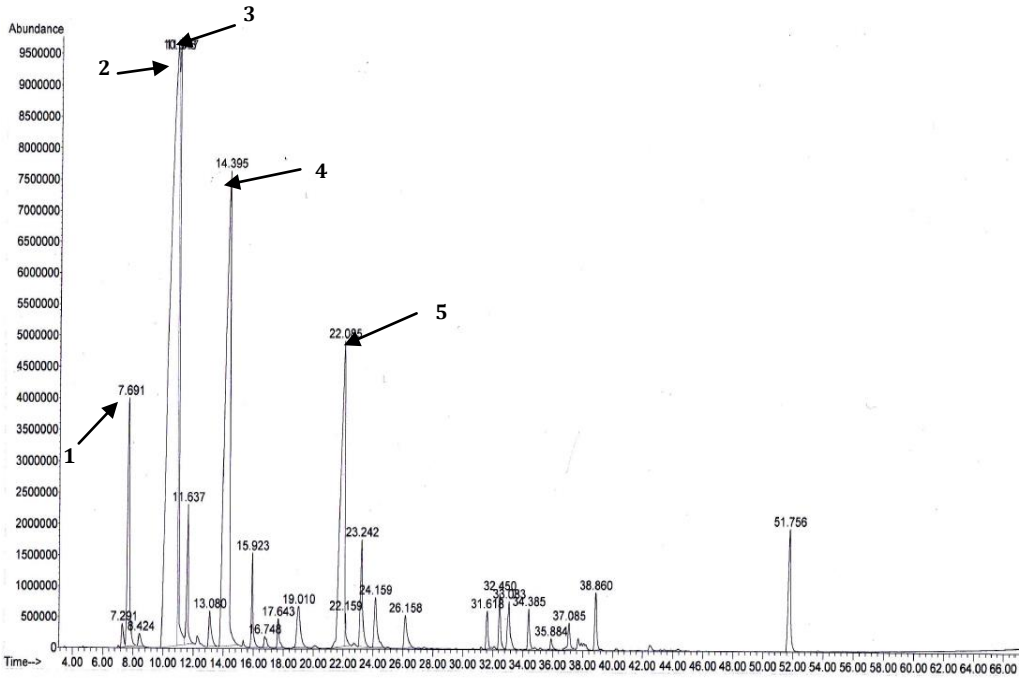


Figure 7. GCMS chromatogram of volatiles compounds from Kaffir lime peels oil (uncontrolled temperature). Major compounds peaks marked: α-Pinene(1), Sabinene(2), β-pinene(3), Limonene(4), Citronellal(5)

The major constituents of Kaffir lime originated from Thailand and Madagascar are listed based on published papers [19-20] respectively and eight major constituents were highlighted. In comparing the quality of Kaffir lime peel with these continents, Table 4 summarized the outcomes. All three regions agreed that three abundance compounds in Kaffir lime peel oil are Limonene, Sabinene and β-pinene. Another study by Abd Majid et. al. [7], also agreed that the main compounds of the oil found were sabinene, limonene, β-pinene, terpinen-4-ol and α-terpineol. Generally, quality of Kaffir lime peel oil is comparable to other regions where major compounds were detected, only slight different in percentage of its concentrations. Therefore, the quality of essential oil in this experiment can be acceptable.

Table 4. Comparison of major compounds of Kaffir lime peel oil with other regions.

Major Constituent	Relative Peak Area (%) **Malaysia** [Current study]	**Thailand** [19]	**Madagascar** [20]
Sabinene	35.2	22.6	11.9
Limonene	19.8	29.2	17.3
β-pinene	16.8	30.6	22.7
Citronellal	7.8	4.2	7.8
α-pinene	3.1	2.5	*nm*
Terpinen-4-ol	2.8	0.2	7.2
Myrcene	1.8	1.4	*nm*
Linalool	1.0	0.5	2.6

**nm = not mentioned*

Conclusion

Returning to the hypothesis posed at the beginning of study, temperature will directly affect the production of essential oil. The analysis on qualitative and quantitative of Kaffir lime peel oil extracted using automated steam distillation had been accomplished successfully. In quantifying oil production rate, the relevance of different temperature response is clearly affects the amount of oil yield. Increase in temperature will speed up oil production rate. In assessing the Kaffir lime peel oil quality; it suggests that temperature regulation from 80^{o}C, 85^{o}C and 90^{o}C, a significant result where most of major constituents are present in the analyzed oil samples. It shown that 85^{o}C of controlled condition can be assumed as an optimal temperature condition, with respect to oil quality, where most of constituents appear at this temperature setting including Citronellol. However during uncontrolled temperature condition, some important compounds were not found in the oil sample. This signifies that extracted oil from uncontrolled temperature (which applied fast heating) can reduce quality of the oil. Further works is also considered to identify optimum conditions for extraction of Kaffir lime essential oil that can maximize the production within efficient means.

Acknowledgement

The authors would like to express most gratitude to Faculty Electrical Engineering, Research Management Institute, Universiti Teknologi MARA for their great contribution in supporting this project.

References

1. Masango P. (2005). Cleaner production of essential oils by steam distillation, *Journal of Cleaner Production*.13: 833-839.
2. Chan S. W., Lee, C. Y., Yap, C. F., Wan Aida, W. M. & Ho, C. W. (2009). Optimisation of extraction conditions for phenolic compounds from limau purut (Citrus hystrix) peels. *International Food Research Journal*. 16: 203-213.
3. Tawatsin A., S. Wratten, R. Scott, U. Thavara, & Y. Techadamrongsin. (2001). Repellency of volatile oils from plants against three mosquito vectors. *Journal of Vector Ecology.* 26: 76-82.
4. Chaisawadi S., D. Thongbutr, & S. Kulamai. (2007). Clean production process of freeze dried Kaffir lime powder for medicinal herb and cosmetic use. *ISHS Acta Horticulturae 786: International Workshop on Medicinal and Aromatic Plants.* pp. 193-200.
5. Hongratanaworakit T., P. Tapaneeyasin, J. Nuamlert, A. Chansiri, & N. Hongrattanavorakit. (2006). Development of skin whitening preparations from kaffir lime oil (Citrus hystrix). *Planta med*, p. 72.
6. Prasart F. & Chonlada W. (2005). Development of anti-dandruff shampoo from kaffir lime which is the by product of food industry. *Kasetsart Journal (Natural Science)(Thailand); Witthayasan Kasetsart (Sakha Witthayasat)*, 39(4). 725-729.
7. Abd Majid J., Nor Azah M. A., Abu Said A., & Mohd Faridz Z. (2005). Teknologi penghasilan minyak pati limau purut (Citrus hystrix) menggunakan kaedah penyulingan hidro berskala besar. *Proceedings on Medicinal and Aromatic Plants: Trends and perspectives, Institut Penyelidikan Perhutanan Malaysia (FRIM),* Malaysia, 214-217.
8. Zaibunnisa A. H., & Chutima W. (2012). Extraction of volatile oil from Kaffir lime leaves (citrus hystrix) using pressurised liquid extraction. *International Journal of Food, Nutrition & Public Health*. 5: 201-210.
9. Catchpole O., J. Grey, K. Mitchell, & J. Lan. (2004). Supercritical antisolvent fractionation of propolis tincture. *The Journal of Supercritical Fluids*. 29: 97-106.
10. Song G., C. Deng, D. Wu, & Y. Hu. (2003). Comparison of Headspace Solid-Phase Microextraction with Solvent Extraction for the Analysis of the Volatile Constituents of Leaf Twigs of Chinese Arborvitae. *Chromatographia.* 58: 769-774.
11. Adegoke G. & B. Odesola. (1996). Storage of maize and cowpea and inhibition of microbial agents of biodeterioration using the powder and essential oil of lemon grass (Cymbopogon citratus). *International Biodeterioration & Biodegradation*. 37: 81-84.
12. Deng C., X. Xu, N. Yao, N. Li, & X. Zhang. (2006). Rapid determination of essential oil compounds in Artemisia Selengensis Turcz by gas chromatography-mass spectrometry with microwave distillation and simultaneous solid-phase microextraction. *Analytica Chimica Acta*. 556: 289-294.

13. Ammann A., D. Hinz, R. Addleman, C. Wai, & B. Wenclawiak. (1999). Superheated water extraction, steam distillation and SFE of peppermint oil. *Fresenius' Journal of Analytical Chemistry*. 364: 650-653.
14. Özel M., F. Gö ü , J. Hamilton, & A. Lewis.2005. Analysis of volatile components from Ziziphora taurica subsp. taurica by steam distillation, superheated-water extraction, and direct thermal desorption with GC× GC–TOFMS. *Analytical and bioanalytical chemistry*. 382: 115-119.
15. Scalia S., L. Giuffreda, & P. Pallado. (1999). Analytical and preparative supercritical fluid extraction of chamomile flowers and its comparison with conventional methods. *Journal of pharmaceutical and biomedical analysis*. 21: 549-558.
16. Li X., S. Tian, Z. Pang, J. Shi, Z. Feng, & Y. Zhang. (2009). Extraction of Cuminum cyminum essential oil by combination technology of organic solvent with low boiling point and steam distillation. *Food Chemistry.* 115: 1114-1119.
17. Silou T., G. Mapola, R. Makany, A. Loumouamou, M. Malanda, & J. Chalchat. (2009). Model of Steam and Water Extraction of Essential Oil of Eucalyptus Citriodora Using a Complete 2n Factorial Plan. *International Journal of Food Engineering*. 5: 9.
18. Nurhani K., M. Yunus, M. Rahiman, S. Aris, & M. Taib. (2009). Essential oil composition of Kaffir lime: Comparative analysis between controlled steam distillation and hydrodistillation extraction process. *IEEE Student Conference on Research and Development (SCOReD).* 479-482.
19. Brian M.L., James W.H. & Stuart J.T. (1971).Constituents of the Leaf and Peel Oils of Citrus Hystrix D.C. *Phytochemistry Reports, England*. 10: 1404-1405.
20. Ishikawa M., S. Hayashi, & S. Hashimoto. (2005). Essential oil components of Combava (Citrus hystrix DC). *Koryo, Terupen oyobi Seiyu Kagaku ni kansuru Toronkai Koen Yoshishu.* 49: 27-29.
21. Adamiec J., C. Borompichaichartkul, G. Srzednicki, W. Panket, S. Piriyapunsakul, & J. Zhao. (2012). Microencapsulation of kaffir lime oil and its functional properties. *Drying Technology*. 30: 914-920.
22. Ozel M. and H. Kaymaz. (2004). Superheated water extraction, steam distillation and Soxhlet extraction of essential oils of Origanum onites. *Analytical and Bioanalytical Chemistry*. 379: 1127-1133
23. Robert P. Adams. (2007). Identification of essential oil components by Gas Chromatography/ Mass Spectrometry. 4th Ed., Illinois, USA: Allured Publishing Corp.

The Malaysian Journal of ANALYTICAL SCIENCES ISSN 1394-2506

EFFECT OF ESSENTIAL OIL OF ATTARASA LEAVES (*Litsea cubeba* Lour. Pers) ON PHYSICO-MECHANICAL AND MICROSTRUCTURAL PROPERTIES OF BREADFRUIT STARCH-ALGINATE EDIBLE FILM

(Kesan Pati Minyak Daun Attarasa (*Litsea Cubeba Lour. Pers*) ke atas Sifat Fiziko-Mekanikal dan Mikrosturktur Pati Sukun-Alginat Filem yang boleh dimakan)

Cut Fatimah Zuhra[1]*, Jamaran Kaban[1], Marpongahtun[1] and Erman Munir[2]

[1.] *Department of Chemistry,*
[2.] *Department of Biology,*
Faculty of Science, Universiti Sumatera Utara, Medan, Indonesia

**Corresponding author: cfatimahzuhra@yahoo.com*

Abstract

Research on preparation of edible film from breadfruit starch and alginate incorporated with essential oil of attarasa leaves (*Litsea cubeba* Lour Pers.) has been done. The film was evaluated of their thickness, tensile strength, elongation at break, water vapor transmission rate (WVTR) and microstructural properties by Scanning Electron Microscopy (SEM). Incorporation of the oil increased thickness of film from 0,033 mm to 0,036 mm, tensile strenght from 32,8 to 37,0 MPa, elongation at break from 48,92% to 50,43% but water vapor transmission rate (WVTR) decreased from 142,9 g/m^2.hour to 120,3 g/m^2.hour. However SEM analysis showed that the surface microstructural of the film was more rough and solid compare with film without incorporation of essential oil.

Keywords : attarasa leaves, essential oil, breadfruit starch, alginate, edible film

Abstrak

Penyelidikan ke atas penyediaan filem yang boleh dimakan dari pati buah Sukun dan alginat digabungkan dengan pati minyak daun attarasa (*Litsea cubeba* Lour Pers.) telah dijalankan. Filem ini dinilai ketebalan, kekuatan tegangan, pemanjangan, kadar pemindahan wap air (WVTR) dan sifat-sifat mikrostruktur oleh Mikroskopi Imbasan Elektron (SEM). Pengabungan minyak telah meningkatkan ketebalan filem dari 0.033 mm hingga 0.036 mm, kekuatan tegangan daripada 32.8 kepada 37.0 MPa, pemanjangan dari 48.92 % kepada 50.4 3% tetapi kadar pemindahan wap air (WVTR) menurun daripada 142.9 g/m2.jam kepada 120.3 g/m2.jam. Walau bagaimanapun analisis SEM menunjukkan bahawa permukaan mikrostruktur filem itu adalah lebih kasar dan kukuh bandingkan dengan filem tanpa pengabungan pati minyak.

Kata kunci: daun attarasa, pati minyak, pati sukun, alginat, filem yang boleh dimakan

Introduction

Polysaccharide, such as starch, alginate, cellulose derivatives and plant gums, has been reported as edible film and coating in food packaging and preservation. They are known to be effective barrier of gas transport (O_2, CO_2), although they posses high water vapor permeability. Generally the main functional properties of these hydrophilic materials strongly depend on their water content and therefore on the surrounding humidity. Particularly, the use of starch could be an interesting reason since this polymer is abundant, cheap, biodegradable and edible [1].

Breadfruit (*Artocarpus artilis*) which belongs to the family Moraceae has been processed into many forms for utilization in the food industry and it has also been processed into starches and flour [2,3]. The breadfruit contains starch up to 18.5 g/100 g with purity of 98.86 % and content of amylose 27.68 % and amylopectin 72.32 %, scanning electron microscopy shows the starch granule is irregular-rounded [4].

Alginic acid and alginate are natural biodegradable, biocompatible, non-toxic and low cost polymer, which have been utilized in various biomedical applications, such as surface modification of biomedical implants and encapsulation of drugs, cells and enzymes [5]. Preparation of edible films from hydrocolloids like alginate forms strong films and exhibits poor water resistance because of their hydrophillics nature. Alginate has a potential to form biopolymer film or coating component because of its unique colloidal properties, which include thickening, stabilizing, suspending, film forming, gel producing and emulsion stabilizing [6].

The ability of edible film or edible coating to carry some food additives such as antioxidants, antimicrobials, colorants, flavors, fortified nutrients and spices has been reported [7,8]. The method is different from direct application, such as the incorporation of antimicrobial agents into edible film or edible coating localizes the functional effect at the food surface. The beneficial effects obtained by using edible film and coating in terms of physical, mechanical, and biochemical benefits have been reported in many publications, including the ability of edible film in retarding moisture, oxygen, aromas, and solute transport [9].

Attarasa (*Litsea cubeba* Lour. Pers) which belongs to the family Lauraceae is also recognized as name ki lemo (Sunda) and krangean (Java). Attarasa leaves contain essential oil with the main component of cineol (13.97 %), γ- elemene (8.27 %), caryophyllene (8.04 %), linalool (6.94 %) and limonene (6.78 %). Furthermore, essential oil of attarasa leaves composes of monoterpene hydrocarbons (32.12 %), oxygenated monoterpenes (27.2 %), sesquiterpene hydrocarbons (22.89 %), "others" (12.91 %), and oxygenated sesquiterpenes (3.75 %) [10]. *L. cubeba* oil also has antimicrobial activity to *Aspergillus niger*, which suggests that the oil directly damages the membrane of *A. niger*, change its structure, viscoelasticity and selective permeability [11].

This paper describes the effect of essential oil attarasa leaves (*L. cubeba* lour. pers) on physico-mechanical and microstructural properties of breadfruit starch-alginate edible film.

Materials and Methods

Preparation of Film

Film forming solutions were prepared from a mixture of breadfruit starch and sodium alginate (4:1) based on total weigth basis (5 g) including glycerol 20 % in 100 mL distilled water. Attarasa leaves essential oil was initially dilute to 4 % v/w concentration using ethanol (95 %) and then incorporated into the edible film forming solution. The mixture was heated to 75 ºC with continuous stirring for 45 min before it was cooled to room temperature. The solutions were casted onto plates (12 x 12 cm) followed by oven drying at 40 ºC for 24 hours. The dry films obtained were carefully peeled off and stored for further analysis [6].

Film Thickness

Film thickness was measured using micrometer to the nearest 0.01-mm accuracy at 5 locations, and the average value was calculated.

Mechanical Properties

The tensile strength and % elongation of the films were investigated using tensile machine according to ASTM 638-1991. Films were cut into strip according ASTM D638 and pinched on tensile machine. Examination were done with five replicates.

Water Vapor Transmission Rate (WVTR)

WVTR was measured using a modified ASTM (American Society for Testing and Materials). The film was sealed on an aluminum permeation cup containing silica gel. The cup was placed at 30 ºC in a desiccator containing the distilled water. It was then weighed at 2 h intervals over 12 h period and determinations were carried out in triplicate. Six films were used for WVTR testing . Weight loss graphs were plotted with respect to time, and the linear least-square method was used to calculate water vapor transmission rate (WVTR) using the equation [12]:

$$WVTR = Slope / film\ area$$

Simultaneous Thermal Analysis (STA) and Scanning Electron Microscopy (SEM)
Thermal characteristic of the film was measured by using a simultaneous thermal analysis (STA) and microstructural was observed using SEM. Films were placed on double-stick tape mounted on specimen holder, coated with 100 to 200 thicknesses of gold and photograped using SEM apparatus.

Results and Discussion

The possibility of edible film or edible coating to carry some food additives such as antioxidants, antimicrobials, colorants, flavors, fortified nutrients and spices has been reported [9]. The essential oil as the antimicrobial additives are introduced into the interstitial (empty) spaces of the polymer matrix by means of a proprietary process, The empty spaces act as reservoirs for the additives, which rise to the surface as needed to police for contaminants [13].

Film Thickness
Thickness of breadfruit starch-alginate edible film was 0.033 mm and breadfruit starch-alginate-attarasa leaves oil edible film was 0.036 mm. Addition of essential oil of attarasa leaves into edible film of breadfruit starch-alginate causes full scale increase of compound which is dissolved in solution edible film. The thickness of edible film increased with increasing of the compound dissolved in breadfruit starch-alginate edible film. Furthermore the addition of essential oil into edible film breadfruit starch-alginate causes intermolecular forces, in this case the dipole-dipole interaction, van der Waals force and hydrogen bonding, these interactions causes the increase thickness.

Mechanical Properties
Tensile strength is a measure of film strength, whereas elongation at break is a measure of film stretch ability prior to breakage. Both properties are important characteristics for packaging material [14]. The tensile strength and elongation at break changes of the edible film incorporated with attarasa leaves oil was higher than that of breadfruit starch-alginate edible film. Breadfruit starch-alginate edible film has tensile strength 32.8 Mpa and elongation at break 48.92 % while breadfruit starch-alginate-attarasa leaves oil edible film has tensile strength 37.0 Mpa and elongation at break 50.43 %. Addition of essential oil causes increased of component which was dissolved in solution edible film then increasingly matrix edible film formed, so that required by larger style to draw edible film so broken. Thus the addition of essential oil into edible film breadfruit starch-alginate cause intermolecular interaction, this thing affects at improvement of tensile strength.

Water Vapor Transmition Rate (WVTR)
The water vapor transmission rate breadfruit starch-alginate edible film was 142.9 g/m^2.hour and breadfruit starch-alginate -attarasa leaves oil edible film was 120.3 g/m^2.hour. Polysacharide-based films are generally rather poor water barriers, due their hydrophilic nature. Addition of essential oil into breadfruit starch-alginate film decreased water vapor transmission rate, because the hydrophobic character of essential oil. Water vapour migration only take place at hydrophilic area edible film and ratio between hydrophobic and hydrophilic side of component edible film affects value of water vapor transmission rate. This result is accordance with previously reported works: the greater of hydrophilicity of edible film, lower of water vapor transmission rate [15]. Essential oil play an important role in water vapor barrier from breadfruit starch-alginate- attarasa leaves oil edible film. The essential oil incorpareted to the breadfruit starch-alginate edible film inhibited the growth of tested microbes [16**].**

Simultaneous Thermal Analysis (STA)
Breadfruit starch-alginate edible film happened mass reduction 4.0 mg (Figure 1), and breadfruit starch-alginate-attarasa leaves oil edible film mass reduction 7 mg (Figure 2). Mass reductions takes its rise at ambient temperature 220 $^{\circ}$C, this thing there because of edible film have experienced process of like melting/ condensation and decomposition. Decomposition caused by heat happened at temperature 220 - 350 $^{\circ}$C. Breadfruit starch-alginate-attarasa leaves oil edible film besides containing the glycerol which starts to vapour at above temperature 200 $^{\circ}$C also there was attrasa leaves oil which represents compound volatil and when heated will soon release of edible film. Glycerol and essential oil will vapour and release of edible film, then process of decomposition edible film also takes place. This event shown by enthalphy change as event of endotherm.

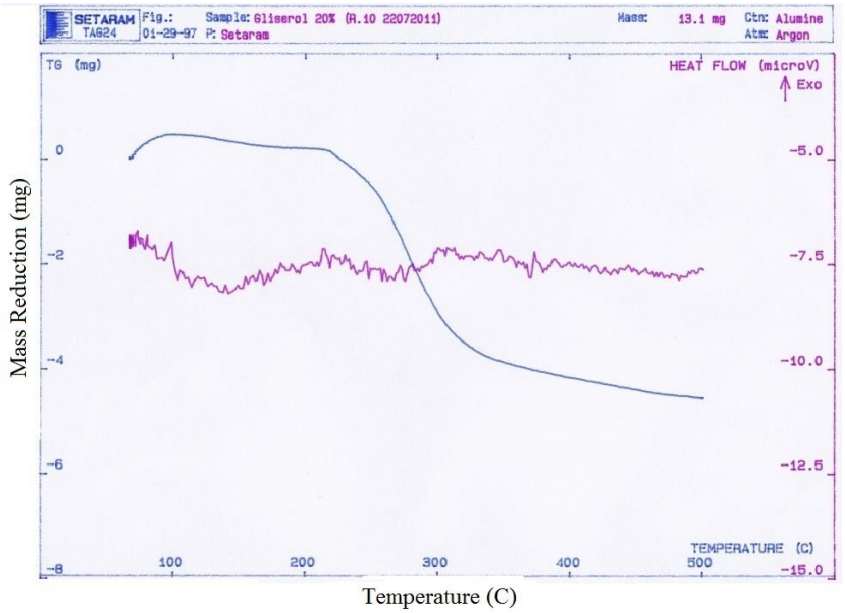


Figure 1. Mass reductions and enthalphy change to breadfruit starch-alginate edible film

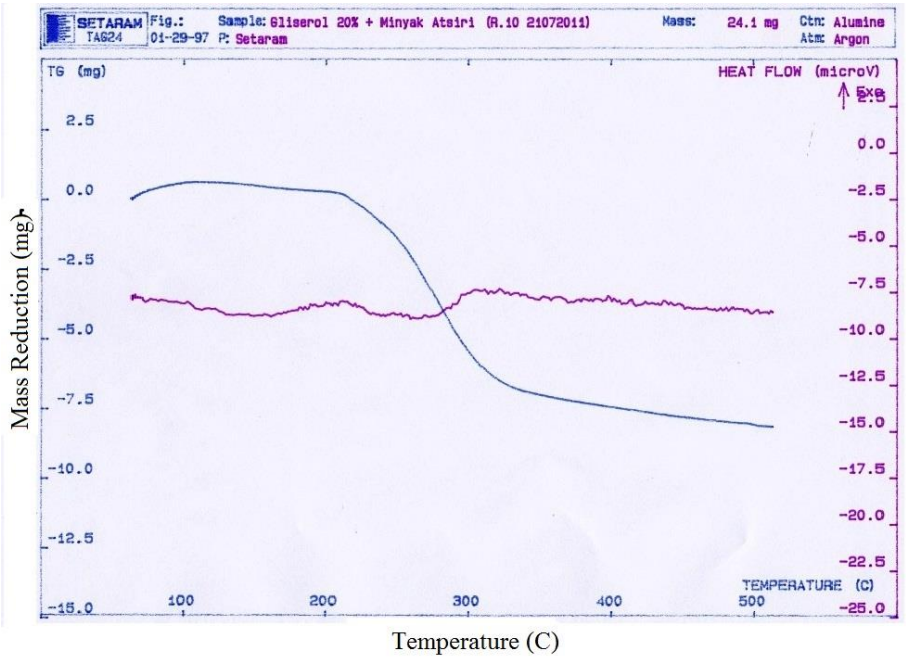


Figure 2. Mass reductions and enthalphy change to breadfruit starch-alginate-attarasa leaves oil edible film

Scanning Electron Microscopy (SEM)

Analysis of SEM breadfruit starch-alginate edible film (Figure 3) seen that surface was smooth and pore which is formed a few, this thing indicates that mixing between material in edible film there mixed with homogeneous.

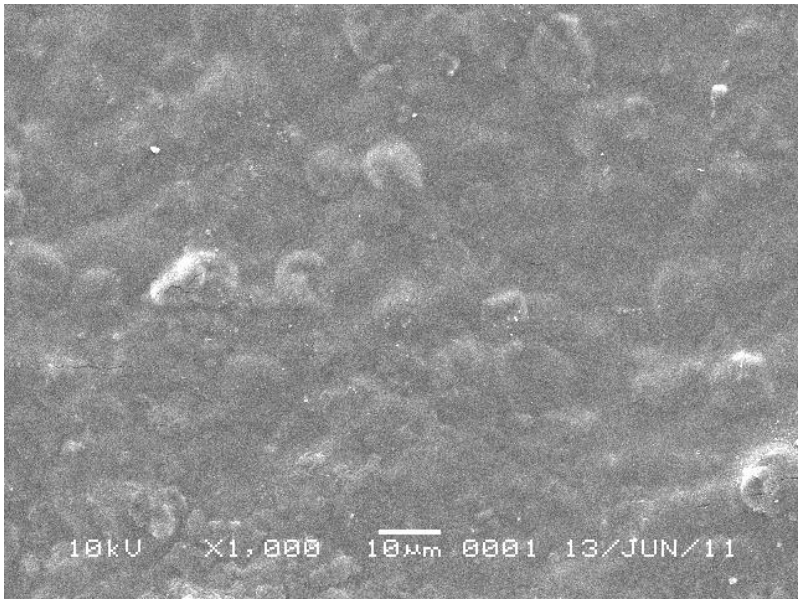


Figure 3. SEM of breadfruit starch-alginate edible film

Analysis of breadfruit starch-alginate edible film which had been incorporated with atarasa leaves oil (Figure 4) seen that surface harsher and more solid, this thing because of addition of essential oil which causes full scale addition of solid edible film.

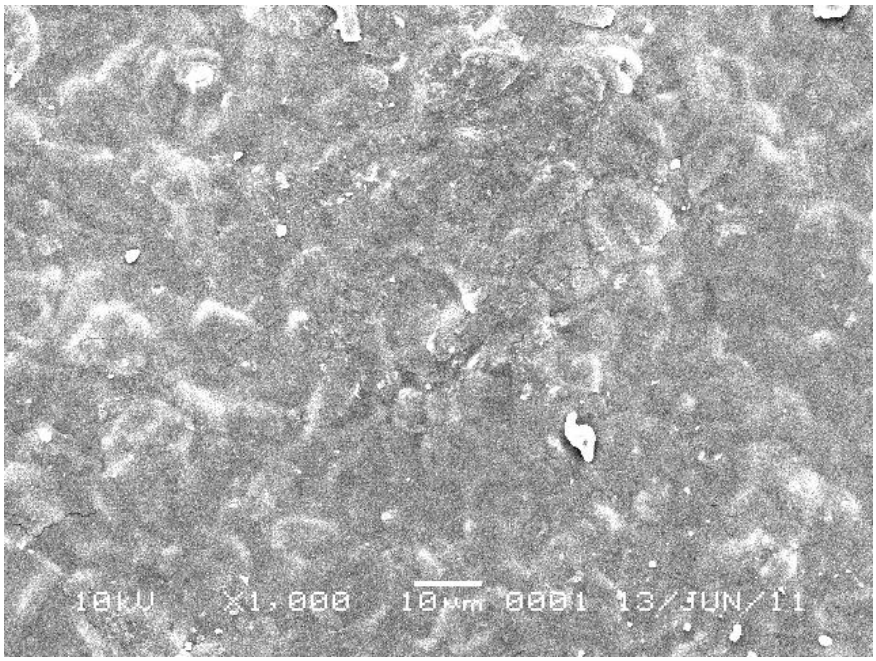


Figure 4. SEM of breadfruit starch-alginate-attarasa leaves oil edible film

Conclusion

The breadfruit starch-alginate edible film was incorporated with attarasa leaves oil have mechanical properties such as thickness of film, tensile strength and elongation of film, mass reduction were higher but water vapor transmission rate (WVTR) was lower than that of breadfruit starch-alginate edible film. SEM analysis showed that the surface microstructural of the edible film was more rough and soild compare with edible film without incorporation of essential oil.

References

1. Bertuzzi, M. A., Vidaurre, E. F. C., Armada, M. & Gottifredi, J.C. (2007). Water Vapor Permeability of Edible Starch Based Films. *Journal of Food Engineering.* 80: 972 – 978.
2. Tridjaja, N. O. (2003). Panduan Teknologi Pengolahan Sukun Sebagai Bahan Pangan Alternatif. Departemen Pertanian. Dirjen Bina Pengolahan dan Pemasaran Hasil Pertanian. Jakarta.
3. Akanbi. T. O., Nazamid S. & Adebowale, A. A. (2009). Functional and Pasting Properties of a Tropical Breadfruit (*Artocarpus altilis*) Starch from Ile-Ife, Osun State, Nigeria. *International Food Research Journal*. 16: 151 - 157.
4. Rincom, A. M. & Fanny, C. P. (2004). Physicochemical Properties of Venezuelan Breadfruit (*Artocarpus altilis*) Starch. *Archivos Latinoamericanos De Nutricion*. 53: 449 - 456.
5. Cheong, M. & Zhitomirsky, I. (2008). Electrodeposition of alginic acid and composite films. *Colloids and Surfaces A: Physicochem. Eng. Aspects*. 328: 73 – 78.
6. Maizura, M., Fazilah, A., Norziah, M. M. & Karim, A. A. (2008). Antibacterial Activity of Starch-Alginate Based Edible Film Incorporated with Lemongrass (*Cymbopogon citrates*) Oil. *International Food Research Journal*. 15: 233 - 236.
7. Han, J. H. 2000. Antimicrobial food packaging. *Food Technology*. 54: 56 – 65.
8. Pena, D. C. R. & Torres, J. A. (1991). Sorbic Acid and Potassium Sorbate Permeability Of an Edible Methylcellulose-Palmitic Acid Films: Water Activity and Ph Effects. *Journal of Food Science* 56: 497 – 499.
9. Pranoto, Y., Vilas, M.S. & Sudi, K.R. (2005). Physical and Bacterial Properties of Alginate-Based Edible Film Incorporated with Garlic Oil. *Food Research International.* 38: 267 - 272.
10. Wang, H. & Liu, Y. (2010). Chemical Composition and Antibacterial Activity of Essential Oil from Different Parts of *Litsea cubeba*. *Chemistry and Biodiversity*. 7: 229 – 235.
11. Man, L., Tang, F., Jiang, L., Huang, Y. & Li, J. (2004). Cytological Mechanism of Antimicrobial Activity of *Litsea cubeba* Oil on *Aspergillus Niger* Growth. *Chin J Appl Environ Biol*, 10: 236 – 238.
12. Srinivasa, P. C., Ramesh, M. N. & Tharanathana, R. N. (2007). Effect of Plasticizers and Fatty Acids on Mechanical and Permeability Characteristics of Chitosan Films. *Food Hydrocolloids*. 21: 1113 - 1122.
13. Kim, Y. T., Kim, K., Han, J. H. & Kimmel, R. M. (2008). Antimicrobial Packaging for Food. *in* Kerry, J. and Butler, P. *at* Smart Packaging Technologies. John Wiley and Sons Ltd. England.
14. Krochta, J. M. & Johnston, C. D. M. (1997). Edible and biodegradable films: challenges and opportunities. *Food Technology* 51: 61–74.
15. Garcia, M. A., Martino, M. N. & Zariky, N. E. 2000. Lipid Addition to Improve Barrier Properties of Edible Starch-Based Film and Coating. *J Food Sci*. 65: 941 – 947.
16. Zuhra, C.F., Kaban, J., Munir, E. & Marpongahtun. (2011). Aktivitas Antimikroba *Edible Film* dari Pati Sukun – Alginat yang di Inkorporasi dengan Minyak Atsiri Daun Attarasa (*Litsea cubeba* Lour. Pers). *Jurnal Biologi Sumatera.* Edisi Juli 2011

The Malaysian Journal of ANALYTICAL SCIENCES ISSN 1394-2506

KAJIAN AWAL PENGGUNAAN JARINGAN NEURAL TIRUAN (ANN) BAGI MENENTUKAN NILAI PEROKSIDA TIGA MINYAK SAWIT KOMERSIL BERDASARKAN SPEKTRUM FTIR

(Preliminary Study on Application of Artificial Neural Networks (ANN) for Determining the Peroxide Value of Three Commercial Palm Oil Based FTIR Spectrum)

Azwan Mat Lazim[1]*, Musa Ahmad[1], Zuriati Zakaria[1], M. Suzeren Jamil[1]
Suria Ramli[1], Faiz Zainuddin[1], Mohd Nasir Taib[2], M. Nasir Mat Arip[3]

[1]Pusat Pengajian Sains Kimia & Teknologi Makanan,
Fakulti Sains dan Teknologi, Universiti Kebangsaan Malaysia, 43600 Bangi, Selangor
[2]Fakulti Kejuruteraan Elektrik,
Universiti Teknologi MARA, 40450 Shah Alam, Selangor
[3]Forest Products Division,
Forest Research Institute Malaysia, 52109 Kepong, Selangor, Malaysia

**Corresponding author: azwani79@ukm.my*

Abstrak

Nilai peroksida sering digunakan bagi menentukan kualiti minyak masak di mana nilai ini mengukur sebatian peroksida dan kumpulan hidroperoksida yang terbentuk di peringkat primer pengoksidaan lipid. Dalam kajian ini sebanyak tiga minyak masak (sawit) komersil telah dipilih dan dilabelkan sebagai A, B dan C. Dua keadaan berbeza telah diaplikasikan ke atas sampel-sampel minyak tersebut. Pertama, sampel minyak telah didedahkan ke udara selama 3 bulan (minyak A) manakala yang kedua sampel minyak telah digunakan untuk menggoreng berulang kali (minyak B dan C). Bagi tujuan latihan ANN, sebanyak dua input telah dipilih daripada spektrum FTIR yang diperoleh, iaitu nilai serapan pada panjang gelombang 3444 cm^{-1} dan 3450 cm^{-1}. Hasil kajian menunjukkan arkitektur yang sesuai bagi jaringan ANN bagi menentukan nilai peroksida bagi sampel minyak komersil adalah 2:20:1. Bagi ujian ramalan, nilai peroksida yang diramalkan oleh ANN adalah hampir menyamai nilai peroksida yang diperoleh daripada kaedah piawai. Keputusan telah menunjukkan bahawa ralat purata yang rendah telah dperoleh, iaitu 0.48 apabila neuron terlindung yang digunakan bagi arkitektur jaringan adalah 20 manakala bilangan ulangan latihan adalah 300.

Kata kunci: nilai peroksida, FTIR, ANN, minyak sawit

Abstract

Peroxide value is one of the measurements that being used to determine the peroxide in oil samples produce from the peroxide compund and hydroperoxide group at the primary level of lipid oxidation. In this study, 3 commercial palm cooking oils were selected and labeled as A, B and C. Two different conditions were applied to the samples. First, the oil sample was exposed to the air for three months (labeled as A) while samples B and C were used for frying for many times. Two inputs from FTIR spectra (3444 cm^{-1} and 3450 cm^{-1}) were chosen for the ANN training. The suitable architecture for this training is 2:20:1. The prediction made by ANN was very accurate and compatible to the result which obtained from the standard method. A low average error (0.48) was obtained when the hidden neuron (20) and the epochs (300) were used.

Keyword: peroxide value, FTIR, ANN, palm oil

Pengenalan

Tanpa kita sedari minyak masak yang telah digunakan beberapa kali atau disimpan dalam persekitaran yang kurang sesuai di mana terdapat interaksi dengan udara, haba, kelembapan dan cahaya boleh menyebabkan kemerosotan kualiti minyak, kandungan nutrisi malah boleh menghasilkan bahan toksik. Dalam keadaan semulajadi, kehadiran oksigen boleh menyebabkan berlakunya pengoksidaan terhadap lemak dan minyak yang mengandungi kandungan

lemak tak tepunya tinggi. Proses pengoksidaan boleh menyebabkan perubahan kepada sifat organoleptik dalam lemak dan minyak kerana kehadiran bahan yang tidak diingini. Ini disebabkan telah berlaku perubahan struktur dalam lemak dan minyak [1].

Terdapat beberapa hasil akhir yang boleh dilihat apabila minyak ini terdegradasi, seperti perubahan warna, bau (tengik) dan rasa. Ini adalah disebabkan oleh terhasilnya bahan-bahan kimia seperti aldehid, keton, polimer, alkohol, asid dan peroksida dalam sampel minyak masak. Kemerosotan kualiti minyak juga boleh dikaitkan dengan nilai peroksida yang tinggi iaitu sebanyak 10 Meq per kilogram lemak dan minyak pengoksidaan [2]. Kaedah titratan merupakan kaedah konvensional yang telah digunapakai sejak dahulu lagi di mana natrium tiosulfat digunakan sebagai titran untuk menentukan kuantiti peroksida yang terbebas. Namun begitu, kaedah ini telah mempunyai beberapa kelemahan seperti masa titratan yang panjang, penggunaan bahan kimia yang banyak, ralat yang tinggi, kebolehulangan yang rendah serta tidak efisien.

Sebagai alternatif dalam menentukan kualiti minyak sawit, salah satu kaedah yang kini diminati oleh para penyelidik ialah menggunakan kaedah FTIR [3]. Melalui kaedah ini, keputusan yang diperoleh adalah lebih cepat dan mudah berbanding dengan kaedah konvensional. Selain daripada kurang penggunaan bahan kimia kaedah ini turut menawarkankan nilai ralat yang rendah [4]. Kaedah ini didapati amat berpotensi dalam aplikasi penentuan status oksidatif bagi minyak makan dan kestabilannya. Seperti yang dilaporkan oleh Van de Voort et al. (1994) [5] dalam kajian mereka terhadap minyak zaitun, apabila pengoksidaan berlaku spektrum minyak akan menunjukkan peningkatan pelebaran serapan jalur O-H (3800-3200 cm^{-1}) manakala pengurangan berlaku pada serapan ester trigliseridik (1744 cm^{-1}) serta regangan C-H (3050-2800 cm^{-1}). Selanjutnya, Fukuzumi dan Kobayashi (1972) [6] mencadangkan pengoksidaan minyak boleh dibandingkan dengan jalur serapan hidroperoksida, yang merujuk kepada regangan OO-H (iaitu pada 3450 cm^{-1}) seperti kajian yang telah dilakukan ke atas sampel metil oktadekadienoat teroksida. Penyataan ini disokong oleh kajian yang dilakukan oleh Van de Voort et al. (1994) [5] di mana getaran regangan OO-H bagi sampel t-butil hidroperoksida berlaku pada 3444 cm^{-1}. Walaubagaimanapun, kemungkinan berlaku gangguan daripada serapan asid lemak bebas yang wujud dalam minyak semasa menentukan nilai peroksida dengan menggunakan spektrum FTIR. Ini berlaku kerana OH daripada kumpulan karboksilik (COOH) turut memberikan serapan pada jalur serapan OH iaitu sekitar 3600-3310 cm^{1}. Tetapi, gangguan yang wujud ini tidak memberi kesan yang besar terhadap kajian yang dijalankan [5, 7].

Dalam kajian yang dibuat oleh Hussain et al. (1996) [8], beliau telah membuktikan bahawa ANN merupakan model yang terbaik dalam menyelesaikan masalah seperti mengesan dan meramalkan nilai bahagian dalam campuran minyak masak. Berdasarkan pencaman corak, ANN dapat menyelesaikan masalah pencampuran minyak yang berkualiti dengan minyak yang tidak berkualiti (*adulteration*) seperti mencampurkan minyak sawit mentah (CPO) dan minyak isirong sawit mentah (CPKO) [9]**.** Selalunya pencampuran dilakukan kerana CPO merupakan minyak yang mahal berbanding dengan CPKO. Biasanya kadar pencampuran adalah antara 1-10% bagi tujuan untuk meminimumkan kos pengeluaran [10]. Namun begitu berdasarkan corak yang diperoleh menggunakan FTIR, ANN dapat meneka kandungan sebenar CPO kerana komposisi kimia bagi minyak campuran telah berubah berbanding dengan komposisi asal [8]. Antara kejayaan lain yang telah dilaporkan dengan menggunakan model ANN dalam penentuan kualiti minyak makan adalah seperti pengklasifikasian antara campuran minyak soya dan minyak *rapeseed*, nilai ketengikan minyak (rancidity) [11], mencirikan nilai pencampuran antara campuran beberapa miyak masak [8].

Bagi analisis kimometrik pula, pencaman corak FTIR daripada setiap sampel minyak dioptimumkan untuk membina model model analisis utama (PCA) dan kuasa dua terkecil separa (PLS). Dalam kajian kami terdahulu, perbandingan keputusan yang dibuat antara nilai pencirian minyak yang diramalkan menggunakan kaedah kemometrik PLS telah dibandingkan dengan nilai pencirian minyak komersial yang ditentukan dalam kaedah konvensional. Keputusan telah menunjukkan kaedah tersebut mampu menentukan kualiti minyak masak setara dengan kaedah konvensional [12]. Lanjutan daripada kajian tersebut, kajian ini akan membincangkan pula tentang pengaplikasian model ANN dalam menentukan nilai peroksida bagi tiga minyak masak komersil yang boleh didapati di pasaran pada keadaan tertentu. Kebolehan ANN akan diuji berdasarkan ketepatan ramalan nilai peroksida bagi setiap minyak berdasarkan pencaman corak spektrum FTIR yang diperolehi berbanding nilai peroksida yang diperoleh berdasarkan kaedah piawaian PORIM (1995) [13].

Bahan dan Kaedah

Sampel minyak

Sebanyak tiga sampel minyak sawit berlainan jenama telah dibeli dari pasaran. Minyak-minyak ini kemudiannya dilabelkan A, B dan C. Beberapa keadaan telah dilakukan terhadap sampel-sampel ini. Minyak A didedahkan ke udara dalam jangka waktu 3 bulan manakala minyak B dan C telah digoreng berulang kali. Ini bertujuan mendapatkan nilai peroksida pada keadaan yang berbeza.

Penentuan Nilai peroksida (kaedah PORIM)

Sebanyak 5.00 g sampel minyak ditimbang dalam kelalang kon 250 mL. Kemudian, sebanyak 30 mL larutan asid asetik glasial : klorofom dalam nisbah 3:2 ditambah ke dalam sampel dan kemudiannya digoncang. Setelah itu, sebanyak 0.5 ml iodida tepu ditambah dan digoncang selama 1 minit. Sebanyak 30 mL air suling yang telah dididih dan disejukkan ditambah ke dalam kelalang. Sampel kemudiannya dititratkan dengan larutan piawai 0.1 natrium tiosulfat. Setiap kali penambahan larutan piawai dilakukan bekas sampel digoncang dengan kuat. Apabila warna kekuningan hampir hilang, beberapa titik larutan penunjuk kanji (1%) ditambah, di mana larutan sampel berubah menjadi biru. Larutan sampel kemudiannya dititrat sehingga larutan biru hilang. Nilai peroksida (militara/kg) dikira mengikut formula berikut:

$$\text{Nilai peroksida} = \frac{(V_1 - V_2) \times N \times 1000}{W} \quad (1)$$

V_1 = isipadu titratan sampel (mL)
V_2 = isipadu titratan pengosong (mL)
N = kenormalan natrium tiosulfat
W = berat sampel

Titratan blank (tanpa sampel) dilakukan sebanyak 2 kali dengan menggunakan kaedah yang sama.

Kaedah transformasi fourier infra merah (FTIR)

Spektrofotometer Perkin Elmer 2000, model GX dengan pengesan *deuterated triglycine sulphate* (DTGS) telah digunakan. Bilangan pengimbas penambah yang digunakan ialah 16 dengan resolusi 4 cm^{-1}. Bagi analisis kualitatif dan kuantitatif, prosedur Hendl et al. (2001) [14] telah digunakan di mana sampel diletakkan di antara dua sel dan ditutup dengan kemas. Kawasan serapan di antara 4000-400 cm^{-1} kemudiannya direkodkan. Pada kawasan ini terdapat serapan kumpulan berfungsi selain daripada kawasan cap jari yang memberikan ciri kepada sesuatu sebatian [15].

Pengoptimuman ANN bagi analisis kualitatif nilai peroksida

Dalam kajian ini ANN telah diaplikasikan dalam penentuan nilai peroksida bagi tiga sampel minyak komersil. Sistem jaringan tiga lapisan suapan hadapan yang mempunyai satu lapisan neuron terlindung telah digunakan dalam proses latihan jaringan dengan algoritma perambatan balik (BP) bagi tujuan memproses data. Lapisan input mengandungi 2 neuron yang mewakili nilai transmisi pada 3450 dan 3444 cm^{-1}. Nombor gelombang ini dipilih berdasarkan kajian terdahulu terhadap jalur hidroperoksida yang merujuk kepada regangan OO-H teroksida bagi metil oktadekadienoat yang memberi serapan pada 3450 cm^{-1} [6]. Dalam kajian Van de Voort et al (1994) [5] pula, mereka menyatakan getaran regangan bagi OO-H bagi t-butil hidroperoksida berlaku pada 3444 cm^{-1} di mana pada jalur ini perubahan peroksida dalam lemak dan minyak dapat dilihat.

Latihan ANN telah menggunakan program *Matlab* 5.3 (1992) di mana bilangan latihan ulangan yang difikirkan sesuai bagi kajian ini adalah di antara 100 hingga 300 manakala bilangan neuron terlindung yang akan digunakan adalah di antara 6 hingga 20. Kedua-dua parameter akan dioptimumkan latihannya melalui kaedah cuba jaya. Selain daripada itu, beberapa parameter lain telah ditetapkan (Jadual 1) sebelum arkitektur terbaik dipilih untuk digunakan dalam bahagian ini.

Keputusan dan Perbincangan

Spektrum serapan FTIR sampel minyak

Berdasarkan spektrum yang diperoleh (Rajah 1 dan Rajah 2) bagi ketiga-tiga sampel minyak, antara intrepretasi yang boleh dibuat terhadap dua spektrum yang diperoleh sebelum berlakunya pengoksidaan dan selepas berlakunya pengoksidaan ialah terdapat serapan frekuensi regangan =CH *cis* ditunjukkan pada jalur 3100- 2990 cm^{-1} [3]. Bagi C=C *cis* serapan regangannya ditunjukkan pada panjang gelombang 1648 cm^{-1} [16]. Apabila berlakunya proses pengoksidaan, spektrum minyak akan memberikan peningkatan serapan pada jalur regangan O-H iaitu sekitar kawasa 3800-3200 cm^{-1}. Pada keadaan ini serapan akan berkurangan berlaku pada jalur rangkaian ester trigliserida (1744 cm^{-1}) dan pada jalur regangan C-H iaitu sekitar 3050-2800 cm^{-1} [5, 7]

Peningkatan nilai peroksida boleh dilihat pada spektrum minyak B dan minyak C, berbanding dengan minyak A didapati peratus transmisi bagi kedua-dua minyak ini adalah rendah berbanding dengan minyak A. Boleh dikatakan kadar pengoksidaan dalam kedua-dua jenis minyak ini adalah tinggi berbanding dengan minyak A kerana minyak-minyak ini telah digunakan untuk menggoreng terlebih dahulu sebelum dianalisis. Menurut Kuntom et al. (1990) [17] pengoksidaan berlaku dengan cepat apabila suhu diberikan kepada minyak melebihi 60 ^{0}C dan setiap peningkatan 15 ^{0}C kadarnya adalah dua kali ganda. Selain daripada itu menurut Sherwin (1978) [18] interaksi dengan udara pada suhu yang tinggi turut kadar pengoksidaan. Kandungan asid oleik (18:1) sebanyak 44% dalam minyak sawit [19] turut menyumbangkan kepada peningkatan pengoksidaan dalam minyak sawit. namun begitu kemerosotan mutu minyak dengan peningkatan nilai peroksida tidak menjejaskan kualiti minyak sawit komersil kerana selain daripada tokoferol dan beta karotena yang menjadi antioksidan semulajasi terdapat antioksidan yang ditambah ke dalam minyak sawit supaya ia tahan lebih lama [20].

Pengoptimuman jaringan ANN

Proses latihan atau pengoptimuman jaringan dijalankan dengan mempelbagaikan lapisan jaringan dengan mengubah bilangan neuron dan lapisan terlindung. Jumlah SSE bagi setiap latihan direkodkan pada setiap penghujung ulangan latihan. Dalam kajian Wesolowski dan Suchacz (2001) [11] bagi mengklasifikasikan minyak, bilangan ulangan latihan yang digunakan adalah anatara 1-300 unit sahaja oleh itu, bilangan ulangan latihan maksimum yang difikirkan sesuai untuk latihan jaringan ANN adalah sebanyak 300 unit. Untuk mendapatkan jaringan yang baik, proses pengoptimuman telah dilakukan terhadap setiap parameter yang terlibat dalam arkitektur ANN. Parameter yang pertama dioptimumkan ialah kadar pembelajaran. Bilangan ulangan latihan dan neuron terlindung yang ditetapkan adalah masing-masing 300 dan 20. Rajah 3 menunjukkan hasil yang diperoleh apabila kadar pembelajaran diubah-ubahkan. Keputusan menunjukkan bahawa kadar pembelajaran pada 0.001 memberikan nilai ralat yang rendah. Oleh kerana didapati nilai ini sesuai, maka kadar pembelajaran ini dipilih untuk pengoptimuman parameter seterusnya.

Bagi mengoptimumkan bilangan ulangan latihan dan neuron terlindung, kadar pembelajaran telah ditetapkan iaitu 0.001, manakal nilai bagi kedua-dua parameter yang ingin dioptimumkan diubah-ubah. Jadual 1 menunjukkan nilai SSE yang direkodkan dengan menggunakan 6, 8, 10, 15 dan 20 neuron terlindung dengan ulang latihan yang digunakan adalah antara 100 hingga 300.

Keputusan yang diperoleh menunjukkan 6 neuron terlindung menghasilkan nilai SSE paling tinggi berbandinga dengan saiz neuron terlindung yang lain. Dalam setiap didapati dengan menambahkan bilangan saiz neuron terlindung SSE yang diperoleh semakin rendah. Perkara ini berlaku kerana berlakunya perubahan parameter perubahan parameter semasa latihan jaringan turut dipengaruhi oleh saiz neuron yang digunakan (Svozil et al. 1997) [21]. Satu corak menarik diperoleh pada setiap latihan apabila menggunakan 20 neuron terlindung dimana nilai SSE yang diperoleh semakin randah apabila bilangan ulangan latihan ditambah (Rajah 4). Menurut Taib et al. (1996) [22] keputusan ini disebabkan oleh hanyutan parameter (parameter drift) semasa latihan dijalankan. Nilai ini akan digunakan untuk kajian selanjutnya.

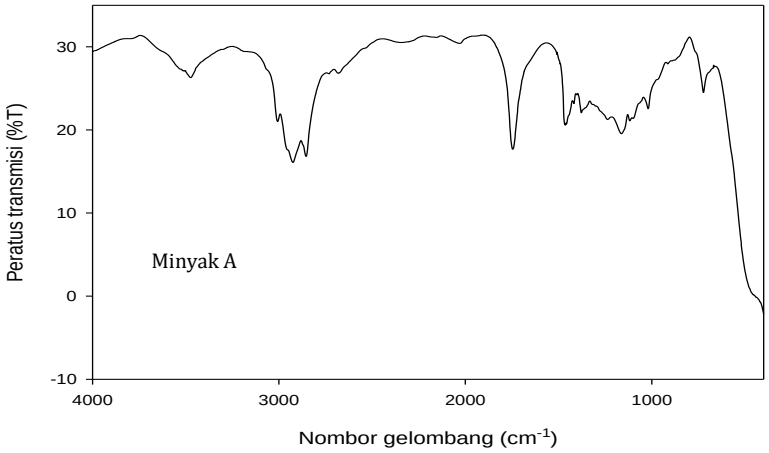
Ujian Ramalan

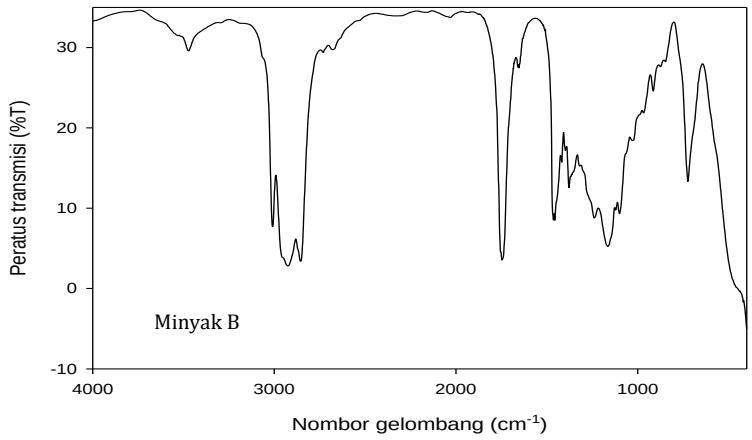
Jaringan ANN yang terlatih dengan 300 bilangan ulangan latihan telah digunakan dalam meramalkan nilai peroksida. Pemilihan jaringan ini kerana ralat yang diperoleh adalah rendah. Menurut Hussain et al. (1996) [8] satu

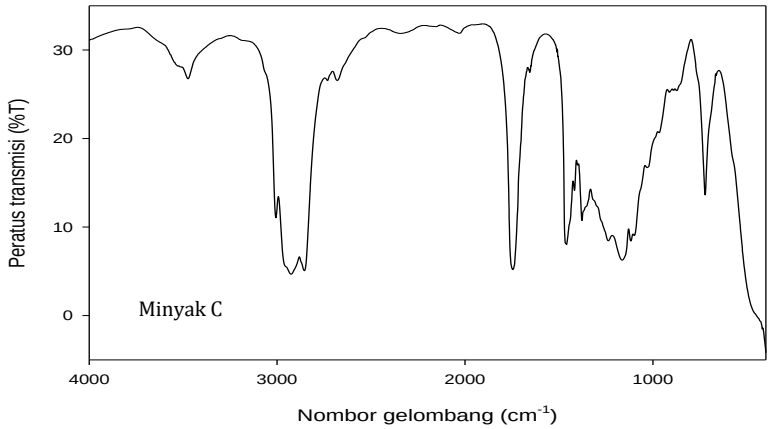
model dengan ralat yang paling minimum akan membuat pencaman yang baik. Nilai yang diramalkan oleh ANN kemudiannnya dibandingkan dengan nilai sebenar yang diperoleh melalui kaedah penitratan PORIM (Jadual 2). Keputusan yang diperoleh menunjukkan purata ralat bagi 20 neuron terlindung adalah yang paling rendah iaitu 0.48 dengan kadar ramalan yang baik dan persis.

Ujian pengesahan

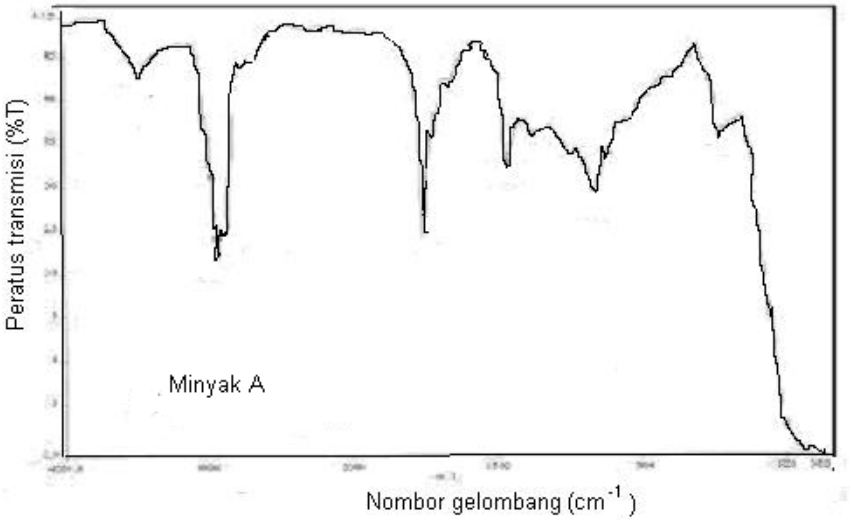
Dalam kajian ini perbandingan telah dibuat antara nilai yang diramalkan oleh ANN dengan nilai sebenar. Satu garis lurus penyesuaian terbaik dengan kecerunan diperoleh 1.1 (Rajah 5). Menurut Miller dan Miller (2000) [22], jika kecerunan garis regrasi yang diperoleh adalah > 1 atau < 1 menunjukkan terdapat ralat yang sistematik yang berlaku dalam dalam salah satu plot kalibrasi yang dibuat. Namun begitu, dengan pintasan pada 0 dan kecerunan menghampiri satu memberikan nilai kepercayaan lebih daripada 95% dimana keputusan yang diperoleh adalah persis [23].

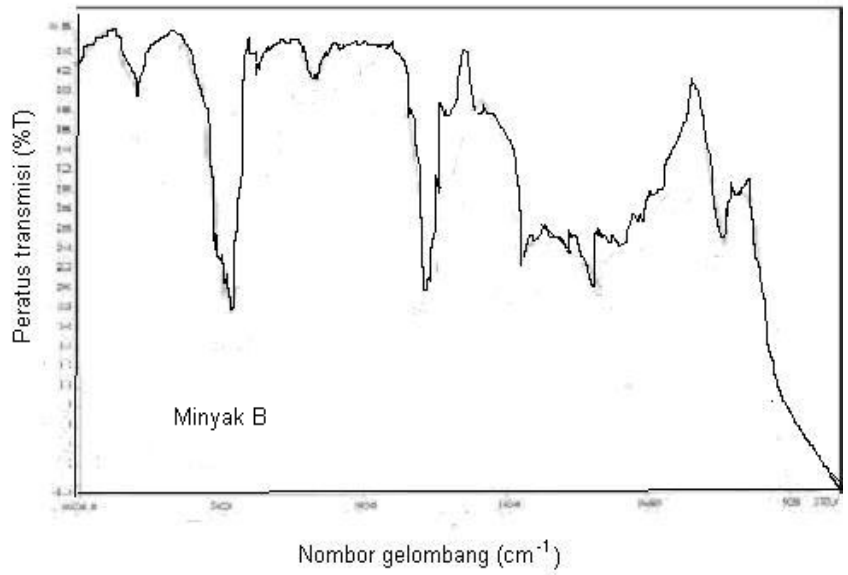


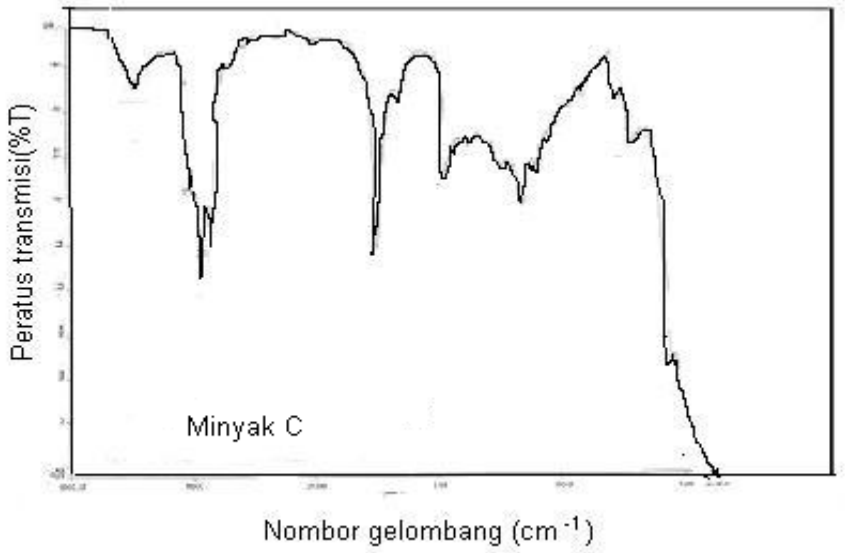




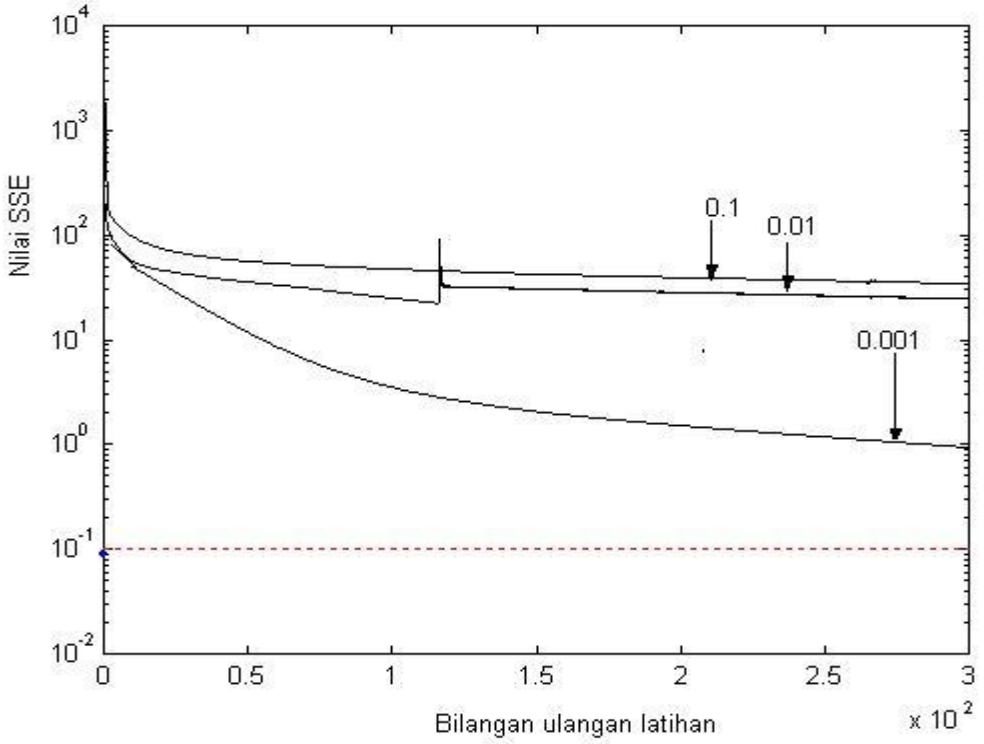
Rajah 1. Serapan FTIR untuk tiga jenis minyak komersil telah teroksida bagi A, B, C



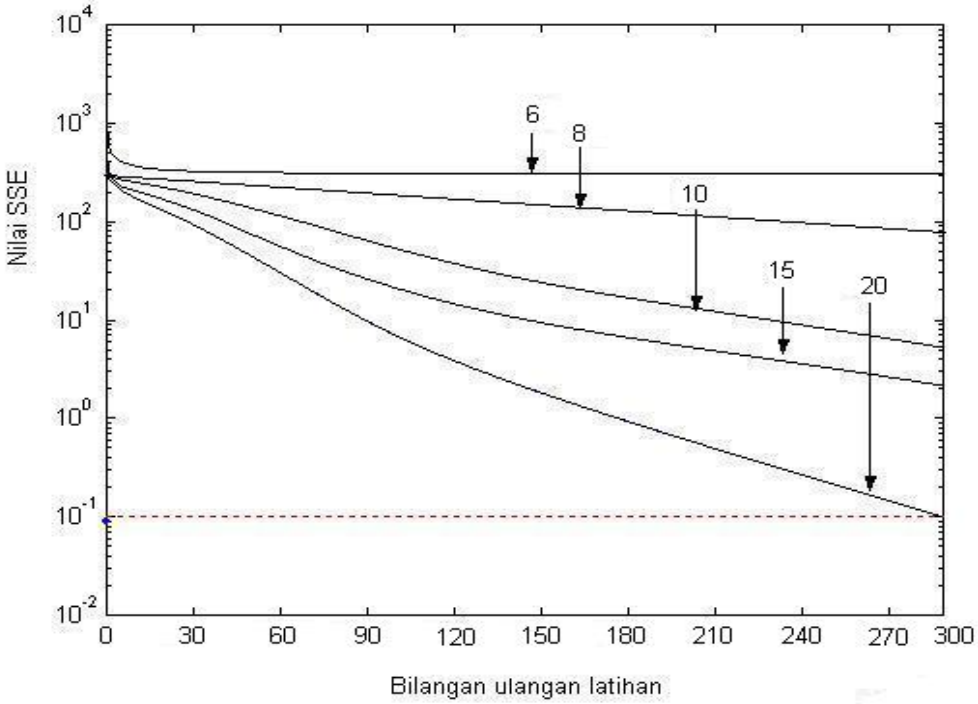




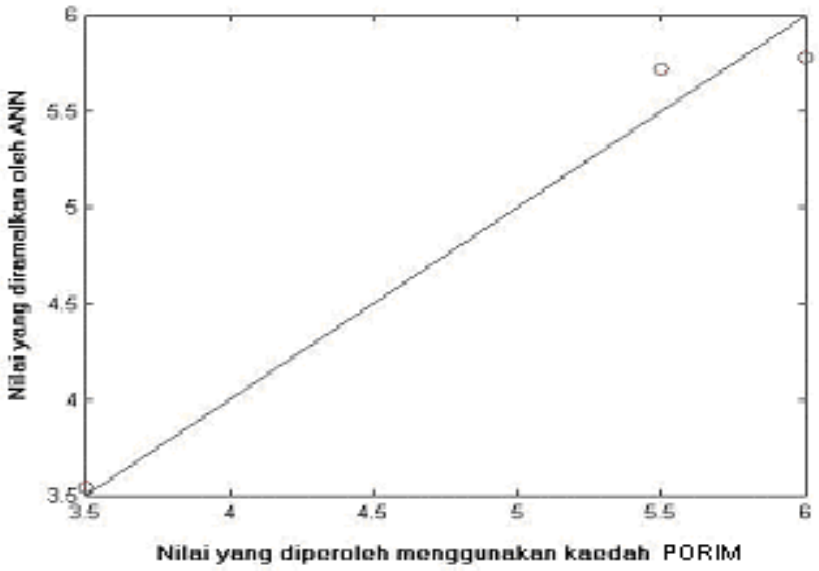
Rajah 2. Spektrum FTIR bagi minyak komersil yang belum teroksidabagi minyak A, B dan C



Rajah 3. SSE yang diperoleh dalam proses pengoptimuman kadar pembelajaran apabila bilangan ulangan latihan 300 dan neuron terlindung 20 ditetapkan



Rajah 4. SSE yangt diperoleh apabila bilangan ulangan latihan ditetapkan 300 dan bilangan neuron terlindung yang berbeza digunakan



Rajah 5. Perbandingan antara ramalan nilai peroksida yang dibuat oleh ANN dengan nilai peroksida sebenar menggunakan kaedah PORIM

Jadual 1. Nilai SSE yang diperoleh dengan menggunakan saiz neuron terlindung yang berbeza pada bilangan ulangan latihan antra 100-300.

Bilangan ulangan latihan	Neuron terlindung				
	6	8	10	15	20
100	3.500	0.147	3.500	3.500	0.243
150	3.500	0.127	3.500	0.846	0.127
200	3.500	3.500	3.500	3.500	0.126
250	3.500	3.500	0.126	0.127	0.116
300	3.500	3.500	0.126	3.500	0.098

Jadual 2. Perbandingan nilai peroksida yang diramalkan oleh ANN dengan nilai peroksida yang diperoleh menggunakan kaedah PORIM

Nilai peroksida (kaedah PORIM)	Bilangan neuron terlindung									
	6		8		10		15		20	
	Ramalan	Ralat	Ramalan	Ralat	Ramalan	Ralat	Ramalan	Ralat	Ramalan	Ralat
3.50	5.00	1.50	5.00	1.50	3.50	0.00	5.00	1.50	3.54	0.04
5.50	5.00	0.50	5.00	0.50	5.75	0.25	5.00	0.50	5.72	0.22
6.00	5.00	1.00	5.00	1.00	5.75	0.25	5.00	1.00	5.78	0.22
Jumlah Ralat		**3.00**		**3.00**		**0.51**		**3.00**		**0.48**

Kesimpulan

Penggunaan ANN dalam menentukan nilai peroksida bagi tiga sampel minyak masak komersil pada keadaan berbeza berjaya dilakukan. Arkitektur jaringan tiga lapisan suapan hadapan dengan kadar pembelajaran sebanyak 0.001 dan bilangan ulangan latihan sebanyak 300 yang mengandungi susunan neuron 2: 20: 1 didapati sesuai digunakan bagi tujuan memproses dan pencaman corak spektrum FTIR. Dalam ujian ramalan, jaringan terlatih ini memberikan ralat purata terendah, iaitu 0.48. Satu garis lurus dengan kecerunan 1.1 telah diperoleh dalam ujian pengesahan. Ini menunjukkan ANN dapat meramalkan sesuatu nilai berdasarkan corak spektrum diperolehi walaupun nilai input yang diberikan adalah sedikit. Selain daripada itu penggunaan ANN adalah mudah tanpa memerlukan penggunaan satu model matematik yang kompleks. Kajian lanjut boleh dilakukan dengan menggunakan ANN sebagai satu alternatif kepada model matematik yang sedia ada.

Rujukan

1. Cornelius, J.A. (1969). Some technical aspects influencing the quality of palm kernels. *J. Sci. Agric.* 17: 57-61.
2. Choo, Y.M. (1999). Speciality products: carotenoids. Dlm. Yusof, B. Jalani, B.S. & Chan, K.W. (pnyt). Advance in oil palm research, hlm. 34-52. Kuala lumpur. PORIM
3. Guillen, M.D & Cabo, N.(1997). Infrared spectroscopy in the study of edible oils and fats, *J. Sci. Food Agric*. 75: 1-11.
4. Moh, M.H. Che Man, Y.B. Badlishah, B.S. Jinap, S. Saad. M.S. & Abdullah, W.J.W. (1999). Quantitative analysis of palm carotene using FTIR and NIR spectroscopy. JAOCS. 76 (2): 249-254.
5. Van de Voort, F.R, Ismail A.A., Sedman, J., Dubois, J. & Nicodemo, T., (1994). The determination of peroxide value by FTIR, *J. Am. Oil Chem. Soc*. 71:921-926
6. Fukuzumi, K. & Kobayashi, E. (1972). Quantitative determination of methyl octadecadienoate hydroperoxide by infrared spectroscopy. *J. Am. Oil Chem. Soc*. 49: 162-165.
7. Moh, M.H & Tang, T.S. (1999). A review on the quantitative analysis of fats and oils using FTIR. *PORIM Bulletin*. 41:30-37.
8. Hussain, S. Devi, K.S. Krishna,D. & Reddy, P.J. (1996). Characterization and identification of edible oil blend and prediction of the composition by ANN- A case study. *Chemmometrics and Intelligent Lab. Syst*. 35:117-126
9. Nora Izma, A.A. (2003). Pembangunan kaedah analisis menggunakan FTIR dan NIR dalam membandingkan minyak tulen dan minyak campuran. Tesis Pusat pengajian Sains Kimia & Teknologi Makanan. UKM, Bangi
10. Basiron, Y. (2001). Global oils and fats business: challenges in new millenium. *Oil Palm Industry Economic Journal*. 11: 1-9.
11. Wesolowski, M. & Suchacz, B. (2001). Classification of rapeseed and soybean oils by use of unsupervised

pattern recognition method and neural networks. *J. Anal. Chem*. 371: 323-330.
12. Azwan Mat Lazim, Mohd Zuli Jaafar, Phang Wei Shong & Suzereen Jamil (2013). Penentuan Kualiti Minyak Masak dan Lemak Komersial Menggunakan Teknik Kimometik. The Malaysian Journal of Analytical Sciences, Vol 17 No 1 (2013): 146 – 152
13. *PORIM Test Method*. (1995). Kuala Lumpur: PORIM
14. Hendl, O., Howell, J., Lowery, J. & William Jones (2001). A rapid and simple method for the determination of iodine values using derivatives FTIR measurements, *Anal.Chim. Acta*. 427:75-81
15. Kamaliah Mahmood & Norsaadah A.R. (1997). *Kaedah spektroskopi dalam pengenalpastian sebatian organik*. Kuala lumpur: Penerbit Universiti Malaya.
16. Che Man, Y.B., Moh, M.H. & Van de Voort, F.R. 1999. Determination of free fatty acid in crude palm oil and refined bleached deodorized palm olein using FTIR. *Journal of American Oil Chemist Society.* 76(4): 485-490.
17. Kuntom, A. (1990). Oxidation and palm oil. *PORIM Bulletin*. 20: 32-40.
18. Sherwin, E.R. (1978). Oxidation and antioxidantin fat and oil processing. *Journal of American Oil Chemist Society.*. 55: 809-814.
19. Fauziah, A. Razali, I. & Nor Aini, S. (2000). Frying performance of palm olein and high oleic sunflower oil during batch frying of potato crisps. *Palm Oil Development*. 33: 2-7.
20. Berger, K.G. (1982). Refined palm oil quality as received. *PORIM Bull.* 4: 19-26.
21. Svozil, D. Kvasnicka, V. & Prospichal, J. (1997). Introduction to multilayer feed-forward neural network. *Chemmom. Intell. Lab. Sys.* 39: 42-62.
22. Taib, M.N & Narayanaswamy, R. (1996). Multichannel calibration technique for optical fibre chemical sensor using ANN. *Sens. Actuators. B*. 38-39:365.
23. Miller, J.N & Miller, J.C. (2000). *Stastistics and chemometrics for analytical chemistry*. Ed. Ke-4. England. Perason Education Ltd.
24. March, J.G., Simonet, B.M. & Grases, F. (1999). Determination of phytic acid by catalytic fluorimetric. *Analyst*. 124:897-900.

The Malaysian Journal of ANALYTICAL SCIENCES ISSN 1394-2506

DEVELOPMENT AND VALIDATION OF RP-HPLC METHOD FOR THE ESTIMATION OF CLOPIDOGREL BISULPHATE

(Pembangunan dan Penentusahkan Kaedah RP-HPLC Terhadap Klopidogrel Bisulfat)

Bhagat Dimple*, Mannur Vinodh, Mastiholimath Vinayak

Department of Quality Assurance,
K.L.E .University's College of Pharmacy, JNMC Campus,
Nehrunagar, Belgaum 590 010, Karnataka, India

**Corresponding author: sukubhagat*@gmail.com

Abstract

A novel, simple, precise, accurate and economical method has been developed and validated for the estimation of Clopidogrel bisulphate. Chromatographic analysis was performed on Hypersil BDS C_{18} (250 × 4.6 mm, 5 µm) column. Mobile phase used was potassium dihydrogen orthophosphate buffer: acetonitrile in a ratio of 32:68, pH was adjusted to 4.0 using orthophosphoric acid and 0.1 ml of triethyl amine was added for peak sharpness. Isocratic analysis was performed on SPD-20A double beam UV spectrophotometer at a detection range of 220 nm with a flow rate of 1.0 ml/min. The retention time for clopidogrel bisulphate was 3.847 min. The linear response was found to be in a concentration range of 50-150 µg/ml with a correlation coefficient of 0.999. The mean recovery was found to be 100.67 %. Intraday and Interday precision variations were found to be 1.88 and 0.863 respectively, which are within the limit of % RSD not more than 2. Hence the developed method is simple, fast, accurate and reproducible. It is suitable for routine quality control analysis of clopidogrel bisulphate.

Keywords: RP-HPLC, validation, clopidogrel bisulphate, linearity, accuracy, precision

Abstrak

Satu kaedah baru yang mudah, tepat, jitu dan ekonomikal telah dibangunkan dan disahkan terhadap analisa klopidogrel bisulfat. Analisis kromatografi telah dijalankan mengunakan turus Hypersil BDS C18 (250 × 4.6 mm, 5 µm). Fasa bergerak yang digunakan ialah larutan penampan kalium dihidrogen ortofosfat : asetonitril dalam nisbah 32 : 68, pH telah diubah kepada nilai 4.0 menggunakan asid ortofosforik dan 0.1 ml larutan trietil amine ditambah untuk ketajaman puncak. Analisis isokratik telah dijalankan ke atas SPD- 20A spektrofotometer UV pada julat pengesanan 220 nm dengan kadar aliran 1.0 ml / min. Retensi masa bagi klopidogrel bisulfat adalah 3. 847 min. Sambutan linear didapati berada dalam julat kepekatan 50-150 µg ml dengan pekali korelasi adalah 0.999. Min perolehan semula adalah 100. 67 %. Variasi kejituan ujian Intra dan Inter-hari didapati masing – masing adalah 1.88 dan 0.863 yang berada dalam julat had % RSD tidak lebih daripada 2. Maka kaedah yang dibangunkan adalah mudah, cepat, tepat dan keboleh ulangan. Ia sesuai untuk analisis rutin kawalan mutu bagi klopidogrel bisulfat.

Kata kunci: RP- HPLC, Penentusahkan, klopidogrel bisulfat., Kelinearan , Ketepatan, Kejituan

Introduction

Clopidogrel bisulphate is an antiplatelet agent or platelet aggregation inhibitor. The IUPAC name of clopidogrel bisulphate is Methyl (+)-(S)-α-(2-chlorophenyl)-6,7dihydrothieno [3,2-c]pyridine-5(4H)acetate sulfate (Figure 1).The drug is practically insoluble in water at neutral pH, but freely soluble at pH 1[1]. It is used to inhibit blood clots in coronary artery disease, peripheral vascular disease, and cerebrovascular disease [2].

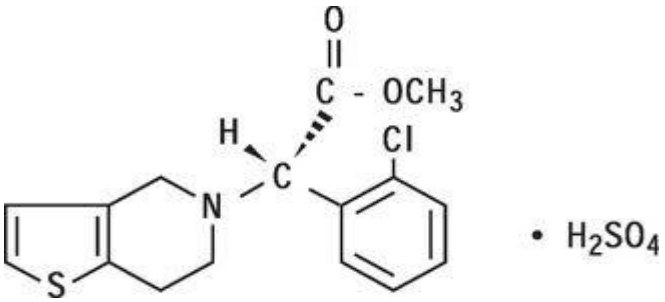


Figure 1. Structure of clopidogrel bisulfate [1]

The quantitative analysis was made on Shimadzu prominence system using reverse phase chromatographic method to obtain less retention time. Hence clopidogrel bisulphate is insoluble in water; RP-HPLC method was used. Several analytical methods which are commonly used to identify the drug concentration and for quantification of drugs for the determination of clopidogrel bisulphate are Spectrofluorometry [3], LC-MS/MS [4], HPLC [5, 6], HPTLC [7, 8] and potentiometry method [9].

The aim of this study was to develop a RP-HPLC method, which could be employed for the routine analysis of the drug clopidogrel bisulphate.

Materials and Methods

Chemicals and Reagents

Working standard of clopidogrel bisulphate was obtained from Sidmak India (pvt) Ltd Valsad, India having purity > 99.2%. HPLC grade Acetonitrile and Water was procured from Merck, Rankem Ltd., Mumbai, India. Phosphate buffer (pH 4.0) used as diluent and all chemical reagents used were HPLC grade.

Instrumentation

Spectral scan was made on a Shimadzu UV 1800 pc double beam spectrophotometer, with spectral bandwidth of 190-800 nm, wavelength accuracy of + 0.3 nm with automatic wavelength corrections using a pair of 10 mm quartz cells. All Spectral measurements were done using Spinchrom software.

Chromatographic Conditions

Chromatographic analysis was performed on Thermo Hypersil BDS C_{18} (250 × 4.6 mm, 5 µm) column with a mobile phase used as potassium dihydrogen orthophosphate buffer adjusted pH 4.0 with orthophosphoric acid: acetonitrile in a ratio of 32:68 and 0.1 ml of triethyl amine was added for peak sharpness. The mobile phase was degassed and filtered through 0.45 µm membrane filter before pumping into HPLC system. Isocratic analysis was performed on SPD-20A double beam UV spectrophotometer at a detection range of 220 nm at a flow rate of 1.0 ml/min. The injection volume was 20 µl.

Preparation of Phosphate Buffer

Dissolve 10 g of Potassium dihydrogen orthophosphate and add 0.1ml of triethyl amine in 1000 ml distilled water. Adjust pH 4.0 with orthophosphoric Acid.

Preparation of Standard Solution

An accurately weighed quantity of 25mg clopidogrel bisulphate transferred in 25ml volumetric flask, dissolved with 10 ml of acetonitrile and volume was made up to the mark with acetonitrile sonicated for 10 min. From that solution pipette out 1 ml in 10 ml volumetric flask and volume was made up to the mark with mobile phase to make final Concentration 100 µg/ml.

Procedure

Equilibrate the column with mobile phase at prescribed condition until a stable baseline is achieved. Separately inject diluent, standard solution and test preparation into liquid chromatography. Measure the response for all peaks.

Results and Discussion

The developed method was validated for parameters like linearity, accuracy, precision, robustness, ruggedness, sensitivity and system suitability [10, 11].

Method development and optimization

Optimized chromatographic conditions for estimation of clopidogrel bisulphate are finalized using Column Thermo Hypersil BDS C_{18} (250×4.6 mm, 5 µm) consisting of mobile phase acetonitrile: phosphate buffer pH 4.0 in a ratio of 68:32. HPLC pump mode was made Isocratic with a flow rate of a 1.0 ml/min over the detection wavelength range of 220 nm. Standard spectrum of clopidogrel bisulphate is as shown in Figure 2.

Injection volume was made with Rheodyne injector 7725i of 20 µl. The run time was 10 min. The retention time for clopidogrel bisulphate was found to be 3.8 min.

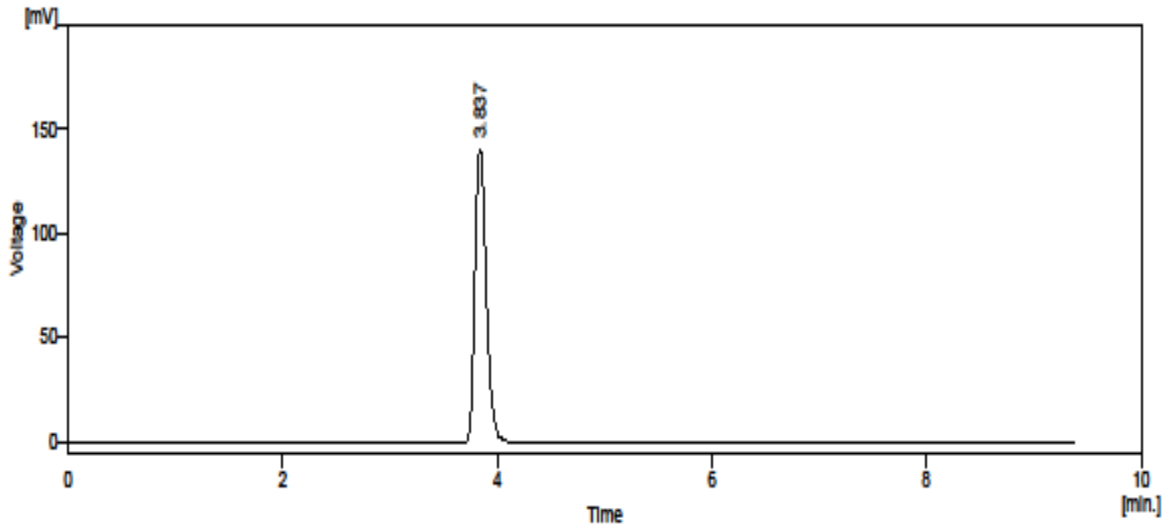


Figure 2. Chromatogram of standard preparation of Clopidogrel bisulphate

System Suitability

In these studies, 5 replicate injections of the drug at a concentration of 100 µg/ml were injected and evaluated for the parameters such as Retention time, theoretical plates and tailing factor. The results obtained from the System Suitability studies were calculated and recorded in Table 1.

Table 1. System suitability parameters for Clopidogrel bisulphate

Name	Retention Time	Area	% Area	Theoretical Plate Count	Tailing Factor
Clopidogrel bisulphate	3.8	1037.18	100	6073	1.63

Linearity

The linear response was found in a concentration range of 50-150 µg/ml. The linearity plot is drawn in figure 3 and the correlation co-efficient (r^2), y-intercept and slope of regression line were found to be 0.999, 9.521, -2.834 respectively and recorded in Table 2.

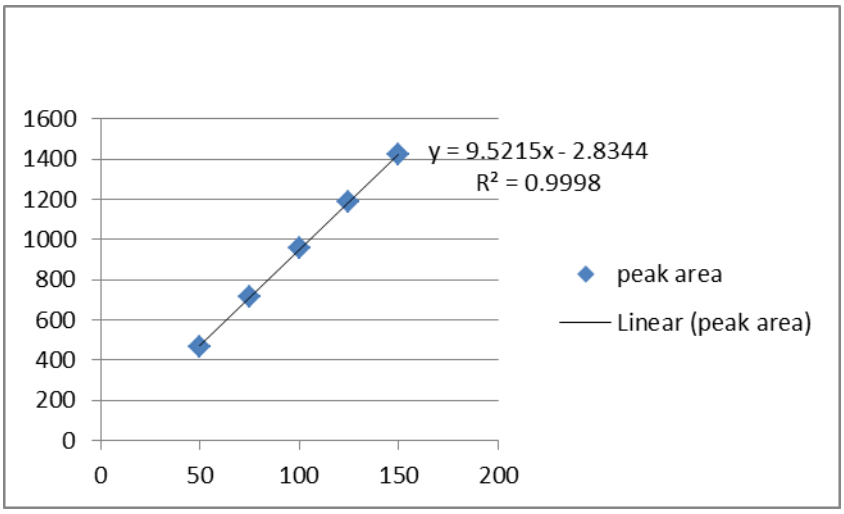


Figure 3. Calibration curve of clopidogrel bisulphate at 220 nm.

Table 2. Linearity study for clopidogrel bisulphate

Injection No.	Concentration (µg/ml)	Area
1	50	467.510
2	75	715.577
3	100	954.103
4	125	1187.576
5	150	1421.576

Accuracy

The accuracy was determined at three levels: 80, 100 and 120 %. From the peak area of the drug, percentage recovery (%) was calculated for 80, 100 and 120 %, which are 99.78, 101.54 and 100.70 % respectively. Percentage recovery was found to be in the limit of 98 – 102 % and recorded in Table 3. Hence, the method termed as accurate.

Precision

The precision expressed as standard deviation or Relative standard deviation.

Intraday Precision

In this study, six injections of standard solution of 100 µg/ml were injected into the chromatographic system in different time intervals within a day. % RSD for retention time was found to be 0.768 and for area 1.88, which are within limit of % RSD not more than 2 and recorded in Table 4.

Table 3. Accuracy study for clopidogrel bisulphate

Accuracy level	Amount added	Area	Amount recovered	% Recovery (Mean)	SD	% RSD
80%		1708.768	80.66			
80%	80	1696.497	79.39	99.78 %	5.71	0.336
80%		1696.798	79.42			
100%		1913.944	101.90			
100%	100	1903.472	100.82	101.54 %	4.94	0.258
100%		1913.944	101.90			
120%		2098.460	121.00			
120%	120	2082.636	119.36	100.70 %	11.02	0.525
120%		2109.498	122.14			

*average of three determinations

Table 4. Intraday precision of clopidogrel bisulphate

Injection No.	Retention Time (min)	Area
1	3.810	952.166
2	3.780	950.675
3	3.780	949.230
4	3.847	975.080
5	3.853	990.675
6	3.830	950.788
Average	3.817	959.135
SD	0.029	18.05
% RSD	0.768	1.88

Interday Precision

In this study, six injections of standard solution of 100 µg/ml were injected into the chromatographic system at different days. % RSD for retention time and for area was found to be 0.863 and 1.99 respectively, % RSD NMT 2 and recorded in Table 5.

Robustness

The robustness was obtained by altering the flow rate by 1.0 ml/min (altered flow rate 0.8 ml/min and 1.2 ml/min) pH 4.0 (altered pH 3.9 and 4.1). The results were obtained from robustness study were calculated. Percentage RSD for flow rate and for pH were found to be 1.49 and 1.03 respectively, % RSD NMT 2, and recorded in Table 6. Hence the method termed as robust.

Table 5. Interday Precision of Clopidogrel bisulphate

Injection No.	Retention Time	Area
1	3.810	952.166
2	3.780	936.951
3	3.780	949.230
4	3.853	995.554
5	3.863	1017.480
6	3.837	970.751
Average	3.821	969.355
SD	0.033	28.96
% RSD	0.863	1.99

Table 6. Robustness study of clopidogrel bisulphate

Condition	Modification	Mean Area ± SD*	% RSD	Mean % RSD
Flow Rate (ml/min)	0.8 ml/min	1041.542 ± 17.83	1.71	1.49
	1.2 ml/min	902.667 ± 11.43	1.27	
pH	3.9	952.471 ± 7.63	0.80	1.03
	4.1	968.01 ± 12.18	1.26	

*average of three determinations

Ruggedness

The ruggedness of the method was determined by carrying out the experiment by different operators. Percentage RSD were calculated and recorded in Table 7. Result obtained by different analyst and different day were found within acceptable limit, which shows that test method is rugged.

Table 7. Ruggedness study of Clopidogrel bisulphate

	Analyst I	Analyst II
Injection no.	**Area**	**Area**
1	479.040	480.981
2	486.911	493.290
Average	482.976	487.136
SD	3.940	6.150
% RSD	0.810	1.260

Limit of Detection and Quantification (LOD and LOQ)

The Limit of Detection and Quantification**,** LOD and LOQ data was calculated and recorded in Table 8. LOD and LOQ were found to be 1.8728, 5.6752 ppm respectively.

Table 8. Limit of Detection and Quantification in this study

Parameters	Clopidogrel bisulphate
LOD (µg/ml)	1.8728
LOQ (µg/ml)	5.6752

Conclusion

The developed analytical method is validated as per ICH guidelines. A rapid and simple RP-HPLC method for determination of clopidogrel bisulphate has been developed and validated. The method involved a mobile phase consisting of acetonitrile: phosphate buffer (pH 4.0) 68:32 used at 220 nm. The retention time was 3.837 min at a flow-rate of 1.0 ml/min and the injection volume was 20 µl. The total run time for an assay was approximately 10 min. This proposed method was validated for parameters including linearity, accuracy, sensitivity, precision, ruggedness and robustness. The present study is concerned for the development and validation of simple, specific, sensitive, accurate and precise RP-HPLC method for the determination of clopidogrel bisulphate for routine analysis work.

Acknowledgement

The authors wish to thank Dr. Anjan Paul from Sidmak India (pvt) Valsad, Gujarat for providing drug sample and Mr. Ketan Patel from Molecule Laboratory, Ahmadabad, Gujarat for providing the facilities to carry out this research work.

References

1. Clopidogel Drug Description on www.rxlist.com/plavix-drug.htm.
2. Clopidogrel Information on en.wikipedia.org/ wiki/ Clopidogrel.
3. Saddet, D., & Erkem, A. (2009). Rapid and accurate determination of clopidogrel in tablets by using spectrophotometric and chromatographic techniques. *Commun Fac Sci Univ Ank Series* B, 55 (1) : 1-16.
4. Venkanna, B., Shreedhara, C., & Ajitha, M. (2011). Rapid and rugged bio analytical method development and validation clopidogrel in human plasma using liquid chromatography/ tandem mass spectroscopy, *American Journal Pharmtech Research*, 1 (2) : 66 - 80.
5. Sahu, S., & Sarangi, S. Development and validation method for the estimation of clopidogrel in bulk and pharmaceutical dosage form, International Journal Research of Pharmaceutical Science, 3 (2) : 224-27.
6. Josh, K., & Jayasehar, P. (2013). Stability indicating HPLC determination of clopidogrel bisulfate in pharmaceutical dosage forms, *International Journal of Comprehensive Pharmacy*, 1 (06): 1 - 5.
7. Himani, A., Kaul, N., Paradkar, A.R., Mahadik, K.R. (2003). Stability indicating HPTLC determination of clopidogrel bisulphate as bulk drug and in pharmaceutical dosage form, *Talanta* 61: 581-89.
8. Sinha, P.K., & Mrinalini, C. (2009). A Validated Stability Indicating HPTLC Method for Determination of Aspirin and Clopidogrel Bisulphate in Combined Dosage Form, *Eurasian J Anal Chem*, 4 (2) : 152-60.
9. SABER, L.A., Elmosallamy, M.A. (2008). Journal of Food and Drug Analysis, Liquid Chromatographic and Potentiometric Methods for Determinations of Clopidogrel, 16 (2): 11-18.
10. Validation of Analytical Procedures: Methodology, ICH Harmonised Tripartite Guidelines, (1996), 1-11.
11. Validation of Analytical Procedures: Methodology, ICH Harmonised Tripartite Guidelines, (1994), 1-7.

The Malaysian Journal of ANALYTICAL SCIENCES ISSN 1394-2506

DETERMINATION OF ANILINE DEGRADED FROM SUDAN I IN CLOTHS

(Penentuan Anilin Yang Terurai Daripada Sudan I Dalam Kain)

Chong Kian Wei*, Loke Chui Fung and Chan Kar Men

Department of Chemistry and Biology,
Faculty of Applied Sciences and Computing,
Tunku Abdul Rahman University College, Jalan Genting Kelang, Setapak, 53300 Kuala Lumpur, Malaysia

**Corresponding author: chongkw@acd.tarc.edu.my*

Abstract

A method development for the determination of an aromatic amine degraded from an azo dye in cloths was carried out. Sodium dithionite was used to cleave the azo bond of Sudan I into its aromatic amines, and the amines, mainly aniline were analyzed using high performance liquid chromatography (HPLC) with UV detection. The efficiency of the reduction process of Sudan I, based on the degree of decolorization of dye, was measured using the spectrophotometer. The optimized values of the reduction process was found effective when 1:1 ratio of 0.30% sodium dithionite to Sudan I (dit/Sud) was used at pH 8. The recovery percentage and relative standard deviation (R.S.D.) of this method was found to be 62.9 – 88.4% and 7.6 – 21.5%, respectively. The proposed method was tested on self-dyed cloth samples with Sudan I. Aniline released from the reduction of Sudan I was detected in the self-dyed cloth samples. The results of this study demonstrate the applicability of sodium dithionite for the reduction of the azo dye in the cloth samples.

Keywords: aniline, Sudan I, sodium dithionite, azo dye

Abstrak

Satu perkembangan kaedah untuk penentuan amina aromatik yang terdegradasi daripada pencelup azo dalam kain-kain telah dijalankan. Natrium ditionit telah digunakan untuk menguraikan ikatan azo Sudan I kepada amina aromatik, dan amina, terutamanya anilina telah dianalisis dengan menggunakan kromatografi cecair prestasi tinggi dengan pengesanan UV. Kecekapan proses penurunan Sudan I, berdasarkan tahap penyahwarnaan warna pencelup, telah diukur dengan menggunakan spektrofotometer. Nilai optimum dalam proses penurunan ini telah didapati berkesan apabila nisbah 0.30% natrium ditionit kepada Sudan I (dit/Sud) digunakan pada pH 8. Peratusan pemulihan dan nilai sisihan piawai relatif (SPR) bagi kaedah ini telah ditentukan sebanyak 62.9 – 88.4% dan 7.6 – 21.5%, masing-masing. Kaedah yang dicadangkan telah diuji ke atas sampel-sampel kain yang telah dicelup sendiri dengan Sudan I. Anilina yang dibebaskan daripada penurunan Sudan I telah dikesan dalam sampel-sampel kain yang dicelup sendiri. Keputusan kajian ini menunjukkan bahawa kebolehan pengunaan natrium ditionit untuk penurunan pencelup azo dalam sampel kain.

Kata kunci: anilina; Sudan I; natrium ditionit; pencelup azo

Introduction

One of the most versatile and largest class of synthetic dyes commonly used today are the azo dyes [1,2]. This is because azo dyes offer a vast spectrum of colors that have good color fastness and are cheaper to be manufactured [3]. Azo dyes are widely used in various industrial application as colorants. Products such as textiles, food, leather, paper, plastics, paints, inks, cosmetics and etc. are known to contain azo colorants [1]. The colors of azo dyes are chracterized by the chromophores associated with the azo groups (-N=N-) [3].

Azo dyes are commonly synthesized by the coupling reaction of a diazotized aromatic amine with another aromatic amine or a phenol [1]. Their structure would contain at least one azo group (-N=N-) bonded to an aromatic ring (R-NH_2) [4]. Not only is the dye itself that is hazardous, but the aromatic amine when it is cleaved from the dye poses as dangerous by-products [5]. The problem with azo dyes arises primarily from the reduction of the azo group causing them to be potentially toxic [1]. This poses a risk to consumers because some of the aromatic amines formed may be confirmed or suspected carcinogens. Azo dyes are easily reduced under anaerobic conditions to

form aromatic amines and are relatively resistant to aerobic degradation [3]. The electron density of the azo bond affects the degree of degradation of the azo dye by reduction. Electron withdrawing groups can be used to reduce the electron density of the azo bond thus, causing degradation of the azo dye and releasing the colorless aromatic amines [5].

In many developing countries where the textile industry is a major industrial sector, which is a major source of discharged dye wastewater that pollutes the natural water source systems. The discharge of this large quantity of industrial wastewater containing azo dyes is a primary concern. The concerns include harming the aquatic life (both flora and fauna) as well as decreasing the aesthetic aspects of the water, since azo dyes are not biodegradable in aerobic conditions, not to mention public human health. Coloured water may reduce light penetration from the sun, causing primary aquatic plant productivity to decrease [4].

One can be exposed to azo dyes via dermal absorption, inhalation and oral ingestion [6]. Furthermore, it was discovered that the azo group can be cleaved by skin microflora, azoreductases in intestinal bacteria and liver cells [3]. Besides that, photochemical reactions through human sweat and dyes on clothings could also form aromatic amines [2]. Sudan I is one of the many types of synthetic azo dyes and it would form aniline when cleaved at the azo bond. Both Sudan I and aniline are classified under the category 3 of carcinogens by the International Agency for Research on Cancer (IARC), which means that these chemicals are harzardous, but their carcinogenicity cannot be specifically classified to humans, although some forms of bladder and liver cancer were observed in mice and rats [7,8].

Given the potential harzardous impact of aniline in daily consumer activities, it is necessary to develop a quick and inexpensive mechanism to detect and measure this compound. This study therefore aims to (i) develop an optimized method to degrade Sudan I and (ii) determine the amount of aniline which can be found in cloths dyed with Sudan I. These objectives enable researchers to measure the potential hazards of dyed textiles based on the amount of aniline that could be released from Sudan I, with the intention of raising awareness to the impacts of these dyes have towards to the consumers and environment.

Several methods have been used to degrade azo dyes to release aromatic amines from different samples such as textiles [5], leather [9], hair dyes [10] and toy products [1]. Other reagents such as hydrogen peroxide (coupled with UV radiation) [11] and Fenton's reagent [4] are oxidizing agent that could also degrade azo dyes. The methods used in these researches were mostly complex and expensive. Biological treatment on azo dyes with azoreductases [12], laccases [13], extracellular fluid protein from *Streptomyces* species [14] and bacterial strain *Shewanellaoneidensis* MR-1 [15] were also possible. However, handling of biological entities or products are demanding as incubation and pretreatment procedures are necessary. Sodium dithionite is commonly used as a reducing agent for the reduction of dye [1,5,9]. Thus, due to the effectiveness of this reagent which had been employed by other researchers in their studies; therefore it was selected to be used to degrade Sudan I azo dye in this study. In this study, the parameters such as concentration of sodium dithionite, dit/Sud ratio, temperature of reduction and pH were studied based on the degree of decolorization which was measured using the spectrophotometer. The optimized values were then applied on self-dyed cloth samples to test the applicability of the proposed method. The determination of the released aniline from the Sudan azo dye was carried out using HPLC.

Experimental

Reagents

The aromatic amine, aniline ($C_6H_5NH_2$, ≥ 98.5% purity) and azo dye, Sudan I ($C_{16}H_{12}N_2O$, pure) were purchased from BDH Chemicals Ltd (England) and Acros Organics (Belgium). The reducing agent, sodium dithionite ($Na_2S_2O_4$) was purchased from Systerm® (Malaysia). Ammonium dihydrogen phosphate ($(NH_4)H_2PO_4$ ≥99% purity) and disodium hydrogen phosphate (Na_2HPO_4, ≥99% purity), which were used to prepare phosphate buffer solution for chromatographic analysis were purchased from Merck (Germany) and Fisher Scientific (United Kingdom). Liquid chromatography (HPLC) grade methanol (Merck, Germany) was used as an organic solvent to dissolve aniline and Sudan I azo dye into solutions. 18 mΩ water was used to prepare HPLC mobile phase throughout the study. Stock solution of 0.1% aniline was prepared by dissolving suitable amount of aniline in 100 mL of HPLC grade methanol. A series of concentration of aniline solution from 2 to 10 ppm were prepared by diluting the stock solution with methanol followed by optimum amount of sodium dithionite solution. The pH of

each prepared standard solution was adjusted to optimum pH before analyzed using HPLC. Sodium dithionite solutions were freshly prepared before used.

Apparatus and operating conditions

The equipment consists of a vacuum degasser, autosampler, UV/Vis Detector and pump (Series 200, Perkin Elmer, United States) was used to determine aniline in the reduced Sudan I azo dye solution. The system is computer-controlled (Windows XP Professional operating system), using the the Total Chrom Navigator software package. HPLC separations were carried out using a reversed phase column of ZORBAX SB-Phenyl column (4.6 mm I.D x 250 mm length, and 5 µm particle size, Agilent Technology, United States). The guard-column was of the same type of separation column (4.6 mm I.D. x 12.5 mm length and 5 µm particle size). The chromatographic eluent consisted of 70% methanol and 30% of ammonium dihydrogen phosphate/disodium hydrogen phosphate buffer solution at pH 6.9. For analysis, 15 µL of the sample solution were injected at a flow-rate of 1 mL/min and at room temperature. The analysis run time was 10 min. The UV-spectra were recorded at 231 nm. MERCK UV-Spectroquant Pharo 100 spectrophotometer was used to measure the color absorption of Sudan I azo dye solution at 476 nm using 10 mL cell tube.

Optimization of dit/Sud ratio, reduction temperature, pH and recovery

Various concentrations of sodium dithionite aqueous solutions were mixed with various amount of 10 ppm Sudan I azo dye solution in methanol to study the effect of the sodium dithionite concentration toward the decolorization of the Sudan I azo dye solution. Each mixture was shaken for 1 minute and left at room temperature for 15 minutes before measured using spectrophotometer at 476 nm. The reduction temperature of Sudan I azo dye to aniline was studied from room temperature to 70 ^{o}C. The effect of the pH of the sodium dithionite solution toward the reduction of the Sudan I azo dye to aniline was studied from pH 2 to 10. 10 - 200 ppm of Sudan I azo dye solutions were treated under the optimum conditions before analyzed using HPLC. The detected aniline amounts were calculated and compared to the stoichiometric amount of aniline released from the reduction of Sudan I. Each concentration was repeated three times.

Sample preparation and extraction

The application of the proposed method was carried out on a self-dyed cloth. Three pieces of 20 x 20 cm of plain white cotton cloth weighted approximately 9 gram were washed in hot distilled water followed by 100 mL of 0.1 M nitric acid to eliminate any possible colorant that adsorbed on the cloths before dried in oven at 100 ^{o}C. Each cloth was soaked in 100 mL of 0.5% Sudan I azo dye solution in methanol for up to 12 hours. The dyed cloths were then air dried at room temperature. Sudan I was extracted from the cloths using 100 mL of methanol at room temperature for 1 hour. 5 mL of the extracted solution containing Sudan I was subjected to the optimum conditions treatment before analyzed using the HPLC.

Results and Discussion

Optimization of sodium dithionite concentration

Sodium dithionite is an effective reducing agent to cleave Sudan I azo dye to aromatic amine compounds. However, the optimum amount needs to be determined. Three different concentrations of sodium dithionite solution were used. Each concentration of sodium dithionite was mixed with different volume of Sudan I azo dye solution. Each mixture absorbance was measured using spectrophotometer to determine the decrement of the absorbance. Measured absorbances were compared with the blank without sodium ditionite. The results are shown in Figure 1. It indicates that higher sodium dithionite concentrations solution decolourized Sudan I azo dye solution at a lower dit/Sud ratio. In general, all three different sodium dithionite concentrations decreased the Sudan I azo dye solution absorbance when the higher ratio of dit/Sud was used. The dit/Sud ratios that completely decolourized the Sudan azo dye solution occurs at 7:3, 5:5 and 3:7 for 0.21%, 0.25% and 0.30% sodium dithionite solution, respectively. This is because higher concentration of reducing agent provides more reducing power to reduce the dye even at lower ratio.

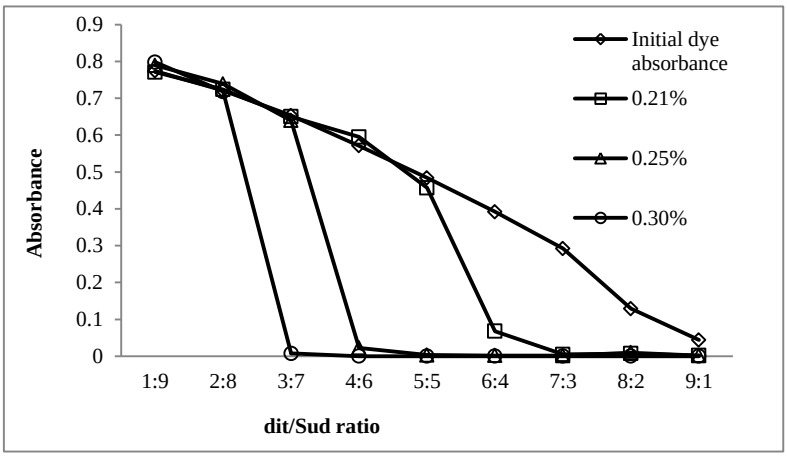


Figure 1. Effect of the sodium dithionite concentration on the reduction of Sudan I azo dye at different ratios of dit/Sud.

Optimization of reduction temperature

The mixtures of various concentrations of sodium dithionite solution with the Sudan I azo dye solution at various ratios were heated at four different temperatures for 15 minutes before spectrophotometry measurement was carried out to study the effect of the temperature on the reduction of Sudan I azo dye to aniline. The obtained results are shown in Figure 2a to Figure 2c. The observed general trend is that Sudan I azo dye absorbances decrease when dit/Sud ratios increase at these four different reduction temperatures. As shown in Figure 2a, fully decolorization of Sudan I azo dye occurred at ratio 7:3 for reduction temperature at room temperature, 40, 50 and 60 ^{o}C. Reduction temperature at 70°C accelerated the Sudan I azo dye fully decolorization from ratio 7:3 to 6:4. Ratios below 6:4 does not show an orderly decrement of absorbance when the reduction temperature increases from room temperature to 70 ^{o}C. The effects of reduction temperature were more obvious (Figure 2b) when 0.25% sodium dithionite was used. The increment of the reduction temperature from room temperature to 70 ^{o}C accelerated the decolorization of the dye from ratio 6:4 to 4:6. However, as shown in Figure 2c, the increasing reduction temperatures does not show any significant effect on the decolorization of dye when 0.30% sodium dithionite solution was used. In this concentration, effect of the concentration is more significant than the temperature toward the decolorization of the Sudan I azo dye. Since there were no obvious temperature effect on the decolorization of the Sudan I azo dye in 0.30% sodium dithionite solution. Therefore, heating is unnecessary to be incorporated into the developed method if 0.30% sodium dithionite was chosen to be used to decolorize the dye.

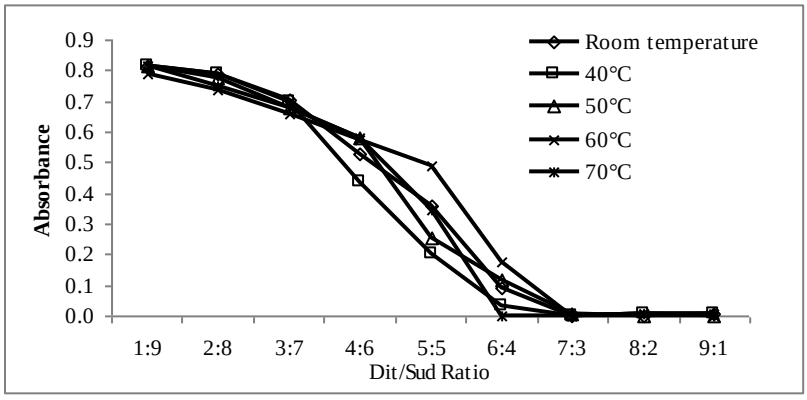


Figure 2a. Effect of temperature on the reduction of dye in 0.21% sodium dithionite.

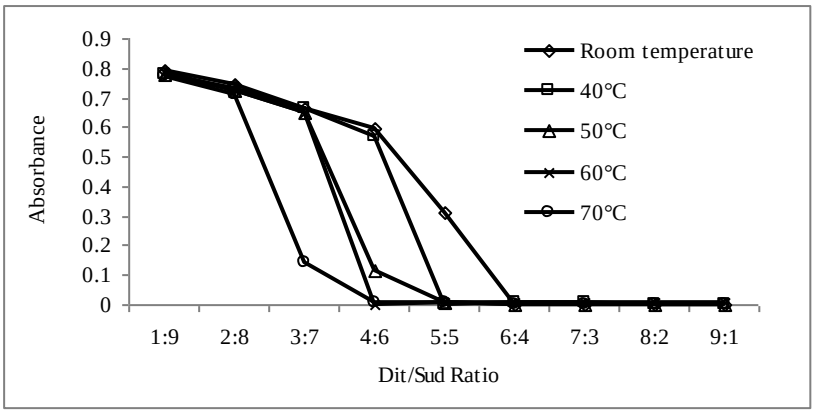


Figure 2b. Effect of temperature on the reduction of dye in 0.25% sodium dithionite.

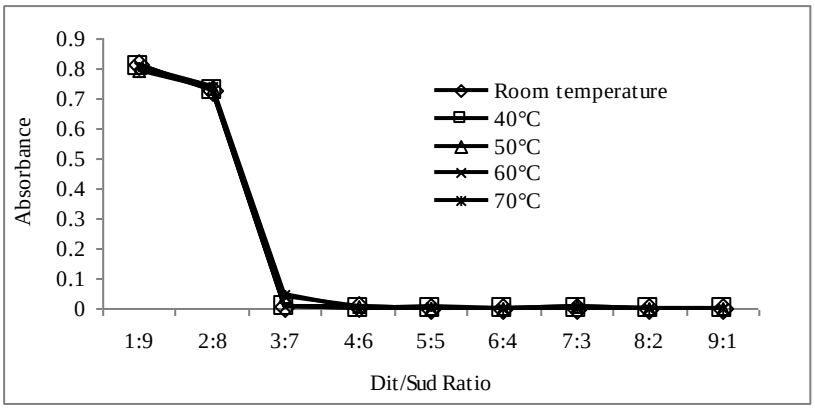


Figure 2c. Effect of temperature on the reduction of dye in 0.30% sodium dithionite.

Optimization of reduction pH

The effects of the reducing agent pH on the Sudan I azo dye decolorization was studied by altering the sodium dithionite solution pH using either HCl or NaOH. The pH ranges from 2 to 10 was studied. The effects of the sodium dithionite pH on the dye decolorization in 0.21% and 0.30% of sodium dithionite solution are presented in Figure 3a, 3b and 3c. All figures show a significant and obvious trend that alkaline sodium dithionite solution decolorized the Sudan I azo dye faster than the acidic sodium dithionite solution. The alkaline curves are slightly below the neutral curve. This shows that alkaline sodium dithionite did not enhance much the reduction of the dye compared to the neutral sodium dithionite solution.. However, curve that produced by pH 2 sodium dithionite shows a significant decrement of the decolorization of the dye in all three concentrations. This is because sodium dithionite is unstable in acidic condition and decomposes to sodium thiosulfate and sodium bisulfate [16]. pH 8 was chosen as optimum value instead of pH 10. This is because it is enough to maintain the stability of the sodium dithionite at pH 8. Moreover, the degrees of decolorization of Sudan I azo dye solution by sodium dithionite at pH 8 and 10 are almost similar in 0.30% sodium dithionite.

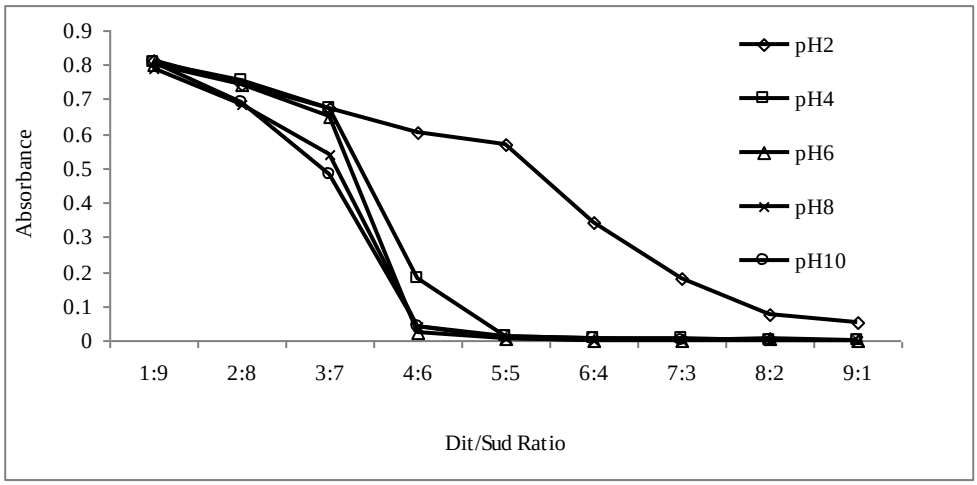


Figure 3a. Effect of the pH on the reduction of dye in 0.21%sodium dithionite.

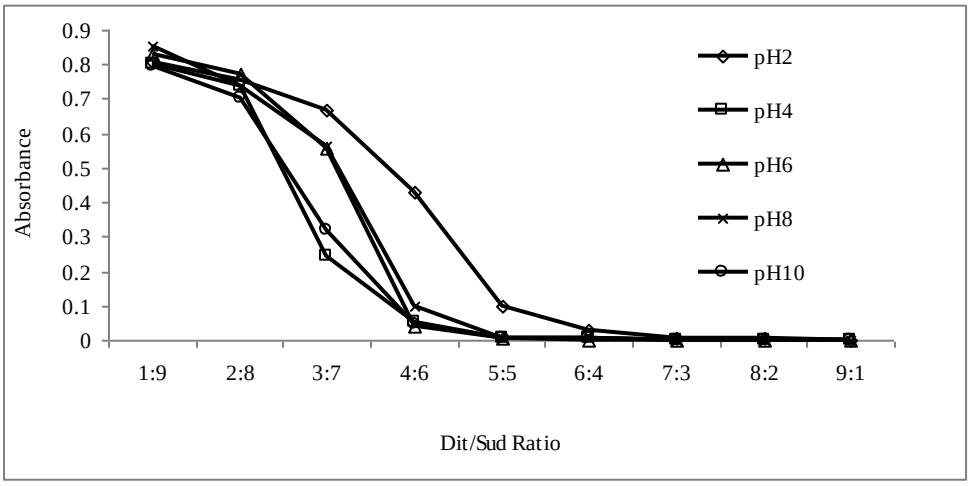


Figure 3b. Effect of the pH on the reduction of dye in 0.25% sodium dithionite.

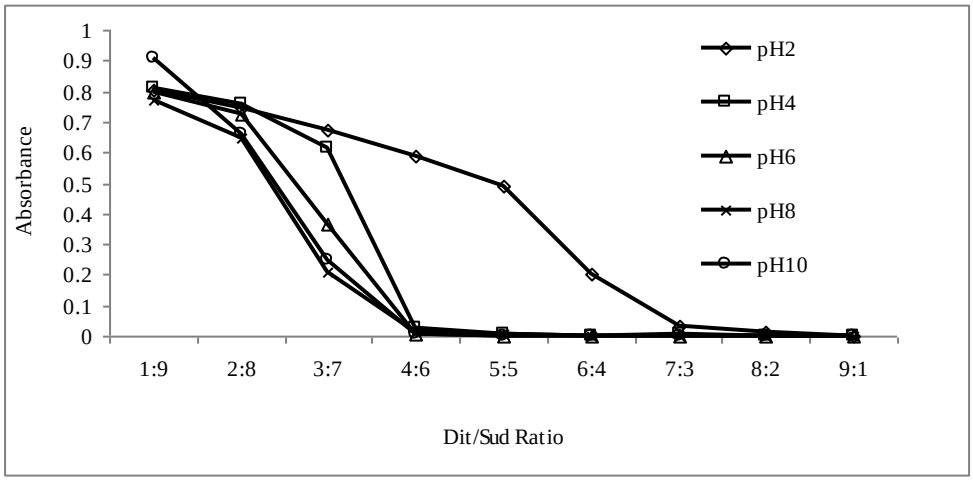


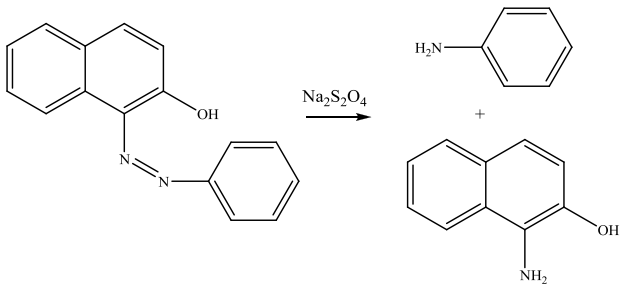
Figure 3c. Effect of the pH on the reduction of dye in 0.30% sodium dithionite.

Optimization of dithionite/Sudan I ratio

The optimization of dit/Sud ratio was studied throughout the optimization process for concentration, temperature and pH parameters. As shown in the results, the dit/Sud ratio where complete decolorization of Sudan I azo dye mostly occurs from ratio 5:5 and above. Therefore, the suitable optimum ratio to be used is 1:1 of dit/Sud (v/v).

Recovery percentage

Five different concentrations of Sudan I azo dye solutions were subjected to sodium dithionite treatment at optimum conditions. Each concentration was repeated three times to obtain each concentration relative standard deviation. The recovery percentage of aniline released from Sudan I azo dye reduction is calculated based on the stoichiometric amount of aniline, which theoretically released from the Sudan I azo dye in accordance to the following chemical equation (1):



(1)

Analyzed results were calibrated using aniline spiked standard in sodium dithionite solution. Aniline peak was detected at around 3.84 min throughout the 10 min run time. The linear correlation value (R^2) obtained from the standard curve is 0.9975 and the minimum detection limit calculated based on the calibration line equation is approximately 0.6 ppm by substituting zero to the y value.

The recovery percentage results are shown in Table 1. The recovery percentage at lower concentrations are slightly below 70%; whereas, higher concentrations are more than 70%. The overall recoveries in the range of concentration from 10 to 200 ppm are within 62.9 - 88.4% with R.S.D. values at 7.6 - 21.5%.

Table 1. The recovery percentages and R.S.D. of different Sudan I concentrations.

Concentration. Of Sudan I (ppm)	Recovery %				R.S.D. (%)
	Duplicate 1	Duplicate 2	Duplicate 3	Average	
10	58.3	67.8	62.7	62.9	7.6
30	72.9	70.7	61.1	68.2	9.2
80	99.1	83.8	64.8	82.6	20.8
150	100.0	82.3	83.1	88.4	11.3
200	82.1	100.2	64.9	82.4	21.5

Note: RSD represents Relative Standard Deviation

Application of the optimized method on self-dyed cloth sample

Sudan I azo dye was extracted from a self-dyed cloth using methanol. The extracted dye solution was treated with sodium dithionite under optimum conditions to reduce the dye into its aromatic amine. Amount of aniline which was released into the solution, was determined using HPLC. The obtained average result is 28.3 mg/kg with 1.2% of the relative standard deviation.

Conclusion

Sodium dithionite is a very effective reducing agent to reduce Sudan I azo dye in alkaline condition. It is able to cleave Sudan I azo dye to 1-aminonaphthalen-2-ol and aniline. In this study, it was found that 0.3% of sodium dithionite needs to be used to decolorize Sudan I azo dye at dit/sud ratio of 1:1 at pH 8. When 0.3% of sodium dithionite was used, heating of the mixture of the sodium dithionite and the Sudan I azo dye is unnecessary because the decolorization of the dye is mostly contributed by the concentration of the sodium dithionite rather than the temperature. Moreover, high heating temperature could decompose sodium dithionite. The minimum amount of the aniline that could be detected by the HPLC is approximately 0.6 ppm equivalent to 6.7 mg/kg if 9 gram of sample was used. Overall recoveries were 62.9 – 88.4% with R.S.D. values at 7.6 – 21.5%. Three pieces of cloths were dyed with Sudan I azo dye before extracted using methanol. Extracted Sudan I azo dye was subjected to optimum conditions treatment before analyzed using HPLC to determine the amount of aniline released from the adsorbed Sudan I azo dye onto the cloths. The obtained average result for the self-dyed cloth is 28.3 mg/kg with R.S.D. value at 1.2%.

Acknowledgement

The authors would like to thank Tunku Abdul Rahman University College for providing the necessary equipments and supporting this research.

References

1. Garrigós, M.C., Reche, F., Marin, M.L., & Jiménez, A. (2002). Determination of Aromatic Amines Formed from Azo Colorants in Toy Products. *J. Chromatogr. A.* 976, 309-317.
2. Li, H., Xiong, Z., Dai, X., & Zeng, Q. (2012). The Effect of Perspiration on Photo-induced Chemical Reaction of Azo Dyes and The Determination of Aromatic Amine Products. *Dyes pigments*. 94, 55-59.
3. Ahlström, L.H., Eskilsson, C.S., & Björklund, E. (2005). Determination of Banned Azo Dyes in Consumer

Goods. *Trend Anal. Chem.*. 24(1), 49-56.
4. Rodrigues, C.S.D., Madeira, L.M., & Boaventura, A.R. (2008). Optimization of The Azo Dye Procion Red H-EXL Degradation by Fenton's Reagent Using Experimental Design. *J. Hazard. Mater.* 164, 987-994.
5. Pielesz, A., Baranowska, I., Rybak, A., & Wlochowicz, A. (2002). Detection and Determination of Aromatic Amines as Products of Reductive Splitting from Selected Azo Dyes. *Ecotoxicol. Environ. Saf.* 53, 42-47.
6. Gómez, J.L., León, G., Hidalgo, A.M., Gómez, M., Murcia, M.D., & Griñàn, G. (2009). Application of Reverse Osmosis to Remove Aniline from Wastewater. *Desalination.* 245, 687-693.
7. International Agency for Research on Cancer. (1975). Monographs on The Evaluation of Carcinogenic Risks to Humans and Their Supplements. *IARC.* 8, 225–241.
8. International Agency for Research on Cancer. (1987). IARC Monographs on The Evaluation of The Carcinogenic Risks to Humans. Overall Evaluations of Carcinogenicity: An Updating of IARC Monographs Volumes 1 to 42. Supplement 7. France; IARC.
9. Eskilsson, C.S., Davidsson, R., & Mathiasson, L. (2002). Harmful Azo Colorants in Leather. Determination Based on Their Cleavage and Extraction of Corresponding Carcinogenic Aromatic Amines Using Modern Extraction Techniques. *J. Chromatogr. A.* 955, 215-227.
10. Pricelius, S., Held, C., Sollner, S., Deller, S., Murkovic, M., Ullrich, R., Hofrichter, M., Cavaco-Paulo, A., Macheroux, P., & Guebitz, G.M. (2007). Enzymatic Reduction and Oxidation of Fiber-bound Azo-dyes. *Enzyme Microb. Technol.* 40, 1732-1738.
11. Shu, H.Y., Chang, M.C., & Fan, H.J. (2004). Decolorization of Azo Dye Acid Black I byThe UV/H_2O_2 Process and Optimization of Operating Parameters. *J. Hazard. Mater.* B113, 201-208.
12. Lui, G., Zhou, J., Wang, J., Zhou. M., Lu, H., & Jin, R. (2009). Acceleration of Azo Dye Decolorization by Using Quinone Reductase Activity of Azoreductase and Quinone Redox Mediator. *Bioresour. Technol.* 100, 2791-2795.
13. Zille, A., Górnacka, B., Rehorek, A., & Cavaco-Paulo, A. (2005). Degradation of Azo Dyes by *Trametes villosa* Laccase Over Long Periods of Oxidative Conditions. *Appl. Environ. Microbiol.* 71(11), 6711-6718.
14. Bhaskar, M., Gnanamani, A., Ganeshjeevan, R.J., Chandrasekar, R., Sadulla, S., & Radhakrishnan, G. (2003). Analyses of Carcinogenic Aromatic Amines Released from Harmful Azo Colorants by *Streptomyces* SP. SS07. *J. Chromatogr. A.* 1018, 117-123.
15. Ji, Q., Lui, G., Zhou, J., Wang, J., Jin, R., & Lv, H. (2012). Removal of Water-insoluble Sudan Dyes by *Shewanella oneidensis* MR-1. *Bioresour. Technol.* 114, 144-148.
16. Lister, M. W. & Garvie, R. C., (1959) Sodium Dithionite, Decomposition in Aqueous Solution and in The Solid State. *Can. J. Chem*. 37, 1567-1574.

The Malaysian Journal of ANALYTICAL SCIENCES ISSN 1394-2506

ANALYSIS OF HIGH QUALITY AGARWOOD OIL CHEMICAL COMPOUNDS BY MEANS OF SPME/GC-MS AND Z-SCORE TECHNIQUE

(Analisa Bahan Minyak Gaharu Berkualiti Tinggi Dengan Cara Z-Score)

Nurlaila Ismail[1]*, Mohd Ali Nor Azah[2], Mailina Jamil[2], Mohd Hezri Fazalul Rahiman[1], Saiful Nizam Tajuddin[3], Mohd Nasir Taib[1]

[1]Faculty of Electrical Engineering,
Universiti Teknologi MARA (UiTM), 40450 Shah Alam, Selangor
[2]Herbal Product Development Programme, Natural Products Division,
Forest Research Institute Malaysia (FRIM), 52109 Kepong, Selangor
[3]Faculty of Industrial Science and Technology,
Universiti Malaysia Pahang (UMP), Lebuhraya Tun Razak, 26300 Gambang, Pahang

**Corresponding author: nrk_my@yahoo.com*

Abstract

Currently, the grading of the agarwood oil to the high and low quality is done using manually such as human trained grader. It was performed based on the agarwood oil physical properties such as human experience and perception and the oil colour, odor and long lasting aroma. Several researchers found that chemical profiles of the oil should be utilized to overcome the problem facing by manual techniques i.e. human nose cannot tolerate with the many oils at the same time, so that accurate result can be obtained in grading the agarwood oil. The analysis involved of SPME/GC-MS and Z-score techniques have been proposed in this study to analyze the chemical compounds especially from the high quality samples of agarwood oil (*Aquilariamalaccensis*) from Malaysia. Two SPME fibers were used such as divinylbenzene-carboxen-polydimethylsiloxane (DVB-CAR-PDMS) and polydimethylsiloxane (PDMS) in extracting the oils' compound under three different sampling temperature conditions such as 40˚C, 60˚C and 80˚C. The chemical compounds extracted by SPME/GC-MS were analyzed. The chemical compounds as identified by Z-score as significant compounds were discussed before the conclusion is made. It was found that 10-epi-ϒ-eudesmol, aromadendrane, β-agarofuran, α-agarofuran and ϒ-eudesmol were highlighted as significant for high quality agarwood oil and can be used as a marker compounds in classifying the agarwood oil.

Keywords: agarwood oil, chemical compounds, high quality, Z-score, solid phase micro-extraction (SPME) and gas chromatography-mass spectrometry (GC-MS)

Abstrak

Pada masa ini, penggredan minyak gaharu kepada kualiti tinggi dan rendah dilakukan secara manual seperti penggreder terlatih oleh manusia. Ia dilakukan berdasarkan ciri-ciri fizikal gaharu minyak seperti pengalaman dan persepsi manusia terhadap minyak tersebut, warna, bau dan ketahanan lama minyak gaharu. Beberapa penyelidik mendapati bahawa profil kimia minyak harus digunakan untuk mengatasi masalah yang dihadapi oleh kaedah manual di mana hidung manusia tidak boleh bertolak ansur dengan minyak yang banyak pada masa yang sama, supaya keputusan yang lebih jitu boleh diperolehi dalam penggredan minyak gaharu. Analisis melibatkan SPME/GC-MS dan teknik Z-skor telah dicadangkan dalam kajian ini untuk analisa bahan kimia minyak gaharu (*Aquilariamalaccensis*) dari Malaysia terutama dari sampel yang berkualiti tinggi. Dua gentian SPME telah digunakan seperti divinylbenzene-carboxen-polydimethylsiloxane (DVB-CAR-PDMS) dan polydimethylsiloxane (PDMS) untuk mengeluarkan kompaun minyak di bawah tiga keadaan suhu persampelan yang berbeza iaitu 40˚C, 60˚C dan 80˚C. Sebatian kimia yang dikeluarkan oleh SPME/GC-MS telah dianalisakan. Sebatian kimia seperti yang dikenalpasti oleh Z-skor sebagai bahan penting telah dibincangkan sebelum kesimpulan dibuat. Penemuan mendapati bahawa 10-epi-Y-eudesmol, aromadendrane, β-agarofuran, α-agarofuran dan Y-eudesmol telah diketengahkan sebagai sebatian kimia penting untuk minyak gaharu berkualiti tinggi dan boleh digunakan sebagai penanda aras dalam mengklasifikasikan minyak gaharu.

Kata kunci: minyak gaharu, bahan kimia, kualiti tinggi, Z-score, fasa pepejal mikro pengekstrakan dan gas kromatografi-spektrometri jisim

Introduction

Agarwood or *gaharu* is the resin impregnated heartwood of the *Aquilaria* species, a genus which belongs taxonomically to the Thymelaeaceae family. The agarwood oil highly demanded in the current world market due to its multiple usage such as an incense in religious ceremony (Buddhism, Hinduism and Islamic), in perfumery ingredient and traditional medicine preparations [1]. In another region, Middle East it is a symbol of wealth and presence in the wedding ceremony [2-7]. Usually, agarwood oil is traded into various qualities but there are countries use grades to classify the agarwood oil. In Malaysia, agarwood oil is classified according to the grade of A, B, C and D [7, 8]. In India, they have four grades too such as A, B, C and D based on color of agarwood oil [1]. In Japan, agarwood oil is categorized as high and low quality where Kanankoh is the highest quality and Jinkoh is low quality [9]. Malaysian labeled Kalambak for good quality and gaharu for the lower one [1]. This shows the classification of agarwood oil is different between countries and the grading system is not standardized. Agarwood oil can be classified according to their properties [10]. Analysis based on their chemical profiles is needed to ensure that agarwood oil can be classified according to their respective classes where the accurate results can be measured [9-12]. In this study, the chemical compounds of high quality agarwood oils were extracted by solid phase micro-extraction (SPME) and gas chromatography-mass spectrometry (GC-MS). The Z-score technique was proposed to identify the significant chemical compounds from the extraction. The findings obtained by all experiments were analyzed and discussed before the conclusion was made.

Materials and Methods

Plant Material

Two agarwood oils, species *Aquilariamalaccensis* known as MA2 and JBD are gathered from Forest Research Institute Malaysia (FRIM), Kepong, Selangor, Malaysia. The samples are regarded by the institution as high quality samples. Firstly, the samples ground is soaked with water for 7 to 21 days. Then, hydrodistillation process is took place for 3 to 5 days to extract the oil. After that, the essential oil is dried using anhydrous sodium sulphate and stored in amber vial for the analysis purposes.

Solid Phase Microextraction (SPME)

The agarwood oil samples, MA2 and JBD are placed into 20mL, tightly capped and screw-top clear vials. In order to extract the odor compound of agarwood oils, two types of SPME Stableflex^{TM} fibers are used. They are a 50/30 µm divinylbenzene-carboxen-polydimethylsiloxane (DVB-CAR-PDMS) and a 100 µm polydimethylsiloxane (PDMS). Both of them and together with the holder are purchased from Supelco (Bellefonte, PA, USA). The DB-CAR-PDMS fiber is placed in an agitator about 10min at incubation temperature of 40˚C, 60˚C and 80˚C. The extraction time is set to 10min to trap the volatile compounds. After that, the fiber is injected immediately into GC port for 10min. The same method is repeated for the PDMS fiber.

GC-MS analysis

GC-MS analysis is carried out using Agilent Technologies 7890A/5975C Series MSD with HP-5MS column (30m x 0.25mm ID x 0.25µm film thickness). At first, the apparatus is set at 60˚C for 10min time duration, followed by 180˚C for 1min at 3˚C/min. The gas carrier helium is injected at a flowrate of 1.0mL/min and the ion-source temperature is programmed at 280˚C. The chemical compounds are identified by matching them to the mass spectral library (HPCH2205.L; Wiley7Nist05a.L; NIST05a.L). The chemical compounds are presented in terms of abundances (%).

Z-score technique

The Z-score is based on the calculation of mean and standard deviation of an attribute. It is a measurement of difference between individual value and the mean population, and then divided by standard deviation of population. The computed, Z-score (*Z*) provides each feature with a zero mean and a unit variance. The foundation of Z-score is where the mathematical Gaussian curve or 'Bell Shaped' curve is applied to the data under study [13].

The Z-score, *Z* as in [14] is expressed as follow:

$$Z = \frac{x_i - \bar{X}}{SD}$$

where x_i is an individual value, $\bar{X}$ is mean of population and SD is standard deviation of population.

Results and Discussion

Table 1 tabulated the chemical compounds extracted by SPME/GC-MS for MA2 and JBD agarwood oils using PDMS fiber at temperatures 40˚C, 60˚C and 80˚C. At least thirty eight chemical compounds were extracted at all temperatures for both samples. Individually, for MA2, twenty seven, twenty four and twenty one chemical compounds were extracted at temperature 40˚C, 60˚C and 80˚C, respectively. It was followed by JBD oil, where twenty eight, twenty six and twenty two chemical compounds were extracted at temperature 40˚C, 60˚C and 80˚C, respectively. It was noticed that the temperature gave effect to the number of chemical compounds extracted in which at high temperature, less chemical compounds was extracted. For MA2 oil, 4-phenyl-2-butanone gave the highest abundances with the percentage of 14.18% at temperature 40˚C, α-bulnesene at temperature 60˚C with the highest abundances of 9.43% and ϒ-eudesmol at temperature 80˚C with the abundances highest of 9.43%. The result was followed by JBD oil where 4-phenyl-2-butanone gave the highest abundances with the percentage of 11.80% at temperature 40˚C, ϒ-eudesmol at temperature 60˚C with the highest abundances of 9.76% and 10-epi-ϒ-eudesmol at temperature 80˚C with the abundances highest of 10.67%. In other observation, there were eighteen and sixteen compounds exist in MA2 and JBD oils, detected by SPME using PDMS fiber in all temperatures. They were 4-phenyl-2-butanone, α-copaene, β-elemene, α-cedrene, α-guaiene, aromadendrane, α-humulene, β-agarofuran, ar-curcumene, cis-β-guaiene, α-selinene, β-dihydroagarofuran, α-bulnesene, α-agarofuran, elemol, β-gurjunene, 10-epi-ϒ-eudesmol and ϒ-eudesmol for MA2 oil. For JBD oil, the responsible compounds were 4-phenyl-2-butanone, α-copaene, β-elemene, α-funebrene, α-cedrene, α-guaiene, α-humulene, β-agarofuran, ar-curcumene, α-bulnesene, δ-cadinene, elemol, β-vetivenene, 10-epi-ϒ-eudesmol, ϒ-eudesmol and alloaromadendrane epoxide. The chemical compounds and its abundances (%) for MA2 and JBD agarwood oils using PDMS fiber is shown in Figure 1.

Figure 1 shows the abundances pattern chemical compounds of MA2 and JBD agarwood oils extracted by SPME using PDMS fiber at temperature 40˚C, 60˚C and 80˚C. The chemical compounds of MA2 and JBD agarwood oils showed a complex mixture of monoterpenes, sesquiterpenes and its chromones derivatives. This finding was in agreement with the finding by Ishihara *et.al* [15]. The behavior of the compounds was showed by variation of the abundances pattern belong to the every compound. From this plot, 4-phenyl-2-butanone has the highest peak of abundances at temperature 40˚C.

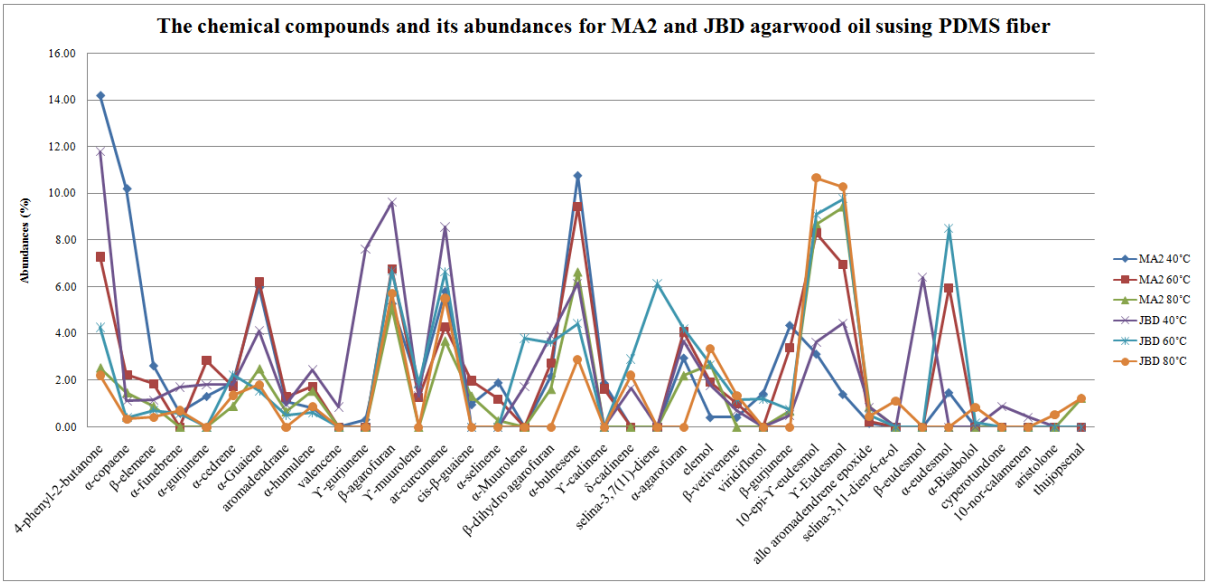


Figure 1. The chemical compounds and its abundances (%) for MA2 and JBD agarwood oils using PDMS fiber

Table 1. The chemical compositions extracted by SPME for MA2 and JBD using PDMS fiber

No.	Chemical compounds	RI	Abundances (%)					
			MA2 40˚C	MA2 60˚C	MA2 80˚C	JBD 40˚C	JBD 60˚C	JBD 80˚C
1	4-phenyl-2-butanone	1241	14.18	7.28	2.54	11.80	4.26	2.22
2	α-copaene	1374	10.20	2.25	1.47	1.11	0.41	0.34
3	β-elemene	1389	2.63	1.85	0.89	1.16	0.72	0.42
4	α-funebrene	1402	0.60	-	-	1.72	0.58	0.71
5	α-gurjunene	1403	1.31	2.85	-	1.81	-	-
6	α-cedrene	1411	1.92	1.75	0.90	1.81	2.24	1.36
7	α-Guaiene	1433	5.98	6.23	2.50	4.13	1.56	1.82
8	aromadendrane	1443	1.08	1.30	0.67	0.97	0.52	-
9	α-humulene	1452	0.82	1.73	1.54	2.45	0.63	0.88
10	valencene	1469	-	-	-	0.87	-	-
11	ϒ-gurjunene	1472	0.32	-	-	7.63	-	-
12	β-agarofuran	1474	5.28	6.77	5.14	9.63	6.67	5.73
13	ϒ-muurolene	1478	1.73	1.28	-	1.33	1.86	-
14	ar-curcumene	1479	5.80	4.30	3.69	8.57	6.64	5.51
15	cis-β-guaiene	1492	0.96	1.99	1.33	-	-	-
16	α-selinene	1498	1.90	1.20	0.27	-	-	-
17	α-Muurolene	1500	-	-	-	1.73	3.80	-
18	β-dihydro agarofuran	1502	2.17	2.73	1.62	3.91	3.61	-
19	α-bulnesene	1509	10.76	9.43	6.64	6.16	4.43	2.89
20	ϒ-cadinene	1513	1.88	1.63	-	-	-	-
21	δ-cadinene	1522	-	-	-	1.66	2.91	2.22
22	selina-3,7(11)-diene	1545	-	-	-	-	6.13	-
23	α-agarofuran	1547	2.96	4.07	2.21	3.67	4.21	-
24	elemol	1550	0.41	1.92	2.68	1.77	2.66	3.36
25	β-vetivenene	1554	0.42	0.99	-	0.71	1.17	1.35
26	viridiflorol	1592	1.42	-	-	-	1.20	-
27	β-gurjunene	1600	4.35	3.40	0.69	0.51	0.74	-
28	10-epi-ϒ-eudesmol	1621	3.12	8.31	8.71	3.63	9.09	10.67
29	ϒ-Eudesmol	1635	1.40	6.96	9.43	4.45	9.76	10.30
30	allo aromadendrene epoxide	1639	0.17	0.24	0.87	0.86	0.50	0.45
31	selina-3,11-dien-6-α-ol	1642	-	-	-	-	-	1.12
32	β-eudesmol	1649	-	-	-	6.42	-	-
33	α-eudesmol	1652	1.48	5.96	-	-	8.49	-
34	α-Bisabolol	1683	-	-	-	-	0.18	0.85
35	cyperotundone	1695	-	-	-	0.89	-	-
36	10-nor-calamenen	1702	-	-	-	0.42	-	-
37	aristolone	1762	-	-	-	-	-	0.53
38	thujopsenal	1887	-	-	1.25	-	-	1.24

Table 2 tabulates the chemical compositions extracted by SPME for MA2 and JBD agarwood oils using DVB-CAR-PDMS fiber at temperatures 40˚C, 60˚C and 80˚C. At least forty seven chemical compounds were extracted at all temperatures for both samples. It can be seen that, for MA2 oil, thirty seven, thirty six and thirty three chemical compounds were extracted at temperature 40˚C, 60˚C and 80˚C, respectively. The result was followed by JBD oil, where forty two, thirty six and thirty five chemical compounds were extracted at temperature 40˚C, 60˚C and 80˚C, respectively. Similarly from the finding in PDMS fiber, in DVB-CAR-PDMS, we can observed that the temperature also give effect to the number of chemical compounds extracted where at high temperature, less chemical compounds was extracted. For MA2 at temperature 40˚C and 60˚C, 4-phenyl-2-butanone gave the highest abundances with the percentage of 14.17% and 11.94%, respectively. At temperature 80˚C, the highest abundances belong to α-eudesmol with the value of 10.23%. The finding was followed by JBD oil where at temperature 40˚C and 60˚C, 4-phenyl-2-butanone gave the highest abundances with the percentage of 11.47% and 8.86%, respectively. At temperature 80˚C, the highest abundances belong to α-eudesmol with the value of 13.00%. We can see here that both agarwood oils have similarity for extracting similar chemical compounds that own the highest abundances at temperature 40˚C, 60˚C and 80˚C. i.e. 4-phenyl-2-butanone at temperature 40˚C and 60˚C and α-eudesmol at temperature 80˚C. In other observation, there were twenty six and twenty seven chemical compounds exist in MA2 and JBD oils, detected by SPME using DVB-CAR-PDMS fiber in all temperatures. For MA2 oil, the compounds were 4-phenyl-2-butanone, α-copaene, β-elemene, α-funebrene, α-cedrene, α-guaiene, α-humulene, E-β-farnesene, ɤ-gurjunene, β-agarofuran, ɤ-muurolene, ar-curcumene, β-selinene, cis-β-guaiene, α-bulnesene, ɤ-cadinene, δ-cadinene, elemol, β-vetivenene, spathulenol, β-gurjunene, 10-epi-ϒ-eudesmol, ϒ-eudesmol, alloaromadendrane epoxide, cyperotundone and thujopsenal. For JBD oil, the responsible compounds were 4-phenyl-2-butanone, methyl decanoate, α-copaene, β-elemene, α-funebrene, α-cedrene, α-guaiene, α-humulene, E-β-farnesene, ɤ-gurjunene, β-agarofuran, ɤ-muurolene, ar-curcumene, α-muurolene, trans-β-guaiene, α-bulnesene, ɤ-cadinene, δ-cadinene, elemol, β-vetivenene, spathulenol, β-gurjunene, guaia-3,10(14)-diene, 9, 11 epoxy, 10-epi-ϒ-eudesmol, ϒ-eudesmol, alloaromadendrane epoxide and α-eudesmol. The chemical compounds and its abundances (%) for MA2 and JBD agarwood oils using DVB-CAR-PDMS fiber is shown in Figure 2.

Table 2. The chemical compositions extracted by SPME for MA2 and JBD using DVB-CAR-PDMS fiber

No.	Chemical compounds	RI	Abundances (%)					
			MA2 40˚C	MA2 60˚C	MA2 80˚C	JBD 40˚C	JBD 60˚C	JBD 80˚C
1	benzaldehyde	952	0.07	-	0.04	-	-	-
2	4-phenyl-2-butanone	1241	14.17	11.94	5.16	11.47	8.86	4.74
3	methyl decanoate	1323	-	-	-	0.04	0.04	0.05
4	α-copaene	1374	3.12	3.20	1.74	0.84	0.73	0.36
5	2-epi-α-funebrene	1380	-	-	-	0.07	0.10	-
6	β-elemene	1389	2.47	1.89	1.04	1.09	0.80	0.41
7	α-funebrene	1402	0.83	0.55	0.37	0.47	0.67	0.68
8	α-gurjunene	1403	1.19	0.31	-	0.45	0.34	-
9	α-cedrene	1411	2.09	2.00	0.97	0.19	2.54	1.20
10	α-guaiene	1433	3.97	5.54	3.14	2.43	2.79	1.19
11	aromadendrane	1443	0.88	1.08	0.21	0.05	-	0.03
12	α-humulene	1452	1.24	2.37	1.68	1.17	1.23	0.79
13	E-β-farnesene	1454	3.35	0.97	0.24	0.38	0.27	0.15
14	valencene	1469	0.10	-	5.03	0.45	-	-
15	ϒ-Gurjunene	1472	0.51	0.24	0.19	0.48	0.13	0.28
16	β-Agarofuran	1474	4.87	7.48	3.20	8.41	8.05	3.32

17	ϒ-muurolene	1478	1.83	0.99	0.11	0.68	0.53	0.23
18	ar-curcumene	1479	4.87	5.51	4.06	7.32	7.31	5.36
19	β-selinene	1489	0.00	2.50	0.23	0.11	-	0.33
20	cis-β-guaiene	1491	0.87	1.36	0.51	0.93	0.88	-
21	δ-selinene	1492	-	-	-	0.52	-	-
22	α-Muurolene	1496	2.23	0.15	-	3.54	6.92	1.78
23	α-selinene	1498	-	0.61	-	-	-	0.10
24	β-dihydro agarofuran	1502	3.04	-	-	3.66	-	-
25	trans-β-guaiene	1502	-	0.56	0.33	0.03	0.69	0.05
26	α-bulnesene	1509	5.89	4.36	2.70	4.36	3.56	2.61
27	ϒ-cadinene	1513	2.47	2.49	2.03	2.14	3.55	2.67
28	trans-calamenen	1521	-	-	-	0.16	0.15	-
29	δ-cadinene	1522	2.11	2.32	0.68	2.47	2.60	2.21
30	α-cadinene	1537	0.08	-	-	0.37	1.37	-
31	selina-3,7(11)-diene	1545	-	1.06	-	0.98	2.86	-
32	α-agarofuran	1547	2.91	3.29	-	3.71	1.26	-
33	elemol	1550	0.92	1.69	3.83	1.86	2.47	4.53
34	β-vetivenene	1554	0.83	1.56	1.52	0.76	1.48	1.30
35	spathulenol	1577	0.63	0.76	1.62	0.22	0.67	2.54
36	viridiflorol	1592	0.62	-	0.06	-	0.71	1.46
37	β-gurjunene	1600	0.11	2.40	1.64	1.64	0.92	3.97
38	guaia-3,10(14)-diene, 9, 11 epoxy	1601	0.05	0.13	-	0.11	0.11	0.06
39	10-epi-ϒ-eudesmol	1621	3.49	5.11	8.42	5.41	6.25	9.02
40	ϒ-eudesmol	1635	2.26	4.74	7.60	4.78	6.73	10.01
41	allo aromadendrene epoxide	1639	0.09	0.69	1.35	0.13	0.55	0.40
42	selina-3,11-dien-6α-ol	1642	-	-	0.84	0.03	-	0.43
43	β-eudesmol	1649	2.71	-	-	6.02	-	-
44	α-eudesmol	1652	-	6.93	10.23	1.70	6.48	13.00
45	cyperotundone	1695	0.17	0.34	0.27	-	-	0.24
46	10-nor-calamenen	1702	-	0.11	-	0.20	-	0.06
47	thujopsenal	1887	0.49	0.66	0.26	-	0.35	0.04

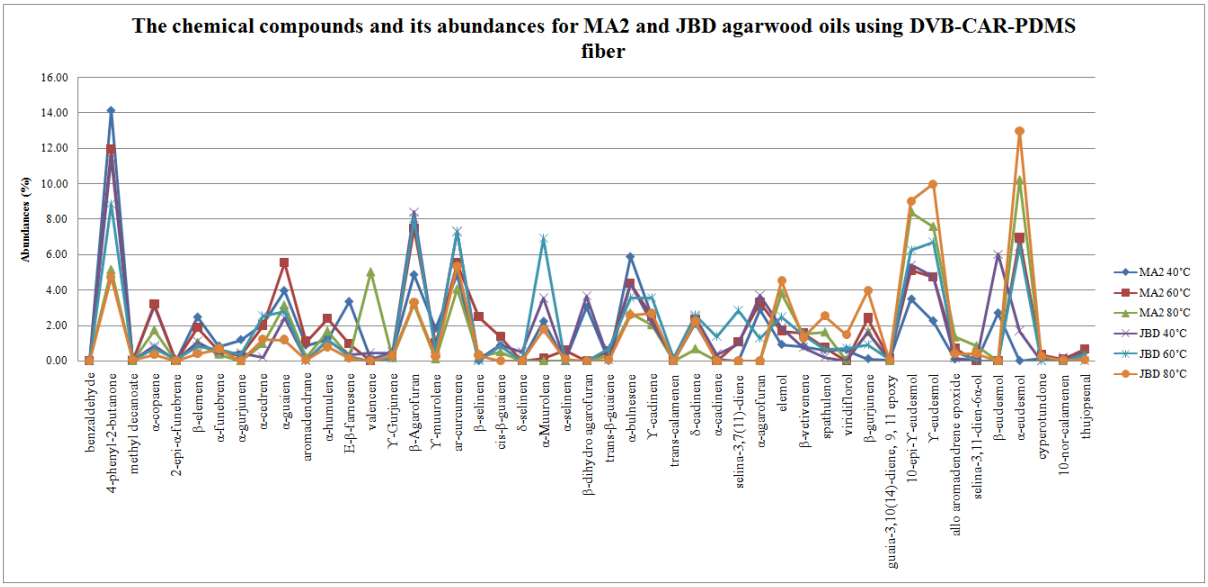


Figure 2. The chemical compounds and its abundances (%) for MA2 and JBD agarwood oils using DVB-CAR-PDMS fiber.

Figure 2 shows the abundances pattern chemical compounds of MA2 and JBD agarwood oils extracted by SPME using DVB-CAR-PDMS fiber at temperature 40˚C, 60˚C and 80˚C. Similar to the result as obtained by PDMS fiber, the chemical compounds of MA2 and JBD oils show a complex mixture of monoterpenes, sesquiterpenes and its chromones derivatives. The behavior of the compounds is showed by variation of the abundances pattern belong to the every compound. From this plot, 4-phenyl-2-butanone has the highest peak of abundances at temperature 40˚C.

It can be noticed from Figure 1 and Figure 2 , 4-phenyl-2-butanone exist as the dominant compound since this compound has the highest average of abundances in two samples i.e. MA2 and JBD using two fibers i.e. DVB-CAR-PDMS and PDMS at temperature 40˚C. This finding shows that SPME is a reliable technique for discriminating high-volatile monoterpenes (4-phenyl-2-butanone as one of the monoterpenes). This finding is supported by the previous researcher, J. Rohloff (1999) [16]. The result also is in agreement with Pripdeevech *et. al.* (2011) where 4-phenyl-2-butanone was recognized as one of the major compounds contributed to the odor of agarwood oil especially species *Aquilariamalaccensis* in their study [17].

As an essential oil, agarwood oil is a complex mixture of multi-component compounds which refer to polar and non polar compounds [18, 19]. Therefore, some of the chemical compounds in this study are lost at high temperature [20]. It is observed that the SPME with the lowest sampling temperature at 40˚C extracted the most compounds among all extraction. This is probably due to more volatile compounds are captured by SPME and are not lost during heating. However, with higher sampling temperature, compounds usually occurred in agarwood oils and are considered as heavy volatile odor-active components were found in higher yields. The relationship between temperature and number of compounds in SPME can be described by as the temperature is increased, the number of compounds extracted by SPME is decreased.

The different number of extraction using different fiber is due to polarity of the fiber. The PDMS (red) fiber is a polar fiber. Thus, it is expecting to be more effective in extracting polar compounds. The DVB-CAR-PDMS (grey) is a non-polar fiber and it is expecting to extract more non-polar compounds. Other factor may influence the difference in chemical compound extraction is the thickness of the fiber used. Thus, the SPME study shows that DVB-CAR-PDMS is more efficient than PDMS fiber since it can extract higher number of compounds. The result

is supported by the review in [17] in which DVB-CAR-PDMS extracted higher number of volatile compounds as compared to PDMS.

Table 3 tabulates the significant compounds identified by Z-score from the many compounds extracted by SPME/GC-MS for MA2 and JBD oils using PDMS fiber. There are five significant chemical compounds identified by Z-score such as aromadendrane, β-agarofuran, α-agarofuran, 10-epi-ɤ-eudesmol and ɤ-eudesmol. At temperature 40˚C, β-agarofuran has the highest abundances with the value of 5.28% for MA2 and 9.63% for JBD. At temperature 60˚C, 10-epi-ɤ-eudesmol has the highest abundances with the percentage of 8.31% for MA2 and ɤ-eudesmol provides the highest abundances for JBD with the value of 9.76%. At temperature 80˚C, ɤ-eudesmol shows the highest percentage of abundances for MA2 with the values of 9.43% and for JBD, the highest abundances belong to 10-epi-ɤ-eudesmol with the value of 10.67%.

Table 3: The significant compounds identified by Z-score for MA2 and JBD using PDMS fiber

No	Chemical compounds	Abundances (%)					
		MA2 40˚C	MA2 60˚C	MA2 80˚C	JBD 40˚C	JBD 60˚C	JBD 80˚C
1	aromadendrane	1.08	0.86	0.67	0.97	0.52	0.00
2	β-agarofuran	5.28	6.77	5.14	9.63	6.67	5.73
3	α-agarofuran	2.96	4.07	2.21	3.67	4.21	0.00
4	10-epi-ϒ-eudesmol	3.12	8.31	8.71	3.63	9.09	10.67
5	ϒ-Eudesmol	1.40	6.96	9.43	4.45	9.76	10.30

Table 4 tabulates the significant compounds identified by Z-score from the many compounds extracted by SPME/GC-MS for MA2 and JBD agarwood oils using DVB-CAR-PDMS fiber. Similar to the Table 3, five chemical compounds were identified as significant. They are aromadendrane, β-agarofuran, α-agarofuran, 10-epi-ɤ-eudesmol and ɤ-eudesmol. At temperature 40˚C, and 60˚C, for both oils, β-agarofuran has the highestabundances with the value of 4.87% and 7.48%, respectively for MA2 and 8.41% and 8.05%, respectively for JBD. At temperature 80˚C, 10-epi-ɤ-eudesmol has the highest abundances i.e. 8.42% for MA2 and ɤ-eudesmol has the highest percentage of abundances for JBD, i.e. 10.01%.

Table 4. The significant compounds identified by Z-score for MA2 and JBD using DVB-CAR-PDMS fiber

No	Chemical compounds	Abundances (%)					
		MA2 40˚C	MA2 60˚C	MA2 80˚C	JBD 40˚C	JBD 60˚C	JBD 80˚C
1	aromadendrane	0.88	1.08	0.21	0.05	0.00	0.03
2	β-agarofuran	4.87	7.48	3.20	8.41	8.05	3.32
3	α-agarofuran	2.91	3.29	0.00	3.71	1.26	0.00
4	10-epi-ϒ-eudesmol	3.49	5.11	8.42	5.41	6.25	9.02
5	ϒ-Eudesmol	2.26	4.74	7.60	4.78	6.73	10.01

Figure 3 (a) and (b) show the abundances pattern from SPME/GC-MS analysis for MA2 and JBD agarwood oils using different fibers at three different sampling temperatures such as 40˚C, 60˚C and 80˚C. Obviously, it can be seen that there is a consistent abundances pattern provided by five significant chemical compounds as identified by Z-score. It is found that three compounds have high peak of abundances in all plots and it applicable for all temperature conditions. These three compounds are 10-epi-ϒ-eudesmol, β-agarofuran and ϒ-eudesmol. Meanwhile, the other two compounds such as aromadendrane and α-agarofuran provide low peak of abundances. The

observation then is followed by the similarity trend provides by abundances pattern even different fibers are used to extract the agarwood oils. The Z-score has highlighted similar chemical compounds but different in their chemical compositions (abundances). These abundances pattern acquired by the significant chemical compounds in SPME/GC-MS contributed to the odor of high quality agarwood oil. They can be used as a benchmark to identify high quality agarwood oil. The chemical compounds such as 10-epi-ϒ-eudesmol, aromadendrane, β-agarofuran, α-agarofuran and ϒ-eudesmol can be used as the marker compounds in high quality agarwood oils.

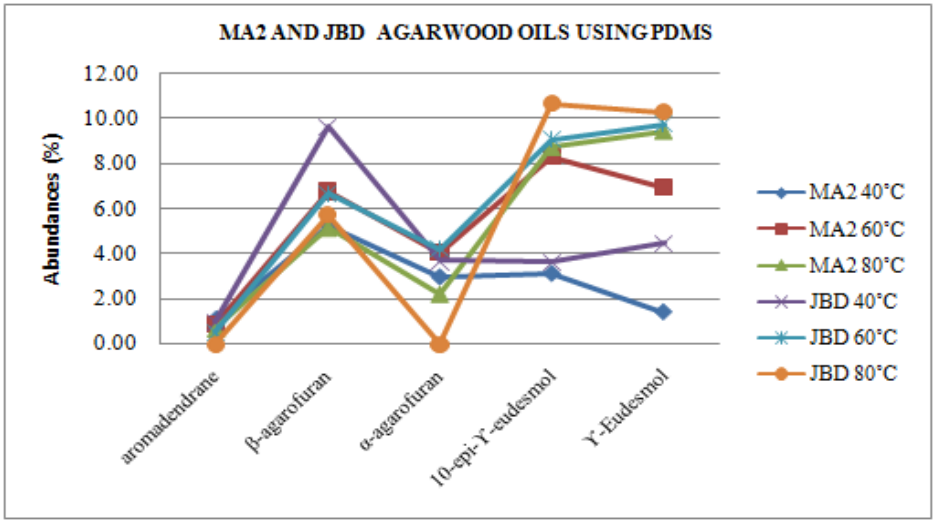


Figure 3 (a). The significant compounds as identified by Z-score at temperature 40˚C, 60˚C and 80˚C for MA2 and JBD using PDMS fiber

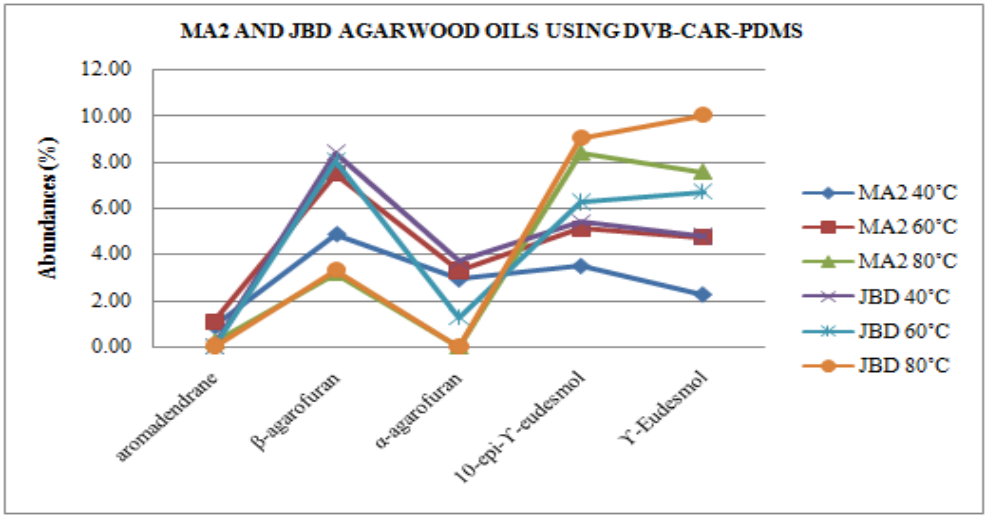


Figure 3 (b). The significant compounds as identified by Z-score at temperature 40˚C, 60˚C and 80˚C for MA2 and JBD using DVB-CAR-PDMS fiber

Conclusion

The study showed that SPME/GC-MS is a reliable technique in extracting the chemical compounds of agarwood oils especially from the high quality. The finding given by proposed Z-score gave a promising result in identifying the significant compounds from many compounds extracted by SPME/GC-MS. The chemical compounds such as 10-epi-ϒ-eudesmol, aromadendrane, β-agarofuran, α-agarofuran and ϒ-eudesmol were highlighted as significant and can be used as a marker compounds in classifying the agarwood oil especially for high quality of oils.

Acknowledgement

The authors would like to acknowledge the financial support given to Nor Azah Mohamad Ali by the Malaysian Ministry of Agriculture and Agrobased Industry (Science fund 05-03-10-SF1017), Mohd Nasir Taib through the RIF Grant Code: 600-RMI/DANA 5/3/RIF (614/2012) and Nurlaila Ismail for MyPhD scholarship by The Ministry of Higher Education, Malaysia.

References

1. R. Naef. (2011). The volatile and semi-volatile constituents of agarwood, the infected heartwood of Aquilaria species: a review, *Flavour and Fragrance Journal* 26: 73-87.
2. M. A. NorAzah, J. A. Majid, J. Mailina, A. A. Said, S. S. Husni, H. N. Hasnida, M. A. M. N. M. Arip, & Y. S. Chang (2009), Profiles of selected supreme Agarwood oils from Malaysia," *Herbal Globalisation: A New Paradigm for Malaysian Herbal Industry (MAPS 2008)* 393-398.
3. W. Hidayat, A. Y. M. Shakaff, M. N. Ahmad, & A. H. Adom, (2010). Classification of Agarwood Oil Using an Electronic Nose, *Sensors*, 10: 4675-468.
4. M. S. Najib, N. A. M. Ali, M. N. M. Arip, A. M. Jalil, & M. N. Taib, (2010). Classification of Agarwood region using ANN," *IEEE Control and System Graduate Research Colloquium (ICSGRC 2011):* 7-13.
5. M. S. Najib, N. A. M. Ali, M. N. M. Arip, A. M. Jalil, M. N. Taib, & N. Kasuan. Classification of Malaysian and Indonesian Agarwood using k-NN, *IEEE Control and System Graduate Research Colloquium (ICSGRC 2011)*.
6. M. S. Najib, M. N. Taib, N. A. M. Ali, M. N. M. Arip, & A. M. Jalil, (2011). Classification of Agarwood Grades using ANN, *International Conference on Electrical, Control and Computer Engineering* 2011.
7. N. A. B. Sidik, (2008). Comparison of Gaharu (Aquilaria Malaccensis) Essential Oil Composition Between Each Country, Bachelor of Chemical Engineering, Faculty of Chemical Engineering and Natural Resources, University Malaysia Pahang.
8. Nor Azah M.A, Chang Y.S., Mailina J., Abu Said A , Abd. Majid J. Saidatul Husni S., Nor Hasnida H. and Nik Yasmin Y. (2008). Comparison of Chemical Profiles of Selected Gaharu Oils from Peninsular Malaysia, *The Malaysian Journal of Analytical Sciences* 12: 338 - 340.
9. M. Ishihara, T. Tsuneya, & K. Uneyama (1993). Components of the agarwood smoke on heating, *Journal of Essential Oil Research* 5: 419-423.
10. A. K. Pravina, (2008). Application of solid phase microextraction in gaharu essential oil analysis, Bachelor of Chemical Engineering, Faculty of Chemical Engineering and Natural Resources, Univerisiti Malaysia Pahang (UMP), Pahang.
11. M. Ishihara, T. Tsuneya, & K. Uneyama, (1993). Fragrant sesquiterpenes from agarwood, *Phytochemistry* 33: 1147-1155.
12. T. Nakanishi, E. Yamagata, K. Yoneda, & T. Nagashima, (1984). Three fragrant sesquiterpenes of agarwood, *Phytochemistry* 23: 2066-2067.
13. R. W. Thatcher, C. J. Biver, & D. M. North, (2004). Z-Score EEG Biofeedback: Technical Foundations, *Applied Neurosciences Inc*.
14. T. C. Brown, T. C. Daniel, & R. M. Forest, (1990). *Scaling of ratings: concepts and methods* 293: USDA Forest Service, Rocky Mountain Forest and Range Experiment Station.
15. M. Ishihara, T. Tsuneya, & K. Uneyama, (1991). Guaiane sesquiterpenes from agarwood, *Phytochemistry*, 30 3343-3347.
16. J. Rohloff, (1999), Monoterpene composition of essential oil from peppermint (Mentha× piperita L.) with regard to leaf position using solid-phase microextraction and gas chromatography/mass spectrometry analysis, *Journal of Agricultural and Food Chemistry* 47: 3782-3786.
17. P. Pripdeevech, W. Khummueng, & S. K. Park, (2011). Identification of Odor-active Components of Agarwood Essential Oils from Thailand by Solid Phase Microextraction-GC/MS and GC-O, *Journal of Essential Oil*

Research, 23: 46-53.
18. S. N. Tajuddin & M. M. Yusoff, (2010), Chemical Composition of Volatile Oils of Aquilaria malaccensis (Thymeleaceae) from Malaysia, *Natural Product Communications* 5: 1965-1968.
19. S. N. Tajuddin, (2011). Resolution of complex sesquiterpene mixture in Aqualaria malaccensis (Gaharu) volatile oils using gas chromatography methods," PhD, Faculty of Industry and Science Technology (FIST), Universiti Malaysia Pahang.
20. P. Masango, (2005). Cleaner production of essential oils by steam distillation, *Journal of Cleaner Production* 13: 833-839.

The Malaysian Journal of ANALYTICAL SCIENCES ISSN 1394-2506

SYNTHESIS OF RUBBER SEED OIL AND TRIMETHYLOLPROPANE BASED BIOLUBRICANT BASE STOCKS

(Penghasilan Stok Asas Biopelincir Berasaskan Minyak Biji Getah dan Trimetilolpropana)

Ainaatul Asmaa' Ishak* and Jumat Salimon

School of Chemical Sciences and Food Technology,
Faculty of Science and Technology,
Universiti Kebangsaan Malaysia, 43600 UKM Bangi, Selangor Darul Ehsan, Malaysia.

**Corresponding author: aina_asmaa88@yahoo.com*

Abstract

Esters derived through a chemical combination of vegetable oil with trimethylolpropane (TMP) have the potential for biolubricants usage due to their biodegradable, non toxic and environmentally friendly nature. The synthesis of ester was carried out via esterification of TMP with fatty acid rubber seed oil (FARSO) for 5 hours of reaction at 150 ^{o}C in the present of concentrated sulphuric acid (2% w/w). A Fourier Transform Infrared Resonance (FTIR) and a Gas Chromatography equipped with a Flame Ionization Detector (GC-FID) was used to determine both the presence of the ester carbonyl group (C=O) as well as the ester composition. The results showed that the esterification process has increased the oil flash point (310 ^{o}C), viscosity indices (283) and lower the pour point (-40 ^{o}C). RSOTMP ester produced has shown comparative physicochemical properties that plausible it to be used as good biolubricant base stock oil.

Keywords: ester, biolubricant; fatty acid rubber seed oil; RSOTMP ester

Abstrak

Ester yang diperolehi melalui kombinasi kimia antara minyak tumbuhan dengan trimetilolpropana (TMP) dipercayai mempunyai potensi untuk kegunaan sebagai biopelincir kerana sifatnya yang mudah terbiodegradasikan, tidak toksik dan mesra alam. Sintesis ester telah dijalankan melalui proses pengesteran TMP dengan asid lemak minyak biji getah (FARSO) selama 5 jam pada suhu 150 ^{o}C dengan kehadiran asid sulfurik pekat (2% w/w). Spektroskopi Penyerapan Inframerah (FTIR) dan Kromatografi Gas yang dilengkapi dengan Pengesan Pengionan Api (GC-FID) telah digunakan untuk menentukan kehadiran kumpulan karbonil ester (C=O) dan komposisi ester. Hasil kajian menunjukkan bahawa proses pengesteran telah meningkatkan takat kilat minyak (310 ^{o}C), indeks kelikatan (283) dan takat tuang (-40 ^{o}C). Ester TMPRSO yang dihasilkan menunjukan sifat pelinciran yang baik dan berpotensi untuk digunakan sebagai stok asas dalam penghasilan biopelincir.

Kata kunci: ester; biopelincir; asid lemak minyak biji getah; ester TMPRSO

Introduction

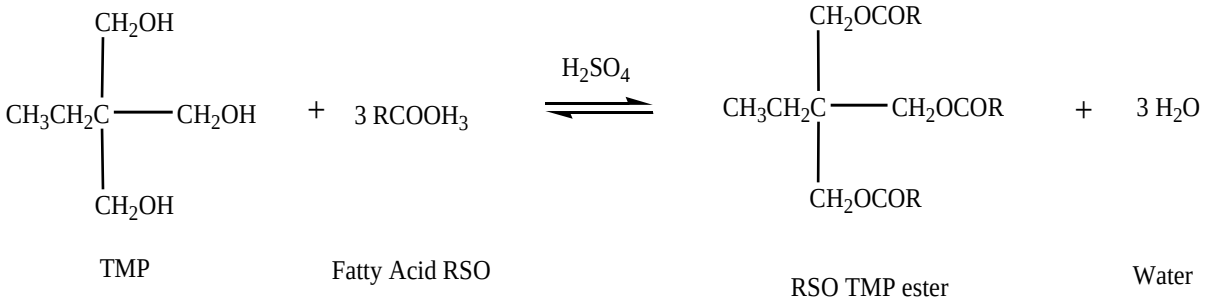
Growing concerns over environmental pollution caused by the use of mineral oil-based lubricants has resulted in lubricant industries expressing interest in environmentally friendly materials that may also be suitable replacements for mineral oil-based lubricants. The nature of vegetable oil that is easily renewable, biodegradable and non toxic makes it the best alternative in replacing mineral oil [1]. It also posses the properties required for lubrication, including excellent lubricity, high flash point and viscosity index, as well as good viscosity [2, 3].

Vegetable oil consists of triacylglycerol molecule which is constructed from three molecules of fatty acid bounded to one molecule of glycerol through ester bonds. However, the existence of β hydrogen on the glycerol backbone in vegetable oil causes few weaknesses which limit its potential use as an industrial lubricant. This includes poor thermal and oxidative stability, [4] easily damaged at high temperature [5] and the fact that it easily undergoes hydrolysis [2]. Chemical modification of vegetable oil, involving the exchanging of glycerol molecule with trimethylolpropane (TMP) forming a typical synthetic ester, has been shown to improve the oil stability [5, 6, 7].

Synthetic esters have been used for many years as base lubricating fluids due to their environmentally friendly nature, despite the high market price of synthetic esters [8]. Synthetic esters are also known for its excellent lubricity such as good thermal and oxidative stability, low volatility, high viscosity index and excellent low temperature fluidity [9].

Typical synthetic esters comprised of vegetable oil with TMP, showed to have good lubrication properties. The esterification of palm kernel oil methyl ester (PKOME) with TMP resulted in a successful conversion of 98 % PKOME to triester (TE) [6]. The esterification between fatty acid *Jatropha curcas* oil with TMP using different catalyst namely nitric acid, perchloric acid, sulphuric acid and *p*-toluenesulfonic acid resulted in TMP ester [4]. The use of perchloric acid produces the highest ester (70 %) with flash point higher than 300 ^{o}C and index viscosity of 150. Esterification of TMP with olive oil, rapeseed oil and lard has shown the resulting TMP ester have good thermal properties [5]. Transesterification of jatropha methyl ester with TMP at 150 ^{o}C using sodium methoxide as the catalyst has improved the oil stability for biolubricant base stock [6]. However the esterification of TMP with rubber seed oil (RSO) has not reported discover.

RSO has many potential in industrial applications, but has not been widely used. Such applications include biodiesel [11, 12], surface coating [13, 14], PVC stabilizer [15] and soap [16]. The oil is rich in polyunsaurated fatty acids, comprising up to 79.45 % of its fatty acid composition. The major fatty acid found in RSO is linolenic acid (C18:2), with a total percentage of 37.28 %, followed by oleic acid (22.95 %) and linolenic acid (19.22 %). The total percentage of saturated fatty acid found in RSO is 19.12 % and is comprised of palmitic and stearic acid [17]. In this paper, we reported the esterification of fatty acid RSO (FARSO) with TMP as shown in Figure 1 for biolubricant application. The finding showed that the typical synthetic ester has good physical properties as a biolubricant based stock.



R = Mixed fatty acid

Figure 1. Esterification of fatty acid rubber seed oil (FARSO) with trimethylolpropane (TMP)

Materials and Methods

Raw Materials

Rubber seeds were obtained from a rubber plantation located in Perak, Malaysia. The TMP utilizes for the esterification process was purchased from Fluka. The sulphuric acid, ethyl acetate, hydrochloric acid, *n*-hexane and toluene were purchased from Systerm whereas N,O-Bis(trimethylsilyl)triflouroacetamide (BSTFA) with 1% trimethylsilyl chloride was purchased from Acros Organic.

Oil Extraction

The collected rubber seeds were dried in an oven for 7 hours sets at 65 ^{o}C. A 500 g of the dried rubber seeds were finely ground and placed in a Soxhlet extraction thimble. The extraction of RSO was performed at 75 ^{o}C for 7 hours period. Hexane was used as an extraction solvent to extract the oil from the rubber seeds and was removed at the end of the process using a rotary evaporator.

Hydrolysis of Rubber Seed Oil (RSO)

The hydrolysis process conducted involves two stages namely saponification and acidification. In the saponification process, 50 g of RSO was mixed with alkaline ethanol and heated in a water bath set at 60 ^{o}C for 2 hours. The mixture then underwent the acidification process in which hydrochloric acid 6 N (HCl 6N) was added to neutralize the alkaline solution. The washing was continued using distilled water and hexane as solvents until the pH was neutral. Solvents were removed at the end using a rotary evaporator and the fatty acid formed was subsequently analysed by FTIR.

Esterification of TMP

The esterification process was conducted by mixing a known quantity of FARSO and TMP at a ratio of 3.9:1 in a 500 mL three neck round bottom flask, equipped with a thermometer and Dean Stark apparatus. Toluene, the azeotropic agent, and 2 % (w/w) sulphuric acid, based on the weight of the fatty acid and acting as a reaction catalyst, were added to the mixture. The reaction was heated for 5 hour at 150 °C with continuous stirring. Mixture was washed thoroughly with alkaline solution and ethyl acetate, followed by distilled water, until pH neutral.

GC-FID Analysis

To determine the percentage composition, the end product was analysed using a gas chromatograph equipped with a flame ionization detector (GC-FID). Sample was prepared by heating a small portion of the sample mixed with ethyl acetate (GC grade) and BSTFA in a 60 °C water bath for 40 minutes. The analysis was performed by using the DB-5HT (30 m x 0.25 mm x 0.10 μm), the injector and detector were set at 380 and 400 °C, respectively. The initial oven temperature was set at 100 °C with 1 minute of initial holding time. Ramping rate was increased for 5 °C/min until it reached 380 °C; and held for 25 minutes.

FTIR Analysis

Identification of functional groups present was determined through Fourier Transform Infrared Resonance (FTIR). FTIR analysis was done by placing the sample on sodium chloride (NaCl) plate (sample holder) forming thin layer of sampel. Second NaCl plate was taken and mounted on the first NaCl plate. Plate was then placed on the sample holder ready for FTIR analysis. The range of wave number used was 4000 cm^{-1} to 700 cm^{-1}.

Physical Characterization

The characterization tests, including flash point (ASTM D92), pour point (ASTM D97), viscosity (ASTM D445) and oxidative stability [20] test were performed on the formed RSOTMP ester.

Results and Discussion

Rubber Seed Oil (RSO)

Rubber seed oil (RSO) is known as non edible vegetable oil. The oil at present has not been used for any major application [12]. The extraction of rubber seed oil shows the seeds contained 48.4% of oil. This value was comparable with other RSO such as 40% by Jumat and Bashar (2009) and 40 – 50% by Ramadhas et al. (2005) [12, 17]. Different in oil content indicates RSO and its fatty acid obtained from the rubber seeds vary depends on the countries and area. Table 1 shows the properties comparison of RSO from different area in Malaysia and from other countries.

Fatty acid composition plays an important role in characteristic formation of the oil. RSO consist from five types of fatty acids. The major fatty acid was linoleic acid with the percentage composition of 40.5 % followed by linolenic acid (13.5 %), oleic acid (28.9 %), stearic acid (9.0 %) and palmitic (7.9 %). This was compareable with Nigeria RSO [18] where 2.2 % of meristic acid was detected in the oil. The high percentage of unsaturated fatty acid in RSO makes up to a total of 82.9 % of its fatty acid composition. This explains the liquid form of the oil at room temperature.

Table 1. Physicochemical properties of Rubber Seed Oil (RSO)

Analysis	**MRSO**	**MRSO [17]**	**IRSO [12]**	**NRSO [18]**
Source of rubber seeds	Malaysia (Perak)	Malaysia (Selangor)	India	Nigeria
Oil content, %	48.4	40	40 – 50	NA
Fatty acid composition, %				
i. Myristic acid	-	-	-	2.2
ii. Palmitic acid	7.9	8.6	10.2	7.6
iii. Stearic acid	9.0	10.6	8.7	10.7
iv. Oleic acid	28.9	22.3	24.6	20.0
v. Linoleic acid	40.5	37.3	39.6	36.0
vi. Linolenic acid	13.5	19.2	16.3	23.5
Iodine value, mgI_2/g	124.2	135.8	NA	155.6
Acid value, mgKOH/g	6.35	15.0	34	23.00
Free fatty acid (as oleic), %	3.19	7.6	NA	11.29

NA – not available

RSOTMP ester

The esterification between FARSO and TMP at high temperature with sulphuric acid as the catalyst has successfully formed ester TMP based on rubber seed oil (RSOTMP ester). The presence of catalyst encourages the protonation of carbonyl oxygen of fatty acid [19] as shown in Figure 2. Increase in electrophilicity of the carbon atom led to alcohol (TMP) nucleophilic attack forming a tetrahedral intermediate. Proton migration of the intermediate eventually forms an ester. Formation of water as by product throughout the process was removed through Dean Stark apparatus to avoid from reverse hydrolysis causing the breakdown of triester (TE) to diester (DE) and monoester (ME).

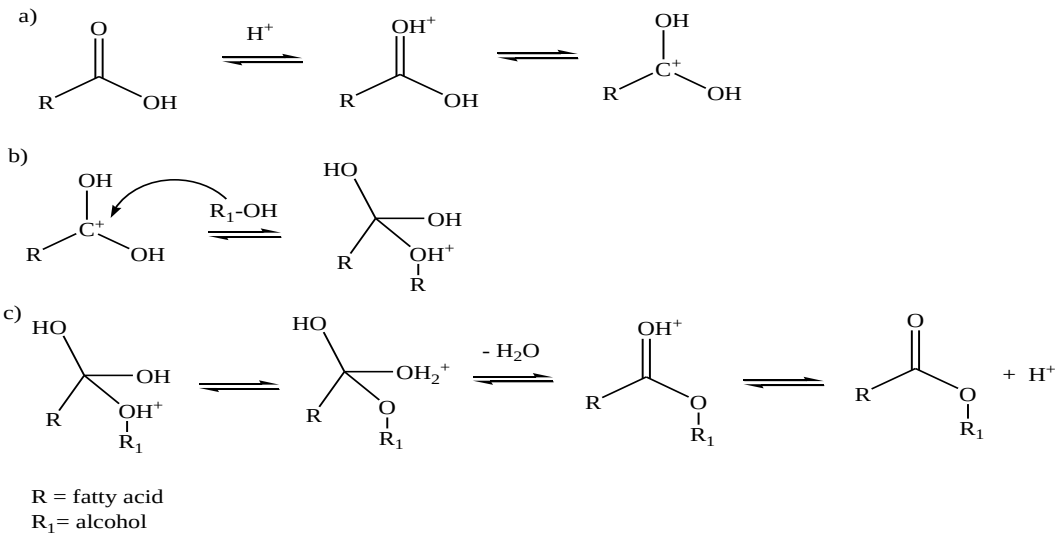


Figure 2. Reaction mechanism for esterification: a) protonation of the carbonyl by acid catalyst; b) nucleophilic attack of alcohol forming tetrahedaral intermediate; c) proton migration of tetrahedral intermediate forming an ester.

The formation of ester was confirmed by the presence of ester groups following FTIR analysis as shown in Figure 3. The IR spectrum of RSOTMP ester shows the emergence of C=O ester peak at a wavenumber 1744 cm^{-1}. This was different from the IR spectrum of the FARSO, whereby the stretching of C=O group of the fatty acid appeared at a wavenumber of 1713 cm^{-1} [21]. The stretching of the C-O ester group exists at wavenumbers of 1239 cm^{-1} and 1164 cm^{-1} in the RSOTMP ester spectrum. The C-O of the fatty acids appears at the wavenumbers of 1285 cm^{-1} and 1247 cm^{-1}. The change in wavenumber indicates that the fatty acid been has reacted with TMP forming RSOTMP ester. In addition, changes in the –OH peak occurred for both spectra in which the peak (3400-2400 cm^{-1}) is no longer visible in the spectrum of RSOTMP ester [21].

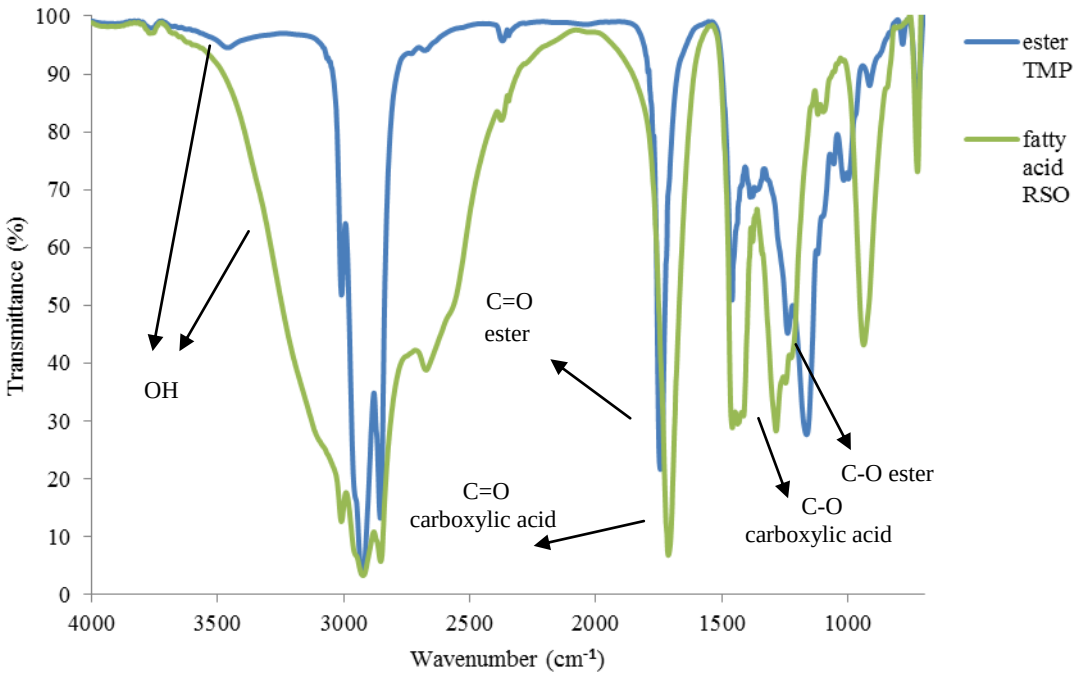


Figure 3. FTIR spectra comparison between fatty acid RSO and RSOTMP ester

The GC-FID chromatogram of RSOTMP ester is shown in Figure 4. The ester consist mixture of TE, DE, unreacted fatty acid and no presence of ME. Table 2 shows the percentage composition of each component. The major component of RSOTMP ester was 79.6% of TE followed by 18.9% of unreacted fatty acid and 1.49% of DE. The peaks in the GC chromatogram refer to the number of carbons from the alkyl group attached to the TMP. Ester of the same carbon number appears as one peak in the chromatogram [22]. Based on Figure 4, TE 54 is a triester which is made up of three fatty acids with the same carbon number, such as C18:0, C18:1, C18:2 or C18:3. TE 48 is also a triester which consists of three C16:0 (palmitic acid) that have a carbon number of 16, bringing the total to 48.

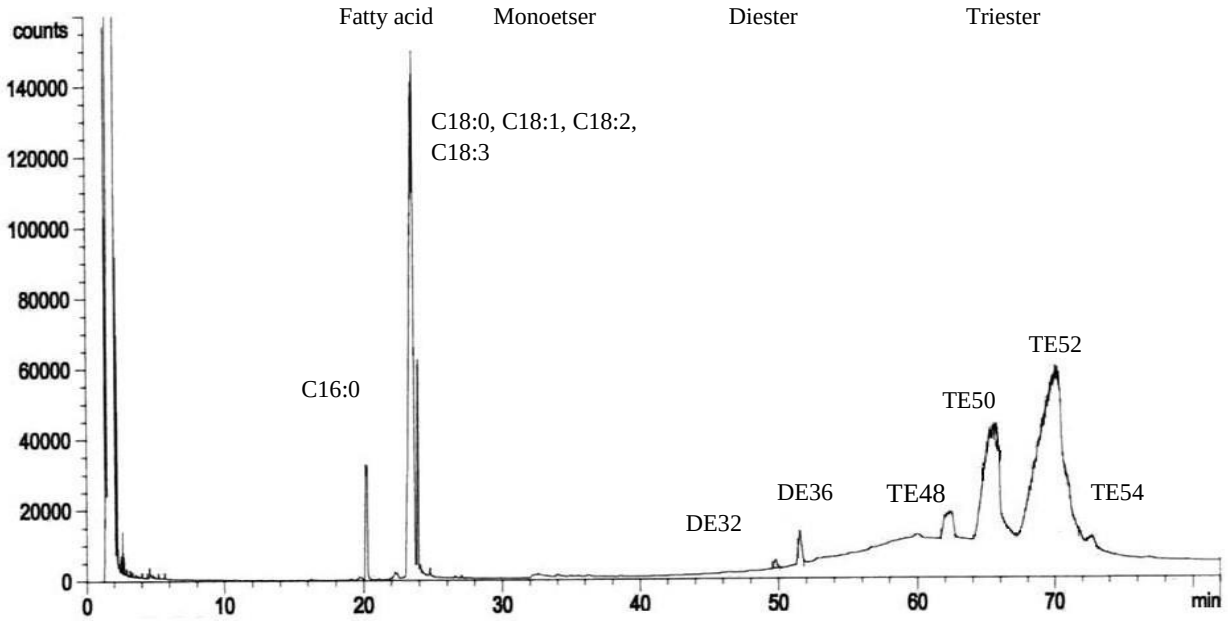


Figure 4. GC-FID chromatogram of RSOTMP ester

Table 2. The composition of RSOTMP ester

Product	Initial	Composition (%)
Unreacted fatty acid	C16:0, C18:0, C18:1, C18:2, C18:3	18.9
Monoester	-	-
Diester	DE32, DE36	1.49
Triester	TE48, TE50, TE52, TE54	79.6

Since the lubricating properties depends on the ester structure [7], the RSOTMP ester was purified by removing any excess fatty acid or monoester as it can affect the lubrication properties. Excess fatty acids were removed from the ester by using methanol extraction.

Lubricant Characterization

The esterification of FARSO with TMP has increased the oil stability. Table 3 shows the lubricant characterization of the RSOTMP ester in comparison with RSO and other synthetic ester. Based on Table 3, the flash point of RSOTMP ester is high at 310 ^{o}C compared to the flash point of RSO which was at 281 ^{o}C. This indicates the esterification with TMP has increase the oil thermal stability due to the absence of β hydrogen in the ester structure. In comparison with other synthetic ester, the obtained flash point was similar to TMP ester of PKOME (310 ^{o}C) but slightly higher than TMP ester of POME (304 ^{o}C) [6]. Typical lubricating oil has flash point around 210 ^{o}C [23]. The high flash point indicates RSOTMP ester has high potential for biolubricant production.

Table 3. The physicochemical properties of RSO, RSOTMP ester and other synthetic ester

Synthetic ester based on natural fats	Flash point, ^{o}C	Pour point, ^{o}C	Oxidative stability, ^{o}C	Viscosity at 40 ^{o}C	Viscosity at 100 ^{o}C	Viscosity index
RSO	281	-36	137	31.5	49	271
RSOTMP ester	310	-40	144	8.6	13.3	283
Palm kernel oil methyl ester (PKOME) + TMP [6]	310	2	NA	39.7	7.7	167
Palm oil methyl ester (POME) + TMP [6]	304	-1	NA	49.7	9.8	187
Olive oil + TMP [5]	NA	-13	NA	36	8.3	218.3
Rapeseed oil + TMP [5]	NA	-15.5	NA	35.3	7.9	209.2

NA – not available

The pour point of the RSOTMP ester is -40 ^{o}C. The obtained pour point was lower than RSO which was -36 ^{o}C. The slight branching structure of RSOTMP ester due to the presence of ethyl group (CH_3CH_2) in the TMP structure has improved the pour point lowering it to -40 ^{o}C. Presence of branch structure can lower the pour point by reducing the crystallization process [24]. This value was comparable with other synthetic ester such as TMP ester of PKOME, POME [6], rapeseed oil and olive oil [5] each recorded a pour point of 2 ^{o}C, -1 ^{o}C, -13 ^{o}C and -15.5 ^{o}C respectively. Esterification with TMP has produced RSOTMP ester with higher oxidative stability than RSO. The esterification has managed to replace glycerol containing β hydrogen, an active site for oxidation, with TMP increasing the oxidative to 144 ^{o}C.

RSOTMP ester has a higher viscosity than RSO. The viscosity of RSOTMP ester at 40 ^{o}C and 100 ^{o}C was 49 cSt and 13.3 cSt. Increase in viscosity was caused by the slight branching and mass increases in the ester structure. From the viscosity reading on both temperatures, the viscosity index was determined. Most refine mineral oil and synthetic oil in the market has the viscosity index around 100 and 150 [23]. The results showed that both RSO and RSOTMP ester have high viscosity index of more than 100. However, RSOTMP ester has a slightly higher viscosity index than RSO. The value of 28 for viscosity index of RSOTMP ester was the highest in comparison with other synthetic ester (PKOME, POME, rapeseed oil and olive oil). High viscosity index indicates little changes in oil viscosity with temperature [5, 23] thus it forms better protective layer or film surrounding the metal surfaces.

Conclusion

The esterification of fatty acid RSO with TMP produces a typical synthetic ester with a slight close to the triacylglycerol of RSO. The absence of β hydrogen in the synthetic ester structure has increase the oil stability. Good physicochemical properties of RSOTMP ester such as viscosity index, high flash point and low pour point made RSOTMP ester of a suitable synthetic ester to be utilised as biolubricant base stock. An excellent lubricity and environmentally nature of the synthetic ester derived from natural oils and fats and TMP made them an appropriate biolubricant base stock for replacing mineral oil based lubricant.

Acknowledgement

The authors would like to thanks to the School of Chemical Science and Food Technology, Faculty of Science and Technology, Universiti Kebangsaan Malaysia of the financial support of this research.

References

1. Erhan, S. Z & Asadauskas, S. (2000). Lubricant basestoocks from vegetable oils. *Industrial Crops and Products* 11:277 – 282.
2. Campanella, A., Rustoy, E., Baldessari, A & Baltanás, M. A. (2010). Lubricant from chemically modified vegetable oils. *Bioresource Technology* 101:245 – 254.
3. Sharma, B. K., Adhwaryu, A., Liu, Z & Erhan, S. Z. (2006). Chemical modification of vegetable oils for lubricant applications. *Journal of the American Oil Chemist's Society* 83:129 – 136.

4. Noor Hafizah Arbain & Jumat Salimon. (2011). The effects of various catalyst on the esterification of *Jatropha curcas* oil based trimethylolpropane ester as biolubricant base stock. *E-Journal of Chemistry*. 8(S1):S33-S40.
5. Gryglewicz, S., Piechocki, W & Gryglewicz, G. (2003). Preparation of polyol esters based on vegetable and animal fats. *Bioresource Tehcnology* 87:35 – 39.
6. R., Fakhru'l-Razi, A., Ooi, T. L., Iyuke, S. E & Idris, A. (2003). Preparation and characterization of trimethylolpropane esters from palm kernel oil methyl esters. *Journal of Oil Palm Research* 15(2): 42 – 49.
7. Eychenne, V., Mouloungui, Z & Gaset, A. (1998). Total and partial erucate of pentaerythritol. Infrared spectroscopy study of relationship between structure, reactivity and thermal properties. *Journal of the American Oil Chemist's Society* 75:293- 299.
8. Nagendramma, P & Kaul, S. (2012). Development of ecofriendly/biodegradable lubricant: An overview. *Renewable and Sustainable Energy Reviews* 16:764 – 774.
9. Kohashi. H. (1990). Application of fatty acid esters for lubricating oil. *Proc. Of the World Conference on Oleochemicals into 21st Century*. American Oil Chemists' Society, Campaign, Illionis. 243-251.
10. Gunam Resul, M. F. M., Mohd. Ghazi, T. I & Idris, A. (2012). Kinetic study of jatropha biolubricant from transesterification of jatropha curcas oil with trimethylolpropane: Effects of temperature. *Industrial Crops and Products* 38:87 – 92.
11. Ikwuagwu, O. E., Ononogbu, I. C & Njoku, O. U. (2000). Production of biodiesel using rubber [*Hevea brasiliensis* (Kunth. Muell.)] seed oil. *Industrial Crops and Products*. 12:57 – 62.
12. Ramadhas, A.S., Jayaraj, S & Muraleedharan. (2005). Biodiesel production from high FFA rubber seed oil. *Fuel*. 84:335 – 340.
13. Aigbodion, A. I & Pillai, C. K. S. (2000). Preparation, analysis and applications of rubber seed oil and its derivatives in surface coatings. *Progress in Organic Coatings*. 38: 187 – 192.
14. Ikhuoria, E. U., Okieimen, F. E., Obazee, E. O & Erhabor, T. (2011). Synthesis and characterization of styrenated rubber seed oil alkyd. *African Journal of Biotechnology*. 10(10):1913 – 1918.
15. Egbuchunam, T. O., Balköse, D & Okieimen, F. E. (2007). Effect of zinc soaps of rubber seed oil (RSO) and/or epoxidised rubber seed oil (ERSO) on thermal stability of PVC plastigels. *Polymer Degradation and Stability* 92:1572 – 1582.
16. Ebewele, R. O., Iyayi, A. F & Hymore, F. K. (2010). Consideration of the extraction process and potential technical applications of Nigerian rubber seed oil. *International Journal of the Physical Sciences*. 5(6):826 – 831.
17. Jumat Salimon & Bashar Mudhaffar Abdullah. (2009). A study on the thermal properties and solid fat content of Malaysian rubber seed oil. *The Malaysian Journal of Analytical Sciences* 13(1):1 – 7.
18. Okieimen, F. E., Bakare, O. I & Okieiman, C. O. (2002). Studies on the epoxidation of rubber seed oil. *Industrial Crops and Products*. 15:139-144.
19. Lotero, E., Liu, Y., Lopez, D. E., Suwannakarn, K., Bruce, D. A & Goodwin Jr, J. G. 2005. Synthesis of biodiesel via acid catalysis. *Industrial Engineering Chemistry Research*. 44(14): 5353 – 5363.
20. Adhvaryu, A., Erhan, S.Z., Liu, Z.S & Perez, J.M. (2000). Oxidation kinetic studies of oils derived from unmodified and genetically modified vegetables using pressurized differential scanning calorimetry and nuclear magnetic resonance spectroscopy. *Thermochimica Acta* 364: 87 – 97
21. Pavia, D. L., Lampman, G. M. & Kriz, G. S. (2010). Introduction to Spectroscopy. 4th ed., United States: Thomson Learning, Inc.
22. Robiah Yunus, Ooi, T.L., A. Fakhru'l-Razi & Shahnor Basri. (2002). Simple capillary column GC method analysis of palm oil-based polyol esters. *Journal of the American Oil Chemists' Society* 79: 1075 – 1080.
23. Stachowiak, G. W & Batchelor, A. W. (2005). *Engineering Tribology*. 3rd edition. Amsterdam: Elsevier Butterworth Heinemann.
24. Cermak, S. C & Isbell, T. A. (2003). Synthesis and physical properties of estolide-based functional fluids. *Industrial Crops and Products*. 18:183 – 196.

The Malaysian Journal of ANALYTICAL SCIENCES ISSN 1394-2506

PREPARATION AND ACTIVATION OF SPIROPYRAN-MEROCYANINE SYSTEM

(Penyediaan dan Pengaktifan bagi Sistem Spiropiran-Merosianin)

Rumaisa Nordin, Azwani Mat Lazim, Atisya Rohadi, Siti Aishah Hasbullah*

School of Chemical Sciences and Food Technology,
Faculty of Science and Technology
Universiti Kebangsaan Malaysia, 43600 Bangi

**Corresponding author: aishah80@ukm.my*

Abstract

A benzospiropyran derivative has been prepared by the condensation of the precursor, methylene indoline derivative with 2,3-dihydroxylbenzaldehye in 1:1 mole ratio. The product, spiro [2H-1-benzopyran-2, 2'-(8'-hydroxy-1', 3', 3'-trimethylindoline)] was able to undergo molecular rearrangement when exposed to UV light, producing an open form merocyanine. Both opened (MC) and closed form (SP) of benzospiropyran were characterized and distinguished by NMR spectroscopy, ATR Infrared and UV-vis absorption. In addition, complexation of metal ions with benzospiropyran in ethanol solution gives rise to colour changes that are visible to the naked eye. Hence, hypsochromic shift in the absorption bands were observed due to the metal ion binding (MC-M).

Keywords: benzospiropyran, photochromic, merocyanine and hypsochromic shift

Abstrak

Terbitan baru benzospiropiran telah berjaya disediakan melalui kondensasi bahan-bahan pemula metilena indolin dan kumpulan aldehid dengan nisbah 1:1. Penghasilan produk, spiro[2H-1-benzopiran-2,2'-(8'-hidroksi-1',3',3'-trimetilindolin)] mampu mengalami perubahan kedudukan molekul apabila diradisi oleh cahaya UV dengan menghasilkan komponen terbuka iaitu merosianin.Pencirian benzospiropiran dalam keadaan tertutup (SP) dan terbuka (MC) dijalankan melalui spekstroskopi NMR, ATR IR dan spektroskopi cahaya tampak (UV). Tambahan pula, pengkompleksanion logam dan benzospiropiran dalam larutan etanol dapat menghasilkan perubahan warna yang dapat dilihat dengan mata kasar. Oleh yang sedemikian, anjakan hipsokromik dalam jalur serapan juga dapat dilihat disebabkan tindak balas bersama ion logam (MC-M).

Kata kunci: benzospiropiran, fotokromik, merosianin dan anjakan hipsokromik

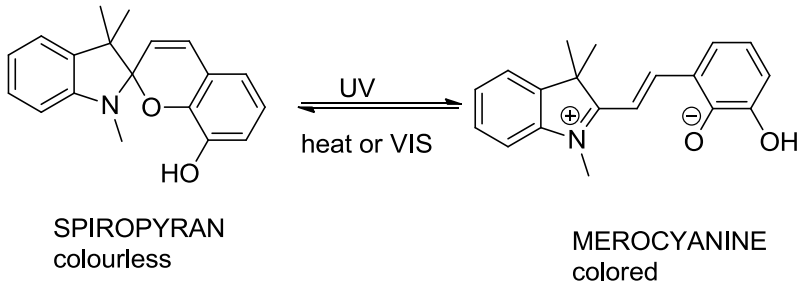
Introduction

Stimuli-responsive polymer is reported to be as the most studied field since decades ago. It has a tremendous demand in sensory [1] as well as biomedical field [2]. This 'smart' polymer is able to elicit responsive behaviour on changes in the environment [3]. Light is one of the stimuli that are capable in performing those conformational and chemical changes in particular system [4].

Light-responding polymer present a fine molecular switch as it is known to be non-destructive, non-contact mode [5], with controlled wavelength, intensity, illuminated specific area and direction [6]. All of these have been observed in nature and the same concept was applied for molecular design of synthetic photoresponsive system [7].

There are few photoreaction compounds that are extensively being investigated in photochromic system such as azobenzene [8], spiropyran [9], fulgides [10], triphenylmethane [11] and their derivatives. Among the structurally diverse photochromic compounds, spiropyrans and spiroozanines have attracted much interest due to their potential application for optical devices and sensors [12].

Spiropyrans (SP) is one of the well-known groups of light-responsive compound, which their properties have been studied extensively. They are able to undergo photo-transformation from closed spiropyran to open- zwitterions merocyanine (MC) when exposed to the UV- light as shown in Scheme 1. The current concept of applying the SP as molecular switch is based on the overall consistency of reversibility [13], rapid response time [14] and reasonably stable [15]. The adherence to those properties therefore leads to a potential molecular devices, sensors and fluorescent switches. However, many suffer from the above characteristics that hinder their wider application [16].



Scheme 1. Photochromism of typical spiropyran

Identification of the above problems has led to the search of new spiropyran derivatives to improve light fatigue resistance for sensory devices system. Hence, this study report on the synthesis and activation in photochromic system by employing metal ions to overcome the problem of stability and selectivity issues. Finally, their photochromic behavior will be investigated with the aid of absorption spectral measurements

Experimental

All the chemicals were purchased from Sigma Aldrich and were used without further purification.NMR spectra were recorded on a Bruker Avance MHz instrument (^{1}H NMR MHz) in deuterated chloroform and tetramethylsilane was used as an internal reference. The observation of functional group for spiropyran was recorded by FT-IR/FT-NIR spectrometer (Perkin Elmer, UK) in nitrogen gas purged environment using the attenuated total reflection (ATR) method for sample preparation technique in the range of 400-4000 cm^{-1}. Purification was performed using flash column chromatography on grade silica gel (Merck, 70-230 mesh). Thin layer chromatography (Merck DC Kieselgel 60 F_{254} plates) was used for detection of all compounds using appropriate solvent system.

Synthesis of benzospiropyran (SP**)**

Spiro [2H-1-benzopyran-2, 2'-(8'-hydroxy-1', 3', 3'-trimethylindoline)] abbreviated as (SP). SP was prepared by following the procedure of [17]. 2,3-dihydroxybenzaldehyde (0.7g, 5mmol) and 1,3,3-trimethyl-2-methyleneindoline (0.87g, 5mmol) were mixed together and dissolved into 50ml anhydrous ethanol. The mixture was refluxed for 5 hours and checked by TLC to confirm the formation of product. The resulting solution was filtered by vacuum filter and crude compound was obtained after purification using flash column chromatography with petroleum – ethyl acetate (4:1) as eluent. Final product (SP) was afforded in purple powder with 70% yield.

^{1}H NMR ($CDCl_3$) : δ 7.19 (t, J_1= 6.6 Hz, J_2= 6.6 Hz, 1H), 7.08 (d, J=6.6 Hz, 1H), 6.8 (d, J= 10.2 Hz, 2H), 6.87 (d, J=6.6 Hz, 1H), 6.75 (t, J_1= 7.2 Hz, J_2=7.8 Hz, 1H), 6.64 (d, =6.0 Hz, 1H), 6.54 (d, J=7.8Hz, 1H), 5.69 (d, J=10.2 Hz, 1H), 5.59 (s, 1H), 2.76 (s, 3H), 1.31 (s, 3H), 1.19 (s, 3H). IR (ATR, cm^{-1}): 3571, 3206, 1605, 1463, 1246, 1075, 933.

Photochromic Study

The spectroscopic measurements were performed with a UV/Vis absorption spectrophotometer. The spiropyran was dissolved in dichloromethane (10μM) and irradiated by high-pressure mercury lamp for 10 minutes. UV-vis spectra were recorded with subsequent times until no change in the maximum absorption of irradiated SP was recorded.

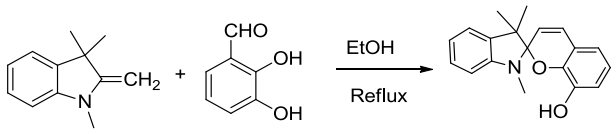
Metal-induced activation of spiropyran

In metal ion activation, standard solution of Zn(II), Cu(II), Co(II), Sn(II) and Fe(II) were prepared in five different concentration (1 x 10^{-2} M, 1 x 10^{-3}M, 1 x 10^{-4}M, 1 x 10^{-5} M and 1 x 10^{-6} M) and dissolved in ethanol and stored in the dark room temperature. The standard solution of SP was prepared in ethanol with fixed concentration of 1 x 10^{-4}M. Solution studies were followed by adding 300µl prepared metal chlorides into 6ml of standard solution of SP. The mixture was placed into a 1cm path length cuvette and the absorption spectra of SP activated in each metals ion were taken.

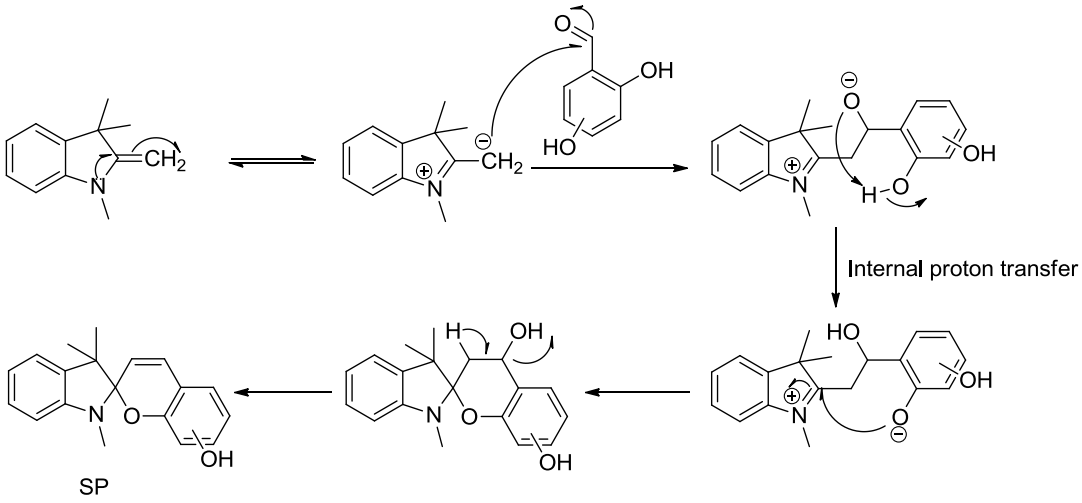
Results and Discussion

Synthesis of benzospiropyran (SP)

Preparation of common benzospiropyran usually dealt with bromination reaction [18] in two consecutive steps. However, the SP prepared in this study is synthesized from the condensation of precursor fisher base and 2, 3-dihydroxylbenzaldehyde in 1:1 mole ratio in one pot reaction (Scheme 2). The reaction mechanism took place when the fisher base formed a carbanion through the mesomeric effect [19]. Thus, the nucleophilic species of fisher base attack to the carbonyl group on the 2,3-dihydroxylbenzaldehyde. This allowed the internal proton transfer of hydroxyl group in the ring [20]. Ring closure through intramolecular addition of the phenolic oxygen to the ammonium group to form the spiro-compound followed by an elimination of water (Scheme 3).



Scheme 2. Synthesis of spiropyran



Scheme 3. Proposed mechanism of SP compound

Spectroscopic studies of benzospiropyran

The chemical structure of both SP and MC were successfully elucidated with the aid of ^{1}H-NMR and IR spectroscopies. Infrared spectroscopy was employed to confirm the structural changes of before and after the irradiation took place of spiropyran compound. The ring opening process of SP is believed to take place after the irradiation which will result in breaking down of C-O bond and appearing of C=O bond in the merocyanine state

[21]. The IR spectrum from 4000 cm^{-1} to 650 cm^{-1} for both SP and MC are presented in Figure 1 and the overall bands observed were simplified in Table 1. The spectrum of SP shows bands around 3296.88 cm^{-1}which assigned to an OH frequency of intramolecular H-band in the salicyldehydes [22]. Approximate stretching ranging from 3100 to 2800 cm^{-1} correspond to the C-H stretching vibration and the C-O-C stretching vibration is assigned at 1246 cm^{-1} and 1075 cm^{-1} respectively [23]. Furthermore, the C-O_{spiro} stretching frequencies were noticed at 990 cm^{-1} - 934 cm^{-1} that signifies the indolinobenzospiropyrans compounds [24]. In despite, the C-O_{spiro} vibration were not visible and strong band exhibited at 1722.85 cm^{-1} associated to the C=O bond that only appears in merocyanine state. These indicate a significant difference in both open and closed state.

Table 2 summarized the ^{1}H NMR of the SP before and after isomerization to the (coloured) MC form. The SP shows signals of the two geminal methyl groups at 1.19 ppm and 1.3 ppm and *N*-methyl peak at 2.97 ppm due to the ring-closed form consisting of orthogonal nature of both indoline and benzopyran halves [25]. Olefinic protons appear at 5.77 and 6.9 ppm for H_3 and H_4, respectively with large coupling constants J=10 Hz indicates for the *cis* configuration. The J value within 7-10Hz is described for *cis* double bond [26]. In contrast, after SP was irradiated under UV light, the corresponding peaks of germinal methyl groups had shifted downfield because of the effect of the positively charged N in the opened form [25]. This effect is attributed to the cleavage C-O bond and observed mainly at the peaks of NCH_3 which newly appeared at 3.41 ppm. Moreover, the conversion to the new species MC also collapsing the *gem*-dimethyl group signals into single peak at 2.08ppm [25]. However, the rest of C-H aromatic peak assignment of merocyanine form was rather complex hence it has not been assigned.

Table 1. Infrared spectral data of both spiropyran and merocyanine

Sample	**Frequency (cm^{-1})**				
	OH	**C=C**	**C-O-C**	**C=O**	**Cspiro-O**
Spiropyran	3206	1605 and 1463	1246 and 1075	-	933
Merocyanine	-	1491	-	1708	-

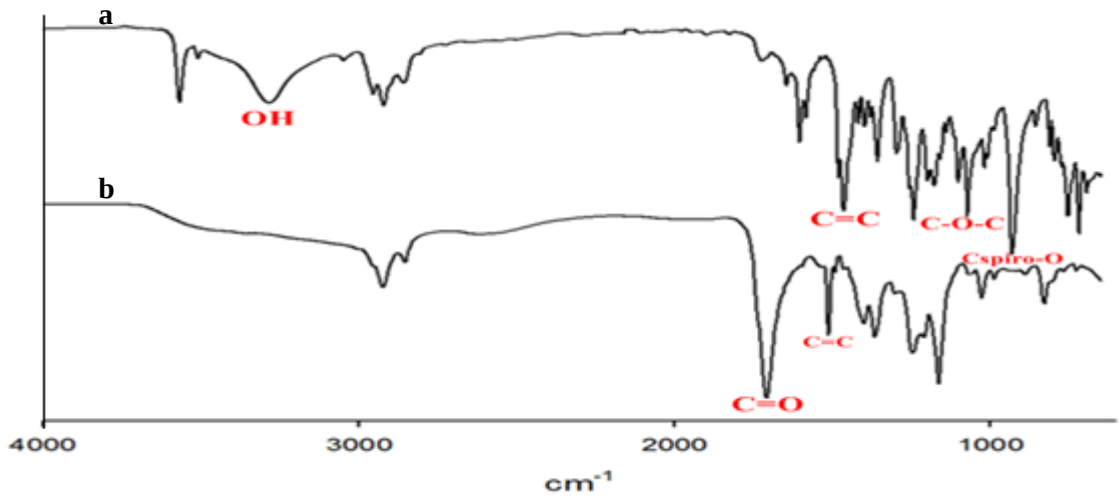


Figure 1. Infrared spectra of (a) spiropyran form (b) merocyanine form

Table 2. Significant ^{1}H NMR spectral data for both SP and MC

Sample	**Assignment (ppm)**			
	H-C aromatic$^{(m)}$	**$CH_3^{(s)}$**	**N-$CH_3^{(s)}$**	**C-OH$^{(s)}$**
Spiropyran	5.69 – 7.19	1.31 and 1.19	2.76	N.D
Merocyanine	8.3	2.0812	3.417	N.D

s, singlet; m, multiplet; and N.D., Not Detected

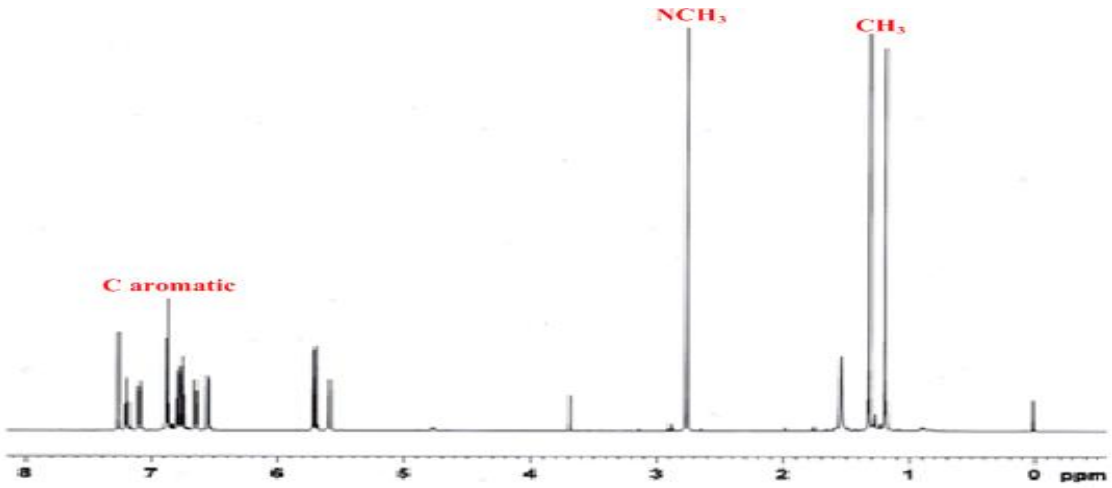


Figure 2. ^{1}H NMR spectrum of spiropyran in $CDCl_3$

Photochromic study

SP prepared which appeared to be colourless after dissolution in dichloromethane was able to exhibit a strong "positive photochromism" and lead to the formation of colored merocyanine. This correspond to the irradiation of spiropyran under UV light for a certain time and triggered the isomerisation to merocyanine form via the photochemical cleavage of the C-O bond [9]. At times zero, there was almost no absorption appears at >430nm, indicating the compound to be at closed form. By contrast, the increase time of UV exposure manifest a build-up of prominent band in the absorption spectrum peaking at 430nm due to hyperchromic effect (Figure 3). Hence, this proved that the conversion of SP → MC in aqueous media can be accelerated in longer time [27].

Metal-induced activation of spiropyran

Upon the addition of various metal cations: Zn^{2+}, Co^{2+}, Cu^{2+}, Fe^{2+} and Sn^{2+}, the colourless spiropyran solution switched to coloured merocyanine metal complex.This binding interaction is in agreement with the previous report [26], that the new absorption peaks observed in the visible region in the presence of metal cations are due to the formation of spiropyran-metal complexes where two different binding sites, a hydroxyl group (position 8') and phenolate anion may be involved (Figure 4). The shifts of the absorption bands were observed in the visible region due to the formation of metal complexes (Figure 5). There is less variation in the response between different ions

although the position of the absorption maxima depends on the nature of the metal ions [28]. For example, MC-Cu, MC-Co and MC-Fe complexes showed maximum absorption at 490 nm, 470 nm and 480 nm respectively. These absorption bands are hypsochromically shifted with respect to the free merocyanine absorption. For MC-Sn complex and MC, changes only occurred in their intensity not in their absorption suggesting the same kinetic energy in both compounds.

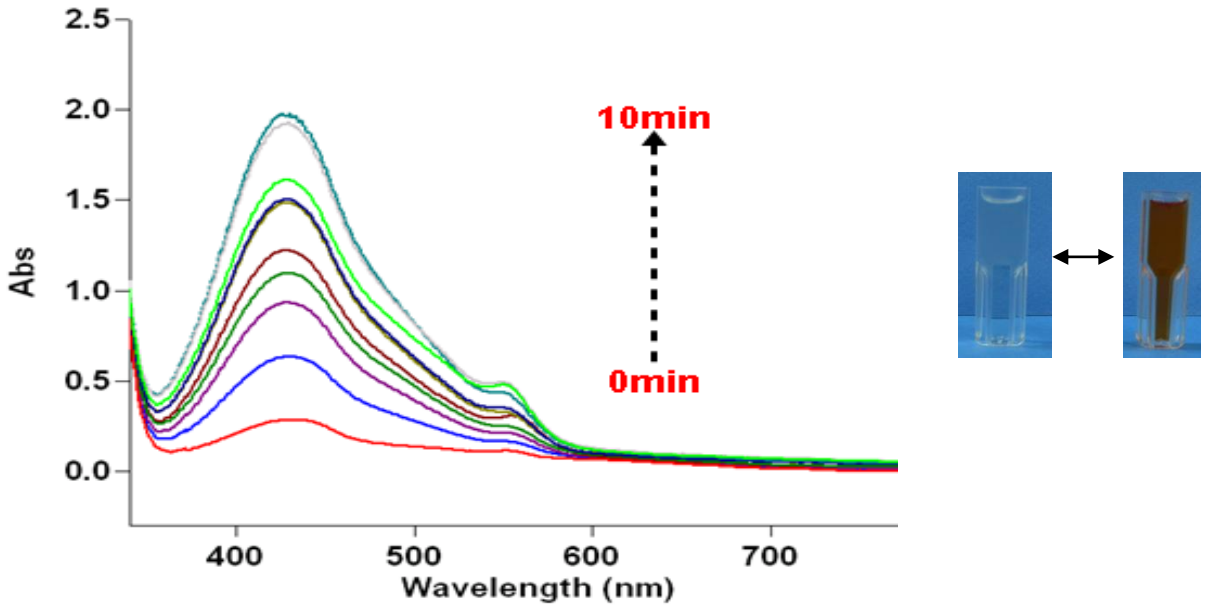


Figure 3: Absorption spectrum of spiropyran after irradiation leads to an increase in absorption at 430nm

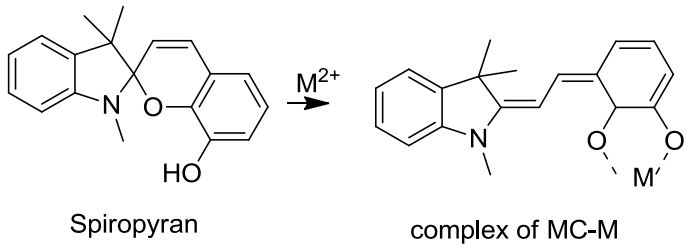


Figure 4. Metal-induced conversion of SP to MC

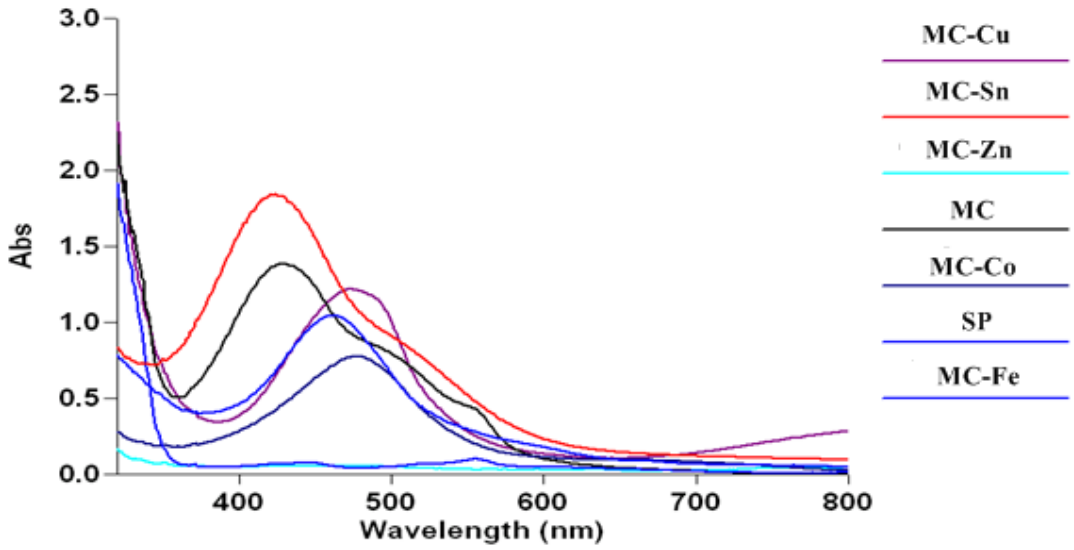


Figure 5: UV-vis absorbance spectra of SP in the presence of different divalent metal ions: Cu, Sn, Fe, Zn, and Co.

Conclusion

New photochromic spiropyrans containing a hydroxyl group were able to undergo cleavage of the weak spiro carbon-oxygen bond and formed a coloured photomerocyanine structure. The interaction between divalent ions Cu^{2+}, Fe^{2+}, Zn^{2+}, Co^{2+} and Sn^{2+} also showed strong spectral and visual changes in all five divalent metal ions. Thus, study proved on the presence of external stimuli such as metal ions can also act as an important factor in heterolytic bond cleavage and ring opening of SP compound. The spectra of all forms are able to exhibit a strong absorption and stabilization with coordination to the metal ions. Lastly, this ionochromic compound is necessary for the basic design of simple and cost-effective chemisensor.

Acknowledgement

This work was financially supported in part by research grants FRGS/1/2011/SG/UKM/02/25 and GGPM-2011-054 given by Universiti Kebangsaan Malaysia and Ministry of Higher Education.

References

1. Jiang, G., Song, Y., Guo, X., Zhang, D. & Zhu, D. (2008). Organic Functional Molecules towards Information Processing and High-Density Information Storage. *Journal of Advanced Materials*, 20 (15):2888 – 2898.
2. Young, D. D. & Deiters, A. (2003). Light-Regulated RNA–Small Molecule Interactions. *Journal of Chemistry BioChemistry*, 9(8): 1225–1228.
3. Raymo, F. M. & Giodani, S. (2001). Signals Processing at the Molecular Level. *Journal of the American Chemical Society*, 123: 4651 – 4652.
4. Zhu, M. Q., Zhu, L., Han, J. J., Wu, W., Hurst, J. K.& Li, A. D. Q. (2005). Spiropyran-based Photochromic Polymer Nanoparticles with Optically Switchable Luminescence. *Journal of the American Chemical Society*, 128: 4303 – 4309.
5. Wang, S., Song, Y. & Jiang, L. (2007). Photoresponsive surfaces with controllable wettability. *Journal of Photochemistry and Photobiology C: Photochemistry Reviews*, 8:18 – 29.
6. Ercole, F., Davis, T. P. & Evans, R. A. (2009). Photo-responsive Systems and Biomaterials: Photochromic Polymers, light-triggered Self-assembly, Surface modification, fluorescence modulation and beyond. *Polymer Chemistry*, 1: 37 – 54.
7. Maurer, M. K., Lednev, I. K. & Asher, S. A. (2005). Photoswitchable Spirobenzopyran- Based Photochemically Controlled Photonic Crystals. *Journal of Advanced Functional Materials*, 15 (9):1401–1406.

8. Anzai, J. I. & Osa, T. (2010). Photosensitive artificial membranes based on azobenzene and spirobenzopyran derivatives. *Journal of Tetrahedron,* 50 (14): 4039 – 4070.
9. Berkovic, G., Krongauz, V. & Weiss, V. (2000). Spiropyran and Spirooxazines for Memories and Switches. *Journal of Chemical Review*, 100 (5): 1741 – 1754.
10. Bowden, S. L., Harris, S. A., Heller, H. G. & Hewlins, M. J. E. (1992). Photochromic heterocyclic fulgides. Part 6. Base-catalysed cyclizations of 1-(2, 5-dimethyl-3-furyl and 2, 5-dimethyl-3-thienyl) ethylidene (isopropylidene) succinic anhydrides and related compounds. *Journal of the Chemical Society, Perkin Transactions 1,* 6: 725 – 728.
11. Oda, H. (1991). Photostabilisation of colorants for imaging and data recording systems: Effects of metal carboxylates on the lightfastness of colour formers. *Journal of Dyes and Pigments,* 16:1 – 10.
12. Shao, N., Zhang, Y., Cheung, S. M., Yang, R. H., Chan, W. H., Mo, T., Li, K. A. & Liu, F. (2005). Copper Ion-selective Fluorescent Sensor based on the inner filter effect using a spiropyran derivative. *Journal of Analytical Chemistry,* 77 (22): 7294 – 7303.
13. Winkler, J. D., Bowen, C. M., and Michelet, V. (1998). Photodynamic Fluorescent metal ion sensors with parts per billion sensitivity. *Journal of the American Chemical Society,* 120:3237 – 3242.
14. Ren, J. & Tian, H. (2007). Thermally Stable Merocyanine Form of Photochromic Spiropyran with Aluminium ions as a reversible photo-driven sensor in aqueous solution. *Sensors* 7:3166 – 3178.
15. Oda, H. (1998). New Developments in the stabilization of Photochromic dyes: counter-ion effects on the light fatigue resistance of spiropyrans. *Journal of Dyes and Pigments,* 38 (4): 243 – 254.
16. Yagi, S., Maeda, K. & Nakazumi, H. (1999). Photochromic properties of cationic merocyanine dyes. Thermal stability of the spiropyran form produced by irradiation with visible light. *Journal of Materials Chemistry,* 9: 2991 – 2997.
17. Han, S. & Chen, Y. (2010). Mercury ion induced activation of the C-O bond in a photo-responsive spiropyran. *Journal of Dyes and Pigments,* 88: 235 – 239.
18. Zakhs, E. R., Zvenigorodskaya, L. A., Leshenyuk, N. G. & Martynova, V. P. (1978). Bromination of spiropyrans and reduction of their nitro derivatives. *Plenum Publishing Corporation,* 10: 1320 – 1326.
19. Scarmagnani, S. (2010). Development of New Adaptive Materials Based On Spiropyran Molecular Photoswitches. *PhD Thesis. Dublin City University*, 32-34.
20. Hecht, S. (2011). Introduction to the Synthesis of Photochromes: Spiropyran and Diarylethenes. *SFB Kolluquium*. Humboldt-Universitat zu Berlin
21. Macuil, R. D., Lopez, M. R., Martinez, M. B. & Pernas, V. C. (2008). ATR- FTIR Spectroscopy and their Applications in the Ring- Opening Reaction of Spiropyran Polymers. *AIP Conference Proceedings,* 992: 1237 – 1241.
22. Keum, S. R., Choi, Y. K., Lee, M. J. & Kim, S. H. (2001). Synthesis and properties of thermo- and photochromic bisindolinobenzospiropyrans linked by thio- and carbonyl groups. *Journal of Dyes and Pigments,* 50: 171-176.
23. Zou, W. X., Huang, H. M., Gao, Y., Matsuura, T. & Meng, J. B. (2004). Structures of Two Spiropyrans in the Open and Closed Form. *Journal of Structural Chemistry,* 15 (4): 317 – 321.
24. Keum, S. R., Choi Y. K., Kim, S. H. & Yoon, C. M. (1999). Symmetric and unsymmetric indolinobenzospiropuran dimmers: synthesis and characterization. *Journal of Dyes and Pigments,* 41:41 – 47.
25. Preigh, M. J., Stauffer, M. T., Lin, F. T. & Weber, S. G. (1996). Anodic oxidation mechanism of a Spiropyran. *Journal of Chemical Society Faraday Trans,* 92 (20):3991 – 3996.
26. Natali, M., Aakeröy, C., Desper, J. & Giordani, S. (2010). The role of metal ions and counterions in the switching behavior of a carboxylic acid functionalized spiropyran. *Dalton Trans,* 39:8269 – 8277.
27. Shiraishi, Y., Itoh, M. & Hirai, T. (2010). Thermal isomerization of spiropyran to merocyanine in aqueous media and its application to colorimetric temperature indication. *Physical Chemistry Chemical Physics,* 12: 13731 – 13745.
28. Nikolaeva, O. G., Tsukanov, A. V., Shepelenko, E. N., Lukyanov, B. S., Metelitsa, A. V., Kostyrina, O. Y., Dubonosov, A. D., Bren, V. A. & Minkin, V. I. (2009). Synthesis of Novel Iono- and Photochromic Spiropyrans Derived from 6, 7-Dihydroxy-8-Formyl-4-Methyl-2H-Chromene-2-One. *International Journal of Photoenergy* 2009: 1 – 6

The Malaysian Journal of ANALYTICAL SCIENCES ISSN 1394-2506

ISOLATION OF ASTILBIN FROM LEAVES OF *CRATOXYLUM ARBORESCENS*

(Pemencilan Komponen Astilbin dari Daun *Cratoxylum arborescens*)

Samsiah Jusoh[1,2], Zuriati Zakaria[3] and Laily B. Din[2]*

[1]*Rice and Industrial Crop Research Centre,*
Malaysian Agricultural Research and Development Institute (MARDI)
P.O.Box 12301, 50774 Kuala Lumpur, Malaysia
[2] *School of Chemical Sciences and Food Technology, Faculty of Science and Technology*
Universiti Kebangsaan Malaysia, 43600 Bangi, Selangor, Malaysia
[3] *Malaysia Japan Institute of Technology,*
Universiti Teknologi Malaysia, 54100 Kuala Lumpur, Malaysia

**Corresponding author: lbdin@ukm.my*

Abstract

Phytochemical studies was conducted on the leaves of *Cratoxylum arborescens* that has been collected from Post Brooke, Gua Musang, Kelantan, Malaysia. Traditionally, latex of the stem bark of *C. arborescens* is being used for the treatment of wound. Extraction of leaves of *C. arborescens* using organic solvents followed by purification using standard procedure of purification yielded known compound, astilbin. This compound was identified by NMR spectral data using various 2D-techniques and comparison with the literature data. Reports showed that this compound has a unique immunosuppressive activity, a selective inhibition against activated T lymphocytes. This characteristic of astilbin is beneficial for the treatment of human immune diseases.

Keywords: guttiferae, *cratoxylum arborescens*, astilbin, leaves, NMR

Abstrak

Kajian fitokimia yang dijalankan ke atas daun *Cratoxylum arborescens* yang dikutip dari Post Brooke, Gua Musang, Kelantan, Malaysia. Secara tradisional, lateks kulit batang *C. arborescens* digunakan untuk mengubat luka. Pengekstrakan ke atas daun *C. arborescens* menggunakan pelarut organik diikuti dengan kaedah lazim penulenan menghasilkan sebatian yang telah dikenal pasti, astilbin. Komponen ini dikenal pasti menggunakan data spektrum RMN dengan teknik variasi 2D dan perbandingan dengan data literatur. Laporan menunjukkan komponen ini menunjukkan aktiviti immunosupresif yang unik, perencatan selektif terhadap limfosit T diaktifkan. Ciri astilbin ini adalah bermanfaat untuk merawat penyakit berkenaan sistem imun.

Kata kunci: guttiferae, *cratoxylum arborescens*, astilbin, daun, RMN

Introduction

Cratoxylum arborescens is known locally as Geronggang. This genus belongs to the family of Guttiferae. It is an emergent tree up to 60 m tall and diameter of about 120 cm. The stem has yellow latex and the leaves are opposite, simple, penni-veined, glabrous and venation is inconspicuous. Flowers are about 8 mm in diameter, white-pink-red and placed in panicles. The fruits are about 8 mm long red-brown-black dehiscent capsule, with many small winged seeds. This plant is normally found in undisturbed to slightly mixed dipterocarp, sub-montane forests up to 1000 m altitude. Geronggang is mostly growing on alluvial sites and along rivers, but also found on ridges. In secondary forests, this plant is usually presents as pre-disturbance remnant tree [1]. A number of studies have already been conducted on *C. arborescens*, where the compound 3-geranyloxy-6-methyl-1,8-dihydroxyanthraquinone was isolated from stem bark [2], while 1,3,8-trihydroxy-2,4-dimethoxyxanthone, 1,7-dihydroxy-2,8-dimethoxyxanthone, 1,3,7-trihydroxy-6-methoxy-4,5-diisoprenylxanthone, euxanthone, friedelin, friedelinol, methoxyemodin, betulinic acid, lup-20(29)-ene-3,30-diol, 3β-hydroxylup-20(29)-en-30-oic acid, 3,4-dihydroxybenzoic acid, eucryphin, astilbin, and isoastilbin from leaves and twigs of *C. arborescens* collected from Narathiwat province, Thailand [3,

4]. Astilbin has also been isolated from the leaves of Chinese folk medicine, *Engelhardia chrysolepis* [5]. Astilbin from stem bark of *Dimorphandra mollis* collected in Rio Claro, Sao Paulo State, Brazil showed insecticidal activity against confined bees [6].

Experimental

Plant Material

The leaves of *Cratoxylum arborescens* was collected at Post Brooke, Gua Musang, Kelantan, Malaysia. The voucher specimen of *C. arborescens* (SK 1932/11) is deposited at Herbarium UPM (UPM), Serdang, Selangor, Malaysia.

Extraction and Isolation

The leaves of *C. arborescens* (GGB, 569.3 g) was dried in oven at 50^{o}C, ground and extracted using solvent extraction at room temperature for five days. The powdered leaves was extracted using methanol (crude extract 45.6 g) and then fractionated with hexane with ratio 1:1. 1.3 g of hexane fraction (GGBA) and 36.8 g of methanol fraction (GGBC) yielded. Chemical components from methanol fraction was separated using vacuum liquid chromatography (VLC). A mixture of solvent ethyl acetate and methanol from 100% ethyl acetate to 100% methanol have been used as mobile phase and 12 fractions were collected. Vial 5-6 from VLC of GGBC have selected for further purification using column chromatography and 148 vials were collected.

Fractions 106-114 were combined for further purification using column chromatography with an internal diameter x length of column is 1.0 cm x 50.0 cm and 27 fractions were collected. The compound was eluted with solvent mixture of ethyl acetate and methanol. The combined fractions was evaporated and gave a greenish crystal (181 mg). The structure of the purified compound was analyzed using Nuclear Magnetic Resonance (NMR) and Infrared (IR) spectrometer.

Astilbin (1)

Greenish needles (181 mg). IR cm^{-1}: 3321 (OH), 2944, 2833, 1648, 1412, 1113 and 1020. ^{1}H NMR (600 MHz, CD_3COCD_3) δ: 5.17 (d, *J*=10.8Hz, H-2), 4.67 (d, *J*=10.8Hz, H-3), 11.92 (s, 5-OH), 5.96 (dd, *J*=1.8, 13.5Hz, H-6, H-8), 9.98 (brs, 7-OH), 7.07 (d, *J*=1.8Hz, H-2'), 6.86 (d, *J*=8.4Hz, H-5'), 6.89 (dd, *J*=1.8, 7.8Hz, H-6'), 4.08 (s, H-1"), 3.55 (s, H-2"), 3.79 (d, *J*=3.0Hz, 2"-OH), 3.64-3.65 (m, H-3"), 3.97 (d, *J*=3.6Hz, 3"-OH), 3.32 (ddd, *J*=3.0, 9.3Hz, H-4"), 3.82 (brs, 4"-OH), 4.20 (dd, *J*=6.0, 9.6Hz, H-5") and 1.13 (d, *J*=6.6Hz, H-6"). ^{13}C NMR (125 MHz, CD_3COCD_3) δ: 195.2 (C-4, C=O), 166.9 (C-5), 164.4 (C-7), 162.8 (C-9), 146.0 (C-3'), 145.2 (C-4'), 128.1 (C-1'), 119.7 (C-6'), 115.2 (C-5'), 114.5 (C-2'), 101.5 (C-10), 100.5 (C-1"), 96.2 (C-6), 95.1 (C-8), 82.5 (C-2), 76.4 (C-3), 72.6 (C-4"), 71.3 (C-3"), 70.6 (C-2"), 69.0 (C-5") and 17.1 (CH_3, C-6").

Results and Discussion

^{1}H NMR showed 5 types of coupling patterns i.e. singlet (s), doublet (d), doublet of doublets (dd), doublet of doublet of doublet (ddd) and multiplet (m). Singlet was shows for H-1" (δ 4.06), two hydroxyl group that attached to C-5 (δ 11.92) and C-7 (δ 9.98) in aglycone structure and one hydroxyl group at C-4" (δ 3.82) in rhamnose structure. There are eight of doublet patterns at chemical shift 1.13 (d, *J*=6.6Hz, 6"-CH_3, neighbour with H-5"), 3.79 (d, *J*=3.0Hz, 2"-OH, neighbour with H-2"), 3.97 (d, *J*=3.6Hz, 3"-OH, neighbour with H-3"), 4.67 (d, *J*=10.8Hz, H-3, neighbour with H-2), 5.17 (d, *J*=10.8Hz, H-2, neighbour with H-3), 6.86 (d, *J*=8.4Hz, H-5', neighbour with H-6'), 7.07 (d, *J*=1.8Hz, H-2', neighbour with H-6') and 8.25 (d, *J*=15.6Hz, 3'-OH, 4'-OH, between them). There are three doublet of doublet patterns. *J* coupling value revealed the proton neighbour is ortho, meta or para coupling. The pattern at δ 5.96 (dd, H-6, H-8) with *J*=13.5Hz revealed ortho coupling with H-7, J_{meta}=1.8Hz between H-6 with H-8. While the dd pattern at δ 6.90 (dd, H-6') revealed J_{ortho}= 7.8Hz with H-5' and J_{meta}=1.8Hz with H-2'. Chemical shift 4.20 (dd, H-5") revealed J_{ortho}=9.6Hz between H-5' with H-6' and para coupling with H-2'. The only one ddd pattern was observed at δ 3.32 (H-4") revealed J_{ortho}=9.3Hz (coupling with H-5" and H-3") and J_{meta}=3.0 Hz (coupling with H-2"). One multiplet pattern is corresponding to H-3" at chemical shift 3.64-3.65. This proton has ortho coupling with H-2" and H-4" and meta coupling with H-1" and H-5".

The spectral data of ^{1}H NMR was supported by a ^{1}H-^{1}H COSY NMR data. COSY is correlated spectroscopy. It indicates which protons are coupling with other proton. The data allowed us to identify a four correlations between six proton. The first correlation could be seen between proton methyl at δ 1.13 (d, *J*=6.6Hz, 6"-CH_3) with proton

attached to C-5" (δ 4.20 (dd, *J*=6.0, 9.6Hz). The other correlation is between δ 3.32 (ddd, *J*=3.0, 9.3Hz, H-4") with δ 3.64-3.65 (m, H-3"), δ 3.32 (ddd, *J*=3.0, 9.3Hz, H-4") with δ 4.20 (dd, *J*=6.0, 9.6Hz, H-5") and δ 4.67 (d, *J*=10.8Hz, H-3) with δ 5.17 (d, *J*=10.8Hz, H-2). There are *J* coupling J_{eq-eq} =1.8Hz between H-4" with H-3" and J_{ax-eq} =3.0Hz between H-3" with H-2". The four correlations were showed in Figure 1.

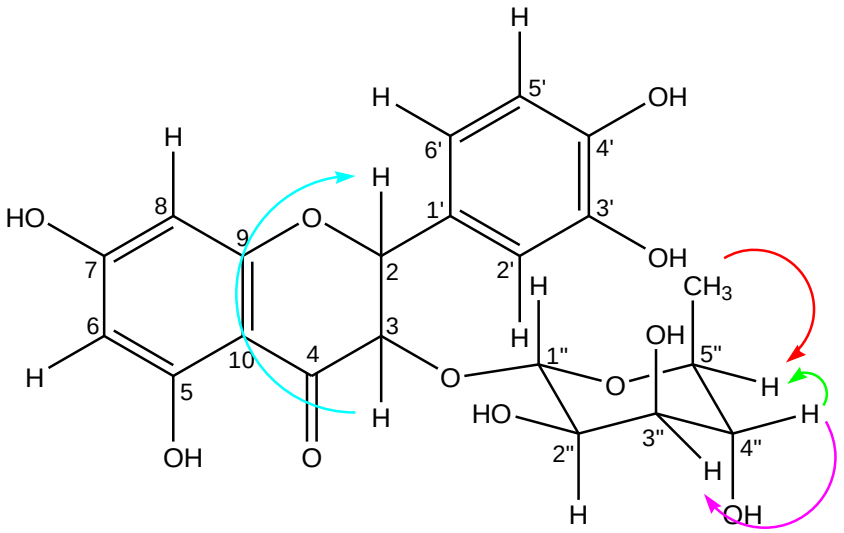


Figure 1. ^{1}H-^{1}H COSY connectivity of GGBC 4

^{13}C-APT is one of the method that showed a carbon attached to the proton, where -CH_3 and CH peaks appear phased in one direction and -CH_2- peaks appear in opposite phase. Quaternary C are seen but may be quite small in size depending on the length of relaxation allowed. There are 21 peaks of carbon for this GGBC 4 compound. From those peaks, 12 peaks of carbon were revealed a correlation with proton in ^{1}H-^{13}C HSQC NMR. The correlation of those peaks are 17.1 (CH_3, C-6") with (1.13 (d, *J*=6.6Hz, 6"-CH_3), 70.6 (C-2") with 3.55 (s, H-2"), 71.3 (C-3") with 3.64-3.65 (m, H-3"), 100.5 (C-1") with 4.08 (s, H-1"), 69.0 (C-5") with 4.20 (dd, *J*=6.0, 9.6Hz, H-5"), 76.4 (C-3) with 4.67 (d, *J*=10.8Hz, H-3), 82.5 (C-2) with 5.17 (d, *J*=10.8Hz, H-2), 96.2 (C-6) and 95.1 (C-8) with 5.96 (dd, *J*=1.8, 13.5Hz, H-6, H-8), 115.2 (C-5') with 6.86 (d, *J*=8.4Hz, H-5'), 119.7 (C-6') with 6.89 (dd, *J*=1.8, 7.8Hz, H-6'), 114.5 (C-2') with 7.07 (d, *J*=1.8Hz, H-2') and 72.6 (C-4") with 3.32 (ddd, *J*=3.0, 9.3Hz, H-4").

Table 1. Correlation of HSQC, HMBC and COSY NMR of GGBC 4

δ_H	HSQC (δ_{H-C})	HMBC (δ_{H-C})	COSY (δ_{H-H})
5.17 (H-2)	82.5 (C-2)	C-2, C-3, C-1', C-2', C-6', C-9, C-4	H-3
4.67 (H-3)	76.4 (C-3)	C-2, C-3, C-4, C-1', C-1"	H-2
5.96 (H-6)	96.2 (C-6)	C-4, C-5, C-6, C-7, C-8, C-9, C-10	
5.96 (H-8)	95.1 (C-8)	C-4, C-5, C-6, C-7, C-8, C-9, C-10	
7.07 (H-2')	114.5 (C-2')	C-2, C-3', C-6'	
6.86 (H-5')	115.2 (C-5')	C-1', C-3'	
6.90 (H-6')	119.7 (C-6')	C-2, C-2', C-3'	
4.08 (H-1")	100.5 (C-1")	C-3, C-1", C-2", C-5"	H-2"
3.55 (H-2")	70.6 (C-2")	C-3", C-4"	H-1"
3.64-3.65 (H-3")	71.3 (C-3")	C-2", C-4"	H-4"
3.32 (H-4")	72.6 (C-4")	C-5", C-3", C-6"	H-3", H-5"
4.20 (H-5")	69.0 (C-5")		H-4", H-6"
1.13 (H-6")	17.1 (C-6")	C-6", C-5", C-4"	H-5"

The spectral data of ^{1}H-^{13}C HMBC NMR was revealed 11 correlations. HMBC is heteronuclear multiple bond correlation. This eleven correlations were showed in Figure 2. The correlations of ^{1}H-^{1}H COSY, ^{1}H-^{13}C HSQC and ^{1}H-^{13}C HMBC of GGBC 4 were showed in Table 1. These NMR data was compared to the astilbin reported data [5, 6, 7, 8]. Table 2 was showed a synchronize data of GGBC 4 with astilbin.

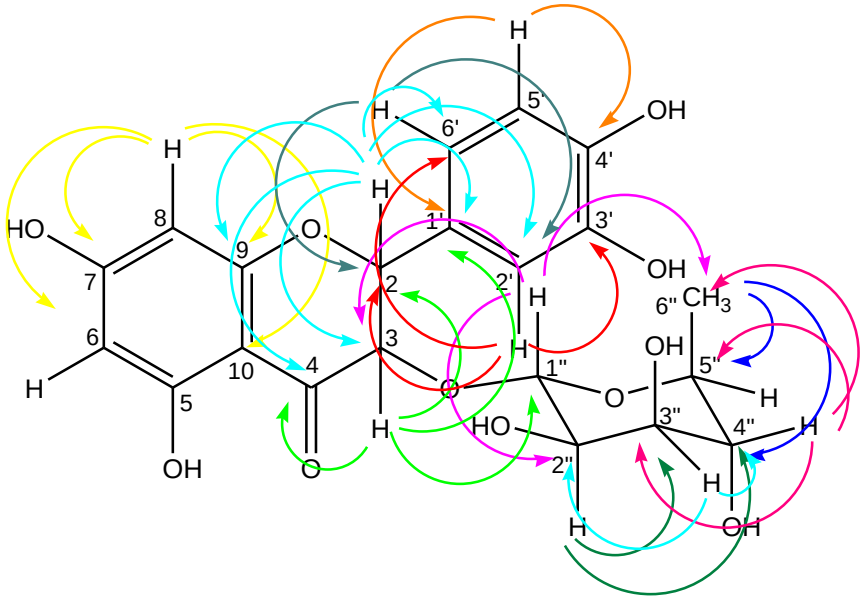


Figure 2. Heteronuclear multiple bond (^{1}H-^{13}C HMBC) connectivity of GGBC 4

Combination of all spectral data of ^{1}H, ^{13}C-APT, ^{1}H-^{1}H COSY, ^{1}H-^{13}C HSQC and ^{1}H-^{13}C HMBC NMR and IR spectrogram could determined the compound GGBC 4 was consistent to astilbin as structured in Figure 3 [5, 6].

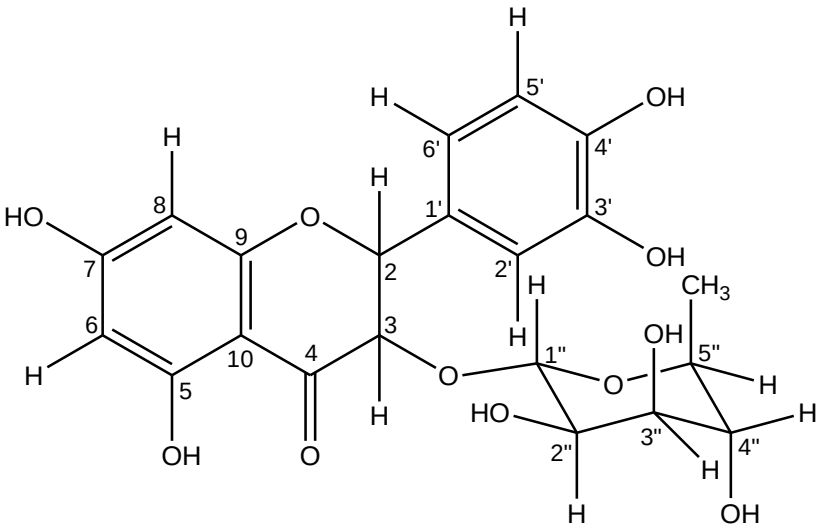


Figure 3. Astilbin

Table 2. ^{1}H and ^{13}C NMR spectral data of GGBC 4 * and astilbin **

Position of carbon and proton	Chemical shift, δ (ppm) carbon GGBC 4 *	Chemical shift, δ (ppm) carbon Astilbin **	Chemical shift, δ (ppm) proton GGBC 4 *	Chemical shift, δ (ppm) proton Astilbin **
Aglycone				
2	82.5	84.8	5.17 (d, *J*=10.8Hz)	5.06 (d, *J*=10.0Hz)
3	76.4	79.4	4.67 (d, *J*=10.8Hz)	4.57 (d, *J*=10.0Hz)
4	195.2	196.7		
5	166.9	166.3	11.92 (s, OH)	
6	96.2	98.2	5.96 (dd, *J*=1.8, 13.5Hz)	5.89 (d, *J*=2.1Hz)
7	164.4	169.7	9.98 (brs, OH)	
8	95.0	97.2	5.96 (dd, *J*=1.8, 13.5Hz)	5.91 (d, *J*=2.1Hz)
9	162.9	164.9		
10	101.5	103.2		
1’	128.1	130.0		
2’	114.5	117.1	7.07 (d, *J*=1.8Hz)	6.95 (d, *J*=1.8Hz)
3’	146.0	147.3	8.25 (d, *J*=15.6Hz, OH)	
4’	145.2	148.1	8.25 (d, *J*=15.6Hz, OH)	
5’	115.2	116.3	6.86 (d, *J*=8.4Hz)	6.80 (d, *J*=8.2Hz)
6’	119.7	121.3	6.89 (dd, *J*=1.8, 7.8Hz)	6.84 (dd, *J*=1.8,8.2Hz)
Rhamnose				
1”	100.5	102.9	4.08 (s)	4.04 (brs)
2”	70.6	72.6	3.79 (d, *J*=3.0Hz, OH), 3.55 (s)	3.53 (brd, *J*=3.3Hz)
3”	71.3	72.9	3.97 (d, *J*=3.6Hz, OH), 3.64-3.65 (m)	3.64 (dd, *J*=3.3,9.6Hz)
4”	72.6	74.6	3.82 (OH), 3.32 (ddd, *J*=3.0, 9.3Hz)	3.32 (t, *J*=9.6Hz)
5”	69.0	71.3	4.20 (dd, *J*=6.0, 9.6Hz)	4.26 (m)
6”	17.1	18.6	1.13 (d, *J*=6.6Hz)	1.18 (d, *J*=6.2Hz)

Reference Astilbin : Guo et al. 2007.

* Recorded in CD_3COCD_3 at 600 MHz, ** Recorded in $CDOD_3$ at 300MHz. Chemical shift, δ values in ppm and coupling constant (*J*) values in Hz. Splitting patterns: s, singlet; brs, broad singlet; d, doublet; dd, doublet of doublets; ddd, doublet of doublet of doublet; brd, broad doublet; t, triplet; m, multiplets.

Conclusion

The identification of compound GGBC 4 only using Nuclear Magnetic Resonance (NMR). It is ^{1}H, ^{13}C-APT, ^{1}H-^{13}C HSQC, ^{1}H-^{1}H COSY and ^{1}H-^{13}C HMBC NMR. Even though only one technique, the compound could be defined as known compound astilbin, a flavonoid glycosides. Therefore, NMR is the most essential tools in structural identification beside other chromatography. NMR spectroscopy also a very useful method in various fields of pharmaceutical sciences like pharmaceutical analysis, medicinal chemistry, natural product chemistry and pharmaceutical technology.

Acknowledgement

This research was financially supported by Ministry of Agriculture and Agro-based Industry (MOA), MARDI, and UKM grant (grant No. UKM-ST-06-FRGS0110-2009, UKM-GUP-2011-205, UKM-DLP-2012-033). We are grateful to Dr Shamsul Khamis for the assistance in identifying plant material and Mr. Mohd. Zahid Md. Yusoff for analyzing NMR.

References

1. www.nationalherbarium.nl. (2009). *Cratoxylum arborescens* (Vahl) Blume, nationalherbarium [cited 25 Oct 2009].
2. Pattanaprateeb, P., Ruangrungsi, N. & Cordell, G. A. (2005). Cytotoxic Constituents from *Cratoxylum arborescens*. *Planta Medica,* 71(2): 181-183.
3. Reutrakul, V., Chanakul, W., Pohmakotr, M., Jaipetch, T., Yoosook, C., Kasisit, J., Napaswat, C., Santisuk, T., Prabpai, S., Kongsaeree, P. & Tuchinda, P. (2006). Anti-HIV-1 Constituents from Leaves and Twigs of *Cratoxylum arborescens. Planta Medica,* 72 : 1433-1435.
4. Reutrakul, V., Chanakul, W., Pohmakotr, M., Jaipetch, T., Yoosook, C., Kasisit, J., Napaswat, C., Santisuk, T., Prabpai, S., Kongsaeree, P. & Tuchinda, P. (2006). Anti-HIV-1 Constituents from Leaves and Twigs of *Cratoxylum arborescens. Planta Medica,* 72 : 383-389.
5. Guo, J., Qian, F., Li, J., Xu, Q. & Chen, T. (2007). Identification of a New Metabolite of Astilbin, 3-*O*-methylastilbin, and its Immunosuppressive Activity Against Contact Dermatitis. *Clinical Chemistry,* 53 (3): *465–471.*
6. Cintra, P., Malaspina, O., Petacci, F., Fernandes, J. B., Bueno, O. C., Vieira, P. C. & Silva, M. F. G. F. (2002). Toxicity of *Dimorphandra mollis* to Workers of *Apis mellifera*. *Journal of the Brazillian Chemical Society*, 13 (1): 115-118.
7. Goetz, G., Fkyerat, A., Metais, N., Kunz, M., Tabacchi, R., Pezet, R. & Pont, V. (1999). Resistance Factors to Grey in Grape Berries: Identification of Some Phenolics Inhibitors of *Botrytis cinerea* Stilbene Oxidase. *Phytochemistry,* 52 : 759-767.
8. Trousdale, E. K. & Singleton,V. L. (1983). Stilbin and Engeltin in Grapes and Wine. *Phytochemistry,* 22 (3): 619-620.

The Malaysian Journal of ANALYTICAL SCIENCES ISSN 1394-2506

DETERMINATION OF HOT SPRINGS PHYSICO-CHEMICAL WATER QUALITY POTENTIALLY USE FOR BALNEOTHERAPY

(Penentuan Kualiti Fizik-Kimia Air Kolam Air Panas Yang Berpotensi Digunakan Untuk Balneoterapi)

Zaini Hamzah[1]*, Nurul Latiffah Abd Rani[1], Ahmad Saat[2] and Ab Khalik Wood[1]

[1]Faculty of Applied Sciences,
[2]Institute of Science (IOS),
Universiti Teknologi MARA, 40450 Shah Alam, Selangor, Malaysia

**Corresponding author: zaini648@salam.uitm.edu.my*

Abstract

Hot springs areas are attractive places for locals and foreigners either for excursion or for medical purposes such as for healing of various types of diseases. This is because the hot spring water is believed rich in salt, sulfur, and sulfate in the water body. For many thousands of years, people have used hot springs water both for cozy bathing and therapy. Balneotherapy is the term used where the patients were immersed in hot mineral water baths emerged as an important treatment in Europe around 1800's. In view of this fact, a study of hot springs water was performed with the objective to determine the concentration of Na^+, K^+, Ca^{2+}, S, SO_4^{2-} and Cl^- in hot springs water around the State of Selangor, Malaysia. Energy dispersive X-ray Fluorescent Spectrometry (EDXRF) was used to measure the concentrations of Na^+, K^+, Ca^{2+} and S meanwhile for SO_4^{2-} and Cl^- anion, Ion Chromatography (IC) was used. The concentration of Na^+ obtained for filtered and unfiltered samples ranged from 33.68 to 80.95 and 37.03 to 81.91 ppm respectively. Meanwhile, the corresponding concentrations of K^+ ranged from 1.47 to 45.72 and 1.70 to 56.81 ppm. Concentrations of Ca^{2+} ranged from 2.44 to 18.45 and 3.75 to 19.77 ppm. The concentration of S obtained for filtered and unfiltered samples ranged from 1.87 to 12.41 and 6.25 to 12.86 ppm. The concentrations for SO_4^{2-} and Cl^- obtained ranged from 0.15 to 1.51 ppm and 7.06 to 20.66 ppm for filtered samples. The data signified higher concentration of salt and other important nutrients in hot spring water.

Keywords: hot springs water, balneotherapy, elemental, anions

Abstrak

Kawasan air panas merupakan tempat tarikan penduduk tempatan dan antarabangsa sama ada untuk pelancongan ataupun mengubati pelbagai jenis penyakit disebabkan oleh kandungan garam, sulfur, dan sulfat di dalam air panas tersebut. Semenjak beribu-ribu tahun, manusia telah menggunakan air panas ini bagi tujuan mandi dan rawatan. Balneoterapi adalah istilah yang digunakan untuk menggambarkan pesakit berendam di dalam kolam air mineral panas dan telah menjadi sebagai satu rawatan penting disekitar tahun 1800 di Eropah. Objektif kajian ini adalah untuk menentukan kepekatan Na^+, K^+, Ca^{2+}, S, SO_4^{2-} dan Cl^- di dalam air panas di Negeri Selangor, Malaysia. Analisis Serakan Tenaga Pendaflur Sinar-X (EDXRF) telah digunakan untuk mengukur kepekatan Na^+, K^+, Ca^{2+} dan S sementara untuk anion SO_4^{2-} dan Cl^-, kaedah ion kromatografi telah digunakan. Kepekatan Na^+ yang diperolehi untuk sampel dituras dan tidak dituras dalam julat 33.68 hingga 80.95 dan 37.03 hingga 81.91 ppm masing-masing. Sementara itu, kepekatan K^+ dalam julat 1.47 hingga 45.72 dan 1.70 hingga 56.81 ppm Kepekatan Ca^{2+} dalam julat 2.44 hingga 18.45 dan 3.75 hingga 19.77 ppm. Kepekatan S yang telah diperolehi untuk sampel dituras dan tidak dituras dalam julat 1.87 hingga 12.41 dan 6.25 hingga 12.86 ppm. Sementara itu, kepekatan untuk SO_4^{2-} dan Cl^- yang diperolehi adalah 0.15 hingga 1.51 ppm dan 7.06 hingga 20.66 ppm bagi sampel yang telah dituras. Data menunjukkan kepekatan garam dan nutrien lain yang tinggi di dalam air panas.

Kata kunci: air panas, balneoterapi, elemental, anion

Introduction

Term of balneotherapy comes from the Latin's word: balneum (bath) which is used for bathing in thermal or mineral waters [1]. Balneotherapy is the practice of using natural mineral hot spring water for the treatment and cure of disease. This therapy has been practiced all over the world from early history [2, 3]. People have used geothermal water and mineral water for cozy bathing, medical purposes and cooking, as being implemented previously in New Zealand, North America and other areas [4]. Presence various of elements and ions, especially sulphur (S) and sulphate ion (SO_4^{2-}) make hot springs water suitable for medical purposes especially for skin therapy. Sulphur is a chemical element and may be present in sulfurated waters as free or combined ion. It may comprise of various combinations of sulphur ions, water and other ions [5]. Initially sulphur and sulphate ion are produced from hydrogen sulphide (H_2SO_4) in underground hot springs water. Meanwhile, sulphide (S^{2-}) will be oxidized when the water rise to the surface [6]. The sulphate ion (SO_4^{2-}) may be originated from the weathering of pyrite or the leaching of other sulphide (S^{2-}) by hypothermal waters of deep origin [7]. The sulphide (S^{2-}) in the form of pyrites (FeS_2) that consist in the hot springs water can react chemically with water to produce H_2S and heat. The H_2S rises with the heated groundwater and gives it the strong odours like a rotten egg [8].

Besides S and SO_4^{2-}, other nutrients and minerals in hot springs water are also important for therapeutic properties. Generally, thermal waters vary greatly in chemical composition depending on geography and geology of the sites. Mineral waters are characterized by physico-chemical dynamism which is based on the study done by Javed *et. al*. (2009) [4], the hot spring water loses most of its ethereal properties when removed from the source. On top of that, the mineral composition of the thermal waters also reflects the geological formations found at the site and the depth of its origin [9]. This paper is focusing on the analysis and data interpretation of Na^+, K^+, Ca^{2+}, S, SO_4^{2-} and Cl^- that present in the hot springs water located around the State of Selangor, Malaysia.

Materials and Methods

Samples of hot springs water were collected from various hot springs in the State of Selangor, Malaysia. The positions of hot springs water were determined using Global Positioning System (GPS) and the coordinates are listed in Table 1. As depicted in Figure 1, the study area lies in the western part of the Peninsular Malaysia. Almost all the hot springs water in the Selangor State are located along the Main Range Granite Batholith but some of the hot springs water located within the area of the granite body and close to sedimentary rock The hot springs water within the granite body give the high concentration of Na^+ as acidic rocks such as sandstone and granitic rocks contain little amount of Ca^{2+} and large amount of Na^+ [10].

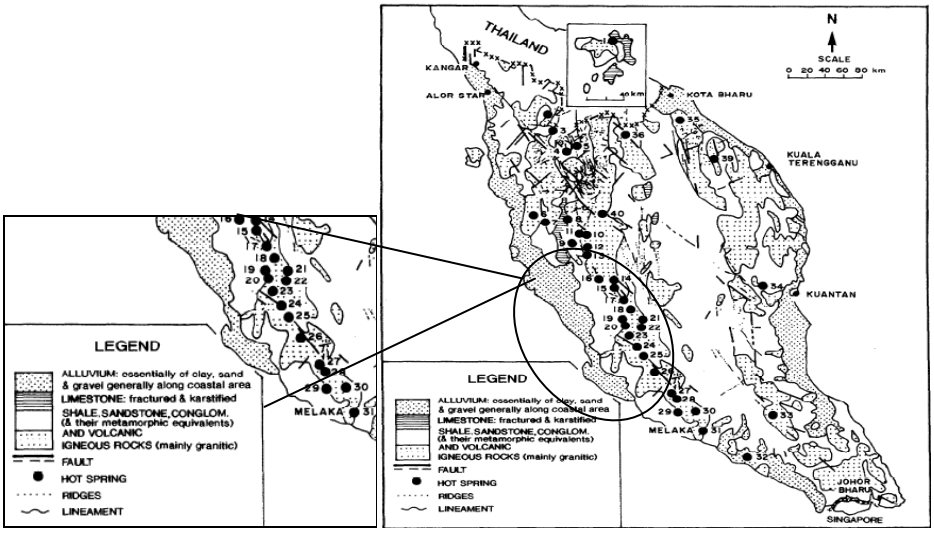


Figure 1. Geological map of the Selangor state, Malaysia hot springs water areas
Source: Abdul Rahim Samsudin *et al*., (1997) [11]

Common parameters such as dissolved oxygen (DO), conductivity, pH, total dissolved solid (TDS) and salinity were measured using calibrated YSI Portable Multi Probes Meter to determine the quality of the hot springs water. The temperature and turbidity of hot springs water were measured using high temperature thermometer and turbidity meter. Water samples for further laboratory analyses were collected from the sampling site in 20 L pre acid-cleaned polyethylene containers.

Table 1. The latitude, longitude and altitude of study areas

Locations	Latitude (N)	Longitude (E)	Altitude (m)
Kerling	03°36.603’	101°36.539’	69
Kuala Kubu Baru	03°33.910’	101°38.753’	68
Hulu Tamu	03°27.838’	101°41.814’	75
Hulu Yam	03°25.549’	101°40.991’	99
Selayang	03°15.542’	101°38.766’	82
Batu 9,Gombak	03°15.246’	101°43.430’	73
Setapak	03°11.384’	101°42.816’	81
IKBN, Hulu Langat	03°08.215’	101°50.072’	59
Sg Serai, Hulu Langat	03°05.445’	101°47.677’	75
Batu 16, Hulu Langat	03°08.343’	101°50.172’	60
Semenyih	03°02.532’	101°52.348’	67

Water samples were then acidified to pH less than 2 using 6 M nitric acid. This was done to prevent any loss of ions fractions by adsorptions onto the wall of containers [12]. Then the water samples were divided into two portions which is filtered and unfiltered. The filtration was done through the 0.45 µm cellulose nitrate membrane filter to separate suspended matter from dissolved portions of the water as suspended solids which has size greater than 0.45 µm retained on filter paper. Elements of Na^+, K^+, Ca^{2+} and S were determined using Energy Dispersive X-ray Fluorescence Spectrometer (EDXRF) (model PW4030) meanwhile SO_4^{2-} and Cl^- were determined using Ion Chromatography (IC) (model ICS-2000).

For elements determined by using EDXRF, 5 mL of filtered and unfiltered samples were pipette into special cups (sample holders) which has a 1.5 µm thin mylar film underneath. The X-ray beam is filtered through an Al-thin filter for determination of K and Ca, kapton filter for S and default for Na. Each sample was analyzed at every 100 s and the spectrums of elements were analyzed by using MiniPal/MiniMate software to determine the elemental concentration.

For anions determined by using IC, 1 mL of sample was injected into the IC column. Eluent used was KOH while SRS (Self-Regenerating Suppressor) was used as suppressor. The function of suppressor is to reduce the conductivity of the eluent and increase the conductivity of the analytes. They are delivered to the conductivity cell in a form that increases response [13].

Results and Discussion

Table 2 shows the value of hot spring water quality parameters in Selangor. Based on the measured parameters as depicted in Table 2, it can be inferred that most of the data comply with the requirement needed for bathing and other body contact activities (Class II B). Nevertheless, some of the water quality parameters values do not conform to water quality guidelines needed as potable water (class I). Salinity for all locations is not fulfilling the requirement needed for class I as the value obtained is above 0.05 mg/L. Similarly, Selayang C and IKBN, Hulu Langat shows the pH and turbidity values that do not fulfil the requirement for with value above 8.5 and 5 NTU respectively.

Apart from immersion in hot springs water, the beneficiary of drinking hot springs water also has been investigated by Dupuy *et al*., (1999)[14] for treatment of dermatologic conditions. Dupuy and his co-workers found out that drinking of low-salt Avene (France) hot spring water (sodium, 4.9 mg/L; magnesium, 22.5 mg/L; calcium, 44.3 mg/L; bicarbonate, 234.8 mg/L) for a period of 18 days was reported to normalized the intestinal permeability in patients with atopic dermatitis. However for the Malaysian hot springs water, it is advice not to drink the water as the water is not meeting the potable water standard as specified in the National Water Quality Standard for Malaysia.

Table 2. Water quality parameters of hot spring

Locations	Temp (^{0}C)	DO (mg/L)	Conductivity (µS/cm)	pH	TDS (mg/L)	Salinity (mg/L)	Turbidity (NTU)	TSS (mg/L)
Hulu Tamu (A)	51.7	2.93	493	7.60	311	0.23	0.22	0.38
Hulu Tamu (B)	50.6	3.07	485	7.58	307	0.23	0.26	0.15
Gombak (A)	56.9	3.00	495	8.50	311	0.23	0.19	1.04
Gombak (B)	52.30	3.50	493	7.54	311	0.23	0.65	1.26
Batu 16, Hulu Langat	67.90	2.64	369	7.86	228	0.17	0.22	1.49
IKBN, Hulu Langat	36.10	2.99	595	7.34	373	0.28	6.75	8.50
Sg Serai, Hulu Langat	45.40	2.80	560	7.73	343	0.25	1.34	0.71
Semenyih	36.70	4.91	559	7.45	364	0.27	0.83	1.00
Kuala Kubu Baru	40.00	3.94	365	7.33	225	0.16	0.20	1.02
Kerling	40.00	3.47	497	7.14	312	0.23	0.24	0.75
Setapak (A)	45.90	5.27	567	7.36	376	0.28	0.23	1.07
Setapak (B)	55.20	1.97	586	7.27	374	0.28	0.19	1.27
Hulu Yam	55.80	4.50	508	7.45	321	0.24	0.18	0.43
Selayang (A)	53.50	2.63	508	7.68	313	0.23	0.26	1.44
Selayang (B)	49.40	3.58	506	7.98	319	0.23	0.78	0.24
Selayang (C)	54.10	2.92	509	8.98	317	0.23	0.14	0.06
Class I, NWQS	**-**	**7**	**1000**	**6.5 – 8.5**	**500**	**0.05**	**5**	**25**
Class II B, NWQS	**-**	**5 - 7**	**-**	**6 - 9**	**1000**	**-**	**50**	**50**

Water temperature has an important role for the metabolic effects of balneotherapy and had been classified as being "cold" (< 20^{o}C), "hypothermal" (20-30^{o}C), "thermal" (30-40^{o}C), or "hyperthermal" (>40^{o}C) [1, 5]. The temperature is ranging from 36.1^{o}C to 67.9^{o}C. Among others, Batu 16, Hulu Langat shows the highest temperature which is 67.9^{o}C and IKBN, Hulu Langat shows the lowest temperature of 36.1^{o}C. The variation in temperature is indicated the geology of a particular site and also the depth from surface of the hot spring water. In Japan, due to volcanic areas, the hot spring water temperature can be much higher. From the data obtained, most of the hot springs water located in Selangor, Malaysia can be categorised as hyperthermal except for IKBN, Semenyih, Kuala Kubu Baru and Kerling as these hot springs water temperature is ranging from 30-40^{o}C. The highest and the lowest temperature are possibly reflecting the depths of waters penetration along faults system in a crust that had been affected by an anomalous geothermal gradient [15]. According to Lambert [16], the water temperature increases from near the surface to the depth of 1000 m from 15ºC to 35ºC. This shows that the deeper the water flow the higher the temperature of the spring's water produced.

Temperature plays an important role for balneotherapy. Study done by Ohtsuka *et al*., (1995) [17], 37.6% of body enzyme activity (erythrocyte aldose reductase) increased after immersion in hot water at 42^{o}C for 10 minutes.

Meanwhile, the body enzyme activity decrease by 52.2% and 47.0% after immersion in hot water for 10 minutes at 39^{o}C and 25^{o}C. However, increasing value of this enzyme activity gave negative effect to the diabetic patients and might aggravate diabetic complications. Besides that, according to Pospisil *et al.*, (2007) [18], heart rate and diastolic blood pressure in patients with Parkinson's disease had been statistically significant decrease after water immersion (32.5^{o}C) up to level of the heart. Literature reported studies show that variations in temperature of hot springs water gave different effect to the human beings and generally depending on the conditions of the individual.

The pH values were from 7.14 – 8.98. This high alkalinity water is primarily assessed by judging through the concentrations of Ca^{2+}, Na^{+} and K^{+} (Table 4). The granitic body in the study areas contributed to the high concentrations of Na^{+} as acidic rocks such as sandstone and granitic rocks contain little amount of Ca^{2+} and large amount of Na^{+} [10].

Pearson correlation had been performed between water quality parameters of hot springs water. There is a good correlation between specific conductivity and total dissolved solid (TDS) with $R^2 = 0.9792$, and salinity with $R^2 = 0.9652$. The correlation between TDS and salinity is $R^2 = 0.9926$. These three parameters were correlated to each other's as there are strong correlations obtained between these three parameters. TDS is solids in water that can pass through a filter (usually with a pore size of 0.45 µm). TDS is a measure of the amount of material dissolved in water. Usually solids can be found in nature in a dissolved form then break into positively and negatively charged ions. The ions include major positively and negatively charged ions such as sodium, (Na^{+}) calcium (Ca^{2+}), potassium (K^{+}) and magnesium (Mg^{2+}) for positively charge ions and chloride (Cl^{-}), sulfate (SO_4^{2-}), carbonate (CO_3^{2-}), and bicarbonate (HCO_3^{-}) for negatively charge ions. The presence of this dissolved salts directly increase the value of salinity and conductivity as salinity is a measure of the amount of salts in the water and conductivity is the ability of water to conduct an electrical current with dissolved ions as the conductors [19].

Table 3. Pearson correlation between water quality parameters of hot springs

	Temp.	**DO**	**Cond.**	**pH**	**TDS**	**Sal.**	**Tur.**	**TSS**
Temp.	1							
DO	0.1865	1						
Cond.	0.1404	0.0038	1					
pH	0.2101	0.0723	0.0183	1				
TDS	0.1455	0.0262	**0.9792**	0.0297	1			
Sal.	0.1247	0.0238	**0.9652**	0.0411	**0.9926**	1		
Tur.	0.2331	0.0096	0.1785	0.0378	0.1402	0.1489	1	
TSS	0.1414	0.0180	0.1069	0.0662	0.0855	0.1013	**0.9022**	1

Turbidity and total suspended solid (TSS) also shows strong correlation ($R^2 = 0.9022$). Turbidity is the measure of the light scattering properties of water and depends on the amount, size and composition of the suspended matter such as clay, silt, colloidal particles, plankton and other microscopic organisms. It is measured in nephelometric turbidity units (NTU) and suspended solids refer to the mass of the suspended matter and are measured as mg/L [20]. According to Mohd Noor Salleh *et al.*, (2011) [21], there are usually a correlation between these two parameters. Other parameters show weak correlation with value of $R^2 < 0.5000$.

Table 4 showed concentration of Ca^{2+}, Na^{+}, K^{+}, S, SO_4^{2-} and Cl^{-} obtained from the analysis. Ca^{2+}, Na^{+}, K^{+}, S were analysed using EDXRF, meanwhile SO_4^{2-} and Cl^{-} were analysed using IC. Results indicate the values of unfiltered samples for each element consistently higher than filtered for EDXRF analysis. This might be due to the ions that attached to the charged site of the suspended solids have been filtered away. From the results, it also shows that the value obtained for concentration of Na^{+} is higher than the concentration of Ca^{2+} in the water samples. This prove that major element composition of the hot water is dominated by Na^{+} meanwhile Ca^{2+} is a minor component [22].

Value obtained for S (filtered and unfiltered) is higher compared with SO_4^{2-} (See Table 4). Their low SO_4^{2-} content suggests that these compounds are converted into S by bacterial reduction of magmatic SO_2 or sulfate [23]. Nevertheless, hot springs water contains SO_4^{2-}, initially in the form of H_2S. As the water rises to the surface, the S^{2-} may be oxidized, especially if the path to the surface is the rise of water is slow through rock fractures rather than faults and S, SO_2, or SO_4^{2-} may be produced [6]. It is important to note that sulfur-rich hot spring water has special interest for dermatological effects [1]. Sulfur also interacts with oxygen radicals in the deeper layers of the epidermis, producing sulfur and disulfur hydrogen, which may be transformed into pentathionic acid and this, may be the source of the anti bactericidal and antifungal activity of sulfur water [5]. This was supported by studied that had done by Inoue *et al*., [24] that *Staphylococcus aureus* on the skin surface decreased in number or disappeared after balneotherapy, the hot-spring water was suspected to act against the microorganism. The concentration range obtained for Cl^- is between 7.06 to 20.66 ppm. Hydrogen sulfide gases dissolved in hot springs water that originates in the magma as well as hydrogen chloride. Thus, chloride ion in geothermal waters can be at high concentrations [6].

The results (see Table 5) showed that most of the Ca^{2+}, Na^+, K^+, S, SO_4^{2-} and Cl^- concentrations for each hot spring water locations in Selangor, Malaysia are comparable with other studies that previously used hot springs water for balneotherapy. Difference concentrations of elements obtained as the locations of the hot springs water in Selangor, Malaysia located at different geological position which on granite body, thus the concentrations of Ca^{2+} obtained is lower compared to others elements.

Table 4. Concentration of Ca^{2+}, Na^+, K^+, S, SO_4^{2-} and Cl^- analyse using EDXRF and IC

Samples	Ca^{2+} (mg/L)	Ca^{2+} (mg/L)	Na^+ (mg/L)	Na^+ (mg/L)	K^+ (mg/L)	K^+ (mg/L)	S (mg/L)	S (mg/L)	SO_4^{2-} (mg/L)	Cl^- (mg/L)
	F	Un-F	F	Un-F	F	Un-F	F	Un-F	F	F
Hulu Tamu (A)	2.44 ± 0.01	5.18 ± 0.02	39.51 ± 0.87	42.40 ± 0.68	1.55 ± 0.04	1.70 ± 0.07	1.87 ± 1.27	6.25 ± 7.02	0.55 ± 0.64	14.19 ± 0.31
Hulu Tamu (B)	2.48 ± 0.02	3.75 ± 0.09	47.68 ± 0.79	52.66 ± 0.40	1.47 ± 0.02	7.82 ± 0.06	11.92 ± 1.35	11.94 ± 1.08	0.79 ± 0.02	20.66 ± 0.43
Gombak (A)	9.53 ± 0.14	10.38 ± 0.19	51.95 ± 0.37	53.86 ± 0.40	18.17 ± 0.05	20.04 ± 0.71	6.78 ± 3.68	8.81 ± 1.44	1.46 ± 0.43	7.06 ± 1.22
Gombak (B)	10.44 ± 0.05	11.31 ± 0.04	37.96 ±0.199	41.15 ± 0.49	3.46 ± 0.07	6.37 ± 0.07	10.96 ± 0.07	11.58 ± 0.17	0.51 ± 0.11	14.66 ± 1.84
Batu 16, Hulu Langat	2.90 ± 0.06	4.73 ± 0.01	55.08 ± 0.38	81.73 ± 0.91	2.75 ± 0.06	2.60 ± 0.05	8.59 ± 0.94	10.11 ± 0.28	0.56 ± 0.37	16.66 ± 1.28
IKBN, Hulu Langat	4.13 ± 0.02	5.61 ± 0.08	61.11 ± 0.62	69.49 ± 0.71	19.35 ± 0.04	24.98 ± 0.93	11.60 ± 1.28	11.02 ± 0.57	0.40 ± 0.01	16.79 ± 0.45
Sg Serai, Hulu Langat	12.60 ± 0.14	15.92 ± 0.13	80.95 ± 0.02	81.91 ± 0.35	13.22 ± 0.02	19.01 ± 0.75	11.53 ± 0.27	11.89 ± 0.80	1.51 ± 0.48	14.05 ± 0.22

Semenyih	14.13 ± 0.13	17.77 ± 0.16	59.69 ± 0.85	60.23 ± 0.68	45.72 ± 0.04	56.81 ± 0.72	7.64 ± 5.66	9.04 ± 4.40	0.76 ± 0.25	9.78 ± 0.19
KKB	9.31 ± 0.02	10.97 ± 0.05	45.23 ± 0.81	46.08 ± 0.97	23.84 ± 0.02	25.27 ± 0.66	10.01 ± 0.56	11.23 ± 0.64	0.23 ± 0.09	12.60 ± 0.19
Kerling	14.82 ± 0.13	16.55 ± 0.15	60.00 ± 0.03	64.94 ± 0.26	20.81 ± 0.09	29.78 ± 0.68	11.58 ± 0.77	11.65 ± 1.30	0.32 ± 0.02	12.13 ± 0.10
Setapak (A)	7.08 ± 0.11	7.83 ± 0.10	66.41 ± 1.27	67.71 ± 0.28	2.85 ± 0.037	8.21 ± 0.07	5.33 ± 1.35	9.33 ± 0.55	0.48 ± 0.09	15.48 ± 0.25
Setapak (B)	7.04 ± 0.03	7.81 ± 0.05	70.33 ± 0.88	71.03 ± 0.53	3.28 ± 0.06	5.97 ± 0.06	10.53 ± 1.30	11.22 ± 0.49	0.16 ± 0.01	20.12 ± 0.39
Ulu Yam	5.67 ± 0.05	6.48 ± 0.07	43.93 ± 0.56	52.22 ± 0.80	2.04 ± 0.02	2.20 ± 0.01	10.39 ± 0.05	11.32 ± 1.14	0.19 ± 0.01	11.78 ± 0.30
Selayang A	17.80 ± 0.06	19.17 ± 0.07	44.30 ± 0.13	48.66 ± 0.67	14.05 ± 0.03	15.16 ± 0.02	11.17 ± 0.01	11.69 ± 0.08	0.15 ± 0.003	11.96 ± 0.34
Selayang B	17.93 ± 0.15	19.77 ± 0.05	40.85 ± 0.02	45.24 ± 0.56	14.53 ± 0.01	15.54 ± 0.01	12.41 ± 0.25	12.86 ± 0.28	0.16 ± 0.02	11.43 ± 0.33
Selayang C	18.45 ± 0.14	18.55 ± 0.12	33.68 ± 1.10	37.03 ± 0.09	2.74 ± 0.02	3.69 ± 0.07	12.38 ± 0.75	12.51 ± 0.37	0.36 ± 0.05	10.09 ± 0.18

[*] F- Filtered, Un-F - Unfiltered

Table 5. Comparison concentration of Ca^{2+}, Na^{+}, K^{+}, S, SO_4^{2-} and Cl^{-} with other studies

Locations	Ca^{2+} (mg/L) Unfiltered	Na^{+} (mg/L) Unfiltered	K^{+} (mg/L) Unfiltered	S (mg/L) Unfiltered	SO_4^{2-} (mg/L) Filtered	Cl^{-} (mg/L) Filtered	References
Kusatsu Hot Spring Water, Japan	72.00	53.70	16.00	-	611.00	343.00	Inoue *et al.*, (1999)[24]
Sulfur baths, Austria	-	-	-	7.30	-	-	Leibetseder *et al.*, (2004) [25]
Atatürk Balneotherapy & Rehabilitation Center, Turkey	91.90	222.50	23.00	-	277.00	2.20	Yurtkuran *et al.*, (2005) [26]
Northern Part of Limpopo Prov., South Africa	1.31-13.73	10.59-156.31	0.99-4.25	-	2.98-53.17	19.47-168.97	Olivier *et al.*, (2011) [27]

Saratoga Spa State Park, USA	32.20 - 872	2.00 –3820	0.15 – 340	-	22.00	4.80 – 6030	Lund., (1996)[3]
Present study Hot springs water in Selangor, Malaysia	**3.75 – 19.77**	**37.03 – 81.91**	**1.70-56.81**	**6.25 – 12.86**	**0.15 – 1.51**	**7.06 – 20.66**	

Conclusion

Hot Springs water all over State of Selangor, Malaysia contains Na^+, K^+, Ca^{2+}, S, SO_4^{2-} and Cl^- which are good for balneotherapy. Chemical composition consist in hot springs water has its own beneficial for the human's health where it generally can increase metabolism, accelerate healing, soothe muscles, improve blood circulation and detoxify the body's lymphatic system [4]. The data shows that hot springs water located in Selangor, Malaysia are suitable for bathing and body contact activities but unsuitable as potable water. The composition and physical properties of various hot springs waters are vary in term of salt, sulphate and chloride content. Generally, the concentrations of chemical compositions of the hot springs water are comparable with literature reported studies and this indicated that the hot springs water in Selangor are potentially qualified for balneotherapy.

Acknowledgement

The authors would like to thank Universiti Teknologi MARA Malaysia particularly the UiTM's Research Management Institute for providing grant, Research Excellence Fund 600-RMI/DANA 5/3/RIF (1/2012) and support to carry out this study.

References

1. Nasermoaddeli, A., and Kagamimori, S., (2005). Balneotherapy in Medicine: A Review. *Environmental Health and Preventive Medicine* 10: 171–179.
2. Kristmannsdóttir, H., and Björnsson, G. O., (2003). Balneological prospects in Iceland using geothermal resources. *International Geothermal Conference, Reykjavík,* 3: 19-26.
3. Lund, J. W., (1996). Balneological use of thermal and mineral waters in the U.S.A. *Geothermics* 25(1): 103-147.
4. Javed, A., Iqbal, J., Asghar, U., Khan, F. A., Munshi, A. B., and Sddiqui, I., (2009). A study to evaluate therapeutic properties of minerals of Manghopir Hot Spring, Karachi. *J.Chem.Soc.Pak* 31(3): 396-401.
5. Matz, H., Orion, E., and Wolf, R., (2003). Balneotheraphy in dermatology. *Dermatologic Theraphy.* 16: 132-140.
6. Hodder, A. P. W., (1999).Geothermal Waters: A Source Of Energy and Metals. *Unit Department of Earth Sciences, University of Waikato .XIII-Water-A-Geothermal;* 1-10.
7. Drogue, C., Cat, N. N., and Dazy, J., (2000). Geological factors affecting the chemical characteristics of the thermal waters of the carbonate karstified aquifers of Northern Vietnam. Hydrology and Earth System Sciences 4(2): 332-340.
8. Thompson, G. R., and Turk, J., (2005). *Earth science and the environment*. Third edition. Brooks/Cole, Thomson Learning, USA.
9. Olivier, J., Niekerk, HJ., and Walt, I., (2008). Physical and chemical characteristics of thermal springs in the Waterberg area in Limpopo Province, South Africa. *Water South Africa* 34(2): 163-174.
10. Homma, A., and Tsukahara, H., (2008). Chemical characteristics of hot springs water and geological environment in the northernmost area of the Itoigawa Shizuoka tectonic line. *Bull. Earthq. Res. Inst. Univ. Tokyo.* 83: 217-225.
11. Abdul Rahim Samsudin., Umar Hamzah., Rakmi Ab. Rahman., Chamhuri Siwar., Mohd Fauzi Mohd. Jani., and Redzuan Othman., (1997). Thermal springs of Malaysia and their potential development. *Journal of Asian Earth Sciences.* 15: 275-284.

12. Kovacs, T., Mate, B., Somlai, J., Kavasi, N., and Jobbagy, V., (2010). Radiochemistry characterization of springs water in Balaton Upland, Hungry, estimation of radiation dose to members of public. *Microchemical Journal* 94(2): 159-165.
13. Dionex., (2010). *Eluent suppressors for ion chromatography*.
14. Dupuy, P., Casse, M., Andre, F., Dhivert-Donnadieu, H., Pinton, J., and Hernandez-Pion, C., (1999). Low-Salt Water Reduces Intestinal Permeability in Atopic Patients. *Dermatology 1999;*198:153–155.
15. Cinti, D., Pizzino, L., Voltattorni, N., Quattrocchi, F., and Walia, V., (2009). Geochemistry of thermal waters along fault segments in the Beas and Parvati valleys (north-west Himalaya, Himachal Pradesh) and in the Sohna town (Haryana), India. *Geochemical Journal*. 43,65-76.
16. David Lambert Group (2007). *The field guide to geology*. Library of Congress Cataloging. pg 29.
17. Ohtsuka, Y., Yabunaka, N., Watanabe, I., Noro, H., Fujisawa, H., and Agishi, Y., (1995). Thermal strees and diabetic complications. *International Journal of Biometeorology*.38(2): 57-59.
18. Pospisil, P., Konecny, L., Zmeskalova, M., Srovnalova, H., Rektorova, I., Nosavcorova, E., Sosikova, M., Dobsak, P., and Siegelova, J., (2007). Balneotherapy in Patients with Parkinson's disease. *SCRIPTA MEDICA (BRNO)* – 80 (5): 233–23.
19. State Water Resources Control Board, Division of Water Quality (2002). Electrical Conductivity/Salinity. *The Clean Water Team Guidance Compendium for Watershed Monitoring and Assessment; 1-5*.
20. National Land and Water Resources Audit., (2008). Turbidity/Suspended Particulate Matter in Aquatic Environments. *Australian Government* 1-9
21. Mohd. Noor Salleh and Zaki Zainudin (2011). Potable Water Quality Characteristics. *JURUTERA; 21-27.*
22. Bucher, K., Zhang, L., and Stober, I., (2009). A hot spring in granite of the Western Tianshan, China. *Applied Geochemistry* 24: 402–410
23. Gebresilassie, S., Tsegab, H., Kabeto, K., Gebreyohannes, T., Sewale, A., Amare, K., Zerabruk, S., Mebrahtu, G., Gebrehiwot, K., and Haile, M., (2011). Preliminary study on geology, mineral potential and characteristics of hot springs from Dallol area, Afar rift, northeastern Ethiopia: implications for natural resource exploration.. *Mekelle University.* 2: 17-3.
24. Inoue, T., Inoue, S., and Kubota, K., (1999). Bactericidal Activity of Manganese and Iodide Ions against Staphylococcus aureus: A Possible Treatment for Acute Atopic Dermatitis. *Acta Derm Venereol*, 79: 360-362.
25. Leibetseder, V., Strauss-Blasche, G., Holzer, F., Wolfgang Marktl, W., and Ekmekcioglu, C., (2004). Improving homocysteine levels through balneotherapy: effects of sulphur baths. *Clinica Chimica Acta* 343: 105– 111
26. Yurtkuran, M., AlevAy and Karakoç, Y., (2005).Improvement of the clinical outcome in Ankylosing Spondylitis by balneotherapy. *Joint Bone Spine* 72:303–308
27. Olivier, J., Venter, J. S., and Jonker, C. Z.,(2011). Thermal and chemical characteristics of hot water springs in the northern part of Limpopo Province, South Africa. *Water South Africa* 37:427-436

The Malaysian Journal of ANALYTICAL SCIENCES ISSN 1394-2506

MORPHOLOGICAL CHARACTERIZATION OF PHOTOSYNTHETIC MICROBIAL GRANULE FROM PALM OIL MILL EFFLUENT (POME)

(Pencirian Morfologi Granul Mikrob Fotosintetik Daripada Efluen Kilang Minyak Sawit (POME))

M.Z. Mohamed Najib[1], Z. Ujang[2], Salmiati[2]*

[1]*Department of Environmental Engineering, Faculty of Civil Engineering,*
[2]*Institute of Environmental and Water Resource Management (IPASA),*
Universiti Teknologi Malaysia (UTM), 81310 Skudai Johor, Malaysia

**Corresponding author: salmiati@utm.my*

Abstract

Presently, global warming is the most highlighted subjects in the environmental issues which relates closely to greenhouse gases (GHG) emissions. In 2007, the Intergovernmental Panel on Climate Change (IPCC) assigns only methane (CH_4) emissions to wastewater treatment rather than GHG emissions specifically carbon dioxide (CO_2) gas from the aerobic treatment processes. Focusing on the palm oil industry in Malaysia, the most commonly used treatment of palm oil mill effluent (POME) which is the conventional ponding system, has caused excessive generation of GHG such as CH_4 and CO_2 gases. To develop a novel, innovative and environmental-friendly mitigation method, this study explores into the possibility of growing the photosynthetic bacteria in the form of granules via the aerobic granulation process with potential applications in reducing CO_2 gases. The cultivation of photosynthetic microbial granules was investigated using POME as the substrate in a sequencing batch reactor (SBR) system via the sequencing cycle of feeding, reacting, settling and decanting. Evidence of the formation of granule was based on microscopic examination of the morphological changes during the development of the granule in the SBR system over a period of 90 days. It shows changes from dispersed loose structure of the sludge merging into small flocs of irregular shapes and finally into dense and compact granular form. The granule was formed by applying an organic loading rate (OLR) at 2.75 kg COD/m^3.day, hydraulic retention time (HRT) at 4 h and superficial air velocity of 2.07 cm/s. The biomass concentration began to decreased first (initial sludge biomass = 16750 mg/L) and then increased steadily to a constant value of 32000 mg/L after 90 days. Besides, the results also demonstrated a good accumulation of biomass as the settleability between raw sludge and granule increased from 0.03 cm/s to 0.94 cm/s. The maximum settling velocity obtained in the reactor was approximately 2.0 cm/s.

Keywords: GHG, CO_2 gas, POME, granulation, photosynthetic bacteria, morphological change

Abstrak

Pada masa ini, pemanasan global adalah subjek yang paling menyerlah dalam isu alam sekitar yang berkait rapat dengan gas rumah hijau (GHG). Pada tahun 2007, *Intergovernmental Panel on Climate Change* (IPCC) menumpukan hanya pelepasan metana (CH_4) untuk rawatan air sisa berbanding pelepasan GHG daripada proses aerobik khususnya gas karbon dioksida (CO_2). Memberi tumpuan kepada industri minyak sawit di Malaysia, rawatan yang paling lazim digunakan untuk rawatan POME iaitu sistem kolam konvensional, telah menghasilkan GHG secara berlebihan seperti gas CH_4 dan CO_2. Untuk membangunkan kaedah mitigasi baru yang lebih inovatif dan mesra alam, kajian ini melihat kepada kemungkinan menghidupkan bakteria fotosintetik dengan menggunakan penggranulan aerobik yang berpotensi untuk mengurangkan gas CO_2. Pembentukan granul mikrob fotosintetik telah disiasat menggunakan POME dalam sistem reaktor kelompok urutan (SBR). Dengan memerhatikan perubahan morfologi granul dalam reaktor, ia memaparkan berlakunya proses penggranulan yang integrasi - penggabungan semula - membesar. Ia menunjukkan perubahan daripada struktur longgar tersebar bergabung kepada floks kecil yang berbentuk tidak teratur dan akhirnya membentuk granul yang lebih mampat dan padat. Granul yang telah terbentuk itu dengan mengenakan kadar muatan organik (OLR) pada 2.75 kg COD/m^3.day, masa tahanan hidraulik (HRT) pada 4 jam dan halaju udara cetek pada 2.07 cm/s. Kepekatan biomas pada mulanya menurun (biomas awal enap cemar = 16750 mg/L) dan kemudian terus meningkat sehingga mencecah nilai 32000 mg/L selepas 90 hari. Selain itu, keputusan juga menunjukkan pengumpulan baik biomas sebagai kebolehan-mendakan antara enap cemar mentah dan granul meningkat daripada 0.03 cm/s hingga 0.94 cm/s. Halaju pemendakan maksimum yang diperoleh dalam reaktor telah mencapai sehingga kira-kira 2.0 cm/s.

Kata kunci: GHG, gas CO_2, POME, penggranulan, bakteria fotosintetik, perubahan morfologi

Introduction

Currently, global warming is the most highlighted subjects in the environmental issues. This climate change is normally related to greenhouse gases (GHG) emissions from anthropogenic activities like the combustion of fossil fuel used for power generation, transportation, and industrial processes [1]. Inefficient wastewater treatment results in excessive production of carbon dioxide (CO_2) and methane (CH_4) continuously which will over time period contribute to global warming. The current Intergovernmental Panel on Climate Change [2] assigns only CH_4 emissions to wastewater treatment, but this approach may overestimate GHG emissions from the highly aerobic processes specifically CO_2. Hence, enhancement of photosynthetic activities in the microenvironment of wastewater is potentially promising for atmospheric CO_2 mitigation in the wastewater.

In Malaysia, one of the major sources of GHG is the palm oil mill wastewater treatment system. Earlier studies have indicated that the end products of the anaerobic digestion of palm oil mill effluent (POME) waste treatment produced biogas with 65% CH_4 [3] A research project prepared by SIRIM [4] discovered that approximately 335.27 kg of CO_2 gases was generated directly from POME treatment of the crude palm oil (CPO). Unfortunately, the biogas is released into the atmosphere from the open ponds and digesters of the waste treatment system. It is estimated that 50 million tonnes of POME are produced annually in Malaysia. In terms of biochemical oxygen demand (BOD) and chemical oxygen demand (COD), these generally exceed 25,000 mg/L and 50,000 mg/L, respectively.

The emissions of CO_2 and CH_4 is presently captured and stored in various anaerobic processes [5, 6, 7, 8]. There is a lot of interest in reducing emissions in anaerobic wastewater treatments especially in the CO_2 biofixation by algae and microalgae. However, the aerobic processes should also be emphasized in research to minimize greenhouse emission from the wastewater. Thus, reduction of emission from aerobically treated wastewater is needed. This can be achieved by utilizing photosynthetic bacteria in a more compact wastewater treatment system.

Aerobic granulation technology is a promising aerobic wastewater treatment system that can overcome the limitations in conventional activated sludge system. This technology provides an excellent characteristic of sludge in granular form with compact structure, good settling rate, high biomass concentration, and simultaneous removal of organic matter, nitrogen and phosphorus [9]. Aerobic granules cultivated via the aerobic granulation process is a form of biofilm in which various microorganisms including photosynthetic bacteria adhere to each other (self-immobilisation) to form a compact structure, which is good for solid-liquid separation in wastewater.

The role of photosynthetic bacteria in the aerobic granules is important for the CO_2 sequestration within the microsystem of wastewater. This will minimize the emission of CO_2 to the environment. Microbial communities in aerobic granules have been shown to be highly distinct from activated sludge, even within a single reactor system. Recent studies imply the importance of gaining an understanding of the functions of microbial communities, as population diversity alone may not be adequate in determining the microbial characteristics. This study focuses on the characterizations of photosynthetic microbial granules developed from POME. The presence of photosynthetic bacteria were determined, the change in morphologies, biomass concentration and settling properties were investigated during growth of the bacteria.

Experimental

Seed Sludge

The reactor was seeded with a 1:2:1 ratio of mixed sludge taken from a local sewage treatment oxidation pond, POME facultative pond treatment system and POME wastewater. Initially, the sludge was sieved (< 3 mm) to remove any debris and large particles. It was then mixed together and acclimatized up to at least 40 days in the reactor by applying anaerobic and aerobic condition similar to SBR operating parameters. After the acclimatisation period, a sludge volume of 0.5 L was filled inside the reactor, making up 50% of the working volume.

Preparation of Growth Medium For Photosynthetic Bacteria

For cell growth of photosynthetic bacteria, the sludge sample was inoculated and grown in two different growth media [10]. The preparation of Succinate Medium and G5 Medium were based on the following compositions. (i)

Succinate Medium consists of the following chemical reagents: 0.33 g K_2HPO_4, 0.33g $MgSO_4.7H_2O$, 0.33 g NaCl, 0.5 g NH_4Cl, 0.05 g $CaCl_2.2H_2O$, 1.0 g sodium and 0.02 g yeast extract; (ii) G5 Medium: 5.0 g peptone, 5.0 g yeast extract, 4.0 g L-glutamic acid, 3.5 g malic acid, 0.12 g KH_2PO_4, and 0.18 g K_2HPO_4. Each medium was adjusted to pH 7.0. Both of the medium were autoclaved at 121^oC, 15 lb/in^2 steam pressure for 15 min. After the temperature has cooled down, the growth media were poured into sterilised petri dishes and allowed to solidify at room temperature. The agar plates were incubated at 30^oC overnight to ensure the plates were not contaminated prior to use.

Culture Conditions

The bacteria used in this study were isolated from the sludge sample. The sludge was inoculated and cultured in both Succinate and G5 medium in stoppered bottles in separate experiments. Then, the cultures were incubated at 28-32 ^oC and illuminated with 3600 lux light source using a 12 h light/ 12 h dark regime for about 1 week.

Pigment Analysis

To detect the presence of photosynthetic bacteria, the colour change of the medium was visually examined during growth of the bacteria. Furthermore, pigment analysis was performed using a UV-Vis spectrophotometer (wavelength ranging between 300-1100 nm) to identify the type of bacteriochlorophyl pigment present in the microorganism according to the wavelength absorption characteristics.

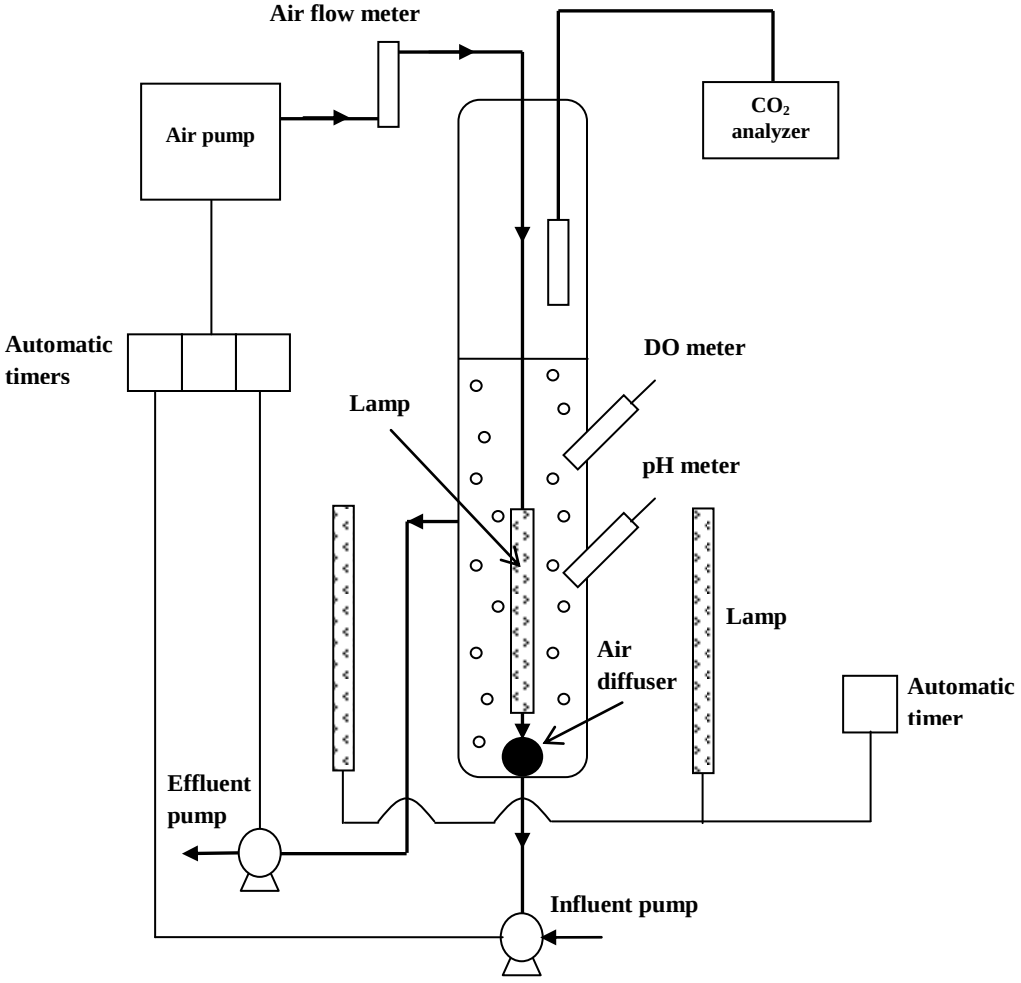


Figure 1. Schematic diagram of SBR system

Characterisation of Granules

During the development period, the morphologies of the photosynthetic microbial granules were examined visually and using the light microscope using PAX-IT™ image analyzing system. All analytical measurements were conducted according to Standard Methods for the Examination of Water and Wastewater [11].

Operation of the Sequencing Batch Reactor (SBR)

The experiment was operated using a 3L double-jacketed cylindrical column type-sequencing batch reactor (SBR) system (diameter = 6.4 cm) with working volume of 1.2 L at an organic loading rate (OLR) of 2.75 kg COD/m^3.day (Figure 1). The SBR was run in a cycle of 4 h per day and consisted of 5 min for filling up of influent, 80 min of anaerobic condition, 130 min for aeration, 15 min for settling of sludge, and 5 min for pumping out of the effluent. Aeration was supplied using an air diffuser by controlling the air flow rate at ± 4 L/min along with maintaining the temperature in the reactor between 20-27^{o}C. Besides, the reactor was equipped with two light sources providing illumination of 3600 lux each (12 h light/ 12 h dark regime) for creating photosynthetic condition. Table 1 summarizes the important operational details of the SBR system.

Table 1. Operating parameters of SBR system

SBR parameter	Unit	Value
HRT	hour	4
Cycle per day	-	6
Working volume	m^3	1200
pH	-	7
Inlet volume	m^3	600
Organic loading rate	kg COD/m^3.day	2.75
Superficial air velocity	cm/s	2.07
Light intensity	lux	3600
Each step of cycle:		
a) Fill	min	5
b) React:		
Anaerobic	min	80
Aerobic	min	130
c) Settle	min	15
d) Decant	min	5
e) Idle	min	5

Results and Discussion

Presence of Photosynthetic Bacteria

To determine the presence of photosynthetic pigment analysis for bacteriochlorophyll α, β and carotenoid pigments were carried out for the cell culture using the UV-Vis spectrophotometer within a range of 380-1100 nm. After 1 week of incubation, the succinate medium showed the appearance of red 'bloom' (Figure 2(a)) while no growth in the G5 medium (Figure 2(b)). This characteristic reddish bloom had implied the presence of photosynthetic bacteria that of purple non-sulfur photosynthetic bacteria and the presence of only bacterichlotophyll b [12]. This was because the average wavelength absorption gained mostly within the range of 976 to 1050 nm as shown in Figure 3.

Bacteria were further isolated and single cultures of bacteria were obtained using the spread plate and dilution streak technique.

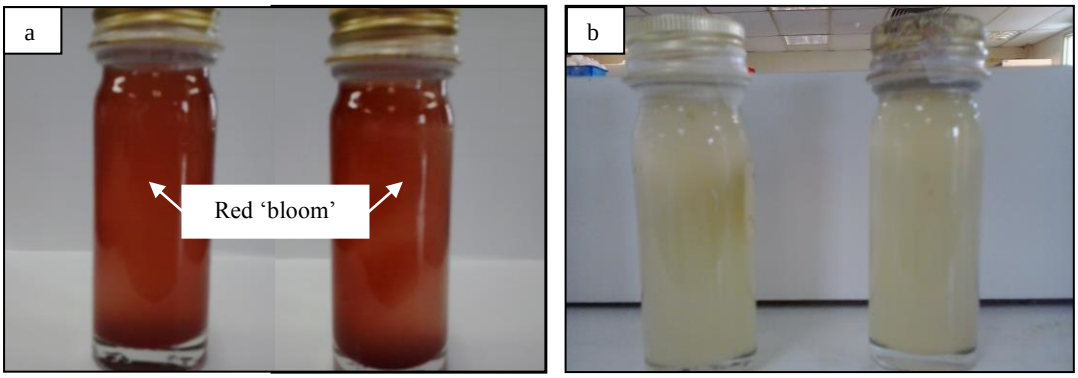


Figure 2. Final results on isolation of bacteria using (a) Succinate and (b) G5 medium.

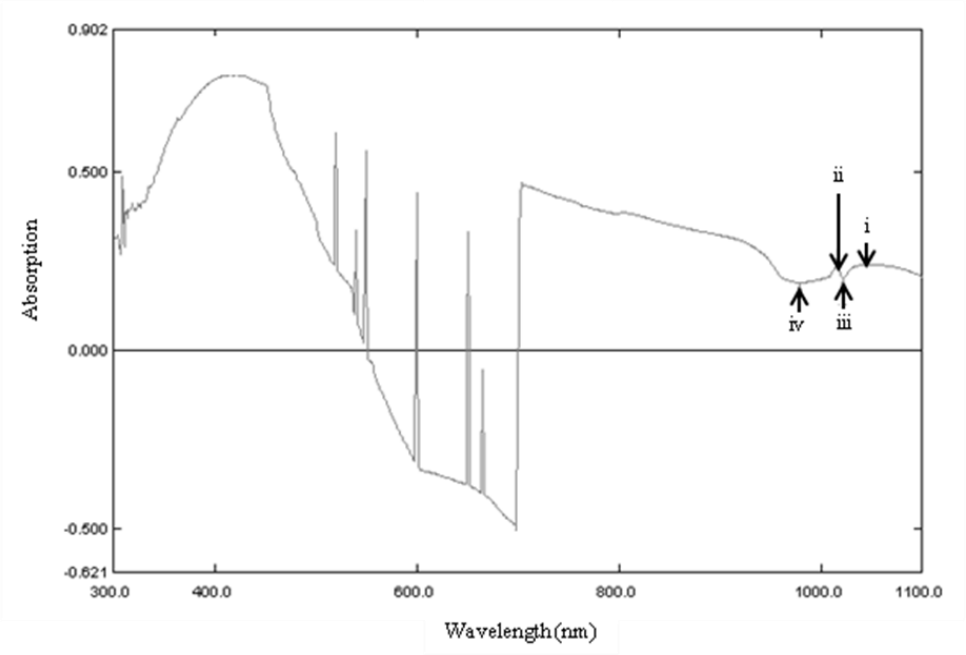


Figure 3. In vivo absorption spectrum for G5 medium. (i) 1046 nm; (ii) 1016 nm; (iii) 1022 nm and (iv) 979 nm.

Morphological Change

Focusing on the morphological characteristics during the development of granules, the initial sludge consisted of mainly dispersed loose structure with an average diameter of 0.07 mm. These were further developed into small flocs after two weeks of cultivation (Figure 4(A)). After 28 days, the flocs began to merge together forming small irregular aggregates with diameter size ranging between 0.02-0.11mm (Figure 4(B)). The number of aggregates was found to increase with time during the experiment. However, after 75 days of operation, the small aggregates had generated into bigger floc size with fluffy shape granular form (Figure 4(C)). Later on, the appearance of smoother non-uniform spherical granule (day 90) was observed as shown in Figure 4(D). During this phase, the maximum

size of mature granule achieved was 1.11 mm with total area of 0.96 mm^2. Based on the morphological variation of granules developed in the reactor, the phenomenon displayed during the granulation process was that of integration – recombination – growing up as described by Linlin *et al.* [13].

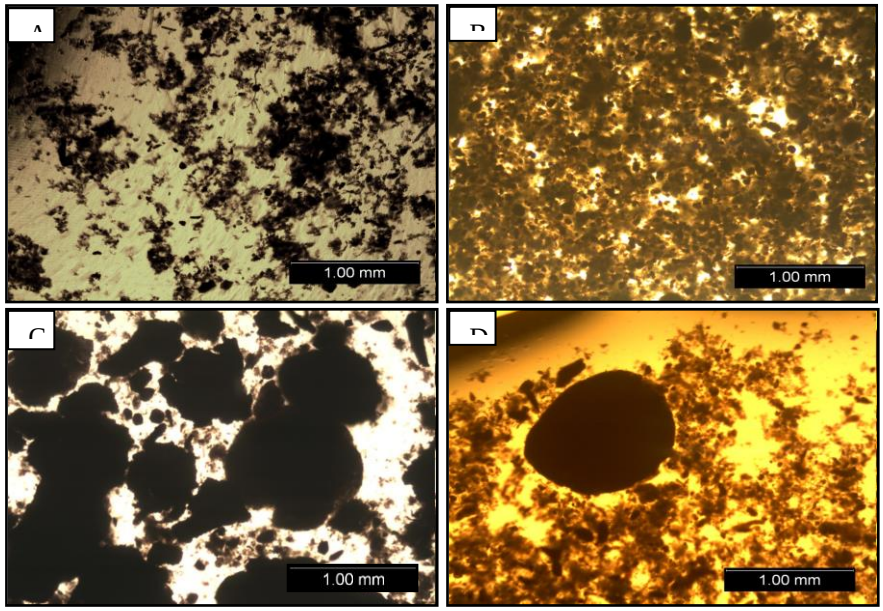


Figure 4. The morphological variation of granules captured using the PAX-IT™ during the experimental period (magnification = 40x). (A) Raw sludge; (B) after 28 days; (C) after 75 days and (D) after 90 days.

After 90 days, however, most of the granules underwent disintegration, forming smaller granules of regular shape and yellow-brownish in colour (Figure 5). This might be probably due to the formation of biogases such as hydrogen [14] and nitrogen gas [15] as secondary metabolites by the photosynthetic bacteria and other bacteria that makes up the granules.

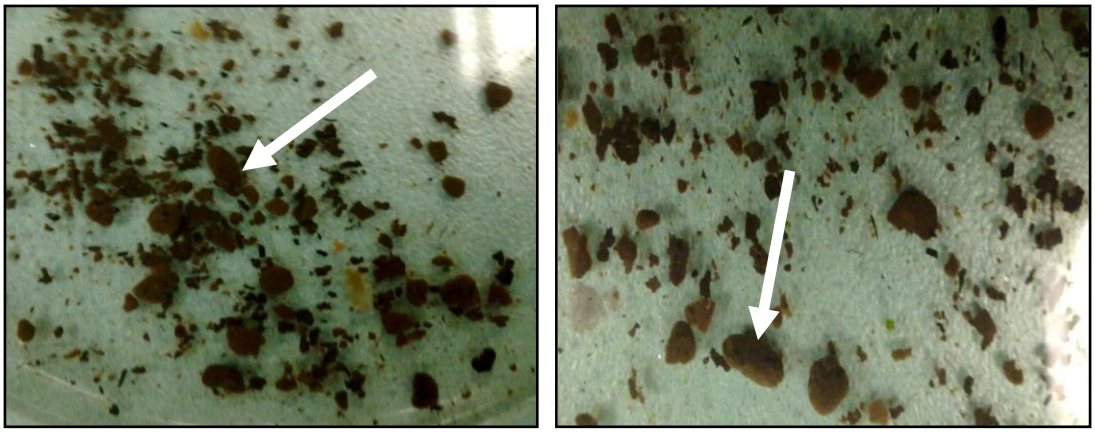


Figure 5. Granules developed at the end of experiment (arrow)

Biomass Properties

During the start-up period, the initial sludge with biomass concentration of mixed liquor suspended solid (MLSS) was 16750 mg/L and physically dispersed form. In the following days, the biomass increased to 17600 mg L^{-1} and continued to do so reaching approximately 32000 mg/L at the end of the experiment. Nevertheless, about 30 percent of the total sludge volume experienced loss of biomass after 14 days of the granule development possibly due to presence of filamentous microorganisms which made it difficult for some of the flocs to settle quickly [16, 17]. The average biomass was attained at about 23700 mg/L between 30 to 80 days with biomass loss up to 12100 mg/L while the highest biomass concentration of developed granule was 32000 mg/L as shown in Figure 6.

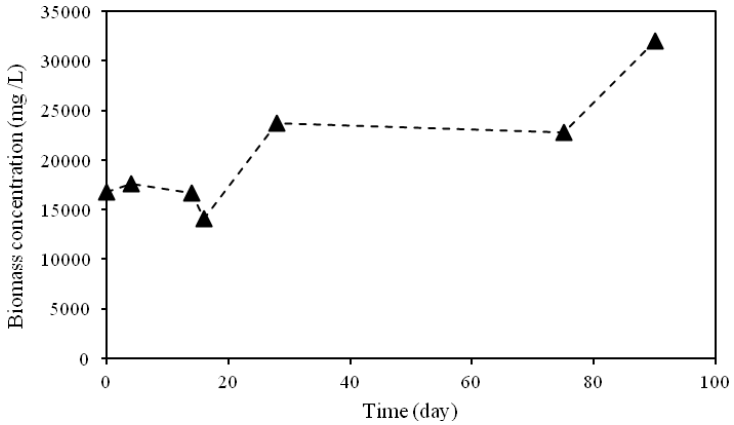


Figure 6. The change of biomass concentration in the reactor

As the relationship between biomass concentrations is proportional to the granule diameter, the settling velocity had also increased gradually (Figure 7). At this point, the maximum settling velocity remained in the reactor had reached approximately 2.0 cm/s. The average settling velocity of the granules were also found to increase linearly with the MLSS values, showing good accumulation of the biomass [18]. Furthermore, the settleability between the initial sludge and developed granule were found to increase (0.03 cm/s to 2.00 cm/s) within the range of 0.5 to 2.5 cm/s as reported by Gao *et al*.[19].

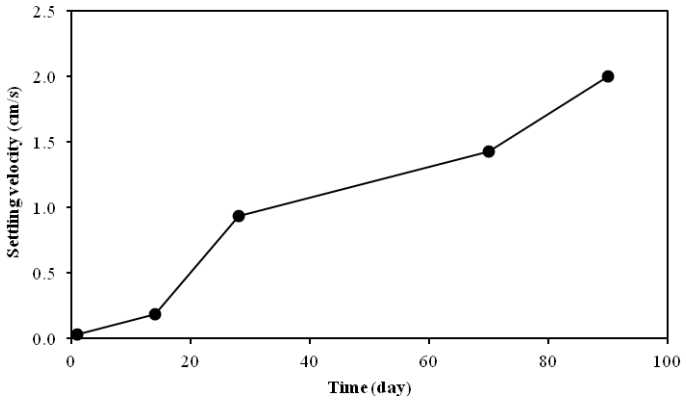


Figure 7. Settling properties of granule from the start-up period till the end of the experiment

Conclusion

In conclusion, the granules containing photosynthetic bacteria were formed after 90 days of cultivation by applying OLR at 2.75 kg COD/m^3.day, HRT of 4 hours and superficial air velocity of 2.07 cm/s. Based on the results, the characteristics of the developed photosynthetic microbial granule were proven better than the conventional sludge with a more compact (MLSS = 3200 mg/L; diameter = 0.40 - 1.11 mm), and higher settling properties of 2.0 cm/s. In addition, from the morphological change of the granules in the reactor, the occurrence of granulation process was that of integration – recombination – growing up. It showed changes from dispersed loose structure merging into small flocs of irregular shapes and finally forming a denser and compact granular form. In general, the granules demonstrated a good accumulation of biomass as well as increased in settleability compared to the conventional sludge (from 0.03 cm/s to 0.94 cm/s). The maximum settling velocity obtained achieved was approximately 2.0 cm/s. Future studies will include optimisation of the operational parameters such as the HRT and organic loading rate to produce granules that are compact, of higher settling abilities and durability. It is also noteworthy to include immediate applications of the granules in wastewater treatment to minimise the emission of GHG.

Acknowledgement

We would like to express our appreciation to Ministry of Higher Education, MOHE (Vot No. R.J130000.7822.4F211) and Universiti Teknologi Malaysia (UTM) for the financial support of this research. The authors would also like to acknowledge the staffs of the Environmental Laboratory, Civil Engineering Faculty for providing the light microscope with PAX-IT software and the assistance of Assoc. Prof. Dr. Zaharah Ibrahim for helpful discussions.

References

1. Chen, S.S. (2008). The LCA Approach to Illustrate Palm Oil's Sustainability Advantage. *International Palm Oil Sustainability Conference 2008.*
2. Intergovernmental Panel on Climate Change (IPCC) (2007). *Climate Change 2007*: The Physical Science Basis. *Contribution Of Working Group I To The Fourth Assessment Report*. Intergovernmental Panel on Climate Change.
3. Hassan, M.A., Yacob, S. & Shirai, Y. (2004). Treatment of Palm Oil Wastewaters. *Handbook of Industrial and Hazardous Waste Treatment (2_{nd} edition), Marcel Dekker Inc., N.Y., pp. 719-735.*
4. SIRIM (2008). Interim National LCI Database, National LCA Project, SIRIM, Shah Alam.
5. Su, F., Lu, C., Chen, W., Bai, H., & Hwang, J. (2009). Capture of CO_2 from Flue Gas via Multiwalled Carbon Nanotubes. *Science Total Environment 407 (8): 3017 - 3023* .
6. Olah, G., Goeppert, A., & Prakash, G. (2009). Chemical Recycling of Carbon Dioxide To Methanol And Dimethyl Ether: From Greenhouse Gas To Renewable, Environmentally Carbon Neutral Fuels And Synthetic Hydrocarbons. *Journal of Organic Chemistry, 74 (2): 487-98.*
7. Huber-Humer, M., Gebert, J., & Hilger, H. (2008). Biotic Systems to Mitigate Landfill Methane Emissions. *Waste Management Resources, 26 (1): 33-46*.
8. Alimahmoodi, M., & Mulligan, C. (2008). Anaerobic Bioconversion of Carbon Dioxide to Biogas in an Upflow Anaerobic Sludge Blanket Reactor. *Journal of Air and Waste Management Association. 58(1): 95-103.*
9. Su, B., Cui, X., & Zua, J. (2012). Optimal Cultivation and Characteristics of Aerobic Granules with Typical Domestic Sewage in an Alternating Anaerobic/Aerobic Sequencing Batch Reactor. *Bioresource Technology Volume 110: 125–129.*
10. Prasertsan, P., Choorit, W. & Suwanno, S. (1993). Isolation, Identification And Growth Conditions of Photosynthetic Found in Seafood Processing Wastewater. *World Journal of Microbiology and Biotechnology*. 9, 590-592.
11. U.S.EPA (1999). Wastewater, Technology Fact Sheet: Sequencing Batch Reactors, U.S Environmental Protection Agency, Office of Water, Washington, D.C., EPA 932-F-99-037.
12. Bhise., A.,D. (2005). Biomimetic Approach for Synthesizing Artificial Light- Harvesting System Using Self-Sssembled. *Institut of Nanotechnology. 5-7*
13. Linlin, H., Jianlong, W., Xianghua, W. & Yi, Q. (2003). The Formation and Characteristics of Aerobic Granules in Sequencing Batch Reactor (SBR) by Seeding Anaerobic Granules. *Process Biochemistry 40, 5–11.*
14. Kaewsuk, J., Thorasampan, Thanuttamavong, M. & Tae, G. (2010). Kinetic Development And Evaluation of Membrane Sequencing Batch Reactor (MSBR) With Mixed Cultures Photosynthetic Bacteria For Dairy Wastewater Treatment. *Journal of Environmental Management 91, 1161-1168.*

15. Dapena, A., Arrojo, B., Campos, J.L., Mosquera, A. & Mendez, R. (2004). Improvement of the Settling Properties of Anammox Sludge in a SBR. *Journal of Chemical Technology and Biotechnology 79, 1417-1420.*
16. Mangrum, R.L. (1998). The effect of anoxic selectors on the control of activated sludge bulking and foaming. Master Thesis. Virginia Polytechnic Institute and State University.
17. Liao, B.Q., Allen, D.G., Droppo, I.G., Leppard, G.G. & Liss, S.N. (2001). Surface Properties of Sludge and Their Role in Bioflocculation and Setteleability. *Water Research Volume 35(2), 339 – 350.*
18. Abdullah, N., Ujang, Z., & Yahya, A. (2011). Aerobic Granular Sludge Formation for High Strength Agro-Based Wastewater Treatment. *Bioresource Technology 102, 6778 – 6781.*
19. Gao, D.W., Lin, L., Liang H., & Wu, W.M. (2011). Aerobic Granular Sludge: Characterization, Mechanism of Granulation and Application to Wastewater Treatment. Critical *Reviews in Biotechnology 31 (2), 137–152.*

The Malaysian Journal of ANALYTICAL SCIENCES ISSN 1394-2506

THE EFFECT OF GAMMA IRRADIATION ON THE CHEMICAL STRUCTURE AND SURFACE CHARACTERISTICS OF DIPALMITOYLPHOSPHATIDYLCHOLINE (DPPC)

(Kesan Sinaran Gama ke atas Struktur Kimia dan Ciri Permukaan Dipalmitoilfosfatidilkolina (DPPC))

Hur Munawar Kabir Mohd[1], Ainee Fatimah Ahmad[1], Faizal Mohamed[1], Nursaidatul Syafadillah Kamaruzaman[1], Ng Wei Ling[1], Poh Roe Jin[1], Muhamad Samudi Yasir[1], Mohd Hafez Mohd Isa[3], Suria Ramli[2], Shahidan Radiman[1] and Irman Abdul Rahman[1]*

[1]*School of Applied Physics,*
[2]*School of Chemical Sciences and Food Technology,*
Faculty of Science & Technology, Universiti Kebangsaan Malaysia, 43600 Bangi, Selangor, Malaysia.
[3]*Industrial Chemistry Technology Program,*
Faculty of Science & Technology,
Universiti Sains Islam Malaysia, Bandar Baru Nilai, 71800 Nilai, Negeri Sembilan.

**Corresponding author: irman@ukm.my*

Abstract

Dipalmitoylphosphatidylcholine (DPPC) is one of the most abundant lipids in the human body and carries out important physiological functions such as liver protection and fighting infections. This study was conducted to investigate the effect of ionising radiation on the chemical structure and surface characteristic of DPPC. Synthetic DPPC was dissolved in chloroform (1mg/ml) and irradiated with Cobalt-60 (dose range of 50 – 200 Gy). The change in surface characteristics due to gamma irradiation was determined by means of monolayer compression isotherms using a Langmuir trough. From the change in the isotherm features, the threshold dose that affected the surface characteristics of the DPPC monolayer was determined to be 60 Gy. With increasing dose value, the plateau feature in the DPPC isotherm became shorter and was shifted to higher surface pressures. Analysis using High Performance Liquid Chromatography (HPLC) and Mass Spectrometry (MS) suggested that gamma irradiation of DPPC destroyed the chemical structure of DPPC and produced two main radiolytic products, namely lisophosphatidylcholine, LPC (~495.3142 g/mol) and phosphatidic acid, PA (~718.916 g/mol) with an average percentage of LPC and PA of 23% and 74%, respectively.

Keywords: dipalmitoylphosphatidylcholine (DPPC), Langmuir monolayer, High Performance Liquid-Chromatography (HPLC), Mass-Spectrometer (MS), gamma radiation

Abstrak

Dipalmitoilfosfatidilkolina (DPPC) adalah antara lipid dengan kelimpahan yang tinggi dalam badan manusia dan terlibat dalam fungsi fisiologi penting seperti perlindungan hati dan penentangan jangkitan. Kajian ini dijalankan untuk menentukan kesan sinaran gama ke atas struktur kimia dan cirian permukaan monolapisan DPPC. DPPC sintetik dilarutkan dalam kloroform (1mg/ml) dan disinarkan dengan punca sinar gama Kobalt-60 (julat dos 50 – 200 Gy). Perubahan pada cirian permukaan isotherma pemampatan monolapisan DPPC akibat kesan sinaran gama ditentukan dengan menggunakan Palung Langmuir. Daripada perubahan ciri pada isoterma pemampatan yang diperolehi, dicadangkan dos ambang yang mula memberikan kesan ke atas kerosakan struktur DPPC bermula pada sekitar 60 Gy. Dengan peningkatan dos dedahan, ciri dataran pada lengkung isoterma DPPC menjadi semakin pendek dan berganjak kepada tekanan permukaan yang lebih tinggi. Analisis dengan menggunakan Kromatografi Cecair Prestasi Tinggi (HPLC) dan Spektrometri Jisim (MS) menentusahkan bahawa struktur kimia asal DPPC termusnah dan membentuk dua hasil radiolitik iaitu lisofosfatidilkolina, LPC (~495.3142 g/mol) dan asid fosfatidik, PA (~718.916 g/mol) dengan purata peratusan LPC dan PA masing-masing adalah 23% dan 74%.

Kata kunci: dipalmitoilfosfatidilkolina (DPPC), monolapisan Langmuir, Kromatografi Cecair Prestasi Tinggi (HPLC), Spektrometri Jisim (MS), sinar gama

Introduction

Ionising radiation has been widely used in medical application as a tool in diagnostic imaging, nuclear medicine and radiotherapy. Living organisms exposed to radiation can undergo tissue deformity and suffer damages which is a major safety concern. However, there are few studies that investigate the effects of gamma radiation on biological system components, in particular phospholipids. In this study, the di-saturated and zwitterionic dipalmitoylphosphatidylcholine (DPPC) was used because it is the most abundant phospholipid and can be found almost everywhere in the body and functions to protect liver, fight toxicity and infection in body system. [1].

Gamma irradiation has been found to be effective in depolymerising and cleaving molecular chains ascribed to the decay processes. This is related to free radicals generated at the primary stage of gamma irradiation, which extends with changes in chemical composition as well as its physiological functions [2]. It has also been reported in previous studies that radiation, given to patients for the purpose of diagnosis and therapy, has caused an onset of joint pain and loss of joint fluidity. This is due to the unacceptable high radiation dose delivered to non-targeted organs because of the leakage from the treated joints [3].

In this study, there are three main objectives. The first objective is to study the effects of ionizing radiation on DPPC monolayer surface structures. A basic technique used to study the phase behavior of monolayers is the so-called Langmuir film balance. The effects are observed from the surface pressure-area isotherms obtained upon compression of lipid spread on aqueous subphase. The second objective is to identify the chemical composition formed from the structural damage of irradiated DPPC at doses range 0 Gy to 200 Gy. High Performance Liquid Chromatography (HPLC) and Mass Spectrometry (MS) were used to obtain and verify chemical composition formed after irradiation. The third objective is to compare the DPPC irradiation results obtained from HPLC method with the results obtained from the Langmuir monolayer compression method. This comparison allows us to determine the threshold dose of gamma radiation damage.

Materials and Methods

Research materials

Synthetic DPPC (1,2-dipalmitoyl-*sn*-glycerol-3-phosphocholine) was purchased from Avanti Polar Lipids Inc. (Alabaster, AL, USA). The samples were dissolved in chloroform to get a concentration of 1 mg/ml and all samples were irradiated with gamma irradiation. The samples irradiated at higher doses (60 Gy to 200 Gy) were supplemented with Fricke dosimetry to determine the exact absorbed dose. All samples were then analysed using Langmuir Blodgett to observe the samples surface structure. HPLC and MS were used to obtain the chemical composition in the samples.

Sample preparation

DPPC monolayer surface were studied using the surface pressure-area isotherms obtained from spreading of lipid on the Langmuir through. All surface pressure-area measurements were performed on deionised water which had a resistivity greater than 18 MΩ m [4]. The chemical composition percentage of irradiated DPPC were analysed with HPLC and MS.

Irradiation Setup

The DPPC was irradiated in 4 ml glass vials with a ^{60}Co source at ambient temperature using a GammaCell 220 Excel irradiator at a dose rate of 4.20kGy/h. Vials containing DPPC were irradiated with 5, 10, 20, 30, 40, 50, 60, 90, 130, 170 and 200 Gy gamma radiation, with 0 Gy as a control. Time required to irradiate each samples were determined by the following equation (1);

$$A = A_0 e^{-\lambda t} \quad (1)$$

Sample Analysis

The DPPC monolayer surface structure damage was determined through the surface pressure-area isotherms and comparisons between plateau region slopes of the graph. Analysis of HPLC and MS will confirm the chemical composition formed after irradiation.

Results and Discussion

Patterns formed from compression of DPPC monolayer

The obtained results for control and irradiated DPPC (Figure 1) exhibits a clear phase transition from liquid expanded to the liquid condensed state. The difference of slope of plateau region between each dose is observed. Each of the DPPC monolayer irradiated from 0 to 50 Gy seems to shift from an expanded to a condensed phase without any significant change in the isotherm slope. Increasing the dose from 60 Gy to 200 Gy gamma radiation exhibit a significant pattern of shifting the isotherms to larger molecular areas.

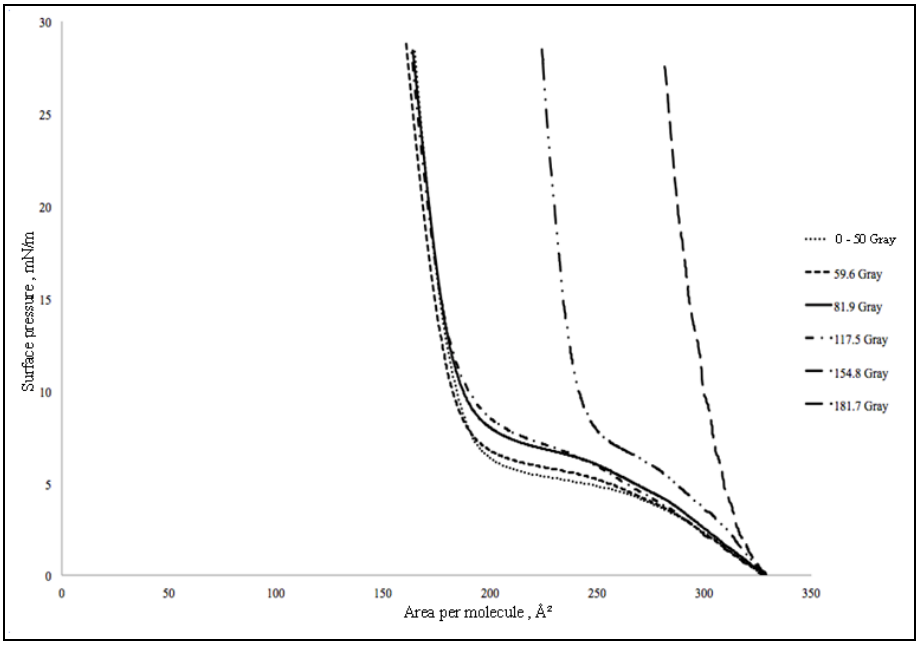


Figure 1. Surface pressure-area isotherms of DPPC monolayer at different radiation dose

As the radiation dose was increased, the slope of the plateau region also eventually increased, as observed in Figure 2. According to Hsu et al. (2009), the characteristics of the plateau's slope are a contribution of several second phase inclusion, impurities and segregation. Charge difference or ion formation on the surface of DPPC also influences the electrostatic interaction characteristic of the air-water interface of DPPC [5, 6].

High Performance Liquid Chromatography studies

HPLC analysis was performed to obtain the chemical composition of irradiated DPPC. Figure 3 displays two linear lines that represents radiolytic products formed i.e lysophosphatidylcholine, LPC and phosphatidic acid, PA [4]. Identification of the chemical compound formed was based on reversed-phase HPLC work principal, where more polar compounds are eluted first [1, 7]. It is known that LPC is a polar compound and PA is a non-polar compound. From the absorption unit versus operation time graph obtained from HPLC analysis, it is found that gamma radiation formed two radiolytic products caused by DPPC structural damage and gave different chemical composition percentage for each dose.

Upon gamma irradiation, phospholipid tends to experience oxidation process and hydrolysis degradation reaction [8]. Oxidation occurs between cells that involve alternative mechanism after phospholipid has been irradiated which will form free radicals and caused damage to cells structure. Hydroxyl radical, •OH are one of the formed radical and it reacts actively with irradiated cell and caused lipid oxidation [9].

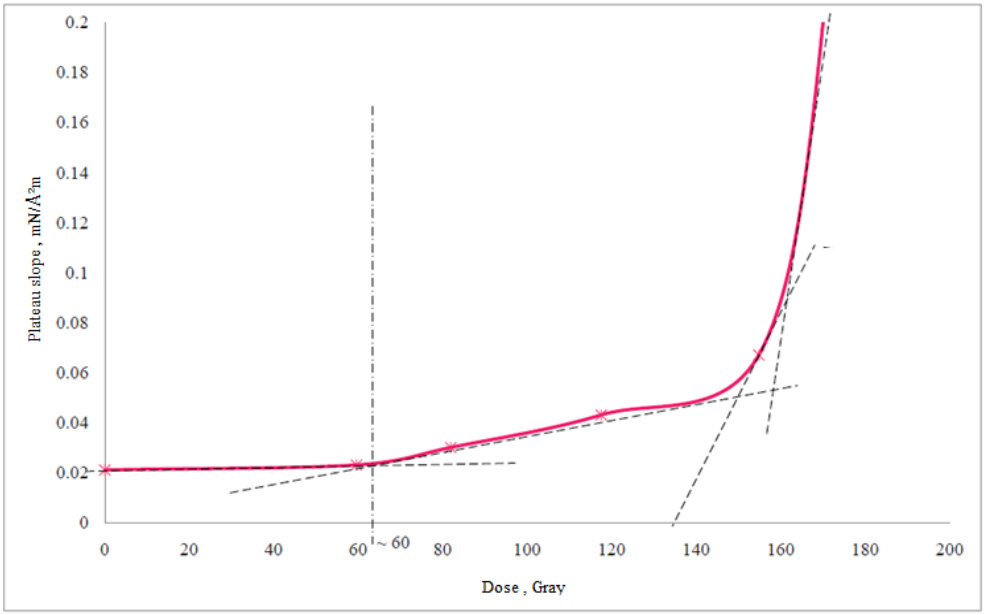


Figure 2. Plateau slope difference between each irradiated doses

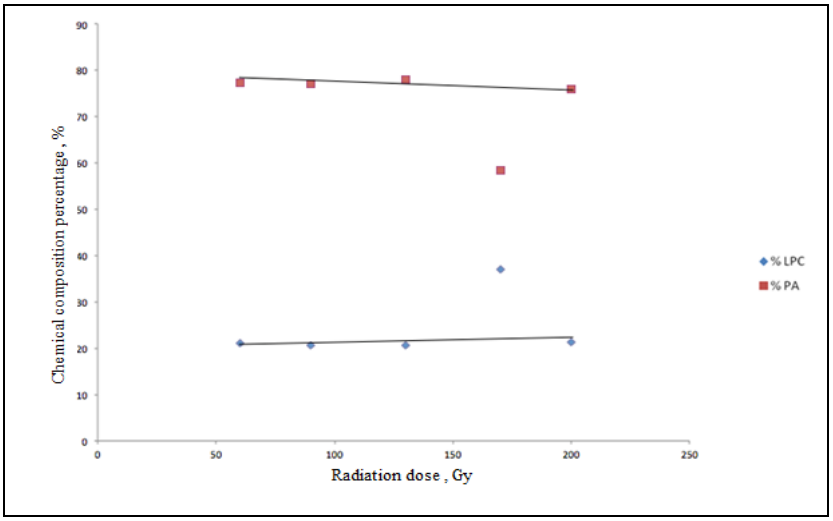
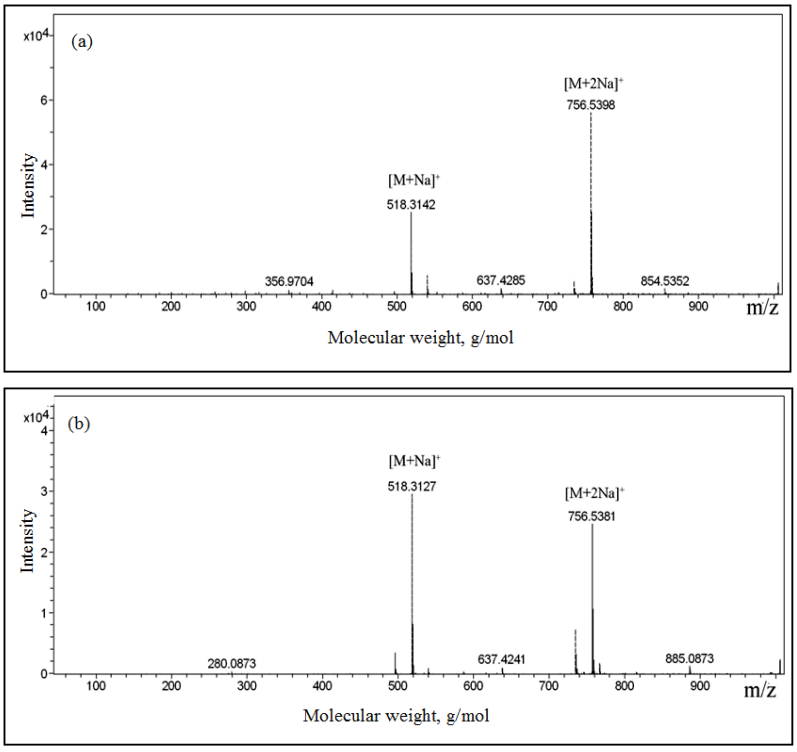


Figure 3. Percentage of chemical compound formed from HPLC separation

Mass Spectrometry studies

MS analysis provides mass spectrum information that can be used to identify molecule. In MS analysis, spectrum peak represents ions that are formed. The peak height depends on the intensity, whilst ions have their own specific abundance [10]. For this analysis, positive ion mode was used. The positive ions used were H^+ and Na^+ and these ions interact with samples to produce mass spectrum information.

Figure 4 shows the spectrum formed together with each individual molecular mass. Each peak represents the chemical compound formed after DPPC was irradiated with gamma radiation. It has been identified that the compounds were combined with Na to form [M+Na^+] at an average peak of 518.31 g/mol (Figure 4(a)-(e)). Hence, the molecules formed at this peak have an average molecular mass of 495.31 g/mol, which is approximate to the LPC molecular mass of 495.63 g/mol. At the average peak of 756.54 g/mol (Figure 4(a)-(e)), it was identified that molecule formed was [M+2Na^+]. With a 46 unit molecular mass difference (molecular mass for every Na is 23 unit), it was identified that the compounds formed at this peak were phosphatidic acid, which has an average molecular mass value of 711.54 g/mol (~718.916 g/mol).



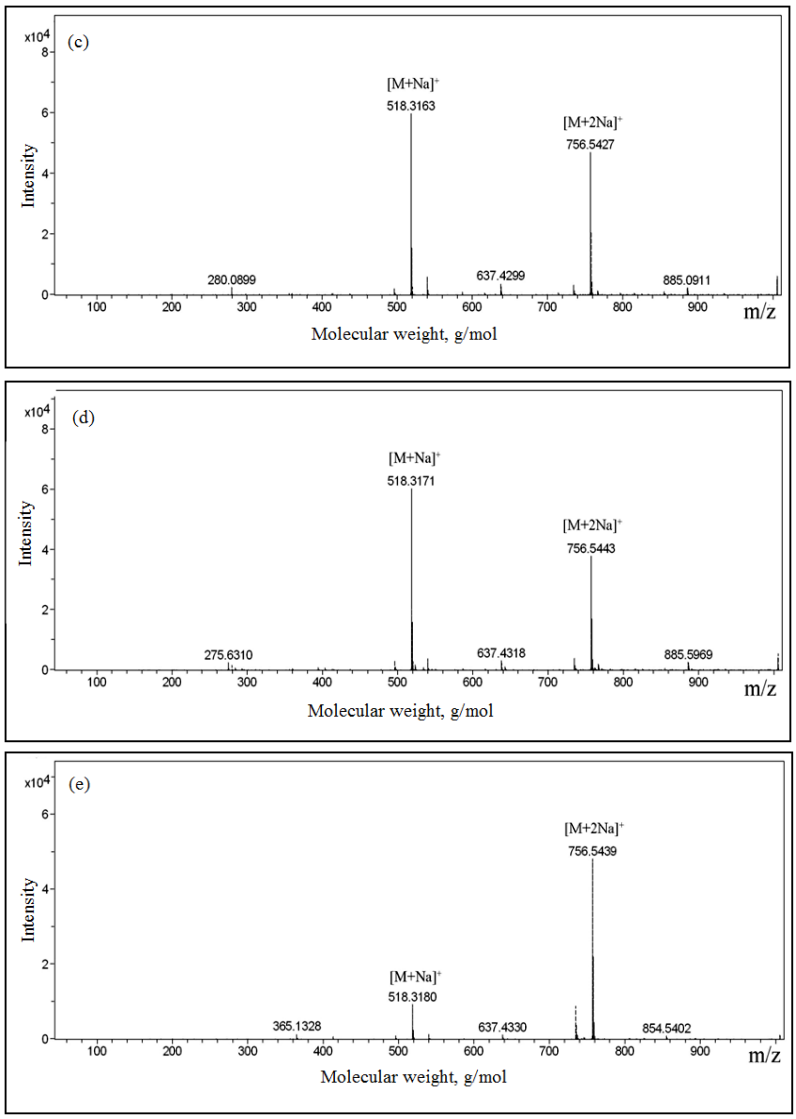


Figure 4. Mass spectrum of samples irradiated with (a) 56.5 Gy, (b) 84.8 Gy, (c) 122.4 Gy, (d) 160.1 Gy and (e) 188.4 Gy dose

Conclusion

Based on the surface pressure-area isotherms data, it is noted that for gamma irradiation lower than 50 Gy does not significantly affect the DPPC monolayer surface structure. At higher dose (59.6, 81.9, 117.5, 154.8 and 181.7 Gy), the results show the existence of the effect of ionising radiation on the characteristics of the DPPC monolayer surface. Based on the plateau slope pattern, the dose effect on the surface characteristics of DPPC monolayer was seen to start at approximately 60 Gy. With increasing dose values, the plateau of the DPPC isotherm curve became shorter and shifted to higher surface pressure. Analysis of MS confirms that the radiolytic products formed were lysophosphatidylcholine, LPC and phosphatidic acid, PA with average percentage 22.94% and 74.38% respectively. A previous study showed that only LPC and PA were formed as the major radiolytic products of gamma irradiation on phospholipids at dose of 9.66 kGy [11]. In summary, our experiments clearly show that DPPC has suffered damage to its chemical compound even at the lower doses (< 50 Gy). However, the surface structure displayed via the Langmuir monolayer remained intact with a gradual shift that depicts structural change starting from the dose of

60 Gy. This suggests the ability of DPPC to sustain its surface structure and functions at higher dose, even though its chemical structures have been altered at the lower doses of 50 Gy.

Acknowledgement

The authors would like to acknowledge funding from UKM in this work through research grants UKM-ST-07-FRGS0023-2010, ERGS/1/2012/STG02/UKM/02/1, UKM-ST-07-FRGS0018-2010 and UKM-PTS-011-2010. We would also like to thank the School of Chemical Sciences and Food Technology for extending their facilities to us.

References

1. Singleton, J., A., Ruan, M., Sanford, J., H., Haney, C., A. & Stikeleather, L., F. (1999). Separation and Characterization of Peanut Phospholipid Molecular Species Using High-Performance Liquid Chromatography and Fast Atom Bombardment Mass Spectrometry. *Journal of the American Oil Chemists' Society*. 76(1): 49-56.
2. Kim, J. K., Srinivasan, P., Kim, J. H., Choi, J., Park, H. J., Byun, M. W. & Lee, J. W. (2008). Structural and antioxidant properties of gamma irradiated hyaluronic acid. *Journal of Food Chemistry*. 109(2008): 763-770.
3. Wang S.J. (2001). Histologic study of effects of radiation synovectomy with Rhenium-1888 microsphere. *Journal of Nuclear Medicine and Biology*. 28(2002): 727-732.
4. Harishchandra, R. K., Saleem, M. & Galla, H. J. (2010). Nanoparticle interaction with model lung surfactant monolayers. *Journal of Royal Society Interface*. 7: 15-26.
5. Garidel, P. & Blume, A. (2005). 1,2-Dimyristoyl-sn-glycero-3-phosphoglycerol (DMPG) monolayers: influence of temperature, pH, ionic strength and binding of alkaline earth cations. *Chemistry and Physics of Lipids*. 138(2005): 50-59.
6. Hsu, S. E., Beibutian, V. M. & Yeh, M. T. (2002). Preparation of hydrogen storage alloys for applications of hydrogen storage and transportation. *Journal of Alloys and Compounds*. 330-332(2002): 882-885.
7. Sanagi, M. M. 1998. Kaedah pemisahan dalam analisis kimia. Skudai: Percetakan Surya Sdn. Bhd.
8. Mengesha, A. E. & Bummer, P. M. (2010). Simple chromatographic method for simultaneous analyses of phosphatidylcholine, lysophosphatidylcholine and free fatty acids. *Journal of American Association of Pharmaceutical Scientists.* 1-8.
9. Hallahan, D. E., Virudachalam, S., Sherman, M.L, Huberman, E., Kufe, D. W. & Weichselbaum. (1991). Tumor necrosis factor gene expression is mediated by protein kinase C following activation by ionizing radiation. *Journal of American Association for Cancer Research*. 51: 4565-4569
10. Watson, J. T. & Sparkman, O. D. (2002). Introduction to mass spectrometry. 4th edition. Chichester: John Wiley & Sons Ltd.
11. Tinsley, P.W. & Maerker, G. (1993). Effect of Low-Dose γ-Radiation on Individual Phospholipids in Aqueous Suspension. *Journal of the American Oil Chemist's Society*. 70(2): 187-191.

The Malaysian Journal of ANALYTICAL SCIENCES ISSN 1394-2506

MINERALOGICAL RESPONSE OF THE POSTHARVEST MANGO (*MANGIFERA INDICA L.)* TO DIFFERENT LEVELS OF BAVISTIN DF

(Tindak balas Minerologi Lepas Tuai Terhadap Mangga (*Mangifera Indica L.*) Pada Tahap Bavistin DF Berbeza)

Md. K. Islam [1]*, N. Absar[2], M. A. R. Sarkar[5], M. Z. H. Khan[4], S. Yeasmin[3] and K. A. Hakim[1]

[1]*Dept. of Crop Science and Technology,*
[2]*Dept. of Biochemistry and Molecular Biology,*
[5]*Dept of Geology and Mining,*
University of Rajshahi, Rajshahi 6205, Bangladesh
[4]*Dept. of Chemical Engineering,*
[5]*Dept. of Genetic Engineering and Biotechnology,*
Jessore Science and Technology University, Jessore 7408, Bangladesh

**Corresponding author: mki_crop@yahoo.com*

Abstract

This study was carried out with the postharvest mangoes (*viz.*, the Langra and the Khirshapat) treating with different levels of Bavistin DF solution (namely, 250, 500, and 750 PPM) for obtaining results on the mineral content changes as well as storability of postharvest mango. The results of the experiments exhibited that only the single effect of varieties was found to be significant in most of the parameters studied. The Langra enriched a greater quantity of magnesium, iron and manganese constituents over the Khirshapat. On the other hand, Khirshapat enriched higher quantities of calcium, copper and zinc content at all the storage duration. Different postharvest treatments subjected to the investigation demonstrated significant variation in most of the mineralogical properties of mango at different days of storage. The result explored that calcium, magnesium, iron, and manganese contents were rapidly increased. On the other hand copper and zinc content drastically decreased from untreated mangoes.

Keywords: mango; postharvest treatment; Bavistin DF; mineral content.

Abstrak

Kajian lepas tuai ini dijalankan terhadap mangga lepas (Langra dan Khirshapat) yang dirawat dengan larutan Bavistin DF pada tahap yang kepekatan berbeza (iaitu, 250, 500 dan 750 ppm) untuk mendapatkan keputusan tentang perubahan kandungan mineral serta tempoh keboleh simpanan mangga lepas tuai. Keputusan eksperimen menunjukkan bahawa hanya kesan tunggal didapati penting dalam kebanyakan parameter yang dikaji. Jenis Langra diperkayakan dengan kuantiti magnesium, ferum dan mangan lebih basar berbanding Khirshapat. Sebaliknya, Khirshapat diperkayakan kuantiti kalsium, kuprum dan zink lebih tinggi kandungannya pada setiap tempoh penyimpanan. Rawatan lepas tuai yang berbeza tertakluk matlamat kajian yang menunjukkan perbezaan ketara di dalam kebanyakan sifat-sifat mineralogi mangga pada perbezaan hari penyimpanan. Hasil kajian mendapati bahawa kandungan kalsium, magnesium, ferum dan mangan meningkat dengan pesat. Sebaliknya kandungan kuprum dan zink menurun secara drastik daripada mangga dirawat.

Kata Kunci : mangga, rawatan lepas tuai, Bavistin DF, kandungan mineral

Introduction

Mango is one of the most important, popular and tasteful fruit crop not only in Bangladesh but also in the world owing to its greater utility, characteristics flavor, attractive color, pleasant aroma, delicious taste and nutritional value. It is consumed as fresh ripe and green fruits. Both the green and ripe fruits are also used to make different varieties of processed products like juice, chutney, pickles, jam, jelly etc. For this reason, it is acknowledged as the king of fruits in Bangladesh as well as in other South-East Asian countries [1]. Nutritionally, it contains substantial quantity of appreciable β carotene, vitamin C, and dietary fibre [2] as well as soluble sugars and different minerals

which are used for good sources of nutrition and readily available and easily assumable in human body and therefore, is capable to prevent many deficiency diseases [3].

Malnutrition and under nutrition have now become an alarming problem of the people of the third world countries affecting their economic and physical development. Protein–energy malnutrition, vitamin and mineral deficiencies are the most serious nutritional disorder in low income groups. Due to these deficiencies, under–weights and high mortality are prevalent in pre- school children and infants. Nutritionally, it contains substantial quantity of appreciable β carotene, vitamin C, and dietary fibre [2] as well as soluble sugars and different minerals which are used for good sources of nutrition and readily available and easily assumable in human body [4] and therefore, is capable to prevent many deficiency diseases [3, 5,]. Approximately 30-50% fruits go waste during postharvest handling, storage and ripening [6]. These treatments strongly impede in ethylene synthesis that resulted in low respiration and delay ripening. These materials also reduced the losses and prolonging the shelf life of mango [7].

In addition, fungicidal treatments like Bavistin DF (BDF) are also excellent ethylene inhibitors. These treatments performed effectively in reduction of postharvest decay, and extension of shelf life of mango [8]. Apparently, these treatments deteriorate the qualities of fruits to some extent, but the reduction of losses and extension of postharvest life of mango will help to increase the market price in the off seasons which play a good role in the economic development. Several researchers used BDF for controlling spoilage of different fruits [9, 10]. The efficacy of Bavistin against the fruit rot pathogen was reported by several workers [11, 12]. In this present study we did investigation on mineralogical constituents of the postharvest mango at various concentrations of BDF treatment during postharvest storage. It was also aimed to reveal the effect of same treatments on target variety.

Materials and Methods

Two mango varieties namely, Langra and Khirshapath were selected as experimental materials. The mango varieties that undertaken for investigation were collected from mango growing areas of Kansart, Shibgonj Upazila of Chapai Nowabgonj district and Chirghat upazila of Rajshahi district and others material used as postharvest treatments *viz*., Bavistin DF (BDF) were collected as analytical grade. The experiment consisted of two factors and was conducted in Randomized Complete Block Design (RCBD) with three replicates. The post-harvest treated fruits were assigned at random in each replication. The required numbers of unblemished physically similar, more or less uniform size, shape and color fruits for the experiment were harvested manually from each plant of the varieties, Langra and Khirshapath. The fruits were carefully selected during harvest. The skin of fruits was cleared with the help of a cloth just after harvesting. The solution of BDF of 250, 500, and 750 ppm were prepared by dissolving 250, 500 and 750 mg of BDF in one litre of distilled water. The fruit of both the varieties were dipped into the BDF solution for a period of 5 minutes. Care was taken to ensure enough quantity of BDF being absorbed by the fruits and stored at ambient condition on brown paper. The collected data was statistically analyzed by analysis of variance method. The means of different parameters was compared using DMRT as described by Gomez and Gomez [13].

Determination of different minerals

Different important minerals of mango pulps were determined following the procedure as stated by Petersen [14].

Preparation of plant sample

Procedure of drying

The cleaned porcelain crucibles were placed in an oven at 105^0 C for overnight. The crucibles were allowed to cool in a desiccator's and these were weighed. The mango pulps were collected with spatula and put into crucible and again weighed. The crucibles were placed in the oven at 105^0 C for 24 hours. Then, the crucibles were allowed to cool in a desiccator and weighed. The crucibles were again placed in the oven at 105^0 for 2 hours. These were cooled in a desiccator and weighed again. Drying, cooling and weighing were accomplished repeatedly until the weight became constant. The dried pulps were stored in airtight plastic container. The moisture content was calculated in the sample.

Procedure of grinding

The dried plant material was ground in a mortar with pestle. These were further kept in an oven at 105^0 C for overnight due to absorption of moisture in the time of grinding for keeping the weight constant.

Determination of calcium content

Ground mango pulp was digested and Ca was released by digestion with nitric acid and it was determined by atomic absorption spectrophotometer. Reagents **a.** HNO_3 (68%) and b. Diluted HNO_3 1: 100. Twenty ml of 68% HNO_3 was transferred to 2000 ml volumetric flask and made the volume with distilled water and mixed well.

$LaCl_3$ solution

The 435 g of $LaCl_3$ $7H_2O$ was weighed into a beaker. One hundred ml of 5 M HNO_3 and 400 ml water were added in it. The salt was heated gently until it was dissolved. After cooling, 300 ml of more 5 M HNO_3 was added and the solution was transferred to 5 l volumetric flasks. It was made to volume with water and mixed. The solution contained 3.25% of La.

Digestion procedure

Ground pulp material (0.3 g) was taken into digestion tube. The two remaining tubes were blanks. Five ml of 68% nitric acid was added to each of all the 40 tubes. The content was mixed in each tube and was kept the tubes overnight. The tubes were placed in the digester and the tubes were covered with the exhaust manifold. The temperature was set at 125^0 C. The digester was turned on and the digestion was continued for 4 hours after boiling started. It was observed that no tubes became dry.

After cooling, the digestion mixture was transferred with distilled water to a 200 ml volumetric flask. The flask was made up to the mark with distilled water and mixed well. It was filtered on a dry filter into a dry bottle which could be closed with a screw cap. The filtrate was kept in the closed bottle and used for estimation of Phosphorus.

Measurement of calcium

20 ml of diluted filtrate was transferred into a 50 ml volumetric flask using a pipette. The $LaCl_3$ solution (5 ml) was added to make a volume with water and mixed well. The content of Ca was measured by atomic absorption spectrometer. When the reading was found to be higher than the reading of the highest standard solution, a larger dilution was made. In this case, 1:100 diluted HNO_3 was added to the volumetric flask to make the total volume of 1:100 HNO_3 and filtrates was equal to 20 ml. Amount of Ca was determined by the following formula:

$$\text{mg per kg mango pulp} = \frac{a \times 25000}{b \times c}$$

where a = mg of Ca per litre, b = amount of filtrate transferred into the 50 ml volumetric flask for determination of Ca, c = g of plant material taken into the digestion tube.

Determination of magnesium content

Ground material of mango pulp was digested and Mg was released by digestion with nitric acid and it was determined by atomic absorption spectrophotometer. Reagents and digestion was used same as describe in calcium procedure.

Measurement of Magnesium

Diluted filtrate (5 ml) was transferred into a 50 ml volumetric flask using a pipette. The $LaCl_3$ solution (5 ml) was added to make a volume with water and mixed well. The content of Mg was measured by atomic absorption spectrometer. When the reading was found to be higher than the reading of the highest standard solution, a larger dilution was made. In this case, 1:100 diluted HNO_3 was added to the volumetric flask to make the total volume of 1:100 diluted HNO_3 and filtrate was equal to 5 ml. Amount of Mg was determined by the following formula:

$$\text{mg per kg mango pulp} = \frac{\text{a} \times 25000}{\text{b} \times \text{c}}$$

where a = mg of Mg per litre, b = ml of diluted filtrate transferred into the 50 ml volumetric flask for determination of Mg, c = g of plant material taken into the digestion tube.

Determination of copper content
Powder form of mango pulp was digested and Cu was released by digestion with nitric acid and it was determined by atomic absorption spectrophotometer. Digestion was used same as describe in calcium procedure.

Measurement of copper
The content of Cu was measured by atomic absorption spectrometer (AAS) directly in the undiluted filtrate. Amount of Cu was determined by the following formula:

$$\text{mg per kg mango pulp} = \frac{d \times 200}{c}$$

where d = mg of Cu per litre, c = g of ground pulp material taken into the digestion tube.

Determination of iron content
Ground mango pulp material was digested and Fe was released by digestion with nitric acid and it was determined by atomic absorption spectrophotometry. Digestion was used same as describe in phosphorus procedure.

Measurement of iron
The content of Fe was measured by atomic absorption spectrometer (AAS) directly in the undiluted filtrate. Amount of Fe was determined by the following formula:

$$\text{mg per kg mango pulp} = \frac{d \times 200}{c}$$

where d = mg of Fe per litre, c = g of ground pulp material taken into the digestion tube.

Determination of manganese content
Ground material of mango pulp was digested and Mn was released by digestion with nitric acid and it was determined by atomic absorption spectrophotometry. Digestion was used same as describe in phosphorus procedure.

Measurement of manganese
The content of Mn was measured by atomic absorption spectrometer directly in the undiluted filtrate. Amount of Mn was determined by the following formula

$$\text{mg per kg mango pulp} = \frac{d \times 200}{c}$$

where d = mg of Mn per litre, c = g of ground pulp material taken into the digestion tube.

Determination of zinc content
Ground mango pulp material was digested and Zn was released by digestion with nitric acid and it was determined by atomic absorption spectrophotometry. Digestion was used same as describe in phosphorus procedure.

Measurement of zinc
The content of Zn was measured by atomic absorption spectrometer directly in the undiluted filtrate. Amount of Zn was determined by the following formula:

$$\text{mg per kg mango pulp} = \frac{d \times 200}{c}$$

where d = mg of Zn per litre, c = g of ground pulp material taken into the digestion tube.

Results and Discussion

The data obtained from different behavior of mineral contents during storage period of mango fruits are presented and fairly interpreted in the following sub-headings.

Calcium content

Analysis of variance of induced varieties to this investigation in connection with Ca content demonstrated highly significant variation at different days after storage. The results were perceived an increasing trend of Ca content with the extending of storage time from both the varieties (Table 1). It also narrated that the Khirshapat was better in accumulation of Ca content as compared to the Langra. At 12^{th} day, higher (22.98 mg/100 g) quantity of Ca was recorded from the Khirshapat and lower (21.25 mg/100 g) was recorded in Langra. These occurrences might be possible due to genetical variation between two varieties.

Different doses of BDF solution on Ca content of mango pulp demonstrated significant variation at different days after storage. At various days of storage, the results of Ca content extended in a continuous stream with the passing of storage time (Figure 1). It also stated that Ca content of control extended sharply from initial to 6^{th} day and then, it extended smoothly and thereafter, it declined due to starting of decomposition. At the same time, Ca content from the fruit treated with B_3 treatment gathered very smoothly. At 9^{th} day, the highest (24.76 mg/100 g) quantity of Ca was recorded from untreated fruit while; the lowest (16.69 mg/100 g) was recorded from the fruit treated with B_3 treatment. These phenomena caused by B_3 treatment might be possible due to delay ripening that caused in lower dissemination of Ca content from peel and stone to pulp of mango [15].

The combined effect of varieties and different doses of BDF solution in terms of Ca content of mango pulp had significant variation at different days after storage except 6^{th} day. The results of Ca content were noticed an increasing trend from various treatment combinations (Table 1). At 9^{th} day, the highest (25.58 mg/100 g) quantity of Ca was observed from the treatment combination of V_2B_0 and the lowest (15.94 mg/100 g) was observed from the treatment combination of V_1B_3. The results of the present investigation annotated that the treatment combination of V_1B_3 was better in mango preservation.

Table 1 Changes of calcium and magnesium content of the postharvest mango pulp between two varieties during storage environments at ambient condition

Treatments	Calcium content (mg/100 g) at different days					Magnesium content (mg/100 g) at different days				
Variety (V)	Initial	3	6	9	12	Initial	3	6	9	12
V_1	10.74b	13.29b	16.63b	19.92b	21.25b	17.01a	17.53a	18.03a	18.08a	17.81a
V_2	12.39a	15.01a	18.44a	21.64a	22.98a	16.02b	16.49b	17.01b	17.11b	16.85b
Level of significance	***	***	***	***	***	***	***	***	***	***

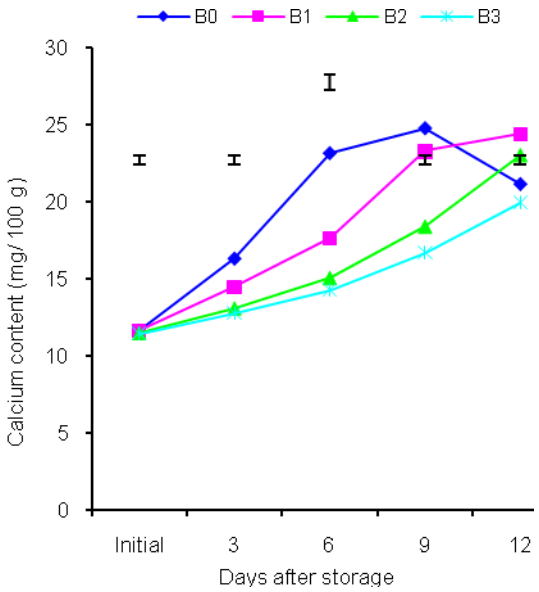


Figure 1. Calcium content of mango pulp as influenced by different doses of BDF at different days after storage. Vertical bars represent LSD at 0.05 levels.

Magnesium content

Highly significant variation was observed in terms of Mg content between the varieties means at different days after storage. The results indicated that Mg content augmented gradually with the advancement of storage period (Table 1). It also denoted that Mg content extended steadily of initial to 9 days thereafter; it came down slightly due to starting decay of the fruit. At 9th day, higher (18.08 mg/100 g) was derived from the Langra and lower (17.11 mg/100 g) was derived from the Khirshapat. These phenomena might be probably due to genetical dissimilarities between the varieties. There were no available research findings in connection with Mg content during storage in the scientific literature. But, the data of the present study revealed that the Langra contained more Mg over the Khirshapat.

Different doses of BDF solution used in this trial exhibited highly significant on Mg content of mango pulp at different days after storage. The results indicated a smooth gathering trend of Mg content of mango pulp with the extension of storage period (Figure 2). It was also noticed that Mg content of control extended gradually from initial to 6 days and then, it abated very sharply. The highest (18.72 and 18.00 mg/100 g) quantity of Mg was obtained from control and B_1 treatment at 6 and 9th day while, the lowest (16.83 and 17.18 mg/100 g) was obtained from the fruit treated with B_3 treatment, respectively. The increasing tendency of Mg content in mango pulp during storage period might have been related to starting of ripening. This result is very much similar to the report of Peter *et al.* [15].

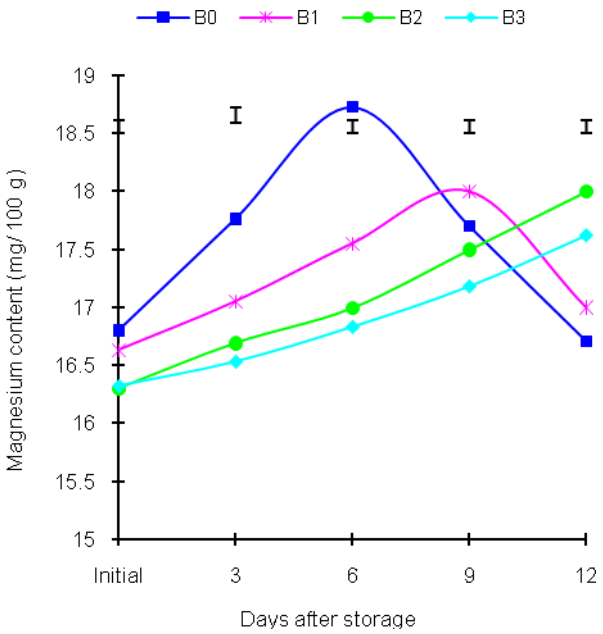


Figure 2. Effect of different doses of BDF on Magnesium content of mango pulp at different days after storage. Vertical bars represent LSD at 0.05 levels.

Copper content

Variation between varieties mean in terms of Cu content of mango pulp demonstrated highly significant at different days after storage. The results denoted that Cu content of mango pulp diminished in a continuous stream with the passing of storage period (Table 3). It also narrated that Cu content of the Khirshapat was higher as compared to Langra. At initial day, higher (0.36 mg/100 g) content of Cu was noted in the Khirshapat and lower (0.33 mg/100 g) was noticed in Langra, respectively. At 12th day, Khirshapat gave higher (0.19 mg/100 g), quantity of Cu and lower (0.16 mg/100 g) was noted in the Langra. These happened might be probably due to genetical dissimilarities between the varieties. There were no available research reports on Cu content of mango pulp at the scientific literature. The results of the present studies revealed that green mangoes contained more copper comparing to stored mangoes and the Khirshapat was fairly good in copper accumulation than the Langra. The present research findings also revealed that Cu content came down gradually during storage period.

Different doses of BDF solution implied to the present study in connection with Cu content of mango pulp exhibited significant variation at different days after storage. The results narrated that Cu content fell off gradually with the advancement of storage period. The diminishing trend from control was higher than the fruit treated with B_1, B_2 and B_3, treatments respectively (Figure 3). At 12th day, higher quantity of Cu (0.24 mg/100 g) was noticed from the fruit treated with B_3 treatment but, it was statistically at par with B_2 treatment while; lower (0.11 mg/100 g) was noticed from control. The data of B_3 treatment recorded from the investigation was fairly good over the other treatments in Cu preservation. So, the present findings revealed that B_3 treatment was much better in mango preservation.

The combined effect of varieties and various doses of BDF solution were observed to be non significant in connection with Mg content at various days after storage. The results were noticed to be slightly extending trend of Mg content of mango pulp with the growing up of storage time (Table 2). At 6th day, the highest quantity (19.15

mg/100 g) of Mg was manifested from the treatment combination of V_1B_0 while; the lowest (16.25 mg/100 g) was reported from the treatment combination of V_2B_3.

Table 2. Combined effects of varieties and different doses of BDF solution on calcium and magnesium content of the postharvest mango pulp during storage at ambient condition

Treatments combination	Calcium content (mg/100 g) at different days					Magnesium content (mg/100 g) at different days				
Varieties × Treatments	Initial	3	6	9	12	Initial	3	6	9	12
V_1B_0	10.75 d	15.48b	22.32	23.93c	20.32g	17.25	18.22	19.15	18.12	17.16
V_1B_1	10.82 d	13.42d	16.62	22.26d	23.35c	17.15	17.55	18.05	18.55	17.55
V_1B_2	10.65 d	12.25e	14.23	17.55f	22.17d	16.75	17.23	17.52	17.92	18.42
V_1B_3	10.72 d	12.02 f	13.34	15.94g	19.16h	16.88	17.12	17.41	17.72	18.12
V_2B_0	12.58 a	17.15a	23.98	25.58a	21.98e	16.35	17.30	18.28	17.28	16.27
V_2B_1	12.48ab	15.48b	18.67	24.32b	25.42a	16.11	16.55	17.05	17.45	16.45
V_2B_2	12.35 b	13.95c	15.92	19.22e	23.84b	15.85	16.15	16.45	17.05	17.55
V_2B_3	12.16 c	13.47d	15.17	17.45f	20.68f	15.75	15.95	16.25	16.65	17.12
Level of significance	*	**	NS	**	**	NS	NS	NS	NS	NS
CV%	0.92	0.75	1.15	0.51	0.48	0.64	0.67	0.61	0.60	0.62

In a column values having the same letter(s) do not differ significantly as per DMRT at 5% level; V_1 = Langra; V_2 = Khirshapat; * and ** indicate 5%, and 1% levels of probability, and NS =non-significant.

Table 3. Pattern of copper and iron content of the postharvest mango pulp between two varieties during storage environments at ambient condition

Treatments	Copper content (mg/100 g) at different days					Iron content (mg/100 g) at different days				
Variety (V)	Initial	3	6	9	12	Initial	3	6	9	12
V_1	0.33 b	0.28 b	0.24 b	0.20 b	0.16 b	2.59 a	3.26 a	4.44 a	5.02 a	4.72 a
V_2	0.36 a	0.32 a	0.27 a	0.23 a	0.19 a	1.70 b	2.32 b	3.50 b	3.80 b	3.30 b
Level of significance	***	***	***	***	***	***	***	***	***	***

Different doses of BDF solution implied to the present study in connection with Cu content of mango pulp exhibited significant variation at different days after storage. The results narrated that Cu content fell off gradually with the advancement of storage period. The diminishing trend from control was higher than the fruit treated with B_1, B_2 and B_3, treatments respectively (Figure 3). At 12th day, higher quantity of Cu (0.24 mg/100 g) was noticed from the fruit treated with B_3 treatment but, it was statistically at par with B_2 treatment while; lower (0.11 mg/100 g) was noticed from control. The data of B_3 treatment recorded from the investigation was fairly good over the other treatments in Cu preservation. So, the present findings revealed that B_3 treatment was much better in mango preservation.

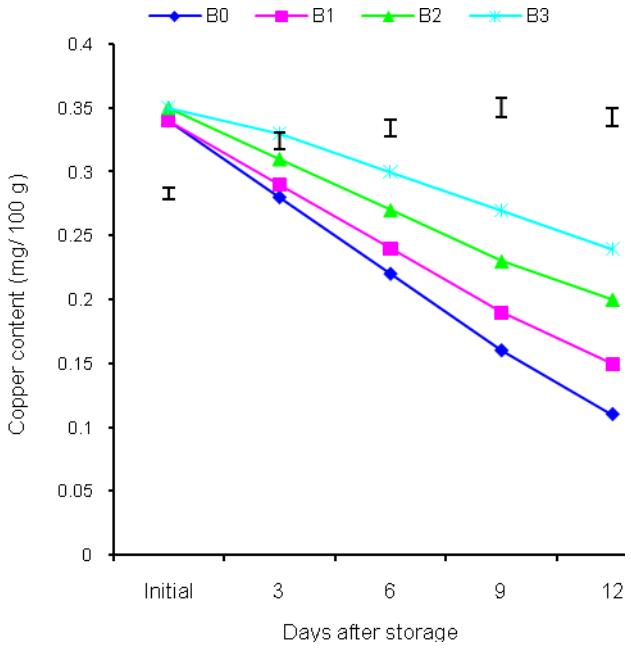


Figure 3. Effect of different doses of BDF on copper content of mango pulp at different days after storage. Vertical bars represent LSD at 0.05 levels.

The combined effect of varieties and applied different doses of BDF solution in relation to Cu content of mango pulp were found to be non significant variation at various days after storage. The results stated that Cu content in different treatment combination came down with the extension of storage duration. At 12th day, the highest (0.24 mg/100 g) was derived from the treatment combination of V_2B_3, which was statistically at par with V_1B_3, V_2B_2 and V_1B_2 and the lowest (0.09 mg/100 g) was derived from the treatment combination of V_1B_0 but, it was statistically at par with V_1B_1 and V_2B_2 (Table 4).

Iron content

The analysis of variance of varieties in connection with Fe content of mango pulp was observed to be highly significant at different days after storage. The results found an extending trend of Fe content with the advancement of storage duration. The growing up trend of Fe content was more or less similar from initial to 9 days thereafter, it abated slightly. At 12th day, higher (4.72 mg/100 g) quantity of Fe was reported from the Langra and lower (3.30 mg/100 g) was reported from the Khirshapat (Table 3). Highly significant variation was noticed to be due to the effect of different doses of BDF solution in connection with Fe content of mango pulp at various days after storage. The results obtained from the study indicated that Fe content was enriched hastily from initial to 6th day and then, it came down significantly at control and similarly B_1 treated fruits abated of Fe content after 9th day. But, Fe content

recorded from the other fruits treated with B_2 and B_3 treatment extended successively up to 12th day (Figure 4). At 12th day, the maximum (4.59 mg/100 g) quantity was derived from the fruit treated with B_2 treatment but, it was statistically at par with B_3 while; the lowest (2.89 mg/100 g) was derived from the untreated fruit due to starting decay. A smaller quantity of Fe obtained from untreated fruits at 12th day might be due to starting decomposition. On the other hand, B_3 treated fruits were fairly good because of its lower achievement of Fe content with the increase of storage duration.

Table 4. Combined effects of varieties and different doses of BDF solution on copper and magnesium content of the postharvest mango pulp at ambient condition

Treatments combination	Copper content (mg/100 g) at different days					Iron content (mg/100 g) at different days				
Varieties × Treatments	Initial	3	6	9	12	Initial	3	6	9	12
V_1B_0	0.31	0.25	0.19	0.14	0.09	2.82	3.82	5.92	5.32 a	3.42 c
V_1B_1	0.32	0.27	0.22	0.17	0.13	2.65	3.35	4.45	5.35 a	4.64 b
V_1B_2	0.34	0.30	0.26	0.22	0.19	2.52	3.12	3.92	5.02 b	5.52 a
V_1B_3	0.33	0.31	0.28	0.25	0.23	2.35	2.75	3.45	4.38 cd	5.31 a
V_2B_0	0.36	0.30	0.24	0.18	0.13	1.88	2.78	4.88	4.25 d	2.35 d
V_2B_1	0.35	0.31	0.26	0.21	0.17	1.73	2.32	3.42	4.45 c	3.75 c
V_2B_2	0.36	0.32	0.28	0.24	0.21	1.64	2.25	3.05	3.15 f	3.65 c
V_2B_3	0.37	0.34	0.31	0.28	0.24	1.53	1.94	2.64	3.35 e	3.46 c
Level of significance	NS	NS	NS	NS	NS	NS	NS	NS	***	***
CV%	3.10	3.54	4.16	5.02	6.10	4.96	3.80	2.67	2.41	4.78

In a column values having the same letter(s) do not differ significantly as per DMRT at 5% level; V_1 = Langra; V_2 = Khirshapat; *** indicates 0.1% level of probability, and NS = non-significant.

The combined effect of varieties and different doses of BDF solution were observed to be non significant variation in relation to Fe content of mango pulp at different days after storage except 9 and 12th day. The results narrated that enhancing trend of Fe content was found from initial to 6 days thereafter, it came down very fast from the treatment combination of V_1B_0 while; the lowest trend was found from the treatment combination of V_2B_3 (Table 4). At 9th day, the highest (5.35 mg/100 g) quantity was recorded from the treatment combination of V_1B_1 and the lowest (3.15 mg/100 g) was recorded from the treatment combination of V_2B_2.

Manganese content

Manganese content of mango pulp was noticed to be differed significantly in both the varieties mean at different days after storage. The results elucidated that Mn content extended gradually with the extension of storage period (Table 5). It also stated that the Langra performed better in Mn accumulation comparing to the Khirshapat. At 9th day, higher (1.20 mg/100 g) quantity of Mn was rnoted in the Langra while; lower (1.05 mg/100 g) was noted in Khirshapat. There were no available research reports in terms of Mn content in the scientific literature. The results of the present research revealed that the Langra was fairly good than the Khirshapat in Mn accumulation and it extended during storage period.

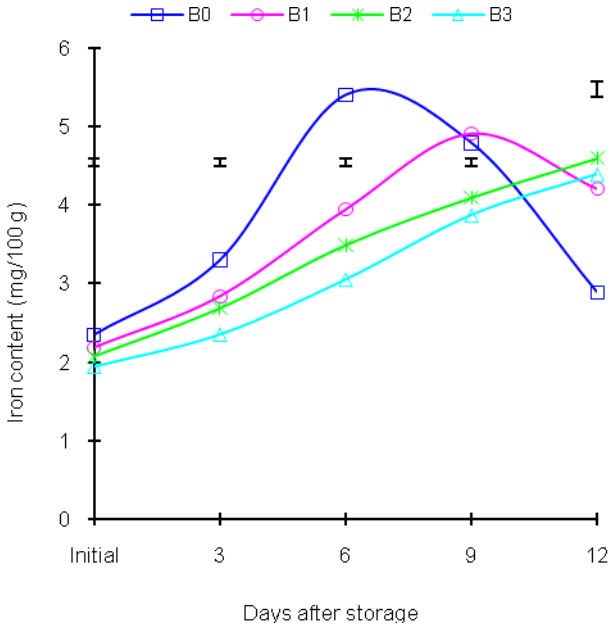


Figure 4. Iron content of mango pulp as influenced by different doses of BDF at different days after storage. Vertical bars represent LSD at 0.05 levels.

Table 5. Behavior of manganese and zinc content of the postharvest mango pulp in two varieties during storage environments at ambient condition

Treatments	Manganese content (mg/100 g) at different days					Zinc content (mg/100 g) At different days				
Variety (V)	Initial	3	6	9	12	Initial	3	6	9	12
V_1	0.63 a	0.84 a	1.07 a	1.21 a	1.20 a	1.26 b	1.19 b	1.06 b	0.90 b	0.73 b
V_2	0.47 b	0.68 b	0.91 b	1.05 b	1.05 b	1.47 a	1.30 a	1.18 a	1.02 a	0.85 a
Level of significance	***	***	***	***	***	***	***	***	***	***

Different doses of BDF solution were found to be highly significant in connection with Mn content of mango pulp at different days after storage. The results explained that Mn content extended continuously from initial to 6th days, and then it came down sharply in control. On the other hand, it increased from initial to 9th day thereafter; it diminished in the fruit treated with B_1 treatment. At the same time, very lesser augmenting trend of Mn content was perceived from the fruit treated with B_3 treatment (Figure 5). At 12th day, Mn content ranged between 0.89 to 1.33 mg per 100 g of fresh mango pulp. The maximum (1.33 mg/100 g) was recorded from B_2 treated fruits and the minimum (0.89 mg/100 g) was recorded from control. There were no available research findings in terms of Mn

content in the scientific literature. But, the data of the present research revealed that B3 treatment showed profound effect in delay ripening which resulted in lesser extending trend of Mn and keeping the quality good in preservation.

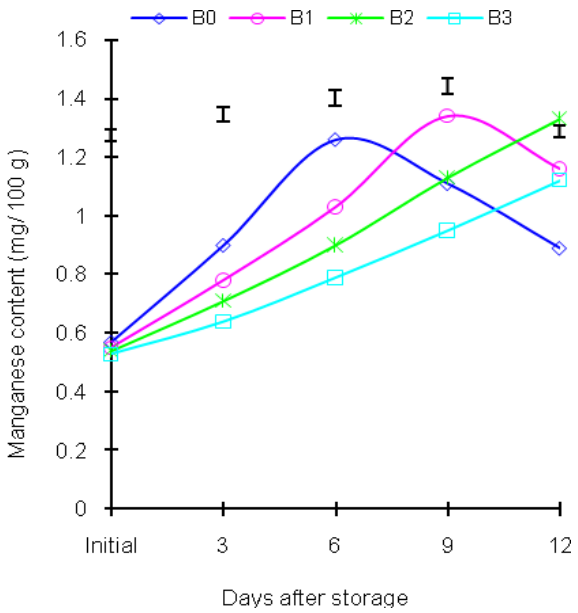


Figure 5. Manganese content of mango pulp as influenced by different doses of BDF at different days after storage. Vertical bars represent LSD at 0.05 levels.

The combined effect of varieties and imposed different doses of BDF solution in relation to Mn content of mango pulp were observed to be non significant at various days after storage. The results were exposited that a growing up trend of Mn content was perceived in different treatment combination with the extension of storage duration (Table 6). At 9th day, the highest (1.42 mg/100 g) was listed from the treatment combination of V_1B_1 and the lowest (0.87 mg/100 g) was listed from the treatment combination of V_2B_3.

Zinc content

Variation in respect of Zinc content of mango pulp due to the effect of varieties showed highly significant at different days after storage. The results indicated that Zn content came down markedly with the extension of storage duration from both the varieties (Table 5). It was also exposited that the Khirshapat was noticed better in Zn content accumulation as compared to the Langra. At initial stage, higher (1.47 mg/100 g) was derived from control and lower (1.26 mg/ 100 g) was derived from the Langra. Again, at 12th day, higher (0.85 mg/100 g) was noticed from Khirshapat and the lesser (0.73 mg/100 g) was recorded from the Langra. There were no available research findings in terms of Zn content in the scientific review. The results of the present studies invented that green mango especially, the Khirshapat received more quantity of Zn than Langra, but, it continuously reduced with the increase of storage duration.

Different doses of BDF solution were found to be significant in connection with Zn content of mango pulp at different days after storage. The results observed an extending trend of Zn content of mango pulp with the advancement of storage period from the fruit treated with different doses of BDF solution. It also stated that the coming down trend was very high in control and very low in the fruit treated with B_3 treatment (Figure 6). At 12th day, the maximum (0.96 mg/100 g) was noticed from the fruit treated with B_3 treatment and the lowest (0.65 mg/100 g) was noticed from control. Zn content of mango pulp decreased during storage period was possibly due to transmission of Zn from pulp to stone and peel at stored condition or Zn content of mango pulp might have been depressed or suppressed as influenced by metabolic activities during storage.

The combined effect of varieties and subjected to different doses of BDF solution on Zn content of mango pulp demonstrated non significant variation at different days after storage except initial day. An expanding trend of Zn content of mango pulp was recorded from various treatment combinations (Table 6). At initial day, the maximum (1.52 mg/100 g) quantity of Zn was obtained from Khirshapat along with B_3 treatment while; the lowest (1.24 mg/100 g) value was obtained from Langra using no treatment.

Table 6. Combined effects of varieties and different doses of BDF solution on iron and manganese content of postharvest mango pulp at ambient condition

Treatments combination	Manganese content (mg/100 g) at different days					Zinc content (mg/100 g) at different days				
Varieties × Treatments	Initial	3	6	9	12	Initial	3	6	9	12
V_1B_0	0.65	0.98	1.34	1.19	0.96	1.26 c	1.13	0.97	0.76	0.53
V_1B_1	0.64	0.87	1.12	1.42	1.24	1.28 c	1.17	1.02	0.85	0.67
V_1B_2	0.62	0.78	0.97	1.21	1.40	1.24 c	1.21	1.10	0.96	0.82
V_1B_3	0.60	0.72	0.86	1.02	1.19	1.25 c	1.25	1.14	1.03	0.91
V_2B_0	0.49	0.82	1.18	1.03	0.82	1.45 b	1.26	1.10	0.89	0.66
V_2B_1	0.46	0.69	0.94	1.25	1.07	1.46 b	1.29	1.15	0.98	0.81
V_2B_2	0.47	0.63	0.82	1.05	1.25	1.44 b	1.32	1.21	1.07	0.93
V_2B_3	0.45	0.56	0.71	0.87	1.05	1.52 a	1.34	1.24	1.13	1.01
Level of significance	NS	NS	NS	NS	NS	*	NS	NS	NS	NS
CV%	3.87	2.81	2.14	1.88	1.89	1.56	1.70	1.90	2.21	2.68

In a column values having the same letter(s) do not differ significantly as per DMRT at 5% level; V_1 = Langra; V_2 = Khirshapat; * and *** indicate 5% and 0.1% level of probability, and NS = non-significant

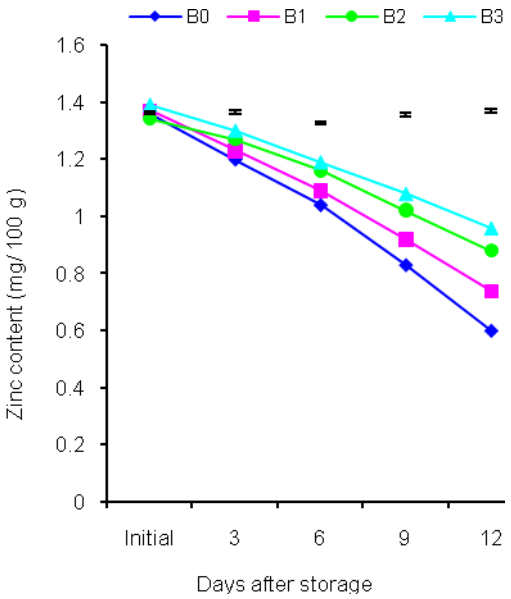


Figure 6. The effect of different doses of BDF on Zinc content of mango pulp at different days

after storage. Vertical bars represent LSD at 0.05 levels.

Conclusion

Results of the interaction effect of varieties and different treatments in different experiments were found to be non-significant in terms of most of the mineralogical properties. The combination of the Langra and control treatment progressively augmented in magnesium and iron content up to a point of ongoing metabolic cycle and thereafter, these compositions decreased. The Khirshapat using no treatment accumulated calcium content up to ongoing metabolic activities but, using 750 ppm of bavistin DF solution strongly interrupted these activities. The Khirshapat along with 750 ppm of Bavistin DF solution extended shelf life up to 17.33 days after storage. Therefore, 750 PPM solution of Bavistin DF was found the best method for preservation and delay ripening of postharvest mango which might be easily adopted by common people for mango preservation.

References

1. Shahjahan, M. S., Sheel, M. A., Zaman, M. A. & Sakur, M. A. (1994). Optimization of harvesting maturities for major mango cultivars in Bangladesh. *Bangladesh J. Sci. Res.* 12: 209-215.
2. Pal, R. K. (1998). Ripening and physiological properties of mango as influenced by ethereal and carbide. *J. Food Sci. Technol.,* 35: 358-360.
3. Purohit, A. G. (1985). Fruit trees for social forestry. *Indian Hort.,* 30: 3-11.
4. Singh, J. N., Pinaki, A. & Singh, B. B. (2000). Effect of GA_3 and plant extracts on storage behavior of mango (*Mangifera indica* L.) cv. Langra. *Haryana J. Hort. Sci.,* 29: 199-200.
5. Samad, M. A., Farruque, A. M. M. & Malek, A. (1975). A Study on the Biochemical Characteristic of the fruit of some mango variety of Bangladesh. *Bangladesh J. Sci. Res.,* 12: 28-32.
6. Lashley, D. (1984). Advances in postharvest technology and new technology in food production. *Proc. Seminar. St. Augustine (Trinidad Tobago),* pp. 173-183.
7. Tefera, A., Seyoum, T. & Worldetsadik, K. (2007). Effect of disinfection, packaging and storage environment on the shelf life of mango. Biosystem Engineering. Oxford, UK: Elsevier, 96: 201-212.
8. Ranjan, A., Raj, R. N. & Prasad, K. K., (2005). Effect of postharvest application of calcium salts and GA_3 on storage life of mango (*Mangifera indica* L.) cv. Langra. *J. Applied Biol. Patna India,*15: 69-73.
9. Sakhale, B. K. & Kapse, B. M. (2012). Studies on shelf life extension of sweet oranges (*Citrus sinensis* L.). *Int. Food Res. Jour.,* 19: 779-781.
10. Sandeep, K. C., Thakur, K. S., Jawa, N. K. & Thakur, K. P. (2012). Botanical formulation and extracts based on plant eaves and flower, a substitute for toxic chemical and waxes for shelf life extension and quality retention of apple cv Starking Delicious in India. *Journal of Hort. and Forestry,* 4: 190-100.
11. Azad, P. (1992). Efficacy of certain fungitoxicants against Colletotrichum capsici (Syd) Butler and Bisby, the incitant of ripe fruit Rot of chilli. *J. Assam Sci. Soc.,* 34: 34–39.
12. Mishra, D. (1988). Fungicides control of anthracnose and fruit rot of chilli. *Indian J. Agric. Sci.,* 58: 147–149.
13. Gomez, K. A. & Gomez, A. A. (1984). Statistical Procedures for Agricultural Research. *John Weley and Sons.* Inc. New York. pp. 67-215.
14. Petersen, L. (2002). Analytical Methods- Soil, Water, Plant material, Fertilizer. Soil Resources Management and Analytical Services, Soil Resource Dev., Inst. Danida, Dhaka. pp. 61-70.
15. Peter, M., Fweja, L., Chove, B., Kinabo, J., George, V. & Mtebe, K. (2007). Physical and chemical characteristics of off vine ripened mango (*Mangifera indica* L.) fruit (Dodo). *African J. Biotech.,* 6: 2477-2483.

The Malaysian Journal of ANALYTICAL SCIENCES ISSN 1394-2506

GRAPHENE COLLOIDAL DISPERSION IN VARIOUS ORGANIC SOLVENTS

(Penyerakan Koloid Grafin dalam Pelbagai Pelarut Organik)

Ainee Fatimah Ahmad[1], Fatin Humaizah Abd Moin[1], Hur Munawar Kabir Mohd[1], Irman Abdul Rahman[1], Faizal Mohamed[1], Chia Chin Hua[1], Suria Ramli[2], Shahidan Radiman[1]*

[1]*School of Applied Physics,*
[2]*School of Chemical Sciences and Food Technology,*
Faculty of Science and Technology,
Universiti Kebangsaan Malaysia, 43600 Bangi, Selangor, Malaysia.

**Corresponding author: shahidan@ukm.my*

Abstract

Graphene is an atom thick carbon-based material that has many intriguing physical and chemicals properties. Since stacks of graphene form graphite, graphene can be produce by chemical exfoliation of graphite in surfactant solution. In this study, the colloidal dispersions of graphene in a variety of organic solvents such as isopropanol, tetrahydrofuran (THF),N-methylpyrrolidone (NMP) and gamma-butyrolactone (GBL) were prepared. Dispersion by bath sonication provides mechanical disruption that breaks apart the graphite flakes, which is then sterically stabilized in the solvent system. FTIR analysis has confirmed the presence of the C=C groups in the samples. By analyzing bright-field TEM images obtained from each dispersion, we have found that the graphene dispersed in isopropanol and THF are multilayered, wrinkled and overlapping graphene sheets; while samples in NMP and GBL are less thick with predominantly folded graphene sheets. The stronger solvents such as NMP and GBL are more effective than isopropanol and THF in obtaining stable graphene dispersions. This will be useful for self-assembly work by dip-coating or monolayer method in the future.

Keywords: graphene, tetrahydrofuran (THF), N-methylpyrrolidone (NMP), gamma-butyrolactone (GBL), Fourier transform infrared spectroscopy (FTIR)

Abstrak

Grafin adalah bahan berasaskan karbon setebal satu atom yang mempunyai ciri-ciri fizikal dan kimia yang menarik. Memandangkan grafit adalah himpunan grafin, ia boleh dihasilkan melalui pengelupasan kimia grafit dalam larutan surfaktan. Dalam kajian ini, serakan koloid grafin telah disediakan dalam pelbagai jenis pelarut organik seperti isopropanol, tetrahidrofuran (THF), N-metilpyrrolidon (NMP) dan butirolakton gama (GBL). Penyerakan oleh sonikasi rendaman memberi gangguan mekanikal yang memisahkan empingan grafit, yang kemudiannya stabil secara sterik dalam sistem pelarut. Analisis FTIR telah mengesahkan kehadiran kumpulan C=C dalam sampel tersebut. Dengan mengkaji imej TEM bagi setiap serakan, didapati sampel dalam larutan isopropanol dan THF merupakan berbilang lapis, berkedut dan helaian grafin yang bertindih; manakala sampel dalam larutan NMP dan GBL adalah kurang tebal dengan sebahagian besarnya dalam bentuk kepingan grafin yang berlipat. Dapat dilihat bahawa pelarut yang lebih kuat seperti NMP dan GBL lebih berkesan daripada isopropanol dan THF dalam menghasilkan penyerakan grafin yang stabil. Hal ini berguna untuk sua-aturan melalui kaedah penyalutan-celup atau kaedah monolapisan pada masa akan datang.

Kata kunci: grafin, tetrahidrofuran (THF), N-Metilpyrrolidon (NMP), butirolakton gama (GBL), Spektoskopi Inframerah Jelmaan Fourier (FTIR).

Introduction

Graphene is a flat monolayer of carbon atoms tightly packed into a two-dimensional honeycomb lattice, and is the basic building block for all carbon nanostructure [1]. Graphene has shown many intriguing properties including high mobility of charge carriers (20000 $cm^2V^{-1}s^{-1}$), high surface area (≈2600 m^2/g), high mechanical strength (≈1 Tpa), and extremely high thermal conductivity (5000 W/mK) [2, 3].

In 2004, Novoselov and Geim developed a micromechanical exfoliation method that consist of repeated peeling of graphite flakes using adhesive tape until the thinnest flakes are obtained which were then transferred onto a clean substrate by gentle pressing of the tape [4]. This method relies on the balance between the inter-layer cohesion and long distance interactions between the tape or the substrate and graphene [1]. In the chemical exfoliation process, the insertion of reactants in the inter-layer space weakens the van der Waals cohesive force. The loosened layer stacking is disrupted when the intercalant decomposition produces a high gas pressure of CO_2 by a rapid annealing to 1050°C. As a result, the sp^2 lattice is partially degraded into sp^2-sp^3 sheet that possesses less π-π stacking stability [1].

Chemical exfoliation can be performed in a suspension known as graphite oxide. The most common method to produce graphite oxide was reported by Hummer [5], where graphite is dispersed into a mixture of concentrated sulfuric acid, sodium nitrate and potassium permanganate at 45°C for a couple of hours. In this compound, the graphite layers remain largely intact and the quest molecules or atoms are located in between. To obtain a few or even single sheet materials, the intercalated reactant is decomposed to produce large amounts of gas in the van der Waals space by chemical or thermal means [6]. Then, rapid annealing to 1050°C generates a CO_2 over pressure and splits the graphite oxide into individual sheets [7]. Graphene oxide solutions are yellow in colour or greenish-blue when non-oxidized graphene sheets are the major constituents [8].

Graphene oxide (GO) shows different electronic properties than individual semi-metallic graphene layer obtained by micromechanical exfoliation because this chemical approach converts a large fraction of the sp^2 carbon into sp^3configuration [1]. Thus, a chemical reduction treatment is required for the recovery of the specific properties of graphene. One of the effective reducing agent for graphene oxide is hydrazine(NH_2-NH_2), which is unfortunately a highly toxic reagent [3,9]. GO could be regarded as graphene functionalized by carboxylic acid, hydroxyl and epoxide groups. Hence, these functionalized groups make GO easily dispersed into a few select polar solvents that form an intercalated composite with polar molecules [10, 11]. The intercalation of solvent causes the graphene sheet to swell and lose its mechanical integrity [12]. Nevertheless, large quantities of structural defects introduced by the oxidation process shifts the physical properties away from pristine graphene [13].

In this study, a more straight forward method based on solvation is used, where graphite is dispersed and sonicated in organic solvents to produce graphene sheets. This method is technically similar to the graphene oxide exfoliation method, minus the oxidation step [1]. Solvent or surfactant stabilised graphene is attractive due to its defect free nature for many applications. However, this method produces graphene with a relatively low single-layered content [3,13]. The dispersed materials remains a concentrated suspension of defect free, un-oxidized sp^2 graphene which can be further homogenized by centrifugation to yield a solutions with 1µm diameter single sheets of graphene [1]. According to Soldano et al. [1], NMP shows the best thermodynamic stabilization and most concentrated suspensions. Furthermore, this colloidal dispersion in solvents is not oxidized to yield genuine graphene.

In this study, graphene was prepared in different solvents under ultrasonic condition and analysed by FTIR and TEM. FTIR analysis of the graphene colloidal dispersion in the NMP solvent was carried out to confirm the presence of C=C bonds of graphene in the sample, while TEM was used to elucidate the morphology of the different graphene sheets.

Materials and Methods

Sample Preparation

In this study, 2mg of sieved graphite powder (Aldrich product 332461) was dispersed in 20ml of isopropanol by bath sonication. Sonication of the dispersion was carried out using a WiseClean WUC-DIOH 200W, 40 kHz, 30% amplitude) ultrasonic bath up to 49 hours. Dispersion by bath sonication provided the mechanical disruption that broke apart the graphite flakes, which was then stabilized by the solvent system [14]. After sonication, the dispersion was grey in color and left to stand for about 24 hours to allow any unstable aggregates to form. To remove these aggregates and stabilise the dispersion, the top 16ml of the dispersion was taken out and consequently centrifuged for 30 minutes at ~15,000 rpm. After this primary centrifugation, the top 13ml of the dispersion was decanted by pipette, forming a homogeneous black dispersion which was retained for use. This procedure was repeated for the three other organic solvents: Tetrahydrofuran (THF), N-Methylpyrrolidone (NMP) and γ-Butyrolactone (GBL). After the final decantation, a small level of sedimentation occurred within 1 week in the isopropanol and THF dispersions and within 2 weeks in NMP and GBL. This suggests that NMP and GBL

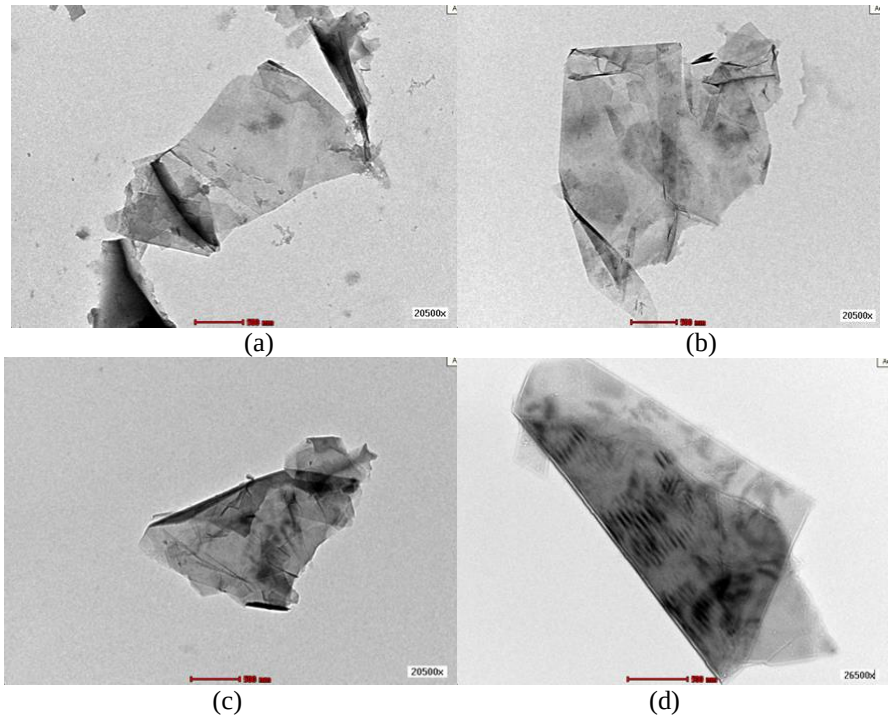
produced more stable dispersions than isopropanol and THF. Isopropanol is inexpensive and easy to use but solvents like THF, NMP, and GBL are expensive and toxic materials, which require special care when handling.

Characterization

Transmission Electron Microscopy (TEM) images were taken in bright field mode on Tecnai Spirit BioTwin microscope using an accelerating voltage of 120kV. Samples were prepared by dropping a small amount of each dispersions onto Formvar grids. Attenuated total reflectance FTIR (Perkin Elmer BX Spectrophotometer) spectra for graphene dispersion in NMP was used as the representative sample to confirm the presence of the C=C bond in the samples. The solvent NMP has been reported to yield high quality graphene sheets because of the strong interaction between NMP and carbon nanotube sidewall that makes the energetic penalty of exfoliation and solvation become small. Hence, a similar effect is suggested to may be occur between this solvents and graphene [3,15].

Results and Discussion

Figure 1 shows the top-view of bright-field transmission electron microscopy (TEM) images of graphene dispersion in isopropanol, THF, NMP and GBL. By analyzing the TEM images of each dispersion, the morphology of graphene in isopropanol (a) and THF (b) are mostly multilayered, wrinkled and overlapping graphene sheets [10]; while graphene in the NMP (c) and GBL (d) dispersions are less thick, with predominantly folded graphene sheets. In all cases, all graphene sheets have lateral sizes between2- 4 µm [3] from high-magnification TEM image and the sheet edges tend to scroll and fold slightly. The lack of any individual monolayer graphene sheetssuggested thatthe graphite is not fully exfoliated.In order to achieve single or double layered graphene, graphite needs to be re-exfoliated, and consequently ultrasonicated up to 168 hours before finally centrifuged to get a uniform distribution [13,16]. Separation of graphene layers depends on the mechanical disruption of the graphene stacking by ultrasonication [1]. From these images, we can conclude that NMP and GBL are better solvents than isopropanol and THF to yield a stable layer dispersion of graphene.



(a) (b)

(c) (d)

Figure 1. Bright field TEM images of graphene sheet in (a) multi-layered/overlapping in isopropanol, (b) wrinkled/scrolled in THF, less thickness with folded layer in (c) NMP and (d) GBL.

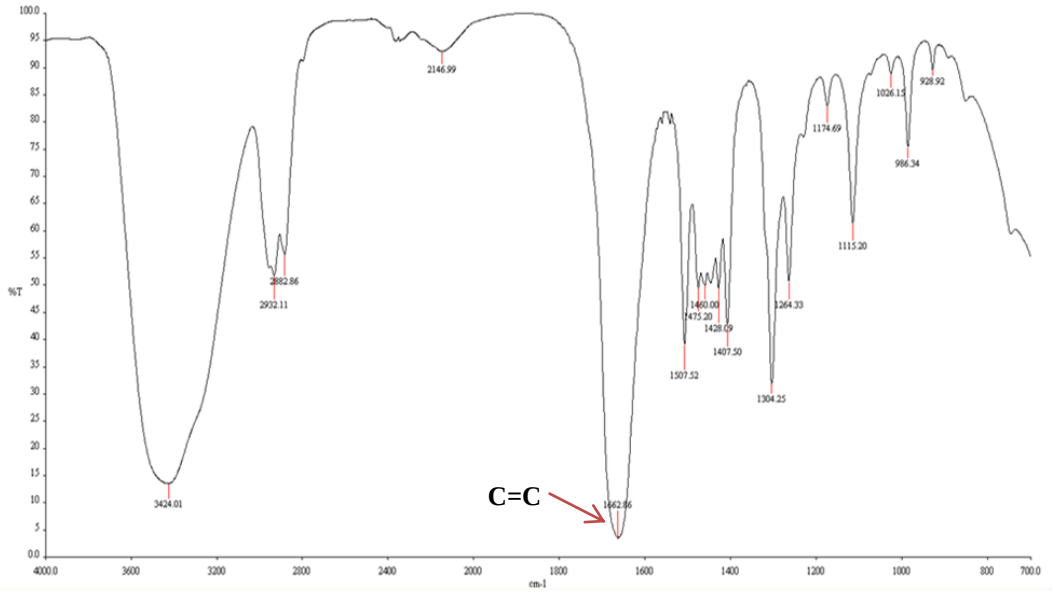


Figure 2. FTIR spectra of graphene dispersion in NMP shows peaks associated with C=C (~1662cm^{-1}) and N-H (~3424cm^{-1}).

FTIR spectra of graphene dispersed in NMP was obtained. The spectra in Figure 2 shows peaks associated with the C=C (~1662cm^{-1}) and N-H (~3424cm^{-1}) bands. The 2932 cm^{-1}, 2882cm^{-1}, 2146 cm^{-1}, 1460 cm^{-1}and 1174 cm^{-1}bands correspond to the C-H stretching vibrations of the hydrocarbon group. The C=C stretch band indicates the presence of graphene in the dispersion, where the C=C stretch band shows the remaining sp^2character [17].

Successful dispersion of graphene monolayers was reported by Hernandez et al. [15], where graphite was almost completely exfoliated to multilayer structures with less than 5 layers in NMP, GBL and N,N'-Dimethylethyleneurea (DMEU), with significant quantities of individual monolayers. The authors estimate that the fraction of monolayer graphene in their NMP dispersion as 28%.

The dispersion in NMP can be improved by intercalating graphite with alkaline metals like potassium [18]. In this compound, electrons from the metallic potassium transfers to graphene and reduces the carbon atoms; forming negatively charged sp^2 graphene. When exposed to NMP, the satked sheets exfoliate and form a stable suspension, even without the ultrasonication process [18]. Polyvinylpyrrolidone, PVP can be used as a graphene dispersion stabilizer in a variety of solvents by preventing reaggregation by adsorbing on the graphene surface. By using PVP, graphene flakes forms a stable solution in comparison to without the PVP and can be easilly sedimented out through centrifugation [19]. Use of PVP as stabilizer will be explored in our future experiment.

Graphene dispersion is stabilized against re-aggregation by the presence of repulsive interactions between nearby surfactant-coated graphene. Surfactant consists of a hydrophilic head group and hydrophobic tail group. The structure of the head group controls the nature of the repulsive interactions [20]. Non-ionic surfactants have a polar head group, while ionic surfactants have an ionic head group. Thus, the repulsions are electrostatic in nature for ionic surfactants [20,21]. For non-ionic surfactants, the repulsions can be due to many sources such as steric interaction [22]. This method will be explored in our future work whilst preparing dispersions of graphene in a range of surfactants, in order to gain understanding the physico-chemistry of the surfactant-stabilization process [20].

Chemical exfoliation acts by weakening the van der Waals (VDW) cohesive forces upon insertion of reactants in the inter-layer space. Surface energy for graphite is defined as the energy per unit area required to overcome the VDW forces when peeling 2 sheets apart, with the literature suggested value of ~70-80 mJm^{-2} [15]. Thus, an energy input of over $2eV/nm^2$ of graphene surface is required to exfoliate pristine graphene into solution [1,14].

Conclusion

Colloidal dispersion in solvent under ultrasonic condition was shown as a simple method to produce graphene of few layers without the need of oxidization with different solvents. The lack of single layered graphene sheets suggests that the graphite used as the feeder material was not fully exfoliated. NMP and GBL were found to be stronger solvents and more effective than isopropanol and THF in yielding stable graphene dispersions. The FTIR spectra obtained from the dispersion in NMP displayed the presence of the C=C bond, which confirmed the presence of graphene in the dispersion. TEM revealedthat the graphene-sheets obtained by sonication and centrifugationwere multilayered, wrinkled and overlapped in the isopropanol and THF solvents, while samples in NMP and GBL were less thick, with predominantly folded graphene sheets.This dispersion method offers a straight forward and low cost alternative to produce graphene for various technological applications like graphene based composites or solar cells [16].

Acknowledgement

The authors would like to acknowledge the financial support from UKM in this study, through grants UKM-GUP-2011-214, ERGS/1/2012/STG02/UKM/02/01, UKM-AP-NBT-15-2010 and UKM-PTS-011-2010.

References

1. Soldano, C., Mahmood, A. & Dujardin, E. (2010). Production, Properties and Potential of Graphene. *Carbon*, 48:2127-2150.
2. Geim, A.K. & Novoselov, K.S. (2007). The Rise of Grapehene. *Nature Materials*, 6:183-191.
3. Park, S. & Ruoff, R.D. (2009). Chemical methods for the production of graphenes. *Nature Nanotechnology* 4:217-224.
4. Novoselov, K.S., Geim, A.K., Morozov, S.V., Jiang, D., Zhang, Y., Dubonos S.V., Grigorieva, I.V. & Firsov, A.A., (2004). Electric Field Effect in Atomically Thin Carbon Films. *Science*, 306:666-669.
5. Hummers, W.S. & Offeman, R.E. (1958). Preparation of Graphite Oxide. *Journal of the American Chemical Society*, 80(6):1339.
6. Dressehaus, M.S. & Dressehaus, D. (2009). Intercalation Compounds of Graphite. *Advance Physics*, 51(1):1-186.
7. Schniepp, H.C., Li, J.L., McAllister, M.J., Sai, H., Herrera-Alonso, M. & Adamson D.H. (2006). Functionalized Single Graphene Sheets Derived from Splitting Graphite Oxide. *Journal of Physical Chemistry B*, 110(17):8535-8539.
8. McAllister, M.J., Li, J.L., Adamson, D.H., Schniepp, H.C., Abdala, A.A. & Liu, J. (2007). Single Sheet Functionalized Graphene by Oxidation and Thermal Expansion of Graphite. *Chemistry of Material*, 19(18):4396-4404.
9. Li, D., Muller, M.B. Gilje, S., Kaner, R.B. & Wallace, G.G. (2008). Processable Aqueous Dispersions of Graphene Nanosheets. *Nature Nanotechnology*, 3(2):101-105.
10. Chen, Y., Qi, Y., Tai, Z., Yan, X., Zhu, F., & Xue, Q. (2012). Preparation, mechanical properties and biocompatibility of graphene oxide/ultrahigh molecular weight polyethylene composites. *European Polymer Journal*, 48:1026-1033.
11. Zhou, X.Z., Huang, X., Qi, X.Y., Wu, S.X., Xue, C., Boey F.Y.C., Yan, Q., Chen, P. & Zhang, H. In situ synthesis of metal nanoparticles on single-layer graphene oxide and reduced graphene oxide surfaces. *Journal of Physical Chemistry C*, 113:10842–6.
12. Stankovich, S., Dikin, D.A., Compton, O.C., Dommett, G.H.B., Ruoff, R.S. & Nguyen S.T. (2010). Systematic Post-assembly Modification of Graphene Oxide Paper with Primary Alkylamines. *Chemistry of Material*, 22:4153-4157.
13. Hernandez, Y., Nicolosi, V., Lotya, M., Blighe, F.M., Sun, Z. & De, S. (2008). High-yield Production of Graphene by Liquid-phase Exfoliation of Graphite. *Nature Nanotechnology*, 3(9):563-568.
14. Khan, U., O'Neill, A., Porwal, H., May, P., Nawaz, K. & Coleman, N.J. (2012). Size of selection of dispersed, exfoliated graphene flakes by controlled centrifugation. *Carbon, 50:*470-475.

15. Green, A.A.& Hersam, M.C. (2010). Emerging Methods for Producing Monodisperse Graphene Dispersions. *The Journal of Physical Chemistry Letters*, 1:544-549.
16. Dhakate, S.R., Chauhan, N., Sharma, S., Tawale, J., Singh, S., Sahare, P.D. & Mathur. (2011). An approach to produce single and double layer graphene from re-exfoliation of expanded graphene. *Carbon 49*,1946-1954.
17. Dato, A., Lee, Z., Jeon, K.J., Erni, R., Radmilovic, V., Richardson, T.J. & Frenklach, M. (2009). Clean and highly ordered graphene synthesized in the gas phase. *Chemical Communications*, 6095-6097.
18. Valles, C., Drummond, C., Saadaoui, H., Furtado, C.A., He, M. & Roubeau, O. (2008). Solutions of Negatively Charged Graphene Sheets and Ribbons. *Journal of the American Chemical Society*, 130(47):15802-15804.
19. Wajid, A.S., Das, S., Irin, F., Tanvir Ahmed H.S., Sherlburne, J.L., Parviz, D., Fullerton, R.J., Jankowski, A.F., Hedden, R.C. & Green M.J. (2012). Polymer-stabilized graphene dispersions at high concentrations in organic solvents for composite production. *Carbon, 50:*526-534.
20. Smith, R.J., Loyta, M. & Coleman, J.N. (2010). The Importance of Repulsive Potential Barriers for the Dispersion of Graphene Using Surfactants. *New Journal of Physics*, 12: 125008.
21. Hunter, R.J. (1993). Interaction to Modern Colloid Science. Oxford: Oxford University Press.
22. Israelachvili, J. (1991). Intermolecular and Surface Forces. New York: Academic Press.

The Malaysian Journal of ANALYTICAL SCIENCES ISSN 1394-2506

SYNTHESIS AND CHARACTERIZATION OF pH SENSITIVE HYDROGEL USING EXTRACTED PECTIN FROM DRAGON FRUIT PEEL

(Sintesis Dan Pencirian Hidrogel pH-Sensitif Berasaskan Ekstrak Pektin Kulit Buah Naga)

Azwan Mat Lazim*, Farahain Mokhtar, Siti Fairus Mohd Yusof , Ishak Ahmad, Adil Hakam

School of Chemical Sciences and Food Technology,
Faculty of Science and Technology, Universiti Kebangsaan Malaysia, 43600 Bangi, Selangor, Malaysia

**Corresponding author: azwani79@ukm.my*

Abstract

The aim of this study is to synthesis pectin-based hydrogel from the dragon fruit peel. The pectin was extracted using acid extraction (pH 3.5) that carried out at 60 ^{o}C for 30 minutes. The extracted compound conformation was analyzed by calculating the degree of esterification (DE) and the analysis was confirmed by the FTIR analysis spectrum. The dragon fruit peel pectin (PcDF) and acrylic acid (AA) hydrogel (AA-PcDF) was fabricated using a free radical polymerization in aqueous solution. Its uptaking efficiency was determined in different pH buffer solutions and their swelling percentage was calculated. Futher characterizations were made by using FTIR and SEM to examine the AA-PcDF hydrogel physicochemical properties. Results obtained showed that this new material has a high potential to be used as biomaterial in pharmaceutical and medical purposes.

Keyword: pectin, dragon fruit peel, hydrogel, *hylocereus polyrhizus*

Abstrak

Tujuan kajian ini dijalankan adalah untuk mensintesis hidrogel beraaskan pektin daripada kulit buah naga. Pengestrakan ini dilakukan menggunakan kaedah pengestrakan asid dalam pH 3.5 pada suhu 60°C selama 30 minit. Perincian susunan kompaun yang telah diestrak telah ditentukan melalui darjah esterifikasi (DE) dan disahkan menggunakan spektrokopi FTIR. Penghasilan hidrogel berasakan pektin kulit buah naga (PcDF) dan akrilik asid (AA) (AA-PcDF) dilakukan melalui proses polimeran radikal bebas dalam larutan akues. Keberkesanan penyerapan dan pengembangan hidrogel ini ditentuksn menggunakan larutan penimbal pada pH yang berbeza iaitu pada pH 3, pH 7 dan pH 12. Pencirian lanjut telah dilakukan menggunakan analisis spektrokopi FTIR dan SEM bagi mengkaji sifat fiziokimia hidrogel AA-PcDF. Keputusan yang diperolehi telah menunjukkan bahan baru ini berpotensi tinggi untuk diaplikasikan dalam bidang farmasi dan perubatan.

Kata kunci: pektin, kulit buah naga, hydrogel, *hylocereus polyrhizus*

Introduction

Dragon fruit (*Hylocereus polyrhizus)* or red pitaya is an exotic tropical fruit which comes from the cactus family, *Cactaceae*. With leathery bright red skin and sweet, its kiwi-like flesh is highly in fiber and vitamins especially C and B. This fruit is widely used in food, jam and beverages. On contrary of the benefits, the dragon fruit waste during the peeling process is unmanageable and leads to environmental problems. Therefore, researches were conducted to utilize these waste materials as a source of pectin [1].

Generally, pectin (Figure 1) is a group of polysaccharides with an extremely diverse set of biopolymers present in all plant primary cell walls specifically, it is a methylated ester of polygalacturonic acid that contains 1,4-linked-α-D-galacturonic acid residues [1,2]. Pectin is characterized by its degree of esterification (DE) either high methoxyl pectin (DE >50 %) or low methoxyl pectin (DE<50 %). Interestingly, the amount of pectin from the dragon fruit is higher than apple pomace (12 %) however it is slightly lower than citrus peels (25%) [3, 4]. Pectin is widely used in food industry as gelling and thickening for jams, meat products, fruit juice and dairy products [5]. Pectin easily degrades by enzyme pectinase and microflora in the colon of the human body [6, 7].

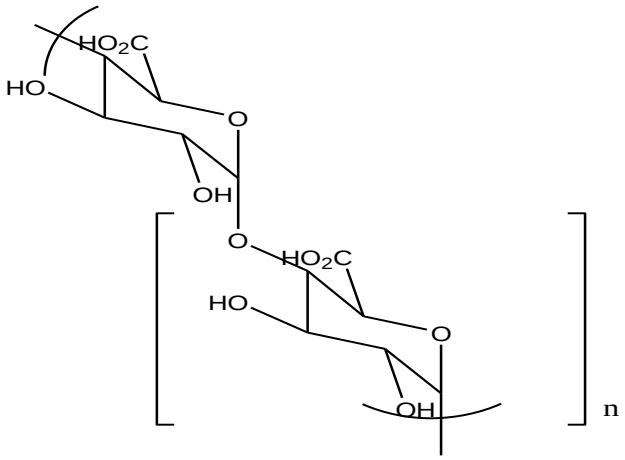


Figure 1. Structure of pectin

In this research extracted pectin from dragon fruit (PcDF) was grafted with acrylic acid (AA) by free radical polymerization. The swelling test of AA-PcDF hydrogel was conducted in three buffer solutions (pH 3, pH 7 and pH 12). Further characterizations and optimizations of AA-PcDF hydrogel were made by using fourier transform infrared (FTIR) spectroscopy, differential scanning calorimeter (DSC) and scanning electron microscopy (SEM) in order to examine the physicochemical properties of synthesized hydrogels. This grafted pectin hydrogel (AA-PcDF) is expecting to produce a biocompatible hydrogel that suitable to be used as colonic drug carrier.

Materials and Methods

Material

All chemicals such as hydrochloric acid (95%), ethanol (95%) and acrylic acid (AA), ammonium persulfate (APS), and N,N'-methylene-bis-acrylamide (MBA) were used as received and supplied by Merck. Dragon fruit was bought at a local store. For extraction hydrochloric acid at 0.1M has been used.

Pectin extraction from dragon fruit (PcDF)

Pectin from dragon fruit peels was extracted using a method modified from [4]. About 2 g dried dragon fruit peels was added to mixture of hydrochloric acid (0.1M) in 30 mL distilled water where the pH was adjusted to 3.5. The extraction process was carried out at 60 ^{o}C for 30 minutes and the final product was filtered using cheesecloth. Ethanol (95%) was added to the extraction solution with a ratio of 0.5: 1.0 for 6 hours. The forming gel was filtered and washed using ethanol (45%) to separate mono-and disaccharides. Pectin was dried in an oven at 40 ^{o}C for 24 hours.

Synthesis of AA-PcDF hydrogels

AA-PcDF hydrogels were synthesized by free radical polymerization using APS as the initiator and MBA as the crosslinker. In a round bottom flask, AA and solution of PcDF (1%) were prepared at different ratios (4:1, 3:2, 2:3 and 1:4). The mixture was purged with nitrogen gas for 10 minutes. Then about 1.6 % of MBA and 1 % of APS were added when the temperature reached at 70 ^{o}C. The synthesis was left for 6 hours to complete the process of radical polymerization. The hydrogel produced was immersed in large amounts of distilled water for 24 hours before it was dried at room temperature for 72 hours.

Pectin characterization

Percentage of extracted pectin was calculated and recorded using this formula (Equation 1):

$$\% \text{ Yield} = P_1/P_0 \times 100 \quad (1)$$

P_0 is the weight of dry dragon fruit skin before extraction; P_1 is the weight of pectin extracted.

Degree of esterification (DE) was calculated using a standard method proposed by [8]. In a 50 mL beaker, 50 mg pectin powder was dissolved in 65 % isopropanol and 10 mL of distilled water. Dropwise, 3 drops of phenolphthalein was added as color indicator. Pectin was titrated with 0.1N NaOH until the solution color changed to pink and the volume was recorded as A mL. After 30 minutes, 30 mL of 0.1N NaOH was added together with 30 mL 0.1N sulfuric acid. Using the same approached the second titration was made using 0.1N NaOH until the solution turned pink and recorded as B mL. Percentage of DE was calculated using a formula (Equation 2) proposed by [5]:

$$\% \text{ DE} = (B / AB) \times 100 \quad (2)$$

A is the first titration volume and B is the volume of the second titration.

Hydrogel AA-PcDF characterization

Percentage of gel fraction was calculated using formula (Equation 3) proposed by [7].

$$\% \text{ Gel fraction} = A_1/A_0 \times 100 \quad (3)$$

A_1 is the dry weight before extraction; A_0 is the dry weight after extracted.

The swelling percentage test of hydrogel was performed in buffer solution ie. pH 3, pH 7 and pH 12 to study the sensitivity of the hydrogel towards external stimuli under different pH factors. The swelling percentage was calculated using a formula (Equation 4) by [8].

$$\% \text{ Swelling} = \frac{G_1 - G_0}{G_0} \times 100 \quad (4)$$

G_1 is the dry weight of hydrogel before swelling. G_0 is the weight of hydrogel after swelling in 24h.

FTIR spectroscopy analyzed was carried out using an Attenuated total reflectance (ATR) technique (Perkin Elmer, USA) while the hydrogel morphology was examined by using the scanning electron microscopy (SEM) technique.

Results and Discussion

Percentage of pectin

The pectin extraction yield obtained from the dragon fruit peel was 18.1%. This result is in significant as reported by [3]. It is also comparable with the commercially available pectin which extracted from citrus (25 %) and apple (12 %) [2-4]. Hence, this result indicates that dragon fruit peel is able to be an alternative source of pectin which is abundance and locally available

Degree of Esterification (DE)

It was found the degree of esterification (DE) for dragon fruit pectin that extracted at pH 3.5 was 36 %. According to Srisagul et. al. (2004) [9] DE is expressed as a percentage of the carboxyl group of the methyl ester on polysaccharides chain of pectic acid. If the DE > 50 % meaning it posess highly degrees of methoxy which is known as high methyl pectin (HM) while if DE < 50 % it is known as low methyl pectin (LM). For HM pectin, it easily forms gels at low pH levels whereas the LM pectin only forms gels in the presence of calcium or any cations. In this study low DE was obtained thus, dragon fruit pectin can be classified as low methoxy (LM) pectin. Therefore, this type of pectin is suitable to be used in colonic applications. As reported by [10], LM was fermented faster in-vivo and in-vitro rather than high methoxy (HM) pectin in colon.

FTIR Spectroscopy analysis

FTIR Spectroscopy analysis (Figure 2) shows that the structure of pectin extracted from dragon fruit is similar to the commercial pectin from citrus peel's spectrum. In order to identify the structure of pectin, the absorbance at 1000-1600cm^{-1} is being focused [2]. The peak at 1600cm^{-1} indicates the presence of carbonyl groups, CO while the

absorption 1740-1760 cm^{-1} indicating the presence of a carboxyl group-COOH de-esterified. The peak at 3200-3600cm^{-1} indicates the presence of hydroxyl-OH groups on galacturonic acid chain and the peak at 1100cm^{-1} is regarding to the position of secondary alcohol.

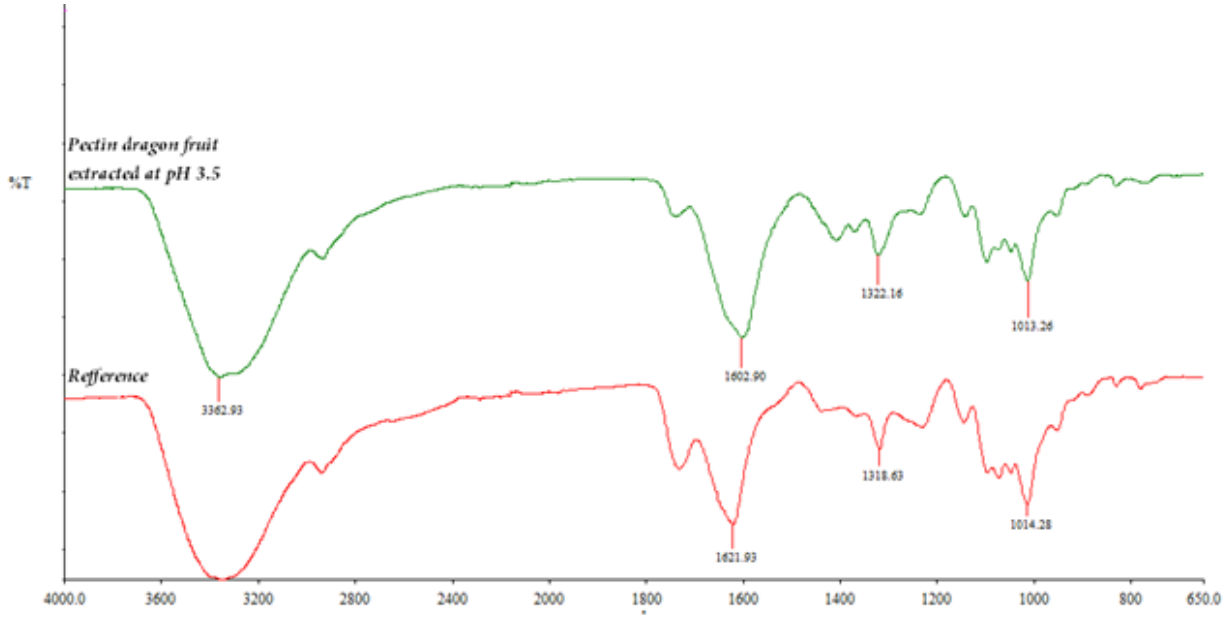


Figure 2. FTIR spectrum from dragon fruit extract pectin (green) at pH 3.5 and commercial pectin (red)

A soft hydrongel was obtained from the synthesis reaction. After being dried for 24 hours at 40 °C, these well-crosslinked gels produced a flexible swollen hydrogel when it immersed in water. The grafting reaction between monomers involved was suggested as shown in Figure 3.

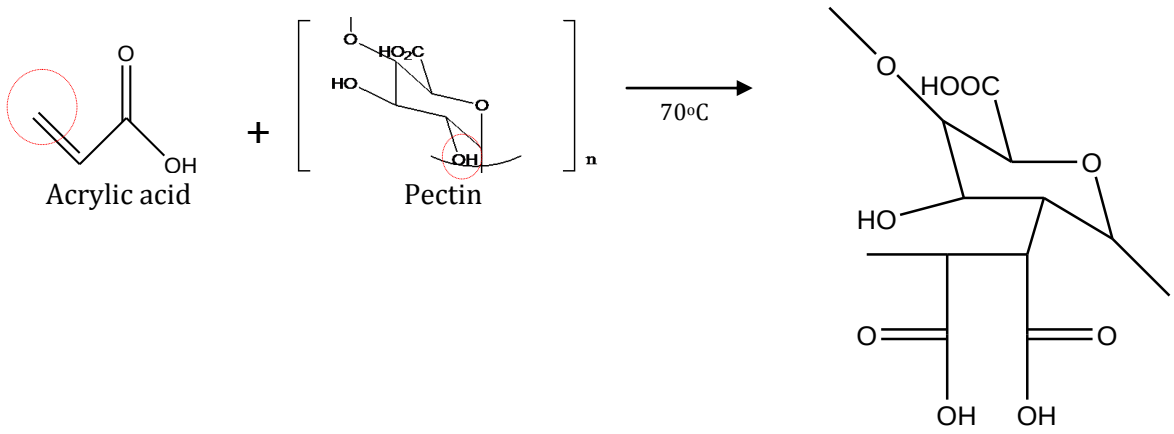


Figure 3. Schematic grafting reaction between monomers AA and PcDF to produce AA-PcDF

Figure 4 shows the structure of AA-PcDF hydrogel in comparison with PcDF and Acrylic acid before polymerization of hydrogel. For PcDF spectra, peaks at 3200 –3260 cm^{-1} indicate the –OH stretching. It clearly shows that the peak of –OH at PcDF spectrum disappears after the polymerization. As be seen at acrylic acid spectrum, a strong peak at 900 cm^{-1} indicated the $C=CH_2$ group disappeared after the polymerization where the absence of any peak at this area suggests pectin dragon fruit and acrylic acid were grafted (Figure 3).

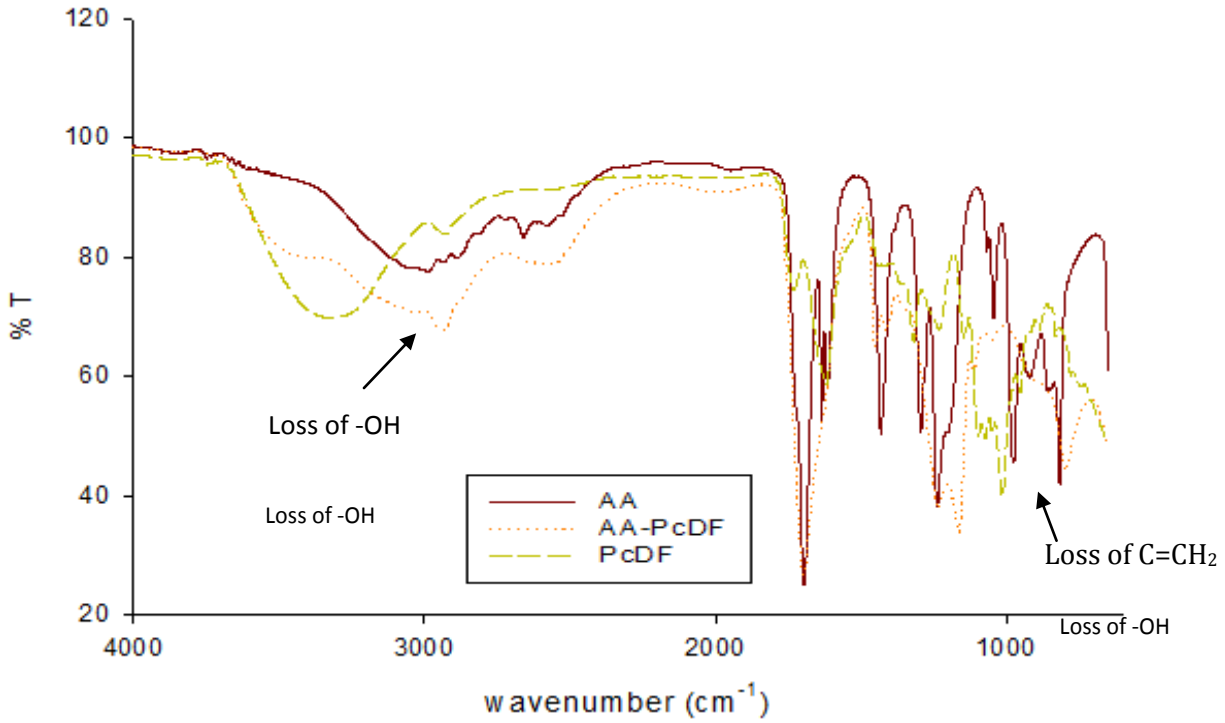


Figure 4. FTIR spectra for AA, PcDF and AA-PcDF

Swelling test

The swelling effects on different weight ratio of AA to PcDF were investigated and the results were shown in Figure 5(a,b,c). It was demonstrated that the AA-PcDF hydrogels highly swelled in pH 7 compared to other pH. This condition occurred due to electrostatic repulsion between the ionized acid groups of poly-acrylic acid. It also being supported by the amount of solvent penetrated the networks. Of all the ratios tested, it was found that hydrogels with 1:4 ratios gave the highest swelling percentage with 3475%. The amount of pectin contributed to the increasing of the hydrogel's expansion due to presence of carboxylic acid in pectin itself. Due to the increasing of charges it leads to electrostatic repulsion between the ionized acid groups and as the result the hydrogel swells [6-8].

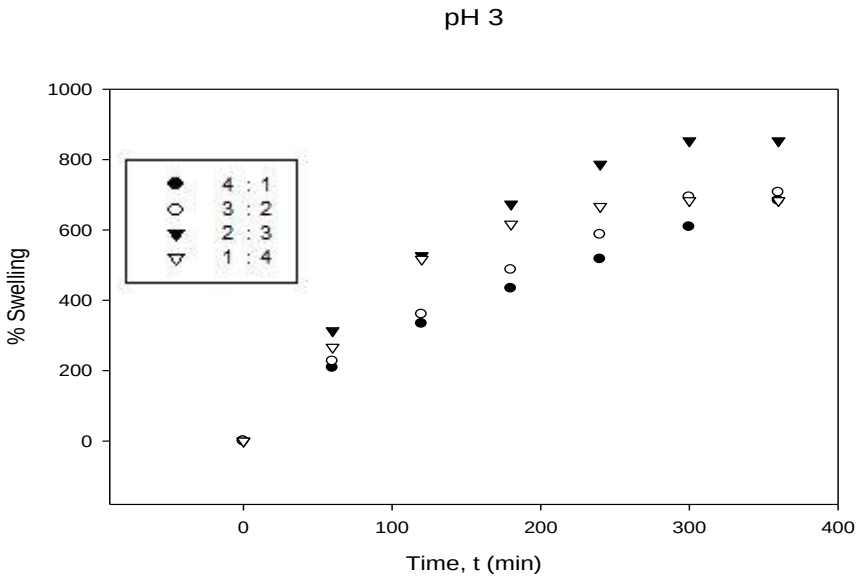


Figure 5(a). Swelling percentages at pH 3

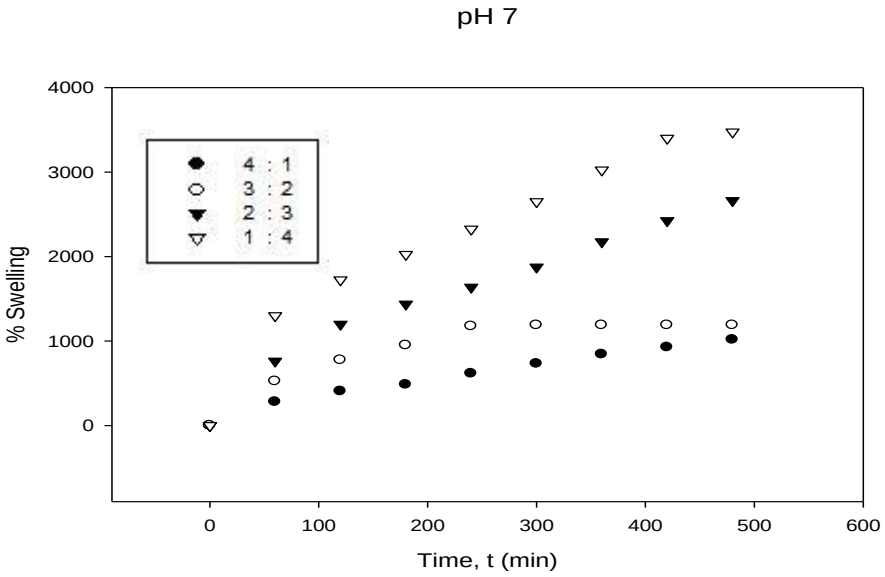


Figure 5(b). Swelling percentages at pH 7

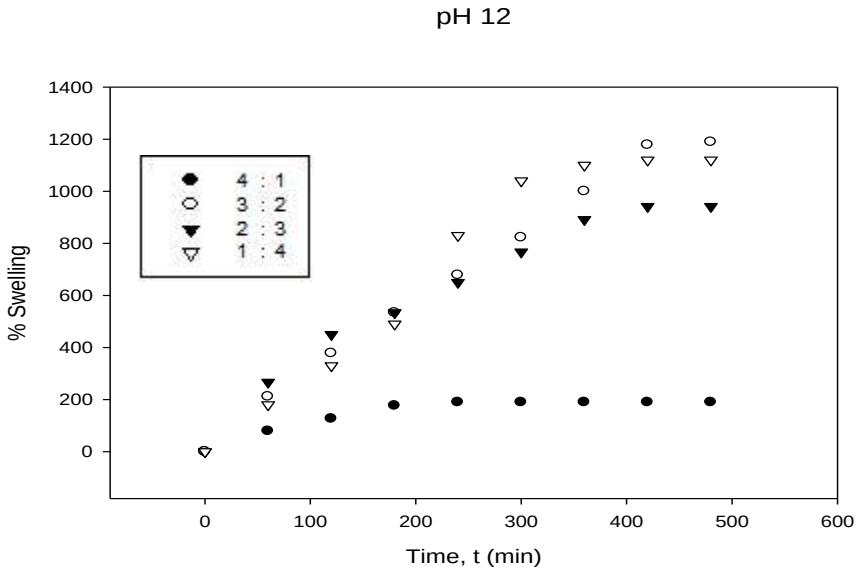
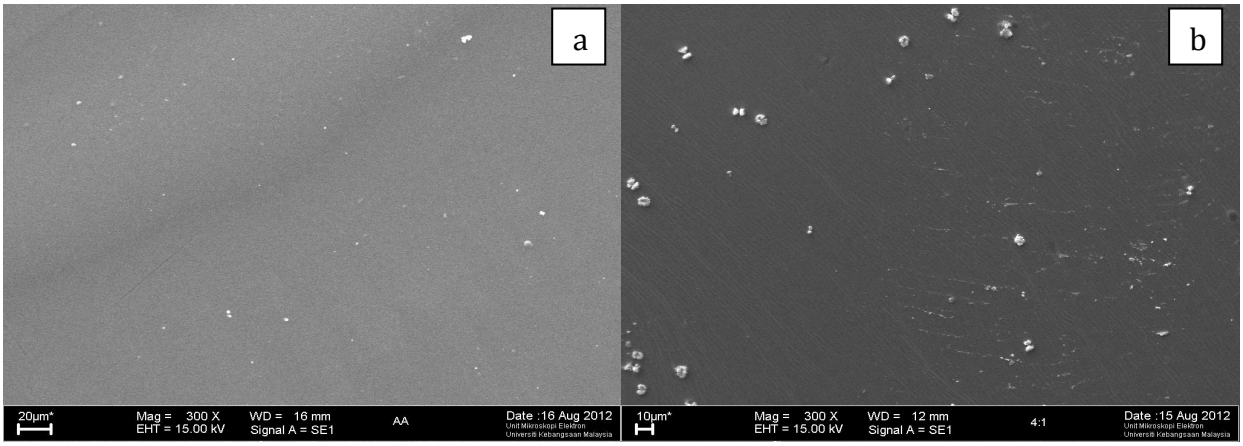


Figure 5(c). Swelling percentages at pH 12

Morphology

Morphology of hydrogel was observed by using the Field Emission Scanning Electron Spectroscopy (FESEM) Zeiss Supra 55VP in dry conditions to investigate the morphology and structure of the hydrogel. The surface image of the hydrogel was taken at 300x magnification. The different images were observed for various samples, AA without pectin, acrylic acid with pectin at ratio of 4:1, 3:2, 2:3, 1:4. A smooth surface was obtained for acrylic acid without pectin as shown in Figure 6a. However, due to the increasing of dragon fruit pectin pores were detected (Figure 6b-6e). Besides elongation of the pectin structure, it also reduces the crosslinking ability between the networks thus porosity sizes increased [9, 10]. This process is simplified as shown in Figure 7.



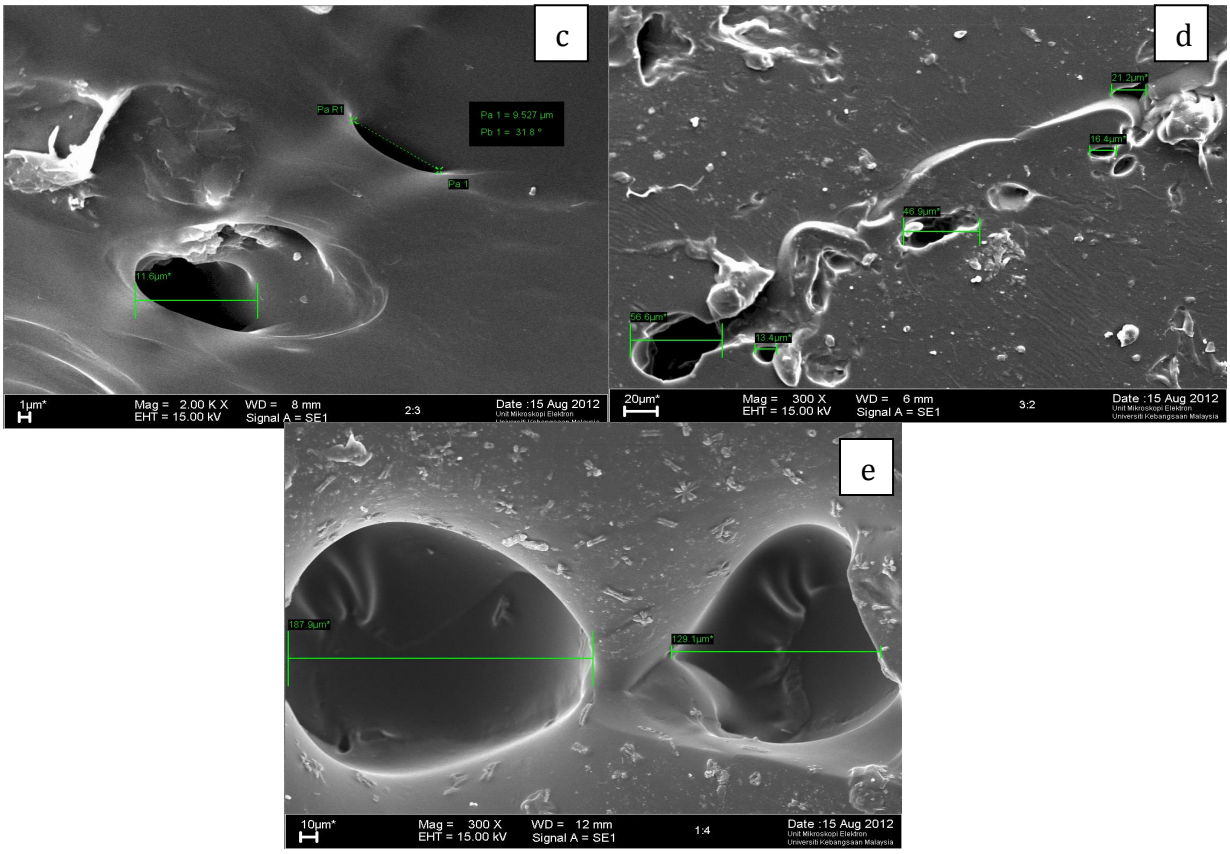
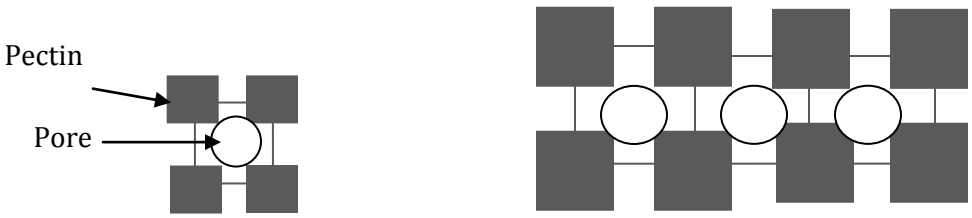


Figure 6. Morphology hydrogel surface in dry conditions. a) Acrylic acid without pectin, while the hydrogel produced with pectin in a ratio of b) 4:1, c) 3:2, d) 2:3 and e)1:4.



AA: PcDF
4: 1

AA: PcDF
1:4

Figure 7. Diagram represent pore size and number of pores of hydrogel with increasing of pectin ratio

Conclusion

A low methoxy (LM) pectin exctracted from dragon fruit peel with 36 % degree esterification of galacturonic acid was able to be grafted with acrylic acid in order to produce a hydrogel. The percentage of swelling capacity was totally depended ratio of hydrogel acrylic acid and pectin being used. It was found that the hydrogels swelled effectively with 3475 % occurred at pH 7 at a ratio of 1:4. These promising results suggest that AA-PcDF hydrogel is a pH sensitive which possibly used as a drug carrier specifically targeted colon area.

Acknowledgment

This work was financially supported in part by research grants FRGS/1/2011/SG/UKM/02/25 and GGPM-2011-054 given by Universiti Kebangsaan Malaysia and Ministry of Higher Education.

References

1. Levigne, S., Ralet, M.C. & Thibault, J.F. (2002). Characterization of pectin extracted from fresh sugar beet under different conditions using an experimental design. *Carbohydrate Polymers* 49 : 145-153.
2. Kalapathy, U & Proctor, A. (2001). Effect of acid extraction and alcohol precipitation conditions on the yield and purity of soy hull pectin. *Food Chemistry* 73 : 393 – 396.
3. Nazaruddin. R, Norazelina S.M.I, Norziah M.H, & zainuddin M. (2011). Pectin from dragon fruit (hylocereus polyrhius) peel. *Malaysian Applied Biology*, 40(1): 19 – 23.
4. Tang P. Y. Wong C. J W. Woo & K. K (2011). Optimization of pectin extraction from peel of dragon fruit (hylocereus polyrhizus). *Asian Journal of Biological Sciences*, 4(2):189 – 195.
5. Jiang C. M, Liu S. C, Wu M. C, Chang W. H. & Chang H.M. (2005). Determination of degree of esterification of alkaline de-esterified pectin by capillary one electrophoresis. *Food Chemistry* 91: 551 – 555.
6. Mizote A, Odagir H, Toei K., & Tanaka K. (1975). Determination of residues of carboxylic acids (mainly galacturonic acid) and their degree of esterification in industrial pectins by colloid titration with Cat-Floc. *Analyst* 100: 822 – 827.
7. Yoshii F., Zhao L., Wach R.A., Nagasawa N., Mitomo H. & Kume T. (2003). Hydrogel of polysaccharide derivatives crosslinked with irradiation at paste-like condition. Nuclear Instruments and Methods in Physics Research (B) Beam Interactions with Materials & Atoms, 208: 320-324
8. Peppas N.A. (1985). Analysis of fickian and non-fickian drug release from polymers. *Pharmceutical Acta Helv*. 60 : 110 – 111.
9. Srisagul S., Pornsak S., Tasana P., Atawit S. & Satit P. (2004). Effect of degree of esterification of pectin and calcium amount on drug release from pectin based matrix tablets. AAPS pharmSciTech, 5(1): Article 9
10. May C.D. (1990). Industrial pectin: Sources, production and applications. *Carbohydrates polymer* 12: 79 – 99.

The Malaysian Journal of ANALYTICAL SCIENCES ISSN 1394-2506

DIFFERENTIATING AGARWOOD OIL QUALITY USING ARTIFICIAL NEURAL NETWORK

(Perbezaan Kualiti Minyak Gaharu Menggunakan Rangkaian Neural Tiruan)

Nurlaila Ismail[1]*, Nor Azah Mohd Ali[2], Mailina Jamil[2], Mohd Hezri Fazalul Rahiman[1], Saiful Nizam Tajuddin[3] and Mohd Nasir Taib[1]

[1]Faculty of Electrical Engineering,
Universiti Teknologi MARA (UiTM), 40450 Shah Alam, Selangor, Malaysia
[2]Herbal Product Development Programme, Natural Products Division,
Forest Research Institute Malaysia (FRIM), 52109 Kepong, Selangor, Malaysia
[3]Faculty of Industrial Science and Technology,
Universiti Malaysia Pahang (UMP), Lebuhraya Tun Razak, 26300 Gambang, Pahang, Malaysia

**Corresponding author: nrk_my@yahoo.com*

Abstract

Agarwood oil is well known as expensive oil extracted from the resinous of fragrant heartwood. The oil is getting high demand in the market especially from the Middle East countries, China and Japan because of its unique odor. As part of an on-going research in grading the agarwood oil quality, the application of Artificial Neural Network (ANN) is proposed in this study to analyze agarwood oil quality using its chemical profiles. The work involves of selected agarwood oil from low and high quality, the extraction of chemical compounds using GC-MS and Z-score to identify of the significant compounds as input to the network. The ANN programming algorithm was developed and computed automatically via Matlab software version R2010a. Back-propagation training algorithm and sigmoid transfer function were used to optimize the parameters in the training network. The result obtained showed the capability of ANN in analyzing the agarwood oil quality hence beneficial for the further application such as grading and classification for agarwood oil.

Keywords: agarwood oil, chemical compounds, quality, gas chromatography-mass spectrometry (GC-MS) and Artificial Neural Network (ANN)

Abstrak

Minyak gaharu dikenali sebagai minyak mahal yang diekstrak daripada resin kayu yang berbau wangi. Minyak ini mendapat permintaan yang tinggi di pasaran terutama dari negara-negara Timur Tengah, China dan Jepun kerana baunya yang unik. Sebagai sebahagian daripada penyelidikan untuk menentukan gred kualiti minyak gaharu, penggunaan rangkaian neural tiruan (ANN) dicadangkan dalam kajian ini untuk menganalisis kualiti minyak gaharu. Kerja ini melibatkan minyak gaharu yang terpilih dari kualiti rendah dan tinggi, pengekstrakan komponen kimia menggunakan GC-MS dan Z-skor untuk mengenalpasti sebatian penting sebagai input kepada rangkaian. Pengaturcaraan algoritma untuk ANN telah dihasilkan dan dilakukan secara automatik melalui perisian Matlab versi R2010a. Algoritma penyebaran undur untuk sesi latihan dan fungsi peralihan sigmoid telah digunakan untuk mengoptimumkan parameter dalam rangkaian latihan. Keputusan yang diperolehi menunjukkan keupayaan ANN dalam menganalisis kualiti minyak gaharu dan seterusnya bermanfaat untuk kegunaan selanjutnya seperti penggredan dan klasifikasi minyak gaharu.

Kata kunci: minyak gaharu, bahan kimia, kualiti, gas kromatografi-spektrometri jisim dan Rangkaian Neural Tiruan

Introduction

Agarwood oil is an expensive oil and is extracted from the resinous of fragrant heartwood of *Aquilaria* species [1]. This species is a genus and belongs taxonomically to the Thymelaeaceae family. The multiples usages of agarwood oil make this oil gets high demand in the market especially from the countries in The Middle East, China and Japan [1-3]. It can be used as incense, in perfume ingredient and medical preparation, during religion and wedding ceremony and also as a symbol of wealth in certain country [1, 4-6]. The agarwood oil has been sold in various

qualities based on its physical appearance such as color and odor. Consumer perception and high fixative properties also give marks in qualifying the agarwood oil thus affect its price in the market [1, 7]. However this conventional technique makes the price of agarwood oil fluctuates and not standardize in the market. A standard is needed to ensure that the agarwood oil can be qualified according to its chemical properties so that accuracy can be trusted [4, 8]. Therefore, as part of an on-going research in grading the agarwood oil quality, the application of ANN is proposed to analyze agarwood oil quality using its chemical profiles. The chemical profiles refer to the complex mixtures of sesquiterpene and its chromone derivatives in agarwood oil [9-11].

Materials and Methods

Plant Material

Fifteen agarwood oil samples obtained at Forest Research Institute Malaysia (FRIM) and Universiti Malaysia Pahang (UMP) were used in this study. The oils are *Aquilariamalaccensis* species were sold as high and low qualities to the institutions by the agarwood traders certified by the Forestry Department, Malaysia [12]. The samples were labeled as LG, RG, HG, CM, MNS, EO3, EO2, EO4, MN, MS, M, MPE, T, MA1, LA, KB, JBD, MA2 and MA for high quality oils and CKE, R5 and HD for low quality oils.

GC-MS analysis

GC-MS analysis is carried out using Agilent Technologies 7890A/5975C Series MSD with HP-5MS column (30m x 0.25mm ID x 0.25µm film thickness). At first, the apparatus is set at 60˚C for 10min time duration, followed by 180˚C for 1min at 3˚C/min. The gas carrier helium is injected at a flowrate of 1.0mL/min and the ion-source temperature is programmed at 280˚C. The chemical compounds are identified by matching them to the mass spectral library (HPCH2205.L; Wiley7Nist05a.L; NIST05a.L). The chemical compounds are presented in terms of abundances (%) [4].

ANN structure and training

The ANN theory applied in this study has been adequately described before[13]. The ANN algorithms were computed by the Matlab software version R2010a for evaluation. It applied feed-forward neural network using back propagation training algorithm. This algorithm is used to adjust the network weights. The input is determined based on the number of input nodes. Therefore in this study the input nodes in number of significant chemical compounds as identified by Z-score. The Z-score application was briefly explained in the previous work [14].

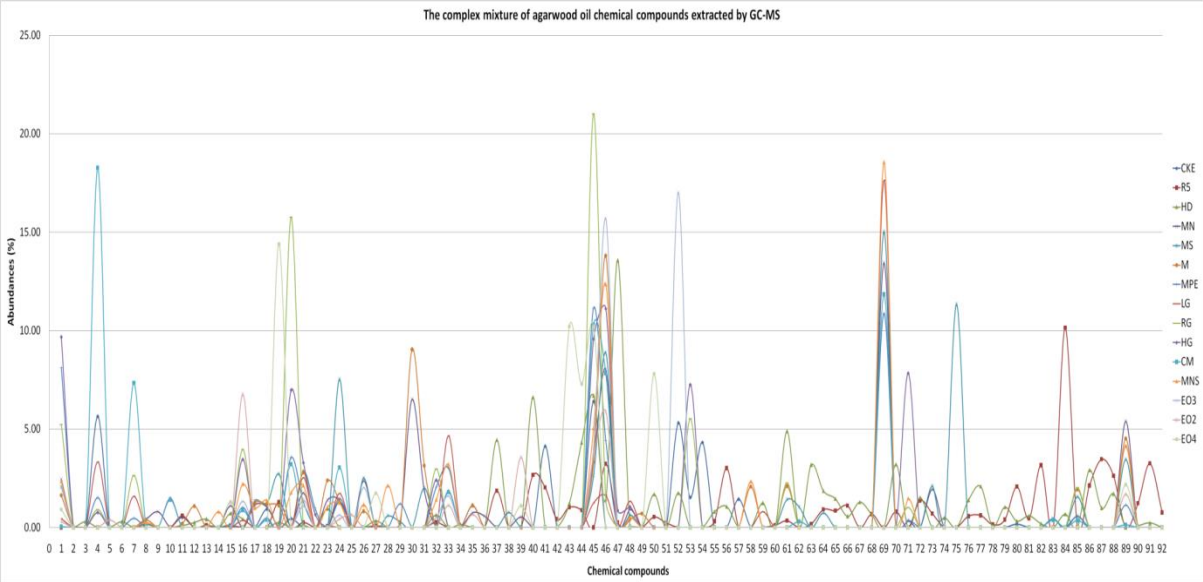
There were ninety six of agarwood oil chemical compounds used as input-output data for ANN analysis. The data were divided into two datasets; training and testing using the ratio of 80%;20% [15]. Seven chemical compounds were used as input for the training data set. The output layer consists of only one node which corresponds to the quality of the agarwood oil, i.e. either high or low. The learning rate, momentum rate and hidden layer size were determined and optimized during the training of the network using the sigmoid transfer function. Mean square error (m.s.e.) was performed to evaluate the ANN performance. After that, the final parameters from ANN training were used for ANN validation.

Results and Discussion

Figure 1 shows the chemical composition or abundances (%) pattern of chemical compounds extracted by GC-MS. It can be seen that there is variation of abundances pattern belong to each of chemical compounds. The abundances for agarwood oil are different to each other. This finding proves that the agarwood oil chemical profile is a complex mixture of sesquiterpenes and its chromone derivatives [9-11] and the difference spotted confirms the finding by other researcher [16]. The pattern variation displays the behavior of the chemical compounds of agarwood oils. It is noticed that, four high peaks of abundances are recognized. They belong to compound no. 4 i.e. α-gurjunene, compound no.20 i.e. cis-β-guaiene, compounds no. 46. i.e. ɤ-eudesmol and compounds no. 71 i.e. β-costol. Different pattern and dissimilarity of abundances (%) amount exist in agarwood oils due to several factors such as ecological condition, environmental and genetic factors of each sample [6].

The chemical compounds and its abundances of agarwood oils as extracted by GC-MS were tabulated in Table 1 and Table 2 for high and low quality, respectively. Table 1 consists of LG, RG, HG, CM, MNS, EO3, EO2, EO4, MN, MS, M, MPE, T, MA1, LA, KB, JBD, MA2 and MA agarwood oils. These agarwood oils are traded as high quality in the market and some of them are published as supreme agarwood oil [17]. There were seven significant

chemical compounds as identified by Z-score. They were β-agarofuran, α-agarofuran, 10-epi-ɤ-eudesmol, ɤ-eudesmol, longifolol, hexadecanol and eudesmol. It was observed that the chemical compounds such as longifolol, hexadecanol and eudesmol are not appear in almost the agarwood oil for this quality. 10-epi-ɤ-eudesmol is found in all samples. β-agarofuran as the most important compound in high quality agarwood oil [2] is found in all agarwood here except for EO4, MN, MS and M.



Notes: 1= 4-phenyl-2-butanone, 2= Nonanoic acid, 3= Decanoic acid, 4= α-gurjunene, 5= α-cedrene, 6= β-maaliene, 7= β-Gurjunene, 8= α-guaiene,9= β-humulene, 10= α-guaiene, 11= aromadendrane, 12= amorpha-4,11-diene, 13= Drima-7,9(11)-diene, 14= valencene, 15= ϒ-gurjunene, 16= β-agarofuran,17= ϒ-muurolene, 18=ar-curcumene, 19=β-selinene, 20=cis-β-guaiene, 21=α-muurolene,22= β-dihydroagarofuran, 23=α-bulnesene, 24=ϒ-cadinene, 25=δ-cadinene, 26=cis-calamenene, 27=α-elemol, 28=(Z)-nerolidol, 29=α-cadinene, 30=selina-3, 7(11)-diene, 31=hedycaryol, 32=α-agarofuran, 33=elemol, 34=nor-keto-agarofuran, 35=β-calacorene, 36=dodecanoic acid, 37=epoxy-bulnesene, 38=spathulenol, 39=viridiflorol, 40=tetradecanal, 41=β-gurjunene, 42=guaiol, 43=hinesol, 44=1,5-epoxy-nor-ketoguaiene, 45=10-epi-ɤ-eudesmol, 46=ɤ-eudesmol, 47=agarospirol, 48=allo aromadendrene epoxide, 49=selina 3,11-dien-6α-ol,50= jinkoh-eremol, 51=kusunol, 52=α-eudesmol, 53=valerianol, 54=selina 11-en-4α-ol, 55=bulnesol, 56=dehydrojinkoh-eremol, 57=β-bisabolol, 58=cadalene, 59=α-bisabolol, 60=selina-3,11-dien-9-one, 61=cyperotundone, 62=10-nor-calamenen-10-one,63= rotundone, 64=longifolol, 65=selina-4,11-dien-14-oic acid, 66=selina-3,11-dien-14-al, 67=9,11-eremophiladiene, 68=selina-3,11-dien-14-ol, 69=α-eudesmol, 70=selina-4,11-dien-14-al, 71=β-costol, 72=guaia-1(10),11-dien-15-ol, 73=selina-3,11-dien-14-oic acid, 74=sinenofuranol, 75=14-hydroxy-α-muurolene, 76=2-hexadecanone, 77=dihyrokaranone, 78=guaia-1(10),11-dien-15-al,79= karanone, 80=oxo-agarospirol, 81=pentadecanoic acid, 82=hexadecanol, 83=hexadecanoic acid, 84=eudesmol, 85=thujopsenal, 86=palmitic acid, 87=2-hydroxyquaia-1(10),11,15-oic acid, 88=9-hydroxyselina-4,11-dien-14-oic acid, 89=dihydrocollumellarin, 90=1,5-diphenyl-2-pentene, 91=guaia-1(10),11-dien-15,2-olide, 92=oleic acid

Figure 1. The abundances pattern for agarwood oil chemical compounds extracted by GC-MS

Table 2 tabulated the low quality of agarwood oils which is comprises of CKE, R5 and HD. As similar to the chemical compounds in high quality oil, there were seven significant chemical compounds as identified by Z-score; β-agarofuran, α-agarofuran, 10-epi-ɤ-eudesmol, ɤ-eudesmol, longifolol, hexadecanol and eudesmol. From this table, it is noticed that only 10-epi-ɤ-eudesmol appears in CKE. The rest of the compounds do not exist in this agarwood oil. As expected, longifolol, hexadecanol and eudesmol are detected as R5 and HD.

Table 1. The high quality of agarwood oils

No.	Chemical compounds	Abundances (%)											
		LG	RG	HG	CM	MNS	EO3	EO2	EO4	MN	MS	M	MPE
C1	β-agarofuran	0.36	3.96	3.47	0.88	2.21	1.33	6.77	0.00	0.00	0.00	0.00	1.02
C2	α-agarofuran	0.00	2.98	2.41	0.00	1.42	0.50	0.00	0.00	0.00	0.00	0.00	2.06
C3	10-epi-ɤeudesmol	1.25	21.01	9.58	10.31	5.04	4.04	3.63	10.21	3.41	2.64	3.33	11.14
C4	ɤ-eudesmol	1.62	1.38	11.11	7.83	12.36	15.67	5.88	0.00	8.03	8.87	13.80	4.40
C5	longifolol	0.00	0.00	0.00	0.00	0.00	0.00	0.00	0.00	0.00	0.75	0.00	0.00
C6	hexadecanol	0.00	0.00	0.00	0.00	0.00	0.00	0.00	0.00	0.00	0.00	0.00	0.00
C7	eudesmol	0.00	0.00	0.00	0.00	0.00	0.00	0.00	0.00	0.00	0.00	0.00	0.00

Table 1 (continued). The high quality of agarwood oils

No.	Chemical compounds	Abundances (%)						
		T	MA1	LA	KB	JBD	MA2	MA
C1	β-agarofuran	4.33	1.73	2.04	1.02	1.02	1.42	5.01
C2	α-agarofuran	3.53	1.72	1.37	1.47	1.76	1.48	2.73
C3	10-epi-ɤ-eudesmol	9.76	10.91	7.65	7.07	8.14	8.28	20.6
C4	ɤ-eudesmol	0.00	8.16	0.00	30.36	14.85	12.93	3.11
C5	longifolol	0.00	0.00	0.00	0.00	0.00	0.00	0.00
C6	hexadecanol	0.00	0.00	0.00	0.00	0.00	0.00	0.00
C7	eudesmol	0.00	0.00	0.00	0.00	0.00	0.00	0.00

Table 2. The low quality of agarwood oils

No.	Chemical compounds	Abundances (%)		
		CKE	R5	HD
C1	β-agarofuran	0.00	0.00	0.43
C2	α-agarofuran	0.00	0.25	0.64
C3	10-epi-ɤ-eudesmol	6.42	0.00	6.70
C4	ɤ-eudesmol	0.00	3.24	1.45
C5	longifolol	0.00	0.91	1.87
C6	hexadecanol	0.00	3.16	0.20
C7	eudesmol	0.00	10.15	0.68

Figure 2 shows the ANN final training errors with varying learning rate. The learning rate is varied from 0.1 to 1. Graphically, it can be seen that learning rate at 0.9 has minimum m.s.e. of 0.0038. The learning rate of 0.9 is used to adjust the next parameter in the training cycle.

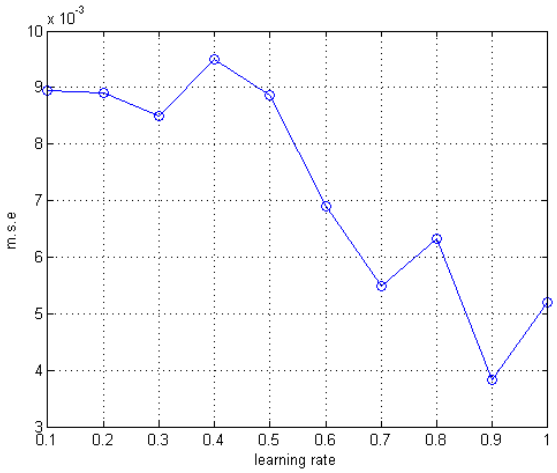


Figure 2. ANN final training errors with varying learning rate

Figure 3 shows the ANN final training errors with varying momentum rate. The momentum rate is varied from 0.1 to 1.0. It is observed that learning rate at 0.7 provides lowest m.s.e. (0.0028). The momentum rate of 0.7 is used to adjust the hidden layer for ANN training network.

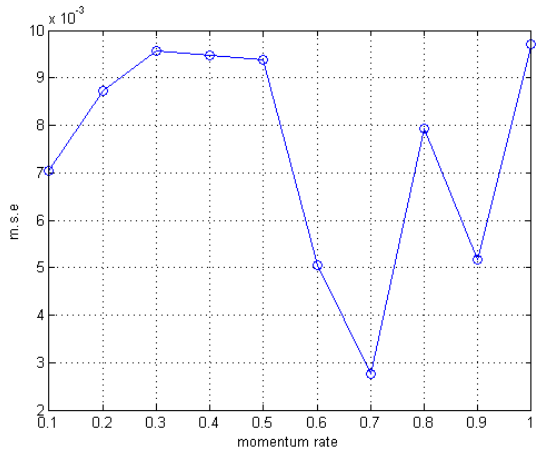


Figure 3. ANN final training errors with varying momentum rate

Figure 4 shows the ANN final training errors with varying hidden layer sizes. The hidden layer size is varied from 1 to 10. The hidden layer size at 2 nodes provides the lowest m.s.e. of 0.0011. The learning rate at 0.9, momentum rate at 0.7 and hidden layer size at 2 nodes were set as final parameters to train the ANN network.

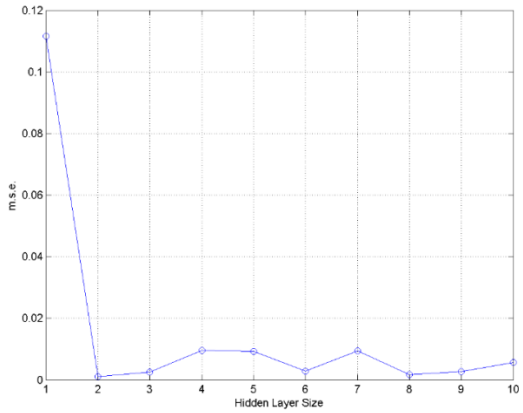


Figure 4. ANN final training errors with varying hidden layer size

Table 3 summarizes the ANN final design parameters for the ANN architecture and training parameters. The nodes in input layer is set as 7, represented by seven significant compounds in agarwood oils (C1 to C7) and the output layer is 1 which is the quality of agarwood oils either high (2) or low (1). The error goal used is 0.01 with the epochs is 100. The other adjusted parameters such as learning rate, momentum rate and nodes in hidden layer are optimum at 0.9, 0.7 and 2, respectively.

Table 3. ANN final design parameters

Parameters	**Value**
Nodes in input layer	7
Nodes in hidden layer size	2
Output layer size	1
Learning rate	0.9
Momentum rate	0.7
Error goal	0.01
Epochs	100

Figure 5 shows the ANN prediction for the training network using the optimised parameters. The training network prediction shows two groups being predicted. Vividly, we can see that the first group, i.e. '1' for low quality, the predicted target is less than 1.4 and for the second group, i.e. '2' for high quality, the predicted target is between 1.8 to 2.0.

Figure 6 shows the prediction of the ANN testing using the optimised training network. It is clear that the predicted targets fall under two groups such as 1 and 2.

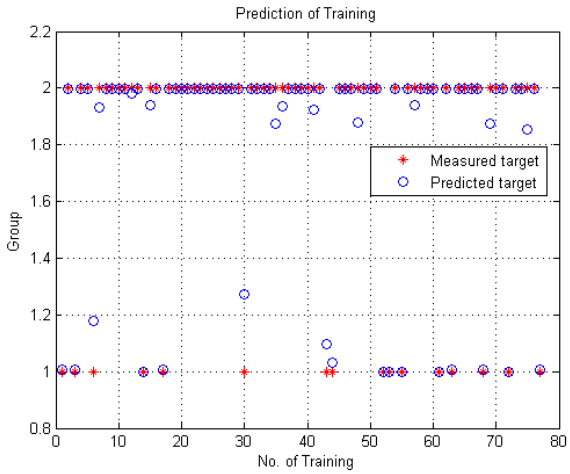


Figure 5. ANN prediction for the training network

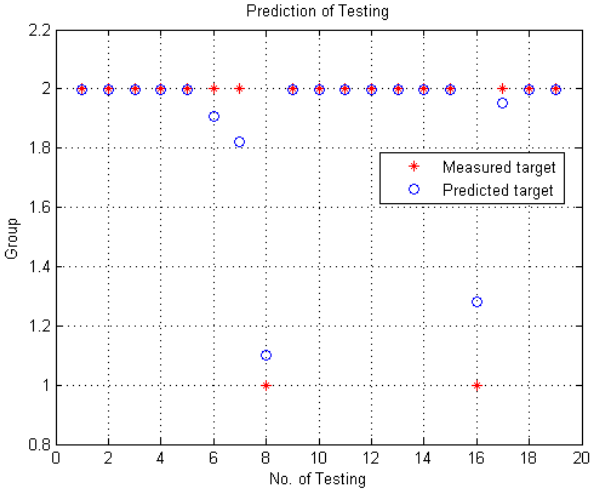


Figure 6. ANN Testing prediction

Figure 7 shows the prediction errors for ANN testing. It is observed that the errors are within -0.03 to 0.02, which is very small and acceptable for nineteen numbers of testing targets of agarwood oil quality.

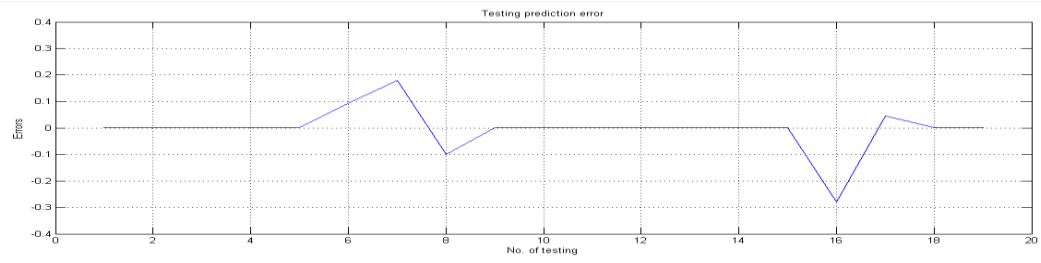


Figure 7. Prediction errors for ANN testing

From the above results, it is clear that the network with 2 nodes in hidden layer size provides one of the best structures for yielding highly accurate prediction of agarwood oil quality. The network successfully differentiated the quality high and low with the worst error of only 0.02 (see Figure 7) with a small error goal i.e. 0.01. The finding proved that the network managed to solve the difficulties in grading the agarwood oil quality using the conventional calibration method as stated before in *Introduction*. Finally, an application of the trained network with 2 hidden neurons was demonstrated by feeding it with seven new significant chemical compounds as identified by z-score technique i.e. β-agarofuran, α-agarofuran, 10-epi-ɤ-eudesmol, ɤ-eudesmol, longifolol, hexadecanol and eudesmol. This is as expected since these significant chemical compounds were identified for both quality of agarwood oil, high and low and they are belonging to the sesquiterpenes compounds.

Conclusion

The study showed that the application of ANN in analyzing the agarwood oil quality has been successful. The result obtained demonstrates the capability of ANN in predicting the quality of agarwood oil. The significant chemical compounds identified i.e. β-agarofuran, α-agarofuran, 10-epi-ɤ-eudesmol, ɤ-eudesmol, longifolol, hexadecanol and eudesmol are useful and beneficial for further analysis such as grading and classification system of agarwood oil.

Acknowledgement

The authors would like to acknowledge the financial support given to Nor Azah Mohamad Ali by the Malaysian Ministry of Agriculture and Agrobased Industry (Science fund 05-03-10-SF1017), Mohd Nasir Taib through the RIF Grant Code: 600-RMI/DANA 5/3/RIF (614/2012) and Nurlaila Ismail for MyPhD scholarship by The Ministry of Higher Education, Malaysia.

References

1. R. Naef (2011). The volatile and semi-volatile constituents of agarwood, the infected heartwood of Aquilaria species: a review, *Flavour and Fragrance Journal* 26: 73-87.
2. P. Tamuli, P. Boruah, S. C. Nath, & P. Leclercq (2005). Essential oil of eaglewood tree: a product of pathogenesis,*Journal of Essential Oil Research* 17: 601-604, 2005.
3. S. N. Tajuddin & M. M. Yusoff (2010). Chemical Composition of Volatile Oils of Aquilaria malaccensis (Thymeleaceae) from Malaysia, *Natural Product Communications* 5: 1965-1968.
4. N. A. B. Sidik (2008).Comparison of Gaharu (Aquilaria Malaccensis) Essential Oil Composition Between Each Country, Bachelor of Chemical Engineering, Faculty of Chemical Engineering and Natural Resources, University Malaysia Pahang.
5. J. Pornpunyapat, P. Chetpattananondh, & C. Tongurai (2011). Mathematical modeling for extraction of essential oil from Aquilaria crassna by hydrodistillation and quality of agarwood oil, *Bangladesh Journal of Pharmacology* 6: 18 - 24.
6. P. Pripdeevech, W. Khummueng, & S. K. Park, (2011). Identification of Odor-active Components of Agarwood Essential Oils from Thailand by Solid Phase Microextraction-GC/MS and GC-O, *Journal of Essential Oil Research* 23: 46-53.
7. M. A. NorAzah, Y. S. Chang, J. Mailina, A. A. Said, J. A. Majid, S. S. Husni, H. N. Hasnida, & Y. N. Yasmin (2008). Comparison of Chemical Profiles of Selected Gaharu Oils from Peninsular Malaysia, *The Malaysian Journal of Analytical Sciences* 12: 338-340.
8. N. A. Latif (2009). Analysis volatile compound of Gaharu oil composition via solid phase micro extraction (SPME), Bachelor of Chemical Engineering, Faculty of Chemical & Natural Resources Engineering, University Malaysia Pahang.
9. M. Ishihara, T. Tsuneya, & K. Uneyama (1993), Fragrant sesquiterpenes from agarwood, *Phytochemistry* 33: 1147-1155.
10. M. Ishihara, T. Tsuneya, & K. Uneyama, (1991). Guaiane sesquiterpenes from agarwood, *Phytochemistry* 30: 3343-3347.
11. M. Ishihara, T. Tsuneya, M. Shiga, & K. Uneyama, (1991). Three sesquiterpenes from agarwood, *Phytochemistry* 30: 563-566.
12. S. N. Tajuddin (2011). Resolution of complex sesquiterpene mixture in Aqualaria malaccensis (Gaharu) volatile oils using gas chromatography methods, PhD, Faculty of Industry and Science Technology (FIST), Universiti Malaysia Pahang (UMP).
13. M. N. Taib, R. Andres, & R. Narayanaswamy (1996). Extending the response range of an optical fibre pH

sensor using an artificial neural network, *Analytica Chimica Acta* 330: 31-40.
14. N. Ismail, M. H. F. Rahiman, M. N. Taib, N. A. M. Ali, M. Jamil & S. N. Tajuddin, (2013). Analysis of Chemical Compounds of Agarwood Oil based on Headspace-Solid Phase Microextraction combined with Gas Chromatography Mass-Spectrometry, *2013 IEEE 9th International Colloquium on Signal Processing and its Applications (CSPA 2013):* 215 - 218, 8-10 March 2013.
15. T. Jayalakshmi & A. Santhakumaran, (2011). Statistical normalization and back propagation for classification, *International Journal of Computer Theory and Engineering* 3: 1793-8201.
16. M. Ishihara, T. Tsuneya, & K. Uneyama (1993). Components of the volatile concentrate of agarwood, *Journal of Essential Oil Research* 5: 283-289.
17. M. A. NorAzah, J. A. Majid, J. Mailina, A. A. Said, S. S. Husni, H. N. Hasnida, M. A. M. N. M. Arip, & Y. S. Chang (2009). Profiles of selected supreme Agarwood oils from Malaysia, *Herbal Globalisation: A New Paradigm for Malaysian Herbal Industry (MAPS 2008):* 393-398.

The Malaysian Journal of ANALYTICAL SCIENCES ISSN 1394-2506

POSTHARVEST QUALITY OF MANGO (*MANGIFERA INDICA* L.) FRUIT AFFECTED BY DIFFERENT LEVELS OF GIBBERELLIC ACID DURING STORAGE

(Kesan Kandungan Asid Giberelik Berbeza ke atas Kualiti Buah Mangga (*Mangifera Indica* L.) Lepas Tuai Semasa Penyimpanan)

Md. K. Islam[1]*, M. Z. H. Khan[3], M. A. R. Sarkar[4], S. Yeasmin[2], Md. K. Ali[1], M. H. Uddin[5]

[1]*Department of Crop Science and Technology,*
[2]*Department of Geology and Mining,*
University of Rajshahi, Bangladesh
[3]*Department of Chemical Engineering,*
[4]*Department of Genetic Engineering and Biotechnology,*
Jessore Science and Technology University, Jessore, Bangladesh
[5]*Department of Applied Chemistry and Chem. Tech.,*
Islamic University, Bangladesh

**Corresponding author: mki_crop@yahoo.com*

Abstract

The experiment consisted of two popular mango varieties in Bangladesh (*viz*., Langra and Khirshapat) and four different levels of Gibberellic acid (GA_3) solution, namely, control, 100, 200 and 400 ppm. The two factors experiment was assigned in randomized complete block design with three replicates. Data obtained from various biochemical analyses in terms of physicochemical properties and shelf life of postharvest mango, were recorded and statistically analyzed for comparison among the mean values using Duncan's Multiple Range Test (DMRT) and Least Significant Difference (LSD). The Khirshapat showed better performance in achieving higher quantity of moisture, progressively lost physiological weight, increased pulp pH, TSS after 6^{th} day of storage, produced more quantity of sugar (total, reducing and non-reducing), as well as extended shelf life and delayed skin color changes than Langra at all the storage duration. Different levels of GA_3 solution subjected to the investigation demonstrated significant variation in most of the physicochemical properties and shelf life of mango at different days after storage. The results explored that some physicochemical properties *viz*., physiological weight loss, moisture content, pulp pH, TSS, sugar (total, reducing and non reducing), were rapidly increased from untreated mangoes. GA_3 at 400 ppm showed better performance in delaying the changes in physicochemical properties and extended shelf life.

Keywords: postharvest, mango, varieties, GA_3, storage

Abstrak

Eksperimen ini melibatkan dua jenis mangga popular di Bangladesh (Langra dan Khirshapat) dan empat tahap kandungan asid Giberelik yang berbeza (GA3) iaitu kawalan, 100, 200 dan 400 ppm. Dua faktor eksperimen ini ditandai secara rawak lengkap pada reka bentuk blok dengan tiga replikasi. Data yang diperolehi daripada pelbagai analisis biokimia dari segi sifat fizikokimia dan jangka hayat mangga lepas tuai telah direkodkan dan dianalisis untuk perbandingan antara nilai min menggunakan ujian DMRT dan LSD. Mangga Khirshapat menunjukkan prestasi yang lebih baik dalam kuantiti kelembapan yang lebih tinggi, kehilangan berat fisiologi secara beransur - ansur, meningkatkan pH pulpa, jumlah pepejal larut selepas hari ke-6 penyimpanan, kuantiti gula yang terhasil lebih banyak (jumlah , penurun dan bukan penurun) serta jangka hayat yang panjang dan perubahan warna kulit lebih lambat berbanding Langra bagi semua tempoh penyimpanan. Tahap kandungan GA3 yang berbeza menunjukkan perbezaan yang ketara dalam kebanyakan sifat-sifat fizikokimia dan jangka hayat mangga pada hari yang berbeza selepas penyimpanan. Keputusan menunjukkan bahawa beberapa ciri-ciri fizikokimia iaitu kehilangan berat fisiologi, tahap kelembapan, pH pulpa, jumlah pepejal larut, kandungan gula (jumlah , penurun dan bukan penurun) telah meningkat dengan pesat berbandiing mangga yang tak terawat. GA3 pada 400 ppm menunjukkan prestasi yang lebih baik dalam proses melambatkan perubahan sifat fizikokimia dan memanjangkan jangka hayat.

Kata kunci : Lepas Tuai , mangga, variasi, GA3 , penyimpanan

Introduction

Mango being a highly perishable fruit possesses a very short shelf life and reach to respiration peak of ripening process on 3rd or 4th day after harvesting at ambient temperature [1]. The shelf life of mango varies among its varieties depending on storage conditions. It ranges from 4 to 8 days at room temperature and 2-3 weeks in cold storage at 13ºC [2]. This short period seriously limits the long distance commercial transport of this fruit [3]. Usually after harvesting, the ripening process in mature green mango takes 9-12 days [4]. The ripening process of mango fruit involves a series of biochemical reactions, resulting into increased respiration, ethylene production, change in structural polysaccharides causing softening, degradation of chlorophyll, developing pigments by Carotenoids biosynthesis, change in carbohydrates or starch conversion into sugars, organic acids, lipids, phenolics and volatile compounds, thus leading to ripening of fruit with softening of texture to acceptable quality [4].

Fruit sensitivity to decay, low temperature and general fruit perishability due to the rapid ripening and softening limits the storage, handling and transport potential [5]. On the other hand, application of modified atmosphere (MA) or controlled atmosphere (CA) is not always compatible with this fruit. Although CA storage has been shown to extend the shelf-life of mango [6], it is cost prohibitive. MA storage was also reported to slow mango ripening, but was often accompanied by high CO_2 and off flavor [7].

Gibberellic acid 2000 ppm gave a highly effective treatment for retarding rate [8]. If mangoes are treated with GA3 150 ppm and Bavistin 1000 ppm, both the treatment slowdown the process of ripening. Significant delay in the ripening of mango fruits was observed with Gibberellic acid [9]. The interaction between post-harvest treatments and storage periods was found to be significant for physical quality parameters and non-significant for chemical quality parameters, whereas storage period significantly affected both type of parameters [10].

In this present investigation, we tried to study the behavioral pattern of physicochemical properties of postharvest mango in the storage conditions. Especially the effects of GA_3 on pH, tritability and sugar contents were studied in details. It was also aimed to find out a desirable technology for extension of storage of mango.

Materials and Methods

Preparation of GA3 solution

The solution of GA3 of 100, 200, and 400 ppm was prepared by dissolving 100, 200, and 400 mg of GA3 in one litre of distilled water. The fruits of both varieties were dipped into the solution for a period of 5 minutes. Care was taken to ensure sufficient absorption of GA3 by the fruits and then they were stored at room temperature on brown paper.

Application of GA3

Different levels of GA_3 used in the experiment were sequentially assigned to the collected fruits. After the application of treatments, the fruits were kept on a brown paper, which was previously laid out in Randomized Complete Block Design and placed on the laboratory floor at ambient condition. Each of the blocks consisted of the experimental type. For each treatment combination of replication, there were six fruits, of which one was kept to record shelf life, changes in weight, color and other external fruit characteristics. The remaining five fruits were preserved in a deep refrigerator (-85^0 C) at Protein and Enzyme Laboratory in the Department of Biochemistry and Molecular Biology, University of Rajshahi, for recording the data periodically at five different dates (at 3 days interval). Five fruits from each treatment combination of every replicate were chemically analyzed for the determination of the changes, total titratable acidity, pulp pH, total soluble solid (TSS), sugar content (total, reducing and non-reducing). To ensure the application of different storage treatment of the fruits for each variety, the following procedures were accomplished.

Parameter Study

Titratable acidity of mango pulp was determined by the method of Ranganna [19] The pH 7 and pH 4 buffer tablets (BDH chemicals Ltd., Poole, England) were used to determine pulp pH of mango. Total soluble solid (TSS) content of mango pulp was estimated by using Abbe Refractometer. Temperature correction was done using the methods as described by Ranganna [19] Total sugar content of mango pulp was determined calorimetrically by the Anthrone method as stated by Jayaraman [20]. Reducing sugar content of mango was determined by Dinitrosalicylic acid

method as denoted by Miller, [21]. Non-reducing sugar content of mango pulp was calculated by using the following formulae: % Non-reducing sugar = % total sugar - % reducing sugar.

Results and Discussion

Titratable acidity

Variation in between varieties means in terms of titratable acidity was observed to be highly significant at different days after storage. At various days during storage, Langra showed higher titratable acid content as compared with Khirshapat. Titratable acidity fell off with the passing of storage period. The diminishing trend was very fast from initial to 3rd day and thereafter, its trend was comparatively slower (Table 1). At initial day, the highest (3.88%) was derived from Langra whereas the lowest (2.60%) was derived from Khirshapat. At 12th day, the highest (0.35%) was reported from langra whereas; Khirshapat produced the lowest amount (0.29%). The abating trend of titratable acidity at storage period was reported by Upadhyay and Tripathi [11]. According to them, acidity was reduced during storage growth on attainment of maturity and ripening. The results of the present investigation might be possibly due to genetical dissimilarities between two varieties.

Table 1. Changes of titratable acidity and pulp pH of postharvest mango pulp between varieties during storage at ambient condition

Treatments	Titratable acidity (%) at different days					Pulp pH at different days				
Variety (V)	Initial	3	6	9	12	Initial	3	6	9	12
V_1	3.88a	1.20a	0.86a	0.61a	0.35a	3.50	4.30b	5.30b	5.93b	6.70
V_2	2.60b	1.03b	0.71b	0.49b	0.29b	3.58	4.55a	5.55a	6.18a	6.80
Level of significance	***	***	***	***	***	NS	***	***	***	NS

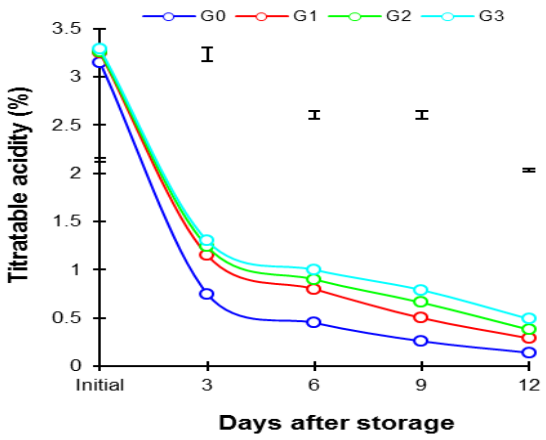


Figure 1. Titratable acidity of mango pulp as influenced by different doses of GA3 at different days after storage. Vertical bars represent LSD at 0.05 level.

Table 2. Combined effects of varieties and different doses of Gibberellic acid solution on titratable acidity and pulp pH of postharvest mango during storage at ambient condition

Treatments combination	Titratable acidity (%) at different days					Pulp pH at different days				
Varieties × Treatments	Initial	3	6	9	12	Initial	3	6	9	12
V_1G_0	3.80 b	0.95d	0.55e	0.30e	0.15g	3.60ab	4.60ab	5.60ab	6.90a	7.00ab
V_1G_1	3.90ab	1.20bc	0.85c	0.58c	0.33e	3.50ab	4.30de	5.30de	5.80cd	6.80bd
V_1G_2	3.82 b	1.28ab	0.95b	0.72b	0.40c	3.50ab	4.20ef	5.20ef	5.60 e	6.60df
V_1G_3	3.98 a	1.35 a	1.10a	0.85a	0.52a	3.40b	4.10f	5.10f	5.40f	6.40f
V_2G_0	2.50d	0.55e	0.35f	0.22f	0.12h	3.70a	4.70a	5.70a	7.00a	7.10a
V_2G_1	2.60 d	1.10 c	0.75d	0.42d	0.25f	3.60ab	4.60ab	5.60ab	6.10 b	6.90ac
V_2G_2	2.70 c	1.20bc	0.85c	0.60c	0.35d	3.50ab	4.50bc	5.50bc	5.90 c	6.70ce
V_2G_3	2.60cd	1.25ab	0.90bc	0.73b	0.45b	3.50 b	4.40cd	5.40cd	5.70de	6.50ef
Level of significance	**	***	*	NS	NS	NS	NS	NS	NS	NS
CV%	1.65	4.82	4.07	5.80	5.26	2.95	2.40	1.96	1.73	1.85

In a column values having the same letter(s) do not differ significantly as per DMRT at 5% level; V_1 = Langra; V_2=Khirshapat; *** indicate at 0.1% level; NS means non-significant

Different doses of GA_3 solution used in this investigation in terms of titratable acidity exhibited significant variation among the means at various days after storage. At various days of storage, titratable acid content came down very sharply from initial to 3 days and then, it came down steadily (Figure 1). In all the storage period, higher titratable acidity (3.29, 1.30, 1.00, 0.79 and 0.49%) was noted at G_3 treatment from initial to 12^{th} days followed by 3.15, 0.75, 0.45, 0.26 and 0.14% from untreated mangoes, respectively. These results are in conformity with the findings of Khumlert [12].

The combined effect of varieties and different doses of GA_3 solution in relation to titratable acidity of mango pulp exhibited significant variation at different days after storage except 9^{th} and 12^{th} days. At different days of storage, there showed a diminishing trend of titratable acid content with the expansion of storage period. At 6^{th} day, the highest (1.10%) quantity was obtained from the treatment combination of V_1G_3 which was statistical similar with the combination of V_1G_2 and the lowest acid concentration (0.35%) obtained from the treatment combination of V_2G_0. These occurrences might be probably due to the reduction of acid oxidation at V_2G_3 combination and, to have genetical variation in between varieties (Table 2).

Pulp pH

The analysis of variance in between the varieties showed significant in respect of pulp pH of mango at different days after storage except initial and 12^{th} day (Table 1). At various days of storage, there noticed an increasing trend of pulp pH with the rising of storage period. In each storage period, pulp pH exposited more in Khirshapat compared with Langra. Higher pulp pH (4.55) was notified from Khirshapat at 3^{rd} day whereas; lower (4.30) was identified from Langra. At 12^{th} day, the highest pH (6.80) was identified with Khirshapat and the lowest value (6.70) was identified with Langra. The growing up trend of pulp pH was also observed by Kumar *et al.* [13] and Shahjahan *et al.*[14]. This phenomenon might be possible due to oxidation of acid during storage resulting in higher pH and also might have genetically dissimilarities between varieties.

Different doses of GA3 solution imposed to this trial demonstrated significant variation in pulp pH at different days after storage .The rising trend of pulp pH was found from different treated and untreated fruits at various days of storage (Figure 2). Pulp pH was higher in control at all stages of storage period followed by the fruits treated with

G_1, G_2 and G_3 treatments. The pH of mango pulp was the highest (7.05) in control whereas the fruits treated with G_3 treatment gave the lowest (6.45) value at 12th day. The results of the present investigation of GA3 solution at G_3 treatment retarded the loss of acid oxidation resulting in lower pH value. These results are in partially supported by the report of Jain and Mukherjee [15].

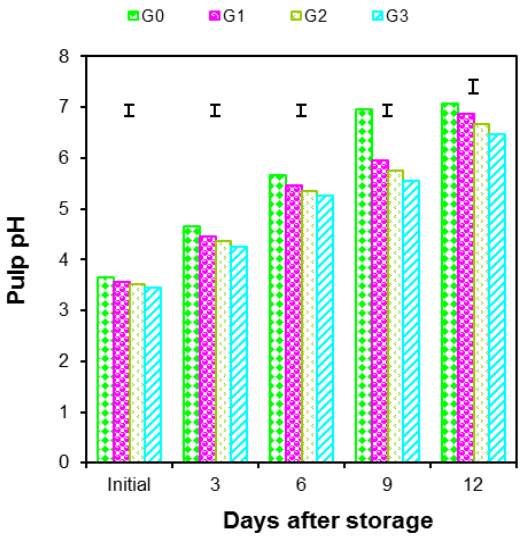


Figure 2. Pulp pH of mango pulp as influenced by different doses of GA3 at different days after storage. Vertical bars represent LSD at 0.05 level

The combined effect of varieties and different doses of GA_3 solution implied to this study in pulp pH were noticed to be non significant at different days after storage. There was the indication of an enhancing trend of pulp pH from various treatment combinations at different days of storage. At 12th day, the highest (7.10) pH value was obtained from the treatment combination of V_2G_0 and the lowest (6.4) was obtained from the treatment of combination of V_1G_3 (Table 2)

Total soluble solid (Brix %) content

Statistically highly significant variation was found in TSS content between two varieties at different days after storage. The results showed that TSS content of mango pulp enlarged continuously with the rising of storage period. The increasing trend was faster from initial to 6th day thereafter; it increased slower. From initial to 6th day, Khirshapat was performed better in TSS accumulation than Langra. But, after 6th day, Langra performed better than Khirshapat up to 12th day. At 9th day, the highest (16.28%) TSS quantity was noticed from Khirshapat and the lowest (16.03%) was noticed from Langra (Table 3).

Different doses of GA_3 solution subjected to the postharvest mangoes in this study were observed to be significant variation in respect of TSS content at different days after storage. At different days of storage, it narrated that TSS accumulation augmented with the expansion of storage duration. The results also illustrated that TSS content was sharply grown up from untreated mangoes from initial to 6th day and then, it fell off significantly (Figure 3). The other treatment such as G_1 also increasingly provided TSS from initial to 9th day and thereafter, it decreased sharply. Mango fruits treated with G_2 also produced more or less similar increasing trend from initial to 12th day. But, the fruits treated with G_3 dose provided very steady rate in TSS accumulation at various days. The highest (19.25, 19.25 and 19.30%) accumulation of TSS was derived from G_0, G_1 and G_2 treatment at 6, 9 and 12th days whereas, the lowest (10.20, 13.00 and 16.00%) was derived from G_3 treatment, respectively. The results of the present study are strongly supported by the findings of Jain and Mukherjee [15]. These happened possibly due to ripening condition

resulting in maximizing TSS gathering in control and 400 ppm of GA3 solution retarded in ethylene synthesis that caused delay ripening and ultimately in lower TSS accumulation. It also explained that TSS gathering is strongly related to ripening and it caused decrease owing to decaying.

Table 3. Changes of total soluble solid and total sugar content of postharvest mango pulp in varieties during storage at ambient condition

Treatments	TSS content (%)at different days					Total sugar content (%) at different days				
Variety (V)	Initial	3	6	9	12	Initial	3	6	9	12
V_1	5.30b	9.28b	13.78b	16.28a	16.35a	5.34b	8.08b	12.80b	16.08b	18.35b
V_2	6.35a	10.33a	14.28a	16.03b	16.05b	5.80a	8.58a	13.28a	16.58a	18.80a
Level of significance	***	***	***	***	***	***	***	***	***	***

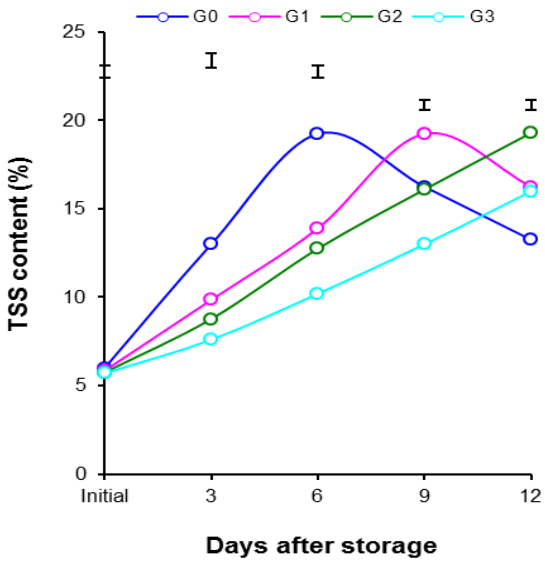


Figure 3. Effect of different doses of GA3 on total soluble solid content of mango pulp at different days after storage. Vertical bars represent LSD at 0.05 level

The combined effect of varieties and imposed different doses of GA_3 solution on TSS content were found to be significant at different days after storage except initial and 3rd day. The result was expounded a rising behavior of TSS content at different days after storage. The highest accumulation (19.50, 19.30 and 19.50) was derived from the treatment combination of V_1G_0, V_1G_1 and V_1G_2 at 6, 9 and 12th days, whereas; the lowest value (10.30, 12.90 and 15.90) was identified from the treatment combination of V_2G_3, respectively (Table 4).

Table 4. Combined effects of varieties and different doses of Gibberellic acid solution on total soluble solid and total sugar content of postharvest mango during storage at ambient condition

Treatments combination	TSS content (%) at different days					Total sugar content (%) at different days				
Varieties × Treatments	Initial	3	6	9	12	Initial	3	6	9	12
V_1G_0	5.50d	12.5b	19.5a	16.5b	13.50f	5.50d	10.2b	18.80b	20.70b	19.80d
V_1G_1	5.30e	9.30d	13.30d	19.30a	16.30c	5.40 d	7.90d	13.20d	18.40d	20.40b
V_1G_2	5.20e	8.20e	12.20e	16.20c	19.50a	5.30de	7.30e	10.30f	13.80f	18.80f
V_1G_3	5.20e	7.10f	10.10g	13.10e	16.10d	5.17e	6.90f	8.90 h	11.40h	14.40h
V_2G_0	6.50a	13.50a	19.00b	16.00d	13.00g	6.00a	10.7a	19.20a	21.20a	20.20c
V_2G_1	6.40ab	10.40c	14.50c	19.20a	16.2cd	5.80b	8.30c	13.60c	18.80c	20.80a
V_2G_2	6.30bc	9.33 d	13.30d	16.00d	19.10b	5.70bc	7.90d	10.90e	14.40e	19.40e
V_2G_3	6.20c	8.10 e	10.30f	12.90f	15.90e	5.68bc	7.40e	9.40 g	11.90g	14.80g
Level of significance	NS	NS	***	**	**	NS	NS	NS	NS	NS
CV%	1.82	1.17	0.76	0.49	0.50	2.05	1.27	0.79	0.76	0.57

In a column values having the same letter(s) do not differ significantly as per DMRT at 5% level. V_1 = Langra; V_2 = Khirshapat; *** indicate at 0.1% level; NS means non-significant

Total sugar content

Highly significant variation was noticed between both the varieties means in terms of total sugar content of mango pulp at different days after storage. The results interpreted that TSC accumulated successively with the rising of storage duration. The accumulating trend was more or less sharp from initial to 9th day in both the varieties, thereafter; it grew up slightly slower. At all days of storage Khirshapat contributed more accumulation of of TSC than Langra. At initial day, Khirshapat gave the highest (5.80%) whereas; Langra produced the lowest (5.34%). At 12th day, Khirshapat produced the highest quantity (18.80%) and the lowest (18.35%) was obtained from the Langra (Table 3). Upadhyay and Tripathi [11] reported that total sugar content was augmented gradually, when stored for 6 days at room temperature. These results are in conformity with the findings of Shahjahan *et al.* [14]. Tsuda *et al.* [16] also found the similar results. The increase in TSC might be due to conversion of complex starch or carbohydrate into simple compound like sucrose, Fructose, galactose etc.

Different doses of GA_3 solution implied to the investigation on total sugar content of mango pulp exhibited significant variation at different days after storage (Appendix 3.5). At different days of storage, the results noticed that TSC augmented markedly with the rising of storage period (Figure 4). The developing trend was very fast in untreated mango followed by other treatments *viz.*, G_1, G_2 and G_3, respectively. The highest quantity of TSC (20.95% and 20.60%) was recorded in control and G_1 treated mangoes at 9 and 12th days, whereas; the lowest (11.64% and 14.60%) was recorded at G_3 treatment. The findings of the present investigation are inconformity with the reports of Jain and Mukherjee [15] and Singh *et al*. [17]. The enhancing trend of total sugar at untreated mangoes might be possible due to breaking down of complex carbohydrate into simple compound but, G_3 treatment made delay ripening at storage period resulting in lower conversion of complex compound into simple molecules.

The combined effect of varieties and used different doses of GA_3 solution in this study in relation to total sugar content of mango pulp showed non-significant variation at different days after storage. These results noted that total sugar content accumulated successively with the rising of storage period. At 12th day the maximum (20.80 %) quantity of TSC was achieved from the treatment combination of V_2G_1 whereas, the minimum (14.40 %) was achieved from the treatment combination of V_1G_3 (Table 4).

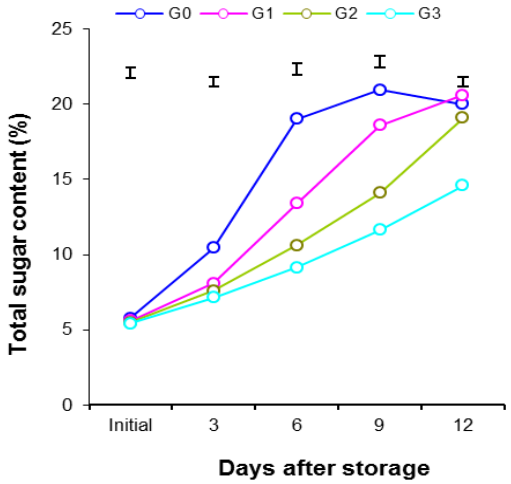


Figure 4. Effect of different doses of GA3 on total sugar content of mango pulp at different days after storage. Vertical bars represent LSD at 0.05 level

Table 5. Changes of reducing and non reducing sugar content of postharvest mango pulp between varieties and influenced by different doses of Gibberellic acid solution during storage at ambient condition

Treatments	Reducing sugar content (%) at different days					Non-reducing sugar content (%) at different days				
Variety (V)	Initial	3	6	9	12	Initial	3	6	9	12
V_1	1.29b	1.96 b	3.82	4.81 b	4.86 b	4.03 b	6.11b	9.29 b	11.26 b	13.46 b
V_2	1.66 a	2.35 a	3.83	5.13 a	5.18 a	4.13 a	6.23 a	9.43 a	11.48 a	13.63 a
Level of significance	***	***	NS	***	***	*	*	**	***	**
Treatments (G)										
G_0	1.55	3.05 a	6.05 a	6.25 a	4.75 c	4.20 a	7.40 a	12.90 a	14.70 a	15.20 a
G_1	1.48	2.03 b	4.14 b	5.98 b	6.18 a	4.10 ab	6.08 b	9.93 b	12.63 b	14.43 b
G_2	1.43	1.83 c	2.88 c	4.38 c	5.38 b	4.05 b	5.78 c	7.73 c	9.73 c	13.73 c
G_3	1.45	1.73 c	2.23 d	3.28 d	3.78 d	3.98 b	5.43 d	6.88 d	8.43 d	10.82 d
Level of significance	NS	***	***	***	***	*	***	***	***	***

In a column values having the same letter(s) do not differ significantly as per DMRT at 5% level. V_1 = Langra; V_2 = Khirshapat; *** indicate at 0.1% level; NS means non-significant

Reducing sugar content

Analysis of variance demonstrated significant variation on reducing sugar content of mango pulp at different days after storage except at 6th day. There was noticed an enhancing trend of reducing sugar with the expanding of storage period (Table 5). It also stated that Khirshapat was better in achieving of reducing sugar than Langra at different days of storage. The highest (5.18%) quantity of this sugar was notified from Khirshapat whereas; the lowest (4.86%) was notified from Langra at 12th days of storage. These results are in agreement with the report of Upadhyay and Tripathi [11]. Castrillo *et al.,* [18] elucidated that reducing sugar was increased during storage

period. Khirshapat producing comparatively more reducing sugar might be possibly due to genetical variation in both the varieties.

Different doses of GA_3 solution applied to this study were found to be significant in respect of reducing sugar content of mango pulp at different storage period except initial day. The results narrated that reducing sugar of mango pulp was grown up continuously at different days after storage. It also revealed that untreated mangoes were performed better in accumulating of reducing sugar as compared to the other treatments. Control treatment was recorded as more successive producer of reducing sugar up to 9^{th} day and then, it fell off due to starting spoilage. At 12^{th} day, the maximum (6.18%) amount of reducing sugar was recorded at G_1 and the lowest (3.78%) was recorded at G_3 treatment (Table 5). The results of the present investigation are in conformity with the findings of Jain and Mukherjee [15]. Lower changing trend of reducing sugar content treated with G_3 treatment might be possibly due to delay ripening which resulted in lower conversion of carbohydrates into simple's molecules.

The combined effect of varieties and used different doses of GA_3 solution of mango pulp exhibited non significant variation in terms of reducing sugar content of mango pulp at different days after storage except 6^{th} day. The results elucidated that reducing sugar content augmented continuously at three days interval up to 9^{th} day thereafter, it abated from the treatment combination of V_2G_0. At 12^{th} day, the highest (6.35%) quantity was obtained from the treatment combination of V_2G_2 and the lowest (3.7%) was obtained from V_1G_3 (Table 6)

Non reducing sugar content

The variation between the varieties means exhibited highly significant in respect of non-reducing sugar content at different days after storage. There appeared an enlarging trend of non reducing sugar content at different days of storage. At all days, it was noticed that the Khirshapat was much better than Langra in achieving of non reducing sugar content (Table 5). At 12^{th} day, higher (13.63%) amount of non reducing sugar was recorded from the Khirshapat and the lowest (13.46%) amount was recorded from the Langra. The results of the present investigation are partially supported by the reports of Islam [22]. The result obtained from the investigation might be possible due to varietals dissimilarities.

Different doses of GA_3 solution subjected to this trial produced the significant variation in respect of non reducing sugar content of mango pulp at different days. The results stated that non reducing sugar content of mango pulp grew up markedly at various days. It also mentioned that untreated fruits were notified better in accumulation of more quantity of non reducing sugar followed by other treatments. This growing up trend was continued up to 9^{th} day and then, it fell off owing to becoming hackneyed. Lower rising trend was noted from the fruit treated with G_3 treatment. The highest result (15.20%) was obtained from control and the lowest value (10.82%) was obtained from G_3 treatment (Table 5). These events might be probably due to G_3 treatment resisted ethylene synthesis of mango pulp resulted in delay ripening and little amount of non reducing sugar deposition. These results are in partially agreement with the reports of Khumlert [12].

The combined effect of varieties and used different doses of GA_3 solution showed not significant variation in terms of non reducing sugar content of mango pulp at different days after storage. There was exposition that a hastening trend of non reducing sugar was notified from different treatment combinations at various days of storage. At 9^{th} day, the highest (14.80%) quantity of non reducing sugar was derived from the treatment combination of V_2G_0 whereas; the lowest (8.20%) was derived from the treatment combination of V_1G_3 (Table 6).

Table 6. Combined effects of varieties and different doses of Gibberellic acid solution on reducing and non reducing sugar content of postharvest mango pulp during storage at ambient condition

Treatments combination	Reducing sugar content (%) at different days					Non-reducing sugar content (%) at different days				
Varieties × Treatments	Initial	3	6	9	12	Initial	3	6	9	12
V_1G_0	1.40 b	2.90 b	5.90 a	6.10b	4.60f	4.10ab	7.30 b	12.80b	14.60b	15.10b
V_1G_1	1.30bc	1.80ef	4.63 b	5.80c	6.00b	4.05 b	6.10 c	9.90 c	12.60c	14.40c
V_1G_2	1.25bc	1.65fg	2.65de	4.15e	5.15d	4.00 b	5.65 e	7.65 d	9.65 d	13.65d
V_1G_3	1.20 c	1.50 g	2.10 e	3.20f	3.70g	3.97 b	5.40 f	6.80 e	8.20 f	10.70f
V_2G_0	1.70 a	3.20 a	6.20 a	6.40a	4.90e	4.30 a	7.50 a	13.00a	14.80a	15.30a
V_2G_1	1.65 a	2.25 c	3.65 c	6.15b	6.35a	4.15ab	6.05cd	9.95c	12.65c	14.45c
V_2G_2	1.60 a	2.00 d	3.10cd	4.60d	5.60c	4.10ab	5.90 d	7.80 d	9.80 d	13.80d
V_2G_3	1.69 a	1.95de	2.35de	3.35f	3.85g	3.98 b	5.45 f	6.95 e	8.65 e	10.95e
Level of significance	NS	NS	*	NS	NS	NS	NS	NS	*	NS
CV%	7.20	4.80	11.14	2.13	2.11	2.63	1.72	1.13	0.93	0.78

In a column values having the same letter(s) do not differ significantly as per DMRT at 5% level. V_1 = Langra; V_2 = Khirshapat; *** indicate at 0.1% level; NS means non-significant

Conclusion

Different doses of GA_3 solution imposed to this investigation in terms of titratable acidity showed significant variation among the means at various days of storage. There appeared a slightly rising trend of pulp pH from various treatment combinations at different days of storage. At different days of storage, the results showed that TSS accumulation increased with the increase of storage duration. The combined effect of varieties and different doses of GA_3 solution exhibited non-significant in terms of non-reducing sugar content of mango pulp at different days after storage.

References

1. Narayana, C. K., Pal, R. K. & Roy, S. K. (1996). Effect of pre-storage treatments and temperature regimes on shelf-life and respiratory behaviour of ripe Baneshan mango. *Journal Food Science Technology* 33: 79 – 82
2. Carrillo, L. A., Ramirez-Bustamante, F. Valdez-Torres, J. B. Rojas-Villegas, R. & Yahia, E. M. (2000). Ripening and quality changes in mango fruit as affected by coating with an edible film. *Journal Food Quality* 23: 479 – 486.
3. Gomer-Lim, M. A. (1997). Post harvest physiology. In: The Mango: Botany, Production and Uses. (Es.): R.E. Litz. , CAB International, New York. pp. 425-446
4. Herianus, J. D. Singh, L. Z. & Tan, S. C. (2003). Aroma volatiles production during fruit ripening of Kensington Pride Mango. *Postharvest Biology Technology* 27: 323 – 336.
5. Hoa, T. T., Duamp, M. N. Lebrun, M. & Baldwin, E. A. (2002). Effect of different coating treatments on the quality of Mango fruit. *Journal Food Quality* 25: 471 – 486.
6. Bender, R. J., Brecht, J. K. Baldwin, E. A. & Malundo, T. M. M. (2000). Aroma volatiles of maturegreen and tree ripe 'Tommy Atkins' mangoes after controlled atmosphere vs air storage. *Horticultural Science* 35: 684 – 686.
7. Gonzalez-Aguilar, G., Zacarias, L. Mulas, M. & Lafuente, M. T. (1997). Temperature and duration of water dips influence chilling injury, decay and polyamine content in Fortune mandarins. *Postharvest Biology Technology* 12: 61 – 69.
8. Parmar, P. B. and Chundawat, B. S. (1989). Effect of various post-harvest treatments on the physiology of Kesar Mango. *Acta Horticultural* (ISHS), 231: 679 – 684.

9. Khader, S. E. S. A. (1992). Effect of Gibberellic acid and vapor guard on ripening, amylase and peroxidase activities and quality of mango fruits during storage. *Journal of Horticultural Science & Biotechnology* 67(6): 855 – 860.
10. Singh A. K., Singh, C. P. Kushwaha, P. S. & Chakraborty, B. (2012). Efficacy of post-harvest treatments on fruit marketability and physico-chemical characteristics of dashehari mango. *Progressive Horticulture* 44: 215-219.
11. Upadhyay, N. P., & Tripathi, B. M. (1985). Postharvest changes during storage and ripening of Gaurjeet mango (*Mangifera indica* L.) fruits. *Progressive Horticultural* 17(1): 25-27.
12. Khumlert, R. (1992). Effect of gibberellic acid (GA3) on some physico-chemical characteristics of 'Kheaw' and 'Sawoey' mango fruit. *Collage Laguna*, Philippines, p. 95.
13. Kumar, P., & Singh, S. (1993). Effect of GA3 and Ethrel on ripening and quality of mango cv. Amrapali. *Horticultural. Journal* 6(1): 19 – 23.
14. Shahjahan, M. S., Sheel, M. A., Zaman, M. A. and Sakur, M. A. (1994). Optimization of harvesting maturities for major mango cultivars in Bangladesh. *Bangladesh Journal Science Research* 12(22): 209 – 215.
15. Jain, S. K. & Mukherjee, S. (2001). Postharvest application of GA3 to delay ripening in mango (*Mangifera indica* L.) cv. Langra. *Journal of Eco-physiology.* 4(12): 27 – 30.
16. Tsuda, T., Chachin, K. & Ueda, Y. (1999). Studies on keeping quality of imported 'Carabao' mango fruit from the Philippines. *Journal Japan Society. Horticultural Science* 68(3): 669 – 674.
17. Singh, S., Kumar, P. Brahmachari, V. S. & Singh, D. M. (1995). Effect of post-harvest spray of GA_3 and Ethrel on storage life of mango cv. Amrapali. Orissa *Journal Horticultural* 23(1/2): 112-118.
18. Castrillo, M., Kruger, N. J. & Whatley, F. R. (1992). Sucrose metabolism in mango during mango ripening. *Plant Science* 84(1): 45 – 51.
19. Ranganna, S. (1979). Manual of analysis of fruits and vegetable products. Tata McGraw Hill Pub. Co. Ltd., New Delhi, p. 634
20. Jayaraman, J. (1981). Laboratory Manual in Biochemistry (Ist ed.) Wiley Eastern Ltd. New Delhi, India.
21. Miller, G.L. (1972). Use of Dinitro Salicylic acid reagent for determination of reducing sugar. *Analytcal Chem*istry, 31: 426-428
22. Islam, M. K. (2013). Behavioral Pattern of Physicochemical Constituents of the Postharvest Mango (*Mangifera indica* L.) Influenced by Storage Stimuli**.** *Pakistan Journal Biology Sci*ence 16 (24):1985 – 1990.